OBTAINING DESIGN INFORMATION FROM FULL-SCALE STRUCTURES

GEOFFREY EUSTICE BLIGHT

Publications submitted to the University of Cape Town in fulfilment of the requirements for the degree of Doctor of Science in Engineering

Field: Civil Engineering

1993

2. THE NEED TO ESTABLISH OR VALIDATE DESIGN PARAMETERS AND PRINCIPLES.

2.1 Blight, G E and Mitchell, M F (1980). The properties of epoxy resin mortars for use in nosings to bridge expansion-joints. The Civil Engineer in South Africa, August 1980, pp 203-210.

The paper describes the results of a project undertaken for the South African Department of Transport. Mr M F Mitchell appears as co-author as a courtesy to the sponsoring body.

2.2 Blight, G E and Barrett, A (1990). Field test of catenary net to protect traffic from mining subsidence. ASCE Journal of Transportation Engineering, vol 116, No. 2, pp 135-144.

This project was carried out for a metropolitan transportation authority via a firm of consulting engineers. Mr Barrett was the liaison person representing the consultants. I carried out all of the investigation and analysis and wrote the paper.

2.3 Blight, G E (1987). Measurements on a tied-back retaining wall. Proceedings, International Conference on Soil-Structure Interactions, Paris, France, pp 513-520.

2.4 Blight, G E (1987). The concept of the master profile for tailings beaches. Proceedings, International Symposium on Prediction and Performance in Geotechnical Engineering, Calgary, Canada, pp 361-365.

2.5 Blight, G E (1987). Lowering of the groundwater table by deep-rooted vegetation - the geotechnical effects of water table recovery. Proceedings, 9th European Conference on Soil Mechanics and Foundation Engineering, Dublin, Ireland,

pp 285-288.

2.6 Blight, G E, Schwartz, K, Weber, H and Wiid, B L (1992). Preheaving of expansive soils by flooding-failures and successes, Proceedings, 7th International Conference on Expansive Soils, Dallas, Texas. Paper accepted for publication.

My co-authors consulted me on each of four case histories described in this review paper, thus involving me in the practical research attached to each case. I wrote the paper and assess my contribution at 60%.

3. DETERIORATION OF REINFORCED EARTH STRUCTURES

3.1 Blight, G E and Dane, M S W (1989). Deterioration of a wall complex constructed or reinforced earth. Geotechnique, vol 39, No 1, pp 47-53.
Discussion and reply: vol 39, No 3, pp 567-570.

This investigation, carried out over a period of six years, was undertaken for a mining house. Mr Dane was the head-office engineer for the mine owning the reinforced earth wall complex. He played the very important role of facilitator in the investigation. I carried out the investigation and wrote the paper.

Seeing the content of the paper as a threat to the reputation of their product, the Reinforced Earth Company Submitted a vigorous discussion of the paper. For the sake of a balanced view, this discussion and my reply have been included.

3.2 Blight, G E (1987). Effects of collapse settlement of fill on reinforced earth walls. Proceedings, 2nd International Conference on Case Histories in Geotechnical Engineering, St. Louis, USA, vol 2 pp 929-934.

4. EROSION OF THE SLOPES AND SURFACES OF TAILINGS DAMS

4.1 Blight, G E (1987). Erosion of the slopes of gold tailings dams. Proceedings, ASCE Conference on Geotechnical Practice for Waste Disposal, Ann Arbor, USA, pp 294-305.

4.2 Blight, G E (1989). Erosion losses from the surfaces of gold-tailings dams. Journal, South African Institute of Mining and Metallurgy, vol 89, No 1, pp 28-29.

4.3 Blight, G E (1991). Erosion and anti-erosion measures for abandoned gold tailings dams. Proceedings, 1991 National Meeting, American Society of Surface Mining and Reclamation, vol 1, pp 323-330.

5. GROUNDWATER POLLUTION CAUSED BY SANITARY LANDFILLS

5.1 Ball J M and Blight, G E (1986). Groundwater pollution downstream of a long established sanitary landfill. Proceedings, International Symposium on Environmental Geotechnology, Allentown, USA, pp 149-157.

This paper is based on work done for the MSc(Eng) degree by Mr J M Ball. I planned and supervised the work and wrote the paper.

5.2 Blight, G E, Vorster, K and Ball, J M (1987). The design of sanitary landfills to reduce groundwater pollution. Proceedings, International Conference on Mining and Industrial Waste Management, Johannesburg, Vol 1, pp 297-305.

The paper is based largely on work done towards a PhD degree by Mr Vorster, but includes material from Mr Ball's MSc(Eng) research. I planned and supervised the work and wrote the paper.

5.3 Blight, G E, Hojem, D J and Ball, J M (1989). Generation of leachate from landfills in water-deficient areas. Proceedings, 2nd ISWA International Landfill Symposium, Sardinia, pp XXVI-15. Also to be published as Chapter 2 of Landfilling of Waste: Leachate, Ed: Christensen, T, Cossu, R and Stegman, R. Elsevier Scientific Publishers (1992).

The paper is based on work for MSc(Eng) degree by mr D J Hojem. Sampling of gas-filled test holes in the landfills was carried out by Mr J M Ball, probably the only person in the world able to do this. I planned and supervised the work and wrote the paper.

5.4 Blight, G E, Ball J M and Blight, J J (1991). Moisture distribution in sanitary landfills. Proceedings, 3rd International Landfill Symposium, Sardinia, Vol 1, pp 813-822. Expanded version accepted for publication by ASCE Journal of Environmental Engineering.

This paper is based on measurements made by Mr J M Ball and Miss J J Blight as part of their MSc(Eng) research, under my supervision. I planned and supervised the work and wrote the paper.

5.5 Blight, G E and Mabula, M C (1992). Designing clay liners for sanitary landfills. Accepted for Proceedings, International ISWA Conference on Solid Waste, Madrid, 10pp.

This paper is based partly on measurements made by Mr M C Mabula towards his MSc(Eng) dissertation. I supervised the research and wrote the paper.

6. THE EFFECTS OF ALKALI-SILICA REACTION ON REINFORCED CONCRETE STRUCTURES

6.1 Blight, G E and Alexander, M G (1988). Evaluating reinforced concrete structures affected by alkali aggregate reaction. Proceedings, International Symposium on Re-evaluation of Concrete Structures, Copenhagen, Denmark, pp 309-317.

Professor M G Alexander is a colleague of mine (and former undergraduate and postgraduate student) who has collaborated with me in work on ASR. I drafted the paper and assess my contribution to it at 80%.

6.2 Blight, G E, Alexander, M G, Ralph, T K and Lewis, B A (1989). Effect of alkali-aggregate reaction on the performance of a reinforced concrete structure over a six-year period. Magazine of Concrete Research, vol 41, No 147, pp 69-77.

This paper is based on work done for the City of Johannesburg via a firm of consulting engineers, represented by Messrs Ralph and Lewis. The consultants carried out the analysis of the structure and arranged the logistics of the two full-scale tests. I planned and supervised the measurements, assisted by Professor Alexander. I also drafted the paper. I assess my contribution to the overall result at 50%.

6.3 Blight, G E (1989). Experiments on waterproofing concrete to inhibit AAR. Proceedings, 8th International Conference on Alkali-Aggregate Reaction, Kyoto, Japan, pp 733-739.

6.4 Blight, G E (1990). Rehabilitation of reinforced concrete structures affected by alkali-silica reaction. Structural Engineering Review, vol 2, pp 1-8.

6.5 Blight, G E (1990). Can concrete structures be waterproofed to inhibit ASR? Proceedings, International Conference on the Protection of Concrete, Dundee, U.K., pp 223-232.

6.6 Blight, G E (1991). A study of four waterproofing systems for concrete. Magazine of Concrete Research, vol 43, no 156, pp 81-87.

6.7 Blight, G E (1992). The moisture condition in an exposed structure damaged by alkali-silica reaction. Magazine of Concrete Research, vol 43, no 157, pp 96-101.

6.8 Alexander, M G, Blight, G E and Lampacher, B J (1992). Pre-demolition tests on structural concrete damaged by AAR. Proceedings, 9th International Conference on Alkali-Aggregate Reaction in Concrete, London. Accepted for publication.

Prof. M G Alexander is a former student of mine and present colleague. B J Lampacher is an Msc(Eng) student. The paper was written by me, based on research by Lampacher, jointly supervised by Alexander and me.

7. ASSESSING DESIGN LOADING ON BINS AND SILOS FOR STORING BULK MATERIALS

7.1 DESIGN LOADING ON SILOS

7.1.1 Blight, G E (1986). Structural loading on the walls of rapidly filled silos. Encyclopedia of Fluid Mechanics, vol 4, Solids and Gas-Solids Flows (N.P. Cheremisinoff, Ed.) pp. 195-219.

7.1.2 Blight, G E (1986). Pressures exerted by materials stored in silos : Part 1, Coarse materials. Geotechnique, vol 36, No 1, pp 33-46.

7.1.3 Blight, G E (1986). Pressures exerted by materials stored in silos : Part 2, Fine powders, Geotechnique, vol 36, No 1, pp 47-56.

7.1.4 Blight, G E (1988). A comparison of measured pressures in silos with code recommendations, Bulk Solids Handling, vol 8, No 2, pp 145-153.

7.1.5 Blight, G E (1988). Design loading for grain silos - intention and reality. International Summer Meeting, American Society of Agricultural Engineers, Rapid City, USA, 12 pp.

7.1.6 Blight, G E (1990). Defects in accepted methods of estimating design loading for silos. Institution of Civil Engineers (London), Proceedings Part 1, vol 88, pp 1015-1036. Discussion and reply, (1991) vol 90, pp 1077-1088.

7.1.7 Blight, G E (1992). Temperature induced loading on silo walls. Structural Engineering Review, vol 4. In press

7.2 MEASUREMENT OF PRESSURES AND LOADS IN SILOS

7.2.1 Blight, G E (1987). Measurements on full size silos Part 1 : Temperatures and strains. Bulk Solids Handling, vol 7, No 6, pp 781-786.

7.2.2 Blight, G E and Bentel, G M (1988). Measurements on full size silos. Part 2 : Pressures. Bulk Solids Handling, vol 8, No 3, pp 343-346.

Dr G M Bentel was, at the time, a PhD student who developed the concept of the zero strain pressure cell under my supervision. I wrote the paper, and assess my contribution at 90%.

7.3 TEMPERATURES AND PRESSURES MEASURED IN SILOS BY MEANS OF PRESSURE CELLS

7.3.1 Blight, G E and Midgley, D (1981). Pressure measured in a 20m diameter coal load-out bin. Journal of Powder and Bulk Solids Technology, vol 5, No 2, pp 21-31.

This study was carried out for a firm of consulting civil engineers. Mr D Midgley was the designer of the silo, I designed and installed the instrumentation, took the measurements and drafted the paper. I estimate my contribution to the paper at 75%.

7.3.2 Blight, G E (1986). A comparison of design and measured lateral pressures in a large coal load-out silo. International Journal of Bulk Solids Storage in Silos, Vol 2, pp 1-8.

7.3.3 Schaffner, R H and Blight, G E (1986). A comparison of design and measured lateral pressures in a large Ibau-type cement storage silo. International Journal of Bulk Solids Storage in Silos, vol 2, No 2, pp 17-24.

The situation for this study was similar to that for paper 7.3.1, Mr Schaffner was the designer of the silo. I estimate my contribution to the paper at 75%.

7.3.4 Fliss, L and Blight G E (1986). A comparison of design and measured lateral pressures and temperatures in a large duo-cell cement storage silo. International Journal of Bulk Solids Storage in Silos, vol 2, No 4, pp 18-28.

The situation was similar to that for papers 7.3.1 and 7.3.3. Mr Fliss was the designer of the silo. I estimate my contribution to the paper at 75%.

7.3.5 Blight, G E (1983). Performance of a 20m diameter steel maize storage bin. Proceedings, 2nd International Conference on Design of Silos for Strength and Flow, Stratford-upon-Avon, UK, pp 179-191.

7.3.6 Blight, G E (1990). Temperature surcharge pressures in reinforced concrete silos. Accepted for publication in Powder Handling and Processing, vol 2, No 3.

7.3.7 Blight, G E (1991). Eccentric emptying of a large coal bin with six outlets. Bulk Solids Handling, vol 11, No 2, pp 451-457.

7.4 MEASUREMENTS OF STRAIN IN THE REINFORCING OF REINFORCED CONCRETE SILOS.

7.4.1 Blight, G E, Schaffner, R H and Gilbert, B (1982). Strains in a reinforced concrete silo during rapid filling with a fine powder. Journal of Powder and Bulk Solids Technology, vol 6, No 2, pp 17-27.

The designer of the silo was Mr Schaffner while Mr Gilbert represents the contractor.

I estimate my contribution to the paper at 80%.

7.4.2 Schaffner, R H and Blight, G E (1983). Comparison of design assumptions and measured performance for cement works silos. Proceedings, 2nd International Conference on Design of Silos for Strength and Flow, Stratford-upon-Avon, UK, pp 207-216.

I was commissioned to write this paper by Mr Schaffner, on behalf of his firm. My contribution to the paper was thus 100%.

7.4.3 Blight, G E and Dreyer, H N (1989). Behaviour of a reinforced concrete coal silo under a design overload. Bulk Solids Handling, vol 9, No 1, pp 21-25.

This study was commissioned for a mining house. Mr Dreyer was head office engineer for the mine. I planned and undertook the investigation and drafted the paper. I estimate my contribution to the paper at 90%.

7.5 MEASUREMENT OF LOADS IN STEEL SILOS VIA ELECTRIC RESISTANCE STRAIN GAUGES

7.5.1 Blight, G E (1985). Temperature changes affect pressures in steel bins. International Journal of Bulk Solids Storage in Silos, vol 1, No 3, pp 1-7.

7.5.2 Blight, G E and Garstang, A (1987). Strains measured in a 7,500t sugar silo. Bulk Solids Handling, vol 7, No 4, pp 573-582.

Mr Garstand was designer of the silo. I planned and carried out the investigation and drafted the paper. My contribution to the paper is assessed at 80%.

7.5.3 Blight, G E (1988). Strains measured in a 7,500t sugar silo, Part II. Bulk Solids Handling, vol 8, No 4, pp 413-419.

7.5.4 Blight, G E (1989). Behaviour of a bolted corrugated steel grain silo. Powder Handling and Processing, vol 1, No 2, pp 143-149.

7.5.5 Blight, G E (1989). Strain and temperature measurements on an externally stiffened corrugated steel grain silo. Powder Handling and Processing, vol 1, No 4, pp 343-347.

7.5.6. Blight, G E (1990). Load and temperature strains of a welded plane plate grain silo. Powder Handling and Processing, vol 2, No 1, pp 25-29.

7.5.7 Blight, G E (1990). Measured loading on a small steel grain silo. Powder Handling and Processing, vol 2, No 2, pp 1-6.

7.5.8 Blight, G E (1991). Structure-fill interaction in steel grain silos. Powder Handling and Processing, vol 3, No 1, pp 43-48.

1. INTRODUCTORY

CONTRIBUTIONS TO LEARNING

1.1 It is believed that this is the first time, or one of the few occasions on which the aims and objectives of field observation and measurement have been analysed to establish principles that should be followed in future exercises of this type.

1.2 Tropical residual soils display certain differences in their behaviour from transported soils. This paper shows that provided these differences are recognized, the behaviour of tropical soils under load can be rationally predicted.

1.3 While the broad behaviour of hydraulic fill soil structures is well understood, certain aspects of the detailed behaviour of hydraulic fill are less well appreciated. A number of these aspects are discussed in the paper in relation to several applications of hydraulic filling.

1.4 The objective of this paper was to show that geotechnical principles can have a wide application in the field of mining.

1.5 This paper set out to show that changes of geological proportions need not only occur over periods of several hundred or thousand millennia, but can occur quite quickly, i.e. within the life-span of a man. Also, the activities of man have now reached such a magnitude that they can be said to be causing geological change. These changes may need to be considered in geotechnical design.

1. INTRODUCTORY

1.1 Blight, G E (1986). Obtaining design information from measurements on full-scale structures. Proceedings, Speciality Geomechanics Symposium, Adelaide, Australia, vol 1, pp 43-44. Keynote Address.

1.2 Blight, G E (1988). Construction in tropical soils. Proceedings, 2nd International Conference on Geomechanics in Tropical Soils, Singapore, vol 2, pp 449-467. Keynote Address.

1.3 Blight, G E (1988). Some less familiar aspects of hydraulic fill structures. Proceedings, Hydraulic Fill Structures, ASCE Speciality Conference, Fort Collins, Colorado, Geotechnical Special Publication, No 21, pp 1000-1064. Postnote (Closing) Address.

1.4 Blight, G E (1989). Geotechnical engineering in mining. Proceedings, 12th International Conference on Soil Mechanics and Foundation Engineering, Rio de Janeiro, vol 4, 11pp. (Still not published at end 1991 because organizing committee had lost French translations of titles and synopses!). Special Plenary Lecture.

1.5 Blight, G E (1989). Tropical processes causing rapid geological change. Proceedings, 25th Annual Conference of the Engineering Group of the British Geological Society, Edinburgh. Geological Society Engineering Special Publication 7, pp 459-471. Theme Lecture.

SPECIALITY GEOMECHANICS SYMPOSIUM

"Interpretation of Field Testing for Design Parameters"

ADELAIDE
18-19 AUGUST, 1986

STATE OF THE ART ADDRESS
KEYNOTE ADDRESSES
SYMPOSIUM DISCUSSION

The Institution of Engineers, Australia
National Conference Publication No 87/8.

Speciality Geomechanics Symposium
Adelaide 18-19 August, 1986

Obtaining Design Information From Measurements on Full—Scale Structures

G.E. BLIGHT
Professor of Construction Materials, University of Witwatersrand, Johannesburg, South Africa

SUMMARY Five case histories are described to illustrate the utility and versatility of using field instrumentation, testing and monitoring of full-scale structures to provide design parameters. It is shown that the geotechnical engineer, by virtue of his training and his unique understanding of the behaviour of particulate materials can make a significant contribution in related fields such as materials handling and storage and engineering related to underground mining.

1 INTRODUCTION

Measurements and observations made on full-scale structures provide an excellent means of obtaining realistic design information. The information obtainable in this way can, with careful planning and execution, provide answers to all-important questions such as the following :

(i) What theory or type of analysis is most appropriate for the design of this type of structure?

Alternatively, are the theory and parameters that are currently accepted for this type of design realistic?

(ii) What type of test should be used to establish design parameters? What correlation is there between parameters measured by means of various types of small-scale test and those obtaining in full-scale situations?

(iii) Are the requirements of appropriate current design codes realistic? If their requirements are met, will the design be unnecessarily conservative? Are there certain situations for which following a code or other accepted practice, could result in an unsafe situation, or even in failure?

There are also certain drawbacks and difficulties associated with field instrumentation and monitoring that must be realised :

(i) Unless the structure under consideration is one of many of similar type yet to be constructed for the same authority, there is usually difficulty in persuading the client that the cost of instrumentation and monitoring is justified, especially when a tight construction schedule is called for. "Why should I pay for tests that will benefit someone else?" "You are the consultant, you should know all the answers" are common client responses to a proposed instrumentation and monitoring programme.

The need for a site investigation is often by no means obvious to a client and that for instrumentation even less so. The costs of both of these activities tend to be viewed in absolute terms and in isolation rather than as a small percentage of a much gr ater overall cost.

(ii) Field instrumentation and monitoring is certainly costly, time-consuming and, for success, requires a lot of "know how" built up by experience. Bearing client suspicion in mind, the engineer must be reasonably certain that instrumentation and monitoring will have a positive outcome before proposing such a course. If he fails to produce the benefits he has promised the client, there will not be a second chance.

This paper will describe five monitoring projects for which the writer has personally been responsible. The object of describing them is to show what can be achieved by field instrumentation and observation, as well as some of the problems that can arise as a result of inadequate planning.

As the theme of this session is "strength parameters", the cases discussed are all concerned with the role played by shear strength in design. However, only two of the cases concern shear strength directly. In the other three cases, shear strength played an important role, although direct stresses were the primary concern of the designers.

The writer has also taken the liberty of extending the definition of "soil" to "soil and soil-like materials". This is deliberate, as it is the writer's belief that the training of a geotechnical engineer peculiarly befits him to play a far wider role in engineering than his traditional one. In particular, the soils engineer can make an important contribution in the fields of materials handling and storage - currently the preserve of the mechanical engineer, and underground mine support technology - currently served almost exclusively by mining engineers.

2 STRESSES IN THE CORE TRENCH OF AN EARTH DAM

This case history is primarily concerned with vertical stresses in a core trench. It does not involve strength parameters directly, although the shear strength and shear stresses in the soil determine the vertical stresses.

During foundation preparation for the Lesapi earth embankment dam in what is now Zimbabwe, an extensive zone of highly weathered rock was discovered running roughly parallel to the length axis of the dam. Once the highly weathered material had been excavated, a deep narrow trench resulted, measuring almost 30m deep and 5m wide at the bottom, opening up to 15m wide at the top. It was decided to backfill the trench with compacted clay fill.

2.1 Instrumentation

The designers were concerned that "hydraulic fracture" of the core might occur on filling of the dam.

To monitor the situation they decided to install three BRS-type vibrating wire pressure cells in the core as well as Bishop-type twin-tube piezometers with high air entry pressure ceramic filters.

It was at this stage that the writer was consulted and visited the site. It was found that all three pressure cells had already been installed, all in a horizontal position so as to measure vertical pressures. Unfortunately, no thought had been given to measuring horizontal pressures in the trench backfill in order to ascertain the lateral stress ratio K. The piezometers had also been installed and all instruments had been placed close to the bottom of the trench. Additional instrumentation could not be obtained in time to install higher up in the trench, so it was necessary to make do with what was already in place.

2.2 Analysis

A theoretical analysis of likely stresses in the trench fill was carried out (Blight(1973)) using data obtained by aughan(1961) for Selset dam and Blight(1970) for Bridle Drift and Manjirenji dams. The analysis was calibrated by applying it to observations for Balderhead dam by Thomas and Ward (1969) and was found to give good agreement with measured vertical effective stresses, as shown in Figure 1.

In the meantime vane shear tests were carried out in the trench backfill at Lesapi to gain some idea of the lateral stress ratio K in the trench (see, eg Blight(1970)). These tests indicated that K was approximately 2 near the surface of the backfill declining to about 1 near the bottom of the trench.

A comparison of measured vertical stresses with those predicted by the theory is given in Figure 2. The theoretical curve is based on the equation (Blight(1973)) :

$$\sigma_v = \frac{1}{A}\left(\gamma - \frac{1}{Fz}(c' - u_o K \tan\phi')\right)\left[1 - e^{-Ah}\right] \qquad (1a)$$

$$A = \frac{K \tan\phi' (1-\bar{B})}{Fz} \qquad (1b)$$

In which

- γ is the bulk unit weight of the fill;
- F is the factor of safety against shear failure of the soil against the walls of the trench;
- $2z$ is the width of the trench;
- h is the depth under consideration;
- c' and ϕ' are the shear strength parameters of the fill;
- u_o is the initial pore pressure (at placement) in the fill;
- K is the ratio of horizontal to vertical effective stresses in the fill: and
- $\bar{B}$ is the ratio of the pore pressure increment in the fill to a corresponding increment in total stress σ_v.

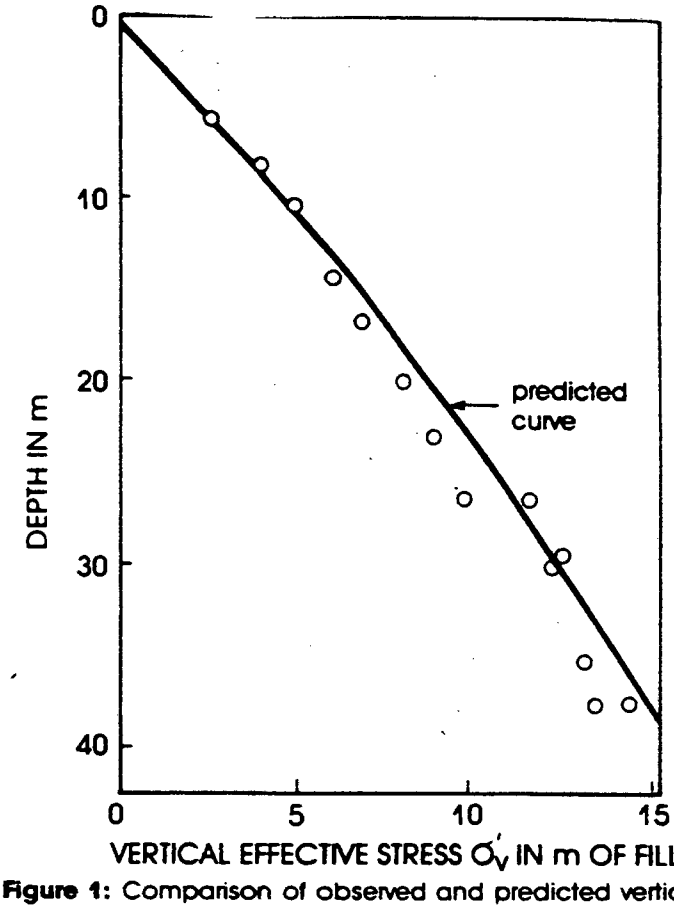

Figure 1: Comparison of observed and predicted vertical effective stresses in Balderhead Dam.

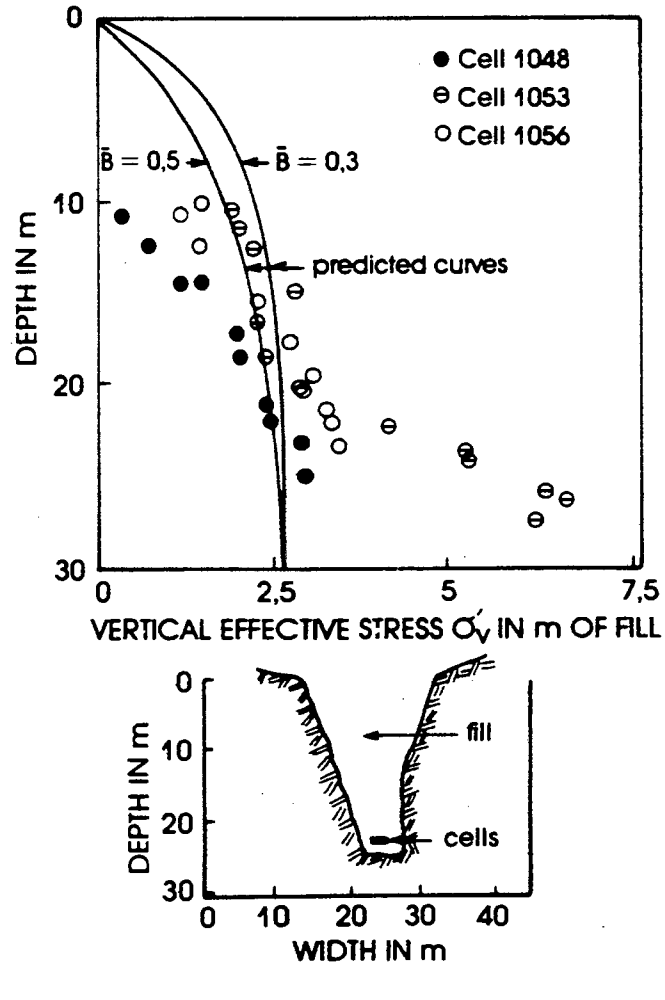

Figure 2: Comparison of observed and predicted vertical effective stresses in Lesapi Dam core trench.

Equations (1a) and (1b) assume undrained compression of the fill in the trench. Agreement of the measured stresses with the theory was fair, the deviation of measurement from theory being probably due to the decrease of K with increasing depth and to lack of a good assessment of the value of K. The theoretical curves were based on the following parameters :

$2z = 6.1m$
$\gamma = 21.3kN/m^3$
$c^1 = 15kPa$
$\phi^1 = 31°$
$u_o = 0$

K was taken as 2 and F as 1.5. The observed value of $\bar{B}$ was 0.3 and Figure 2 also shows a curve for $\bar{B} = 0.5$

The theoretical analysis had also indicated that tensile cleavage of the trench fill would be possible under certain circumstances even before the core was subjected to seepage. The condition for tensile cleavage if K exceeds unity was found to be

$$\sigma_v^1 < \frac{c^1}{(1+\tan^2\phi^1)} \quad (2)$$

2.3 Further field tests

As it appeared from equation (2) and measured values of σ_v^1 that there was a possibility of tensile cleavage occurring in the Lesapi trench, two holes were drilled in the fill, primarily to install two standpipe piezometers, but also to seek evidence of tensile cleavage. The holes were wetdrilled using a wagondrill and a 76mm bit and the water return was monitored for evidence of cleavage fissures. There was a full return of water from both holes until a depth of 24m was reached when there was a sudden and complete loss of drill water. Fortunately, the fissure at this depth did not appear to penetrate the full width of the trench as the rate of water flow into the holes decreased with time, apparently as the clay fill swelled, closing off the fissure. A back analysis of the Balderhead case history (Vaughan, et al (1970)) showed that tensile cleavage during construction had also been a distinct possibility in that case.

2.4 Further analysis

If equations (1a) and (1b) are re-written with the pore pressure u as a variable

$$\sigma_v = \frac{1}{A^1}\{\gamma - \frac{1}{Fz}(c^1 - K\tan\phi^1 u)\}[1-e^{-A^1 h}] \quad (3a)$$

$$A^1 = \frac{K\tan\phi^1}{Fz} \quad (3b)$$

Once the trench had been filled, h became a constant for any point under consideration, while u would vary as construction pore pressures dissipated and seepage pore pressures were established.

If equation (3a) is differentiated partially with respect to u, the result is :

$$\frac{\partial\sigma_v}{\partial u} = 1 \quad (4)$$

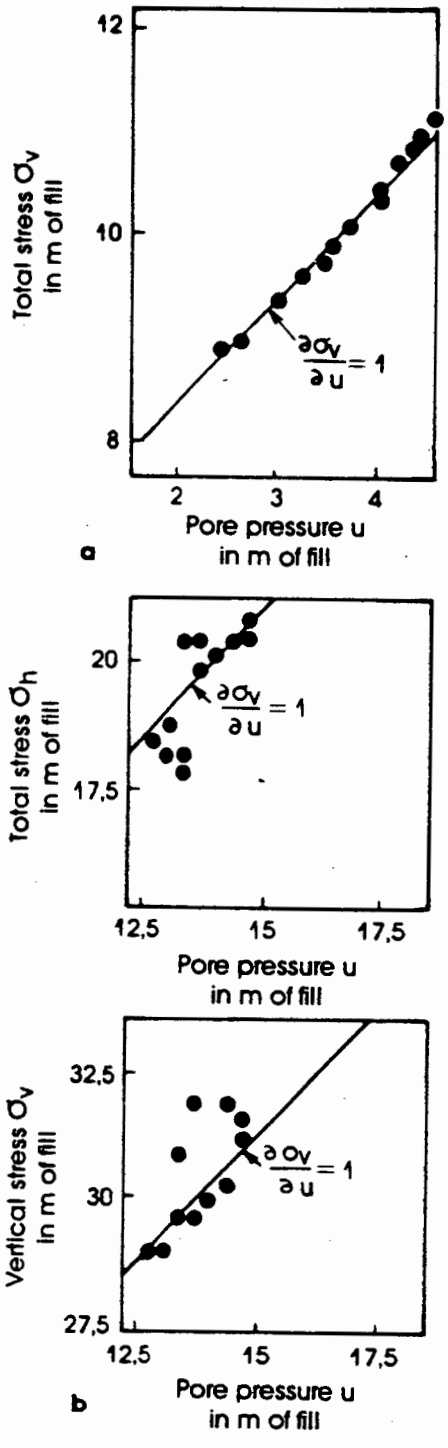

Figure 3: Observed relationships between vertical total stress and pore pressure for (a) the core trench of Lesapi Dam and (b) the core of Balderhead Dam.

That is, any change in vertical stress will be accompanied by an equal change in pore pressure and the effective stress will be unchanged. If, in terms of equation (2), the effective vertical stress σ_v^1 in the fill at the end of construction is every where more than the critical value for tensile cleavage and if σ_v^1 remains constant as seepage occurs, then tensile cleavage of the soil cannot occur, ie "hydraulic fracture" will not take place on reservoir filling.

Figure 3a shows the relationship between pore pressure and vertical stress observed in the Lesapi trench, which agrees remarkably well with the predictions of equation (4). Figure 3b shows similar data taken from the paper by Vaughan et al (1970) for Balderhead dam. Here also, there is a strong suggestion that equation (4) applies, and

that tensile cleavage did not occur as a result of rising pore pressure.

2.5 Conclusions

The lessons of this case history are as follows :

(i) The layout of instrumentation should be carefully planned. The type of instrument and its position should be chosen to yield specific information which preferably has been predicted theoretically during the design.

(ii) Nevertheless, even inadequate instrumentation, if it is working correctly, is very much better than no instruments at all.

(iii) It is only by making measurements that one is able to investigate the validity of unexpected theoretical results.

As a postscript, the core trench of Lesapi dam gave no trouble when the reservoir was filled and has given no trouble since. It is assumed that the tensile fissures located in the fill during construction swelled closed and have since remained so.

3 THE BACK ANALYSIS OF WASTE ROCK DUMP FAILURES

This investigation was undertaken during the mid 1960's (Blight(1969)). The reasons for the study were as follows :

(i) Failures of waste rock dumps in the South African gold mining area were relatively common and frequently disrupted production schedules. At that time the mechanics of the failures had not been studied and there was therefore uncertainty as to how to analyse and design a rock dump for shear stability.

(ii) Failures invariably involved shearing through the relatively thin soil foundation strata. The soil was known to be fissured and slickensided. Studies on stiff fissured soils elsewhere in the world (eg Ward, Marsland and Samuels(1965)) and Skempton and La Rochelle(1965) had indicated that the strength of these materials was dependent on the scale of the test used to determine the strength. The concept of residual strength was beginning to take shape. There was therefore also uncertainty as to what method of shear testing would give realistic shear strength parameters. Were laboratory triaxial or shear box tests on undisturbed specimens appropriate, and if so, what minimum size of specimen should be used? Could in situ tests be used, and if so, what type of in situ test was appropriate?

Four failed rock dumps were chosen for the investigation. Of these, two were "first-time" slides which had occurred as the dumps were being raised in height. The other two dumps had suffered repeated slides. After each slide had occurred, rock was dumped over the failure until a new slide occurred.

In each of the four cases, the surface features of the slide were surveyed and the failure surface located, both on top of the rock dump and by drilling at its toe. Figure 4 shows the details of a typical first-time slide, including the failure surface and the profile of the foundation stratum, while Figure 5 shows similar details for a dump that has slid repeatedly. The Figure shows profiles of the dump after two successive slides that occurred within just over 2 years of each other. It will be seen from the figure that the failure surface through the waste rock remained in roughly the same position, even though the tipping face of the dump had advanced 37m between the successive slides. Successive failures appear merely to extend the horizontal portion of the failure surface, the failure through the rockfill remaining in the same position.

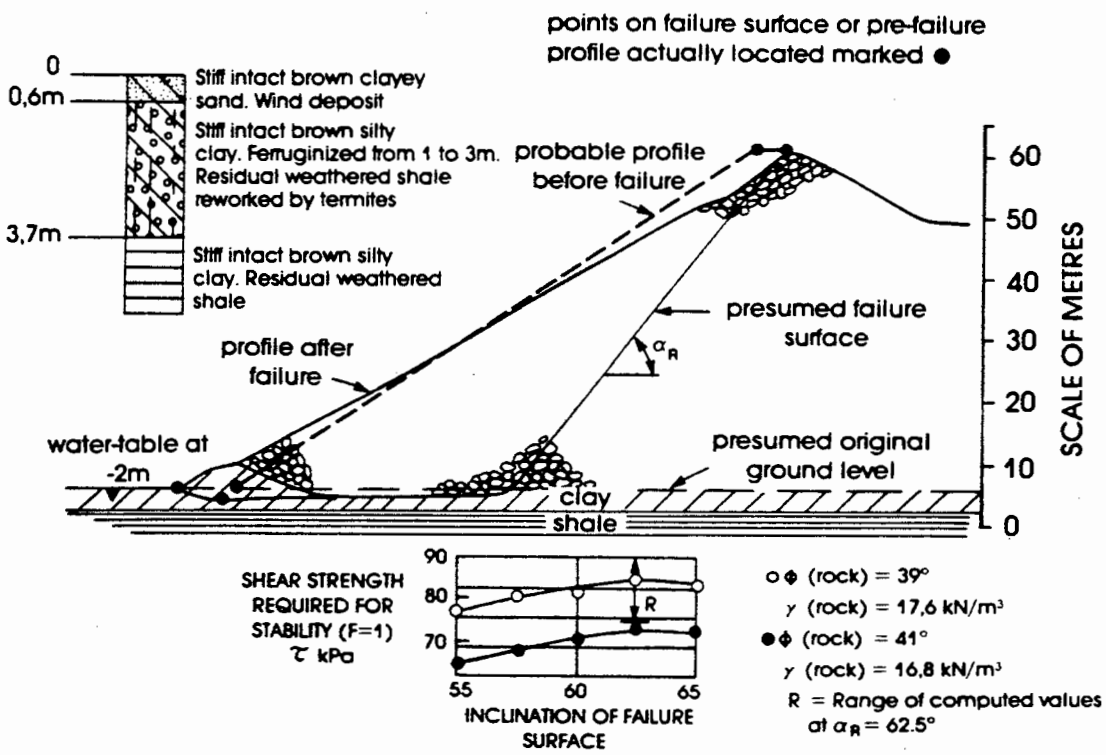

Figure 4: Section through a typical first-time slide in a rock dump on a clay foundation.

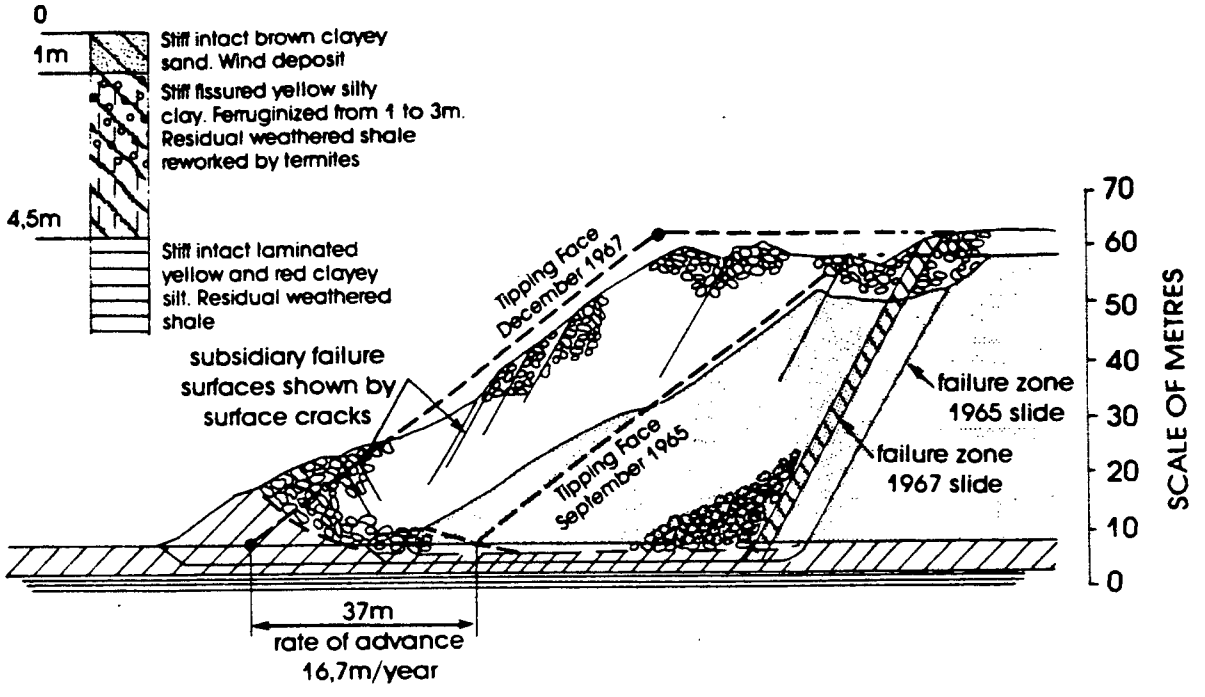

Figure 5: Section through a rock-dump that has failed repeatedly.

3.1 Mechanics of the slides

The surveys of the slides and model tests in the laboratory confirmed that the sliding mass in each case consists of a series of apex-down active driving wedges resisted by apex-up passive resisting wedges, as shown in Figure 6. The base of each passive wedge consists of a roughly horizontal failure surface through the foundation soil. As shown in Figures 4 and 5, the basal failure plane was constrained to be horizontal in each case by the limited depth of foundation soil overlying hard material.

Based on this investigation, the stability of the dumps could be analysed, either by a sliding wedge analysis or by a method such as Janbu's(1957). A number of different analyses were tried, and all gave essentially similar values for the base shear strength in the slides (see 'R' in Figure 4).

3.2 Measurements of shear strength of foundation stratum

It was established from the rate of advance of the dumps that very little consolidation of the foundation strata could be occurring and that failure of the soil was taking place in an essentially unconsolidated undrained mode. The laboratory shear tests used in the investigation were performed on undisturbed samples taken from near the toe of each dump with a 76mm diameter thin-walled open-drive sampler and consisted of unconsolidated undrained triaxial tests on the untrimmed 76mm diameter samples and quick shear box tests, also on 76mm diameter specimens. Field vane shear tests were also carried out. Results of these measurements for the first time slide shown in Figure 4 are given in Figure 7 and for the repeated slide shown in Figure 5, in Figure 8.

This type of comparison has since been performed by many others and hardly needs discussion. Because the spacing of the fissures in the foundation soil under consideration is very close (of the order of 10mm to 20mm), the shear strength of the soil in bulk for a first time failure can be represented quite closely by laboratory triaxial and shear box tests on 76mm diameter specimens, or by the remoulded vane shear strength, as shown in Figure 7.

(a) Active and Passive Wedges in first-time failure

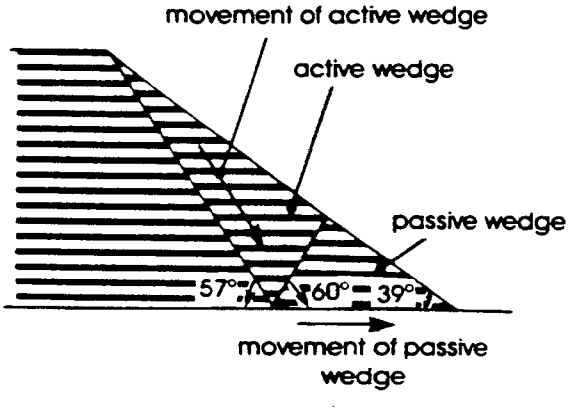

(b) Active and Passive Wedges in subsequent failures

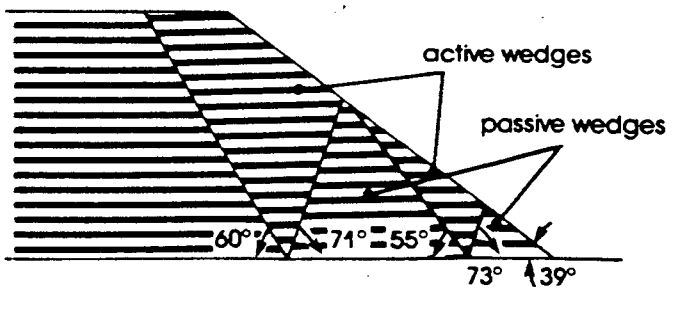

Figure 6: Diagrammatic representation of failures of model slopes on thin horizontal cohesive foundations.

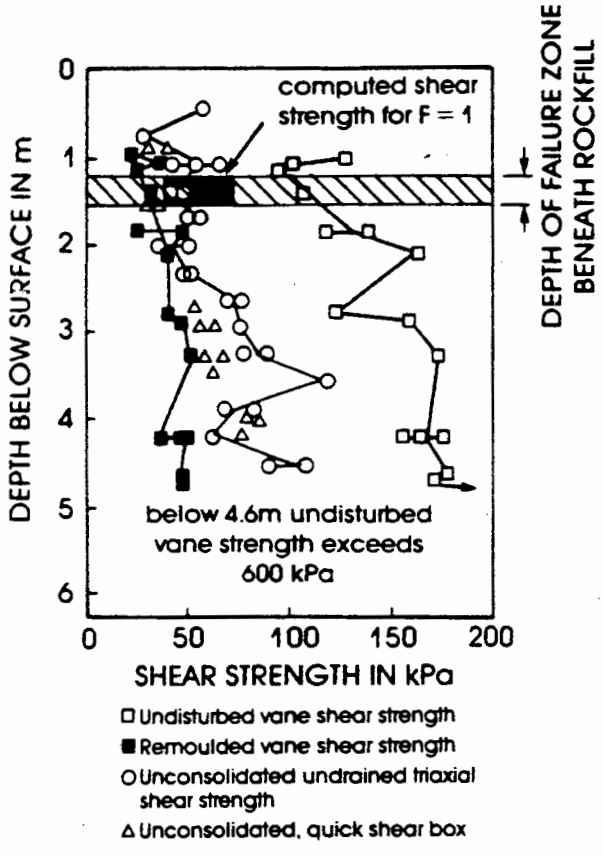

Figure 7: Comparison of measured and calculated foundation strengths for first-time slide in rock dump.

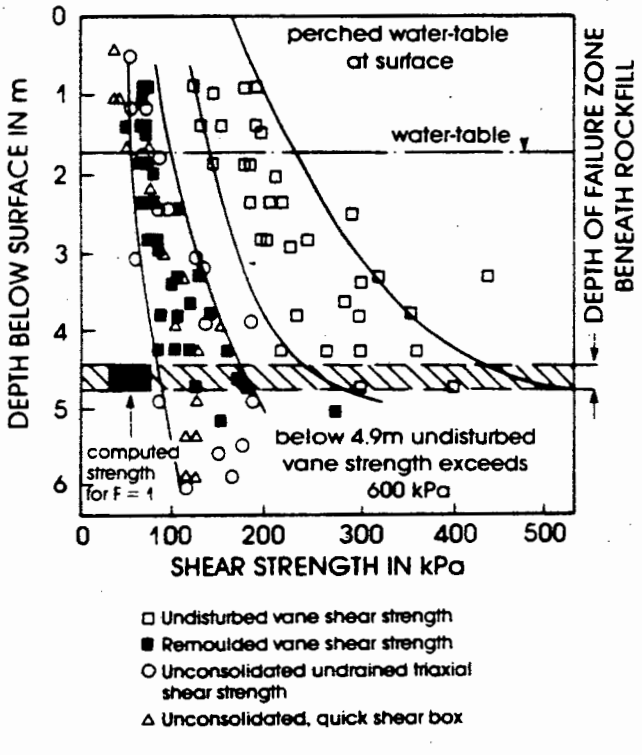

Figure 8: Comparison of measured and calculated foundation strengths for repeated slides in rock dump.

As shown in Figure 8, when repeated failures have taken place the shear strength along the failure surface reduces to a residual value which is somewhat less than the minimum strength value established by means of small-scale tests.

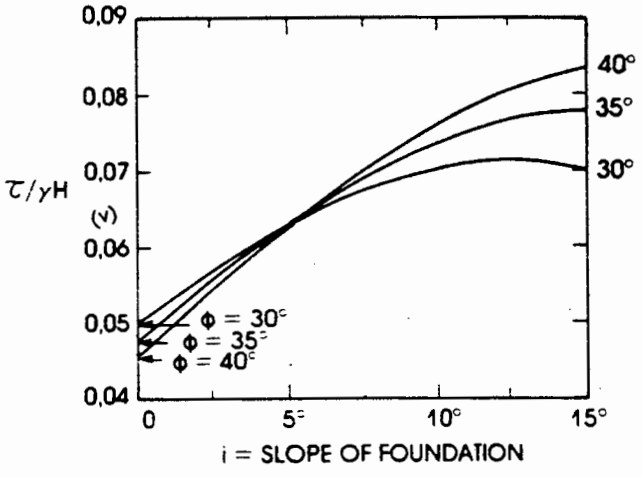

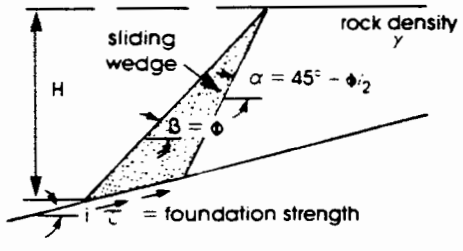

Figure 9: Foundation strength corresponding to failure of dump on shallow cohesive foundation according to sliding wedge analysis.

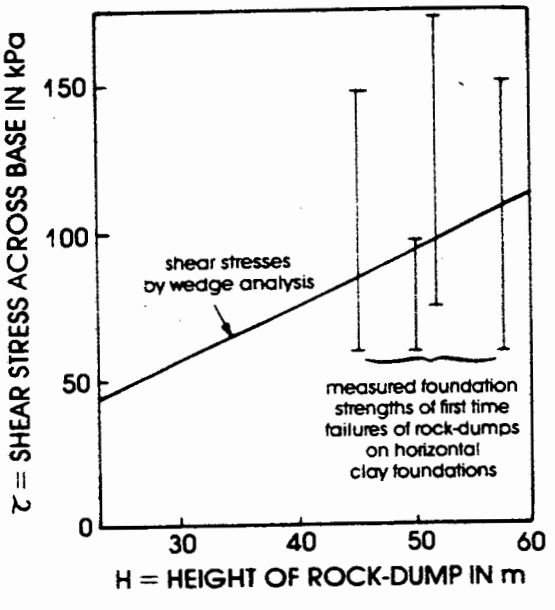

Figure 10: Comparison of measured foundation strengths with strengths required for stability according to wedge analysis

3.3 Design of rock dumps

The situation to be designed against is clearly the first-time slide. This can be analysed in general terms by means of a sliding wedge analysis and hence a stability chart drawn up. The relevant chart (Blight(1979)) is shown in Figure 9. This enables the unconsolidated undrained shear strength of the foundation required for a factor of safety of unity to be identified for any required height of dump. Alternatively, knowing the shear strength of the foundation stratum, the maximum safe height of dump can be found.

The applicability of the chart has been checked against back analyses of four first-time rock-dump failures, the original two investigated and two subsequent slides. The comparison of the stability chart's predictions and the range of shear strengths measured in the field is shown in Figure 10.

3.4 Conclusions

This study produced the following design information :

(i) it established the mode of failure of waste rock dumps on thin cohesive soil foundations;

(ii) this enabled a method of analysis and design to be formulated; and

(iii) it established acceptable means whereby the shear strength of the foundation strata for a proposed rock dump may be measured for the purposes of design.

In this connection, it should be noted that soils in the gold mining areas of South Africa are particularly intensely fissured by repeated desiccation. The conclusions regarding acceptable methods of assessing shear strength may not be valid in other parts of the world. If London clay, for instance, were being considered, the scale of the tests would be too small for reliable strength results to be obtained (see, eg Powell and Quarterman(1986)).

4 PRESSURES IN A CEMENT SILO OF UNUSUAL DESIGN

Like the first case history, this one does not involve shear strength parameters directly. However, the shear strength of the material stored in a silo to a large extent determines the pressures exerted on its walls, and measured shear strength parameters are essential to the accepted method of estimating a design pressure envelope. Cement powder is not soil, but behaves as a highly frictional fine-grained dry silt-like material and obeys the rules of soil mechanics, including the principal of effective stress.

The case concerns a 14000m³ capacity cement silo of unusual design in that the base of the silo consists of an inverted cone which forms a ring-conical hopper. The shape of the silo and its principal dimensions are shown in Figure 11.

The silo was designed in accordance with the German silo design code DIN 1055 (Martens(1980)) which specifies the following properties for cement powder :

Unit weight, γ = 17kN/m³
Angle of shearing resistance, ϕ^1=28°. $\tan\phi^1$=0.53
Angle of wall friction,
cement on concrete, δ=22°. $\tan\delta$=0.40
Cohesion, c^1 = 0
Coefficient of lateral pressure
K (for filling) = 0.5
K (for emptying) = 1.0

In contrast, the measured properties of the cement powder actually stored in the silo are :

Unit weight, γ = 12kN/m³
Angle of shearing resistance, ϕ^1=42°. $\tan\phi^1$=0.90
Angle of wall friction, δ=39°. $\tan\delta$=0.81
Cohesion after precompression to 500kPa, the maximum expected vertical stress, c^1 = 25kPa.

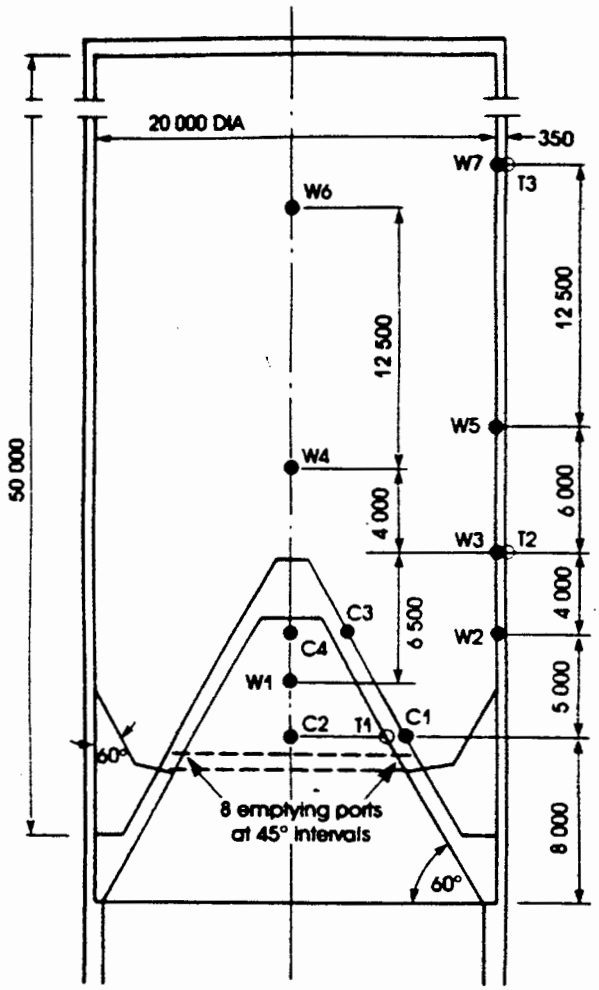

W1 to W7 are pressure cells in walls
C1 to C4 are pressure cells in cone
T1 to T3 are thermo couple pairs
Dimensions are mm

Figure 11: Layout of instrumentation in silo

Coefficient of lateral pressure
K_o (zero lateral yield) = 0.35 (loading)
K_o = up to 1.5 (unloading)
K_A (active condition) = 0.20

This was an example of a structure designed and built for a client (the Pretoria Portland Cement Company) that expects to build many more silos for storing cement and other materials in the future. The client was very willing to pay for instrumentation of the structure, but only up to a limit that was set at the early planning stage. By the time the instruments came to be ordered, inflation and changing currency values had reduced the value of the sum set aside, and the extent of the instrumentation had to be curtailed. The immediate objective of the instrumentation was to check on the design pressures and in particular, to check on pressures exerted on the base cone and on the vertical walls within the ring-conical hopper. The ultimate objective was to obtain information that (hopefully) would enable silos to be designed and built more economically in the future.

4.1 INSTRUMENTATION

Figure 11 shows the layout of pressure cells (W1 to W7 and C1 to C4) and thermocouple pairs (T1 to T3) in the silo. Pressure cells were of the mercury-filled strain gauged diaphragm type, with 200mm diameter sensitive faces.

The pressure cells were calibrated using cement powder in the way described by Blight(1983) and were carefully installed so that their sensitive faces were flush with the inner surface of the silo walls. After grouting in the cells, the sensitive faces were painted with epoxy resin and strewn with fine sand so that the surface texture of the cells was similar to that of the concrete wall surrounding them.

Thermocouples were copper-constantan, arranged in pairs with a junction just below the inner and outer surfaces of the wall.

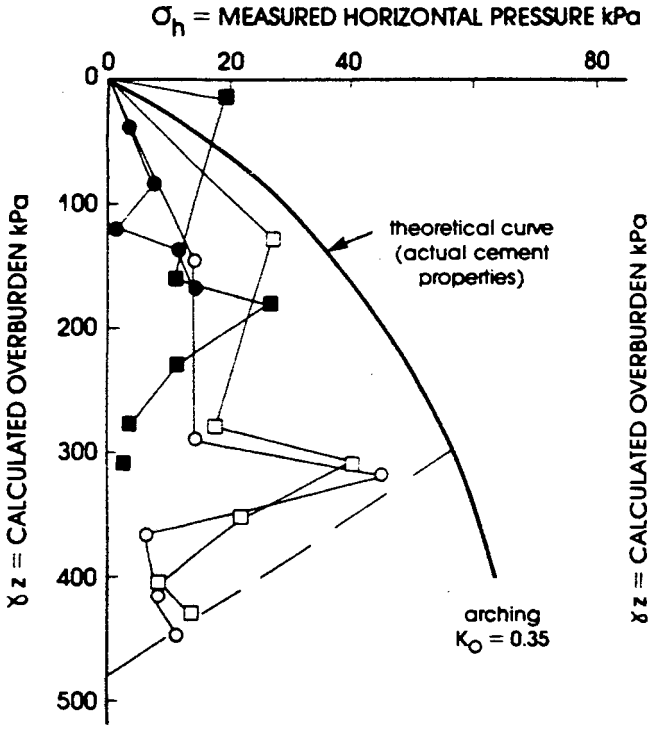

Figure 12a: Individual profiles for pressure on wall

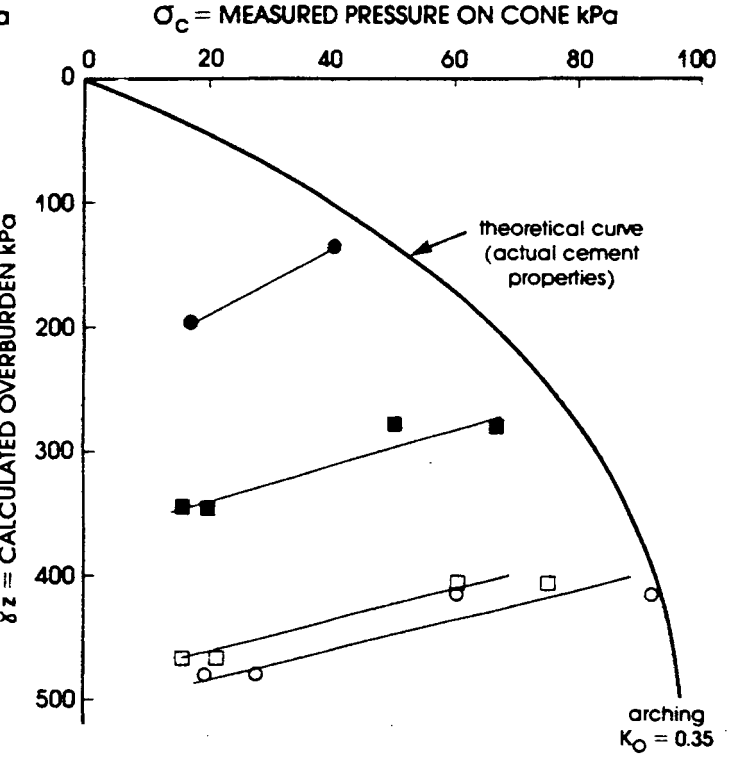

Figure 12b: Individual profiles for pressure on cone

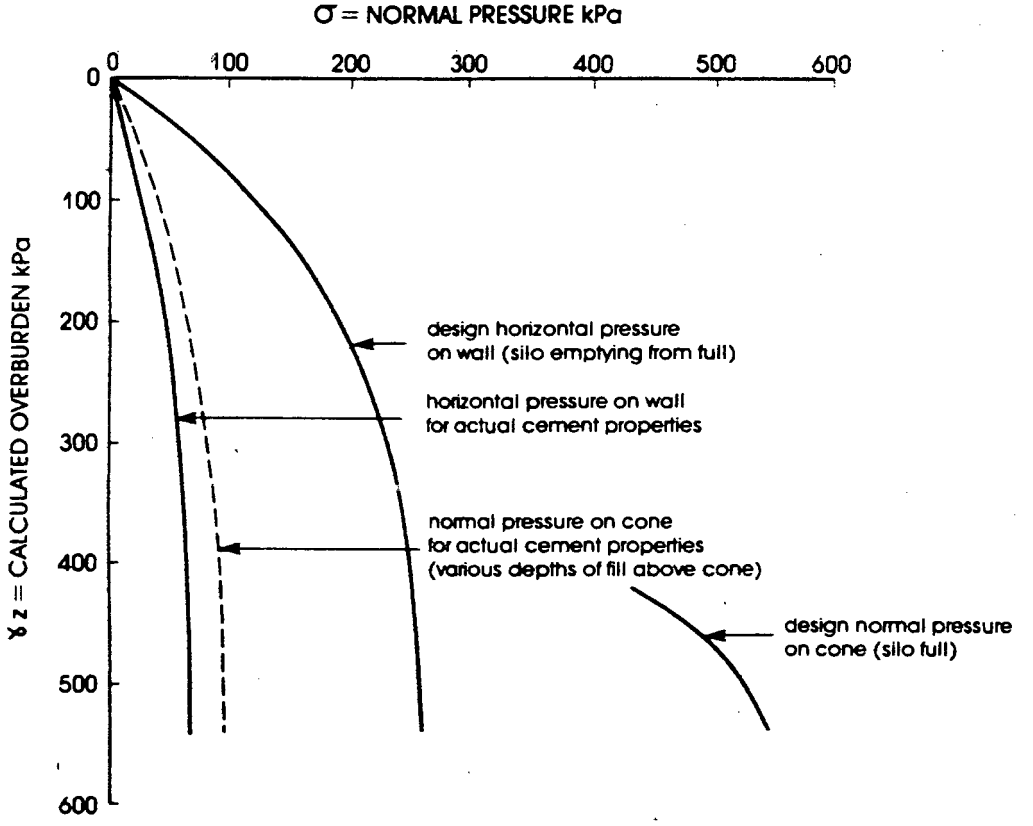

Figure 13: Comparison of design pressures with pressures calculated for actual cement properties

4.2 Theory used for design

The accepted theoretical basis for the design of silos to DIN 1055 is the Janssen arching theory which is very similar to that which was applied to stresses in the trench fill at Lesapi dam. According to this theory, the vertical pressure at depth z below the surface of the fill in a silo is given by :

$$\frac{\sigma_v}{\sigma_v(max)} = 1 - \exp\left[-\frac{\gamma z}{\sigma_v(max)}\right] \qquad (4a)$$

$$\sigma_v(max) = \frac{D\gamma}{4K\tan\delta} \qquad (4b)$$

In which D is the diameter of the silo and the other symbols have their usual meaning. The horizontal pressure on the silo walls is then

$$\sigma_h = K\sigma_v \qquad (4c)$$

The resulting horizontal pressures were then factored by 1.73 to allow for the possible existence of local pressure peaks, and the effects of slightly eccentric discharge.

The cone was designed for a normal pressure calculated as

$$\sigma_N = \sigma_v \left[\cos^2\alpha + K\sin^2\alpha\right] \qquad (5)$$

in which α is the cone angle of 60°, and σ_v was calculated by means of equations (4)

The resulting pressure was then factored by 1.14 to allow for possible variations in material unit weight.

4.3 Measured pressures

Figure 12 shows some profiles of pressure measured on the vertical walls of the silo (Figure 12a) and on the surface of the cone (Figure 12b). Many more measurements than those shown in Figure 12 are available and have been published elsewhere (Blight (1986)). However, the measurements shown in the figure are typical.

The solid curves shown in the figure correspond to pressure profiles calculated by means of equations (4) and (5) using the measured properties of the cement powder given earlier. Note that most of the observations fall within the calculated pressure envelopes. There is a sharp gradient of pressure on the vertical walls once the ring-conical hopper section is entered (see dashed line in Figure 12a). The pressures on the cone show a similar sharp gradient from roughly the theoretically predicted pressure near the apex of the cone to values approaching zero at the level of the outlet ports. The theoretical pressure envelopes calculated for the actual cement properties, shown in Figure 12, are compared with the design pressure envelopes in Figure 13.

It is quite obvious that the design assumptions were quite unrealistic, especially as factors of safety on the strength of the construction materials were applied over and above the design stresses. The main reason for the excessive design pressures is the adoption of unrealistic design parameters for cement powder - a combination of a high unit weight, low angles of shearing resistance and wall friction and a high lateral pressure coefficient. (The design lateral pressure coefficient was 1.0).

4.4 Conclusions

It became clear from the results of the measurements that :

(i) The theory used for calculating pressures in cement silos is generally adequate, provided realistic cement properties are used. (However, see Blight(1986a) and Blight(1986b) for qualifications to this conclusion as it applies to stored materials in general.)

ii) Existing codes of practice for silos can give ridiculous over-estimates of the lateral pressures exerted on silo walls. (See Schaffner and Blight (1983) for another example that supports this statement.)

(iii) It follows that the object of the investigation had been achieved - safe cement silos can be built considerably more economically than was the case in this instance.

5 THE PERFORMANCE OF TENSION PILES SUBJECTED TO UPLIFT BY EXPANSIVE CLAYS

The Lethabo power station (Blight(1984a), Blight (1984b)) is founded on a deep profile of desiccated clayey silt residual from weathered siltstone. The water table at the site is at a depth of about 20m. Studies of the potential heave of the site had indicated that a surface heave of up to 120mm could be expected to occur.

The operation of power station plant and other installations such as cooling towers and cooling water ducts is very sensitive to differential movement. For this reason, an early design decision was to found all structures on bored cast-in-situ reinforced concrete piles. The piles were to penetrate the residual siltstone and be founded in a less weathered dimensionally stable carbonaceous shale that underlies the expansive weathered siltstone. All structures would be supported on piles with a 300mm void between the soil and the underside of the structure. The design of piles for heavy loads would not be problematic, as the carbonaceous shale provides a high bearing capacity. Lightly loaded piles would have to be anchored in the carbonaceous shale and resist the uplift forces imposed on them by the surrounding expansive soil. This would also apply to piles that ultimately would be heavily loaded, but which would be in the ground for long enough to be affected by heave before the loads were applied.

There were three basic problems associated with the pile design :

Collins(1953) had proposed a procedure for designing piles subject to uplift by expansive clays. This method had been widely used in the intervening 30 years, without ever having been properly checked. Donaldson(1967) had, indeed, carried out measurements of the load distribution in an instrumented pile of 230mm diameter 10m in length. These measurements confirmed the form of Collins' expression for pile tension which is :

$$P = \pi D \int_0^L (c' + K\sigma_v' \tan\phi')dz \qquad (6)$$

In which

P is the tension in the pile;
D is the pile shaft diameter;

L is the length of the pile subjected to uplift; and
c^1 and ϕ^1 have their usual meaning.

However . :

(i) There was uncertainty as to whether the expression would apply to the very large piles that would be needed at Lethabo (35m long and up to 2000mm in diameter).

(ii) There was uncertainty as to the values of c^1 and ϕ^1 to use.

(iii) What value of K should be used?

Donaldson's study had not attempted to compare measured pile tensions with tensions predicted from measured shear strengths.

A simple paper exercise showed that with so many piles to be constructed, even small economies on each pile would make a field testing exercise a financially viable proposition. It was therefore decided to embark on such an exercise.

5.1 Shear strength

It was known from published work (eg Burland et al (1966) and O'Riordan(1982)) that the appropriate strength to use in designing the piles probably corresponded to the lower limit of laboratory strength measurements. But, should an adhesion factor be applied and what was the value of K?

To answer these questions a series of plug pulling tests was arranged. The plugs were of 1050mm diameter and 2m length and were constructed as shown in Figure 14. The plugs were installed at a series of depths and the surrounding soil was soaked by filling the hole with water. After a period of 4 weeks the water was allowed to drain away until there was no free water in the standpipe. This ensured that the effective stress in the soil surrounding the plugs was close to the value of the total stress as the pore pressure must have been close to zero. The plugs were then pulled by jacking up a beam around which the cables from the plug were fastened.

Figure 15 shows the resultant load displacement curves. Note the difference between the two plugs centred at a depth of 6m, one of which was pulled dry, the other after soaking.

Figure 16 summarizes all the available results of laboratory drained shear strength tests on the siltstone, as well as showing the results of the plug-pulling tests. With the exception of one test, the strengths from the plugs coincided quite closely with the lower limit to the laboratory strength measurements. This result confirmed expectations, in the light of previously published work. However, the way in which the tests had been performed and the fact that at a given depth in Figure 16, the laboratory shear tests correspond to the same effective stress as the plug tests, eliminated the need to know values for either the adhesion factor or the lateral stress ratio K. In fact, the indication was that both of these factors equalled unity.

5.2 Design of piles

The piles could be designed using Collins' expression in terms of the changing effective stress and the progressive heave predicted for the site. Whereas the laboratory shear tests had shown a pronounced peak in the stress displacement curve, the field curves showed no peak. As shown by Figure 17, using strengths derived from the plug-pulling tests rather than the mean laboratory curves had a very considerable effect on the maximum design tension.

5.3 Field test on an instrumented pile group

The one question remaining was whether the Collins expression correctly represented the distribution of tension in the shaft of a pile subjected to uplift and whether the uplift forces could correctly be predicted from the measured shear strengths. All piles were straight-shafted, 1050mm in diameter and 33m long. Referring to Figure 18, the positions of the three instrumented piles were selected so that they represented a corner pile, a side pile and an interior pile in a typical pile group. For details of the instrumentation, the reader is referred to Blight(1984b).

The soil surrounding the test pile group was flooded by means of a grid of boreholes and the strain at various depths in each instrumented pile was recorded as the soil took up water and swelled.

Figure 19 shows the variation at various times of the recorded tension in pile 2 (see Figure 18). Tensions were calculated from the recorded strains on the assumption that the concrete had cracked and the steel reinforcing was carrying the entire load. Strains at depths of up to 5m and more than 22m were not sufficient to crack the concrete and the tensions were therefore underestimated at either end of the pile.

The design tension curve calculated from the results of the plug-pulling tests via Collins' equation has been superimposed on Figure 19 and shows quite reasonable agreement with the measured pile tensions.

Figure 20 shows the variation of shaft shear stresses down the three test piles. The diagram shows

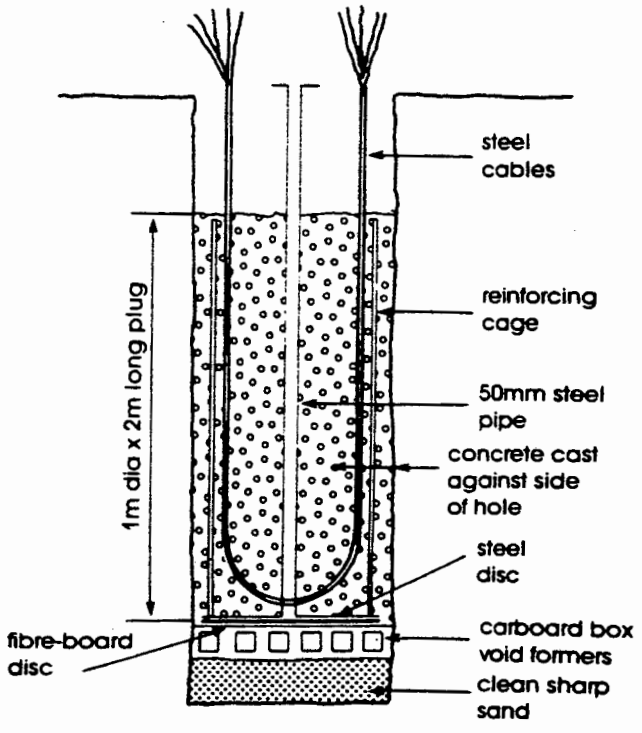

Figure 14: Design of plugs to measure insitu strength on pile shafts.

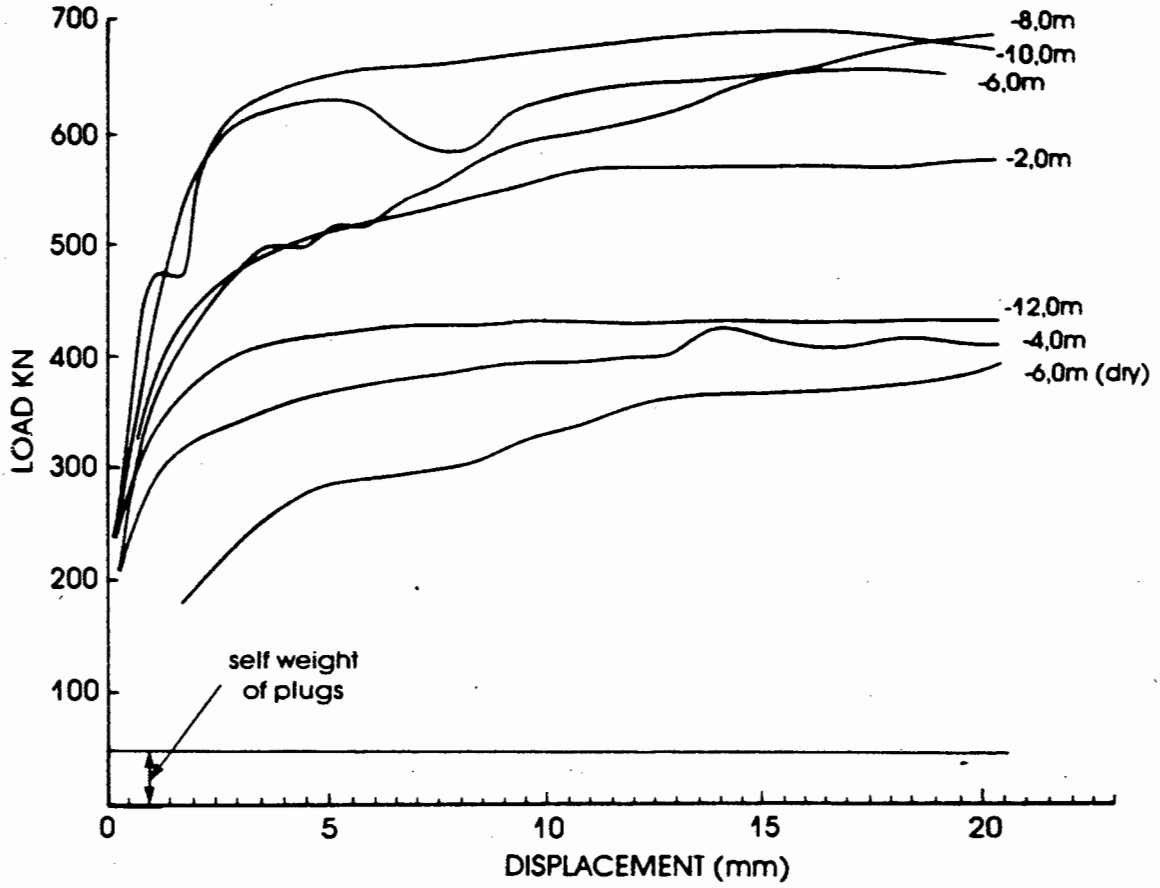

Figure 15: Load-displacement curves for plug-pulling tests in weathered silt-stone.

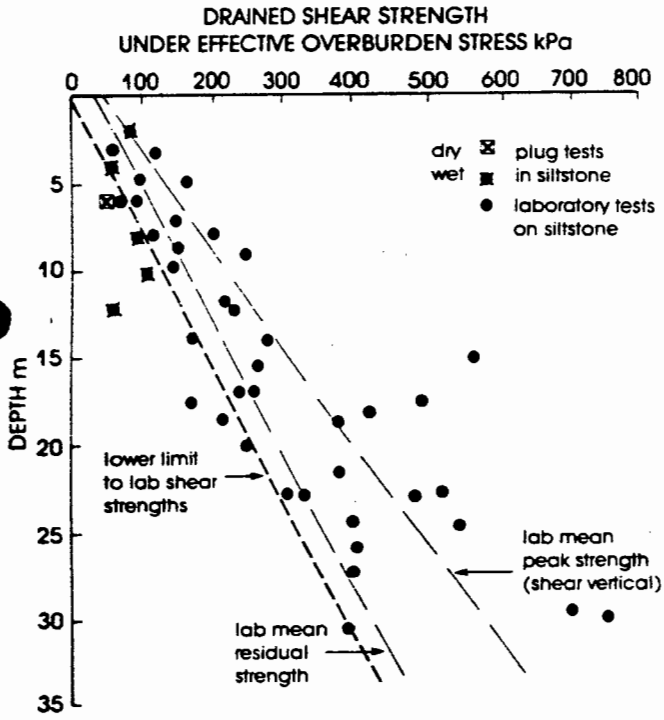

Figure 16: Summary of laboratory and insitu strength measurements made on silt stone.

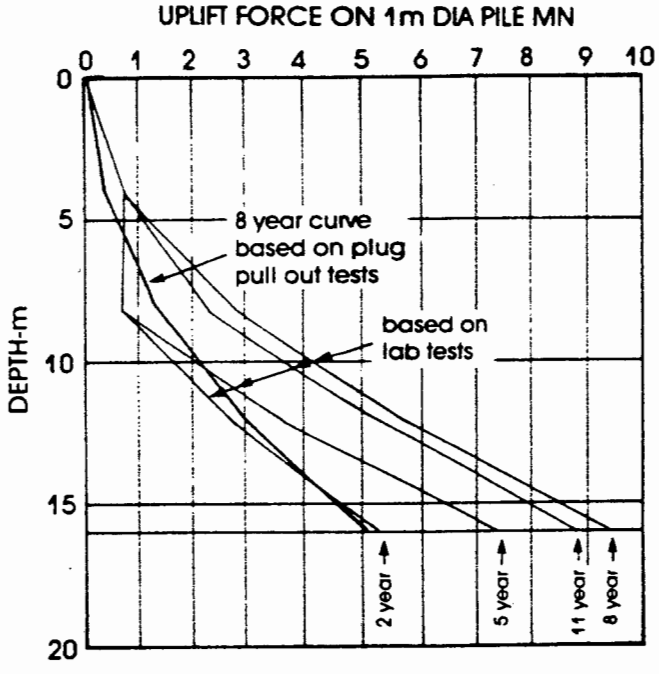

Figure 17: Pile design curves based on Collins' formula. Curves based on lab tests take account of progression of heave with time and effect of peak in stress-displacement curve.

how uplift shears developed above a depth of about 10m are counteracted by anchorage shears on the lower part of the pile shaft. This diagram also provides a check on the validity of the tension measurements, as the area under the uplift shear curve must equal that under the anchorage shear curve if vertical equilibrium is to be preserved.

The strength versus depth relationship established from the plug-pulling tests has been superimposed on the upper part of Figure 20. This agrees reasonably with the shear stress-depth curves calculated for the piles if one bears in mind that the pile shaft shear stresses were underestimated at depths of less than 5m.

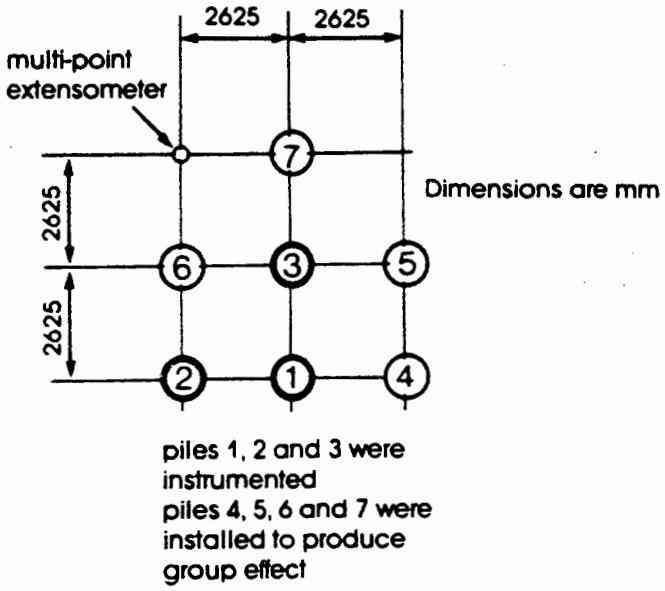

Figure 18: Layout of piles in test pile group.

5.5 Effect of loading a pile previously subjected to uplift

As many of the piles would be installed two to three years prior to being loaded, it was decided to study the effect of this delayed loading by applying a compression load to two of the instrumented piles after full tension had developed in them. A 1000kN compressive load was applied by installing anchors into the carbonaceous shale and jacking off the anchors. As had been expected, the applied load was resisted by shears on the pile shafts and was completely carried by the upper 6m of pile. Tensions in the shafts below this depth were unaffected.

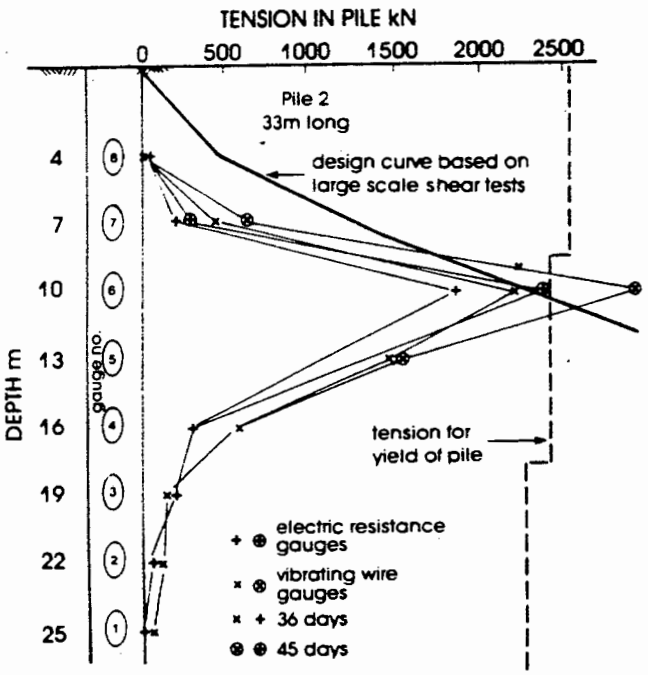

Figure 19: Development of tension in test pile 2 with time and comparison of measured and predicted depth-tension relationships.

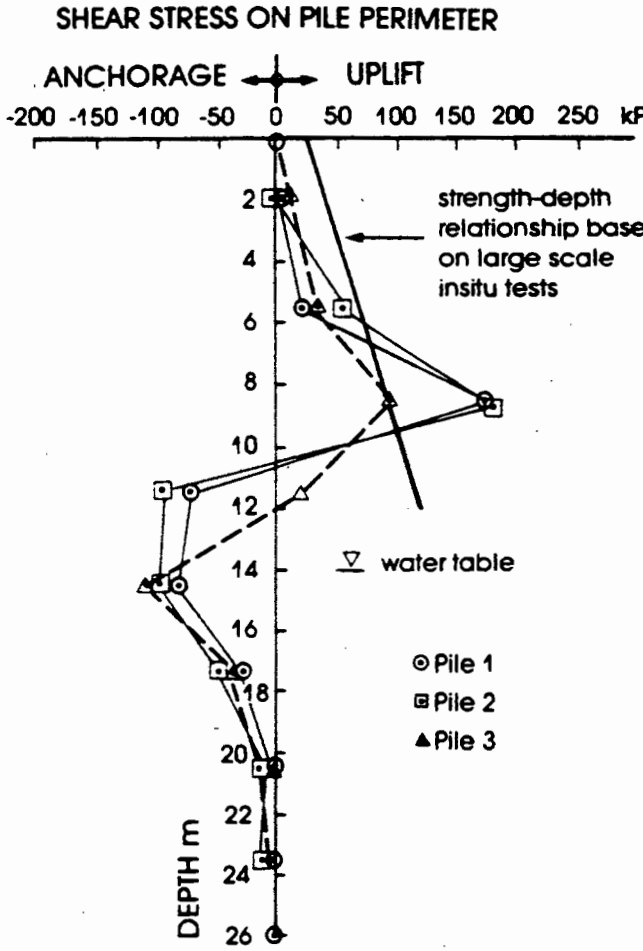

Figure 20: Shear stresses developed down length of p and comparison with measured shear strength-depth relationship.

5.3 Conclusions

The programme of field testing and monitoring achieved all its objectives :

(i) The Collins expression for pile shaft tensio was validated for the large diameter piles used at Lethabo.

(ii) Appropriate design parameters for the piles were established.

So far, the piles at Lethabo appear to have perfor med as expected. Problems were experienced when one of the cooling water ducts started to lift. When the supporting piles were opened up, it was found that the void between the underside of the duct and the soil had carelessly been allowed to fill up with soil washed in by a thunderstorm before the sides of the duct were backfilled. The underlying soil had heaved and lifted the duct off the piles, but the piles had not moved.

6 IN SITU MEASUREMENTS OF THE CHARACTERISTICS OF UNDERGROUND FILL

The following case history is not as extensive as the previous ones, but has been included to illustrate the role that both geotechnics and in situ testing may play in providing design parameters for mining.

Gold mining in South Africa takes place at depths of up to 3.5km. The gold-bearing reef is tabular and usually dips moderately at up to 30°. As mining proceeds, a tabular excavation or stope is formed which is usually 1m to 1.2m in height and which traditionally has been supported by timber grillages or "packs".

For the following reasons, the gold mining industry is attempting to replace the timber supports by support provided by alternative materials.

(i) Timber is expensive and the building of packs in situ is labour-intensive.

(ii) The large quantities of timber in the mine constitute a fire hazard.

(iii) As mining activities expand, the available supply of timber is being exhausted.

One means of providing support is by mass backfilling with barren tailings. This process has been described by Blight et al(1976). The tailings may be cemented or uncemented and both run-of-mill material and cyclone underflow have been used in various mines.

Friction on the hanging and foot walls prevents the fill from being squeezed laterally out of the stope as the excavation converges elastically. Hence it is likely that fill near the edges is subjected to uniaxial compression and that away from the edges to confined compression with zero lateral strain. Early tests to establish the compressibility of fill materials used model slabs of fill that were geometrically similar in shape and proportion to the prototype fills. These were compressed between the platens of a testing machine and the resultant load-compression curve recorded. These tests provided comparisons of the load-compression characteristics of various candidate fill materials. However, it had to be accepted that tests on model slabs probably did not provide absolute information on fill performance under load. Confined compression tests in the laboratory were an obvious alternative, but it was thought that their results would be over-optimistic. The only means of checking the realism of model slab tests was to measure the load-compression curve of a fill in situ and to compare this curve with the corresponding laboratory characteristic. An opportunity to do this arose at the Stilfontein mine in South Africa when it was decided to use a fill to support the area around a shaft when the gold-rich shaft pillar was mined out.

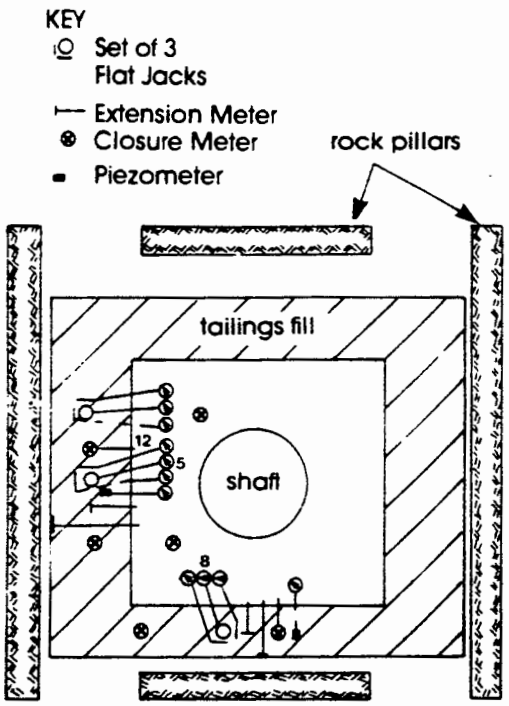

Figure 21: Layout of instrumentation in shaft pillar replacement fill.

The pillar existed at a depth of 1900m below surface and was mined out and replaced by a pumped cemented tailings fill containing 10 per cent of ordinary Portland cement. Figure 21 shows a plan of the area surrounding the shaft, as well as the instrumentation installed in the tailings fill. The flat jacks referred to in the figure were 200mm diameter oil-filled Freyssinet flat jacks connected by copper tubing to Bourdon pressure gauges, and pre-pressurized to 1MPa. The jacks were installed so as to measure vertical stress as well as horizontal stress in two orthogonal directions.

Figure 22 shows the field compression curve, as recorded on two of the jacks and the closure meters compared with a laboratory compression curve for a model fill slab. The figure shows that the fill performed considerably better in the field than would have been predicted from the laboratory model tests.

Unfortunately, the in situ stress-compression curve could not be followed beyond 25 per cent compression as the site became inaccessible.

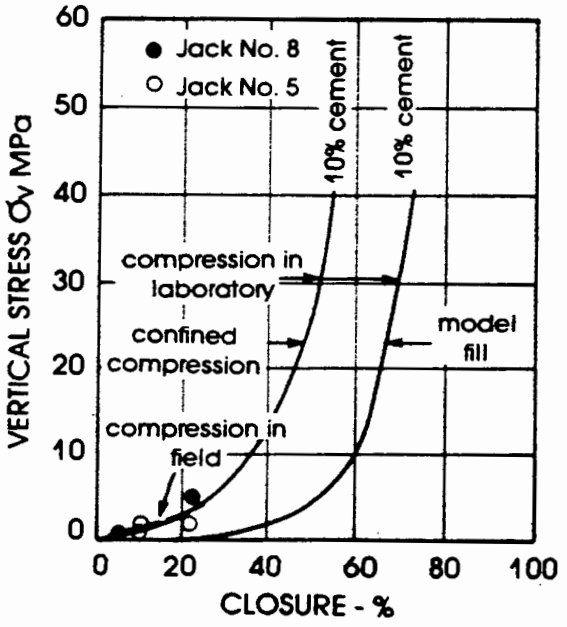

Figure 22: Comparison of field compression curve of fill with laboratory compression curves

As Figure 22 also shows, a compression curve for the fill determined by means of confined compression in which the fill was compressed in a steel cylinder which allowed of no lateral strain agreed very well with the observed field compression curve. This showed that the characteristics of a mine fill should be assessed in the laboratory by means of confined compression tests, and not by tests on model slabs. The former is the method currently employed.

7 CONCLUDING STATEMENT

The case histories described above have illustrated the utility and versatility of using field instrumentation and monitoring, not only to provide parameters for design but also to assist understanding the mechanics of processes such as : tensile cleavage of fill in core trenches, the failure of rockfill slopes, the development of uplift forces in piles, pressures exerted by materials in silos and the compression of load-bearing fill in underground mines.

The important principles to follow in carrying out field instrumentation are :

(i) Select, design and locate the instrumentation to provide the information required for the design. A careful theoretical analysis should form the basis for any instrumentation project.

(ii) Field instrumentation is subject to a high casualty rate. Make it simple and robust, and wherever possible duplicate or even triplicate important instruments. Not only does redundancy insure against instrument casualties, but it provides checks on the correctness of the readings.

(iii) Do not leave either instrument installation or readings to technicians who, without a theoretical awareness of the problem, may not appreciate the significance either of occurrences during instrument installation or the behaviour of instruments during the taking of readings. The designer should personally supervise every stage of instrument installation and if possible either take the readings himself or closely supervise the taking of readings.

(iv) Reduce and plot all observations as soon as they have been taken. It is only by doing this that unexpected trends or behaviour will be detected while there is time to take corrective action if necessary.

The above principles do not only apply to geotechnical projects but are of general application in engineering.

8 REFERENCES

BLIGHT, G.E. (1969). Foundation failures of four rockfill slopes. Jour.Soil Mech.and Found.Eng. Div., ASCE, Vol. 95, No.SM3, pp 743-767.

BLIGHT, G.E. (1970a). Construction pore pressures in two sloping-core rockfill dams. Proc.10th Congr. Large Dams, Montreal, Q.36, R.18, pp 269-290.

BLIGHT, G.E. (1970b). In situ strength of rolled and hydraulic fill. Jour. Soil Mech. and Found. Eng. Div., ASCE, Vol. 96, No.SM3, pp 881-899.

BLIGHT, G.E. (1973). Stresses in narrow cores and core trenches of dams. Proc.11th Congr. Large Dams, Madrid, Q.43, R.5, pp 63-79.

BLIGHT, G.E., MORE O'FERRAL, R.C. and AVALLE, D.L. (1976). Cemented tailings fill for mining excavations. Proc.9th Int. Conf. on Soil Mech. and Found. Eng., Tokyo, Vol. 1, pp 47-54.

BLIGHT, G.E. (1983a). Measuring pressures in silos with pressure cells. Proc.2nd Int. Conf. Design of Silos for Strength and Flow, London : Powder Advisory Centre, pp 217-229.

BLIGHT, G.E., and SCHAFFNER, R.H. (1983b). Comparison of design assumptions and measured performance for cement works silos. Proc.2nd Int. Conf. Design of Silos for Strength and Flow, London : Powder Advisory Centre, pp 207-216.

BLIGHT, G.E. (1984a). Power station foundations in deep expansive soil. Proc.Int. Conf. on Case Histories in Geotechnical Engineering, St Louis, U.S.A., Vol. 1, pp 353-362.

BLIGHT, G.E. (1984b). Uplift forces measured in piles in expansive clay. Proc.5th Int. Conf. on Expansive Soils, Adelaide, pp 363-367

BLIGHT, G.E. (1986a). Pressures exerted by materials stored in silos : Part I, coarse materials. Geotechnique, Vol. 36, No. 1, pp 33-46.

BLIGHT, G.E. (1986b). Pressures exerted by materials stored in silos : Part II, fine powders. Geotechnique, Vol. 36, No. 1, pp 47-56.

BURLAND, J.B., BUTLER, F.G.B. and DUNICAN, P. (1966) The behaviour and design of large diameter bored piles in stiff clay. Symposium on Large Bored Piles, I.C.E., London, pp 51-71.

COLLINS, L.E. (1953). A preliminary theory for the design of underreamed piles in expansive clay. Transactions, South African Inst. Civ. Engrs., Vol. 3, No. 11.

DONALDSON, G.W. (1967). The measurement of stresses in anchor piles. Proc.4th Reg. Conf. for Africa on Soil Mech.and Found.Eng. Cape Town, pp 253-256.

JANBU, N. (1967). Earth pressures and bearing capacity calculations by generalized procedure of slices. Proc.4th Int. Conf. on Soil Mech. and Found. Eng., London, Vol. 2, pp 103-107.

MARTENS, P. (1980). DIN 1055 Part 6 : The performance of the old norm and a progress report on the revised edition. Proc.Int. Conf. Design of Silos for Strength and Flow, London : Powder Advisory Centre.

O'RIORDAN, N.J. (1982). The mobilization of shaft adhesion down a bored, cast-in-situ pile in the Woolwich and Reading beds, Ground Engineering, April, pp 17-26.

POWELL, J.J.M. and QUARTERMAN, R.S.T. (1986). Evaluating the screw plate test in stiff clay soils in the U.K. Proceedings of this Conference.

THOMAS, H.S.H. and WARD, W.H. (1969). The design, construction and performance of a vibrating-wire earth pressure cell, Geotechnique, Vol. 19, No. 1, pp 39-51.

VAUGHAN, P.R., KLUTH, D.J., LEONARD, M.W. and PRADOURA, H.H.M. (1970). Cracking and erosion of the rolled clay core of Balderhead dam and the remedial works adopted for its repair. Proc.10th Congr. Large Dams, Montreal, Vol.1, pp 73-94.

PROCEEDINGS OF THE SECOND INTERNATIONAL CONFERENCE ON GEOMECHANICS IN TROPICAL SOILS
SINGAPORE / 12-14 DECEMBER 1988

GEOMECHANICS IN TROPICAL SOILS

Editors
PUBLICATIONS COMMITTEE OF 2 ICOTS
School of Civil and Structural Engineering, Nanyang Technological Institute

OFFPRINT

co-sponsored by
Nanyang Technological Institute
International Society for Soil Mechanics and Foundation Engineering
South East Asian Geotechnical Society

A.A.BALKEMA / ROTTERDAM / BROOKFIELD / 1988

Keynote paper: Construction in tropical soils

G.E.BLIGHT, University of the Witwatersrand, Johannesburg, South Africa

ABSTRACT

The process of formation of tropical soils is reviewed and typical properties of tropical residual soil profiles are described. The failure modes of natural and cut slopes in tropical soils are summarized and it is shown that slopes in tropical soils can be rationally analysed and designed. Examples are cited to show that the settlement of raft and spread footings on tropical soils can be satisfactorily predicted. This conclusion applies also to the design of deep foundations in tropical soils. Some of the peculiarities of tropical soils, when used as construction materials, are described.

1 INTRODUCTION : INTERPRETATION OF THE TITLE

As the title would indicate this paper is intended to deal with "construction in tropical soils" which immediately raises the twin questions of what is meant by "tropical soils" and by "construction"?

The fact that a class of soils receives a distinctive title must indicate that it has some special characteristics or properties that distinguish it from other "non-tropical" soils. Marine clays and river sands and gravels, for instance, occur widely in the tropics, but would not be expected to have properties any different from similar soils located outside of the tropics. Is it perhaps the climate, past and present that distinguishes "tropical" from "non-tropical" soils? Reference to a household atlas (Reader's Digest, 1973) and to Figure 1 shows that the tropics, that span of latitudes around the earth's circumference between the tropic of Cancer in the north (23½°N) and the tropic of Capricorn in the south (23½°S), does have a special climate. It is generally warm to hot all year round and includes many of the more humid climatic regions of the world, for example the Amazon and Congo basins and the islands of Indonesia. However, it also includes some of the driest areas on earth, for instance, the Atacama and Great Western deserts of the Americas, the Sahara and Kalahari deserts of Africa and the Australian desert.

In considering the formation of soils, we talk of a geological time span. It is known that the earth's poles have shifted position in the distant geological past. The situation is complicated by the fact that the continents have also drifted (see, for example Stacey, 1970). However, there has been no glaciation of the tropical regions since before the cretaceous era which ended one to two hundred million years ago. Hence it is possible that areas no longer in the tropics at present may have deposits of palaeo-tropical soil.

The desert areas may perhaps be ruled out as possible homes for tropical soils. With the exception of the Persian Gulf, where oil has artificially concentrated the population and development, deserts are sparsely populated and underdeveloped. There is therefore less reason for concern with the soils of deserts. This does not say that desert soils do not have their own peculiar geotechnical difficulties. The various problems associated with desert soils such as sabkha have been described by various authors, e.g. Akili and Torrance (1981), Fookes (1978) and Stipho (1984).

The more humid and sub-humid regions of the tropics, however, support and can support large population densities and are becoming increasingly subject to development, especially those areas bordering the sea or with access to the sea via navigable rivers. A combination of warm to hot, and humid to sub-humid climate and an ancient surface geology strongly points to the conclusion that the tropical soils referred to by the title must be residual soils occurring in the tropics or palaeo-tropics.

Quite apart from any past wandering of the poles, and referring again to Figure 1, it will be seen that the two tropics do not impose a rigid bound to the region within which one would expect to find tropical soils. Humid and sub-humid, warm to hot climates occur well outside the tropical limits. Much of Queensland, Australia for example, lies south of the tropic of Capricorn, yet tropical-type soils are found there. Georgia, in the USA, lies well north of the tropic of Cancer, but tropical-type soils are also found there.

The term "construction" also poses some queries of definition. It could be taken to mean "techniques used in construction", or alternatively "problems experienced in construction", or yet again "the behaviour of structures". In this paper the last definition has been adopted in the main, but the other two definitions will also be used.

Hence if one were to follow the Victorian custom of amplifying titles (e.g. "Eric, or Little by Little") the paper might be entitled "Construction in tropical soils, and especially the behaviour and problems associated with structures built on or in residual soils of the tropical and sub-tropical regions".

However, before proceeding to describe the

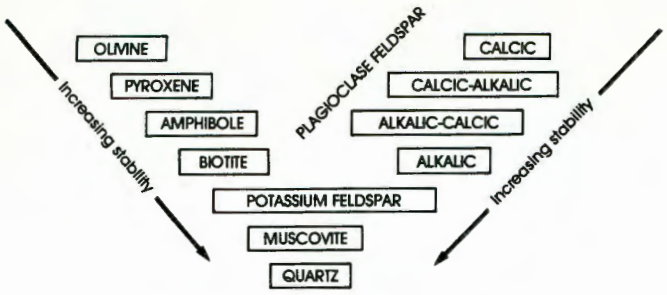

Figure 2: Weathering order of minerals

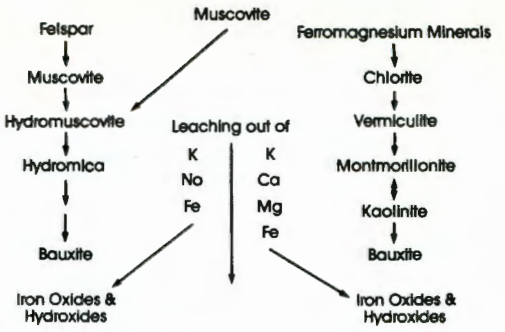

Figure 3a: Suggested sequence of weathering leading to formation of clay minerals

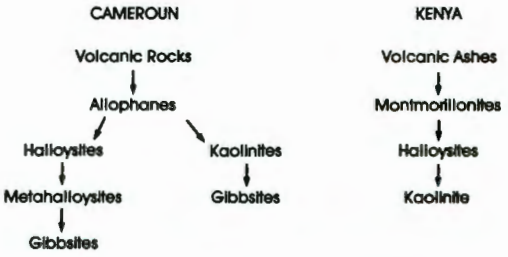

Figure 3b: Sequences in the formation of clay minerals from volcanic materials in Africa

but not entirely, on the parent rock type. Onodera, (1976) describes how granitic residual soils in Japan may vary in colour from light grey to red depending on the quantity of limonite present, while the clay content may vary from 2% to 26% depending on the relative quantities of feldspar, mica and quartz in the parent rock. Ruddock (1967) finds that, in Ghana, granitic rocks weather to deep profiles of sand containing feldspar crystals and that the "boulder" weathering reported by Ruxton and Berry (1957) from Hong Kong does not occur. Ruddock attributes the difference to the lack of a regular jointing pattern in the Ghanaian granites, but the difference may also be partly due to mineralogical, climatic, topographical and age differences.

Van der Merwe (1965) has shown that reddish kaolinitic soils develop in well drained situations over norite gabbro, whereas blackish montmorillonitic clays develop from identical parent rock in poorly drained situations.

Wesley (1973) concluded that the dark-coloured andosols and red latosols found in Java originate from much the same volcanic parent material but occur in profiles of different ages.

It is evident that apart from a few generalizations, it is difficult to relate the properties of a residual soil directly to its parent rock. Each situation requires individual consideration and it is rarely possible to extrapolate from experience in one area to predict conditions in another even if the underlying hard rock geology in the two areas is similar. The chemical changes and sequence of minerals formed during weathering are extremely complex. For example, one suggested weathering sequence leading to the formation of clay minerals is shown in Figure 3a (van der Merwe, 1965). The sequence may be arrested at any stage and certain stages may be reversed as a result of changes in climate or conditions of drainage.

Figure 3b (Gonzalez de Vallejo et al, 1981) shows weathering sequences for volcanic rocks observed in Cameroun (West Africa) and Kenya (East Africa). Apart from unknown differences in mineralogy, Cameroun has a hotter, moister climate than does Kenya, which may explain the difference in weathering sequence.

Occasionally, residual soils may form by the in situ weathering of unconsolidated sediments. The commonest example of this is the loess or collapsing sand formed by the weathering of feldspars in deposits of windblown sand (Knight, 1961, Dudley, 1970, Schwartz and Yates, 1980). Shirasu, found in Japan (Yamanouchi and Haruyama, 1969) is an unconsolidated volcanic sediment, partly weathered in situ, whose engineering properties have much in common with loess.

A survey by Brand and Phillipson (1985) showed that colluvium mantling a residual soil profile is regarded as a residual soil by many authorities.

2.2 The role of climate

Climate exerts a considerable influence on the rate of weathering and on the resultant weathering products (Weinert, 1963 and 1974. Morin and Ayetey, 1971). Physical weathering is more predominant in dry climates while the extent and rate of chemical weathering is largely controlled by the availability of moisture and by temperature. (Chemical reaction rates approximately double for each 10°C rise in average temperature).

According to Uehara (1982) the clay mineralogy of the soils of the world changes in a predictable way with distance from the equator, as indicated by Figure 4. This must be an oversimplification, because as shown by Figure 1, climates do not vary predictably with distance from the equator. Nevertheless, Figure 4 gives a useful concept of the influence of climate on the products of weathering. Uehara says that near the equator, high temperatures and year-round rainfall favour the formation of low activity kaolin and oxides (Skempton's Activity 0.3 to 0.5). As one moves towards the limits of the tropics, rainfall decreases and high activity smectitic clays predominate (Skempton's Activity 1.5 to 7).

The influence of temperature and moisture on rock weathering in South Africa is shown by Weinert's (1974) climatic index

$$N = \frac{12Ej}{Pa}$$

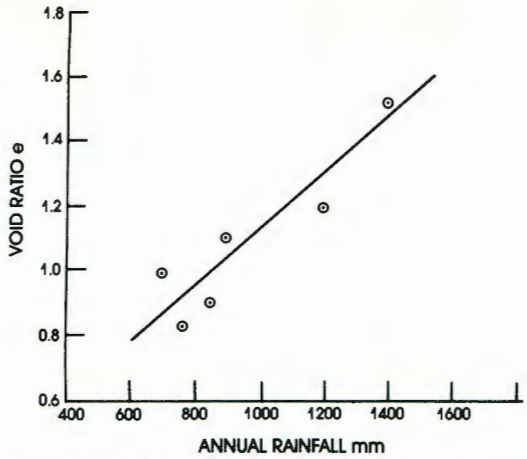

Figure 6: Relationship between void ratio and annual rainfall for highly weathered and leached granites in South Africa.

mechanism of rock weathering. Highly weathered residual granites, for instance become more porous and therefore more compressible as the annual precipitation and therefore the leaching increases. This is illustrated by Figure 6 which shows some data of Brink and Kantey (1961) relating void ratio to annual rainfall for weathered granites in South Africa.

2.4 The role of time

Other things being equal, the older a residual profile, the deeper and more weathered it will be. In Southern Africa, for example, six ancient erosion surfaces may be identified (King, 1975, Brink, 1979) each of which formed as a result of uplift and a consequent acceleration of the erosion process. The oldest of these erosion surfaces, the Gondwana surface, predates the break-up of the original super-continent and now exists only as isolated remnants on high ground dating back more than 190 million years. However, the 100 million year old African erosion surface covers extensive parts of the country and is underlain by depths of highly weathered residual material upwards of 50m deep. The most recent erosion surface, the 2 million year old Quarternary, in contrast, is underlain by a relatively thin residual cover.

3 TYPICAL CHARACTERISTICS OF TROPICAL SOIL PROFILES

Because weathering proceeds from the surface down and inwards from joint surfaces and other percolation paths, the intensity of weathering generally reduces with increasing depth and there is also usually a variation in weathering intensity in the material between joint surfaces. In profiles residual from igneous rocks, core stones or boulders of sound parent rock are very often found enclosed within blocks of weathered rock (e.g. Lumb, 1975).

Typically, a profile of residual soil will consist of three indistinctly divided zones (Vargas and Pichler, 1957, Ruxton and Berry, 1957, Little, 1969) as illustrated in Figure 7.

The upper zone will consist of highly weathered and leached soil often reworked by burrowing animals and insects or by cultivation, and intersected by root channels. This zone has always been subjected to at least some transport process.

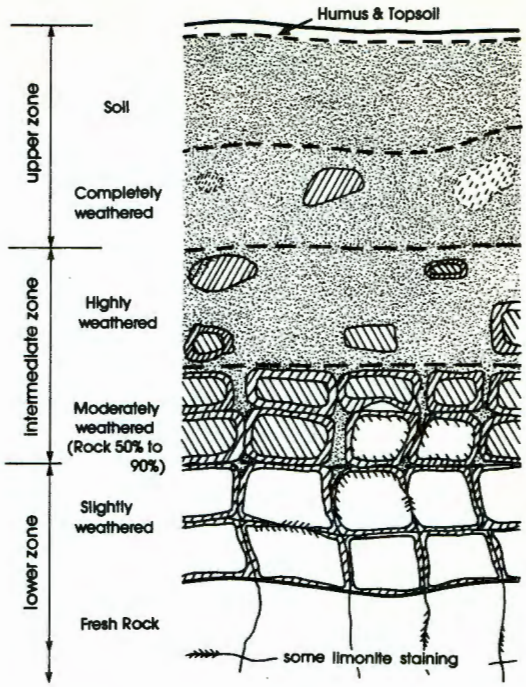

Figure 7: Schematic Diagram of Typical Tropical Residual Soil Profile (after Little, 1969)

The intermediate zone also consists of highly weathered material but exhibits some features of the structure of the parent rock and may contain core stones. This zone often contains pedogenic material such as nodules of calcium or iron salts which may give it a mottled or spotted appearance.

The lower zone consists of physically disintegrated and partially to slightly weathered material often having the appearance of a mass of interlocking blocks of soft rock. The lower zone merges into fractured or jointed, almost unweathered parent rock. An example of a typical soil profile residual from an igneous rock (andesite lava) is shown in Figure 8.

According to Tuncer and Lohnes (1977), a basalt-derived tropical soil may go through six stages of weathering, as illustrated in Figure 9. These stages may be summarized as follows:

Stage 1 - Parent rock with very low void ratio and high cohesion.

Stage 2 - Weathering causes rock disintegration, increase in void ratio, and decreases in cohesion and friction angle.

Stage 3 - Increase in clay content causes increase in cohesion, decrease in void ratio and permeability. Specific gravity begins to increase because of increase in sesquioxide (Fe_2O_3 and Al_2O_3) content.

Stage 4 - Oxide content continues to increase, kaolinite content decreases through conversion to gibbsite. Sesquioxides cement clay particles and cause soil

kaolin increasing in quantity towards the surface. This has plainly either not occurred, or the clay minerals have been redistributed by leaching in the profile since their formation, or the minerals in the parent rock were such that they did not give rise to the expected sequence. The complete absence of quartz below the water table is also inexplicable, unless it is accepted that the minerals comprising the separate lava flows that make up the profile could have varied widely one from another.

Figure 11 shows the variation of void ratio e_o, compression index C_c and rebound index C_r in a profile of Ventersdorp lava. There is a general tendency for all three parameters to decrease with depth (with a local anomaly at about 16m) which indicates that the degree of weathering decreases with depth. The strong similarity in the shapes of the three curves suggests that both C_c and C_r should correlate with void ratio as indeed, Figure 12 shows they do. The data from a second site about 5km away shows that the relationships in Figure 12 are of fairly general applicability and that the void ratio of the weathered material gives a good indication of its compressibility.

Because of the residual bonds between the weathered mineral particles, most tropical soils behave as if overconsolidated, with the degree of overconsolidation, as represented by the equivalent preconsolidation pressure P_c, increasing with depth as the degree of weathering decreases. This tendency is illustrated by Figure 13 which shows the variation of P_c and e_o with depth at the second site referred to in Figure 12. The variation of void ratio shows that the degree of weathering is decreasing with depth, while the equivalent preconsolidation pressure increases roughly linearly with depth.

Figure 14 shows the variation with depth at this site of the effective stress σ'_s measured in undisturbed soil samples immediately after sampling. The ratio R_s of σ'_s/σ'_{vo} (σ'_{vo} = effective overburden stress) gives an indication of K_o in the profile. It is clear from the observed values of R_s and the laboratory measurements of K_o that K_o in the profile has a relatively low value of about 0.4. This would not be unexpected at a site with the high void ratios shown in Figure 13.

The strength of tropical residual soils is also dependent on their void ratio or density. This is illustrated by Figure 15 which shows the variation of shear strength with bulk density for weathered Ventersdorp lava. As the density approaches that of the unweathered rock the strength increases rapidly. Conversely, once the density falls below about 1900 kg/m³ there is not much reduction in strength with further reducing density.

Because of saprolitic features such as relict rock jointing and superimposed features such as fissures caused by swelling and shrinkage, the shear strength in mass of tropical soils tends to be governed by the strength along joints and fissures. Strengths measured in the laboratory on conventional sized specimens (75mm or 100mm diameter) tend to be erratic, as do strengths measured in situ by means of small scale in situ tests (e.g. the field vane). The sort of result obtained is shown by Figure 16 which summarizes the results of triaxial shear tests on samples taken from four sites in the Johannesburg graben. However, if the results are looked at site by

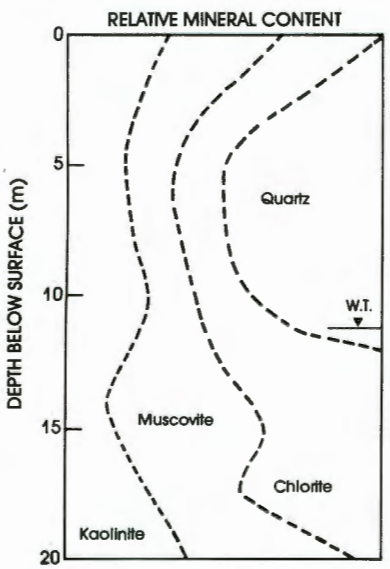

Figure 10: Mineral distribution profile for weathered andesite lava

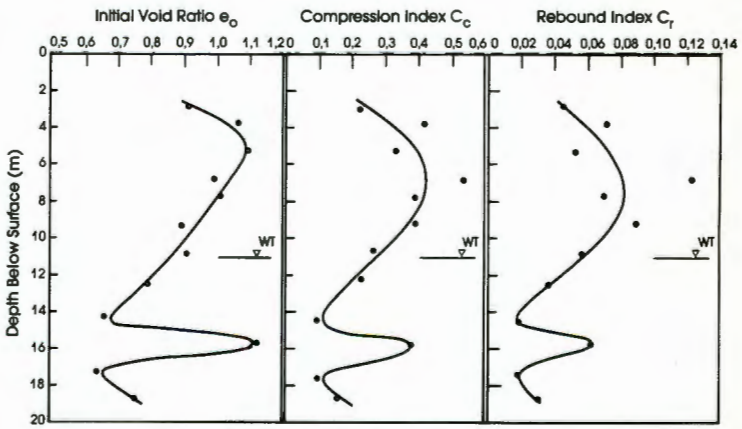

Figure 11: Variation of initial void ratio, compression index, rebound index and preconsolidation pressure with depth in profile of residual weathered andesite lava

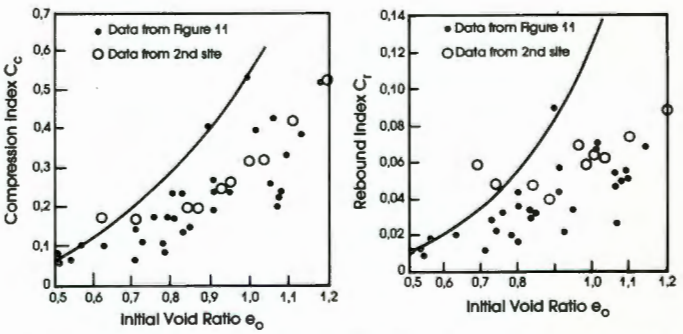

Figure 12: Correlations between initial void ratio and compression and rebound indices

slopes of residual soil exist in an unsaturated condition and their margin of safety against sliding depends on the capillary tensions which exist in the pore water and enhance the strength of the soil. In a natural slope of weathered mudstone (Blight et al, 1970), the capillary tension was found to vary, after light rain, from zero at the surface to 100kPa at a depth of 3m. Infiltration during prolonged rainfall can reduce capillary tensions to a point where the slope becomes unstable. Brand (1982) has observed suctions in residual soil slopes in Hong Kong. At shallow depths, suctions have been observed to decrease to zero during prolonged rain.

According to Lumb (1975), the rate of infiltration of rain into a homogeneous soil in the absence of surface ponding is numerically equal to the saturated permeability of the soil. The water advances into the soil as a wetting front which travels at a velocity of $v = k/(1-S)n$ where k is the permeability, S the initial degree of saturation and n the porosity. Using typical values for soil permeability and rainfall intensity, Lumb shows that such a wetting front could reach a potentially critical depth in a slope (such as the contact between soil and rock) within a few hours. Open cracks and fissures in a soil have the effect of accelerating the advance of such a wetting front.

Yong et al, (1982) have shown how varying duration of rainfall of an intensity at least equal to the saturated surface permeability reduces the factor of safety of a slope. Figure 17 shows some of the results of their analysis plotted as factor of safety versus depth of rainfall penetration. In the example, failure occurs after 20 hours in the one case and after 36 hours in the other. Rainfall of this sort of duration is by no means uncommon in many parts of the tropics, even though it may represent a 10 to 100 year event in other parts.

One of the most extensive series of storm-associated slides on record was that which occurred in the Serra das Araras district of Brazil in 1967 (Da Costa Nunes, 1969). During and following a single night in which the rainfall intensity reached 70mm/hour, an area 24 km long and 7.5km wide was devastated by a series of landslides that killed an estimated 1000 people and caused untold damage to property.

4.1.2 Seismic events:
Yamanouchi and Murata (1973) describe a number of failures in slopes of shirasu that occurred during the 1968 Ebino earthquake. As shirasu is a relatively rigid, brittle material, the earthquake loading produced multitudinous shear cracks in the soil which caused slabs of material to slough off.

Although natural slopes appear to have been affected, cut slopes suffered more severe damage.

4.1.3 Human interference:
There are many types of human interference that may affect the stability of natural slopes in residual soil. Of those the following are probably the most common:

° Removal of toe support by cutting or erosion may precipitate a failure.

The introduction of a cut at the toe of a long natural slope may precipitate a slide. The slide that occurred at Bethlehem, South Africa (Blight et al, 1970) is a typical example of this type of failure (see Figure 18). The slide occurred when a shallow road cut was made in a hillside

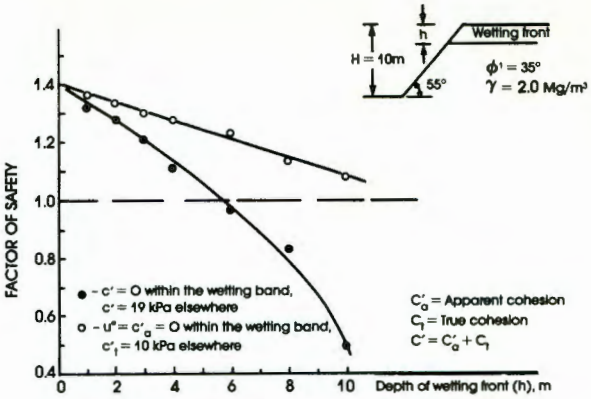

Figure 17a: Effect of rainwater infiltration on Factor of Safety

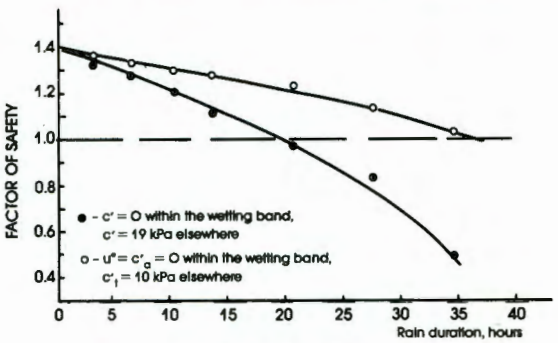

Figure 17b: Effect of rainfall duration on Factor of Safety of a slope

which slopes at a gentle 8°. On investigation it was found that the slide involved a block of weathered sand-stone that was sliding on its contact with an underlying stratum of weathered mudstone. Conditions for failure were exacerbated by a high water table and the existence at the sandstone-mudstone contact of a concentration of illite and montmorillonite clays leached out of the sandstone layer.

Material removed from the toe of a slope by erosion can also cause a previously stable slope to become unstable (e.g. Yamanouchi and Murata, 1973).

° Changes in the soil water regime of a slope may cause instability:

If the soil water regime of a slope is drastically altered by irrigation, the removal of vegetation or partial inundation, instability may ensue (Richards, 1985).

° The most spectacular and tragic recorded example of instability by raised water levels in a natural residual soil slope is the failure in the Vaiont valley described by Muller (1964) and Mencl (1966). During the impounding of water by a new dam, a slope some 600m high, forming one side of the reservoir valley began to creep. After creeping for a period of over three years during which certain observed points were displaced by 4m, the sliding mass suddenly accelerated and the entire slope slumped into the reservoir.

° The effect of deforestation may also be to cause slope instability:

Gray (1974) and Brown and Sheu (1975) identified a number of ways in which deforestation may affect the stability of natural slopes: The following appear to be the more important:

If deep-rooted vegetation is removed, capillary tensions will be reduced and the phreatic

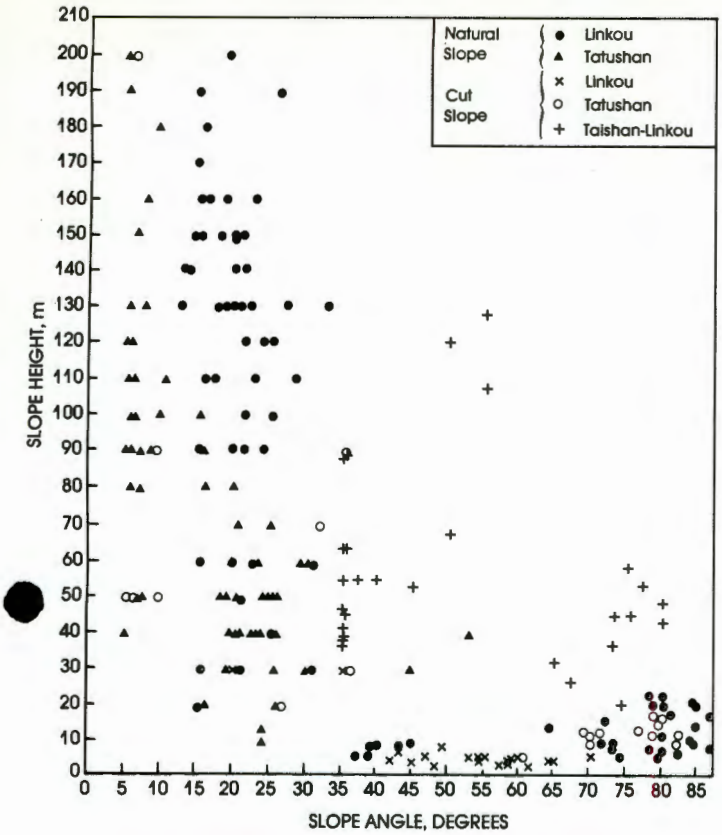

Figure 20: Slope height versus slope angle for the slopes of gravel deposits in north western Taiwan

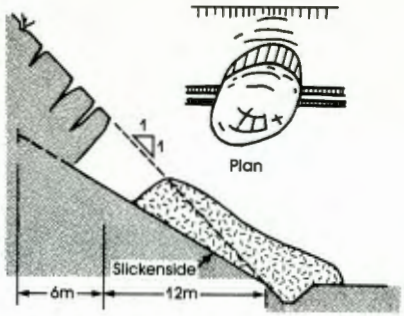

Figure 21a: Slide on slickensided surface flatter than cut slope in weathered tuff (after St. John et al (1969))

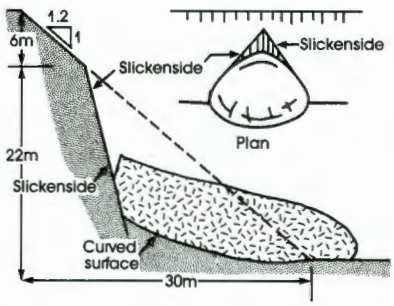

Figure 21b: Slide on intersecting slickensided surfaces steeper than cut slope in weathered tuff (after St. John et al (1969))

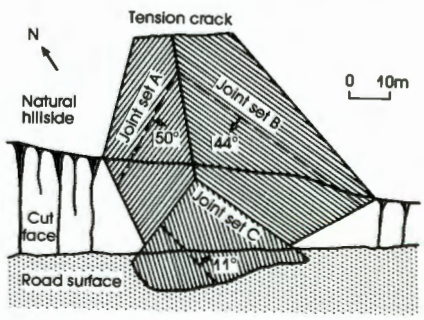

Figure 22: Plan showing three dimensional nature of slip in weathered diabase (after Pells and Maurenbrecher (1974))

In less confined situations such as road or rail cuts, slopes are often cut to a nominal angle and if slides occur, ad hoc remedial measures are taken.

As the surfaces exposed by a slide in residual soil are often stable even though steeper than the original cut face (e.g. St John et al) remedial measures may consist simply of clearing away the fallen debris.

In other cases drainage measures of varying complexity may be required (e.g. Kezdi, 1969) or the provision of toe support in the form of retaining walls of various types. Da Costa Nunes (1969) describes the use of gravity, counterfort, cantilever and crib walls. Gabion or reinforced earth walls are other possibilities. In certain cases it may be necessary to tie back the slope using stressed soil anchors (e.g. Wagener and Neely, 1975).

If rational design and analysis methods are to be applied to slopes in tropical residual soils, a decision has to be made as to what the shear strength of the soil is in bulk, so that this value may be used in the design. Lumb (1975) suggested a design procedure for cuts in which it is assumed that either:

(a) stability is controlled by the cumulative peak strength over the whole potential failure surface; or

(b) stability is controlled by the least peak strength anywhere along the potential failure surface. This procedure provides bounds within which the actual soil behaviour should lie. Because of the effects of seasonal wet weather, peak strengths are established in terms of effective stresses for saturated conditions.

There is considerable evidence (e.g. Burland et al, 1966, Blight, 1969) that the shear strength of a stiff fissured material in bulk corresponds to the lower limit of strengths measured in small-scale laboratory or in situ tests. This was shown by Blight (1969) by back analysing failures of four waste rock dumps founded on residual soil profiles. It was also demonstrated by Blight et al (1970) in relation to series of slides that took place in a mantle

rafts and spread foundations have been used to transfer load to tropical residual soil in a number of countries, including Brazil, Hong Kong, India, Nigeria, Singapore, South Africa and Sri Lanka. These types of foundation are also widely used in the United States (e.g. Barksdale et al, 1982) and Australia (Moore 1982).

As stated earlier, tropical soils behave as if overconsolidated, the degree of overconsolidation depending on the degree of weathering. Williams (1975) found that conventional oedometer tests could successfully be used to predict settlement on residual soils provided the Schmertman corrections were applied as well as the Skempton-Bjerrum correction for overconsolidation.

Barksdale et al (1982) used a number of methods to predict the settlement of a large water tower founded on a weathered biotite gneiss. They found that methods based on in situ tests considerably overestimated the settlement whereas those based on laboratory tests could give excellent predictions.

Working in the same geographical area, Wilmer et al (1982) reported on five settlement studies of spread footings on residual soils. Using conventional one-dimensional oedometer tests, they concluded that calculated settlements for residual soils would normally be about 30 per cent in excess of measured movements.

Barksdale et al have observed that differential settlement on residual soils may be as much as 75% of total settlement, but averages less than 25% of total settlement. Their observations tend in fact to be rather more favourable than those of Burland et al, (1977) on differential settlement of buildings on transported clays.

Two detailed settlement studies have been made for structures founded on Ventersdorp lava in the Johannesburg graben, on the residual profile described in 3 above. (See Figure 25).

Jaros (1978) used a pseudo-elastic finite element method to predict the settlement of two multi-storey structures on Ventersdorp lava with reasonable success. Recognizing that the material behaved as if over consolidated, he used rebound curves from oedometer tests to derive his pseudo-elastic constants. He did not however, attempt a full time-settlement analysis.

The time settlement records for the two buildings, Total House and Guardian Liberty Centre which are both founded on rafts at depths of 18m and 15m respectively, are given in Figures 26 and 27. Both of these records show that most of the settlement occurred during construction with post-construction settlement amounting to only 10 per cent to 20 per cent of total settlement. If the settlement measurements had been commenced after construction, very little movement would have been recorded.

As far as the amount of settlement is concerned both analyses proved reasonably accurate. In the case of Total House, Jaros overpredicted the actual settlement by 26%, while for Guardian Liberty Centre, he underpredicted by 21%. Jaros ascribed the discrepancy in the case of Total House to the presence of large quartzite inclusions or floaters (see Figure 25) in the lava, the effect of which could not adequately be considered in the analysis.

Pavlakis (1983) re-analyzed the settlement records for the two buildings. Using a conventional analysis based on pressuremeter tests,

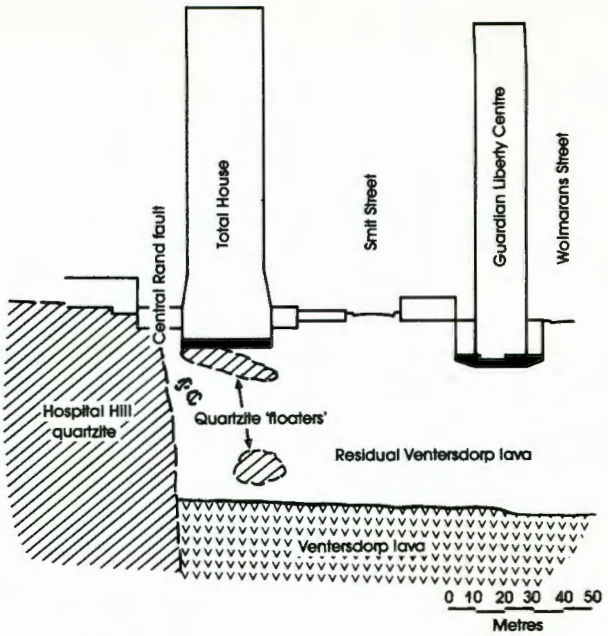

Figure 25: Section through the Total House and Guardian Liberty Centre buildings (Jaros, 1978)

and correcting for the presence of the quartzite floaters,he was able to predict the measured settlements very closely, as recorded on Figures 26 and 27.

5.3 Deep foundations

According to the Brand and Phillipson survey, deep foundations of various types are widely used in tropical residual soils. Driven displacement piles and driven steel tube piles have been used in Brazil, but bored piles and caissons of various types appear to be more widely used in tropical soils. Hand dug caissons are widely used in Hong Kong, with bored contiguous piles frequently used to support the sides of building excavations. Bored piles are also used in India, Nigeria and Singapore. Driven H piles and precast concrete piles are used in Singapore. In South Africa the commonest type of pile in residual soils is the bored cast in situ pile, although driven and driven displacement piles are also used. The situation in Sri Lanka is similar.

When designing bored cast in situ piles in tropical soils, the question of what strength represents that of the soil in bulk must again be answered. Basically, the answer is the same as that given before - the lower limit to strengths measured by small scale means will represent the strength of the soil in bulk. However, in certain cases this is not a low enough value. For example, Figure 28a shows that strengths measured by means of large scale plug-pulling tests in an expansive residual siltstone (Blight, 1984) were less than half of the lower limit to strengths measured by small scale means. Figure 28b shows a comparison of the predicted tension versus depth curve for a pile designed on the basis of the large scale shear tests, and tensions measured in a test pile. The comparison shows that the large scale test

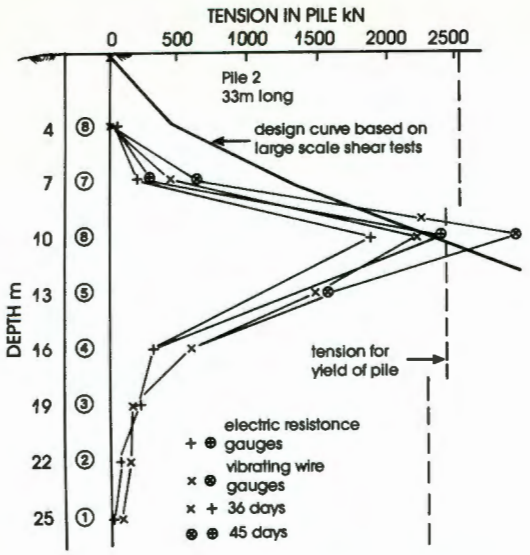

Figure 28b: Comparison of predicted and measured tensions in a bored cast-in-situ pile installed in expansive residual siltstone

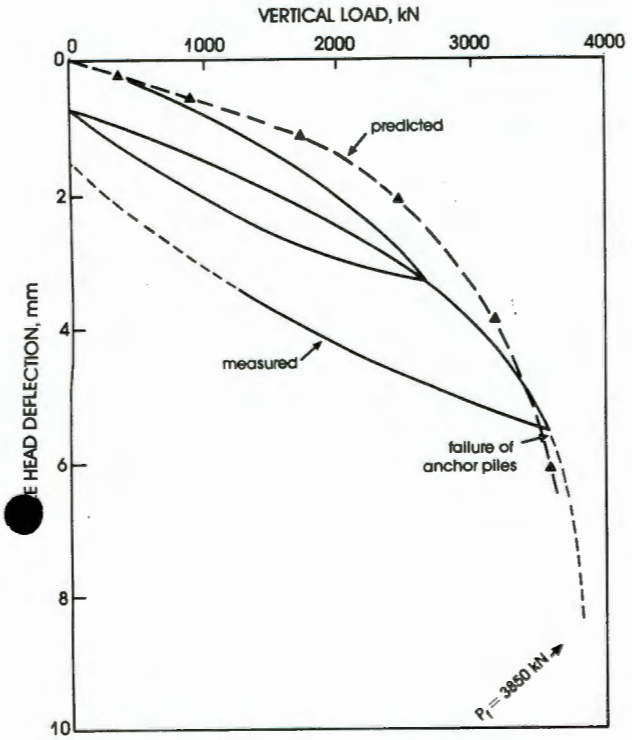

Figure 29a: Measured and predicted load-deflection behaviour for a single driven cast-in-situ pile

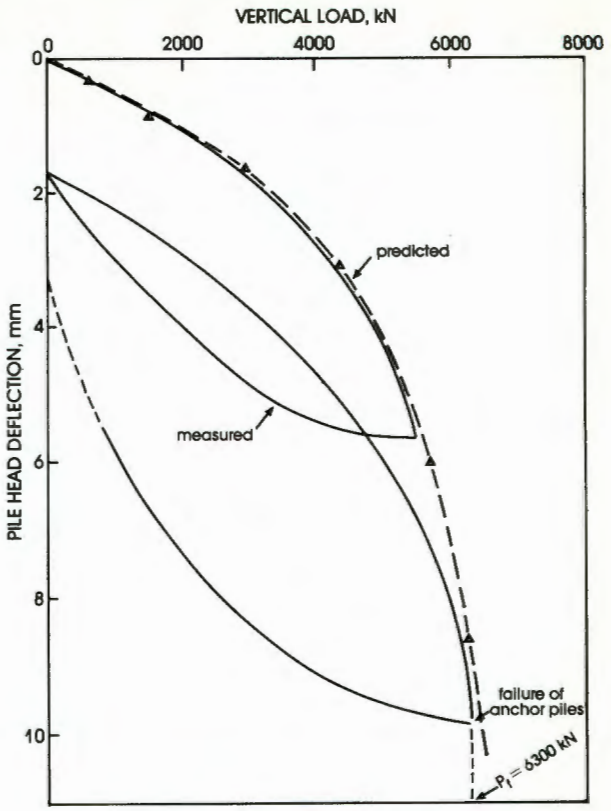

Figure 29b: Measured and predicted load-settlement behaviour of 2 driven cast-in-situ piles under one pile cap

1980 and Horn and Schweitzer, 1982).

A number of general problems in the use of residual soils as construction materials have been identified by various authors:

° As a result of variability in both parent rock and extent of weathering, borrow areas in residual soils usually exhibit variability both laterally and vertically. Hence quality control becomes difficult and materials must either be mixed or selected or both to maintain homogeneity of material in the soil structure.

° Drying of the soil from its in situ moisture content has the effect of changing the soil properties. Hence in many cases, standard soil testing procedures in which the soil is air-dried before testing cannot be used. Also, specimens cannot be remixed and re-compacted but fresh soil must be used for each compacted specimen.

° Aggregates of soil particles and soil particles themselves tend to breakdown with mechanical working, thus changing the properties of the soil.

Figure 30 (after Gidigasu, 1974) illustrates some of the effects of drying and reworking by compaction on the compaction properties of a lateritic soil. Figure 31 (Gidigasu and Dogbey, 1980) illustrates the progressive breakdown in particle size under compaction of a quartzitic gravel and a lateritic gravel both residual from the weathering of granite.

One of the most important results of the above effects is that laboratory compaction behaviour may not correlate with the behaviour of the soil under roller compaction in the field. (This often applies with transported soils as well, as roller compaction characteristics are generally different from the characteristics of laboratory compaction).

Figures 32a and b (Blight, 1962) show two comparisons of roller compaction curves for a soil residual from a granite pegmatite in northern Zambia.

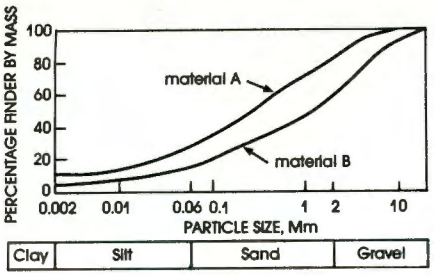

Figure 33: Average grading curves for materials A and B of Fig. 32.

7.3 Natural slopes appear generally to be stable, but may be precariously so. Failures that do occur are often preceded by some unusual natural event, or by man's intervention. Events that have led to failures include:

- unusually heavy or prolonged rainfall,
- seismic events,
- removal of toe support by cutting or erosion
- changes in the soil water regime
- deforestation.

7.4 The stability of cut slopes is affected by many of the factors that affect the stability of natural slopes. Stability is very sensitive to structural features in the soil, and can be greatly influenced by the presence of capillary water stresses. Rational design of cut slopes is beset with difficulties, but the strength in mass of tropical residual soils can be assessed as the lower limit to the results of small scale in situ or laboratory measurements.

7.5 The settlement of raft and spread foundations on tropical soils can be predicted with acceptable accuracy. In certain instances, notwithstanding the heterogeneity of tropical profiles, differential settlements may be less than with transported clays.

7.6 Deep foundations in tropical soils can successfully be designed on a rational basis. Again, there is a difficulty in assessing the strength of the soil in mass, and it may be necessary to use large-scale in situ tests or full-scale pile loading tests to do this.

7.7 Tropical residual soils are widely used as construction materials for building roads and embankments. Apart from inherent variability in the borrow pit, the properties of the soil may change as a result of the effects of drying or particle breakdown during working and compaction.

REFERENCES

Akili,W. and Torrance, J.C., 1981. The development and geotechnical problems of sabkha, with preliminary experiments on static penetration resistance of cemented sand. Quarterly J. Eng. Geol. 14(1):59-74.

Arnold, M., 1984. The genesis, mineralogy and identification of expansive soils. Proc. 5th Int. Conf. Expansive Soils, Adelaide, Australia. 32-36.

Barksdale, R.D., Bachus, R.C. and Calnan, M.B., 1982. Settlements of a tower on residual soil. Engineering and Construction in Tropical and Residual Soils, ASCE Geotech. Div. Spec. Conf. Honolulu, Hawaii, 647-664.

Bishop, A.W., and Blight, G.E., 1963. Some aspects of effective stress in saturated and partly saturated soils. Geotechnique 13(3) 177-197.

Blight, G.E., 1962. Controlling earth-dam compaction under arid conditions. ASCE Civ. Engin. 54-55.

Blight, G.E., 1967. Effective stress evaluation for unsaturated soils. Jour.Soil Mech. & Found. Eng. Div., ASCE. 93(SM2). 125-148.

Blight G.E., 1969. Foundation failures in four rockfill slopes, Jour. Soil Mech & Found. Eng. Div., ASCE, 95(SM3) 743-767.

Blight, G.E., 1980. Partial saturation can assist the soil engineer. Proc. 6th Southeast Asian Conf. on Soil Eng. Taipeh, Taiwan. 1. 15-29.

Blight, G.E., 1983. Aspects of the capillary model for unsaturated soils. Proc. Asia Reg. Conf. Soil Mech. & Found. Eng. Haifa, Israel, 1. 5pp.

Blight, G.E., 1984. Uplift forces measured in piles in expansive clay. Proc. 5th Int. Conf. Expansive Soils, Adelaide, Australia, 1. 240-244.

Blight, G.E. and Brummer, R.K. 1980. Compressibility and strength of weathered andesite lava. Civ.Eng. in. S. Africa. 22(10). 271-278.

Blight, G.E., Van Heerden A and Brackley I.J.S., 1970. Landslides at Amsterdamhoek and Bethlehem - an examination of the mechanics of stiff fissured clays, Civ. Eng. in S. Africa, 129-140.

Brand, E.W. 1982. Analysis and design in residual soils, Engineering and Construction in Tropical and Residual Soils. ASCE Geotech. Div. Spec. Conf. Honolulu, Hawaii, 89-143.

Brand, E.W. and Phillipson, H.B., 1985. Sampling and testing of residual soils. Southeast Asian Geotechnical Society, Scorpion Press, Hong Kong.

Brink, A.B.A., 1979. Engineering geology of Southern Africa. Building Publications, Pretoria, South Africa.

Brink, A.B.A., and Kantey B.A., 1961. Collapsible grain structure in residual granite soils in Southern Africa. Proc. 5th Int. Conf.Soil Mech. & Found. Eng., Paris. 1. 611-614.

Brown, C.B., & Sheu, M.S., 1975, Effects of deforestation on slopes, Jour. Geotech.Div. ASCE 101 (GT2) 147-165.

Brummer, R.K. 1980. The engineering properties of deep highly weathered residual soil profiles. MSc(Eng) Thesis, University of Witwatersrand, Johannesburg.

Burland, J.B., Butler F.G.B. and Dunican, P., 1966. The behaviour and design of large diameter bored piles in stiff clay. Symp. Large Bored Piles. Instn. Civ. Engrs, London. 51-71.

Burland, J.B., Broms, B.B. and de Mello, V.F.B. Behaviour of foundations and structures. State-of-the-Art Report. 9th Int. Conf. Soil Mech. & Found. Eng. Tokyo, Japan 2. 495-546.

Da Costa Nunes, A.J., 1969. Landslides in soils of decomposed rock due to intense rainstorms, Proc. 7th Int. Conf. on Soil Mech. & Found. Eng., Mexico City 2. 547-554.

de Beer, J.H., 1965. A detailed geological and soil map of Johannesburg city area. MSc Thesis

Terzaghi, K., 1958. Design and performance of Sasumua dam. Proc. Inst. Civ. Engrs. (London) 9. 369-394.
Tuncer, A.L., 1969. An engineering classification of certain basalt-derived lateritic soils Eng. Geol. 11(4). 319-339.
Uehara, G., 1982. Soil science for the tropics. Engineering and construction in tropical and residual soils. ASCE Geotech. Div. Spec. Conf. Honolulu, Hawaii. 13-26.
van der Merwe, D.H., 1965. The soils and their engineering properties of an area between Pretoria North and Brits, Transvaal. DSc Thesis, University of Pretoria.
Vargas, M., and Pichler, E., 1957. Residual soil and rock slides in Santos, Brazil. Proc. 4th Int. Conf. for Soil Mech. & Found. Eng. London II. 394-398.
Wagener, F. von M. and Neely, W.J., 1975. Stability of a railway cutting in micaceous silt stones. Proc. 6th Reg. Conf. for Africa Soil Mech. & Found. Eng. I. 213-218.
Weinert, H.H., 1974. A climatic index of weathering and its application in road construction. Geotechnique. 24(4). 475-488.
Wesley, L.D., 1973. Some basic engineering properties of halloysite and allophane clays in Java, Indonesia. Geotechnique. 23(4). 471-494.
Williams, A.A.B., 1975. The settlement of three embankments on ancient residual soils. Proc. 6th Reg. Conf. for Africa on Soil Mech. & Found. Eng. Durban, S. Africa. 1. 255-262.
Willmer, J.L., Futrell, G.E. and Langfelder, J., 1982. Settlement predictions in Piedmont residual soil. Engineering and Construction in Tropical and Residual Soils. ASCE Geotech. Div. Spec. Conf. Honolulu, Hawaii. 629-646.
Woo, S.M., Guo, W.S., Yu, K. and Moh, Z.C., 1982. Engineering problems of gravel deposits in Taiwan. Engineering and Construction in Tropical and Residual Soils. ASCE Geotech. Div. Spec. Conf. Honolulu, Hawaii. 500-518.
Yamanouchi, T. and Haruyama, M., 1969. Shear characteristics of such granular soil as *shirasu*. Memoirs. Faculty of Eng. Kyushu University. 29(1). 63-64.
Yamanouchi, T. and Murata, H., 1973. Brittle failure of a volcanic ash soil - shirasu. Proc. 8th Int. Conf. on Soil Mech. & Found. Eng. Moscow. 1. 495-500.
Yong, R.N., Siu, S.K.H. and Sciadas, N., 1982. Stability analysis of unsaturated soil slopes. Engineering and Construction in Tropical and Residual Soils. ASCE Geotech. Div. Spec. Conf. Honolulu, Hawaii. 483-499.
Zaruba, O. and Mencl, V., 1976. Engineering Geology. Elsevier Scientific, Amsterdam.

HYDRAULIC FILL STRUCTURES

A speciality conference sponsored by
the Geotechnical Engineering Division of the
American Society of Civil Engineers

Co-sponsored by the
Society of Mining Engineers of AIME

Colorado State University
Fort Collins, Colorado
August 15-18, 1988

Edited by D.J.A. Van Zyl and Steven G. Vick

Geotechnical Special Publication No. 21

Published by the
American Society of Civil Engineers
345 East 47th Street
New York, New York 10017

SOME LESS FAMILIAR ASPECTS OF HYDRAULIC FILL STRUCTURES

by

Geoffrey E Blight[a], MASCE

ABSTRACT

There are many aspects of hydraulics fill structures that may be of great importance in particular cases and circumstances, even though they may not be considered of general importance and may be less familiar to the geotechnical engineer. This paper selects ten such aspects and gives a brief discussion of each. The object is to widen the readers' perspective and knowledge of hydraulic fill structures beyond what is usually covered in papers and conferences dealing with this subject.

1. INTRODUCTION

Hydraulic fill structures form an important class of geotechnical construction in the fields of civil and mining engineering, in the mineral extraction industry, the electricity generating industry and to a lesser extent, in the chemical processing industry. Within these fields, hydraulic fill structures of various types are used for the following general functions:

.1 To provide access and support, e.g. reclamation fills, artificial islands for off-shore drilling, backfill in underground mines;

.2 To provide storage for low grade mineral ores and for water.

It will be noted that no direct reference has been made to "waste disposal". This is because, with rapidly advancing techniques of mineral extraction and energy utilization, most deposits of what was formerly considered to be mineral waste must now be regarded as low grade ore or a mineral resource awaiting a favourable economic and technological opportunity for its re-exploitation.

---

[a] Professor of Construction Materials, Department of Civil Engineering, University of the Witwatersrand, Johannesburg, South Africa.

Many papers have been written describing the macro-aspects of the design and construction of hydraulic fill structures of various types. For example, the design, construction, maintenance and reclamation of what are termed mine waste deposits have been codified and extensively described by authorities such as the British National Coal Board(1970), the Canada Centre for Mineral and Energy Technology(1977), the Australian Department of Home Affairs and Environment(1982) and the Chamber of Mines of South Africa(1979). However, there are aspects of hydraulic filling that have received less attention in the literature, but which may often be of equal importance to the macro-aspects of a particular operation.

This paper will select ten of these less well known and researched aspects and examine them in limited detail with the purpose to inform and broaden the perspective of the engineer with an interest in hydraulic fill construction.

The aspects that have been selected for examination are the following:

.1 the flow properties of mineral slurries;
.2 the flow of slurry escaping from a breached containment;
.3 the beaching behaviour of slurries;
.4 the effects of desiccation on the construction of hydraulic fills;
.5 tailoring the composition of a fill to improve its qualities;
.6 stiff underground fills;
.7 horizontally reinforced hydraulic fill mine supports;
.8 effects of underground mine filling on surface storage of residue;
.9 the effect of desiccation on hydraulic fill structures;
.10 surface erosion of hydraulic fill mineral deposits.

The material for these discussions has mainly been taken from the writer's own published experience, [e.g. Blight(1979), Blight(1980), Blight(1984), Blight(1987), Blight and Bentel(1983), Blight and Clarke(1983), Blight, McPhail and Fourie(1986), Blight, Robinson and Diering(1981), Blight, Thomson and Vorster(1985), Hahn, Blight and Dison(1982)]. It is freely admitted that the selection of topics and the material itself has been strongly biased by the writer's background and the practice in the area in which he works.

2. ASPECTS OF HYDRAULIC FILLING

.1 FLOW PROPERTIES OF MINERAL SLURRIES

The construction of hydraulic fill structures involves the transportation and deposition of mineral material in the form of water-borne slurries. Hence the flow of slurry through pipelines, launders or other channels, as well as the distribution of the slurry to build the structure are subjects of great importance. All of these operations depend on the rheological behaviour of mineral slurries. The water content at which slurries are transported and placed varies widely, depending on the material being moved and the application. As

examples, the water content of mine tailings during transportation from the mill to the storage dam is typically in the range from 150 to 100 per cent by mass of dry solids[b]. For the hydraulic filling of underground mine excavations, the water content is typically 50 per cent or less.

The rheological behaviour of mineral slurries is complex, but can be approximated by that of a Bingham plastic for which the Newtonian viscosity η is related to the shear strength τ by

$$\tau = \tau_0 + d\gamma/dt \cdot \eta \qquad [1]$$

Where τ_0 is a yield shear strength that applies when the rate of shear strain $d\gamma/dt$ is zero.

Slurry viscosities are commonly measured by observing the variation of torque with water content and rate of shear strain using a co-axial cylinder viscometer. Any single torque measurement can be interpreted in terms of an apparent viscosity η_a where

$$\eta_a = \eta + \frac{\tau_0}{d\gamma/dt} \qquad [2]$$

The apparent viscosity at a specific water content and rate of shear strain is usually sufficient for the purpose. If the true viscosity is required, the value of τ_0 has first to be established.

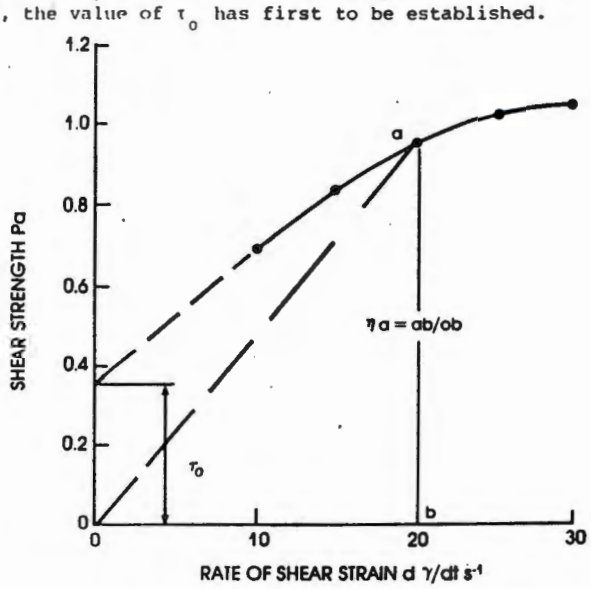

Figure 1a: Relationship between shear strength and rate of shear strain for diamond tailings at a water content of 125 per cent

[b] It should be noted that in the mining and mineral industries, it is more common to express water contents as a percentage of the wet mass.

Figure 1a illustrates the concepts of η_a and τ_0 as applied to a slurry of diamond tailings. For a true Bingham plastic the relationship between τ and $d\gamma/dt$ would be linear and the slope of this line would represent the true viscosity η. Figure 1b shows the relationship between τ and $d\gamma/dt$ calculated for Figure 1a. Calculated values of η are also shown. For a true Bingham plastic, η would, of course, be independent of $d\gamma/dt$. Figure 1 relates to a single water content whereas one is usually interested in the effect of varying water content on flow properties. This effect is shown in Figures 2a and 2b for a platinum tailings. Further data on the rheological properties of mineral slurries have been published by Whitney et al(1977), Jeyapalan(1980) and Lucia et al(1981).

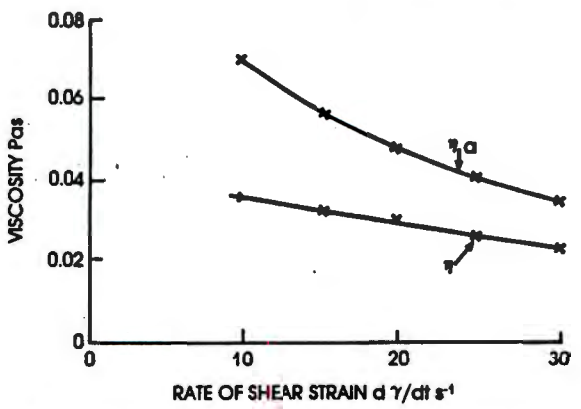

Figure 1b: Relationship between viscosity and rate of shear strain for diamond tailings at a water content of 125 per cent
η_a = apparent viscosity η = 'true' viscosity

Once the rheological properties of a slurry have been established, they can be used to estimate friction losses in pipelines, flow rates in open channels, etc. via established flow theory [e.g. Graf(1971) and Verkerk(1987)]. It is interesting to note that none of the accepted flow equations actually use viscosity as a basic parameter. Viscosity is always converted back to an estimated shear resistance. From the geotechnical engineers' viewpoint, therefore, it would be preferable to use rheological data in terms of shear strength, as given in Figures 1a and 2a rather than to convert it to terms of viscosity, a far more difficult concept to grasp and use.

Note also that the range of shear strengths for slurries is smaller than the range of strengths of solid soils by a factor of a thousand. The increase of strength from Pascals to kiloPascals takes place after deposition and consolidation of the slurry in the hydraulic fill structure.

Perhaps the most important point to note is that the shear strength of slurries and the soil-like materials that they form after draining are affected in a complex way by both water content and rate of shearing.

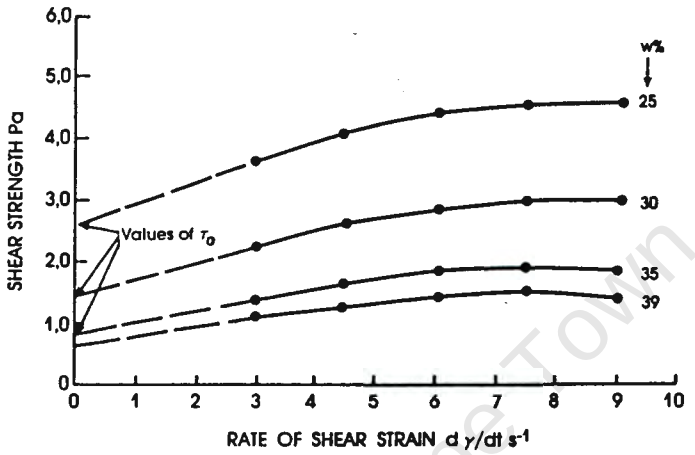

Figure 2a: Measurements of shear strength on platinum tailings, showing the influence of varying water content
w = water content of the slurry

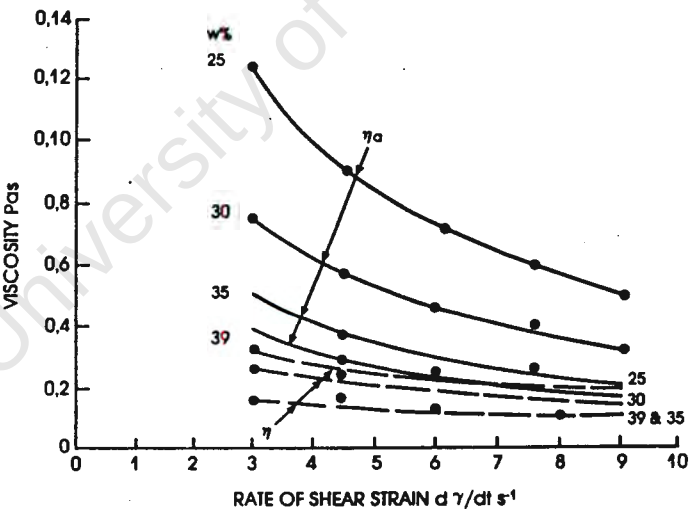

Figure 2b: Measurements of viscosity on platinum tailings, showing the influence of varying water content
w = water content of the slurry ηa = apparent viscosity η = 'true' viscosity

The effect of water content is well known, but the effect of rate of shearing is far less recognized.

.2 THE FLOW OF SLURRIES ESCAPING FROM BREACHED CONTAINMENTS

In the past, and even very recently, hydraulic fill structures have suffered from their share of failures. The usual consequence of such an accident is that the outer containment has breached and the liquid slurry contents have escaped to wreak terrible damage. Examples of such failures in recent years have been the breaching of the Mochikoshi tailings dam in Japan in 1978 [Marcuson et al(1979)], the Stava tailings dam in Italy in 1985 [Berti et al(1988)] and the Bafokeng tailings dam in South Africa in 1974 [Jennings(1979)]. All of these events were accompanied by tragic loss of life and damage to property.

To give an idea of the potential mobility of a mineral slurry accidently released in this way, the 3 million m^3 of slurry that escaped from the Bafokeng tailings dam entered a small water course and flowed down it for 42km. The flow was only stopped because it entered a water storage reservoir at that point. An estimated 2 million m^3 of slurry reached and almost filled the reservoir, slopping the water it contained over the dam wall.

Relatively little research seems to have been done on this problem. Jeyapalan et al(1983), Lucia et al(1981) and the writer and colleagues are among the few that have investigated the matter, although work along similar lines has been done on natural mudflows [Hutchinson and Bandari(1971)] and submarine slurry flows [Morgenstern(1967)].

Blight et al(1981) concentrated on finding a method of predicting flow depths and flow velocities downstream of a hypothetical breach. The object was to be able to assume that a ringdyke tailings dam would breach in various positions and then to analyse the effect of the ensuing flood of slurry on surface installations, shafts, nearby housing, etc. If, as a result of the analysis, it became clear that a particular structure or group of structures was at risk, a protective bund could be constructed to deflect the possible flood, or the installation could be re-located.

The proposed analysis proceeds step-wise from the breach by applying the general equation of motion to the element of moving slurry depicted by Figure 3:

> Downstream forces on element - upstream forces
> = (mass of slurry in element) x acceleration. [3]

This, together with the equation of continuity, namely that the mass of slurry passing any cross-section is the same at any instant and an assumed surface profile for the flow, enables the flow depth and velocity to be estimated progressively along its course.

The analysis was calibrated by applying it to the failure of the Bafokeng tailings dam and comparing calculated flow depths and velocities with slurry depths observed on various structures affected by the flow and with eye-witness accounts. Figure 4 is a plan showing the complex form taken by the flow as it issued from the breach in the dam. The figure shows the sections analysed and some of the structures affected by the flood.

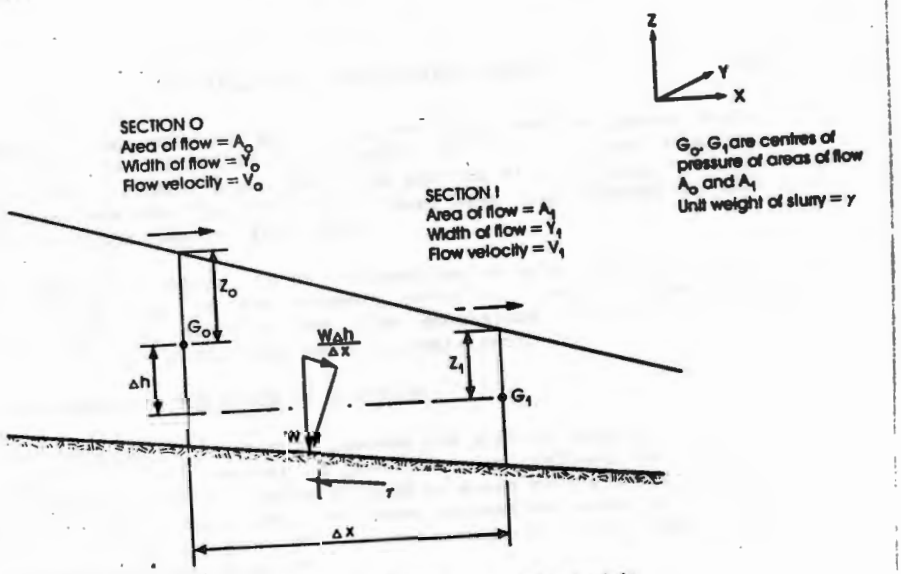

Figure 3: Free body diagram of the flow of slurry at steady state

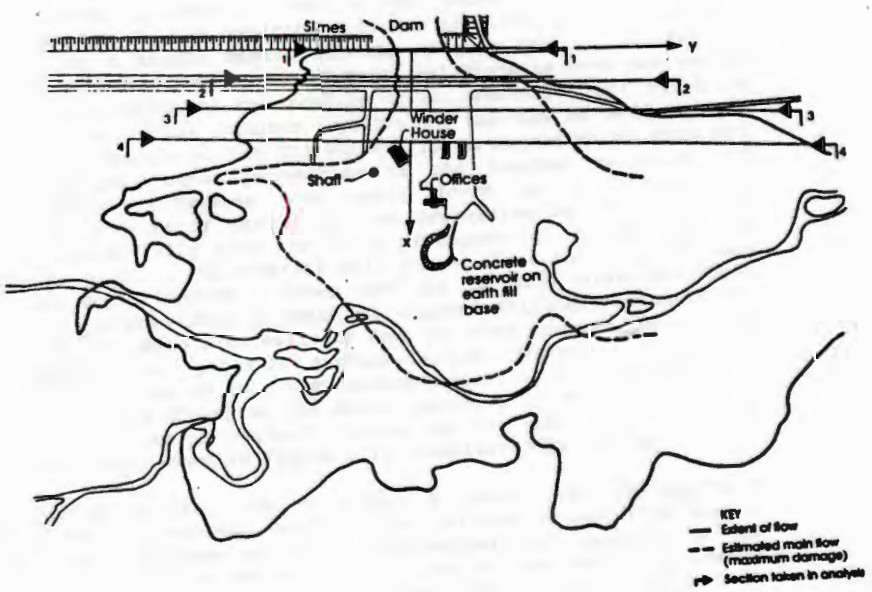

Figure 4: Failure of Bafokeng slimes dam

watertables. The effect on shear stability of the force is extremely adverse. Walls in this condition have failed at heights as low as 3m.

Recent work on very fine tailings (cyclone overflow gold mine tailings) has shown that material deposited on a beach settles appreciably after it has come to rest. This has the effect of

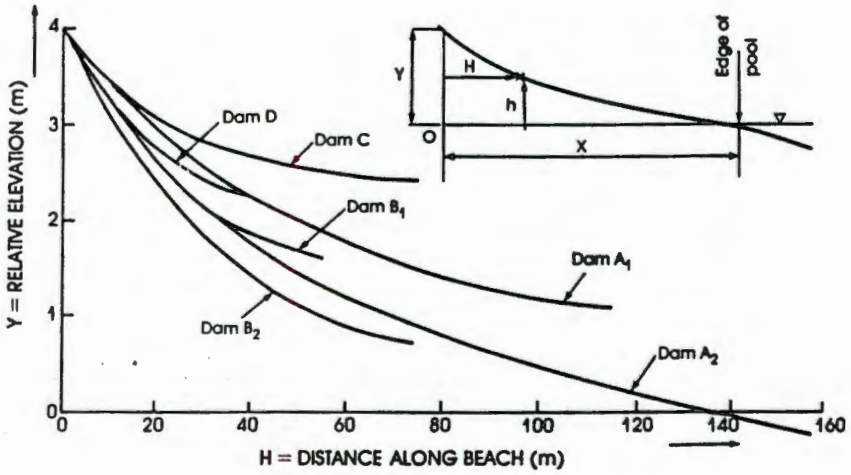

Figure 5a: Measured beach profiles on six platinum-tailings dams

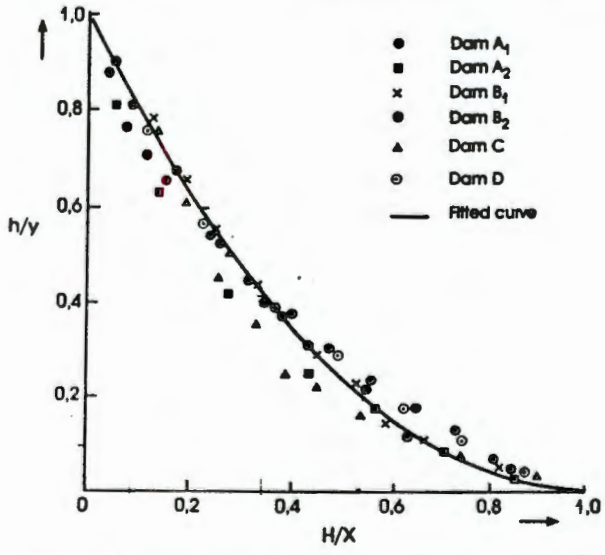

Figure 5b: Dimensionless beach profiles for platinum tailings

flattening the beach profile. Hence it is not just particle sorting that determines the profile, but settlement as well. This conclusion is supported by Wates et al(1987).

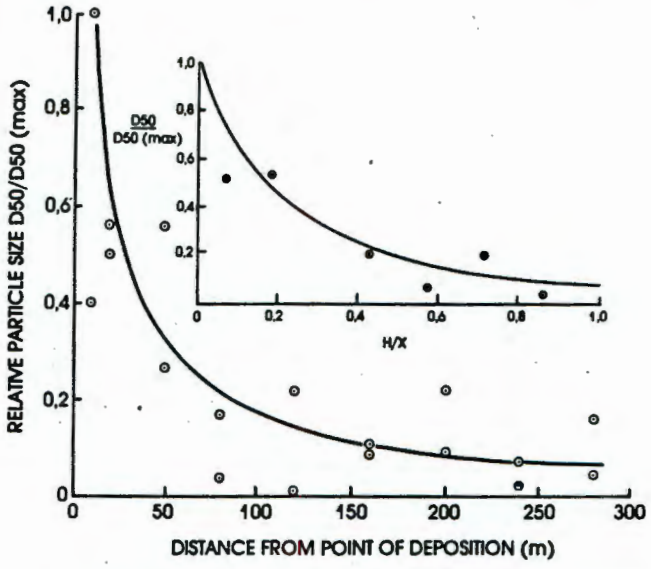

Figure 6: Particle size sorting that occurs on a hydraulic beach

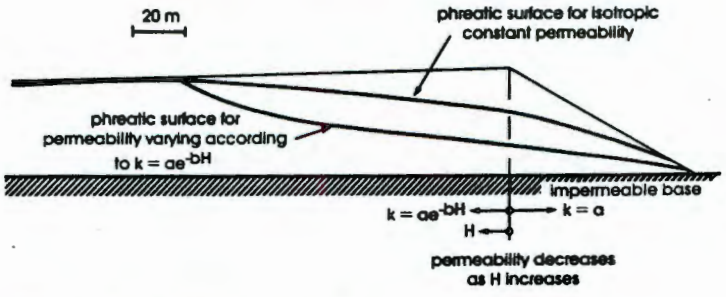

Figure 7: Effect of varying permeability on position of phreatic surface in a tailings dam

4 THE EFFECT OF DESICCATION DURING CONSTRUCTION

In many climates of the world, evaporation from a free water surface considerably exceeds precipitation in the form of rainfall. The water deficit may apply either seasonally or throughout the year. This favourable climatic condition is often deliberately exploited by allowing each layer of hydraulically deposited material to dry out

before placing the next layer. This is known as the "semi-dry" process of deposition [Blight and Steffen(1979)]. The practice of sundrying has the effect of considerably reducing the void ratio of the deposited material and correspondingly increasing the solids storage capacity of the impoundment. Figure 8 shows the effect of desiccation on reducing the void ratio of a gold slimes dam.

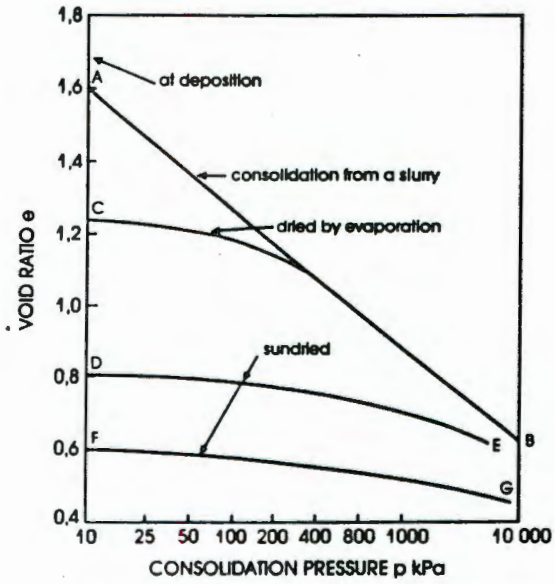

Figure 8: Effect of sundrying on void ratio and consolidation characteristics of slimes

It may be unwise to design and rely on the volume reduction caused by dessication if there is any possibility that as a result of operating errors, the sundrying will not take place. In one case known to the writer, the volumetric design of a tailings deposit (a valley dam behind a pre-built earth embankment) depended for its five-year life on volume reduction by sundrying. When the mill was commissioned, loss of control resulted in the tailings impoundment almost filling with tailings at a very high water content. Decanting the water once the solids had settled did not help, as only the surface of the saturated tailings could be affected by subsequent sundrying. The effect of this failure to operate the deposit as designed was the loss of half its useful life.

The practice of allowing successive layers to shrink to their maximum may also have negative effects, as vertical desiccation cracks may open up in each layer. These cracks may form a network of incipient piping channels within the deposit and later result in piping failures that could put the deposit out of commission temporarily, or in severe cases result in a failure of the complete impoundment. The Bafokeng

failure is believed to have resulted from a combination of desiccation cracking and horizontal layering by fine material followed by a piping failure.

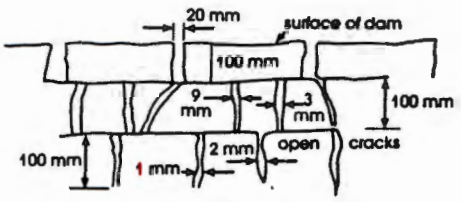

OPEN VERITCAL CRACKS DOWN TO 500 mm

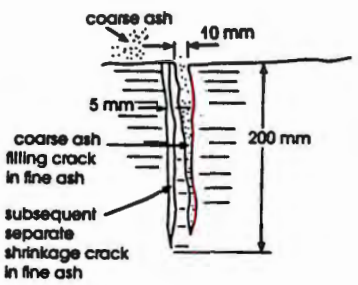

Figure 9a: Systems of shrinkage cracks near the surface of hydraulically deposited power-station fly ash

Figure 9a illustrates the sort of cracking that occurs in a deposit of pulverized fuel ash that has suffered repeated piping failures over the course of its life. The most dangerous situation arises when the pool on the deposit becomes enlarged in size either because of rain, lack of control by the operating staff or the deliberate storage of water on the dam. Once water enters the crack network, the pool empties into the cracks and erodes long deep subterranean channels that every so often emerge from the outer slopes of the deposit and result in a localized failure. Figure 9b shows some of the piping channels that have been observed to form in the material of Figure 9a.

The only remedy for this situation appears to be to avoid desiccation of the beaches by a more frequent deposition cycle, tight control over the size of the pool, or, as a more certain solution, by changing the method of deposition or the properties of the material being deposited.

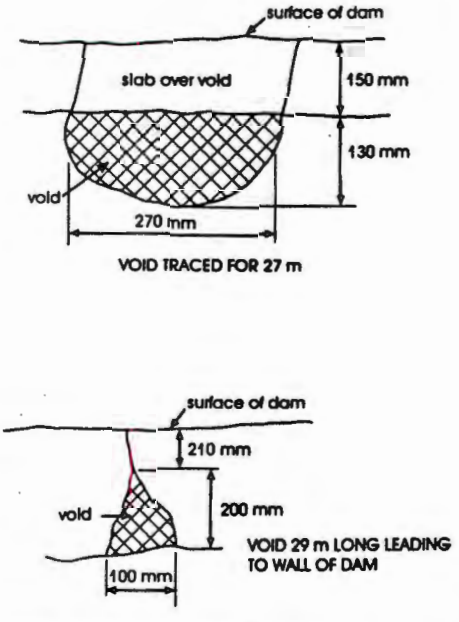

Figure 9b: Erosion pipes located beneath the surface of hydraulically deposited fly ash

.5 TAILORING THE PROPERTIES OF A FILL

It is a well-established geotechnical principle that the strength and compressibility of a soil-like material depend on its density. Strength increases and compressibility reduces as density is increased. It is perhaps not always remembered that this principle is the sole reason for the geotechnical engineer's pre-occupation with moisture and density control in earthworks construction. The density of a particulate material is dependent on its particle size distribution and it is often possible to tailor the size distribution by combining available materials or by removing certain size fractions so that the fill will settle into a maximum or improved density state.

Size distribution curves may be subdivided into two general categories:

.1 Straight line gradings that give approximate straight line plots on the conventional percentage passing versus log particle size chart, and

.2 gap gradings which consist of two sections of straight lines separated by a size gap in which there are no or few particles present.

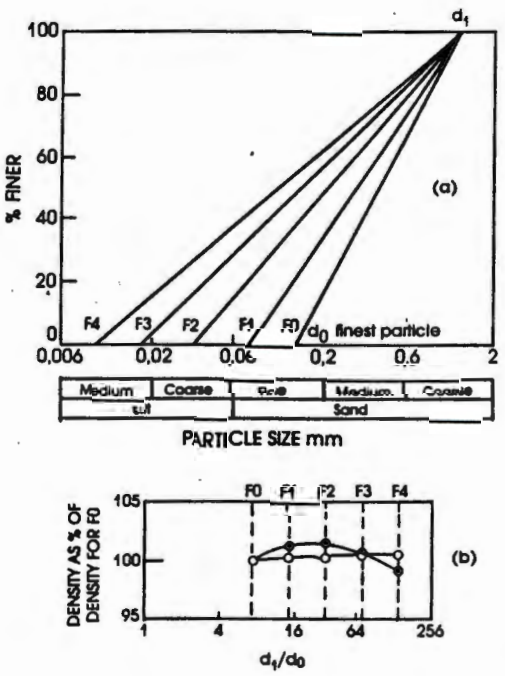

Figure 10: (a) Series of continuous gradings F0, F1, F2, F3, F4
(b) Settled densities of two materials made up in gradings F0 to F4

Figures 10a and 10b illustrate the effect on settled density of varying the slope of a straight line grading while keeping the maximum particle size constant. The various materials were all allowed to settle out from a slurry under identical conditions. It is obvious that the slope of the grading has a relatively minor effect on the density.

Figures 11a and 11b show the effect of varying the maximum particle size while keeping the slope of the grading constant. It appears that the maximum particle size has a far greater influence on density than does the slope of the grading.

Thirdly, Figure 11b also shows a number of gap gradings in which the gap between the uniform gradings F0 and F5 is bridged at various percentages finer, to give, for example grading F0-G0-G0-F5. Figure 12 shows the effect on settled density of varying the percentage of finer

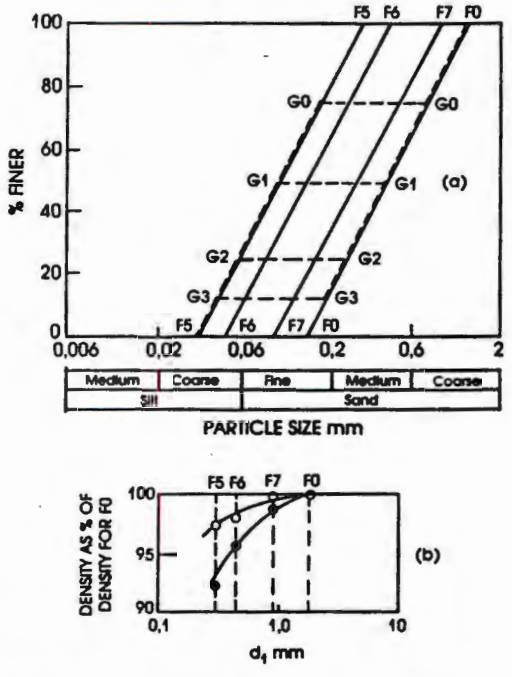

Figure 11: (a) Series of continuous gradings F0, F5, F6, F7, and gap gradings G0, G1, G2, G3
(b) Settled densities of two materials made up in gradings F0, F5, F6, F7

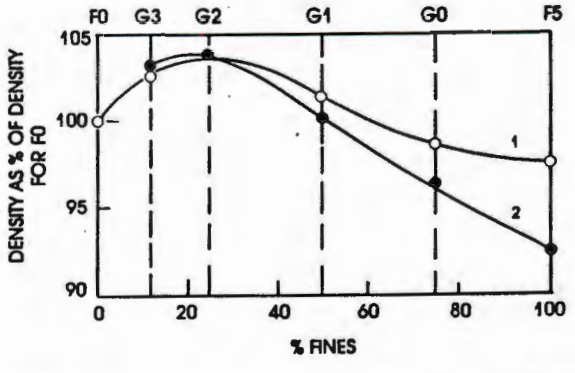

Figure 12: Settled densities of two materials made up in gradings F0, G0 to G3, and F5

material in this way. This manipulation produced the greatest variation of density. For example, the addition of 20 per cent of fines to a material with grading F0 can increase the density by 4 per cent, whereas the density of the fines alone would be 5 per cent less than the density obtainable with grading F0.

These illustrations of the effect of tailoring the properties of a fill do not provide a set of rules for obtaining maximum settled density in a hydraulic fill, as there are other variables such as particle shape, particle surface texture and particle density that also affect the settled density of a slurry. The examples do, however, illustrate the scope that exists for improving the properties of a fill by manipulating the grading.

As a ridiculous example, cement is often added to pumped mining fills with a resultant improvement of density and strength which is ascribed to cementing action. In reality, the water/cement ratio may be so large that the cement bonds have a negligible strength. The improvement of properties arises mostly from the modification of the material grading by the addition of the cement fines. An equal percentage of similar, but chemically inert fines would have almost be same effect.

Density is obviously not the only property of an hydraulic fill that it may be desirable to optimize. Permeability may be improved or even optimized by cycloning to remove much of the fine fraction of a fill. This process also has the effect of reducing in place shrinkage (and hence the piping problems referred to in .4 above) by reducing the water content at placement and removing most of the material that is the source of the shrinkage.

.6 STIFF UNDERGROUND FILLS

The concept of tailored fills is taken to an extreme in the design of stiff underground mining fills.

The stiff fill is designed primarily to provide lateral restraint to ore pillars, thus strengthening the pillars and enabling them to be made smaller. Smaller ore pillars mean a greater ore extraction ratio and hence a more profitable mining operation. The design concept is to create a rigid in situ skeleton of rock particles with the voids just filled with cemented tailings. In addition to the requirement of in situ rigidity, the fill has to be pumped into place and the fresh mix must therefore have a low enough viscosity to be pumped and placed. This is done by means of positive displacement concrete pumps [see Verkerk(1987)]. The as-placed density of such a fill is extremely high and can be more than 90 per cent of the density of the solid constituents. The maximum possible volumetric compression of such a stiff fill is thus less than 10 per cent.

Figure 13 compares the confined (i.e. K_o) compression characteristics of stiff fills with those of conventional "soft" cemented tailings fills. The cement content is similar in each case. It will be seen that the stiff fills become virtually incompressible beyond a limit of

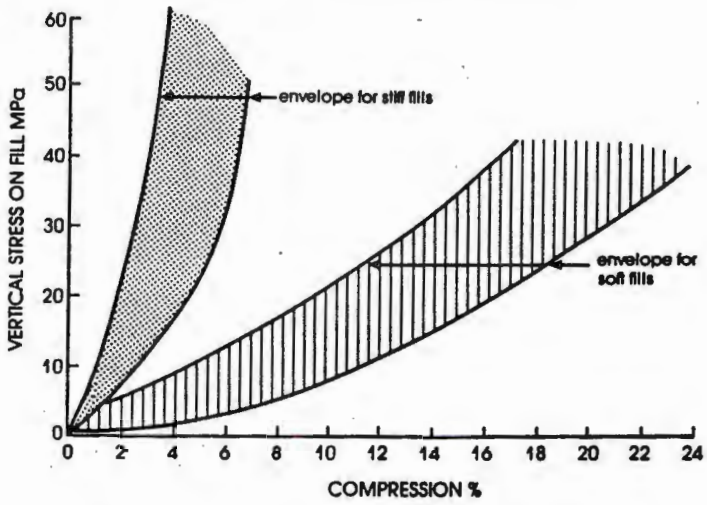

Figure 13: Confined compression tests on stiff and soft fills: stress-compression envelopes

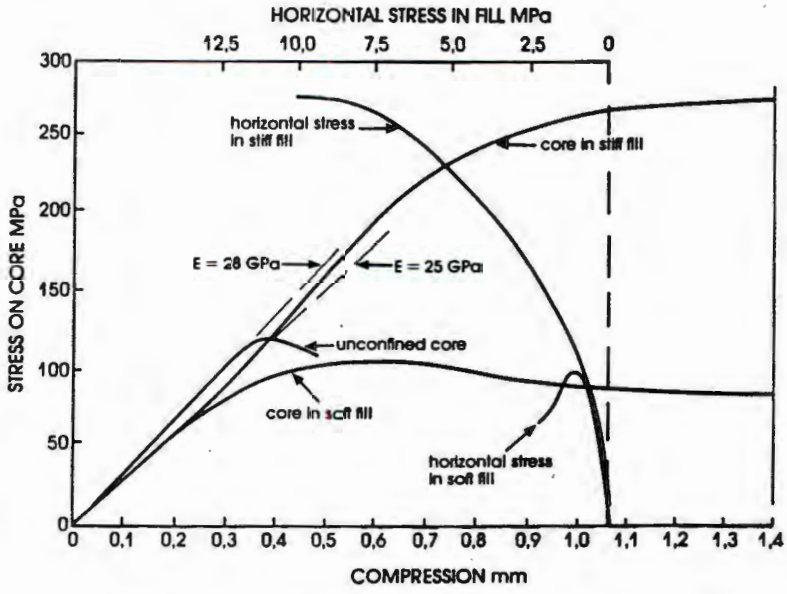

Figure 14: Comparison of stress-compression behaviour of unconfined core with fill-supported cores

about 7 per cent compression. Note in particular the stress range for the figure which is roughly 1000 times larger than that for conventional surface geotechnics.

The extent to which a stiff fill can provide lateral support and strengthening to a rock pillar is illustrated by the results of model tests shown in Figure 14. The ore pillars were represented by drill cores of quartzite conglomerate ore and the cores were embedded in either stiff or conventional soft fill contained in cylindrical steel moulds to provide lateral constraint. The composite core-fill system was loaded by means of a rigid piston that caused fill and model pillar to strain by the same amount. Figure 14 shows that the soft fill provided very little lateral support to the model pillar, as the strengths of the unconfined core and the core supported by the soft fill were almost identical. However, enough lateral support was generated to maintain a post-failure strength in the pillar of 85 per cent of the peak strength.

The presence of the stiff fill considerably augmented the strength of the model pillar. As the figure shows, a peak strength was not reached by the model pillar/stiff fill system even at a compression of 1.75 per cent which is a large strain for a system as rigid as this.

It therefore appears that surrounding a highly stressed pillar with a soft fill will not materially improve the strength of the pillar, but will ensure a high level of residual resistance. A stiff fill, in contrast, can be used considerably to increase the strength of a pillar.

.7 HORIZONTALLY REINFORCED HYDRAULIC FILL MINE SUPPORTS

Apart from providing regional roof or hanging wall support and lateral support to ore pillars, hydraulic fill methods have also been adapted to provide point supports in the form of yielding horizontally reinforced cemented tailings packs in the narrow tabular stopes of South African gold mines.

The concept of such a support is illustrated by Figure 15 [Dison and Blight(1986)]. The porous bag, with the steel mesh mats sewn into it at a pre-determined spacing, is transported underground and positioned in the stope it is intended to support. The sides of the bag are braced with steel mesh shutters and the bag is then pumped full of a carefully designed cemented tailings fill. Excess water drains from the bag and the fill hardens within 24 hours. The support now carries an increasing load as the working face advances away from it and the stope converges.

The pack carries the load in the following manner:

The vertical load on the pack tends to cause a horizontal strain that is resisted by tension in the horizontal reinforcing. If the reinforcing steel has a cross-section of area A_R, a vertical spacing v and a horizontal spacing h, then

$$\sigma_h vh = A_R \sigma_R \qquad [4]$$

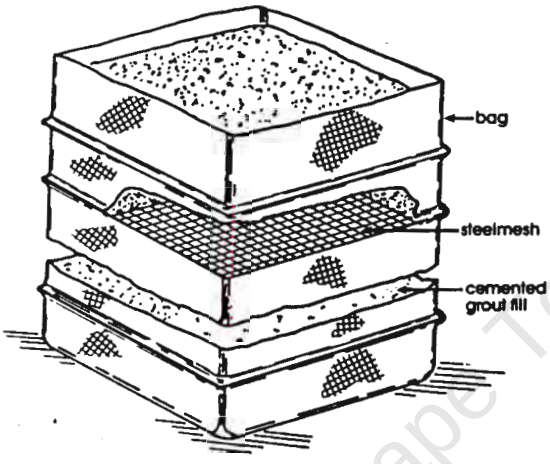

Figure 15: Diagrammatic view of pack assembly

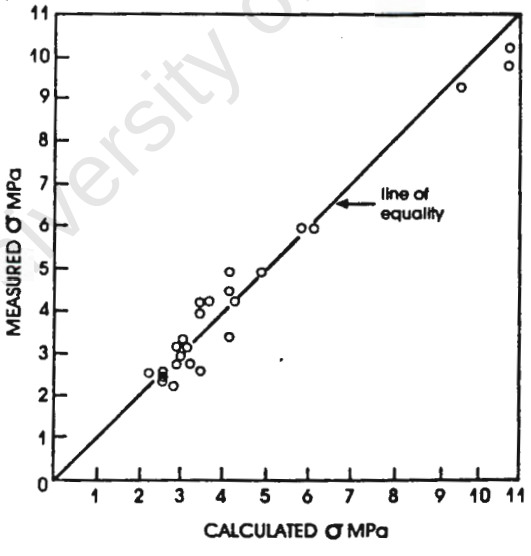

Figure 16: Relationship between calculated and measured strengths of walls built of horizontally reinforced granular material

where σ_h is the horizontal stress in the cemented tailings fill and σ_R is the reinforcing.

Ultimately, the fill fails in shear and the reinforcing yields. Equation[4] then becomes

$$\sigma_h = \frac{A_R \sigma_{yR}}{vh} \qquad [4a]$$

in which σ_{yR} is the yield strength of the reinforcing. σ_v, the vertical stress carried by the pack is then related to σ_h by

$$\sigma_v = \sigma_h \tan^2(45+\phi/2) + 2c \tan(45+\phi/2) \qquad [4b]$$

where 2c is the unconfined compression strength of the cemented fill and ϕ is the angle of shearing resistance. There is a considerable capillary stress component in the strength of the cemented fill and c and ϕ are total stress parameters that incorporate this component of strength.

The validity of equations[4a] and [4b] has been established by means of an exhaustive series of tests using a wide variety of fill materials and types and specimens of steel reinforcing. Figure 16 shows the excellent correlation between measured and calculated strengths for some of these tests.

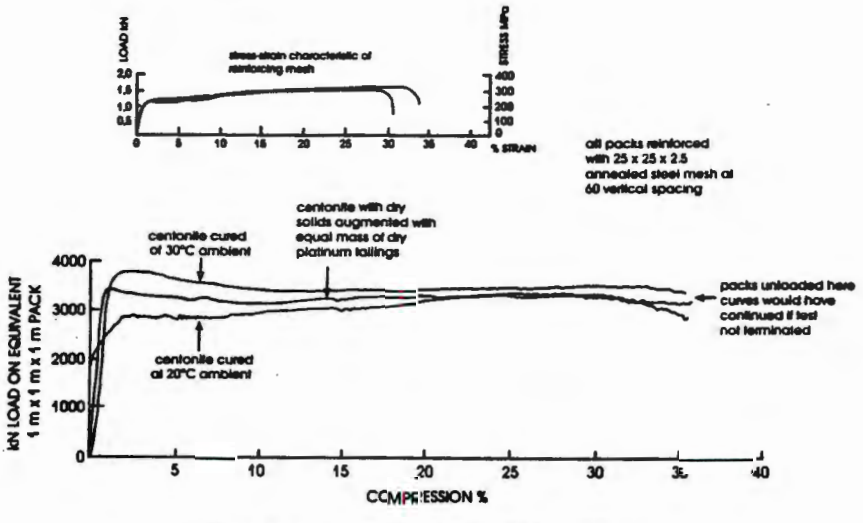

Figure 17: Compression characteristics of 300mm cubes of centonite reinforced with annealed steel mesh

The performance required from yielding supports is that they initially be as stiff as possible, reach a predetermined load at which the reinforcing yields, and then maintain that load over as great a range of compression as possible.

To obtain the long-sustained yield load, the mesh reinforcing is annealed after fabrication. Figure 17 shows typical stress-strain curves for annealed mesh reinforcing and also for three packs reinforced with annealed steel mesh. It will be noted that whereas normal mild steel fails at a strain of about 20 per cent, annealed mild steel fails at strains of up to 50 per cent. The load-compression characteristic illustrated in Figure 17 is nearly ideal. The filling material in this case was a new development known as Hydropak which consists largely of water, bentonite and a quick-setting cement. With this material, strengths of up to 3MPa are attainable 4 hours after casting. The tests illustrated in Figure 17 were made 24 hours after casting.

.8 EFFECTS OF HYDRAULIC FILLING OF UNDERGROUND EXCAVATIONS ON SURFACE STORAGE OF TAILINGS

Many mines engaged in deep level (3 to 4km below surface) gold mining in South Africa are experimenting on a large pilot scale with the use of pumped cycloned tailings fills to provide regional underground support. The cyclone underflow is placed underground and the finer overflow, together with most of the water from the tailings stream must be stored on surface.

The density of solid gold ore is about 2700kg/m^3 and the dry density of deposited cyclone underflow tailings is only 1400kg/m^3. Hence the volume of tailings required to fill a given rock excavation is about half of that actually available, and the remainder must continue to be stored on surface.

A closer analysis of the situation shows that, allowing for space underground that cannot be backfilled for reasons of maintaining permanent access, the residue requiring storage on surface will comprise at least 60 per cent by mass of run of mill tailings and at most 40 per cent of cyclone overflow material.

Hence if large scale, complete underground filling is adopted, the problems of surface storage of residues do not go away. Rather, they become exacerbated by the finer grade of material to be handled and the great proportion of water it will inevitably contain.

A recent investigation [Blight, McPhail and Fourie(1986)] has shown that the geotechnical properties of the surface tailings stream do not change dramatically, but do become less favourable. Shear strength parameters in terms of effective stresses remain almost unchanged. Coefficients of consolidation, however, reduce by a factor of 3, indicating that lower rates of rise for outer impoundments slopes may be necessary.

In the field, beach profiles will flatten, which means that pool areas will enlarge. This in turn may mean higher phreatic surfaces and possibly require flatter outer slopes to achieve the same factor of safety against shear failure.

In the worst analysis, the storing of tailings underground may actually require more, rather than less, surface area to be devoted to tailings storage.

.9 THE EFFECTS OF DESICCATION ON THE SAFETY OF HYDRAULIC FILL STRUCTURES

A previous section (.4) considered the benefits and some of the problems of desiccation of hydraulic fill tailings during deposition. This section will consider the benefits and effects of desiccation on the stability of hydraulic fill structures built in favourable climates - those where there is a seasonal or perennial water deficit.

Hydraulic fill gold tailings impoundments in South Africa are all operated by the semi-dry process whereby a long rotation of deposition is adopted that allows each layer to dry out before the next is deposited over it. Outer impoundment slopes are usually underdrained and the pool is kept to an absolute minimum size. The effect is considerably to depress the phreatic surface in the outer slopes with the result that these dams are remarkably stable.

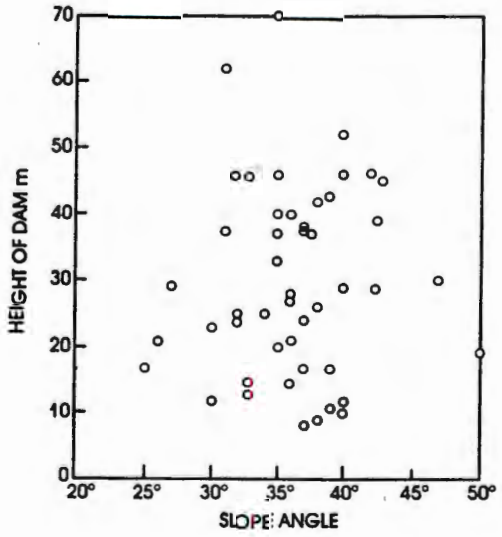

Figure 18: Heights and slope angles of 46 stable gold mine tailings dams

Figure 18 shows a plot of height versus slope angle for 46 stable gold tailings dams in South Africa. The average slope angle is 35° while

heights range up to 70m and some slopes exceed 40° at heights in excess of 40m. What makes these slopes remarkable is that they are constructed of a cohesionless material having an effective stress angle of shearing resistance of between 27° and 35°. Their stability is due almost entirely to the permanent capillary tensions that act within the tailings.

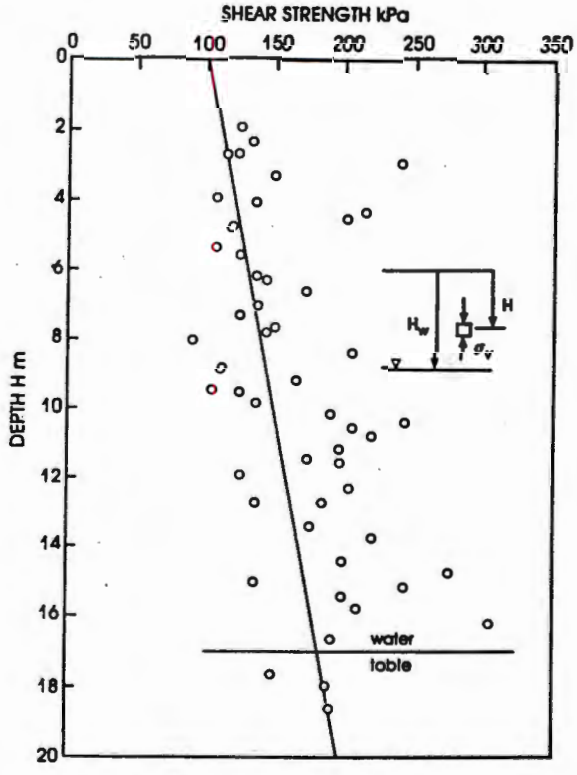

Figure 19: Profile of vane shear strength in a tailings deposit where the water table was 17 m deep

The effect of the capillary stresses on enhancing the strength of a tailings deposit is illustrated by Figure 19 which shows a vane strength profile measured in a hydraulic fill gold tailings deposit in which the phreatic surface was at a depth of 17m. The line of best fit to the measured vane strengths has the equation

$$\tau = [\gamma H + \gamma_w (H_w - H)] \tan \phi' \qquad [5]$$

where H and H_w are as defined in Figure 19 and ϕ' has a value of 29°. This value of ϕ' is well within the range of 27° to 35° mentioned earlier for the angle of shearing resistance of gold tailings. Hence the capillary stresses in the tailings are virtually fully effective in their contribution to effective stresses in the tailings.

.10 SURFACE EROSION OF HYDRAULIC FILL TAILINGS DEPOSITS

Pollution of air and water by particulate matter eroded off the surface of tailings deposits constitutes a serious threat to the environment, and as such must be minimized. The problem is especially severe with ringdyke structures that project above the general level of the countryside. Rates of erosion from the slopes of gold tailings dams of as much as 500T/ha/y (dry tons of tailings per hectare per year) have been published [Blight(1987)]. However, rates as high as 950T/ha/y have since been measured. Under South African conditions where most of the rainfall occurs in summer and winters are dry, erosion by wind appears to constitute about one third of the total loss of solids.

Erosion from the steep slopes of tailings dams appears to be affected by much the same factors as are incorporated in the Universal Soil Loss Equation [e.g. Blight(1987)], principally slope length and slope angle, as well as a measure of surface shear strength. Figure 20, for example, shows a correlation between surface shear strength and erosion loss for gold tailings dams.

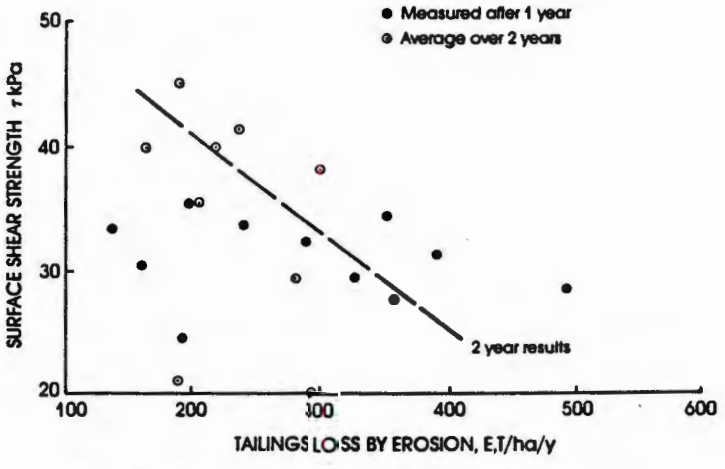

Figure 20: Correlation between surface shear strength and tailings loss by erosion

Experiments have been made to stabilize the top surfaces of tailings dams with cement and lime in order to reduce rates of water and wind erosion [Blight and Caldwell(1984)]. Initially, it was thought that this treatment was unsuccessful as the strength of the stabilized

tailings deteriorated rapidly in the first three years as a result of attack by sulphate and salt crystallization [e.g. Blight(1976)]. However, recent measurements on 9 year old horizontal areas of cement and lime stabilized tailings have shown zero erosion loss over a full year, while an adjacent untreated control area lost 65T/ha/y over the same period.

Pebble mulches consisting of a single particle layer of 10mm or 13mm gravel spread over the surface have also shown some promise as a means of reducing rates of erosion on horizontal or gently sloping surfaces. Two pebble mulched surfaces sloping at 5° lost an average of 70T/ha/y over a full year period. An untreated control area between the two pebble mulched surfaces lost no less than 900T/ha/y over the same period.

The outer slopes of most tailings dams in South Africa are too steep to allow of access by mechanical plant and hence cannot be treated by, for example, cement stabilization. They are also too steep to retain a pebble mulch. The only alternatives at present are to leave the slopes untreated and catch the eroded material at the foot of the slope, or to cover them with vegetation - this may be the obvious course in humid climates, but is not easy in arid areas.

Measurements of rates of erosion from grassed slopes indicate that losses may be just as high as from untreated slopes. However, this preliminary conclusion needs confirmation.

3. CONCLUDING REMARKS

It is hoped that the material presented in this paper has proved of interest to the reader. As stated earlier, the object was to bring to attention some of the less familiar aspects of hydraulic fill structures. All of the aspects described above are of importance although not of general importance. If the readers' perspective of hydraulic fill structures has been widened, the object of the paper will have been achieved.

4. REFERENCES

Abadjiev, C.B., "Estimation of the physical characteristics of deposited tailings in the tailings dam of non-ferrous metallurgy", Proceedings, 11th International Conference on Soil Mechanics and Foundation Engineering, San Francisco, 1985, vol 3, pp 1231-1234.

Berti, G., Villa, F., Dovera, O., Genevois, R and Brauns, J., "The disaster of Stava/Northern Italy", ASCE Geotechnical Division Specialty Conference on Hydraulic Fill Structures, Fort Collins, Colorado, USA, 1988.

Blight, G.E., "Properties of pumped tailings fill", Journal of the South African Institute of Mining and Metallurgy, vol 79, no 10, 1979, pp 446-453.

Blight, G.E., "Partial saturation can assist the soil engineer", Proceedings, 6th South East Asian Conference on Soil Engineering, Taipeh, Taiwan, 1980, vol 1, pp 15-29.

Blight, G.E., "The concept of the master profile for tailings dam beaches", Prediction and Performance in Geotechnical Engineering, Balkema, 1987, pp 361-368.

Blight, G.E., "Erosion of the slopes of gold tailings dams", Geotechnical Practice for Waste Disposal '87, ASCE Geotechnical Special Publication No 13, 1987, pp 294-305.

Blight, G.E. and Bentel, G.M., "The behaviour of mine tailings during hydraulic deposition", Journal of the South African Institute of Mining and Metallurgy, vol 83, no 4, 1983, pp 73-86.

Blight, G.E. and Caldwell, J.A., "The abatement of pollution from abandoned gold-residue dams", Journal of the South African Institute of Mining and Metallurgy, vol 84, no 1, 1984, pp 1-9.

Blight, G.E. and Clarke, I.E., "Design and properties of stiff fill for lateral support of pillars", Proceedings, International Symposium on Mining with Backfill, Lulea, Sweden, 1983, pp 303-307.

Blight, G.E., McPhail, G.I. and Fourie, J., "Possible difficulties with building tailings dams of cyclone overflow product", Association f Mine Managers of South Africa, Symposium on Backfill, 1986, 14pp.

Blight, G.E., Robinson, M.J. and Diering, J.A.C., "The flow of tailings slurry from a breached dam", Journal of the South African Institute of Mining and Metallurgy, vol 81, no 1, 1981, pp 1-8.

Blight, G.E., and Steffen, O.K.H., "Geotechnics of gold mining waste disposal", Current geotechnical Practice in Mine Waste Disposal, ASCE, 1979, pp 1-52.

Blight, G.E., Thomson, R.R. and Vorster, K., "Profiles of hydraulic fill beaches and seepage through hydraulically sorted tailings", Journal of the South African Institute of Mining and Metallurgy, vol 85, no 5, 1985, pp 157-161.

Canada Centre for Mineral and Energy Technology, "Pit and Slope Manual, Chapter 9, Waste Embankments", Canmet Report 77-01, 1977.

Chamber of Mines of South Africa, "Handbook of guidelines for environmental protection", vol 1/1979, revised 1983, "The design, operation and closure of metalliferous and coal residue deposits", The Chamber, 1983.

Commonwealth of Australia, Department of Home Affairs and Environment, "Code of practice on the management of radioacative wastes from the mining and milling of radioactive ores", Australian Government Publishing Service, Canberra, 1982.

Dison, L. and Blight, G.E., "Reinforced cemented tailings fill", Proceedings, Association of Mine Managers of South Africa Symposium on Backfill, Johannesburg, South Africa, 1986, 13pp.

Fourie, A.B., "A laboratory study of the beaching and consolidation characteristics of two hydraulically placed soils", ASCE Geotechnical Division Speciality Conference on Hydraulic Fill Structures, Fort Collins, Colorado, USA, 1988.

Graf, W.H., "Hydraulics of sediment transport", McGraw-Hill, New York, 1971, pp 455-461.

International Commission on Large Dams, "Manual on tailings dams and dumps", ICOLD Bulletin 45, 1982.

Hahn, J.A., Blight, G.E. and Dison, L., "Support in shallow mines using horizontally reinforced systems", Journal of the South African Institute of Mining and Metallurgy, vol 82, no 10, 1982, pp 277-290.

Hutchinson, J.N. and Bhandari, R.I., "Undrained loading: A fundamental mechanism of mudflows and other mass movements", Geotechnique, vol 21, no 4, 1971, pp 353-358.

Jennings, J.E., "The failure of a slimes dam at Bafokeng", The Civil Engineer in South Africa, vol 21, no 6, 1979, pp 135-141.

Jeyapalan, J.K., Duncan, J.M. and Seed, H.B., "Analysis of flow failures of mines tailings dams", Journal of Geotechnical Engineering, ASCE, vol 109, no 2, 1983, pp 150-171.

Jeyapalan, J.K., "Analysis of flow failures of mine tailings impoundments", PhD Thesis, University of California, Berkley, 1980.

Lucia, P.C, Duncan, J.M. and Seed, H.B., "Summary of research on case histories of flow failures of mine tailings", Mine Waste Disposal Technology, U.S. Bureau of Mines Information Circular IC8857/1987, pp 46-53.

Marcuson, W.F., Ballard, R.F. and Ledbetter, R.H.G., "Liquefaction failure of tailings dams resulting from the new Izu Oshima earthquake, 14 and 15 February, 1978", Proceedings, 6th Pan American Conference on Soil Mechanics and Foundation Engineering, Lima, Peru, 1979.

Melent'ev, V.A., Kolpashnikov, N.P. and Volnin, B.A., "Hydraulic fill structures", Energy (Moscow) 1973. (English translation of original Russian).

Morgenstern, N.R., "Submarine slumping and initiation of turbidity currents", Marine Geotechnique, A.R. Richards, ed., University of Illinois Press, Urbana, Illinois, 1967, pp 189-220.

National Coal Board (UK), "Spoil heaps and lagoons", 1970.

Smith, G.M., Abt, S.R. and Nelson, J.D., "Profile prediction of hydraulically deposited tailings", Transactions, Society of Mining Engineers of AIME, vol 80, 1987, pp 2024-2027.

Verkerk, C.G., "The hydraulic transportation of gold mine waste", Proceedings, International Conference on Mining and Industrial Waste Management, Johannesburg, South Africa, 1987, pp 139-145.

Wates, J.A., Stevenson, C. and Purchase, A.R., "The effect of relative densities on beaching angles and segregation on gold and uranium tailings", Proceedings, International Conference on Mining and Industrial Waste Management, Johannesburg, South Africa, 1987, pp 89-93.

Whitney, E.D., Moudgil, B.M. and Onoda, G.Y., "Dewatering of phosphate clay wastes", Department of Material Science and Engineering, University of Florida, 1977.

PROCEEDINGS OF THE TWELFTH INTERNATIONAL CONFERENCE ON SOIL MECHANICS AND FOUNDATION ENGINEERING

RIO DE JANEIRO / 13-18 AUGUST 1989

EDITOR: PUBLICATIONS COMMITTEE OF XII ICSMFE

TECHNICAL PAPERS
EXPOSES TECHNIQUES

COMPTES RENDUS DU DOUZIEME CONGRES INTERNATIONAL DE MECANIQUE DES SOLS ET DES TRAVAUX DE FONDATIONS

RIO DE JANEIRO / 13-18 AOUT 1989

EDITEUR: COMITE DES PUBLICATIONS DU XII CIMSTF

A.A.BALKEMA / ROTTERDAM / BROOKFIELD / 1989

Geotechnical engineering in mining

G.E.Blight
University of the Witwatersrand, Johannesburg.

SYNOPSIS: The object of this paper is to review the field of application of geotechnical engineering in mining, and to give some examples of the type of projects in which geotechnical engineers may become engaged.

After a brief review of current applications the following developments are described in more detail:

- Design and measured pressures in coal storage silos.
- The design of box fronts to underground ore passes.
- Catenary membranes for crossing ground subject to mining subsidence, and
- Rapid deterioration of a reinforced soil supporting a mill structure.

1 INTRODUCTION - A BRIEF REVIEW OF GEOTECHNICS IN MINING

The title of this paper, "Geotechnical Engineering in Mining", could potentially embrace an astonishingly wide range of topics especially if the definition of geotechnical engineering is widened to include the rock mechanics of cut slopes and underground excavations. For the present purpose, geotechnical engineering will be defined as engineering applied to the behaviour and properties of soil, soil-like and other particulate materials. Even with this narrowed definition, the field of geotechnical engineering in mining is potentially vast:

1.1 There is the geotechnical engineering associated with the establishment of the infrastructure for a new mine, or extensions to an existing mine. This includes the design and construction of:

- access roads and service roads within the mine area;
- terraces and platforms for plant;
- water supply dams;
- earthworks for water purification and sewage works;
- foundations for plant and buildings associated with these works;
- foundations for the houses for the staff of the mine (e.g. Jennings and Kerrich, 1962);
- sanitary landfills to dispose of the community's domestic refuse (e.g. Ball, Vorster and Blight, 1987).

1.2 Then there is the geotechnical engineering associated with the surface installations of the mine. This could include the design and construction of:

- heavy foundations for shaft head-gears, winders, crushers, ball and rod mills and similar items of heavy plant;
- approach cuts to inclined shafts;
- haul roads for ultra-heavy mine haulers and dump trucks
- storage structures for crushed or milled materials such as bins, silos and stock piles (e.g. Blight, 1988);
- foundations for thickeners and tanks of various types;
- support structures for gravity feed mill complexes (e.g.Blight and Dane, 1988), etc.

With the exception of the design of storage structures, the geotechnics involved with the above items is of a fairly conventional and recognized civil engineering nature. The topics that follow are of a somewhat more unusual type:

1.3 Still dealing with surface geotechnics, a growing section of geotechnical practice is concerned with what is generally termed the "disposal" of mine waste. Mine waste may comprise a wide range of materials, from coarse broken rock (e.g. Blight, 1969), through sandy and silty mill tailings (see various publications of the American Society of Civil Engineers, e.g. 1979, 1988) to fine muds and clays (e.g. Carrier 1982, Glenister and Cooling, 1984).

The mine waste disposal field is fraught with technical and operational difficulties and several disasters involving the failure of mine waste storage structures are on record (e.g. Jeyapalan, Duncan and Seed 1983, Jennings 1979, Marcuson et al 1979, Berti et al, 1988). As a result, the design and construction of these containments is now strictly codified in several countries (e.g. Canmet in Canada 1977, National Coal Board in United Kingdom 1970, Chamber of Mines in South Africa 1979, and Department of Home Affairs and Environment in Australia, 1982).

There is a world-wide trend towards tightened environmental control over mining operations.

This has resulted in geotechnical engineers becoming involved in rehabilitation, reclamation and other "clean-up" operations (e.g. Blight and Caldwell 1982, Blight 1988, Barth et al, 1989) including those under the current U.S. Uranium Mill Tailings Remedial Action (UMTRA) programme (e.g. Larson and Keshion, 1988).

1.4 Geotechnical engineering in underground mining is a relatively new and underdeveloped field that will offer many opportunities to the geotechnical engineer in future. The area in which there is the greatest activity at present is that of underground filling and the provision of underground support.

The backfilling of mining excavations to achieve various objectives has long been practised in the mining industry. Recently, there has been an intensification of research into the use of fill in underground mining (e.g. Blight et al 1977, Mitchell 1983, Blight 1979a). Waste or tailings, placed as an underground fill:

- provides support to the excavation and makes the mining operation safer by preventing bed separation and block fall-out (e.g. Hahn, Blight and Dison, 1982).
- reduces the convergence of excavations, thus reducing the release of gravitational potential energy from the superincumbent strata and reducing the incidence of rockbursts (explosive failures) (Blight, 1979b);
- can be used to provide access for mining wide or high orebodies (e.g. Knutsson, 1980).
- provides lateral support to rock pillars thus enhancing their load-carrying capacities (e.g. Blight and Clarke, 1983).
- reduces the fire hazard associated with using conventional timber supports underground;
- can be used to direct and channel ventilation air, thus reducing air losses and heat gained by the air from the country rock (also replacing the flammable materials conventionally used for ventilation curtains and ducting); and
- reduces surface subsidence in the case of shallow mining, and stabilizes the surface in the case of long-abandoned shallow workings.

In addition, tailings fill can be used to build underground structures such as flood-control plugs and shaft pillar replacements (Blight, 1988a). It was originally considered that the stowing of large quantities of tailings underground would reduce pressures on the surface environment by

- releasing area at the surface for more productive use than the storing of tailings, and
- reducing problems of air, water and visual pollution.

However, a recent more careful investigation (Blight, McPhail and Fourie, 1986) has shown that environmental problems on the surface are likely to increase, rather than decrease as the practice of underground filling expands. This is because the material that remains to be stored on surface is geotechnically less suitable for surface storage.

After this brief overview, the remainder of the paper will be devoted to describing in more detail four topics illustrating rather unusual applications of geotechnical principles in mining. These will be:

- a comparison of design and measured pressures in large coal storage silos,
- the design of "box fronts" to underground ore passes,
- the use of catenary membranes as a safety feature for roads crossing ground undermined at shallow depth, and
- the deterioration of a gravity-flow-process mill support structure.

2 A COMPARISON OF DESIGN AND MEASURED PRESSURES IN COAL STORAGE SILOS.

Storage structures for bulk materials such as bins, bunkers and silos are indispensable to the operation of any mine. The estimation of design pressures for these structures is not usually regarded as part of geotechnical engineering, and has over the past three decades fallen into the hands of mechanical and structural engineers most of whom lack a fundamental understanding of the mechanics of granular media. This has resulted in a proliferation of theories that predict the generation of very large horizontal

Figure 1: The Optimum Colliery load-out silos.

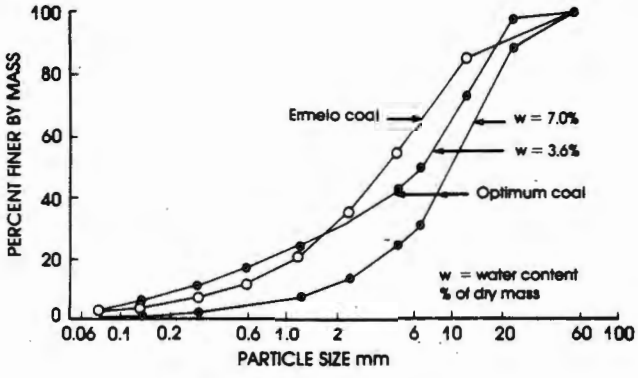

Figure 2: Grain size analysis of coal

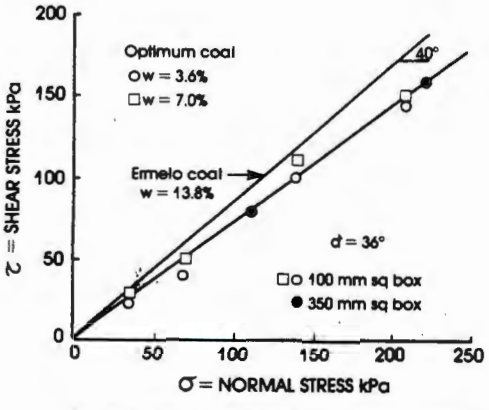

Figure 3: Measurements of angle of wall friction, coal on concrete, at two water contents

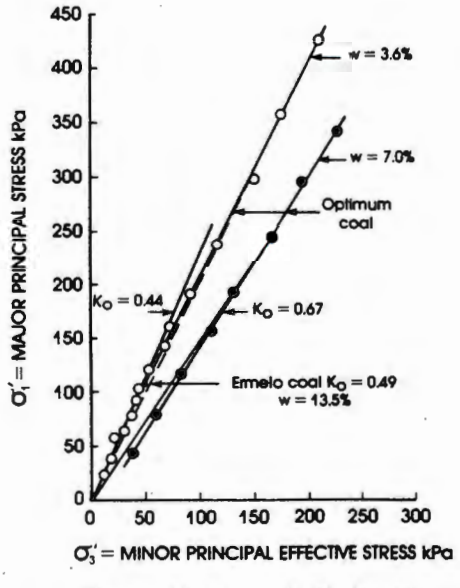

Figure 4: Measurements of Ko in coal at two water contents

"overpressures" or "peak pressures" that may exceed the passive pressure for the corresponding overburden. The most widely used of these theories are due to Jenike, Johanson and Carson (1972) and Walker (1966). Their theoretical predictions have been incorporated into widely used codes of practice for silo loading such as the German DIN 1055 (1964 to 1984), the American Concrete Institute ACI 313 (1975) and the Institution of Engineers, Australia's Guidelines (1986).

Over the past decade the author has had the opportunity of installing instruments in a number of large bunkers, bins and silos in order to measure the pressures actually experienced by the walls of these structures (e.g. Blight 1986). Bins and silos may be very large. For example, the silo at Optimum colliery, shown in Figure 1, has an internal diameter of 20m, stores a height of coal of 54m and has a capacity of nearly 12 000 T of coal.

Figures 2, 3 and 4 summarize the geotechnical properties of the washed, low ash coal which is stored in the two structures that will be dealt with here, those at Optimum and Ermelo Collieries. Figure 2 shows that the coal is predominantly of gravel particle size. The grading varies somewhat from mine to mine and with time at a given mine, but is governed within the limits of the purchaser's specification. Figure 3 shows the angle of wall friction, coal on concrete, established by means of special shear box tests. The coal is a highly frictional material and water content has relatively little effect on wall friction. The data shown in the figure relates to a condition of motion of the coal across a concrete surface. The static angle of friction is 2° to 3° less than the dynamic angle. Figure 4 shows the relationship between major and minor principal stresses under K_o conditions in triaxial compression tests on coal. Water content clearly does have some effect and the value of K_o which may vary from about 0.4 to 0.7.

Pressures on the walls of the silos were measured by means of conventional mercury-filled strain-gauged diaphragm earth pressure cells (Blight and Bentel, 1988). A set of measured pressure profiles for the Optimum silo is shown in Figure 5. The measurements were made on three separate occasions during which the silo was filled from empty without interruption and then emptied. The measurements are compared with a pressure profile corresponding to the relationship

$$\sigma_h = K_A \gamma z \qquad (1)$$

in which σ_h is the horizontal pressure, K_A the active pressure coefficient and γz the coal overburden pressure.

A comparison is also given with the design horizontal pressure envelope according to the ACI loading code. It will be seen that the measured pressures are only about one third of those predicted by the loading code. An examination of code predictions and pressures measured in eight full-scale silos (Blight 1988b) has shown that this overestimation by silo

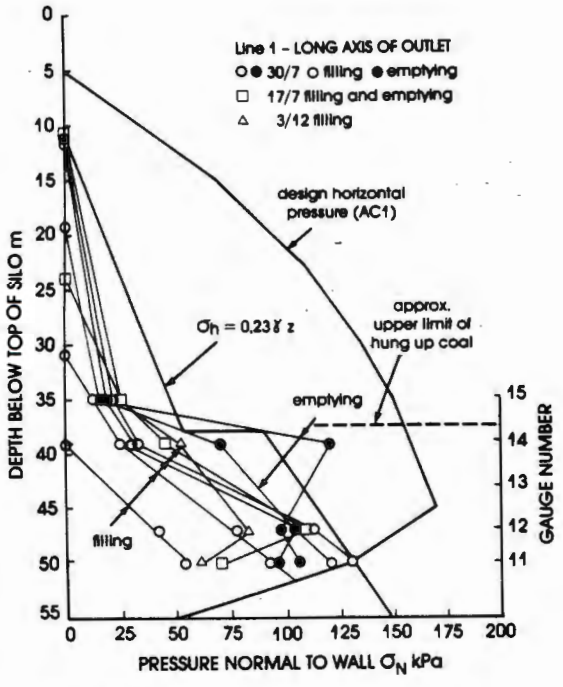

Figure 5: Pressures observed on long axis of slot outlet

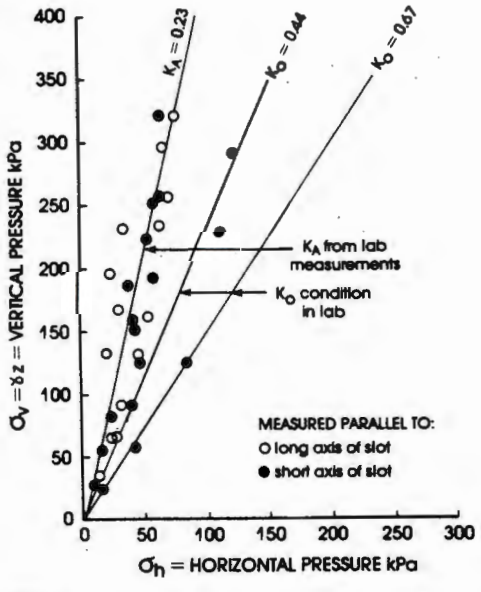

Figure 6: Relationship between measured horizontal stress and calculated vertical stress during filling

loading codes is by no means unusual. The commonly used silo loading codes (the German DIN 1055 and American ACI 313) may be conservative to the point of being ridiculous.

Figures 6 and 7 show observed relationships between horizontal pressure and vertical overburden for the Optimum and Ermelo load-out silos. The Ermelo silo has the same diameter as that at Optimum, but only half the storage capacity. It will be noted that in both cases, the horizontal pressure corresponds, on average, to the active condition. The upper limit to measured pressures in each case corresponds to the K_o condition. This is easily understandable: the coal pours into the silos off an overhead conveyor. It forms a central cone in the silo, slides down the cone and comes to rest in an active state. Coal deposited at a particular level is then consolidated under an increasing overburden. The silo walls prevent lateral strain, and hence the stress-state tends to move from the active (K_A) towards the at rest (K_o) condition. There is a small increase in horizontal pressure at the start of emptying of the silo, but the upper (K_o) limit to the pressure is not exceeded. Note that there is no evidence of any soil arching within either silo. However, this is not very surprising as the height to diameter ratio is only about 2 at the most.

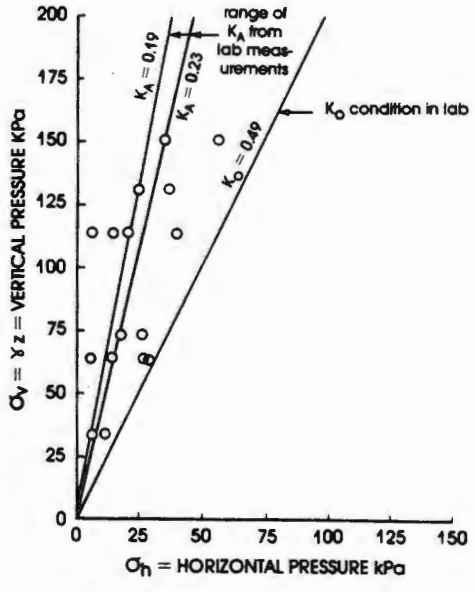

Figure 7: Ermelo mines silo: relationship between measured horizontal stress and calculated vertical stress during filling

The conclusion that may be drawn is that horizontal pressures within a silo subjected to concentric filling, and emptied through a central outlet will not exceed values given by

$$\sigma_h = K_o \gamma z \qquad (2)$$

This conclusion does not hold, however, if the silo is emptied via an eccentric outlet (e.g. Jenike, 1967).

The above conclusion has been shown to apply generally to silos storing coarse materials (e.g. ores and grain). It appears that soil arching occurs to a greater extent in silos storing fine powders (Blight 1988b), even at height to diameter ratios as low as 2.

3 THE DESIGN OF BOX FRONTS TO UNDERGROUND ORE PASSES

An underground ore pass consists of a vertical or steeply inclined shaft that connects one level of a mine with another. Ore mined at the higher level is loaded into the ore pass and gravitates to the lower level. Here it is extracted from the ore pass, usually by means of a belt conveyor, and conveyed to a shaft which is used to haul the material to the surface for processing. There may be a primary crushing process before hauling the ore to the surface.

Ore passes are usually maintained full, or nearly full of ore to limit the impact of lumps of rock falling through a great height. Hence they operate like underground, rock-walled silos. The box front is located at the lower end of the ore pass and serves as a transition between the ore pass and the conveyor belt.

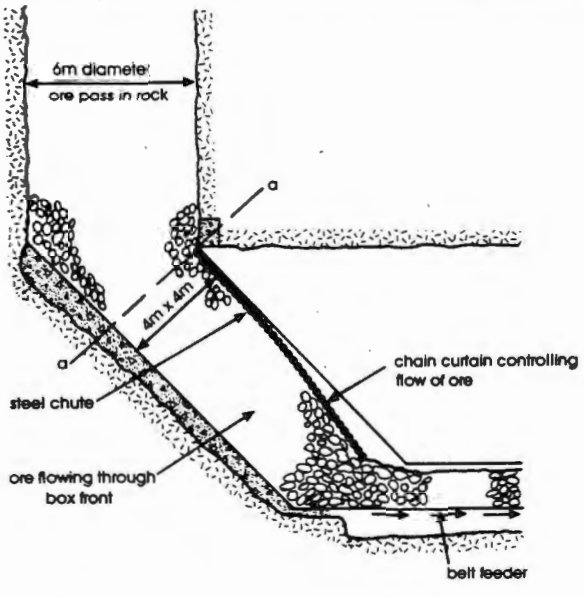

Figure 8: Principle of "box front" controlling flow of ore from ore pass on to belt feeder

Figure 8 shows the features of a box front diagrammatically. Flow of ore from the ore pass is controlled by the chain curtain. The weight of the curtain is such that if it is lifted, ore will flow out of the ore pass. If the curtain is dropped, the flow is choked off.

Ore passes have always been designed by rule of thumb. If the chain curtain did not prove heavy enough, extra weight was added until control of the flow of ore was achieved. However, because explosive rock-breaking is not as energy-efficient as crushing, the current tendency is to fragment the ore less by explosive and to crush the resulting larger blocks of ore underground before hoisting it to the surface. This has resulted in a need for larger ore passes and hence larger box fronts and wider conveyors. The industry now perceives a need for a rational method of designing box fronts so that the flow of the ore will be correctly controlled and the dimensions of the feeding chute will also be adequate.

The first component of the design is to calculate the tension generated in the chain curtain as the ore flows under it. The chain tension turns out to be given by a very simple expression

If w is the weight per unit length of chain and δ_c is the angle of friction between the chain and the ore surface, the chain tension

T = w x (vertical projected length of chain)
+ $\tan\delta_c$ x (horizontal projected length of chain)

This applies regardless of the shape adopted by the chain.

The second component of the design is to calculate the profile of the chain and the required depth of chute to contain the ore without spillage as it flows out of the ore pass.

The procedure is as follows:

.1 The pressure of the ore at the exit from the ore pass is calculated. As the height to diameter ratio of an ore pass may be 10 or more, the pressure is calculated as the asymptotic pressure according to the conventional soil arching theory, namely:

$$\sigma_v = \frac{\gamma D}{4K\tan\delta} \qquad (3)$$

where σ_v is the vertical pressure in the ore, D is the ore pass diameter, K is the lateral pressure ratio (taken as K_A to get a maximum value for σ_v) and δ is the angle of wall friction, ore on rock.

.2 The normal presssure across the entry to the chute (line aa in Figure 8) is assessed.

.3 Referring to the forces indicated in Figure 9, the forces resisting flow, which result from friction with the chain (τ_c), walls (τ_w) and base (τ_b) of the first horizontal metre of chute, are assessed. Hence the residual thrust at the start of the second horizontal metre of chute is calculated.

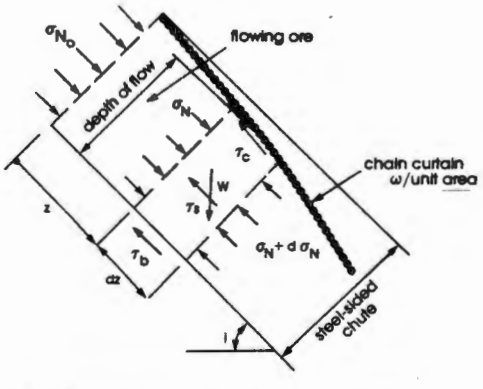

Figure 9: Principle of calculating chain profile

.4 The depth of ore necessary to provide this thrust is calculated next, allowing for the surcharge weight of the chain. If this exceeds the physical depth of the chute, the chain surcharge must be increased, or the chute must be roofed to limit the depth. If the calculated ore depth is less than the physical depth of the chute, the depth of the chute is adequate.

.5 The procedure is repeated stepwise until the calculated unbalanced thrust becomes zero. Beyond this point, the chain curtain is no longer necessary. The calculated heights of ore give the profile the chain will assume.

The procedure has been applied to the design of a box front to a new 6m diameter ore pass in a diamond mine which is intended to handle material with a maximum lump size of 1m. The chute will measure 4m wide by 4m deep. Figure 10 summarizes the calculated dimensions of the flowing broken ore. The first two horizontal metres of chute will be roofed, with a chain curtain weighing 5kN/m² hanging inside it. The calculated profile of the chain is also shown in Figure 10.

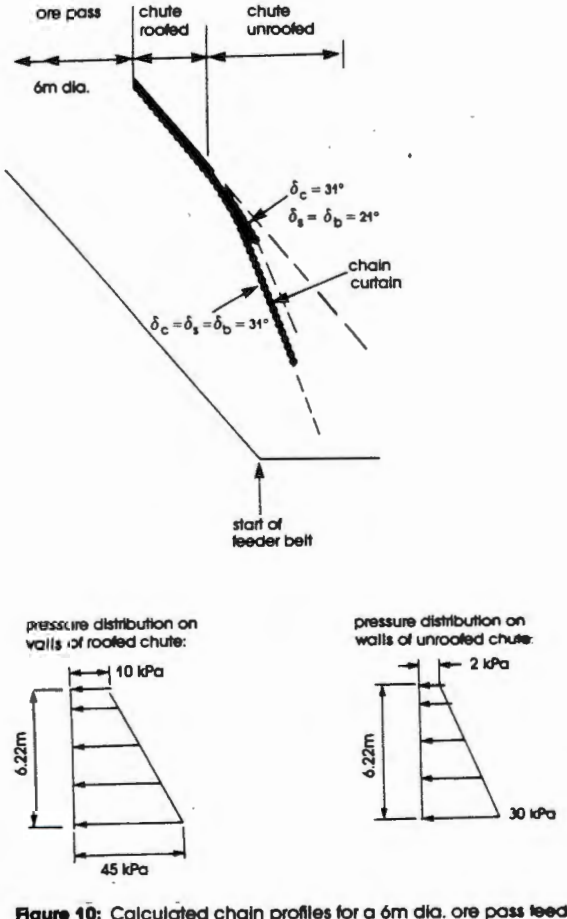

Figure 10: Calculated chain profiles for a 6m dia. ore pass feeding a chain curtained box front

The tension in the chain turns out to be quite small and its effect in limiting flow of the ore is also fairly small, the major effect coming from friction between the ore and the sides of the chute. In order to achieve the length of transition and chain profile shown in Figure 10, it will be necessary to provide the chute with transverse ribs to increase the effective angle of wall friction to that of ore on ore rather than ore on steel.

The box front is being constructed at the time of writing and will be strain-gauged in situ to check the estimated pressures on the walls of the chute. It will then also be possible to check the profile assumed by the chain curtain (for which each link will weigh 250kg).

4 CATENARY MEMBRANES TO PROVIDE SAFETY FOR ROADS CROSSING GROUND UNDERMINED AT SHALLOW DEPTH

There are many areas in the world where mining, especially for coal, has taken place at depths as shallow as 10m to 15m or less below surface. The areas may be extensive, or may only constitute a relatively narrow band along the outcrop of a reef. Both conditions exist in the Witwatersrand area of South Africa where rich coal deposits overly even richer deposits of gold. In the central Witwatersrand area, mining of the shallow gold and coal took place 80 to 100 years ago. There is now growing pressure to extend urban and industrial development over these shallowly undermined areas.

There are many different ways of stabilizing ground undermined at shallow depth. One method is to fill the voids with mine tailings or pulverized fuel ash, another is to drill into the void, place explosives down the holes and blast out the supporting pillars thus filling the void with bulked broken material. A third method, particularly applicable to the protection of isolated buildings or roads crossing undermined areas, is illustrated in Figure 11. A layer of welded steel mesh is incorporated into the road structure or into a foundation raft for a building. If a sink-hole forms as a result of collapse of a pillar or of progressive collapse of the roof of the old workings, the mesh is designed to act as a catenary safety net, as indicated by Figure 11.

An opportunity has recently arisen to design a road on the catenary net principle. The road crosses an area undermined for coal where several sinkholes and surface subsidences have occurred in recent years. The road is designed to carry 200 equivalent 80kN axle loads per day with an annual growth rate of 8 per cent, giving a total design traffic of 3.2 million equivalent 80kN axle loads over the 20 year design life. The pavement has been designed conventionally and has the section shown in Figure 12. The catenary net is incorporated in the 300mm thick cement stabilized sub-base. The cement stabilization is intended to have the double function of improving the load bearing properties and elastic modulus of the sub-base and protecting the weld-mesh from corrosion. Stabilization will be by means of 5 per cent of ordinary Portland cement which, tests show, will provide a CBR of 100 per cent. Eades tests have

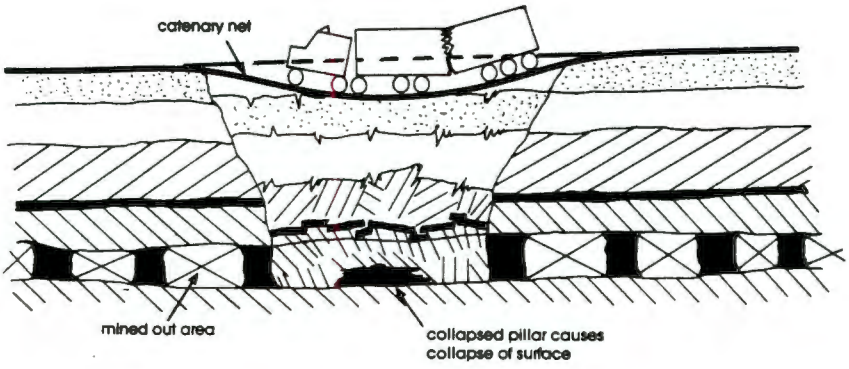

Figure 11: Principle of catenary net to protect traffic on road crossing undermined area

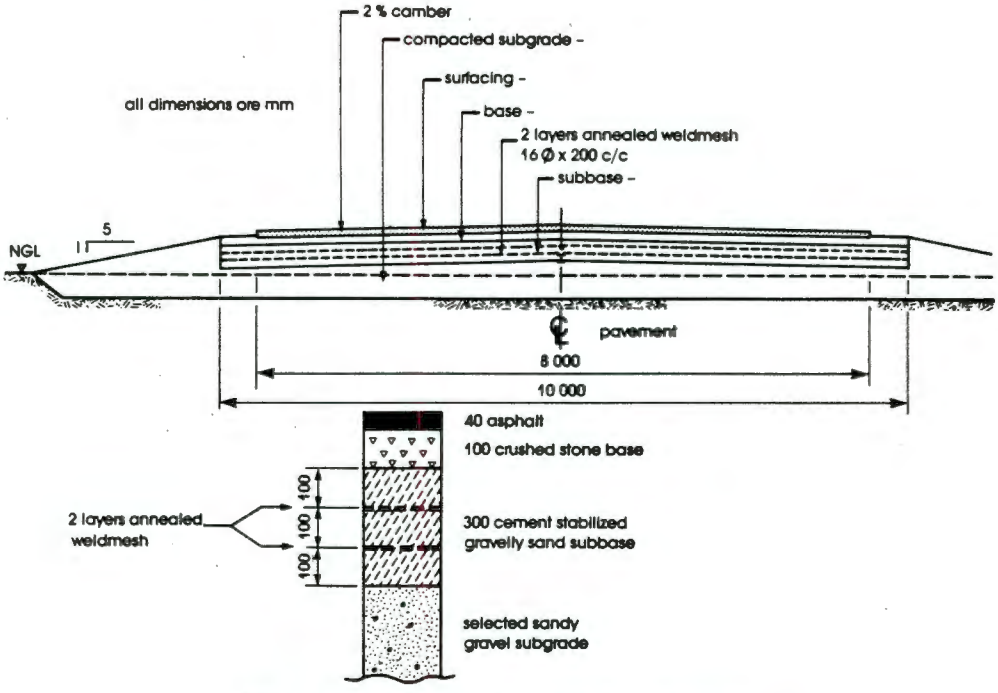

Figure 12: Section through road incorporating catenary net

shown that a 5 per cent cement addition will ensure a pH of 11.7 which is sufficiently high to passivate the steel against corrosion.

The catenary net will consist of a double layer of annealed weld-mesh with individual sheets lap-welded together so as to form an integral continuous net. The bar diameter for the mesh is 16mm and the bar spacing 200mm. The weld mesh is annealed after welding so as to heat-treat the welds and improve the ductility of the mesh. The elongation at failure over a 200mm gauge length before annealing is 15 per cent and failure invariably takes place at a welded node. After annealing, the elongation at failure varies from 35 per cent to 45 per cent with a mean yield stress of 255MPa and an ultimate tensile strength of 315MPa. The failures occur randomly, seldom at a welded node. The average permanent elongation after failure over an original length of 1m is 26 per cent.

Tests on 100mm long lap joints welded from the top only, showed that failure always occurs away from the lap. Hence the lapped welds do not weaken the mesh.

The design of the catenary net caters for the possible formation of a 10m diameter circular void occurring under the roadway. Under this circumstance, the net can carry a superimposed load of 6.6kPa over the entire 10m diameter area at a steel stress of 230MPa. This is equivalent to a total load of 518kN or 50 tons.

If the load is concentrated towards the centre of the collapsed area, the mesh will yield. However, the maximum depth of coal removed in mining is 2½m. The mesh can sag by 3.2m before attaining an average elongation of 26 per cent. Hence if a sinkhole occurs, the load will at worst be gently let down to rest on the bottom of the sinkhole.

A full-scale field trial is currently underway

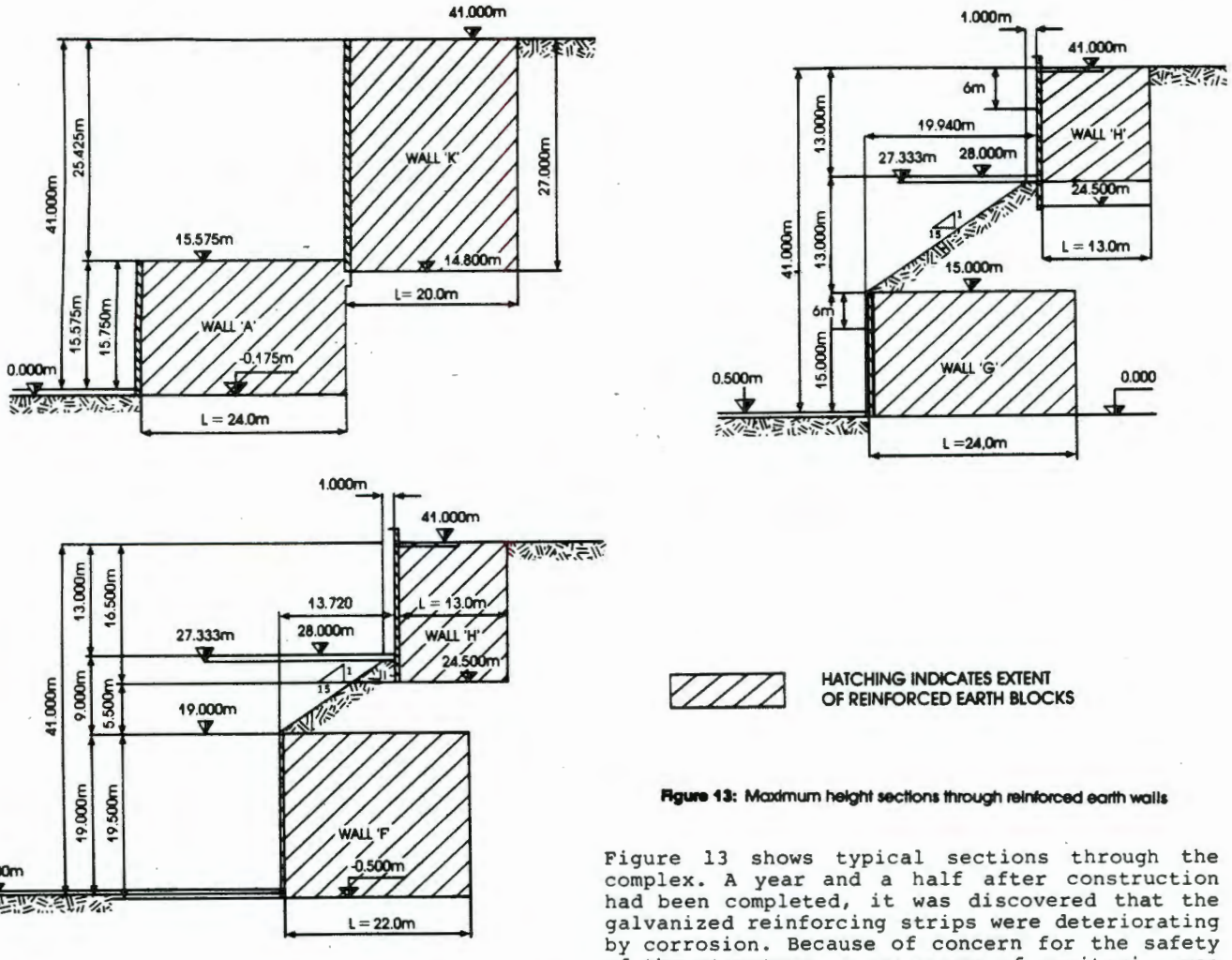

Figure 13: Maximum height sections through reinforced earth walls

to test the catenary net concept, prior to constructing the prototype road.

5 THE DETERIORATION OF A REINFORCED SOIL MILL-SUPPORT STRUCTURE

Engineers are usually concerned with the design of new structures and it is the success or failure of these new designs that is reported in the technical literature. Most structures deteriorate with time, use and exposure to the elements and sooner or later require maintenance and repair, or even complete reconstruction. Far less is published concerning reasons for, and mechanisms of deterioration, even though the lessons learnt from such experience should be incorporated into new designs. The case history that will now follow describes the dramatically rapid deterioration of a structure. The design life was variously claimed by the designers to be 50 years and 30 years but the structure had to be demolished and rebuilt as it had deteriorated beyond the limits of safety after only 8 years. A gravity separation mill at the Tweepad diamond mine on the west coast of South Africa is supported by a complex of reinforced soil walls having a maximum overall height of 41m.

Figure 13 shows typical sections through the complex. A year and a half after construction had been completed, it was discovered that the galvanized reinforcing strips were deteriorating by corrosion. Because of concern for the safety of the structure, a programme of monitoring was embarked on.

The climate of the area is desert with an average annual precipitation of only 90mm and annual evaporation from a free water surface of 1940mm. However, the area is subject to salt-laden sea fogs, and the sparse rainfall deposits some salt with it.

Available backfill materials consisted of sands from ancient raised beach deposits. The specification for the backfill was:

100% finer than	300mm
More than 75% finer than	150mm
Less than 20% finer than	15 microns (0.015mm)

The geotechnical requirements were:

pH	5 to 10
Resistivity greater than	500 ohm cm
Chlorides less than	1500mg/kg
Sulphates less than	800mg/kg

Because of the shortage of fresh water, sea water was used for compaction of the fill.

At the time of design, the fill specification obviously appeared adequate, even though it was dictated to a large extent by expediency and

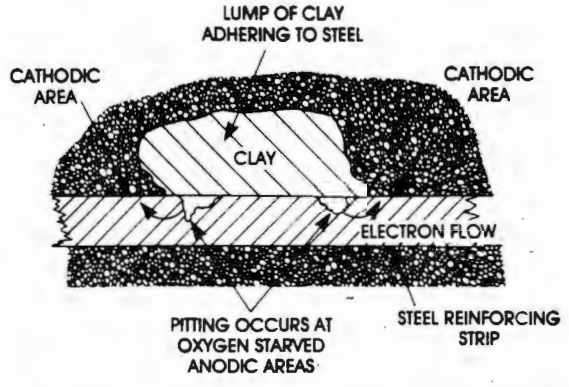

Figure 14: Mechanisms of pitting corrosion of reinforcing strips

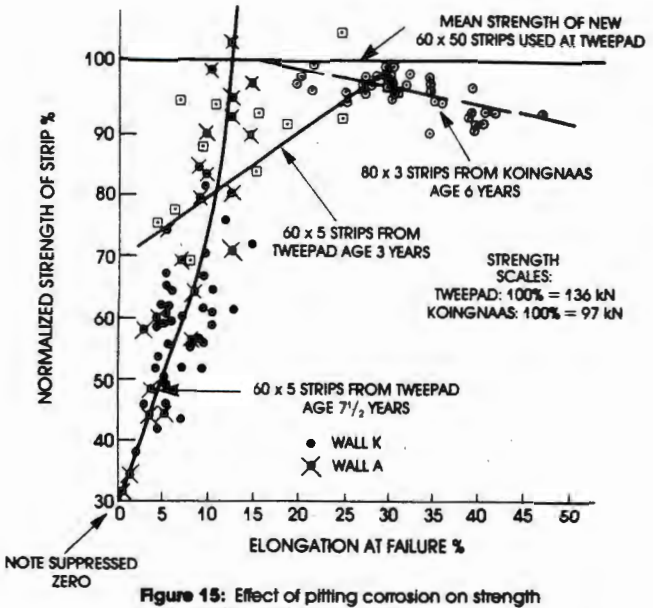

Figure 15: Effect of pitting corrosion on strength and ductility of reinforcing strips

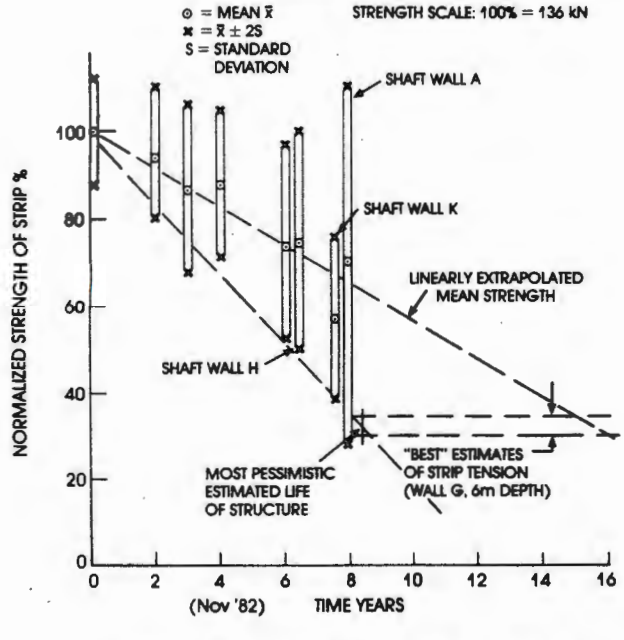

Figure 16: Deterioration of strip strength with time for 60mm x 5mm reinforcing strips

cost considerations.

Early in the corrosion monitoring programme, it became apparent that the fine fraction of the fill occurred as discrete lumps of clay. Wherever a lump of clay rested in contact with a reinforcing strip, severe pitting corrosion had occurred. This was because of the formation of differential aeration cells, as illustrated by Figure 14. The effect of the pitting was not only to reduce the load-bearing cross-section of the reinforcing strips, but also to embrittle them by introducing stress concentrators in the form of the irregularly shaped corrosion pits.

The effect of the corrosion on the strength and ductility of the reinforcing is shown in Figure 15. The reduced ductility and strength was already apparent in the results of tests on the three year old strips. The 7½ year-old strips showed severely reduced strengths and some strips showed a negligible elongation at failure.

For comparison, Figure 15 shows the results of tests on 6 year-old reinforcing strips from a similar reinforced soil mill-support structure at the Koingnaas mine, 60km down the coast. Here, the fill material had been a uniform sized dune sand containing no fines at all. Even though the moisture and chloride contents of the sand were considerably higher than at Tweepad, absolutely no corrosion had occurred and the strips remained very ductile.

Figure 16 summarizes the results of the strength monitoring. It became apparent that the life of the Tweepad structure would be reached at about 8 to 8½ years. Because of the low ductility of the corroded reinforcing strips, no warning of imminent failure, such as that given by an acceleration of the rate of deformation of the structure, could be expected. It was therefore decided to demolish the structure, one half at a time, and to rebuild it in reinforced soil. This was done in such a way that the plant could be kept fully operational during the demolition and rebuilding.

The decision to rebuild the complex in reinforced soil was a brave one, but was again dictated by cost and by the remoteness of the site. The specification for the backfill was, however, tightened considerably. The particle size requirements became:

100% finer than	300mm
More than 75% finer than	150mm
Less than 10% finer than	75 microns
Nothing finer than	2 microns

This eliminated the possibility of clay lumps occurring in the fill. The geochemical specification was also tightened to:

pH	7 to 9
Resistivity greater than	2000 ohm cm
Chlorides less than	200mg/kg
Sulphates less than	200mg/kg

Fresh water was used for compaction, even though it had to be trucked in for the purpose. The rebuilt structure will continue to be monitored lest it too deteriorates.

6 CONCLUDING REMARKS

Existing applications for geotechnical engineering in mining are many and various, as this paper has shown. They range from the completely conventional, to activities that might hardly be considered part of geotechnical engineering. It is hoped that this review will contribute to greater awareness among geotechnical engineers of the potential and excitement of working on mining projects. The demands of mining may frequently take the geotechnical engineer beyond the bounds of current practice and require him to apply his knowledge fundamentally and with innovation.

7 ACKNOWLEDGEMENTS

The subject matter of this paper is published by kind permission of the Anglo American Corporation of South Africa Limited, Gencor Limited and the City Engineer of Springs, Transvaal.

8 REFERENCES

American Concrete Institute, ACI Committee 313 (1975). Proposed ACI Standard, Recommended Practice for the Design and Construction of Concrete Bins, Silos and Bunkers for Storing Granular Materials, Title no 72-37, ACI Journal, 529-548.

American Society of Civil Engineers (1979). Current Geotechnical Practice in Mine Waste Disposal, ASCE, New York, USA.

American Society of Civil Engineers (1988). Hydraulic Fill Structures '88, Geotechnical Division Special Conference, Fort Collins, Colorado, USA.

Ball, J .M., Vorster, K. and Blight, G.E.,(1987) Computer-Assisted Landfill Design Considering Local Climate, Proc. ISWA Symposium on Process, Technology and Environmental Impact of Sanitary Landfill, Cagliari, Sardinia, 2, XLIX1-XLIX-11.

Barth, R.C., Bengson, S.A. and van Zyl, D.J.A. (Eds) (1988). Principles and Practices of Tailings Reclamation, American Society for Surface Mining and Reclamation, Denver, USA.

Berti, G., Villa, F., Dovera, D., Genevois, R. and Brauns, J. (1988). The Disaster of Stava, Northern Italy. Proc. Hydraulic Fill Structures '88, ASCE Geotechnical Division Speciality Conference, Fort Collins, USA 17 pp.

Blight, G.E. (1969). Foundation Failures of Four Rockfill Slopes, Journal of the Soil Mechanics and Foundations Division, ASCE, (95), SM3, 743-767.

Blight, G.E. (1979a). Properties of Pumped Tailings Fill, Journal of the South African Institute of Mining and Metallurgy, (79), 10, 446-453.

Blight, G.E. (1979b). Geotechnics of Gold Mining Waste Disposal, Current Geotechnical Practice in Mine Waste Disposal, ASCE, New York 1-52.

Blight, G.E. (1986). A Comparison of Design and Measured Lateral Pressures in a Large Coal Load-Out Silo, International Journal of Bulk Solids Storage in Silos (2), 2, 1-8.

Blight, G.E. (1987). Erosion of the Slopes of Gold Tailings Dams, Geotechnical Practice for Waste Disposal '87, ASCE Geotechnical Division Special Publication (13), 294-305.

Blight, G.E. (1988a). Soil Mechanics Principles in Underground Mining, Chapter 16 (3), Handbook of Civil Engineering, N.P. and P.N. Cheremisinoff (Eds) Technomic Publishing, New Jersey, USA 54 pp.

Blight, G.E. (1988b). A Comparison of Measured Pressures in Silos with Code Recommendations, Bulk Solids Handling (8), 2, 1-9.

Blight, G.E. and Bentel, G.M. (1988). Measurements on Full Size Silos, Part 2: Pressures, Bulk Solids Handling (8), 2, 4 pp.

Blight, G.E. and Caldwell, J.A. (1984). The Abatement of Pollution from Abandoned Gold-Residue Dams, Journal of the South African Institute of Mining and Metallurgy, (84), 1, 1-9.

Blight, G.E. and Clarke, I.E. (1983). Design and Properties of Stiff Fill for Lateral Support of Pillars, Proc. International Symposium on Mining with Backfill, Lulea, Sweden, 303-307.

Blight, G.E. and Dane, M.S.W. (1988). Deterioration of a Wall Complex Constructed of Reinforced Earth, Geotechnique, in press.

Blight, G.E., McPhail, G.I. and Fourie, J. (1986). Possible Difficulties with Building Tailings Dams of Cyclone Overflow Product, Association of Mine Managers of South Africa, Symposium on Backfill, 14 pp.

Blight, G.E., More O'Ferral, R.C. and Avalle, D.L. (1977). Cemented Tailings Fill for Mining Excavations, Proc. 9th International Conference on Soil Mechanics and Foundation Engineering, Tokyo, (1) 47-54.

Canada Centre for Mineral and Energy Technology (1977). Pit and Slope Manual, Chapter 9, Waste Embankments, Canmet Report 77-01.

Carrier, W.D. (1982). Predicting Consolidation of Phosphatic Clay Waste, Conference on Consolidation and Dewatering of Fine Grained Particles, University of Alabama, Tuscaloosa.

Chamber of Mines of South Africa, (1983). Handbook of Guidelines for Environmental Protection, (1/1979), Revised 1983, The Design, Operation and Closure of Metalliferous and Coal Residue Deposits, Chamber of Mines, South Africa.

Commonwealth of Australia, Department of Home Affairs and Environment (1982). Code of Practice on the Management of Radioactive Wastes from the Mining and Milling of Radioactive Ores, Australian Government Publishing Service, Canberra.

German Standards Institute (1964 to 1984). Design Loadings for Buildings, DIN 1055, Sheet 6 - Silos.

Glenister, D.J. and Cooling, D.J. (1984). Gravity Underdrainage as an Aid to the Consolidation of Red Mud Residue from the Alumina Industry, Proc. 4th Australia New Zealand Conference on Geomechanics, Perth, (1), 198-202.

Hahn, J.A., Blight, G.E. and Dison, L. (1982). Support in Shallow Mines Using Horizontally Reinforced Systems, Journal of the South African Institute of Mining and Metallurgy, (82), 10, 277-290.

Institution of Engineers, Australia (1986). Guidelines for the Assessment of Loads on Bulk Solids Containers, Canberra, Australia.

Jenike, A.W. (1967). Denting of Circular Bins with Eccentric Drawpoints, Journal of the Structural Division, ASCE, (93) ST1, 27-35.

Jenike, A.W., Johansen, J.R. and Carson, J.W. (1972). Bin Loads Part 3: Mass-Flow Bins,

Journal of Engineering for Industry, ASME Paper 72-MH-2, 1-7.
Jennings, J.E. and Kerrich, J.E. (1962). The Heave of Buildings and the Associated Economic Consequences With particular Reference to the Orange Free State Goldfields, Trans. South African Institution of Civil Engineers, (11), 221-248.
Jennings, J.E. (1979). The Failure of a Slimes Dam at Bafokeng, The Civil Engineer in South Africa, (21), 6, 135-141.
Jeyapalan, J.K., Duncan, J.M. and Seed, H.B. (1983). Analysis of Flow Failures of Mine Tailings Dams, Journal of Geotechnical Engineering, ASCE, (109), 2, 150-171.
Knutsson, S. (1980). The Näsliden Project - Stresses in the Hydraulic Backfill from Analytical Calculations and In Situ Measurements, Proc. Conference on Application of Rock Mechanics to Cut-and-Fill Mining, Lulea, Sweden (2) 283-306.
Larson, N.B. and Keshion, B. (1988). Prediction of Strains in Earthern Covers, Proc. Hydraulic Fill Structures,'88, ASCE, Geotechnical Division Specialty Conference, Fort Collins, USA, 24 pp.
Marcuson, W.F., Ballard, R.F. and Ledbetter, R.H.G. (1979). Liquefaction Failure of Tailings Dams Resulting From The New Izu Oshima Earthquake, 14 and 15 February, 1978, Proc. 6th Pan American Conference on Soil Mechanics and Foundation Engineering, Lima, Peru.
Mitchell, R.J. (1983). Chapter 6 of Earth Structures Engineering, Allen & Unwin, Boston, USA.
National Coal Board (UK) (1970). Spoil Heaps and Lagoons.
Walker, D.M. (1966). An Approximate Theory for Pressures and Arching in Hoppers, Chemical Engineering Science, (21) 975-997.

Theme lecture: Tropical processes causing rapid geological change

G. E. Blight

University of the Witwatersrand, P O Wits, 2050, South Africa.

ABSTRACT. Geological conditions and processes in the tropics may differ considerably from those in temperate climates. After briefly considering the nature of tropical soils, the paper describes some of the geological processes, occurring in the tropics, that may result in rapid geological change. These processes may act sufficiently quickly to produce significant change in a lifetime or at the very least, in a few centuries.

INTRODUCTION

The tropics, that span of latitudes around the earth's circumference between the tropic of Cancer in the north (23½°N) and the tropic of Capricorn in the south (23½°S), has a special climate. It is generally warm to hot all year round and the tropics include many of the more humid climatic regions of the world, for example the Amazon and Congo basins and the islands of Indonesia (Figure 1). However, they also include some of the driest areas on earth, for instance, the Atacama and Great Western deserts of the Americas, the Sahara and Kalahari deserts of Africa and the Australian desert.

In considering the formation of soils, we are usually concerned with a geological time span. It is known that the earth's poles have shifted position in the distant geological past. The situation is complicated by the fact that the continents have also drifted (see, for example Stacey, 1970). However, there has been no glaciation of the tropical regions since before the cretaceous era which ended one to two hundred million years ago. Hence it is possible that areas no longer in the tropics at present may have deposits of palaeo-tropical soil.

With the exception of the Persian Gulf, where oil has artificially concentrated population and development, deserts are sparsely populated and underdeveloped. There is therefore less reason for concern with the soils of deserts. This does not say that desert soils do not have their own peculiar geotechnical difficulties. The various problems associated with desert soils such as sabkha have been described by various authors, e.g. Akili and Torrance (1981), Fookes (1978) and Stipho (1984).

Many engineering geologists and geotechnical engineers have been taught, and believe that all geological processes happen imperceptibly over time spans of millions, or at least hundreds of thousands, of years. While this is true of many geological processes, it may be quite untrue of others. If one takes the trouble to measure the rate at which certain natural processes occur, or considers the changes wrought by natural disasters, it becomes apparent that changes of sufficient magnitude to affect the activities of the engineering geologist or geotechnical engineer and hence, by extension, the activities of man may occur within the span of a human lifetime, and certainly may have occurred within recent historical times. An example of such a process is provided by the well-known observation by Charles Darwin that pieces of chalk that as a young man he had observed on the surface of a field, had been transported below the surface by the activity of earthworms when he re-examined the field in his old age.

According to various general references, we currently live in the Quaternary Era, "the last of the eras of geological time; it includes the Pleistocene and Holocene Periods (i.e. the last 1 000 000 years) and is still in progress". This paper will concentrate on some of the processes, operating on tropical soils, that are "still in progress". and particularly those that can and have wrought perceptible changes during the recent history of man. In this context, man himself must be recognised as a significant agent of rapid geological change.

TROPICAL SOILS

Because the processes to be described operate mainly on tropical soils, a deviation will be made to consider the nature and formation of these materials. Soils that are distinctly tropical in nature include saprolites, laterites and desert dune sands.

From FORSTER, A., CULSHAW, M. G., CRIPPS, J. C., LITTLE, J. A. & MOON, C. F. (eds)
1991, *Quaternary Engineering Geology*, Geological Society Engineering Geology Special Publication No 7, pp 459-471

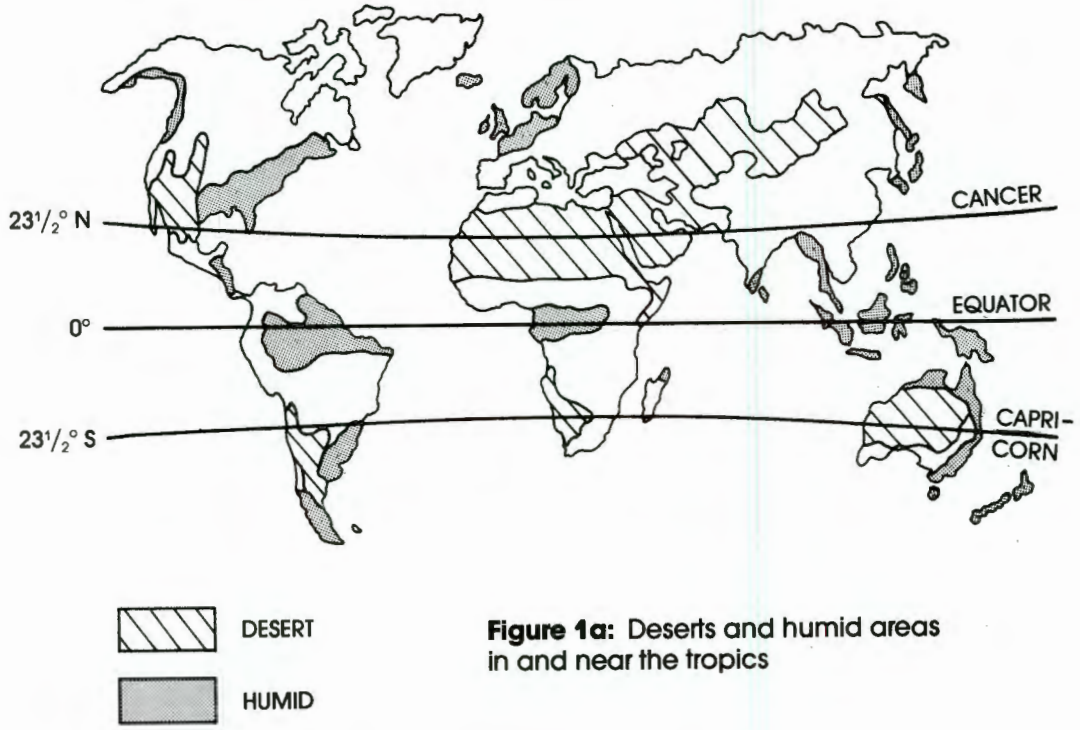

Figure 1a: Deserts and humid areas in and near the tropics

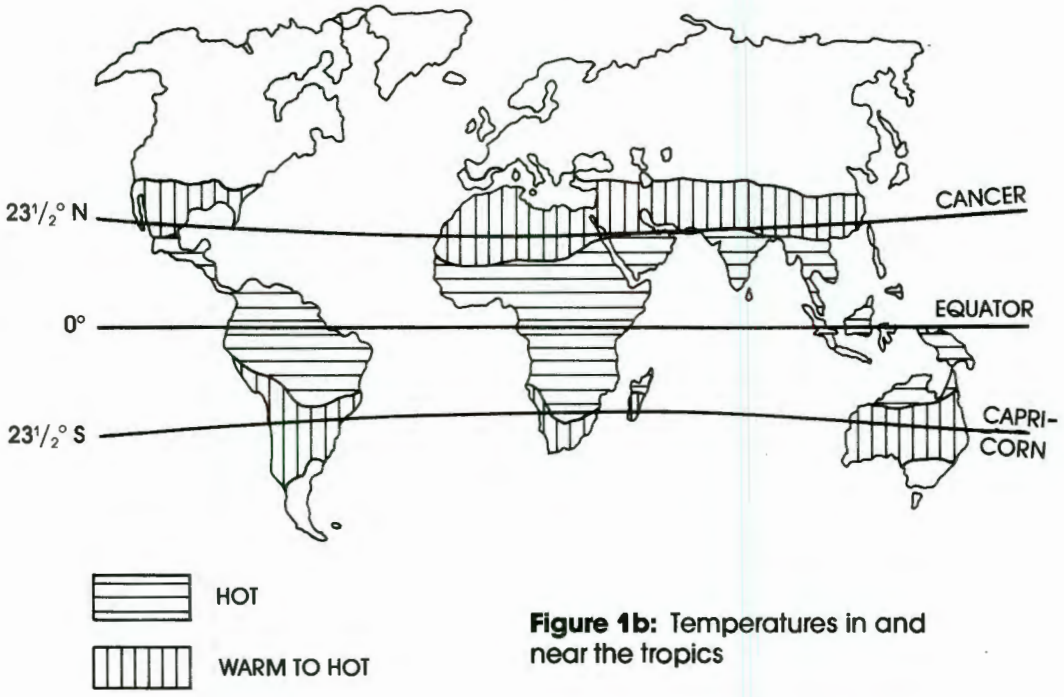

Figure 1b: Temperatures in and near the tropics

Saprolites are materials that have soil-like strength or consistency, but retain modified but recognisable relics of the physical features or fabric of the parent rock. For example a saprolite derived from the weathering of lava may retain the flow structure and amygdales of the parent rock. One derived from a shale may retain the bedding and jointing pattern of its parent rock.

Laterites are usually highly weathered and altered residual soils, low in silica, that contain a sufficient concentration of the sesquioxides of iron and aluminium to have been cemented to some degree. These salts are secondary emplacements resulting from the evaporation of iron- or aluminium-bearing near-surface ground waters. Depending on the extent of the emplacement, the material could be described as lateritic or as laterite. Lateritization usually occurs in residual soils, but ancient transported soils may also have been lateritized. Desai (1985) given definitions of the degree of lateritization in terms of the

silica/alumina ratio SiO_2/Al_2O_3. In terms of this ratio, non lateritic soils have S_iO_2/Al_2O_3 greater than 2. For lateritic soils SiO_2/Al_2O_3 lies between 1.3 and 2 and for true laterites the ratio is less than 1.3.

Figure 2 (adapted from Tuncer and Lohnes (1977) and Sueoka (1988) shows in schematic form the progression from fresh rock through saprolite to laterite. Note that the progression from residual soil to laterite is not inevitable, but depends on conditions being favourable for lateritization. Saprolites may occur in profiles of almost any depth. Because of their mode of formation, laterites usually occur as fairly near-surface strata of limited depth.

and compaction. The permeability of a transported soil can usually be related to its granulometry (e.g. by the well-known Hazen formula). For the reason just explained, this may not be so with tropical soils. The permeability of tropical soils is usually governed by its micro- and macro- fabrics and by superimposed features such as slickensiding, termite or other bio-channels (see, e.g. de Mello et al, 1988). For the above, and other reasons, the design assessment of a tropical residual soil requires far more attention to visually discernable features of the soil profile, selection of in situ and laboratory test methods and particularly to the scale on which such tests are

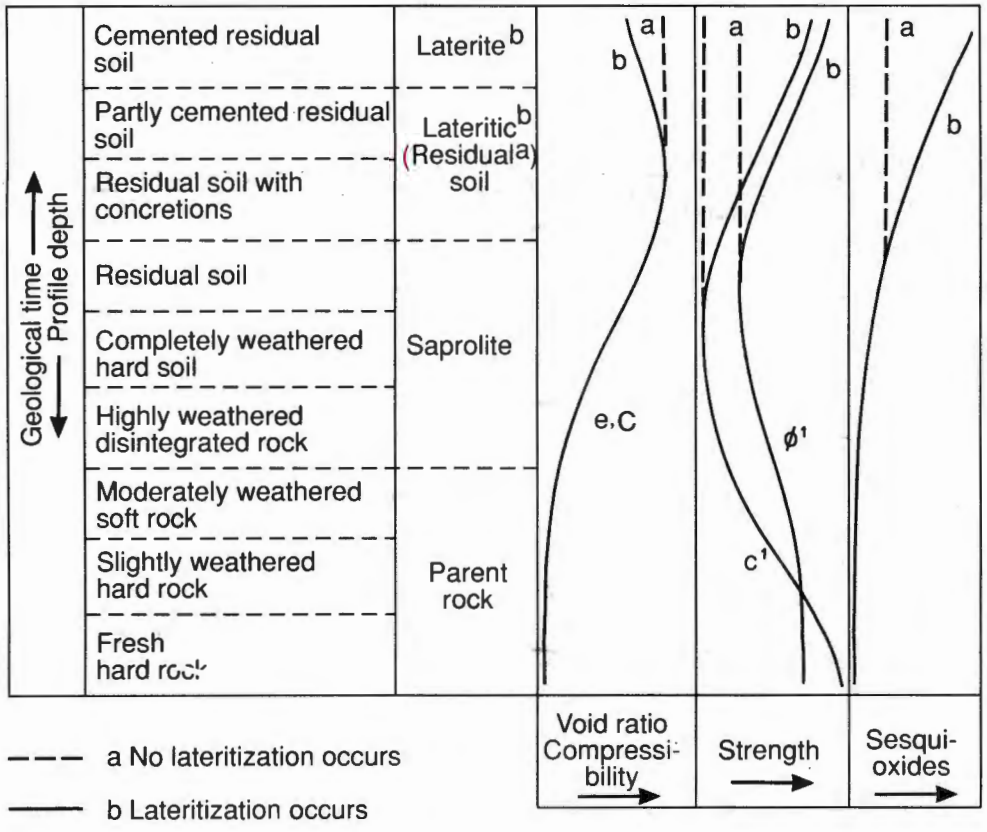

Figure 2: Changes occuring in a weathering profile
(Adapted from Tuncer and Lohnes (1977) and Sueoka (1988))

Saprolites and laterites can have characteristics that are quite distinctively different from those of the transported soils commonly occurring in temperate zones. For example, the conventional concept of a soil grain or a particle size is inapplicable to many tropical soils. Particles of tropical soil often consist of aggregates of weathered mineral matter that break down and become progressively finer if the soil is manipulated. What appears in situ to be a coarse sandy gravel may deteriorate to a fine sandy silt during excavation, mixing

performed, than is usually the case with transported soils.

With that brief introduction to tropical soils, the ongoing processes that can produce surprisingly rapid geological changes in soil profiles in the tropics will now be described.

BIOPERTURBATION OF SOIL BY TERMITES

Most termites live in tropical and subtropical regions, but they extend in range between about 45°N and 45°S, i.e. between the latitudes of Milan and Toronto, in the north to Christchurch, New Zealand in the south; a span of latitudes that covers two-thirds of the earth's land surface. Termites are insects of the order Isoptera. Often called "white ants), they are more closely related to cockroaches than ants, even though their lifestyle superficially resembles that of ants. Like the honeybee, termites have been the subject of popular scientific writing, as Figure 3 indicates. The central figure in

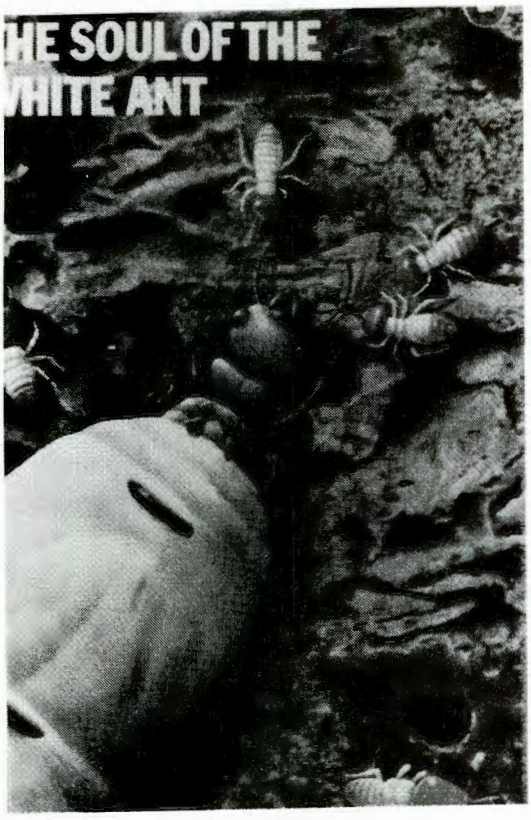

Figure 3 : The termite or white ant.

Figure 3 is the queen termite, attended by workers (upper right).

Termites live on vegetable matter - grass, wood and other plants and plant litter. Their significance to engineering geology and geotechnical engineering arises from the fact that they are burrowing insects that construct both underground food storage chambers and above surface mounds, with extensive galleries and tunnels serving the colony's food gathering, fungus farming and water-fetching activities. Figure 4 (after Lee and Wood, 1971) diagrammatically illustrates the form taken by a typical termitary.

Depending on species and climate, mounds may vary from modest, roughly hemispherical domes 300 to 500 mm in diameter to monstrous fantastically shaped structures up to 9 m or more in height and 30 m diameter at the base. (Harris, 1955). Figures 5 and 6 illustrate two of the many forms taken by termite mounds.

The activities of a single colony may cover a radius in plan of 60 to 75 m (Ratcliff and Greaves, 1940) and termite channels have been observed by the writer in test holes in South Africa at depths exceeding 20m.

The mass of material contained in termite mounds per unit of surface area has been measured by a number of authors. Figures from Australia are typically in the range from 5 to 50 tons per hectare (T/ha). Figures have been reported from central Asia of as much as 285 T/ha. (Lee and Wood, 1971). While Meyer (1960) has reported up to 2400 T/ha in termite mounds from the Congo. This latter figure is equivalent to a layer of soil 200 mm deep spread uniformly over the surface.

The rate at which these mounds are built and eroded is nothing short of amazing. Nye (1955) has reported that in West Africa a mound 600 mm high was built in a month while one 1500 mm high was built in a single season. In South Africa, the writer has observed a mound 600 mm high built in 2 years.

Termite mounds readily erode during spells of prolonged heavy rain,thus redistributing the soil over the surface. The rate at which soil is distributed over the surface has been estimated by Lee and Wood in Australia to vary between 0.1 and 0.4 mm per year, of which varying amounts are transported further afield by erosion. It would appear from the figures given for the mass per hectare of termite mounds that rates of distribution may be as much as fifty times these figures (5 to 20 mm per year) in certain areas. Thus it is quite possible for termites to turn over a full metre of the soil profile per century.

Two important geotechnical effects of termites have been identified. These relate to

- the settlement of structures, and
- the permeability of soils.

Settlement of Structures

There two ways in which termite activity may affect the settlement of structures:

In an area infested with termites, the soil profile may be riddled with termite

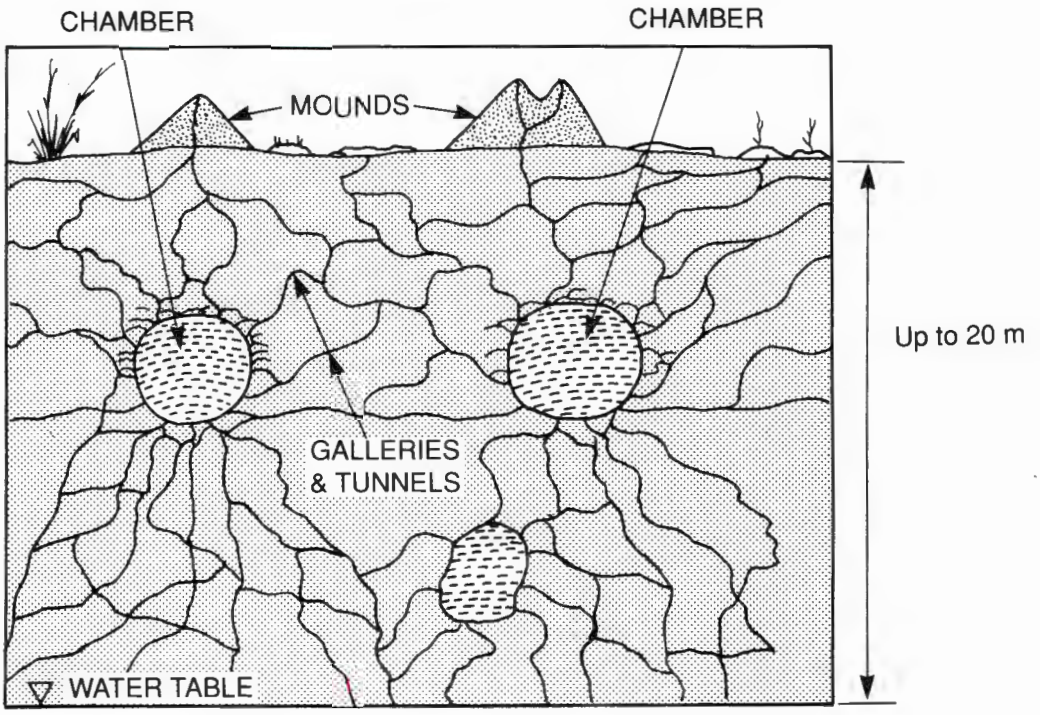

Figure 4: Form taken by typical termitary *(After Lee and Wood, 1971)*

Figure 5 : Termite mound in the Transvaal

channels, thus materially increasing both the macro void ratio of the soil and its compressibility.

Unfortunately, this effect does not appear to have been quantified,but it is an effect that should be recognised when examining, sampling and testing soil profiles. It is important to note that termite channels may be present in the soil even though there is no sign of termite mounds on the surface. The termites may have left the area decades or more ago, but the effects of their tunnelling will remain in the soil.

Figure 6: Termite mound in Botswana.

Because termites carry soil fines to the surface, large objects such as boulders and shallow foundations tend to be carried downwards. In the case of a foundation, the settlement may be sufficient to cause structural distress.

Partridge (1989) has reported that termite activity may result in the formation of a collapsible soil structure which may be subject to severe settlement if loaded during a dry period of the year and subsequently wetted by infiltrating water.

Case Histories of Settlement

Settlement of a pile

In Johannesburg, one of a pair of augered cast in situ piles 10 m deep, supporting a pile cap, started to settle as load came on to it with the result that the pile cap rotated. A 750 mm diameter auger hole was drilled next to the pile to determine the cause of the settlement. It was discovered that the pile had been founded directly above the food storage chamber of a termitary. This highly compressible spherical structure, about 500 mm in diameter was responsible for the settlement.

Ruination of a precise survey base (Watt and Brink, 1985)

In 1974 a precise survey base was constructed at Pienaarsriver, Transvaal by Finnish geodesists. It was intended for the calibration of electro-optical and electronic distance measuring instruments to an accuracy of 1 part in 10 million. The monuments supporting the calibration marks were mass concrete blocks measuring 1 m square and founded at depths of 2.5 to 3 m on a yellow to reddish brown very stiff to very soft rock consistency silty sand, residual from the in situ decomposition of dolerite.

Within two months it was found that certain of the monuments had settled by as much as 6 mm and had tilted slightly. This small movement could have been caused by shrinkage of the concrete, hence measurements were continued until 1976 when the precise distances were set out. At this time settlements of up to 16 mm had occurred. The movement continued and by 1980 it was found that the distance between the zero and 432 m marks had shortened by 12 mm (1 part in 36 000). The base was quite clearly unable to meet the accuracy requirements. Figure 7 shows settlement records for some of the monuments, indicating that settlements of more than 150 mm had taken place over a period of 11 years.

There was abundant surface evidence of termite activity in the area and test pits showed the existence of subterranean cavities, channels and food stores. A stone-age core of unweathered quartzite thought to be about 100 000 years old was found lodged in a biotic stone layer in the residual dolerite profile at a depth of

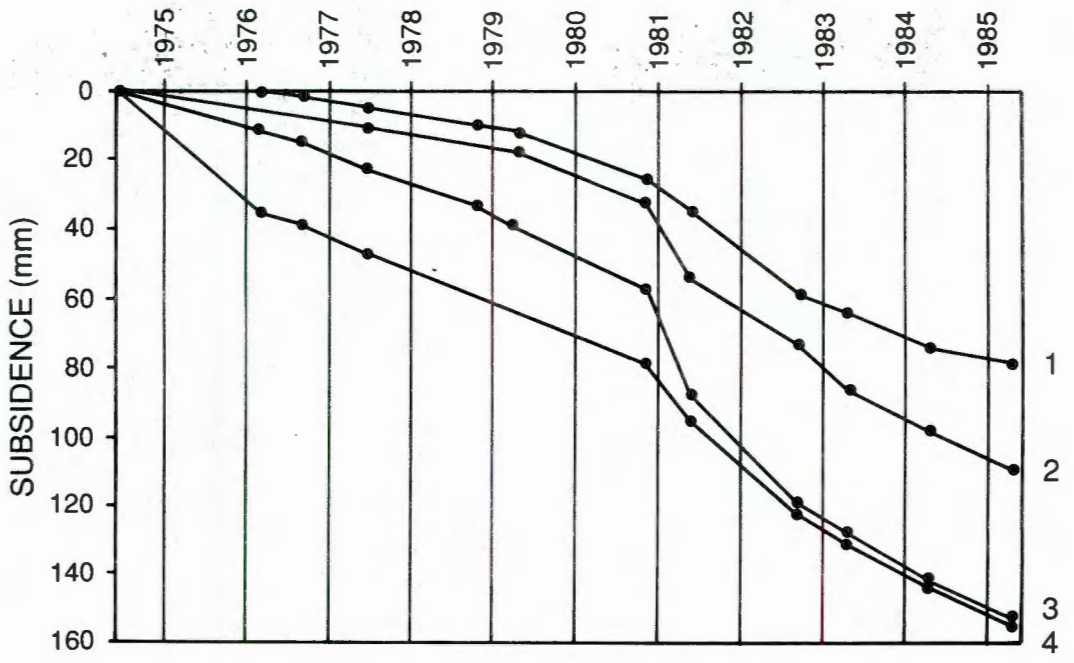

Figure 7: Subsidence of various surface monuments as a result of termite activity *(After Watt and Brink, 1985)*

1.4 m. This was further evidence of the longstanding activity of the termites. Five genera of termites were identified as being active at the site. It is interesting to note that none of these produce large surface mounds. Three genera produce no mounds at all, and the other two build modest mounds of about 1 m diameter and height.

Permeability

Because termite channels increase the void ratio of soil and provide pathways that may be continuous for tens of metres, termite activity can have a huge effect on the permeability of soils.

A series of evaporation ponds was built near Johannesburg on a gentle 5° slope. After completion of the compacted earth walls, the cascade of ponds was filled from the top, each pond overflowing in turn into the next lower pond. In several areas severe leakage from one pond to the next was discovered. On examination it was found that the leakage was occurring through ancient termite channels contained in the lateritized surface layer of the hillside. These had not been discovered during the site investigation and there were no termite mounds at the surface or any other signs of the presence of termites. The flow was clear, thanks to the lateritization of the soil through which the channels ran.

As the ponds had been designed to decant downhill, it was decided not to attempt to stop the leakage, but to guard against the effects of a possible enlargement of the channels by internal erosion To do this, each area from which leakage was emerging was covered by a reverse filter blanket, two of which are shown in Figure 8.

Figure 8 : Filter blanket protecting point of exit of seepage from termite channels

EROSION OF SOIL BY WIND AND RAIN

The loss of topsoil by water and wind erosion is a well-recognised and extensively researched hazard of agriculture. The main factors affecting erosion losses from agricultural land are the slope length and inclination, the agricultural practice and the surface cover

Figure 9 : Eroded surfaces in Badlands of South Dakota

Figure 10 : Eroded surface of a gold tailings dam.

(e.g. Evans and Kalkanis, 1977). Agricultural fields rarely exceed an inclination of 10° to 12°. Much less is known of rates of erosion from steeper slopes, and in particular, from man-made slopes, e.g. highway cuts and fills, the slopes of tailings dams, etc. Whereas loss of soil from agricultural fields rarely exceeds 10 to 15 T/ha/year, losses from man-made or engineered slopes may be measured in hundreds of T/ha/year. Rates of erosion as large as this are probably not common in nature, but in areas where the soils are highly erodable and the climate and topography unfavourable, e.g. the Badlands of South Dakota, it is likely that rates of erosion are also of this order. Figure 9 shows a typical eroded landscape in the South Dakota badlands. The similarity of this landform with the appearance of the eroded slope of a tailings dam (Figure 10) is striking.

The total erosion loss from a surface is made up of material removed by water and that removed by wind. The enormous sand dunes that occur in some of the deserts of the world give evidence of the capacity of the wind to transport solid material. Figure 11, for example shows a 350 m high dune in the Namib sand sea. Figure 12 (Blight, 1989) shows measurements of seasonal erosion losses from gold tailings, dams on the Witwatersrand. The erosion loss has been plotted against the ETCOM index which is a measure of the strength of the slope's surface crust. The significance of the measurements shown in Figure 12 is that the Witwatersrand is a summer rainfall area with very little rain falling in the dry winter months when the only agent of erosion is wind. Hence the measurements show that soil losses caused by wind erosion can be of the same order of size as losses by water erosion. Note the absolute magnitude of the losses whether expressed

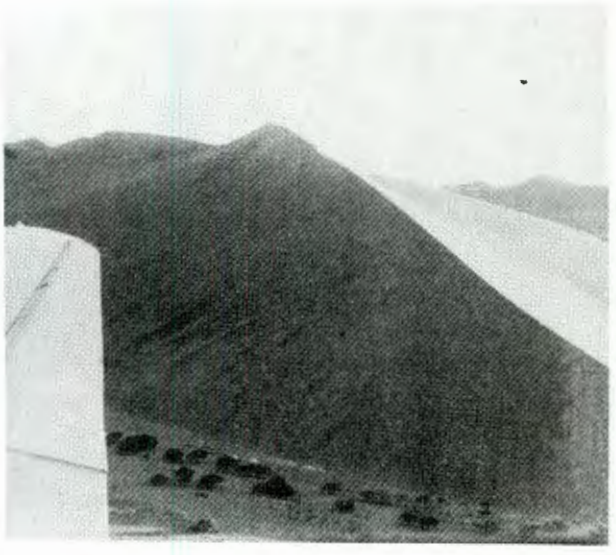

Figure 11 : 350m high dune in the Namib sand sea

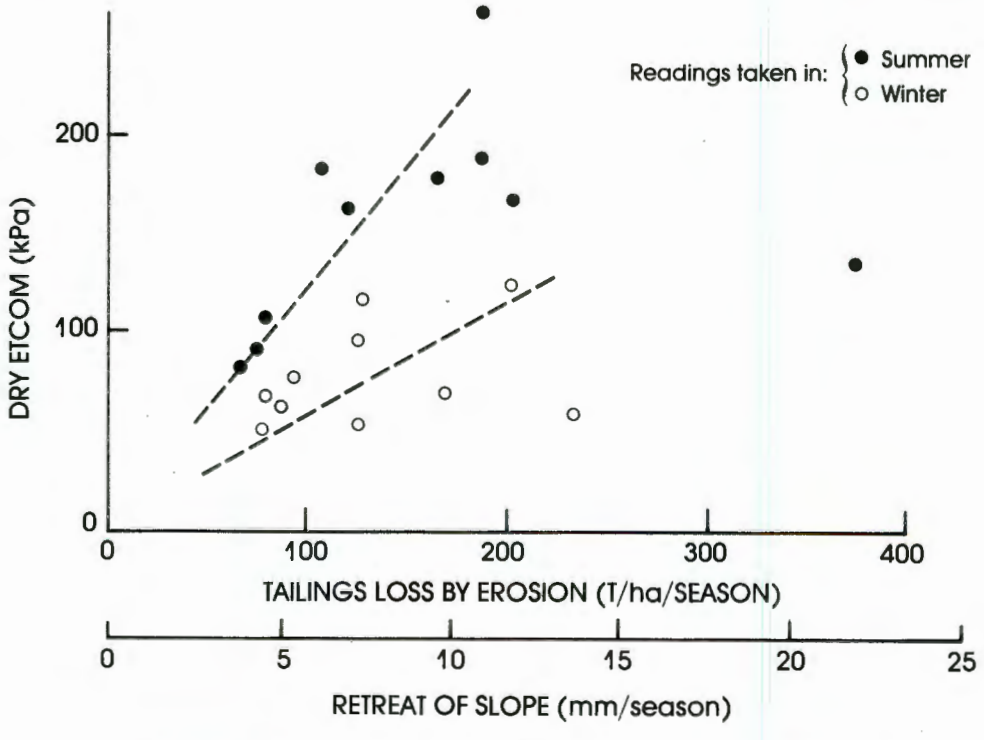

Figure 12: Correlation between ETCOM erosion index and tailings loss by erosion.

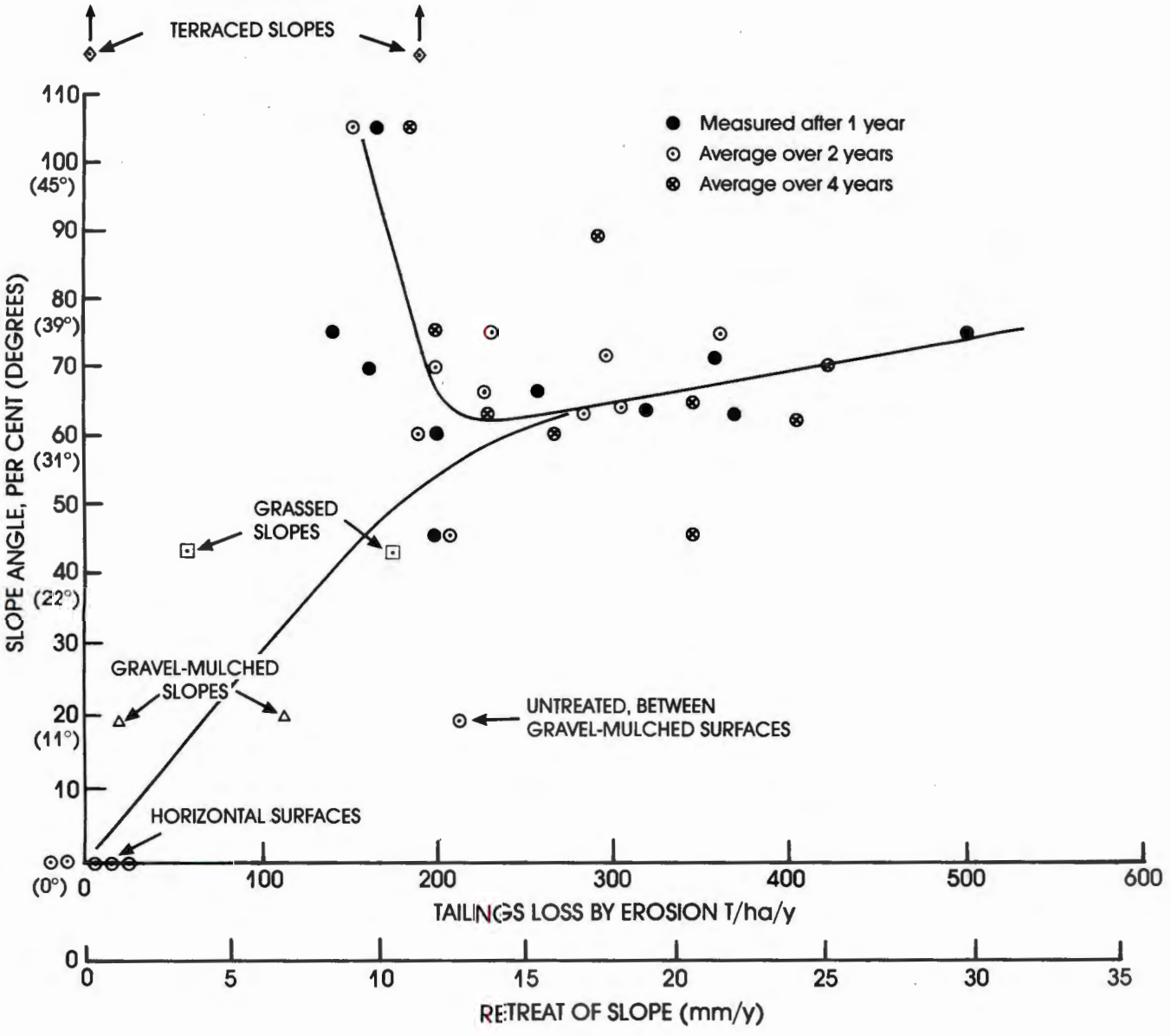

Figure 13: Correlation between slope angle and tailings loss by erosion.

as T/ha/year or as mm of slope retreat.

Figure 13 shows a collection of data relating losses from the slopes of tailings dams to slope angle. The two-branched correlation between slope angle and erosion loss has long been established (e.g. Renner, 1936) and shows that relatively little erosion occurs on very flat or very steep slopes. Most of the measurements in Figure 13 relate to bare, ungrassed slopes. The evidence is limited, but it is interesting to note that grassed slopes appear to erode at much the same rate as ungrassed slopes.

EROSION AND DEPOSITION OF MATERIAL BY FLOODS

Each year tropical cyclones develop along the coast of the world's continents. In the southern hemisphere cyclones usually develop along the east coasts. If such a storm crosses the coastline, severe storm damage is almost inevitable. Over the past 150 years for which partial or complete records have been kept, 934 cyclones have been observed in the South West Indian Ocean. Since 1950 ten tropical cyclones have crossed the coastline of Southern Africa to wreak havoc inland. The estimated volume of water dumped by these storms on South Africa alone has varied from 2000 million cubic metres to over 40 000 million cubic metres dumped by cyclone Domoina in January 1984. (Kovacs, et al, 1985). Figure 14 is a satellite photo of cyclone Domoina as it crossed the Southern African coast.

Fortunately these storms rarely occur outside of latitudes 30°N to 30°S and very few cross their adjacent coastlines.

The flooding caused by a tropical

Figure 14 : Cyclone Domoina crossing the coast of Southern Africa

cyclone is quite sufficient to cause erosion or deposition that constitutes a significant geological event.

Figure 15 illustrates the extent of erosion that can be caused by a single storm. It shows before and after cross-sections of the Mfolozi river at the site of a bridge destroyed by the storm. It will be seen that as much as 10 m of material was removed by this single event, although the maximum depth of the river channel was increased by only 2 m. Clearly large depths of deposition can occur further down a river channel where the section widens and the flow velocity drops. Figure 16 shows sections through the basin of the Pongolapoort reservoir (on the Pongola river) which indicate depths of deposition of as much as 15 m of silt. Although some of the siltation had probably occurred between the date of completion of the dam (1970) and the arrival of Domoina, most of the siltation is believed to have occurred in this single storm. The total volume of sediment estimated to have been deposited in this one reservoir by Domoina is 125 million cubic metres. In addition extensive areas along river banks were covered by silt and debris many metres deep.

Failures of man-made structures may also result in extensive erosion and deposition. In 1982, the Lawn Lake dam on the Roaring River in the Rocky Mountain National Park, Colorado, failed (Jarrett and Costa, 1986) initiating a catastrophic flood. Where the Roaring River debouches into the larger Fall River, an extensive alluvial fan was deposited within a period of only 5 hours. The fan covers an area of 0.25 km^2, has a radial length of up to 0.7 km and consists of bolders,gravel and sand. The depth of deposition is up to 14 m, and the volume of deposition approximately 3.6 million cubic metres.

On 11 November 1974, the wall of a tailings dam at Bafokeng, Transvaal failed by overtopping (Blight et al, 1981). Before

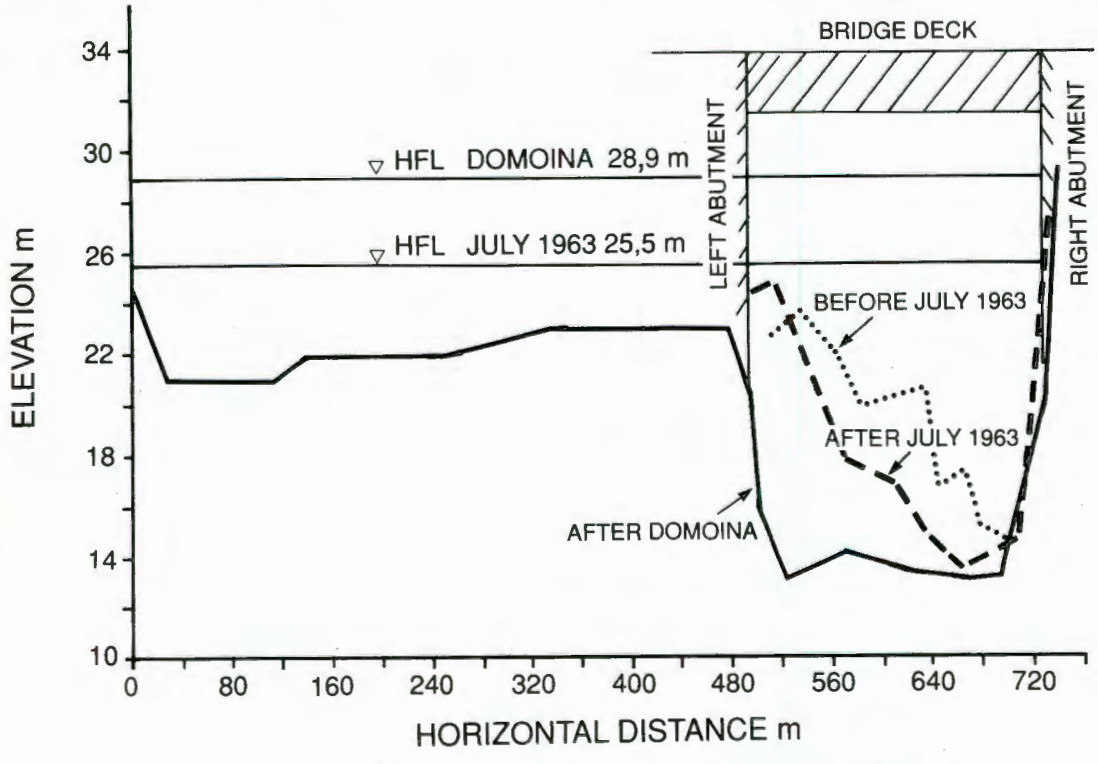

Figure 15: Erosion caused at site of bridge over Mfolozi river by Cyclone Demoina *(After Kovacs, et al, 1985)*

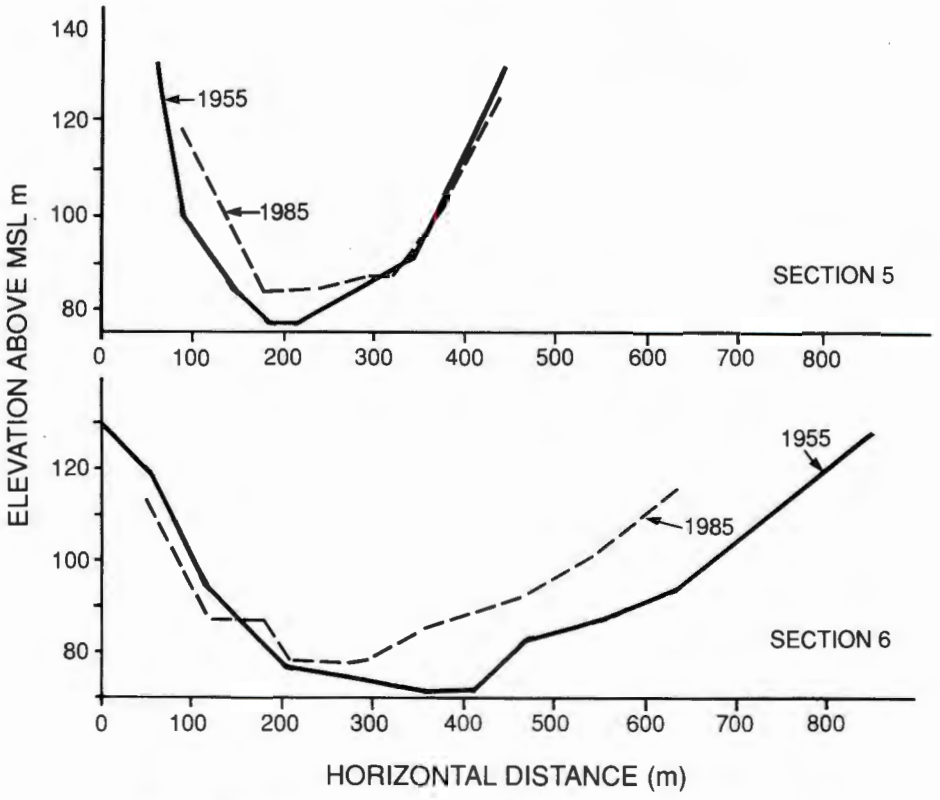

Figure 16: Siltation in the basin of the Pongolapoort reservoir caused by Cyclone Demoina. *(After Kovacs et al, 1985)*

the failure, the dam (900 m by 900 m in plan and 20 m high) contained 13 million cubic metres of tailings. About 3 million cubic metres of liquified tailings flowed out through the breach in the wall, engulfed a vertical shaft of the mine and flowed down the valley of the Kwa-Leragane stream. At a distance of 4 km from the dam the flood of slurry had spread to a width of 0.8 km, was 10 m deep and moving at an estimated speed of 30 km/h. The flood continued into the Elands river and an estimated 2 million cubic metres of tailings eventually flowed into the reservoir of the Vaalkop dam, 45 km downstream of Bafokeng. Figure 17 shows a stretch of the Elands river after the flood had passed showing the light-coloured tailings deposited along the river banks.

Although the quantities of material transported in these two man-made disasters were not nearly as large as may occur in a natural event, the examples show that man must consider himself to be an agent of significant geological change.

Mudflows

In recent years, catastrophic mudflows of volcanic ash have been reported from various parts of the world - Mount St Helens in Washington State, and Nevado del Ruiz in Colombia are examples of the sites of recent flows.

Volcanic mudflows or lahars occur when a snow or ice-capped volcano erupts large quantities of ash. The hot ash melts the snow-cap, thus saturating the ash. As the material will usually have been deposited at its dry angle of repose, the inevitable consequence is that the saturated material slides, liquifies, and then flows down the mountainside.

The Nevado del Ruiz flow (McDowell, 1986) formed a 40 m high mud-wave that

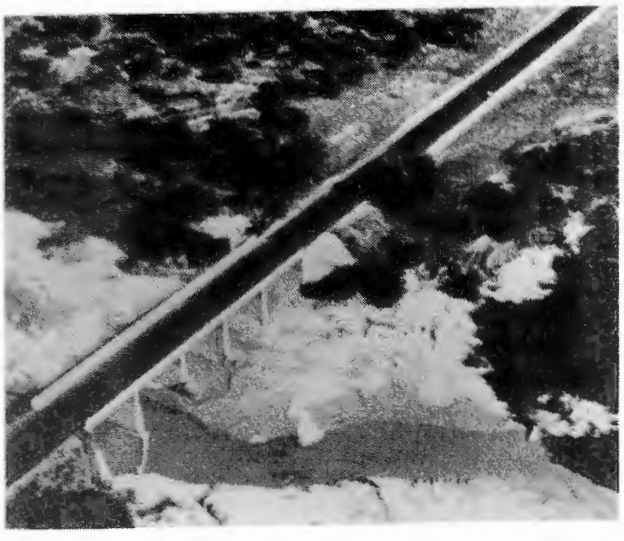

Figure 17 : Tailings flow deposited along the banks of a river

Figure 18 : Rapid weathering of a lava flow that has crossed a road on Hawaii

Figure 19 : Black beach sand formed by rapid weathering of lava in Hawaii

flowed down the Lagunilla river and, pouring over the plain below, annihilated the town of Armero with a loss of life of some 23 000. The mudflow eventually covered an area of 40 km^2 to depths of up to 3.5 m. The flow appears to have moved at about 20 km/h.

Lava Flows

The Hawaiian islands are possibly the best example of an area where the geology consists almost entirely of recent lava flows.

According to Bigelow (1982) and (Lum 1982), the islands were formed as the Pacific crustal plate slowly traversed a hot spot or plume of magma below the crust. Each volcano (and therefore island) originated and became active as its site arrived over the plume and then became extinct as it moved away. In this way a chain of islands was formed, ranging in age for 5 million years for Kauai to three million for Oahu to less than 1 million years for Hawaii. Hence the island of Hawaii is truly a product of the Quarternary Era, and is the only state of the United States that is still increasing in area as successive lava flows encroach into the sea.

The lava on Hawaii weathers surprisingly quickly. Figure 18 shows a recent lava flow that crossed a road on Hawaii. The freshness of the painted line on the road shows how recently the flow occurred, yet already there is sufficient weathered material present to support plant life. The black sand beaches of the island (Figure 19) further indicate the rapidity with which the lava is weathered.

This weathering is mainly physical. However, Lum reports that layers and lenses of ash interbedded with the lavas have weathered to form seams of almost pure montmorillonite clay. The presence of these clay seams can lead to stability problems in road cuts and the sides of foundation excavations.

CONCLUSIONS

This wide-ranging and necessarily superficial review has set out to illustrate that the Quaternary Era is indeed still in progress and its geological processes on-going. It has also shown by illustration that geological changes significant to the engineering geologist and geotechnical engineer can take place in surprisingly short periods of time and that the works of man can be regarded as significant to geological change. There are many other examples in the world around us that support these theses.

REFERENCES

Akili, W. and Torrance, J.C., 1981. The development and geotechnical problems of sabkha, with preliminary experiments on static penetration resistance of cemented sand. Quarterly Journal of Engineering Geology, 14(1):59-74.

Bigelow, G.E., 1982. Geology of the Hawaiian Islands, Engineering and Construction in Tropical and Residual

Soils, ASCE Speciality Conference, Honolulu, 27-29.

Blight, G.E., 1989. Erosion losses from the surfaces of gold-tailings dams, Journal of the South African Institute of Mining and Metallurgy, January, 23-29.

Blight, G.E., Robinson, M.J. and Diering, J.A.C., 1989. The flow of slurry from a breached tailings dam, Journal of the South African Institute of Mining and Metallurgy, January, 1-8.

de Mello, L.G.F.S., Franco, J.M.M. and Alvise, C.R., 1988. Grouting of canaliculae in residual soils and behaviour of the foundations of Balbina dam, 385-390.

Desai, M.D., 1985. Geotechnical aspects of residual soils (ed. Brand, E.W. and Phillipson, H.B.) Scorpion Press, Hong Kong, 83-98.

Evans, W.R. and Kalkanis, G., 1977. Use of the universal soil loss equation in California. Soil Erosion: Prediction and Control. Proceedings, National Soil Erosion Conference. Soil Conservation Society of America, 31-40.

Fookes, P.G., 1978. Middle East inherent foundation problems. Quarterly Journal of Engineering Geology, 11(1) : 33-49.

Harris, W.V., 1955. Termites and the soil. In Soil Zoology, D.K.M. Kevan, ed. Butterworth, London, 62-72.

Jarrett, R.D. and Costa, J.E., 1984. Hydrology, geomorphology and dam-break modelling of the July 15, 1982, Lawn Lake Dam and Cascade Lake Dam failures, Larimer Country, Colorado. U.S. Geological Survey Open-File Report No.OF 84-0612.

Kovacs, Z.P., Du Plessis, D.B., Bracher, P.R., Dunn, P and Mallory, G.C.L. 1985. Documentation of the 1984 Domoina Floods, Technical Report TR122, S.A. Department of Water Affairs, Pretoria, R.S.A.

Lee, K.E. and Wood, T.G. 1971. Termites and soils, Academic Press, London.

Lumm, W.B. 1982. Engineering problems in tropical and residual soils in Hawaii, Engineering and Construction in Tropical and Residual Soils, ASCE Specialty Conference, Honolulu, 1-12.

McDowell, B. 1986. Eruption in Colombia, National Geographic, 169, (5) 641-652.

Meyer, J.A. 1960. Quoted by Lee and Wood, 1971.

Nye, P.H. 1955. Some soil-forming processes in the humid tropics, IV. The action of soil fauna. Journal of Soil Science, 6, 73-83.

Partridge, T.C. 1989. The significance of origin for the identification of engineering problems in transported Quaternary soils. Applied Quaternary Research (De Mulder and Hageman, Eds). Balkema, Rotterdam, 119-128.

Ratcliff, F.N. and Greaves, T. 1940. The subterranean foraging galleries of Captotermes lacteus. Journal, Council for Scientific and Industrial Research, Australia, 13, 150-161.

Renner, F.G. 1936. Conditions influencing erosion on the Boise river watershed. U.S. Department of Agriculture, Technical Bulletin 528.

Stacey, F.D. 1970. Geomagnetism in global gephysics, English Universities Press, London.

Stipho, A. 1984. Soil conditions and foundation problems in the desert regions of the Middle East. Proceedings, International Conference on Case Histories in Geotechnical Engineering. St Louis, U.S.A. 1: 21-25.

Sueoka, T. (1988). Identification and classification of granitic residual soils using chemical weathering index. 55-62.

Tuncer, E.R. & Lohnes, R.A. (1977). An engineering classification for certain basalt-derived lateritic soils. Engineering Geology, II, (4) 319-339.

Watt, I.B. and Brink, A.B.A. 1985. Movement of benchmarks at the Pienaarsriver survey base. Case history 28 in Engineering Geology of Southern Africa, A.B.A. Brink, Ed. 4, Post-Gondwana Deposits, Building Publications, Pretoria, RSA, 199-204.

2. THE NEED TO ESTABLISH OR VALIDATE DESIGN PARAMETERS AND PRINCIPLES

CONTRIBUTIONS TO LEARNING

In each of the papers 2.1 to 2.6 field observations and measurements were used to establish design principles and requirements that had not been known or were not apparent prior to the field investigation:

2.1 The properties of epoxy resin mortars for use in nosings to bridge expansion joints:
The over-riding importance of differential thermal strains and the necessity to accommodate these by creep and relaxation at the epoxy mortar to concrete interface was not realized until the field trials were performed.

2.2 Field test of a catenary net to protect traffic from mining subsidence:
Here, the magnitude and importance of the straightening sag of the catenary net in reducing loads in the net was not appreciated until the field trial. The concept of using a low yield stress, highly ductile annealed steel in contrast to the more usual high tensile steel is also novel.

2.3 Measurements on a tied-back retaining wall:
While it was appreciated that the distribution of earth pressure behind the wall was unlikely to be the classical active distribution, it was only when the field measurements were analysed that the roughly trapezoidal distribution could be established.

2.4 The concept of the master profile for tailings dam beaches:
This work was not entirely original as it was based on earlier Russian work published

in Russian. The measurements confirmed the existence of a master beach profile, showed that it could be reproduced or established in the laboratory (this was original) and demonstrated its consequences for the stability of tailings dam slopes.

2.5 Lowering of the groundwater table by deep-rooted vegetation-the geotechnical effects of water table recovery:

It is believed that this was the first time that the extensive groundwater lowering that is possible with deep-rooted vegetation had been documented in the geotechnical literature. It is also believed to be the first time that the consequences of water table re-establishment have been identified and analysed. The form of the predicted concave-up time-heave curve is quite different to that of the conventional concave-down time-heave curve. Since writing this paper, observations at the site have confirmed the general shape of the predicted time-heave curve, as illustrated by the observations of heave at Lethabo Power Station included with the paper.

2.6 This paper reviews the use of preheaving of expansive clay profiles by flooding. The technique is not widely used, possibly because it is not well understood, and also because its application needs careful pre-planning. The record shows that the procedure is viable and can be completely successful if correctly carried out.

2. THE NEED TO ESTABLISH OR VALIDATE DESIGN PARAMETERS AND PRINCIPLES.

2.1 Blight, G E and Mitchell, M F (1980). The properties of epoxy resin mortars for use in nosings to bridge expansion-joints. The Civil Engineer in South Africa, August 1980, pp 203-210.

The paper describes the results of a project undertaken for the South African Department of Transport. Mr M F Mitchell appears as co-author as a courtesy to the sponsoring body.

2.2 Blight, G E and Barrett, A (1990). Field test of catenary net to protect traffic from mining subsidence. ASCE Journal of Transportation Engineering, vol 116, No. 2, pp 135-144.

This project was carried out for a metropolitan transportation authority via a firm of consulting engineers. Mr Barrett was the liaison person representing the consultants. I carried out all of the investigation and analysis and wrote the paper.

2.3 Blight, G E (1987). Measurements on a tied-back retaining wall. Proceedings, International Conference on Soil-Structure Interactions, Paris, France, pp 513-520.

2.4 Blight, G E (1987). The concept of the master profile for tailings beaches. Proceedings, International Symposium on Prediction and Performance in Geotechnical Engineering, Calgary, Canada, pp 361-365.

2.5 Blight, G E (1987). Lowering of the groundwater table by deep-rooted vegetation - the geotechnical effects of water table recovery. Proceedings, 9th European Conference on Soil Mechanics and Foundation Engineering, Dublin, Ireland,

pp 285-288.

2.6 Blight, G E, Schwartz, K, Weber, H and Wiid, B L (1992). Preheaving of expansive soils by flooding-failures and successes, Proceedings, 7th International Conference on Expansive Soils, Dallas, Texas. Paper accepted for publication.

My co-authors consulted me on each of four case histories described in this review paper, thus involving me in the practical research attached to each case. I wrote the paper and assess my contribution at 60%.

The properties of epoxy resin mortars for use in nosings to bridge expansion joints

G E BLIGHT* and M F MITCHELL**

Geoff Blight, *PrEng, graduated from the University of the Witwatersrand in 1955 and studied for the MSc(Eng) degree during 1956. In 1957 and 1958 he was employed as a pupil engineer under the tutelage of Mr G H H Legge. He subsequently proceeded to the Imperial College, London, where he developed his interest in unsaturated soils, being awarded the degree of PhD for a thesis entitled 'Strength and consolidation characteristics of compacted soils'. On his return from the UK he spent a period in the Department of Civil Engineering at Wits, followed by six years in the Geotechnical Division of the National Building Research Institute working on the design of waste disposal dams. Blight was appointed to the Chair of Construction Materials at Wits in 1969, a position which he still holds. His current technical interests cover the fields of geotechnics and the mechanics of civil engineering materials.*

M F Mitchell, *PrEng, graduated in Civil Engineering at Natal University. Since then he has been engaged in the construction of railways, roads and tunnels, in the geometric design of roads and, for 15 years in geotechnical and pavement engineering. He is currently Chief Engineer (Programming) in the National Roads Branch of the Department of Transport and a member of both the Geotechnical and the Highway and Traffic Engineering Divisions of the Institution.*

Introduction

In many ways, epoxy resin mortars are ideal materials for the construction of nosings to bridge expansion joints. They are strong and gain their strength very quickly, thus enabling a nosing to be installed or repaired and the road to be reopened to traffic with a minimum of delay. A successfully installed bridge nosing is extremely durable and will withstand the effects of many years of heavy traffic with little or no signs of wear and tear.

On the other hand, failures of epoxy resin mortar bridge nosings are not uncommon. In the United Kingdom, for instance, Reader and Shaw[1] reported that epoxy resin mortar bridge nosings were subject to a failure rate of over 15 per cent in the two years preceding 1971 and a more recent report[2] indicates that the situation has not improved in latter years. As epoxy resins are oil-based, their price has risen spectacularly in the recent past and there is a strong move to abandon epoxy resin mortar nosings in favour of cheaper but less convenient concrete nosings. In the United Kingdom[2] nosings of steel fibre reinforced concrete are being used as an alternative to epoxy resin mortar.

A meeting held by the Department of Transport in 1976 decided that the apparent increased incidence in South Africa of failures of epoxy mortar bridge nosings within a short period from installation required the establishment of a suitable specification for epoxy resin mortars for this use. As it was known that similar problems were being experienced overseas, representatives of the epoxy resin industry were requested to collect as much information on the subject as possible from their overseas parent companies or other overseas connections and to send the information to the Department of Transport for analysis.

It soon became apparent that although certain relevant information was available, it was of a qualitative rather than a quantitative nature. It was then decided to generate information on epoxy resin mortars made with South African materials. Once a suitable spectrum of information had been generated, field trials would be instituted to assess the field behaviour of the potentially most suitable epoxy resin mortars.

It was decided that laboratory tests should be undertaken to establish the following properties for a range of epoxy resin mortars:

1. **The effect of aggregate grading on mortar properties**
2. **The effect of mix proportions on the following: coefficient of thermal expansion, flexural strength and failure strain, air permeability and bonding properties.**

It appeared from available literature that the above properties represented the most relevant parameters for the success of an epoxy resin mortar bridge nosing. Once the range of attainable properties had been established it would be possible to prepare a preliminary draft specification on which the field trials could be based.

Information collected from overseas literature

Dimensions and proportions of nosings

The British Ministry of Transport[3] specifies a minimum width for a nosing of 180 mm and a minimum thickness of 50 mm.

Differential shrinkage and thermal movement

Shaw[4] states that failure of epoxy resin bridge nosings occurs mostly by detachment of the epoxy mortar from the deck because of the difference in coefficients of thermal expansion between the epoxy resin mortar and the deck concrete. Curing shrinkage was stated to be unimportant as 'most of the cure shrinkage occurs while the epoxy resin mortar is still plastic'***. This observation resulted in the evolving of a simple test in which a specimen of epoxy resin mortar 6 mm thick, 50 mm wide and 150 mm long is bonded to a degreased glass panel. After curing the composite glass epoxy specimen is thermally cycled from 0°C to 50°C over 10 cycles and any signs of debonding are regarded as grounds for rejection of that particular formulation.

The suggested[3] design temperature range for bridges in the United Kingdom is from 32°C to -7°C and the design differential temperature between any two parts of a bridge is 8°C.

Loads or stresses sustained by bridge nosings under traffic loading

The British Ministry of Transport[3] states that a bridge expansion joint should be capable of carrying two vertical loads, each of 112 kN, 0,91 m apart, having a contact area of 380 mm long by 76 mm wide for each load. The load is to be applied to the edge of the expansion gap. In addition a horizontal load of 81,6 kN/m should be applied at road level.

Required properties of materials

The British Ministry of Transport[3] requires that an epoxy resin mortar for use in bridge nosings should contain not more than 6,5 parts by weight of suitable fine aggregate to one part by weight of resin. Unfilled resins develop large strength but are relatively brittle. A moderate strength and increased toughness can be obtained by adding a mineral aggregate. A later statement[5] requires information on the following materials properties:

1. Classification and source of aggregate
2. Grading curve for 'all-in' aggregate
3. Water absorption, impact and abrasion properties of aggregate

Trade literature on the properties of epoxy mortars recommended for use in bridge nosings gives the following range of required properties:

* University of the Witwatersrand, Johannesburg
** Chief Engineer, Programming, National Roads Branch, Department of Transport

***Data given later in this paper contradict this statement.

One-week bending strength, 15 to 30 MPa
One-week tensile strength, 10 to 20 MPa
Thermal expansion from -30°C to + 25°C, 35 x 10^{-6} per °C
Compressive strength, 45 to 60 MPa
Density, 2 200 to 2 400 kgm^{-3}

Trials or tests of epoxy mortars for bridge nosings

The British Ministry of Transport[5] requires a successful field trial before approving an epoxy resin mortar for use as a bridge nosing material, as follows:

A complete expansion joint, using the formulation under test, must be installed on a bridge carrying not less than 12 000 vehicles per day on a single carriage-way of a dual two lane road or equivalent. The trial period for epoxy mortar nosings is a minimum of 12 months under these traffic conditions. After this period the nosings are inspected for defects.

Laboratory tests on epoxy resin mortars made from South African materials

Tests on aggregate materials

Two resin suppliers supplied samples of aggregate for use in the laboratory tests. These were:

1. Fine, medium and coarse aggregates consisting of white silicious material with a cubical grain shape. Fig 1(a) shows the gradings of these three aggregates (A) individually and also the gradings of a 1:1:1 mixture of coarse, medium and fine aggregate and a 2:1 mixture of coarse and fine aggregate.
2. Fine, medium and coarse aggregates of which the fine aggregate was a natural river sand and the medium and coarse aggregates were angular crushed dolerites. Fig 1(b) shows the gradings of the second (B) fine medium and coarse aggregates as well as combined gradings for a 1:1:1 coarse, medium and fine mixture and a 2:1 coarse and fine mixture of the aggregates.

As a guide to the suitability of the different gradings a series of dry compaction tests were carried out in which a standard proctor mould of known mass was loosely filled with aggregate of each grading and then weighed. The mould was heavily vibrated for 5 minutes, adding material to keep the mould full. The mould of vibrated material was then weighed. Hence the loose and compacted densities for each aggregate grading were calculated. The results are as shown in Table 1.

Table 1
Loose and vibrated densities of various dry aggregates

Aggregate	*Overall particle specific mass* G_s	*Description of grading*	*Loose density* γ_{min} kgm^{-3}	*Vibrated density* γ_{max} kgm^{-3}	$\frac{\gamma_{min}}{G_s}$ kgm^{-3}	$\frac{\gamma_{max}}{G_s}$ kgm^{-3}
A	2,64	Fine	1 572	1 729	595	655
		1:1:1/Coarse:Medium: Fine	1 645	1 794	623	680
		2:1/Coarse:Fine	1 679	1 807	636	684
B	2,72	Fine	1 391	1 593	511	586
		1:1:1/Coarse:Medium: Fine	1 942	2 114	714	777
		2:1/Coarse:Fine	1 994	2 047	733	753

It will be seen from Table 1 that grading has a considerable effect on both loose and vibrated density of the dry sands, even allowing for the effect of differing particle specific gravity (G_s) by dividing the densities by the relevant value of G_s. As a result of these preliminary tests it was decided to use a 1:1:1 coarse : medium : fine mix of aggregate A (see Figure 1(a)) which represents a continuously but steeply graded sand and a 1:1:1 coarse : medium : fine mix of aggregate B (see Fig 1(b)) which represents a flat grading with a double gap. Table 1 shows that these gradings do not give the extremes of the density range but are probably representative of gradings that are likely to be used in practice.

Resins used in the tests

Five resin suppliers volunteered to supply samples of resin

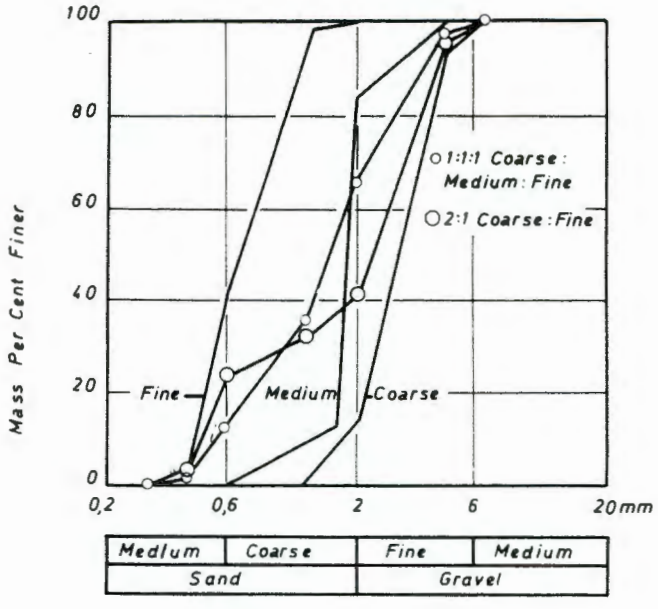

Fig 1 (a): Aggregate A

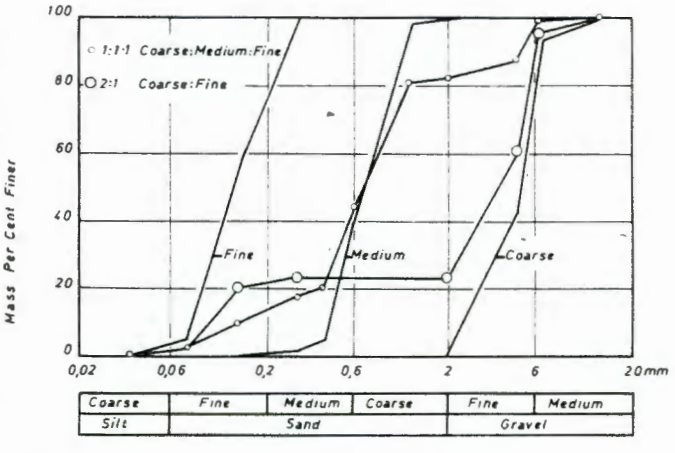

Fig 1 (b): Aggregate B

Fig 1: Grading curves for aggregates used in laboratory test programme

which they considered suitable for use in epoxy resin mortar bridge nosings.

Test programme

Beams measuring 40 mm by 40 mm in cross section and 160 mm long were cast using proportions of aggregate to resin of 2:1, 4:1, 6:1 and 8:1 by mass. It soon became apparent that a 2:1 mixture is too resin-rich as severe segregation occurred of the aggregate from the resin. The result was a beam with almost all resin at the top and the bulk of the aggregate concentrated at the bottom of the beam. As a result of this segregation erratic test results were experienced with the 2:1 ratio beams. All the beams were cured at 24°C for a minimum period of 3 weeks, which in all cases exceeds the minimum curing period specified by the manufacturers. After the beams were fully cured they were faced on a diamond saw and a diamond face grinder and the following test programme was performed:

1. *Coefficient of thermal expansion and contraction:* At the curing temperature of 24°C the length of each beam was measured to the nearest 0,01 mm using Vernier callipers. The beams were then placed in a freezer at 0°C and allowed to equilibrate to this temperature (a 24-hour period was used), after which the length was remeasured. The beams were then removed from the freezer and allowed to recover to curing temperature. At this stage their length was again measured. Typical results of these tests are shown in Fig 2.

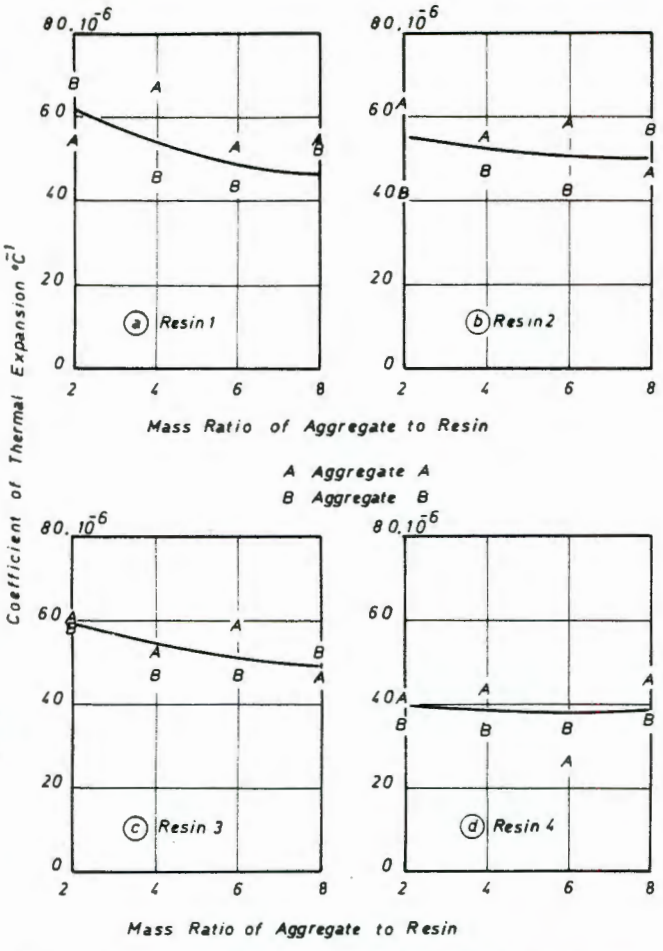

Fig 2: Variation of coefficient of thermal expansion for four resins and two aggregates at various aggregate : resin ratios

2. *Flexural strength and failure strain:* The beams were tested in 4-point bending using a span of 150 mm with equal loads applied at the third points of the span. The load-deflection curve for the beam was autographically recorded in each case and from the autographic recording and the maximum recorded deflection and load, the bending strength and bending strain at maximum load were computed. To assess the effect of temperature on strength and failure strain, bending tests were carried out at temperatures of 0°C and 24°C. Typical results of these tests are shown in Fig 3.

3. *Air permeability:* As an indication of the permeability of the resin mortar, air permeability tests were carried out on broken halves of beams of each resin and aggregate to resin ratio. To do this half-beams measuring 80 mm long by 40 mm square were sealed into a square steel tube and air pressure was applied to one of the 40 mm square faces so that the air tended to percolate along the axis of the specimen. Permeability could then be measured by means of the 'falling-head' method.[6]

4. *Differential thermal expansion – bond tests:* All specimens subjected to this test were made up at an aggregate to resin ratio of 6:1. The glass plates were of approximately the same thickness as the epoxy resin specimens (5 mm as against 6 mm for the epoxy resin). By means of thermocouples buried in the epoxy resin mortar at the epoxy-glass interface it was ascertained that the specimens required three hours to come to equilibrium with a new temperature. Cycling was carried out as follows:

   Ambient (about 20°C) to 0°C (3 hours)
   0°C to ambient (3 hours)
   Ambient to 50°C (3 hours)
   50°C to ambient (3 hours), etc

   It was noted that some debonding had occurred during curing of the mortars. This was recorded and the specimens were re-examined after 10 thermal cycles. After assessing the debonded area visually through the glass from the back of the specimens, they were pried loose from the glass and the debonded area was again checked visually.

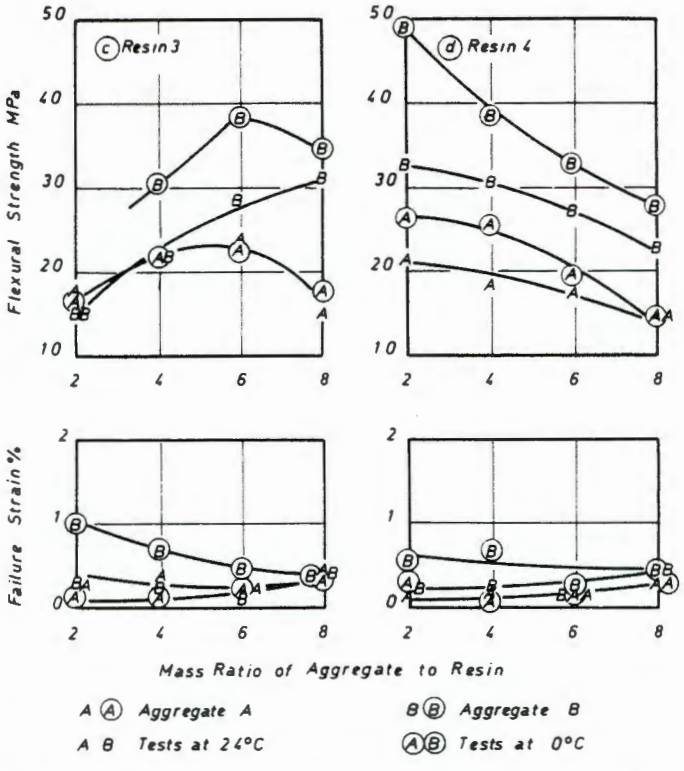

Fig 3: Variation of flexural strength and failure strain for four resins and two aggregates at various aggregate : resin ratios

Discussion of results from laboratory tests

1. *Coefficient of thermal expansion and contraction*

   Figs 2(a), (b), (c) and (d) show the results of measured coefficients of thermal expansion and contraction. It will be seen that for all resins the coefficient of thermal expansion tends to decrease with increasing aggregate to resin ratio; however, the decrease is marginal when one considers that most of the coefficients of expansion are in the range from 40 to 70 x 10^{-6} per °C while the coefficient of thermal expansion of reinforced concrete is only 10 to 12 x 10^{-6} per °C. It is therefore clear that relatively large differential thermal strains will develop in an epoxy resin bridge nosing as it cools from an average ambient temperature of say 20°C to 0°C.

   The resin showing the lowest coefficient of thermal expansion had a coefficient of about 40 x 10^{-6} per °C. In cooling from 20°C to 0°C a mortar with a coefficient of thermal contraction of 42 x 10^{-6} per °C would experience a strain differential with respect to reinforced concrete of 0,06 per cent whereas a mortar with a coefficient of thermal expansion of 72 x 10^{-6} °C would experience a differential strain of 0,12 per cent in cooling through the same temperature range. This will be looked at later when considering failure strains in tension of the epoxy resin mortars.

2. *Flexural strength and failure strain*

   The results of typical beam bending tests are shown in Figs 3(a), (b), (c) and (d).

   Flexural strength: The flexural strength at 0°C was generally greater than corresponding values at 24°C. In most cases flexural strength increased to a maximum at an aggregate to resin ratio of about 6:1 with larger increases being recorded using aggregate B than aggregate A. The highest bending strengths were recorded with resin 4; however, the bending strength using this resin declines as the aggregate to resin ratio is increased. These tests showed that at aggregate to resin ratios of 6:1 and 8:1 flexural strengths can be very large with 20 MPa easily attainable.

Failure strains: Failure strains are generally much less than 1 per cent but it will be noted from Figs 3(a), (b) (c) and (d) that it is perfectly possible to achieve a failure strain that is greater than the value of 0,12 per cent quoted in an earlier section as the differential thermal strain that would be experienced between an epoxy resin mortar bridge nosing and the reinforced concrete bridge structure in cooling from 20°C to 0°C. Surprisingly, with certain of the mortars (notably those using resins 3 and 4 together with aggregate B) the failure strain at 0°C was found to exceed that at 24°C. This is a factor very much in favour of the use of this type of formulation. It is again noteworthy that the performance of mortars made with aggregate B tended to be superior to that of mortars made with aggregate A.

3. *Air permeability*
   All of the mortars tested in this series were completely impervious to air.

4. *Differential thermal expansion – bond tests*
   This appeared to be an extremely severe test. The thermal changes are so severe that in several cases the glass to which the epoxy was bonded cracked. As the test appeared to be so stringent, it was not included in the preliminary draft specification.

The laboratory work illustrated the importance of the grading of the aggregate used for epoxy resin mortar. Gradings can cause large differences in the behaviour of mortars which are otherwise identical. It also illustrated that the coefficient of thermal expansion or contraction of epoxy resin mortars is very large compared with that of reinforced concrete. This showed that one of the major potential sources of trouble with epoxy resin mortar bridge nosings is the differential thermal strain of the epoxy resin mortar relative to the reinforced concrete bridge structure.

The tests showed that the effect of low temperatures is to increase the strength of epoxy mortars and usually to lower their failure strain. However, the use of combinations of certain resins and aggregates can provide a mortar, the failure strain of which is actually increased at lower temperatures. Finally, well compacted epoxy resin mortar can be completely impervious.

The preliminary specification, based on the laboratory tests, called for minimum values of the:

1. Density of the compacted dry aggregate
2. Coefficient of thermal contraction from 25°C to 0°
3. Flexural strength and failure strain
4. Air permeability.

It also specified the:

5. Minimum dimensions and shape of nosings.

In addition, acceptable test methods for aggregate and mortar were described and acceptable methods of installation were also given.

Field trials based on the preliminary draft specification

A bridge on the Johannesburg Western Bypass was made available for field trials on nosings constructed in accordance with the first draft specification. The bridge had three expansion joints on each carriageway giving a possibility of six trial bridge nosings. The five suppliers who had provided resins for the laboratory programme were invited to install trial bridge nosings in accordance with the draft specification. All accepted the invitation and after preliminary acceptance tests on the materials they proposed using, the trial nosings were installed during September and October 1978. A number of defects became apparent within the first month after installation. The most important of these were:

1. Disbonding of the nosings from the concrete bridge structure
2. Interlayer bond failures where the epoxy mortar had been placed in two layers
3. Transverse shrinkage cracking of the nosings.

Disbonding from the concrete

Four of the six nosings became disbonded from the concrete to such an extent that repairs had to be effected. Three of the nosings became so badly disbonded that they were removed and replaced while the remaining nosing was partially replaced.

In every case the disbonding had occurred by a horizontal fracture through the concrete leaving a 10 mm to 20 mm layer of concrete adhering to the epoxy mortar. This is clearly illustrated by Fig 4. This experience indicated that the failures had occurred as a result either of differential thermal movement between the epoxy mortar and the concrete or, possibly, as a result of curing shrinkage of the epoxy mortar. It also showed that the shear strength of the epoxy mortar exceeded that of the bridge concrete after a relatively short period of curing.

Fig 4: Thin layer of concrete adhering to underside of epoxy mortar nosing after disbonding failure

The fact that two of the nosings did not suffer disbonding even though their coefficients of thermal contraction were similar to those that had become disbonded indicated that properties, additional to those that had been included in the draft specification, are required for an epoxy mortar to function satisfactorily when bonded to concrete. In fact, it appears that an epoxy mortar must be able to accommodate by creep the differential thermal movement that occurs daily (and possibly also curing shrinkage). If sufficient creep does not occur, the concrete will inevitably be fractured in shear as shown in Fig 4.

Interlayer bond failure

One of the experimental nosings that had been placed in two layers suffered an interlayer bond failure as shown in Fig 5. The nosing was placed on an exceptionally hot day and it is suspected that the heat caused the surface of the lower layer to partly cure before the top layer was placed. The lack of bond between the two layers became apparent within 14 days of placing.

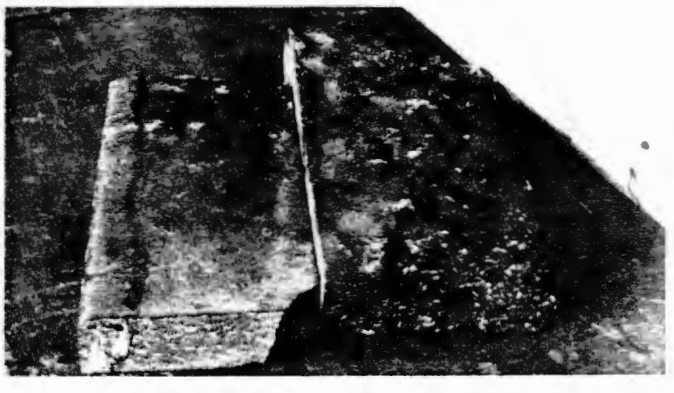

Fig 5: Interlayer bond failure of a nosing placed in two layers

Transverse cracking

One of the nosings developed transverse cracks over its entire length with a spacing of about 0,5 m (see Fig 6). The crack widths were measured by means of feeler gauges and the strain derived from these measurements was found to amount to nearly 0,1 per cent. Curing shrinkage appeared to be the most likely explanation for the cracking and a series of measurements were made in the laboratory to investigate this.

Fig 6: Transverse cracking of nosing as a result of curing shrinkage

Beams of epoxy mortar were cast and immediately stored at 25°C. As soon as the mortar was hard enough, strain measuring targets were fixed to a pair of opposite sides of each beam and the shortening of the beams was observed (at constant temperature) for a period of a month. The results of these measurements are shown in Fig 7. The findings contradicted the statement by Shaw[4], quoted earlier, as it was found that very significant curing shrinkage occurs within the first five days of casting. It was also found that the mortar that had cracked (Fig 6) so badly did not by any means display the worst curing shrinkage. This reinforced the view that creep within a mortar is important as a means of relieving stresses resulting from thermal and curing movement.

Comparison of results of acceptance tests with those of tests on field samples

Prior to installing the trial nosings, the suppliers had submitted details of the mixes they proposed using and samples of their materials for acceptance testing in accordance with the preliminary specification. During the installation of the nosings samples of the mortar were taken for laboratory check testing. For convenience, 150 mm cube moulds were used for this sampling and, after curing, each cube was sawn into four beamlets measuring 40 mm square and 150 mm long. These were tested for density, coefficient of contraction, flexural strength, failure strain and, finally, resin content. The latter was established by igniting samples of the mortar and separate samples of the aggregate at 1 000°C.

A comparison of the results of the preliminary acceptance tests and the control tests is shown in Table 2. It will be seen that large discrepancies between specified and actual properties occurred in the resin contents. In one case the field resin content was only 63 per cent of the specified value. Field flexural strengths and failure strains were generally larger than those established in the laboratory acceptance tests, as were field coefficients of contraction.

Table 2 both shows the difficulties of field control of materials

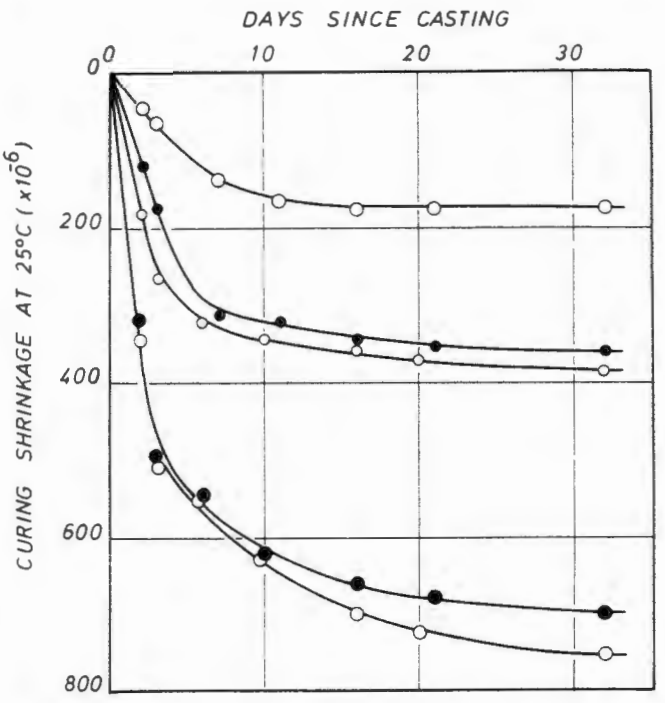

Fig 7: Curing shrinkage of epoxy resin mortar beams stored at 25°C

and emphasizes its importance. The last material entered in the table, for instance, performed unsatisfactorily but would probably have performed adequately, had it been to specification.

Reintroduction of the thermal cycling test

Prior to the experience of the field trials, the thermal cycling test[4] had been rejected as being too severe. It was later realized that this test is probably a good simulation of the stresses undergone by a nosing in the field and it was decided to perform thermal cycling tests on all of the materials used in the trial nosings. The results of these tests are shown in Table 2 and it will be seen that there is an excellent correlation between a low percentage debonding in the thermal cycling test and satisfactory performance of a nosing. It was therefore decided to incorporate the thermal cycling test into the specification.

Concluding remarks

At the time of writing, the trial bridge nosings have been in place for 16 months. Most of the defects showed up in the first month after installation, whereafter the condition of the nosings appeared to stabilize. In recent months only secondary faults appear to be manifesting themselves. For example, the nosing with the low resin content is now chipping at the edges and beginning to crack trans-

Table 2
Summary of results of tests on cubes taken from material laid as experimental bridge nosings
(All figures are the mean of four separate determinations)

Mean density of mortar kgm⁻³		*Mean coefficient of contraction 25°C to 0°C x 10⁻⁶ °C⁻¹*		*Mean flexural strength MPa*		*Mean failure strain %*		*Resin content (by mass)*		*Shrinkage at 25°C after 30 days με (με=1.10⁻⁶)*	*Debonding after thermal cycling test % of area*	*Performance of nosing on bridge*
Laboratory	*Field*	*Laboratory*	*Field*	*Laboratory*	*Field*	*Laboratory*	*Field*	*Specified*	*Actual*			
2 083	2 071	36	37	23,4	33,6	0,58	0,89	Volume mix	14,9%	380	4,8%	Satisfactory after minor repairs
2 103	2 119	25	25	22,8	37,4	0,41	0,82	14,3%	12,6%	360	21,8%	Unsatisfactory
1 947	1 947	39	41*	18,6*	36,1	0,56	1,16	16,7%	17,4%	180	82,8%	Unsatisfactory
2 123	2 112	38	50*	16,5*	26,4	0,58	1,93	Volume mix	15,1%	700	4,3%	Satisfactory
2 146	2 129	31	35	22,4	35,8	0,56	1,09	12,5%	10,6%	370	0	Satisfactory
2 250	2 243	17	20	26,4	33,3	0,44	0,69	12,5%	7,9%	190	0	Unsatisfactory

* Did not comply with draft specifications

versely, signs of debonding are developing next to some of the cross cuts* in other nosings, etc.

Only time will tell whether the long-term behaviour of the nosings will be satisfactory. However, it is believed that the specification in its latest form (the latest draft is attached as Appendix 1) goes a long way to resolving the problems of the epoxy resin mortar bridge nosing.

Acknowledgement

We gratefully acknowledge the help and active co-operation we have received from the epoxy resin suppliers and installers who have been associated with this investigation.

References

1. Reader, C E L, and Shaw, J D N. Epoxy resin compositions in concrete construction repair, *Proceedings,* Symposium on Resin and Concrete, University of Newcastle-upon-Tyne, 1973. (Available as Shell Chemicals Literature.)
2. *New Civil Engineer,* 11 May, 1978. Noses that were put out of joint, pp 23 & 24.
3. British Ministry of Transport. *Expansion joints for use in highway bridge decks,* Technical Memorandum (Bridges) No BE6, 1967.
4. Shaw, J D N. Epikote resin expansion gap nosings, Shell Chemicals Literature, 1975.
5. British Ministry of Transport. *Expansion joints for use in highway bridge decks (Amendment No. 4),* Technical Memorandum No. BE3/72, 1972.
6. Blight, G E. A falling head air permeameter for testing asphalt, *The Civil Engineer in South Africa,* vol 19, No. 6, 1977, pp 123 – 126.

Appendix

Draft specification for epoxy resin mortars for use in nosings to bridge expansion joints

1. Scope of specification

This specification covers the required properties of

(i) *aggregate*
(ii) *epoxy resin mortars*

for use in nosings to bridge expansion joints and also the *minimum dimensions* of such nosings.

In addition to the mandatory clauses of the specification which follow, notes for the guidance of the supplier and the contractor are given which deal with:

(a) acceptable test methods for aggregate and mortar; and
(b) acceptable methods for the installation of epoxy mortar bridge nosings.

2. Materials – general

Aggregate and resin shall be supplied in pre-packed kits with clear instructions for mixing. The aggregate shall be supplied ready-mixed as a single material.

3. Aggregate

3.1 General

A sample of the aggregate it is proposed to use in the epoxy mortar shall be submitted to the engineer for inspection before proceeding with further testing. All testing shall be performed by a laboratory which is acceptable to the engineer and independent of the resin supplier and contractor.

3.2 Aggregate particles

Aggregate particles shall consist of fresh unweathered crushed rock or clean river sand containing no weathered particles. For example, sound quartzite, dolerite, granite and dolomite are acceptable materials for crushed aggregates. Shales, schists, mudstones and any materials showing visible signs of weathering are unacceptable. River sands and washed pit sands shall consist of quartz particles only. Sand containing particles of shale and particles of any weathered rock are unacceptable.

3.3 Aggregate grading

Aggregates shall be graded from the largest to the finest particle size. The largest particle size shall be 9,5 mm and no aggregate shall contain more than 5 per cent by mass of particles which pass a 0,075 mm mesh. If material finer than this is required as a filler, only quartz flour shall be used for this purpose.

* There is now some doubt as to the efficacy of these cross-cuts. They may actually do little to relieve differential thermal strains, but instead act as starter flaws for the propagation of disbonding.

3.4 Compacted density of aggregate

A sample of the graded aggregate shall be compacted in accordance with *Method 1* described in Appendix 1: *Acceptable Test Methods.* The ratio of the mass per unit volume of the compacted aggregate to the average mass per unit volume of the aggregate particles shall be not less than 0,7.

4. Epoxy resin mortars

4.1 Mix proportions

The ratio by mass of aggregate to resin in an epoxy resin mortar proposed for use in a bridge nosing shall be stated by the supplier and the contents of kits shall be in these proportions.

4.2 Thermal cycling performance

The mean of the disbonded areas of three separate specimens which have been subjected to the thermal cycling test described in Appendix 1: *Acceptable Test Methods* shall not exceed 5 per cent.

4.3 Bending strength

The bending strength of the fully cured mortar measured in a four point bending test as described in Appendix 1: *Acceptable Test Methods* shall be not less than 20 MPa at a test temperature of 25°C.

4.4 Failure strain in bending

The failure strain in the bending test described in 4.3 above shall not be less than 0,40 per cent.

4.5 Compacted density

The compacted density of the epoxy resin mortar test specimens shall be recorded for comparison with the density of test specimens taken during installation of the nosings. The density of the field compacted specimens shall be at least 90 per cent of the mean density of the specimens compacted in the laboratory.

5. Minimum dimensions of bridge nosings

The minimum width of a nosing measured normal to the expansion joint shall be 180 mm. The minimum thickness measured normal to the road surface shall be 50 mm. In the event that it becomes necessary to place a nosing in two or more layers of material, the delay between the placing of successive layers shall be minimized as far as possible. If the preceding layer is no longer workable by the time the next layer is placed, the interface between the two layers must be lightly primed with freshly mixed epoxy resin immediately before placing the next layer.

6. Shape of bridge nosings

The ratio of the width of a nosing to its maximum thickness shall not be less than three.

Appendix 1: Acceptable test methods

A1.1 Density of compacted dry aggregate

The object of using an aggregate which is graded and not single sized is to achieve a high compacted density. There are many types of grading which will achieve a high density, eg a continuous grading or a single or double gap grading. The grading selected in a particular case will depend on the aggregate available. For this reason the specification calls only for a minimum compacted dry density but does not specify the grading curve which is to be used to achieve this. A standard proctor mould of measured mass is filled with the graded aggregate and then placed on the table of a Vebe* vibrator. The mould is vibrated for 5 minutes, adding material to keep the mould full. After 5 minutes the material is struck off level with the top of the mould and the mass of the mould of vibrated material is measured. Hence the mass per unit volume of the compacted aggregate is determined. To allow for differences in the mass per unit volume of the aggregate particles from one material to another, the mass per unit volume of the compacted aggregate is divided by the mass per unit volume of the aggregate particles (the particle specific gravity) and the resultant figure should be not less than 0,7.

A1.2 Pre-acceptance tests on epoxy mortar resins

Thermal cycling tests are carried out on specimens of epoxy resin mortar that measure 150 mm long by 50 mm wide by 15 mm deep. The specimens are bonded in threes to pieces of 6 mm thick plate glass. Specimens for the thermal cycling tests are cast in a sheet metal mould such as that shown in Fig 1. The inside surfaces of the mould are wiped or sprayed with a releasing agent before placing the epoxy resin mortar. The surface of the plate glass is carefully de-greased by washing in tri-chlorethylene which is allowed to dry off before casting the specimens.

Measurements of the bending strength and the bending strain at failure are carried out on prisms of epoxy resin mortar measuring

* BS1881: Part 2, 1970

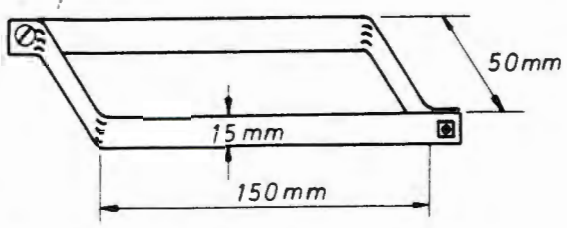

Fig 1: Strip-metal mould for thermal cycling tests

40 mm square in cross-section and 160 mm in length. For this purpose machined steel moulds with plane smooth surfaces should be used. The interior surfaces of the mould should be wiped or sprayed with a releasing agent before filling.

After drying the graded aggregate at 105°C for 16 hours and then cooling to room temperature it is thoroughly mixed with the correct proportion by mass of resin.

The moulds are then filled, the mix being compacted into the mould by means of rodding and vibration for a minimum time of 5 minutes. After completing the compaction the upper surface of each thermal cycling specimen or prism is trowelled to as smooth a finish as possible.

Alternatively, a slab of epoxy resin mortar 40 mm in thickness may be cast and, after curing, sawn into beams measuring 40 mm square by 160 mm long for thermal contraction and strength testing.

A1.2.1 Thermal cycling test

After casting the thermal cycling specimens they are cured at 25°C for 21 days to allow all curing shrinkage to take place. The specimens are then placed in a refrigerator at 0°C for 8 hours, allowed to return to ambient temperature, placed in an oven at 50°C for 8 hours and again allowed to return to ambient temperature. The specimens are taken through 10 such cycles of cooling and heating.

The areas of mortar that have become disbonded from the glass can be observed through the glass to which the specimens are adhering. The disbonded areas are outlined using a marking pen and the perimeter of the specimen and the outlines of the disbonded areas are transfered onto tracing paper. The shape of the specimen is cut out of the tracing paper and this piece of paper weighed. The disbonded areas are then cut out and the paper is re-weighed. The loss of mass divided by the original mass represents the percentage of disbonded area.

A minimum of three specimens of each mortar should be tested and the results of all three tests reported.

A1.2.2 Measurement of bending strength and failure strain in bending

The prisms are supported on rollers over a span of 150 mm. One of the moulded sides of the beam should be placed in contact with the supporting rollers. A spreader beam with a pair of loading rollers having a spacing of 50 mm is placed symmetrically on the upper surface of the beam and a dial gauge graduated to 0,01 mm is arranged so as to record the mid-span deflection of the beam. (See Fig 2. The arrangement

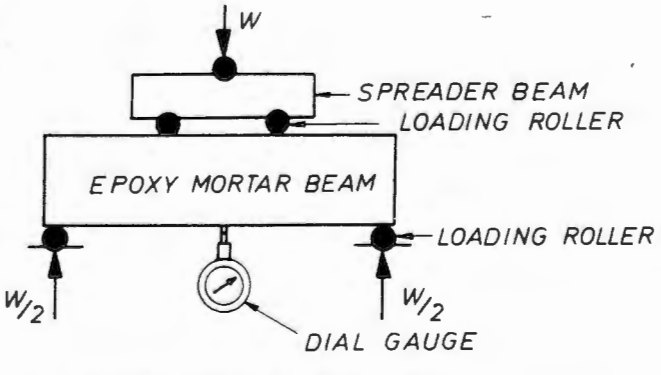

Fig 2: Loading arrangement – bending tests

of the dial gauge will differ depending on the testing system available.) The beam is then loaded to failure and the maximum load and the mid span deflection at maximum load recorded. The rate of loading should be adjusted to 5 000 kN per minute so that failure occurs within a period of 1,5 to 2 minutes. The bending strength of the beam is then calculated from the relationship

$$\sigma_b = 2{,}34 \times 10^{-3} W \text{ MPa}$$

where W is the failure load measured in Newtons.

The failure strain in bending is calculated from the relationship

$$\varepsilon_b = 0{,}71\delta \text{ per cent}$$

where δ = the mid span deflection of the beam at failure, in mm.

In this test, also, the bending strength and failure strain in bending should be measured on at least 5 specimens and the results of all 5 tests should be reported.

Appendix 2: Placement of epoxy resin mortar bridge nosings

A2.1 Preparation of joint

(a) The expansion joint in the concrete structure is located by chopping away the premix over the joint in three areas, ie one at each kerb and one in the centre.

(b) Once it has been established that the joint is straight, the desired width of premix to be removed is marked using a 3 mm nylon rope and white spray paint. Care must be taken to include the eventual expansion joint with the desired widths of the proposed nosings on either side of it.

(c) The premix is then cut right through to the concrete and removed.

(d) The exposed concrete is lightly bush-hammered to remove all premix primer and laitance and to expose the aggregate in the concrete. Care must be taken in this operation to prevent spalling of the concrete at the joint faces. An absolute minimum of the structural concrete must be removed in this operation. Any loose or cracked pieces resulting from spalling or other breakage should be removed prior to priming the area.

A2.2 Mixing of epoxy mortar

(a) Mixing is to be carried out strictly in accordance with the resin supplier's instructions. These instructions shall be clearly marked on all containers in which the pre-measured components of the mix are supplied.

(b) No hand mixing shall be allowed.

(c) Mixing machines shall be approved by the engineer and shall be specially suited to mixing epoxy resin mortars.

(d) The two parts of the epoxy resin are mixed to the manufacturer's instructions and then added to the aggregate in the mixer. A minimum mixing time of four minutes is required for adequate dispersal of the resin and thorough coating of the aggregate particles.

(e) While (d) is being carried out, the concrete surface which is to accept the mortar is cleaned of dust preferably by a jet of compressed air. Immediately before placing the mortar, a mixture of the activated resin is applied to the clean dry concrete surface as a primer. The primer must be fresh enough to adhere to the fingers when the mortar is placed on it.
Under no circumstances is the epoxy primer to be placed on a wet concrete surface.

A2.3 Placing of the mortar

(a) Where the joint former used in the construction of the bridge has been removed, rolled up paper is inserted into the expansion joint to prevent the mortar from falling into it. Where the ends of the nosing abut against the kerb or the concrete parapet walls of the bridge a strip of impregnated soft-board should be provided to prevent any bond developing between the epoxy mortar and the kerb or parapet.

(b) The mortar is now placed on the primed surface and compacted with a road stamper in layers of not less than 25 mm and not more than 50 mm. The compaction should be vigorous enough to compact the mortar but not so violent as to crush the aggregate.

(c) After placing and compaction the mortar is floated level with the premix surface with a steel floating trowel and left to cure.

(d) *As soon as the mortar has cured sufficiently to carry the weight of the cutting machine* (the mortar should have hardened sufficiently at this stage to ring when tapped with a hammer) a 6 mm cut is made down the centre line of the mortar for the full length of the joint. This cut must be *made to the full depth of the epoxy mortar and must be made on the same day as the mortar is placed* to allow overnight movement of the structure to occur without cracking the partly cured mortar. Alternatively, a strip of hard-board may be placed down the centreline of the nosing to act as a bond-breaker between the two halves of the nosing. In this case care must be taken that there is no difference in level of the epoxy mortar on either side of the bond-breaker strip. The mortar is now left to cure overnight.

(e) *On the following day* the expansion joint in the mortar is cut to the specified width and the material in the joint space is removed.

(f) *Also on the following day* 6 mm transverse cuts are made in the

epoxy mortar nosing starting from the centre of the roadway and at a spacing not exceeding 2 m.

(g) The specified neoprene seal is installed with a neoprene adhesive which is applied to the joint surfaces as well as the seal. Under no circumstances is the seal to be stretched during installation.

(h) For joint spaces of up to 35 mm in width it is recommended that the seals be installed with their upper surfaces 6 mm below the riding surface whereas joints with spaces in excess of 35 mm should have the seals installed with their upper surfaces 12 mm below the riding surface.

(i) Before the contractor leaves the site the nosing should be tested for soundness of bond to the underlying concrete by lightly tapping with a hammer. A clear sharp ring indicates good bond whereas a dull hollow ring indicates the presence of disbonding.

A2.4 Sampling of mortar

A sample of the epoxy resin mortar should be taken for check testing in the laboratory. Ideally, beam moulds of the same dimensions as those used for laboratory testing (see A1.2 above) should be used. If not available, 100 mm or preferably 150 mm cube moulds may be used. A minimum of two beam samples or one cube sample of mortar should be taken from the material used for each nosing. After compacting the mortar into the mould or moulds the sample should (if possible) be stored on the bridge, adjacent to the nosing from which it was taken, for a period of 24 hours so that it experiences similar early curing conditions. After stripping the moulds, samples should be sent to the laboratory for testing.

The tests to be carried out will consist of:

(a) A comparison of the density of the field-mixed and compacted mortar with that of the laboratory specimens (see 4.5 above)

(b) The bending strength (4.3 above) and failure strain in bending (4.4 above) should be measured either on moulded beams or on beam specimens cut from test cubes.

(i) If 100 mm cubes have been taken, beam specimens measuring 40 mm by 40 mm by 100 mm long can be cut from them and tested in bending with a central point load over a span of 90 mm.

(ii) If 150 mm cubes have been used, beam specimens measuring 40 mm by 40 mm by 150 mm long can be cut from them and tested in bending over a span of 140 mm with a symmetrical pair of point loads spaced 50 mm apart.

(iii) For (i) above $\sigma_b = 2{,}11 \times 10^{-3}\ W$MPa

$$\varepsilon_b = 1{,}98\delta \text{ per cent}$$

For (ii) above $\sigma_b = 2{,}11 \times 10^{-3}\ W$MPa

$$\varepsilon_b = 0{,}82\delta \text{ per cent}$$

Where W is the measured load at failure and$\delta$is the midspan deflection at failure: W is measured in Newtons andδin mm.

Notices

Innovation in industry

This will be the theme of a conference organized by SEIFSA and the CSIR in Pretoria on 25 and 26 February 1981. The aim of the conference is the promotion of research and development and innovation in the steel and engineering industry in South Africa.

All enquiries should be addressed to The Symposium Secretariat S. 233, CSIR, P O Box 395, Pretoria, 0001

Water supply and drainage services in developing countries

This CIB seminar, organized by the NBRI, will be held at the CSIR in Pretoria from 30 September to 2 October 1980. Further information from the NBRI at tel (012) 86-9211 x 3868.

Tunnelling '82

The British Institution of Mining and Metallurgy, with the co-operation of the British Tunnelling Society, the Institution of Mining Engineers and the Transport and Road Research Laboratory, will hold the third international symposium, Tunnelling '82, at the Metropole Hotel, Brighton, England, from 7 to 11 June 1982. An associated exhibition will feature plant, equipment, material processes and ancillary services for all types of tunnelling and underground excavation.

Papers are invited on practical developments in safety, technology and cost-effectiveness of all types of tunnelling. The programme of technical sessions will include the following principal topics:

Methods and machines – shields, full-face boring machines, drilling and blasting methods
Geotechnical topics – site investigation, dewatering, grouting, freezing, lining and support, ground stability and practical measurements
Services – planning and surveying, contractual and legal aspects, ventilation, safety and health
Complete projects – tunnels for mining and civil engineering purposes worldwide

Abstracts (250 – 300 words) should be submitted to the Secretary, The Institution of Mining and Metallurgy, 44 Portland Place, London, W1N 4BR, England, before 1 November 1980. Completed manuscripts of approved papers will be required in November 1981. Further information is available from the South African member of the Organizing Committee, A A T Wilson, Keeve Steyn and Partners, 26th Floor, Durban Bay House, 333 Smith Street, Durban.

Konferensie oor ingenieursmannekragontwikkeling in die RSA vir die 21ste eeu

Een van die grootste uitdagings waarmee die Republiek te kampe het en in toenemende mate gaan hê, is dié van werkverskaffing aan 'n snelgroeiende bevolking. Dit is seker die belangrikste vereiste vir vreedsame ontwikkeling in ons veelvolkige land. Die tegnologie kan hierin onteenseglik 'n belangrike en trouens onmisbare bydrae lewer.

Om te besin oor hierdie bydrae en die optimale voorsiening, seleksie, opleiding en benutting van die nodige tegnologiese mannekrag word 'n konferensie gereël deur die FVPI in samewerking met die Universiteit van Pretoria en die Ingenieursafdeling van die SA Akademie vir Wetenskap en Kuns. Die konferensie sal gehou word by die Universiteit van Pretoria van 4 tot 7 November 1980. Dit sal deel uitmaak van die halfeeufeesviering van die Universiteit van Pretoria en die kwarteeufeesviering van die universiteit se Fakulteit van Ingenieurswese. Ses sessies word beoog:

1. Die paradoks van toenemende ongeskoolde werkloosheid en gelyktydig 'n toenemende tekort aan opgeleide werkers en die totale strategie nodig om die probleem die hoof te bied.
2. Die rol wat tegnologie kan speel in die totale strategie om werkloosheid binne perke te hou, die behoefte aan opgeleide tegnologiese mannekrag en die opleidingsfasiliteite wat nodig is.
3. Akademiese opleiding van blanke ingenieurstegnoloë en tegnici.
4. Opleiding en benutting van ingenieursmannekrag in die praktyk.
5. Opleiding van nie-blanke tegnologiese mannekrag, in diens, by nywerheidsopleidingsentra, by tegnikons en universiteite.
6. Voorligting vir en keuring van tegnologiese mannekrag: die inligting en toetse ter beskikking van skoliere en skoolverlaters om hulle te help met die keuse van hulle hoër skoolvakke en loopbane.

Die reëlingskomitee vertrou dat sinvolle voorstelle vir implimentering uit die konferensie sal vloei, tov:

1. Die voorsiening van 'n gebalanseerde tegnologiese mannekraggarde van ingenieurstegnoloë, tegnici, ambags- en ander geskoolde werksmanne om in die land se behoeftes te voldoen.
2. Beter voorligting aan skoliere en skoolverlaters.
3. Die doeltreffende opleiding van leerlinge en studente vir die verskillende funksies.
4. Die benutting van opgeleides.

Verdere inligting kan verkry word van Mev M Cronjé, Wenningstraat 37, Groenkloof, 0181 Pretoria (Tel 012-78 3719).

Field Test of Catenary Net to Protect Traffic from Mining Subsidence

By Geoffrey Blight,[1] Member, ASCE, and Andrew Barrett[2]

(Reviewed by the Highway Division)

Abstract: It is often necessary to construct roads across areas that have been undermined at shallow depth or that are subject to surface subsidence from other causes. Surface subsidences can be bridged by incorporating a continuous steel net into the road structure. If a subsidence occurs, the net will form a catenary over the void and allow vehicles to pass safely. The paper describe the requirements for the design of such a catenary net and reports on the results of a near full-size field test. The design depends for its safety on the use of ductile annealed steel for the net and is intrinsically safe, as an increase in the sag of the net reduces the forces it has to carry. The field test showed that theoretical expectations can be realized in practice. It is concluded that on the basis of the field test a prototype catenary-supported road can be constructed.

Introduction

There are many areas in the world where mining, especially for coal, has taken place at depths as shallow as 10–15 m or less below surface. The areas may be extensive, or may only constitute a relatively narrow band along the outcrop of a reef. Both conditions exist in the Witwatersrand area of South Africa, where rich coal deposits overlie even richer deposits of gold. In the central Witwatersrand area, mining of the shallow gold and coal took place 80–100 years ago. There is now growing pressure to extend urban and industrial development over these shallowly undermined areas.

There are many different ways of stabilizing ground undermined at shallow depth. One method is to fill the voids with mine tailings or pulverized fuel ash [e.g., Blight (1984), Healy and Head (1984), and Stacey (1983)], another is to drill into the void, place explosives down the holes, and blast out the supporting pillars, thus filling the void with bulked broken material [e.g., Braithwaite and Cole (1986)]. A third method, particularly applicable to the protection of isolated buildings or roads crossing undermined areas, is illustrated in Fig. 1. A layer of welded steel mesh is incorporated into the road structure or into a foundation raft for a building. If a sinkhole forms as a result of collapse of a pillar or of progressive collapse of the roof of the old workings, the mesh is designed to act as a catenary safety net, as indicated by Fig. 1. This method has previously been considered by Parry (1983).

Full-Scale Design

An opportunity has recently arisen to design a road supported on the catenary net principle. The road will cross an area undermined for coal where

[1]Prof. of Constr. Materials, Univ. of the Witwatersrand, Johannesburg, P.O. WITS, 2050, South Africa.

[2]Partner, Steffen Robertson and Kirsten, Inc., P.O. Box 8856, Johannesburg 2000, South Africa.

Note. Discussion open until August 1, 1990. To extend the closing date one month, a written request must be filed with the ASCE Manager of Journals. The manuscript for this paper was submitted for review and possible publication on December 16, 1988. This paper is part of the ***Journal of Transportation Engineering***, Vol. 116, No. 2, March/April, 1990. ©ASCE, ISSN 0733-947X/90/0002-0135/$1.00 + $.15 per page. Paper No. 24414.

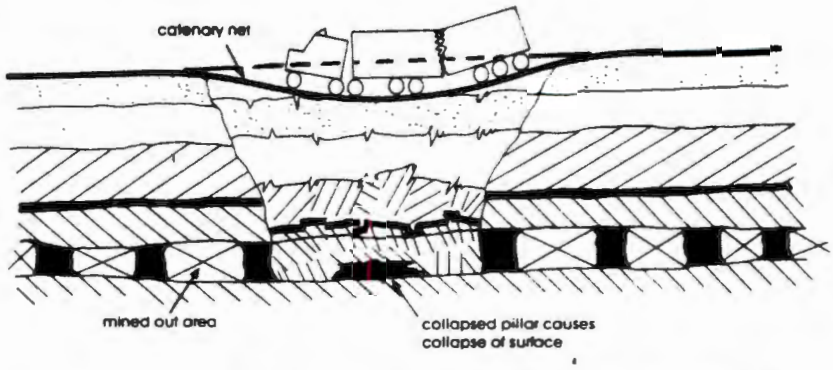

FIG. 1. Principal of Catenary Net to Protect Traffic on Road Crossing Undermined Area

several sinkholes and surface subsidences have occurred in recent years. The road has been designed to carry 200 equivalent 80-kN (8-ton) axle loads per day with an annual growth of 8%, giving a total design traffic of 3,200,000 equivalent 80-kN axle loads over the 20-year design life. The pavement has been designed conventionally and will have the section shown in Fig. 2. The catenary net will be incorporated in the 300-mm-thick cement-stabilized subbase. The cement stabilization is intended to have the double function of improving the load-bearing properties and elastic modulus of the subbase and protecting the weldmesh from corrosion. Stabilization will be by means of 5% of ordinary Portland cement which, tests show, will provide a California bearing ratio (CBR) of 100%. Eades tests have shown that a 5% cement addition will ensure a pH of 11.7 that is sufficiently high to passivate the steel against corrosion.

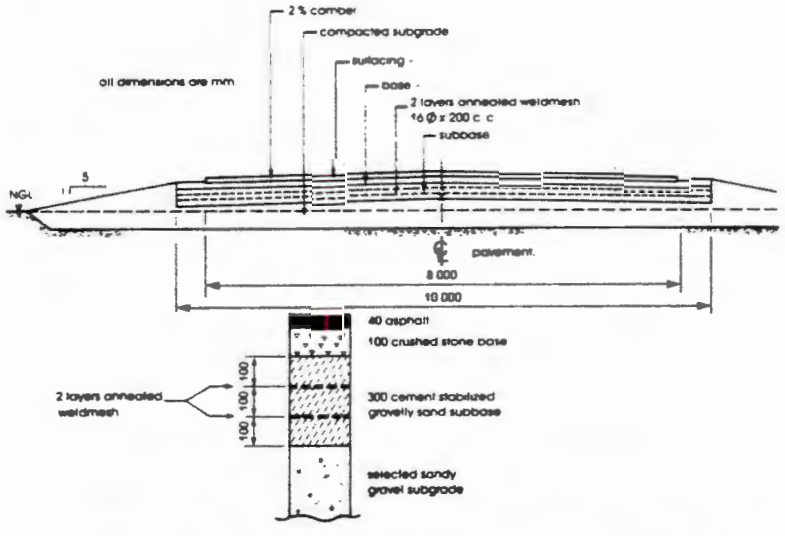

FIG. 2. Section through Road Incorporating Catenary Net

The catenary net will consist of a double layer of annealed weldmesh with individual sheets lap-welded together so as to form an integral continuous net. The bar diameter for the mesh will be 16 mm and the bar spacing 200 mm. The weld mesh will be annealed after welding so as to heat-treat the welds and improve the ductility of the mesh. The elongation at failure for the weld mesh over a 200-mm gauge length is 15% before annealing and failure invariably takes place at a welded node. After annealing, the elongation at failure varies from 35 to 45% with a mean yield stress of 255 MPa (37,000 psi) and an ultimate tensile strength of 315 MPa (45,000 psi). The failures occur randomly, seldom at a welded node. The average permanent elongation after failure over an original length of 1 m is 26%.

Tests on 100-mm-long lap joints welded from the top only, showed that failure always occurs away from the lap. Hence the lapped welds do not weaken the mesh.

The design of the catenary net caters for the possible formation of a 10-m-diameter circular void occurring under the roadway. Under this circumstance, the net can carry a superimposed load of 6.6 kPa (140 psf) over the entire 10-m-diameter area at a steel stress of 230 MPa (33,000 psi). This is equivalent to a total load of 518 kN or 50 tons.

If the load is concentrated towards the center of the collapsed area, the mesh may yield. However, the maximum depth of coal removed in mining is 2-1/2 m in this area. The mesh can sag by 3.2 m before attaining an average elongation of 26%. Hence, if a sinkhole occurs, the load will at worst be gently let down to rest on the bottom of the sinkhole. At best, it will roll across the depression in the road surface and continue safely on its way. Before constructing the first prototype catenary supported road, it was decided to test the concept by carrying out a near–full-scale trial. This experiment and its results will be described next.

Reasons for Choosing Steel Catenary Net System

Consideration was given to two possible systems for spanning the surface cavity formed by a sinkhole.

In the "slab system," the road structure and any traffic loads would be supported by means of a reinforced soil-cement beam or slab that would span any sinkhole that might form up to a preselected design diameter. This system would carry its loads in bending. The system would be reasonably efficient, in that load support would arise from a combination of compression in the soil cement and tension in the reinforcement. However, it would have the disadvantage of initially being a rigid system.

Voids of up to a certain size could form below the reinforced layer without being detected from the surface. If the void subsequently enlarged sufficiently, a combination of a heavy vehicle load and a critical span could cause the slab to fail. Once the slab had failed, the reinforced layer would act as a catenary membrane with a reduced load-carrying capacity.

In the catenary net system, the net of reinforcing is incorporated into the road structure at approximately the neutral axis for bending. If a cavity should form under the road surface, the road structure would span the cavity until it failed as an unreinforced slab. This should occur for voids of quite small span, probably less than 2 m. The surface depression arising from such a failure would be evidence of the cavity underneath, and steps could be taken

to fill in the hole and repair the road surface. Provided the cavity did not develop to a diameter that exceeded the failure diameter for the design load, a safe situation would exist until remedial measures could be taken.

A number of materials was considered as candidates for the catenary net. Polymeric materials were eventually rejected because of their low elastic modulus and doubts as to their long-term durability when buried in soil. The only viable alternative material is steel. This also has the disadvantage of having a limited life when buried in soil. However, it is intended always to incorporate the steel net into a layer of cement-stabilized soil where the high pH environment will protect against corrosion by the same mechanism that protects the steel in reinforced concrete.

Because loads and spans are difficult to estimate in this application, annealed mild steel weldmesh will be used to given an additional margin of safety to the design.

Construction of Experiment

Rather than search for a real mining cavity with which to experiment, a simulated cavity of 6 m span was created. This was done as illustrated in Fig. 3. A hole measuring 6 m^2 in plan, and 4-m deep was excavated and

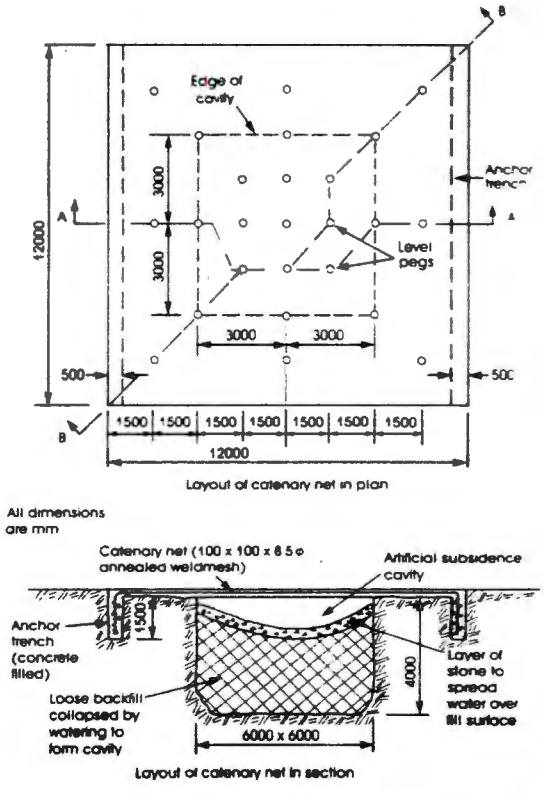

FIG. 3. Layout of Field Experiment in Plan and Section

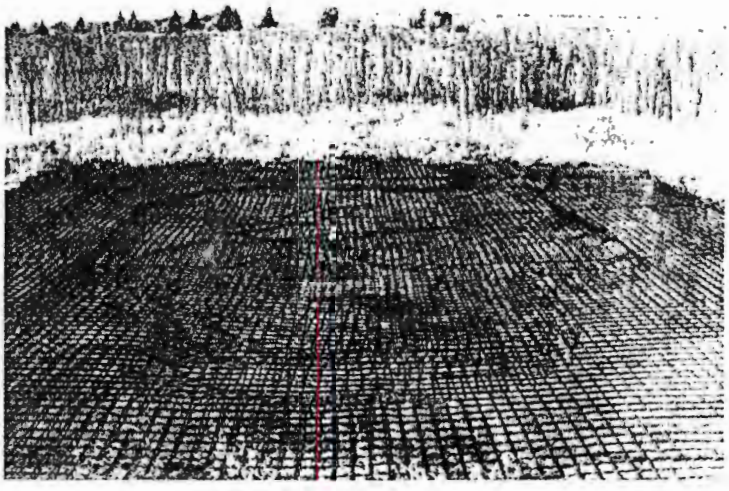

FIG. 4(*a*). Surface Depression Caused under Catenary Net by Collapse-Settlement of Fill

then loosely backfilled to within 400 mm of the ground surface. After leveling the surface of the backfill, a 200-mm-thick layer of concrete-aggregate was placed on it. This was followed by a 100-mm thick layer of cement-stabilized soil. A pair of anchor trenches was then excavated parallel to one pair of sides of the hole. A 100-mm^2 mesh formed of 8.5-mm-diameter bars was used. This was too heavy for the purpose, but was the only annealed weldmesh that could be obtained at the time. The annealed weldmesh was laid out with one opposite pair of edges turned down into the anchor trenches, which were then backfilled with concrete. The direction at right angles to the anchor trenches represented the direction of the continuous catenary-supported roadway that was being modeled. After welding and anchoring the steel net, a 100-mm cover layer of soil-element was placed.

The loose backfill in the hole was settled by cutting holes through the cement-stabilized soil layer and flooding the backfill from a water tanker. The layer of concrete stone assisted in distributing the water over the surface of the backfill. The resultant void under the slab was 400–500-mm deep. The experiment was now ready for load testing.

Fig. 4(*a*) shows subsidence under the catenary net that occurred after heavy unseasonal rains had saturated the backfill in the hole and caused the surface to collapse prematurely. This shows the extent and nature of the artificial surface subsidence. After this had occurred the net had to be cut away, the hole was reexcavated and the construction of the experiment was repeated.

Fig. 4(*b*) shows the cavity produced under the catenary-supported slab by collapsing the backfill of the reinstated experiment. The cavity was 450–500-mm deep.

Load Tests

The set of level pegs at the surface of the soil cement slab was leveled

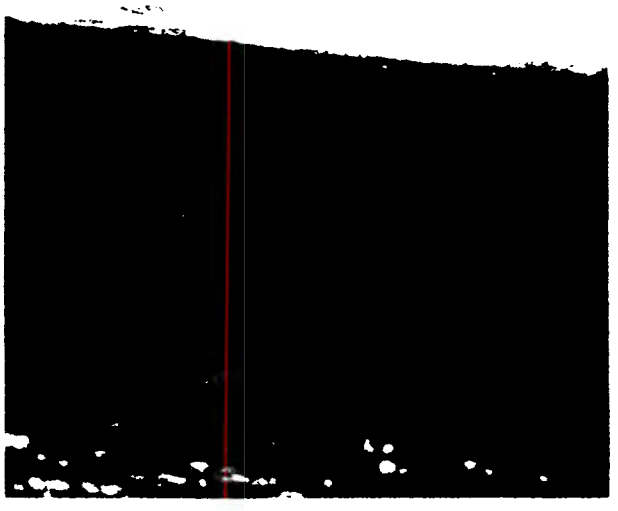

FIG. 4(*b*). Cavity under Catenary Net; Light Area above is Catenary Supported Roof; Dark Area below is Collapsed Top of Fill

to determine the shape of the catenary-supported slab under its self-weight. A light truck was then driven onto the slab as a preliminary test and the leveling repeated.

A twin-axle truck with a rear axle load of 64 kN was then reversed onto the slab. The long axis of the truck was orientated at right angles to the anchor trenches and the rear dual wheels were stopped at the midspan of the catenary net. Thus the loading on the catenary net consisted of the 100-mm layer of surfacing material, plus 64 kN. The surface of the net was leveled again while the truck was in place, and residual deflections were recorded once the load had been removed. This procedure was repeated with a truck having a rear axle load of 81 kN.

Not all of the surface points on the catenary net could be observed while

the trucks were in place as certain of the pegs were under the vehicles. In the cases of both the 64- and 81-kN loads, a check was made to ensure that the underside of the net had not bottomed on the backfill in the hole. In both cases there was a clear 150 mm between the underside of the net and the top of the backfill.

Analysis of Results

The results of the load tests have been recorded in Fig. 5 in the form of level profiles for the catenary slab. The line of the profiles AA and BB is shown in plan in Fig. 3.

The tension T in a catenary net of width a spanning a distance L in one direction only is given approximately by:

$$T = \frac{(W + waL)L}{4\delta} \qquad (1)$$

in which w is the uniformly distributed load carried by the net, W is the concentrated load, δ is the midspan sag (and waL is small compared with W). The greatest difficulty in designing a catenary net lies in estimating the value of δ. Clearly, other things being equal, the larger δ becomes, the smaller T will be. The approach that has been adopted so far, is to calculate the value of δ corresponding to yield stress in the steel and then calculate the corresponding value of $(W + waL)$ and hence, by comparing with the design load to be carried, to establish the load factor for the net.

In the present case, the sag δ corresponding to yield of the catenary net is 300 mm, which quite by chance equals the actual maximum measured sag. For the mesh used in the load test, the value of $(W + waL)$ at yield

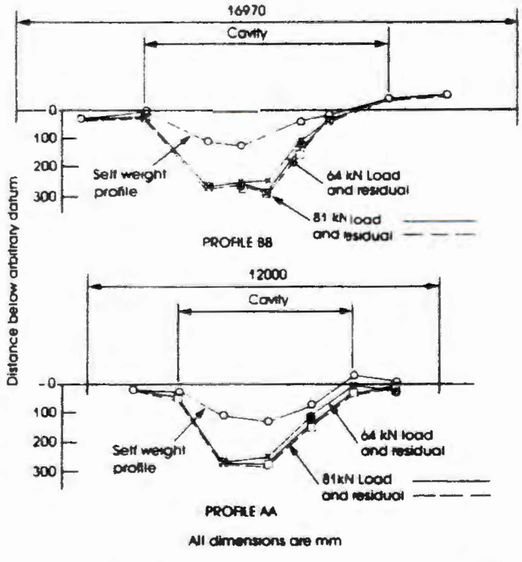

FIG. 5. Profiles A-A and B-B of Catenary Net under Load

FIG. 6. 81-kN Axle Load Supported over Cavity by Catenary Net

would have been 723 kN as compared with an actual load of 110 kN. Hence the load factor was 6.6.

Note that for both the 64- and 81-kN loads, the profile under load and the profile of residual deflection were almost the same, and the maximum deflections for the two loads were not very different (270 and 300 mm, respectively). The maximum stress in the net under the 81-kN load was only 38 MPa (5,500 psi), whereas the yield stress was 250 MPa (36,000 psi) and that under the 64-kN load was 36 MPa (5,200 psi). Hence the movement of the net arose almost entirely from irreversible sources such as yielding of the anchor trenches, compression of the edges of the hole, and straightening of the steel forming the net. As the original estimate of the midspan sag of the net cannot take these additional sources of sag into account, the estimated load carrying capacity of the net will always be conservative.

Fig. 6 shows the catenary net successfully supporting an axle load at midspan of 81 kN.

Effect on Vehicle Driving into Catenary Net-Supported Depression

If a vehicle were to drive through a depression spanned by a catenary net, it would be subject to: (1) Downward acceleration as its wheels entered the dip; and (2) upward acceleration as it emerged on the opposite side.

The downward acceleration cannot exceed 1 g, but the upward acceleration would depend on the speed of the vehicle, the maximum sag of the net, and the distance over which the vehicle would climb out of that sag.

A complicating factor would be that the net itself would change shape as the wheels rolled across it. An approximate analysis is given by:

$$f = \left(\frac{v^2}{l}\right)\delta \quad \ldots\ldots (2)$$

in which f = the vertically upward acceleration of the vehicle; v = the constant velocity of the vehicle in a horizontal direction; l = the distance over which the vehicle climbs out of the depression; and δ = the depth of depression climbed out of over distance l.

This expression shows that the vertical acceleration can be severe and is approximately 2.5 g at a speed of 50 km/h (31 mph) and 10 g at a speed of 100 km/h (62 mph). These accelerations would, of course, be of short duration (0.1 s at 50 km/h and 0.05 s at 100 km/h). Because of the springing of the vehicle, the driver and any passengers would be subjected to less acceleration than the vehicle.

To place these accelerations into perspective, a human blacks out if subjected to a sustained acceleration of at least 8 g. Passengers in commercial aircraft are often subjected to short-term accelerations of 2 g without adverse effects. An acceleration of 8 g can be tolerated without ill effects if it is of short duration (less than 0.50 s).

The answer to the acceleration problem appears to lie in placing a permanent speed restriction of, say, 60 km/h (40 mph) on any road crossing undermined ground. This would limit accelerations to not much more than 2.5 g for durations less than 0.1 s. This level of acceleration should be tolerable to both driver and vehicle.

Conclusions

The load test on the experimental catenary net has shown the following:

1. Steel catenary nets can be used to support vehicles crossing surface cavities arising from mining subsidence.
2. Almost all of the sagging deflection of the net in the case of the experiment resulted from sources other than the extension of the net under load. These extraneous sources of sag increase the margin of safety of the net for carrying load.
3. The acceleration to which a vehicle crossing a depression in a catenary net will be subjected will not be excessive provided speeds are limited to about 60 km/h.

On the basis of this successful field test, construction of the prototype catenary-supported road can proceed.

Acknowledgments

The design and experiment were sponsored by the East Rand Metropolitan Transport Area and the City Council of Springs. The authors thank these bodies for permission to publish the note.

Appendix I. References

Blight, G. E. (1984). "Soil mechanics principles in underground mining." *J. Geotech. Engrg. Div.*, ASCE, 110(5), 567–581.
Braithwaite, P. A., and Cole, J. W. (1986). "Subsurface investigations of abandoned

limestone workings in the West Midlands of England by use of remote sensors." *Trans.*, Institute of Mining and Metallurgy, Section A, 95, 181–190.
Healy, P. R., and Head, J. M. (1984). "Construction over abandoned mine workings." *Special Publication 32*, Constr. Industry Res. and Information Association, United Kingdom.
Parry, H. J. (1983). "Coping with Fife's mining industrial heritage." *Municipal Engineer*, London, England, 110(7/8), 231–240.
Stacey, T. R. (1983). "Railway development over undermined area at Witbank." *Engineering geology of Southern Africa*, A. B. A. Brink, ed., Building Publications, Pretoria, Republic of South Africa, 145–147.

Appendix II. Notation

The following symbols are used in this paper:

- a = width of catenary net;
- f = vertically upward acceleration;
- L = span of catenary net;
- l = distance over which vehicle climbs out of depression;
- T = tension in catenary net;
- v = velocity of vehicle in horizontal direction;
- W = concentrated load;
- w = uniformly distributed load; and
- δ = midspan sag of catenary net.

INTERACTIONS SOLS-STRUCTURES

SOIL STRUCTURE INTERACTIONS

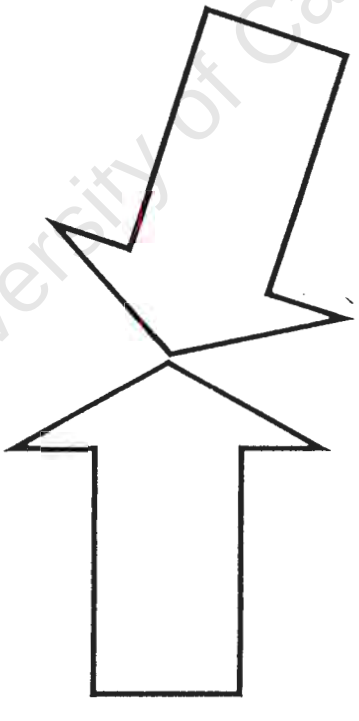

Actes du colloque organisé par
l'Ecole Nationale des Ponts et Chaussées
Paris, 5-7 mai 1987

Presses de l'école nationale des Ponts et chaussées

PROCEEDINGS OF THE NINTH EUROPEAN CONFERENCE ON SOIL MECHANICS AND FOUNDATION ENGINEERING
DUBLIN / 31 AUGUST-3 SEPTEMBER 1987

GROUNDWATER EFFECTS IN GEOTECHNICAL ENGINEERING

Editors
E.T.HANRAHAN, T.L.L.ORR & T.F.WIDDIS

OFFPRINT

A.A.BALKEMA / ROTTERDAM / BROOKFIELD / 1987

Lowering of the groundwater table by deep-rooted vegetation – The geotechnical effects of water table recovery

Abaissement de la nappe phréatique par la végétation à racines profondes – Les effets géotechniques du relèvement de la nappe

G.E.BLIGHT, University of the Witwatersrand, Johannesburg, RSA

SYNOPSIS: It has been found that deep-rooted trees such as eucalyptus species growing in semi-arid environments, may depress the water table in their immediate vicinity by many metres. When planted as a forest, the water table may be severely depressed over an extensive area. When the trees are removed, as a prelude to building development, the water table starts to recover. Swelling of the soil resulting from the decrease in effective stress in the soil profile as the water rises, may cause serious damage to structures. The paper will describe four case histories of such occurrences in South Africa and identify procedures for predicting the rate of recovery of the water table and the quantity and rate of heave of the soil profile.

INTRODUCTION

Desiccation caused by trees

If the supply of water is not limiting, water losses from the surface of extensive treed areas may exceed evaporation losses from a water surface under comparable climatic conditions (Penman, 1963). If the water supply is limiting, trees will continue to extract moisture over the depth of their root zone until their wilting point is reached. This corresponds to a soil suction of about 1500kPa although it is known that some trees and plants can continue extracting water from the soil at suctions greater than this.

Even at the wilting point, the work required for roots to extract water from the soil is only about 2J/g of water extracted whereas 2500J/g is required to evaporate water from the leaves of a tree. Hence if the evaporative energy is available, the extractive energy is easily supplied.

It is also known that trees are capable of extending their root systems in search of water. To quote Penman (1963) "If root development is such that the roots can continue to grow downwards in pursuit of a retreating water table, it will be possible to lower the water table permanently, provided that the mean annual transpiration is a little greater from the deep-rooted vegetation than that of any shallow-rooted vegetation it has replaced: and in silty soils of high specific yield "little" need be only a few millimetres per year".

This situation - depression of the water table over an extensive area - is difficult to recognize in a conventional site investigation. If the investigation covers only a small area, the water table depth will be reasonably uniform over the site. Even though the desiccation caused by the trees may be identified and noted as such, the potential problems associated with

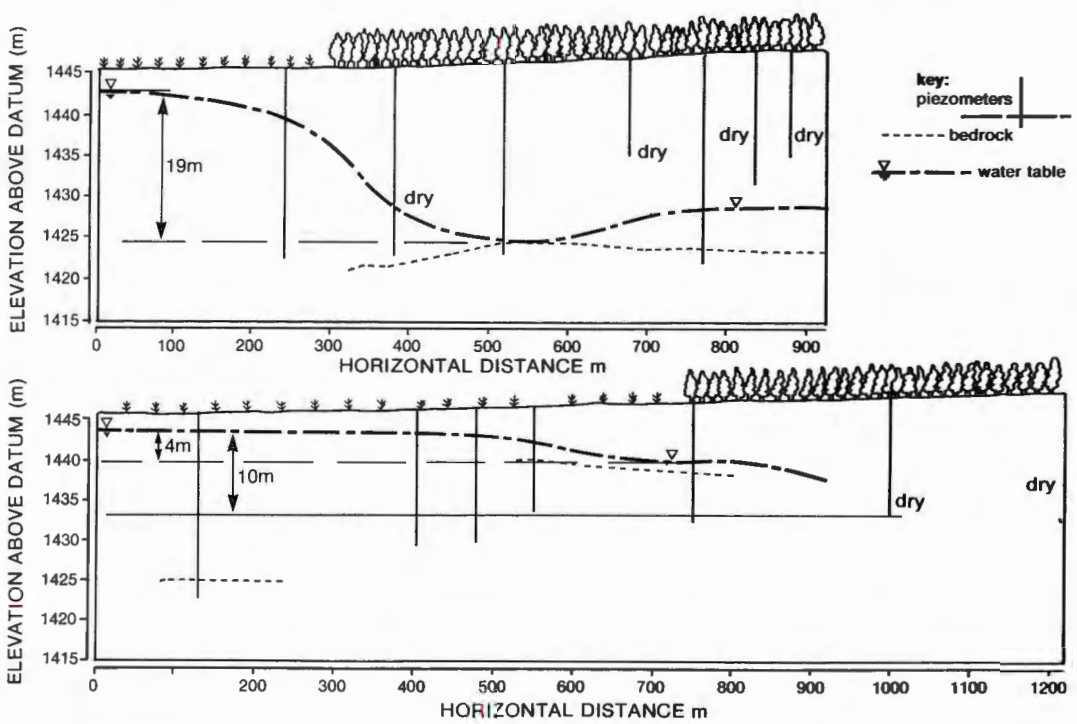

Figure 1. Examples of water table depression caused by eucalyptus trees in an area having an average annual precipitation of 650mm

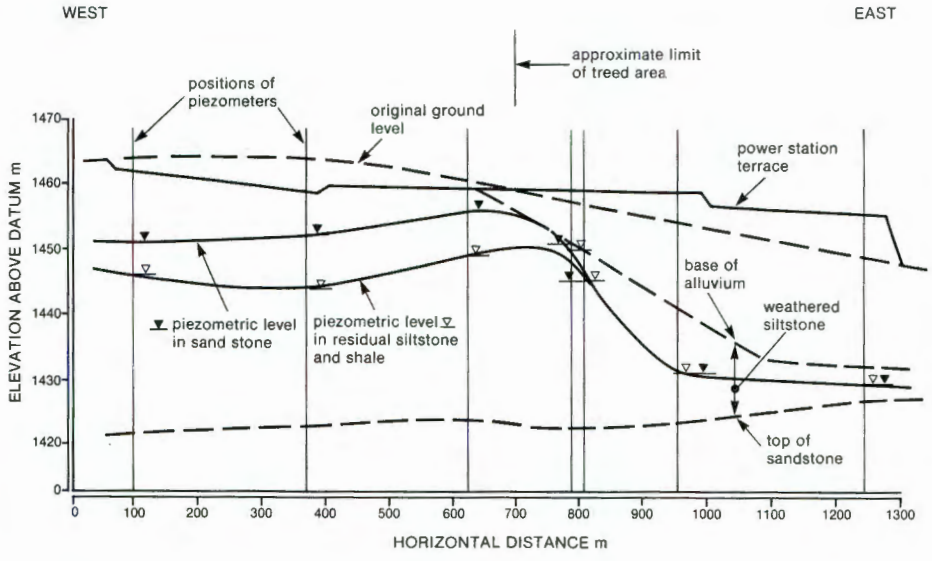

Figure 2. East-West section through power station site showing depression of water table under area formerly covered by trees.

a depressed water table may not be realized. Only if the site investigation extends beyond the limits of the treed area and a gradient in the water table is revealed, will the depression caused by the trees become evident.

EXAMPLES OF WATER TABLES DEPRESSED BY TREES

Figure 1 shows two examples of water-tables observed under treed areas and adjoining cultivated (but not irrigated) land. In both cases the trees were eucalypts and the adjoining fields were used to grow maize in summer and lay fallow in winter.

The upper diagram shows an astonishing water table depression of 19m while the lower diagram shows a depression of at least 10m.

Figure 2 shows groundwater conditions under a power station site which, prior to terracing, had been partly covered by a eucalyptus plantation. Under the treed zone the water table has been depressed by upwards of 20m. Live tree roots have been found in pile holes down to a depth of 15m below natural ground level. It is possible that hair roots extend to an even greater depth.

In another case, less well documented, the water table rose, after felling a eucalypt plantation, by at least 13m over a period of 15 years. At this site tree roots were observed to have penetrated to a depth of 27m below surface (Wolpert, 1952).

Among trees grown commercially in South Africa, eucalypt species appear to be particularly thirsty. Henrici (1946) for instance, quoted a rate of transpiration of 500ℓ/day for a eucalypus tree (Eucalyptus macarthuri), while black wattle (Acacia mollissima) transpired at 250ℓ/day and a typical grass (Themeda) at 1ℓ per m^2 per day. The size of the trees observed by Henrici is unknown. If the canopies are assumed to have covered a diameter of 5 to 6m, the rate of transpiration of the eucalypt would have been about 20ℓ per m^2 per day while that of the wattle would have been 10ℓ per m^2 per day, ie rates of transpiration of 10 to 20 times that from grassland.

PROBLEMS ASSOCIATED WITH A DEPRESSED WATER TABLE

Problems do not arise from the water table depression itself, but from the fact that if the trees are partially or completely felled over an extensive area in order to accommodate an alternative land use, eg a housing or industrial estate or a power station, the water table will inevitably rise with time, as illustrated by the fourth example above. Not only will heave associated with the relief of desiccation occur, but the entire cleared area will heave as the effective stress is reduced at all depths in the profile. The situation is illustrated by the pore pressure and suction profiles in Figure 3.

These profiles represent conditions under a treed surface and subsequently when the trees have been felled and the ground water has come to a new equilibrium with a different land use.

ad represents the suction in the root zone of the trees

bd represents the hydrostatic suction profile over the depressed water table, and

ce the hydrostatic suction profile in equilibrium with the recovered water table.

Dimension 1 represents the suction that would be relieved if the trees were felled and the water table remained in its depressed position.

Dimension 2 represents the suction that would be relieved as the water table rose to its new equilibrium position.

If one were calculating the amount of heave for the profile on the basis of a static water table, the calculated heave would correspond to a decrease of suction = suction 1, whereas if the potential rise of the water table were recognized, one would calculate the heave corresponding to a decrease of suction = (suction 1 + suction 2).

What is particularly insidious about this situation is that the rise in water table reduces the effective stress over the whole depth of the soil profile, above and below the depressed position of the water table.

Hence not only is the depth to which expansion occurs unexpectedly large, but the initial position of the water table no longer represents a level below which expansion will not occur. Hence, for example, tension piles anchored below the level of the depressed water table will heave as they will not be anchored in stable material.

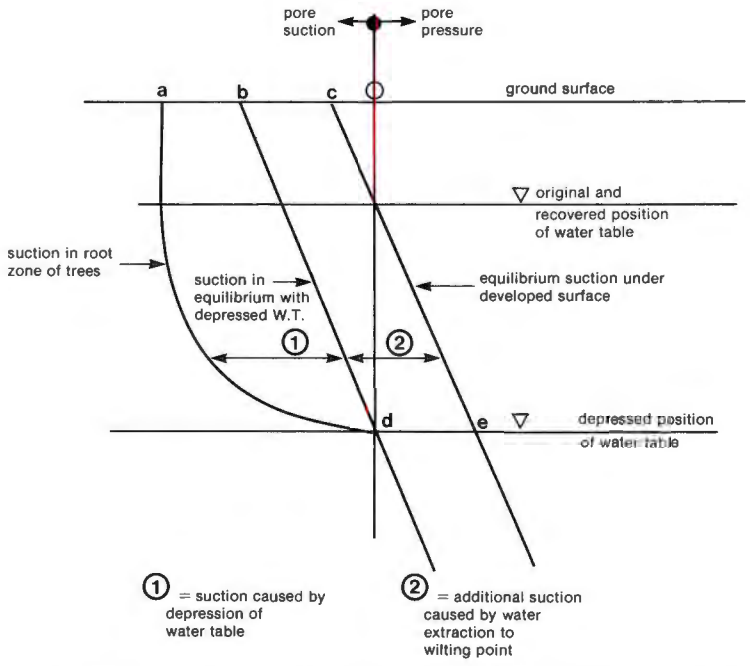

Figure 3. Suction and pore pressure profiles illustrating the effects of recovery of a depressed water table.

CALCULATION OF THE EFFECTS OF RECOVERY OF A DEPRESSED WATER TABLE

The quantity of heave likely to occur as the water table rises to its new equilibrium position can be calculated from the compressibility characteristics of the soil, the initial effective stress profile and the expected change of effective stress as the water table recovers.

The initial effective stress profile may be estimated from measurements of swelling pressure. The compressibility characteristics may be represented by, for example, the swelling index C_s, ie the slope of the void ratio versus log (effective stress) rebound line in an oedometer test on the saturated soil.

It is difficult to estimate the final equilibrium position of the recovered water table, as this will depend on the character of the new land use. However, if evidence (such as that shown in Figure 1) is available as to the depth of the "undisturbed" water table, this will serve as a valuable guide to the estimation of the equilibrium water table position.

The quantity of heave is important, but the time over which it will occur may be equally so. The relationship between time and heave for a structure such as a road or an isolated building over a stable water table can be calculated by assuming boundary conditions and applying the theory of water flow in soils (eg Blight, 1965).

This method breaks down when considering the heave of an extensive area such as that of an industrial township or a power station. In cases like this, the only feasible approach seems to be to calculate a water balance for the site and hence to estimate the rate at which water will accumulate in the profile. Hence the "rate model" usually used for problems of this type must be replaced by a "capacity model".

If the water is deep (as it will be if considering a depressed water table), the contribution to the accumulation of water in the profile from the water table itself will be negligible. The major component of recharge must be the net infiltration (ie infiltration minus evapotranspiration losses) into the soil through the ground surface.

Water recharging the profile from the surface

$$Vs/V = \frac{\Delta e_s}{1+e}$$

$$Va/V = \frac{e\,(1-S)}{1+e}$$

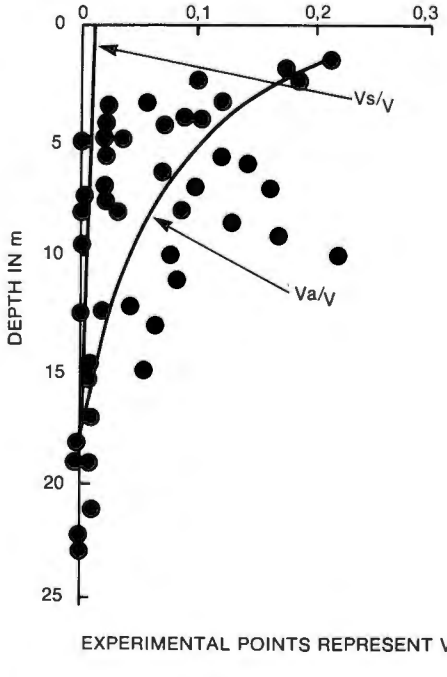

Figure 4. Profile of void space available for recharge in a residual mudstone profile.

is assumed to do so in the form of a sharply defined wetting front (eg Morgenstern and de Matos 1975). The time taken for the recharge to occur can be assessed by calculating the time necessary for the available recharge to fill:

(a) air-filled pore space in the profile above the water table; and

(b) additional void space created by swelling.

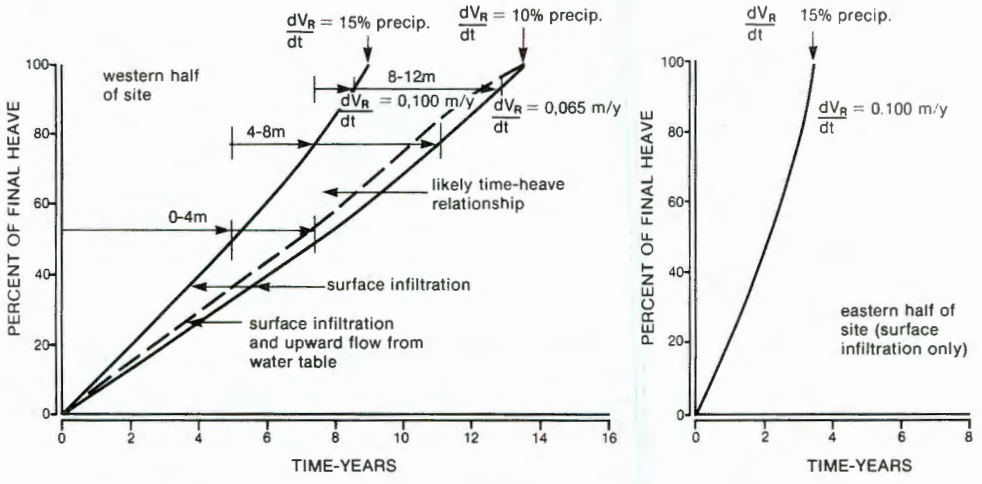

Figure 5. Predicted time-heave curves for power station site shown in Figure 2.

The air-filled void space per unit volume of soil is given by

$$\frac{V_a}{V} = \frac{e(1-S)}{1+e} \qquad (1)$$

The additional void space resulting from swell is

$$\frac{Vs}{V} = \frac{\Delta e_s}{1+e} \qquad (2)$$

In which V_a = volume of air-filled pore space;
V_s = void space resulting from swell;
V = volume of soil;
e = void ratio;
Δe_s = increase in void ratio resulting from swell;
and S = degree of pore space saturation.

Figure 4 shows typical profiles of V_a/V and Vs/V for the residual mudstone profile at the site illustrated in Figure 2. It will be seen from Figure 4 that the contribution of V_s/V is very small and when one considers the scatter of measured values of Va/V, neglect of Vs/V is justifiable.

The time taken for the available recharge to fill the available void space is calculated by dividing the available void space by the recharge rate, ie

$$\text{time to fill pore space} = \frac{\text{Available space}}{\text{Recharge rate}}$$

$$\text{or } t = \frac{Va/_V + Vs/_V}{1/_V \cdot dV_R/_{dt}} \qquad (3)$$

in which $\frac{dV_R}{dt}$ is the rate of recharge estimated from the water balance model.

To calculate the time-heave curve, the profile is subdivided into horizons and the time taken to recharge each horizon is calculated together with the contribution to heave of that horizon. Typical time-heave curves calculated on this basis are given for the site shown in Figure 2 in Figure 5.

It will be noted that the major portion of the heave occurs from the surface downwards. In the case of any isolated structure on the surface, heave will have to occur by lateral flow from adjacent recharged soil. Hence the heave of such a structure will usually occur more slowly than that of the area as a whole.

Once the profile has been recharged, the water table will rise very quickly to its final equilibrium position. Figure 5 also indicates the uncertainty attached to estimating dV_R/dt from a water balance model when the rate of recharge is unknown with any great precision.

CONCLUSION

This paper illustrated how the water table under an extensive treed area can become depressed and how the depression may be difficult to identify during the course of a site investigation. The effects of recovery of the water table once the trees have been felled have been described and a method given for calculating the distribution of heave in time as the soil water is recharged.

REFERENCES

Blight, G.E. 1965. The Time-Rate of Heave of Structures on Expansive Soils. Moisture Equilibria and Moisture Changes in Soils Beneath Covered Areas. Butterworth, Australia, p.33-67.

Henrici, M. 1947. Transpiration of South African plant associations. Science Bulletins Nos.247 and 248, Department of Agriculture and Forestry, Pretoria, South Africa.

Morgenstern, N.R. & M de Matos 1975. Stability of Slopes in Residual Soils. Proceedings, Fifth Pan American Conference on Soil Mechanics and Foundation Engineering. Buenos Aires, Vol.3, p.369-384.

Penman, H.L. 1963. Vegetation and Hydrology. Technical Communication No.53, Commonwealth Bureau of Soils. Harpenden, U.K.

Wolpert, L. 1952. The direct measurement of the natural moisture content of unsaturated soils. N.B.R.I. Bulletin No.9. C.S.I.R. Pretoria, South Africa.

Hanrahan, E.T., T.L.L.Orr & T.F.Widdis (eds.) 90 6191 720 4
Groundwater effects in geotechnical engineering – *Proceedings of the ninth European conference on soil mechanics and foundation engineering, Dublin, 31.08 – 03.09.1987*
Les actions de l'eau souterraine en géotechnique – *Comptes-rendus du neuvième congrès de mécanique des sols et des travaux de fondations, Dublin, 31.08 – 03.09.1987*
1987–88, 30 cm, 3 vols, c.1300 pp., Hfl.520 / $265.00 / £156
Field & laboratory testing; Special problem soils; Groundwater problems in embankments, dams & natural slopes; Groundwater in foundations & excavations; Environmental problems & seepage; Groundwater modelling; Groundwater control; Dynamic effects. About 220 contributions.

FROM THE SAME PUBLISHER

Rathmayer, H.G. & K.H.O.Saari (eds.) 90 6191 240 7
Improvement of ground – *Proceedings of the eighth European conference on soil mechanics and foundation engineering, Helsinki, 23–26 May 1983*
1983–84, 30 cm, 1398 pp., 3 vols., Hfl.520 / $265.00 / £156
In-situ testing for design & control of ground improvement; Soil grouting; Deep compaction; Laboratory testing for design & control of ground improvement; Soil reinforcement; Speeding up of consolidation; Improvement of special soils; Soil improvement under water; Soil stabilization. 400 papers. Editors: Technical Research Centre of Finland, Espoo.

List of members 1986 90 6191 585 6
International Society for Soil Mechanics & Foundation Engineering
1986, 22 cm, 250 pp., paper, Hfl.75 / $38.50 / £22.50
About 16000 addresses. Addresses or selections are also available on Cheshire or on self adhesive lables at Hfl.12 per 100.

90 6191 560 0
Proceedings of the 11th international conference on soil mechanics and foundation engineering – *San Francisco, 12–16 August 1985* / **Comptes-rendus du 11ème congrès international de mécanique des sols et des travaux de fondations** – *San Francisco, 12–16 août 1985*
1985–87, 28 cm, c.3700 pp., 5 vols., Hfl.1250 / £375
The most important conference on soil mechanics & foundation engineering, held every 4 years. *Soil mechanics: Property characterization & analysis procedures:* Constitutive relationships for soil behavior; Numerical methods; Decision theory & probability. *New developments in field & laboratory testing of soils:* In-situ testing techniques; Centrifuge testing & its application; Laboratory testing; New procedures & data acquisition techniques; Field instrumentation & field measurements. *Geotechnical aspects of environmental control:* Ground water modelling & soil-waste interaction; Seepage control; Tailing dams. *Piles & other deep foundations:* Pile foundation design-methods; Pier foundations; Foundations for offshore structures. *Geotechnical engineered construction:* Influence of earthwork construction on structures; Earth strengthening; Applications of geotextiles. *Evaluating seismic risk in engineering practice:* Seismic geology & risk analysis; Seismic safety of earth structures. *Stability of natural deposits during earthquakes:* Soil liquefaction; Seismic stability in natural slopes. *Comparison of prediction & performance of earth structures:* Earth & rockfill dams; Excavation support; Foundations; Non-technical constraints on engineering practice. *Geological aspects of geotechnical engineering:* Earth dam engineering; Problems in areas with special geological conditions.

90 6191 566 X
Proceedings of the 11th international conference on soil mechanics and foundation engineering – *San Francisco, 12–16 August 1985* Golden jubilee volume
1985, 28 cm, 168 pp., Hfl.65 / $20.00 / £19.50
The history of geotechnical engineering until 1700 (J. Kerisel); A history of soil properties, 1717-1927 (A.W.Skempton); The last 60 years (R.B.Peck); The first Terzaghi Oration: Amuay landslides (T.William Lambe). (Also in French).

90 6191 210 5
Soil mechanics and foundation engineering – *Proceedings of the 10th international conference on soil mechanics and foundation engineering, Stockholm 15–19 June 1981*
Mécanique des sols et des travaux de fondations – *Comptes-rendus du 10ème congrès internationale de mécanique des sols et des travaux de fondations, Stockholm, 15–19 juin 1981*
1981–82, 28 cm, 3542 pp., 4 vols., Hfl.1250 / $640.00 / £375
Papers are selected & reviewed by the national societies of ISSMFE. *Prediction & performance:* Accuracy of prediction & its determination, application of probability & decision theory design, factors governing the performance of buildings & other structures; *Tunnelling in soils:* Case records, effects of different excavation/construction techniques, new calculation methods, mapping & control systems; *Ground water & seepage problems:* Prediction & measurement of ground water conditions & flow, internal erosion & piping, hydraulic fracturing, etc., control of ground water, effects of changes in ground water level; *Laboratory testing:* Relevance of laboratory soil testing methods, standardization of laboratory tests for practical application; new laboratory testing methods; model tests.

Kerisel, Jean 90 6191 688 7
Down to earth – *Foundations past and present: The invisible art of the builder*
1987, 28 cm, 162 pp., 52 photos, Hfl.60 / $29.50 / £18
Written in a straightforward non-technical language, with numerous diagrams & photographs, the book takes a look at 'the invisible art' of the great builders; how they founded their constructions in the earth & strove to understand & combat the natural forces. Many examples are used to illustrate various aspects of this long battle. The final part of the book looks into the future & discusses the threats to a number of great cities & the attempts to counter them. Author: Former President of the Intl. Society for Soil Mechanics & Foundation Engineering.

Ramiah, B.K. & L.L.Chickanagappa (eds.) 90 6191 404 3
Soil mechanics and foundation engineering
(Indian edition series, 3) (No rights India)
1986, 25 cm, 706 pp., Hfl.50 / $25.50 / £15
Handbook for students & practising engineers. Engineering properties of soils; Properties of rocks; Stress distribution & deformation; Earth pressures & retaining structures; Shallow foundations; Deep foundations; Stability of natural slopes & embankments; Earth dams; Ground water & seepage; Vibration of foundation; Subsoil exploration; References; Index.

Pells, P.J.N., A.Mac G.Robertson & J.A.Caldwell (eds.)
0 86961 085 6
Soil mechanics and foundation engineering – *Proceedings of the 6th regional conference for Africa, Durban, 1975*
1975–76, 28 cm, 628 pp., 2 vols., Hfl.275 / $140.00 / £82.50
Engineering geology & geomorphology; Properties of soils & construction materials; Engineering in rock; Embankments.

All books available from your bookseller or directly from the publisher:
A.A.Balkema, P.O.Box 1675, NL-3000 BR Rotterdam, Netherlands
A.A.Balkema Publishers, Old Post Road, Brookfield, VT 05036, USA

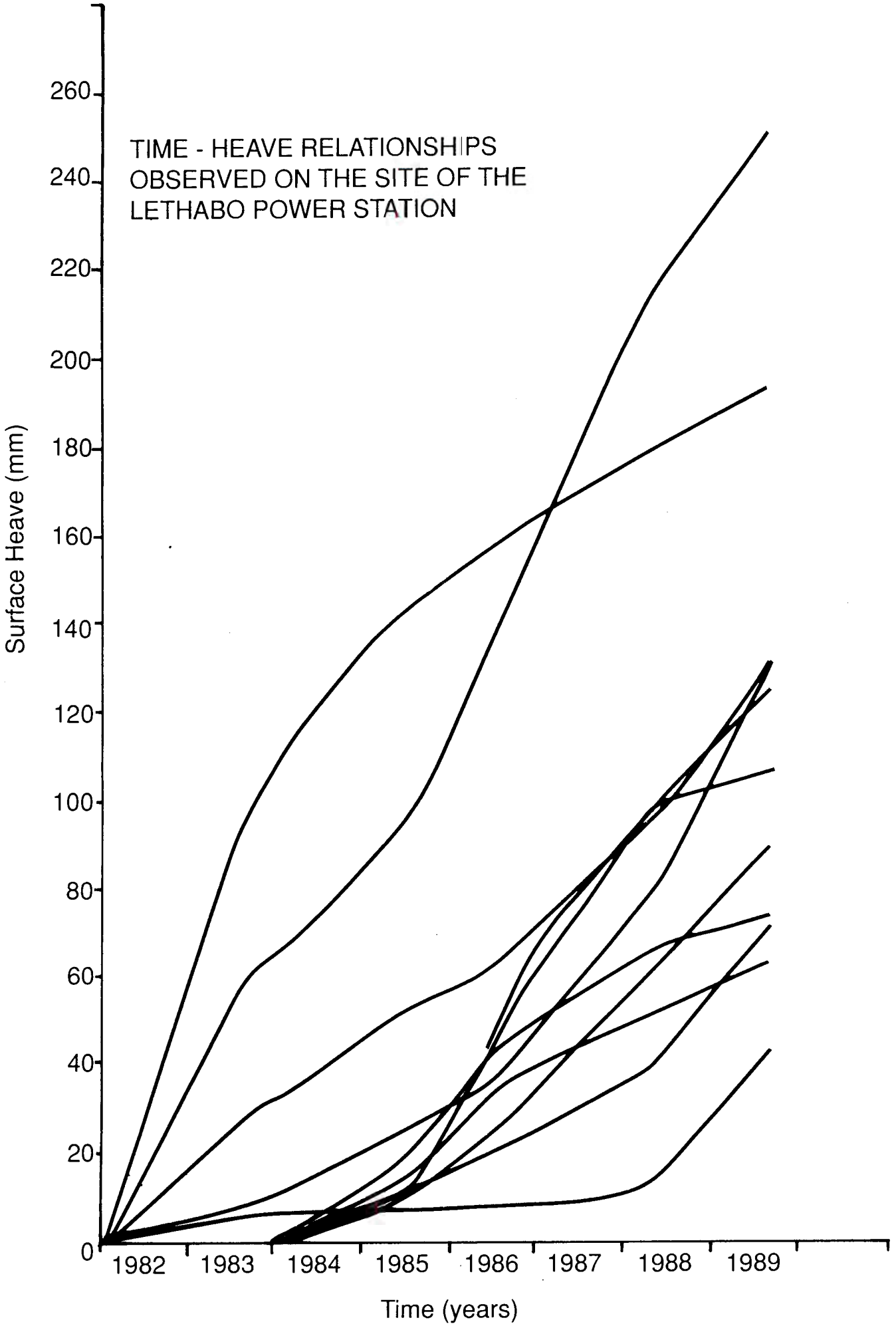
TIME - HEAVE RELATIONSHIPS
OBSERVED ON THE SITE OF THE
LETHABO POWER STATION
Surface Heave (mm)
0
20
40
60
80
100
120
140
160
180
200
220
240
260
1982
1983
1984
1985
1986
1987
1988
1989
Time (years)

TEXAS TECH
UNIVERSITY
DEPARTMENT OF CIVIL ENGINEERING
Box 4089 • Lubbock, Texas 79409-1023
Telephone (806) 742-3523 • Fax (806) 742-3488

December 20, 1991

G.E. Blight
University of the Witwatersrand
P O Wits
Johannesburg - 2050
South Africa

Dear Mr. Blight:

The paper which you submitted for the 7th International Conference on Expansive Soils entitled:

"Preheaving of Expansive Soils by Flooding-Failures and Successes"

has been peer-reviewed and I am pleased to inform you that the paper has been accepted for publication in the conference proceedings without any changes. If your paper has a co-author, I would appreciate it if you would inform your co-author(s) of the paper's acceptance.

The second bulletin for the conference will be mailed in February, 1992. The bulletin will include the conference schedule and will indicate when you are to present your paper. Good visual aids make a technical presentation successful. This is particularly important at an international conference where English (the conference language) is a second language for many of the attendees. Overhead projectors and 35mm slide projectors will be available for all presentations. Please try to make your projection material conform with the enclosed visual aid preparation recommendations.

Specific information on hotel arrangements, conference registration, planned social activities, and information on things to do and see in Dallas and Fort Worth will be forwarded to you at the time the 2nd conference bulletin is mailed. As always, if you have questions on any aspect of the conference, please contact me. I am looking forward to the conference and to meeting you.

Sincerely yours,

Warren K. Wray

Warren K. Wray, Ph.D., P.E.
Chairman, Conference Organizing Committee

Encl: Visual Aids Guide

WKW:jh

PREHEAVING OF EXPANSIVE SOILS BY FLOODING - FAILURES AND SUCCESSES

G.E. BLIGHT, K. SCHWARTZ, H. WEBER and B.L. WIID
Witwatersrand University, Private Bag 3, Wits, 2050, Johannesburg, South Africa

7th INTERNATIONAL CONFERENCE ON EXPANSIVE SOILS

DALLAS, TEXAS (USA)
AUGUST 3 - 5, 1992

SUMMARY: The technique of pre-heaving a site by flooding the soil with water was first applied nearly 40 years ago. Since then it has not proved a very popular measure. However, six case studies show that if the fundamental mechanics of preheaving are understood, and if the technique is applied correctly, with adequate monitoring, it can be very successful. The technique can be used both to precondition a site for new construction, or be applied as a remedial measure to structures damaged by differential heave movement.

1. INTRODUCTION

It became apparent, in the early 1950's, that heave of a covered surface occurs because of gradual moisture accumulation in a previously desiccated underlying soil profile. Preheaving of expansive soil by pre-construction flooding then became an obvious candidate solution to the problem of founding on expansive soils. Because of the low permeability of most expansive soils, early attempts to implement preheaving were not entirely successful. For example, Dawson (1959) flooded the 1.5m deep foundation trenches for a building on expansive clay in Texas. After four months of flooding, only limited penetration of water into the soil was found. McDowell (1959) attempted to preheave highway formations in Texas by surface flooding, but reported that water contents had increased to a depth of only 1200mm after a month of flooding. However, in a later paper, McDowell (1965) showed that changes of water content had actually occurred down to a depth of 6m, while quite major changes had occurred to 3.4m.

A large-scale field experiment, started in 1957 and reported by Blight and de Wet in 1965, was successful in demonstrating the essential requirements for effective preheaving by flooding, as well as illustrating the mechanism of preheaving. de Wet, who conceived the experiment, recognized that the only simple way to accelerate the penetration of water into an impervious soil is to reduce the length of the maximum flow path. In the experiment, this was achieved by drilling a grid of vertical holes to facilitate the entry of water into the soil by horizontal radial flow. By this means, de Wet was able to induce almost full heave of a 7.5m deep expansive clay profile within 3 months. This demonstrated that preheaving by flooding can be a practical pre-construction procedure. Later work by Williams (1980) showed that flooding can also be used as a remedial measure.

Preheaving by flooding does have two potential practical drawbacks. These are:

(i) The time necessary to achieve substantially full heave of a profile is of the order of two to three months, even if a grid of holes is used to accelerate entry of water into the soil. Careful planning is required to enable a period as long as this to be included at the start of the construction schedule.

(ii) At the end of flooding the soil surface is soft, muddy and untrafficable. To provide immediate access to the site a pioneer layer consisting of a geofabric separation layer covered by a layer of crushed rock, clinker or similar free-draining, highly frictional material must be provided. Alternatively, a working platform of lime stabilized soil can be constructed (eg McDowell, 1959). Possibly because of these disadvantages, flooding has not become a popular method of dealing with expansive soils.

2. CHARACTERISTICS OF THE PREHEAVING PROCESS

Figure 1 (from Blight and de Wet) illustrates the changes in effective stress that occur during and after the preheaving process:
In the virgin desiccated profile the pore water pressure at depth z is u_o (point a in Figure 1a). u_o is in dynamic equilibrium with the water table at depth h below the surface. The corresponding point on an effective stress versus movement relationship (Figure 1b) would be A. At the end of flooding a temporary perched water table has been established at the ground surface and the pore water pressure is u_f (point d in Figure 1a). The surface has heaved and the effective stress has been reduced Point B in Figure 1b describes the state of the soil in terms of effective stress and heave. When the soil surface is covered by the structure, the profile will contain an excess of moisture which will gradually drain away until static equilibrium is established with the permanent water table. The pore water pressure will then be u_s (point b in Figure 1a). The effective stress will have increased somewhat, and the surface will have settled, bringing the soil to point C in Figure 1b. The effects of the surface loading imposed by the structure (ef in Figure 1a) will be to increase the effective stress further and cause further settlement to take place to point D in Figure 1b.

Figure 2 shows the time-heave-settlement curve observed in the de Wet experiment:
Flooding was maintained for 96 days, after which period the surface of the test area was covered by a concrete slab. Heave was observed to continue for a further year, after which a slow settlement commenced. After 7.5 years the settlement had virtually ceased. In this particular case, post-flooding settlement amounted to about 20 per cent of maximum heave. It is likely that post-flooding

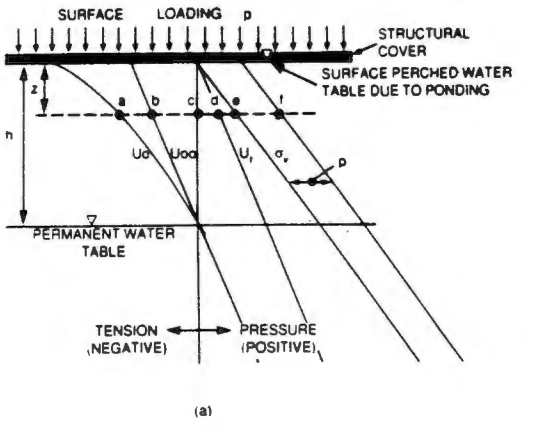

(a)

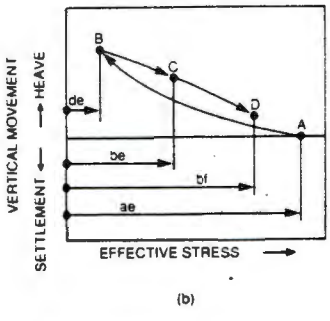

(b)

Figure 1(a) Changes in pore pressure and total stress during flooding of a profile
(b) Changes in effective stress and vertical movement.

settlement will be more in cases where the permanent water table is deeper or the superimposed loading is greater. It would appear that particular care is necessary not to plant any deep-rooted vegetation with a high evapo-transpiration requirement (eg eucalyptus or poplar trees) near to the preheaved area. By re-desiccating the soil and causing localized settlement, such plantings could be disastrous for a light structure founded at the surface of a pre-heaved area. The broken curve superimposed on Figure 2 shows the time-heave curve for a house constructed on the same heaving profile. Here, heave occurred by gradual seasonal accumulation of moisture under the house. A comparison of this curve with the experimental time-heave curve shows the marked acceleration of the heave process that can be brought about by flooding.

3. OTHER EXAMPLES OF ACCELERATING HEAVE BY FLOODING

As stated earlier, the process of accelerating heave by flooding has not become very widely used. Apart from early experiments in the United States, the technique appears to have found most application in Southern Africa. Here, some attempts to apply the technique have resulted in dismal failures. On closer examination it has invariably been found that failure of the technique resulted from a lack of appreciation of the soil mechanics and the time involved in the process.

3.1 DOMESTIC HOUSING

A notable failure of the method occurred when four brick-built single storey houses were constructed on residual mudstone in the Odendaalsrust area of South Africa. The profile consisted of 0.5 to 1m of sandy surface soil overlying the expansive weathered mudstone. The site had formerly been covered by eucalyptus trees. This tree species is notorious for the deep and intense desiccation it is capable of causing. For example Blight and Lyell, 1984, reported drawdowns of the water table of up to 19m under eucalyptus plantations.

The engineer's specification for preheaving the site of each house read in part as follows:
"2. It is recommended that the desiccated clays over the area to be built on be first pre-expanded by means of drilling holes at approximately 3m centres into and through the topsoil down to the clay strata. These holes thereafter to be continuously filled with water for approximately 3 weeks or longer if possible."
"9. Only trees and shrubs with tap roots should be planted in the vicinity of the dwelling."

No monitoring of the heave was specified and none appears to have been carried out.

The houses were built on conventional strip footings and were completed and occupied between September and October of 1981. The first signs of distress were recorded in mid-December 1981. By January 1983 all four houses were damaged, two of them seriously.

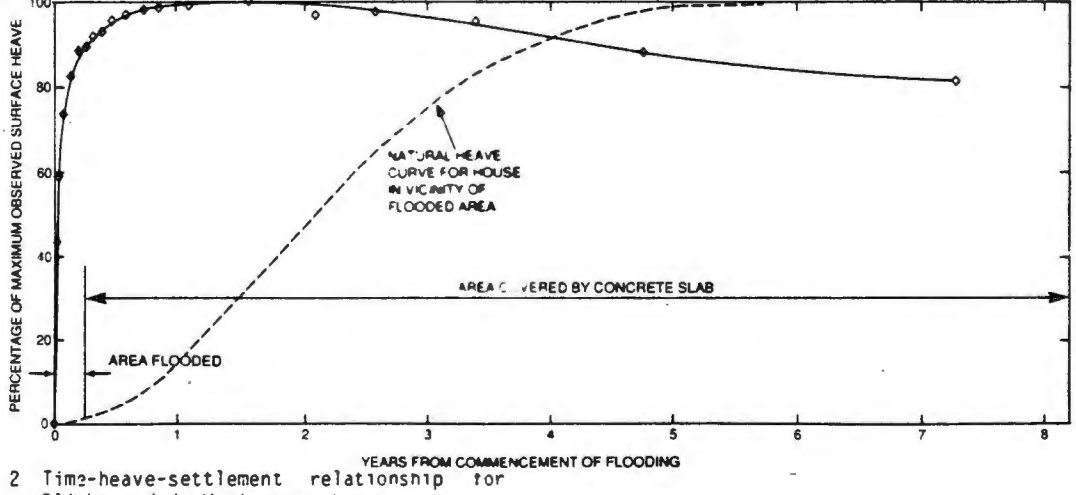

Figure 2 Time-heave-settlement relationship for Blight and de Wet's experiment

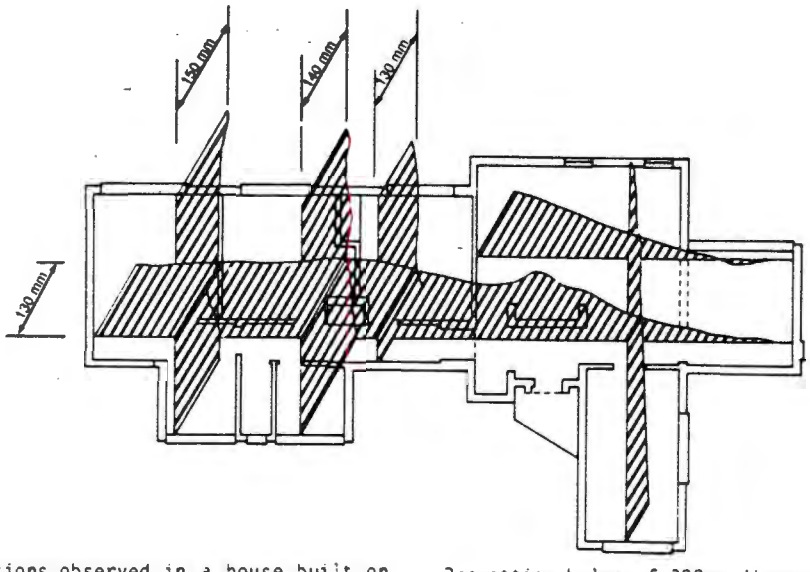

Figure 3 Distortions observed in a house built on a 'pre-expanded' site

Figure 3 shows the relative movement in January 1983 of the most seriously damaged house. The heave shown at the left hand side of the diagram was up to 150mm more than that of the right hand side. The differential movement was either caused or exacerbated by the presence of a large eucalyptus tree that had been left near the right hand side of the house to provide shade, and by leaking drains, broken by the heave movement, as well as a soak-away drain, at the left hand side.

It is fairly obvious that the procedure for flooding outlined by the engineer was quite inadequate, even if it was implemented to the letter. The flooding holes did not penetrate the expansive strata and the recommended procedure was tantamount to rather inefficiently flooding the sub-surface of the residual mudstone. The recommended period of flooding was much too short for significant pre-heaving of the expansive material to have occurred. The engineer also obviously did not understand the implication of allowing 'only trees and shrubs with tap roots' to be planted close to the house. Most plants that are capable of extracting water from soil against a high suction have tap roots. Indeed, the eucalyptus tree that assisted in causing the severe differential heave had a tap root system that probably extended 15m or more into the expansive soil.

This case history illustrates the great danger inherent in only half understanding an engineering concept, and then misapplying it.

3.2 SHOPPING COMPLEXES

The pre-heaving technique has been successfully applied in constructing a large shopping complex on expansive clay in the town of Vereeniging, South Africa. The soil profile consists of a thin surface layer of fill underlain by 1.5m to 2m of stiff, slickensided sandy clay alluvium. The alluvium in turn, rests on 9m to 10m of residual shale, weathered to a stiff, slickensided clayey silt. This overlies less weathered shale. The water table before flooding was at a depth of 11m.

The main structure was to be supported on piles, and the pre-heaving was intended to stabilize the soil underlying the slab-on-grade floors. Prewetting holes of 300mm diameter and 6m deep were drilled on a 3m grid with a wider spacing of 3.6m adjacent to main column grid-lines. The holes were filled with crushed rock to prevent them from collapsing.

Expansion of the soil was monitored by means of surface pegs and 4 multidepth extensometers. The extensometers enabled the progression of heave at various depths in the profile to be monitored. Flooding was maintained for a period of 2½ months between early June 1983 and late August 1983. Figure 4 shows available records of surface heave versus time, while Figure 5 shows profiles of heave recorded at the four extensometers shortly before flooding was terminated.

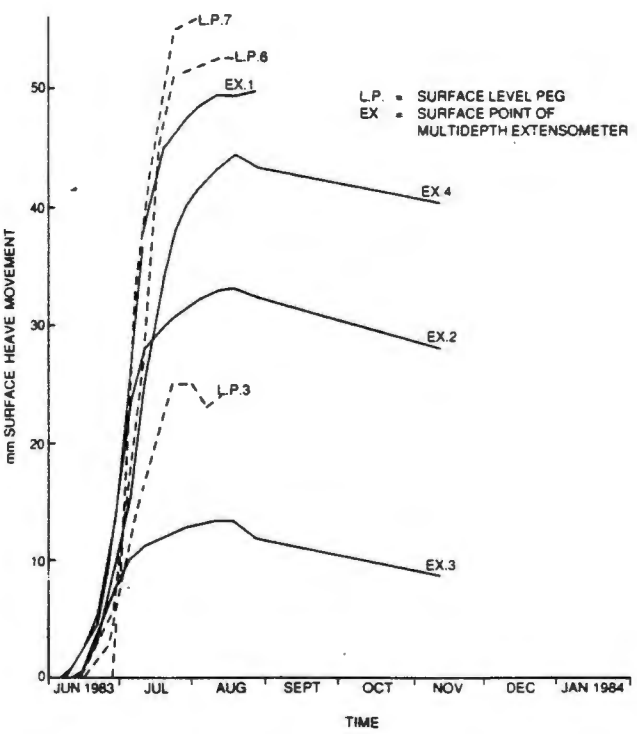

Figure 4 Time-surface heave relationships observed during flooding of the site for a shopping complex in Vereeniging, South Africa.

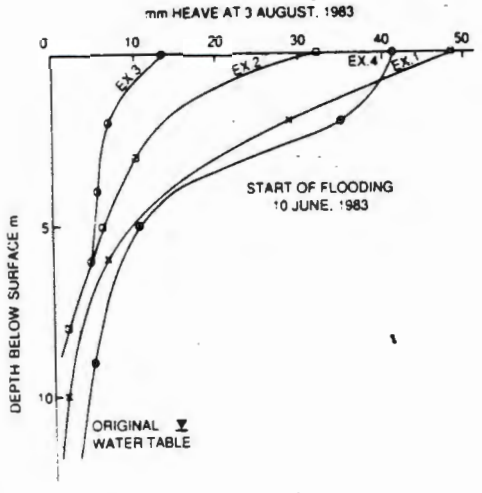

Figure 5 Heave-depth relationships after flooding of the site for a shopping complex in Vereeniging, South Africa.

The maximum recorded surface heave varied from 12mm to 55mm over the 11000m² area of the site. The time-heave curves given in Figure 4 show very similar features to those of the Blight and de Wet time-heave curve (Figure 2). Unfortunately, the surface pegs were destroyed once construction was started and the extensometers were destroyed shortly thereafter. By this time, the extensometer curves were showing a steady settlement as the excess water drained out of the soil.

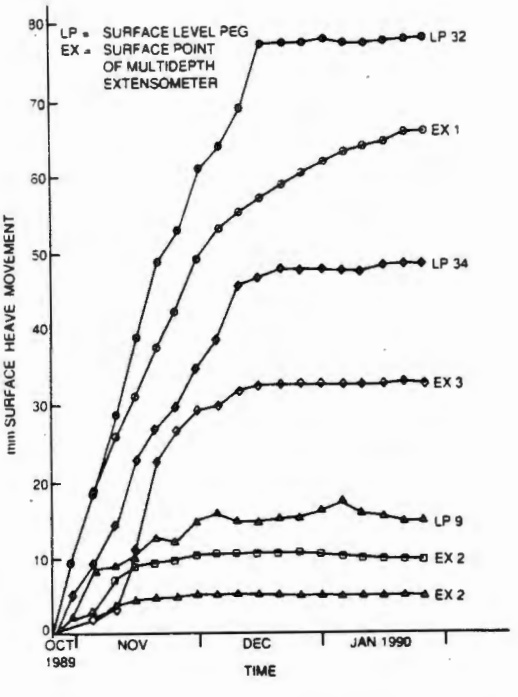

Figure 6 Time-surface heave relationships observed during flooding of the site for a shopping complex in Standerton, South Africa.

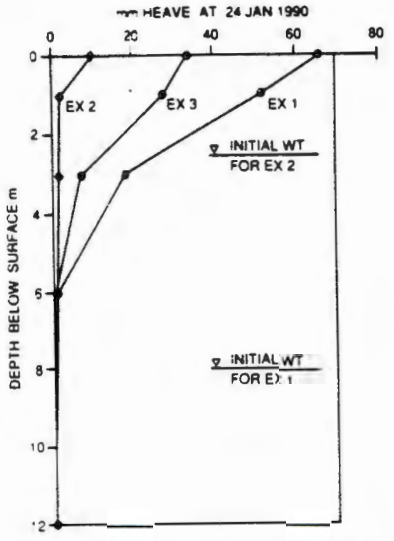

Figure 7 Heave-depth relationship after flooding of the site for a shopping complex in Standerton, South Africa.

Figure 5 shows the variation of heave with depth recorded by the four extensometers. These curves show that most of the heave took place within the upper 5m of the profile where desiccation should have been greatest. Unfortunately, no post-construction monitoring has been carried out on the structure. It is understood, however, that no problems of excessive settlement have been experienced and that the owners of the complex are satisfied with the result.

The pre-flooding technique was also used for a shopping complex in the town of Standerton, South Africa. The site was covered by 0.3m to 1.2m of fill underlain by transported soils to depths of 2.1m to 4.6m. The transported soils, in turn, rested on residual soils derived from the weathering of mudstones.

The transported soils consisted of firm to stiff silty clays and gravels of various colours which were slickensided and potentially expansive. The residual mudstone had weathered to a stiff, grey to black, silty to sandy clay with slickensides and occasional shattering (closely spaced open cracks). This was potentially expansive to highly expansive. The deepest test hole penetrated to 9.5m and the depth of the water table varied from 2.5m to 8.2m. Total heave movements of 55mm to 65mm were predicted on the basis of oedometer tests on undisturbed specimens from the profile.

Here also, the main structure of the shopping complex was to be supported on piles, while the pre- heaving was used to stabilize the soil underlying the slab-on-grade floors. The gravel-filled pre- wetting holes were 4m deep and spaced on a 4m square grid.

Figure 6 shows curves of surface heave versus time from the start of flooding for three multi-depth extensometers and three of the surface movement monitoring pegs. The diagram shows the wide range of surface heave values that were recorded on the site (10mm to 80mm) and also that full heave had occurred within 50 days of the start of flooding. Figure 7 shows the distribution of heave with depth, as recorded by the three multi-depth extensometers. Most of the heave at this site took place in the top 2m to 3m of the profile.

The shopping complex was subsequently successfully completed. Again, no post-construction monitoring figures are available, but the performance of the complex over the year-and-a-half since the end of flooding has been very satisfactory.

3.3 ACCELERATED HEAVING OF EXPERIMENTAL PILE SITE

Blight (1984a, 1984b) described a large scale experiment on a group of seven anchored tension piles. The piles were all 1050mm diameter and 33m long. They were installed in a profile of residual siltstone that has weathered to a stiff fissured clayey silt. The water table before flooding was at a depth of 14m.

The object of the experiment was to measure the uplift tensions induced in the piles as the profile heaved. Flooding was used to accelerate the heave. The piles were installed on a 2.63m grid and the flooding holes bisected the grid. The flooding holes were 75mm in diameter and 25m deep. Each flooding hole contained a perforated hose pipe over its full depth. Heave of the soil was monitored by a single multipoint extensometer.

The pile group was first flooded for 10 days. After a 50 day interval to study the effects of this initial wetting, flooding was resumed, and maintained for a further 50 days.

Figure 8 shows a record of movement with time, at the surface and at 7m and 14m below surface. The diagram also shows the volume of water injected via the watering system. There is a very clear correlation between the volume of water injected and the heave curves. Unfortunately, the volume of soil absorbing the injected water is not known with any precision. Hence a meaningful relationship or ratio between the volume of water injected and the volume of heave induced cannot be established. Approximate calculations show that up to half of the flooding water must have been lost from the test area by lateral seepage into the surrounding soil.

Figure 9 shows relationships between depth and heave at various times after the start of flooding. The data is rather similar in form to that shown in Figures 5 and 7.

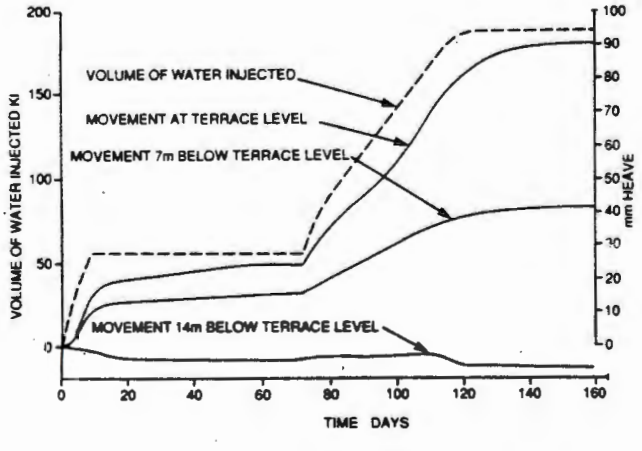

Figure 8 Relationships between time and heave and time and water injected for flooding of experimental pile site.

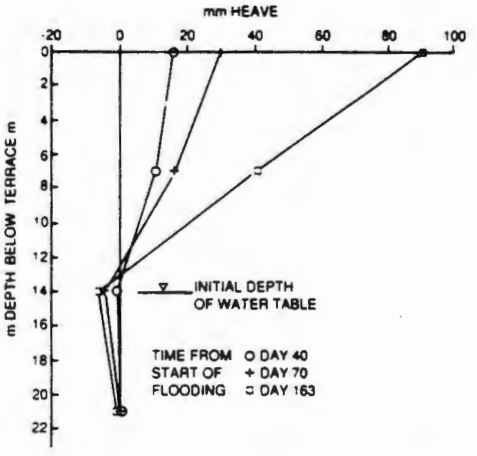

Figure 9 Heave-depth relationships during flooding of experimental pile site.

In this case, therefore, the technique of flooding proved very successful as a means of accelerating the development of uplift tensions in the piles.

3.4 REMEDIAL FLOODING OF AN APARTMENT BUILDING

Much of the heave at a particular site will take place in the upper 2m to 3m of the soil profile, where desiccation effects are likely to be most severe (Figures 5, 7 and 9). This indicates that surface flooding or irrigation should also be effective for preheaving, provided sufficient time is allowed for the water to penetrate the soil. The time required will probably also be of the order of 2 to 3 months. Williams (1980) describes the use of surface irrigation as a remedial measure for an apartment building damaged by heave:
A three storey load-bearing brick apartment block was erected on shallow strip footings on a soil profile that consists of 1m of calcareous windblown

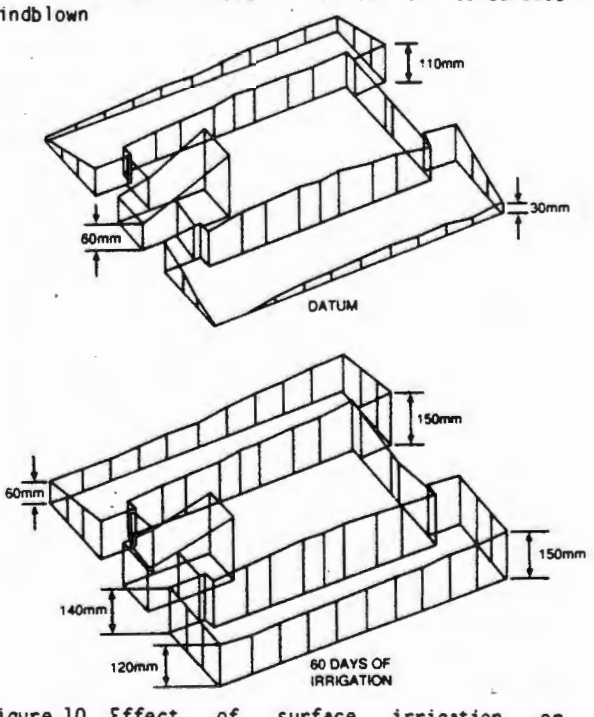

Figure 10 Effect of surface irrigation on distortion of apartment block damaged by heave.

sand overlying a great depth of desiccated weathered shale. No water table was found within 23m of the surface. The apartment block consisted of two buildings on either side of a courtyard, the two being linked by walkways on either side to form a hollow square . The courtyard was surfaced with asphalt concrete.

Cracking of the buildings was noticed before they were occupied and occupation was delayed because of this. Within three years the structures were so severely distorted and cracked that it was feared they would have to be demolished. Examination of the complex, and level measurements showed that the two apartment buildings had heaved and tilted outwards, moisture having accumulated under the buildings and the paved courtyard.

It was decided to attempt to reduce the distortion by wetting the whole area using spray irrigation. This was undertaken and within 60 days the distortion had been much reduced. Figure 10 shows the progressive changes of level of the perimeter of the complex, while Figure 11 shows typical transverse sections of the site before and after irrigation. However, it will be noted from Figure 10 that some of the differential movements were maintained, e.g. 30mm across the front side of the building in Figure 10 and 110mm between the right and left hand corners at the back. To maintain the site in a heaved condition, the area around the apartments was paved with open-jointed concrete blocks bedded in a sand layer. This type of surfacing allows rainfall to penetrate into the soil, but minimizes water losses by evaporation from the surface.

Ten years later the remedial measures continue successful, although there has been a slow settlement of the area since irrigation ceased.

4. CONCLUSIONS

The original de Wet experiment, as well as the case histories described by 3.2 and 3.3 have shown that preheaving of expansive sites by flooding can be successfully carried out. Preheaving is a useful technique if done rationally, with careful monitoring of the effects. There are certain disadvantages, the principal of which is the time taken for the water to penetrate the soil. However, careful planning and scheduling can overcome this shortcoming.

Case history 3.4 shows that surface flooding or irrigation can also successfully be used as a remedial or pretreatment measure.

On the other hand, case history 3.1 illustrates the futility of trying to apply a technique that is not understood.

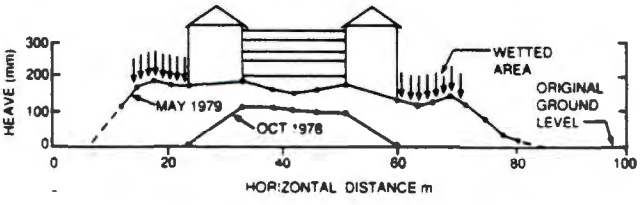

Figure 11 Effect of surface irrigation on ground profile under apartment block.

5. REFERENCES

Blight, G.E. 1984a. Uplift Forces Measured in Piles in Expansive Clay. Proc. 5th Int. Conf. Expansive Clay Soils, Adelaide, Australia, Vol 1, pp 240-244.

Blight, G.E. 1984b. Power Station Foundations in Deep Expansive Clay. Proc. Int. Conf. on Case Histories in Geotech. Eng. St. Louis, Missouri, Vol 1, pp 77-86.

Blight, G.E. and de Wet, J.A. 1965. The Acceleration of Heave by Flooding. Moisture Equilibria and Moisture Changes in Soils Beneath Covered Areas. Butterworth, Australia, pp 89-92.

Blight, G.E. and Lyell, K. 1984. Water Table Depression Under Treed Areas and Swell Subsequent to Felling. Proc. 5th Int. Conf. Expansive Clay Soils, Adelaide, Australia, Vol 1, pp 245-249.

Dawson, R.F. 1959. Modern Practices Used in the Design of Foundations for Structures on Expansive Soils. Quarterly, Colorado School of Mines, Vol 54, No 4, pp 67-87.

McDowell, C. 1959. The Relation of Laboratory Testing to Design for Pavements and Structures on Expansive Soils. Quarterly, Colorado School of Mines, Vol 54, No 4, pp 127-153.

McDowell, C. 1965. Remedial Measures Used in the Reduction of Detrimental Effects of Swelling Soils. Proceedings, Int. Res. and Eng. Conf. on Expansive Clay Soils, Texas A&M Press, pp 239-254.

Williams, A.A.B. 1980. Severe Heaving of a Block of Flats Near Kimberley. Proc. 7th Reg. Conf. for Africa on Soil Mech. and Found. Eng. Vol 1, pp 301-310.

3. DETERIORATION OF REINFORCED EARTH STRUCTURES

CONTRIBUTION TO LEARNING

The Tweepad walls were not the first in the world to fail as a result of corrosion of the reinforcing, but this failure, of the highest complex of reinforced earth walls built so far, is the first to be described in the open literature. The occurrence and details of other failures have been suppressed. Collapse settlement of the backfill to a reinforced earth wall has also not been publicly identified before. It is believed that it will be to the eventual benefit of reinforced earth technology to expose these weaknesses in the technique so that they can be avoided in future.

3. DETERIORATION OF REINFORCED EARTH STRUCTURES

3.1 Blight, G E and Dane, M S W (1989). Deterioration of a wall complex constructed or reinforced earth. Geotechnique, vol 39, No 1, pp 47-53.
Discussion and reply: vol 39, No 3, pp 567-570.

This investigation, carried out over a period of six years, was undertaken for a mining house. Mr Dane was the head-office engineer for the mine owning the reinforced earth wall complex. He played the very important role of facilitator in the investigation. I carried out the investigation and wrote the paper.

Seeing the content of the paper as a threat to the reputation of their product, the Reinforced Earth Company Submitted a vigorous discussion of the paper. For the sake of a balanced view, this discussion and my reply have been included.

3.2 Blight, G E (1987). Effects of collapse settlement of fill on reinforced earth walls. Proceedings, 2nd International Conference on Case Histories in Geotechnical Engineering, St. Louis, USA, vol 2 pp 929-934.

Blight, G. E. & Djane, M. S. W. (1989). *Géotechnique* **39**, No. 1, 47–53

Deterioration of a wall complex constructed of reinforced earth

G. E. BLIGHT* and M. S. W. DANE†

A gravity separation plant at a mine on the west coast of South Africa is flanked by a complex of reinforced earth walls having a maximum overall height of 41 m. Eighteen months after construction had been completed, it was discovered that the galvanized reinforcing strips were deteriorating as a result of galvanic corrosion caused by the aggressive nature of the backfill. The process of deterioration was monitored until the walls were demolished and rebuilt 8 years later. The progressive deterioration of the wall complex is described in terms of the reducing strength of the reinforcement and the continuing movement of the wall facings. The results of in-situ measurements of tensions in the reinforcing strips are also presented. The Paper gives an important insight into the process of corrosion affecting steel buried in soil, and also into the behaviour of large reinforced earth walls.

Une installation pour la séparation par gravité située dans une mine sur la côte ouest de l'Afrique du Sud est entourée d'un complexe de murs en terre armée ayant une hauteur totale maximale de 41 m. Un an et demi après l'achèvement de la construction on découvrit que les armatures galvanisées s'altéraient par la corrosion galvanique causée par la nature aggressive du remblai. La détérioration fut mesurée jusqu'à ce que les murs soient démolis et rebâtis huit années plus tard. L'article explique la détérioration progressive du complexe de murs par la résistance amoindrie du renforcement et le mouvement continu des parements des murs et présente aussi les résultats des mesures en place des tensions dans les bandes de renforcement. Ceci donne un aperçu important sur la corrosion des aciers enrobés dans le sol et aussi sur le comportement des grands murs en terre renforcés.

KEYWORDS: Case history; deterioration; field tests; reinforced soil; retaining walls.

INTRODUCTION

A complex of reinforced earth walls was built to support a gravity separation plant at the Tweepad mine on the west coast of South Africa (29°S, 21°E). The walls were designed by the Reinforced Earth Company and were reinforced with galvanized ribbed mild steel strips. Fig. 1 shows maximum height cross-sections through the walls. The blocks of reinforced earth have been indicated by cross-hatching. Fig. 2 shows walls H and G. Construction of the complex started in 1978 and was completed in 1979.

During 1980 a failure of a reinforced earth wall at another mine on the coast resulted from corrosion of the reinforcing strips. As a result, it was decided to investigate the more recently constructed walls at Tweepad for signs of similar deterioration. It was found that the reinforcement of these walls was also deteriorating, as a result of severe pitting corrosion. Monitoring exercises were subsequently carried out at regular intervals to follow the process of deterioration and to assess the safety of the walls. The walls were finally demolished and rebuilt in 1986, after 8 years of the 30-year design life.

Discussion on this Paper closes on 3 July 1989. For further details, see p. ii.

* University of the Witwatersrand, Johannesburg.
† Anglo American Corporation of South Africa Limited, Johannesburg.

SPECIFICATIONS FOR FILL AND REINFORCING

The Tweepad area has a desert climate, with an average annual precipitation of 92 mm during the years 1978–86. The annual mean temperature at 14.00 h is 26°C, with a minimum of 18°C and a maximum of 34°C. Evaporation from a free water surface averages 1940 mm.

Available backfill materials consisted of ancient raised beach deposits of sands. The specification accepted for the wall backfill was: 100% passing the 300 mm sieve; more than 75% passing the 150 mm sieve; less than 20% passing the 15 μm sieve. This specification was not always met as far as the fraction finer than 15 μm was concerned. The usual Reinforced Earth Company specification for the electrochemical properties of back-

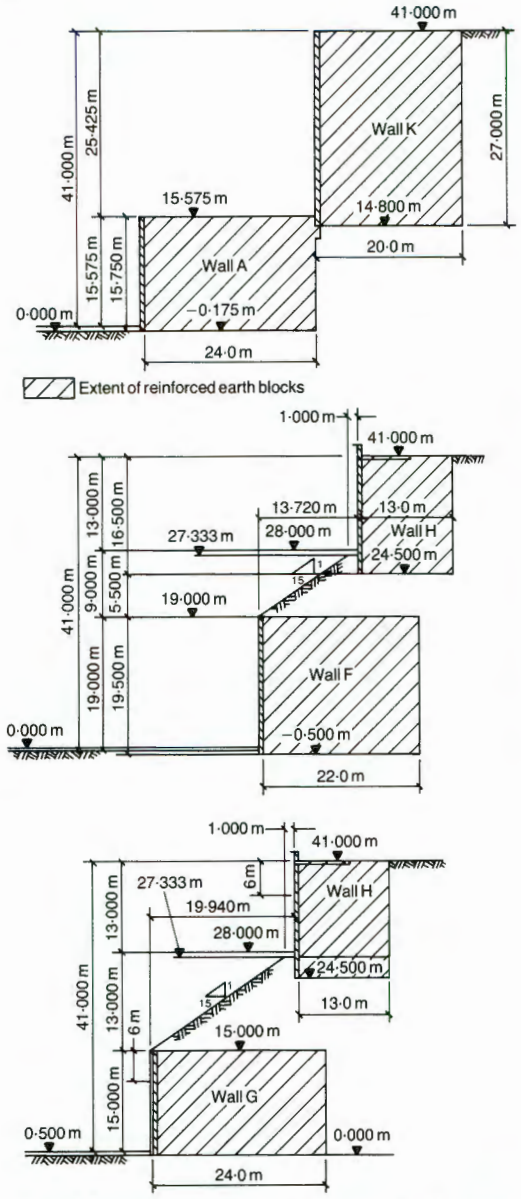

Fig. 1. Maximum height sections through reinforced earth walls

fill (French Ministry of Transport, 1978) at the time of the design was: pH 5–10; resistivity greater than 1000 Ωcm; chlorides less than 200 mg/kg; sulphates less than 1000 mg/kg. As a result of difficulty with meeting this specification using easily available fill, the following relaxed specification was accepted: pH 5–10; resistivity greater than 500 Ωcm; chlorides less than 1500 mg/kg; sulphates less than 800 mg/kg. These requirements were expected to be adequate to give a working life of 30 years, instead of the 70-year life expectancy of the more rigorous specification. The use of sea water for compaction of the backfill was agreed to by the Reinforced Earth Company. The reinforcing strips were designed with 1 mm of sacrificial steel all round and were galvanized.

The ultimate tensile strength of the reinforcing strips was specified as 350 MPa. In fact, the average ultimate tensile strength of the strips as installed proved to be 450 MPa.

MECHANISM OF ACCELERATED CORROSION

Once monitoring of the progress of deterioration was started, it soon became apparent that the fine fraction of the fill occurred as discrete lumps of clay, and was not uniformly disseminated through the soil. Wherever a clay lump rested in contact with a reinforcing strip, severe pitting corrosion occurred. It was obvious that corrosion was occurring mainly as a result of the formation of differential aeration cells (Allen & Lewis, 1979) as shown in Fig. 3. The contact between the relatively pervious sand and the steel was well oxygenated, whereas that between the clay and the steel was oxygen-starved. This caused the steel near the perimeter of the clay lump to become anodic and corrode over a limited area, forming pits.

This conclusion was confirmed when it was found that the reinforcement of a second reinforced earth wall complex (at the nearby Koingnaas mine) that had been backfilled with a uniform clean sand was quite free of corrosion, even though the chloride content was much higher than at Tweepad.

EFFECT OF CORROSION ON THE REINFORCING STRIPS

Initially, monitoring of the progress of corrosion was accomplished by breaking out facing panels and retrieving strips from behind the wall face. Replacement strips were then welded into place. As the safety condition of the walls became more critical, it was decided to sink a shaft behind each wall, located approximately on the locus of maximum strip tension, i.e. one third of the length of the reinforcing strips back from the wall facing. As each set of strips was exposed, usually two at each level, targets for a demountable Demec strain gauge were glued on. After taking an initial reading, the strip was cut at one end by means of an oxy-acetylene torch. The elastic shortening of the strip was then measured, and hence the in-situ tension deduced. Once the shaft had been completed, the shaft casing was progressively withdrawn and replacement strips were welded into place. The recovered strips were

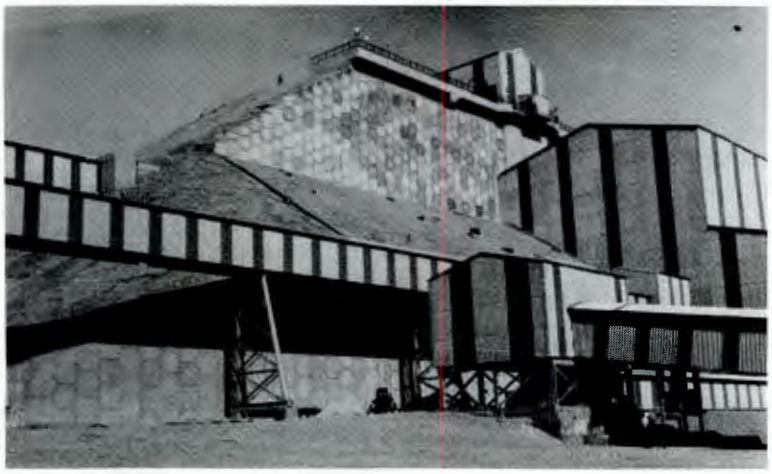

Fig. 2. View of reinforced earth walls H (above) and G (below)

tested for strength, and elongation at failure was measured over a 100 mm gauge length straddling the break. The effect of the pitting corrosion was not only to reduce the load-bearing cross-section of the reinforcing strips, but also to embrittle them by introducing stress concentrators in the form of the irregularly-shaped corrosion pits.

The influence of the corrosion on both strength and ductility is illustrated in Fig. 4, in which the strength values have been normalized with respect to the mean strength of new strips. The uncorroded strips taken from the Koingnaas wall show the usually expected relationship between ultimate tensile strength and ductility: an increase in ductility corresponds to a slight decrease in strength.

Strips sampled from Tweepad after 3 years already showed a marked reduction in strength. They also showed the effect of embrittlement by the presence of corrosion pitting, in that ductility decreased with decreasing strength. The results of tests on $7\frac{1}{2}$-year-old strips showed this tendency even more markedly. The strength of certain strips was then only 30% of the original value, with negligible ductility.

Figure 5 shows the observed deterioration of strip strength with time for 60 mm × 5 mm reinforcing strips. As in Fig. 4, the strength axis of the diagram has been normalized with respect to the mean strength of new strips. It is interesting to note that the 'most pessimistic estimated life of structure' was determined after a time of 4 years on a basis of linear extrapolation. This estimate did not require subsequent revision. Fig. 5 relates to average conditions for all the walls of the complex. Diagrams similar to this were drawn up

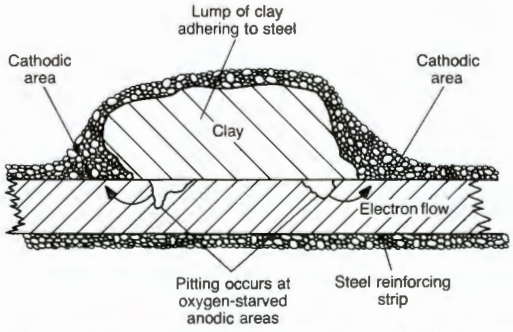

Fig. 3. Mechanism of pitting corrosion of reinforcing strips

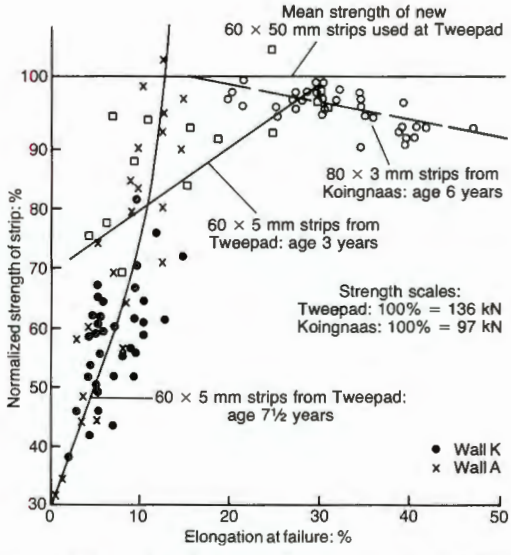

Fig. 4. Effect of pitting corrosion on strength and ductility of reinforcing strips

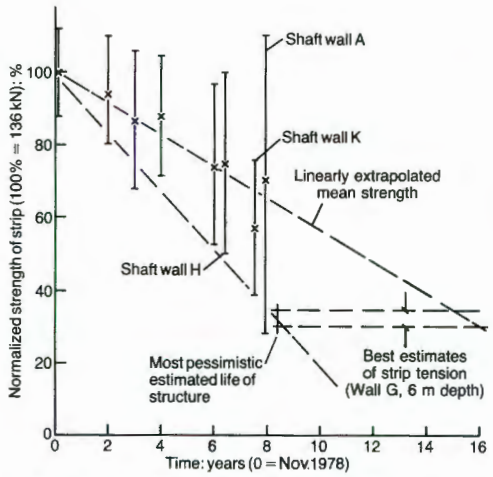

Fig. 5. Deterioration of strip strength with time for 60 mm × 5 mm reinforcing strips (error bars show standard deviation × 2)

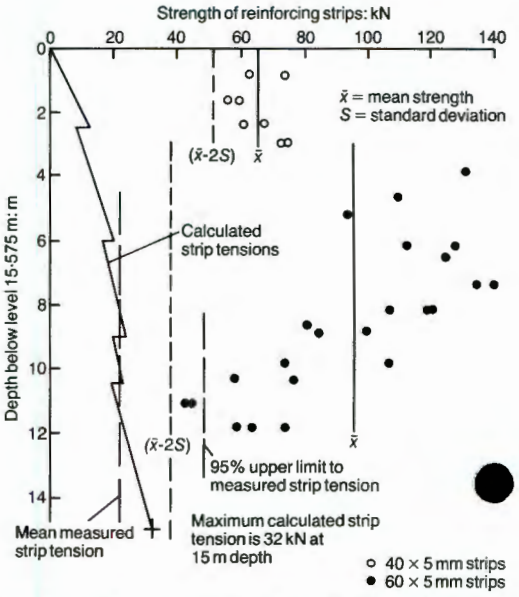

Fig. 6. Results of strength tests on reinforcing strips taken from shaft behind wall A

for each individual wall, and the sequence of demolition and reconstruction was decided on the basis of the estimated residual life for each wall. In Fig. 5 the best estimates of strip tension were based on the Reinforced Earth Company's conventional analysis of strip tensions in the walls (McKittrick, 1978).

DISTRIBUTION OF STRIP STRENGTH WITH DEPTH

Figure 6 shows a profile of strip strengths with depth, as measured on strips recovered from the shaft behind wall A. The shafts behind walls H and K gave similar results. The diagram illustrates the large scatter in measurements, which is also reflected in Fig. 5. The shaft results showed that the deterioration of strength was by no means uniform with either depth or lateral extent.

In the case of Fig. 6, relatively little deterioration is shown down to a depth of 8 m. Below 8 m, however, the deterioration became severe. The observed deterioration did not correlate with the salt content of the fill, or variations of moisture content. The salt content varied roughly linearly with depth from 0·5% by dry mass of fill at the surface to 0·3% at a depth of 12 m. The moisture content also varied roughly linearly with depth, from 11% at the surface to 6% at 12 m. Hence the more severe corrosion between depths of 8 m and 12 m is not obviously explained by correlation with fill characteristics. In Fig. 6, the line representing calculated tensions was determined by conventional analysis of the wall (McKittrick, 1978). The steps in the line result from changes in the number of reinforcing strips at a particular level.

Figure 6 also shows that the upper limit to the measured strip tensions in the reinforced earth at a 95% confidence level (see Fig. 11) exceeds two of the measured strip strengths. Hence, at the time this data was gathered, there was a danger that wall A could have failed within a short time.

PROGRESSIVE MOVEMENT OF WALLS

Monitoring of outward movement of the walls was started as soon as it was realized that the reinforcement was deteriorating. Initially, measurements were made by conventional survey methods, observing targets fixed to the wall surface. Later, use was made of short-range photogrammetry. It was soon realized, however, that because of the increasing brittleness of the reinforcing strips as the pitting corrosion progressed (Fig. 4), it was unlikely that a record of wall movement would give any warning of imminent failure of one of the walls by an acceleration of the rate of wall movement. It was therefore decided to base the decision on when to decommission and demolish a particular wall on relationships such as that shown by Fig. 5.

Figure 7 illustrates some of the observed movements of wall K, the highest single wall in the complex. The movements shown are for two points at the same height on the wall. As the record shows, except for a few interruptions apparently resulting from survey errors, the wall moved steadily outward throughout the period of observation. Depending on the height of the

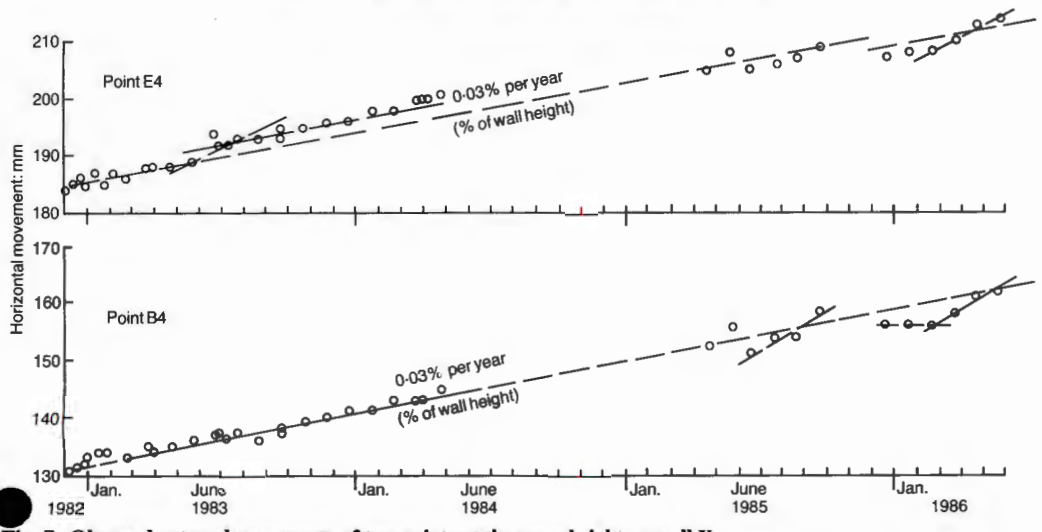

Fig. 7. Observed outward movements of two points at the same height on wall K

point observed, the rate of movement varied from near zero at the base of each wall to a maximum at the top, indicating that the walls were undergoing rotational or leaning movement with little or no translation. This pattern was typical of the movement of all of the walls in the complex.

Figure 8 shows a comparison of profiles measured in 1982 for wall K by conventional survey methods and by photogrammetry. The profiles of the lower walls in the complex were similar to those shown in Fig. 8, but the movements were less.

Walls A, F and G were founded on rock (Fig. 1), hence progressive leaning of these walls is thought to have resulted from continuing elongation of the reinforcing strips as corrosion progressed and the strain in the strips increased accordingly. Walls H and K each rested on a considerable thickness of fill. As the conventional view of a reinforced earth wall is that the pressure under the reinforced earth block is greater towards the toe, differential settlement was also thought to have contributed to the outward

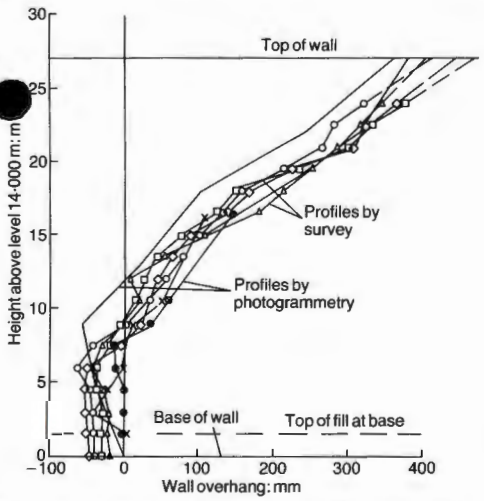

Fig. 8. Comparison of profiles for wall K measured by two methods

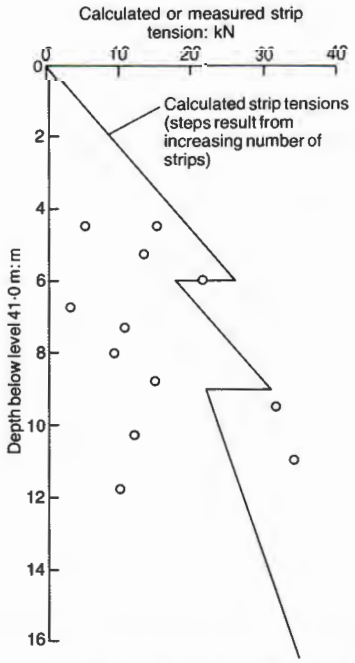

Fig. 9. Comparison of calculated strip loads with strip loads deduced from strain release measurements made in shaft behind wall H

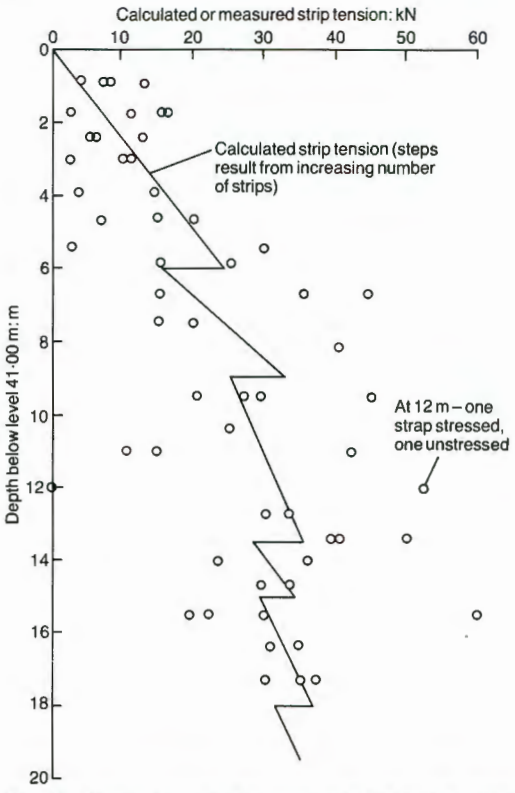

Fig. 10. Comparison of calculated strip loads with loads deduced from strain release measurements made in shaft behind wall K

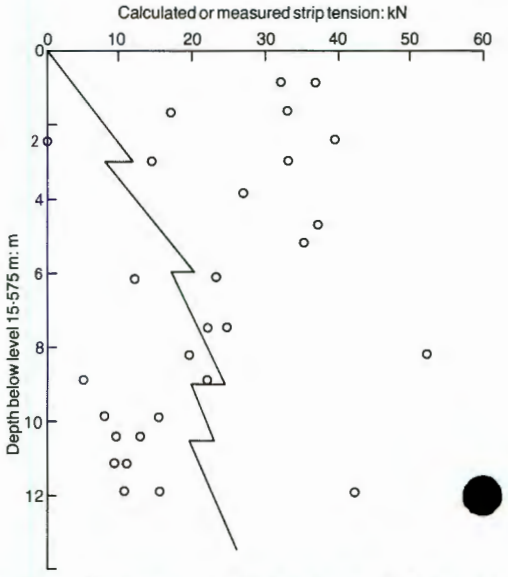

Fig. 11. Comparison of calculated strip loads deduced from strain release measurements made in shaft behind wall A

leaning. As the fill employed was basically a fine sand, this source of movement should not have been of a continuing nature.

DISTRIBUTION OF STRIP TENSION WITH DEPTH

Results (in chronological order) obtained for shafts sunk behind walls H, K and A are shown in Figs 9–11 and 7 respectively. Each figure also shows the variation of strip tension with depth, calculated by conventional means. In each case a considerable scatter occurred in measured tensions. It was quite common to find one of a pair of adjacent strips highly stressed while the other carried almost no load. This was evident not only from the spring-back measurements, but also from the note given out by individual strips when struck with a spade. This appears to be almost an inherent characteristic of reinforced earth that results from the method of construction. If a strip is bent by the passage of a piece of earth-moving machinery, while an adjacent strip is not, the bent strip, being effectively shortened, will carry more load. Time and again, a more heavily loaded strip would spring back into a bent position, while a lightly loaded strip would remain straight.

The general trend of the measurements follows the calculated line. This was particularly so in the case of wall K, where the calculated line forms a good average to the measured tensions.

The data in Fig. 7 for wall A show unusually large tensions in the strips from the surface down to a depth of 5 m. This was initially thought to be due to stresses distributed downwards from wall K, which is supported by wall A (Fig. 11). However, on the basis of conventional load distribution theory, the tensions in the reinforcing strips of wall A should not be affected by [illegible] distributed from wall K above a depth of 10 m. Hence the high stresses found above this depth cannot easily be explained.

RECONSTRUCTION OF WALLS

The walls have now been reconstructed in reinforced earth, this being both the most economical option and the one that most easily allowed the plant to be kept operational during demolition and rebuilding. The specification for the backfill was changed to the following: 100% passing the 300 mm sieve; more than 75% passing the 150 mm sieve; less than 10% passing the 75 μm sieve; nothing finer than 2 μm. This specification eliminates the possibility of clay lumps occurring in the fill.

The geochemical specification was changed to the following: pH 7–9; resistivity greater than 2000 Ωcm; chlorides less than 200 mg/kg; sulphates less than 200 mg/kg. Sea water was banned for compaction of the backfill. Instead, fresh water was trucked in for this purpose over a distance of 60 km. The concentration of dissolved solids in this water was 118 mg/l, including 17 mg/l chlorides and 8 mg/l sulphates.

CONCLUSIONS

The Tweepad experience has been a traumatic demonstration of the importance that must be attached to corrosion processes when designing and constructing structures that incorporate buried steel structural elements. It has also demonstrated that it is not always realistic to assume that corrosive metal loss will be uniformly distributed, or that the corrosion process will decelerate with time. These were commonly accepted views at the time of design.

The experience has also emphasized the great importance of having a completely homogeneous fill. Unfortunately, a grading curve says nothing about how the particle size fractions are likely to be distributed within the soil mass. Only careful examination of the placed in-situ material will give this information.

The monitoring studies have illustrated that pitting corrosion results in embrittlement of the reinforcement and that observations of wall movement alone may not be sufficient to evaluate the state of safety of a wall. It is imperative to monitor the actual state of the reinforcement.

The observations have also illustrated the statistical nature of the tensions generated in the reinforcing strips. The conventional method of calculation predicts the trends of the mean tension, but tensions in individual strips can be expected to vary widely about any calculated value.

It has often been said that failures are the greatest source of advance in engineering. It is hoped that the Tweepad experience will help materially to advance the practice of soil reinforcing.

ACKNOWLEDGEMENT

This Paper is published by kind permission of De Beers Consolidated Mines Limited and the Anglo American Corporation of South Africa Limited.

REFERENCES

Allen, M. D. & Lewis, D. A. (1979). Cathodic protection in civil engineering. *Corrosion in civil engineering*, pp. 79–94. London: The Institution of Civil Engineers.

French Ministry of Transport (1978). Quality of materials. *Reinforced earth structures recommendations—rules of the art* (English translation). pp 97–106. Paris: French Ministry of Transport.

McKittrick, D. P. (1978). Reinforced earth: application of theory and research to practice. *Proc. Symp. on Soil reinforcing and stabilizing techniques in engineering practice*, Sydney: University of New South Wales, separate paper, 44 pp.

Blight, G. E. & Dane, M. S. W. (1989). *Géotechnique* **39**, No. 3, 567–570

DISCUSSION

Deterioration of a wall complex constructed of reinforced earth

G. E. BLIGHT and M. S. W. DANE (1989). *Géotechnique* **39**, No. 1, 47–53

A. C. S. Smith, *Reinforced Earth (Pty) Ltd.*

The design and supply of components for the Reinforced Earth structure was undertaken by the Writer's company Reinforced Earth (Pty) Ltd in South Africa. The Reinforced Earth group has also undertaken extensive research on the question of corrosion for 13 years and the Writer's comments include some salient points on this topic generally. As a result the Writer hopes the brief comment in this contribution will enable engineers to draw fairly based conclusions on the Tweepad structure and corrosion in aggressive backfills.

The Writer feels it important to point out that the failure of the other Reinforced Earth wall to which the Authors refer, was, in fact, caused by the failure of an impressed cathodic protection system designed by a specialist consultant selected by the same Employer. The Authors might have given the impression that the two cases were similar.

LOCALITY AND CONSTRUCTION ENVIRONMENT

The project was constructed under particular and unusual conditions. Tweepad is situated in a vast and remote diamond mine on the desolate west coast of South Africa. The whole region is a high security area, and access to the site is restricted. Because of this kind of logistical difficulty, the Employer was responsible for the supply of backfill to the Contractor who was responsible only for the construction of the structure according to the specifications for the erection. The Writer's company was not responsible within the contract for the construction nor the supervision of the construction.

BACKFILL CHARACTERISTICS

At both the feasibility and design stages, the backfill material of the site was known to be free-draining (less than 5% passing the 80 μm sieve) with high chloride contents ranging between 100 and 800 ppm. This material was outside standard Reinforced Earth chemical specifications but was considered suitable on account of its uniform free-draining nature and the relatively short service life requirement of 30 years. At the request of the Employer the specification was amended to permit the use of sea water as opposed to fresh water for compaction purposes.

This amendment was accepted on the assumption that the sand was free-draining and because of the Reinforced Earth group's experience at that time which was

(*a*) experience of a large temporary industrial structure, constructed in France where sea water was used for compaction of a self-draining marine sand—good results had been recorded after four years of use (these walls, now 20 years old, are still in service, have been recently inspected and are performing well)

(*b*) a one year laboratory test on corrosion cells and box tests using free-draining sand moistened with sea water—the test results did not indicate that there would be a corrosion problem.

Before the construction stage, several samples of backfill material had been taken from the site and its vicinity. These samples were mainly free-draining wind blown sands with less than 5% by weight passing the 80 μm sieve. One 'calcrete' sample tested by the Employer with 13% passing the 80 μm sieve had also been approved by the Writer's company since the draining properties were still considered to be satisfactory.

A test sample of the 'calcrete' type material with 32% passing the 80 μm sieve was rejected by Reinforced Earth (Pty) Ltd for use as Reinforced Earth backfill.

After completion of the structure in 1980, further tests were carried out on the backfill and it became evident that the backfill was out of specification. It turned out that the backfill contained up to 20% clay (less than 2 μm) in the form of lumps in the sand.

CORROSION

Ten years after completion and a great deal of analysis it is clear that the problem encountered

at Tweepad was caused by the combination of two factors

(*a*) the presence of an irregular and excessive quantity of clay in the soil which was not in accordance with the Writer's company's specifications and
(*b*) the use of salt water during compaction.

The irregular distribution of the clay induced high local corrosion rates.

This point is confirmed by comparison of Figs 6 with Fig. 12. The first seems to suggest that corrosion increases with depth, while the average salt content has been found to decrease slightly. The second diagram, relative to wall *H* and not included by the Authors, suggests on the contrary that corrosion decreases with depth, whereas the salt content remains in the same range. This discrepancy can only be attributed to the random distribution of clay.

An extensive study has been made of the behaviour of galvanized steel in aggressive environments. The study relates to soils containing up to 2000 ppm of sulphates and chlorides (Darbin, Jailloux & Montuelle, 1988). The Tweepad experience is in line with the results of the study.

From this study it can be seen that a soil containing 1300 ppm of chlorides and 600 ppm of sulphates (the average salt content found at Tweepad) is expected to corrode galvanized steel at a rate given by $P = (100 + 20)T^{0.65}$ (where P, in μm, is the loss of metal, zinc and iron, for one side; T is the time in years; 0·65 is the deceleration of the corrosion with time). In fact the average corrosion rate measured in the samples

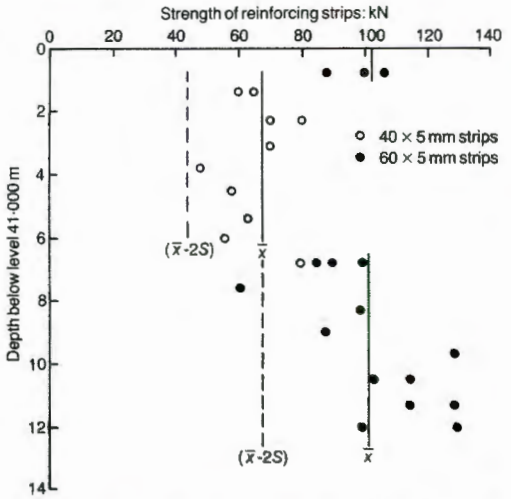

Fig. 12. Results of strength tests on reinforcing strips taken from shaft sunk behind wall H

Table 1.

Time: years T	Number of samples	Average loss (iron and zinc per side: μm	
		Calculated P	Actual P
2	12	188	250
3	15	245	245
4	22	295	297
6	21	385	392
8		404	NA

retrieved from Tweepad closely follows this equation, as shown in Table 1. This Table shows that the laws governing the corrosion of steel in aggressive environments are now defined with a greater degree of precision and understand[illegible] than was possible at the time the Tweepad structure was designed.

MOVEMENTS

The Authors make a number of comments concerning movement of structures at the site and corrosion. The comments are unsubstantiated. The facts are

(*a*) post construction rotational movements took place on wall K, which is 27 m high and founded on top of another 15 m high Reinforced Earth wall; over the monitored period, the top of this wall moved out at the rate of 8 mm per year
(*b*) wall H founded on top of a 25 m high fill, moved in the same way
(*c*) negligible post construction movement was measured on walls A, G and F which are founded on rock.

The only conclusion is that walls K and H moved because of the normal amount of consolidation of the fill beneath it, and that no relationship ex[illegible] between movement and corrosion of the reinforcing strips.

TENSION IN REINFORCING STRIPS

Over the years, a considerable number of measurements of tension forces in reinforcing strips have been carried out by the Reinforced Earth group and by highway administrations in many structures and in many parts of the world. This type of measurement always requires the use of two strain gauges (one on each side of the strip in order to eliminate the effects of bending). The accuracy and consistency of the results are totally satisfactory and have enabled reliable design methods to be formulated for all types of structures including surcharged walls.

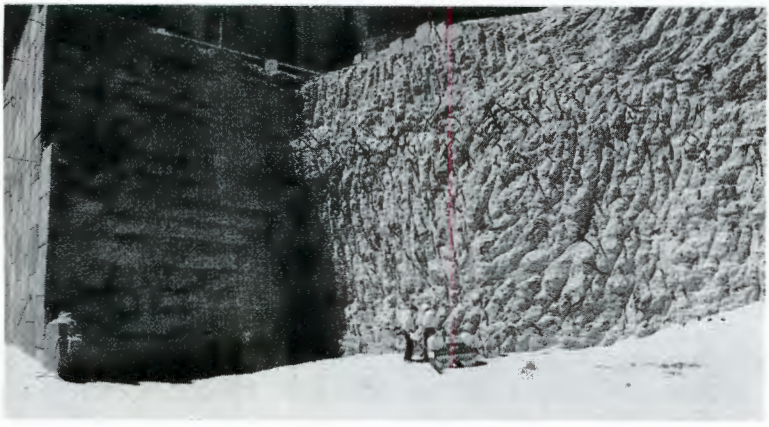

Fig. 13. Excavation on wall A—15 m high

The strain in the reinforcing strips at Tweepad, after excavating a shaft within the wall, was only estimated by measuring the relaxation of the tension on one side of the reinforcing strips, which does not give accurate results. In addition, the excavation of the shaft among the strips changed the state of stress in the strips and there is no basis to support that measurement made in such conditions can provide reliable results.

RECONSTRUCTION OF WALLS

Despite the problems and costs incurred through the use of corrosive backfill, it was decided to reconstruct the affected walls using Reinforced Earth for all structures where this was possible. One of the walls was completely dismantled and a new Reinforced Earth structure built in its place and other walls were buttressed with new Reinforced Earth structures. The Writer's company designed and supplied the components for all the additional Reinforced Earth structures. Specifications complying with standard Reinforced Earth company requirements were strictly enforced, and it is interesting to note that a suitable backfill source was located close to the site of the works.

During reconstruction deep and high excavations in the Reinforced Earth structures indicated that failure of the total structure was not imminent. Fig. 13 shows a 15 m high excavation in wall A.

CONCLUSION

There is nothing in the Tweepad experience which contradicts accepted theory and knowledge derived from the extensive research and practical applications of Reinforced Earth technology in around 12 000 structures designed and built worldwide.

Authors' reply

Although the discussion appears under the name of A. C. S. Smith, it seems to the Authors that this is a corporate discussion by Terre Armée Internationale. We apologise if this supposition is incorrrect. Much of the discussion confirms and amplifies information given in the Paper. However, the Authors, in reply, do have some comments to make.

The information given in Table 1 is interesting but quite irrelevant. Information or accurate predictions of average rates of thickness loss are of no value at all if galloping corrosion is occurring or is likely to occur at various isolated points, and will reduce the strength and ductility of the steel at rates five times quicker than average. The importance of the Tweepad experience is that it demonstrates the potentially disastrous consequences of processes that do not proceed uniformly at average rates. Darbin *et al.* (1988) must have been aware of the Tweepad failure at the time their paper was finalized, yet they give support to the notion that the corrosion of galvanized steel buried in earth always follows a predictable course. Their information on corrosion heterogeneity is dismissed as 'unreliable', whereas it was probably of greater significance than their well-behaved data. In common with many engineers, they appear obsessed with strength, whereas ductility may be a parameter of equal, or greater importance. An almost complete loss of ductility combined with severe localized loss of strength can spell disaster in a relatively short time, even if a formula based on average behaviour predicts a service life of many decades. This is a lesson that should be learned and publicized.

The Authors freely admit that they cannot completely account for the observed continuing movement of the Tweepad walls. However, to deny that the movement could have had anything to do with corrosion of the steel reinforcing seems akin to denying that the steel was corroding.

The well-behaved measurements of strain in reinforcing strips referred to by Smith were no doubt made on carefully prepared and handled test strips that were then as carefully buried and compacted over. The diagrams in the Paper, showing observed variations of strip tension with depth, are, like it or not, what actually happens in a reinforced earth structure. The observations cannot simply be swept under the carpet and ignored because they do not fit in with preconceived ideas of how Reinforced Earth behaves. Unpalatable as the fact may be, the performance of real structures depends on how they are constructed. The reality seldom matches neat, oversimplified drawing-board notions. Those concerned with the design and reinforced fill structures would do well to note the statistical nature of the design concepts, as typified by the measurements made at Tweepad.

It should be noted that the mode of failure most feared at Tweepad was fall-out of a facing panel. Had one of these panels crashed down, people working below could have been killed or injured. There was always less concern at the possibility of a general shear failure within the fill, for the simple reason that Tweepad is situated in a desert. The shafts sunk behind the wall had shown that the fill had considerable capillary cohesion in it. Smith's photograph shows a vertical face that probably owed its apparent stability more to capillary cohesion than to the badly corroded reinforcing strips embedded in the fill.

Finally, if Smith and his colleagues really have learned nothing from Tweepad, we urge that they read the Paper carefully again.

REFERENCE

Darbin, M., Jailloux, J. M. & Montuelle, J. (1988). Durability of Reinforced Earth structures: the results of a long-term study conducted on galvanized steel. *Proc. Instn Civ. Engrs*, Part 1, **84**, Oct., 1029–1057.

Second International Conference on Case Histories in Geotechnical Engineering

June 1-5, 1988

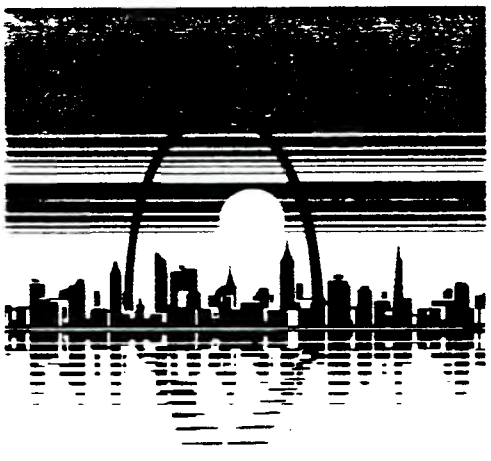

Geotechnical Engineering
St. Louis 1988

Vol. II

Editor: Shamsher Prakash

University of Missouri-Rolla
Rolla, Missouri

Proceedings: Second International Conference on Case Histories in Geotechnical Engineering, June 1-5, 1988, St. Louis, Mo., Paper No. 5.06

Effects of Collapse Settlement of Fill on Reinforced Earth Walls

G.E. Blight
Professor of Construction Materials, University of the Witwatersrand,
Johannesburg, South Africa

SYNOPSIS

Two case histories illustrate the effects that collapse settlement of the fill forming a Reinforced Earth wall can have on the structure.

Pre-requisites for collapse settlement are inadequate compaction, compaction at too low a water content, or a combination of these. Collapse settlement occurs subsequently when the water content of the fill is increased by infiltration.

The effects of collapse settlement identified in this paper are:

(i) a temporary release of friction on the reinforcing strips with the result that the wall facing moves outwards; and

(ii) relative settlement between the fill and the wall facing with the result that the reinforcing strips become inclined to the horizontal and their tension increases.

EFFECTS OF COLLAPSE SETTLEMENT OF FILL ON STRIP FRICTION

A loose fill has an unstable structure that is maintained by capillary stresses. In clayey fills the structure will consist of an assemblage of clods that behaves like a granular mass. Each clod maintains its integrity by means of strength imparted by capillary stresses acting within it. The void space between clods is large relative to the void space within each clod, i.e. individual clods are compact relative to the overall soil. In sand fills the unstable structure will be maintained by capillary stresses between individual grains or groups of grains.

When water later infiltrates the fill, the capillary stresses are released. Clods lose strength and compact into the surrounding voids and sand grain assemblages break down. The net effect is a settlement of the fill that has been defined as collapse settlement. The amount of collapse settlement that occurs depends on the quantity of water infiltrating and the time-settlement relationship depends on the distribution of the infiltration with time. The transient effect of the settlement on friction between the reinforcing strips and the soil will be illustrated by a case history:

A reinforced earth wall was built at Koingnaas on the west coast of South Africa. The climate is desert with an average annual precipitation of 90 mm and an annual pan evaporation of 1950mm. The wall supports a fill of uniform fine dune sand which was placed without control on moisture content and with little compaction. Shortly after a high pressure sea water hose had burst on the platform at the top of the wall, the wall abruptly moved forward a distance of 150mm to 200mm and then again came to rest.

The sand was uniform in grading, having a d_{10} size of 0.1mm and a ratio $d_{60}/d_{10} = 3.2$. An investigation in the laboratory showed that the angle of shearing resistance of the sand was high ($\phi' = 43°$) although the angle of friction of the loose dry sand on the surfaces of the smooth galvanized steel reinforcing strips was surprisingly low ($\delta=13°$). When the sand was inundated in the shear box, the angle of friction increased to 19°.

A re-analysis of the stability of the wall showed that for $\delta = 13°$ the factor of safety against pull-out of the strips from the fill would be as low as 1.1 at a distance of 2.5m below the top of the wall, increasing to 1.5 at 4.5m and to close to 2.0 at 6m, the base of the wall. Because the effect of wetting was ultimately to increase the factor of safety against a pull-out of the strips, it appeared that some transient phenomenon had occurred, presumably as the wetting front, arising from the burst hose, passed through the fill.

The phenomenon was modeled in the laboratory by loading a dry sand-to-galvanized steel surface in the shear box, to a factor of safety of 2 against shear failure. The sand was then inundated and the movement of the sand and the shear load were recorded on a UV recorder. A typical result of such a test is shown in Figure 1.

AB in the figure represents the stage during which the dry sand was loaded to a factor of safety of about 2 (actual $\delta = 6.1°$). At B the loading was stopped and the sand inundated. At C it appears that the water reached the sand-galvanized steel interface and the shear stress reduced (C to D) to an angle of friction of less than 1°. Simultaneously the sand settled, although most

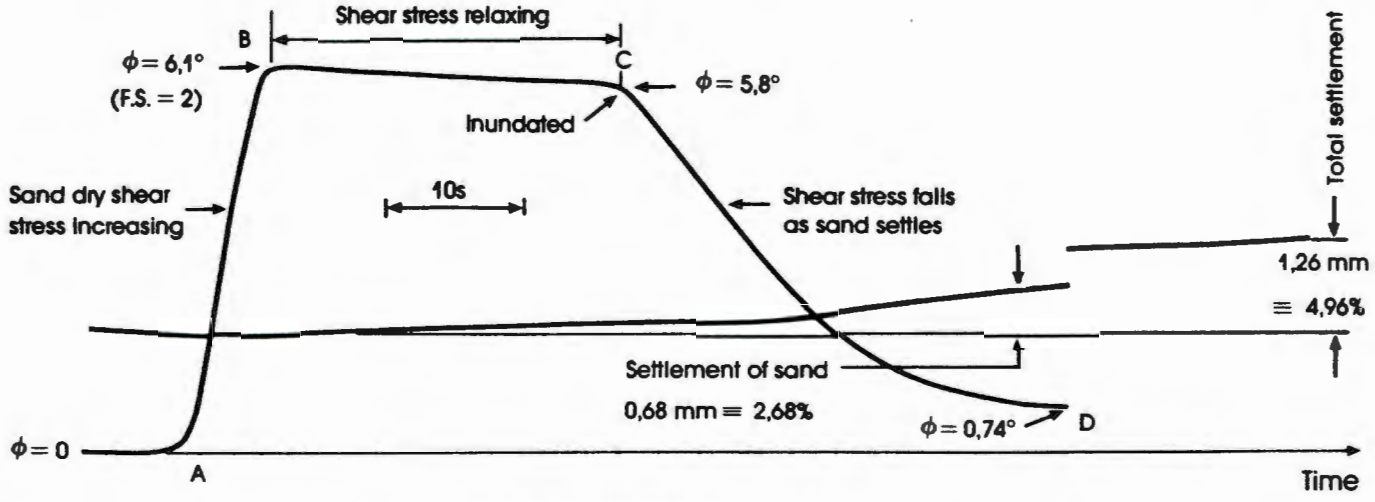

Figure 1: Variation of shear load at sand-steel interface when dry sand is inundated.

of the settlement occurred after the frictional resistance at the sand-steel interface had been lost.

It can be inferred from Figure 1 that as the wetting front moved downwards through the fill, successive layers of reinforcing strips temporarily lost their shear resistance and allowed the pressure in the fill to move the wall facing forward. As the wetting front passed, shear resistance was re-established, possibly at a greater angle of friction, and the wall facing re-stabilized.

The effect of saturating the fill on strip friction has previously been investigated by the Reinforced Earth Company. Although they found that saturation reduces the frictional coefficient between a dune sand and a steel reinforcing strip, the transient phenomenon illustrated in Figure 1 appears not to have been identified at that time.

A possible secondary effect of water entry is that water pressure may develop in the fill, thus reducing its shear strength and precipitating a rotational shear failure. In the Koingnaas case, this did not occur because the quantity of water was limited and the fill was relatively free-draining.

EFFECT OF COLLAPSE SETTLEMENT OF FILL ON STRIP TENSION

The collapse settlement of a poorly compacted fill has its effect on strip tension by dragging the reinforcing strips down relative to the wall facing. If the latter consists of concrete panels, the facing is stiff in a vertical plane, relative to the fill, once the 20mm joints between the concrete elements have closed up. This closure corresponds to 1.3% of post construction settlement of the fill.

There is also the possible secondary effect of water pressure to consider, if sufficient water enters the fill and if the fill is not free-draining.

The effect of collapse settlement on strip tension is a complex geometrical one, which depends on:

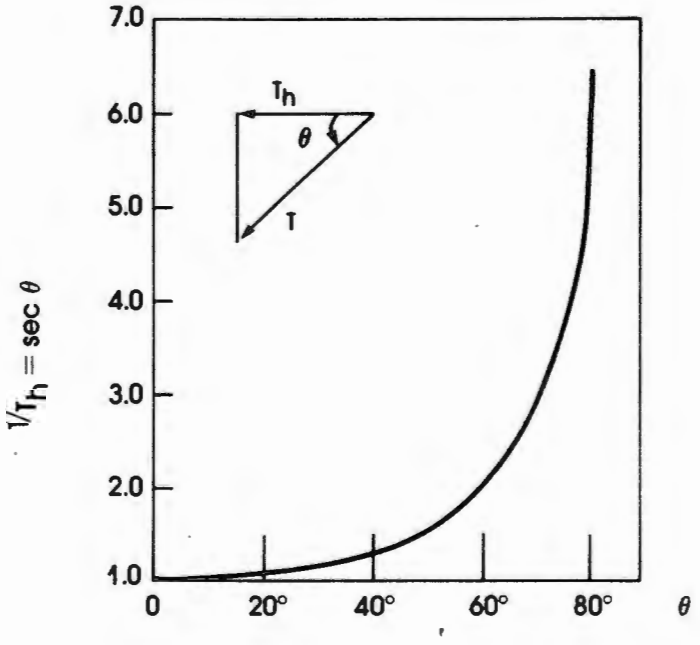

Figure 2: Strip tension T required to exert horizontal component T_h for various inclinations θ.

- the relative settlement of the reinforcing strip to the tie strip taking into account the ability of the cladding to compress in the vertical plane
- the movement of the reinforcing strip required to mobilise the friction in the loose fill along the length of the strip.

G E BLIGHT
Professor of Construction Materials, University of the Witwatersrand, Johannesburg, South Africa

EFFECTS OF COLLAPSE SETTLEMENT OF FILL ON REINFORCED EARTH WALLS

As a result of the relative settlement, the strips become inclined adjacent to the wall. For an inclined strip to exert a horizontal tension component T_h, the tension in the strip has to be (see Figure 2)

$$T = T_h \sec \theta$$

As shown by Figure 2, T increases rapidly with increasing θ. If the design factor of safety against yield of a reinforcing strip is 1.6, a strip inclination of 51° will cause yield. If the factor of safety against tensile fracture is 2, an inclination of 60° will result in fracture.

The occurrence of this effect of fill settlement will also be illustrated by a case history:

At the Grootgeluk Coal Mine in the north-west Transvaal province of South Africa, the two arms of a U-shaped crusher complex were constructed of Reinforced Earth walls.

The walls support the earth ramps that provide access for 250T haul trucks to tip their loads from the base of the U into a primary crusher. Eight years after construction one of the side walls (the south wall) of the U failed, a wedge of fill sliding out together with a section of the concrete panel facing. The height of the section that failed was 16m. A view of the failure is shown in Figure 3.

Early in the life of the wall complex there had been concern because the facing of the north arm of the U had been found to be moving outwards. The movement of the wall was monitored for fifteen months, but when the rate of movement was seen to be moderate (between 5 and 20mm per year), measurements were stopped. At the same time, the wall that ultimately failed was monitored over a period of five months. The observed movement was only 1mm and hence measurements were stopped. The observed movements of the north wall over the period 1979 to 1984 are illustrated in Figure 4. The 1984 measurements seem to show that the rate of movement of the wall had been almost constant with time.

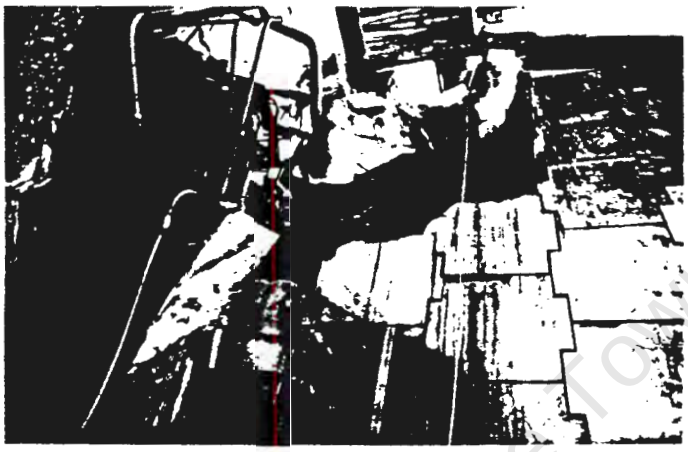

Figure 3: Frontal view of the failure at Grootgeluk Mine

An examination of the failure showed the following:

(i) A water pipe in the failed area had been leaking for an unknown period, discharging water into the fill.

(ii) The fill consisted of a sandy gravel which contains a considerable proportion of clay. It was certainly not free-draining but had an estimated permeability of only 1m/year. Penetration of water into the fill by infiltration of rainwater would have been slow. Equally, water fed into the fill by the leaking pipe would not readily have dispersed.

(iii) Several reinforcing strips had never been placed in the wall. For example, one facing panel was attached to four instead of the required six strips. In other cases 60mm x 3mm strips had been used instead of 80mm x 3mm strips.

(iv) Strips in the wall adjacent to the failed section were found to be inclined at steep angles to the horizontal. Inclinations as steep as 80° were found. It is surmised that a similar situation applied to the section of wall that failed. Figure 5 shows a row of inclined strips uncovered in the post-failure examination.

G E BLIGHT
Professor of Construction Materials, University of the Witwatersrand, Johannesburg, South Africa

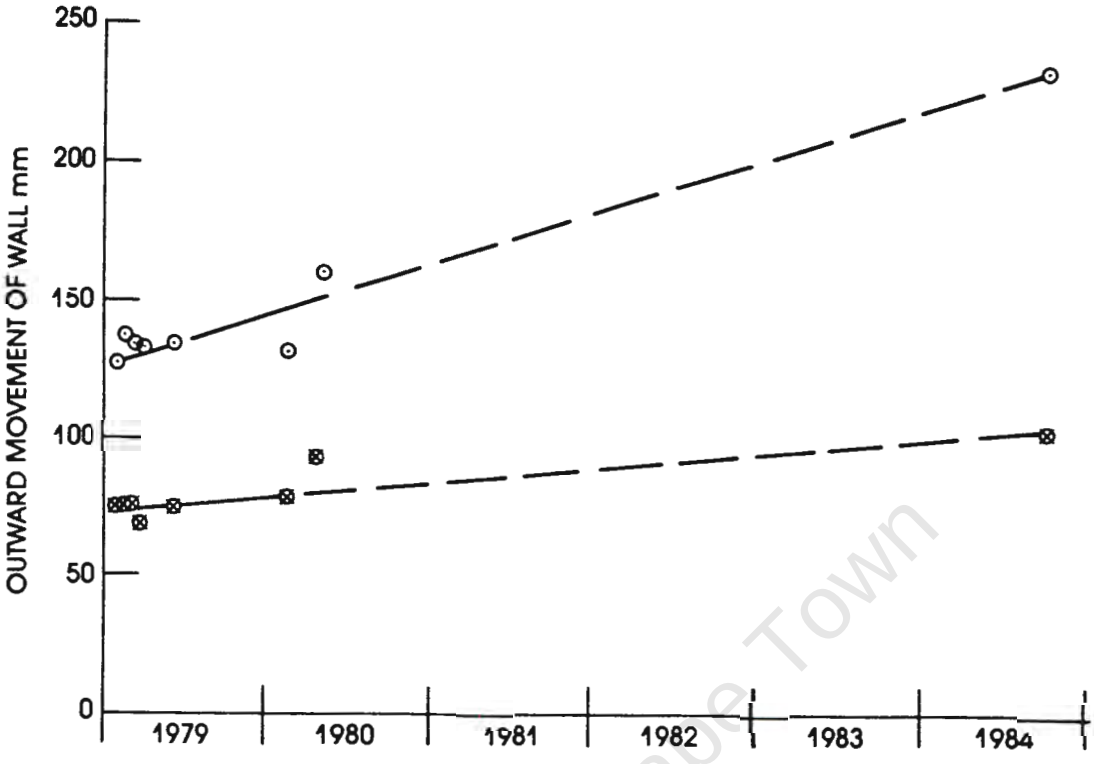

Figure 4: Observed movements of north wall at Grootgeluk Primary Crushing Plant.

The inclination of the strips may have resulted from setting the facing slabs too far ahead of the fill with the result that the unsupported reinforcing strips drooped down to rest on the fill surface. On the other hand, the observed progressive movements of the north wall were probably caused by a similar mechanism, involving collapse settlement, to the movement of the Koningnaas wall. Because of the relatively low permeability of the fill, the process of progressive release of friction would have taken place slowly over the years as each seasonal wetting front progressed through the fill. The same process was probably taking place on the south wall, but was unobserved.

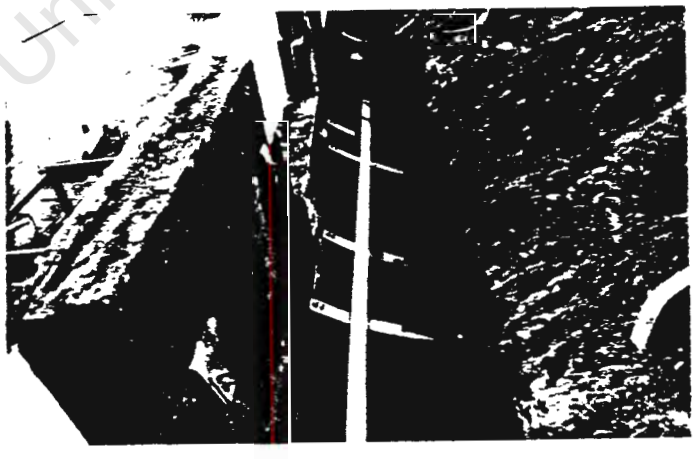

Figure 5: Inclined reinforcing strips uncovered during post-failure examination

(v) A deep rut in the surface of the fill showed that a heavy wheel load had been applied to the surface of the failed area shortly before the failure occurred.

(vi) Several of the strips supporting the failed section had clearly broken some time previously, as the fracture surfaces had rusted.

An engineering failure seldom stems from a single cause. It is usually the concatenation of a number of circumstances that results in a failure. The Grootgeluk failure was obviously no exception. All the above factors would have pushed the condition of the wall nearer to failure.

Accepting the various construction errors mentioned above, a likely scenario for the failure is the following:

Because of progressive collapse settlement and construction errors, the factor of safety of the section of wall that failed may have been close to unity before the water pipe started to leak. The penetration of the fill by water from the leak would have resulted in further collapse settlement and an increasing inclination of the reinforcing strips in this zone. Simultaneously, the accumulation of water would have reduced the shear strength of the fill. The last straw may have been the straying of a heavy vehicle onto the surface of the fill above this zone, now in a critical state. As often happens in engineering failures, there was no coherent eye-witness account of the failure.

Observations at Grootgeluk indicated that reinforcing strips were dragged down over a distance of 500mm to 750mm back from the wall facing. If one sets the acceptable angle of inclination at 37° (a 25 per cent increase in strip tension), then the maximum permissible settlement of the backfill relative to the wall facings is 375mm. Hence the limitation on settlement or misplacement of strips in elevation is not severe. Relative displacements of less than 375mm over a fill height of 16m should be easily possible with good supervision and careful compaction.

CONCLUDING REMARKS

The case histories described above, illustrate the importance of applying the usual control norms during the construction of Reinforced Earth structures, as well as the necessity for adequate compaction of the fill. As shown by measurements on Reinforced Earth structures, the tensions in reinforcing strips at a particular level can vary widely (Blight, Dane and Smith (1)). Circumstances that result in increasing strip tensions may cause certain strips to break, thus reducing the overall factor of safety of the structure. Recognition of these facts will lead to the building of safe, durable structures.

ACKNOWLEDGEMENTS

The information on the Koningnaas wall is published by kind permission of the Anglo American Corporation of South Africa Limited.

The Grootgeluk case history is published by permission of Iscor Limited.

REFERENCES

1. Blight, G.E., Dane, M.S.W. and Smith, A.C.S., "The progressive deterioration of a Reinforced Earth wall complex", submitted to Geotechnique. 1987.

4. EROSION OF THE SLOPES AND SURFACES OF TAILINGS DAMS

CONTRIBUTION TO LEARNING

Prior to the study described in these three papers, no information was available on the rates of removal of material from tailings dams by wind and water. Actual erosion rates turned out to be very much larger than generally thought. It was also a great surprise to many to find that:

.1 most of the material is eroded from the slopes and very little from the tops of dams; and that

.2 almost as much erosion results from wind action as from rain.

The third paper describes the current South African guidelines for environmental protection of tailings dams and the impact on these guidelines of measured rates and distributions of erosion.

4. EROSION OF THE SLOPES AND SURFACES OF TAILINGS DAMS

4.1 Blight, G E (1987). Erosion of the slopes of gold tailings dams. Proceedings, ASCE Conference on Geotechnical Practice for Waste Disposal, Ann Arbor, USA, pp 294-305.

4.2 Blight, G E (1989). Erosion losses from the surfaces of gold-tailings dams. Journal, South African Institute of Mining and Metallurgy, vol 89, No 1, pp 28-29.

4.3 Blight, G E (1991). Erosion and anti-erosion measures for abandoned gold tailings dams. Proceedings, 1991 National Meeting, American Society of Surface Mining and Reclamation, vol 1, pp 323-330.

GEOTECHNICAL PRACTICE FOR WASTE DISPOSAL '87

Proceedings of a Specialty Conference
sponsored by the Geotechnical
Engineering Division of the American
Society of Civil Engineers

University of Michigan
Ann Arbor, Michigan
June 15-17, 1987

Geotechnical Special Publication No. 13

Edited by Richard D. Woods

Published by the
American Society of Civil Engineers
345 East 47th Street
New York, New York 10017-2398

EROSION OF THE SLOPES OF GOLD TAILINGS DAMS

by

Geoffrey E Blight[a], MASCE

ABSTRACT

A study has been made of rates of erosion from the slopes of gold-residue dams in the South African Highveld region. Data is available for two years at this time and conclusions must therefore be regarded as tentative. Nevertheless, some useful correlations have been established that enable quantitative predictions to be made of the annual tonnage of residue that will be lost from a slope. This information can be used for designing the capacity of erosion-containing structures, estimating desilting requirements and deciding on whether or not a slope will require protection against erosion.

INTRODUCTION

Gold residue or tailings is a highly erodible, silty material which, if it escapes from the confines of a tailings dam, can cause extensive siltation of streams, rivers, low-lying areas and adjacent agricultural land. Dust pollution emanating from gold tailings dams may also reach unacceptable levels.

The bulk of the tailings particles fall into the silt particle size range. The mass proportion finer than 74 microns is typically 70 to 90 per cent and that finer than 2 microns is 5 to 25 per cent.

The topography of the South African gold mining areas is relatively flat with virtually no sites suitable for valley dam tailings impoundments. As a result, the tailings dams serving the thirty-odd gold mines are all of the ring-dyke impoundment type. The dams are raised by the upstream method and maximum use is made of sun-drying to consolidate the slopes and outer beaches of the impoundments. One consequence of this is that a large area of tailings is maintained in a dry state and is susceptible to dust generation.

Figure 1 shows a typical large (200 hectare or 480 acre) gold tailings dam. The dam is divided in two, each half having its own decant facility and being capable of separate operation. It will be appreciated that the large flat top surface of such a dam provides a considerable potential for dust pick-up by wind. The exposed slopes of the

---

[a] Professor of Construction Materials, Department of Civil Engineering, University of the Witwatersrand, Johannesburg, South Africa.

ring-dyke are susceptible to both wind and water erosion.

The slopes of gold tailings dams cannot be vegetated to provide protection against erosion as the dam rises. Pyrite contained by the tailings oxidizes near the surface, creating an acid environment that is hostile to plant life. Until the period of acid generation has passed (typically between 5 and 10 years), it is only possible to contain the material eroded from the slopes by water by means of a series of toe paddocks or silt traps such as those to be seen encircling the dam in Figure 1.

The purpose of the work described here was to investigate actual rates of erosion from gold tailings dams with the object of acquiring data for the design of erosion-containing structures, estimating desilting requirements for these containments and deciding on whether or not a slope requires protection against erosion over and above vegetating.

MECHANICS OF SOIL EROSION

Extensive research into the mechanics of soil erosion has been carried out in the field of agricultural science, river mechanics and related areas.

Because agricultural fields, river beds, etc invariably have flat slopes, it is generally not possible to extrapolate the results of agricultural or riverine erosion studies to the very steep slopes of mine

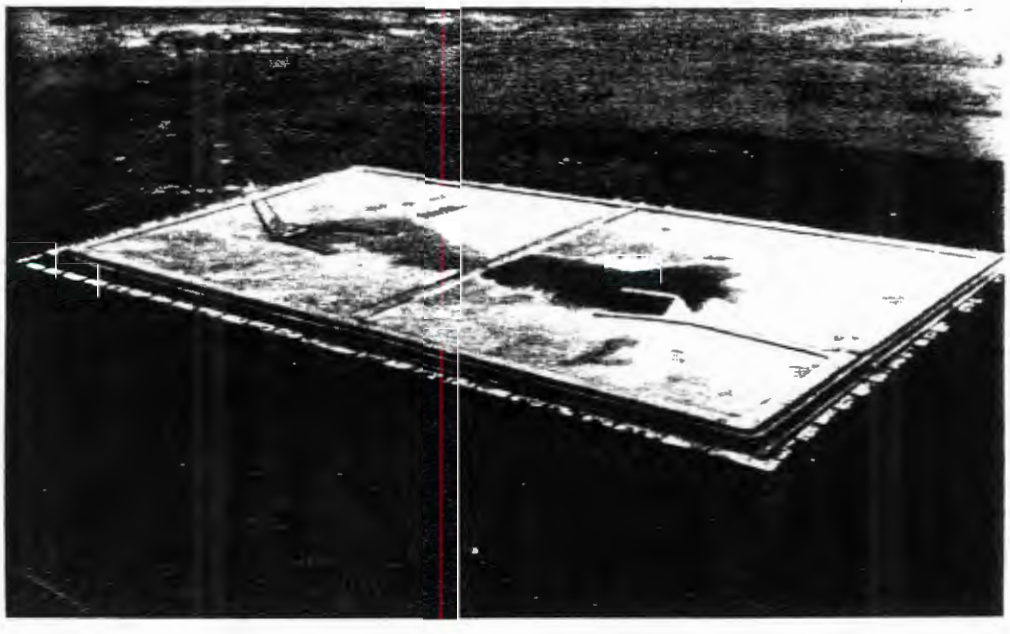

Figure 1 Aerial view of ring-dyke gold tailings (residue) dam. Note large top and slope area exposed to wind and water erosion. Dam is ringed by silt catchment paddocks

tailings dams. For example, a slope of 15° would be excessively steep in agricultural practice, but impractically flat for the sides of a tailings dam.

Lack of space precludes an exhaustive survey of the literature on soil erosion. What follows is a brief introduction to the mechanisms of soil erosion and the factors that affect it.

Erosion by water can be defined by two sub-processes :

detachment by rainfall
detachment by runoff.

Raindrops hitting the surface dislodge particles which are then carried downslope in increasing quantities as the flow rate increases. A single drop falling on a slope in still air conditions has components of momentum normal to, and down the slope. The downslope component of the weight of the drop is transferred in full to the surface but only a small proportion of the component normal to the surface is transferred, the remainder being reflected. The transference of momentum to the particles has two effects :

It provides an impact force, compacting the surface; and it imparts a velocity to some of the loosened particles and launches them into the air. This process of saltation or skipping of particles is continued down the slope by transfer of momentum and the saltating process is repeated.

The bulk of the water erosion from residue dams probably arises from detachment by runoff. Runoff occurs during a rainstorm when the moisture storage or infiltration capacity has been exceeded. For the flow of water to detach the particles a certain tractive force, related to the flow velocity has to be reached.

Bagnold (1974) related the tractive force to the flow velocity and particle size. He found that the critical flow velocity required for particles to become detached decreases with decreasing grain size, but below a certain particle size (about 0,1mm, and the bulk of gold tailings particles are finer than this), the critical velocity increases again.

Hjulstrom (1976) determined a relationship between particle size and critical velocity for erosion. His data supports that of Bagnold and shows, for instance, that the critical velocity for a particle size of 0,1mm is about 0,2m/s, for 1mm it is 0,3m/s, but for 0,01mm the critical velocity rises to 0,8m/s.

The process of erosion by wind is basically similar to that by water. In order to be eroded, a particle must be detached by tractive forces. To be transported, it must acquire kinetic energy from the wind. Once this has occurred, solid particles above a certain size will saltate and finer particles may be carried in suspension.

Bagnold (1959) showed that the rate of saltation in wind is directly proportional to the square root of the particle size and to the cube

MEASUREMENTS ON A TIED-BACK RETAINING WALL

MESURES IN SITU EFFECTUÉES SUR UN MUR DE SOUTÈNEMENT ANCRÉ PAR TIRANTS

G.E. BLIGHT
University of the Witwatersrand, Johannesburg (South Africa)

In order temporarily to retain the embankment on either side of a new rail-over-road bridge being constructed under an operating suburban railway line, the contractors designed a flexible tiedback retaining wall. The paper will describe the instrumentation of the 10 m high wall and give the results of the measurements. The bending moments in the vertical channels and the loads in the tied bars were used to deduce the pressure distribution on the back of the wall.

Afin de retenir, temporairement, le talus de part et d'autre d'un nouveau pont pour voie ferrée suburbaine, franchissant une voie routière, la construction du pont se faisant avec la ligne ferroviaire restant active, les entrepreneurs ont conçu un mur de soutènement souple ancré par tirants. Cet article décrit la procédure d'instrumentation du mur, haut de 10 mètres, et donne les résultats des mesures effectuées. Les moments fléchissants dans les fers en U verticaux et les forces dans les barres d'ancrage furent utilisés pour déduire la répartition des pression au dos du mur.

INTRODUCTION

In order temporarily to retain the embankment on either side of a new rail-over-road bridge being constructed under an operating suburban railway line the contractors designed a flexible tied-back retaining wall. The wall consisted of vertical double channel members at a horizontal spacing of 915mm supporting horizontally laid 76mm thick by 300mm wide prestressed concrete planks. The vertical channels were supported at their lower ends on two layers of galvanized steel sheet resting on concrete strip footings and were tied back by means of mild steel tie rods to beams buried at two levels in the retained fill. The anchor beams were located well beyond the 'active' zone of the fill, as indicated in Figure 1.

At short notice it was decided to instrument the walls in order to measure the actual forces and bending moments developed in the tie-bars and vertical channel members.

Figure 1 shows a section of the portion of wall that was instrumented

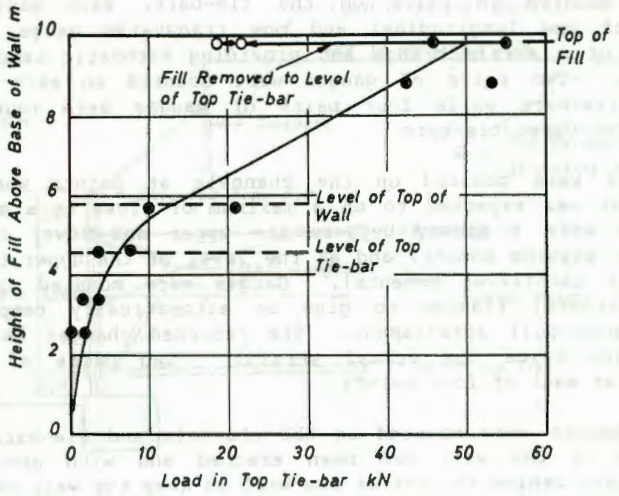

Figure 2

(a) *Variation of load in top tie-bars with height of retained fill.*

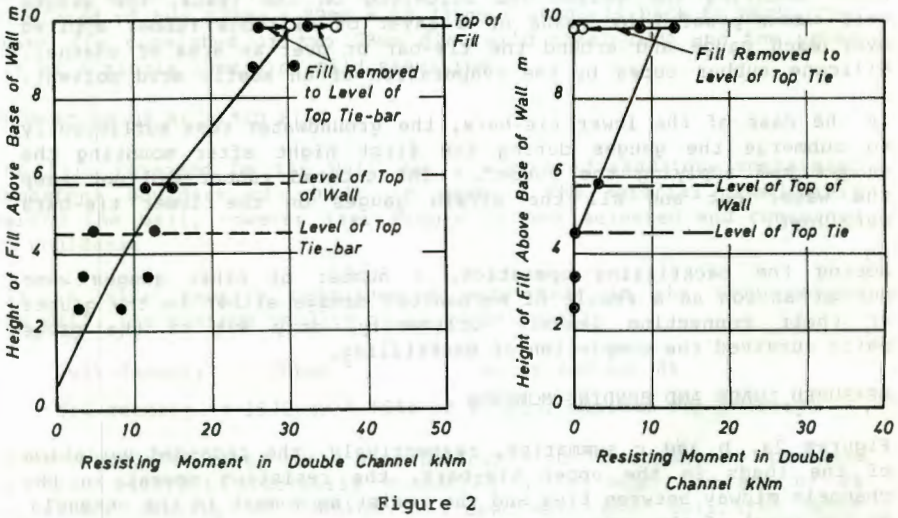

Figure 2

(b) *Variation of resisting moment in double channels with height of retained fill at a point midway between upper and lower tie-bars.*

(c) *Variation of resisting moment in double channels with height of retained fill at level of upper tie-bars.*

The fill was replaced with only nominal compaction and it is interesting to note that replacement of the fill had relatively little immediate effect on tie-bar loads and bending moments.

The fill reached its full height within 10 days. Subsequent to this, strains were monitored for a further 98 days after which the wall was dismantled. Figure 3 shows the variation with time of the top tie-bar load and of the bending moment in the channels midway between ties. In both cases very little change occurred,

indicating that the relatively non-plastic fill retained by the wall crept very little in the three-month period of observation. The effect of the removal and replacement of fill on tie-bar loads and channel bending moments is also illustrated in Figure 3.

The load in the lower tie-bars was determined by transferring the load from the tie-bar to a jack and noting the load at which the slope of the load-deflection curve changed. This was at a load of 45kN. The total wall deflection at a 45kN load was 1,19mm which corresponds closely to the calculated elastic extension of the 7m long tie-bars of 1,22mm under this load.

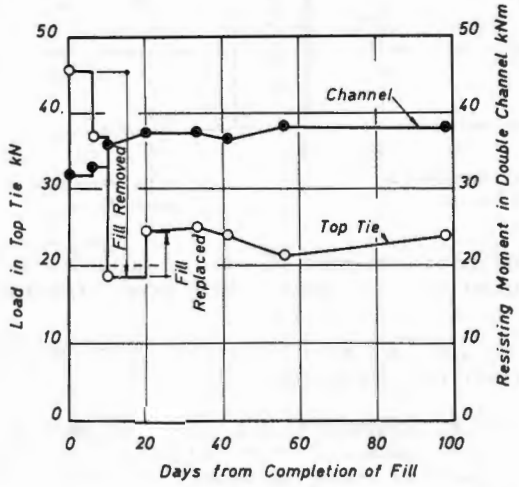

Figure 3

Effect of time and removal and replacement of fill on load in top tie-bars and resisting moment in channels midway between upper and lower tie-bars.

MEASURED MOVEMENTS OF WALL

Horizontal movements of the wall were monitored by means of an optical plummet. To make the measurements of each channel member, the plummet was set up over a reference peg in a concrete datum slab at the toe of the wall. Offsets from reference points on each channel to the vertical line of sight of the plummet were then measured by holding a steel rule graduated in millimetres against the channel so that it projected horizontally and reading the offset through the plummet. In this way it proved possible to measure offsets with a repeatability of less than ± 0,5mm.

Figures 4a and 4b show the progression of the wall movement as the level of the fill rose. Although the movements appear to be fairly large (20mm) they represent only a small average strain in the backfill when expressed as a percentage of the tie-bar length or the wall height (about 0,3%). Figure 4a shows the elastic extension of the top tie-bars as the level of the fill rose (calculated from Figure 2a). It is obvious from a comparison of the wall movements with the tie-bar extensions that the anchor beams must have slightly moved within the fill as the anchorage force developed. The curvature of the wall between the upper and lower tie-bars

from the analysis as it could not affect the value of H). Hence for horizontal equilibrium of the wall

$$H = (W \sin\alpha - [W \cos\alpha - \frac{\bar{u}h}{\sin\alpha}]\tan\phi^1)\cos\alpha \qquad (6)$$

If H can potentially exceed the right hand side of equation (6) the term $\tan\phi^1$ need not be fully developed, ie shear strains in the fill may be (and probably were) less than failure strains.

Equation (6) can be used to evaluate the average pore pressure on the potential sliding surface that would correspond to the measured tie-bar loads. If α is taken as $45° + \phi^1/2 = 62,3°$ and full development of $\tan\phi^1$ is assumed, the pore pressure ratio

$$r_u = \frac{\bar{u}}{\gamma h} = 0,05$$

Considering that seepage was issuing from the lower part of the wall this is an entirely reasonable value. At the time of installing the strain gauges, the phreatic surface in the partly completed fill was about 2m above the base of the wall. If it maintained this height once the fill was complete, r_u would in fact have had a value of 0,05. If $\tan\phi^1$ is assumed to have been only half developed, $r_u = 0.06$ showing that r_u is not particularly sensitive to the angle of friction actually developed.

RECOMMENDATION FOR DESIGN OF SIMILAR WALLS

In view of the reasonable values given by the wedge analysis outlined above, the author would be satisfied to adopt this approach for the design of similar walls in future. The most important question to be answered at the design stage is, "What value of r_u should be used"? As shown by Equation (6), H increases linearly as r_u increases. It is therefore important to carefully assess groundwater conditions in the vicinity of a proposed wall so that a value of r_u can be chosen that is conservative, but not unrealistically large. The apportionment of H between individual tie-bars obviously depends on the location and number of ties and the profile of the retained fill. Experience with this wall indicates that apportionment of H should be based on the assumption of either a trapezoidal or rectangular earth pressure distribution on the wall.

PROCEEDINGS OF THE INTERNATIONAL SYMPOSIUM ON PREDICTION AND PERFORMANCE IN GEOTECHNICAL ENGINEERING / CALGARY / 17-19 JUNE 1987

Prediction and Performance in Geotechnical Engineering

Edited by
RAMESH C.JOSHI & FRED J.GRIFFITHS
University of Calgary, Alberta, Canada

OFFPRINT

Sponsored by the Department of Civil Engineering and the Faculty of Continuing Education at the University of Calgary, and the Canadian Geotechnical Society, Calgary Chapter

A.A.BALKEMA / ROTTERDAM / 1987

Prediction and Performance in Geotechnical Engineering / Calgary / 17-19 June 1987

The concept of the master profile for tailings dam beaches

G.E.Blight
University of the Witwatersrand, Johannesburg, South Africa

ABSTRACT: The profile of an hydraulic fill beach may be non-dimensionalized to give a master profile which is the same for all beaches of a specific material deposited at a specific solids concentration. Hydraulic particle sorting along a beach may also be predicted from a simple expression and hence the variation of tailings permeability may be found. From this, the position of the phreatic surface in a dam may be predicted.

INTRODUCTION

Studies in Russia (eg Melent'ev et al 1973) which are not generally known or available in the West, have shown that the profile of an hydraulic fill beach for a particular fill material, solids concentration at placing and (probably) rate of placing, can be represented by a single dimensionless "master profile". The master profile applies regardless of the length of the beach or (within limits) the difference in elevation between the point of deposition and the pool. Reference to this phenomenon was discovered by the author and colleagues in an English translation of Melent'ev's paper. As the concept appeared to be a most useful one, research into the subject was started.

This paper is a summary of the present state of knowledge of master profiles (Blight and Bentel (1983), Blight, Thomson and Vorster (1985), Abadjiev (1985)).

There are two other phenomena which are closely related to the master profile concept:

(i) The profile appears to be generated by gravitational sorting of particle sizes as the tailings slurry moves down the beach.

(ii) The resultant gradient of particle sizes down the beach produces a gradient of permeability, the permeability of the tailings deposit decreasing from the point of deposition towards the pool.

The latter phenomenon, in particular, has important consequences for the stability of a tailings deposit.

THE MASTER PROFILE

Figure 1 shows beach profiles measured at six different locations on a large complex of platinum tailings dams. It will be noted that each profile has a different length H and a difference in elevation Y between the point of deposition and the pool. In Figure 2 the profiles have been non-dimensionalized by normalizing the elevation and distance down the beach of each point on the profile. The result is a single master beach profile with the equation

$$h/_y = (1-H/_X)^n \qquad (1)$$

Each different tailings product can be characterized by a different exponent n, as illustrated in Figure 3. The exponent is also affected by the solids concentration of the slurry and the fineness of the material.

The concept of a master profile enables the designer to predict the position of the pool, to assess the storm-water capacity of the top of the dam and more accurately to assess the tailings storage capacity.

What makes the concept practically useful is the fact that the master profile appears to apply almost regardless of the length of the beach. As a result the master profile for a new product can be established by means of beaching tests in a small laboratory flume. This enables the designer to establish the master profile on samples of tailings produced during pilot plant operations. What is more, the influence of such variables as solids concentration at deposition, fineness of grind and the presence

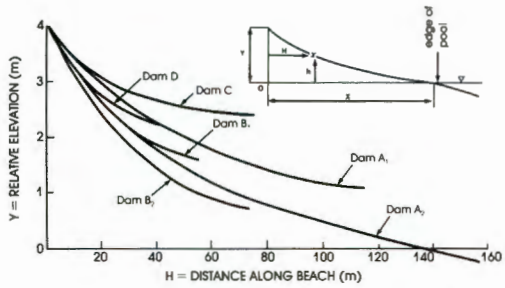

Figure 1: Measured beach profiles on 6 platinum tailings dams

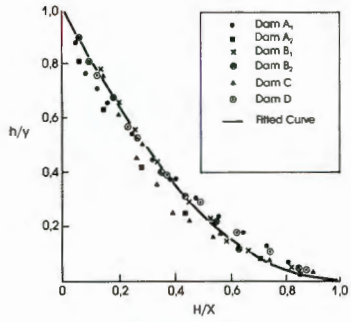

Figure 2: Dimensionless beach profiles for 6 platinum tailings dams

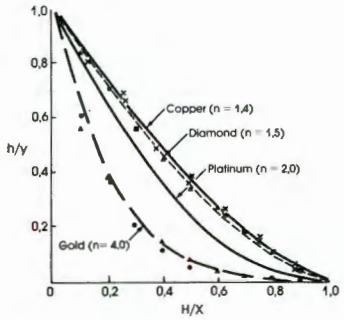

Figure 3: Dimensionless beach profiles for dams of various types of tailings

of flocculation can easily be studied.

Figure 4 shows a set of observations that illustrate the above statement. The field profile in these figures was established on a gold tailings dam where the beach length was 125m and the difference in elevation between the point of deposition and the pool was 0.7m. The solids concentration at deposition was 50 per cent. The other profiles in Figure 4 were established in a laboratory flume only 1.82m in overall length with an actual beach length of 1.5m and a difference in elevation of 100mm.

Figure 4a shows that the model-scale beach profile almost exactly matches the

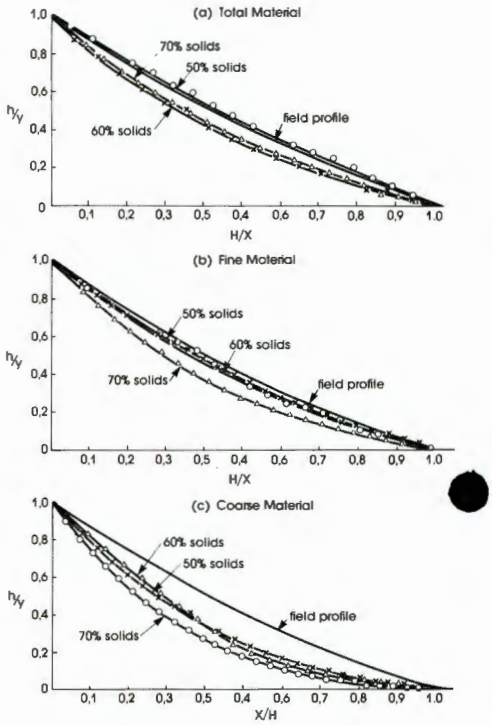

Figure 4: Comparison of field and model beach profiles for gold tailings

field profile, if the same material and solids concentration are used. As the solids concentration is increased, the exponent n in the equation to the profile (see Figure 3) increases. Varying the solids concentration produces the same effect if material either finer or coarser than the total tailings of the prototype beach is deposited, (Figures 4b and 4c). A beach of finer material has, in this example, almost the same profile as a beach of total tailings, whereas a beach of coarser material has a greater exponent n.

MECHANICS OF PROFILE FORMATION

As the tailings slurry flows down the beach there is a tendency for particles to gravitate to the bottom of the slurry stream and to deposit out. According to the laws of gravitational settling, larger particles will settle out higher up the beach while finer particles will travel further towards the pool. At any point along the beach, the beach slope i will be given by the equation for the stability of an infinite slope

$$i = \frac{1}{2} \sin^{-1} \frac{\tau_o}{\gamma \delta} \qquad (2)$$

in which τ_o is the shear strength of the

just-settled tailings, γ is its unit weight and δ the thickness of material having shear strength τ_o. Because the coarser material will tend to drain more easily, it will have a higher strength as it deposits and the slope i of the beach will decrease continuously from the point of deposition to the pool.

Figure 5 shows the variation of shear strength down a model beach of gold tailings just after deposition. Unfortunately, the corresponding beach slopes cannot be calculated via equation (2) as the thickness δ is not known with any precision. It is known, however, that the average slope of a beach, expressed by Y/X in Figure 1, increases with the solids concentration. Also, as the solids concentration increases, there is an increasing degree of interference between particles in the slurry which inhibits the settling process described

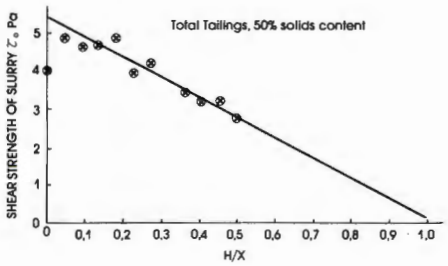

Figure 5: Variation of shear strength down a model beach of gold tailings

above. Ultimately, beyond a certain solids concentration, the flow regime changes and instead of progressive particle sorting occurring, with the average particle size decreasing towards the pool, the slurry starts to flow as a homogeneous material. This change of regime is illustrated in Figure 6 which shows the variation of Y/X for model beaches as the solids concentration of a fly ash slurry is progressively increased. The pronounced maximum slope that occurs at a solids concentration of 40 per cent marks the change from a "particle settling" to a "mud-flow" regime. Note the sudden decrease in Y/X as the "mud-flow" condition is established between solids concentrations of 40 and 50 per cent. As the solids concentration is increased further, it is surmised that Y/X will again increase progressively. To the left of the maximum slope in Figure 6, the particle settling regime, under which most conventional tailings dams operate, applies. To the right, the mud-flow regime, under which thickened discharge type dams (eg Robinsky (1978)) operate, applies.

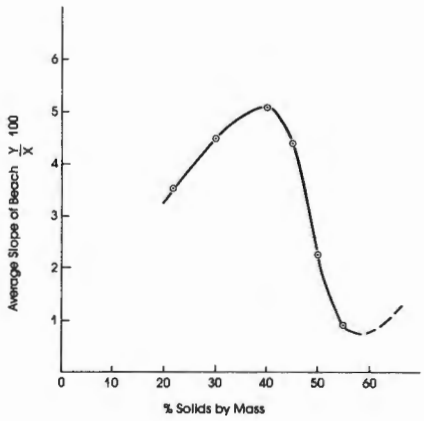

Figure 6: Variation of average beach slope with solids concentration for model beaches of fly ash slurry

It appears likely that as the rate of deposition on a beach increases, as measured in terms of tonnage discharged per unit of beach area, so the discontinuity between regimes will occur at progressively lower solids concentrations. This would follow because the velocity of flow down the beach would increase, and probably also the depth of flow. There would therefore be less opportunity for a "particle settling" regime to become established.

PARTICLE SORTING ALONG A BEACH AND ITS CONSEQUENCE

Figure 7 illustrates the particle size sorting that has taken place along a 280m long beach of diamond tailings. The inset shows similar information for the same beach taken 12 months later and expressed in dimensionless form. It will be noted that, although there is a lot of scatter, the profile of relative particle sizes is very similar in shape to that of a beach profile.

A study of particle size profiles such as those shown in Figure 7 has indicated that the size of particle at a distance H along an hydraulic fill beach from the point of deposition can be roughly predicted from the relationship

$$A = e^{-B.H/X} \qquad (3)$$

in which A is given by

$$A = \frac{D50 \text{ (at H down the beach)}}{D50 \text{ (of total product)}}$$

B is a characteristic of the tailings (and probably also of the rate of deposition)

Joshi, R.C. & F.J.Griffiths (eds.) 90 6191 707 7
Prediction and performance in geotechnical engineering – *Proceedings of an international symposium on prediction and performance in geotechnical engineering, Calgary, 17–19 June 1987*
1987, 25 cm, 464 pp., Hfl.95 / $48.50 / £28.50
Invited papers; Prediction & performance of pile foundations; Soil improvement; General prediction & performance of soils, unique soils, retaining structure behaviour & tunnels; Environmental geotechnology; Triaxial testing of soils; Centrifuge model testing; Risk analysis. 51 papers

FROM THE SAME PUBLISHER

Balasubramaniam, A.S., S.Chandra, D.T.Bergado & G.Rantucci (eds.) 90 6191 686 0
Geotechnical aspects of mass and material transportation – *Proceedings of the international symposium, Bangkok, 3–14 December 1984*
1987, 25 cm, 544 pp., Hfl.170 / $88.00 / £51
Soil exploration & testing; Geotechnical aspects of transportation; Shallow & pile foundation practices; Landslide, slope stability & subsidence problems; Tunnelling. 41 papers.

Hanrahan, E.T., T.L.L.Orr & T.F.Widdis (eds.) 90 6191 720 4
Groundwater effects in geotechnical engineering – *Proceedings of the ninth European conference on soil mechanics and foundation engineering, Dublin, 31.08 – 03.09.1987*
Les actions de l'eau souterraine en géotechnique – *Comptes-rendus du neuvième congrès de mécanique des sols et des travaux de fondations, Dublin, 31.08 – 03.09.1987*
1987–88, 30 cm, 3 vols, c.1300 pp., Hfl.520 / $265.00 / £156
Field & laboratory testing; Special problem soils; Groundwater problems in embankments, dams & natural slopes; Groundwater in foundations & excavations; Environmental problems & seepage; Groundwater modelling; Groundwater control; Dynamic effects. About 220 contributions.

Balasubramaniam, A.A., S.Chandra & D.T.Bergado (eds.) 90 6191 623 2
Recent developments in laboratory and field tests and analysis of geotechnical problems – *Proceedings of international symposium, Bangkok, 6–9 December 1983*
1986, 25 cm, 632 pp., Hfl. 195 / $99.50 / £58.50
Laboratory & field tests; Analysis of test data; Stress strain modeling; Analysis of geotechnical problems. 39 papers.

Balasubramaniam, A.S., S.Chandra, D.T.Bergado, J.S.Younger & F.Prinzl (eds.) 90 6191 568 6
Recent developments in ground improvement techniques – *Proceedings of the international symposium held at Asian Institute of Technology, Bangkok, 29.11–03.12.1982*
1985, 25 cm, 598 pp., Hfl.190 / $95.00 / £57
45 papers: Ground improvement by deep compaction & piling; Reinforced earth, soil fabrics & geotextiles; Grouting ground anchors & soil nailing; Root piles, micropiles & ground freezing; Blasting operation, seepage problems & case histories.

Balasubramaniam, A.S., D.T.Bergado & S.Chandra (eds.) 90 6191 599 6
Geotechnical engineering in Southeast Asia – *A commemorative volume of the Southeast Asian Geotechnical Society*
1985, 28 cm, 352 pp., Hfl.165 / $85.00 / £49.50
11 comprehensive invited lectures on site investigations, engineering behavior of soils, ground improvements, pile foundations, settlement of structures, landslides, environmental geotechnics, & developments is rock mechanics.

Amir, Joram M. 90 6191 596 4
Piling in rock
1985, 25 cm, 112 pp., Hfl.105 / $50.00 / £31.50
Piles are usually used to bypass soft formations. For typical conditions, piling in rock leads to considerable savings in terms of construction duration, labor, concrete, steel & energy. First comprehensive text devoted to piling in rock. Dr.Amir is consulting geotechnical engineer in Tel-Aviv.

Balasubramaniam, A.S., Yudhbir, A.Tomiolo & J.S.Younger (eds.) 90 6191 265 2
Geotechnical problems and practice of dam engineering – *Proceedings of the international symposium held at Asian Institute of Technology, Bangkok 1–15 December 1980*
1982, 25 cm, 400 pp., Hfl.180 / $90.00 / £54
Principles & practice; Investigations, instrumentation & foundation treatment; Environmental considerations; Geological control & case histories; Country reports: Pakistan Philippines, Taiwan, Indonesia, Singapore & W Malaysia, & Korea.

Desai, Mahesh (ed.) 90 6191 226 1
Construction practices and instrumentation in geotechnical engineering – *Proceedings of the international conference, Surat, India, 20–23 December 1982* (No rights India)
1982–84, 28 cm, 559 pp., 2 vols., Hfl.180 / $92.00 / £54
Embankments & embankment dams; Tunnels, mining & deep cuts; Coastal & offshore structures; Foundations on soils & rocks; Environ controls.

90 6191 560 0
Proceedings of the 11th international conference on soil mechanics and foundation engineering – *San Francisco, 12–16 August 1985* / **Comptes-rendus du 11ème congrès international de mécanique des sols et des travaux de fondations** – *San Francisco, 12–16 août 1985*
1985–87, 28 cm, c.3700 pp., 5 vols., Hfl.1250/$380.00/£375
The most important conference on soil mechanics & foundation engineering, held every 4 years. *Soil mechanics: Property characterization & analysis procedures:* Constitutive relationships for soil behavior; Numerical methods; Decision theory & probability. *New developments in field & laboratory testing of soils:* In-situ testing techniques; Centrifuge testing & its application; Laboratory testing; New procedures & data acquisition techniques; Field instrumentation & field measurements. *Geotechnical aspects of environmental control:* Ground water modelling & soil-waste interaction; Seepage control; Tailing dams. *Piles & other deep foundations:* Pile foundation design methods; Pier foundations; Foundations for offshore structures. *Geotechnical engineered construction:* Influence of earthwork construction on structures; Earth strenghtening; Applications of geotextiles. *Evaluating seismic risk in engineering practice:* Seismic geology & risk analysis; Seismic safety of earth structures. *Stability of natural deposits during earthquakes:* Soil liquefaction; Seismic stability in natural slopes. *Comparison of prediction & performance of earth structures:* Earth & rockfill dams; Excavation support; Foundations; Non-technical constraints on engineering practice. *Geological aspects of geotechnical engineering:* Earth dam engineering; Problems in areas with special geological conditions.

90 6191 566 X
Proceedings of the 11th international conference on soil mechanics and foundation engineering – *San Francisco, 12–16 August 1985* Golden jubilee volume
1985, 28 cm, 168 pp., Hfl.65 / $20.00 / £19.50
The history of geotechnical engineering until 1700 (J. Kerisel); A history of soil properties, 1717-1927 (A.W.Skempton); The last 60 years (R.B.Peck); The first Terzaghi oration: Amuay landslides (T.William Lambe).

All books available from your bookseller or directly from the publisher:
A.A.Balkema, P.O.Box 1675, NL-3000 BR Rotterdam, Netherlands

of the difference between the wind speed and the threshold wind speed for particle pick-up. The threshold wind speed is directly proportional to the particle size or diameter. However, this only applies to particles larger in size than about 0,1mm. Finer material becomes airborne when kinetic energy is imparted to it by saltating larger grains. The rate at which dust goes into suspension thus becomes roughly proportional to the rate at which larger particles are saltating (Gilette et al (1972)).

By far the most widely used method of predicting soil erosion is by means of the semi-empirical Universal Soil Loss Equation (USLE) developed by soil conservationists in the United States and modified for regional use (eg Evans and Kalkanis (1976)). The equation is :

$$E = ARKLSCP \qquad (1)$$

In which

- E is the soil loss in mass per area units.
- A is a constant usually taken as 2,24.
- R is a rainfall factor related to the kinetic energy of falling rain.
- K is an erodibility index.
- LS is a topographic factor accounting for the combined effect of slope length L and slope angle S.
- C is a cropping-management factor

and P an erosion control factor.

Of these factors R is the most important as AR represents the soil loss whereas K, LS, C and P are all modifying factors.

Although it was not intended to establish a USLE for gold tailings dams, it was decided to use the terms in the USLE as a guide to parameters that would probably be important in the study.

For the present investigation, it was decided to select those slope parameters that can be controlled or measured by the engineer and to attempt to establish correlations between them and measured rates of erosion.

The parameters and dimensions selected for correlation were the :

- shear strength of the slope (probably analogous to K);
- slope length;
- slope angle; and
- ETCOM erosion index (formerly the COMET index mentioned by Blight et al, 1981).

The ETCOM instrument directs a jet of water 0,8mm in diameter onto

the soil surface. The pressure behind the jet is increased until the surface is penetrated. The pressure required for penetration, in kPa, is the erosion index. Figure 2 shows the ETCOM in use.

Figure 2 ETCOM erosion tester in use

EXPERIMENTAL WORK

Ten experimental plots were set up on seven gold tailings dams on the Highveld. The plots each measured 9m by 9m and were chosen to have differing aspects, slope lengths and slope angles.

8mm Diameter steel pegs, each 1m in length were driven normal to the slope at 3m intervals giving a 4 x 4 peg array of 16 pegs in total. 250mm Of each peg, accurately measured, was left proud of the ground surface. The erosion loss could then be assessed by measuring the retreat of the slope surface against the datum of the top of the pegs. The positioning of the plot is important if measurements are to be representative, so plots were positioned approximately in the middle of the slope length. It was assumed that erosion would be least at the top of the slope and most at the bottom. Therefore an average value should be

obtained at the centre of the slope. Pegs were driven on an exact grid. As a result, some were located in erosion rills, some on the ridges between rills and some in intermediate positions. Observations confirmed the expectation that rates of erosion would be higher for pegs located further down the slope and also that more rapid erosion occurs in rills, where the quantity of runoff is larger, than on the ridges between rills.

From the average measured surface retreat on the experimental plots and the measured tailings dry density at each plot, the rate of erosion in T/ha/y[b] was calculated for both summer and winter. (Summer was defined for this purpose as the months of October to March[c] while winter was taken as the months April to September.) Most of the rain falls in summer. Winters are generally dry.

In addition to measuring the retreat of the residue surfaces, measurements were also made of the ETCOM erosion index and of the shear strength of the residue surfaces.

Shear strengths were measured by means of a handheld miniature vane (Torvane) which penetrates the surface to a depth of 5mm and thus measures the shear strength of the surface skin that is directly affected by erosion. To eliminate capillary stresses that would have unrealistically increased the shear strength, the test area was pre-soaked by pouring water over it and allowing this to seep away before using the vane. Apart from strength imparted by capillary stresses, the surface of a gold tailings slope is usually weakly cemented by gypsum produced by the reaction of weathered pyrite in the tailings with lime residual from gold extraction.

At the time of writing, only two calendar years' results are available. These span from April 1984 to March 1986. The total rainfall for the test period was 600mm for the first year and 760mm for the second. The average rainfall for these two years was 7 per cent less than the local 30 year average, hence the rainfall for the test period while below average, does not appear to have been abnormal.

Surprisingly, the measured erosion rates showed that erosion in the first winter averaged only slightly less than that in the first summer. Although winter rainfall was only 10 per cent of summer rainfall, winter erosion exceeded summer erosion in some cases. For the ten test plots, the average summer erosion was 145T/ha whereas the average winter erosion was 120T/ha, ie the winter erosion averaged 83 per cent of the summer erosion. For individual plots, winter erosion varied between 45 and 138 per cent of summer erosion. Hence there is a large component of wind erosion in the total erosion figure. It is likely that wind action also causes a significant proportion of summer erosion.

CORRELATIONS BETWEEN EROSION LOSS AND VARIOUS PARAMETERS

Erosion versus ETCOM erosion index

---

b T/ha/y = metric ton per hectare per year. 10T/ha/y = 1 kg/m²/y.
c Southern hemisphere seasons.

Figure 3 shows two correlations - between average ETCOM erosion index measured in summer and in winter and residue loss by erosion. (In this case expressed as erosion loss per season.)

It will be noted that ETCOM readings taken in summer are generally higher than those taken in winter. This is indicative of the generally higher capillary stresses at the slope surface when the weather is hot and rates of evaporation high. Unlike the vane measurements, ETCOM measurements are not made on a pre-wetted surface.

The correlations are positive, showing that erosion loss increases with increasing ETCOM reading. The explanation for this is not entirely clear. ETCOM measurements are made on a desiccated surface for which much of the strength and penetration resistance probably arises from capillary stresses. Hence finer material in which capillary stresses can be larger would be expected to give higher ETCOM readings. When rain wets the surface, the capillary stresses disappear and finer materials then become more erodible than coarser.

Figure 4 shows annual residue loss plotted against the mean of the average summer and winter ETCOM readings. Although there is a lot of scatter and some outlying points, the dashed correlation line could be used as a basis for predicting erosion losses.

Erosion versus shear strength

The correlation between erosion loss and surface shear strength measured by hand vane on a saturated surface, is shown in Figure 5.

The measurements made over the first year gave a poor correlation,

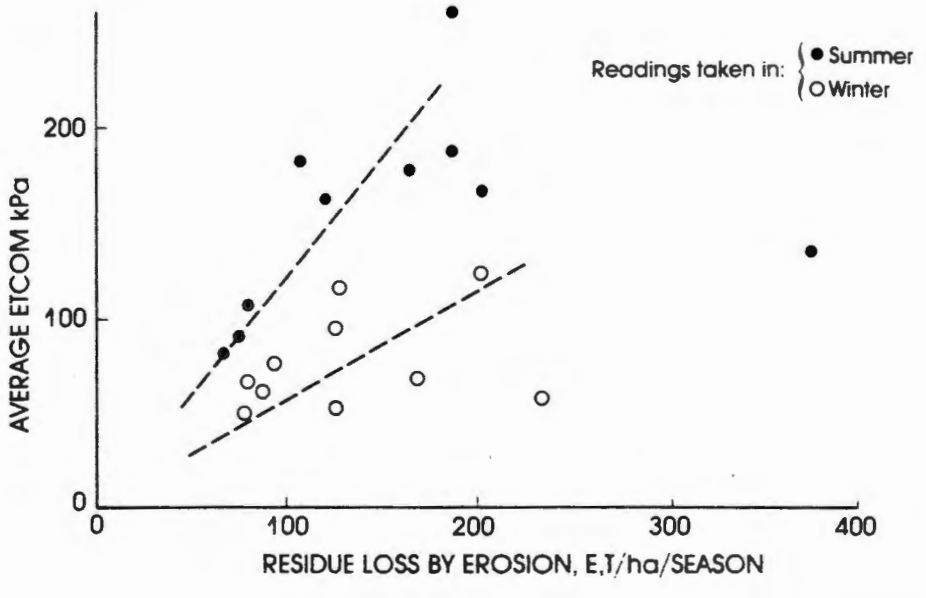

Figure 3 Correlation between ETCOM erosion index and residue loss by erosion

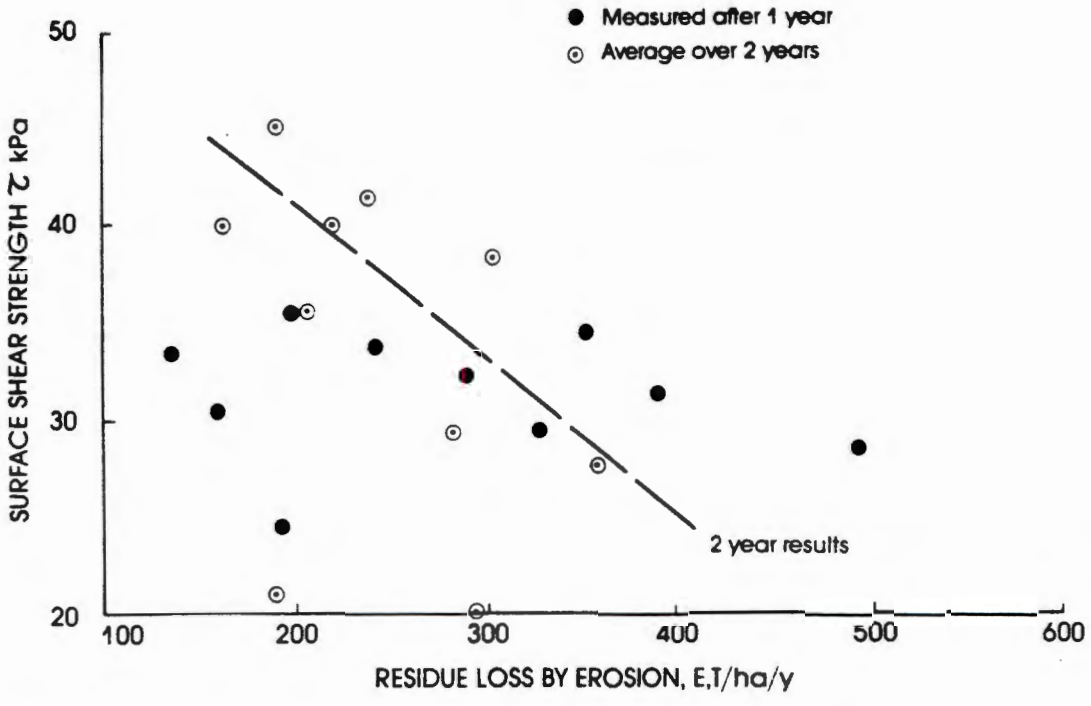

Figure 5 Correlation between surface shear strength and residue loss by erosion

Erosion versus slope *angle*

The correlation between slope angle and erosion loss is shown in Figure 7. In this diagram the slope angle has been expressed as a gradient in per cent, (which is how S in the USLE is expressed) eg an angle of 45° corresponds to 100 per cent.

As the figure shows, the correlation is double valued. For a slope angle of 70 per cent, for example, the average erosion loss could either be of the order of 200T/ha/y or 400T/ha/y.

A similar dependence of rate of erosion on slope angle was identified 50 years ago by Renner (1936) who observed that very little erosion occurred on natural slopes steeper than 80 per cent or flatter than 5 per cent. Other things being equal, progressively steeper slopes will present ever decreasing catchment areas. Very little precipitation will impinge directly on a vertical slope, and if no runoff cascades over the slope from above, there should be no water erosion. Wind erosion could, of course, still occur.

USING CORRELATIONS TO PREDICT EROSION RATES

Because of the uncertainty in the correlations that have been established so far, it is recommended that Figures 4, 5, 6 and 7 be used in conjunction to predict erosion rates. For example, for a typical slope :

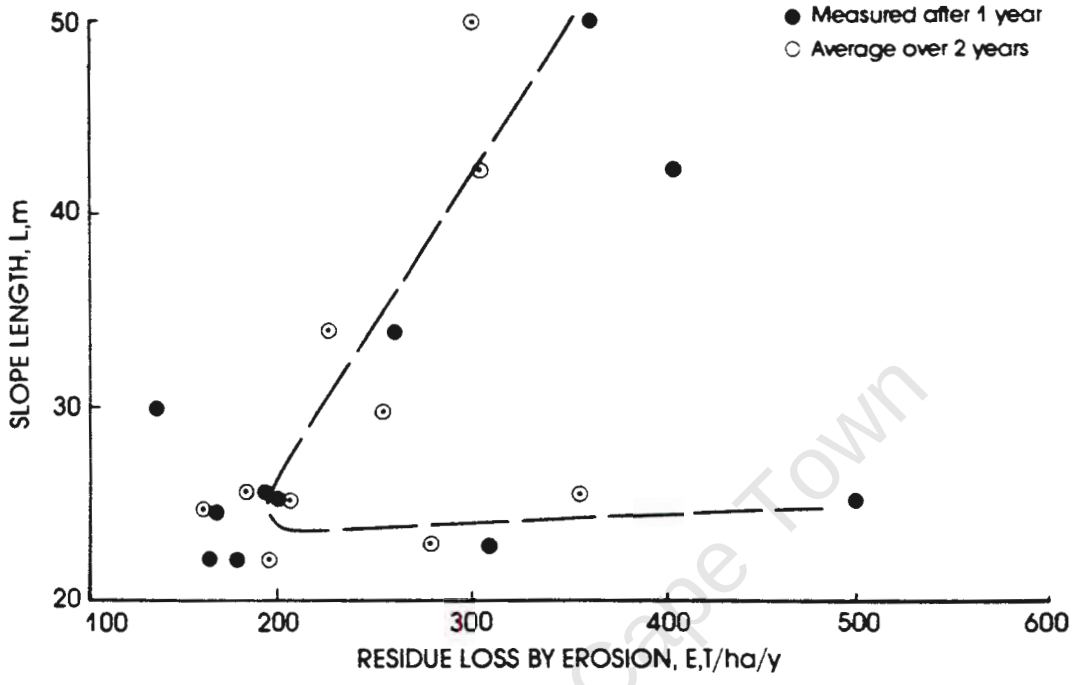

Figure 6 Correlation between slope length and residue loss by erosion

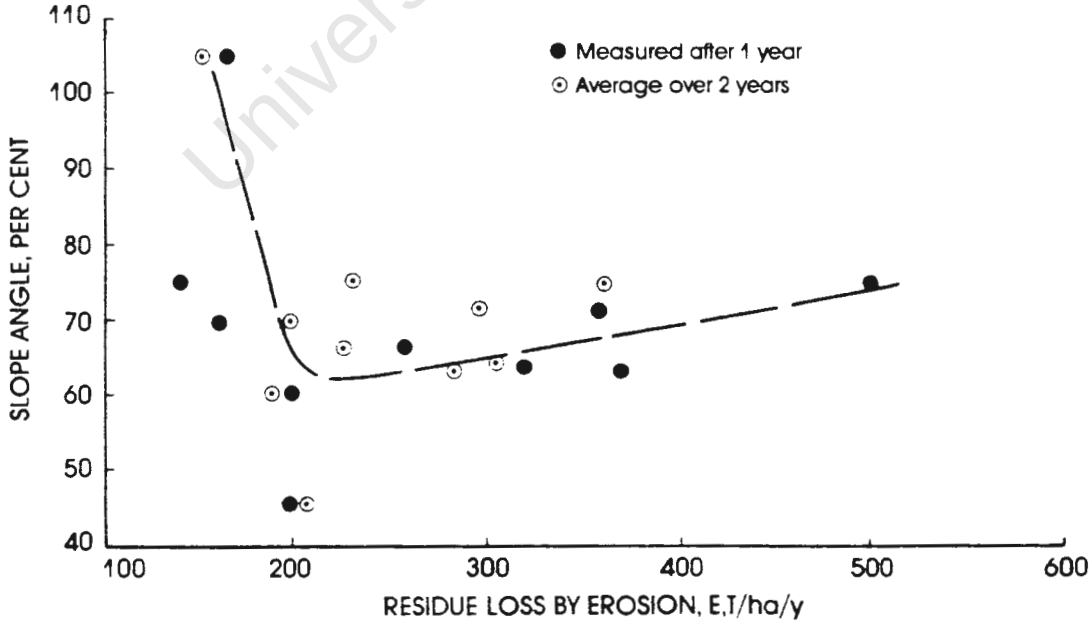

Figure 7 Correlation between slope angle and residue loss by erosion

ETCOM = 209kPa ∴ E = 380T/ha/y from Figure 4

Mean τ = 260kPa ∴ E = 390T/ha/y from Figure 5

L = 49m ∴ E = 350T/ha/y from Figure 6

S = 64% ∴ E = 290T/ha/y from Figure 7
(ignoring lower value on graph)

Mean estimated E = 350T/ha/y

Observed 2 year average E = 294T/ha/y

As indicated earlier, the value of erosion rate given above includes components of wind and water erosion. The present state of knowledge does not allow of accurate apportionment of the total between the two components. As an interim measure it is suggested that two thirds of the total erosion rate be assigned to water erosion and one third to wind erosion. Silt containments would obviously have to be designed to contain the water erosion component, but not that due to wind erosion.

As a design value, two thirds of either the mean estimated, or the largest estimated E could be adopted for designing the capacity of silt containing structures such as toe paddock dams. The data could also be used as a basis for estimating de-silting requirements and hence maintenance costs for erosion-containing structures and for deciding on whether or not a given dam or slope needs to be protected, by some means, against erosion.

The correlation may also in principle be used to optimise the profile of a slope to reduce erosion losses. Figure 6 indicates that it may be preferable to break a long continuous slope up into a series of shorter, steeper slopes separated by berms. However, the designer would have to be sure which branch of the correlation in Figure 7 applied to the original slope before taking this step. Measures would also need to be taken to prevent water from cascading over the edge of a berm onto the slope below.

CONCLUSIONS

The research described inthis paper has identified the more important factors affecting erosion from the slopes of gold-residue dams. It has demonstrated that wind erosion must be a very significant component of the total annual erosion from a slope. It has, for the first time, provided quantitative information on rates of erosion from gold-residue dams.

This information is, as yet, tentative and may apply both qualitatively and quantitatively, only to conditions in the Highveld region of South Africa.

CURRENT RESEARCH

As stated earlier, this paper is based on the data for only two

years. Measurements at the various sites will be continued for at least another three years to confirm these preliminary findings. Additional sites have been set up to measure rates of accretion in silt containments, Not only should these measurements support those made on the slopes from which the silt is derived, but should give a useful indication of the split, both in summer and winter, between wind and water erosion.

Measurements of erosion rates from the top surfaces of dams are also being made, including some on cement-stabilized and stone-mulched surfaces and others on vegetated surfaces. A number of vegetated slopes are also being monitored. The results will be reported when they become available.

ACKNOWLEDGEMENTS

The writer acknowledges the support and assistance received from the Chamber of Mines of South Africa Vegetation Unit, and in particular, from Mr Don Marsden. Most of the field work was done by Mr Douglas Dorren as research for a Masters degree.

REFERENCES

Bagnold, R.A., The physics of blown land and desert dunes, Methuen, London, 1959.

Bagnold, R.A., Fluid Forces on a Body in Shear Flow; Experimental Use of"Stationary Flow", Proceedings, Royal Society, London, A.340, 1974, pp. 147-171.

Blight, G.E., Rea, C.E., Caldwell, J.A. and Davidson, K.W., Environmental protection of abandoned tailings dams. Proceedings, 10th International Conference on Soil Mechanics and Foundation Engineering, Stockholm, 1981, vol.2, pp. 303-308.

Chamber of Mines of South Africa. Guidelines for Environmental protection, vol.1/1979 (Revised 1983), The design, operation and closure of residue deposits, Johannesburg, The Chamber, 1979.

Evans, W.R. and Kalkanis, G., Use of the universal soil loss equation in California, Soil Erosion : Prediction and Control, Soil Conservation Society of America, 1976, pp. 31-40.

Gillete, D.A.,Blifford,I.H. and Fenster, C.R., Measurements of aerosol size distributions and vertical fluxes of aerosols on land subject to wind erosion,Journal of Applied Meteorology, vol.11,1972, pp.977-982.

Hjulstrom, F., The morphological activity of rivers as illustrated by river Fyris, Bulletin of the Geological Institute of Uppsala, Chapter III, 1976.

Renner, F.G., Conditions influencing erosion on the Boise river watershed, U.S. Department of Agriculture, Technical Bulletin 528, 1936.

J. S. Afr. Inst. Min. Metall., vol. 89, no. 1.
Jan. 1989. pp. 23-29.

Erosion losses from the surfaces of gold-tailings dams

by G.E. BLIGHT*

SYNOPSIS

Rates of erosion have been measured for the slopes and top surfaces of a number of gold-tailings dams in the Germiston–Johannesburg–Roodepoort area of the Transvaal. Preliminary results were given in an earlier paper. The present paper gives results for a four-year period of observation, and identifies the major factors affecting the rates of erosion from the surfaces of gold-tailings dams.

SAMEVATTING

Erosietempos is vir die hellings en bokante van 'n aantal gouduitskotdamme in die Germiston–Johannesburg–Roodepoort gebied van Transvaal gemeet. Die voorlopige resultate is in 'n vroeëre referaat verstrek. Hierdie referaat gee die resultate vir 'n waarnemingstydperk van vier jaar en identifiseer die belangrikste faktore wat die erosietempo van die oppervlakke van gouduitskotdamme bepaal.

Introduction

Ways and means of preventing surface erosion from gold-tailings dams and the difficulties of doing so were described in two papers by Blight *et al.*[2] and Blight and Caldwell[3]. Those papers describe various defences that were devised to reduce erosion losses and the problems that arise with their implementation. At that time it became clear that not enough was known regarding the rate at which material can be removed by erosion, or the relative importance of wind and water erosion. The distribution of erosion losses over the slopes and top surfaces of tailings dams was also not known. There was an impression, gained from the observation of dust clouds emanating from tailings dams during windy weather, that wind erosion affected mainly the top surfaces of tailings dams and water erosion the slopes. This impression was reinforced by the observation that the slopes of gold-tailings dams are usually hard and crusted, and are apparently impervious to the effects of wind, whereas there are often pockets and areas of loose material lying on the top surfaces of dams. Finally, the efficacy of various measures proposed to reduce erosion losses was not known.

In 1984 the writer, with the assistance of the Chamber of Mines of South Africa, initiated a programme to measure erosion losses from the slopes of gold-tailings dams in the Transvaal. The programme was subsequently extended to include measurements of erosion losses from the top surfaces of dams, and the rates of accretion of material lost from slopes and caught in erosion catch-paddocks. The preliminary results of these observations were published after two years by Dorren and Blight[1] and by Blight[4].

The purpose of the present paper is to give the results of four years of observations. Whereas the previous two papers described only the rates of loss from the unprotected slopes of tailings dams, this paper also describes the rates of loss from top surfaces and grassed slopes. It also discusses the efficacy of some measures that have been proposed to reduce erosion losses.

The Measurement Programme

The two previous papers[1,4] summarized the theoretical mechanics of erosion by water and wind, and the reader is referred to those papers and others[5–9]. In brief, the variables under the control of the engineer that, according to theory and empirical knowledge, affect the rate of erosion of a soil are as follows:

- the strength of the soil surface,
- the length of a slope, and
- the slope angle or inclination of the surface.

The surface roughness or micro-relief is also known to affect rates of erosion (e.g. Jennings and Jarrett[10]).

Two means have been used to measure the strength of tailings surfaces.

ETCOM Penetration Resistance

The ETCOM instrument directs a jet of water 0,8 mm in diameter to impinge normally on the tailings surface. The pressure behind the jet is increased until the surface is penetrated, and the pressure in kilopascals at which penetration occurs is used as an index of erosivity. At first, correlations were made with values of ETCOM measured on initially dry tailings surfaces. Later, ETCOM values were also measured on surfaces that had been prewetted by having water poured over them and had then been allowed to drain of free water before measurement of the index. This was to eliminate capillary stresses that may falsely have enhanced the strength of the surfaces.

When the ETCOM instrument was developed, it was expected that the erosion resistance of a surface would be directly related to the ETCOM reading, and that erosion loss would decrease as the ETCOM reading increased. However, it has since been found that high ETCOM readings correspond to high erosion losses, and *vice versa*. The reasons for this apparently anomalous result were

* Head of Department of Civil Engineering, University of the Witwatersrand, 1 Jan Smuts Avenue, Johannesburg 2001.

ISSN 0038–223X/$3.00 + 0.00. Paper received 3rd August, 1988.

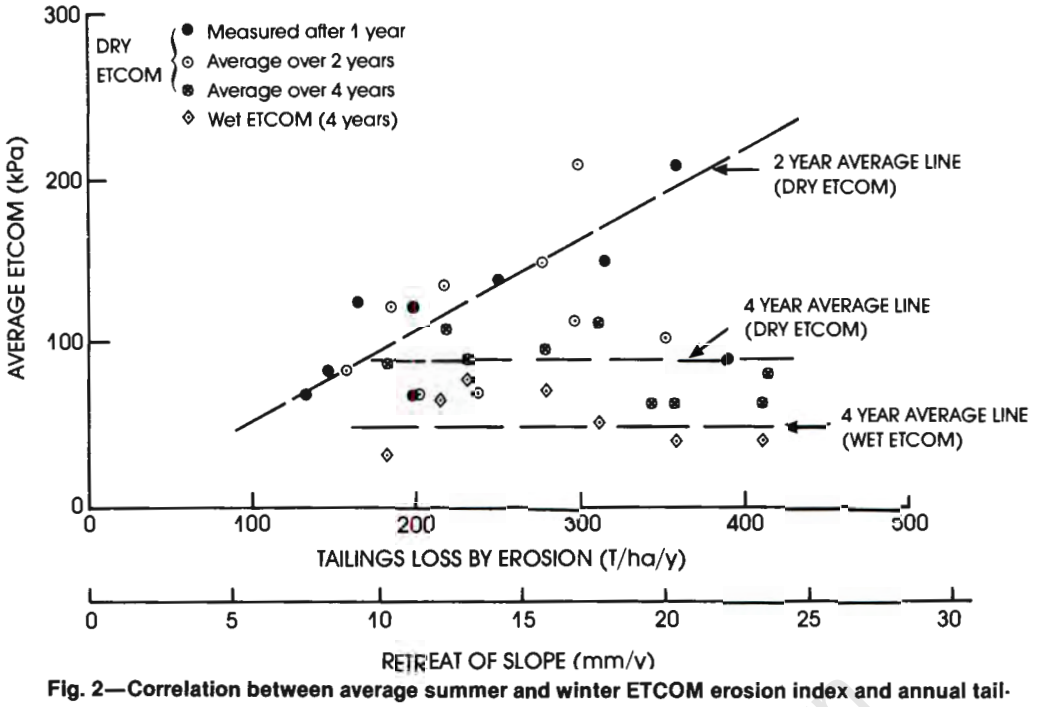

Fig. 2—Correlation between average summer and winter ETCOM erosion index and annual tailings loss by erosion

3 had much lower maximum values, but also higher minimum values, than those measured in year 1. The reason for this effect is not clear. It is probably because the slope surfaces were not as dry in year 3 as they were in year 1, and were therefore generally not as resistant to penetration by the water jet. Whatever the reason, the change in ETCOM values converted correlation to independence for these data.

Surface Shear Strength and Erosion Loss

The correlation between surface shear strength and erosion loss is shown in Fig. 3.

The surface shear strength was measured at the end of each summer and winter period, and the values represent a running average over 1, 2, or 4 years as the case may be. The data show a similar trend to that for dry ETCOM, i.e. shear strength shows a progressive decrease with time.

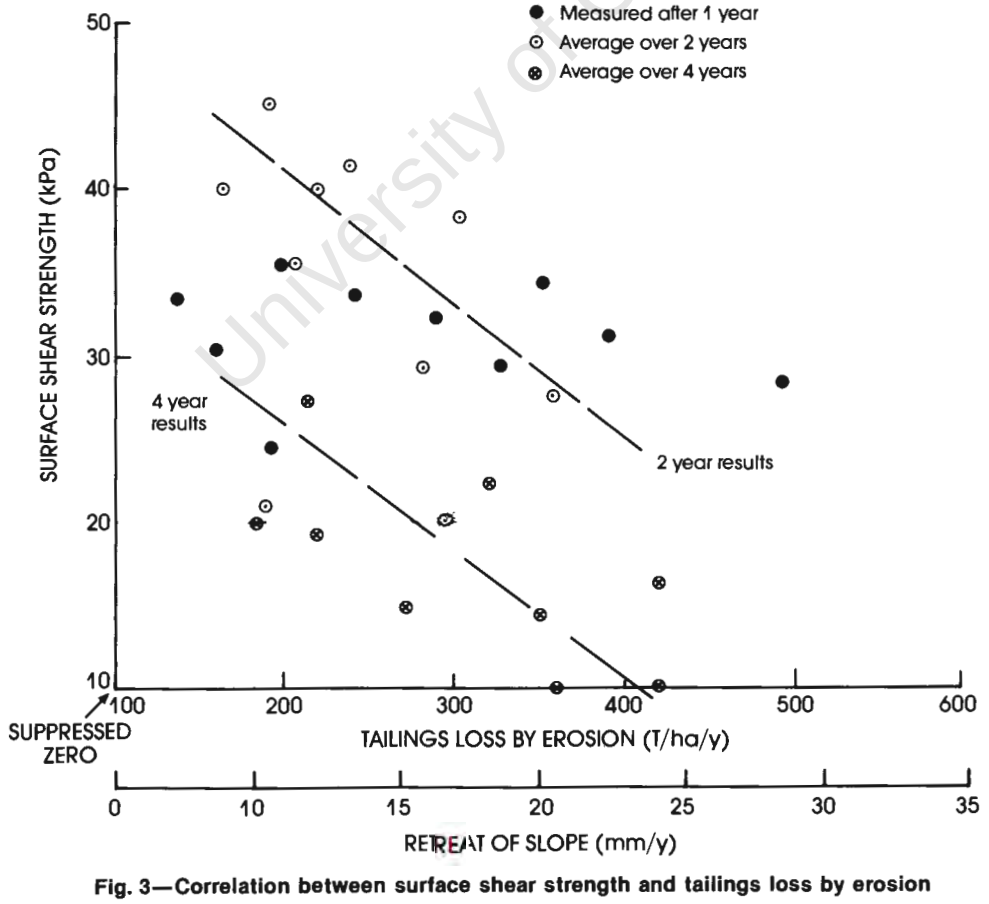

Fig. 3—Correlation between surface shear strength and tailings loss by erosion

distributed over the entire length of each slope, instead of being located at midslope.

Grassed Slopes

Three grassed slopes were included in the programme. Fig. 4 shows 2-year average results for the erosion of two of those slopes, a west- and a south-facing slope. The results lie well to the left of the data for untreated slopes. The result for the third slope, north-facing, is not shown because it is not eroding but is accreting at an annual rate of 35 t/ha (2 mm). Material blown off the other slopes of the dam is apparently trapped by the grass on the north face, and the rate of erosion by water is insufficient to remove this entrapped material. The maximum observed accretion rate for this slope during the winter was 90 t/ha per year (or 5 mm per year).

Slope Angle and Erosion Loss

Bare Slopes

All the available data relating erosion loss to slope angle are shown in Fig. 6. Once again, the data can be regarded as showing no correlation at all, or they can be regarded as showing the two-branched relationship indicated in the diagram. As pointed out earlier, the USLE indicates that a positive correlation can be expected between slope angle and erosion loss. A qualitative two-branched correlation between slope angle and erosion loss was previously noted by Renner[11], who observed that very little erosion occurs on natural slopes steeper than 80 per cent (39 degrees) or flatter than 5 per cent (3 degrees).

Terraced Slopes

Blight *et al.*[2] and Blight and Caldwell[3] suggested that the erosion of a slope can be reduced if it is terraced in a series of steps with vertical and sub-horizontal surfaces, as illustrated in Fig. 7. Each sub-horizontal surface slopes back towards the vertical step above, and is hydrologically designed to retain precipitation on it without spilling down to the next step. The erosion of two terraced slopes was observed as part of this programme.

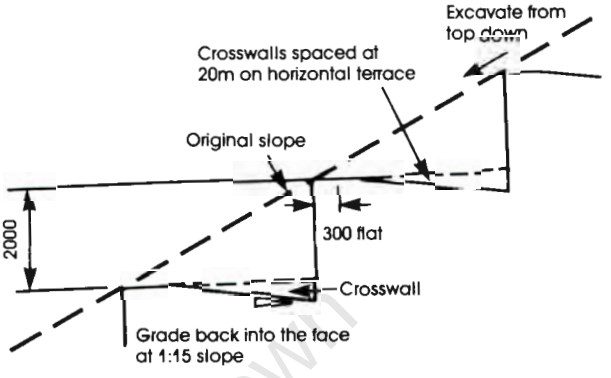

Fig. 7—Design section for a terraced slope

The results of the measurements, shown in Fig. 6, confirm that erosion losses from terraced slopes are relatively

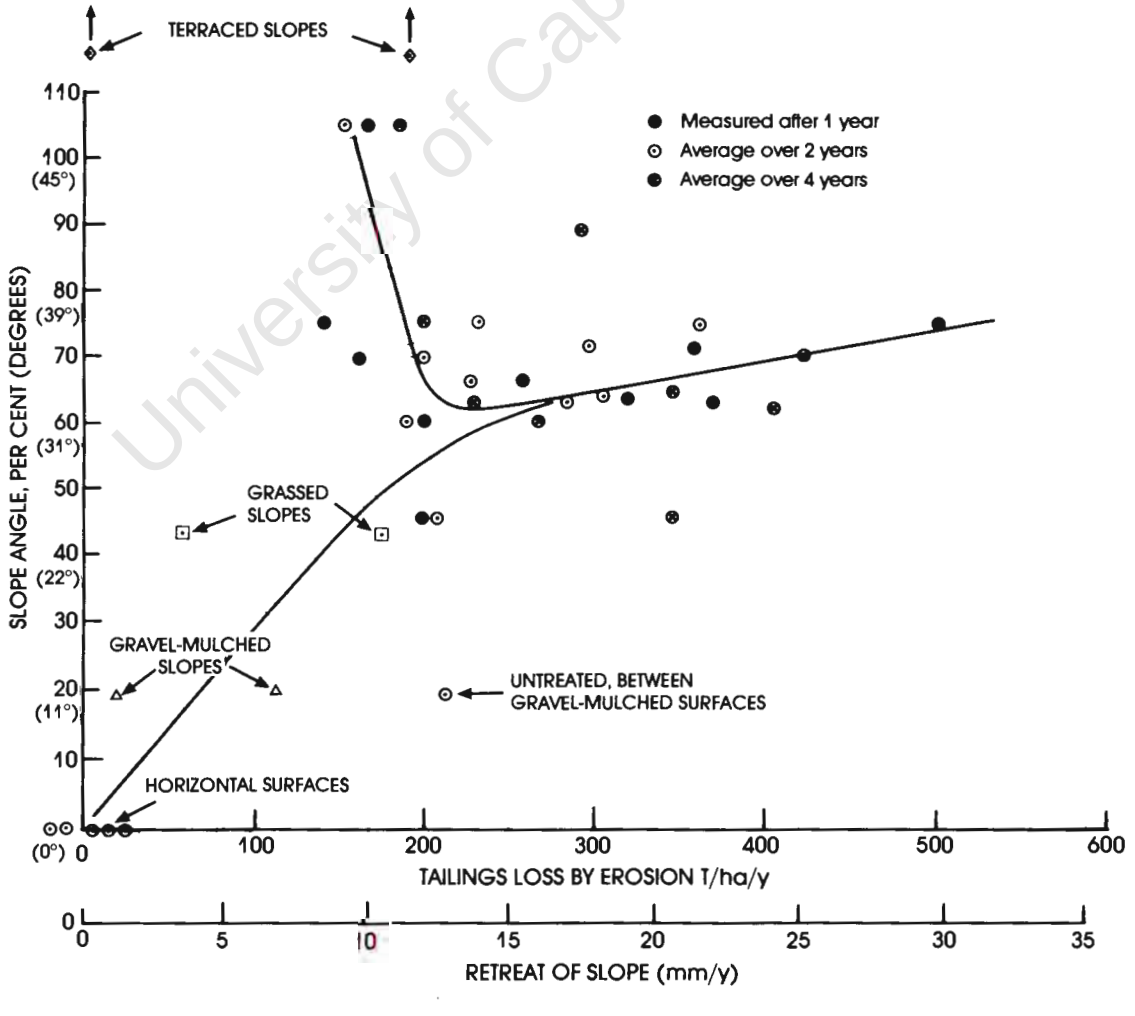

Fig. 6—Correlation between slope angle and tailings loss by erosion

4. BLIGHT, G.E. Erosion of the slopes of gold tailings dams. *Geotechnical practice for waste disposal.* ASCE Publication, 1987. pp. 294–305.
5. BAGNOLD, R.A. *The physics of blown sand and desert dunes.* London, Methuen, 1959.
6. EVANS, W.R., and KALKANIS, G. Use of the universal soil loss equation in California. *Soil Erosion: Prediction and Control, Proceedings, National Soil Erosion Conference.* Soil Conservation Society of America, 1977. pp. 31–40.
7. GREGORY, J.M., BORRELI, J., and FEDLER, C.B. Team: Texas erosion analysis model. Summer Meeting, American Society of Agricultural Engineers, Rapid City, S.D., 1988. Paper 88–2121.
8. KIRBY, M.J., and MORGAN, R.P.C. *Soil erosion.* New York, Wiley, 1980.
9. WOODRUFF, N.P., and SIDDOWAY, F.H. A wind erosion equation. *J. Soil Sci. Amer.*, vol. 25, no. 5. 1965. pp. 602–608.
10. JENNINGS, G.D., and JARRET, A.R. Laboratory evaluation of mulches in reducing erosion. *Trans. Am. Soc. Agric. Engrs,* vol. 28, no. 5. 1985. pp. 1466–1470.
11. RENNER, F.G. Conditions influencing erosion on the Boise River watershed. US Department of Agriculture, *Tech. Bull.* 528. 1936.
12. JOHNSON, C.B., MANNERING, J.V., and MOLDENHAUER, W.C. Influence of surface roughness and clod size and stability on soil and water losses. *J. Soil Sci. Amer.,* vol. 43, 1979. pp. 772–777.

The SAIMM Council 1988/1989

Council Members 1988/1989, left to right:

Row 1 (seated): H.E. James, P.W.J. van Rensburg, Dr H. Wagner, B.C. Alberts, C.E. Fivaz (President), H.G. Mosenthal, R.D. Beck, Professor A.N. Brown, Dr P.R. Jochens

Row 2 (standing): P.C. van Aswegen, J.P. Hoffman, D. Wilson, P.M.T. White, K.A. van Gessel, Dr L.A. Cramer, J.S. Freer, V.J. Moore, G.A. Brown, R.A. Snodgrass, J.D. Austin

Row 3 (standing): Dr G.A. Fourie, Dr J. Lurie, A.M.P. Henderson, R.P. Mohring, J.A. Cruise, J.L. Nel, H. Scott Russell, J.P. Deetlefs, D.A.J. Ross-Watt

Inserts, top row: K.R. Beard, N.J. Devine, R.J. Dippenaar, G.T.G. Emère, Dr J–P. Franzidis, Professor R.P. King, J.G. McCallum.

Bottom row: G.Y. Nisbit, Professor R.P. Plewman, Dr R.E. Robinson, Dr O.K.H. Steffen, P.A. von Wielligh

PROCEEDINGS OF THE 1991 NATIONAL MEETING OF THE AMERICAN SOCIETY OF SURFACE MINING AND RECLAMATION

VOLUME I

Editors:

Wendall Oaks
Joe Bowden

EROSION AND ANTI-EROSION MEASURES FOR ABANDONED GOLD TAILINGS DAMS[1]

by
Geoffrey E. Blight[2]

Abstract. This paper briefly describes geotechnical measures for the abatement of air and water pollution from abandoned gold-residue dams. The measures were specified by a set of guidelines for environmental protection formulated for the Chamber of Mines of South Africa in 1979. The results of measured rates of erosion of unprotected tailings surfaces are then given and the effect of various anti-erosion treatments is reported. These treatments include surface stabilization with cement, grassing, and gravel mulching.

Introduction

Unlike Canada and the United States of America, the Republic of South Africa has no legislation specifically directed towards the protection of the environment from the effects of mining. However,there are a number of statutes that affect the design, operation, and abandonment of tailings deposits. To comply with the requirements of these statutes and to achieve effective environmental control over the tailings deposits owned by its members, the Chamber of Mines of South Africa, in 1978, commissioned the author to draft a comprehensive set of guidelines for the design, operation, and closure of tailings deposits. These guidelines were adopted in 1979 and revised in 1983.

Whereas valley dams are common in the United States, most tailings dams in South Africa are ring-dyke structures constructed on relatively flat ground. Because they protrude above the natural ground contours, these dams are particularly exposed to the erosive forces of the atmosphere. Figure 1 shows the layout of a typical ring-dyke gold tailings dam.

The guidelines for the closure of tailings deposits require, prior to the closure of any tailings deposit, an inspection by a geotechnical engineer, who should report on the existing state of the deposit and list all actions needed to ensure that the deposit complies with the provisions of the guidelines. In addition to the state of the tailings deposit itself, the report should note the presence of any adjacent structures or development, and the extent to which they may be affected by abandonment of the deposit. Recommendations to minimize the impact of abandonment, or of possible failures of the deposit after abandonment, should also be made in consultation with professionals of appropriate related disciplines

Specific Requirements of the Guidelines

The Chamber of Mines Guidelines have a number of specific requirements.

Erosion of Top Surfaces.The guidelines require the best practicable means to be adopted to prevent erosion of top surfaces. Among the measures that have been suggested for control of wind erosion are the following:

(a) the establishment of vegetation on top of a deposit, either by planting directly into the tailings material or by first covering the surface with a layer of top soil of suitable thickness.

(b) covering the top of the deposit with a suitable thickness of broken waste rock.

Water erosion of top surfaces, as well as a requirement that all precipitation should be held on the dam and not discharged into any stream, has been addressed by a system of crest walls that subdivide the surface of the dam into a series of paddocks as shown in Figure 2. The crest walls also prevent precipitation

---

[1] Paper presented at the 1991 National Meeting of the American Society for Surface Mining and Reclamation, Durango, Colorado, May 14-17, 1991.

[2] Geoff Blight is Professor of Construction Materials and Head, Department of Civil Engineering, Witwatersrand University, Johannesburg, Private Bag 3, 2050, South Africa.

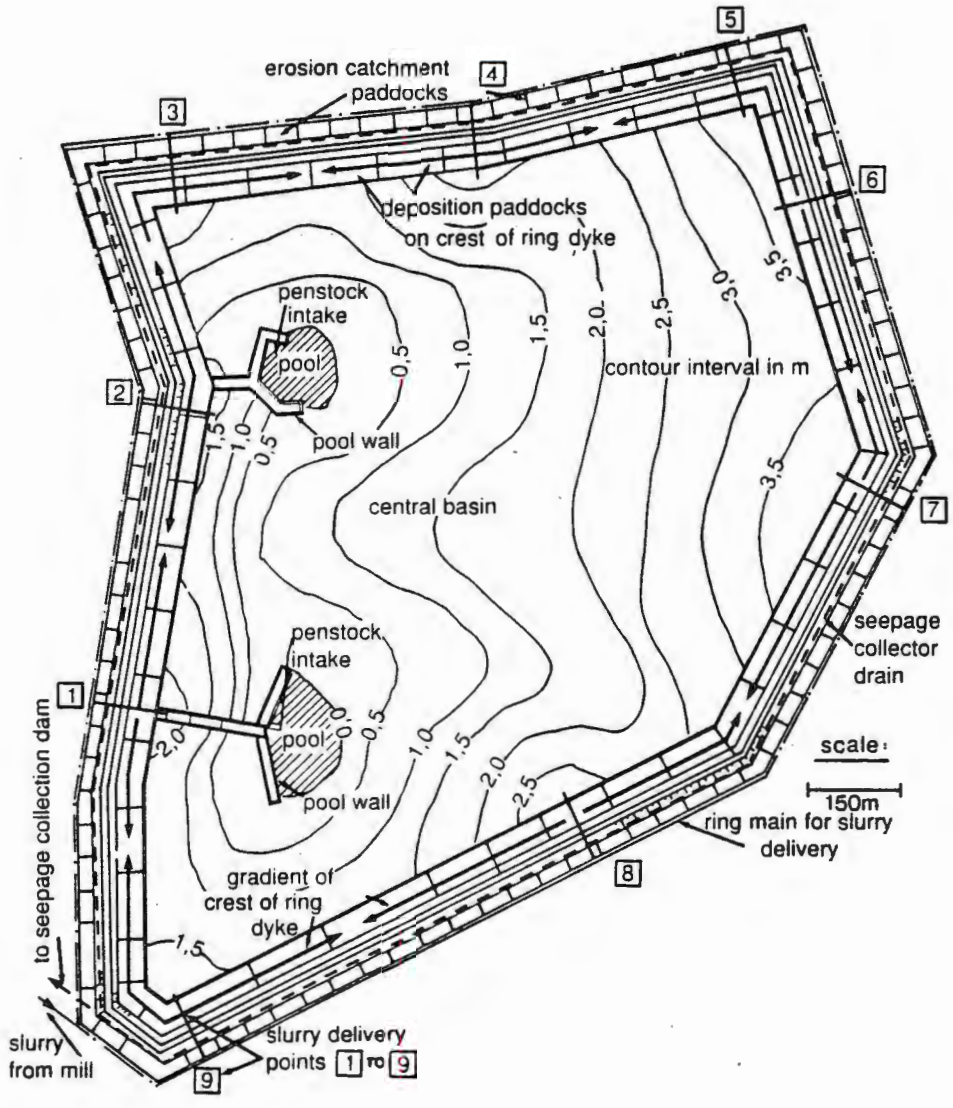

Figure 1 Layout of a typical ring-dyke tailings dam.

on top of the dam from cascading down the outer slopes and increasing the potential for slope erosion. The height of the crest and division walls is designed hydrologically so that the walls will contain the maximum probable precipitation over a period of 24 hours, with a frequency of once in a 100 years. A freeboard of 0.5 m is required throughout the system above the predicted maximum water level. In the Witwatersrand area, as the annual evaporation from a free-water surface vastly exceeds the annual precipitation, there is usually no need to decant water from the top surface of a deposit.

Paddocks must be carefully shaped to prevent water from standing near the crest wall of a dam. Numerous cases of piping erosion have occurred when water has been held on the surface near to the crest of a dam.

The penstocks used to decant water during the operation of a residue dam are plugged when the dam is closed because they otherwise tend to collapse and provide channels for piping erosion. Old dams often have a number of steel delivery or penstock pipes buried in them at various positions. The steel has usually corroded away and the resulting void has been enlarged by erosion. Such a collapsed pipe can result in severe internal erosion and gulleying of the tailings dam.

Erosion of Slopes. The slopes of old residue dams are extremely steep (usually 35° or more) and the

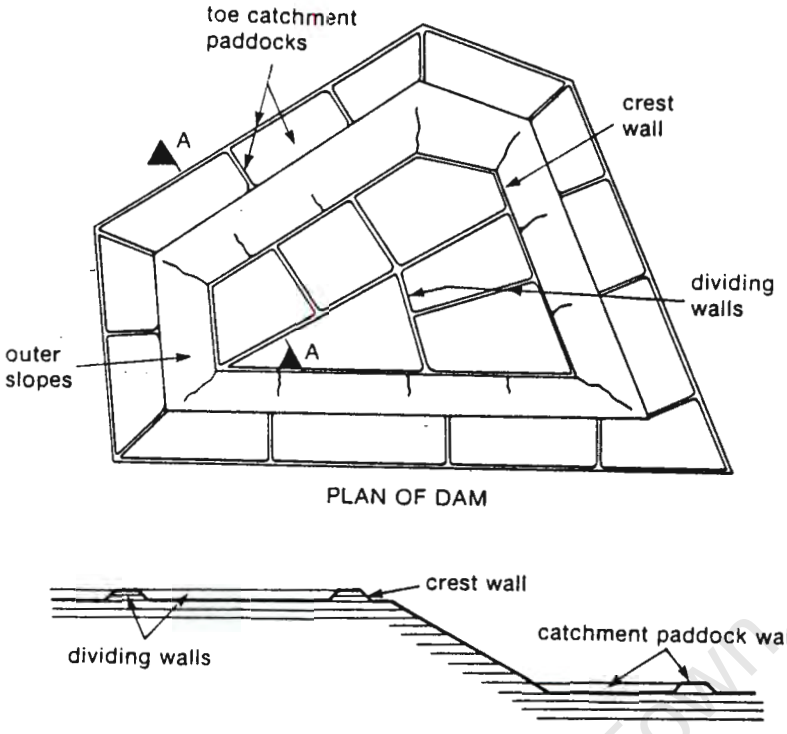

Figure 2 Anti-erosion walls and cathchment paddocks on an abondoned ring-dyke tailings dam

protection of these steep slopes against erosion is very difficult. Sheet erosion of the slopes can be reduced, and gulley erosion virtually eliminated, by the provision of crest walls, which prevent water from cascading off the top and down the slopes of a residue deposit. Slopes can be protected against erosion by being covered with a layer of waste rock. However, this requires a large quantity of rock because the angle of repose of the rock seldom, if ever, equals the slope angle. Vegetation has also been used to provide protection against erosion. This practice has not proved entirely successful: some of the steeper slopes are gradually denuded of grass as erosion progresses.

Containment of Precipitation and Eroded Material. Run-off and eroded material are contained by a series of catchment paddocks around the perimeter of a dam. These paddocks are designed hydrologically to ensure a freeboard of at least 0.5 m above the maximum predicted water level, which is based on the average monthly rainfall for the area concerned, less the gross mean evaporation for the area plus the maximum precipitation to be expected over a period of 24 hours for a frequency of once in 100 years. To this is added an additional capacity to allow for the siltation resulting from erosion off the slopes.

Control of Access. It has been found essential to prevent access to abandoned tailings deposits by the public, especially those seeking recreation by horseriding or cross-country motorcycling. The trails left by these activities often reduce the freeboard of paddock walls and result in gulley erosion. It is, therefore, considered essential that each abandoned tailings deposit be surrounded by a properly constructed, well-maintained security fence.

Stability of Slopes. The retention of water on the top surface of a tailings deposit, as well as measures such as erosion protection by covering of slopes with rock, may lead to instability of the slopes. The guidelines require an investigation of potential slope instability as part of the closure report.

Preparation of the guidelines exposed a number of areas in which knowledge was either inadequate or non-existent. The most important of the areas of ignorance were the actual rate of erosion of tailings dams, the parameters that affect erosion, and means of preventing erosion. Rates of accretion in silt-trapping structures were not known either. The relative importance of wind and water as agents of erosion was also unknown. There was an impression,

gained from the observation of dust clouds emanating from tailings dams during windy weather, that wind erosion affected mainly the top surfaces of tailings dams and water erosion the slopes. This impression was reinforced by the observation that the slopes of gold-tailings dams are usually hard and crusted, and are apparently impervious to the effects of wind, whereas there are often pockets and areas of loose material lying on the top surfaces of dams.

Rates of Erosion from Gold Tailings Dams

In 1984, the author initiated a programme to measure erosion losses from the slopes of gold-tailings dams. The programme was subsequently extended to include measurements of erosion losses from the top surfaces of dams, and the rates of accretion of material lost from slopes and caught in erosion catch-paddocks.

Measurements of the rates of erosion were made in the field at 10 different sites. At many of these, measurements were made on more than one slope or surface. This was because it was initially thought that the aspect of the slope with respect to the direction of the sun and prevailing winds might be important. However, in only 1 case was such an influence detected.

The experimental measurement plots were each 9 m by 9 m in plan, and consisted of a grid of steel pegs 1 m long and 8 mm in diameter. These were driven in normal to the surface at 3 m intervals to give a 4 x 4 array of 16 pegs. 50 mm of each peg was left protruding from the ground. The erosion loss (or gain) could then be gauged simply from measurements taken at successive times of the distance from the tip of each peg to the tailings surface.

The erosion-measurement plots on slopes were positioned approximately in the middle of the slope length. All pegs were driven in an exact grid. Thus, some were located in erosion rills, some on ridges between rills, and others in intermediate positions.

The results are reported as average values for the whole of each plot. However, observations on individual pegs confirmed the expectation that rates of erosion tend to be progressively higher from the top to the bottom of a slope, and also higher in rills, where the quantity of runoff is larger. In each case, a crest wall was present at the crest of the slope to ensure that no water cascaded down the slope from the top of the dam and that any measured erosion was thus the effect only of water precipitated directly onto the slope.

Originally, each test area was equipped with a rain gauge. However, these were all vandalized within a few weeks of installation, and information from the nearest official meteorological stations was therefore relied on for rainfall data.

For the first year of the experiment, April 1984 to March 1985, the rainfall was 20 % less than the local 30-year average of 750 mm. For the second year, up to March 1986, the rainfall was almost equal to the 30-year average. For the final 2 years, from April 1986 to May 1988, the rainfall was 11 % and 29 % above the 30-year average. For this reason, most of the results are reported in terms of 1-year, 2-year, and 4-year averages.

Distribution of Erosion between Seasons. Figure 3 shows the seasonal distribution of erosion loss from tailings slopes observed over the first year of the experiment. Most of the rainfall occcurs in summer, but there are usually at least 1 or 2 precipitation events during winter. These account for about 10 % of annual precipitation. In Figure 3, the erosion loss quoted in terms of retreat of the slope in millimeters per season, and tons lost per hectare per season has been plotted against the ETCOM index measured on dry surfaces.

The ETCOM index is measured by directing a jet of water 0.8 mm in diameter to impinge normally on the tailings surface. The pressure behind the jet is increased until the surface is penetrated and the pressure (in kilopascals) at which penetration occurs is used as an index of erosivity.

When the ETCOM instrument was developed (by the Chamber of Mines of South Africa), it was expected that the erosion resistance of a surface would be directly related to the ETCOM reading, and that erosion loss would decrease as the ETCOM reading increased. However, it has since been found that high ETCOM readings correspond to high erosion losses, and vice versa.

This is essentially because high ETCOM indices occur on surfaces of fine-grained, desiccated material. Once such a surface has been wetted by rain, it becomes soft and easily eroded. Probably for similar reasons, no correlation was found between the shear strength of tailings surfaces and erosion losses. As Figure 3 shows, erosion loss during the winter amounted to about 80 % of the loss during the summer. For individual plots, the winter erosion was measured at between 40 and 140 % of the summer erosion. This shows that there is a large component of wind erosion in the total annual erosion loss. The visual impression referred to earlier is thus erroneous, and the slopes of tailings dams are indeed subject to considerable erosion by wind.

Figure 3 also shows that erosion losses are very considerable, whether reported in terms of slope

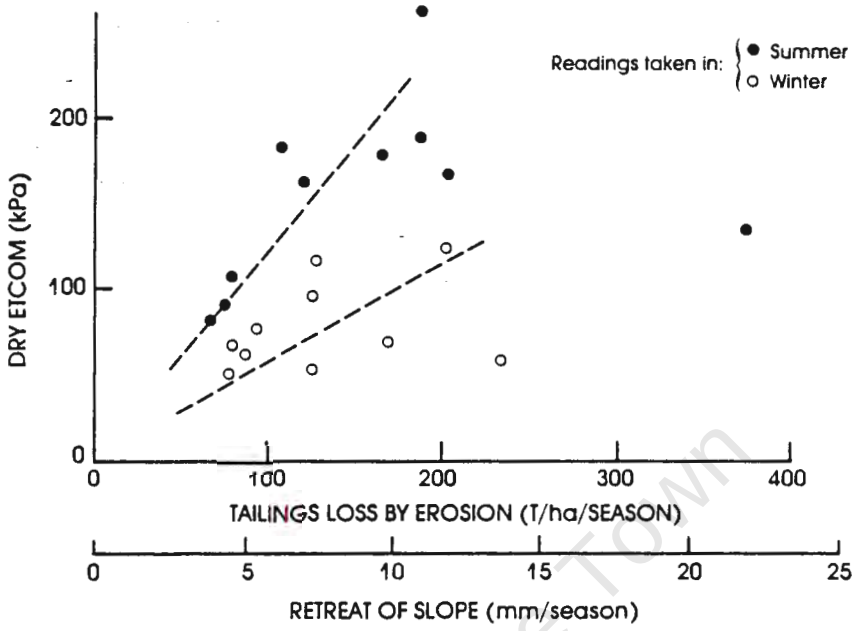

Figure 3 Correlation between seasonal erosion loss and ETCOM erosion index

retreat or tons/ha/yr. Annual erosion losses from agricultural fields rarely exceed 10 to 15 t/ha, whereas annual losses from the slopes of tailings dams are measured in 100 tons/ha.

Slope Length and Erosion Loss. The Universal Soil Loss Equation (USLE) gives the soil loss E as

$$E = ARKLSCP,$$

(e.g. Evans and Kalkanis 1977) in which LS is a topographic factor to account for the combined effect of slope length (L) and slope angle (S) and A, R, K, C, and P are factors accounting for other effects. Because the slopes of agricultural land are generally flat, the USLE is not regarded as being valid for slopes steeper than 25 % (about 14°).

Figure 4 shows the measured relationship between slope length and erosion loss. Part of the data show a positive correlation between slope length and erosion loss, and part do not.

The portion of Figure 4 that indicates no correlation between slope length and erosion loss is believed to arise because of the stronger influence of other factors such as surface shear strength or slope angle. It may also arise because certain of the test plots were too small to adequately represent average erosion over the length of some of the slopes, or simply because certain slopes were subjected to more precipitation and, therefore, eroded more than others.

Three grassed slopes were included in the programme. Figure 4 shows 2-year average results for the erosion of 2 of those slopes, a west- and a south-facing slope. The results lie well to the left of the data for bare slopes. The results for the third slope (north-facing) is not shown because it is not eroding but is accreting at an annual rate of 35 t/ha (2 mm). Material blown off the other slopes of the dam is apparently trapped by the grass on the north face, and the rate of erosion by water is insufficient to remove this entrapped material. The maximum observed accretion rate for this slope during the dry winter was 90 t/ha per year (or 5 mm/yr).

Slope Angle and Erosion Loss. All the available data relating erosion loss to slope angle are shown in Figure 5. The data can be regarded as showing the 2-branched relationship indicated in the diagram. As pointed out earlier, the USLE indicates that a positive correlation can be expected between slope angle and erosion loss. A qualitative 2-branched correlation between slope angle and erosion loss was previously noted by Renner (1936), who observed that very little erosion occurs on natural slopes steeper than 80 % (39°) or flatter than 5 % (3°).

The reduced erosion loss at steep slope angles suggested that the erosion of a slope can be reduced if it is terraced in a series of steps with vertical and sub-horizontal surfaces. Each sub-horizontal surface

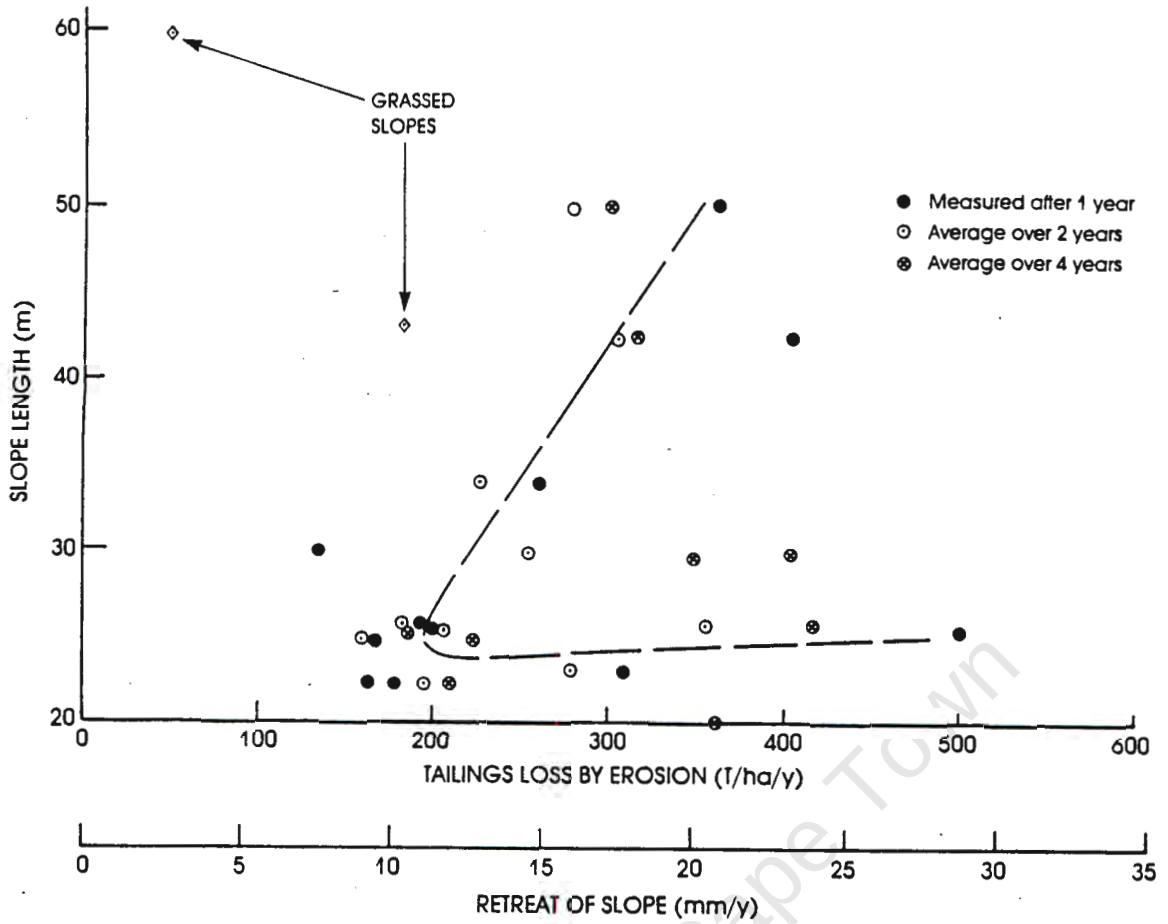

Figure 4 Correlation between slope and tailings loss by erosion

slopes back towards the vertical step above, and is hydrologically designed to retain precipitation on it without spilling down to the next step. The erosion of 2 terraced slopes was observed as part of this programme.

The results of the measurements, shown in Figure 5, confirm that erosion losses from terraced slopes are relatively small. However, the measure is not very practical as severe gulleying occurs if one of the steps overflows. A terraced slope is also not visually pleasing.

Five test plots were established on the untreated horizontal top surfaces of dams. The results of these measurements (see Figure 5) show that there is little or no erosion loss from untreated top surfaces. In some cases, a small accretion occurred. These measurements represent an average over years 3 and 4 of the experiment.

These results, taken with those shown in Figure 3, appear to indicate that the major losses from tailings dams due to wind and water erosion take place from the slopes and not from the flat top surfaces. The dust clouds that appear to emanate from the top surfaces are in reality blown off the windward slope and other slopes that are subjected to a component of wind shear.

The Effect of Anti-erosion Measures

Grassed Slopes. The data for grassed slopes are also shown in Figure 5. Losses for the west and south-facing slopes do not appear to be unusually low when compared with the trend of the other data. (Prevailing winds in winter are south to southwest).

However, the north-facing grassed slope is the only non-horizontal slope for which an accretion was recorded during this investigation.

Gravel-mulched Surfaces. Two sets of measurements are available for the rates of erosion of gently sloping surfaces (11°) that were covered by a layer 1 particle thick of 16 mm crushed rock. As shown in Figure 5, the gravel-mulched surfaces eroded considerably less than the untreated adjacent control plot. However, the position of the data in relation to that for other

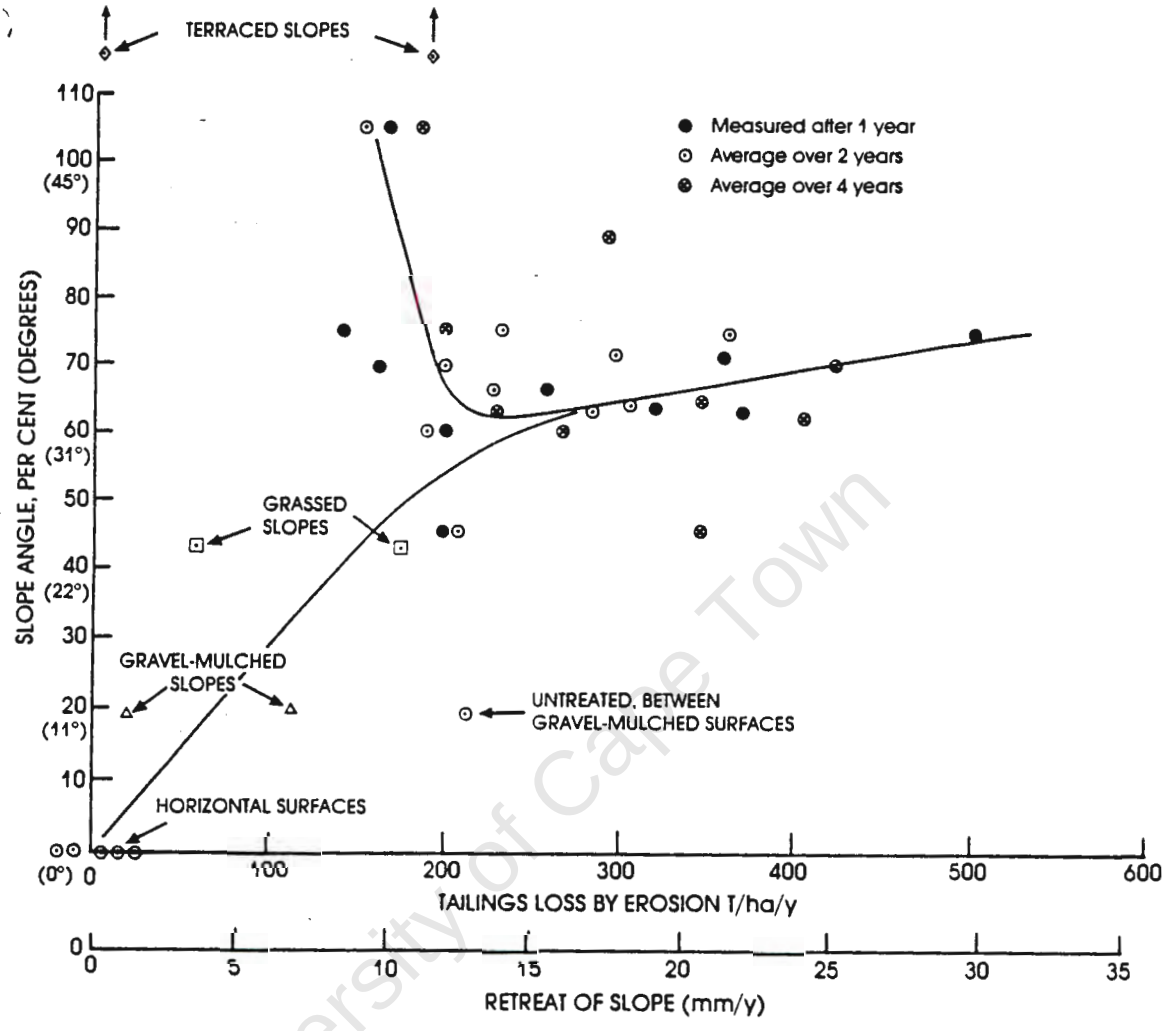

Figure 5 Correlation between slope angle and tailings loss by erosion.

slopes suggests that the control plot was unusually erosive, rather than that the gravel mulch was very effective in preventing erosion. However, there is evidence in the literature that surface obstructions such as closely spaced gravel particles and clods decrease the rates of erosion of soil surfaces by reducing the kinetic energy of runoff passing over the surface (Johnson et al 1979, Jennings and Jarret 1985).

Effect of Stabilizing Dam Top Surfaces. Blight et al(1981) and Blight and Caldwell (1984) reported on the experimental stabilization of the horizontal surface of a tailings dam with Portland cement and road lime. Erosion-measuring plots were set up on these surfaces and on an intervening untreated surface. Measurements on these plots over years 3 and 4 gave the result that the cement-stabilized surface is eroding at a rate of 18 t/ha/yr (a rate of retreat of slightly more than 1 mm/yr). The lime-stabilized surface is eroding at a rate of 3 t/ha/yr, and the adjacent untreated surface is accreting at 6 t/ha/yr. This set of measurements has simply confirmed the conclusion reached above that near-horizontal surfaces are relatively unaffected by erosion.

Accretion in Erosion Catch-paddocks. Rates of accretion were measured in a number of erosion catch-paddocks at the toes of tailings-dam slopes. The measured rates varied from 70 to 150 mm/yr. These accretion rates could not be reconciled with, and generally appeared to be greater than, the losses from the slopes above the paddocks. This is presumably because more material is eroded from near the toe of a slope than from the mid-length area. With

hindsight, it would have been better to have measured erosion losses over the full length of the slopes.

Retreat of Crest Walls. The top surfaces of crest walls made of compacted, unstabilized tailings decreased in height by up to 200 mm/yr. The rate of height reduction of crest walls with cement-stabilized crests (5 % nominal cement content) is only about 1 mm/yr. Cement stabilization of the tops of crest walls therefore appears to be well worthwhile as a stabilizing measure.

Conclusions

The main conclusions drawn from this study are as follows:

(1) Both wind and water are major agents in eroding the slopes of gold-tailings dams. Under South African conditions, roughly half of the total erosion loss may result from wind action. Annual erosion losses may exceed 500 t/ha/y (a rate of retreat of 30 mm/yr).

(2) The horizontal top surfaces of gold-tailings dams are relatively little-affected by erosion.

(3) There is a weak positive correlation between the length of a slope and the rate of erosion. The rate of erosion appears to increase from top to bottom of a slope as the volume of run-off increases.

(4) A 2-branched correlation exists between the slope angles of gold-tailings dams and the rate of erosion. Very flat slopes and very steep slopes erode less than slopes of intermediate angle. At the limits of slope, horizontal and vertical surfaces erode very little.

(5) While more data is needed on anti-erosion measures, it appears that grassing, gravel-mulching, or terracing of slopes can considerably reduce erosion losses.

Literature Cited

Blight, G.E.; C.E. Rea; J.A..Caldwell; and K.W. Davidson. 1981. Environmental protection of abandoned tailings dams. Proceedings, 10th International Conference on Soil Mechanics and Foundation Engineering, Stockholm, vol.2. 303-308.

Blight, G.E.; and J.A. Caldwell 1984. The abatement of pollution from abandoned gold-residue dams. Journal of the South African Institute of Mining and Metallurgy, 84,(1) 1-9.

CHAMBER OF MINES OF SOUTH AFRICA .1979. Guidelines for environmental protection, vol 1/1979, The design, operation and closure of residue deposits, Johannesburg, The Chamber (Revised 1983).

Evans, W.R.; and G. Kalkanis 1977. Use of the universal soil loss equation in California. Soil Erosion: Prediction and Control, Proceedings, National Soil Erosion Conference, Soil Conservation Society of America, 1977. 31-40.

Jennings, G.D.; and A.R. Jarret 1985. Laboratory evaluation of mulches in reducing erosion. Transactions of the American Society of Agricultural Engineers, 28(5), 1466-1470.

Johnson, C.B.; J.V. Mannering, and W.C. Moldenhauer 1979 Influence of surface roughness and clod size and stability on soil and water losses. Journal of Soil Science of America. 43, 772-777.

Renner, F.G. 1936. Conditions influencing erosion on the Boise River watershed. US Department of Agriculture, Technical Bulletin; 528. 1936.

5. GROUNDWATER POLLUTION CAUSED BY SANITARY LANDFILLS

CONTRIBUTION TO LEARNING

The first paper shows that with correct siting in areas of perennial water deficit, it is possible to operate a sanitary landfill without generating leachate, and therefore without causing pollution of the groundwater. The second and third papers explore this theme further and the third paper shows how the water balance for a site can be used to predict the generation of leachate. This last is not original, but it is believed to be the first time that predictions based on the water balance have been tested by direct sampling of landfills. The second paper also explores the leakage of leachate from sanitary landfills and shows that this can only be predicted if the complete flow system is considered.

These findings will be incorporated in new regulations for sanitary landfilling in South Africa.

The fourth paper starts to examine the complexity of moisture movement through landfills and the effects of the differing field capacities or moisture storage capacities of refuse and cover material. The fifth and final paper considers the design of clay liners for sanitary landfills and sets out a method of analysis whereby large-scale ponding tests can be analysed and liners designed.

5. GROUNDWATER POLLUTION CAUSED BY SANITARY LANDFILLS

5.1 Ball J M and Blight, G E (1986). Groundwater pollution downstream of a long established sanitary landfill. Proceedings, International Symposium on Environmental Geotechnology, Allentown, USA, pp 149-157.

This paper is based on work done for the MSc(Eng) degree by Mr J M Ball. I planned and supervised the work and wrote the paper.

5.2 Blight, G E, Vorster, K and Ball, J M (1987). The design of sanitary landfills to reduce groundwater pollution. Proceedings, International Conference on Mining and Industrial Waste Management, Johannesburg, Vol 1, pp 297-305.

The paper is based largely on work done towards a PhD degree by Mr Vorster, but includes material from Mr Ball's MSc(Eng) research. I planned and supervised the work and wrote the paper.

5.3 Blight, G E, Hojem, D J and Ball, J M (1989). Generation of leachate from landfills in water-deficient areas. Proceedings, 2nd ISWA International Landfill Symposium, Sardinia, pp XXVI-15. Also to be published as Chapter 2 of Landfilling of Waste: Leachate, Ed: Christensen, T, Cossu, R and Stegman, R. Elsevier Scientific Publishers (1992).

The paper is based on work for MSc(Eng) degree by mr D J Hojem. Sampling of gas-filled test holes in the landfills was carried out by Mr J M Ball, probably the only person in the world able to do this. I planned and supervised the work and wrote the paper.

5.4 Blight, G E, Ball J M and Blight, J J (1991). Moisture distribution in sanitary landfills. Proceedings, 3rd International Landfill Symposium, Sardinia, Vol 1, pp 813-822. Expanded version accepted for publication by ASCE Journal of Environmental Engineering.

This paper is based on measurements made by Mr J M Ball and Miss J J Blight as part of their MSc(Eng) research, under my supervision. I planned and supervised the work and wrote the paper.

5.5 Blight, G E and Mabula, M C (1992). Designing clay liners for sanitary landfills. Accepted for Proceedings, International ISWA Conference on Solid Waste, Madrid, 10pp.

This paper is based partly on measurements made by Mr M C Mabula towards his MSc(Eng) dissertation. I supervised the research and wrote the paper.

International Symposium

on

ENVIRONMENTAL GEOTECHNOLOGY

Volume I

Edited by

Hsai-Yang Fang

Department of Civil Engineering
Lehigh University
Bethlehem, PA U.S.A.

ENVO PUBLISHING COMPANY, INC.
1986

International Symposium on Environmental Geotechnology

GROUND WATER POLLUTION DOWNSTREAM OF A LONG ESTABLISHED SANITARY LANDFILL

J. M. Ball
G. E. Blight
University of the Witwatersrand, SOUTH AFRICA

ABSTRACT

The Waterval landfill was established in 1928 and was operated for 50 years, until closed in 1978. Operations started by primitive "wet-tipping" into abandoned water-filled brick pits and concluded with a well-managed sanitary landfill operation that was well separated from the water table. The study described in this paper shows that the early operations produced significant pollution of the groundwater downstream of the landfill. In contrast, the later operation produced no, or at worst, negligible groundwater pollution.

INTRODUCTION

In South Africa, as in many other countries, landfill has been found to be the most cost-effective method of refuse disposal. 95 Per cent of the 11 million tons of domestic solid waste generated annually in South Africa is disposed of in landfills, which are operated by both the public and private sectors.

Noble (1976) drew attention to the need to establish whether or not otherwise acceptable landfilling procedures are adequate to prevent the pollution of underground water in South Africa, and the study described in this paper was initiated in the following year, in order to answer this need in the inland area of the country.

THE STUDY SITE

As pollution of groundwater can occur both by the generation of leachate and by groundwater encroachment into a fill, a site was chosen where both mechanisms are possible and one, groundwater encroachment, certainly does occur.

According to van Onselen (1982), the Waterval site was operated as a brick pit from 1896 until abandoned for this purpose in 1906. Fitzgerald (1974) records that landfilling, by "wet-tipping" into the partially water-filled brick pit commenced in 1928, and the landfill remained in operation until closed in 1978. The estimated volume of the landfill is between 3 and 4.5 million cubic metres. Waterval received predominantly urban domestic refuse as well as garden refuse and small amounts of business and industrial refuse. Liquid wastes were never (officially) accepted at the site.

In the latter years of its life the composition of the refuse was as shown in Table 1. Early in its operation, the content of plastic would have been negligible, and that of ash considerably greater.

Table 1

Refuse Composition

Fraction	Percent by Mass
Organic putrescible	33
Paper	38
Plastic	4
Glass	9
Metal	4
Ash	3
Rags	2
Bones	2
Unclassified	3
Tailings	2
TOTAL	100

The floor of the Waterval valley is composed of clays and sandy clays residual from dioritic gneisses and ultramafic schists. The valley forms a catchment, drained by a small stream that runs through the site of the landfill, and trends towards the north-east. The study of groundwater pollution was made along the banks of this stream.

Figure 1 shows the position of the landfill in relation to the geology and surface contours. Where the stream crosses the landfill site, it is now culverted, but the culvert contains weepholes to prevent flotation. Hence, any leachate generated in the fill has direct access to the stream.

GROUNDWATER POLLUTION

A series of boreholes, equipped with slotted casings, wrapped in filter fabric and surrounded by clean sand were put down on either side of the stream downstream of the landfill site. Figure 2 shows the location of the boreholes GW1 to GW21, as well as the position of a 1.2m diameter auger hole (mentioned later) and an indication of the urban development surrounding the fill.

To assess the permeability of the soil downstream of the fill, bailing and recovery tests were carried out on 6 of the boreholes with the results shown in Table 2.

Table 2

In situ permeabilities of soil downstream of Waterval site

Borehole No.	Permeability m/y
GW 7	6.8
10	15.6
14	37.2
15	14.8
16	11.0
18	7.7
Mean 15.5 m/y	Std. Devn : 11.2 m/y

Figure 3 shows contours of conductivity (an indication of total dissolved salts) in mS/m for the boreholes. The contours were drawn up as average values recorded over a period of two years during which there was little change in observed values. Figure 4 shows contours of chloride in mgC1/ℓ for the same samples, while Figure 5 shows corresponding contours of ammonia expressed as mgN/ℓ.

It is quite clear from Figures 3, 4 and 5 that significant pollution of the groundwater has occurred downstream of the fill. The shape of the contours indicates that given a general downstream movement of the groundwater, far less pollution is currently entering the groundwater than was the case some years ago.

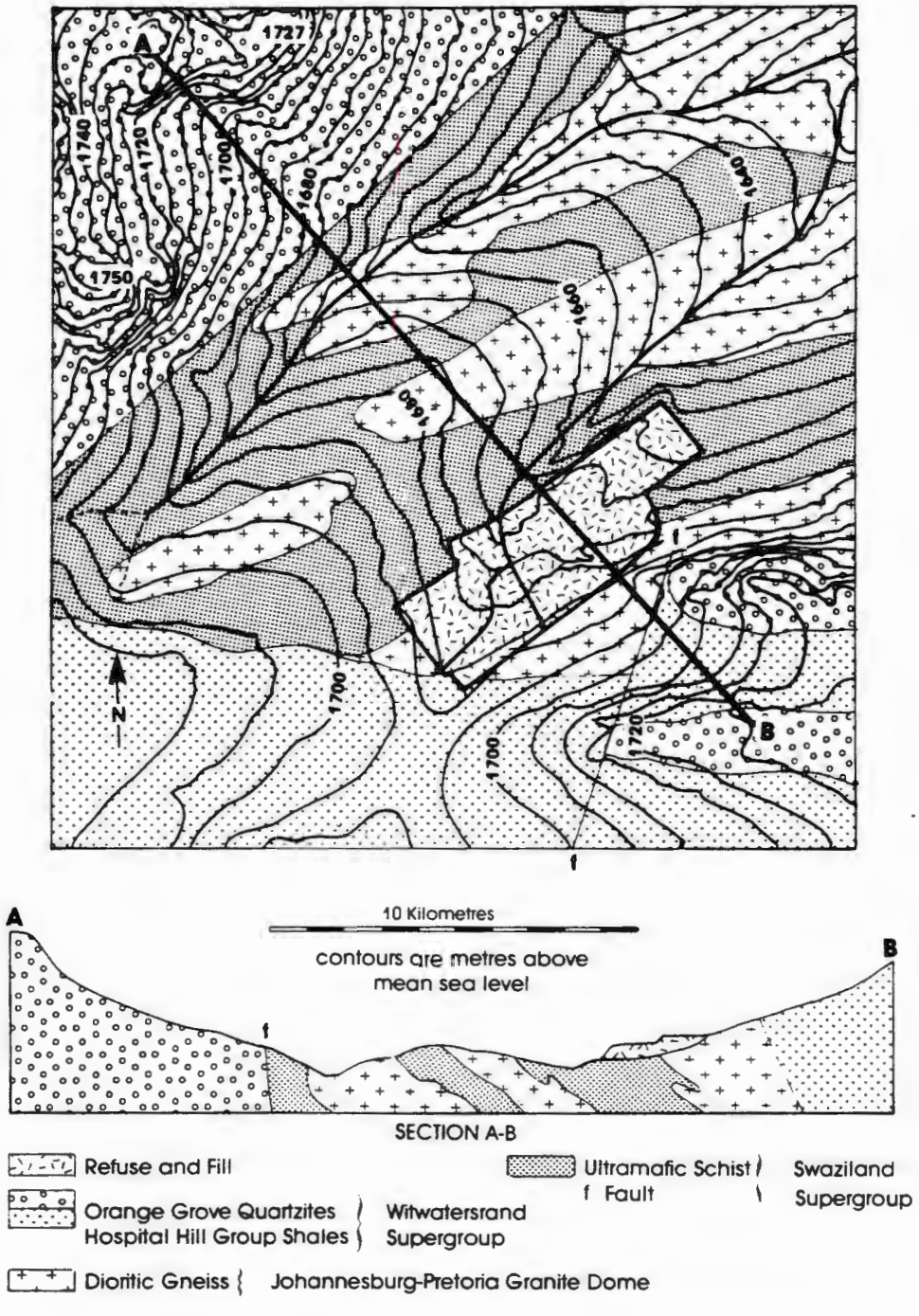

FIGURE 1: Waterval valley topography and geology

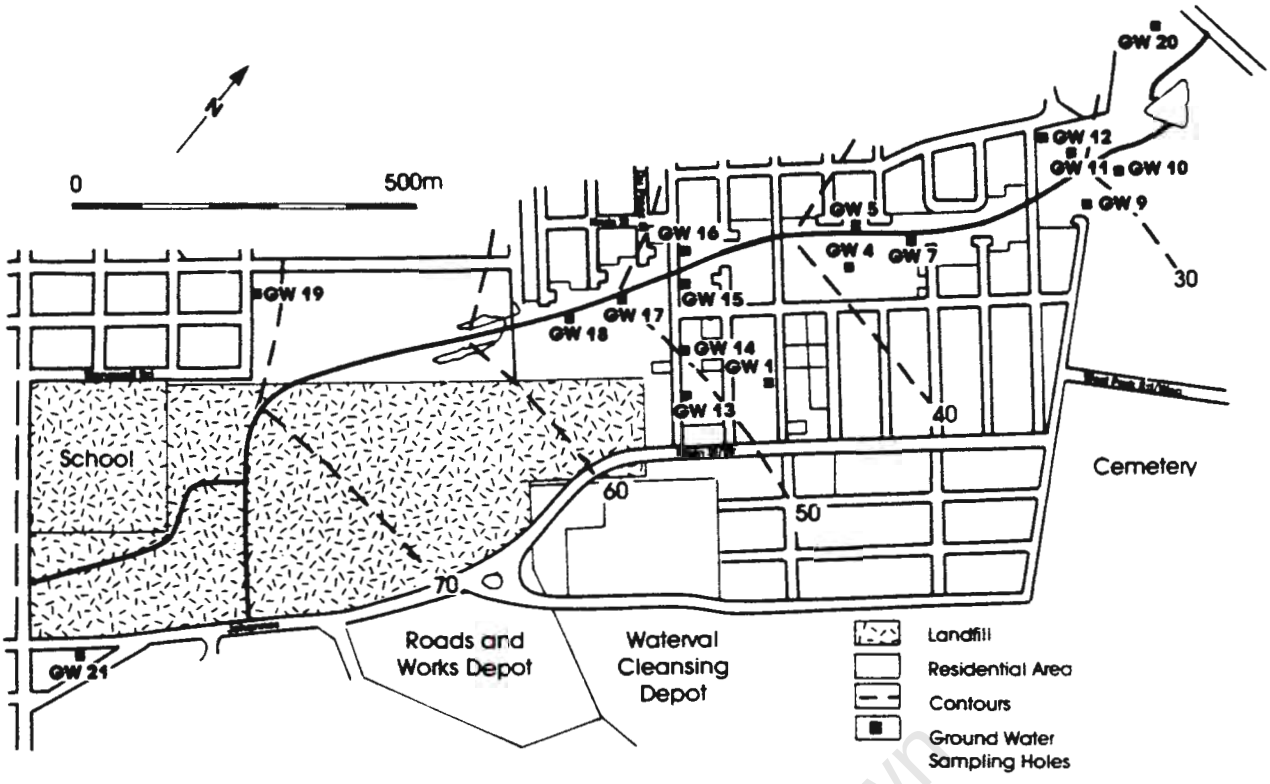

FIGURE 2: Water sampling boreholes and phreatic surface contours downstream of Waterval Landfill

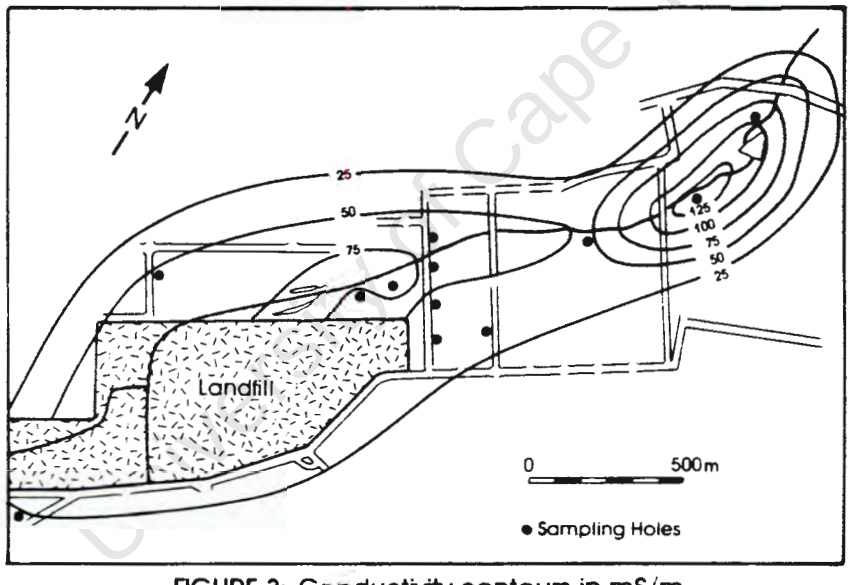

FIGURE 3: Conductivity contours in mS/m in the groundwater

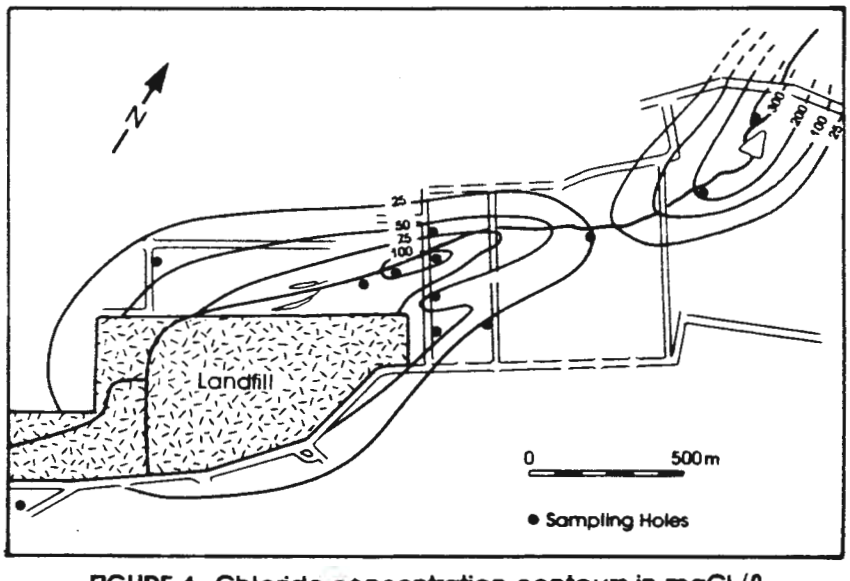

FIGURE 4: Chloride concentration contours in mgCl/ℓ in the groundwater

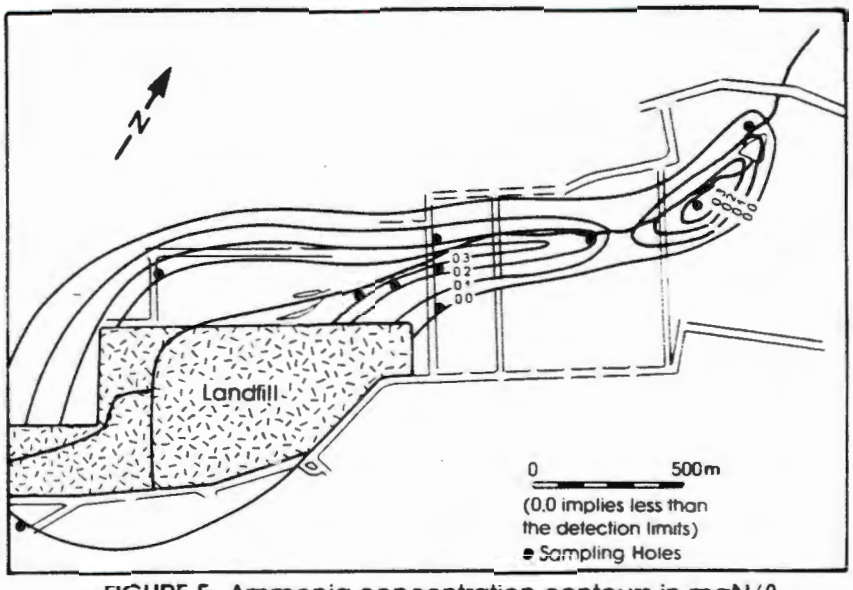

FIGURE 5: Ammonia concentration contours in mgN/ℓ in the groundwater

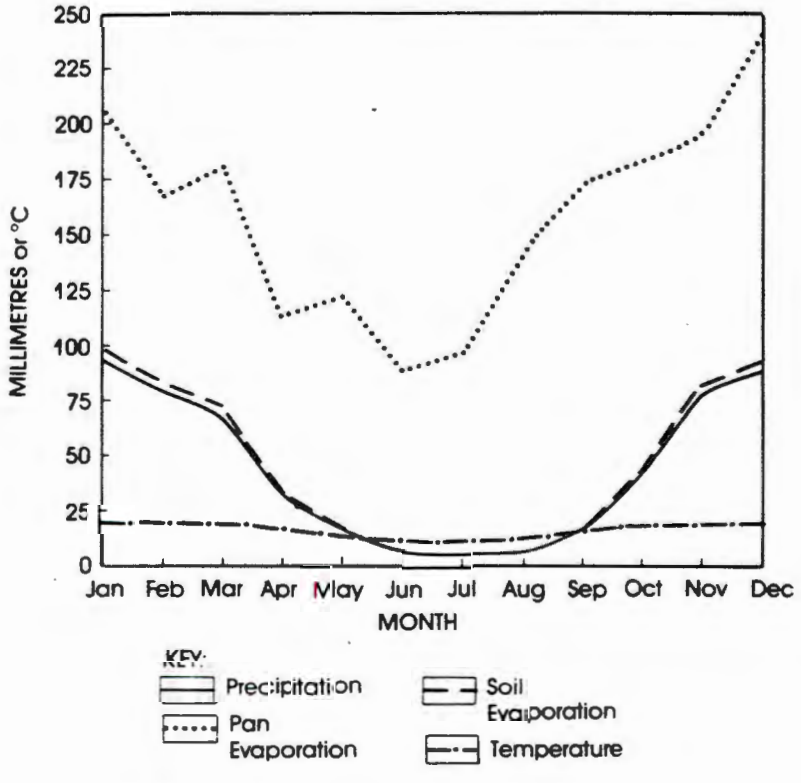

FIGURE 6: Water balance data for Waterval

A concentrated "slug" of pollution shown by all three sets of measurements at a distance of about 1500m downstream of the fill is of particular interest. Figure 2 shows approximate contours of the phreatic surface downstream of the landfill. These indicate that the downstream flow gradient is approximately 1 in 30. Hence, assuming that the likely upper limit to the macro-permeability of the soil strata equals the measured mean value plus two standard deviations, i.e. about 40 m/y, the average calculated flow velocity down the valley is 1.3 m/y. It is not possible to reconcile the actual average minimum flow velocity of 1500m in 50 years (or 30 m/y) with this calculated velocity. However, the conclusion is inescapable that the slug of pollution was released from the landfill approximately 50 years ago, when tipping of refuse into the flooded brick pits was commenced. The level of pollution then appears to have decreased, presumably because the level of the refuse rose above the water level in the pits and the rate of production of pollutant from the deeper material decreased. However, the contours also show a secondary slug of pollution situated about 500m downstream of the fill site. This must have been released about the year 1960, but the reason for its occurrence is not known.

THE WATER BALANCE AT THE SITE

The water balance for the fill can be expressed in the following terms :

Gain in fill moisture + Percolation = Precipitation (rainfall) - (Runoff + Soil evaporation + Transpiration)

At Waterval, the soil cover was bare of vegetation, hence the "transpiration" term can be disregarded. Figure 6 shows monthly variations for the site of :

pan evaporation,
precipitation or rainfall,
temperature and
soil evaporation.

Soil evaporation was calculated from Turc's equation (e.g. Penman (1963)).

As figure 6 shows, calculated soil evaporation is generally either equal to, or exceeds precipitation, while potential evaporation (i.e. pan evaporation) always far exceeds precipitation. Hence, on this basis alone (neglecting runoff) percolation and gain in fill moisture should have been negligible. It follows that any groundwater pollution must in general, occur through direct contact between refuse and groundwater, although there is always a possibility that rain falling on an uncovered cell of refuse could produce percolation locally and for a short time.

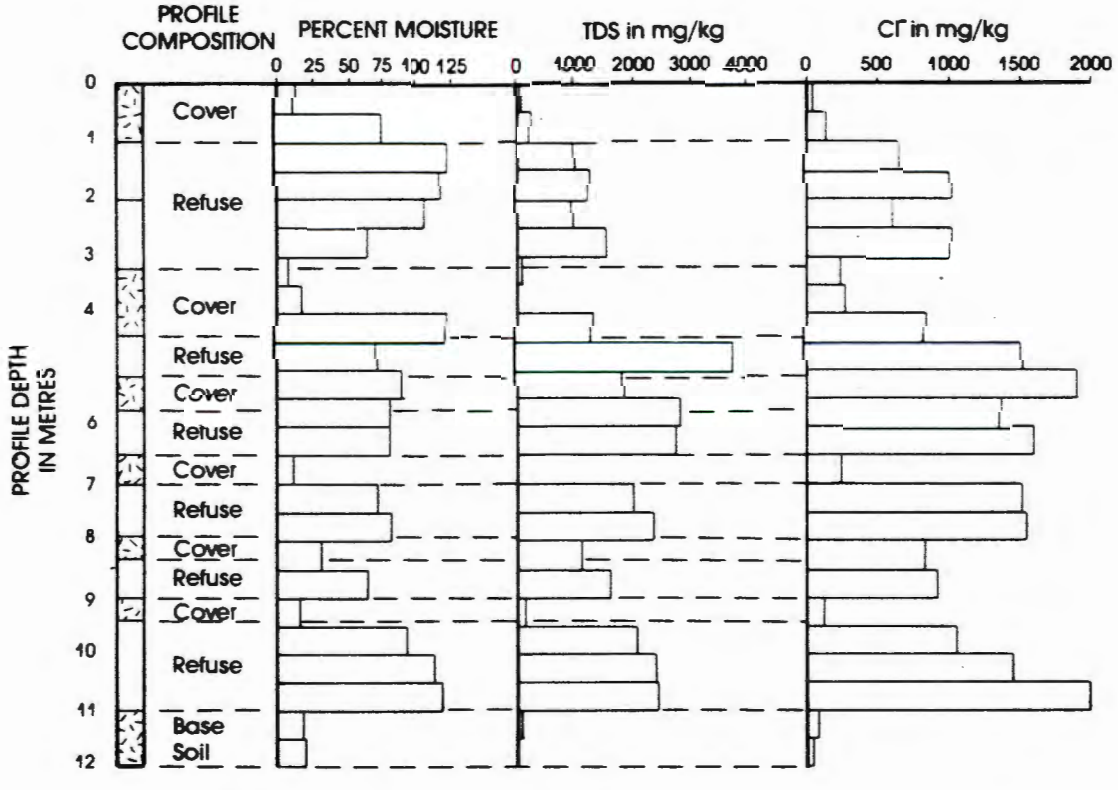

FIGURE 7: Moisture and solute profiles for 1.2m DIA auger hole

MOISTURE AND DISSOLVED SALT PROFILES IN FILL

To substantiate the above conclusion, a 1.2m diameter hole was augered through the fill and the hole sampled and carefully profiled.

The profile and the results of tests on the samples are shown in Figure 7. The hole was augered and sampled in October 1977, but only profiled (and re-sampled) in July 1978. The reason for the delay was concern for the safety of anyone entering the hole. The hole was entered eventually, after keeping it carefully covered for nine months, by means of a metal plate and a collar that fitted the entrance to the hole. A cage welded from large diameter reinforcing bars was lowered down the shaft and the first author profiled the hole wearing a self-contained breathing apparatus. A similar descent, during which further samples were taken, took place in September 1978. Because of the delay between drilling and sampling, care was taken to remove the samples from about 0.5m back from the side of the hole, to avoid as far as possible, the influence of any moisture and salt migration towards the hole.

The moisture profile shows a very low moisture content in the upper 0.5m of cover as well as a tendency for moisture to decrease with depth in the upper 2m thick cell of refuse. These observations are indicative of seasonal upward flow of moisture under an evaporation gradient after earlier seasonal wetting. The total dissolved solids (TDS) and chloride (Cl) profiles do not show evidence of upward flow in the top cell of refuse, but neither are they indicative of downward flow.

Below a depth of 3m, one would not expect much seasonal variation of either moisture or dissolved salts to occur. There appears to be no clear trend of either upward or downward movement of moisture or dissolved salts, except in the lowest cell of refuse and the base soil. Here there appears to be evidence of slight downward movement of both moisture and dissolved salts and the uppermost 0.5m of base soil seems to have gained salts from the refuse.

However, the general impression is that of a reasonably static situation in which there may be localized seasonal movement of moisture and dissolved salts, either upwards or downwards, but there is no evidence for a continuing downward leaching of dissolved salts into the soil underlying the fill.

The water table in the hole stabilized at a depth of 13.5m. Hence, at the time of sampling, at least 2.5m of soil separated the refuse from the groundwater. It should be noted that this portion of the landfill does not overly the brickpit area.

It is interesting to note, that the refuse could be dated precisely from the dates of newspapers included in the sampled material. These dates varied from 1969 at the bottom of the profile to 1970 at the top. Hence the refuse was 7 to 8 years old when sampled.

The evidence presented in Figure 7 reinforces the conclusion arrived at by considering the water balance for the site, namely that given the climatic conditions prevailing at Waterval, leachate should not percolate from the base of the landfill, and if any groundwater pollution is occurring, it must occur as a result of direct contact between refuse and groundwater.

CONCLUSIONS

The observations made in this study bear out the work of other researchers, e.g. Fenn et al (1975), Burns and Karpinski (1980) and Holmes (1980), to the effect that if climatic conditions are such that a net water deficit exists at the site of a landfill, no percolation will exit from the base of the fill. Hence, if there is an adequate separation between the lowest level of refuse and the highest level of the phreatic surface or water table, no groundwater pollution will occur.

In contrast, if refuse is placed directly in contact with the groundwater body, pollution of the groundwater downstream of the fill is inevitable. This reiterates the conclusions of Zerone et al (1975), of the Sumner Report 1978) and others.

Finally, the investigation shows how difficult it is to predict the rate of advance of a pollution plume. In the present case, the rate of advance on the basis of in situ permeability measurements is underestimated by a factor of 30, even allowing for the effects of hydrodynamic-dispersion (e.g. Freeze and Cherry (1979)).

REFERENCES

1. Burns, J. and Karpinski, G., 1980. Water balance method estimates how much leachate a site will produce. Solid Waste Management, August, 1980, pp 54-84.

2. Fenn, D.G., Hanley, K.J. and De Geare, T.V., 1975. Use of the water balance method for predicting leachate generation from solid waste disposal sites. US Environmental Protection Agency. Solid Waste Management Series SW168.

3. Fitzgerald, P., 1974. Recording and mapping of refuse disposal sites. Internal report, Cleansing Branch, City Engineer's Department, Johannesburg.

4. Freeze, R.A. and Cherry, J.A., 1979. Groundwater. Prentice-Hall, Englewood Cliffs.

5. Holmes, R., 1980. The water balance method of estimating leachate production from landfill sites. Solid Waste, January, 1980, pp 20-33.

6. Noble, R.G., 1976. Solid waste research in South Africa, South African National Scientific Programmes Report No. 4, p 3.

7. Penman, H.L., 1963. Vegetation and hydrology. Commonwealth Bureau of Soils, Harpenden, England, Technical Communication No. 53.

8. United Kingdom Department of the Environment, 1978. Co-operation programme of research on the behaviour of hazardous wastes in landfill sites (The 1978 Sumner Report) HMSO, London.

9. van Onselen, C., 1982. Studies in the social and economic history of the Witwatersrand, Ravan Press, Johannesburg, pp 19 and 35.

10. Zenone, et al, 1975. Groundwater quality beneath solid waste disposal sites at Anchorage, Alaska. Groundwater, vol 13, No. 2, pp 182-190.

PROCEEDINGS OF THE INTERNATIONAL CONFERENCE ON MINING AND INDUSTRIAL WASTE MANAGEMENT / JOHANNESBURG / AUGUST 1987

Mining and Industrial Waste Management *International Conference*

VOLUME ONE

Technical editors

J.A. WATES / D. BRINK

SOUTH AFRICAN INSTITUTION OF CIVIL ENGINEERS
Division of Geotechnical Engineering
Division of Urban Engineering

JOHANNESBURG 1987

ISBN 0 620 10968 8

Proceedings of the International Conference on Mining and Industrial Waste Management Johannesburg / 1987

On the design of sanitary landfills to reduce groundwater pollution

G.E. BLIGHT
University of the Witwatersrand, Johannesburg, South Africa
K. VORSTER
Technicon Pretoria, Pretoria, South Africa
J.M. BALL
Ball Lombard Associates, Johannesburg, South Africa

SYNOPSIS

The provisions of the recently drafted "Guidelines for the effective disposal and control of waste" (which relate to the proposed Regulations under the Environment Conservation Act of 1982) are examined in relation to their advice on the prevention of groundwater pollution. It is shown that the water balance for a waste disposal site is all-important for design against groundwater pollution and that the rules of thumb for acceptable site permeability given in the guidelines are inadequate.

INTRODUCTION

At a recent workshop organized by the National Research Programme for Waste Management of the CSIR Foundation for Research Development, a set of "Draft guidelines for the effective disposal and control of waste" was drawn up to "assist control bodies, local authorities and private companies to comply with control measures regarding waste disposal". The "control measures" were specifically those relating to draft regulations in terms of Section 12(2)(a) of the Environment Conservation Act, 1982 (Act 100 of 1982).

In these guidelines, waste disposal sites are divided into three classes :

"Class I - A containment site for the disposal of special waste," which is described as:

> "material in this category is considered to be dangerous and detrimental to man and/or the environment and causes serious pollution if released uncontrolled".

The guideline continues : "This class site requires an impermeable membrane or a relative impermeable strata (sic) that will efficiently contain both the waste and the leachate in the site or in the immediate surroundings thereof :

- In the case of a relative impermeable strata being used, the nature and thickness of the material will be the deciding factor.
- An acceptable bottom layer can also be acquired (sic) through engineering by means of compaction techniques.
- A rule of thumb is that a site must have an in situ permeability of less than 10^{-6} cm/s to qualify as a Class I site".

"Class II - A site for the disposal of general waste", which is defined by: "Material in this category consists of material of low toxicity/pathogens that have (sic) a limited pollution potential".

The guideline then continues : "This site is known to emit leachate very slowly and continuously. Because of this an unsaturated zone is required under the site that can act as a biological filter that will allow air oxidation that will decompose the leachate.

An acceptable rule of thumb is that a site with a permeability higher than 10^{-4} cm/s will be classified as a class II site."

There appears to be an error in the previous line which should presumably state "a site with a permeability of less than 10^{-4} cm/s will be classified as a Class II site".

"Class III - A site for the disposal of waste with an insignificant pollution potential (ie building material). This site is usually in hydraulic continuity with the groundwater and will emit any leachate that is formed in the site".

In the section on "Siting of a Class I and Class II site", the guideline states :

"The essential property of the design of both a Class I and Class II site is to ensure that pollution of the aquifer through seepage is limited to an acceptable level. The prescribed level that will be acceptable in most cases can be found in the general standards for waste water under the Water act.

In calculating the acceptable minimum flow of leachate from the site the water balance of the whole site with cover material, the disposed waste, the attenuation zone and the groundwater must be taken into account".

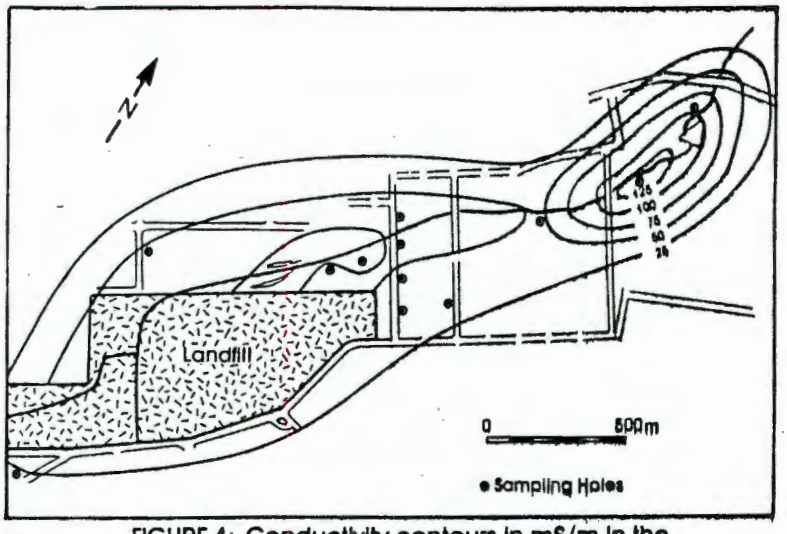

FIGURE 1: Conductivity contours in mS/m in the groundwater downstream of a landfill

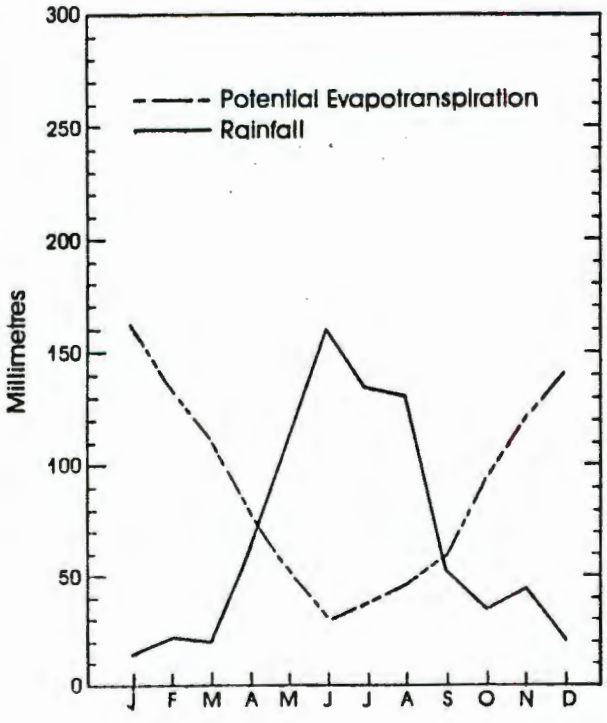

FIGURE 2a: Typical rainfall and evaporation distribution for the Cape Flats

The object of this paper is to explore the validity of the guideline recommendations outlined above. In particular, the implications of the water balance for a site will be assessed, as well as the consequence of adopting the two rules of thumb relating to the permeability of the liner or impermeable strata of a Class I site and the attenuation zone permeability of a Class II site in cases where the water balance is unfavourable.

THE CLASS III SITE

The Class III site can be dismissed in fairly short order :

Either the waste to be disposed of is inert and innocuous or if this is not the case, then the site is unacceptable.

However, it is worth emphasizing the truth of the statement to the effect that if a site is "in hydraulic continuity with the groundwater", ie if the groundwater level either permanently or seasonally, is above the lowest level of the refuse, then the site "will emit any leachate that is formed".

Numerous examples of this type of pollution are known from other parts of the world. In South Africa, a landfill in the Transvaal[4] provides a prime example. Here "wet-tipping" of refuse into an abandoned, partially water-filled brick pit commenced in 1926. An investigation of groundwater quality downstream of the site carried out between 1978 and 1984 brought to light the extensive groundwater pollution plume illustrated in Figure 1. The conductivity contours in the figure indicate the variation of dissolved solids in the groundwater against a background value of less than 10m s/m. The zone of high conductivity located about 1,6 km to the north east of the tip is indicative of a "slug" of pollution that entered the groundwater at the time of the wet-tipping operation, 50 years ago and has been slowly moving downstream ever since. There must be many cases of similar groundwater pollution in the towns and cities of South Africa. Figure 1 graphically shows why Class III sites are unacceptable for any but the most inert and innocuous wastes.

THE SIGNIFICANCE OF THE WATER BALANCE

The water balance for a site can be expressed in the following terms :

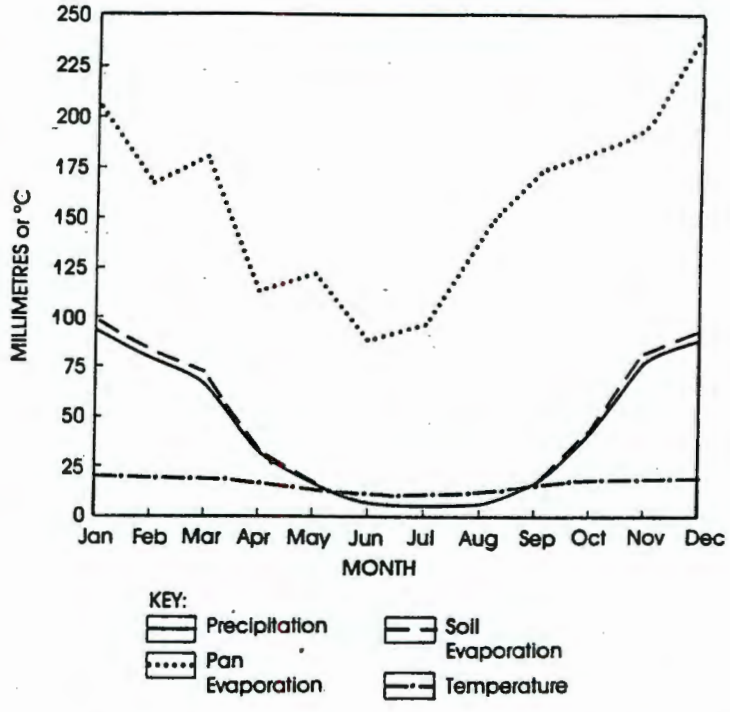

FIGURE 2b: Water balance data for Transvaal Site

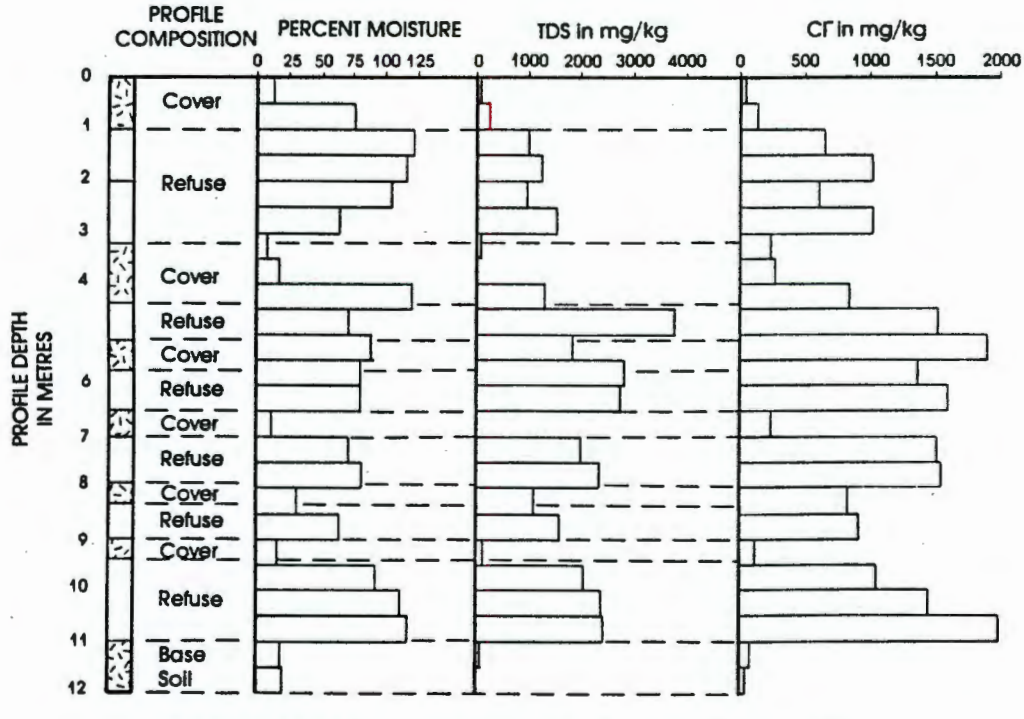

FIGURE 3: Moisture and solute profiles for 1.2m DIA auger hole in landfill referred to by Figure 2b

(Gain in fill moisture) + (leachate lost through base of fill) = (Precipitation or rainfall) + (Added liquids) - Runoff - (Soil evaporation) - (Transpiration by any plant cover).

Figure 2a shows monthly variations in "potential evapotranspiration" and rainfall for a site near Cape Town[3]. (The term potential evapotranspiration is not defined in the reference, but can probably be equated to pan evaporation or evaporation from a free water surface). The important aspect of Figure 2a is that from April to August each year, precipitation far exceeds potential evapotranspiration. It follows from the water balance equation that during this period the fill will gain in moisture and there will be a potential for the escape of leachate from the base of the landfill.

In contrast, Figure 2b shows similar data for a site on the Transvaal highveld. It will be seen that soil evaporation alone generally either equals or exceeds precipitation, and pan evaporation or potential evaporation always far exceeds precipitation. Hence, providing there is no ponding of water in any low-lying areas on the surface, there can be no potential for either a gain in fill moisture or for the generation of leachate by infiltration. This conclusion is substantiated by the data shown in Figure 3. This represents profiles of moisture content, total dissolved solids (TDS) and chlorides as Cl measured in material taken from a hole drilled through the sanitary landfill for which Figure 2b illustrates the water balance. Sampling occurred in October, 1972.

The moisture profile shows a very low moisture content in the upper 0,5m of cover as well as a tendency for moisture to decrease with depth in the upper 2m of refuse. This seems to indicate a pattern of residual moisture from infiltration during the previous wet season. Below 4m, the moisture profile appears random with no clear trend discernable. The profiles of TDS and Cl show a similar lack of systematic variation. Values in the top cell of refuse are somewhat less than those lower down, but the low values recorded in all of the intermediate layers of cover material show that there has been no downward leaching of soluble salts. The reasonably large values of TDS and Cl at the base of the top cover layer and the highest intermediate cover layer indicate that if anything, the soluble salts are tending to rise in the fill.
Most importantly, there is no evidence of salt contamination of the soil forming the base of the landfill, and hence no evidence of the formation or escape of leachate.

Hence it may be concluded that the water balance for a Class I or Class II site is of prime importance. If there is a water surplus (as in Figure 2a), then there is a potential for the formation of leachate and for contamination of the groundwater. If there is a water deficit (as in

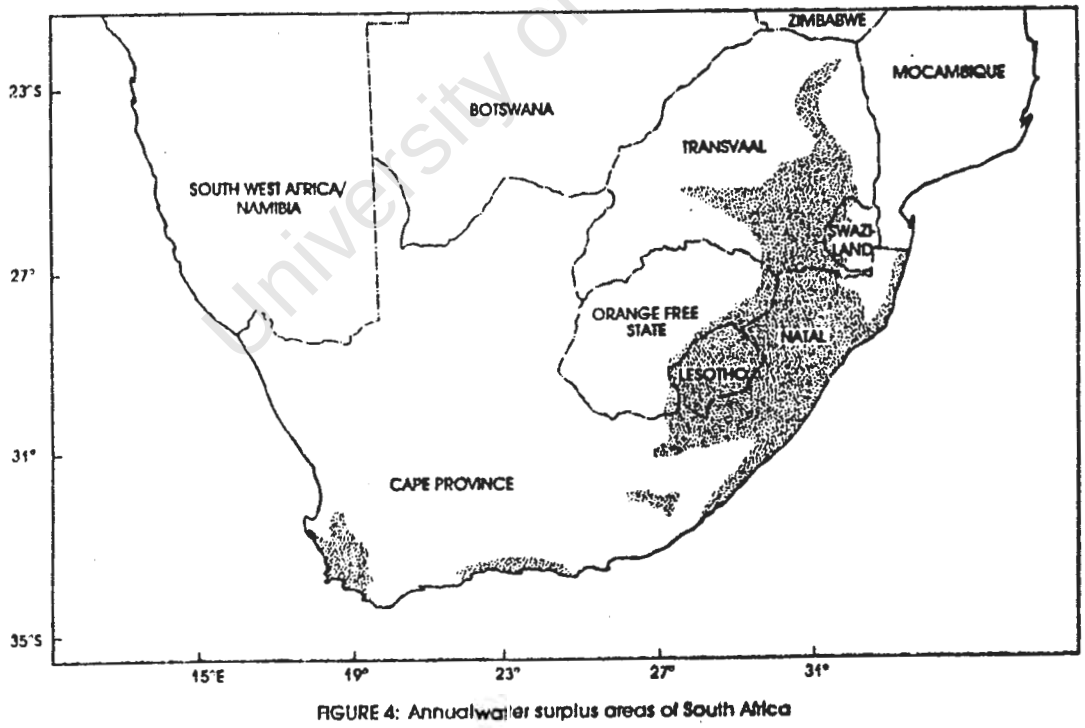

FIGURE 4: Annual water surplus areas of South Africa

Figure 2b) then the potential for leachate formation and for groundwater pollution is almost eliminated.

However, it must be emphasized that this conclusion may not be valid under the following circumstances:

(i) after an unusually wet season;

(ii) if the surface of the landfill is sufficiently irregular to allow rainwater to pond locally; and

(iii) if sufficient liquid waste is co-disposed to change the water balance to a surplus, either on an annual basis or for lesser periods.

By and large, therefore, it should be possible to satisfy the requirements of a Class I or II site without much difficulty, except in those areas of the country where there is either an annual or a seasonal water surplus.

As preliminary guide, Figure 4 illustrates those areas of South Africa where an annual water surplus exists. Each case should, however, be treated on its merits, as many areas do exist that have an annual water deficit, but seasonal water surpluses, as illustrated in Figure 2a. Note that Cape Town is not an area of annual water surplus.

CLASS I AND II SITES IN AREAS OF SEASONAL OR ANNUAL WATER SURPLUS

A parametric study has been carried out to test the rules of thumb relating to the limiting permeabilities for Class I and II sites that were referred to earlier.

It is likely that the rules came about from the assumption that if the permeability of a stratum is k m/y, then the outflow from the site into the groundwater can be no more than k m/y. For example, if $k = 10^{-6}$ cm/s (or 0.3 m/y), the out flow on this basis would not exceed 300 mm/y. This conclusion, which assumes a maximum hydraulic gradient of unity is usually quite incorrect, as the following examples will show.

Figure 5 represents the results of flow analyses for the situation of a landfill consisting of 10m of refuse resting on a 0,5m thick liner which in turn overlies a 2m thick unsaturated zone. The refuse may or may not be covered by a 0,5m thick cover layer having the same permeability as the soil of the unsaturated zone.

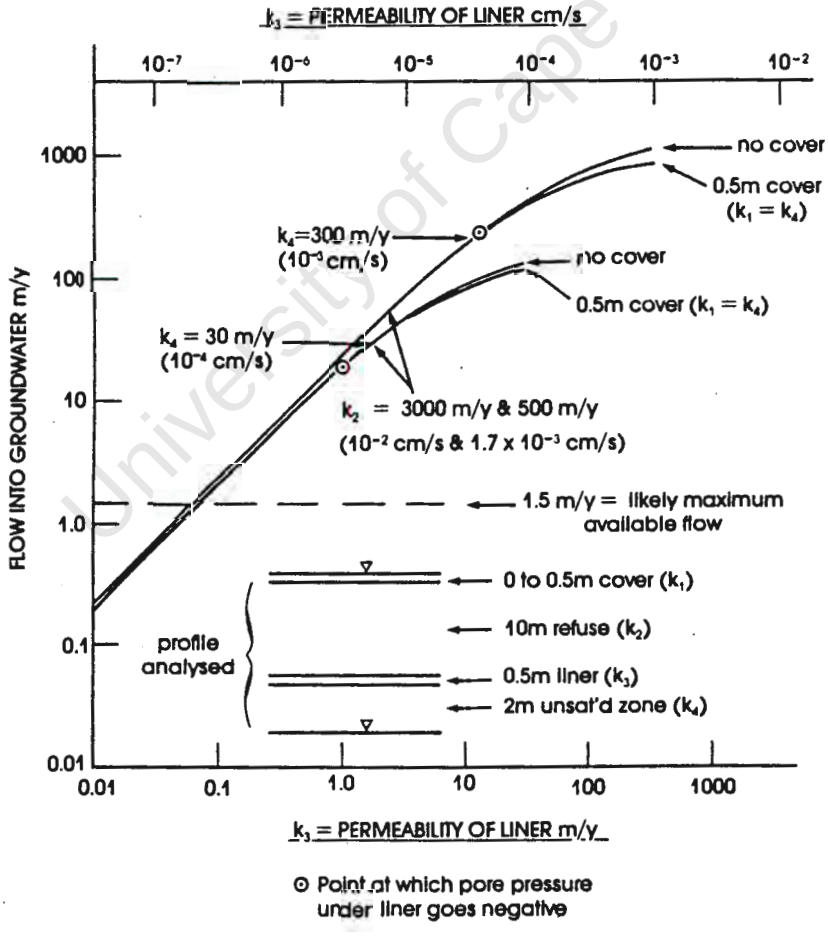

FIGURE 5: Variation of flow into the groundwater with liner permeability for a typical landfill profile

A search of the literature showed that very little seems to be known of the permeability characteristics of refuse. Oweis and Kera[4] give the following values :

Maximum permeability : $k_2(max) = 1500$ m/y

Minimum permeability : $k_2(min) = 200$ m/y

Field average : $\bar{k}_2 = 800$ m/y

For the present study limiting values of k_2 of 3000 m/y and 500 m/y were selected. (Note : 1 m/y=3.10^{-6} cm/s).

In the analysis, the permeability of the liner (k_3) was varied over a ragge of 0.01 m/y to 300 m/y (3.10^{-8} cm/s to 1.10^{-3} cm/s). The permeability of the cover material (k_1) and that of the unsaturated zone (k_4) were taken as either 300 m/y or 30 m/y (1.10^{-3} cm/s or 1.10^{-4} cm/s).

The method of calculation will not be described here (see Appendix), but follows the analysis given by Blight[5]. A free water surface was assumed at the top of either the refuse or the cover layer and initially, saturated flow conditions have been assumed. In other words, the refuse has been saturated to its field capacity and leachate is passing through the liner, into the unsaturated zone and thence into the groundwater.

As Figure 5 shows, for a liner permeability of 1.10^{-6} cm/s, the potential flow under these circumstances is of the order of 8 m/y which is a far cry from the 300mm/y mentioned above. To reduce the flow to 300mm/y either the liner permeability would have to be reduced to 6.10^{-7} cm/s, or the liner would would have to be thickened to more than 10m.

In reality, the situation would not be as bad as this because even in a water surplus area, the maximum excess water available to generate leachate is most unlikely to exceed 1500 mm/y. But basically, in this situation, the liner will pass all the leachate that reaches it. The actual quantity of leachate generated will be decided by the water balance.

Various other interesting points are also evident from Figure 5:

(i) The presence of a cover layer has very little effect on the potential leachate flow.

ii) The permeability of the refuse plays little part in limiting the flow.

iii) The permeability of the unsaturated zone has a moderating effect on the flow, but only if it has more or less the same value as that of the liner.

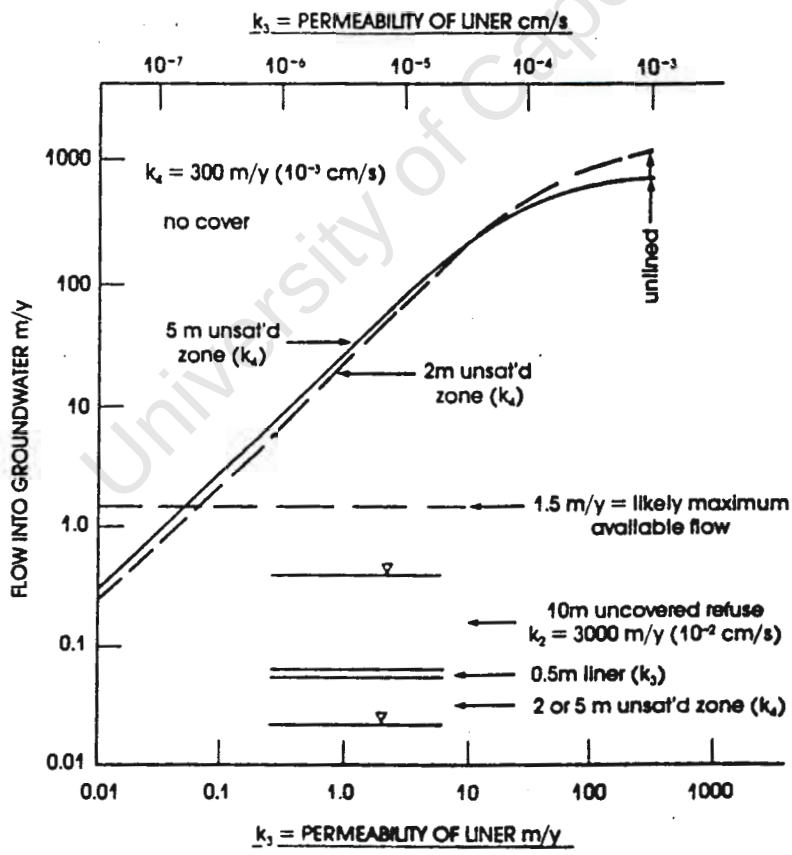

FIGURE 6: Effect on flow into the groundwater of increasing the thickness of the unsaturated zone

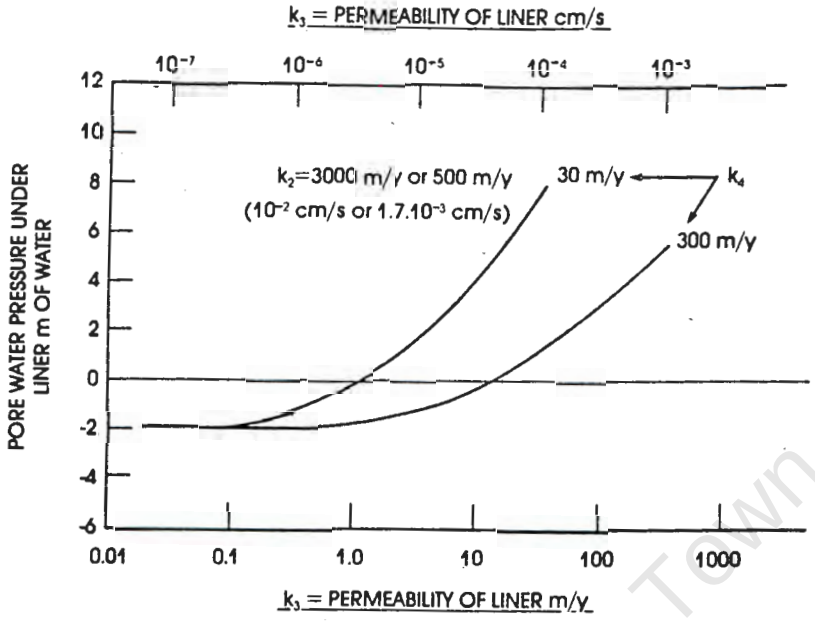

FIGURE 7: Variation of pore water pressure at liner underside with liner permeability for situation of Figure 5

Figure 6 shows the effect of changing the thickness of the unsaturated zone from 2m to 5m. Thickening a relatively permeable unsaturated zone slightly increases the flow because of the increase of seepage head. Although the term "unsaturated zone" has been used above, the zone between the underside of the liner and the water table will only remain unsaturated if the pore water pressure in this zone is negative. If the pore pressure is positive, this zone will become saturated.

Figure 7 shows how the pore pressure at the underside of the liner varies with liner permeability for the situation illustrated by Figure 5. The points at which the pore pressure becomes negative have also been marked in Figure 5. Figure 7 shows that for this situation a liner permeability of 10^{-6} cm/s is sufficiently low to induce and maintain a state of unsaturation in the "unsaturated zone".

It is known that a state of unsaturation can have a dramatic effect on the permeability of a soil. For example, Figure 8 (reproduced from Blight[3]) shows the effect of negative water pressure on the permeability of a sand, a silt and a heavy clay. In the case of the sand and silt, a few metres of negative water pressure dramatically reduce the permeability, whereas there is relatively little effect on the permeability of a heavy clay.

It might be thought therefore, that the effect of unsaturation would cause an equally dramatic decrease in the flow through the unsaturated zone. This, however, is not necessarily the case. Calculations were made for the situation of Figure 5 assuming :

(i) a constant liner permeability of 3 m/y (10^{-5} cm/s) and a variable permeability for the unsaturated zone corresponding to the curve for "sand" in Figure 8; and

(ii) a constant liner permeability of 0.3 m/y (10^{-6} cm/s) and a variable permeability for the unsaturated zone corresponding to the curve for "silt" in Figure 8.

For case (i), assuming the saturated permeability was maintained led to a calculated outflow of 74 m/y, whereas taking the variable unsaturated permeability values reduced the outflow by only 14 per cent to 64 m/y.

For case (ii) the completely saturated flow was 7.4 m/y whereas the flow reduced by unsaturation was 6.9 m/y (a 7 per cent reduction).

The reason that unsaturation has such a small effect is that the flow gradient through the liner remains relatively unaffected and also that appreciable negative pore pressures are only induced in a relatively thin zone of soil immediately under the liner.

CONCLUSIONS

The analyses just described have emphasized the following important point :

The two rules of thumb relating to limiting permeabilities for Class I and II sites are meaningless statements unless they are read in conjunction with the later statement in the section on "Siting" which should read more correctly and comprehensively :

(i) In calculating the likely flow of leachate from a site the water balance should first be established from meteorological data for the area and operating characteristics for the site. If there is a water deficit at all

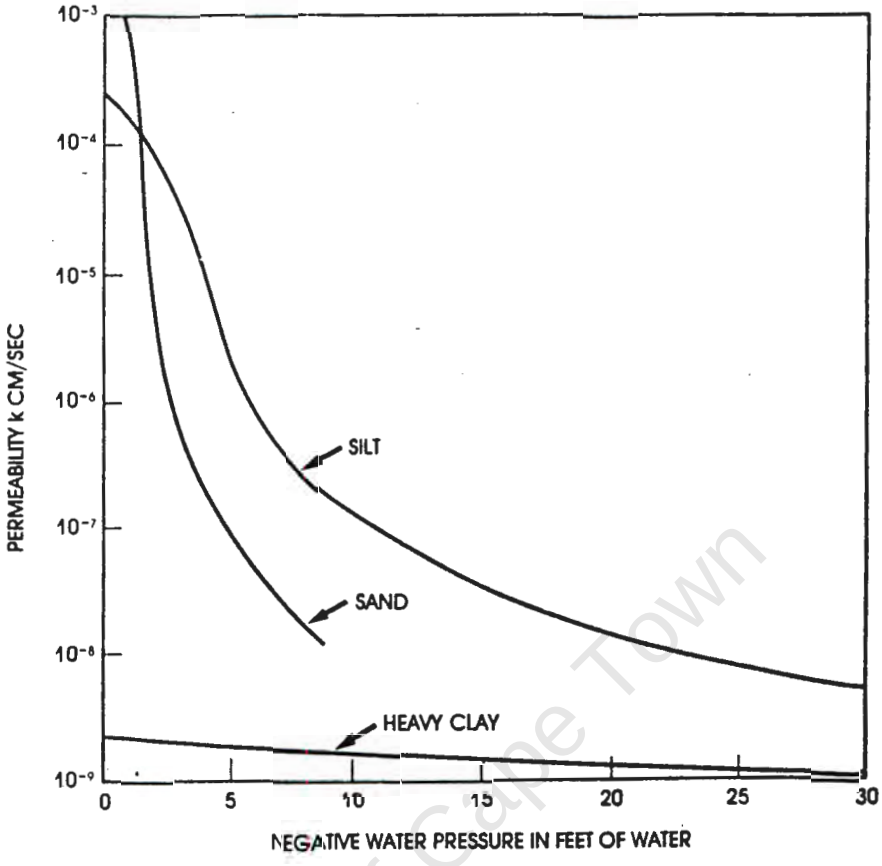

FIGURE 8: Effect of negative pore pressure on permeability of typical soils

times of the year, no leachate will be formed. If there is a seasonal water surplus, leachate will form, the quantity of which can be calculated from the water balance.

(ii) In calculating the rate of outflow of leachate, the thicknesses and permeabilities of cover, disposed waste, any liner and the unsaturated or attenuation zone must be considered as an integral flow system.

ACKNOWLEDGEMENT

The investigation described in this paper forms part of a research project funded by the Foundation for Research Development. The authors wish to thank Mr J J Malan and Dr R G Noble of the Foundation and the project steering committee chaired by Mr S J Verrier, for their support and encouragement.

REFERENCES

1. FRD National Research Programme for Waste Management Workshop, "Draft guidelines for the effective disposal and control of waste", 1986.

2. Ball, J M and Blight, G E, "Groundwater pollution downstream of a long established sanitary landfill". Proceedings, International Symposium on Environmental Geotechnology, Allentown, Penn, USA, Vol 1, pp 149-157.

3. Tredoux, G, "the Groundwater pollution hazard in the Cape Flats". Proceedings, Biennial Conference, Southern African Branch, Institute of Water Pollution Control, 1984, pp 473-483.

4. Oweis, I and Kera, R, "Criteria for geotechnical construction of sanitary landfills". Proceedings, International Symposium on Environmental Geotechnology, Allentown, Penn, USA, Vol 1, 1986, pp 205-222.

5. Blight, G E, "Seepage from clay-lined ponds", The Civil Engineer in South Africa, Vol 8, 1966, pp 215-221.

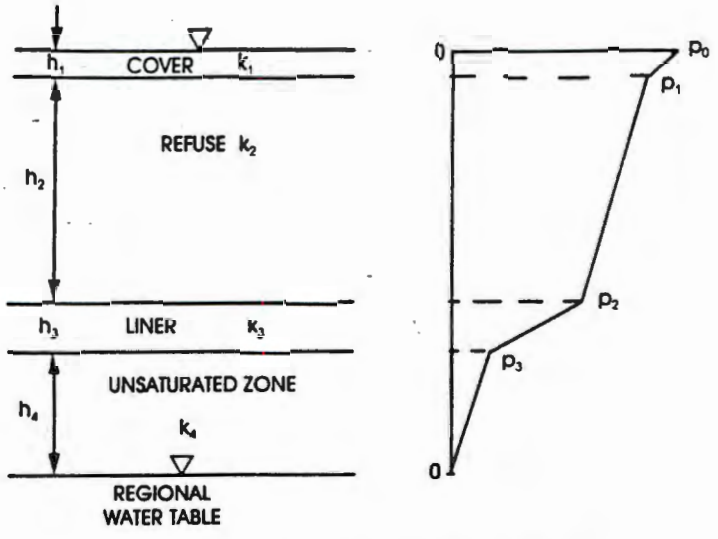

FIGURE 9: Dimensions and potential profile for landfill in water surplus situation

APPENDIX - CALCULATION OF LEACHATE FLOW FROM A LANDFILL SITE

Figure 9 illustrates the dimensions and properties of the situation to be analysed. The potentials p_0, p_2, etc represent the sum of pressure and elevational head at the boundaries of the various layers.

For continuity of flow in a steady state situation:

$$q = k_1 \frac{(p_0 - p_1)}{h_1} = k_2 \frac{(p_1 - p_2)}{h_2} = k_3 \frac{(p_2 - p_3)}{h_3} = \frac{k_4 p_3}{h_4}$$

Also $P_0 = h_1 + h_2 + h_3 + h_4$

The unknowns are the four potentials and the outflow from the system, q. Having solved the system of equations, the pore pressure at any elevation is the potential minus the elevation, eg at the underside of the liner the pore pressure is

$$u = p_3 - h_4$$

The perched water table in the landfill can be set at the highest seasonal level indicated by the water balance calculations.

SARDINIA 89

Second International Landfill Symposium

"Landfill Concepts, Environmental Aspects, Lining Technology, Leachate Management, Industrial Waste and Combustion Residues Disposal"

9-13 October 1989
Porto Conte (Alghero) - Italy

PROCEEDINGS – VOLUME 1

Organized by:
University of Cagliari
Technical University of Denmark
Technical University of Hamburg-Harburg
University of Sassari
CISA - Sanitary Environmental Engineering Centre, Sardinia

Promoted by:
Regional Government of Sardinia
ISWA (International Solid Wastes and Public Cleansing Association)
ANDIS (Italian Association of Sanitary Engineering)

Under the aegis of:
Italian Ministry of Environment

SARDINIA '89 - 2nd International Landfill Symposium

GENERATION OF LEACHATE FROM LANDFILLS IN WATER-DEFICIENT AREAS

G.E. Blight, D.J. Hojem, J.M. Ball

University of the Witwatersrand, Johannesburg, P.O. Wits., 2050, South Africa

SUMMARY : The water balance method has been used to predict the time taken for two sanitary landfills, sited in water deficient areas, to reach their overall field capacity. These predictions have been checked by direct sampling of the landfills. It is concluded that the water balance method is a useful design tool.

1. INTRODUCTION

Water is a scarce commodity in arid and semi-arid areas and pollution of surface and underground water resources can be disastrous to communities and households depending on these sources for domestic supply.

As the Southern African continent is largely a water deficient area, concern has arisen lest existing and future sanitary landfills were causing, or had the potential to cause unacceptable water pollution. Such pollution is also most costly and difficult to clear up once it has occurred. If nothing is done to ameliorate the situation, the pollution may persist in the groundwater for decades (Ball and Blight, 1986) even though the source of the pollution has been removed.

A preliminary study (Ball and Blight, 1986, Blight, Vorster and Ball, 1987) produced strong evidence that if climatic conditions are such that a perpetual water deficit exists at the site of a landfill, no or very little leachate will be formed or exit the base of the landfill. Hence, if there is an adequate separation between the lowest level of refuse and the highest level of the regional phreatic surface, no groundwater pollution will occur. By extension, surface water replenished by the groundwater will also remain unpolluted by leachate from the landfill.

There is considerable support for this view in the literature. For example, Keenan (1986) give figures indicating that landfills receiving more than 750mm of precipitation per annum will eventually produce leachate, while those in arid regions receiving less than an annual 325mm are likely never to exude pollution. Saxton (1983) states that for climates where annual precipitation is less than 400mm, virtually all precipitation is evapotranspired.

Earlier, Fenn et al (1975), Burns and Karpinski (1980) and Holmes (1980) all agreed that if a net annual water deficit exists at the site of a landfill, little if any leachate will exit its base.

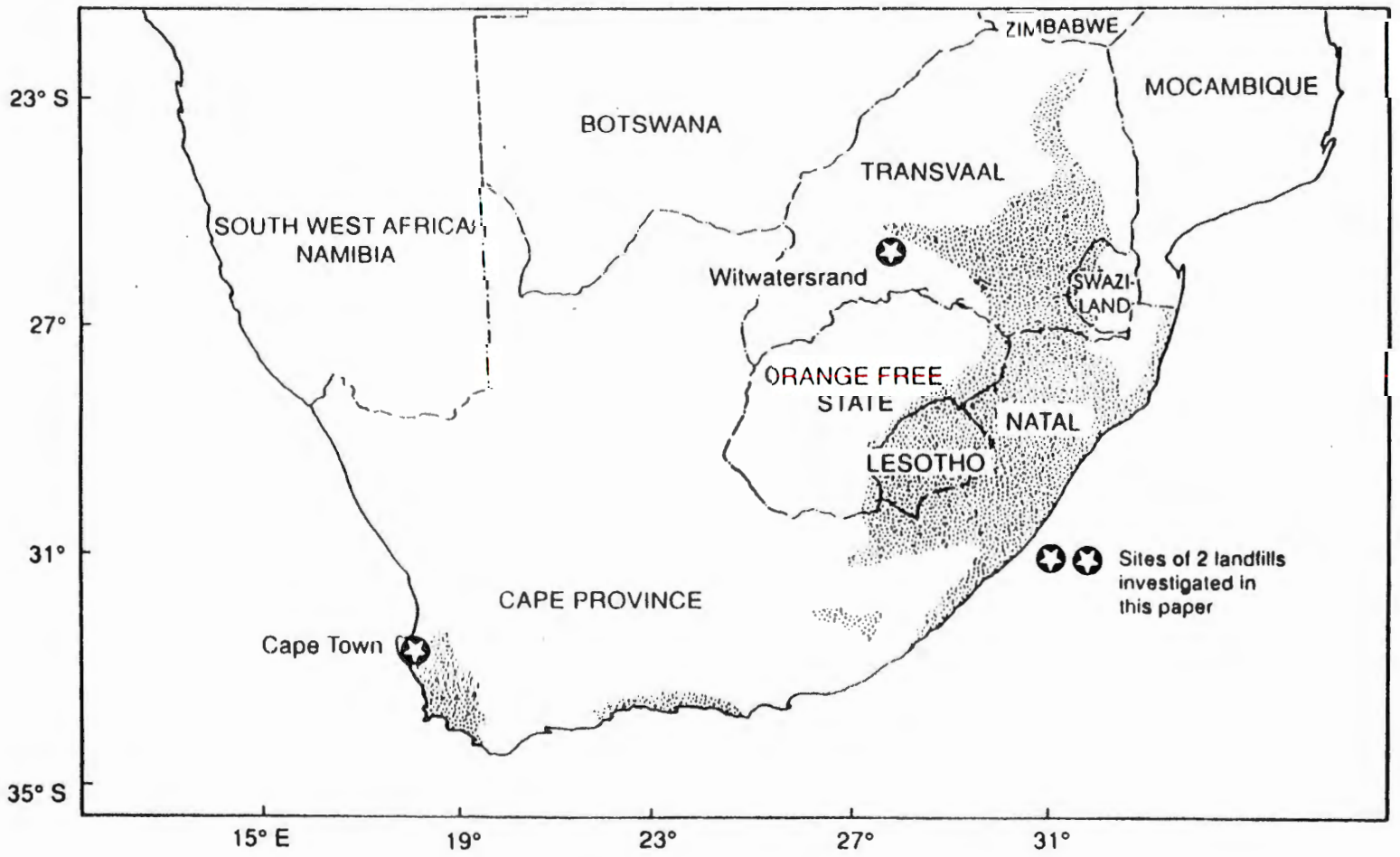

FIGURE 1: Annual water surplus areas of South Africa

Southern Africa includes a wide range of climatic zones, from those on the arid west coast receiving less than 120mm of precipitation and having a potential evapotranspiration of 3 000mm, to those with over 1 000mm of precipitation and almost equal potential evapotranspiration on the humid east coast. However, only 10 per cent of the land surface receives more than 750mm of annual precipitation. Figure 1 shows the limited areas of annual water surplus (i.e. precipitation in excess of potential evaporation) in Southern Africa.

It must also be recognised that good engineering and management of a landfill can be used to maintain a perennial water deficit within the fill even though there may actually be an excess of precipitation over potential evaporation. This can be done by maximizing run-off and minimizing infiltration into the refuse. A suitably sloping surface and the installation of a carefully designed impervious cover layer can achieve this (e.g. Lundgren and Elander, 1987).

This paper will describe a recent detailed investigation into the movement and retention of water within two sanitary landfills in South Africa. The results largely corroborate the evidence outlined above and have formed the basis for a set of guidelines for the design of sanitary landfills in the Southern African region, to avoid water pollution.

2. THE WATER BALANCE FOR A LANDFILL

The water balance for a landfill can be stated as follows:

Water Input + Water Production = Water Output + Water Retained

In this equation, each term represents a rate of accumulation or loss. Water input includes precipitation (P) and the water content of the incoming waste (W). W, however, only makes a once-off contribution to the annual water balance of a given mass of landfill. Water production is that produced by biochemical processes (B). Water output includes evapotranspiration (E), water vapour entrained by gas (G), water lost in leachate (L), and runoff (V). Finally, there is water absorbed and retained by the waste (S). I.e. for an annual water balance:

$$P + W + B = E + G + L + V + S \qquad (1)$$

In the present study B and G have been ignored, as they are understood to be small in comparison with the other terms and the annual water balance equation, as applied to an established landfill, has been simplified to:

$$P = E + L + V + S \qquad (1a)$$

Figure 2 (after Naylor et al, 1978) illustrates the components of the water balance for a landfill in greater detail. In equation (1a), the only component that can be directly controlled by the engineer is the runoff V, and by limiting infiltration, the term S. In terms of equation (1a) the leachate production L is given by:

$$L = P - E - V - S \qquad (1b)$$

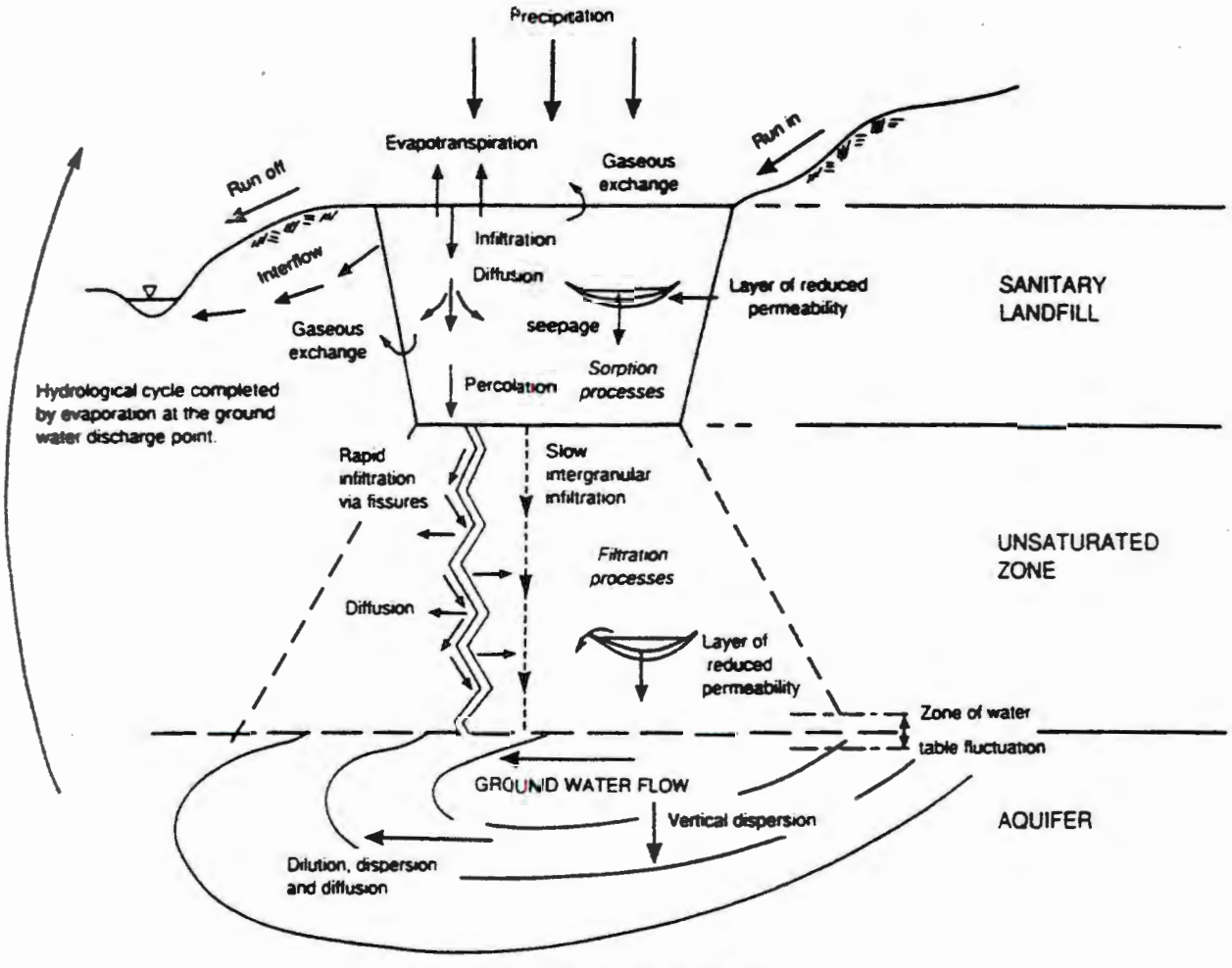

FIGURE 2: Details of water balance in a sanitary landfill

Obviously the smaller the precipitation (P) and the larger the evapotranspiration (E) and runoff (V), the less the potential for the generation of leachate (L). These terms are particularly favourable in water deficient areas.

3. THE FIELD CAPACITY OF REFUSE AND LANDFILLS

The field capacity is that water content (by mass of dry solids) which the refuse will absorb and store or retain by capillarity.

In concept, for an annual water balance, the term S will persist and the term L will be zero until the field capacity of the refuse has been reached. At this stage, the refuse will absorb no more moisture, the term S will disappear and the term L will appear in its place.

It is obvious that as decomposition and compaction of refuse occurs in a landfill, the field capacity will progressively decrease. The literature records values for the field capacity of refuse that vary from 80% for fresh refuse (Campbell, 1983) to between 63% and 74% for refuse more than 4 years old (Holmes, 1980). These figures obviously depend both on the composition of the refuse and the method of determining the dry mass.

It was considered worthwhile to make a separate study of the field capacity of refuse from Johannesburg and the results of two

independent studies by Roper and Fongoqa and by the second author are summarized in Figure 3. The analysis of the refuse was carried out by Roper and Fongoqa (1988) and was as follows:

Component	Percentage of Dry Mass*
Organic	54
Paper	23
Glass	9
Plastic	8
Metal	6

(*Dried at 50°C until constant mass was reached).

Figure 3 shows an even wider variation of field capacity than that recorded above. As a conservative working figure, a field capacity of 60% by dry (50°C) mass of refuse has been assumed in this study.

The theoretical concept that refuse will continue to absorb moisture until the field capacity is reached and will thereafter release moisture at the same rate as it receives it, is obviously an over-simplification. It can be deduced from Figure 3 that the field capacity of refuse itself can be reached because of the accumulation of moisture, or because the field capacity is changing as the age and state of compaction and decomposition of the refuse increase, or by a combination of the two processes.

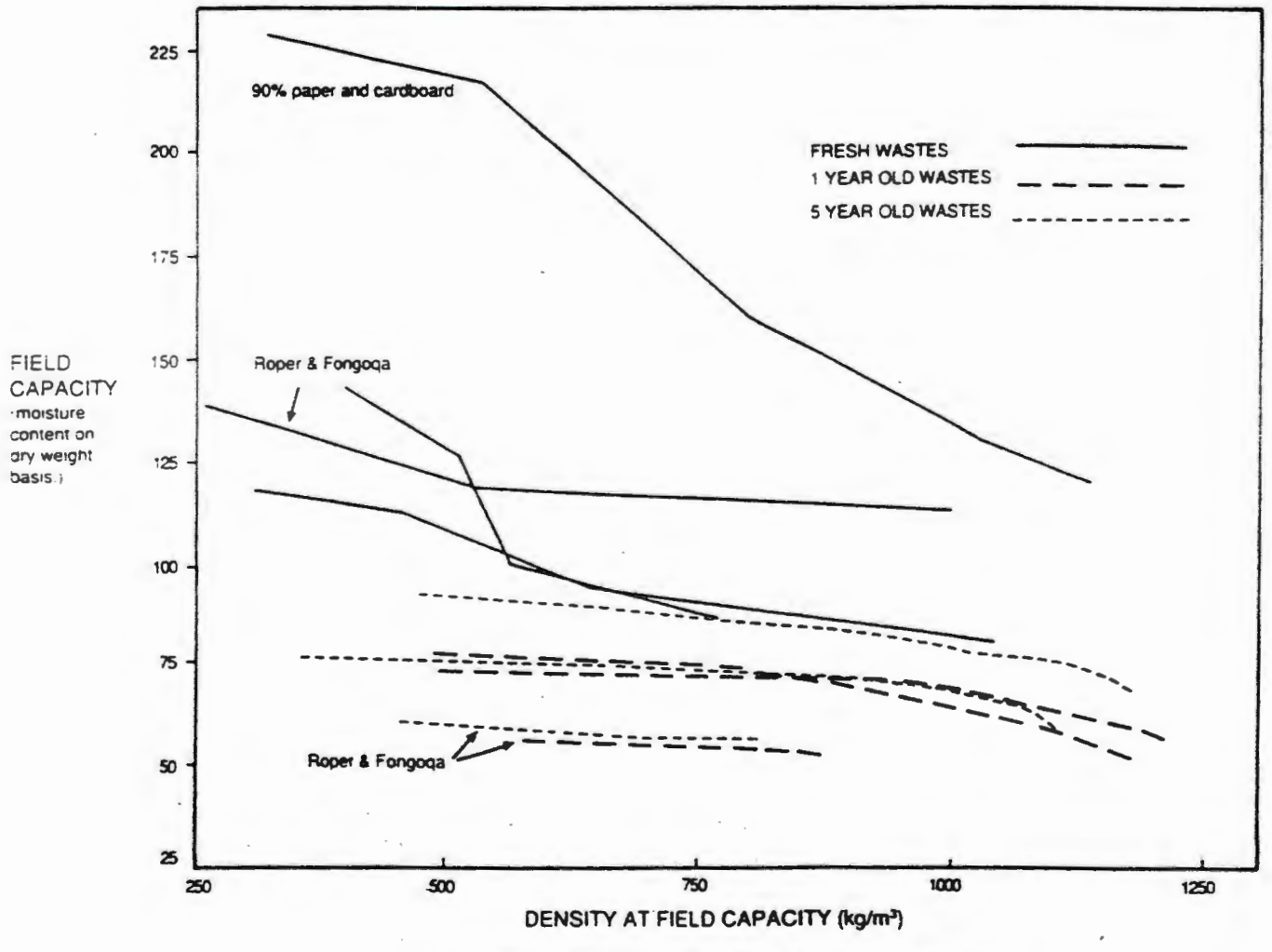

FIGURE 3: Measurements of the field capacity of refuse.

A landfill may start to release leachate long before its overall field capacity has been reached because certain interconnected zones within it have a lower field capacity than others. This is well illustrated by Figure 4 which shows a record of the precipitation on the surface and the corresponding release of leachate from a 20m square and 5m deep cell of refuse at a landfill near Cape Town.

The cell was underlined with a plastic sheet that trapped all leachate exiting the refuse and channelled it into a container, which enabled the leachate production to be measured.

As at the end of 1988 the landfill had received over 1500mm of precipitation, and had released less than 150mm of leachate over a 2½ year period. The water balance calculation (to be described later) predicted that once the field capacity of the landfill has been reached, the annual output of leachate will be 200mm per year or 500mm in 2½ years. It is therefore clear that the overall field capacity has not yet been reached. At the same time, certain zones in the cell are releasing leachate and therefore must have reached their localized field capacity. Leachate is, however, only generated during the cool wet winter months when there is a seasonal water surplus.

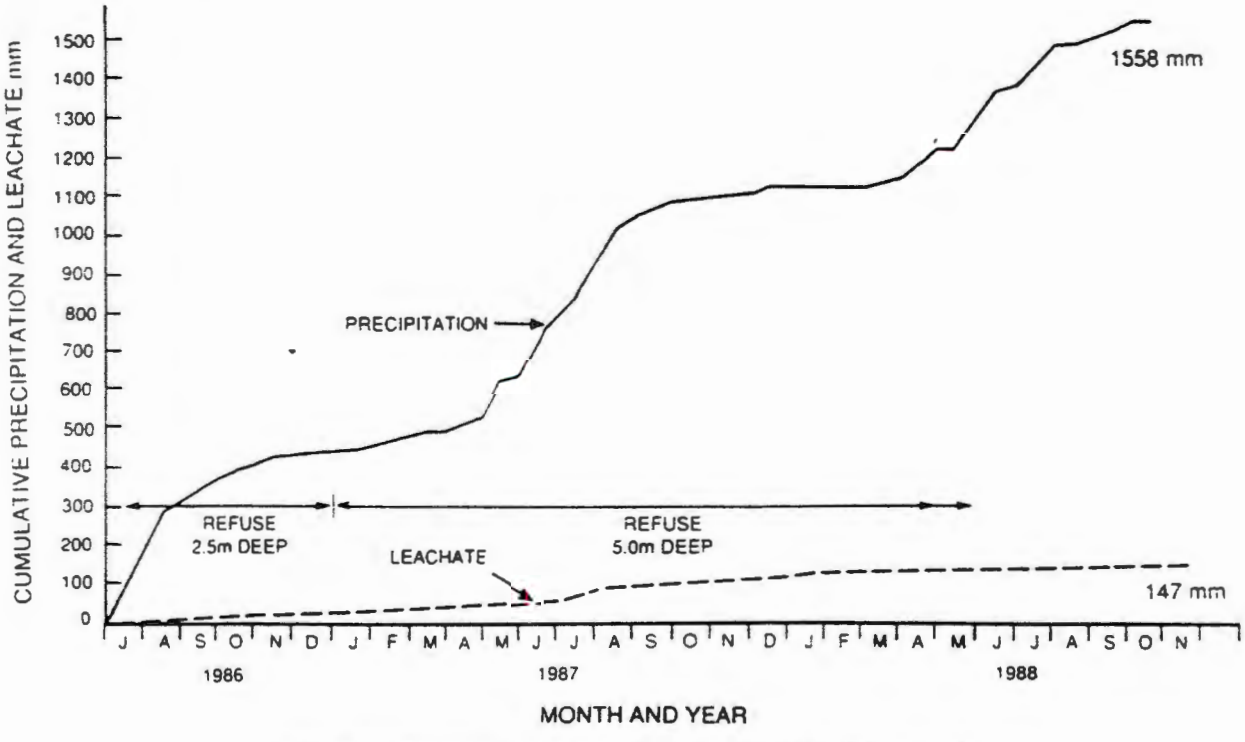

FIGURE 4: Precipitation and leachate production at landfill in Cape Town

4. WATER BALANCE FOR TEST LANDFILLS

The experimental work to be described in this paper was performed at a landfill on the Witwatersrand and one near Cape Town (see Figure 1). The Witwatersrand landfill is in a summer rainfall area while that at Cape Town is in a winter rainfall area. The climatic parameters for the two sites have been summarized in Figure 5.

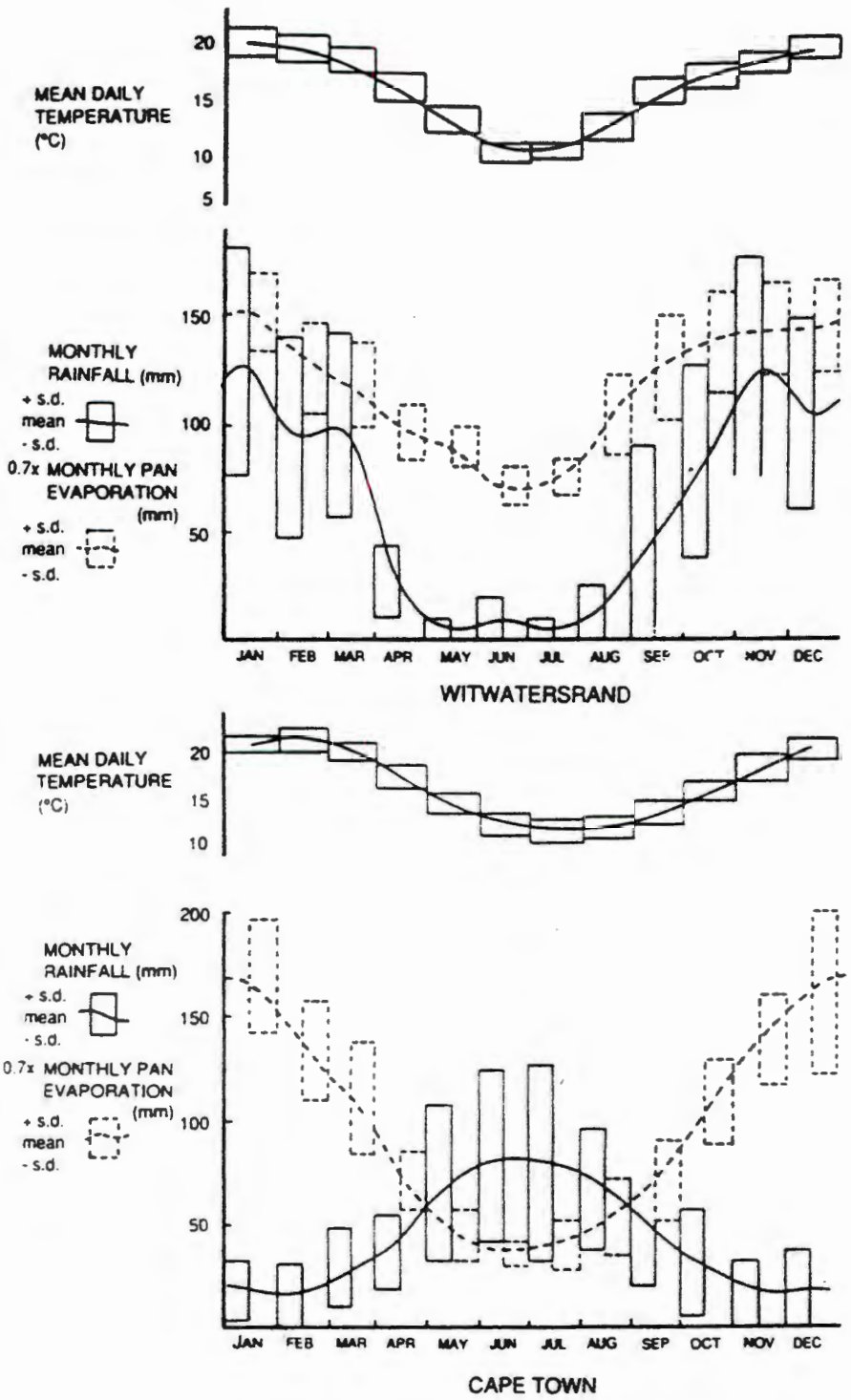

FIGURE 5: Summary of climatic parameters at two test landfills.

At the Witwatersrand landfill, pan evaporation exceeds precipitation throughout the year, while at Cape Town precipitation exceeds evaporation during the 3½ to 4 winter months. 30-year average annual figures for precipitation and rainfall at the two sites are:

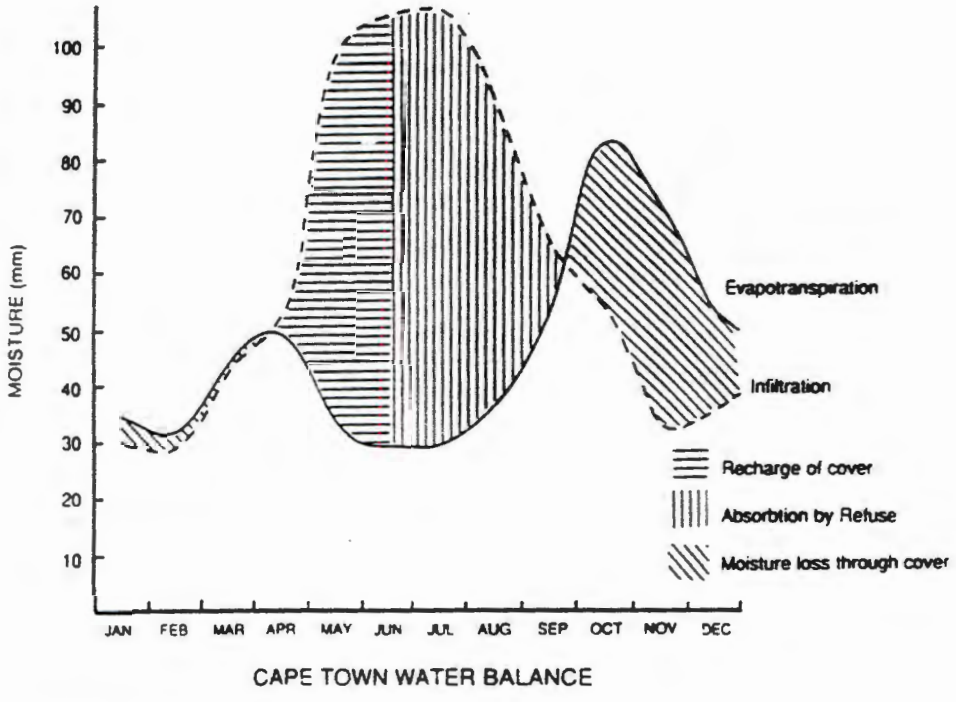

FIGURE 6: Water balances for Cape Town and Witwatersrand landfills.

Witwatersrand	:	Precipitation	= 745mm
		Pan Evaporation	= 1550mm
Cape Town	:	Precipitation	= 510mm
		Pan Evaporation	= 1110mm

Hence both sites are nominally in water deficit areas with potential evaporation exceeding precipitation by some 600 to 800mm.

Figure 6 shows detailed water balances for the two sites calculated by Fenn et al's, (1975) adaptation of the method of Thornwaite and Mather (1957), and based on a weekly calculation interval.

Assumptions for both sites were the same, namely 1000mm of top cover with 100mm of available storage in the cover. Precipitation was taken as:

$$P = (\text{mean rainfall} + 1 \text{ standard deviation})$$

and evapotranspiration as:

$$E = 0.7 (\text{mean pan evaporation} - 1 \text{ standard deviation}).$$

Hence some conservatism was built into the calculations.

Runoff for the Witwatersrand site, where the cover material is a clayey sand, was taken as:

$$V = 0.11 P$$

while that at Cape Town, where the cover is a clean fine sand, was taken as:

$$V = 0.08 P$$

Both of these are probably also conservative figures.

Figure 6 indicates that at Witwatersrand it is only in the 2-month mid-February to mid-April period, that the refuse will be gaining in moisture, while at Cape Town, moisture is gained for 3 months from mid-June to mid-September. As mentioned previously, these calculated annual water balances will usually be conservative, and will inevitably vary from year to year. For example, the precipitation at the Witwatersrand site in 1984 was only 46% of the 30 year average. In 1986 it was equal to the average, while in 1988 it was 130% of the 30 year average. On one day in October 1985 the landfill received 110mm of rainfall, nearly 12% of the annual figure, most of which must have run off. These extreme figures illustrate the uncertainties inherent in water balance calculations.

On the basis of these water balances, a time for each landfill to reach field capacity can be calculated, as can the ensuing rate of generation of leachate. The calculations showed that the Witwatersrand landfill can be expected to reach a field capacity of 60% moisture around the year 2000, after which leachate is likely to be generated at a rate of about 130mm per year. However, as the calculations are based on conservative figures, these approach worst case estimates. 130mm per year is equivalent to 4×10^{-7} cm/s, which is about one tenth of the coefficient of permeability of the base of the landfill. Hence any leachate that is generated will disperse into the underlying unsaturated zone.

It should also be emphasized that the result of a water balance calculation depends on the interval adopted for the calculation. For example, for Witwatersrand a weekly calculation interval gives 70% of the figures based on a daily interval.

At Cape Town, overall field capacity is predicted in 1993 whereafter the predicted rate of leachate production is 200mm per year. As recorded earlier, this compares with the currently measured leachate production of 60mm per year.

5. DIRECT SAMPLING OF LANDFILLS

A direct sampling of both the Witwatersrand and Cape Town landfills was carried out in order to examine in detail the distributions of moisture and solutes in the two landfills. An analysis of these, both at the end of the wet season and at the end of the dry season would give an indication of the accuracy of the predictions based on water balance.

Sampling was performed from 1200mm diameter holes augered in the landfills by means of a pile augering machine. Each hole was cased against possible collapse of the sides with a cylindrical cage made of heavy reinforcing steel. A steel collar and hinged lid was fitted to each hole to exclude surface water and retain the landfill gas. The level of each lid was kept above the surface of the landfill and surrounded by a mound, further to exclude surface water.

Two holes were drilled at the Witwatersrand site, one in a well-drained area (the South hole), the other in a slight depression where water ponds to a shallow depth (the North hole). One hole was drilled at Cape Town, adjacent to the lined leacnate collection cell.

The actual sampling was carried out by the third author who descended the holes on a bosun's chair, wearing a full-face diving mask, and extracted the samples from the sides of the holes through the apertures in the casing cage.

The results of the analyses of the holes is shown in Figure 7a (Witwatersrand North), Figure 7b (Witwatersrand South), and Figure 8 (Cape Town). Each figure shows profiles of water content, TDS and chloride (both in mg per kg of dry refuse). A number of other parameters were also measured but have not been shown in the figures.

6. RESULTS OF DIRECT SAMPLING

6.1 Witwatersrand

The Witwatersrand North hole shows a definite seasonal fluctuation of water content. All the measurements except two were well below the assumed average field capacity of 60%. There appears to be an isolated wet layer at a depth of 15m, and the water content of the soil at the base of the landfill rose to over 40% at the end of the wet season. This is well in excess of the field capacity of this soil, estimated at 15%. Hence this profile shows evidence of some leachate exiting from the base of the fill.

The South hole shows a greater fluctuation of water content down to about 5m and also a zone in excess of the field capacity between depths of 3 and 5m. There was also a wet season concentration of water near the base of the landfill. Both profiles are thus generally below the field capacity but show evidence of some outflow of leachate near the base.

The TDS in both profiles changed little from season to season. At about 5m depth, the North hole shows a concentration of TDS which

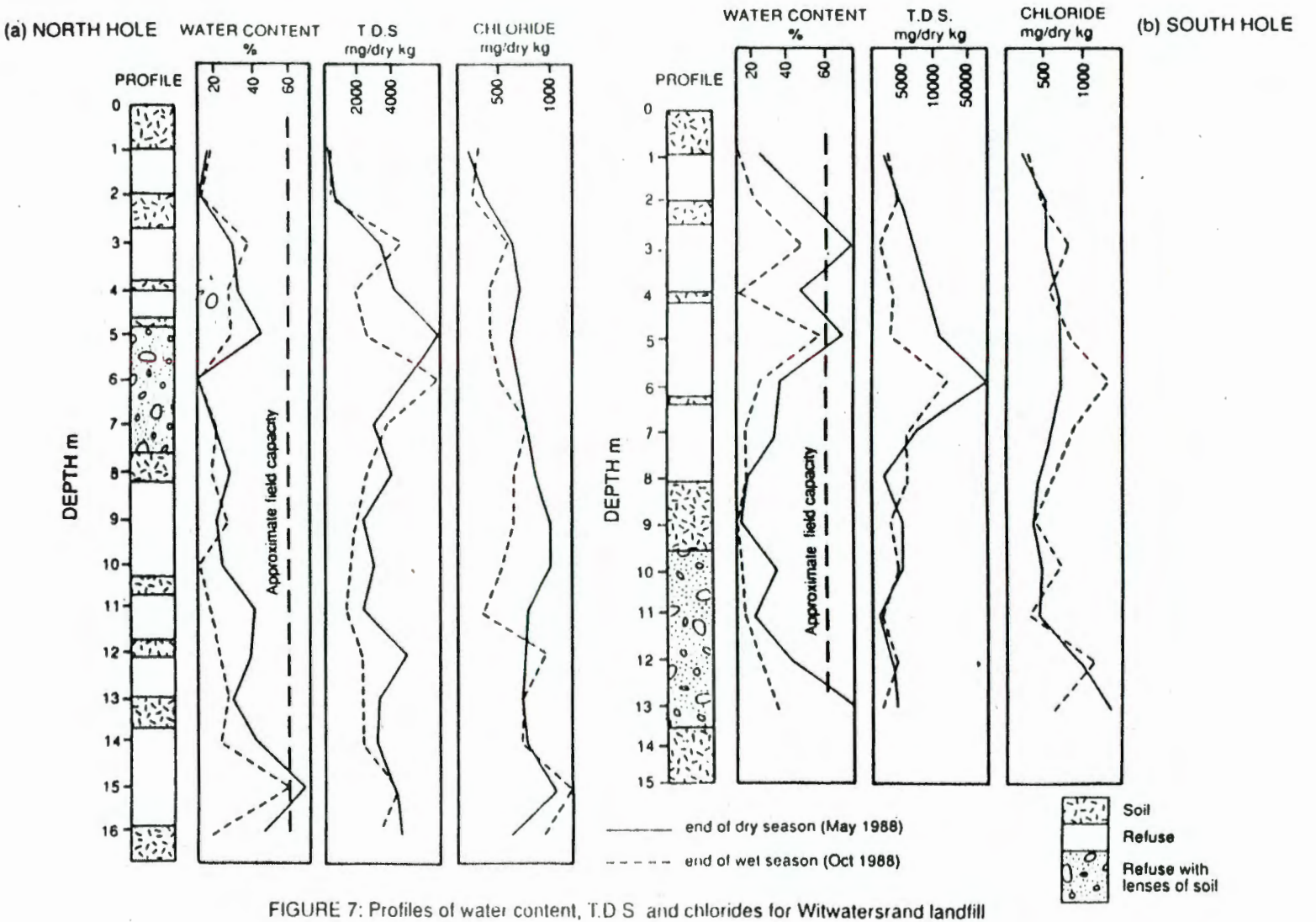

FIGURE 7: Profiles of water content, T.D.S and chlorides for Witwatersrand landfill

may be related to corresponding peak in the water content profile. This may correspond to the 30% above average rainfall that fell in the 1988 wet season immediately preceding the sampling. This unusual precipitation may also account for the high TDS at about 6m deep in the South hole.

Neither hole shows a tendency for TDS to accumulate at the base of the profile. Equally, neither shows a tendence for a concentration towards the top of the profile during the dry season.

The profiles of chloride at Witwatersrand show similar trends to the TDS profiles. However, there does appear to be an increase of chloride content with depth.

The overall impression is one of a fairly stable, but seasonally fluctuating water and solute profile with evidence of some outflow at the base of the landfill. Strangely enough, the profile underlying the area where ponding occurs is drier than that under the well-drained area. This may be because the cover is more pervious at the South hole, but this has not been established.

The water content profiles can be used to estimate the total moisture accumulation in the refuse since placing, if inital water contents for refuse and cover material are assumed. On average, at the end of the 1988 wet season, the profiles for the two holes had accumulated 3000mm of water since placing. This reduced to 1750mm at the end of the ensuing dry season. Bearing in mind that 1988 had an unusually wet season, it thus appears that the seasonal fluctuation of moisture in the profile is of the same order as the average annual precipitation of 950mm.

Because the profile is mostly well dry of the field capacity, this moisture must mainly be moving in and out of the top cover, and the quantity of leachate escaping from the base can only be very small. Hence there is fair agreement between the results of the direct sampling and the prediction based on a water balance, with the water balance calculation likely to be pessimistic.

6.2 Cape Town

The end of the wet season water content was mostly below the field capacity, but there was a zone of material at a depth of 4m, that was above field capacity and one at 2m that was at field capacity. There were also concentrations of TDS and Chloride coinciding with this wet zone in the profile. These peak values probably represent a wetting front moving through the landfill.

The end of dry season water content profile was well below the field capacity, which must indicate that moisture moves up the profile and out through the cover during the dry season. Moisture moving downward by gravity flow could be expected to leave material at the field capacity above it.

The profile appears to have accumulated about 900mm of water since placing at the end of the wet season and 650mm at the end of the dry season. Hence taking runoff at 40mm per annum, the moisture available for increasing the water content of the landfill and ultimately for producing leachate amounts to about 200mm per year

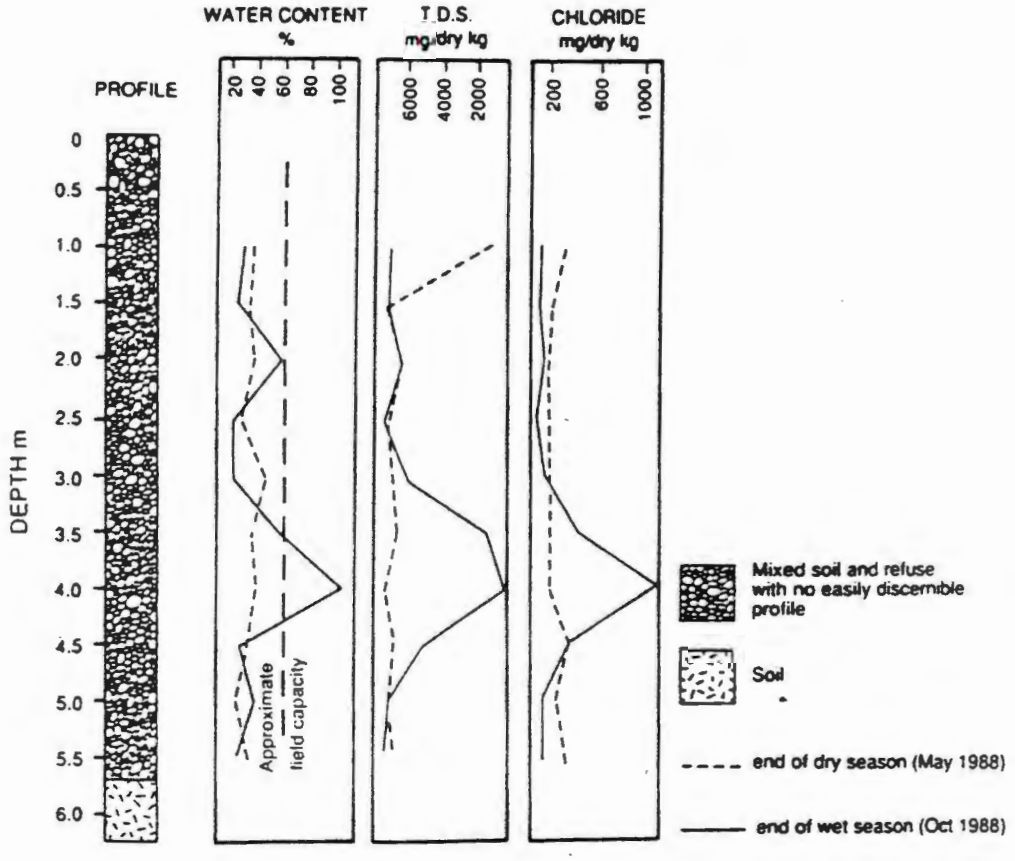

FIGURE 8: Profiles of water content, T.D.S. and chlorides for Cape Town landfill.

which agrees with the prediction based on the water balance.

7. SUMMARY AND CONCLUSIONS

7.1 Calculations based on considerations of the water balance for a landfill can be used to predict the time likely to be taken for the landfill to reach its overall field capacity. The results of such calculations are liable to uncertainty because of the highly variable nature of the weather and the variable properties of the refuse and cover material. Uncertainties in the estimation of runoff and evapotranspiration add to the uncertainty of the prediction.

7.2 A comparison between the results of direct sampling of two landfills and predictions based on their water balance showed that the water balance method is realistic and as accurate as can be expected, given the uncertainty of the input data.

7.3 In order to predict whether or not a landfill sited in an arid or semi-arid area will produce leachate, it is essential to consider the detailed distributions of precipitation and evaporation through the year, and to carry out a full water balance calculation.

In the examples examined here, both landfills are sited in areas of nominal water deficit, with the annual deficit being between 600 and 800mm. Neither landfill is producing very much leachate at

present, but it seems that the Cape Town landfill has the potential to produce more than twice the leachate possibly to be produced by the landfill at Witwatersrand.

8. ACKNOWLEDGEMENTS

The research on which this paper is based was funded by the South African Foundation for Research Development as part of their programme of research into waste management. The second author was seconded to Witwatersrand University by the City Engineer's Department, Johannesburg for the purpose of undertaking the study. The authors gratefully acknowledge the assistance of the City Engineer's Departments of Johannesburg and Cape Town.

9. REFERENCES

BALL, J.M and BLIGHT, G.E. "Groundwater pollution downstream of a long established sanitary landfill". Proceedings, International Symposium on Environmental Geotechnology, Allentown, Pa, USA, (H.V. Fang, Ed.) 1986, pp 149-157.

BLIGHT, G.E., VORSTER,K and BALL, J.M. "The design of sanitary landfills to reduce groundwater pollution". Proceedings, International Conference on Mining and Industrial Waste Management". S A Institution of Civil Engineers, Johannesburg, 1987, pp 297-306.

BURNS, J and KARPINSKI, G. "Water balance method estimates how much leachate a site will produce". Solid Waste Management, August 1980, pp 54-84.

CAMPBELL, D.J.V. "Understanding water balance in landfill sites". Waste Management, November 1983, pp 594-605.

FENN, D.G., HANLEY, K.J. and DE GEARE, T.V. "Use of the water balance method for predicting leachate generation for solid waste disposal sites". U.S. Environmental Protection Agency, Report No.EPA/530/SW168, 1975.

HOLMES, R. "The water balance method for estmating leachate production from landfill sites". Solid Wastes, Vol.LXX, No.1, 1980, pp 20-33.

KEENAN, J.D. "Landfill leachate management". Journal of Resource Management and Technology, Vol.14, No.3, 1986, pp 177-188.

LUNDGREN, T and ELANDER, P. "Environmental Control in Disposal and Utilization of Combustion Residues". Swedish Geotechnical Institute Report No.28E, 1987.

NAYLOR, J.A., ROWLAND, C.D., YOUNG, C.P. and BARBER, C. "The investigation of landfill sites". Water Research Centre, Technical Report TR9, 1978.

ROPER, K and FONGOQA, F. "Determination of the field capacity of domestic refuse". Final year project report, Department of Civil Engineering, Witwatersrand University, 1988.

SAXTON, K.E. "Soil water hydrology : simulation for water balance computations". Proceedings, Workshop on New Approaches in Water Balance Computations, Hamburg, 1983.

THORNWAITE, C.W. and MATHER, J.R. "Instructions and tables for computing potential evapotranspiration and the water balance". Publications in Climatology, Vol.X, No.3, Drexel Institute of Technology, 1957.

SARDINIA 91

Third International Landfill Symposium
"Biogas disposal and utilization, choice of material and quality control, landfill completion and aftercare, environmental monitoring"

14 - 18 October 1991, S.Margherita di Pula (Cagliari), Sardinia, Italy

PROCEEDINGS

VOLUME I

MOISTURE DISTRIBUTION IN SANITARY LANDFILLS

G.E. BLIGHT, J.M. BALL AND J.J. BLIGHT

Witwatersrand University, P.O. Wits, 2050, Johannesburg, South Africa

SUMMARY:

This study examines the detail of moisture profiles in three landfills located in semi-arid climates and concludes that one of the components of the water balance that is most difficult to estimate is the storage capacity of the refuse body. This appears to be greatly influenced by the properties and disposition of the layers of intermediate cover.

1. INTRODUCTION

The water balance technique has been developed with the aim of allowing the pollution potential of a landfill to be assessed from a knowledge of climatic parameters and with some assumptions regarding the properties of the landfill. These relate mainly to the moisture storage capacity of the refuse and capping layer, and the percentage of precipitation that will infiltrate the cap.

The usual main defence against leachate pollution is a well designed under-liner. The primary defence against the generation of leachate within the landfill is the final landfill cover or cap. With design attention focused on excluding moisture from landfills by means of the cap system, or retaining and re-circulating leachate within landfills by means of the under-liner, less attention has been directed towards the moisture absorbtion and retention capacity of the stored refuse and the intermediate cover layers. The water retained within refuse represents by far the largest volume of moisture in the landfill system. Moreover, a certain minimum of moisture is required within the refuse to allow microbiological decomposition processes to proceed. If the objectives of the landfill management system include rapid consolidation of the waste body, or the generation and extraction of landfill gas, then the retention of an optimum water content for microbiological activity within the waste body is essential.

The present study has explored the water retention capacity of three landfills situated in semi-arid areas. The paper will show how the water content of the refuse changes seasonally, and point out the important effect of the intermediate cover layers. It will show that the moisture storage capacity of a landfill is very difficult to quantify. Finally, it will present data on the moisture suction in two landfills, and show that even though these are situated in semi-arid areas, suction is always sufficiently low for microbiological activity to proceed.

Proceedings Sardinia 91, Third International Landfill Symposium
S. Margherita di Pula, Cagliari, Italy; 14 - 18 October 1991

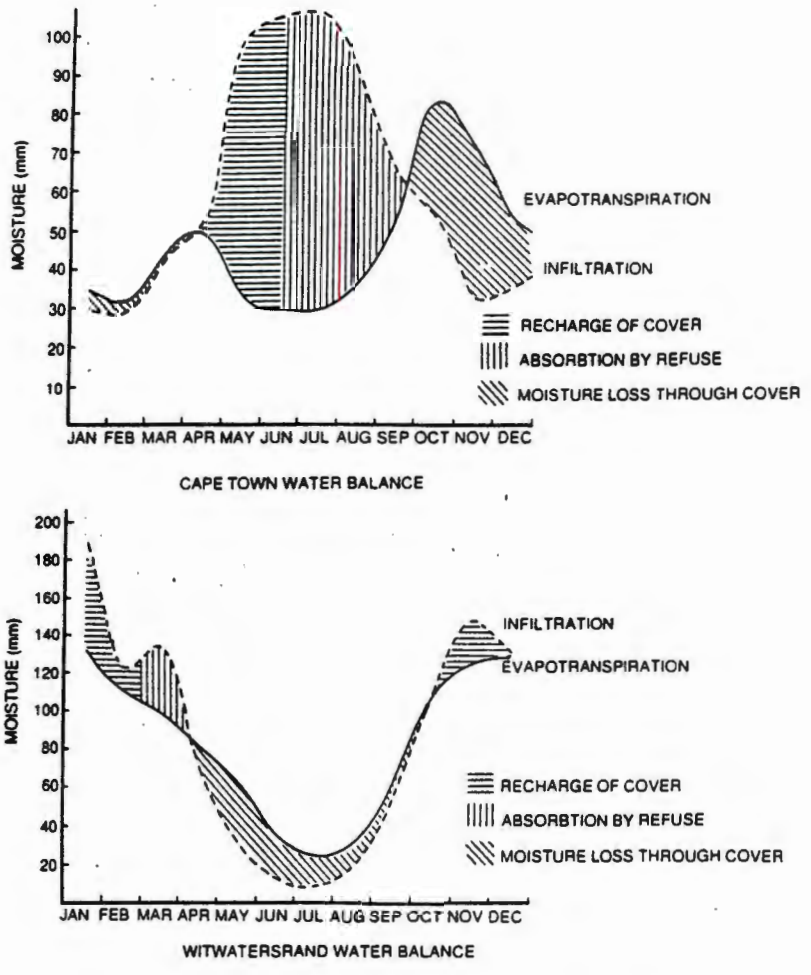

FIGURE 1: Water balances for landfills at Cape Town and Witwatersrand

store within its pores by capillarity. In terms of a water balance one might imagine the water stored in a landfill gradually accumulating until the overall moisture storage capacity had been reached. Thereafter any further water added at the top of the landfill would result in the production of an equal quantity of leachate at the base. However, the concept, as stated here, is a gross over-simplification.

The storage capacity of refuse has been measured in the laboratory by a number of workers [eg Campbell (1983) and Holmes (1980)]. Measured storage capacities range from 225 per cent for fresh waste predominantly of paper and cardboard, to around 55 per cent for 1 to 5 year old wastes after compression to high densities. It must not be forgotten that intermediate cover layers have a different storage capacity, usually far less than that of refuse.

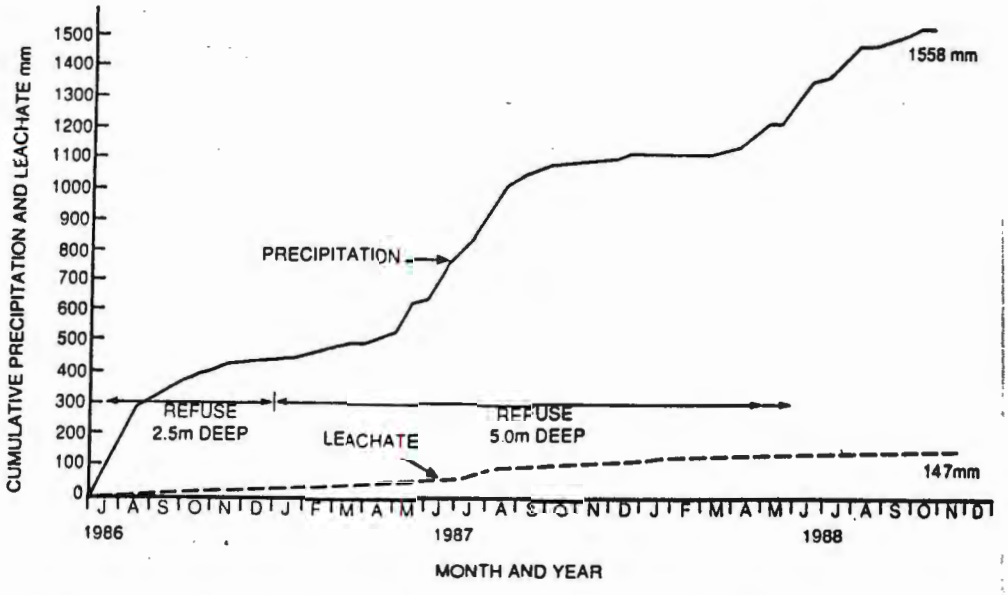

FIGURE 2: Precipitation and leachate production at Cape Town landfill

Figure 2 illustrates how the observed water balance behaviour of the Cape Town landfill differs from the simplified ideal. The figure compares the cumulative precipitation at the Cape Town landfill with the cumulative leachate flow from a 5m deep layer of refuse, starting from the time of deposition. Leachate started appearing during the first wet season and has continued seasonally ever since.

This behaviour contradicts the classical concept of storage capacity and shows that the results of water balance calculations, especially as they relate to time-dependent effects, must be viewed with caution. Assuming an overall storage capacity of 60 per cent for the landfill, water balance calculations predict that the Cape Town landfill will reach its storage capacity in 1993. It is however obvious from Figure 2 that zones of the landfill actually achieved storage capacity within a few months of being deposited.

4. MOISTURE CONDITIONS IN LANDFILLS REVEALED BY SAMPLING

4.1 Waterval Landfill

Figure 3 shows water content and total soluble solids (TDS) profiles for the Waterval landfill near Johannesburg [Ball and Blight (1986)]. The samples were taken at the end of the dry season and the profile was 7 to 8 years old at this time. The intermediate cover material was a clayey silt with a permeability of about 10m/y. The positions of the cover layers have been marked in the Figure. They generally correspond to low water contents and low TDS values.

It appears that the low permeability cover layers effectively divide the landfill into a series of sealed cells with very little moisture or soluble solids transfer occurring from one cell to another. Note in particular that the TDS content below the base of the landfill is negligible, indicating a negligible seepage of leachate from the base of the landfill. In general, the TDS profile is a reflexion of the water content profile. No measurements of the storage capacity of the refuse were made. However it seems likely that the storage capacity of the refuse was at least 125 per cent, the highest water content in the upper part of the profile, while that of the cover layers was about 30 per cent.

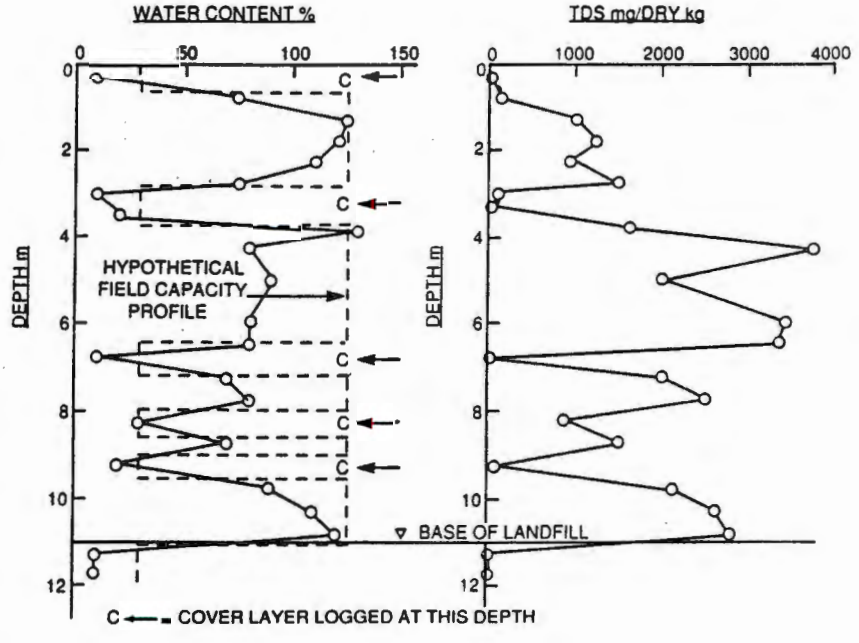

FIGURE 3: Water content and TDS profiles for Waterval landfill at end of dry season

4.2 Coastal Park Landfill

Figure 4a shows profiles of water content measured for the end of the dry season and the end of the wet season at Coastal Park landfill near Cape Town. The intermediate and top cover material is a fine dune sand. It is interesting to note that with the exception of the high water contents measured at 2m and between 3 and 4.5m, water contents recorded at the end of the wet season were actually slightly less than those at the end of the dry season.

Of particular interest are the measured values of storage capacity. The storage capacity for the sand cover almost coincides with the lower limit

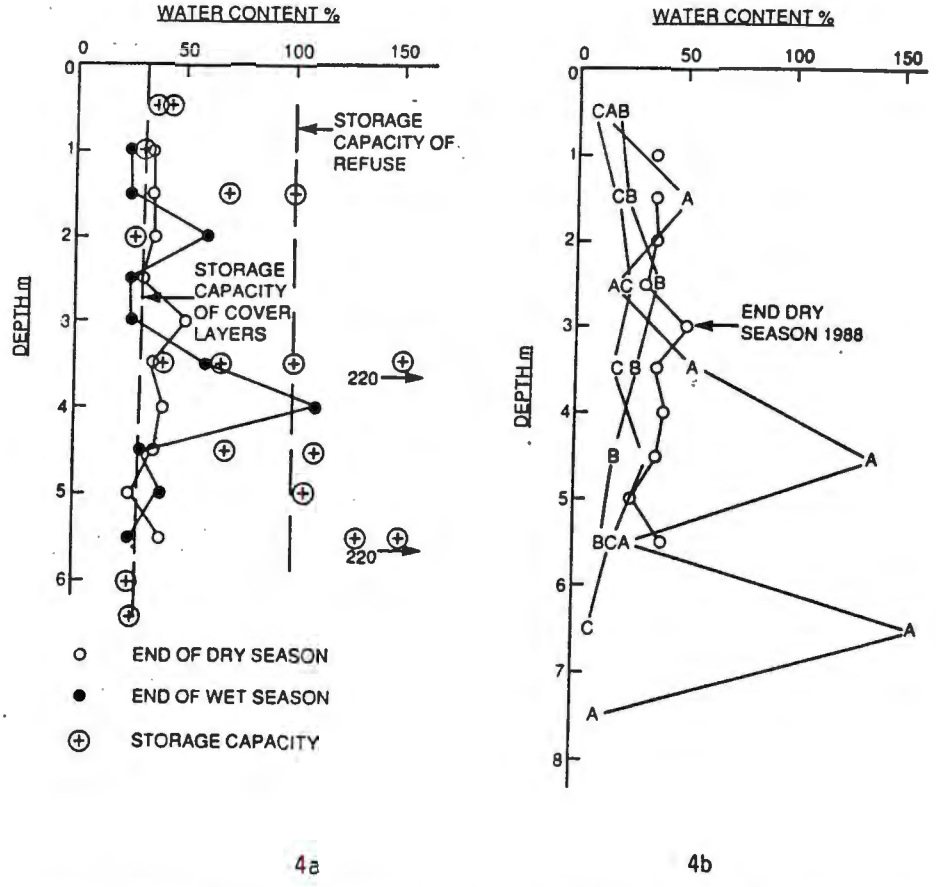

4a 4b

FIGURE 4: Water content profiles for Coastal Park landfill
a: End of wet and dry seasons 1988 b: End of dry season 1990

of water content in the profile, but the higher storage capacities in the refuse (up to 220 per cent) far exceed the maximum water contents. Samples for which the storage capacity was about 70 per cent consisted of a mixture of refuse and sand. The landfill does produce leachate during the wet season (Figure 2). As the storage capacity of the refuse has not been reached it appears that this leachate must be channeling through the relatively permeable layers of intermediate cover.

Thus at Waterval the low permeability intermediate cover layers act to encapsulate the cells of refuse and prevent the generation of leachate, while at Coastal Park, the high permeability cover layers actually promote the generation of leachate by reducing the effective storage capacity of the landfill. However they also reduce the volume of refuse subject to leaching.

The results of Figure 4a, in which end of dry season water contents slightly exceeded end of wet season values, raised doubts as to the validity of comparing measurements on a single set of samples taken at the

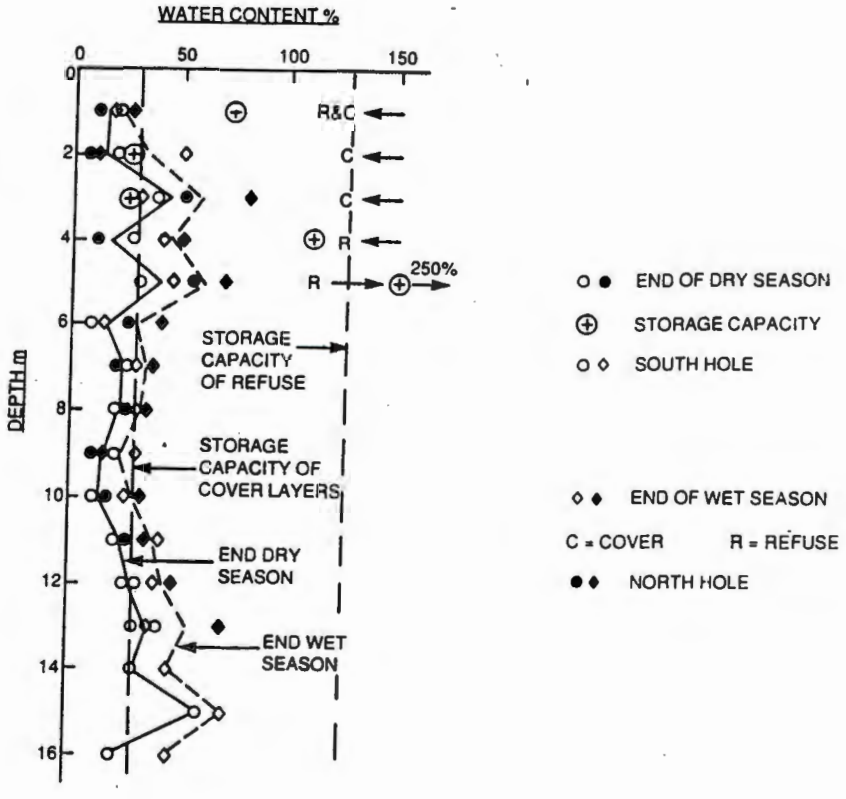

FIGURE 5: Water content profiles for Linbro Park Landfill.
End of Wet and dry seasons 1988

end of one season with a second set taken 6 months later. For this reason, at the end of the wet season two years later, a set of three widely separated holes (A, B and C) was drilled and sampled at Coastal Park. The results of these three samplings are compared in Figure 4b with the end of dry season values of two years previously. It will be seen that with the exception of two measurements for hole A, the four sets of water content measurements agree very well, at least as well as would be expected in normal comparisons of adjacent geotechnical profiles. The correspondence between sets of measurements taken two years apart and from different locations gives confidence that valid conclusions can indeed be drawn by comparing the data of single holes.

4.3 Linbro Park Landfill

Figure 5 compares end of wet season and end of dry season samplings from two separate holes at Linbro Park landfill.

Each of the pairs of water content measurements agrees very well with its fellow, even though the holes from which the samples were taken were 300m apart. There is a change in water content over the whole depth of the landfill between wet and dry seasons. At this site the cover material is a silty sand intermediate in permeability (1000m/y) between the cover at Waterval and Coastal Park. Again, the end of wet season water contents are well below the storage capacity of the refuse, but very close to the storage capacity of the cover material.

The situation at Linbro Park appears similar to that at Coastal Park. If leachate is being generated seasonally, it will be channeled along the relatively pervious intermediate cover layers, bypassing a large proportion of the refuse.

5. CONCLUSION FROM MOISTURE PROFILES

It is apparent from this examination of the detail of moisture profiles in landfills that it is extremely difficult to define an overall storage capacity for a landfill. The storage capacity is very much influenced by the location and properties of the intermediate cover layers and as such, almost impossible to predict from a knowledge of the separate storage capacities of refuse and cover material.

It is also apparent that using either highly pervious or completely impervious intermediate cover material in a landfill could have advantages. In the first place, highly pervious layers will channel infiltrating water past cells of refuse thus resulting in a less concentrated leachate. Completely impervious cover layers will seal off refuse from percolating water thus preventing the evolution of leachate. However, these sealing layers might adversely affect landfill gas production, if it is intended to exploit this as an energy source.

6. MOISTURE SUCTION IN LANDFILLS

With the increasing tendency to exploit landfill gas as a source of energy [eg papers to this conference], concern was felt that landfills in semi-arid climates such as the Witwatersrand might be too dry for optimal bacteriological activity. For this reason it was decided to measure suction profiles when resampling the Coastal Park and Linbro Park landfills in 1990. Figure 6 shows the results of these suction measurements. As they were taken at the end of the dry season in each case, the profiles should represent maximum suctions likely to occur in the respective landfills.

The suctions were measured using psychrometers and the readings therefore represent total suction, the sum of the osmotic and matrix components [eg Savage and Cass (1984)].

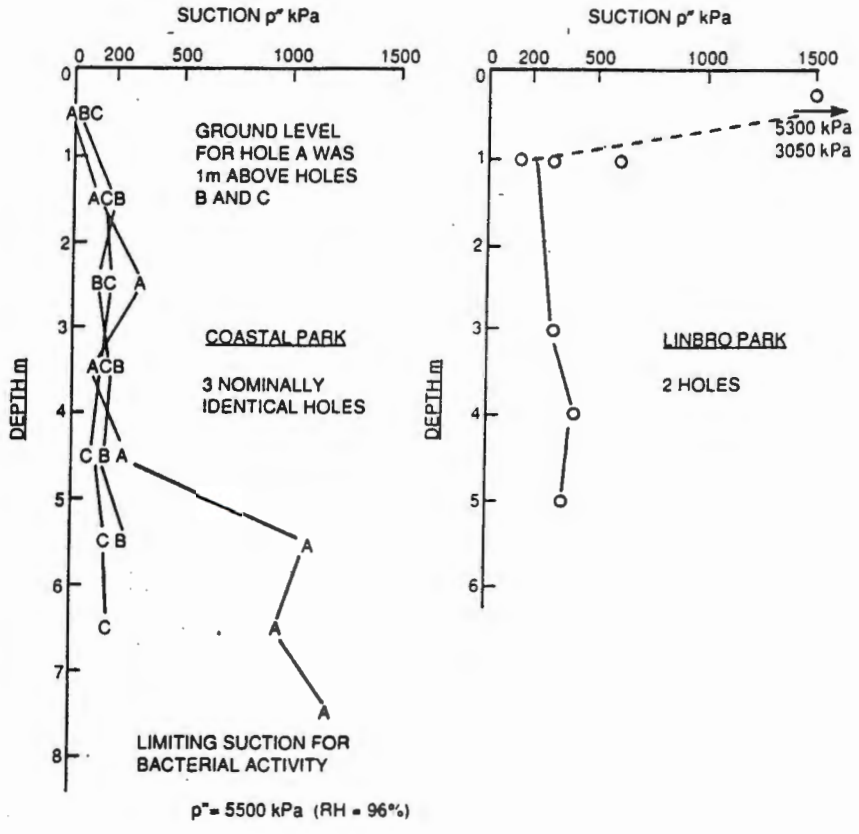

FIGURE 6: Suction profiles at end of dry season in Coastal Park and Linbro Park landfills

The three profiles measured at Coastal Park show suctions consistently below 300 kPa (a relative humidity in the pores of the refuse of 99.8 per cent). Only three suction measurements in hole A exceed this. At Linbro Park, with the exception of the near surface measurements, the maximum suction was 400 kPa (a relative humidity of 99.7 per cent). The suction beyond which microbiological activity is inhibited is about 5000 kPa (a relative humidity of 96 per cent) [Senior (1990)]. Hence apart from the dried crust of the cover layer at the top of the Linbro Park landfill, all the measured suctions would permit of uninhibited bacteriological activity.

7. CONCLUSIONS

This detailed examination of moisture and suction profiles in landfills situated in semi-arid climates has enabled the following conclusions to be drawn:

7.1 The overall storage capacity of a landfill is very difficult to predict, as it depends a great deal on the properties and disposition of the intermediate cover layers. The emission of leachate from a landfill is greatly affected by either the channeling or sealing effect of the intermediate cover layers.

7.2 Even in semi-arid climates, landfills contain sufficient moisture to sustain uninhibited bacteriological activity.

ACKNOWLEDGEMENT

The research described in this paper was sponsored and supported by the South African Foundation for Research Development and the City Engineers of Cape Town and Johannesburg.

REFERENCES

Ball, J.M. and Blight, G.E. (1986). "Groundwater pollution downstream of a long-established sanitary landfill". Proc. Int. Symp. Environmental Geotechnology, Allentown, Pa.(H.V. Fang, Ed.) 144-157.

Blakey, N.C (1989) "Predicting landfill leachate production and use of a computer model". Proc. 2nd Int. Landfill Symposium, Sardinia, I, XXV-1 - XXV-15.

Blight, G.E, Hojem, D.J and Ball, J.M (1989). "Generation of leachate from landfills in water-deficient areas". Proc. 2nd Int. Landfill Symposium, Sardinia, I, XXVI-1-XXVI-15.

Campbell, DJV (1983). "Understanding water balance in landfill sites". Waste Management (UK), November, 594-605.

Fenn, D.G, Hanley, K.J and De Geare, T.V (1975). "Use of the water balance method for predicting leachate generation for solid waste disposal sites". US. Environmental Protection Agency, Report No EPA/530/SW168.

Holmes, R (1980). "The water balance method for estimating leachate production from landfill sites". Solid Wastes (UK), LXX(1) 20-33.

Savage, M.J and Cass, A (1984). "Measurement of water potential using in situ thermocouple hygrometers". Advances in Agronomy, 37, 73-126.

Senior, E (1990). Personal communication to authors.

6º CONGRESO Y EXPOSICION INTERNACIONAL DE RESIDUOS SOLIDOS

ISWA 92 MADRID

25th. March 1991

Dear Sir,

On behalf of the PMC of ISWA we would like to inform you that your conference titled " Properties of cappings and underseals for sanitary landfills" has been approved by the PMC of ISWA for ORAL PRESENTATION at ISWA´92.

The full text of the conference should be sent to us before September 30th. 1991, following the instructions of the enclosure.

Now the Intermediate Program of the Congress is to be printed, and we would like to receive before May, 3th. 1991 your agreement to present the conference and the exact titled and your position, as you want to be printed in this Program.

Looking forward to receiving your news before May 3th.,

Yours sincerely,

M. Edurne Torre

Ms. Edurne Torre
Technical Sec. ISWA´92

GENERAL CONDITIONS FOR CONFERENCE SPEAKERS

- registration at not fee.
- travel to and from Madrid at your own expense .
- hotel accomodation at your own charge.
- lunch and refreshments during the congress as well as participation in all official arrangements free of charge.
- one copy of the Proceedings free of charge.

ISWA
General Secretariat
V. Farimagsgade, 29
DK-1606 Copengagen V
Tel.: 45 15 65 65
DENMARK

ATEGRUS
Secretaría Técnica Congreso
Chairman ISWA 92
Apartado de Correos 1668
Tel.: (94) 464 19 90
Fax: (94) 464 44 34

IFEMA - TEM
Secretaría Gral. del Congre
Apartado de Correos 110
Tels.: 470 10 14 - 463 90
Fax: 470 22 53
28080 MADRID

ISWA '92
6TH INTERNATIONAL CONGRESS
AND EXHIBITION ON SOLID WASTES
14 - 19 June 1992, Madrid Spain

DESIGNING CLAY LINERS FOR SANITARY LANDFILLS

BY
G E Blight and M C Mabula
Witwatersrand University
P O Wits, 2050,
South Africa

ABSTRACT

There are two principal parts to the design of clay underseals or liners for sanitary landfills. The first concerns the method of calculating the potential outflow of leachate through the seal or liner. The second concerns measuring the coefficient of permeability of the clay. This paper considers both parts of the problem and makes recommendations for design in terms of the results of a literature survey and of recent field and laboratory measurements.

1. INTRODUCTION

If, during the design of a sanitary landfill, it is established that leachate will be generated, it will be necessary not only to provide the landfill with a rationally designed underliner, but also to contour and shape the base of the landfill so that leachate is directed towards collection areas from which it can be pumped and either re-circulated, or treated and discharged. Hence, if the landfill is properly designed, the depth of leachate over the liner should never exceed a few centimetres. In its simplest form, therefore, a clay liner must be designed for the situation illustrated in Figure 1.

Usually, a specified maximum permissible outflow rate q per unit area will have to be met. To do this it will be necessary either to determine d_C (in Figure 1) for a given value of k_C, or to establish the necessary value of k_C for a predetermined d_C. In either case, it will be

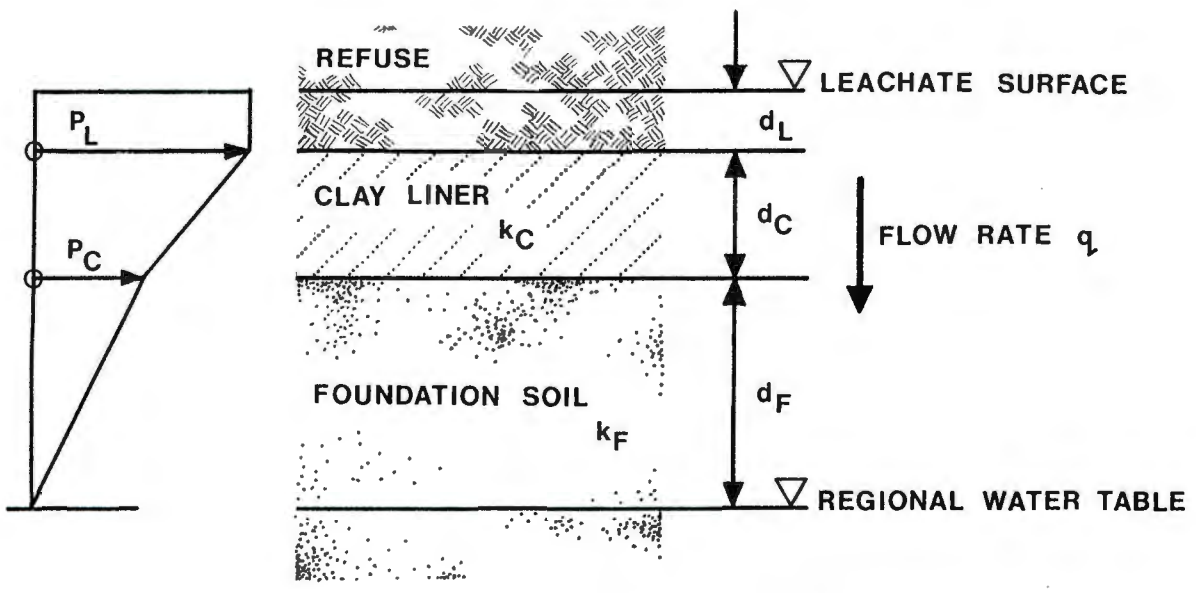

Figure 1
Basis for Estimating Rate of Seepage Through a Clay Liner

necessary to calculate q from the dimensions and parameters indicated in Figure 1. In what follows, both the calculation of q and the measurement of k_C will be considered.

2. CALCULATION OF THE RATE OF SEEPAGE THROUGH A CLAY LINER

Under steady-state conditions, the seepage flow through the liner and the foundation soil will be the same. By applying Darcy's law,

$$q = k\, i \tag{1}$$

(where k is the coefficient of permeability and i the seepage gradient) the outflow per unit plan area through the liner can be shown to be:

$$q = \frac{k_C k_F (d_F + d_C)}{k_C d_F + k_F d_C} \tag{2}$$

Alternatively, the liner permeability k_C is related to q by:

$$k_C = \frac{q\, d_C}{(d_C + d_F) - \frac{q d_F}{k_F}} \tag{3}$$

The pore water pressure at the underside of the liner is given by

$$u = (k_C - k_F)\left(\frac{d_F d_C}{k_C d_F + k_F d_C}\right) \tag{4}$$

It follows from (4) that if the permeability of the foundation soil exceeds that of the liner (which will usually be the case), the pore pressure under the liner will be negative. This will usually result in the foundation soil becoming unsaturated immediately below the liner. Because the permeability of a soil decreases when it becomes unsaturated, this will further decrease q.

Figure 2 shows a typical pore pressure profile through a clay liner and the underlying foundation soil, as well as the modification to the profile caused by unsaturation.

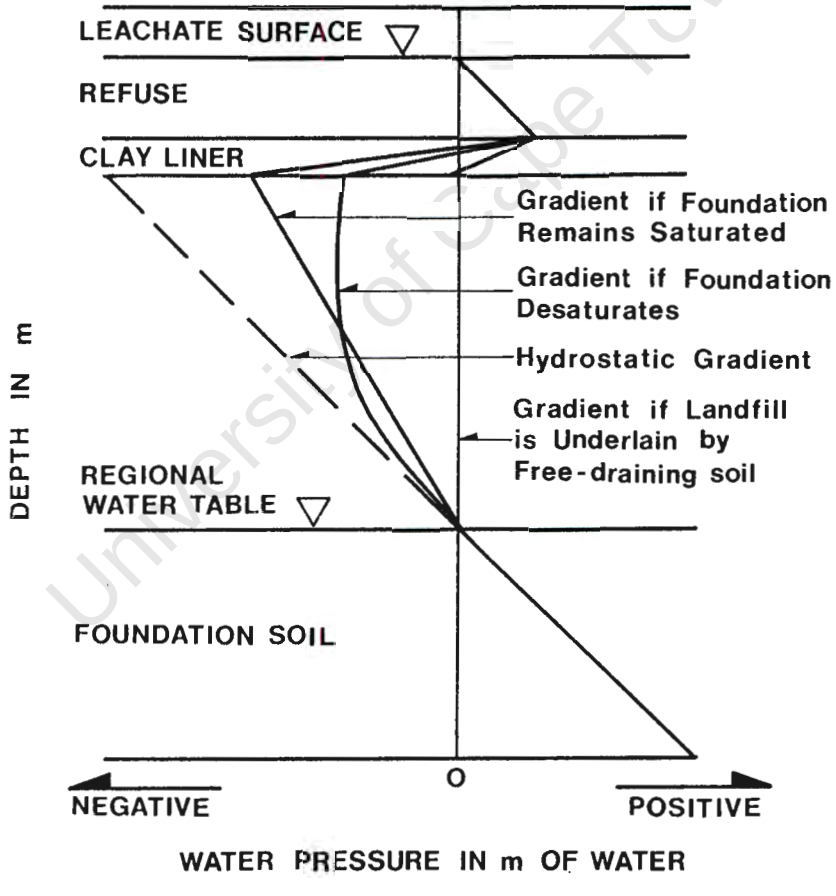

Figure 2
Typical Pore Pressure Profiles Through a Clay Liner

3. MEASUREMENT OF PERMEABILITY IN SITU AND IN THE LABORATORY

Although Darcy's law is usually applied to calculating the outflow through a clay liner, there is considerable uncertainty as to how best to measure the Darcy coefficient of permeability *k*:

Day and Daniel (1985) conducted comparative field and laboratory measurements of permeability on two clays. Test ponds were constructed in the field, and samples were later retrieved from the test liners for laboratory measurements. Measurements of seepage rate were made for the pond as a whole, and by means of single and double ring infiltrometers. Tests using both rigid and flexible walled permeameters were made on block and tube samples of the clay compacted in situ, and also on samples compacted in the laboratory. Effective confining stresses in the laboratory were about 100 kPa and seepage gradients ranged from 20 to 200. Day and Daniel found that values of permeability deduced from seepage losses from the ponds were 900 to 2000 times larger than permeabilities measured in the laboratory, but only 1.2 to 1.9 times larger than field infiltrometer measurements.

Chen and Yamamoto (1987) also carried out a comparison of field and laboratory permeability measurements, using infiltrometers and porous probes in situ and flexible-walled permeameters in the laboratory. For the laboratory tests, effective stresses were about 200 kPa and the seepage gradient was 180. They found that field permeabilities were 10 times larger than laboratory values.

Elsbury et al (1990) made a comparison of field and laboratory permeability measurements on a highly plastic clay. They found that double ring infiltrometer tests gave slightly lower permeabilities than did seepage rates from a test pond. However, compaction in the field with a vibratory roller resulted in a liner with a permeability ten times larger than one compacted using the same roller without vibration. Permeabilities measured in the laboratory used seepage gradients of 20 to 100 and effective stresses of 15 to 70 kPa. Permeabilities measured in the field proved to be between 10 000 and 100 000 times greater than values measured in the laboratory.

Finally, Pregl (1987) has stated that a permeability measured in the laboratory serves as an index of material quality but is not directly related to the permeability of a lining in the field.

The permeability in the field will always be less than that measured in the laboratory, says Pregl, because the seepage gradient used in laboratory tests is usually of the order of 30 whereas that in the field approximates to unity.

It is apparent from these studies that there are several possible reasons why a permeability measured in the field may differ from one measured in the laboratory:

•1 A large area exposed to seepage is more likely to contain defects in the form of more permeable zones than is a small area.

•2 If the Darcy coefficient of permeability is not constant, the use of different seepage gradients in the field and laboratory will result in different field and laboratory values.

•3 A similar remark applies to effective stresses. A specimen subjected to a high effective stress can be expected to show a lower permeability than a similar one with a low effective stress.

•4 The interpretation of the field permeability test: It will be noted from equation (3) that the permeability of the liner, k_C, cannot be evaluated without a knowledge of d_F and k_F, whereas d_L, the depth of leachate, does not enter the expression. The literature shows various other interpretations for k_C. The most common is to assume that the seepage gradient $i = 1$, in which case $q = k_C$. This is clearly not always logical because by the same argument, k_F in Figure 1 would also equal q. Daniel (1987) uses the expression

$$k_C = \frac{q\, d_C}{(d_L + d_C)} \qquad (5)$$

To get some notion of the errors involved with this expression suppose that

$$k_F = 10\, k_C, \quad d_F = d_C \quad \text{and} \quad d_L = d_C/10$$

If $i = 1$	$k_C = q$
According to Daniel (equation (5)):	$k_C = 0.91q$
According to equation (3)	$k_C = 0.55q$

(The larger the ratio of k_F/k_C, the nearer the value of k_C approaches 0.5q).
If, however, $k_F = k_C$ or $d_F = 0$, then according to equation (3) $k_C = q$.

One of the probable reasons, therefore, for the wide discrepancy between Daniel's field and laboratory measurements is that his field measurements appear to have been misinterpreted.

4. THE DARCY COEFFICIENT OF PERMEABILITY

According to the classical form of the Darcy equation (1), one is led to believe that k is a constant for all i. Pregl (1987) has pointed out that this is not so for compacted clays, but rather that k increases with increasing i. The set of measurements shown in Figure 3 confirm this observation. The soil was a clayey sand residual from weathered granite and the measurements show that the seepage flow rate increases at a greater rate than the hydraulic gradient. For this set of data, the value of k at an hydraulic gradient of 1 was 1×10^{-4} cm/s while at an hydraulic gradient of 20, k was 3×10^{-4} cm/s.

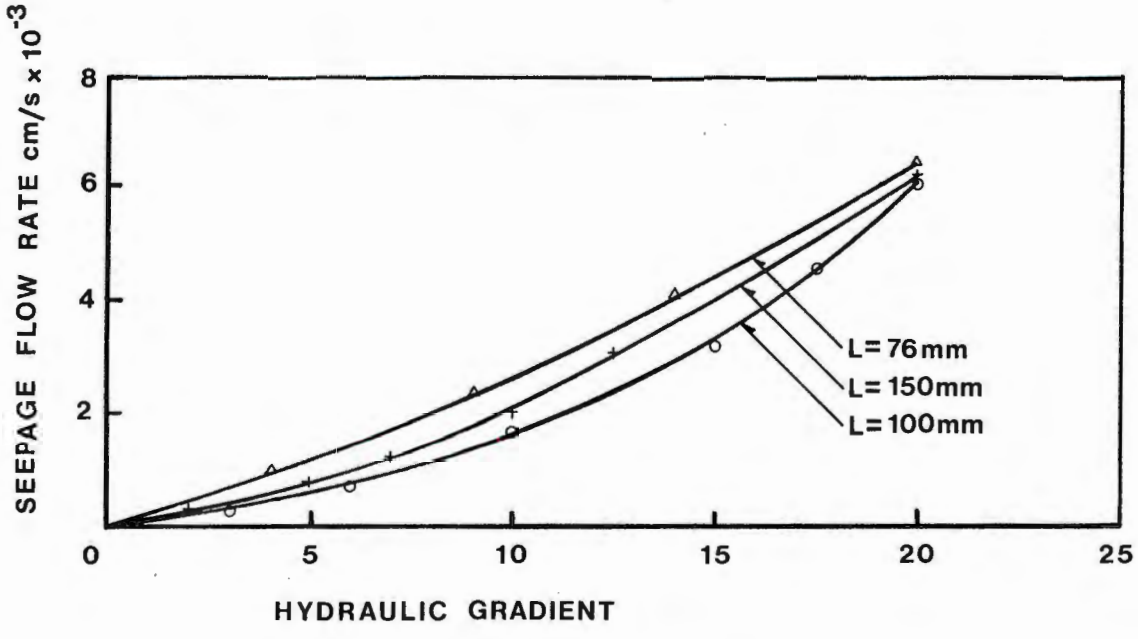

Figure 3
Observed Relationships Between q and i

Figure 3 also shows that reducing the seepage path length from 150 mm to 75 mm had relatively little effect on the seepage flow rate at a particular hydraulic gradient. In other words, k was not particularly sensitive to specimen size, in this case.

5. POND SEEPAGE TESTS

Following on from other workers, e.g. Daniel (1985, 1987) and Elsbury et al (1990), it was decided to perform a series of pond seepage tests and companion laboratory tests to compare permeabilities measured in the field and in the laboratory for a situation where the field test could be correctly interpreted.

Four 3 m square ponds were constructed on a profile of clayey sand residual from weathered granite. The water table lay at a depth of 2 m below the bottom of the ponds.

Figure 4
View of Test Ponds

The liner consisted of the compacted in situ soil and the ponds were surrounded by a perimeter moat to eliminate lateral flow from the pond edges as far as possible. Figure 4 shows a view of the ponds. One of the four ponds was lined with a geomembrane so that it could be used to measure evaporation losses, and all four ponds were filled with a coarse

clinker ash to provide some overburden on the pond bottoms to eliminate wave formation in the water and also to reduce evaporation*.

The rates of seepage were measured by observing the water levels in four perforated observation pipes that were installed in each pond.

Referring to Figure 1 and equation (3): because k_F was close in value to k_C, or alternatively, because d_F was zero, it could truly be said in this case that $k_C = q$.

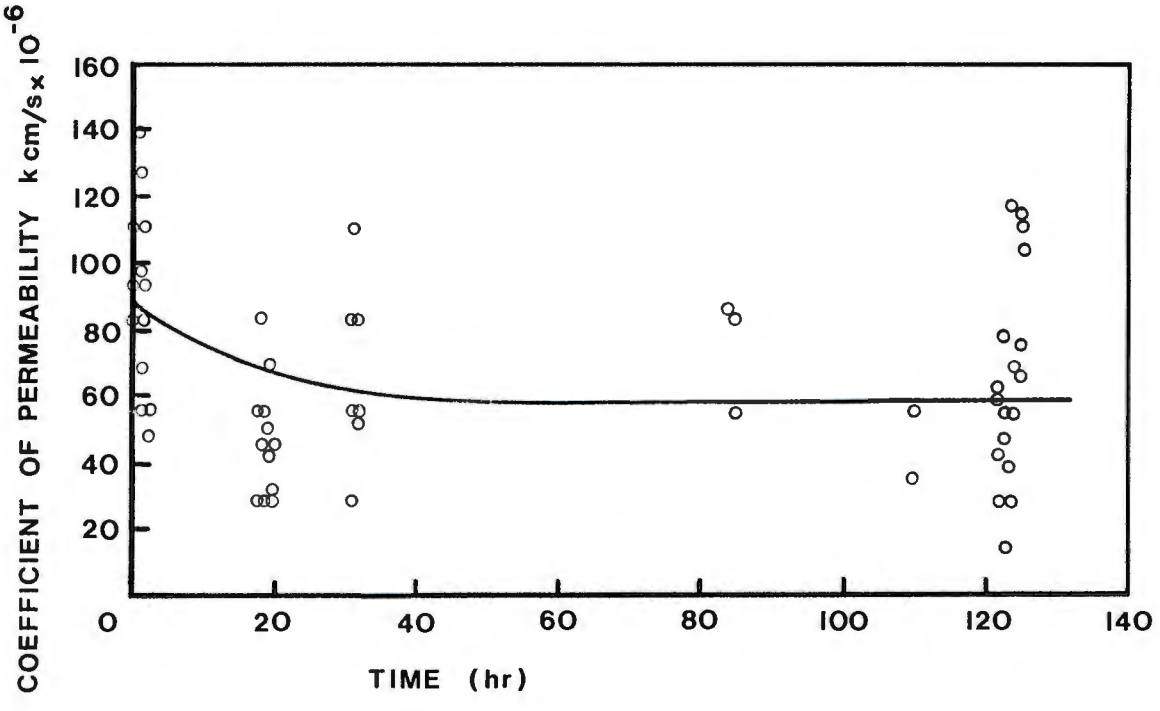

Figure 5 shows a set of measured k_C values for one of the ponds. It will be seen that there is a considerable scatter in the measurements, with values on any particular day varying by factors of up to 6. The scatter appeared to result from the difficulty of measuring small changes of water level accurately and difficulty in compensating the measured seepages for evaporation losses which also depend on measuring small changes of water level. Temperature changes also affected the accuracy of the measurements by causing the plastic measuring pipes to change in length, thus an increase in temperature caused an apparent increase in seepage rate, and vice versa.

*It was found however, that because of its dark colour and large surface area, the ash actually increased the evaporation rates from the ponds.

6. LABORATORY PERMEABILITY TESTS

In the classic design situation the clay liner to a landfill must be designed on the basis of the results of laboratory permeability tests. For this reason, a comparison of pond seepage test results and laboratory permeability measurements is of particular interest. Also, as seen in Section 4, the laboratory tests should be carried out at a seepage gradient of 1.0 if they are to be meaningful.

All laboratory permeability tests were of the constant head flexible wall triaxial cell type and the average effective stress was kept at 35 kPa for all tests. This stress was the lowest value that could be controlled reliably in the laboratory, but was still much more than the effective overburden stress in the pond tests of 0.5 m of submerged ash, or only 4 to 5 kPa.

The following table compares the permeability values measured in the laboratory on specimens compacted to the same dry density as the upper 150 mm of soil in the ponds:

Table 1

Range of Mean Permeability from Pond Tests (cm/s x 10^{-6})	Range of Mean Permeability from Laboratory Tests (cm/s x 10^{-6})
59 to 81	37 to 93

Hence this set of measurements shows that it is possible, with correct interpretation and correct testing to estimate in situ permeabilities very closely from the results of laboratory tests.

However, it must be noted that the permeability of this granite soil is higher than what would usually be used for a liner. It is also noted from the literature that discrepancies between field and laboratory permeabilities appear to increase as the soil becomes less permeable.

It was also found in this series of tests that double ring infiltrometer tests gave values of permeability that were considerably less than those recorded in Table 1. The reason for this has not been discovered, but possibly also lies in a misinterpretation of the measurements.

7. CONCLUSIONS

7.1 This paper has set out a method for estimating the seepage flow through a clay liner from a knowledge of the depth to the regional water table, the thickness of the liner and the coefficients of permeability of the liner and the foundation soil.

7.2 A review of the literature has shown that some uncertainty exists concerning the relationship between permeability measured in the field in large-scale pond tests and permeability measured in the laboratory.

7.3 It has been pointed out that because the Darcy coefficient of permeability is not constant with hydraulic gradient, permeabilities should be measured in the laboratory at a gradient close to the likely seepage gradient in the field.

7.4 The results of pond seepage tests must be correctly interpreted, when used to evaluate Darcy coefficients of permeability. Equally, seepage rates must be correctly calculated for design purposes, as stated in 7.1.

8. REFERENCES

1. Chen, H.W. and Yamamoto, L.D. (1987). Permeability tests for hazardous waste management with clay liners. Geotechnical and Geohydrological Aspects of Waste Management, Lewis Publishers, U.S.A., pp 229-243.

2. Daniel, D.E. (1987). Earthen liners for land disposal facilities. Proceedings, ASCE Specialty Conference on Geotechnical Practice for Waste Disposal, pp 21-39.

3. Day, S.R. and Daniel, D.E. (1985). Hydraulic conductivity of two prototype clay liners, ASCE Journal of Geotechnical Engineering, vol 111, no 8, pp 957-970.

4. Elsbury, B.R., Daniel, D.E., Sraders, G.A. and Anderson, D.C. (1990). Lessons learned from compacted earth liners, ASCE Journal of Geotechnical Engineering, vol 116, no 11, pp 1641-1659.

5. Pregl, O. (1987). Natural lining materials. Proceedings, International Symposium on Process, Technology and Environmental Impact of Sanitary Landfill, Cagliari, Sardinia, vII,pp XXVI - 1 to 7.

ISWA '92
6TH INTERNATIONAL CONGRESS
AND EXHIBITION ON SOLID WASTES
14 - 19 June 1992, Madrid Spain

DESIGNING CLAY LINERS FOR SANITARY LANDFILLS

BY
G E Blight and M C Mabula
Witwatersrand University
P O Wits, 2050,
South Africa

ABSTRACT

There are two principal parts to the design of clay underseals or liners for sanitary landfills. The first concerns the method of calculating the potential outflow of leachate through the seal or liner. The second concerns measuring the coefficient of permeability of the clay. This paper considers both parts of the problem and makes recommendations for design in terms of the results of a literature survey and of recent field and laboratory measurements.

1. INTRODUCTION

If, during the design of a sanitary landfill, it is established that leachate will be generated, it will be necessary not only to provide the landfill with a rationally designed underliner, but also to contour and shape the base of the landfill so that leachate is directed towards collection areas from which it can be pumped and either re-circulated, or treated and discharged. Hence, if the landfill is properly designed, the depth of leachate over the liner should never exceed a few centimetres. In its simplest form, therefore, a clay liner must be designed for the situation illustrated in Figure 1.

Usually, a specified maximum permissible outflow rate q per unit area will have to be met. To do this it will be necessary either to determine d_C (in Figure 1) for a given value of k_C, or to establish the necessary value of k_C for a predetermined d_C. In either case, it will be

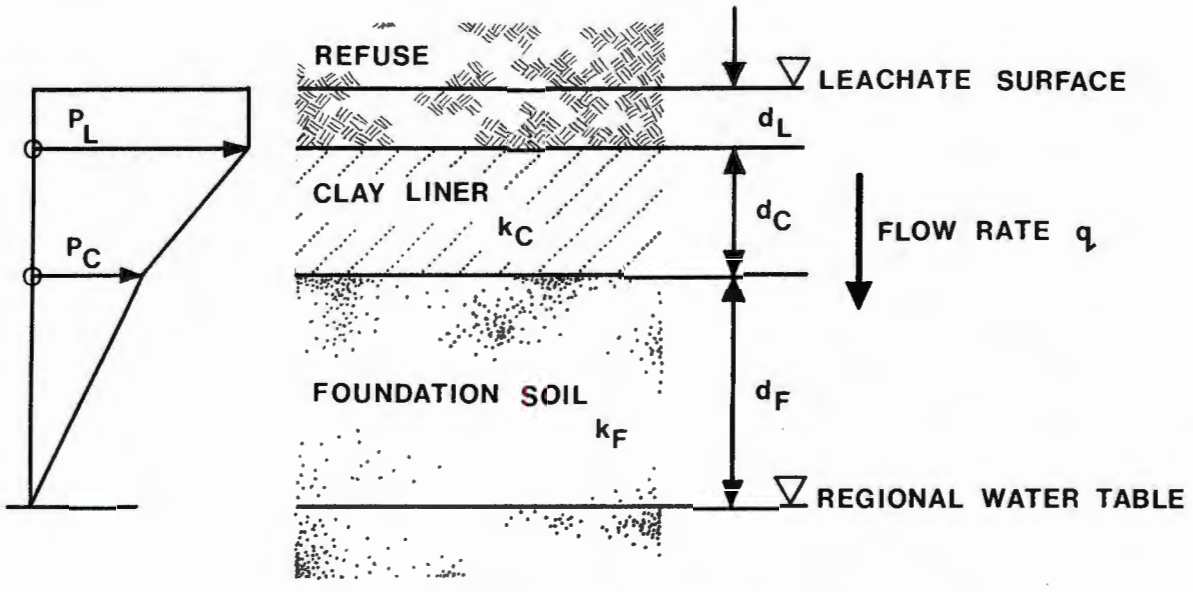

Figure 1
Basis for Estimating Rate of Seepage Through a Clay Liner

necessary to calculate q from the dimensions and parameters indicated in Figure 1. In what follows, both the calculation of q and the measurement of k_C will be considered.

2. CALCULATION OF THE RATE OF SEEPAGE THROUGH A CLAY LINER

Under steady-state conditions, the seepage flow through the liner and the foundation soil will be the same. By applying Darcy's law,

$$q = k\,i \tag{1}$$

(where k is the coefficient of permeability and i the seepage gradient) the outflow per unit plan area through the liner can be shown to be:

$$q = \frac{k_C k_F (d_F + d_C)}{k_C d_F + k_F d_C} \tag{2}$$

Alternatively, the liner permeability k_C is related to q by:

$$k_C = \frac{q\,d_C}{(d_C + d_F) - \dfrac{q d_F}{k_F}} \tag{3}$$

The pore water pressure at the underside of the liner is given by

$$u = (k_C - k_F)\left(\frac{d_F d_C}{k_C d_F + k_F d_C}\right) \tag{4}$$

It follows from (4) that if the permeability of the foundation soil exceeds that of the liner (which will usually be the case), the pore pressure under the liner will be negative. This will usually result in the foundation soil becoming unsaturated immediately below the liner. Because the permeability of a soil decreases when it becomes unsaturated, this will further decrease q.

Figure 2 shows a typical pore pressure profile through a clay liner and the underlying foundation soil, as well as the modification to the profile caused by unsaturation.

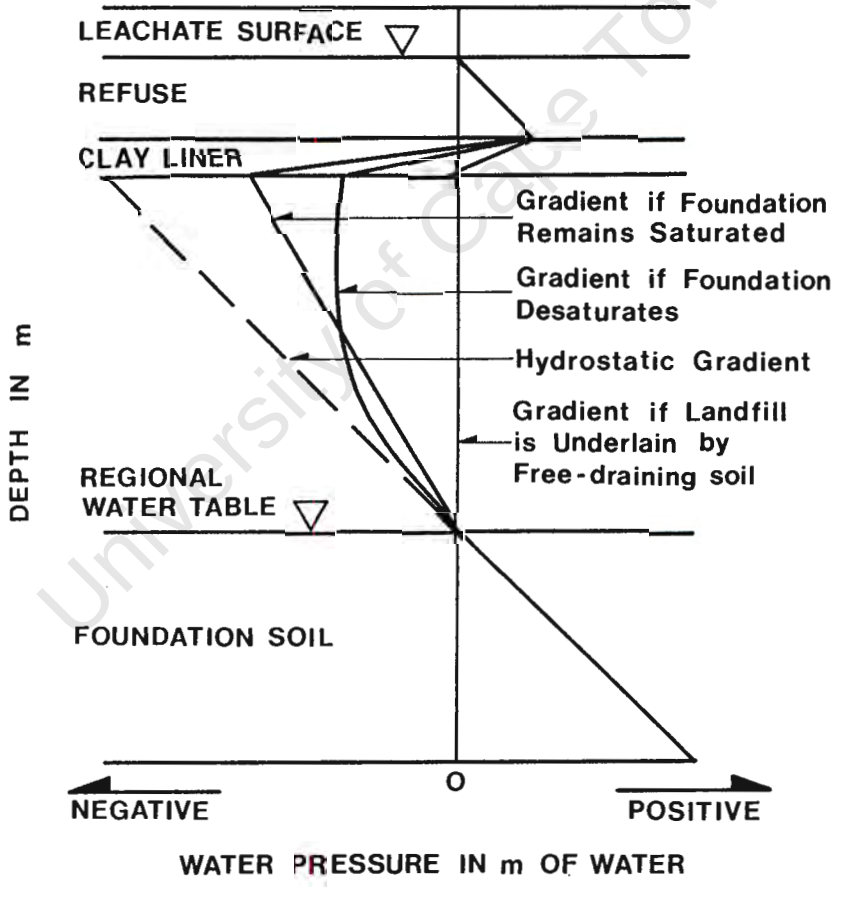

Figure 2
Typical Pore Pressure Profiles Through a Clay Liner

3. MEASUREMENT OF PERMEABILITY IN SITU AND IN THE LABORATORY

Although Darcy's law is usually applied to calculating the outflow through a clay liner, there is considerable uncertainty as to how best to measure the Darcy coefficient of permeability *k*:

Day and Daniel (1985) conducted comparative field and laboratory measurements of permeability on two clays. Test ponds were constructed in the field, and samples were later retrieved from the test liners for laboratory measurements. Measurements of seepage rate were made for the pond as a whole, and by means of single and double ring infiltrometers. Tests using both rigid and flexible walled permeameters were made on block and tube samples of the clay compacted in situ, and also on samples compacted in the laboratory. Effective confining stresses in the laboratory were about 100 kPa and seepage gradients ranged from 20 to 200. Day and Daniel found that values of permeability deduced from seepage losses from the ponds were 900 to 2000 times larger than permeabilities measured in the laboratory, but only 1.2 to 1.9 times larger than field infiltrometer measurements.

Chen and Yamamoto (1987) also carried out a comparison of field and laboratory permeability measurements, using infiltrometers and porous probes in situ and flexible-walled permeameters in the laboratory. For the laboratory tests, effective stresses were about 200 kPa and the seepage gradient was 180. They found that field permeabilities were 10 times larger than laboratory values.

Elsbury et al (1990) made a comparison of field and laboratory permeability measurements on a highly plastic clay. They found that double ring infiltrometer tests gave slightly lower permeabilities than did seepage rates from a test pond. However, compaction in the field with a vibratory roller resulted in a liner with a permeability ten times larger than one compacted using the same roller without vibration. Permeabilities measured in the laboratory used seepage gradients of 20 to 100 and effective stresses of 15 to 70 kPa. Permeabilities measured in the field proved to be between 10 000 and 100 000 times greater than values measured in the laboratory.

Finally, Pregl (1987) has stated that a permeability measured in the laboratory serves as an index of material quality but is not directly related to the permeability of a lining in the field.

The permeability in the field will always be less than that measured in the laboratory, says Pregl, because the seepage gradient used in laboratory tests is usually of the order of 30 whereas that in the field approximates to unity.

It is apparent from these studies that there are several possible reasons why a permeability measured in the field may differ from one measured in the laboratory:

•1 A large area exposed to seepage is more likely to contain defects in the form of more permeable zones than is a small area.

•2 If the Darcy coefficient of permeability is not constant, the use of different seepage gradients in the field and laboratory will result in different field and laboratory values.

•3 A similar remark applies to effective stresses. A specimen subjected to a high effective stress can be expected to show a lower permeability than a similar one with a low effective stress.

•4 The interpretation of the field permeability test: It will be noted from equation (3) that the permeability of the liner, k_C, cannot be evaluated without a knowledge of d_F and k_F, whereas d_L, the depth of leachate, does not enter the expression. The literature shows various other interpretations for k_C. The most common is to assume that the seepage gradient $i = 1$, in which case $q = k_C$. This is clearly not always logical because by the same argument, k_F in Figure 1 would also equal q. Daniel (1987) uses the expression

$$k_C = \frac{q\, d_C}{(d_L + d_C)} \qquad (5)$$

To get some notion of the errors involved with this expression suppose that

$$k_F = 10\, k_C, \quad d_F = d_C \quad \text{and} \quad d_L = d_C/10$$

If $i = 1$	$k_C = q$
According to Daniel (equation (5)):	$k_C = 0.91q$
According to equation (3)	$k_C = 0.55q$

(The larger the ratio of k_F/k_C, the nearer the value of k_C approaches 0.5q).
If, however, $k_F = k_C$ or $d_F = 0$, then according to equation (3) $k_C = q$.

One of the probable reasons, therefore, for the wide discrepancy between Daniel's field and laboratory measurements is that his field measurements appear to have been misinterpreted.

4. THE DARCY COEFFICIENT OF PERMEABILITY

According to the classical form of the Darcy equation (1), one is led to believe that k is a constant for all i. Pregl (1987) has pointed out that this is not so for compacted clays, but rather that k increases with increasing i. The set of measurements shown in Figure 3 confirm this observation. The soil was a clayey sand residual from weathered granite and the measurements show that the seepage flow rate increases at a greater rate than the hydraulic gradient. For this set of data, the value of k at an hydraulic gradient of 1 was 1 x 10^{-4} cm/s while at an hydraulic gradient of 20, k was 3 x 10^{-4} cm/s.

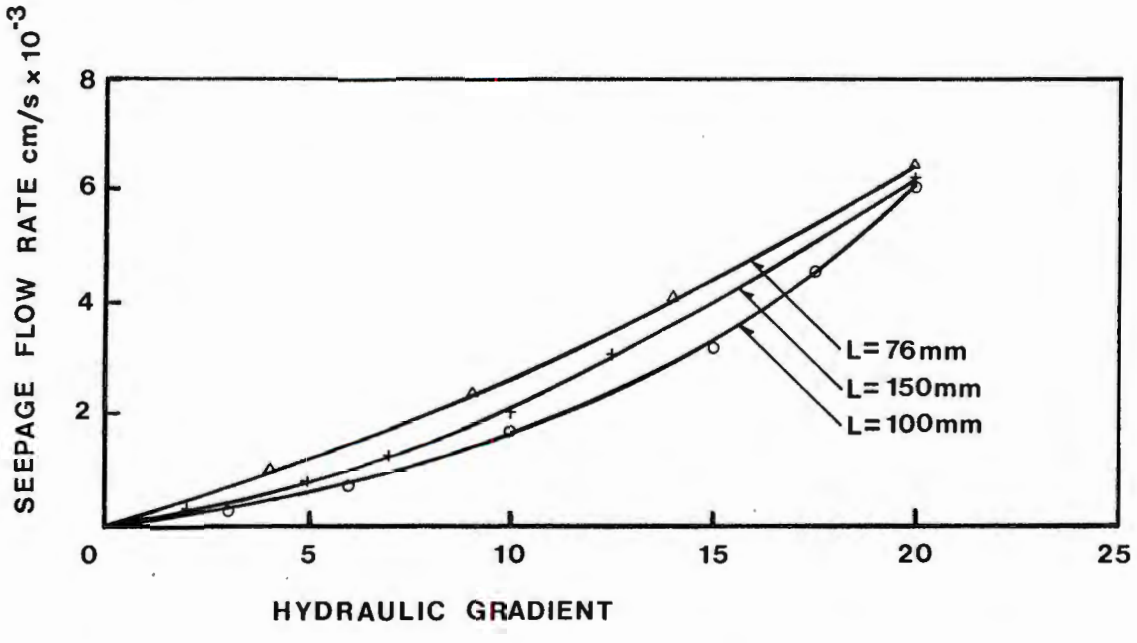

Figure 3
Observed Relationships Between q and i

Figure 3 also shows that reducing the seepage path length from 150 mm to 75 mm had relatively little effect on the seepage flow rate at a particular hydraulic gradient. In other words, k was not particularly sensitive to specimen size, in this case.

5. POND SEEPAGE TESTS

Following on from other workers, e.g. Daniel (1985, 1987) and Elsbury et al (1990), it was decided to perform a series of pond seepage tests and companion laboratory tests to compare permeabilities measured in the field and in the laboratory for a situation where the field test could be correctly interpreted.

Four 3 m square ponds were constructed on a profile of clayey sand residual from weathered granite. The water table lay at a depth of 2 m below the bottom of the ponds.

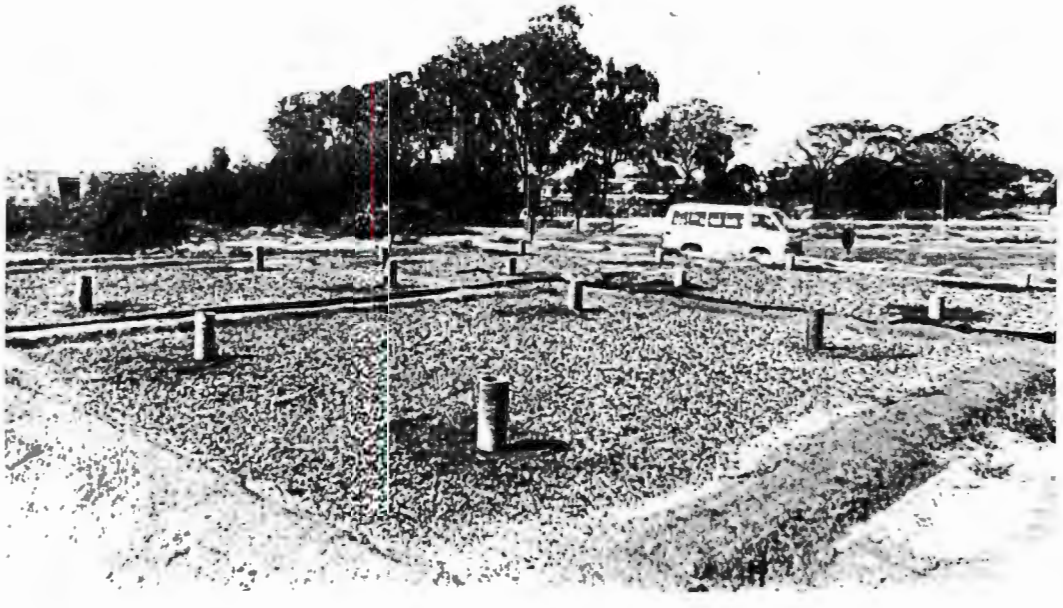

Figure 4
View of Test Ponds

The liner consisted of the compacted in situ soil and the ponds were surrounded by a perimeter moat to eliminate lateral flow from the pond edges as far as possible. Figure 4 shows a view of the ponds. One of the four ponds was lined with a geomembrane so that it could be used to measure evaporation losses, and all four ponds were filled with a coarse

clinker ash to provide some overburden on the pond bottoms to eliminate wave formation in the water and also to reduce evaporation*.

The rates of seepage were measured by observing the water levels in four perforated observation pipes that were installed in each pond.

Referring to Figure 1 and equation (3): because k_F was close in value to k_C, or alternatively, because d_F was zero, it could truly be said in this case that $k_C = q$.

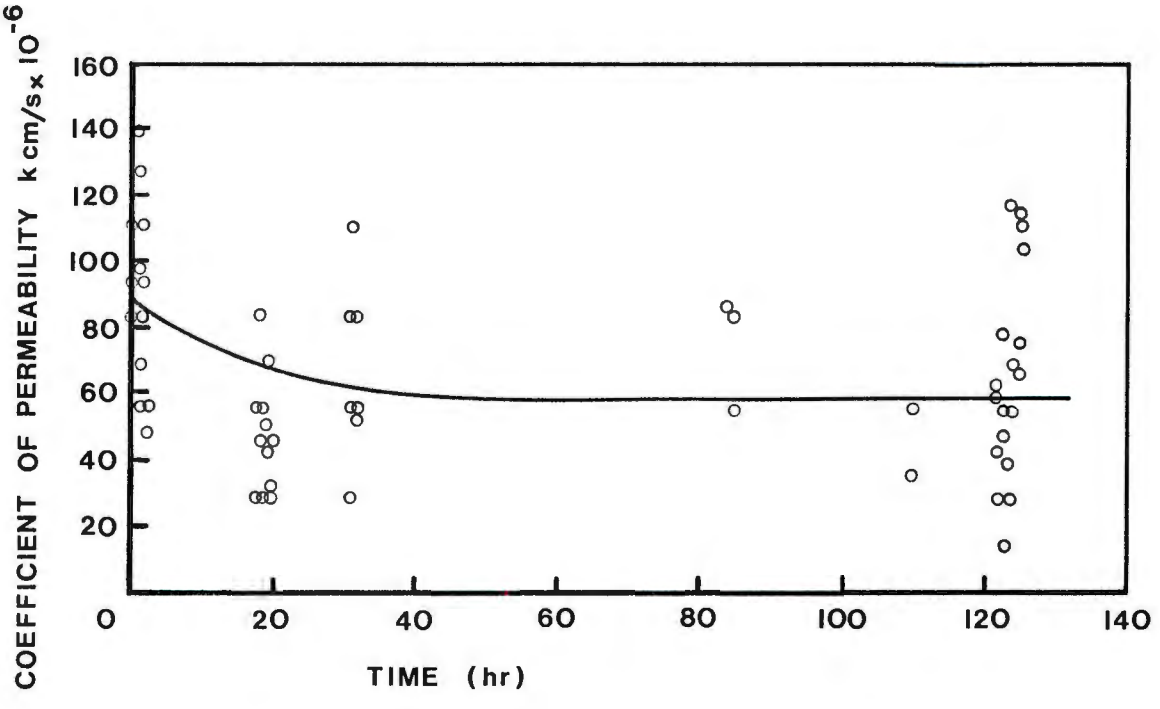

Figure 5 shows a set of measured k_C values for one of the ponds. It will be seen that there is a considerable scatter in the measurements, with values on any particular day varying by factors of up to 6. The scatter appeared to result from the difficulty of measuring small changes of water level accurately and difficulty in compensating the measured seepages for evaporation losses which also depend on measuring small changes of water level. Temperature changes also affected the accuracy of the measurements by causing the plastic measuring pipes to change in length, thus an increase in temperature caused an apparent increase in seepage rate, and vice versa.

*It was found however, that because of its dark colour and large surface area, the ash actually increased the evaporation rates from the ponds.

6. LABORATORY PERMEABILITY TESTS

In the classic design situation the clay liner to a landfill must be designed on the basis of the results of laboratory permeability tests. For this reason, a comparison of pond seepage test results and laboratory permeability measurements is of particular interest. Also, as seen in Section 4, the laboratory tests should be carried out at a seepage gradient of 1.0 if they are to be meaningful.

All laboratory permeability tests were of the constant head flexible wall triaxial cell type and the average effective stress was kept at 35 kPa for all tests. This stress was the lowest value that could be controlled reliably in the laboratory, but was still much more than the effective overburden stress in the pond tests of 0.5 m of submerged ash, or only 4 to 5 kPa.

The following table compares the permeability values measured in the laboratory on specimens compacted to the same dry density as the upper 150 mm of soil in the ponds:

Table 1

Range of Mean Permeability from Pond Tests (cm/s x 10^{-6})	Range of Mean Permeability from Laboratory Tests (cm/s x 10^{-6})
59 to 81	37 to 93

Hence this set of measurements shows that it is possible, with correct interpretation and correct testing to estimate in situ permeabilities very closely from the results of laboratory tests.

However, it must be noted that the permeability of this granite soil is higher than what would usually be used for a liner. It is also noted from the literature that discrepancies between field and laboratory permeabilities appear to increase as the soil becomes less permeable.

It was also found in this series of tests that double ring infiltrometer tests gave values of permeability that were considerably less than those recorded in Table 1. The reason for this has not been discovered, but possibly also lies in a misinterpretation of the measurements.

7. CONCLUSIONS

7.1 This paper has set out a method for estimating the seepage flow through a clay liner from a knowledge of the depth to the regional water table, the thickness of the liner and the coefficients of permeability of the liner and the foundation soil.

7.2 A review of the literature has shown that some uncertainty exists concerning the relationship between permeability measured in the field in large-scale pond tests and permeability measured in the laboratory.

7.3 It has been pointed out that because the Darcy coefficient of permeability is not constant with hydraulic gradient, permeabilities should be measured in the laboratory at a gradient close to the likely seepage gradient in the field.

7.4 The results of pond seepage tests must be correctly interpreted, when used to evaluate Darcy coefficients of permeability. Equally, seepage rates must be correctly calculated for design purposes, as stated in 7.1.

8. REFERENCES

1. Chen, H.W. and Yamamoto, L.D. (1987). Permeability tests for hazardous waste management with clay liners. Geotechnical and Geohydrological Aspects of Waste Management, Lewis Publishers, U.S.A., pp 229-243.

2. Daniel, D.E. (1987). Earthen liners for land disposal facilities. Proceedings, ASCE Specialty Conference on Geotechnical Practice for Waste Disposal, pp 21-39.

3. Day, S.R. and Daniel, D.E. (1985). Hydraulic conductivity of two prototype clay liners, ASCE Journal of Geotechnical Engineering, vol 111, no 8, pp 957-970.

4. Elsbury, B.R., Daniel, D.E., Sraders, G.A. and Anderson, D.C. (1990). Lessons learned from compacted earth liners, ASCE Journal of Geotechnical Engineering, vol 116, no 11, pp 1641-1659.

5. Pregl, O. (1987). Natural lining materials. Proceedings, International Symposium on Process, Technology and Environmental Impact of Sanitary Landfill, Cagliari, Sardinia, vII,pp XXVI - 1 to 7.

Postnote

Designing Clay Liners for Sanitary Landfills

G E Blight and M C Mabula

This paper was written on the assumption that the depth of leachate over the liner would be a small fraction of the liner thickness. If the depth of leachate is not negligible, the equations contained by the paper should be modified as follows:

$$q = \frac{k_c k_F (d_L + d_c + d_F)}{(k_c d_F + k_F d_c)} \qquad (2)$$

$$k_c = \frac{q d_c}{(d_L + d_c + d_F) - \frac{q d_F}{k_F}} \qquad (3)$$

$$u = \frac{(k_c - k_F)\, d_F d_c + k_c d_F d_L}{k_c d_F + k_F d_c} \qquad (4)$$

6. THE EFFECTS OF ALKALI-SILICA REACTION ON REINFORCED CONCRETE STRUCTURES

CONTRIBUTION TO LEARNING

The effects of alkali-aggregate reaction (AAR) or alkali-silica reaction (ASR) were identified in South Africa for the first time in the late 1970's. The author was fortunate to become involved in assessing the engineering effects of ASR on structures early in 1977. At that time most of the knowledge of ASR related to the physics and chemistry of the reaction and research was entirely laboratory-based. Very little research had been directed at assessing the engineering consequences of ASR.

The research of the author was directed from the outset at assessing the effects of ASR on the safety and serviceability of engineering structures, at formulating repair measures, and later, at practical measures to inhibit the alkali-silica reaction in structures in service. The repairs were probably the first of their kind to be applied to ASR-affected structures and the full-scale load tests described in paper 6.2 are believed to be the first to be done on an ASR-affected structure. However, the major contribution of the research has been to show that the structural effects of ASR are not nearly as serious as once thought, and that ASR affected structures can safely be kept in service almost indefinitely.

Notwithstanding this last statement, the final paper in this section describes the results of precursive tests to the rehabilitation of a structure, damaged by AAR, by partial demolition and rebuilding. The decision to demolish rather than maintain was, however, a management and not an engineering one.

6. THE EFFECTS OF ALKALI-SILICA REACTION ON REINFORCED CONCRETE STRUCTURES

6.1 Blight, G E and Alexander, M G (1988). Evaluating reinforced concrete structures affected by alkali aggregate reaction. Proceedings, International Symposium on Re-evaluation of Concrete Structures, Copenhagen, Denmark, pp 309-317.

Professor M G Alexander is a colleague of mine (and former undergraduate and postgraduate student) who has collaborated with me in work on ASR. I drafted the paper and assess my contribution to it at 80%.

6.2 Blight, G E, Alexander, M G, Ralph, T K and Lewis, B A (1989). Effect of alkali-aggregate reaction on the performance of a reinforced concrete structure over a six-year period. Magazine of Concrete Research, vol 41, No 147, pp 69-77.

This paper is based on work done for the City of Johannesburg via a firm of consulting engineers, represented by Messrs Ralph and Lewis. The consultants carried out the analysis of the structure and arranged the logistics of the two full-scale tests. I planned and supervised the measurements, assisted by Professor Alexander. I also drafted the paper. I assess my contribution to the overall result at 50%.

6.3 Blight, G E (1989). Experiments on waterproofing concrete to inhibit AAR. Proceedings, 8th International Conference on Alkali-Aggregate Reaction, Kyoto, Japan, pp 733-739.

6.4 Blight, G E (1990). Rehabilitation of reinforced concrete structures affected by alkali-silica reaction. Structural Engineering Review, vol 2, pp 1-8.

6.5 Blight, G E (1990). Can concrete structures be waterproofed to inhibit ASR? Proceedings, International Conference on the Protection of Concrete, Dundee, U.K., pp 223-232.

6.6 Blight, G E (1991). A study of four waterproofing systems for concrete. Magazine of Concrete Research, vol 43, no 156, pp 81-87.

6.7 Blight, G E (1992). The moisture condition in an exposed structure damaged by alkali-silica reaction. Magazine of Concrete Research, vol 43, no 157, pp 96-101.

6.8 Alexander, M G, Blight, G E and Lampacher, B J (1992). Pre-demolition tests on structural concrete damaged by AAR. Proceedings, 9th International Conference on Alkali-Aggregate Reaction in Concrete, London. Accepted for publication.

Prof. M G Alexander is a former student of mine and present colleague. B J Lampacher is an Msc(Eng) student. The paper was written by me, based on research by Lampacher, jointly supervised by Alexander and me.

10th Anniversary of

DABI | Dansk Beton Institut | 1978-1988 | Danish Concrete Institute

International Symposium

RE-EVALUATION OF CONCRETE STRUCTURES

Reliability and Load Carrying Capacity

PROCEEDINGS

Editors: Steen Rostam & M.W. Bræstrup

TECHNICAL UNIVERSITY of Denmark
Copenhagen – Lyngby
13th – 15th June, 1988

Co-sponsored by:
- ACI, American Concrete Institute
- CEB, Comité Euro-International du Béton
- IABSE, International Assocition for Bridge and Structural Engineering
- DBF, Danish Concrete Association
- DSBy, Danish Society for Structural Science and Engineering

EVALUATING REINFORCED CONCRETE STRUCTURES AFFECTED BY ALKALI AGGREGATE REACTION

by

G E BLIGHT and M G ALEXANDER
UNIVERSITY OF THE WITWATERSRAND, JOHANNESBURG
P O WITS, 2050, SOUTH AFRICA

ABSTRACT

Although alkali aggregate reaction or AAR is not a new phenomenon, the bulk of research so far has been aimed at investigating the mechanisms of deterioration, the identification of materials susceptible to reaction and methods of preventing AAR from occurring in structures yet to be built. There is relatively little information on the effect of AAR on the strength and deformation properties of concrete. In order to assess the strength margin of structures that have deteriorated, and to formulate measures for repairing and strengthening them, a knowledge of the strength of the deteriorated concrete as well as its elastic and time-dependent deformation properties is required. This review will describe the effects of AAR on these properties, as well as means for assessing the extent of the deterioration of full scale structures.

KEY WORDS: Alkali Aggregate Reaction, Reinforced Concrete.

1. INTRODUCTION: THE AAR PHENOMENON

As the name implies, AAR occurs when the alkali associated with the cement content of a concrete reacts with the concrete aggregate. The reaction is expansive and results in disruption of the concrete. The reaction occurs very slowly and signs of damage are unlikely to appear until five to fifteen years after construction. This makes the cause of the problem (in a particular case) very difficult to identify as by this time, detailed construction records have often been destroyed.

Damage caused by AAR may vary from continuous cracks aligned parallel to the direction of the major principal compressive stress in a structural member to severe block cracking of the surface (see Figure 1a). Cracks are usually not static, but progressively widen as time proceeds.

Figure 1b shows some crack width-time relationships that have been observed on the surface shown in Figure 1a. The growth in width of the cracks is influenced by the weather. It will be noted from Figure 1b that an acceleration of movement occurs at the start of each rainy season (September/October) and that the rate of expansion slows during the dry season (May to August).

The necessary conditions for AAR to occur are a combination of an AAR-susceptible aggregate and an alkali content in the concrete which exceeds a certain threshold. The threshold is usually assumed to be an equivalent Na_2O content of 0.6 per cent of the cement*. The fulfilment of these two conditions, however, is not sufficient for AAR to take place. Moisture must also be present in the concrete. Concrete that remains or can be kept permanently dry is not susceptible to attack/1/.

2. ENGINEERING CHARACTERISTICS OF AAR-DETERIORATED CONCRETE

Because AAR causes an expansive disruption of concrete, the main effects of cracking caused by the attack are to decrease the elastic modulus and

* Equivalent Na_2O content = (% Na_2O + 0.66% K_2O)

Figure 1a: Block-cracked surface of motorway column which is subject to AAR

strength of the material. If AAR-affected concrete is subsequently subjected to long-term loading, creep strains become abnormally large as the expansion caused by AAR is reversed by the applied stress.

The strength of concrete that has been disrupted by AAR is, however, decreased to a suprisingly small degree. Figure 2 shows the results of a series of compression and splitting tensile strength tests on sets of cores from two series of concrete structures having different mix designs, but the same design concrete strength of 30MPa. Although the cores were taken from structures that had apparently been badly affected by AAR,

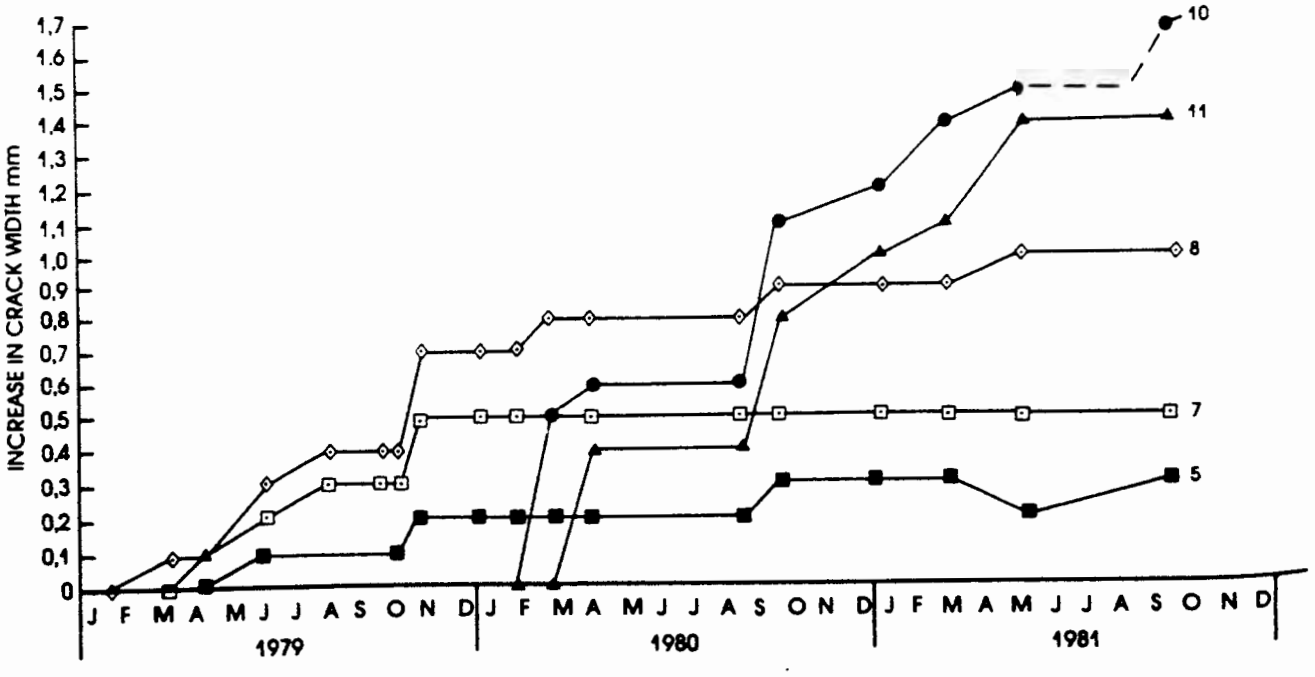

Figure 1b: Growth of surface crack widths with time. Observations taken on column supporting motorway structure.

Figure 2 shows that the mean strength for concrete 1 still exceeded the design strength. The mean compressive strength for concrete 2 was still up to specification, although the splitting tensile strength had been reduced.

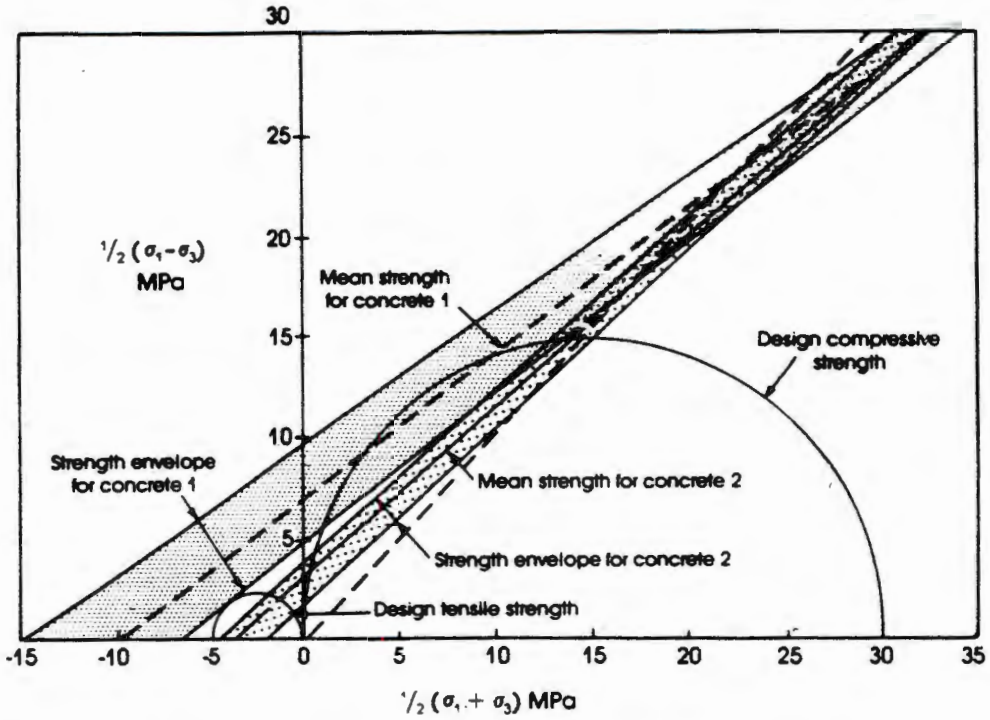

Figure 2: Comparison of strength of concrete that has deteriorated by AAR with specified strength

Figure 3 compares the instantaneous and creep strains measured on three cores of concrete, all of which were subjected to a stress of 15MPa, i.e. half the design strength. Specimen A was of sound concrete showing no signs of AAR attack while cores B and C had deteriorated by AAR. The results show that the elastic deformations of the deteriorated concrete were about three times as large as those of sound concrete, while the creep strain was two and a half to four times as large.

3. ASSESSMENT OF THE EXTENT OF DAMAGE BY AAR TO A STRUCTURE

3.1 Indirect Methods

3.1.1 Ultrasonic Pulse Transmission

Blight et al/2/ showed that ultrasonic pulse transmissions may be used to assess the extent of damage by AAR to a reinforced concrete structure. They showed the results of calibration measurements which demonstrate the usefulness of the technique for exploring the depth to which damage, visible on the surface of the concrete, extends.

An ultrasonic pulse velocity survey conducted on the beam of a reinforced concrete portal frame (Blight et al/3/) indicated as shown by Figure 4 that almost the entire beam had been badly affected by AAR. Nevertheless, a subsequent full-scale load test showed that the structural integrity of the beam had been little affected. It then became apparent that the observed retardation of the ultrasonic pulse velocity was caused by a relatively thin shell of deteriorated concrete that surrounded the almost unaffected heart of the member. A similar experience occurred with a large badly cracked foundation block. Ultrasonic pulse velocity measurements

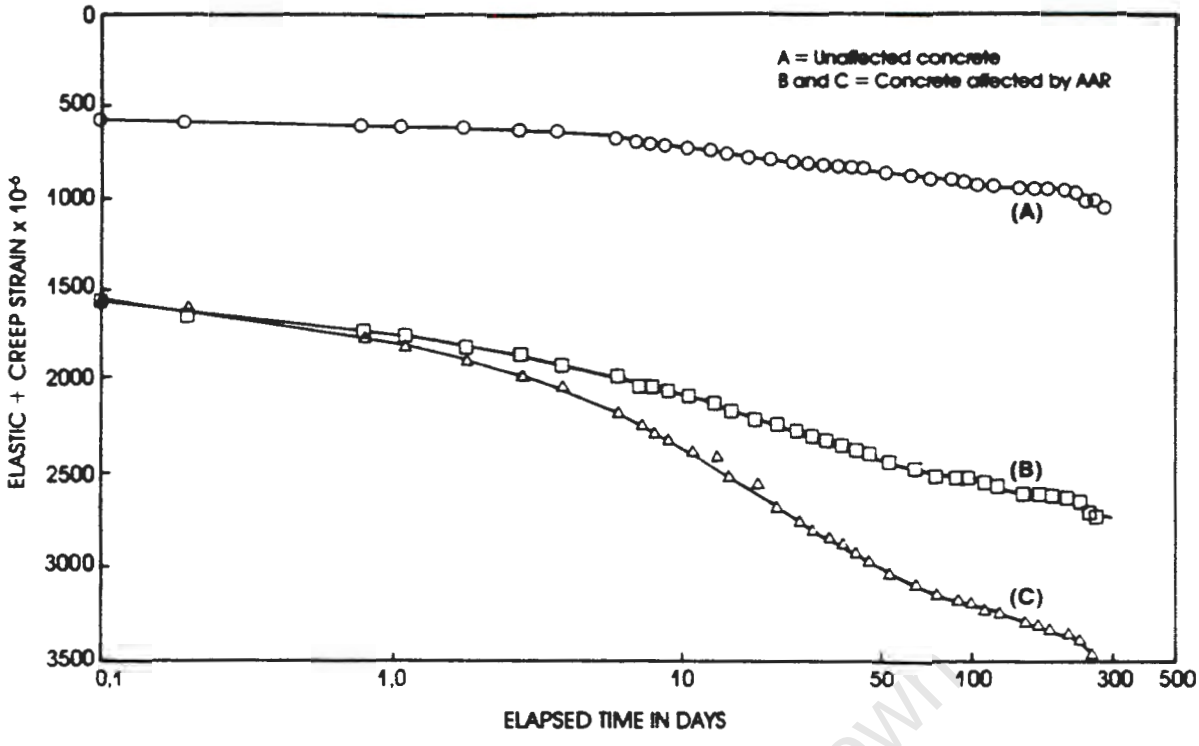

Figure 3: Illustration of effect of damage by AAR on elastic and creep properties of concrete.

indicated extreme deterioration. However, coring showed that the deterioration extended no more than 300mm below the surface of the block. Ultrasonic pulses transmitted from the bottom of a core hole and received from a similar hole on the opposite side of the block showed that the heart of the block had not deteriorated significantly.

It may be concluded that an ultrasonic pulse velocity survey can be a useful method of exploring the extent of deterioration by AAR. However, the method should not be used without calibration against a more direct physical method such as the examination of cores, or load tests on similar structures.

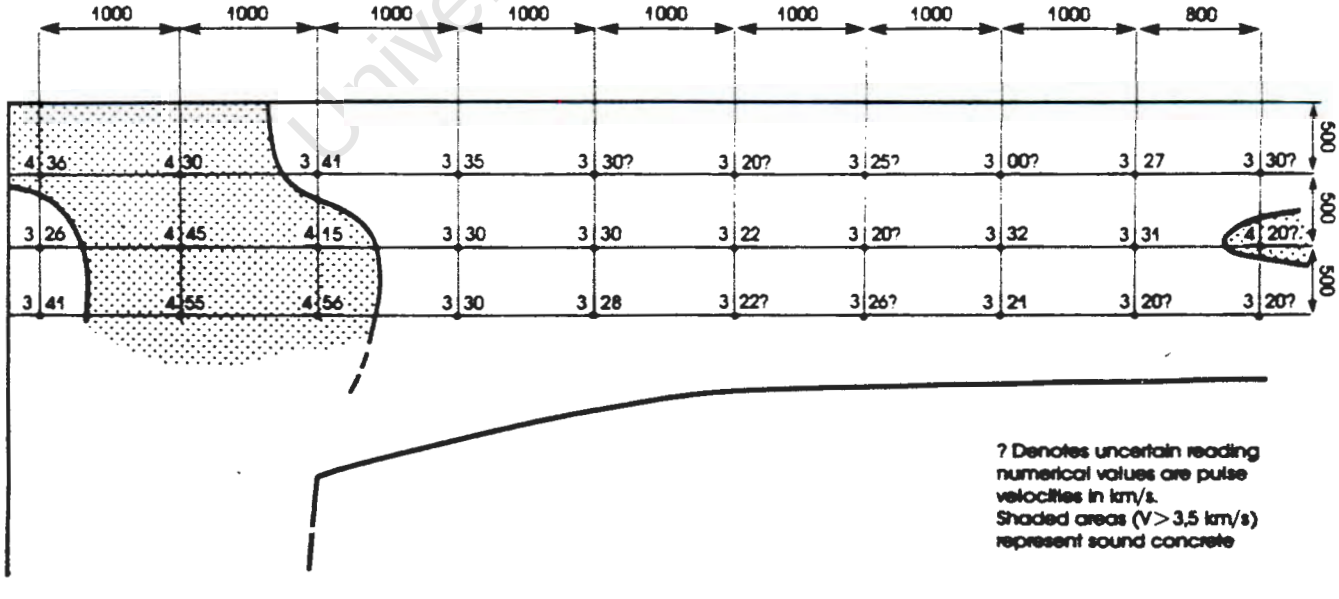

Figure 4: Result of ultrasonic pulse velocity survey on beam of portal frame damaged by AAR.

3.1.2 Visual Examination of Cores

Blight et al/2/ suggested a "petrographic examination score" which rated the extent of deterioration of concrete on the basis of the presence of various manifestations of AAR attack. This can be a useful technique if it is used to compare the condition of one structure with that of another. A semi-quantitative means of comparison may be necessary, for instance, to decide on priorities for a repair and rehabilitation programme for a structure or a series of structures.

To establish the petrographic examination score, the concrete is examined for the presence and extent of five features that are typical of deterioration by alkali-aggregate reaction. These are:

1. the presence of dark reaction rims around the perimeter of aggregate particles;
2. the presence of white or translucent reaction products in voids or cracks in the concrete;
3. the presence of cracks in the aggregate particles;
4. the presence of cracks in the mortar; and
5. loss of bond between mortar and aggregate.

The scoring system is as follows:

1 = feature present, but occasional
2 = feature occurs fairly frequently
3 = feature present in abundance.

The maximum score, corresponding to the worst state of deterioration, is thus 15.

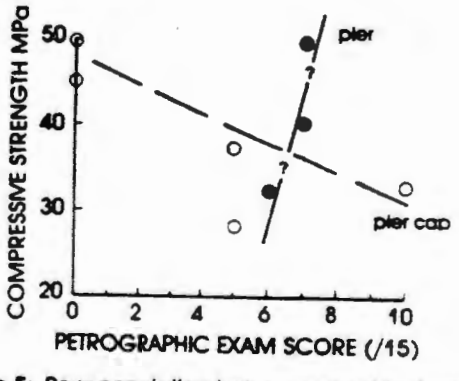

Figure 5: Poor correlation between visual features and strength of concrete.

This approach has been found very useful, but it must be emphasized that the correlation with measured concrete properties is tenuous. Figure 5 for example shows the petrographic examination score for a series of concrete cores, plotted against compressive strength. As the diagram shows, the cores taken from a bridge column show a weak negative correlation, which is to be expected. The cores taken from the foundation pier which supports the column, however, shows a positive correlation, if considered in isolation.

3.1.3 Mechanical Testing of Cores

The deteriorative effects of AAR as measured on cores may also be used to assess the extent and severity of the attack. The selection of core sites will usually bias the results optimistically. For example, a core having a large crack through it will not be taken or tested unless it is to explore the depth of the crack. Although such a core might have zero strength in the laboratory, under field loading the crack may partially close, and the concrete on either side of it carry some stress.

Notwithstanding the benefit of selection, it is recognized that the strength of any specimen depends on its size (Neville/4/). Boundary restraints applied by the testing machine tend to increase the measured strength of a small specimen. Also, there is a statistically greater chance of including a strength-reducing defect the larger the specimen size.

Figure 6 gives some typical results of tests on cores taken from an AAR-deteriorated structure. The data are for the same cores that were described in Figure 5. The results show very clear relationships between compressive strength and elastic modulus and between compressive strength and Poisson' ratio. It will also be noted that the design strength of the concrete was 30MPa, and that only one of the cores tested was below this strength.

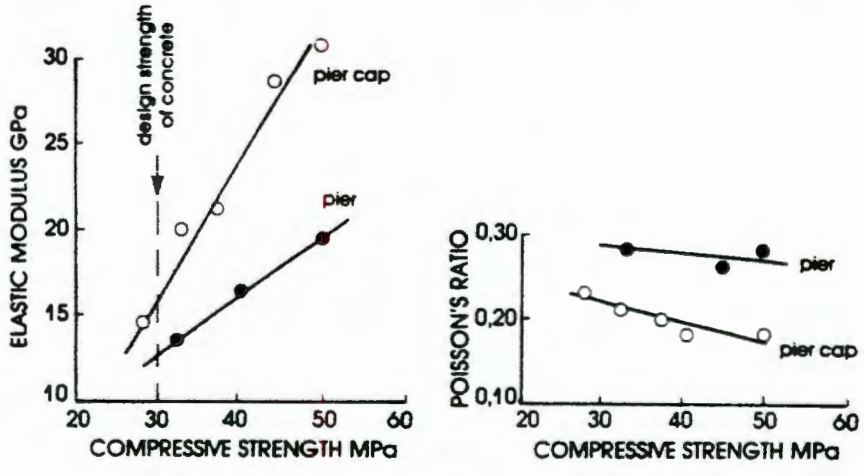

Figure 6: Relationship between Elastic Modulus, Poisson's Ratio and strength for AAR-Affected Concrete.

3.2 Direct Methods

Full-scale load testing must be regarded as the ultimate criterion of the safety and serviceability of an AAR-deteriorated structure. If the structure behaves predictably and in accordance with the design requirements, and if strains and deformations are of reasonable magnitude and recoverability, there can be little doubt that structural adequacy has been preserved. Such testing is, however, extremely expensive. In many cases it may be sufficient to instrument the structure, or part of the structure, and observe its behaviour in service, rather than mount a special test to full design load.

3.2.1 Full-Scale Loading Testing

A full-scale field loading test was carried out on a reinforced concrete portal frame that was showing severe deterioration as a result of AAR/5/. Prior to the loading tests an elastic finite element analysis of the frame was made using a reduced value of elastic modulus for the concrete that had been established by means of laboratory measurements on cores taken from the structure. Measured deflections, rotations and strains were then compared with the previously predicted quantities. In every case, close agreement was found between prediction and measurement. Over the short time duration of the tests, the structure behaved almost completely elastically and deformations were nearly fully recovered on removal of the load. Figure 7 is a view of the portal during the field test while Figure 8 shows the predicted and measured load-deflection curves for two points

Figure 7: View of portal frame being prepared for full-scale load test

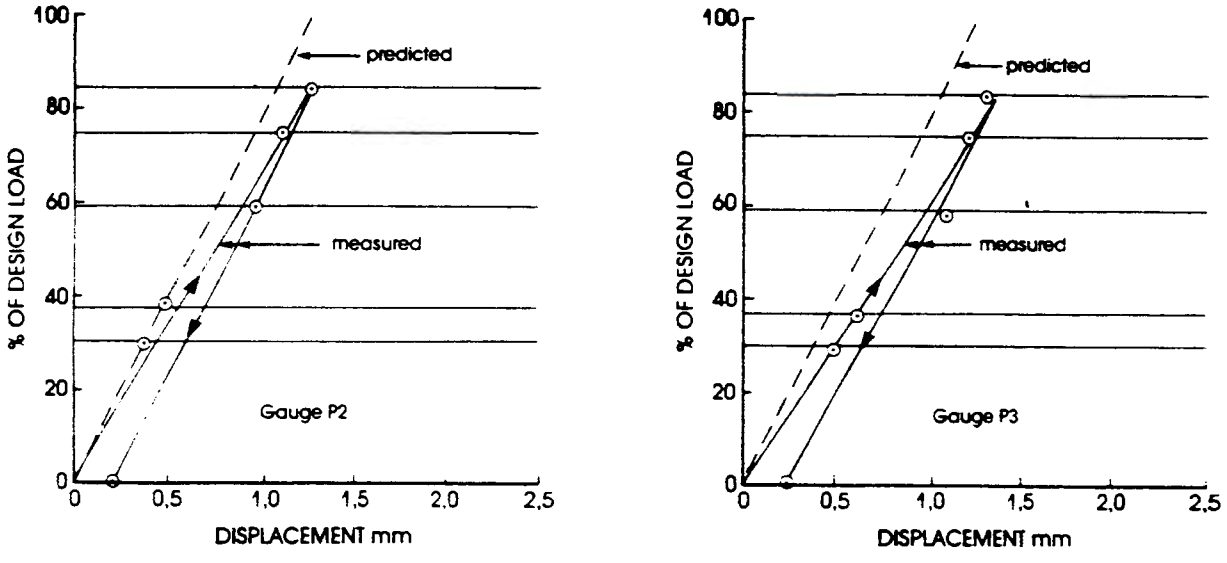

Figure 8: Comparison of predicted and measured load - displacement relationships for beam referred to in Fig. 4.

on the beam of the asymmetrical portal. The agreement obtained between strains, rotations and displacements predicted by analysis on one hand and observation on the other was surprisingly good.

The conservatism of design loading codes also works in favour of safety: It will be noted that only 85 per cent of the design load was applied to the structure, which supports an overhead motorway. Loading was by means of trucks overloaded to the extent of 10 per cent. Even with the trucks almost touching side to side and nose to tail, the full design load could not physically be accommodated on the structure.

3.2.2 Observation of In-Service Behaviour

Figure 9 shows the results of observing the in-service behaviour of a bridge pier that had cracked severely as a result of AAR (although there was a theory that the cracking was caused by dynamic overloading). This is the same pier referred to in 3.1.3.

Strain gauges affixed to the pier showed that in normal service, the live load stresses amounted to a maximum of only 0.4MPa. This is illustrated in Figure 9, which refers to measurements taken during a normal peak traffic period. This information, together with the reassuringly large core strengths (Figure 6) was sufficient to demonstrate that the structure remained adequately strong even in its deteriorated condition. Note that the stresses are based on a value of elastic modulus of 30GPa, which according to the data of Figure 6 is a conservatively high value for the pier.

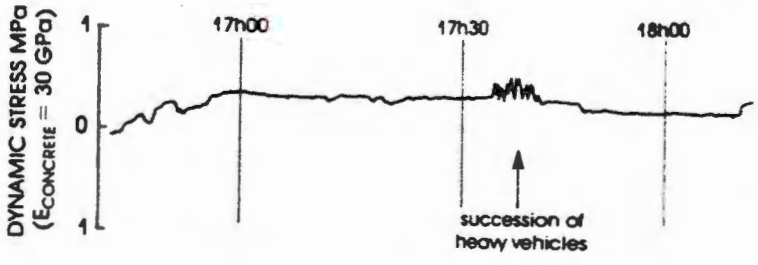

Figure 9: Dynamic strains recorded on pier below pile cap.

4. CONCLUSIONS

The main effect of AAR is expansive cracking which results in a reduced elastic modulus, reduced strength and increased creep if long term load is applied subsequent to occurrence of the damage. There are many ways of assessing the effects of this deterioration on the integrity of a reinforced concrete structure. Of the indirect methods of assessment:

4.1 Ultrasonic pulse transmission is a useful method of assessing the condition of concrete affected by AAR. However, the results of such measurement should be calibrated with reference to a direct physical method such as the examination of cores.

4.2 The visual condition of cores, quantified by the petrographic examination score, provides a useful means of comparing the state of damage of one structure with another. However, the correlation between the examination score and the strength of the concrete is poor.

4.3 Mechanical strength and stress-strain testing of carefully sited cores provides a good means of assessing the degree of damage to concrete caused by AAR.

However, the ideal method of assessment must be via direct measurements of the behaviour of the structure supported by the evidence of indirect tests.

4.4 Either a full-scale load test can be carried out and measured deflections, rotations and strains compared with those predicted, or

4.5 the structure can be instrumented and its behaviour observed under service loading.

There are, however, two important factors to be considered that have not yet been mentioned:

4.6 The structures investigated so far have had members of massive section. Hence the AAR has been a comparatively skin-deep effect. The deterioration could become much more important in the case of members of lesser section, or in the case of massive sections wetted internally, eg. by leaking drainage ducts.

4.7 Where the cover of deteriorated concrete was stripped off the reinforcing steel of the portal frame, the steel was found to be in excellent condition with no corrosion in evidence. Apparently, the environment in the concrete was still sufficiently alkaline to passivate the steel. This was the case in a geographical area where annual potential evaporation far exceeds rainfall. In moist, humid industrial or coastal climates, it is possible that steel that has become exposed to the atmosphere as a result of AAR could corrode catastrophically.

5. REFERENCES

/1/ VIVIAN, H.E: The effect on mortar expansion of amount of available water in mortar, Studies in cement-aggregate reaction XI, CSIRO Australia, Bulletin 256, (1950).

/2/ BLIGHT, G.E., McIVER, J.R., SCHUTTE, W.K. and RIMMER, R: The effects of alkali-aggregate reaction on reinforced concrete structures made with Witwatersrand quartzite aggregate, Proceedings, 5th International Conference on Alkali-Aggregate Reaction in Concrete, Cape Town, South Africa, (1981) 13pp.

/3/ BLIGHT, G.E., ALEXANDER, M.G., SCHUTTE, W.K. and RALPH, T.K: The effects of alkali-aggregate reaction on the strength and deformation of a reinforced concrete structure, Proceedings, 6th International Concrete on Alkalis in Concrete, Copenhagen (1983), pp. 401-410.

/4/ NEVILLE, A.M: The influence of size of concrete test cubes on mean strength and standard deviation, Magazine of Concrete Research vol. 8, no. 23 (1956), pp. 101-110.

/5/ BLIGHT, G.E. and ALEXANDER, M.G: Damage by alkali-aggregate reaction to reinforced concrete structures made with Witwatersrand quartzite aggregate and examples of repair measurements, Concrete Beton, Vol.38 no.10 (1985), pp. 14-23.

Magazine of Concrete Research, 1989, **41**, No. 147, June, 69–77

Effect of alkali-aggregate reaction on the performance of a reinforced concrete structure over a six-year period

G. E. Blight,* M. G. Alexander,* T. K. Ralph† and B. A. Lewis†

UNIVERSITY OF WITWATERSRAND; SODERLUND & SCHUTTE INC.

Two full-scale load tests have been carried out, with a six-year intervening period, on a reinforced concrete portal frame supporting an overhead motorway structure. The results of the tests show that the portal has slightly deteriorated since the first test was performed. The structure, however, remains safe and fully able to carry out its function. It continues to behave predictably under load. Plans have been made to arrest the progress of the alkali-aggregate reaction, rather than to carry out extensive or radical repairs to the structure.

Introduction

A portal that forms part of a major double-deck road structure in Johannesburg, South Africa, has deteriorated, as a result of alkali-aggregate reaction (AAR), to an extent that is visually alarming. The upper portions of the columns and the upper beam of the portal show the greatest degree of deterioration, and ultrasonic pulse velocity surveys have indicated that the visible surface deterioration penetrates the concrete to a considerable depth.

In 1982 it was decided that an assessment of the safety of the structure was required prior to taking a decision either to repair and seal the surface of the concrete against moisture ingress or to partially demolish and rebuild the portal. To assess the structural safety, it was decided to carry out a full-scale load test.

Prior to performing the load test, a finite-element analysis of the portal was carried out. This was to provide a basis of reference for the performance of the structure under load. The analysis was made using elastic moduli for the deteriorated concrete that had been measured in the laboratory on cores taken from the portal.

This is believed to have been the first time that the effects of alkali-aggregate reaction on the strength of a major structure had been assessed quantitatively by means of a full-scale field loading test. This test was fully reported in 1983[1] and showed that the margin of safety of the structure was still very adequate. Subsequently techniques similar to those described in this Paper were used to assess the condition of a motorway structure in Japan.[2]

While experiments were being performed to determine the most effective way of repairing the structure, a programme started in 1979 to monitor the movements of the larger surface cracks in the vicinity of the beam-to-column joint continued. In 1982 these records (see Fig. 1) had indicated that the rate of opening of the cracks was decreasing. However, the rate has since increased for some of the cracks. One of the larger cracks has increased in width by some 5.5 mm between 1980 and 1988 to an overall width of 15 mm. A view of the deteriorated concrete and of this major crack is shown in Fig. 2. Furthermore, the main steel reinforcement in the west face of the west portal column has become exposed in this and other cracks. The climate of Johannesburg is mild to warm (minimum temperature −5°C, maximum 30°C) and dry. The annual rainfall occurs in summer and amounts to 750 mm, while the potential evaporation is 1500 mm. In this climate, there has been minimal rusting of exposed reinforcing, and no spalling of concrete has occurred as result of either AAR or corrosion of the reinforcing.

As a result of the obvious continuing deterioration, it was decided that a further full-scale load test should be carried out with a view to determining to what extent the structure had deteriorated since the previous load test. It was also necessary to assess

*Department of Civil Engineering, University of Witwatersrand, 1 Jan Smuts Avenue, Johannesburg, South Africa.
†Soderlund & Schutte Inc., Johannesburg, South Africa.

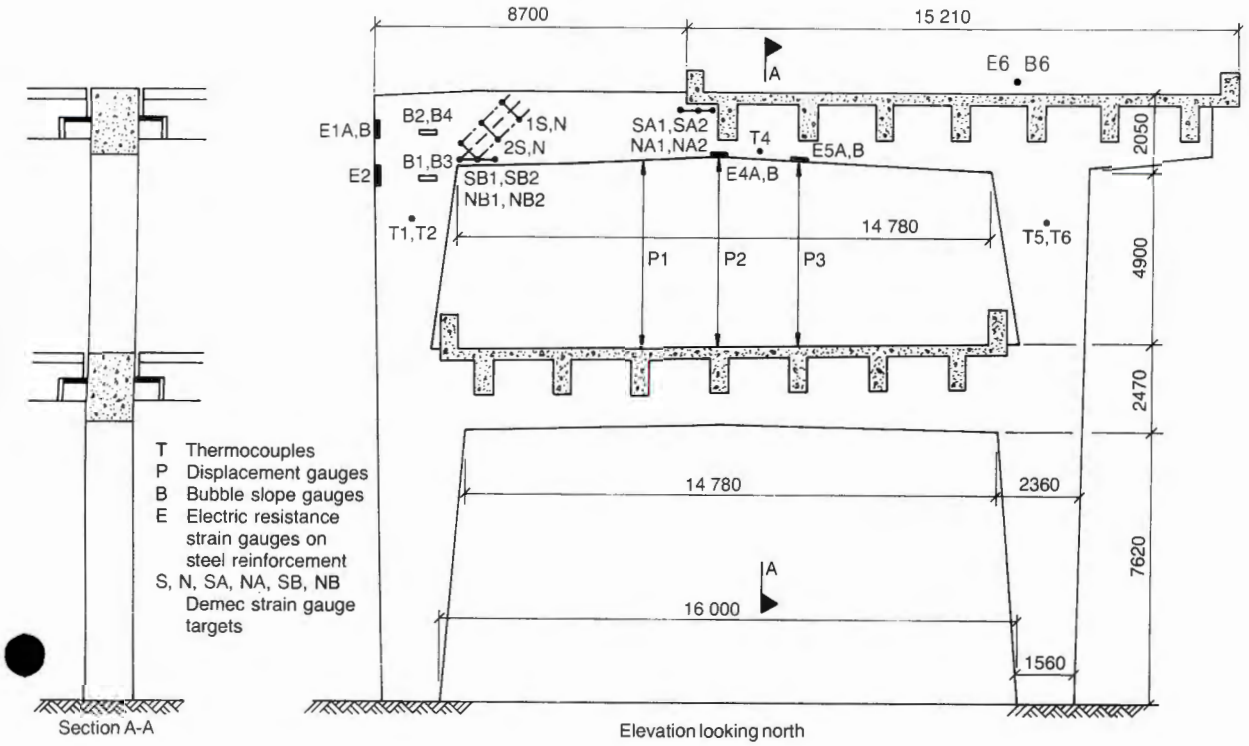

Fig. 3. Elevations of portal frame showing positions and types of instruments used in load test

the column appears to be of comparable quality to the better areas of the beam.

(*c*) Finally, the inability to correlate the two surveys, even though they were carried out by the same people and the two instruments could be directly compared, must throw some doubt on the reliability of ultrasonic pulse velocity measurements.

Finite-element analysis

The finite-element analysis was originally performed in 1982 on an elastic basis. Second moments of area for the portal were determined for the gross concrete section. Tests on cores from the portal and other related structures had shown that the elastic modulus for the concrete varied from 32 GPa for a sound material to 11 GPa for badly deteriorated concrete. An intermediate value of 18 GPa was chosen for the analysis. The results of the computed deflections are shown in Fig. 5. In the first series of analyses full continuity was assumed at every joint of the portal.

Because of the severe deterioration at the west end of the top portal beam, concern was felt lest moment continuity had been partially or completely lost at this point (J in Fig. 5). For this reason, the analysis was repeated assuming no moment continuity at J. Loss of continuity at J would have the effect of causing the portal to sway to the west.

What is measured in a load test is the difference between displacements or slopes under dead load and those under dead plus live load. For this structure, these differences are very small. The maximum expected displacement of the top beam was only 1·2 mm. The maximum rotation at point J was expected to be only 70×10^{-6} rad if full moment continuity existed and 365×10^{-6} rad if continuity had ceased to exist.

Objectives of the load test

The object of load testing the portal was to compare the behaviour of the structure under load with that determined analytically. For the second test in 1988 there was the additional object to ascertain whether or not the deterioration that had occurred since the previous load test had affected the structural behaviour of the portal frame, and if so to ascertain whether or not the structure was still capable of supporting the design loading with adequate safety.

The structure had been designed for type HA loading according to BS 153.[3] In the case of this particular structure, type HA loading amounts to uniformly distributed loads of 33 kN/m and 7 kN/m plus concentrated live loads of 1223 kN and 31 kN over two traffic lanes each 3·66 m wide and a third lane 2·33 m wide, respectively. In the 1982 load test it was found impossible to achieve full HA loading using road trucks loaded to capacity with sand and positioned on the deck as close to each other as possible; the total loading applied amounted to only 84% of HA loading.

The code of practice currently in use in South Africa for highway loading is TMH7.[4] According to this code, the normal live loading due to traffic on highway

where L is the effective loaded length in metres and Qa is the average load per metre of notional lane in kilonewtons.

1.2 One nominal axle load of $120/n$ kN per notional lane, where n is the loading sequence number of the relevant lane (i.e. $n = 1$ for the first lane loaded with the axle load, $n = 2$ for the second lane etc.).

The latter loading is applied in conjunction with the former loading in such a way as to cause the most adverse effect on the structure.'

It is not possible to compare type HA loading with type NA loading directly. By comparing predicted deflections at mid-span of the upper transverse beam, however, type NA loading was found to be equivalent to about 81% of type HA loading.

Load test

Because of the small magnitude of the movements it was intended to measure, temperature differences between different parts of the structure had to be avoided as far as possible. For this reason, it was decided to set up the instrumentation during daylight and to complete the test between midnight and dawn, when temperature conditions could be expected to be stable. Loading was to be applied by means of trucks loaded with sand to their maximum legal weight of either 20 t or 10 t.

The instrumentation was selected and placed so as to monitor those aspects of the behaviour of the portal frame that the finite-element analysis had suggested might be critical. These were as follows.

Displacement of the beam

Displacement was measured at four points on the beam (gauges P1–P4 in Fig. 3) by means of the instruments illustrated in Fig. 6. An invar wire was attached to the soffit of the beam at the point of measurement by means of a masonry bolt. The lower end of the wire was attached to a heavy weight that was able to slide freely in a vertical direction guided by a ball bushing. The bushing, in turn, was attached to a base that was bedded down on the road surface of the lower deck vertically below the point of measurement. Fig. 6 shows the lower extremity of the invar wire attached to the cylindrical weight. The bushing was attached to the base, the channel legs of which were bedded down in the white plaster of Paris visible in the photograph. The underside of the weight was attached to a spindle, the vertical movement of which was measured to the nearest 0·01 mm by means of the dial gauge visible in Fig. 6. Because of possible displacements of the lower deck (see Figs 3 and 5) the arrangement of wires and displacement gauges was repeated between the soffit of the lower beam of the portal and the road surface at ground level.

In the 1982 load test it was established that the deflections of the lower deck were negligible. The lower gauges were therefore omitted for the 1988 test.

Rotation of the joints

Rotations were measured at points B1–B6 (Fig. 3) by means of bubble slope gauges. Each gauge consists of a sensitive bubble that can be levelled to an accuracy of 50×10^{-6} rad, and the change in slope was measured to the same accuracy. Gauges B1 to B5 all measured the rotation at or near J. If moment continuity at J had been partially or completely lost, B2 and B4 would register different rotations to B1 and B3. Gauge B6 was mounted to measure out-of-plane rotations of the portal when only one span of the deck was loaded.

Tensile strain in the main reinforcing

Because of the deterioration of the concrete it was considered essential to measure the strain in the tensile reinforcing of the portal. The main reinforcing bars were exposed by chipping away the cover at the points E1, E2, E4 and E5 shown in Fig. 3. Temperature compensated pairs of electric resistance strain gauges were then bonded to two exposed steel bars at each location.

Figure 7 shows the main vertical reinforcement exposed in the west column near the beam-column

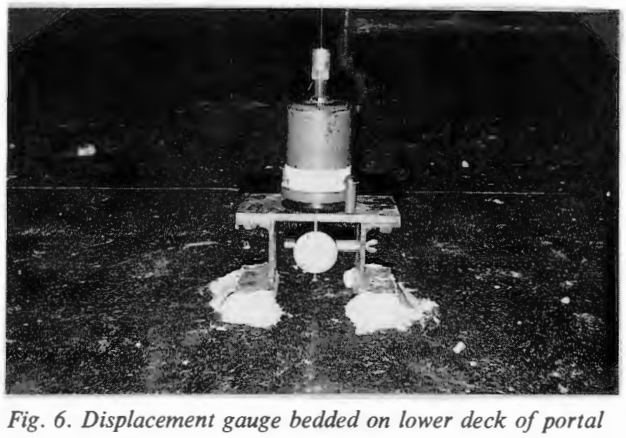

Fig. 6. Displacement gauge bedded on lower deck of portal

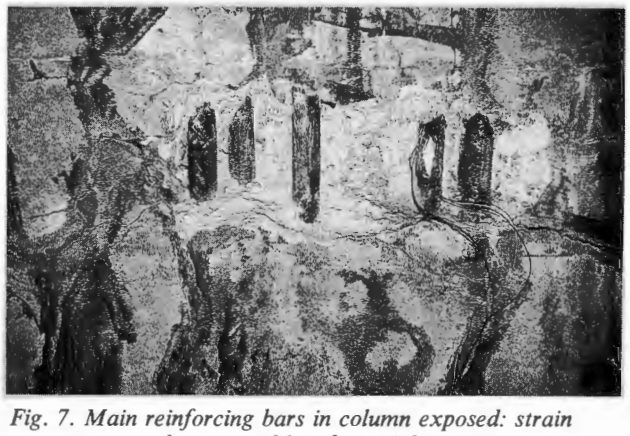

Fig. 7. Main reinforcing bars in column exposed: strain gauges mounted on second bar from right

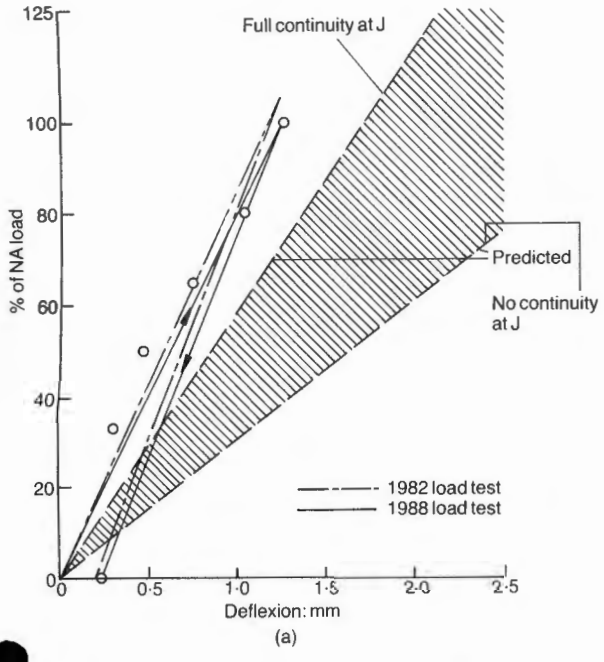

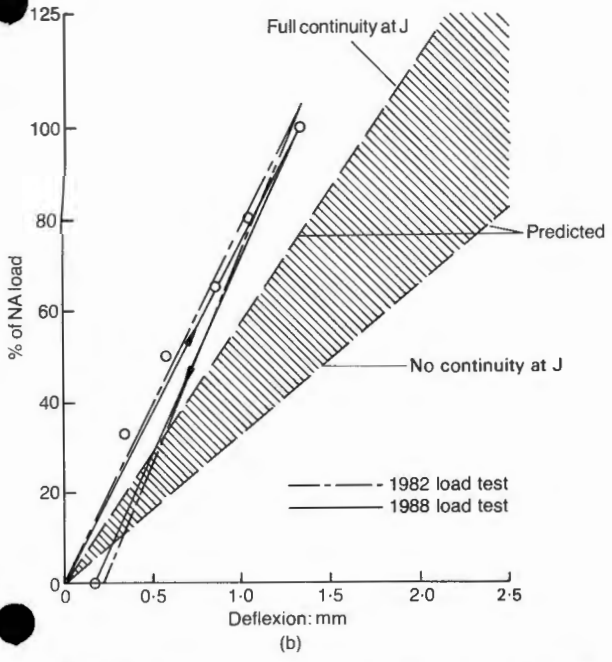

Fig. 10. Comparison of measured and predicted deflections of upper transverse beam: (a) gauge P2; (b) gauge P3; 125% NA load = BS 153 100% HA load

Tensile strains in reinforcing

Figure 12(*a*) shows strains measured in the reinforcing at the west beam to column joint (J). As far as continuity at J is concerned, a lack of continuity would be indicated by low or zero strains at E1 and E3 and a difference in strains between E1 and E2. In fact, the readings taken at all three locations cannot be distinguished, although strains at E2 are slightly lower than predicted if full continuity applies. As shown in Fig. 12(*b*), measured strains at mid-span agree almost exactly with those predicted assuming that the concrete is capable of resisting tension, thus supporting the conclusion that full continuity exists at J. Once again it appears that a very slight deterioration of the portal has taken place in the six-year interval between tests.

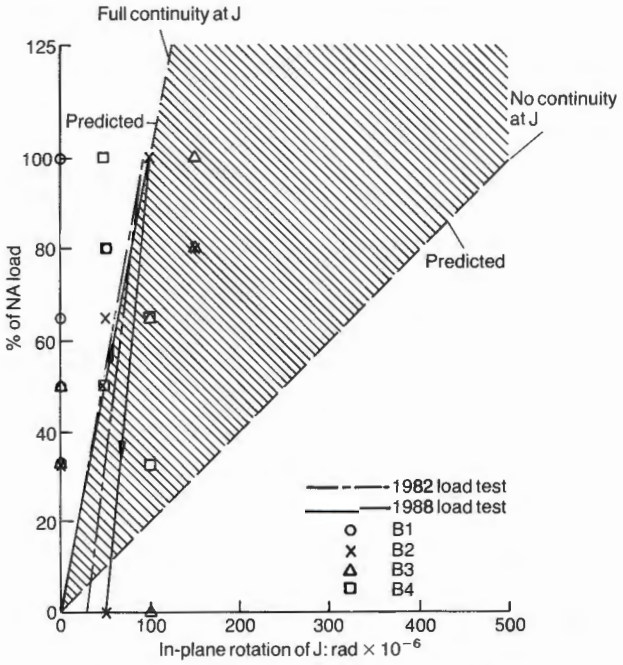

Fig. 11. Comparison of measured and predicted rotations at western beam-column joint (point J in Fig. 5); 125% NA load = BS 153 100% HA load

Surface compressive strains in concrete

In Fig. 13(*a*) the measured surface compressive strains at mid-span of the upper beam are compared with the strains predicted by analysis of the transformed section.

In Fig. 13(*b*) the measured surface compressive strains at the beam-column joint are compared with the strains predicted using both the transformed section and the conventional straightline no-tension theory.

At the mid-span of the upper beam, the compressive strains in the concrete are only half of the predicted strains. The concrete and steel strains measured at this point are, however, reasonably consistent with the strains predicted using the transformed section.

At point J, the concrete compressive strains slightly exceed the strains predicted using the transformed section. At two of the strain gauge positions, permanent strains of around 500×10^{-6} took place during the first load increment of the 1988 test. However, strain changes that took place in subsequent load increments were small and close to predicted values. In 1982, this 'crack closure strain' was observed at all the strain gauge positions. The residual strains after excluding the crack closure strain were less than 30×10^{-6}.

Permanent deformation of the structure

After applying each load increment a set of measure-

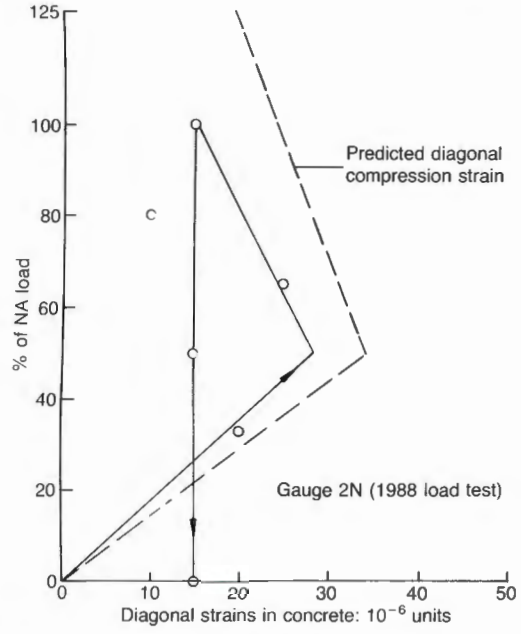

Fig. 14. Comparison of measured and predicted surface diagonal strains in concrete; 125% NA load = BS 153 100% HA load

strains are reasonably similar to the anticipated strains.

Unfortunately, the readings obtained at the remaining gauge stations were random and could not be meaningfully interpreted. This may be due to the deteriorated state of the concrete leading to an internal non-linear redistribution of shear stresses within the beam, as well as the very complex way in which reinforced concrete members resist shear.

Conclusions

The load tests both supported the view, formulated prior to 1982 on the basis of laboratory tests,[5] that deterioration of concrete as a result of alkali-aggregate reaction may be alarming in appearance but not necessarily structurally dangerous. Moreover, structures that have deteriorated behave predictably and their elastic behaviour can be predicted on the basis of laboratory tests on cores taken from the structure.

The major effect of alkali-aggregate deterioration appears to be to increase the deformation of a structure by reducing the elastic modulus of the concrete. With normal design practice where the design load usually far exceeds loads actually applied to a structure, safety appears not to be a serious problem. (With certain other classes of structure, where design loads can be determined with greater certainty and where the structures carry more of their design load, this conclusion may not be valid.)

The load tests have shown that the structure has deteriorated as a result of the AAR, but that the rate of deterioration was very slow between 1982 and 1988. In 1982 it was recommended that nothing drastic be done to the structure, but that sources of water ingress to the concrete be eliminated. Essentially the same recommendations were made in 1988. It is now planned to jacket the beam and column in a water-excluding but non-structural tube. The precise form of this jacket has yet to be determined.

Acknowledgement

This Paper is published by kind permission of the City Engineer of Johannesburg.

References

1. BLIGHT G. E. *et al.* The effect of alkali-aggregate reaction on the strength and deformation of a reinforced concrete structure. *Proc. 6th Int. Conf. Alk. Concr., Copenhagen, June 1983*, (edited by G. M. Idorn and S. Rostam). Danish Concrete Association, Copenhagen, 1983, 401–410.
2. AMAI H. *et al.* The deterioration by alkali-silicate reaction of Hanshin expressway concrete structures—investigation and repair. *Proc. 7th Int. Conf. Concr. Alk.-Aggr. React. Concr., Ottawa, 18–22 Aug. 1986*, (edited by P. E. Grattan-Bellew). Noyes Publications, NJ, USA, 1987, 131–135.
3. BRITISH STANDARDS INSTITUTION. *Girder bridges*. BSI, London, 1954, BS 153, Part 3A Loads and stresses.
4. NATIONAL INSTITUTE FOR TRANSPORT AND ROAD RESEARCH. *Code of practice for the design of highway bridges and culverts in South Africa*. National Institute for Transport and Road Research, Pretoria, 1981, TMH7, Parts 1 and 2.
5. BLIGHT G. E. *et al.* The effects of alkali-aggregate reaction on reinforced concrete structures made with Witwatersrand quartzite aggregate. *Proc. 5th Int. Conf. Alk.-Aggr. React. Concr., Cape Town, 30 Mar.–3 Apr. 1981*, National Building Research Institute, Pretoria, 1981, S25/15/1–12.

Discussion contributions on this Paper should reach the Editor not later than 2 January 1990.

Alkali-Aggregate Reaction

8th International Conference

EDITED BY

K. Okada, S. Nishibayashi and M. Kawamura

8th ICAAR 1989 KYOTO 8th International Conference on Alkali-Aggregate Reaction

EXPERIMENTS ON WATERPROOFING CONCRETE TO INHIBIT AAR

BY

G E Blight

University of the Witwatersrand, Johannesburg,
P O WITS 2050, South Africa

ABSTRACT

Laboratory experiments were undertaken to test the effectiveness of four surface treatments for waterproofing concrete. These were two coatings and two pore liner penetrants (a silicone and a silane). The results showed that none of the treatments waterproof concrete. Subsequent field trials showed that in the South African climate it is not necessary to surface treat sound concrete. Also, that if the surface is cracked, water can enter through the cracks even if the surface has been treated.

INTRODUCTION

It has long been known qualitatively that AAR in concrete can proceed only if water is present to sustain it. Vivian[1] showed 40 years ago that the amount of expansion that occurs in mortars depends on the amount of removable water in the mortar. Vivian's original results are shown in Figure 1. If the removable water is less than about 4 per cent by dry mass, no expansion due to AAR occurs. Once the removable water exceeds 4 per cent the expansion becomes directly proportional to the excess of removable water over 4 per cent (the available water).

Vivian defined removable water as the water lost after prolonged storage over calcium chloride (a relative humidity of 32 per cent). The available water is that part of the total water that is loosely held in capillaries in the mortar. Note from Figure 1 that the available water may be contained within the concrete ab initio (sealed specimens) or be allowed to penetrate the mortar from outside (unsealed specimens) after some drying has occurred. Assuming that Vivian's results on mortar are applicable to concrete, it is clear that if the available water in concrete can be kept to zero, expansion by AAR will be minimized or even eliminated.

The above statement does not define available water with any precision. What is needed is a criterion in terms of a measurable moisture tension-related variable. Possible variables would be the relative humidity (RH) or the pore water suction (p").

The evidence[2,3,4,5], shows that if the relative humidity in the atmosphere surrounding a concrete structure can be maintained at below 95 per cent, AAR will be inhibited. However, the relative humidity of the surroundings is usually not the same as the relative humidity in the pores of the concrete where the AAR occurs.

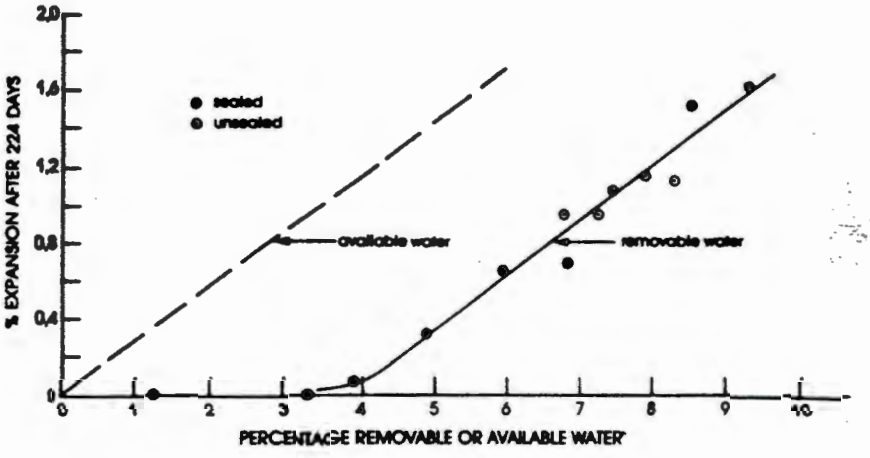

Figure 1: Vivian's observed relationship between removable water and expansion

Relative humidity in a material like concrete can be related to the pore water suction p" by the Kelvin equation[eg. 6,7]:

$$p" = 311 \log_{10}(RH) \text{ in MPa}$$

where RH is expressed as a fraction of unity, eg. 0.95.

Even at a RH of 0.95, the suction is nearly 7MPa. This moisture stress exerts an equal isotropic compressive stress on the concrete. Even if the suction is not completely effective, the concrete must, at RH = 0.95, be subjected to an isotropic compressive stress of several MPa.

The only recorded measurements of the swelling pressure exerted by AAR are due to McGowan and Vivian[7]. Their measurements indicated swelling pressures of no more than 500kPa. Clearly, concrete can only expand if the swelling pressure exceeds the moisture stress. As the moisture stress is so large at RH = 0.95 and below, it appears unlikely that the cut-off RH could be less than 0.95 per cent in the pores of the concrete.

One obvious way of inhibiting AAR is to dry the interior of the concrete out to below the cut-off RH and then maintain it in that condition by means of a waterproofing layer or coating.

The climate in South Africa is relatively dry. The highest RH recorded has been 0.96, while the average maximum is only 0.75. Hence a concrete structure should dry out to below RH = 0.95 provided a) it is protected from rain; b) water cannot accumulate in or on it via faulty drainage; and c) the concrete is not situated in an artificially high humidity environment.

The above considerations have led to the following investigations:

.1 a laboratory investigation of various types of waterproofing and;

.2 an extension of this investigation to structures in the field.

TYPES OF WATERPROOFERS USED IN INVESTIGATION

Two major studies[8,9] list five types of waterproofers for concrete:

.1 Pore liner penetrants, usually operating as water repellants.
.2 Pore blocker penetrants that seal surface pores.
.3 Sealers that form an impervious surface skin on the concrete
.4 Coatings that form a thicker impervious surface skin.
.5 Renderings which are thick coatings, usually applied by trowel.

The four waterproofers tested in this work were two coatings and two pore liner penetrants, described as:
Coating 1: a cementitious slurry.
Coating 2: an aqueous dispersion of synthetic resins.
Penetrant 1: silicones in hydrocarbon solution.
Penetrant 2: alkyl alkoxy silane.

LABORATORY TESTS

100x100x200 mm concrete prisms were treated with each of the four waterproofers. The treated prisms were then subjected to two moisture regimes. Three prisms for each of the four treatments were submitted to each regime. The efficacy of the treatment was judged by weighing the prisms to assess progressive gain or loss of moisture.

Regime A tested the waterproofing of the coatings. Coatings were applied to oven dried specimens. After curing, the prisms were weighed and placed on racks where they were subjected to a wet atmosphere in a fog room. The results showed that none of the coatings were waterproof. The best performance was that of Penetrant 2 (silane), but it was clear that the moisture content of the other three sets of specimens was heading towards an equilibrium water content (probably close to saturation), when the tests were terminated after 110 days. The results of this set of tests is shown in Figure 2.

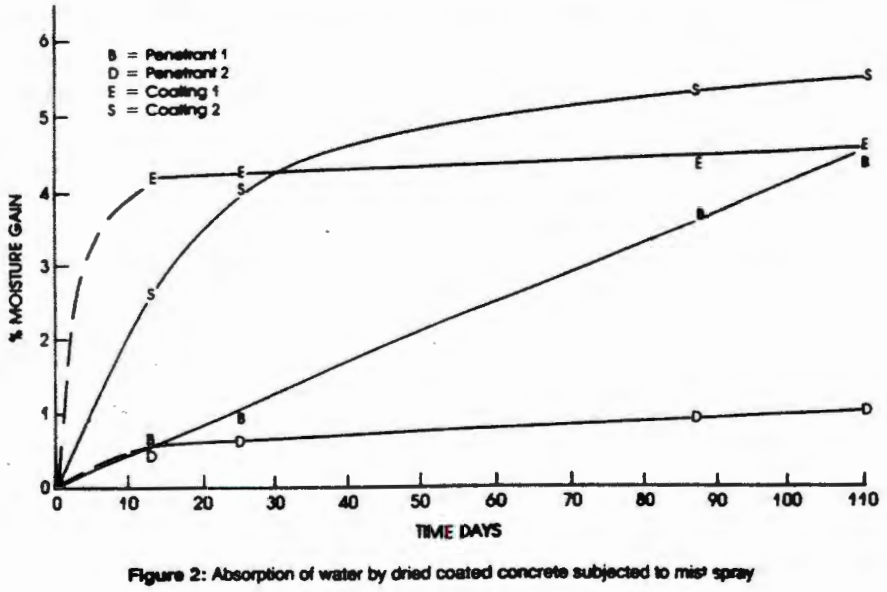

Figure 2: Absorption of water by dried coated concrete subjected to mist spray

Regime B tested the ability for moisture to be lost through the coating from concrete that is already wet, when the concrete is exposed to a low RH environment. The uncoated specimens were soaked in water for 7 days, allowed to surface dry for one day and were then coated. The specimens were stored

over calcium chloride to give an ambient atmosphere RH = 0.32. The prisms were periodically weighed.

The results showed that the water repellent penetrants, and Coating 1 proved most effective in allowing water to pass out of the concrete. All specimens lost moisture more slowly than they gained it.

The next series simulated the South African climate in the laboratory. The coated specimens originally subjected to Regime B were stored in the fog room for 7 days. A cyclic drying-wetting regime simulating a climate of short wet periods followed by much longer drying periods was then started. The specimens were stored in a drying atmosphere at RH = 0.32 for 7 days, then at RH = 1.0 for 6 hours, then at RH = 0.32, and so on.

The results of this treatment are shown in Figure 3. After an initial uptake of moisture, all, including the untreated controls, dried out progressively and approached the initial moisture content.

There were two possible conclusions relating to concrete structures exposed to the South African climate:

.1 Either it is not necessary to waterproof exposed concrete because it will dry out completely between the brief wet spells it experiences; or

.2 the waterproofing need not be 100 per cent effective. Provided most of the precipitation is excluded, the concrete will subsequently dry out.

To examine these tentative conclusions, it was decided to test some reinforced concrete structures in the field.

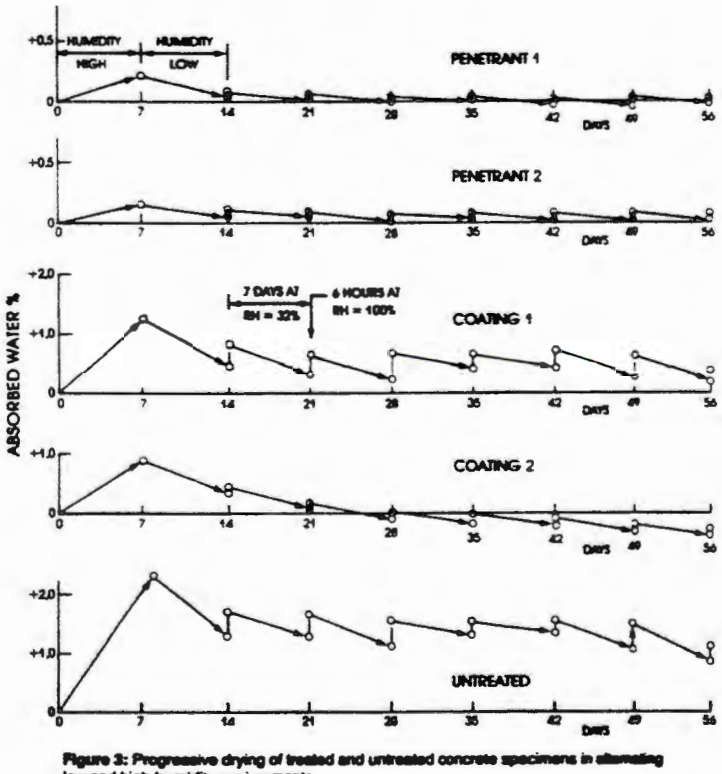

Figure 3: Progressive drying of treated and untreated concrete specimens in alternating low and high humidity environments
(Low = RH 32% High = RH 100%)

FIELD EXPERIMENTS INVOLVING WETTING FOLLOWED BY DRYING

A group of columns supporting an overhead structure was selected for the field trials. The columns were washed down with high pressure water jets and were then coated with the four waterproofers. The column shafts are completely protected from impinging rain by the overhead structures they support. This situation was chosen deliberately so that the moisture condition of the column surfaces could be controlled artificially. The effect of wetting and drying was assessed by inserting thermocouple psychrometer probes to a depth of 100mm into holes drilled into the columns.

A psychrometer probe[10] consists of a thermocouple sealed into a cavity in the concrete. The air surrounding the probe comes to thermal and moisture equilibrium with the air in the cavity. A current is passed through the thermocouple which cools by the Peltier effect until the temperature falls below the dew point of the moisture in the surrounding air. Moisture then condenses on the thermocouple junction. The cooling current is interrupted and the condensed moisture starts to evaporate at the dew point temperature. The thermocouple is used to measure this temperature and hence the relative humidity in the cavity and the related pore water suction (p") in the concrete can be determined via the Kelvin equation.

The measuring range of the psychrometer is from RH = 100 to about RH = 0.96. Below RH = 0.96 it is not possible to condense water out of the atmosphere by cooling the air. The range does not quite cover the RH interval of 0.95 to 1.00, but the actual range of interest is probably less than this.

Figure 4 shows the results of two sets of measurements on the untreated control column and the column treated with Penetrant 1 (silicone). Not all of the columns are in the same physical condition. Some are completely sound, but

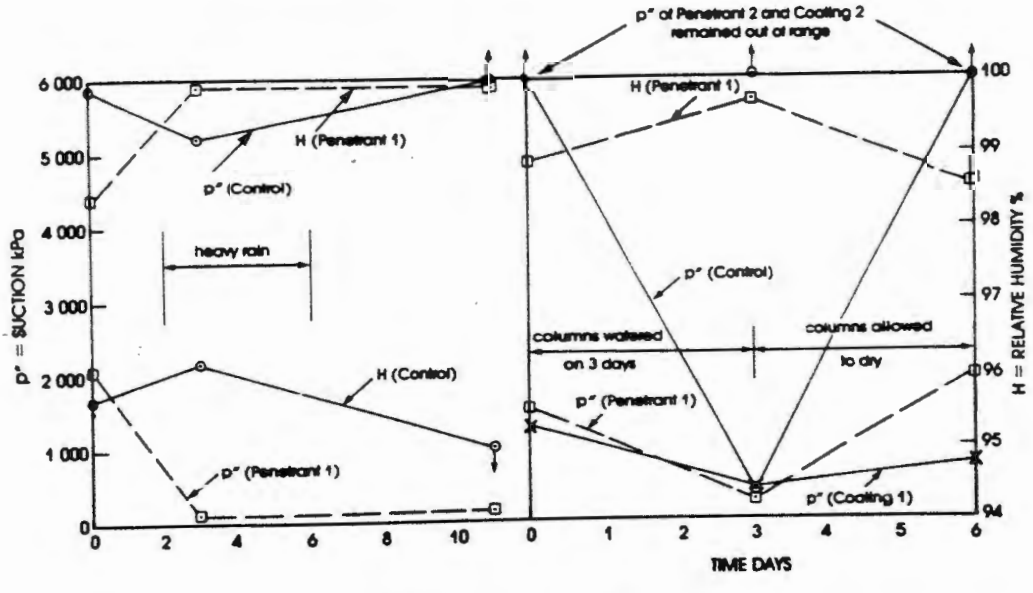

Figure 4: In situ psychrometer measurements in two columns supporting overhead structure.

others show signs of AAR attack, in the form of cracks in the columns, or in the mushroom slabs they support, or both. As it happened, the control column is completely sound whereas the silicone-treated column has a badly cracked mushroom slab, although the column itself has only minor cracks in it.

The left hand section of Figure 4 shows results of preliminary measurements on the two columns to establish the range of p" or RH to be expected. p" in the control column was very high (more than 5000kPa) and the measurements eventually went out of range. p" in the silicone-treated column, however, was unexpectedly low (2000kPa) and after a spell of heavy rain, reduced even further. A few days later streaks of white AAR gel appeared through cracks in the column and ran down the surface. This showed that water was entering the column via the structure it supports and causing further AAR.

In a second series of tests conducted during very hot dry weather, initial p" readings were taken and the columns were then watered by hose over a period of six hours on three consecutive days to represent as severe a condition of wetting as is ever likely to occur on an outside structure.

The wetting caused p" in the control column to fall from beyond the range of the psychrometer to only 350kPa (Figure 4). After 3 days of drying, the p" was again out of range.

p" in the silicone treated column started at 1500kPa, fell to 250kPa after 3 days watering and then rose again to 1900kPa after 3 days of drying. This indicated that water was entering the concrete through pre-existing cracks, even though the surface had been treated. There was no rain during the test and the water could not have been entering through the superstructure. However, atmospheric drying removed the water relatively quickly.

These tests confirmed the conclusions drawn earlier:

.1 If there is no internal source of water from, for example a blocked internal drainage pipe, etc, sound concrete will quickly dry out after being surface wetted. It probably does not need to be waterproofed.
.2 If there is an internal source of water it is pointless to waterproof the concrete.

The column treated with Coating 1 is also cracked by AAR. p" in the column started at 1200kPa, but fell to 300kPa after the period of watering. Three days later p" had increased but was still at a relatively low 800kPa. These results confirm that water can enter a concrete member through surface cracks, even if the surface has been treated. The rate at which the structure dries again depends on the type of treatment.

The column treated with Coating 2 is in sound condition. That treated by Penetrant 2 is cracked, but the psychrometer probe was inserted in an area of sound concrete. p" recorded in these two columns started out of measuring range and remained out of range even after the watering.

GENERAL CONCLUSIONS

.1 None of the surface treatments tested proved able to waterproof concrete.
.2 Conversely, once the concrete was wet the surface treatments were sufficiently permeable to allow it to dry out again.
.3 When surface treated concrete that is wet internally is subjected to short periods of wetting followed by longer periods of drying, it is possible progressively to dry out concrete. This is directly applicable

in climates where brief wet spells are followed by longer dry spells.

.4 Provided the concrete is sound, exposed reinforced concrete structures in South Africa quickly dry out after surface wetting, and do not need to be waterproofed.

.5 If there is an internal source of water in the concrete, waterproofing the exterior of a structure is obviously ineffective.

.6 Even if the surface of cracked concrete is surface treated, water can still enter through the cracks.

ACKNOWLEDGEMENT

The study described in this paper was sponsored by the City Engineer of Johannesburg who has kindly permitted the information to be published.

REFERENCES

[1] Vivian, H.E, The effect on mortar expansion of amount of available water in mortar, Studies in Cement-Aggregate Reaction XI, CSIRO, Australia, Bull. 256, 1950.

[2] Gudmundsson, G and Asgeirsson, H, Parameters affecting alkali expansion in Icelandic concretes, Proc. 6th Int. Conf. Alkalis in Concrete, Copenhagen, 217-222, 1983.

[3] Nilsson, L.O, Moisture effects on the alkali-silica reaction, Proc. 6th Int Conf Alkalis in Concrete, Copenhagen, 201-208, 1983.

[4] Addis, B.J, (Ed), Fulton's Concrete Technology, Portland Cement Institute, South Africa, 474, 1986.

[5] Hawkins, M.R, (Chairman), Minimizing the risk of alkali-silica reaction, Report of Working Party, Cement and Concrete Association, UK, 1, 1983.

[6] Blight, G.E, Strength characteristics of desiccated clays, Jour. Soil Mech and Found Div, ASCE, 92, SM6, 19-37, 1966.

[7] McGowan, J.K and Vivian, H.E, The effect of superincumbent load on mortar bar expansion, Studies in Cement-Aggregate Reaction, XXIII, Austr. Jour. of Appl. Sci., 6, 1, 94-99, 1955.

[8] Pfeifer, D. W and Scali, M.J, Concrete sealers for protection of bridge structures, Nat. Co-op. Highway Rec. Prog., Rep. 244, US Transportation Research Board, Washington, DC, 1981.

[9] Leeming, M.B and O,Brien, T.P, Protection of reinforced concrete by surface treatments, CIRIA (UK) Technical Note 130, London, 1987.

[10] Savage, M.J and Cass, A, Measurement of water potential using in situ thermocouple hygrometers, Advances in Agronomy, 37, 73-126, 1984.

Structural Engineering Review, 1990, **2**, 113–120

Rehabilitation of reinforced concrete structures affected by alkali-silica reaction

G.E. BLIGHT

Department of Civil Engineering, Witwatersrand University, P.O. Wits, 2050, South Africa

The appearance of a reinforced concrete structure that has deteriorated as a result of alkali-silica reaction (ASR) may be alarming. However, it is known that in most cases the concrete retains useful strength and elastic modulus properties, and that ASR-affected structures can be successfully repaired.

This paper reviews the literature on the repair and rehabilitation of structures damaged by ASR under the following headings: arresting the ASR process; correcting structural deficiencies by resin injection and post-stressing; and partial demolition and reconstruction.

It concludes that much remains to be learned of the first two approaches, and that the third will rarely be necessary for purely technical reasons.

1. INTRODUCTION

Although the cracking caused in concrete by alkali-silica reaction (ASR), may be visually alarming, there is strong evidence that the effects of the deterioration may be less serious in terms of structural safety than appearances might suggest. This is at least partly because most structural loading codes are almost unrealistically conservative. Thus building and highway structures are hardly ever required to carry more than a small proportion of their design loads during service, and actual service stresses are generally low. The latter statement has been demonstrated by measuring dynamic strains in a bridge pier under real service loading [1]. Visually the pier had deteriorated severely as a result of ASR. However, the actual service live load stresses amounted to a maximum of only 0.4 MPa. As the minimum strength measured for cores taken from the pier was 28 MPa it was most unlikely that there could be an immediate safety problem. Full-scale load tests on structures showing ASR deterioration have been carried out in Japan [2] and in South Africa [3, 4]. In both cases the structures were found to behave predictably with little apparent loss in serviceability as a result of the deterioration. In the South African case two successive full-scale loading tests at an interval of 6 years, showed that the structure (a double deck highway portal frame) had undergone little, if any, deterioration in the period between tests.

If the margin of safety of a structure that has been attacked by ASR remains reasonably adequate, rehabilitation of the structure and repair of the ASR-related damage must inevitably come under consideration. The object of this paper is to survey the small amount of experience that appears in the literature concerning the repair of ASR damage to reinforced concrete structures. The paucity of the available information is illustrated by the observation that in a recent book on ASR [5] the text dealing with repair occupies less than two pages of the 174 page book.

ASR has been rather dramatically described as 'concrete cancer'. However experience has shown that ASR need not be a terminal disease. Although it cannot be cured, corrective measures can be taken. As with cancer, these can vary from therapy and cosmetic treatment to minor corrective surgery, to radical surgery with partial reconstruction and the fitting of prostheses.

The types of repair that will be discussed and evaluated here will be:

(1) Therapeutic and cosmetic — arresting the ASR process and hiding its effects;

(2) Corrective surgery — correcting structural deficiencies that have resulted from ASR; and

(3) Radical surgery — partial or complete demolition and reconstruction.

2. ARRESTING THE ASR PROCESS

In most cases, arrest of the ASR process may be a prerequisite to other forms of treatment. There is, for instance, little point in applying a cosmetic treatment if cracking will recur within a few years. In many cases, arrest of ASR may be the only treatment required, together with surface cosmetic treatment. Unfortunately, it is the form of treatment which is least understood and which has the least satisfactory record of success. It is also the field most frequented by commercial opportunists peddling instant but unproven remedies and preparations. It has long been known [6] that ASR can

0952-5807/90 $03.00+.12

be arrested if the concrete can be dried out to below a certain moisture level. Other evidence [7, 8, 9] suggests that the threshold moisture level below which ASR will not proceed can be defined by a relative humidity in the atmosphere surrounding the concrete of about 95%. A mechanistic explanation of these observations is that the relative humidity within the pores of the concrete is related to the tension in the pore moisture [10]. The pore moisture tension p″ exerts an internal isotropic compressive stress on the concrete (which is one of the reasons that concrete shrinks as it dries). Provided the moisture tension exceeds any expansive stress or swelling pressure exerted by ASR, the concrete should not expand.

Very little seems to be known of the magnitude of the swelling pressure developed in concrete by ASR. The earliest measured swelling pressures appear to be due to McGowan and Vivian [11]. Their tests showed swelling pressures of no more than 0.5 MPa. Tests conducted by Wood *et al.* [12], although full details are not given, suggest that swelling pressures of up to 4 MPa are possible in concrete. Data collected by Hobbs [5] also suggests that swelling pressures of up to 4 MPa are possible, although in one case a swelling pressure of 13.5 MPa was recorded. However, all of these measurements were made in accelerated laboratory tests. Under field conditions where the reaction takes place over years rather than weeks, relaxation of stress can be expected to reduce swelling pressures to less than the quoted values. Hence a realistic swelling pressure in the field might be 3 MPa. The Kelvin equation [10]

$$p'' = 311 \log_{10} (RH)$$

shows that a pore moisture tension (p″) of 3 MPa corresponds to a relative humidity (RH) of between 97 and 98 per cent. This is likely to be the level to which the relative humidity in the pores of the concrete must be reduced to suppress ASR expansion.

A number of authors have advocated and in some cases applied remedial measures designed to prevent the ingress of moisture into concrete structures and (hopefully) allow them to dry out to below the threshold internal relative humidity. Measures have included sealing surface cracks, injecting cracks with epoxy and other resins, and applying various surface treatments such as resin coatings or water repellent impregnations. In some cases the measures have not been completely successful in arresting the ASR [2] and in others [13] adequate follow-ups have not been made to assess the effectiveness of the treatment.

Tests of various surface treatments on a laboratory scale [10, 5, 14] have shown that none of the available surface treatments completely prevents the ingress of moisture into concrete, but that pore liner penetrants, operating as water repellents (e.g. silanes and silicones), appear to be the most effective, not only in preventing water absorption, but also in allowing water already within the concrete to dry out. Figure 1, for example [10], shows a comparison of the performance of two penetrants and two coatings applied to concrete prisms that were subjected to a regime in which misting for 6 hours was followed by drying in an ambient relative humidity of 32% for 7 days. Penetrant 1 was a silicone, penetrant 2 was an alkyl alkoxy silane, coating 1 was a cementitious slurry and coating 2 an aqueous dispersion of synthetic resins. It will be noted that regardless of the comments concerning water repellents, the drying performance of coating 2 exceeded that of the other three treatments.

Two further gaps in knowledge relating to the use of surface treatments to inhibit ASR is that little is known of how effective surface treatments are when applied to ASR-cracked concrete. Also, little is known of how concrete structures in the field dry out under natural ambient conditions. Field tests [10] have indicated that silicones are less effective at preventing moisture penetration when applied to ASR-cracked concrete than when applied to sound concrete.

Figure 2 shows interim results of an experiment (which is still in progress) to study variations in moisture in a reinforced concrete structure exposed to the weather. In this case the structure is the portal frame previously described by Blight *et al.* [3, 4]. The most severely damaged area of the portal is at the junction of the upper beam and the column. Figure 3 shows the state of the concrete surface in this area and also the results of previous unsuccessful attempts to seal the cracks by means of epoxy resin.

Thermocouple psychrometers* to measure the internal relative humidity in the concrete have been inserted at depths of 150 mm and 400 mm in the north, west and south faces of this portion of the structure. The original intention was to study variations in internal relative humidity for a complete year, then to fill the surface cracks and see what effect this had, and finally to treat the surface of the area with a silane and observe the change brought about by this procedure.

Figure 2 shows the observed variations of internal relative humidity, expressed via the Kelvin equation as pore moisture tension. The April measurements were taken at the end of the wet season and showed the concrete to be near-saturated. Over the ensuing six-month dry season, the concrete dried out progressively, with a fall in moisture tension observed during July, following unseasonal rainfall in June. In Fig. 2, the labels 150 W, 400 S, etc. refer to the depth of the psychrometer probe and the orientation of the concrete surface. It will be noted that the shallower (150) psychrometers indicated more rapid drying of the concrete nearer the surface. Also that the north face (which, being in the southern hemisphere, faces the sun) dried out more rapidly than the south face (in perpetual shade). Appreciable rain fell in October, depressing the moisture tensions once more.

*A psychrometer is a device to measure relative humidity or moisture tension.

of Concrete Caused by Alkali–Aggregate Reaction under Natural Environmental Conditions. National Building Research Institute, Pretoria, South Africa.

15. Wood, J.G.M., Johnson, A. and Norris, P. (1986) 'Management strategies for buildings and bridges subject to degradation from alkali–aggregate reaction', in Proceedings of the 7th International Conference on Concrete Alkali–Aggregate Reaction, Ottawa, Canada, pp. 178–82.
16. Blight, G.E. and Mitchell, M.F. (1980) The properties of epoxy resin mortars for use in nosings to bridge expansion joints, *Civil Engineer in South Africa*, August, pp. 203–10.
17. Blight, G.E., McIver, J.R., Schutte, W.K. and Rimmer, R. (1981) 'The effects of alkali–aggregate reaction on reinforced concrete structures made with Witwatersrand quartzite aggregate', in Proceedings of the 5th International Conference on Alkali–Aggregate Reaction in Concrete, Cape Town, South Africa, S252/15, 12 pp.
18. Vanderstraeten, A.T. (1986) 'Repair of alkali–aggregate reaction damage to the motorway structures of the Pell Street interchange, Port Elizabeth, Republic of South Africa', in Proceedings of the 7th International Conference on Concrete Alkali–Aggregate Reactions, Ottawa, Canada, pp. 194–8.
19. Houde, J., Lacroix, P. and Morneau, M. (1986) 'Rehabilitation of railway bridge piers heavily damaged by alkali–aggregate reaction', in Proceedings of the 7th International Conference on Concrete Alkali–Aggregate Reactions, Ottawa, Canada, pp. 163–7.

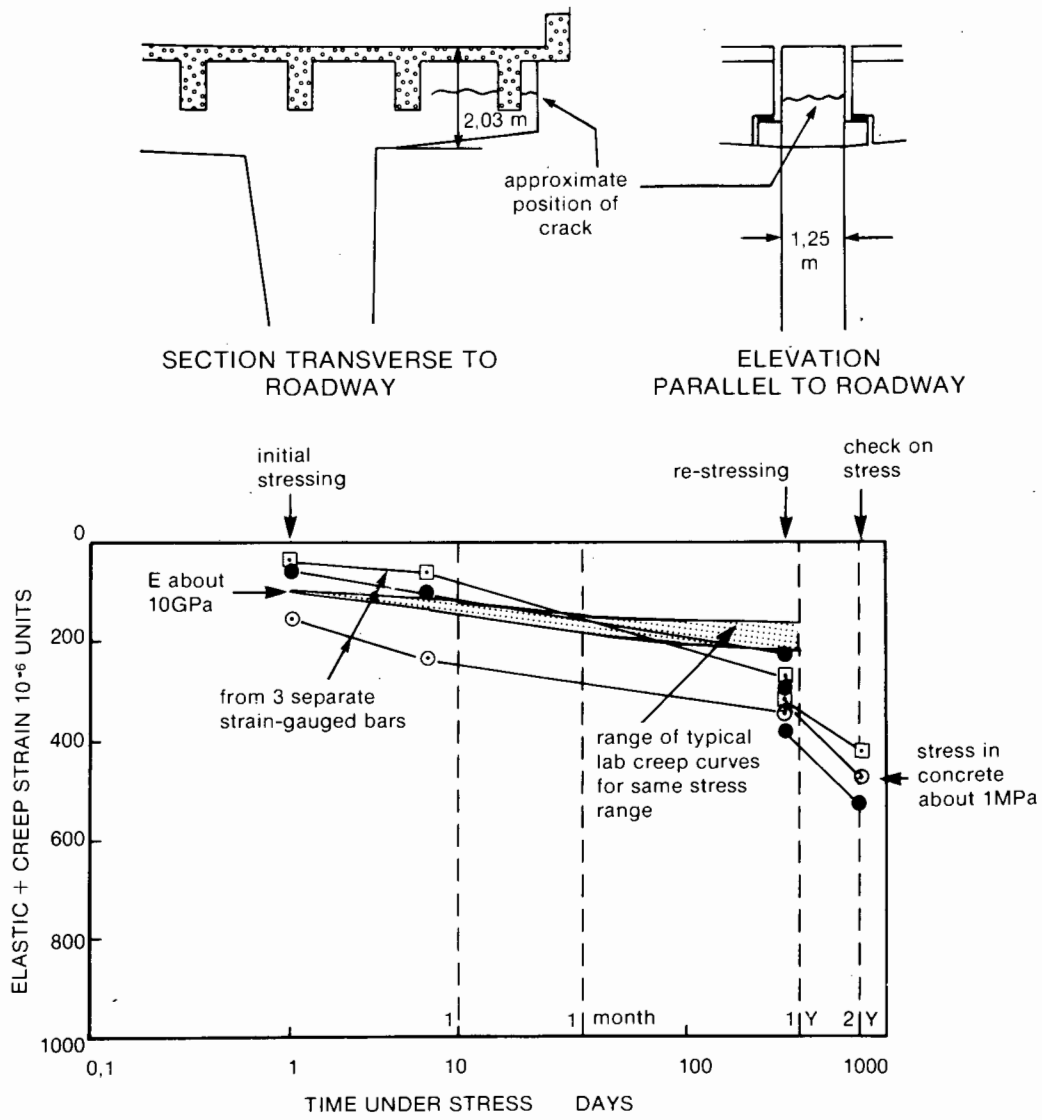

Fig. 5. Details of dimensions (above) and measurements of field creep curve (below) for concrete cantilever damaged by ASR.

external and one pair of internal high tensile steel stressing bars. Electric resistance strain gauges were glued to the concrete and used to monitor strains in order to control the stressing operation. The monitoring was continued to observe creep in the stressed concrete and also to control the subsequent re-stressing after an interval of a year.

The modulus of elasticity of the concrete, once the crack had been closed, was measured as 10 GPa which agreed with the lower limit to values of the modulus measured on cores taken from the cantilever. During the subsequent checking and adjusting of the post-stress, the loss of post-stress was used to estimate the creep that had occurred in the concrete. Figure 5 shows the resulting field creep curve which is compared with a range of laboratory creep curves measured on cores from the cantilever. The agreement between field and laboratory measurements was reasonable up to about 100 days. Thereafter, the field creep considerably exceeded that measured in the laboratory. When the measurements were terminated after 2 years, the effective modulus of elasticity of the concrete had declined from 10 GPa to just over 2 GPa. As time has been shown on a log scale in Fig. 5, it is not obvious that the field rate of creep strain actually declined from 160 × 10^{-6}/y in year 1 to 100 × 10^{-6}/y in year 2.

At the time of writing, 7 years after the repair was effected, there has been no further visual deterioration of the cantilever. Other similar repairs carried out by stressing have been reported from Japan [5] and from South Africa [17, 18]. In the one case [17] where moment continuity at a beam-to-column connection was restored by post-stressing, the post-stress was checked and adjusted twice at yearly intervals. On both occasions the loss of post-stress in the preceding year was small. In a second case [18], post-stressing was used to tie together a pile cap that had cracked as a result of ASR. Here, no monitoring of the repair seems to have been carried out.

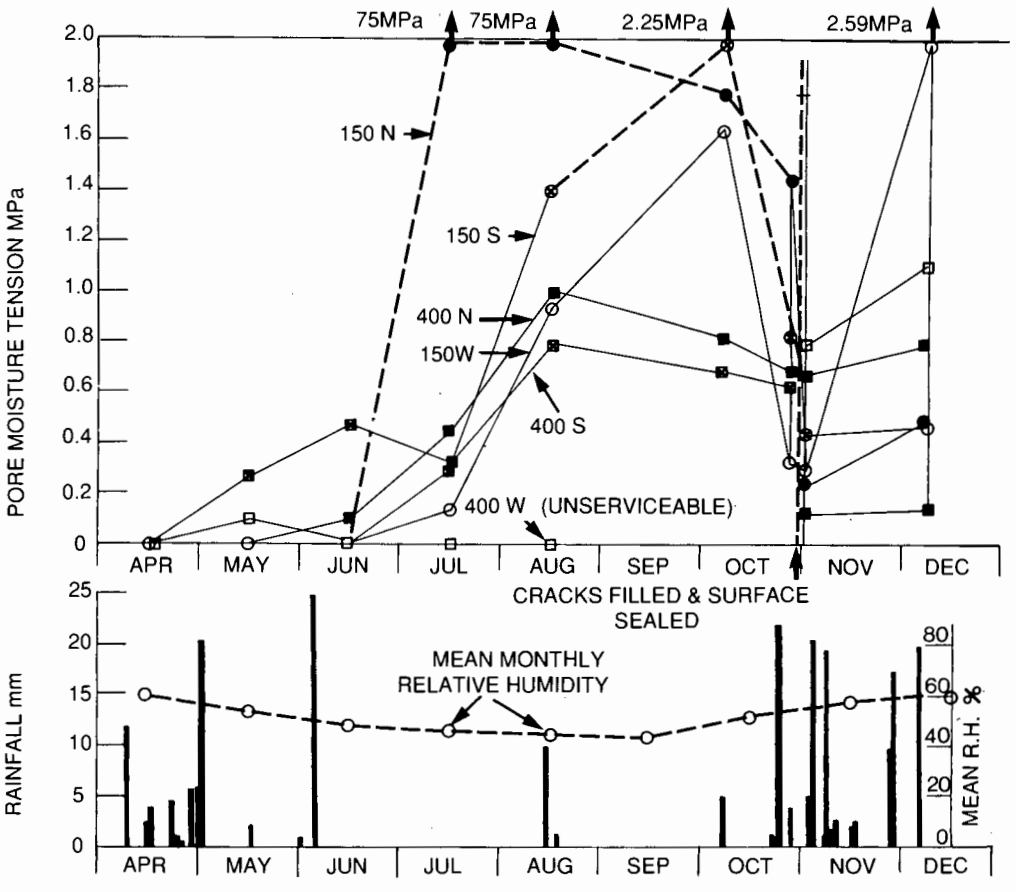

Fig. 2. Moisture tensions observed during seasonal drying of ASR-damaged concrete in the natural environment of Johannesburg, South Africa.

Obviously, any ASR expansion occurring after grouting would undo much of the work of the grout. Imai *et al.* [2] used epoxy resin injection grouting to restore the integrity of a double cantilever beam supporting an expressway that had deteriorated by ASR. Before the repair ultrasonic pulse velocity (UPV) measurements made on the concrete averaged 2.7 km/s (although it is not clear if the measurements were made in situ or on cores). After grouting, Imai *et al.* report that the UPV had been restored to above 3 km/s and on this basis regarded the repair as having been successful.

Without questioning the validity of their measurements, it must be pointed out that while the increase in UPV certainly showed that the sonic discontinuities in the concrete had been reduced, the mechanical properties may not have been much improved, as a similar result would probably have ensued if the cracks had been injected full of a low strength material such as grease.

Portland cement grout would probably be an ideal material for injection grouting ASR-cracked concrete were it not for two factors:

1. Injection with Portland cement would increase the alkali content of the concrete and possibly accelerate or reactivate the ASR; and
2. the particles of Portland cement powder (even rapid-hardening cement) are of too large a size to penetrate very fine cracks.

Hence it is necessary to consider resin grouting for repairs to ASR-damaged concrete. There are a number of requirements that a resin used for injecting ASR-damaged concrete should meet:

1. It should have a sufficiently low viscosity to enable it to penetrate fine hair cracks using very moderate injection pressures.
2. It should nevertheless not have such a low viscosity that it becomes absorbed into the pores of the concrete on either side of a crack so that the crack empties when injection ceases.
3. Cracks generated by ASR can be expected to contain powdery or gel-like reaction products. The resin should have excellent wetting properties so that it can penetrate these products and wet the intact concrete forming the crack sides.
4. Cured resins generally have coefficients of thermal expansion that are as much as 50 times that of concrete. In the exposed field situation, cyclic thermal stresses will therefore be set up at the resin–concrete interface. The resin must be able to accommodate this movement by creep, otherwise it will debond from the concrete [16].
5. If the injection is to improve the mechanical properties of the concrete, its shear and elastic moduli should equal or exceed those of the intact concrete.

Unfortunately requirements 4 and 5 are probably incompatible.

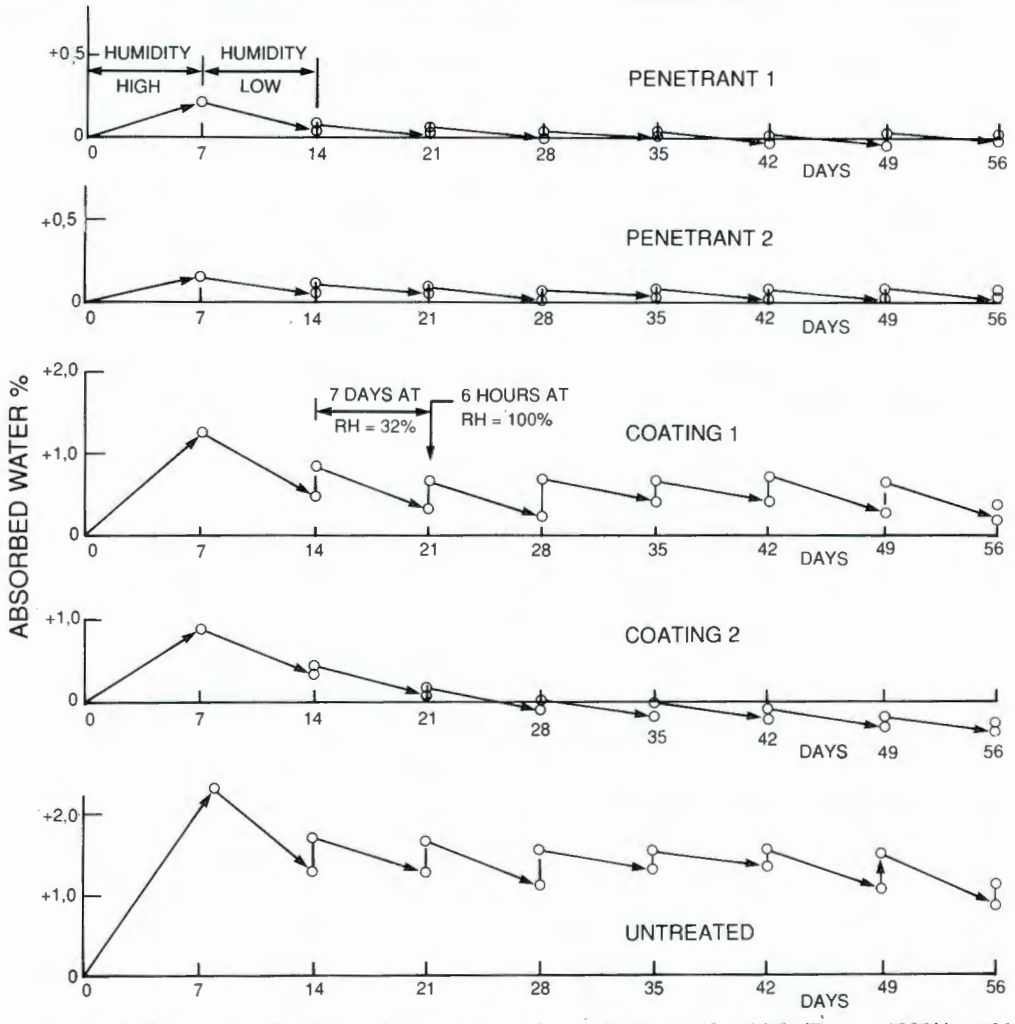

Fig. 1. Progressive drying of treated and untreated concrete specimens in alternating high (RH = 100%) and low (RH = 32%) humidity environments

It should be noted particularly that even in the very dry winter climate of Johannesburg, where the relative humidity averages less than 50%, only the 150 N-probe on the north face indicated a moisture stress sufficiently high to arrest ASR.

In late October, the owners of the structure decided to fill in the larger surface cracks in the portal using a quick-setting Portland cement-based mortar, and to paint over the fine surface cracks with a slurry of the same material. As Fig. 2 shows, this treatment seems to have had a beneficial effect as the pore moisture tension increased in the November–December period even though there was a lot of rain.

Although the experiment is incomplete, the results throw doubt on whether it is possible to dry the concrete of an exposed ASR-damaged structure in a climate wetter than that of Johannesburg, for example the damp climate of the UK, without taking special measures to exclude impinging rain.

It must be concluded that not enough is yet known of how to arrest the ASR in full-scale field situations. The writer's personal opinion is that only one type of solution has any chance of long-term success. This is the use of what Wood *et al.* [15] describe as ventilated claddings, although the option may be costly. In the case of the Johannesburg portal it has been proposed to clad the entire upper portal beam in a ventilated tube constructed of sheet metal and supported by the portal. The structure can easily carry the additional load. The cladding would allow the concrete it encloses to dry out over a period of a few years, thus arresting the ASR. Unfortunately, in this case the provision of cladding appears to cost much the same as solutions involving partial demolition and reconstruction. For the reasons given later the ventilated cladding solution seems unlikely to be put into effect in this case.

3. CORRECTING STRUCTURAL DEFICIENCIES

By its deteriorative nature, ASR inevitably causes structural deficiencies to develop that may necessitate remedial action. The type of repair may take several possible forms. Two types of limited repair will be discussed here: injection grouting and post-stressing.

3.1 Repair by Injection Grouting

A pre-requisite for this type of treatment is that the ASR should have been arrested or should have ceased.

Fig. 3. Appearance of portion of structure referred to in Fig. 2.

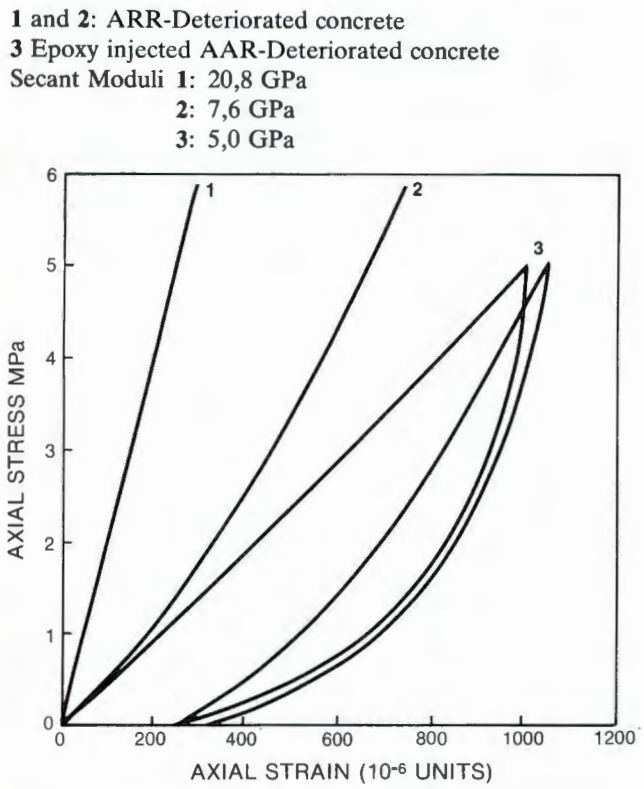

Fig. 4. Comparison of stress–strain curves for ASR-damaged concrete and ASR-damaged concrete that has been injected with epoxy resin.

A large (5 m by 5 m by 2.5 m deep) reinforced concrete foundation block in Johannesburg showed severe cracking as a result of ASR. It was decided to attempt a repair by means of epoxy resin injection grouting. Cores of the affected concrete were taken prior to injection and further cores were taken after injection to examine the success of the operation. The resin was carefully formulated to comply with requirements 1–4 above with 4 being tested by means of the Shaw test [16].

The results of the post-injection examination were disappointing. Penetration of the cracks was poor because the low allowable injection pressures were not enough to force the resin into the fine cracks. Many wide cracks also remained unpenetrated because they were not interconnected with cracks along which resin was able to flow. The resin had in many places not wetted the sides of the cracks and had not bonded to the concrete.

Figure 4 shows the results of a compression test on a core of epoxy-injected concrete from the foundation block. The test is compared with the results of two tests made on cores taken before the injection.

The results were again disappointing. The injected core was divided in two by a wide diagonal resin-filled crack. The resin had obviously imparted a reasonable strength to the core, but the compression modulus (5 GPa) and the residual deformation were clearly not acceptable.

It may be concluded that considerable development is still required before resin injection grouting becomes an acceptable and reliable means of repairing ASR-affected concrete. In particular, the incompatibility between the necessary creep characteristics and the required mechanical properties of the resin needs to be eliminated or substantially reduced.

3.2 Repair by Post-stressing

A cantilever projection on the side of a portal frame supporting an elevated highway had, as a result of ASR, developed a horizontal crack. The layout of the cantilever and the position of the crack are shown in Fig. 5. The cantilever supports a series of simply supported beams, as shown in elevation in Fig. 5, and a repair therefore had to be effected without delay. As an interim safety measure, the traffic lane adjacent to the cracked cantilever (which happened to be the slow lane) was closed to traffic.

The repair was made by stressing the upper and lower portions of the cantilever together with one pair of

4. REPAIR BY PARTIAL DEMOLITION AND RECONSTRUCTION

When structures that are in the public eye are considered, a decision to demolish and rebuild rather than to repair or attempt to arrest the ASR may be taken at least partly for non-technical reasons. The official reason for radical action is usually that it is in the interests of public safety. However, such a decision often arises partly out of officialdom's desire to be seen as people of action who do not procrastinate when there is a problem to be solved. The decision to strengthen the Charles Cross parking garage in Plymouth, after loading tests had shown that the strength of the structure was little affected by ASR, probably falls into this category.

The method of rehabilitation chosen for a series of railway bridge piers in Canada [19] also appears to fall within the category of a partly political decision. The 40-year-old concrete exposed above the water line showed severe ASR deterioration compounded by freeze–thaw damage. Coring of the piers was undertaken to establish the properties of the deteriorated concrete. The lowest values of strength and elastic modulus occurred in the top 3 metres of the approximately 16 m high piers. The minimum compressive strength measured on cores was 22.8 MPa, and ranged up to 31.6 MPa. The elastic modulus varied between 13 GPa and 22.8 GPa, and the splitting tensile strength averaged 2.5 MPa. The piers were massive, and these mechanical properties must have been adequate to support the applied loads. Also, the concrete was 40 years old and the rate of further deterioration must at that stage have been minimal. Nevertheless, a decision was made to demolish the piers above the water level and to reconstruct them.

As far as the writer knows, there has so far been no case of repair by partial demolition and re-building that could be justified purely on technical grounds. As mentioned earlier, a public relations based decision may well also decide the fate of the highway portal frame described by Blight *et al.* [4].

5. CONCLUSIONS

Existing published experience of the repair and rehabilitation of reinforced concrete structures damaged by ASR has been reviewed under the headings of: arresting the ASR process; correcting structural deficiencies; and partial demolition and reconstruction. It is concluded that not enough is known of how to arrest ASR in the field situation, although, in combination with surface cosmetic treatment, this is potentially the most useful way of rehabilitating ASR-damaged structures. The correction of structural deficiencies has been attempted by means of resin injection and by the application of post-stressing. Where its application is appropriate, post-stressing appears a viable way of repairing damage caused by ASR. Resin injection has not been proved successful, but is potentially a useful repair procedure.

Finally, although few cases of partial demolition and reconstruction are on record, it appears that the decision to take this option will usually be at least partly motivated by local politics and considerations related to maintaining a good public image.

REFERENCES

1. Blight, G.E. and Alexander, M.G. (1986) 'Assessment of AAR damage to concrete structures', in Proceedings of the 7th International Conference on Concrete Alkali–Aggregate Reactions, Ottawa, Canada, pp. 121–5.
2. Imai, H., Yamasaki, T., Maehara, H. and Miyagawa, T. (1986) 'The deterioration by alkali–silica reaction of Hanshin expressway concrete structures – investigation and repair', in Proceedings of the 7th International Conference on Concrete Alkali–Aggregate Reactions, Ottawa, Canada, pp. 131–5.
3. Blight, G.E., Alexander, M.G., Schutte, W.K. and Ralph, T.K. (1983) 'The effects of alkali–aggregate reaction on the strength and deformation of a reinforced concrete structure', in Proceedings of the 6th International Conference on Alkalis in Concrete, Copenhagen, Denmark, pp. 401–10.
4. Blight, G.E., Alexander, M.G., Ralph, T.K. and Lewis, B.A. (1989) Effect of alkali–aggregate reaction on the performance of a reinforced concrete structure over a six-year period. *Magazine of Concrete Research*, **41** (147) 69–77.
5. Hobbs, D.W. (1988) *Alkali–silica Reaction in Concrete*. Thomas Telford, London.
6. Vivian, H.E. (1950) The effect on mortar expansion of amount of available water in mortar. *Studies in Cement Aggregate Reaction XI*, CSIRO, Australia, Bulletin 256.
7. Gudmundsson, G. and Asgeirsson, H. (1983) 'Parameters affecting alkali expansion in Icelandic concretes', in Proceedings of the 6th International Conference on Alkalis in Concrete, Copenhagen, Denmark, pp. 217–22.
8. Nilsson, L.O. (1983) 'Moisture effects on the alkali–silica reaction', in Proceedings of the 6th International Conference on Alkalis in Concrete, Copenhagen, Denmark, pp. 201–8.
9. Hawkins, M.R. (Chairman) (1983) 'Minimizing the risk of alkali–silicate reaction'. Report of Working Party, Cement and Concrete Association, UK.
10. Blight, G.E. (1989) 'Experiments on waterproofing concrete to inhibit AAR', in Proceedings of the 8th International Conference on Alkali–Aggregate Reaction, Kyoto, Japan, pp. 733–9.
11. McGowan, J.K. and Vivian, H.E. (1955) The effect of superincumbent load on mortar bar expansion. *Studies in Cement–Aggregate Reaction XXIII, Australian Journal of Applied Science*, **6** (1) 94–9.
12. Wood, J.G.M., Young, J.S. and Ward, D.E. (1986) 'The structural effects of alkali–aggregate reaction on reinforced concrete', in Proceedings of the 7th International Conference on Concrete Alkali–Aggregate Reactions, Ottawa, Canada, pp. 157–62.
13. Hoppe, G.E. (1986) 'Rehabilitation of an arch bridge', in Proceedings of the 7th International Conference on Concrete Alkali–Aggregate Reactions, Ottawa, Canada, pp. 199–203.
14. Putterill, K.E. and Oberholster, R.E. (1985) *Investigations of Different Variables that Influence the Expansion*

Protection of Concrete

Proceedings of the International Conference,
held at the University of Dundee, Scotland, UK,
on 11-13 September 1990

Edited by

Ravindra K. Dhir
Director, Concrete Technology Unit,
University of Dundee
and
Jeffrey W. Green
Industrial Consultant in Concrete Technology,
University of Dundee

E. & F.N. SPON
An Imprint of Chapman and Hall
LONDON . NEW YORK . TOKYO . MELBOURNE . MADRAS

CAN CONCRETE STRUCTURES BE WATERPROOFED TO INHIBIT ASR?

G E Blight

University of the Witwatersrand,

South Africa

ABSTRACT. The hypothesis is advanced that if concrete can be dried out so that the relative humidity in its pores is less than about 97%, expansion resulting from alkali silica reaction (ASR) will be inhibited or eliminated. The paper then goes on to explore the possibility of maintaining reinforced concrete structures that are exposed to the weather, in the necessary state of desiccation. The observations raise severe doubts as to the practicality of successfully applying the hypothesis, especially to structures that have already suffered damage from ASR.

Keywords: Alkali silica reaction, moisture, humidity, waterproofing, drying.

Geoffrey E Blight is Professor of Construction Materials and Head of the Department of Civil Engineering at the University of the Witwatersrand, Johannesburg, South Africa. His research interests include the behaviour of ASR - affected structures, loading on bins and silos, the disposal of mining and industrial solid waste and the properties and behaviour of tropical and residual soils.

INTRODUCTION

Forty years ago Vivian[1] showed that the amount of expansion that occurs in cement mortars as a result of alkali silica reaction (ASR) depends on the amount of removable water in the mortar. Vivian's original results are reproduced in Figure 1. If the removable water was less than 4% by dry mass, no expansion due to ASR occurred. Once the removable water exceeded 4% the expansion became directly proportional to the excess of removable water over 4%. Vivian called this excess the available water. Removable water was defined as the water lost after prolonged storage over calcium chloride (a relative humidity of 32%). The available water is that part of the total water that is loosely held in capillaries in the mortar. Note from Figure 1 that the available water may be contained within the concrete ab initio (sealed specimens) or be allowed to penetrate the mortar from outside (unsealed specimens) after some drying has occurred. Assuming that Vivian's results on mortar are applicable to concrete, it would appear that if the available water in concrete can be kept to zero, expansion by ASR will be minimized.

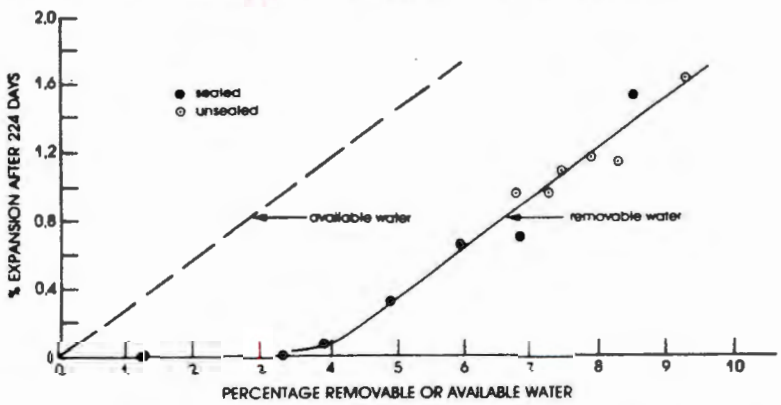

Figure 1: Vivian's observed relationship between removable water and expansion

Other evidence[2,3,4,5] has shown that if the relative humidity in the atmosphere surrounding a concrete structure can be maintained at below 95%, ASR will be inhibited. However, the relative humidity of the surroundings is unlikely to be the same as the relative humidity in the pores of the concrete where the ASR takes place. Water in the pores of concrete maintained at a relative humidity of less that 100% is in a state of tension or suction. The pore water tension is balanced by compressive stress in the solid components of the concrete. The net effect is that any expansive stresses are counterbalanced, partly or completely, by the pore water tension or suction.

The relative humidity (RH) in a porous material can be related to the pore water suction p^- by the Kelvin equation[6]:

$$p^- = 311000 \log_{10}(RH) \text{ in kPa}$$

where RH is expressed as a fraction of unity, eg 0.95.

At a RH of 0.95, the suction is nearly 7000 kPa. Even if the suction is not completely effective in compressing the concrete there must, at RH = 0.95, be an isotropic compressive stress in the concrete of several thousands of kPa.

Hence one obvious way of inhibiting ASR is to dry the interior of the concrete out until the suction exceeds the swelling pressure developed by the ASR, and then maintain it in that condition by means of a waterproofing layer or coating. Based on observed values of the swelling pressure exerted by ASR, it appears that if the suction within the concrete can be maintained at above 5000 kPa (RH below 0.97) expansion caused by ASR should be eliminated or much reduced.

This paper describes two field experiments to probe the practicality of maintaining full-scale structures, exposed to the weather, in the required state of desiccation.

It should be emphasized that the climate of Johannesburg, where the tests were performed, is particularly favourable for this type of approach. The highest short period atmospheric relative humidity is 96% while the average maximum is only 75%. During the dry winter months, the average maximum relative humidity is below 65% and the average minimum relative humidity is less that 40%.

FIELD EXPERIMENTS INVOLVING ARTIFICIAL WETTING FOLLOWED BY DRYING

A group of columns supporting an overhead motorway was selected for the first field trial. The column shafts are completely protected from impinging rain by the overhead structures they support. This situation was chosen deliberately so that the moisture condition of the column surfaces could be controlled artificially. The columns were cleared down with high pressure water jets. Four columns, selected at random were each waterproofed with a different waterproofer, under the supervision of the suppliers of the preparations. A fifth column was left untreated as a control. The waterproofers consisted of :

Coating 1: A Portland cement - based resin - modified slurry.

Coating 2: An aqueous emulsion of synthetic resins.

Penetrant 1: A silicone in a hydrocarbon solution.

Penetrant 2: An alkyl alkoxy silane solution.

All preparations were applied by brush.

The effect of wetting and drying was assessed by inserting thermocouple psychrometer probes to a depth of 100mm into holes drilled into the columns. A psychrometer probe[7] consists of a thermocouple sealed into a cavity in the concrete. The air in the cavity comes to thermal and moisture equilibrium with the atmosphere in the concrete. A current is passed thorough the thermocouple which cools by the Peltier effect until the temperature falls below the dew point of the moisture in the surrounding air. Moisture then condenses on the thermocouple junction. The cooling current is interrupted and the condensed moisture starts to evaporate at the dew point temperature. The thermocouple is used to measure this temperature and hence the relative humidity in the cavity and the related pore water suction (p^-) in the concrete can be determined via the Kelvin equation. The measuring range of the psychrometer is from RH = 1.00 to about RH = 0.96. Below RH = 0.96 it is not possible to condense water out of the atmosphere by cooling the air. The range covers the RH range of interest of 0.97 to 1.00.

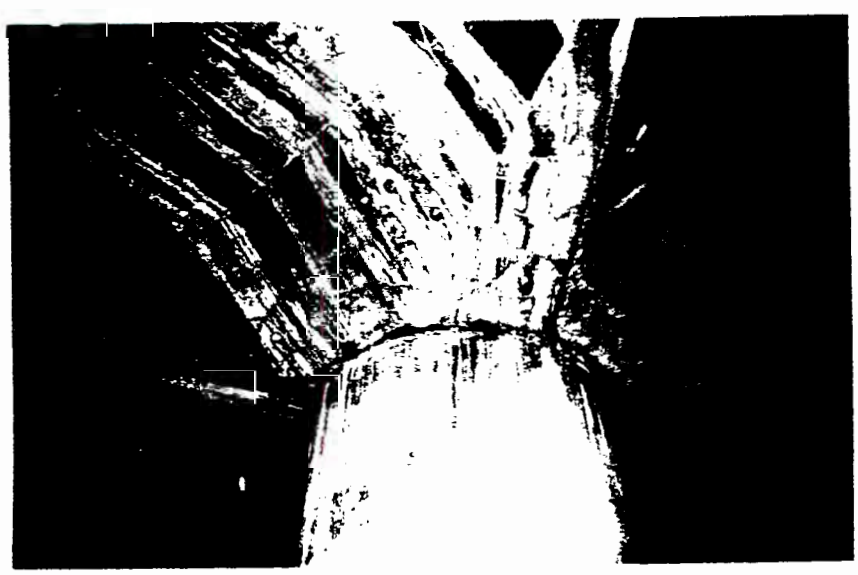

Figure 2: Test column that was waterproofed and subjected to artificial wetting. Note cracks from ASR in shaft and mushroom slab.

Figure 2 shows one of the columns that were the subject of the experiment and Figure 3 shows a psychrometer installed in one of the columns. Figure 4 shows the results of two sets of measurements on the untreated control column and the column treated with Penetrant 1 (silicone). Not all of the columns are in the same physical condition. Some are completely sound, but others show signs of ASR

attack, in the form of cracks in the columns, or in the mushroom slabs they support, or both. As it happened, the control column is completely sound whereas the silicone-treated column has a badly cracked mushroom slab, although the column itself has only minor cracks in it.

Figure 3: Psychrometer probe installed in side of column, and protected from water by clear plastic cylinder

The left hand section of Figure 4 Shows results of preliminary measurements on the two columns to establish the range of $\bar{p}$ or RH to be expected. $\bar{p}$ in the control column was very high (more than 5000 kPa) and the measurements eventually went out of range. $\bar{p}$ in the silicone-treated column, however, was unexpectedly low (2000 kPa) and after a spell of heavy rain, reduced even further. A few days later streaks of white ASR gel appeared through cracks in the column and ran down the surface. This showed that water was entering the column via the structure it supports and causing further ASR. The silicone treatment was quite ineffective as the water was not entering through the surface of the column. In a second series of tests conducted during very hot dry weather, initial $\bar{p}$ readings were taken and the columns were then watered continually by hose over a period of six hours on three consecutive days to represent as severe a condition of wetting as is ever likely to occur on an outside structure.

The wetting caused $\bar{p}$ in the control column to fall from beyond the range of the psychrometer to only 350 kPa (Figure 4). After 3 days of drying, the $\bar{p}$ was again out of range.

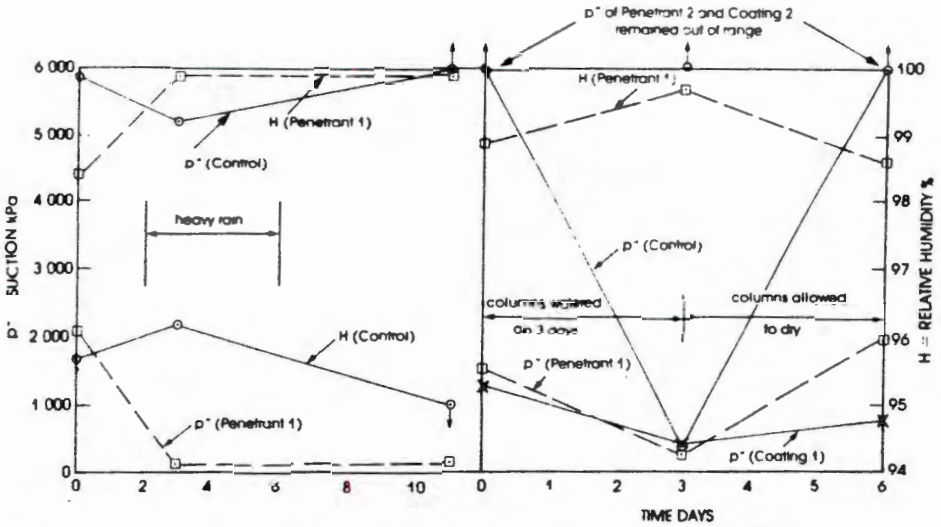

Figure 4: In-situ psychrometer measurements in two columns supporting overhead structure

p^- in the silicone treated column started at 1500 kPa, fell to 250 kPa after 3 days watering and then rose again to 1900 kPa after 3 days of drying. This indicated that water was entering the concrete through pre-existing cracks, even though the surface had been treated. There was no rain during the test and the water could not have been entering through the superstructure. However, atmospheric drying removed the water relatively quickly.

These tests led to the following conclusions:

1. If there is no internal source of water from, for example a blocked internal drainage pipe, etc, sound concrete in a dry climate will quickly dry out after being surface wetted. It probably does not need to be waterproofed.

2. If there is an internal source of water it is pointless to waterproof the exterior of the concrete.

3. Water will probably enter the surface of cracked concrete even if the surface has been treated with a water repellent.

The column treated with Coating 1 is also cracked by ASR. p^- in the column started at 1200 kPa, but fell to 300 kPa after the period of watering. Three days later p^- has increased but was still at a relatively low 800 kPa. These results confirm that water can enter a concrete member through surface cracks, even if the surface has been treated. The rate at which the structure dries again will depend on the type of treatment and the climate.

The column treated with Coating 2 is in sound condition. That treated by Penetrant 2 is cracked, but the psychrometer probe was inserted in an area of sound concrete. p^- recorded in these two columns started out of measuring range and remained out of range even after the watering. This shows that waterproofing treatments can assist in preventing concrete from absorbing water. However, a previous investigation by the author[8] has shown that many preparations sold as "waterproofers" for concrete are not really effective as such.

FIELD OBSERVATIONS OF A STRUCTURE EXPOSED TO THE WEATHER

For the second stage of this study, variations of suction with time were observed within portion of a reinforced concrete portal frame that had deteriorated severely as a result of ASR. Full details of this structure have been published elsewhere[9]. The variation of suction in the damaged concrete was observed for six months, after which the larger surface cracks were filled using quick-setting Portland cement-based mortar and the finer cracks were painted over with a slurry of the same material. Figure 5 shows the structure as it appeared after application of the surface coating.

Figure 5: Knee of portal frame that is subject of measurements shown in Figure 6. Dark areas show where large cracks were filled.

Psychrometers were installed from faces of the portal oriented north, west and south, at depths of 150mm and 400mm from each face. As the thickness of concrete in the north-south direction is 1250mm, the deeper psychrometers were close to the axis of the structure.

Figure 6 summarizes the observed variations of suction. In this diagram 150S, 400S etc represent the depth of the psychrometer (150mm or 400mm) and the orientation (N,S,W) of the face from which it is installed. The first two months of observation were dry and suctions recorded at 150 mm depth rose to about 2000 kPa. At 400mm, however, the suction did not rise above 1000 kPa. Rain at the end of October caused the suction to plummet to the region of 500 kPa.

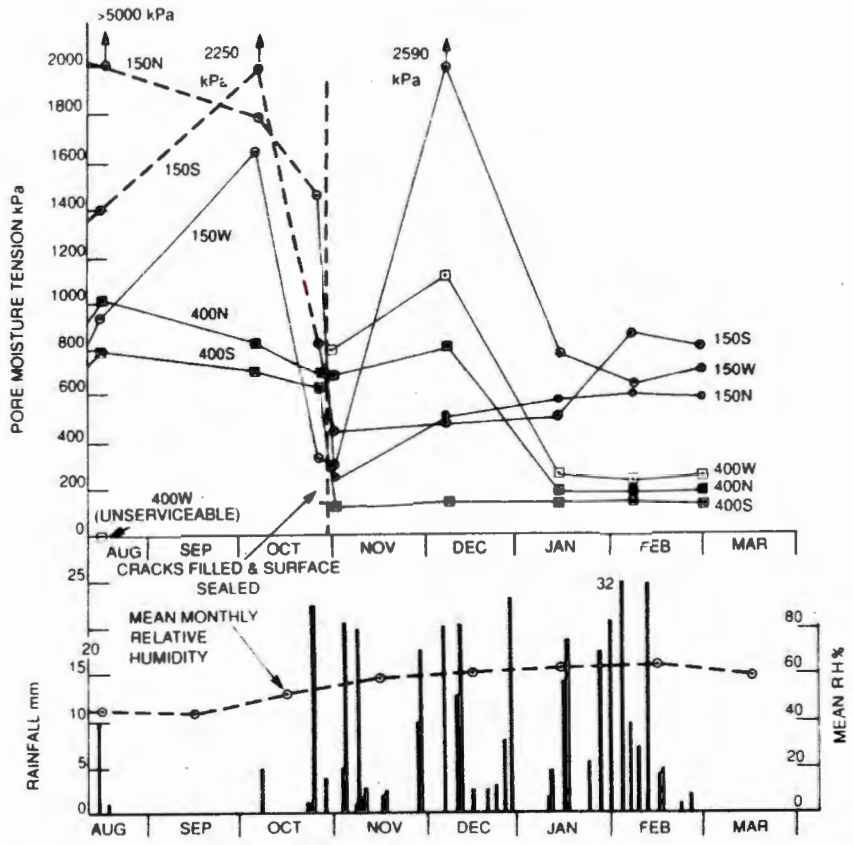

Figure 6: Variations of suction observed in the knee of the portal frame shown in Figure 5

At the end of October the crack repairs and surface sealing were carried out. At this time the psychrometers were overhauled and 400W which had been unserviceable, was replaced. After an initial period of rather wide fluctuation, the suctions have now settled down into two groups. At 150mm depth the suction is 400 to 800 kPa, while at 400mm depth it is much lower, at about 200 kPa. There seems to be little doubt that sealing the cracks when suctions were low has entrapped moisture within the concrete. Over the four months since sealing, this moisture has distributed itself and the moisture regime within the concrete is now relatively stable.

Figure 6 shows that the suction is essentially unaffected by incident rainfall, even if this is heavy and of frequent occurrence.

However, it will be noted that during the dry months, the suction did not reach the level of 5000 kPa considered necessary to inhibit ASR. Now that the surface has been sealed, the suction has stabilized at well below the level necessary for inhibition. Hence, it does appear that even if the sealing had been carried out before the first rain of the season, when the suction was at its maximum, the resultant suction in the sealed structure would still have been well below 5000 kPa.

Hence it may be concluded that even in the relatively dry climate of Johannesburg, it is unlikely that a structure that has been damaged by ASR and which is exposed to the weather, will dry out sufficiently in dry weather to reach a suction sufficient to inhibit ASR. Sealing the surface of an exposed structure damaged by ASR will result in stabilization and evening out of the moisture within the structure, but a suction level sufficient to inhibit ASR is unlikely to be reached.

GENERAL CONCLUSIONS

The hypothesis has been advanced that a reinforced concrete structure subject to ASR attack can be protected by waterproofing it, thus maintaining the concrete in a dry enough state to inhibit the ASR.

However, the measurements described in this paper show that there are serious practical difficulties in attaining this ideal condition. The only really practical way of protecting an ASR - damaged structure appears to be to shield it from incident rainfall by means of a specially constructed canopy or enclosure. The provision of such external protection would allow the concrete to dry out progressively over a period of several years, until a level of moisture sufficiently low to inhibit ASR is reached.

REFERENCES

1 VIVIAN H E. The effect on mortar expansion of amount of available water in mortar. Studies in Cement-Aggregate Reaction XI, CSIRO, Australia, Bulletin 256, 1950.

2 GUDMUNDSSON G and ASGEIRSSON H. Parameters affecting alkali expansion in Icelandic concretes. Proc. 6th International Conference Alkalis in Concrete, Copenhagen, 1983, pp 217-222.

3 NILSSON L O. Moisture effects on the alkali-silica reaction. Proc. 6th International Conference Alkalis in Concrete, Copenhagen, 1983, pp 201-208.

4 LUDWIG U. Effects of environmental conditions on alkali-aggregate reaction and preventative measures. Proc. 8th International Conference Alkali-Aggregate Reaction, Kyoto, Japan, 1989, pp 503-596.

5 HAWKING M R (Chairman). Minimizing the risk of alkali-silica reaction. Report of Working Party, Cement and Concrete Association, UK, 1983.

6 BLIGHT G E. Strength characteristics of desiccated clays. Journal Soil Mech and Found Div, ASCE, 92, SM6, 1966, pp 19-37.

7 SAVAGE M J and CASS A. Measurement of water potential using in-situ thermocouple hygrometers. Advances in Agronomy, 37, 1984, pp 73-126.

8 BLIGHT G E. Experiments on waterproofing concrete to inhibit AAR. Proc. 8th International Conference Alkali-Aggregate Reaction, Kyoto, Japan, 1989, pp 733-740.

9 BLIGHT G E, ALEXANDER M G, RALPH T K and LEWIS B N. Effect of alkali-aggregate reaction on the performance of a reinforced concrete structure over a six-year period. Magazine of Concrete Research, 41 (147), 1989, pp 69-77.

Magazine of Concrete Research, 1991, **43**, No. 156, Sept., 197–203

A study of four waterproofing systems for concrete

G. E. Blight*

WITWATERSRAND UNIVERSITY, SOUTH AFRICA

As part of a study of possible mitigatory measures for concrete structures damaged by alkali–aggregate reaction, four treatments for waterproofing concrete (two coatings and two pore liner penetrants), have been compared. Tests were performed both on small specimens in the laboratory and on full-size structures in the field. It was found that none of the systems waterproofed concrete completely, but that three of them initially reduced the rate of water penetration, particularly under field conditions. Following initial tests, the laboratory specimens were exposed to the weather for four years, after which time the earlier tests were repeated. The effectiveness of the treatments applied in the field was also reassessed after four years. On the laboratory specimens, all treatments had apparently become more effective. In the field, the treatments had evidently retained moisture in the concrete, i.e. they had done precisely the opposite of what is required of a waterproofing system.

Introduction

It has long been known from laboratory tests that alkali–silica reaction (ASR) in concrete can be prevented or halted if the concrete is kept dry. Available evidence (e.g. Refs 1–4) shows that if the relative humidity surrounding concrete can be maintained at below 95%, ASR will cease. It is therefore tempting to speculate that if concrete susceptible to ASR were first dried to below the critical internal relative humidity and then waterproofed, existing ASR would cease and potential ASR would not occur. However, this ideal state of affairs is not easy to achieve in practice.

A series of laboratory experiments was performed on concrete specimens waterproofed by means of four commercially-promoted treatments. The experiments were performed shortly after the treatments had been applied, and were repeated after the treated specimens had been exposed to the weather for four years.

Simultaneously, a programme of field experiments was undertaken on a series of reinforced concrete columns supporting a motorway structure. These experiments were also reassessed after four years. The early results of this programme were reported by Blight.[5]

Types of waterproofer used in investigation

References 6 and 7 identify five types of waterproofer for concrete:

(*a*) pore liner penetrants, usually operating as water repellents
(*b*) pore blocker penetrants that seal surface pores
(*c*) sealers that form an impervious surface skin on the concrete
(*d*) coatings that form a thick impervious surface skin
(*e*) renderings (thick coatings), usually applied by trowel.

Two pore liner penetrants and two coatings were used in the present study. The descriptions given by the suppliers (with brand names in parentheses) were

(*a*) silicone—a silicone in a hydrocarbon solvent (Barrasil)
(*b*) silane—an alkyl alkoxy silane (Dynamit Nobel)
(*c*) cement slurry—a cement-based resin-modified slurry (Embecon)
(*d*) resin emulsion—an aqueous emulsion of synthetic resins (Sika).

Laboratory tests

100 mm × 100 mm × 200 mm prisms of concrete were oven dried to constant mass at 50°C. A set of

*Witwatersrand University, Johannesburg, PO Wits, 2050, South Africa.

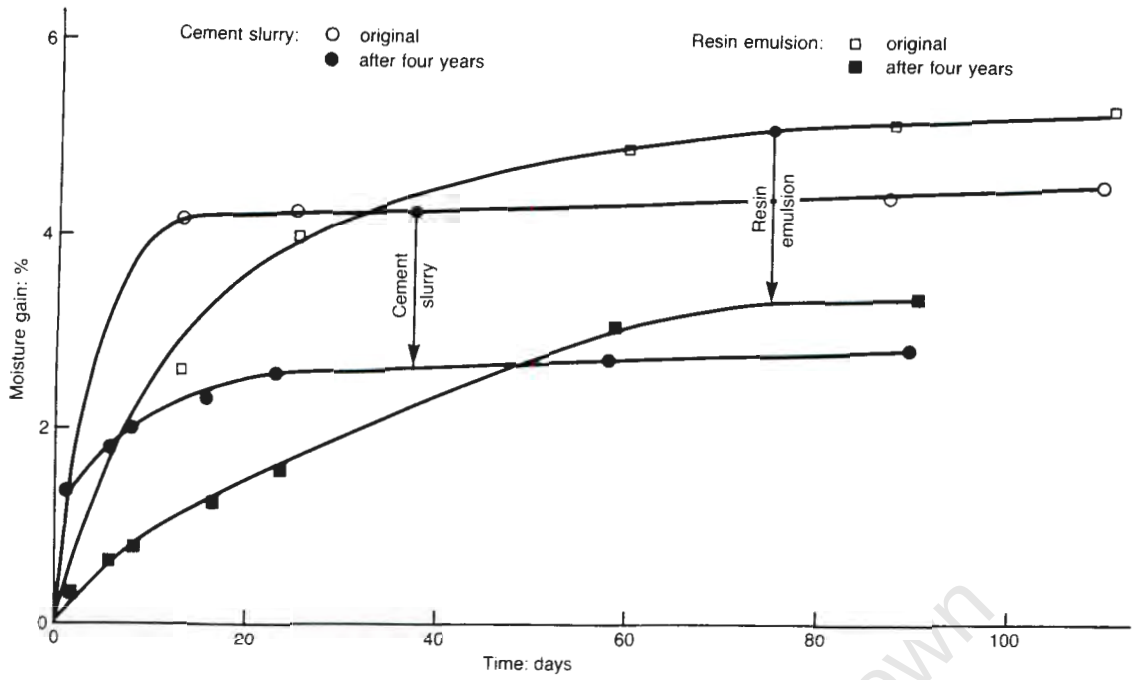

Fig. 2. Variation of moisture gain with time for specimens treated with cement slurry and resin emulsion

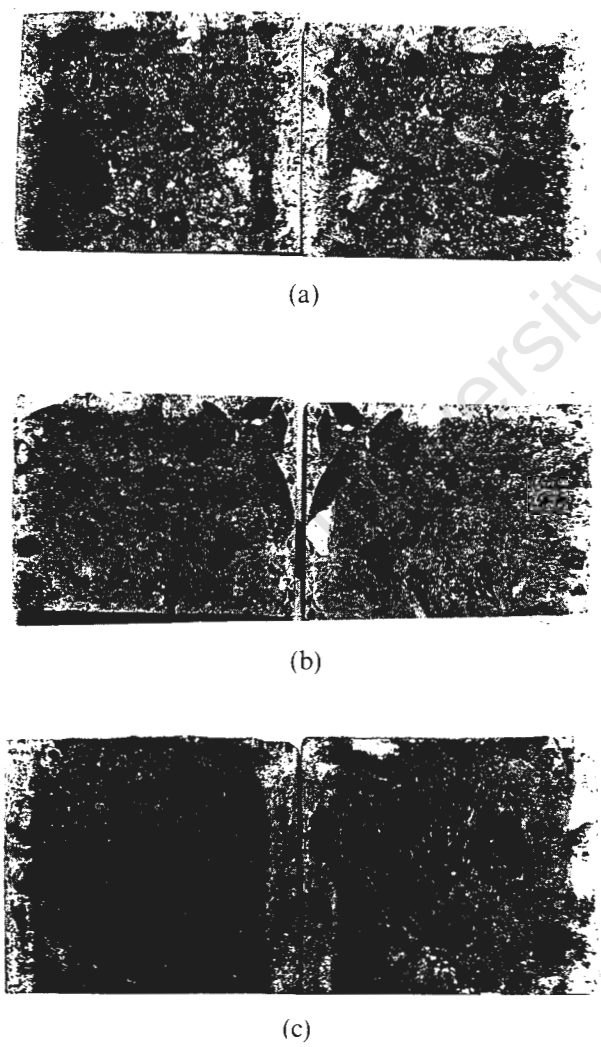

Fig. 3. Depths of carbonation in test prisms treated with (a) silicone; (b) silane and (c) cement slurry

directed normal to their exterior surfaces, indicated that the permeability of untreated uncarbonated concrete was about five times that of the carbonated exterior surfaces of the control specimens, and that the oxygen permeability of the silane-treated surfaces was about twice that of the other surfaces. The silane was thus, after four years, still acting as a water repellent, as well as inhibiting carbonation. On the assumption that water permeability is proportional to oxygen permeability, it is postulated that carbonation has resulted in the reduced water absorption. The depth of carbonation of the silicone-treated specimens was slightly less than that of the controls, which may account for the higher water absorption of the former.

Preparation for field tests

For an earlier series of laboratory tests which simulated the effects of the South African climate, specimens were prepared by soaking in water for seven days. They were then allowed to dry for one day, after which the surface treatments were applied. The specimens were subjected to a cycle starting with seven days in the fog room followed by seven days over calcium chloride at a relative humidity (RH) of 0·32. Thereafter, to simulate a climate of short wet spells followed by much longer dry spells, the cycle comprised 6 h in the fog followed by seven days at RH = 0·32. The results of this treatment are shown in Fig. 4. It can be seen that all of the specimens, including the untreated control, dried out progressively.

These tests encouraged the tentative conclusions that in a semi-arid climate, either

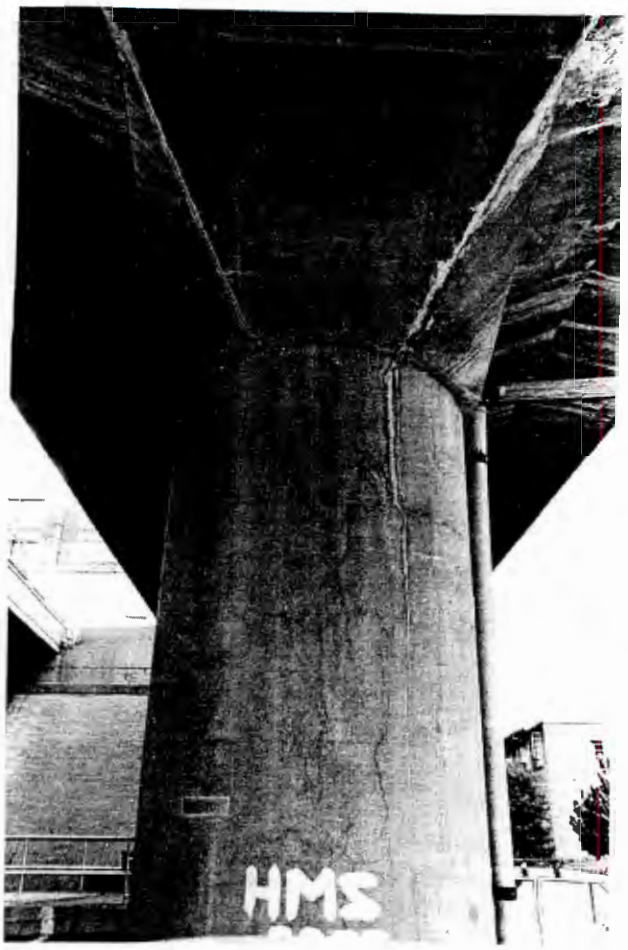

Fig. 5. One of the columns used in the field experiment

Below RH = 0·96 it is difficult to condense water out of the atmosphere by cooling the air.

The relative humidity in the pores of a porous material can be related to the tension or suction p'' in the pore water by means of the Kelvin equation (see for example Ref. 9)

$$p'' = 311\,000 \log_{10} \text{RH}$$

where p'' is in kPa.

Even at RH = 0·96, the suction is 5500 kPa. This can be thought of as the tensile stress with which the concrete draws in any water available on its surface. Hence, a low p'' corresponds to moist concrete and a high p'' to dry concrete.

It should be noted that p'' has two components, a matrix component that arises from capillary tension forces in the concrete and an osmotic component arising from the dissolved salts in the pore water. The osmotic component in concrete can be as high as 2000 kPa.

Field tests

Figure 6(a) shows some preliminary measurements on the control and the silicone-treated columns. Initial readings were taken at the end of the dry season during a period of hot sunny weather. The suction in the control column was almost at the limit of measurement, but that in the silicone-treated column was much less. A spell of heavy rain followed, during which the suction in the control column decreased slightly while that in the silicone-treated column almost disappeared. Shortly afterwards, streaks of what was assumed to be silica gel from the ASR exuded from cracks in the column and mushroom head. Similar streaks had appeared previously and were visible on some of the other columns. It appeared that water was entering the concrete from above, probably by way of the imperfectly sealed central drainage duct. When the rain was succeeded by sunny weather the suction in the control column increased and went out of range, while that in the silicone–treated column remained low.

A few weeks later, during a spell of hot dry weather, the suction in each of the columns was measured. It was found that p'' in the control, silane- and resin emulsion-treated columns was out of range. In the silicone- and cement slurry-treated columns, p'' was ~ 1500 kPa. The exterior surfaces of the columns were then sprayed with water and kept wet for 8 h/day on three consecutive days to simulate a spell of natural wet weather (Fig. 6(b)). The suction in the silane- and resin emulsion-treated columns remained out of range, while that in the control fell to 350 kPa. The suction in the silicone- and cement slurry-treated columns also responded by falling to low values. Four days later, the suction in the control column was again out of range, while that in the silicone- and cement slurry-treated columns had partially recovered.

These tests showed that if there is no internal source of water, sound concrete will quickly dry out after being surface wetted. Concrete probably does not need to be waterproofed in semi-arid climatic conditions.

Four years later the suction in the five columns was measured over a period of 28 days during a hot dry spell. (Fig. 7) The suction in all of the treated columns was low, and remained depressed throughout the period of measurement. The suction in the control column was at its level of four years previously. These results were so surprising that at first the psychrometers were thought to be defective. They were all changed, with replacements being tested before installation, but the measurements remained the same. When the final reading was made on the silicone-treated column, water actually ran out of the psychrometer hole. Although the suctions recorded in Fig. 7 are not zero, it is believed that the matrix suction is very close to zero and that the low values in Fig. 7 mainly represent osmotic suction.

In the light of the earlier observations on the silicone-treated column, and the exudation of gel from some of the other columns, the only possible conclusion seems to be that defective seals at the top of the internal drainage ducts were allowing small quantities

dry out quickly after surface wetting, and do not need to be waterproofed.

4. If there is an internal source of water in the concrete, waterproofing the exterior of a structure may serve to retain moisture so that the interior of the concrete becomes progressively wetter.

Acknowledgements

The studies described in this Paper were sponsored by the City Engineer of Johannesburg. The Author was assisted by Bob van der Merwe and Bob Anderson. Yunus Ballim measured the oxygen permeabilities.

References

1. GUDMUNDSSON G. and ASGEIRSSON H. Parameters affecting alkali expansion in Icelandic concretes. *Proc. 6th int. conf. on alkalis in concrete, Copenhagen, 1983*, pp. 217–222.
2. NILSSON L. O. Moisture effects on the alkali–silica reaction. *Proc. 6th int. conf. on alkalis in concrete, Copenhagen, 1983* pp. 201–208.
3. HAWKINS M. R. (CHAIRMAN) *Minimizing the risk of alkali–silica reaction.* Cement and Concrete Association, Slough, 1983. Report of working party.
4. LUDWIG U. Effects of environmental conditions on alkali–aggregate reaction and preventive measures. *Proc. 8th int. conf. on alkali–aggregate reaction, Kyoto, 1989*, pp. 503–596.
5. BLIGHT G. E. *Experiments on waterproofing concrete to inhibit AAR. Proc. 8th int. conf. on alkali–aggregate reaction, Kyoto, 1989*, pp. 733–738.
6. PFEIFER D. W. and SCALI M. J. *Concrete sealers for protection of bridge structures.* US Transportation Research Board, Washington, D.C., 1981, National Co-operative Highway Research Programme Report 244.
7. LEEMING M. B and O'BRIEN T. P. *Protection of reinforced concrete by surface treatments.* CIRIA, London, 1987, technical note 130.
8. SAVAGE M. J. and CASS A. Measurement of water potential using in situ thermocouple hygrometers. *Advances in Agronomy*, 1984, **37**, 73–126.
9. BLIGHT G. E. Strength characteristics of desiccated clays. *J. Soil Mech. Fdns Div. Am. Soc. Civ. Engrs*, 1966, **92** No. SM6, 19–37.
10. BLIGHT G. E. Can concrete structures be waterproofed to inhibit ASR? *Protection of concrete*, E. and F. N. Spon, London, 1990, pp. 223–232.

Discussion contributions on this Paper should reach the Editor not later than 29 March 1992.

Magazine of Concrete Research, 1991, **43**, No. 157, Dec., 249–255

The moisture condition in an exposed structure damaged by alkali–silica reaction

G. E. Blight*

WITWATERSRAND UNIVERSITY

This study demonstrates the difficulty of attempting to exclude moisture from concrete in structures exposed to the weather, especially if they have been cracked by ASR. Once the concrete has gained moisture it does not easily dry out, even if there is a well-defined dry season. If a waterproofing treatment is applied, the moisture may be sealed into the concrete. If present, leaking internal drainage ducts may exacerbate the problem, and promote the accumulation of moisture.

Introduction

In 1975 a double-storied portal frame supporting a motorway structure in Johannesburg was found to have suffered severe cracking. The dimensions and layout of this portal are shown in Fig. 1. Some of the cracks were sealed with epoxy resin, but a few months later they were found to have opened again. Fig. 2(a), taken in 1977, shows these epoxy-daubed cracks. An investigation into the cracking of this and other exposed reinforced concrete structures in Johannesburg eventually led to the conclusion that an alkali–silica reaction (ASR) was the cause of the damage. Since 1978 the portal has been the subject of intensive investigation, firstly to establish its structural safety, then to investigate means of halting the reaction, and finally to repair and rehabilitate the structure.

The length of beam marked A′A in Fig. 1 suffered the most severe damage, in the form of closely spaced cracking; the haunch, where upper beam and column join, was particularly badly affected. Fig. 2(b) shows the appearance of this concrete in 1990. A horizontal crack in the cantilever projection (marked B in Fig. 1) was repaired by post-stressing[1,2] in 1981. At about the same time internal storm water drainage ducts (marked by broken lines in Fig. 1), that led from kerb inlets along the upper and lower beams and down the insides of the columns, were plugged at their inlets. The ground-level outlets were left open to allow any water that might find its way into the concrete to drain away.

In 1982[3] and again in 1988[4] the portal was subjected to full-scale loading tests to check on its structural adquacy. On both occasions, the structure was found to behave predictably, with acceptable deflexions and joint rotations and very little irrecoverable deformation. However, there did appear to have been a slight deterioration of the performance of the portal under load in the six years between the two load tests. The structure had also deteriorated in outward appearance. New cracks had appeared and existing cracks had continued to widen. It was therefore decided by the owners that the structure would be rehabilitated, and investigations were started to find the most effective form of rehabilitation.

A number of possible solutions to the repair and rehabilitation of the section A′A of beam were considered. These included

(*a*) filling the major surface cracks with an elastomeric sealer and sealing the surface of the exposed concrete to exclude moisture from the surface and from minor surface cracks
(*b*) encasing the beam in a ventilated metal sheath to exclude incident rain, but allow the concrete to dry out gradually to the surrounding atmosphere
(*c*) demolishing length A′A of the upper beam and reconstructing it in reinforced concrete
(*d*) various variations of (*c*) above, including augmenting the strength of the upper beam with bolt-on steel members, and replacing length A′A with a bolt-on steel beam.

The rationale for measures (*a*) and (*b*) was as follows.

*Witwatersrand University, Private Bag 3, WITS 2050, Johannesburg, South Africa.

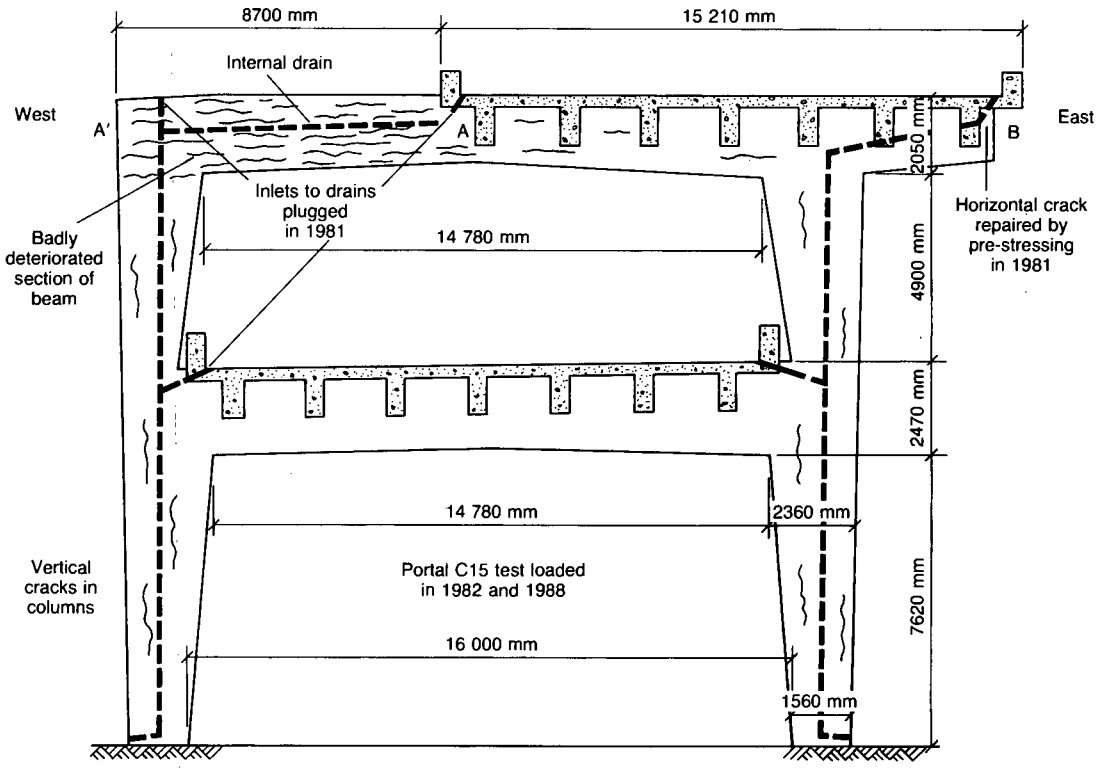

Fig. 1. Elevation looking north of portal showing location of deteriorated concrete and internal drainage ducts

A series of experiments carried out by Vivian[5] showed that the expansion caused by ASR in cement mortar can be halted if the moisture content of the mortar can be sufficiently reduced. Vivian's results were given in terms of the removable water content, which he defined as that water lost after prolonged storage over calcium chloride. In his experiments he showed that if the removable water content is less than about 4% expansion caused by ASR ceases. More recent work by Tomasawa *et al.*[6] and Kurihara and Katawaki[7] have broadly confirmed that Vivian's results also apply to concrete. They conclude that expansion caused by ASR ceases when the water content of concrete (dried at 105–110°C) falls below a range of 4–8%. This corresponds to an ambient relative humidity of about 85%.

In a review of the effects of environmental conditions on ASR, Ludwig[8] also concluded that ASR expansion ceases once the ambient relative humidity falls below 80–85%. Other estimates of the level of ambient relative humidity necessary to inhibit ASR expansion vary from 75%,[9] 83%,[10] to 90%.[11]

The available evidence therefore indicates that if the concrete in a structure subject to ASR can be dried out to or maintained at a moisture content that would be compatible with an ambient relative humidity of about 90%, expansion caused by ASR should be inhibited.

The implementation of measures (*a*) and (*b*) required a knowledge of the moisture condition in the concrete. If measure (*a*) was to be adopted it would be important to seal the cracks and concrete surface at a time of the year when the concrete was at its driest. Johannesburg has well-defined wet and dry seasons, and the obvious time appeared to be August/September, at the end of the dry season. However, it was not known to what extent the moisture in the concrete varied seasonally, or if the concrete dried out to any significant extent during the dry season. To provide this information, the programme of measurements described in this Paper was undertaken.

The instrumentation

The instruments used were thermocouple psychrometers, which were installed in the north, south and west faces of the western haunch of portal C15 (A′ in Fig. 1).

Thermocouple psychrometers were originally used for measuring moisture conditions in soil[12] and have only recently been adapted for use in concrete. A thermocouple psychrometer consists of a thermocouple junction sealed into a cavity in the concrete. In this case the cavity was formed by drilling a 10 mm dia. hole to the required depth (100 or 400 mm). The probe was inserted into the hole at the end of a wooden dowel stick that had been heavily varnished with polyurethane varnish. The varnish prevented absorption of water by the dowel, which was a push fit in the hole. A soft rubber disc attached to the end of

the dowel, through which the psychrometer lead was passed, further helped to seal off the cavity at its end.

The air at the end of the hole comes to thermal and moisture equilibrium with the atmosphere in the concrete. This may take several hours or days to occur, and for this reason the psychrometers are left installed permanently in situ. To read the psychrometer a current is passed through the thermocouple junction, which cools by the Peltier effect, until the temperature falls *below* the dew point of the atmosphere in the cavity; moisture then condenses on the cool junction. The cooling current is stopped and the condensed moisture starts to evaporate at the dew point temperature. The thermocouple is used to measure this temperature, and hence the relative humidity in the cavity (and by inference in the concrete) can be determined. The relative humidity can be expressed in terms of the pore moisture suction p'' in the concrete via the well-known Kelvin equation

$$p'' = 311\,000 \log_{10}(\mathrm{RH}) \quad (\mathrm{kPa}) \qquad (1)$$

where the relative humidity RH is expressed as a decimal of unity.

The width of the portal beam and columns is 1250 mm. To ensure that information would be available for most of the thickness of the concrete, the psychrometers were installed in pairs at depths of 150 and 400 mm in from the concrete surface. As the psychrometers were installed at a height of 16 m above ground level they had to be installed and accessed for reading via a truck-mounted hydraulic boom designed for repairing power lines. Fig. 2(b) is a photograph taken from this boom. The faintly visible 150 and 400 on the concrete show where psychrometers have been installed.

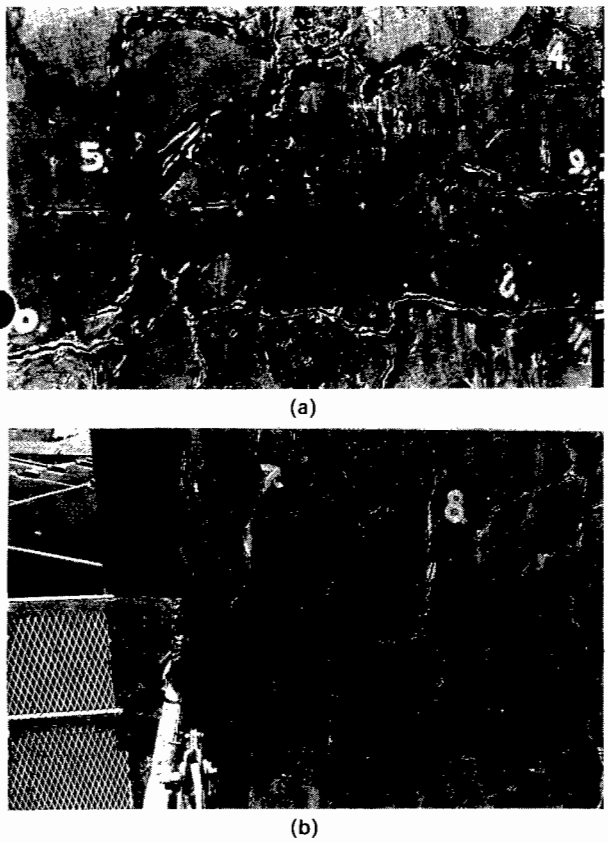

(a)

(b)

Fig. 2. (a) Appearance of cracked concrete surface in 1977 after attempt to seal cracks with epoxy resin; (b) appearance of concrete in 1990

The useful range of the psychrometer is RH = 1·0–0·96, or p'' = 0–5000 kPa. Although this may sound restrictive, it is the main range of interest for concrete structures exposed to the weather. The psychrometer has the advantage that it simultaneously measures the suction and the temperature in the concrete. It is particularly important to know the temperature if strain measurements are being made.

Equation (1) provides an explanation of why a low relative humidity inhibits expansion caused by ASR. The pore moisture suction p'' exerts an internal isotropic compressive stress on the concrete. Provided this compressive stress exceeds the swelling pressure generated by the ASR, the concrete does not expand. Data collected by Hobbs[13] show that swelling pressures of up to 4000 kPa are possible as a result of ASR. All of these measurements were made in accelerated laboratory tests. In a real structure where ASR develops over years, rather than weeks, stress relaxation can be expected to reduce swelling pressures to less than 4000 kPa; 3000 kPa might be a realistic value. This corresponds to a relative humidity of between 97 and 98%.

Results of moisture measurements

Measurements were taken at intervals for a period of 20 months and the results have been summarized in Figs 3(a) (period from April to December 1989) and 3(b) (period from January to November 1990). Readings were discontinued after it was decided, on the basis of the measurements, to rehabilitate the portal by demolishing and reconstructing length A′A the upper portal beam. Portions of these results have been published previously[2,14] but this is the first time that the complete results have appeared.

The upper portion of each set of results shows the variation of moisture suction with time, while the lower portion shows the corresponding rainfall, plotted on a daily basis, and the 30-year mean monthly relative humidity (plotted for only one year). The measurements are identified by the depth of installation and the direction faced by the side of the haunch, e.g. 150 N is installed at 150 mm depth on the north-facing side of the beam. The measurements were started in April 1989, towards the end of the wet season, and it was found that suctions were negligible, indicating that the concrete was extremely wet. However, it is possible that at this stage the psychrometers were not yet in moisture equilibrium with the concrete.

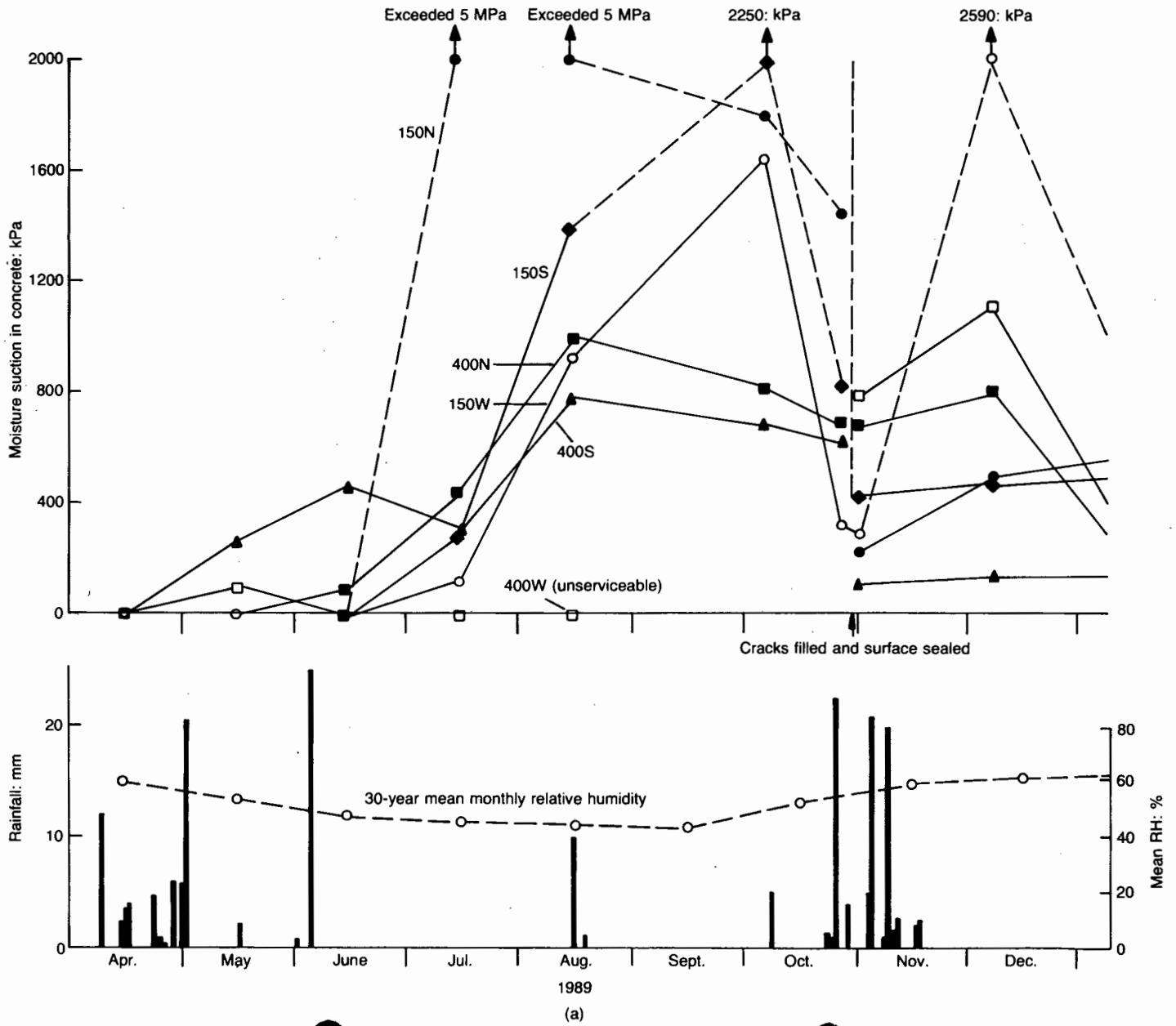
Exceeded 5 MPa
Exceeded 5 MPa
2250: kPa
2590: kPa
150N
150S
400N
150W
400S
400W (unserviceable)
Moisture suction in concrete: kPa
2000
1600
1200
800
400
0
Cracks filled and surface sealed
Rainfall: mm
20
10
0
30-year mean monthly relative humidity
Mean RH: %
80
60
40
20
0
Apr.
May
June
Jul.
Aug.
Sept.
Oct.
Nov.
Dec.
1989
(a)

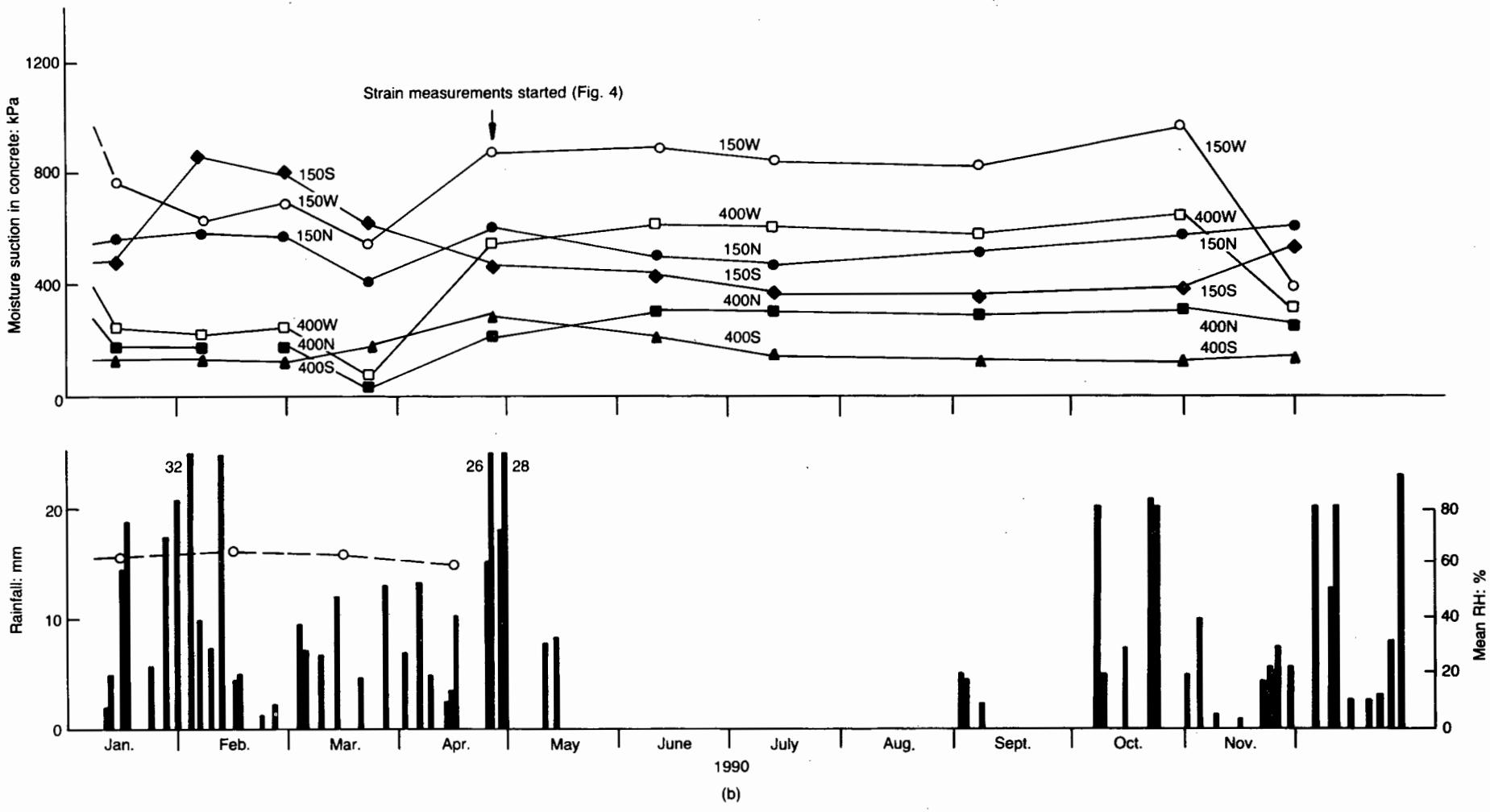

Fig. 3. (a) Measurements of moisture suction and rainfall for (a) April 1989–December 1989; (b) January 1990–November 1990

During the 1989 dry season the 150 mm-deep psychrometers recorded large suctions, with 150 N (which faces the sun in winter) going out of the range of measurement and 150 S (permanently in shade in winter) recording 2250 kPa. 150 W showed a disappointingly low maximum suction of 1600 kPa. Only two of the 400 mm-deep psychrometers were in working order, and they too showed very disappointing maximum suctions of less than 1000 kPa. On the evidence presented in Fig. 3(a), concrete that has cracked as a result of ASR will not dry out to below the limiting relative humidity of 97% in a single dry season. Once the 1989 dry season was ended by rain in October, suctions plummeted once again to low values.

At the end of October (although this was not part of the agreed programme of observation) the major surface cracks were caulked with a dry cement mortar and all surfaces of the beam A′A were treated with a cement-slurry-based waterproofing coating. This seemed, on the face of it, the worst possible time to carry out such a treatment, as the concrete was moist and the waterproofing treatment would serve to seal the moisture into the concrete; subsequent measurements (Fig. 3(b)) were to confirm this. After some wide fluctuations in suction between November 1989 and January 1990, conditions in the concrete stabilized and suctions remained virtually constant for the ensuing 11 months. Very little change in suction occurred during the 1990 dry season, even though there was no rain for 14 weeks. A very stable moisture region had been established as a result of sealing the surface of the structure.

Results of strain measurements

Measurements of crack widths had shown that the concrete was still swelling in mid-October when its surface was sealed. Once it had been confirmed that suctions had stabilized at a low level, it was decided to measure surface strains in the vicinity of the psychrometers to see if the sealed-in moisture had affected the swelling.

Figure 4 shows the results of the strain measurements made near the psychrometers. A 400 mm gauge length DEMEC strain gauge was used, and the measurements plotted in Fig. 4 have been corrected to a temperature of 20°C. The measurements confirmed that expansion was still occurring 28 years after the portal was constructed. Strains measured on the beam (S and N) showed hardly any movement parallel to the beam axis (S- and N-horizontal) and up to 200 $\mu\varepsilon$ over 7 months normal to the beam axis (S- and N-vertical). Strains measured on the western face of the haunch showed mainly horizontal expansion (W-horizontal), although anomalously large strains were recorded

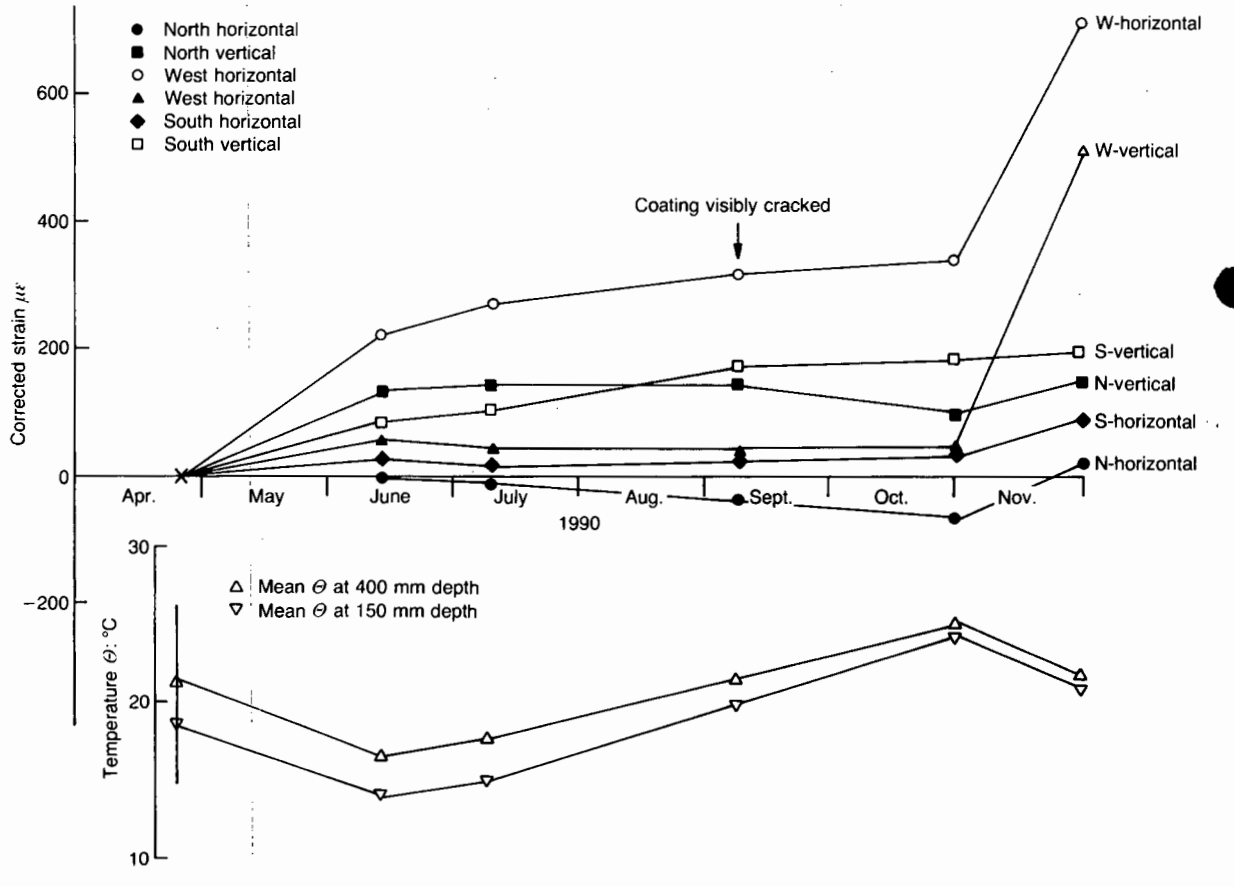

Fig. 4. Measurements of surface strain from April 1990–November 1990

between October and November 1990. The waterproof coating had visibly cracked by mid-September 1990, 10 months after it was applied.

Because previous measurements[4] had recorded crack widths and not strains, it is not known if sealing and concrete accelerated the swelling, or had no effect on it.

Conclusions and decision based on measurements

The results of the psychrometer measurements, taken in conjuction with a separate study of waterproofers for concrete,[15] demonstrated that it is very difficult to control moisture conditions in concrete structures exposed to the elements, particularly if they have cracked as a result of ASR. After much consideration, it was decided to adopt solution (*c*)—and to demolish and rebuild beam A′A. The decision was basically a political one based on a reluctance to appear indecisive about a solution to the problem, as well as a reluctance to continue indefinitely with a programme of monitoring.

When the beam was demolished it was found that the concrete around the internal drainage ducts was visibly wet. Clearly what had happened in the companion study[15] had happened here as well. The plugging of the inlets to the drains had not been successful and water continued to be fed into the interior of the concrete throughout the life of the structure.

The conclusions for this study are thus as follows. Concrete cracked by ASR readily admits water through the cracks. This water penetrates deeply into the concrete, and does not dry out by evaporation even if there is a well-defined annual dry season. Previous tests[15] have shown that sound concrete absorbs incident water but then relatively quickly dries out again. Waterproofing such a structure by means of a coating may seal moisture in. The accumulation of moisture within the concrete can be exacerbated by leaking internal drainage ducts.

References

1. BLIGHT G. E. *et al.* The repair of reinforced concrete structures affected by alkali-aggregate reaction. *Civ. Engr S. Afr.*, 1984, No. 11, 525–538.
2. BLIGHT G. E. Rehabilitation of reinforced concrete structures affected by alkali-silica reaction. *Struct. Engng Rev.*, 1990, **2**, 113–120.
3. BLIGHT G. E. *et al.* (IDORN G. M. and ROSTAM S. (eds)) The effect of alkali-aggregate reaction on the strength and deformation of a reinforced concrete structure. *Proceedings of the 6th International Conference on Alkalis in Concrete.* Copenhagen, 1983, Danish Concrete Association, Copenhagen, 1983, 401–410.
4. BLIGHT G. E. *et al.* Effect of alkali-aggregate reaction on the performance of a reinforced concrete structure over a six-year period. *Mag. Concr. Res.*, 1989, **41**, No. 147, June, 69–77.
5. VIVIAN H. E. The effect on mortar expansion of amount of available water in mortar. *Studies in Cement–Aggregate Reaction XI.* Commonwealth Scientific and Industrial Research Organization, Australia, Bulletin 256, 1950.
6. TOMASAWA F. *et al.* Influence of water content of concrete on alkali-aggregate reaction. *Proceedings of the 8th International Conference on Alkali Aggregate Reaction.* Kyoto, 1989, 881–885.
7. KURIHARA T. and KATAWAKI K. Effects of moisture control and inhibition on alkali-silica reaction. *Proceedings of the 8th International Conference on Alkali Aggregate Reaction.* Kyoto, 1989, 629–634.
8. LUDWIG U. Effects of environmental conditions on alkali-aggregate reaction and preventitive measures. *Proceedings of the 8th International Conference on Alkali Aggregate Reaction.* Kyoto, 1989, 583–596.
9. HAWKINS M. R. (Chairman) Minimizing the risk of alkali-silica reaction. Report of Working Party, Cement and Concrete Association, 1983.
10. GUDMUNDSSON G. and ASGEIRSSON H. Parameters affecting alkali expansion in Icelandic concretes. *Proceedings of the 6th International Conference on Alkalis in Concrete.* Copenhagen, 1983, 217–222.
11. NILSSON L. O. Moisture effects on the alkali-silica reaction. *Proceedings of the 6th International Conference on Alkalis in Concrete.* Copenhagen, 1983, 201–208.
12. MONTEITH J. L. and OWEN P. C. A thermocouple method of measuring relative humidity in the range 95–100%. *J. Sci. Instrum.*, 1958, No. 35, 443–446.
13. HOBBS D. W. *Alkali-silica reaction in concrete.* Thomas Telford, London, 1988.
14. BLIGHT G. E. (DHIR R. K. and GREEN J. W. (eds)) Can concrete structures be waterproofed to inhibit ASR? *Proceedings of the International Conference on Protection of Concrete.* Spon, London, 1990, 223–232.
15. BLIGHT G. E. A study of four waterproofing systems for concrete. *Mag. Concr. Res.*, 1991, **43**, 197–204.

Discussion contributions on this paper should reach the Editor by 30 June 1992.

Concrete Society

Framewood Road
Wexham
Slough
SL3 6PJ
Telephone
0753 662226
Fax
0753 662126

President M. R. Hawkins OBE

8.1.92.

Dear Colleague,

9TH INTERNATIONAL AAR CONFERENCE

I now have pleasure in enclosing a set of instructions for the preparation of your manuscript together with examples of a typed manuscript and A5 papers in which form the conference proceedings will be prepared.

Please follow the instructions as closely as possible using the paper provided.

The Technical Presentations Committee asks that, if possible, you restrict the length of your paper to 8 pages including diagrams. May I remind you that final date for receipt of the completed manuscript is 31 March 1992.

Happy New Year!

Yours faithfully,

GERALD YOUNG
AAR Conference Secretariat

Limited by Guarantee
Registered London 884419
Registered Office
Framewood Road
Wexham
Slough SL3 6PJ

PRE-DEMOLITION TESTS ON STRUCTURAL CONCRETE DAMAGED BY AAR

M G Alexander, G E Blight, B J Lampacher
Witwatersrand University, P O Wits, 2050, Johannesburg, South Africa

A reinforced concrete double storey portal frame that was damaged by AAR was recently rehabilitated by demolishing part of the upper beam and reconstructing it. After outlining the history of the portal and the various investigations made on it in the past 13 years, the paper describes the results of a series of pre-demolition tests carried out on the concrete.

INTRODUCTION - THE HISTORY OF THE CONCRETE

In 1977 it was discovered that several of the reinforced concrete portal frames supporting an overhead section of the Johannesburg urban motorway system were severely cracked (1). An examination of cores taken from the damaged structures, as well as the form of the crack patterns, resulted in a diagnosis of alkali aggregate reaction as the cause of the damages. One portal (number C15), was particularly badly damaged and became the subject of intense investigation. Figure 1 shows the dimensions of portal C15 and records the various tests and remedial measures carried out in the period of 13 years that the portal was under investigation.

The concrete is made of Witwatersrand quartzite fine and coarse aggregate. This quartzite is a mine waste rock that has been brought to the surface from depths of 1000 to 3000m. An analysis of the rock showed that its equivalent Na_2O content varies between 0.1 and 0.7 percent. Analysis of the AAR-affected concrete, allowing for the alkali content of the aggregate, indicated that the equivalent Na_2O content of the cement varied between 0.3 and 2.6 percent with a mean for 13 analyses of 1.3 percent and a standard deviation of 0.8 percent. As the concrete was 15 years old when the damage was discovered, and the construction records had been destroyed, the source of the abnormally high alkali cement has never been discovered.

Full-scale Load Tests

Because of concern for the structural safety of portal C15, a full-scale load test was carried out in 1982 (2). Part of the preparation for the test consisted of an elastic finite element analysis to predict the behaviour of the structure under load. The elastic modulus used in the analysis was based on laboratory measurements on cores taken from the structure, and

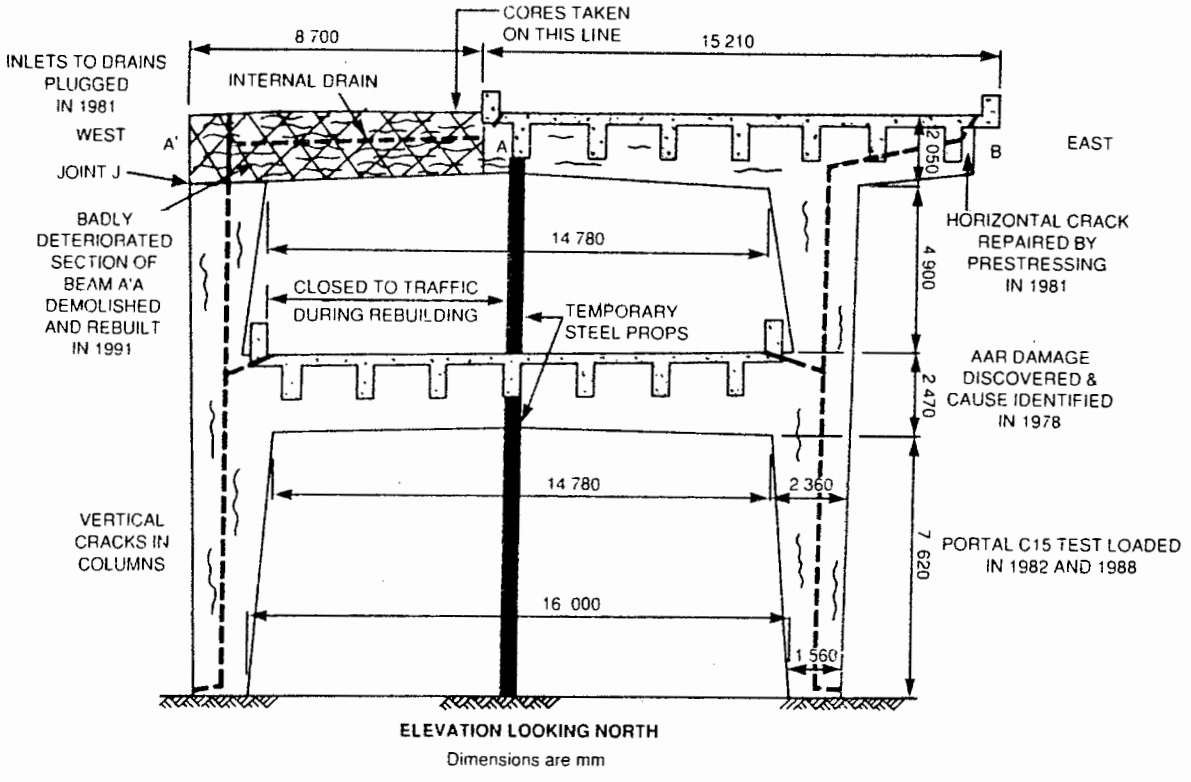

FIGURE 1 Portal C15 - principal dimensions, test history and method of rehabilitation

was determined at 18 GPa. It was concluded from the test that the appearance of the deterioration was more alarming than serious. The structure was at that time fully capable of carrying its design load and behaved predictably and elastically under load.

Continuing measurements of crack widths showed that the AAR expansion was proceeding in the portal with ever-widening cracks, as well as the appearance of new cracks. A second full-scale loadtest was carried out in 1988 (3). The results were very much the same as those of the test carried out 6 years earlier. Figure 2 shows the predicted and observed relationships between midspan deflection of the upper beam of the portal and load. The load is expressed as a percentage of South African NA loading (125 percent of NA load corresponds to about 100 percent of British BS153 HA loading). Predictions were made on the two assumptions that (a) full moment continuity had been retained at the upper left hand (or west) joint of the portal (J in Figure 1) and (b) that continuity had been lost. The figure shows that the portal performed better than the prediction assuming full continuity at J. It also shows how well the results of the 1982 and 1988 load tests agreed, and how close to elastic was the behaviour of the portal under load. The actual modulus of elasticity of the portal was about 24 GPa, as compared with 18 GPa assessed from tests on cores.

Moisture Measurements

A series of measurements was started in April of 1989 to find if it would be possible to dry out the beam of the portal during the dry season and then coat it with a waterproof or water repellent preparation. In this way it was hoped to slow down, or even stop the AAR. Psychrometer moisture sensors were embedded in the concrete and a series of measurements was made over the next 19 months (4,5). The measurements showed that it is very difficult to control moisture conditions in concrete structures exposed to the elements and that short of jacketing the portal in a ventilated metal tube, it would be almost

impossible to dry it out permanently.

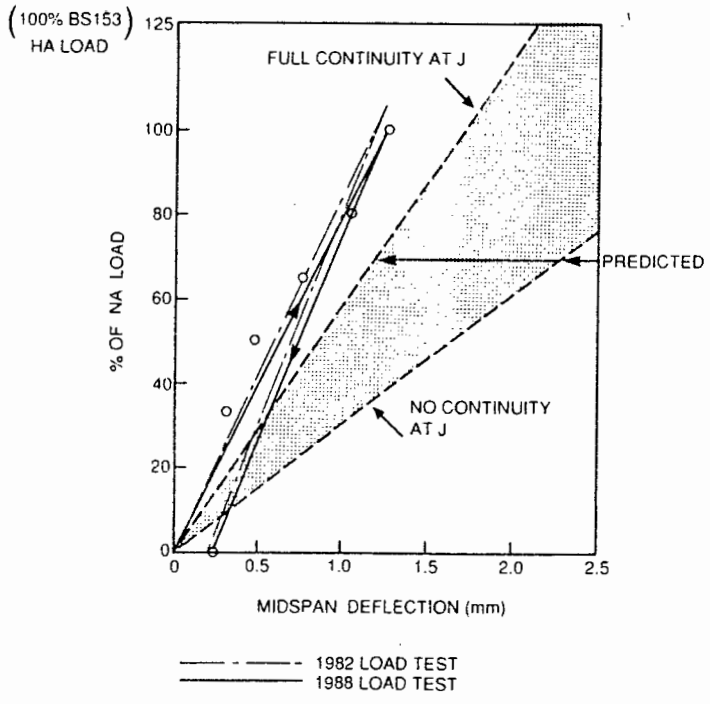

FIGURE 2 Typical results recorded in two full scale load tests on Portal C15

Continued Swelling of the Concrete

Although crack widths had been measured on the structure since cracking was first discovered, no-one thought to measure swelling strains until April 1990, when the concrete was 25 years old. The measurements were carried out with a 400 mm Demec gauge and were corrected for temperature by means of thermocouples embedded in the portal. The results, shown in Figure 3, indicated that the concrete was still expanding (5). The expansion had probably been re-activated when the owners of the structure sealed its surface while the concrete was wet (4) thus sealing in the moisture and preventing the concrete from drying out.

The cause of the continuing expansion was queried by Hobbs (6) who suggested that delayed ettringite formation (7) might be responsible. However a careful examination of concrete from the portal was unable to find ettringite or the structures and crystal growth patterns associated with delayed ettringite formation.

Other Remedial Measures

While the moisture condition of the portal was being studied, other more drastic measures were also under consideration. These included

(a) Demolishing length A'A of the upper beam (see Figure 1) and reconstructing it in reinforced concrete exactly as before, except that low alkali cement and non-reactive aggregate would be used.

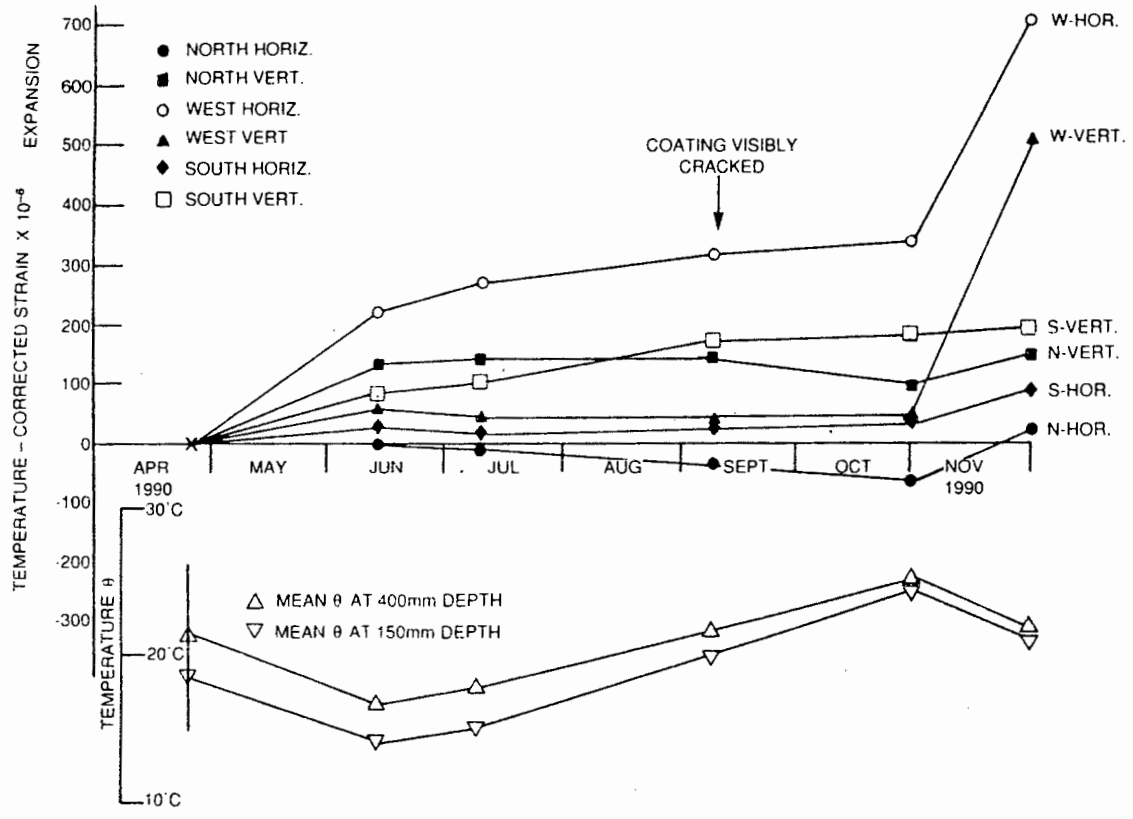

FIGURE 3 Measured expansion on beam of Portal C15 recorded shortly before demolition

(b) Augmenting the strength of A'A by means of bolt-on steel splints; and

(c) Replacing A'A with a bolt-on steel beam.

Eventually it was decided to adopt course (a) and to demolish and rebuild A'A in reinforced concrete. The decision was not taken for purely technical reasons -it being accepted that the structure was adequately safe and would continue to be so for many years to come. It was basically a management decision based on a reluctance to appear indecisive about a solution to the problem, as well as a reluctance to continue indefinitely with a programme of monitoring.

PRE-DEMOLITION OBSERVATIONS

Prior to defining the extent of demolition of beam A'A, tests were made to establish the properties of the existing concrete at the proposed junction of the new and old sections. Three horizontal cores were taken on the vertical line indicated in Figure 1. The cores penetrated the full 1240mm thickness of the beam and were drilled at roughly 500mm vertical intervals.

Compressive Strength

The cores were divided into suitable lengths for testing and one piece from each core was tested for compressive strength. Considering the results of earlier tests, it was not surprising to find

a mean compressive strength of 31 MPa, whereas the design strength had been 4500 psi or 31 MPa. Although the concrete showed signs of deterioration, the cores appeared to be in better condition than some of the concrete in A'A.

Ultrasonic Pulse Velocities

A measurement of ultrasonic pulse velocity (UPV) was made on each piece of core prior to further testing. The ultrasound pulse was transmitted along the axis of the core in each case, thus simulating horizontal transmission through the thickness of the beam.

The results of the measurements are shown in Figure 4(a) where they are compared with the mean UPV established for the better quality concrete in beam A'A during the 1988 tests (3). As the figure shows, the mean UPV of 4.09 km/s measured on the cores was very close to the mean UPV of 4.07 km/s measured in situ in 1988, prior to the second full-scale loading test.

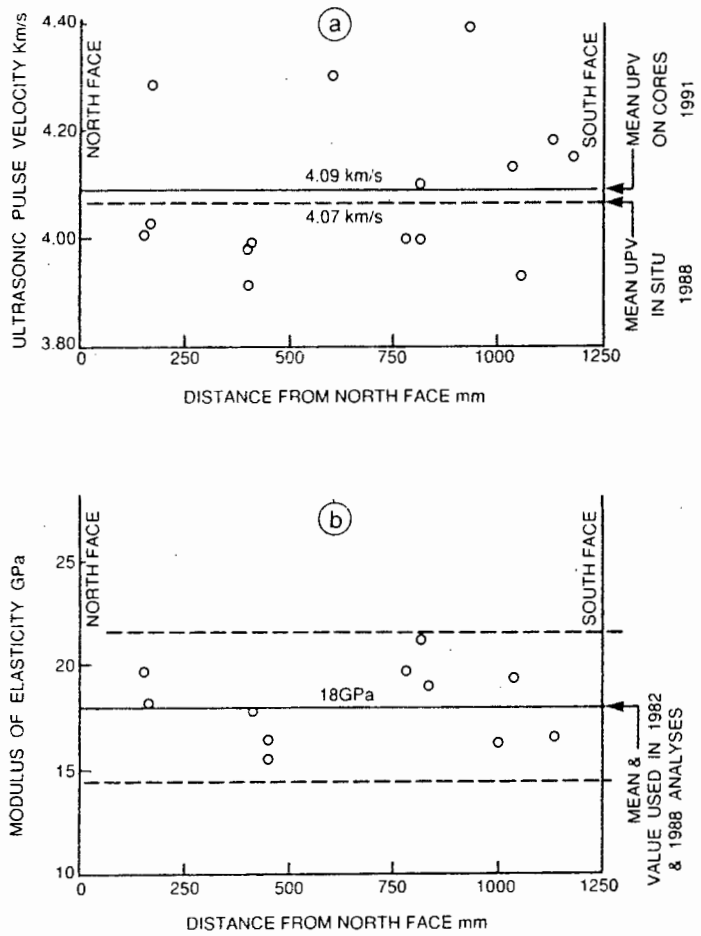

FIGURE 4 (a) Ultrasonic pulse velocity and (b) modulus of elasticity measurement on cores from Portal C15

Figure 4(a) shows the measured UPVs plotted against the position of the cores in the thickness of the beam. There appears to be no particular pattern in the measurements, no indication, for example, that concrete from the heart of the member had deteriorated less than concrete from close to the surface.

Modulus of Elasticity

The static modulus of elasticity was also measured on the cores. These results are plotted in Figure 4. In considering Figure 4, it must be remembered that the measurements represent moduli measured in what would have been a horizontal transverse direction in situ.

Individual measurements ranged from 15.5 GPa to 21.1 GPa with a mean value of 18.1 GPa. This is close to the value of elastic modulus of 18 GPa chosen in 1982 and again in 1988 for the finite element analyses and shown by the loading tests to be reasonably representative of the structure's behaviour (although the elastic modulus for the structure exceeded 18 GPa). Here again, there is no indication that the heart concrete was of any better quality than concrete from closer to the surface of the member.

Swell-Under-Load

Some of the cores were subjected to swell-under-load tests to assess if the concrete was still expansive, and if so, to estimate the residual swelling pressure.

The cores were mounted in modified soil testing oedometers which enabled a constant axial stress to be applied via dead weights and a lever system. The axial strain of the specimens could be measured by means of dial gauges reading to 0.001mm, enabling a strain of 5 x 10^{-6} or 5 $\mu\varepsilon$ to be resolved on a specimen 200mm long. The specimens were enclosed in a jacket over distilled water, and the tests were carried out at a constant temperature of 23°C.

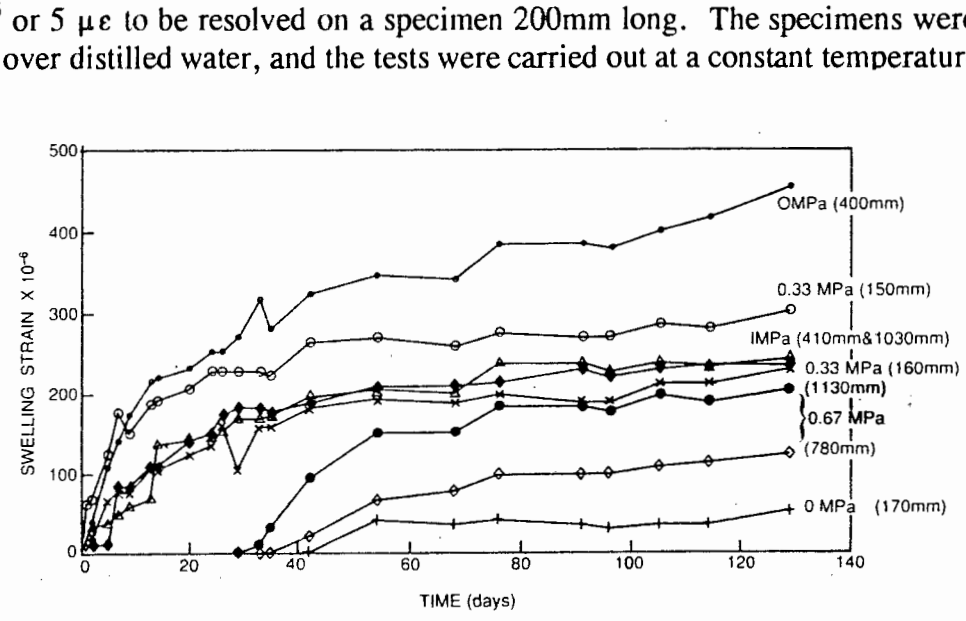

FIGURE 5 Swell under load versus time relationships for cores taken from Portal C15

Figure 5 shows the observed relationships between swell-under-load and time. The constant stress applied to each specimen is indicated next to each curve, and so is the distance from the north face of the beam at which the core was taken. It will be seen that free swells of over 450 $\mu\varepsilon$ were recorded and that strains of close to 250 $\mu\varepsilon$ occurred under a confining stress of 1 MPa. Swelling strains over a period of 4 months were of the same order as those observed previously over a similar period on the surface of the beam (Figure 3).

Figure 6 shows the approximate equilibrium swell strains plotted against the corresponding confining stresses. Extrapolating the trend lines of swell versus stress to zero

swell strain gives an indication that the fully restrained swelling pressure of the concrete was in the range of 1 to 2 MPa, even after 25 years of exposure to the elements. Again, there is no indication that the samples from closer to the axis of the beam were more expansive than samples from close to the surface.

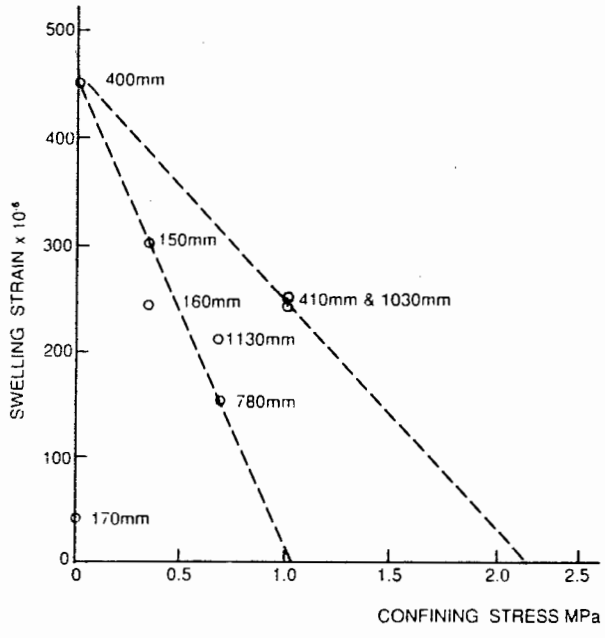

FIGURE 6 Relationships between equilibrium swell strain and confining stress for cores from Portal C15

CONCLUSIONS

The results of the pre-demolition tests have largely confirmed the conclusions reached on the basis of earlier laboratory tests on cores from the structure and the two full-scale load tests:

The strength of the concrete generally remained above the design strength of 31 MPa. This conclusion had been reached in 1981 (1) and was confirmed a number of times in later years. There were, however, zones of concrete where the strength fell below 31 MPa. Even in the pre-1981 tests, the strengths of certain cores were as low as 12 MPa.

Ultrasonic pulse velocities have been used by the authors primarily as an indication of the degree of internal disruption of the concrete. The agreement between UPVs measured on cores and the in situ measurements made in 1988 supports the view that this is a valid and repeatable procedure. However, the in situ measurements made in 1982 and 1988 could not be reconciled, for reasons that remain unknown.

The agreement between elastic moduli measured on cores and the value that could be deduced from the full-scale loading tests shows that the properties of the concrete were reasonably isotropic and non-directional. It also demonstrates that valid predictions of the behaviour of full scale reinforced concrete structures can be made on the basis of engineering properties established by sampling from the structure. This is a most important conclusion, for it shows that the behaviour of AAR-affected structures can be predicted on the basis of properties measured on sample cores.

The measurements shown in Figure 3 indicated that the concrete was still swelling in situ shortly before beam A'A was demolished. Although this swell had probably been re-activated by sealing the surface of the beam at a time when the concrete was wet, it showed that relatively old concrete may retain a swell potential.

This observation has been confirmed by the results of the swelling tests shown in Figures 5 and 6. Given access to moisture, the concrete is not only capable of swelling by up to 500 $\mu\varepsilon$, but can exert fully restrained swelling pressures of between 1 and 2 MPa.

Finally, it appears that the whole volume of concrete comprising beam A'A was more or less equally affected by AAR. There do not seem to be any gradients of properties that would indicate a progression of the reaction from the outside of the concrete towards the axis. However, this may be because during the relatively long period for which the concrete has been subjected to AAR, these gradients have formed and disappeared.

REFERENCES

1. Blight, G E, McIver, J R, Schutte, W K and Rimmer, R, 1981. "The effects of alkali-aggregate reaction on reinforced concrete structures made with Witwatersrand quartzite aggregate". Conference on Alkali-Aggregate Reaction in Concrete, Proceedings, Cape Town, South Africa, 11pp.

2. Blight, G E, Alexander, M G, Schutte, W K and Ralph, T K, 1983. "The effect of alkali-aggregate reaction on the strength and deformation of a reinforced concrete structure". 6th International Conference on Alkalis in Concrete, Proceedings, Copenhagen, Denmark, 401-410.

3. Blight, G E, Alexander, M G, Ralph, T K and Lewis, B A, 1989. "Effect of alkali-aggregate reaction on the performance of a reinforced concrete structure over a six-year period". Magazine of Concrete Research, 41, (147), 69-77.

4. Blight, G E, 1990. "Rehabilitation of reinforced concrete structures affected by alkali-silica reaction". Structural Engineering Review, 2, 1-8.

5. Blight, G E, 1992. "The moisture conditions in an exposed structure damaged by alkali-silica reaction". Magazine of Concrete Research, 43, (157), 96-101.

6. Hobbs, D W, 1991. Personal communication with G E Blight.

7. Lawrence, C D, Dalziel, C D and Hobbs, D W, 1990. "Sulphate attack arising from delayed ettringite formation". Interim Technical Note 12, British Concrete Association.

7. ASSESSING DESIGN LOADING ON BINS AND SILOS FOR STORING BULK MATERIALS

CONTRIBUTION TO LEARNING

Pressures in silos have been measured before. It has been unusual to embark on the measurement of pressures in a full-scale silo, and very few researchers have measured pressures in more than one full-scale storage structure. The author has embarked on a systematic campaign of measurement during the course of which twenty full size structures have been studied. These have varied from 5.5m in diameter to 25m in diameter and from 250 tons to 15000 tons in storage capacity. Materials stored have included coal, grain of various types, sugar, cement powder, and asbestos ore.

Out of the work has come a very much improved understanding of the pressures exerted by particulate materials on storage structures. The picture that has emerged is a much simpler and more rational one than that embodied in current silo design codes, even codes that are presently still in draft form.

7.1 DESIGN LOADING ON SILOS

CONTRIBUTION TO LEARNING

The seven papers in this section progressively summarize the results of measurements as they became available and compare these results with the predictions of current silo design codes. The series culminates in papers 7.1.6 and 7.1.7. Paper 7.1.6 advances a very simple view of design pressures in silos. It points out that

- Arching is unreliable and may or may not occur in a silo;

  hence the design pressure distribution should be linear with depth.
- Pressures in the hopper portion of a silo should be treated as an extension of

those in the cylindrical portion.

- Temperature surcharge pressures may form a substantial proportion of the load carried by a silo.
- Pressure distributions are likely to be non-uniform and this non-uniformity should be allowed for in design.

This paper drew a great deal of criticism in discussion. To present a balanced view, both the discussion and my reply have been included.

The view that the design pressure distribution in a silo should be taken as linear has recently been vindicated by the failure of a reinforced concrete coal silo that was designed in 1981 for a pressure distribution calculated according to the Walker theory. The Walker theory is a version of the Janssen arching theory, and also allows for a concentrated overpressure at the junction of the hopper and cylindrical portions of the silo. This pressure distribution is far less in magnitude then that advocated by 7.1.6, even with the overpressure. The silo cracked very extensively over a height of nearly 30m but was kept in use for a period of nearly 10 years, because (incredibly) no-one appears to have noticed the cracks. The attached diagram shows that if the linear pressure distribution according to 7.1.6 had been operative, the hoop steel provided in the silo wall would have yielded or have been close to yield at three points up the height of the silo. This is what seems to have actually happened in this case. The silo is currently under repair by constructing an outside reinforced concrete shell to augment the strength of the existing shell.

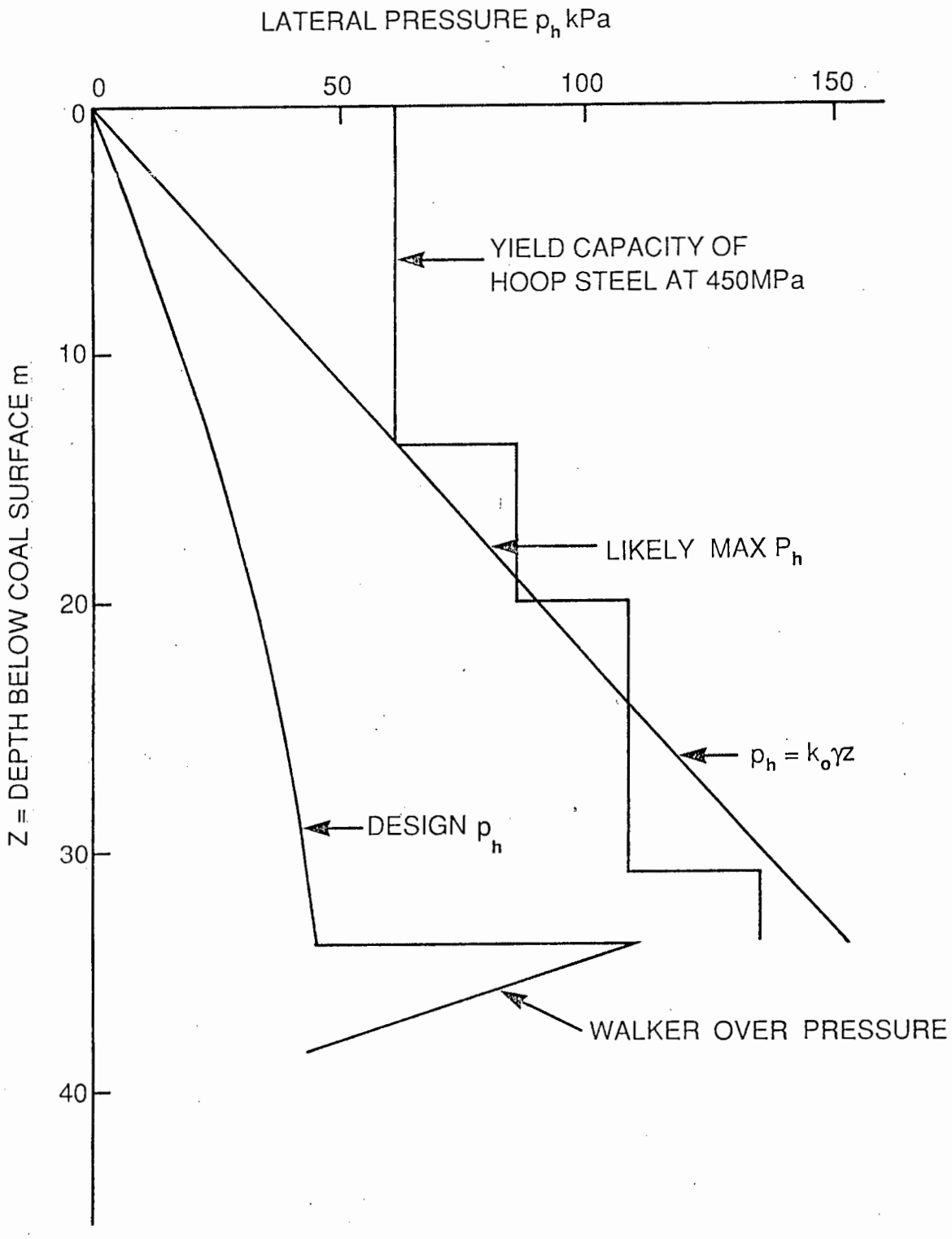
LATERAL PRESSURE p_h kPa
0
50
100
150
0
10
20
30
40
Z = DEPTH BELOW COAL SURFACE m
YIELD CAPACITY OF
HOOP STEEL AT 450MPa
LIKELY MAX P_h
$p_h = k_o \gamma z$
DESIGN p_h
WALKER OVER PRESSURE

7. ASSESSING DESIGN LOADING ON BINS AND SILOS FOR STORING BULK MATERIALS

7.1 DESIGN LOADING ON SILOS

7.1.1 Blight, G E (1986). Structural loading on the walls of rapidly filled silos. Encyclopedia of Fluid Mechanics, vol 4, Solids and Gas-Solids Flows (N.P. Cheremisinoff, Ed.) pp. 195-219.

7.1.2 Blight, G E (1986). Pressures exerted by materials stored in silos : Part 1, Coarse materials. Geotechnique, vol 36, No 1, pp 33-46.

7.1.3 Blight, G E (1986). Pressures exerted by materials stored in silos : Part 2, Fine powders, Geotechnique, vol 36, No 1, pp 47-56.

7.1.4 Blight, G E (1988). A comparison of measured pressures in silos with code recommendations, Bulk Solids Handling, vol 8, No 2, pp 145-153.

7.1.5 Blight, G E (1988). Design loading for grain silos - intention and reality. International Summer Meeting, American Society of Agricultural Engineers, Rapid City, USA, 12 pp.

7.1.6 Blight, G E (1990). Defects in accepted methods of estimating design loading for silos. Institution of Civil Engineers (London), Proceedings Part 1, vol 88, pp 1015-1036. Discussion and reply, (1991) vol 90, pp 1077-1088.

7.1.7 Blight, G E (1992). Temperature induced loading on silo walls. Structural Engineering Review, vol 4. In press

Encyclopedia of Fluid Mechanics

VOLUME 4

Solids and Gas-Solids Flows

N. P. Cheremisinoff, Editor

in collaboration with–

H. Arastoopour
Y. Arkun
W. H. Ayers
G. E. Blight
M. Bohnet
F. Boysan
T. E. Broadhurst
R. Chandran
J. C. Chen
L. H. Chen
P. N. Cheremisinoff
S. Chiba
T. Chiba
Y. O. Chong
M. Y. Dedegil
A. O. Denloye
J. Dirgo
R. P. Donovan
R. J. Dry
R. Echigo
H. Enomoto
K. Funatsu
W. E. Genetti
F. J. Gerchow
W. Gregor
N. S. Grewal
P. Guigon
M. Hartman
S. Hasegawa
M. Ishida
T. Ishikura
J. Kawabata
M. Kawahara
I. V. Klumpar
K. Kuramitsu
J. F. Large
D. Leith
L. S. Leung
H. Littman
K. Makino
T. Matsuda
S. Matsumoto
O. Molerus
Y. Molodtsof
M. H. Morgan III
A. Nishiwaki
E. Obata
T. A. Ring
F. Rizk
H. Seager
A. Shimizu
T. Shingles
H. Shinohara
K. Svoboda
J. Swithenbank
C. S. Teo
J. R. Too
Y. Tsuji
D. W. VanOsdell
H. Watanabe
B. R. White
K. E. Wirth
M. Yamada
W. C. Yang

CHAPTER 6

STRUCTURAL LOADING ON THE WALLS OF RAPIDLY FILLED SILOS

G. E. Blight

University of the Witwatersrand
Johannesburg, South Africa

CONTENTS

INTRODUCTION

This chapter deals with the pressures exerted on the walls of storage silos when they are rapidly filled with fine powders. There are many fine powders that are of commercial importance and which are produced and stored in large volumes. Examples are cement powder, cement raw meal, wheat

flour and powdered limestone or chalk. Figure 1 shows particle size distribution curves for some typical fine products. Generally 80 to 90% of the particles are in the size range between 0.1 mm and 0.001 mm. The rate at which fine powders are loaded into storage silos may be very large, especially if the decantation is intended to produce a measure of blending. For example, in a recently commissioned facility [1] the storage silos were designed for a maximum rate of rise of the fill surface of 35 m/h (115 ft/h) during filling. When a fine powder is rapidly loaded into a silo it entrains a large proportion by volume of air. The powder is deposited in a very loose state and then compresses as further overburden is deposited on top of it.

The pressure exerted on the silo walls at any depth below the fill surface is made up of two components: that exerted by pressure in the entrained air and that exerted by the solid particles, the intergranular pressure. The total horizontal pressure σ_h can thus be written as the sum of the intergranular pressure σ_h^1 and the pressure in the entrained air, or pore air pressure, p_a:

$$\sigma_h = p_a + \sigma_h^1 \tag{1a}$$

The compression or change in volume of the powder and its internal friction and friction against the walls of the silo is controlled by the intergranular pressure, not the total pressure. This is a sufficiently important point to warrant re-writing Equation 1a as

$$\sigma_h^1 = \sigma_h - p_a \tag{1b}$$

The relative magnitude of the initial value of p_a varies with the speed of filling and with the fineness of the powder. With extremely rapid rates of filling, p_a may be large enough to support much of the weight of the solid particles. In this case σ_h^1 will be small and the powder will be partly fluidized. As time passes after the deposition of a particular layer of fill in a silo, the entrained air will gradually escape, p_a will diminish and σ_h^1 will increase. Ultimately, all the entrained air will have escaped,

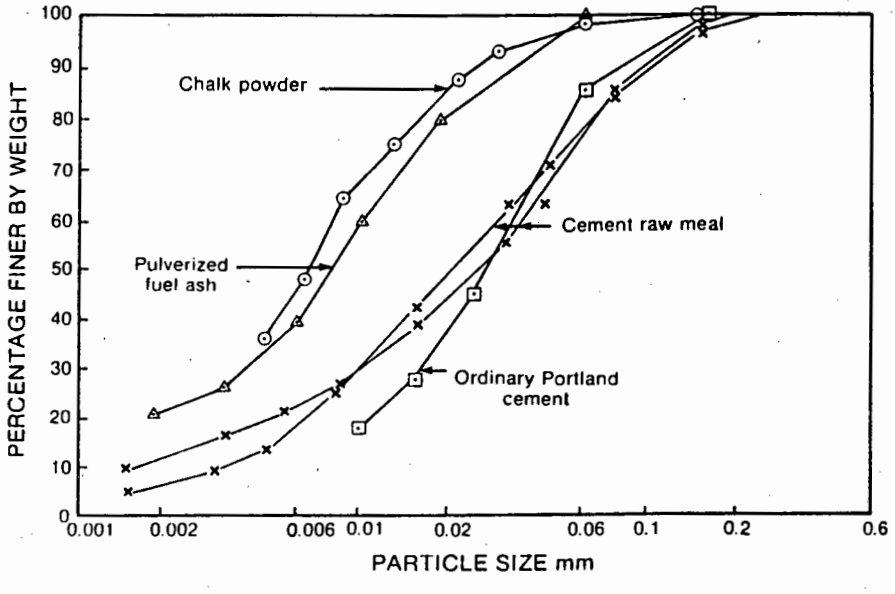

Figure 1. Particle size distribution curves for typical fine powders.

p_a will equal atmospheric pressive (zero gauge) and

$$\sigma_h^1 = \sigma_h \tag{1c}$$

The pressure for which the wall of a silo requires to be designed depends on the complex relationship between the rate of filling, and hence the rate at which over-burden stress builds up in the silo at a given level, the compression of the fill, and hence the generation of pore air pressure within its voids, and the rate at which the pore air pressure can dissipate. These processes decide on the build-up of friction on the silo walls which in turn, has a considerable effect on the horizontal pressure.

Before proceeding to consider the silo problem, therefore, it is necessary to consider some of the fundamentals of solids—void space geometry in powders and of the compression and the flow of air through powdery materials.

Throughout this chapter, reference will be made to measured parameters that are in common use in geotechnical and silo engineering. Because methods of measuring these are described in detail in a number of standard geotechnical engineering texts, the reader is referred to books such as those by Lambe and Whitman [2], Lee, White and Ingles [3] and Harr [4] rather than repeat descriptions of test apparatus and methods here.

SOLIDS—VOID SPACE RELATIONSHIPS FOR POWDERS

The state of packing of the particles in a powder can be described in terms of four parameters: the particle relative density or specific gravity G_s, the void ratio e, the porosity n, and the density or unit weight γ. The particle relative density G_s is the ratio of the mass of unit volume of solid particle to the mass of an equal volume of water. The void ratio e is the ratio of the volume of void space in a given mass of powder to the volume occupied by the solid particles. The porosity n is the ratio of the volume of void space to the total volume of powder. The unit weight γ is the weight of unit volume of powder.

The solid-to-void space relationships for a powder can be idealized as shown in Figure 2 in which all the void space has been lumped together to give void volume e while the solids have been lumped together to give unit solids volume. The relationships between the four parameters G_s, e, n, and γ can then be summarized as:

$$n = \frac{e}{1+e} \tag{2a}$$

$$\gamma = \frac{G_s \gamma_w}{1+e} \tag{2b}$$

In Equation 2b, γ_w is the unit weight of water and γ has units of kN/m^3, lbf/ft^3, kPa/m or $lbf/ft^2/ft$.

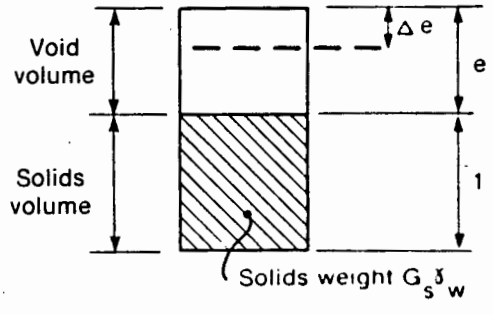

Figure 2. Solid-void space relationships for powders.

THE COMPRESSION OF FINE POWDERS

The compression of a fine powder is governed by the increase of intergranular pressure according to the equation

$$\frac{\Delta e}{1+e} = -C\,\Delta\sigma^1 \tag{3a}$$

where e = the void ratio,
Δe = the change in void ratio resulting from a change in intergranular stress $\Delta\sigma^1$
C = the variable compressibility of the powder
$\Delta e/1+e$ = the volumetric strain of the powder

If the void ratio of a powder is plotted against the logarithm of the intergranular stress, a linear relationship results as shown in Figure 3 [5]. It is evident from the parallelism of the four experimental curves in Figure 3 that the compressibility of a powder at a given intergranular stress is only slightly affected by the initial void ratio. The curves in Figure 3 all start from an initial intergranular stress of 25 kPa (3.6 psi). Separate measurements indicate that most powders have void ratios of about 1.7 to 1.8 at zero intergranular stress i.e. when deposited. When a powder is compressed without allowing the pore air to escape, (i.e. if the compression is undrained) the pore air pressure increases according to Boyle's law. Hence, it can be shown that the change of air pressure Δp_a produced by a change of void ratio Δe is given by:

$$\frac{\Delta p_a}{p_a} = \frac{-\Delta e}{e+\Delta e} \tag{3b}$$

Usually, Δe would be negative in sign, hence compression of the powder will result in an increase in p_a.

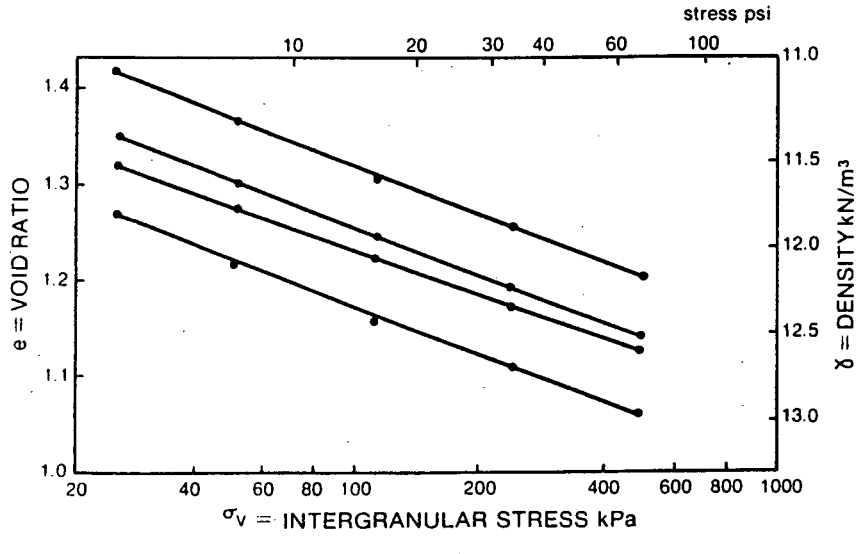

Figure 3. Compression curves for a fine powder (cement raw meal).

It is frequently useful to express the pore air pressure generated by an undrained compression Δe, in terms of the corresponding increment of total stress $\Delta\sigma$, thus:

$$\Delta p_a = B_a \Delta\sigma \quad \text{or} \quad B_a = \frac{\Delta p_a}{\Delta\sigma} \tag{3c}$$

B_a is known as a pore air pressure parameter. From Equation 3b:

$$B_a = -\frac{p_a}{\Delta\sigma} \cdot \frac{\Delta e}{e + \Delta e} \tag{3d}$$

Values of B_a for fine powders are generally in the range from 0.05 to 0.2 although measurements by Murfitt and Bransby [6] indicate that B_a could approach 0.5 in very loose powders. An indication of how compressible a powder has to be before B_a can approach 0.5 is given by the following analysis: Suppose $\Delta\sigma = p_a = 100$ kPa (1 atmosphere) and $B_a = 0.5$. Then from Equation 3d $\Delta e = -e/3$ or $\Delta e = -0,6$ if $e = 1.8$. A glance at Figure 3 will show that a change of void ratio of this magnitude is extremely large.

THE FLOW OF AIR THROUGH FINE POWDERS

Steady flow

The steady-state flow of air through the pores of a fine powder can be described by Fick's law [7], according to which

$$\frac{\partial m_a}{\partial t} = -F \frac{\partial p_a}{\partial z} \tag{4a}$$

where $\frac{\partial m_a}{\partial t}$ = the mass velocity of flow, i.e. the mass of air flowing normal to unit area of powder cross-section per unit time

$\frac{\partial p_a}{\partial z}$ = the pressure gradient in the direction of flow, the z-direction, and

F = a transmission constant having units of time (e.g. seconds or hours) if the pressure gradient is expressed in units of force per unit area per unit time

As shown by Figure 4A, Equation 4a only holds approximately as the relationship between mass velocity and pressure gradient is not completely linear. However, provided the range of pressure gradients or mass velocities that is of interest is not too large, Equation 4a gives a reasonably accurate representation of the steady-state flow of air through a fine powder. If the equation of state of air is taken to be

$$p_a v_a = \frac{R\theta m_a}{w_a} \tag{4b}$$

where p_a is the absolute pore air pressure, V_a the volume of air, w_a the molecular mass of mass m_a of air; θ is the absolute temperature and R the universal gas constant, Equation 4a can be rewritten in terms of a linear flow velocity, v_a as

$$v_a = -F \frac{R\theta}{w_a} \frac{1}{p_a} \frac{\partial p_a}{\partial z} \tag{4c}$$

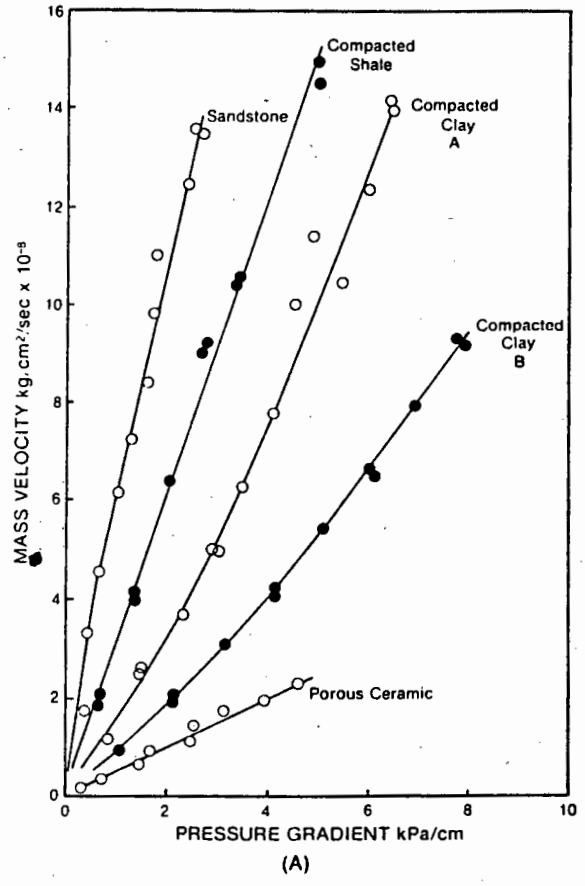

(A)

Figure 4. (A) Relationships between pressure gradient and mass velocity for flow of air through dry porous solids.

Unsteady Flow

When considering the escape of entrained air from the pores of a powdery silo fill, one is concerned with the phenomenon of unsteady flow of air from the pores of a material that compresses as the air escapes. In the case of steady flow, it did not matter whether the powder was compressible or rigid. Because steady-state conditions were being considered, the void ratio of the powder was not changing.

Consider an elemental volume of fixed size dxdydz in a powder through which air at constant temperature is flowing in the z-direction only.

The boundaries of the element are fixed in space and the powder within the element has a porosity n. If m_a is the mass of air entering the element in the z-direction in unit time, then using Fick's law,

$$m_a = nF \frac{\partial p_a}{\partial z} dxdy \qquad (4d)$$

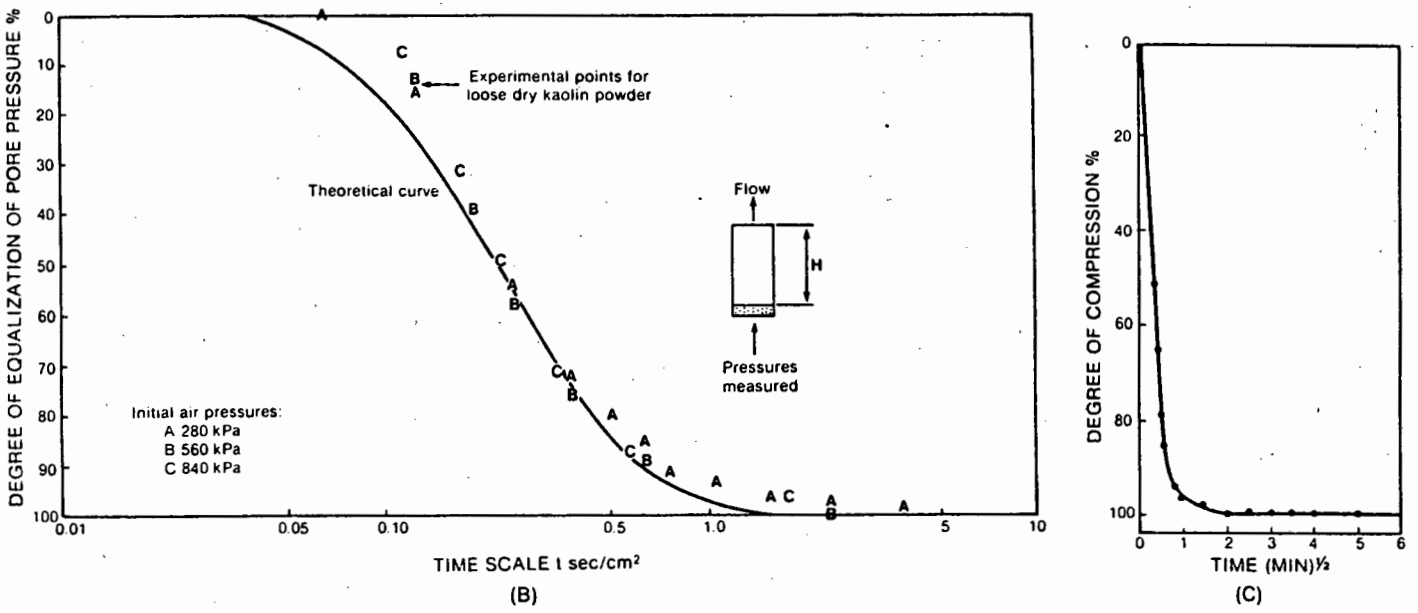

Figure 4. (B) Pressure equalization curves for unsteady flow of air through a compressible fine powder. (c) Compression time curve for fine powder subjected to stress increment.

If m_a is the mass of air contained in the element at any time, then for mass continuity of air,

$$\frac{\partial m_a}{\partial t} = \frac{\partial m_a}{\partial z} dz \tag{4e}$$

From the equation of state for air,

$$m_a = \frac{w_a}{R\theta} n p_a \, dxdydz \tag{4f}$$

and hence from Equations 4d and 4e,

$$\frac{\partial}{\partial t} n p_a = \frac{FR\theta}{w_a} \frac{\partial}{\partial z} n \frac{\partial p_a}{\partial z} \tag{4g}$$

This differential equation describes the unsteady flow of air through a compressing powder.

To solve Equation 4g, it is necessary to relate changes of the porosity n to changes in pore air pressure p_a, which can be done by using Equations 2a and 3d. However, a closed form solution cannot be obtained and each situation requires its own numerical solution.

Fortunately, however, the effect of the powder compressibility is small. If the powder is assumed for the moment to be rigid, Equation 4g reduces to

$$\frac{\partial p_a}{\partial t} = \frac{FR\theta}{w_a} \frac{\partial^2 p_a}{\partial z^2} \tag{4h}$$

This equation is linear and solutions for a number of initial and boundary conditions have been published. Figure 4B [7] compares the results of three sets of measurements taken during the unsteady one-dimensional flow or dissipation of air from the pores of three separate specimens of fine kaolin powder. The theoretical flow solution corresponding to Equation 4h has been fitted to the observations at a time corresponding to 50% equalization with atmospheric pressure of the air pressure at the impervious base of the specimen. Actually, the time t divided by the square of the maximum drainage path length H has been used as abscissa in Figure 4B. t/H^2 is plotted to a logarithmic scale to compress the time axis. In each case the specimen was compressed isotropically under undrained conditions. Drainage of air was then allowed to proceed from one end of the specimen while changes in pore air pressure were measured at the opposite (impermeable) boundary. The experimental results deviate from the theoretical curve by a maximum of 14% at a given time. Hence, an acceptable error is incurred if Equation 4h is used to describe the unsteady flow of air through a compressible powder, rather than the rigorously correct Equation 4g. Figure 4B also illustrates one method of evaluating the constant

$$c = \frac{FR\theta}{w_a} \tag{4i}$$

in Equation 4g. The actual value of t/H^2 at which 50% dissipation of pore air pressure occurs is compared with the corresponding theoretical value of ct/H^2 and hence c is found.

Alternatively, because the pore air pressure and the compression of the powder are related via Equations 1b and 3a, the process of pore air pressure dissipation can be followed by observing the time compression curve for the powder as shown in Figure 4C. The degree of equalization is simply taken as the compression at time t divided by the total compression undergone by the powder. In Figure 4C the time scale has been compressed by plotting to a square root scale. c is again found by comparing the observed t/H^2 with the theoretical value of ct/H^2 for a given degree of equalization.

For fine powders, values of c typically fall within the range 5 m^2h^{-1} to 50 m^2h^{-1}.

STRAIN CONDITIONS IN A POWDER DURING FILLING OF A SILO

When a fine powder is rapidly decanted into a silo, it is able to compress or strain vertically, but is prevented from straining laterally by the relatively rigid walls of the silo. The powder is thus subjected to one-dimensional compression with zero lateral strain.

An approximate relationship can be obtained between the horizontal and vertical intergranular stresses in the powder during this process if the grain skeleton of the powder is assumed to be elastic, or more correctly, if a linear relationship is assumed between intergranular stress and strain. The corresponding relationship between horizontal stress and strain is then

$$E\varepsilon_h = \sigma_h^1 - \nu(\sigma_v^1 + \sigma_h^1) = 0 \tag{5a}$$

in which E and ν are respectively the equivalent Young's modulus and Poisson's ratio of the powder, and ε_h is the (zero) lateral strain. Hence,

$$\frac{\sigma_h^1}{\sigma_v^1} = K_0 = \frac{\nu}{1-\nu} \tag{5b}$$

K_0, the ratio of horizontal to vertical intergranular stresses, is known as the "coefficient of lateral pressure at rest" in which the words "at rest" indicate the condition of zero lateral strain. For an incompressible material, $\nu = \frac{1}{2}$ and $K_0 = 1$, while for $\nu = \frac{1}{3}$, $K_0 = \frac{1}{2}$.

Several empirical relationships have been suggested between K_0 and the angle of shearing resistance ϕ^1 of granular materials. The most commonly used of these are due to Jaky,

$$K_0 = 1 - \sin\phi^1 \tag{5c}$$

and Reimbert,

$$K_0 = \frac{90° - \phi^1}{90° + \phi^1} \tag{5d}$$

See, for example, Harr [4].

If $\phi^1 = 30°$, $K_0 = \frac{1}{2}$ for Equations 5c and 5d, whereas if $\phi^1 = 20°$, $K_0 = 0.66$ by Jaky and 0.64 by Reimbert. In practice, it is more reliable to measure K_0 in the laboratory, especially as Equations 5c and 5d apply only to the first loading of a material. If the material is unloaded, K_0 ceases to be a constant ratio, and increases considerably.

There are many methods of measuring K_0 for fine powders [8], but all involve the principle of compressing a material vertically under a series of measured stresses, while simultaneously preventing lateral strain and measuring the lateral stress that is generated. During this process the pore air pressure must be controlled or measured so that the intergranular stresses can be determined in accordance with Equation 1b.

Figures 5A and 5B show measured relationships between σ_v^1 and σ_h^1 in cement powder and cement raw meal. In neither case is the ratio K_0 constant over the entire stress range, but tends to decrease from a value of about 0.7 at low stresses to 0.5 at higher stresses. The effects of unloading or stress reversal are not relevant to this chapter, but it should be noted that K_0 increases immediately unloading occurs.

Figures 5A and 5B each compare results obtained using the oedometer apparatus with those obtained by means of the triaxial cell. The reader is referred to the paper by Ofer and Blight [8] for full details of the test methods.

INTERNAL FRICTION AND WALL FRICTION IN SILOS

Both internal friction (or shearing resistance) and friction on the walls of a silo are a function of the intergranular stress σ^1 on the shearing surface. Internal shearing resistance τ can be characterized

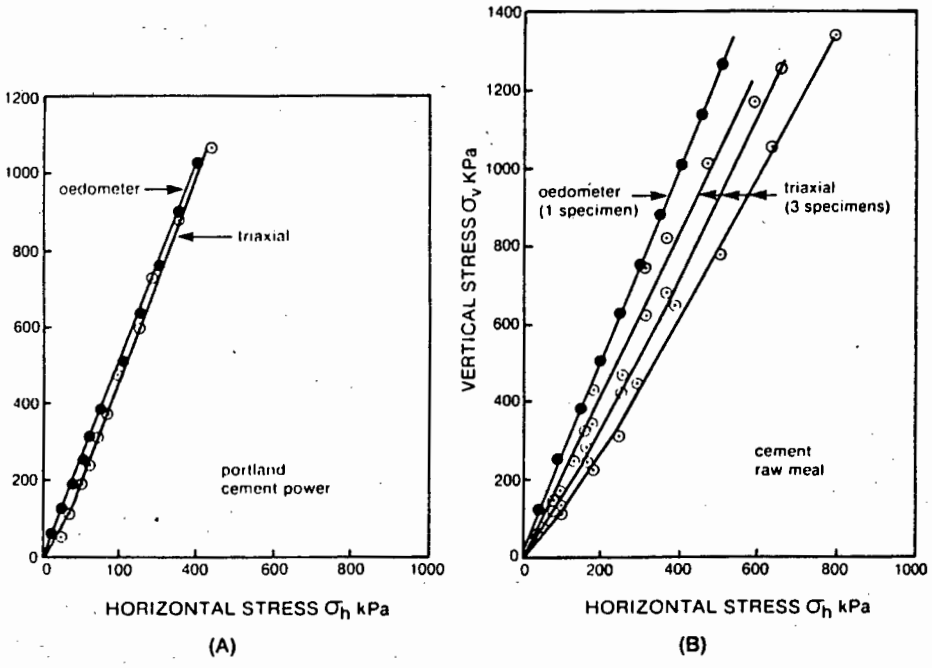

Figure 5. (A) Relationship between vertical and horizontal intergranular stresses for K_0 compression of cement powder. (B) Relationship between vertical and horizontal intergranular stresses for K_0 compression of cement raw meal.

by the equation

$$\tau = \sigma^1 \tan \phi^1 = (\sigma - p_a) \tan \phi^1 \tag{6a}$$

in which ϕ^1 is the angle of shearing resistance. Shearing resistance generated on the wall of a silo can be described by

$$\tau = \sigma^1 \tan \delta^1 = (\sigma - p_a) \tan \delta^1 \tag{6b}$$

in which δ^1 is the angle of wall friction. Note in both Equations 6a and 6b that if $p_a = \sigma$, the shearing resistance will be zero. (Reference to this point is made later.)

δ^1 and ϕ^1 are not generally equal as δ^1 depends on both the characteristics of the wall surface and the powder, while ϕ^1 depends only on the characteristics of the powder. However, for walls that are rough relative to the particle size of the powder, such as those of a reinforced concrete silo, δ^1 and ϕ^1 can be equated with little error.

Figure 6A shows the shearing characteristics of a typical fine powder, in this case, a cement raw meal.

Figure 6B shows a typical stress-strain characteristic measured in a triaxial shear test while Figure 6A also compares the internal shearing characteristic of the meal with the wall friction characteristic for meal on concrete.

Figure 6C shows the influence of relative movement between the fill and the wall on the angle of wall friction. When the fill is moving relative to the wall, the angle of wall friction increases to

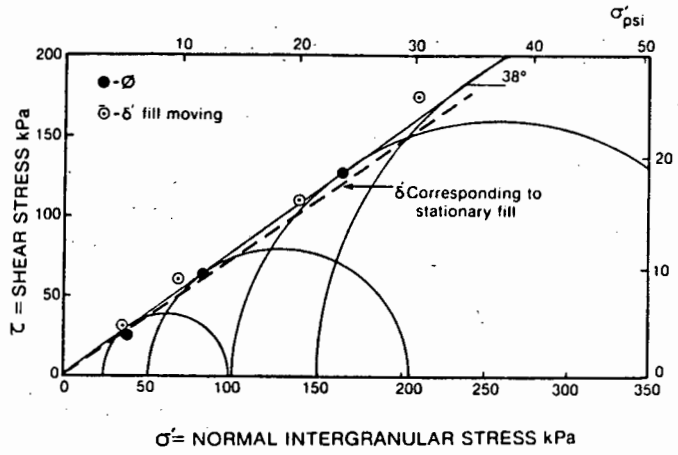

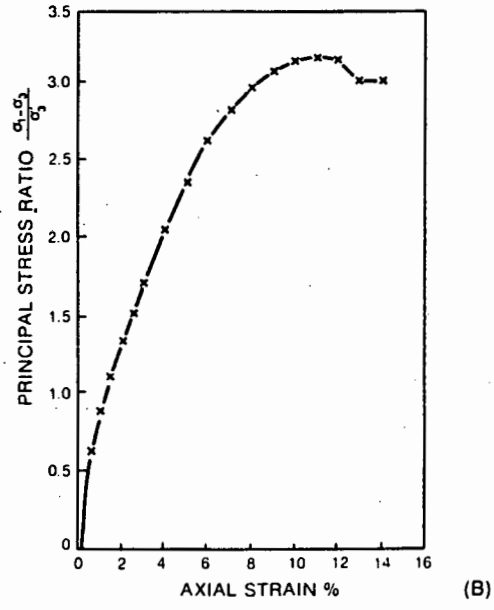

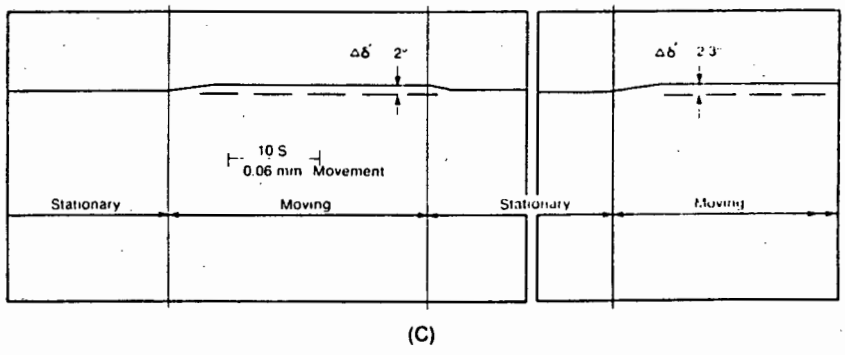

Figure 6. (A) Shearing characteristics of cement raw meal. (B) Stress-strain characteristic for triaxial shear of cement raw meal. (C) Effect of relative motion on angle of wall friction between cement raw meal and concrete surface.

above the static value, in this case by 2°. As the angle of wall friction appears as the tangent in Equation 6b this corresponds to a deviation of only about 4% from the static value. Values of ϕ^1 are similarly affected, static ϕ^1 values for powders being slightly less than dynamic values.

LOAD TRANSFER TO THE WALLS OF SILOS

As described in earlier, when a silo is filled, the fill is able to compress vertically, but lateral strain is prevented by the presence of the walls. The ratio of lateral to vertical intergranular stresses is therefore represented by K_0. Because the fill moves downward relative to the silo walls, wall friction is generated, which transfers some of the vertical stress into the silo walls. This action is illustrated by Figure 7, which shows the stresses acting on a typical elemental slice of fill at depth z below the fill surface in a cylindrical silo having diameter D. By considering vertical equilibrium of the element, the following differential equation may be derived:

$$\frac{d\sigma_v}{dz} = \gamma - \frac{4K_0}{D}(\sigma_v - p_a)\tan\delta^1 \tag{7a}$$

or

$$\frac{d\sigma_v}{dz} = \gamma\left\{1 - \frac{(\sigma_v - p_a)}{(\sigma_v - p_a)_{max}}\right\} \tag{7b}$$

where

$$(\sigma_v - p_a)\,max = \frac{\gamma D}{4K_0}\tan\delta^1 \tag{7c}$$

Equation 7b may be integrated to obtain the distribution of σ_v for any given distribution of p_a with z. For example, if p_a is zero, the differential equation integrates to the well-known Janssen equation:

$$\frac{\sigma_v}{\sigma_v(max)} = \{1 - e^{-\gamma z/\sigma_v(max)}\} \tag{7d}$$

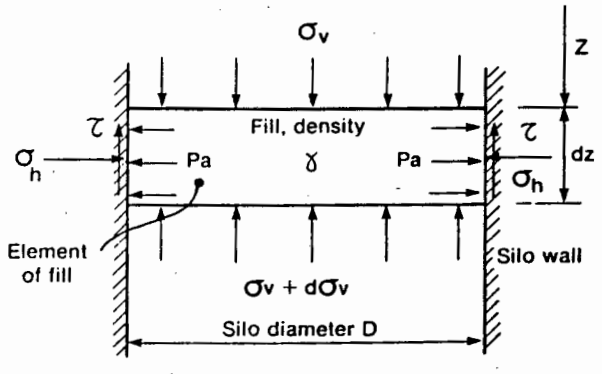

Figure 7. Stresses acting on an element of fill in a silo.

$$\text{in which } \sigma_v(\max) = \frac{\gamma D}{4K_0 \tan \delta} \tag{7e}$$

In this case

$$\sigma_h = K_0 \sigma_v \tag{7f}$$

whereas in the more general case of $p_a \neq 0$

$$\sigma_h = K_0(\sigma_v - p_a) + p_a \tag{7g}$$

It is clear from the form of Equations 7d and 7e that σ_v increases exponentially from zero at the fill surface towards an asymptotic value $\sigma_v(\max)$. When $\sigma_v(\max)$ is attained, the weight of the fill element in Figure 7 is just supported by the frictional forces on the walls of the silo. Examples of pressure-depth curves calculated from Equations 7d and 7e are given later.

The effect of σ_h is to induce hoop tension in the walls of a circular silo and bending and axial tension in the walls of a rectangular one. At a given depth z, the total load to be supported is the weight of the fill above z, plus the weight of the silo walls. The difference between the vertical load carried by the fill, namely

$$(\pi D^2/4) \cdot \sigma_v$$

and the weight of fill plus walls is carried by an axial stress σ_w in the walls which amounts to

$$\sigma_w = \frac{D}{4t}(\gamma z - \sigma_v) \tag{7h}$$

where t is the wall thickness (and the weight of the walls has been neglected).

If the silo walls are constructed of reinforced concrete, t is relatively large and σ_w generally of no consequence. However, in the case of a steel silo t is usually only a few millimeters (or eighths of an inch) and σ_w is often the stress that governs the design of the silo.

For the case of particular concern in this chapter, p_a varies both with time, according to Equation 4g or 4h and with stress, according to Equation 3d. For an analytical solution to silo pressures, it is therefore necessary to solve Equations 3d, 4h, and 7a simultaneously.

EMPIRICAL SOLUTION TO PRESSURES IN A RAPIDLY FILLED SILO

Martens [9] carried out laboratory-scale research into the effects of rapid filling of silos with fine powders. He used an instrumented model silo of 0.8 m (2.62 ft) diameter and 5.5 m (18.04 ft) high, but was apparently only able to measure total horizontal pressures, σ_h. No attempt was made to measure pore air pressures. The materials used consisted of powdered limestone, cement powder, and wheat flour. He came to the conclusion that the profile of σ_h in the zone affected by the speed of filling could be represented empirically by two straight-line relationships:

$$\sigma_h = 0.8\,\gamma z \tag{8a}$$

with a vertical cut-off at depth z given by

$$z = (v - v_0)t \tag{8b}$$

In the above, γ is the density of the powder in its loosest state, v is the filling speed or rate of rise of the fill surface in the silo; and v_0 is a limiting filling speed. If v and v_0 are expressed in mh^{-1}, t is taken as 1 hour. Table 1 summarizes the values of γ and v_0 established by Martens for his three materials.

Table 1
Properties of Materials Tested by Martens [10]

Material	Minimum Density γ		Limiting filling speed v_0	
	(kN/m³)	(lb/ft³)	(m/h)	(ft/h)
Powdered limestone	13.5	84	1.40	4.6
Cement powder	15.5	97	2.60	8.5
Wheat flour	7.0	44	4.80	15.7

Some of Marten's detailed results were published by Pieper [10] and are shown in Figures 8 and 9, which also show pressure-depth curves calculated according to the German standard for silo design DIN 1055 (1964), which is based on Equations 7d and 7e. It will be noted from Figures 8 and 9 that Martens did not investigate pressures *during* rapid filling but only the conditions at the completion of rapid filling, and subsequent pressure changes as the entrained air escaped.

Martens' work was subsequently extended by Nothdurft et al [11], who proposed a second empirical relationship:

$$\sigma_{ho} = (\min\gamma)\dot{v}t_a K_f \sqrt{R}\ 3.6 \text{ (in units of kPa)} \tag{8c}$$

where σ_{ho} = the maximum horizontal pressure
$(\min\gamma)$ = the minimum density of the powder
v = the rate of rise of the fill surface
t_a = a characteristic settling or de-aeration time for the powder
R = the hydraulic radius of the silo (the ratio of cross-sectional area to perimeter), and
K_f = the ratio of the total horizontal to vertical stresses in the fill

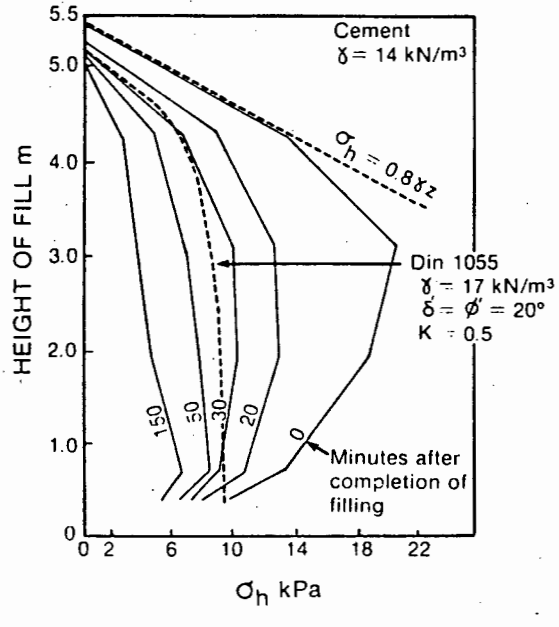

Figure 8. Variation of horizontal stress with time after completion of model silo filling with a fine powder (after Pieper [10]).

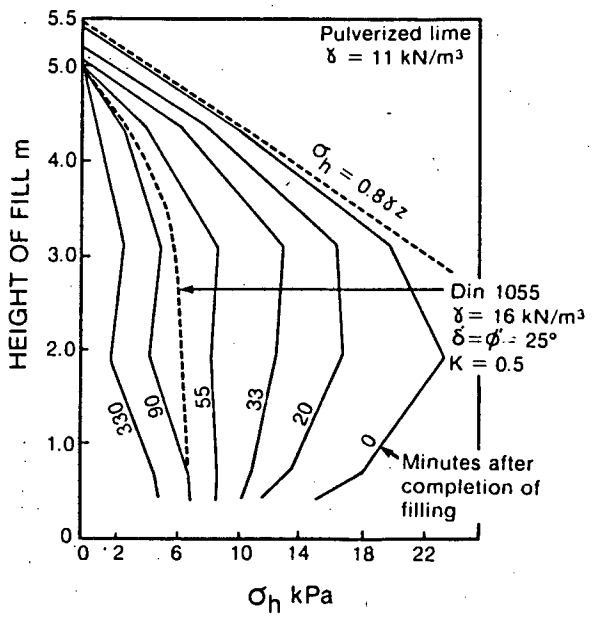

Figure 9. Variation of horizontal stress with time after completion of model silo filling with a fine powder (after Pieper [10]).

Values for these variables, recommended by Pieper, Martens, and Nothdurft [11] are given in Table 2.

Recently, Martens [12] has expressed the opinion that Equation 8a could be relaxed to

$$\sigma_h = 0.6\gamma z \tag{8d}$$

Note that the implication of both Martens' and Nothdurft's equations (8a-d) is that if the filling velocity is high enough, the fill will remain semi-fluidized (i.e., $\sigma_h = 0.6\gamma z$ to $0.8\gamma z$) throughout filling, no matter how deep the silo. If $\sigma_h = \lambda\gamma z$ and $\sigma_v = \gamma z$ (i.e. if the silo action described earlier is ignored), it can be shown from Equations 1a and 5b that

$$p_a = \frac{\lambda - K_0}{1 - K_0}\gamma z \tag{8e}$$

Table 2
Values of (min γ), t_a and K_f According to Nothdurft et al [11]

Material	(min γ) (kN/m³)	(min γ) (lb/ft³)	t_a (h)	K_f
Powdered limestone	11	62	0.24	0.55
Cement powder	13	81	0.19	0.53
Wheat flour	6	37	0.14	0.31

Hence, if $K_0 = 0,5$

$$p_a = (2\lambda - 1)\gamma z \tag{8f}$$

Note that only if $\lambda = 1$ will $p_a = \gamma z$. In other words, according to Equation 6b, only if $\lambda = 1$ will no frictional transfer of load to the wall of the silo occur. Conversely, if $\lambda < 1$ as suggested by Martens and Nothdurft, the gradient of σ_h with depth must decrease continuously and cannot be represented by a constant gradient λ.

MEASURED AIR PRESSURES IN RAPIDLY FILLED MODEL SILOS

Some seven years after the publication of Nothdurft's results, Murfitt and Bransby [6, 13] reported the results of a series of tests on two model silos, 1.83 m (6 ft) diameter by 4.24 m (13.91 ft) high and 2.44 m (8 ft) diameter by 4.21 m (13.8 ft) high. The silos were rapidly filled with a fine chalk powder, and the dissipation of pore air pressures with time after filling was studied. It was observed that the pore air pressure at completion of filling could be as much as 60% of the total stress measured at the silo wall. Thereafter, the dissipation of pore air pressure followed the predictions of Equation 4h fairly closely.

As a result of their measurements, Murfitt and Bransby [6] recommended that silos that are rapidly filled with fine powders should be designed to withstand hydrostatic pressures, i.e. that the horizontal pressure at the end of filling should be calculated as

$$\sigma_h = \gamma z \tag{9a}$$

It is strange that neither Murfitt and Bransby, Martens, nor Nothdurft attempted to scale the filling rates used for their model silos so that they would accord reasonably with filling rates that are practically attainable in full-scale silos. Sets of measurements in all three investigations commenced at the completion of filling and no attention appears to have been paid either to the rate of filling or the potential for the dissipation of pore air pressure during filling. At the time of writing, no published results on the build-up of pore air pressure in silos during filling exist.

MEASUREMENTS DURING RAPID FILLING OF A FULL-SCALE SILO WITH FINE POWDER

At the time of writing, only one set of measurements of pressures in a full-scale silo filled at various rates with a fine powder has been published [5]. The measurements were made on a cement raw meal silo at the Slurry works of the Pretoria Portland Cement Company. The assessment of pressures was made via strains measured in the hoop reinforcement of a silo 15 m (49.2 ft) in diameter by 43 m (141 ft) high. The silo forms part of a blending and storage complex for cement raw meal consisting of twin blending and storage silos.

Figure 10A shows a vertical section through one of the pair of silos. The blending silos form the upper one third of the storage height of the structure. When both blending silos are full, their contents can be discharged simultaneously into one of the two storage silos at filling rates of up to 10 m.h^{-1} (33 ft/h).

A description of the instrumentation and the method of interpretation of the strain readings is beyond the scope of this chapter and the reader is referred to the original paper for details.

Figure 10B summarizes the results of the investigation and also shows the maximum pressure line given by Equation 8d and the vertical cut-off line derived from Equation 8c for a filling velocity of 4.2 m/h (14 ft/h). The theoretical curves in Figure 10B have been derived by simultaneously solving equations 3d, 4h, and 7a as explained in the following section.

The effects of a variable filling speed are shown very clearly by the measurements that show certain similarities with the results of Martens' work (Figures 8 and 9). Although pressures increase as filling rates increase, there are certain puzzling features of the measurements that cannot yet be

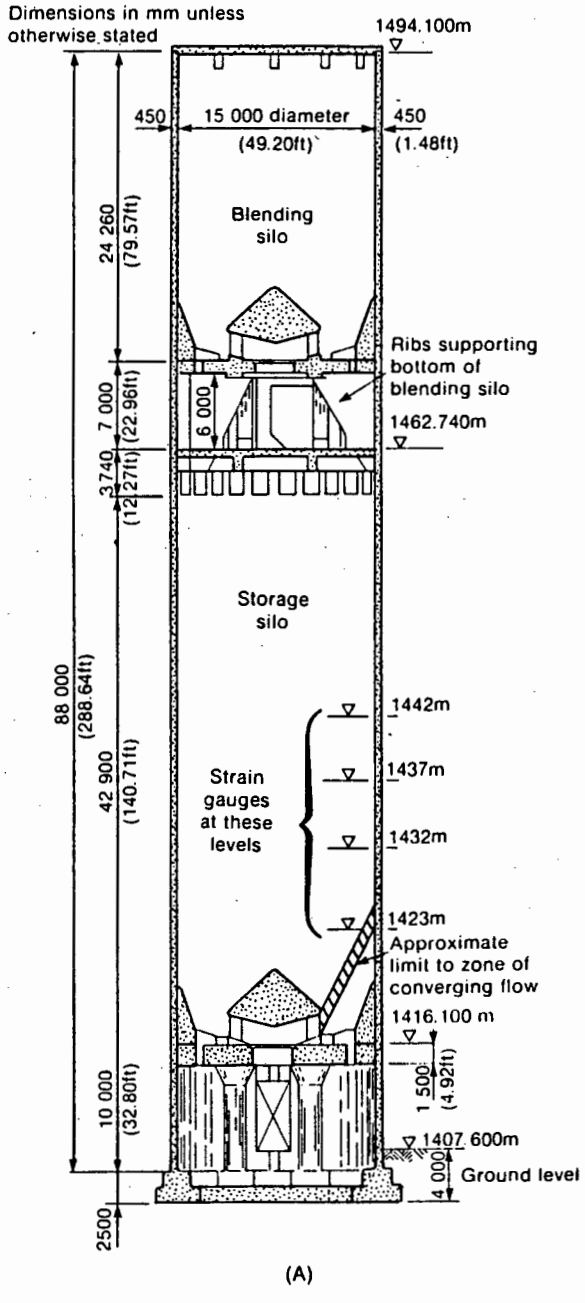

Figure 10. (A) Section through combined blending and storage silo in which pressures during rapid filling were investigated.

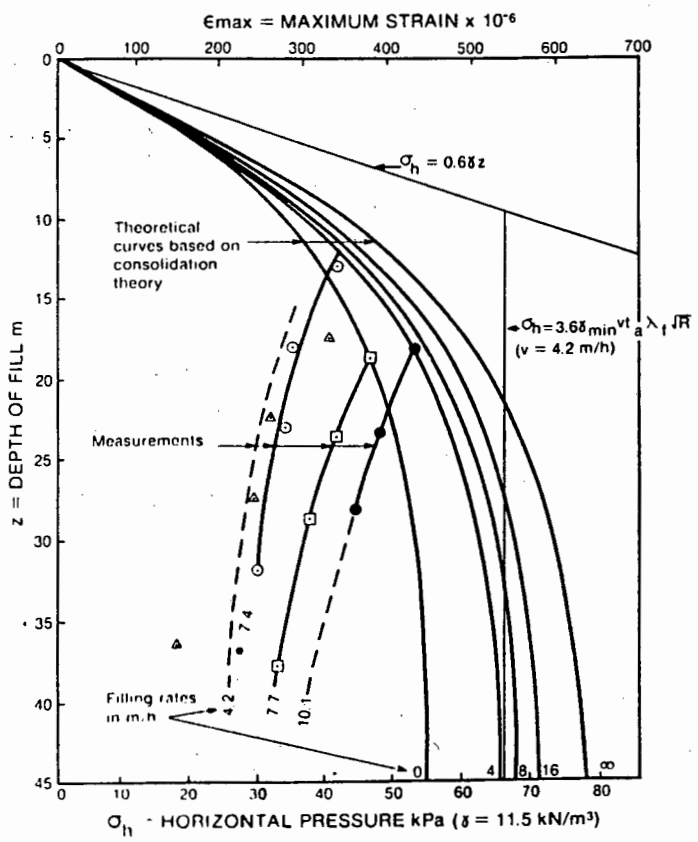

(B)

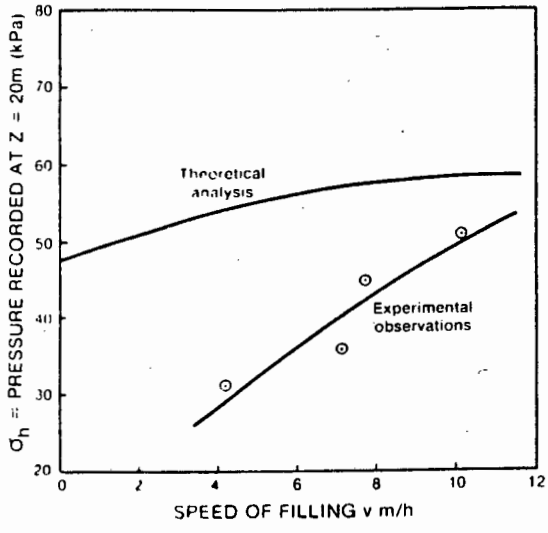

(C)

Figure 10. (B) Observed and calculated horizontal pressures during rapid filling of storage silo shown in Figure 10A. (C) Variation with speed of filling of pressure estimated and recorded in storage silo shown in Figure 10A.

explained. Why, for instance, do the pressures apparently decrease with increasing depth? (This feature is also shown by Martens' measurements and by some, but not all, of Murfitt and Bransby's). One possible explanation is that the angle of wall friction δ increases with depth, thus transferring more load into the walls and decreasing vertical and lateral pressures. Why are the pressures less even than those calculated from Equations 7d and 7e, which assume pore air pressures to be zero? (This same feature is evident in Martens' results). Only further research and field and laboratory measurements will provide an explanation.

From the designer's point of view, the importance of the Slurry results is that the maximum recorded pressures agree reasonably with those predicted on a rational basis. The results do not indicate that maximum pressures increase linearly with filling rate as this rate is increased, as predicted by Equations 8b and 8c.

Figure 10C compares measured and calculated pressures at a depth of 20 m below the fill surface at the completion of filling at various filling speeds. The theoretical analysis indicates an upper limit to the horizontal pressure of 60 kPa and the experimental observations tend towards a similar limit.

THEORETICAL SOLUTION TO SILO PRESSURES DURING RAPID FILLING

Equation 3d can be incorporated in Equation 4h by adding a term that accounts for the generation of pore air pressure as fill overburden builds up in a silo. With this modification, Equation 4h becomes

$$\frac{\partial p_a}{\partial t} = c\frac{\partial^2 p_a}{\partial z^2} + \gamma B_a \frac{dh}{dt} \tag{11a}$$

in which dh/dt is the rate of rise of the fill surface, i.e. the filling rate. Equation 11a must be solved simultaneously with Equation 7a,

$$\frac{d\sigma_v}{dz} = \gamma - \frac{4K_o}{D}(\sigma_v - p_a)\tan\delta' \tag{7a}$$

which can be accomplished by writing the equations in finite difference form with reference to the finite difference grid shown in Figure 11.

$$p_1 = p_0 + \frac{c\,\Delta t}{(\Delta z)^2}(p_2 + p_3 - 2p_0) + B_a\,\Delta\sigma_v \tag{11b}$$

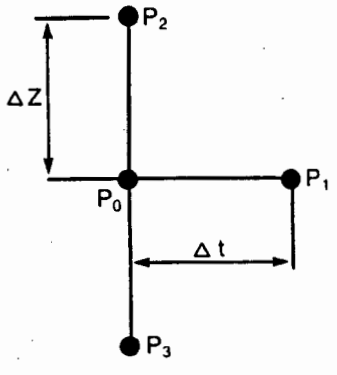

Figure 11. Finite difference grid used to calculate pressure during rapid filling.

$$\Delta\sigma_v = \Delta z\left\{\gamma - \frac{4K_0}{D}\tan\delta^1(\sigma_v - p_0)\right\} \qquad (11c)$$

in which p_1, p_0, etc. are the values of p_a at the nodes of the grid, Δz is a suitable depth differential and Δt a suitable time step. Once Δt has been chosen, Δh is fixed by the filling rate.

The actual solution of the equations is beyond the scope of this chapter, but the reader is referred to Lee, White and Ingles [3] for examples of the solution process for similar problems in geotechnical engineering.

Figure 10B shows the results of solving Equations 11b and 11c for the Slurry raw meal silo referred to earlier. It should be noted particularly that the range of pressures covered by the theoretical curves is about 50% of the maximum pressure at a filling rate of zero.

It should also be noted that the Nøthdurft-Martens envelope gives very reasonable agreement with the theoretical curves in this instance (i.e. a filling speed of 4.2 m/h). However, as the cut-off pressure (σ_{h_0} in Equation 8c) is directly proportional to the filling speed v, the corresponding envelope for a filling speed of 10 m/h would have predicted a maximum pressure of 10/4.2 = 2.4 times that shown in Figure 10B. This would have been quite unrealistic when compared with the measured pressures.

The largest of the measured pressures, on the other hand, agree quite well with the theoretical curves.

DESIGN ASSUMPTIONS FOR THE SILOS AT SLURRY

It is instructive to compare the assumptions used in the design of the Slurry silos with the pressures actually measured. The silos at Slurry were designed at a time (1974) when the only known work on the effects of rapid filling of silos with fine powders was that of Martens [9, 10]. The following filling possibilities were assumed for the silo [1]:

1. Discharge into an empty storage silo at a rate of 35 m/h from two full blending silos until the blending silo directly above the storage silo was empty, followed by transverse discharge at 5 m/h until the adjacent blending silo was empty.
2. Filling of an empty storage silo by vertical discharge at 30 m/h followed by filling at 5 m/h by transverse discharge.
3. The reverse of 2.
4. Starting at any fill level and then filling at any rate from 5 m/h to 35 m/h.

Once the material had been deposited in the silo, the horizontal pressure was assumed to revert to that corresponding to the Janssen Equations 7d and 7e with K taken not as K_0, but a lesser value, $K_A = (1 - \sin\phi^1)/(1 + \sin\phi^1)$.

In the absence of direct measurements, the angles of internal friction ϕ^1 and wall friction δ^1 were both taken as 20° while the density of the raw meal was taken as 1.7 T/m³ (17 kN/m³).

Martens gave v_0 (Equation 8b) for limestone as 1.4 m/h and this was assumed to be applicable also to cement raw meal.

In addition to the normal filling and emptying pressures in the storage silo, it was considered prudent to design the walls to withstand a nominal minimum pressure of 100 kPa that could be transmitted from the blending silo above. Figure 12A shows the resultant design pressure envelope.

The pressure envelope is made up as follows:

1. ab represents the pressure produced by filling the silo to just more than half at a rate of 35 m/h (z_0 = 33.6 m).
2. bcd represents the pressure produced by filling the upper half of an initially half-full silo at a rate of 35 m/h.
3. de represents portion of the static (Janssen) curve.
4. ef represents the minimum 100 kPa pressure.

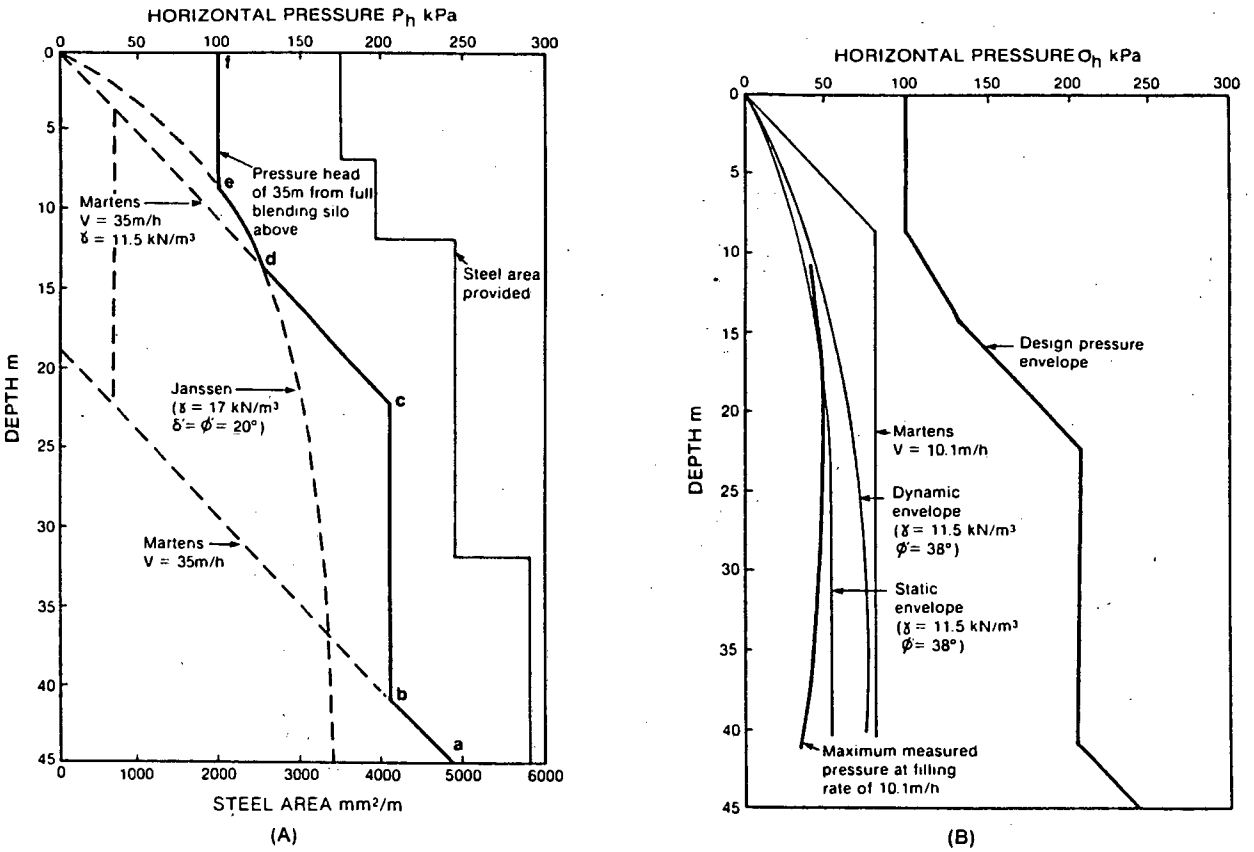

Figure 12. (A) Design pressure envelope for storage silo shown in Figure 10A. (B) Comparison of design pressure envelope (Figure 12A) with observed and calculated pressure envelopes (Figure 12B).

Figure 12B compares the design pressure envelope with the maximum measured pressures (v = 10.1 m/h) the static (v = 0) envelope, the dynamic (v = ∞) envelope and the Martens' envelope for v = 10.1 m/h.

In retrospect, there are several reasons for the large discrepancy between design assumptions and actual pressures:

1. The maximum filling rate turned out to be limited by the ducting connecting the silos and was only 10.1 m/h rather than the design figure of 35 m/h. (Figure 10C indicates that this would actually have made little difference to maximum pressures).
2. The actual settled density of the raw meal was 11.5 kN/m^3 rather than the assumed 17 kN/m^3.
3. The actual angles of shearing resistance and wall friction were 38° rather than the assumed 20°.

All of these differences, if known at the design stage, would have resulted in a lesser design pressure envelope, but the biggest source of discrepancy, by far, arose from assumption, necessary at the time, that Martens' model test results could be extrapolated to the full-scale situation. It is now clear that the reasonable agreement between the observed and theoretically predicted pressure envelopes and the Martens-Nothdurft envelopes in the filling speed range 4 to 10 m/h was largely coincidental.

PROPOSED DESIGN METHOD FOR RAPIDLY FILLED SILOS

The design method is based on the observation in Figure 10B that the increase in calculated horizontal pressure between the static condition (v = 0 and $p_a = 0$) and the fully dynamic condition (v = ∞ and $\Delta p_a = B_a \Delta\sigma_v$ is less than 100% of the static pressure. For design purposes, the fully dynamic condition will give a conservative but not unrealistic over estimate of horizontal pressures.

If both the pore air pressure and the vertical stresses are assumed to have datum values of zero, Equation 7a can be rewritten as

$$\frac{d\sigma_v}{dz} = \gamma - \frac{4K_0(1 - B_a)\tan\delta'}{D}\sigma_v \tag{13a}$$

or

$$\frac{d\sigma_v}{dz} = \gamma\left\{1 - \frac{\sigma_v}{\sigma_v(\max)}\right\} \tag{13b}$$

$$\text{in which } \sigma_v(\max) = \frac{\gamma D}{4K_0\tan\delta'}(1 - B_a) \tag{13c}$$

The solution to this equation is simply

$$\frac{\sigma_v}{\sigma_v(\max)} = \{1 - e^{-\gamma z/\sigma_v(\max)}\} \tag{13d}$$

which is identical to Equation 7d, although, of course $\sigma_v(\max)$ is different. Also,

$$\sigma_h = \sigma_v[K_0(1 - B_a) + B_a] \tag{13e}$$

γ, K_0 and δ' should be established by direct testing of the powder product it is proposed to store. If the product is not available, tests should be performed on the closest available approximation to

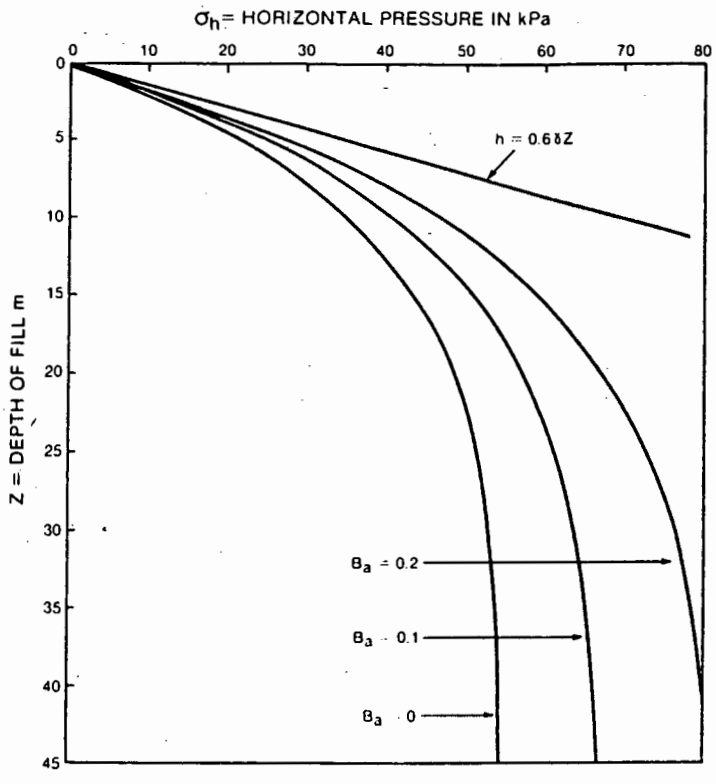

Figure 13. Design curves for storage silo shown in Figure 10A showing the effect of the pore pressure parameter B_a on pressure (Calculated from Equations 13c, 13d, and 13e).

the product. Only as a last resort should a design be based on parameters taken from the literature, although these are useful as a check on the reality of actual test results.

B_a can either be established by direct test, compressing the powder under a series of total stresses in an undrained condition and measuring the resultant pore air pressures (see Equation 3c) or B_a can be assessed from the results of drained compression curves, yielding a relationship between σ_1' and e, via Equation 3d. Figure 13 shows a family of design curves calculated for the Slurry silo for a range of values of B_a. (If the curves for $B_a = 0$ and $B_a = 0.1$ are compared with those for filling rates of zero and ∞ in Figure 10B, slight discrepancies will be noted. This is because the two sets of curves were calculated for slightly different values of γ: 12.0 kN/m^3 in Figure 10B and 11.5 kN/m^3 in Figure 13. Also, the curves in Figure 10B were derived by numerical integration and not from a formal expression).

CONCLUSION

When referring to knowledge of a particular subject, the term "encyclopedic" usually denotes an all-embracing exhaustive state of knowledge. Engineering knowledge, of course, is not like that. It is continually being added to, corrected, and enlarged and is continually sprouting side-shoots of

knowledge that either die and are forgotten when they outlive their usefulness, or flourish, grow and in due course push out their own side-shoots of specialized knowledge. The subject dealt here is a side-shoot of the main branch of knowledge of silo design. It is a specialized, and currently important avenue of knowledge which is, however, unlikely ever to have a similar effort expended on it as the main field of silo design. It is hoped that the foregoing summary of available knowledge of the subject will prove adequate as a frame-work within which the present-day designer of silos intended for rapid filling with fine powders can operate.

NOTATION

B_a	pore air pressure parameter	m	mass
C	compressibility	n	porosity
c	constant defined by Equation 4i	p_a	pore air pressure
D	diameter	R	universal gas constant; also hydraulic radius of silo
E	Young's modulus		
e	void ratio	t	wall thickness or time
F	transmission constant	t_a	characteristic settling or de-aeration time for powder
G_s	particle relative density		
H	height	V_a	volume of air
K_f	ratio of total horizontal to vertical stress in the fill	v_0	filling speed
		w_a	molecular mass
K_0	ratio of horizontal to vertical intergranular stresses	z	depth

Greek Symbols

γ	specific weight	σ_{ho}	maximum horizontal pressure
δ'	angle of wall friction	σ_w	axial stress
ε	strain	σ'	intergranular pressure
θ	absolute temperature	τ	shearing resistance
ν	Poisson's ratio	ϕ'	angle of shearing resistance
σ	pressure		

REFERENCES

1. Schaffner, R. H., and Blight, G. E., "Comparison of Design Assumptions and Measured Performance for Cement Works Silos", *Proceedings, 2nd International Conference on Design of Silos for Strength and Flow*. Stratford-upon-Avon, U.K., 1983, vol. 1, pp. 207–216.
2. Lambe, T. W., and Whitman, R. V., *Soil Mechanics*, New York, Wiley, 1969.
3. Lee, I. K., White, W., and Ingles, O. G., *Geotechnical Engineering*, Melbourne, Pitman, 1983.
4. Harr, M. E., *Mechanics of Particulate Media*, New York, McGraw-Hill, 1977.
5. Blight, G. E., Schaffner, R. H., and Gilbert, B., "Strains in a Reinforced Concrete Silo During Rapid Filling with a Fine Powder," *Journal of Powder and Bulk Solids Technology*, vol. 6, No. 2, 1982, pp. 17–27.
6. Murfitt, P. G., and Bransby, P. L., "Pressures in Hoppers Filled with Fine Powders," *Proceedings, 1st International Conference on Design of Silos for Strength and Flow*. Lancaster, U.K. 1980, vol. 1, 51 pp.
7. Blight, G. E., "Flow of Air Through Soils," *Journal of the Soil Mechanics and Foundations Division* ASCE, vol. 97, No. SM4, 1971, pp. 607–624.
8. Ofer, Z., and Blight, G. E., "Laboratory Determination of K_0 and Comparison with Prototype Silo Observations," *Proceedings, 4th Australia-New Zealand Conference on Geomechanics*, Perth, Western Australia, 1984.

9. Martens, P., "*Silolasten Aus Staubförmiger Schuttgütern und aus Luftzufuhr*," Dr. Ing Dissertation, Technische Universität Carolo-Wilhelmina zu Braunschweig, West Germany, 1969.
10. Pieper, K., "Investigation of Silo Loads in Measuring Models," *Journal of Engineering for Industry*, ASME, May 1969, pp. 365–372.
11. Pieper, K., Martens, P., and Nothdurft, K., "Silolasten aus Mehl, *Aufbereitungs-Technik*, vol. 16, No. 11, 1975, pp. 579–585.
12. Martens, P, personal communication.
13. Murfitt, P. G., and Bransby, P. L., "Deaeration of Powders in Hoppers," *Proceedings, Powder Europa 80 Conference*, Wiesbaden, West Germany, 1980.

BLIGHT, G. E. (1986). *Géotechnique* **36**, No. 1, 33–46

Pressures exerted by materials stored in silos: part I, coarse materials

G. E. BLIGHT*

Silos are usually designed on the basis of simple theory which is used to predict horizontal pressures on the walls. The pressures generated depend on many factors, including the pattern of flow within the contained material, the method of operating the silo and also the mechanical characteristics of the material. This Paper compares pressures measured in a number of full-scale silos containing coarse materials with the predictions of commonly accepted design theory. It shows that, although the silo arching theory gives an acceptable estimate of the average pressure on a silo wall, it does not always provide an adequate design envelope. It is preferable to use a simple straight line variation of pressures with depth for design.

Les silos sont généralement calculé sur la base d'une théorie très simple utilisée pour prévoir les pressions horizontales sur les murs. Les pressions réellement exercées dépendent de plusieurs facteurs, dont la forme de l'écoulement à l'intérieur de la matière, le principe du fonctionement du silo et aussi les caractéristiques mécaniques de la matière ensilée. L'article compare les pressions mesurées dans quelques grands silos contenant des matières à gros grains avec les prévisions de la théorie classique. Bien que la théorie de l'effet de voûte dans un silo donne une évaluation acceptable de la pression moyenne sur la paroi mur, cette théorie ne fournit pas toujours une enveloppe acceptable. Il paraît préférable d'utiliser pour les calculs des pressions proportionelles à la profondeur.

KEYWORDS: case history; design; earth pressures; field instrumentation; granular materials; silos.

INTRODUCTION

Storage silos form a class of structure that is subject to an unusually high rate of structural and functional failure. The extent of structural failure varies from cracking of the walls of reinforced concrete silos to localized denting or buckling of the walls of steel silos and to complete splitting or collapse of the walls. Functional failure may be represented by the inability to extract the contents of the silo, spoiling of the contents by leakage of rain-water through cracks in the walls, excessive vibration leading to cracking and a variety of similar shortcomings. Foundation problems may also result in either functional or structural problems arising from differential settlement or, in several recorded instances, in toppling of the structure.

Theimer (1969) described failure by toppling or partial or complete collapse experienced by 14 reinforced concrete grain silo complexes and records less spectacular, but equally serious, problems that arose in eight other cases. Sadler (1980) described 15 cases of partial or complete collapse of silos built in the US to store materials as diverse as raw or washed coal, polyethylene pellets, grain, silage and coke.

An extensive inventory of failures in steel, reinforced brickwork and reinforced concrete silos in Europe has also been given by Ravenet (1981).

The denting of steel silos has been described by Jenike (1967). In a recent survey of grain storage silos in Scandinavia (Wigram, 1980), 34% of the reinforced concrete silos examined were found to have suffered vertical cracking of the walls.

Most functional failures of silos arise because they will not empty or because they empty in an unforeseen way. Functional failure may lead to structural failure. For example, Sadler (1980) described how emptying of a steel silage silo caused a void to form at the base of the silo while the material above arched across the void. As a result of the increased axial load in the walls, the walls buckled and the silo collapsed.

The frequent and continuing problems experienced with silos of all types may be ascribed to the following: silos are one of the few classes of structure that are subjected to their full or more than full design load over most of their life-span; the estimation of loads and pressures is uncertain because

(*a*) pressures are dependent on the flow pattern that develops in the silo, which may be difficult to determine at the design stage, or may not be appreciated by the designer: the flow pattern may also be affected by the way in which a silo is operated

(*b*) pressures depend on the characteristics of the stored material: very often, silos have to be designed before the material they are to store is available or has been produced; consequently, the design must be based on assumed

Discussion on this Paper closes on 1 July 1986. For further details see inside back cover.

* University of the Witwatersrand.

rather than measured material properties; also, the properties of stored materials may (and probably will) vary to an unpredictable extent during the operating life of the silo

(*c*) relatively slight deviations during construction from the designed form and dimensions of a silo may have unexpectedly large effects on the pressures (Jenike, 1980; Nielsen & Kristiansen, 1980), e.g. a localized internal ridge may cause a substantial pressure increase at that point

(*d*) slight variations in material properties, moisture content, storage time, etc. may result in the formation of arches in a silo: it is impossible to predict the positions at which arches will form and almost impossible to predict the pressure concentrations that will result from the arch action, and most importantly it is uneconomic to design a silo to resist either the arching pressures or the shock loading that may result when an arch collapses

(*e*) the accuracy of theories from which silo pressures can be calculated is limited by the assumptions on which they are based: the situations to which the theories are applied frequently do not match up to these assumptions, and it is because of the uncertainties that there has been a steady increase over the years in the design pressures called for by various authorities, e.g. the 1980 draft revision of the German design standard, DIN 1055, required design pressures about 18% in excess of those of the 1964 version (Martens, 1980).

Because of the complexities and uncertainties involved, it is not generally considered to be worthwhile to attempt to apply sophisticated theory or analysis to the estimation of wall loads in silos and hoppers. Silo design codes, of which the most widely used are the German DIN 1055 (Martens, 1980) and that of the American Concrete Institute (1975), are based on relatively simple theories—those of Janssen (1895), Reimbert & Reimbert (1956) and Walker (1966).

The object of this Paper is to present the results of a series of cases in which pressures have been measured in full-scale operating silos and to compare the measured pressures with the predictions of simple theory. This comparison will show whether currently accepted theory, when used in conjunction with realistic materials parameters, is adequate to predict pressures in operating silos. Some of the measurements have previously been published (e.g. Hartlen, Nielsen & Ljunggren, 1984; Blight, 1983a; Blight & Midgley, 1980) but others have not.

The use of the term 'coarse materials' in the title indicates that the Paper will be concerned entirely with materials in which pore air pressures will not develop during filling, and compressed air is not used as an aid to emptying, i.e. total and effective stresses become synonymous throughout the Paper.

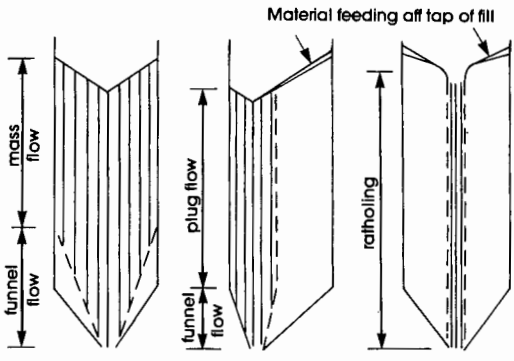

Fig. 1. Four principal types of flow occurring in silos

A companion paper (Blight, 1986) will deal with horizontal pressures exerted by fine powders stored in silos.

THEORETICAL BACKGROUND

Patterns of flow within silos

In designing a silo, at least two operational conditions must be considered—those of filling and emptying. It is apparently during the emptying phase that most problems develop, and many silo collapses have reportedly occurred at the first attempt to empty the structure.

With most materials a 'first in, first out' sequence of flow is desirable. This is particularly so with materials that spoil with time, e.g. foodstuffs, cement and coal (which may become subject to spontaneous combustion if stored undisturbed for a lengthy period). With other materials, e.g. ores, sand, etc., it may not matter whether a storage structure contains extensive zones of 'dead' material that will not emerge until the structure is completely emptied.

Figure 1 illustrates the four principal types of flow occurring in a silo. The first in, first out sequence is best obtained by mass flow in which the entire body of material contained within the parallel-sided portion of the silo moves through as a mass.

In order for the contents to emerge from the silo, flow must converge towards the outlet, resulting in a funnel flow. Depending on the configuration of the bottom of the silo, the boundary of the convergent flow will either coincide with the solid hopper wall of the silo, or else 'live' material will slide over 'dead' material at the base of the silo.

Plug flow usually occurs when the outlet to a silo is eccentric. Within the boundaries of the

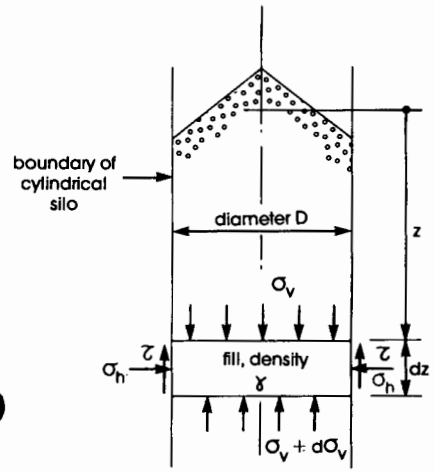

Fig. 2. Basis of the Janssen arching theory for pressure in parallel-sided silos

plug, mass flow occurs, but the plug is fed off the top of the stored material, resulting in a 'first in, last out' flow sequence. At the boundary of the plug, live material again slides over dead material. Plug flow is a special case of funnel flow. In some silos funnel flow will extend up to the top surface of the fill and may be fed off the top. Rat holing is a special case of plug flow in which the diameter of the plug is approximately the same size as the silo outlet. A rat hole may be fed off the top of the fill, or in cohesive material may become a stable empty hole, in which case the silo will not further empty. Multiple rat hole flow is sometimes designed for in blending silos in which the silo is first completely filled and then emptied in such a way that the successive layers that occupy a potential rat hole emerge in quick succession a blending chamber.

Simple theory of silo pressures

Janssen arching theory (1895). Fig. 2 represents an element of fill of density γ in the parallel-sided portion of a cylindrical silo. The element is moving down relative to the silo wall. It can be imagined that as the depth z of the element increases the shear stresses on the boundaries of the element will increase until the weight of the fill element is balanced by the boundary shear force. At this stage

$$\frac{\pi D^2}{4}\gamma\,dz = \pi D\tau\,dz$$

or

$$\tau = \frac{D\gamma}{4}$$

Writing

$$\tau = K\sigma_v \tan\delta$$

where

$$K = \sigma_h/\sigma_v$$

$$\sigma_v = \frac{D\gamma}{4K\tan\delta} = \sigma_v(\max) \qquad (1)$$

This represents the maximum vertical stress in the silo fill. If the element shown in Fig. 2 is sliding relative to the solid walls of the silo δ will represent the angle of wall friction between the silo wall and the filling. If the element is sliding relative to dead fill (as in plug flow) $\delta = \phi$, the angle of shearing resistance of the fill. At lesser depths, the vertical stress will be governed by the requirement for vertical equilibrium of the element which is

$$\frac{d\sigma_v}{dz} = \gamma\left[1 - \frac{\sigma_v}{\sigma_v(\max)}\right] \qquad (2a)$$

This can be integrated to give

$$\frac{\sigma_v}{\sigma_v(\max)} = 1 - \exp\left[-\frac{\gamma z}{\sigma_v(\max)}\right] \qquad (2b)$$

Also

$$\sigma_h = K\sigma_v \qquad (2c)$$

This is the simple Janssen theory on which most silo design codes are based. The alternative common theory, due to Reimbert & Reimbert (1956) recognizes the existence of $\sigma_v(\max)$ and then postulates that the pressure increases hyperbolically from zero at the surface of the fill to the $\sigma_v(\max)$.

It should be noted that Janssen's and Reimberts' theories apply strictly only to parallel-sided silos of infinite depth.

The value of K in equation (2c) has so far not been defined. Janssen's original theory defines K as K_A, the active pressure coefficient. When a granular fill is poured into a silo, it forms a conical pile in which conditions are probably active. As the fill deposited at a particular level is buried, it becomes subject to one-dimensional consolidation. It is therefore reasonable to expect the pressure coefficient to increase and approach K_0, the coefficient of earth pressure at rest for the normally consolidated material.

Walker theory (1966). The basis of Walker's theory is illustrated in Fig. 3.

The requirement for equilibrium of the element of fill at height h above the apex of the conical hopper is

$$\frac{d\sigma_v}{dh} = \frac{2K\sigma_v \tan\delta}{h\tan\alpha} - \gamma \qquad (3)$$

which can be integrated for the boundary condition

$$\sigma_v = 0 \quad \text{at } h = 0$$

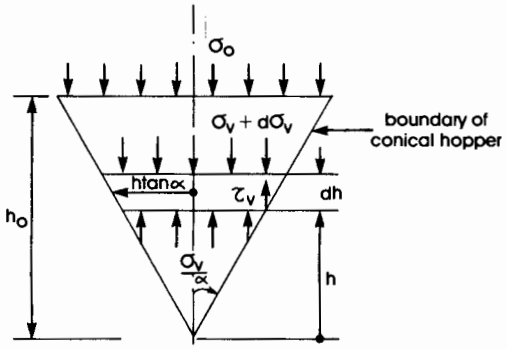

Fig. 3. Basis of the Walker arching theory for pressures in convergent hoppers

to give

$$\sigma_v = \frac{\gamma h}{C-1}\left[1-\left(\frac{h}{h_0}\right)^{C-1}\right] + \sigma_0\left(\frac{h}{h_0}\right)^{C} \quad (4a)$$

$$C = \frac{2K\tan\delta}{\tan\alpha} \quad (4b)$$

Because of the imposed boundary condition, equations (4) apply to emptying of the hopper. It is implicit that the pressure will decrease to zero at the outlet.

Once again, K has not been defined. Because the vertical stress must decrease as the material moves towards the outlet, material in a hopper becomes overconsolidated. K must therefore, increase and can be expected to approach K_0 for the overconsolidated material.

Filling and emptying conditions

The theory outlined above assumes that the fill has settled relative to its boundaries sufficiently to mobilize full wall shear (for a solid boundary) or full internal shear (when sliding over dead material). Wall shear can be fully mobilized by a shear displacement of 2–5 mm. Full internal shear can be fully mobilized by a shear displacement of 5–10 mm. The contents of a large silo will compress by at least 1% (10 mm per metre). Hence, when a silo is filled without interruption, it must be expected that boundary shear stresses such as those shown in Figs 2 and 3 will be fully developed.

When a silo is filled without interruption, the trajectories of major principal stress σ_1 will be as shown in Fig. 4. On the axis of the silo, the major

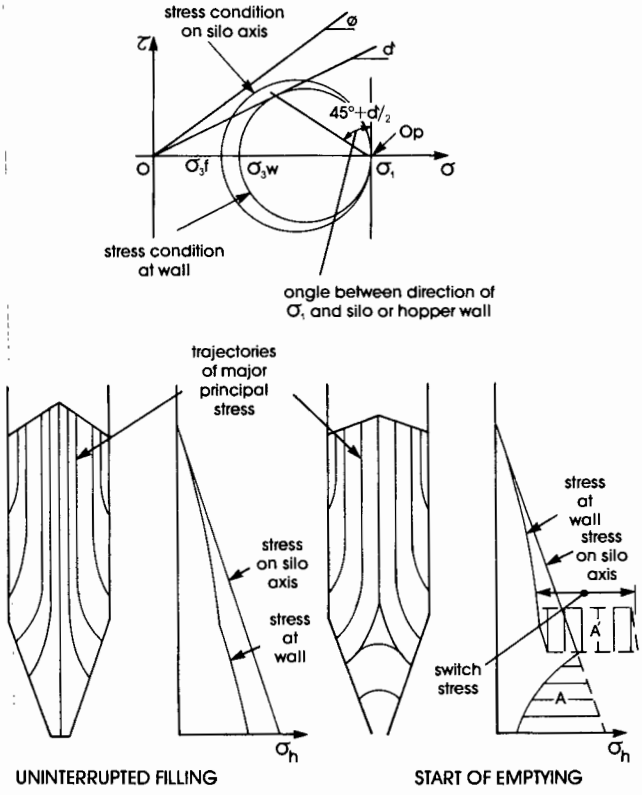

Fig. 4. Expected trajectories of major principal stress and distributions of horizontal pressure in silos

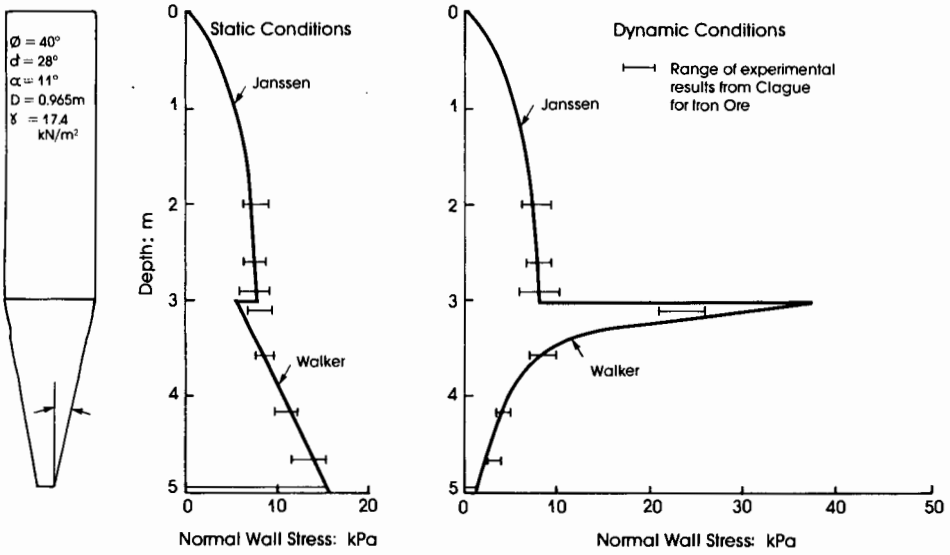

Fig. 5. Measurements by Clague (1973) of pressures normal to the wall of a small silo

principal stress will be vertical, whereas at the walls sufficient compression of the fill will normally occur to mobilize full wall friction. The trajectories of σ_1 will therefore intercept the wall at an angle of $45° + \delta/2$. At the wall, part of the weight of the fill will be supported by friction; hence the vertical stress will be reduced relative to the stress on the axis of the silo. Provided that the stress ratio K at the wall is not much different from that on the axis, the horizontal stress will also be reduced as indicated on Fig. 4. It is unrealistic to believe (as assumed in Janssen's theory) that wall friction affects stresses in more than a narrow annular zone near the wall.

When emptying is started, the material is caused to converge towards the outlet. The horizontal stress may increase, while simultaneously, because the stress at the outlet must be low, the vertical stress in the zone of convergent flow must decrease. Conditions therefore approach those assumed by the Walker theory, with the major principal stress in this zone tending to the horizontal.

In the zone of convergent flow, the weight of fill previously supported by vertical stress (area A in Fig. 4) has to be transferred to the walls where it is carried in friction to preserve vertical equilibrium. This transferred load is indicated by A' in Fig. 4 and must result in an increased horizontal stress in the area of transition between static fill and fill in which convergent flow is beginning.

There is some argument about the existence and magnitude of this 'switch stress' as well as about whether it becomes 'locked' in position at the transition between the parallel and convergent flow zones in the silo (the view of Jenike, Johansen & Carson (1972) and Nanninga (1956)) or travels up throughout the height of the silo (Walters' view (1973)).

It is only in certain special purpose silos, e.g. train or ship load-out silos, that the idealized states of uninterrupted filling followed by emptying are realized in practice. Most practical silos are subjected to mixed filling and emptying in which partial filling or refilling is followed or accompanied by partial emptying.

The idealized conditions discussed in this section are borne out by a limited number of tests on model or small-scale silos. Fig. 5, for example, shows the results of measurements by Clague (1973) on a small silo 5 m in height and 1 m in diameter. It should be noted that Clague's results are shown in terms of stress normal to the silo wall, rather than horizontal stress. This explains the discontinuity in the stresses measured on the cylindrical and hopper portions of the silo. Jenike *et al.* (1972) and Walker (1966) have presented similar measurements for small diameter model silos.

PRESSURES OBSERVED IN FULL-SCALE SILOS

Many of the studies reported in the literature, of pressures measured in silos, are suspect because of what appears to be inadequate instrumentation, inadequate use of instrumentation or incorrect interpretation of experimental readings.

Care has been taken in this Paper, and its companion (Blight, 1986), to include only cases where there is confidence that experimental readings

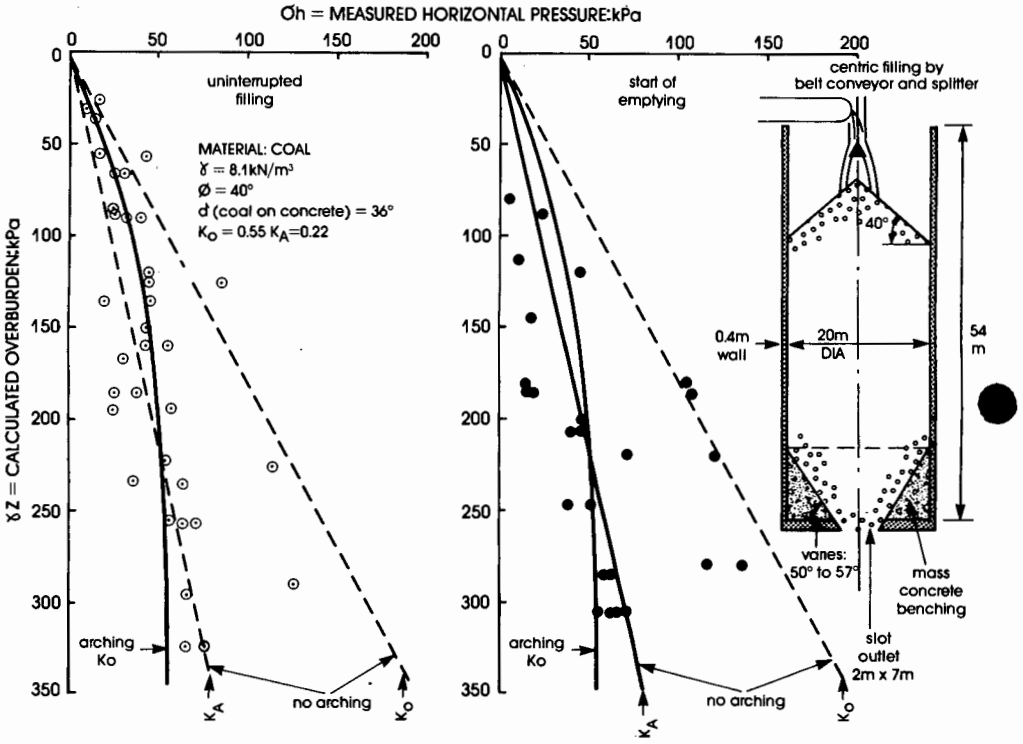

Fig. 6. Pressures measured in a coal load-out silo 20 m in diameter and 54 m high

and their interpretation are accurate. A small number of studies concerning the measurement of pressures with pressure cells and in particular the measurement of pressures in silos are particularly relevant.

Most useful general studies of the action, desirable characteristics and correct use of pressure cells have been described by Hvorslev (1976) and Peattie & Sparrow (1954). The specific use of pressure cells to measure pressures in silos has been studied by Askegaard (1963) and by Blight (1983).

The following are particularly important points.

(*a*) The face of the pressure cell should be as coplanar as possible with the inside of the silo wall and should have a similar surface texture to that of the wall.

(*b*) The stiffness of the cell should be as close to that of the wall as possible: in practice this means that the pressure cell should be as incompressible as possible.

(*c*) The calibration of a pressure cell depends on the material in contact with it, and on whether the material is stationary with respect to the cell face, or moving tangentially across it: all pressure cells used in silos should therefore be calibrated by applying pressure to the sensitive face via a sample of the silo fill and observing the cell readings as the fill slides across the face.

(*d*) The maximum particle size in the silo fill should not exceed one-tenth of the size of the pressure cell's sensitive face: in all the studies by the Author, appearing in this Paper, the diameter of the pressure-sensitive face of the pressure cells is 200 mm.

Cylindrical silos with uninterrupted filling followed by emptying

Figure 6 shows the results of stress measurements in a full-scale reinforced concrete mass flow coal silo used to load trains with export coal. This is one of the special purpose silos referred to earlier which is filled without interruption and then completely emptied before being refilled. Although the silo has a slot outlet, its dimensions are sufficiently small for the silo to behave reasonably concentrically and to discharge in mass flow. Pressures were measured using pressure cells set flush with the silo walls. A detailed description of the type of instrumentation, its calibration, installation and performance has previously been given by Blight (1983b).

The results have been presented as a plot of horizontal pressure versus calculated overburden γz, i.e. the depth of fill above a particular pressure

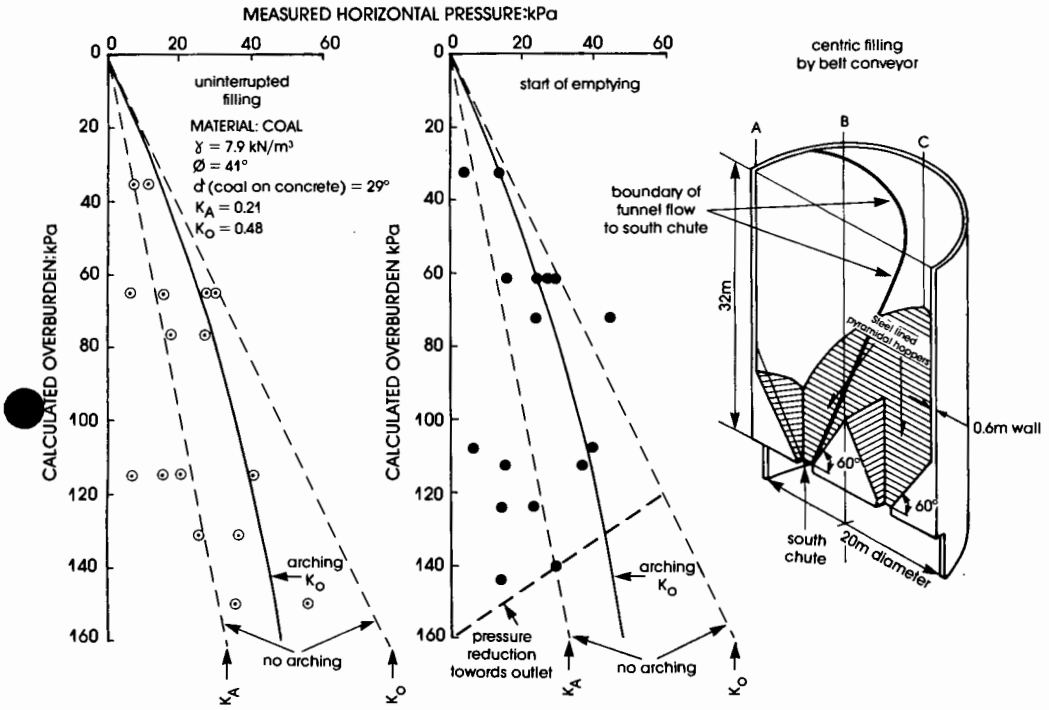

Fig. 7. Pressures measured in a coal load-out silo 20 m in diameter and 32 m high

cell times the bulk density of the fill. The parameters γ, ϕ, δ and K_0 were determined using established soil mechanics test methods (Blight & Ofer, 1984).

It will be seen that the results exhibit a considerable scatter corresponding to a slight variability in the coal, segregation of particle sizes, etc. For design, therefore, it would be desirable to seek a relationship between overburden and horizontal pressure that provides a containing envelope to the measurements. For uninterrupted filling, the arching theory (Janssen's theory with $K = K_0$) fits the mean of the measurements reasonably well. A significant number of measured pressures are large enough to fall outside the envelope defined by

$$\sigma_h = K_A \gamma z \tag{5a}$$

Only two, however, fall outside the envelope defined by

$$\sigma_h = K_0 \gamma z \tag{5b}$$

This confirms the expectation, noted earlier, that stress conditions in a silo will approach the at-rest state during filling.

Turning to conditions at the start of emptying, it will be seen that the scatter of observations increases, but similar conclusions apply—the Janssen theory with $K = K_0$ gives a good fit to the observations but equation (5b) gives a better containing envelope.

It should be noted from Fig. 6 that horizontal pressures generally increase moderately at the start of emptying. However, there is no dramatic increase such as might result in the failure of an otherwise adequately designed silo.

Figure 7 shows similar data for a second reinforced concrete coal load-out bin. (This bin and its instrumentation have been fully described by Blight & Midgley (1980)). The bin is more complex than the first because, although it is filled concentrically, it has two outlets, only one of which can be used at a time. The silo therefore discharges in funnel or core flow with some of the flowing material bounded by the silo wall and the rest by dead material.

The pattern of the results is very similar to that of Fig. 6, with Janssen's theory for $K = K_0$ giving a good fit to the observations and equation (5b) providing an adequate containing envelope.

Again, there is a moderate increase in pressure at the start of emptying. Also, at the start of emptying, horizontal pressures are reduced by the proximity of the outlet and modified by the onset of funnel flow, as indicated in Fig. 7.

Figure 8 shows a set of measurements for a third reinforced concrete silo subjected to uninterrupted filling followed by emptying. It is an

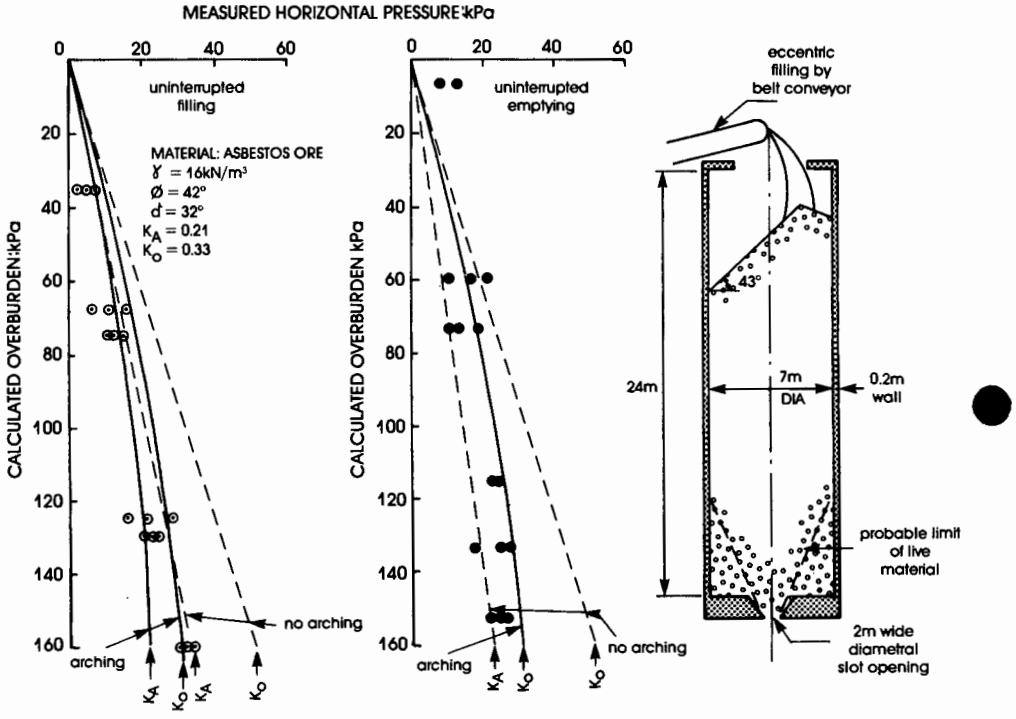

Fig. 8. Pressure measured in an asbestos ore silo 7 m in diameter and 24 m high

asbestos storage silo that is filled eccentrically because the head pulley of the filling conveyor is located concentrically and no allowance was made for the trajectory of the falling ore. It is also emptied eccentrically by means of a diametral slot across the whole of its flat bottom. In this case, the instrumentation consisted of strain gauges mounted on the hoop reinforcing of the silo. The pressures shown in Fig. 8 were calculated from the measured hoop strains. This procedure has previously been justified experimentally (Blight, Schaffner & Gilbert, 1982). The results for this silo are similar to those for the first two cases. The arching theory with $K = K_A$ provides a line of good fit to the data for uninterrupted filling, while equation (5a) provides a reasonable containing envelope. At the start of emptying the arching theory again provides a line of good fit (with K having a value between K_A and K_0), but equation (5b) provides a reasonable containing envelope.

Figure 9 refers to the fourth case of uninterrupted filling followed by emptying. The data have been abstracted from Hartlen *et al.* (1984). This reinforced concrete silo, used for storing barley and wheat grain, has a much larger ratio of height to diameter than in the previous cases, and arching of the fill could therefore be expected to have a greater influence on lateral pressures. This was certainly so for uninterrupted filling, although equation (5a) provides a good containing envelope to the data. The pressures at the start of emptying obviously increased. The arching envelopes do not fit the data well, but equation (5b) contains it. In this case, it should be noted that the large pressures recorded at a calculated overburden of 220 kPa probably coincide with the start of funnel flow to the outlet. Here the increase in lateral pressure coefficient caused by convergent flow has more than offset the pressure-reducing effect of the outlet.

Cylindrical silo subjected to mixed filling and emptying

Many silos are daily subjected to partial filling or emptying or simultaneous filling and emptying. Therefore stress states in the silo cannot be neatly divided into filling and emptying categories. Results for one such silo, a 20 m dia. steel maize grain storage facility, are shown in Fig. 10. The silo, its instrumentation and performance have been described by Blight (1983a).

The measured pressures are subject to far more scatter than in the previous cases, although the Janssen theory with $K = K_0$ again provides a line of good average fit to the data.

Being a steel silo which responds rapidly to changes in ambient temperature, the pressures are

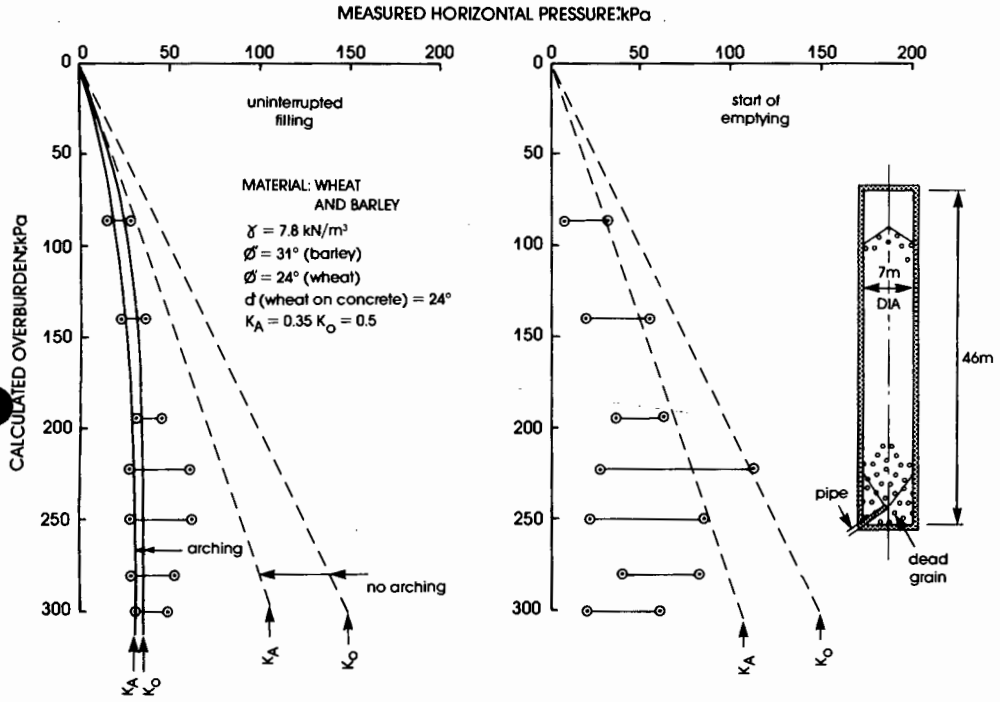

Fig. 9. Measurements by Hartlen *et al.* (1984) of pressures in a grain silo 7 m in diameter and 46 m high

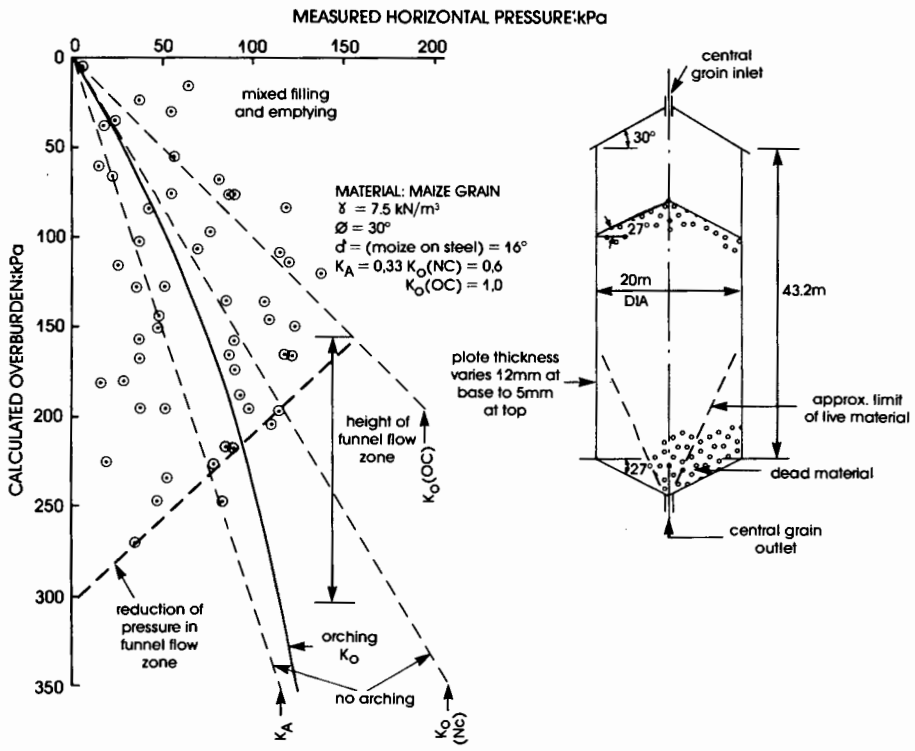

Fig. 10. Pressures measured in a maize storage silo 20 m in diameter and 43·2 m high

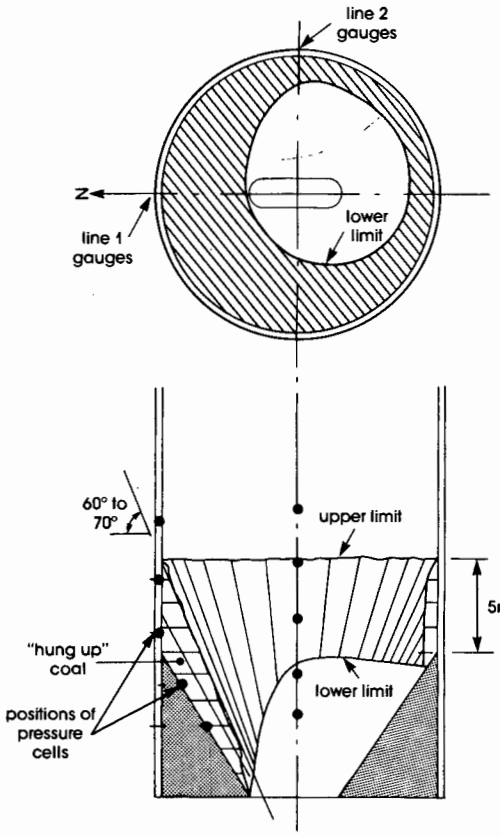

Fig. 11. Detail of the effective hopper section of a coal load-out bin.

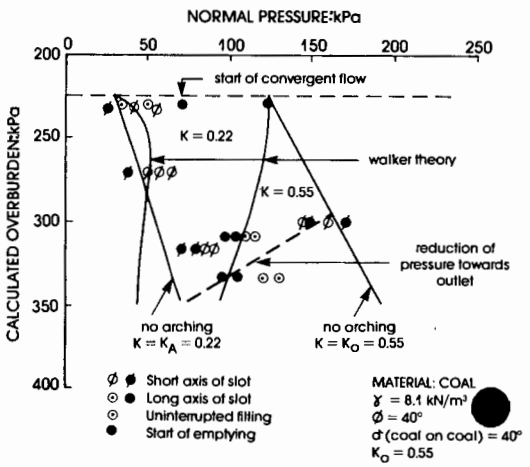

Fig. 12. Pressures measured in the hopper described by Fig. 11

also very much influenced by temperature. A fall in temperature results in a rise in pressure and vice versa. The large pressures recorded in Fig. 10 correspond to periods during which the temperature had fallen. The pressure-reducing effect of funnel flow towards the outlet is again evident, as indicated in Fig. 10.

K_0 for the normally consolidated maize is 0·60 (K_0(NC)) while overconsolidation results in K_0 increasing asymptotically to 1·0 (K_0(OC)).

From Fig. 10 the combined effects of overconsolidation and temperature are such that the horizontal pressure coefficient at times rises to well above 1·0, and even a K_0(OC) pressure line will not envelope all possible pressures. (A detailed study of the effects of temperature changes on pressures in steel silos has recently been reported by Blight (1985)).

Pressures in converging hoppers

Measurements of pressures in full-scale hoppers are difficult to obtain. The hopper portions of most reinforced concrete silos are formed in mass concrete benching either lined or unlined (see Figs 6 and 7) or allowed to form in dead fill (see Figs 8 and 9). In steel silos dead fill is also often used to form the hopper (Fig. 10). Hence it is difficult or impossible to install pressure-measuring devices.

Pressure cells, however, were installed in the hopper section of the silo referred to in Fig. 6. Fig. 11 shows the layout of the pressure cells in this area. Because the mass concrete benching had not been made steep enough, coal packed or 'hung up' on the benching to form an effective hopper surface as shown in the figure.

Figure 12 shows measurements made on cells in the effective hopper both at the end of uninterrupted filling and at the start of emptying. The pressures have been converted to equivalent horizontal pressures on the assumption that the coal was sliding across the effective hopper surface.

Figure 12 shows that the pressures changed as emptying was started, but that the change was relatively minor. It should be noted from Fig. 12 that pressures measured on the long axis of the slot outlet increased near the start of convergent flow and decreased towards the outlet. On the short axis of the slot, pressures generally decreased.

The K_A and K_0 stress lines given by equations (5a) and (5b) bracket the measured data with the K_0 stress line forming an upper limit to the observations.

The Walker theory, in contrast, gives a poor representation of the observed pressures. The inclined broken line in Fig. 12 indicates a reasonable limit or cut-off to the pressure diagram caused by the proximity of the outlet. Hence the pressure diagram within the hopper is made up of a continuation of that in the cylindrical silo

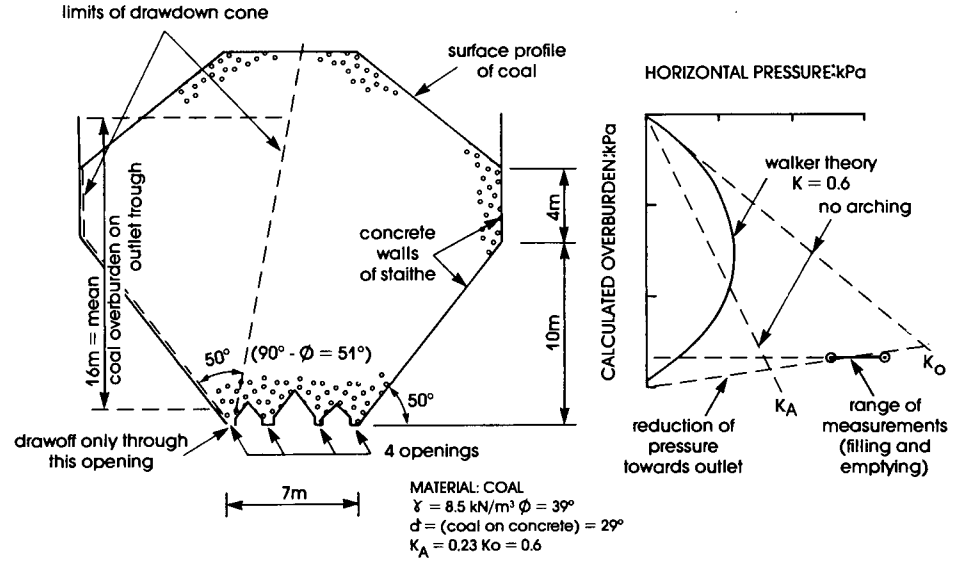

Fig. 13. Pressure deduced at the outlet chute of a large coal staithe

above, terminated by a sharp transition over the lower 1 m or so of the hopper to near zero pressure at the outlet.

The second case concerns the coal staithe illustrated in Fig. 13. Here measurements were made of the strains in one of the steel outlet troughs as the staithe was filled from empty without interruption and emptying then started. As the trough consisted of vertical, horizontally spanning, simply supported components, it was simple to calculate the average horizontal pressure at that level. The range covered by six independent measurements is shown in Fig. 13. Once again, the measurements are bracketed by the K_A and K_0 str[illegible] lines and the Walker theory gives a poor prediction. A continuous recording of the strains was made at the start of emptying, but no significant change in pressure occurred as the drawdown cone developed above the outlet trough.

This is particularly surprising in view of the fact that a stress-free opening existed just over 1 m from the points of measurement. The vertical stress must have been much reduced as a consequence of the nearby outlet. Hence the horizontal pressure coefficient must have increased to a value far greater than 0·6 to keep the horizontal pressure substantially constant. The flatly inclined broken line on the pressure diagram in Fig. 13 indicates the steep gradient of pressure that must occur within the outlet trough of the staithe.

The measurements shown in Figs 7, 9 and 10 all show a decrease in horizontal pressure in the vicinity of an outlet. However, because this decrease may occur over a very short vertical distance, and probably does not occur at all at the end of uninterrupted filling, hoppers should be designed assuming that the relationship (5b)

$$\sigma_h = K_0 \gamma z$$

applies over their entire height.

Radial distribution of pressure

Unless there is an obvious reason for horizontal pressures to be radially non-uniform, any theory must assume radial uniformity. However, actual pressures may depart widely from this ideal. Fig. 14 shows two radial distributions of horizontal pressure measured in the coal load-out bin referred to in Fig. 7. The distributions were measured at the transition between the cylindrical bin and the pyramidal hoppers. It will be seen that in both the cases illustrated the pressure was radially non-uniform. Discharge from the chute remote from the pressure cells affected the distribution relatively little (Fig. 14(a)), whereas discharge from the adjacent chute produced a large change in radial distribution as the pattern of funnel flow developed (Fig. 14(b)).

In contrast, Fig. 15 shows the radial distribution of horizontal pressure in the asbestos ore silo referred to in Fig. 8. Here, even though the silo is filled eccentrically and emptied eccentrically through the slot at the base, measured pressures were almost perfectly radially uniform. The points of measurement were above the zone of convergent flow and therefore unaffected by it. Eccentric filling also had no effect on the radial pressure.

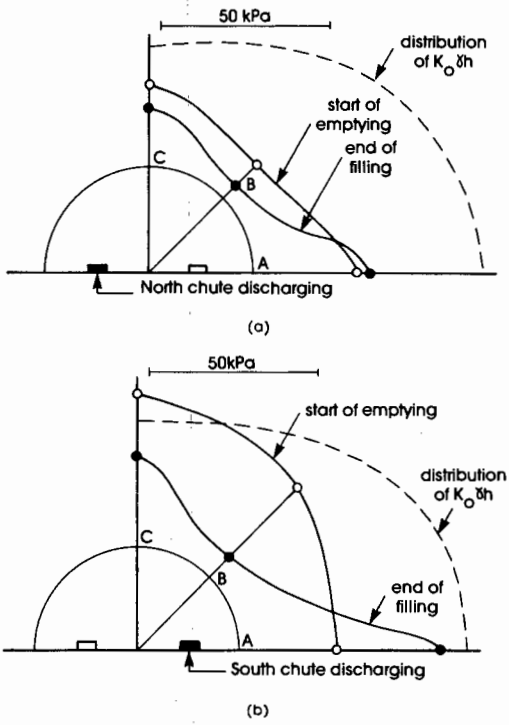

Fig. 14. Radial distribution of horizontal pressure in a coal storage silo

Effects of eccentric flow

Funnel flow, such as that which takes place in the coal load-out bin referred to in Figs 7 and 14, or plug flow (see Fig. 1), results in a radial non-uniformity of horizontal pressure. The simplest mechanistic explanation of this phenomenon is that given by Jenike (1967): Fig. 16 represents a silo of internal diameter D in which plug or funnel flow is taking place over a diameter d. The flow zone impinges on the silo wall. Applying equation (1) to the static and flowing zones of fill

$$\sigma_{hD} = \frac{D\gamma}{4 \tan \delta} \tag{6a}$$

$$\sigma_{hd} = \frac{d\gamma}{4 \tan \delta} \tag{6b}$$

Hence

$$\frac{\sigma_{hd}}{\sigma_{hD}} = \frac{d}{D} \tag{6c}$$

Thus the horizontal pressure in the flowing fill will be less than that in the static fill and additional forces Q will have to be generated by horizontal friction along the walls of the silo to maintain horizontal equilibrium.

Turning again to the silo illustrated in Fig. 7, when the silo is emptied through one chute, the

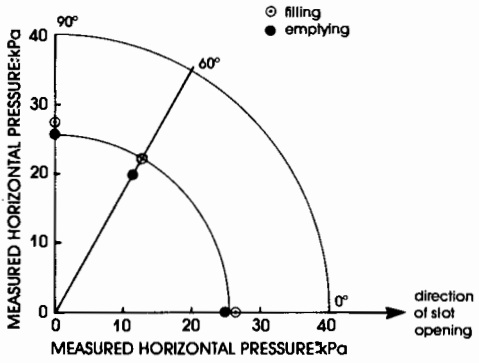

Fig. 15. Radial distribution of horizontal pressure in an asbestos ore silo

horizontal pressure on the wall adjacent to that chute should decrease. This effect is shown in Fig. 17. Pressure cells A1–A4 are mounted on line A (see Fig. 7) adjacent to the south chute. Line A fell within the zone of funnel flow and pressures would therefore be expected to decrease. Line B fell just outside the funnel flow zone so that pressures would not be expected to change by much.

In Fig. 17 the numbers 1–3 each represent one series of measurements. As the figure shows, the expectations expressed above were realized, except at gauge A4, where there was an unexplained slight increase in pressure. Although there is qualitative agreement with the predictions of equation (5c), it is difficult to check on the quantitative agreement. However, the diameter of the funnel flow zone must decrease with increasing depth z and therefore the decrease in pressure along line A should increase with z. As Fig. 17 shows, this was so.

Occurrence of switch pressures

Clague's (1973) model test data (Fig. 5) as well as those of Jenike *et al.* (1972) (and others) show what appear to be clearly defined and relatively

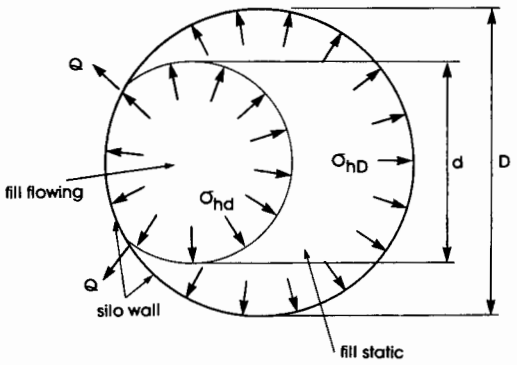

Fig. 16. Effects of funnel or plug flow on horizontal pressure in a silo

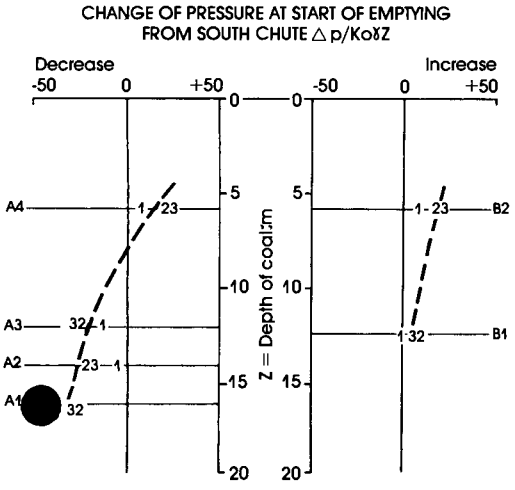

Fig. 17. Modification of horizontal pressure in a coal load-out bin by funnel flow

large switch pressures in the vicinity of the transition from parallel mass flow to convergent funnel flow. In the four full-scale silos monitored by the Author, no switch pressures have been observed, although horizontal pressures do increase at the start of emptying.

It has been suggested that switch pressures are a dynamic phenomenon. Because they appear, travel up the height of a silo and disappear within a few seconds is why static measurements do not record them. However, continuous recordings of pressure immediately after the start of discharge on several silos have failed to disclose any switch pressures.

Figure 18 gives an example of such a recording made on the coal load-out bin illustrated in Fig. 7 on two separate occasions for discharge through the south chute. In each case, the initial 20 s of the record corresponds to the loading of 60 tons of coal into the first wagon of the train. The chute then closes and reopens 10 s later for the second 20 s loading period. There clearly are dynamic effects, but the horizontal pressure changes are relatively small. There is no evidence of a large switch pressure either locked in position or travelling up the silo.

GENERAL CONCLUSIONS

The data presented here show that for the classical design conditions of 'end of filling' and 'start of emptying' the simple Janssen arching theory provides a good estimate of the mean trend of horizontal pressure with depth in a cylindrical silo if used in conjunction with realistic material parameters. However, pressures are highly variable, and for design what is required is a relationship between pressure and depth that will contain all pressure values. For the range of silo geometries considered in this Paper, this is provided by the simple relationship

$$\sigma_h = K_0 \gamma z \qquad (5b)$$

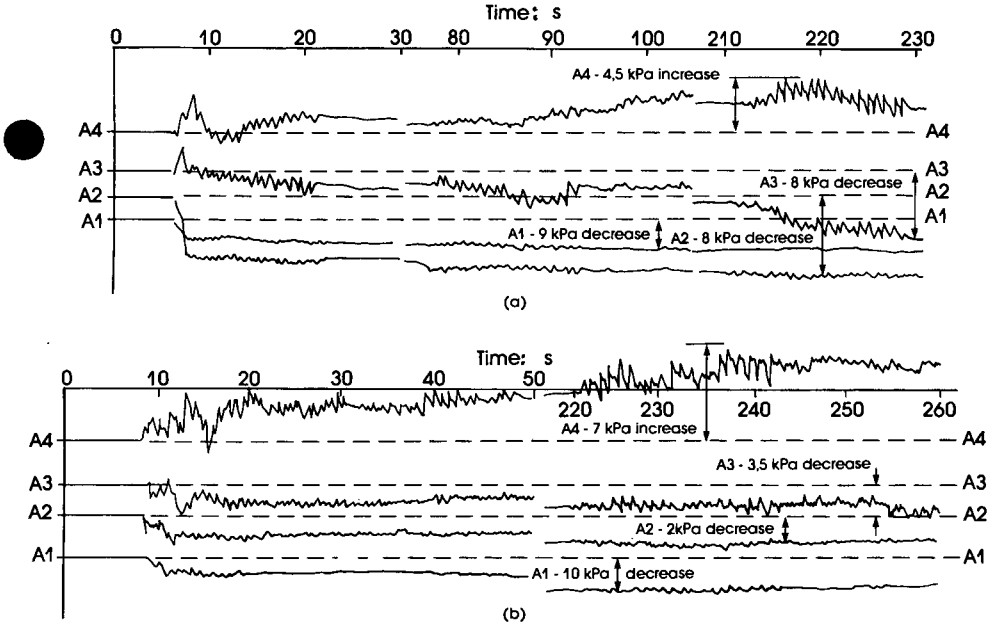

Fig. 18. Recording of changes in horizontal pressure in a coal load-out bin at the start of emptying

in which K_0 is the at-rest pressure coefficient for the normally consolidated fill.

This relationship provides an envelope to the pressures that are likely to occur in hoppers and the hopper portions of silos. The Walker arching theory for convergent containers has not been found to fit observed pressures.

In silos subjected to mixed filling and emptying, horizontal pressures may far exceed those experienced at the start of emptying after uninterrupted filling. This is particularly so for steel silos in which pressures are much affected by temperature cycles. Here equation (5b), in which K_0 is the at-rest pressure coefficient for the overconsolidated fill, will contain most, but not necessarily all, expected pressures.

Horizontal pressures in silos are not necessarily radially uniform as assumed in theory. If nonuniformity is caused by a predictable flow condition, e.g. funnel flow to an eccentric outlet, the effects of the flow on pressure can be predicted, at least qualitatively.

Horizontal pressures generally increase at the start of emptying. However, the increase is moderate and significant switch pressures have not, as far as is known, been observed in full-scale silos.

These conclusions are essentially the same as those reached for silos used to store fine powders (Blight, 1986).

REFERENCES

American Concrete Institute Committee 313 (1975). Recommended practice for design and construction of concrete bins, silos and bunkers for storing granular materials. *Am. Concr. Inst. J.* **71,** Oct. 529–565.

Askegaard, V. (1963). *Measurement of pressure in solids by means of pressure cells.* Bulletin 17, Structural Research Laboratory, Technical University of Denmark.

Blight, G. E. (1983a). Performance of a 20 m diameter steel maize storage bin. *Proc. 2nd Int. Conf. Design of Silos for Strength and Flow*, pp. 179–191. London: Powder Advisory Centre.

Blight, G. E. (1983b). Measuring pressures in silos with pressure cells. *Proc. 2nd Int. Conf. Design of Silos for Strength and Flow*, pp. 217–229. London: Powder Advisory Centre.

Blight, G. E. (1985). Temperature changes affect pressures in steel bins. *Int. J. Bulk Solids Stor. Silos* **1,** No. 4.

Blight, G. E. (1986). Pressures exerted by materials stored in silos: part II, fine powders. *Géotechnique* **36,** No. 1, 47–56.

Blight, G. E. & Midgley, D. (1980). Pressure measured in a 20 m diameter coal load-out bin. *Proc. Int. Conf. Design of Silos for Strength and Flow* **1**. London: Powder Advisory Centre.

Blight, G. E. & Ofer, Z. (1984). Laboratory determination of K_0 and comparison with prototype silo observations. *Proc. 4th Aust.–N.Z. Conf. Geomechanics, Perth* **1,** 83–87.

Blight, G. E., Schaffner, R. H. & Gilbert, B. (1982). Strains in a reinforced concrete silo during rapid filling with a fine powder. *J. Powd. Bulk Solids Technol.* **6,** 17–27.

Clague, K. (1973) *The effects of stresses in bunkers.* PhD thesis, University of Nottingham.

Hartlen, J., Nielsen, J. & Ljunggren, L. (1984). *The wall pressure in large grain silos.* Stockholm: Swedish Council for Building Research.

Hvorslev, M. J. (1976). *The changeable interaction between soils and pressure cells; tests and reviews at the Waterways Experiment Station.* Technical Report S-76-7, US Army Engineer Waterways Experiment Station.

Janssen, H. A. (1895). Versuche über Getreidedruck in Silozellen. *Z. Ver. Dt. Ing.*, 1045–1050.

Jenike, A. W. (1967). Denting of circular bins with eccentric drawpoints. *J. Struct. Div. Am. Soc. Civ. Engrs* **93,** ST1, 27–35.

Jenike, A. W. (1980). Effect of solids flow properties and the hopper-feeder unit on silo loads. *Proc. Int. Conf. Design of Silos for Strength and Flow* **1**. London: Powder Advisory Centre.

Jenike, A. W., Johansen, J. R. & Carson, J. W. (1972). Bin loads part 3: mass-flow bins. *J. Engng Ind. Am. Soc. Mech. Engrs*, 1–7.

Martens, P. (1980). DIN 1055 part 6: The performance of the old norm and a progress report on the revised edition. *Proc. Int. Conf. Design of Silos for Strength and Flow* **1**. London: Powder Advisory Centre.

Nanninga, K. (1956). Gibt die übliche Berechnungsart der Drücke auf die Wände und den Boden von Silobauten sichere Ergebenisse. *Ingenieur*, Nov.

Nielsen, J. & Kristiansen, N. O. (1980). Related measurements of pressure and conditions in full-scale barley silo and in model silo. *Proc. Int. Conf. Design of Silos for Strength and Flow* **1,** 22. London: Powder Advisory Centre.

Peattie, K. R. & Sparrow, R. R. (1954). The fundamental action of earth pressure cells. *J. Mech. Phys. Solids* **2,** 141–155.

Ravenet, J. (1981). Silo problems. *Bulk Solids Handl.* **1,** No. 4, 667–679.

Reimbert, M. & Reimbert, A. (1956). *Silos, traité théorique et pratique.* Paris: Eyrolles.

Sadler, J. S. (1980). Silo problems. *Proc. Int. Conf. Design of Silos for Strength and Flow.* **1, 2**. London: Powder Advisory Centre.

Theimer, O. F. (1969). Failures of reinforced concrete grain silos. *Trans. Am. Soc. Mech. Engrs*, 460–477.

Walker, D. M. (1966). An approximate theory for pressures and arching in hoppers. *Chem. Engng Sci.* **21,** 975–997.

Walters, J. K. (1973). A theoretical analysis of stresses in axially-symmetric hoppers and bunkers. *Chem. Engng Sci.* **28,** 13–20.

Wigram, S. (1980). Report on an inventory of Swedish grain silos. *Proc. Int. Conf. Design of Silos for Strength and Flow* **1**. London: Powder Advisory Centre.

BLIGHT, G. E. (1986). *Géotechnique* **36**, No. 1, 47–56

Pressures exerted by materials stored in silos: part II, fine powders

G. E. BLIGHT*

The Paper compares pressures measured in several silos used to store fine powders with the predictions of commonly accepted design theory. In most cases, the silo arching theory provides an adequate containing envelope to the observed pressures. Nevertheless, it is preferable to use a simple straight line variation in pressure with depth to cover all eventualities. These conclusions agree with those reached for silos used to store coarse materials. The Paper also describes the radial distribution of pressure in silos and transient pressures during emptying.

L'article compare les pressions mesurées dans divers silos contenant des poudres fines avec les prévisions de la théorie classique. Dans la plupart des cas la théorie de l'effet de voûte dans un silo fournit une enveloppante acceptable pour les pressions observées. Cependant, pour couvrir tous les cas il serait préférable d'utiliser des pressions proportionnelles à la profondeur. Ces conclusions s'accordent avec celles tirées pour les silos utilisés pour le stockage des matières à gros grains. L'article décrit aussi la distribution radiale de la pression dans les silos qui se produit au cours du déchargement.

KEYWORDS: case history; design; earth pressures; field instrumentation; granular materials; silos.

INTRODUCTION

A companion paper (Blight, 1986a) has described the pressures exerted by coarse materials stored in silos. For that paper, coarse materials were defined as materials in which pore air pressures would not develop during filling of the silo and for which compressed air is not used as an aid to emptying. Examples of coarse materials commonly stored in silos are grains (wheat, maize, etc.), granulated sugar, mineral ores and coal.

Many types of fine powder are produced in bulk and stored in silos. Examples are Portland cement powder, cement raw meal, grain flour and pulverized fuel ash. These powders typically have 100% by mass of their particles passing a 0·147 mm sieve, and as much as 80–90% passing a 0·074 mm sieve. Because of their fineness, they entrap air if filled rapidly into a silo. It is also usual to empty powder storage silos by aerating and locally fluidizing the powder near the outlet by means of compressed air.

This Paper will consider four case histories of pressures measured in full-scale operating silos. The measurements will be compared with the predictions of the simple arching theory conventionally used to design silos in accordance with commonly accepted design codes (e.g. the German DIN 1055 (Martens, 1980) and the American Concrete Institute Committee 313 (1975)). In this way the adequacy of the theory for assessing wall pressures in silos will be assessed. Wherever appropriate, the findings of this Paper will be compared with those of the companion paper (Blight, 1986a).

Pressures developed in silos rapidly filled with fine powders that entrain air have been fairly comprehensively described in a series of papers by Pieper, Martins & Nothdurft (1975), Murfitt & Bransby (1980a, b), Blight, Schaffner & Gilbert (1982) and Blight (1986b). This aspect of the subject will not be dealt with in detail, but a summary of findings will be given here.

THEORETICAL BACKGROUND

As stated in the companion paper (Blight, 1986a) the theory conventionally used in silo design is the arching theory due to Janssen (1895). In its original form, the theory did not recognize a possible role for air pressures and was derived in terms of total stresses. The version that follows has been written in terms of effective stresses: when a silo is filled with a powder, the powder is initially deposited in a conical pile in which active conditions probably apply. The ratio of lateral to vertical effective stresses is therefore represented by K_A, the active lateral pressure coefficient.

As further fill accumulates, the fill compresses vertically, and the stress state approaches that of compression with zero lateral strain. The lateral pressure coefficient therefore approaches the at-rest value K_0. Because the fill moves downwards relative to the silo walls, wall friction is generated which transfers some of the vertical stress into the silo walls. This action is illustrated by Fig. 1 which shows the stresses acting on an element of fill at depth z below the fill surface in a cylindrical silo of diameter D. For vertical equi-

Discussion on this Paper closes on 1 July 1986. For further details see inside back cover.

* University of the Witwatersrand.

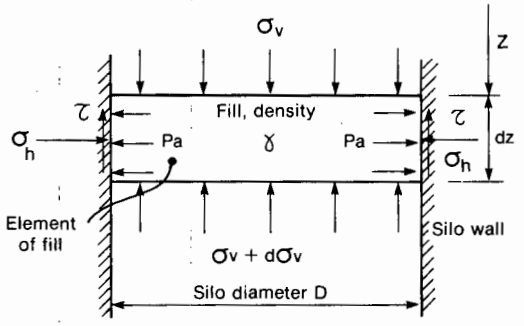

Fig. 1. Basis of the arching theory for wall pressures in silos

librium of the element, the following differential equation applies

$$\frac{d\sigma_v}{dz} = \gamma - \frac{4K}{D}(\sigma_v - p_a)\tan\delta' \qquad (1)$$

In equation (1) γ is the unit weight of the fill, K is the lateral pressure coefficient, p_a is the pore air pressure in the fill and δ' is the angle of wall friction between the fill and the silo wall, evaluated in terms of effective stresses.

In general $\sigma_v - p_a$ will increase with increasing z until the weight of the element is entirely supported by wall friction. At this stage

$$\frac{d\sigma_v}{dz} = 0$$

and

$$(\sigma_v - p_a)_{max} = \frac{\gamma D}{4K}\tan\delta' \qquad (2)$$

i.e.

$$\frac{d\sigma_v}{dz} = \gamma\left[1 - \frac{(\sigma_v - p_a)}{(\sigma_v - p_a)_{max}}\right] \qquad (3)$$

Equation (3) can be integrated to obtain the variation in σ_v with z for any given distribution of p_a with z, and the corresponding horizontal stress on the wall is

$$\sigma_h = K(\sigma_v - p_a) + p_a \qquad (4)$$

To illustrate the influence of pore air pressures on lateral pressures, consider the case of undrained compression for which p_a is related to σ_v by the relationship

$$p_a = B_a\sigma_v \qquad (5)$$

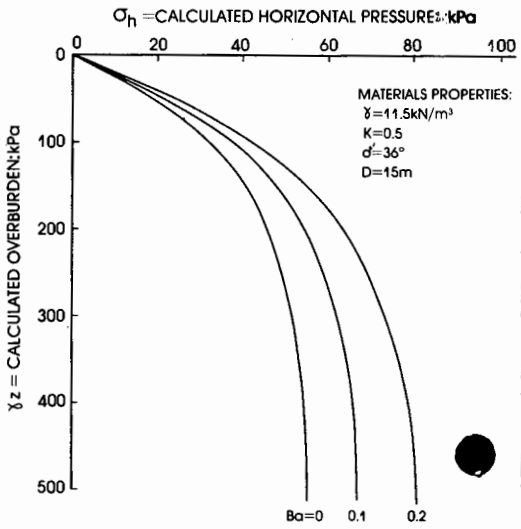

Fig. 2. Role of pore air pressure in silo pressures under undrained conditions

In this case equations (1)–(3) can be rewritten as

$$\frac{d\sigma_v}{dz} = \gamma - \frac{4K(1 - B_a)\tan\delta'}{D}\sigma_v \qquad (6)$$

$$\sigma_v(max) = \frac{\gamma D}{4K\tan\delta'(1 - B_a)} \qquad (7)$$

$$\frac{d\sigma_v}{dz} = \gamma\left[1 - \frac{\sigma_v}{\sigma_v(max)}\right] \qquad (8)$$

The solution to equation (8) for the boundary condition $\sigma_v = 0$ when $z = 0$ is

$$\frac{\sigma_v}{\sigma_v(max)} = 1 - \exp\left[-\frac{\gamma z}{\sigma_v(max)}\right] \qquad (9)$$

Equation (4) becomes

$$\sigma_h = \sigma_v[K(1 - B_a) + B_a] \qquad (10)$$

Figure 2 shows a family of curves calculated from equations (9) and (10) for a case where $\gamma = 11{\cdot}5$ kN/m^3, $\delta' = 36°$, $K = 0{\cdot}5$ and for successive B_a values of 0, 0·1 and 0·2.

In Fig. 2, values of the calculated horizontal stress σ_h have been plotted against the calculated overburden γz. Because of the compressibility of air, B_a is unlikely ever to exceed a value of 0·2 (Murfitt & Bransby, 1980b). It should be noted that even under the completely undrained conditions assumed for example the pore air pressure does not add more than 30% to the value of the horizontal pressure. In silos that are not filled rapidly, the contribution of pore air pressure to the horizontal pressure will be less than this. The

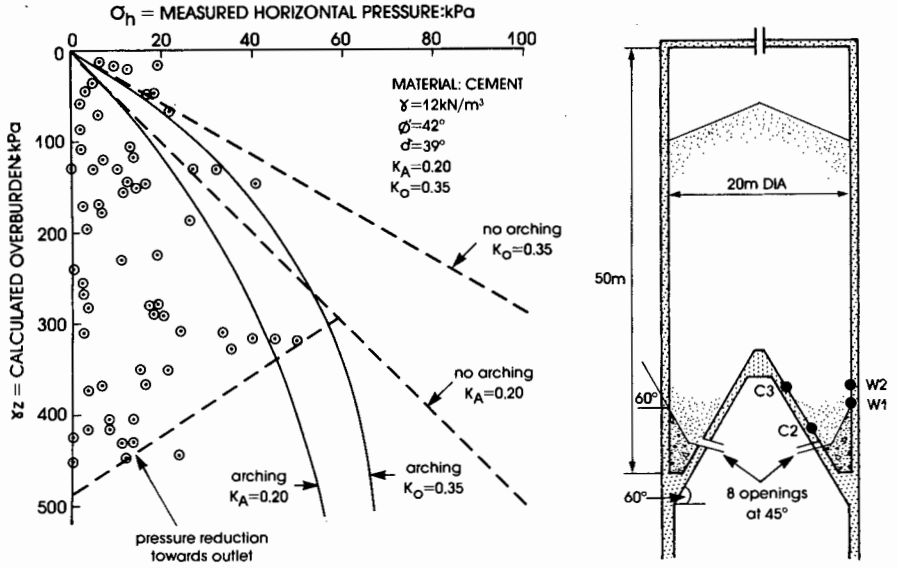

Fig. 3. Pressures measured in a 20 m dia. cement silo with an inverted conical base

effect of air pressure injected to empty a silo will be considered later.

PRESSURES ON VERTICAL WALLS

The first two case histories concern cement silos of two very different types. Sections through the silos are shown in Figs 3 and 4.

Figure 3 shows the results of pressure measurements made in a cement silo 20 m in diameter and 50 m high with an inverted ring–conical hopper bottom. The silo is filled through a single central opening in the top and is emptied via eight symmetrically disposed openings at 45° to each other around the perimeter of the cone. The

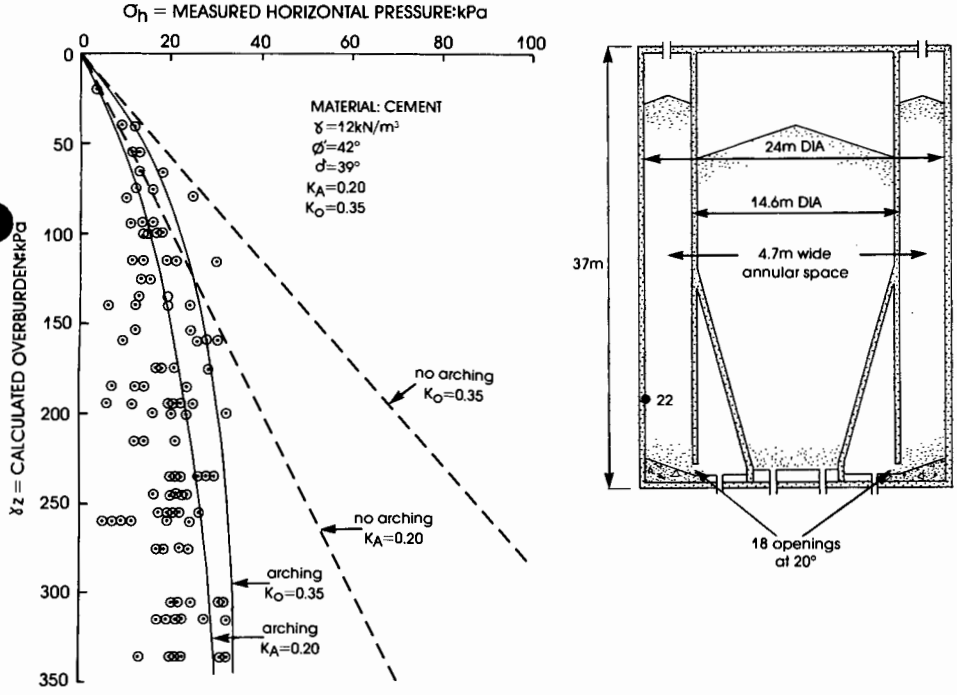

Fig. 4. Pressures measured in a 'duocell' ring cement silo

openings are operated in diametrically opposed pairs. To keep the fill level reasonably uniform around the silo perimeter, each pair of openings is operated for 15 min before rotating to the next pair.

The contents of the silo are added to daily, while simultaneously cement is loaded from its outlets into road tankers. The traditional loading conditions of uninterrupted filling followed by emptying therefore do not apply.

The instrumentation consisted of 200 mm dia. mercury-filled strain-gauged pressure cells. The method of installation has previously been described by Blight & Midgley (1980) and the characteristics of the cells as well as the method of calibrating them by Blight (1983).

The results in Fig. 3 represent pressures measured on the vertical walls of the silo. Pressures measured on the cone will be presented separately. The measurements are very scattered with a large proportion of low values. However, this is characteristic of measured silo pressures (see, for example, Blight (1986a)).

For design, what is required is a relationship between overburden and horizontal pressure that will envelope the observed pressures. The line for $K = K_0$ contains the data reasonably well, although at small overburdens the straight line relationship

$$\sigma_h = K_0 \gamma z \tag{11}$$

is a slightly better containing envelope.

Figure 3 also shows a line joining measurements made on the highest and lowest pressure cells on the cylindrical wall within the zone of convergent flow towards the outlet. This represents (approximately) the gradient of wall pressure as the outlet is approached. However, if the silo had been filled without interruption, this pressure gradient would not have been established.

The second case concerns a so-called 'duocell' silo consisting of a 14 m dia. cylindrical inner chamber surrounded by a ring silo 4·7 m wide and 24 m outside diameter. The ring silo is emptied through 18 openings on its inner perimeter, each operating for a 2 min period to maintain the fill at approximately the same level around the ring.

The outer wall of the outer ring silo was instrumented with pressure cells and the measurements shown in Fig. 4 were taken during normal operation of the silo, which also consists of daily simultaneous filling and emptying. The scattered nature of the measurements is similar to those shown in Fig. 3. The 'arching' curves in Fig. 4 were calculated from equations (7), (9) and (10) with $B_a = 0$ and modified for the ring shape of the silo, i.e. equation (7) becomes

$$\sigma_v(\max) = \frac{\gamma(D_o - D_i)}{4K \tan \delta'(1 - B_a)} \tag{12}$$

in which D_o is the outside diameter of the ring silo and D_i is the inside diameter.

As with the results shown in Fig. 3, the measurements show a considerable scatter but are contained fairly well by the arching curve for $K = K_0 = 0{\cdot}35$.

The third case concerns the cement raw meal silo illustrated in Fig. 5. This silo is filled from two adjacent blending silos, completely emptied and then refilled. The measurements shown in Fig. 5 correspond to the classical design conditions of 'end of uninterrupted filling' and 'start of emptying'.

The instrumentation consisted of electric resistance strain gauges attached to the hoop reinforcing of the silo at four different levels. The justification for using strain gauges has been investigated and reported by Blight *et al.* (1982).

As in Figs 3 and 4, the measured pressures again show considerable scatter, but most are enveloped by the arching curve for $K = K_0$. Once again, pressures measured at low overburdens are perhaps better enveloped by the straight line relationship of equation (11). There is no clearly defined increase in pressure at the start of emptying.

The fourth case concerns a 16 m dia. silo for storing pulverized fuel ash, described by Nielsen (1983) (Fig. 6). The instrumentation consisted of pressure cells set in the walls of the silo. Unfortunately, all the properties of the ash have not been established. The unit weight is given as 12 kN/m^3 and assumed values of $K_0 = 0{\cdot}58$ and $\delta' = 31°$ are used. If it is further assumed that ϕ' is slightly larger than δ, say $\phi' = 33°$, $K_A = 0{\cdot}30$. These values have been used in drawing Fig. 6. The reported measurements are for 'filling' and 'start of discharge'. Unfortunately, it is not stated whether or not filling is uninterrupted.

The two lines for the arching theory give reasonable agreement with the observed pressures during filling. However, at the start of emptying, pressures increase, the arch action appears to break down and the results are contained by the line described by equation (11).

When examining pressures exerted by coarse materials contained in silos (Blight, 1986a), it was found that, for the classical design conditions of 'end of filling' and 'start of emptying', the Janssen theory provided a good estimate to the mean trend of horizontal pressures with depth. An acceptable containing envelope to the results, however, was provided by the straight line

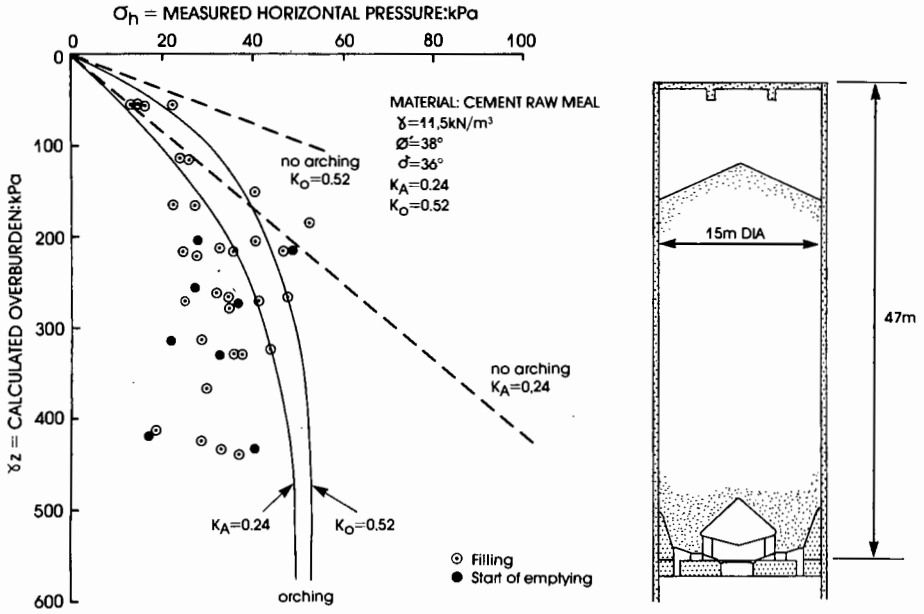

Fig. 5. Pressures measured in a 15 m dia. cement raw meal silo

relationship of equation (11). In three of the four cases examined here, the modified Janssen theory given by equations (7), (9) and (10) with $B_a = 0$ and $K = K_0$ has provided a satisfactory containing envelope to the observed pressures, except at small overburdens where equation (11) has been applicable. In the fourth case, the conclusion is the same as that reached for coarse materials. Hence in general the conclusions reached for coarse materials apply also to powders.

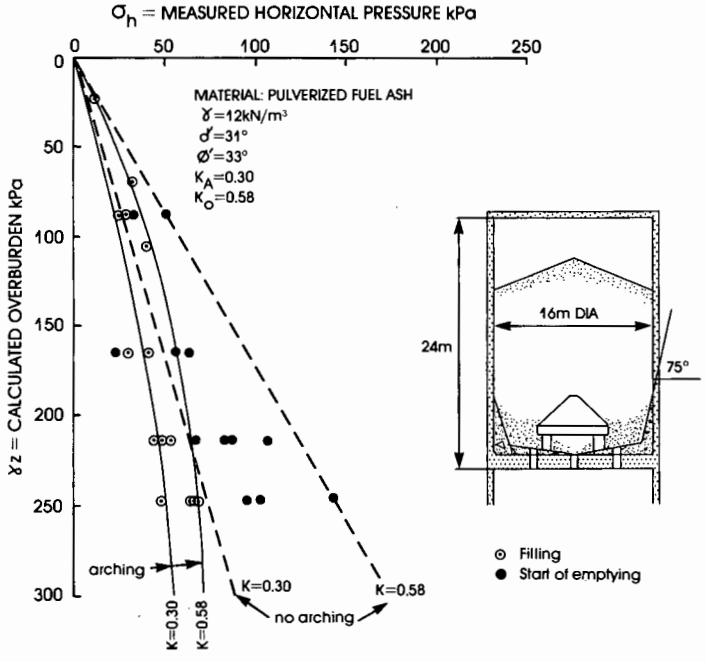

Fig. 6. Pressure measured in a 16 m dia. pulverized fuel ash silo (after Nielsen (1983))

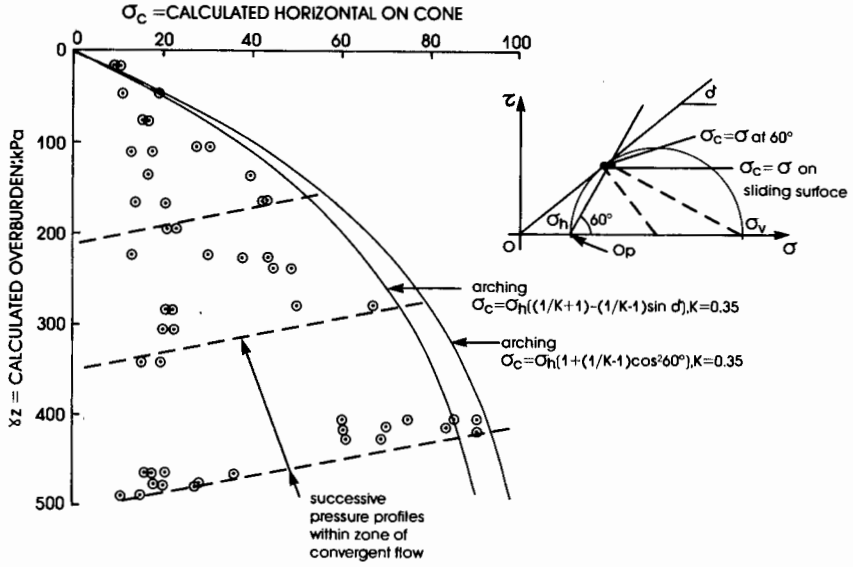

Fig. 7. Pressures measured on the inverted cone of the cement silo illustrated in Fig. 3

PRESSURES ON INCLINED SURFACES

The cone of the ring–conical hopper in the silo illustrated in Fig. 3 is equipped with pressure cells. Measured pressures on the cone for various overburdens are shown in Fig. 7. In this diagram, the inclined broken lines join measurements made via the highest and lowest pressure cells on the cone and thus indicate the reduction in pressure that occurs in the zone of convergent flow towards the outlets.

The lines enveloping the observed pressures represent the arching line for $K_0 = 0{\cdot}35$ modified to represent the pressure on the inclined surface of the cone. The modification has been made on two bases

(*a*) assuming that the cement slides on the surface of the cone
(*b*) assuming that sliding occurs through the cement.

Pressure cell readings are also available for the steeply inclined benching of the ash silo illustrated in Fig. 6. These have been plotted in Fig. 8. The measurements for filling are fairly well contained by the line given by equation (11) with $K_0 = 0{\cdot}58$. The pressures at the start of discharge, however, indicate that K_0 must have increased to 1·0 as a result of the unloading caused by the decline in pressure towards the outlet.

When studying pressures in zones of convergent flow in coarse materials (Blight, 1986a), it was concluded that the pressure diagram within a hopper or other zone of convergent flow consists of a continuation of that in the zone of parallel flow above, terminated by a sharp transition to the pressure at the outlet. The same conclusion is valid for powders.

RADIAL DISTRIBUTION OF PRESSURE

It was shown in the companion paper that the radial distribution of pressure in a silo may be uniform but in general is not. In particular, the radial pressure distribution is affected by the flow pattern within the silo.

Figure 9 shows radial distributions of pressure measured in the duocell cement silo illustrated by Fig. 4. The two sets of readings, A and B, were taken at different times at three levels 1, 2 and 3 where level 1 is 1·5 m above the aeration pad on the base of the silo, level 2 is 5 m above level 1 and level 3 is 10 m above level 1.

In set A, draw-off has recently occurred adjacent to the pressure cells at 0°, 90° and 180°. At level 2, 5 m above, the radial pressure distribution is unaffected by the draw-off. Another 5 m up, at level 3, the radial pressure distribution is again different.

In contrast, in set B, the radial pressure distribution, although far from uniform, remains similar with height.

Hence the general conclusion reached for coarse materials applies also to powders.

TRANSIENT PRESSURE VARIATIONS

Continuous recordings of pressures showing transient fluctuations are available for the two cement silos referred to by Figs 3 and 4. Because

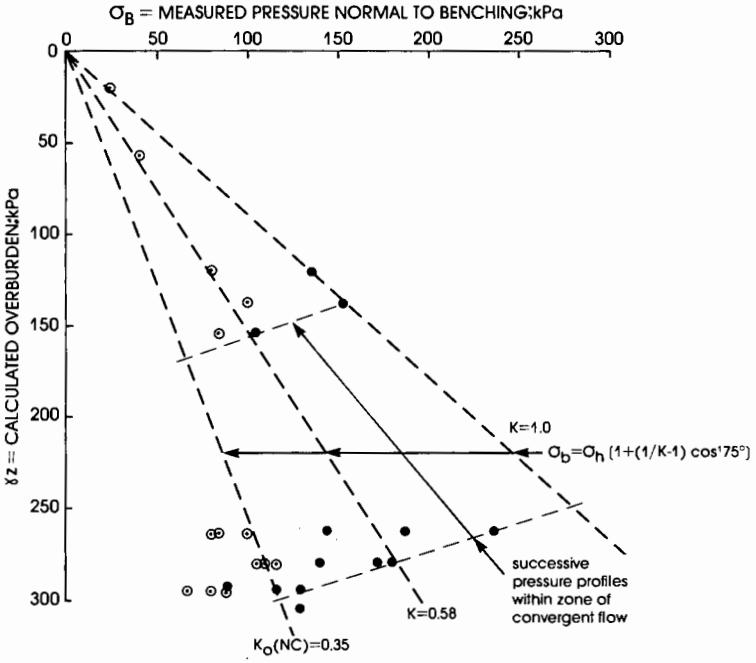

Fig. 8. Pressures measured on the inclined benching of the pulverized fuel ash silo illustrated in Fig. 6

the silos are operated on a simultaneous filling and emptying basis, the presence of a concentrated switch pressure (referred to in the companion paper) would not be expected. Transient pressures arising from the injection of compressed air would be expected to occur.

Figure 10 shows a continuous recording of pressures at gauge 22 in the duocell silo referred to by Fig. 4. The position of gauge 22 is shown in Fig. 4 and is 6·5 m above the level of the aeration pads on the benching at the base of the silo. The record covers just over 2 days during which the

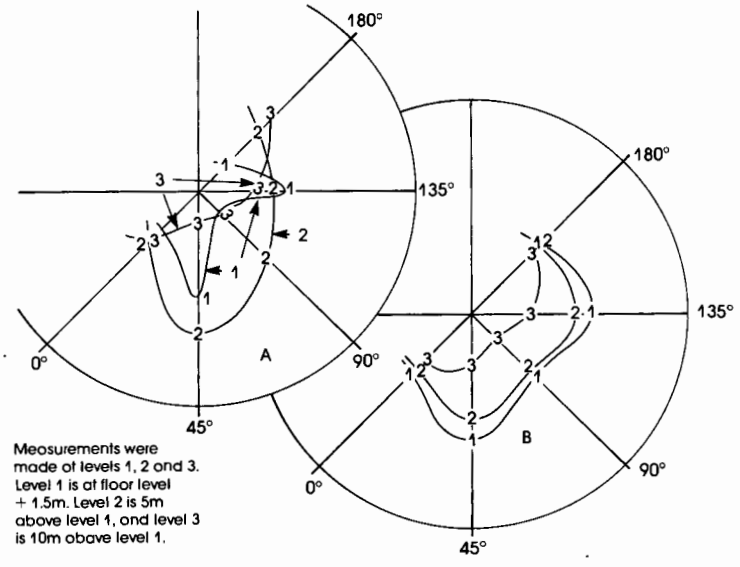

Fig. 9. Typical radial distributions of horizontal pressure in the duocell cement silo illustrated in Fig. 4

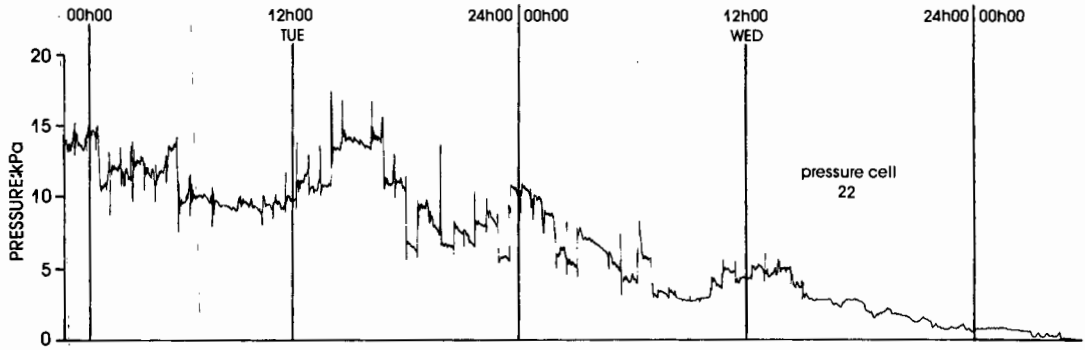

Fig. 10. Continuous recording of pressures 6·5 m above the base of the duocell cement silo

level of the fill was drawn down to below the level of gauge 22. The record is characteristically irregular with pressure spikes at regular intervals of 36 min. These represent the effect of periodic air injection adjacent to gauge 22 as each opening at the base of the silo is used in rotation. The air injection continues on a 24 h basis as the silo feeds road and rail tankers, as well as a bagging plant which operates continuously.

As Fig. 10 shows, the magnitude of the air pressure reacting on the pressure gauge is variable, being 7 kPa or less. After air has been injected, the pressure may either increase or decrease depending on how the fill settles in response to the draw-off. Fig. 10 gives a graphic illustration of why pressures measured at random times are so much more variable than changes in the top level of the fill would lead one to expe

Figure 11 shows two pairs of pressure recordings made for pressure gauges in the cement silo referred to in Fig. 3. The positions of the pairs of gauges W1 and C2 and W2 and C3, one each on the cone and the vertical wall, are indicated in Fig. 3. In this case cement is drawn from the silo into a surge hopper which is used to fill road tankers. The surge hopper is filled on demand and hence emptying of the silo occurs irregularly.

Figure 11 is recorded with a much larger timescale than Fig. 10 and indicates in fine detail the irregular nature of pressure variations in a silo. It should be noted that the discharge of cement can be accompanied by either an increase or a

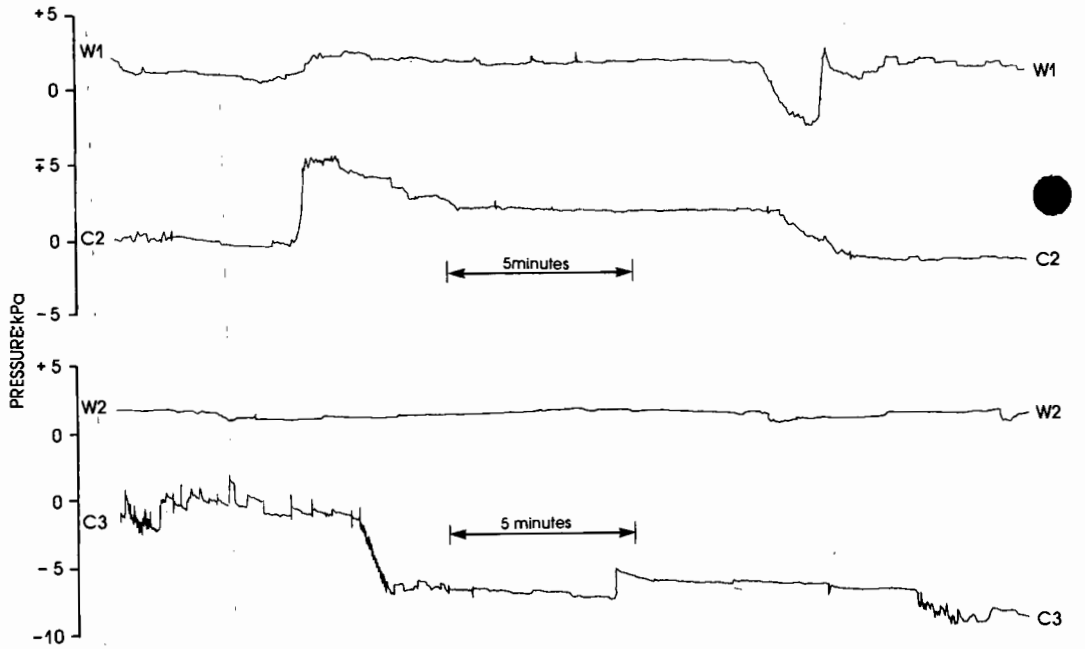

Fig. 11. Typical variations in pressure on the wall and cone of the cement silo illustrated in Fig. 3

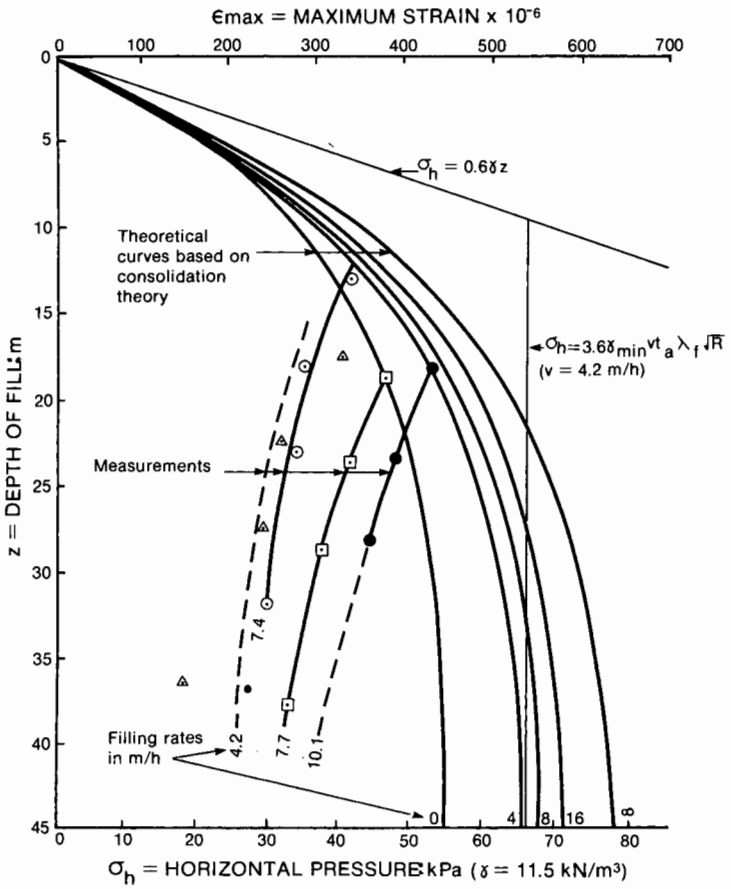

Fig. 12. Pressures measured at the end of rapid filling of a silo with a fine powder

decrease in pressure on the cone or the wall (W1 and C2). Pressure changes at adjacent points on the wall and cone may be in the same or opposite senses. As the point of measurement on the wall becomes more remote from the opening (W2 and C3), pressure changes decrease.

Figures 10 and 11 show that pressure changes within silos are highly irregular and random and certainly not amenable to analysis in any detail.

EFFECTS OF RAPID FILLING

When powder is rapidly loaded into a silo it entrains air and, depending on the rate of loading, the fill may act as a semifluidized mass. The German silo design code DIN 1055 (Martens, 1980) treats the fill as an equivalent fluid, down to a depth related to the filling velocity, and assumes a constant horizontal pressure below that depth. As far as is known, only one set of experimental data exists for pressures in a silo rapidly filled with a fine powder. These data have been presented by Blight *et al.* (1982) and were obtained for the silo described in Fig. 5.

The results of these measurements are presented in Fig. 12. The figure shows the empirical pressure envelope obtained by Pieper *et al.* (1975) which is the basis of the DIN 1055 recommendation, as well as a set of theoretical curves obtained by applying consolidation theory simultaneously with the differential equation for the pressure–depth relationship (equation (6)).

Measured pressures proved to be considerably lower than those predicted, although both the empirical relationship and the theoretical line provided containing envelopes to the observed data.

In Fig. 12, the theoretical curve corresponding to an infinite filling rate is identical with the type of curve shown in Fig. 2 for a constant value of B_a. It appears from Fig. 12 that no serious error would be incurred if the pressures for rapid filling were to be calculated on the assumption that no drainage of pore air takes place during filling, i.e. pressures can be calculated from equations (9) and (10) using an appropriate measured value for B_a.

CONCLUSIONS

For three of the four silos examined in this Paper, the Janssen arching theory, ignoring the possible existence of pore air pressures, provides an adequate containing or design envelope to pressures measured on the vertical walls of the silos, although at small overburdens the straight line relationship

$$\sigma_h = K_0 \gamma z \qquad (11)$$

represents a better containing envelope. For the fourth silo, the straight line relationship provided the best design pressure envelope. The effect of pore air pressures resulting from the injection of compressed air is small enough to be neglected.

The pressure distribution within a zone of convergent flow consists of a continuation of the pressure distribution in the parallel flow zone above, terminated by a sharp transition to the pressure at the outlet. Because of over-consolidation resulting from a decrease in the vertical stress, the lateral pressure coefficient in a zone of convergent flow may increase above the value of K_0 for the normally consolidated material.

Horizontal pressures in silos may be radially non-uniform. The non-uniformity is related to the flow pattern within the silo.

Pressure variations at a point on the wall of an operating silo are highly irregular. This irregularity contributes to the scatter of results experienced when pressures are being measured.

In a silo which is rapidly filled with a fine powder, the pressure distribution can be calculated on the assumption that the fill is subjected to undrained compression, i.e. equations (9) and (10) may be used with an appropriate measured value for B_a.

These conclusions are essentially similar to those reached in the study of pressures in s filled with coarse materials.

REFERENCES

American Concrete Institute Committee 313 (197 Recommended practice for design and constructi of concrete bins, silos and bunkers for storing gran lar materials. *Am. Concr. Inst. J.* **71,** Oct. 529–565.

Blight, G. E. (1983). Measuring pressures in silos wi pressure cells. *Proc. 2nd Int. Conf. Design of Silos f Strength and Flow*, pp. 217–229. London: Powe Advisory Centre.

Blight, G. E. (1986a). Pressures exerted by mater stored in silos: part I, coarse materials. *Géotechni* **36,** No. 1, 33–46.

Blight, G. E. (1986b). Structural loading on the walls rapidly filled silos. In *Encyclopaedia of fluid mech nics*, vol. IV, s. I, ch. 8. New Jersey: Gulf.

Blight, G. E. & Midgley, D. (1980). Pressure mea in a 20 m diameter coal load-out bin. *Proc. Int Conf. Design of Silos for Strength and Flow* **1.** London: Powder Advisory Centre.

Blight, G. E., Schaffner, R. H. & Gilbert, B. (1982 Strains in a reinforced concrete silo during rap filling with a fine powder. *J. Powd. Bulk Soli Technol.* **6,** No. 2, 17–27.

Janssen, H. A. (1895). Versuche über Getreidedruck Silozellen. *Z. Ver. Dt. Ing.* **1,** 1045–1050.

Martens, P. (1980). DIN 1055 part 6: The performanc of the old norm and a progress report on the revise edition. *Proc. Int. Conf. Design of Silos for Strengt and Flow* **1.** London: Powder Advisory Centre.

Murfitt, P. G. & Bransby, P. L. (1980a). Pressures i hoppers filled with fine powders. *Proc. Int. Con Design of Silos for Strength and Flow* **1.** Londor Powder Advisory Centre.

Murfitt, P. G. & Bransby, P. L. (1980b). Deaeration c powders in hoppers. *Proc. Powder Europa 80 Con Wiesbaden.*

Nielsen, J. (1983). Pressure measurements in a full-scal fly ash silo. *Proc. Conf. Silos, Hawaii.*

Pieper, K., Martens, P. & Nothdurft, K. (1975). Silolas ten aus Mehl. *Aufbereitungs-Tech.* **16,** No. 11, 579–585

Proc. Instn Civ. Engrs, Part 1, 1990, **88**, Dec., 1015–1036
9593 STRUCTURAL ENGINEERING GROUP

Defects in accepted methods of estimating design loading for silos

G. E. BLIGHT DSc(Eng)(London), DSc(Eng)(Witwatersrand)*

Current codes of practice and guidelines for assessing design loading on silos and hoppers are lacking in a number of respects. Firstly, it is not generally recognized that arching in silo [illegible] is a phenomenon that may or may not occur. Even when it does occur, arching may [illegible]eak down, with the result that higher than estimated pressures are applied to the silo. Secondly, horizontal pressures in silos are not always radially uniform. This is another aspect that needs to be recognized and taken into account in design. Finally, temperature surcharge pressures should, where appropriate, be included in estimates of design loading. A method of calculating temperature surcharge pressures is proposed.

Introduction

Several codes of practice or guidelines for estimating design loading on silos are in common use throughout the world. The most widely known of these codes are those of the American Concrete Institute (ACI Committee 313, 1975),[1] the German Standards Institute (DIN 1055, 1987),[2] the Institution of Engineers, Australia's Guidelines (1986)[3] and the recent American Society of Agricultural Engineers' standard EP 433 (1989).[4]

2. No engineering code can be perfect. However, all of the codes mentioned are based in part on assumptions which measurements on full-size silos show to be unrealistic. The object of this paper is to point out these defects and to suggest how the design approach can be improved.

Stress paths for vertical and horizontal pressures in silos

3. All of the codes and the guidelines listed base the calculation of horizontal wall pressures (and vertical bottom loads) on the arching theories of Janssen[5] or Reimbert.[6] However, there is a general caution expressed towards this approach, [illegible]ich is well summarized by this quotation from the commentary on the ACI [illegible]de.

> Silo failures have alerted design engineers to the danger of designing silos for only static pressures due to stored material at rest. The research thus far has established beyond doubt that pressures during withdrawal may greatly exceed those present when the material is at rest. There is evidence that one of the causes of overpressure is the switch from active to passive conditions which occurs during material withdrawal.

4. The realization that silo pressures at the start of emptying may exceed those at the end of filling long pre-dates the publication of the ACI Code in 1975. Here,

Written discussion closes 15 February 1991; for further details see p. ii.
* Professor of Construction Materials, Civil Engineering Department, Witwatersrand University, Johannesburg.

for example, is a quotation referring to silo pressures, from the 1932 edition of a well-known design handbook.[7]

> During the emptying process the arching action on which the reduction of pressure depends is completely or partially destroyed, and pressures appreciably in excess of the theoretically determined pressures are obtained.

As this Paper will show, the 1932 statement explains the phenomena occurring in a silo more closely than does the statement in the ACI commentary.

5. Figure 1(a) illustrates the concepts of the active (A), at rest (0) and passive (P) pressure states in a particulate material. Imagine a cylindrical container which is full of particulate material. The container is open at the top, closed at the base, and its diameter can be expanded or contracted. If the upper surface of the material is uniformly loaded and the diameter of the cylinder kept constant, the material will compress vertically, but there will be no overall horizontal strain. The ratio of the horizontal stress on the walls σ_h to the applied vertical stress σ_v will assume a characteristic value K_0 known as the 'at rest pressure coefficient' (σ_h and σ_v are both assumed to be principal stresses). If the diameter of the container is allowed to extend while maintaining the vertical stress σ_v constant, the horizontal stress σ_h will reduce to a minimum constant value after a horizontal extensive strain of 1–2% has occurred. At this stage, the ratio of σ_h to σ_v will have assumed a second characteristic value K_A, the active pressure coefficient. If, however, the diameter of the container is compressed while keeping σ_v constant, the horizontal pressure will increase to a constant maximum value after a horizontal compressive strain of 5–10% has occurred. The ratio of σ_h to σ_v will now be K_p, the passive pressure coefficient.

6. If ϕ is the angle of shearing resistance of the particulate material, then K_A and K_P will be given by the well-known expressions

$$K_A = \tan^2 (45° - \phi/2) \tag{1a}$$

$$K_P = \tan^2 (45° + \phi/2) \tag{1b}$$

K_0 is given empirically and approximately by

$$K_0 = (45° - \phi/2)/(45° + \phi/2) \tag{1c}$$

The numerical values of K in Fig. 1(*a*) are illustrative only, and correspond approximately to $\phi = 30°$.

7. In the context of this Paper, arching is a process whereby sufficient of the weight of the silo fill is supported by friction on the walls to reduce the horizontal stress. Fig. 1(b) indicates how these concepts apply in a silo in which no arching is occurring.

8. The fill material is usually poured into the silo off a conveyor belt or through a spout or chute. It comes to rest at a point represented by 0 in Fig. 1(b). As overburden or vertical stress builds up above a particular element of fill, the element will be compressed vertically and some horizontal extensive strain will occur. The material will therefore follow a stress path such as OA or OA′, and the pressure coefficient will be somewhere between K_A and K_0. The stress path may be modified by the occurrence of arching, depending on the proportions of the silo (i.e. the ratio of height to diameter) and the characteristics of the silo filling.

9. Along stress path OA or OA′, the silo fill is in a metastable stress state. The stress ratio K is less than that corresponding to the stable at rest or K_0 condition.

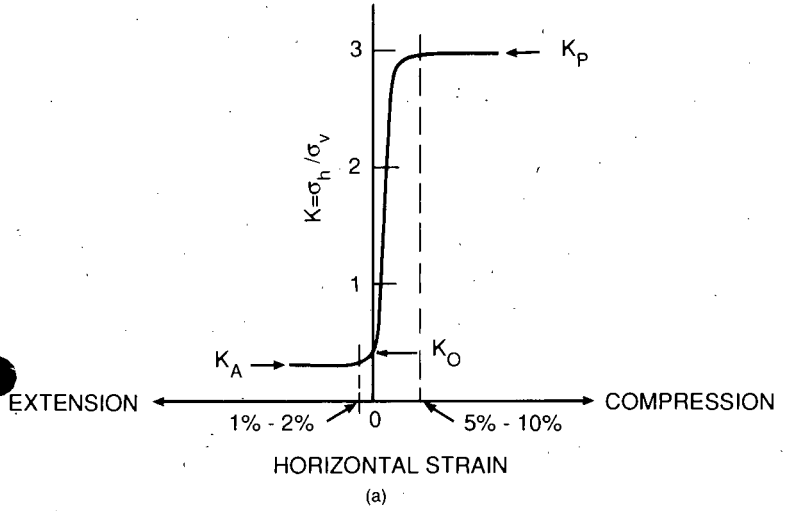

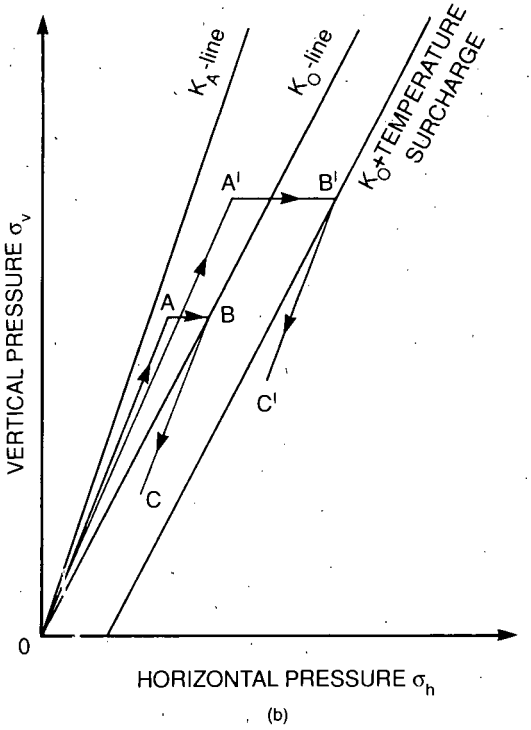

Fig. 1.(a) The at rest, active and passive pressure coefficients in relation to horizontal strain in a silo fill; (b) hypothetical stress paths for material contained in a silo

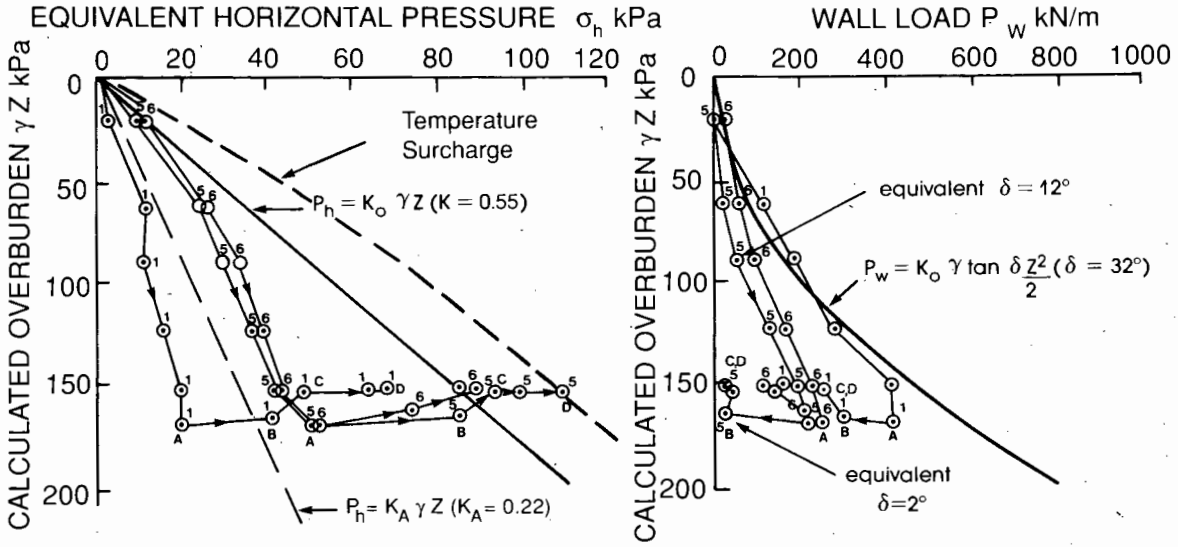

Fig. 2. Stress paths for horizontal pressure and wall load observed for a 20 m dia. by 31·5 m high insulated steel sugar silo

If the fill is allowed to undergo vertical strain, while lateral strain is prevented, it will tend to assume the K_0 condition. In other words, the stress path will deviate from OA along AB. The start of emptying provides an opportunity for strain to occur in the K_0 condition, and therefore the horizontal stress in a silo can be expected to increase at the start of emptying. These strains may also result in a breakdown of arching in the silo.

10. The stress path OA′ is similar to OA, but applies to a silo that is filled and then subjected to diurnal temperature changes. The alternate expansion and contraction of the silo shell causes the stress path to deviate from A′ to B′. The horizontal stress corresponding to B′ exceeds the corresponding K_0 stress by an amount that is related to the horizontal thermal strain, and which will be referred to as the temperature surcharge pressure TS.

11. The concepts outlined above will now be illustrated by the results of measurements on full-size silos. It will be shown that one defect of current design codes is that they assume that arching will always occur in a silo, whereas arching may or may not occur and may break down as a result of disturbances such as fill movement at the start of emptying or temperature cycling. Current codes allow for the effects of non-arching behaviour or the breakdown of arching by applying empirical overpressure factors. It would be more rational to recognize and design for the processes observed to occur within a silo.

Stress paths observed in a steel sugar silo

12. Figure 2[8] shows stress paths, similar to those sketched in Fig. 1(b), observed during uninterrupted filling of a 20 m diameter by 31·5 m high steel sugar silo. Measurements were made by means of electric resistance strain gauges mounted on the steel shell, and relationships between the equivalent horizontal pressure σ_h, the frictional wall load P_ω and the overburden (which approximates to σ_v) are shown. The calculated horizontal pressure depends on the assumption that the silo cross-section is truly circular. For this reason, it is referred to as an equivalent pressure.

13. It will be noted that the stress path OA is quite variable, depending on the local frictional characteristic and the local unloaded radius of the silo wall. Also, that a lower horizontal pressure is associated with a higher frictional wall load (path 1–1) and vice versa (paths 5–5 and 6–6). The slight convex-up curvature of the stress paths shows that some arching was occurring, as does the fact that OA for stress path 1–1 lies below the K_A stress path. Paths 1–1, 5–5 and 6–6 have been chosen for display as they represent measurements spaced at 90° to each other in plan.

14. At A, filling was terminated and emptying started. Immediately, σ_h increased along AB while the wall load decreased correspondingly. Both sets of measurements are consistent with the breakdown of arching which was postulated earlier.

15. The drawdowns that resulted in AB and BC in Fig. 2 each took place over the course of a few hours, with an interval of a day between. A further increase in horizontal pressure, with very little change in wall load, then took place over the course of the next few weeks (to point D) as the silo and the static contents were subjected to diurnal temperature cycles, and the temperature surcharge pressure built up. (Although the silo is insulated, the wall is still subject to a subdued diurnal temperature wave.) All of these observations are completely consistent

with Fig. 1(b) and illustrate that arching in a silo cannot be regarded as an ever-present phenomenon.

16. It will be noted that the angle of wall friction developed on path 5–5 during filling was about 12°, as compared with the full angle of wall friction of 32°. The low angle arose because the shear displacement was limited to vertical compression of the sugar, and also, as discovered later,[9] the measurements were taken when the silo wall was cooling and contracting relative to the fill. The very low value of $\delta = 2°$ can also be ascribed to cooling contraction of the silo wall relative to the fill.

Examples of pressure envelopes and stress paths observed in other silos

17. Figure 3 shows a set of horizontal pressures measured in a 7 m dia. by 46 m high reinforced concrete wheat silo.[10] The figure shows the spread of pressures

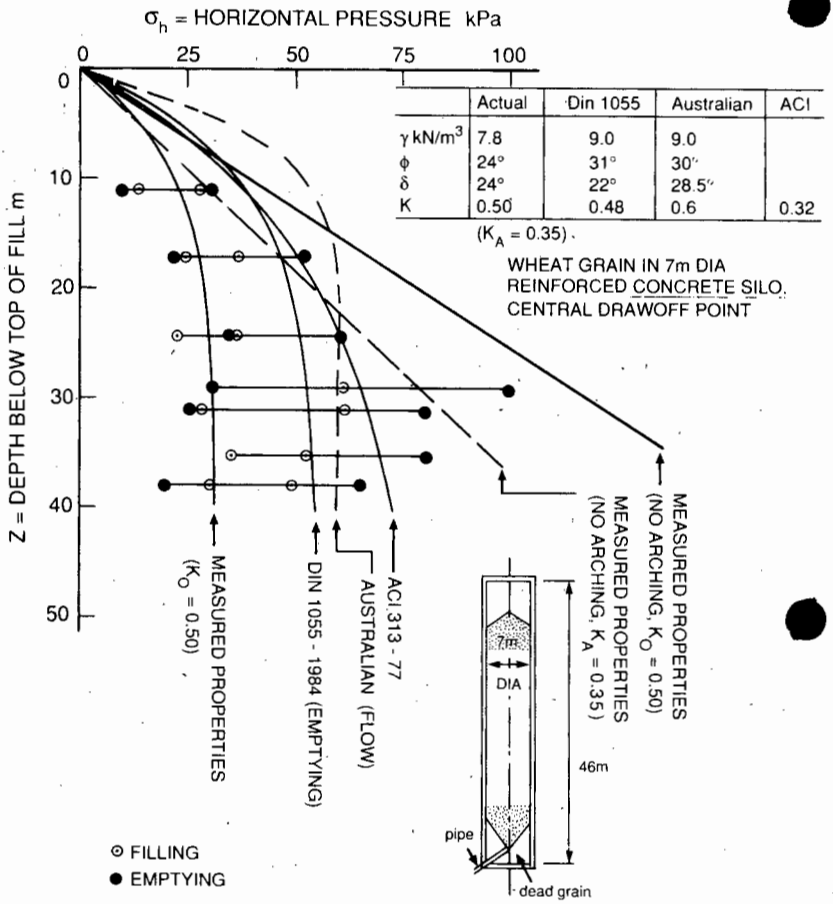

Fig. 3. Horizontal pressures measured at the end of filling and the start of emptying in a 7 m dia. by 46 m high reinforced concrete wheat silo

measured at various levels in the silo at the end of filling and after the start of emptying. The measurements were made by means of pressure cells built into the wall of the silo. The figure again illustrates the highly variable nature of pressures measured in silos.

18. Comparing the measurements with the envelope based on the Janssen theory (labelled 'measured properties') shows that arching certainly did occur during filling. However, at a depth of 30 m, the upper limit to the measured horizontal pressures reveals that there was relatively little arching at this depth. At the start of emptying, the lower limit to the pressures was relatively unchanged, but the upper limit increased considerably and coincided roughly with the K_A line, with pressures approaching the K_0 condition at two levels. The data in Fig. 3 illustrate the breakdown of arching that may occur at the start of emptying, and the unreliability of the arching phenomenon.

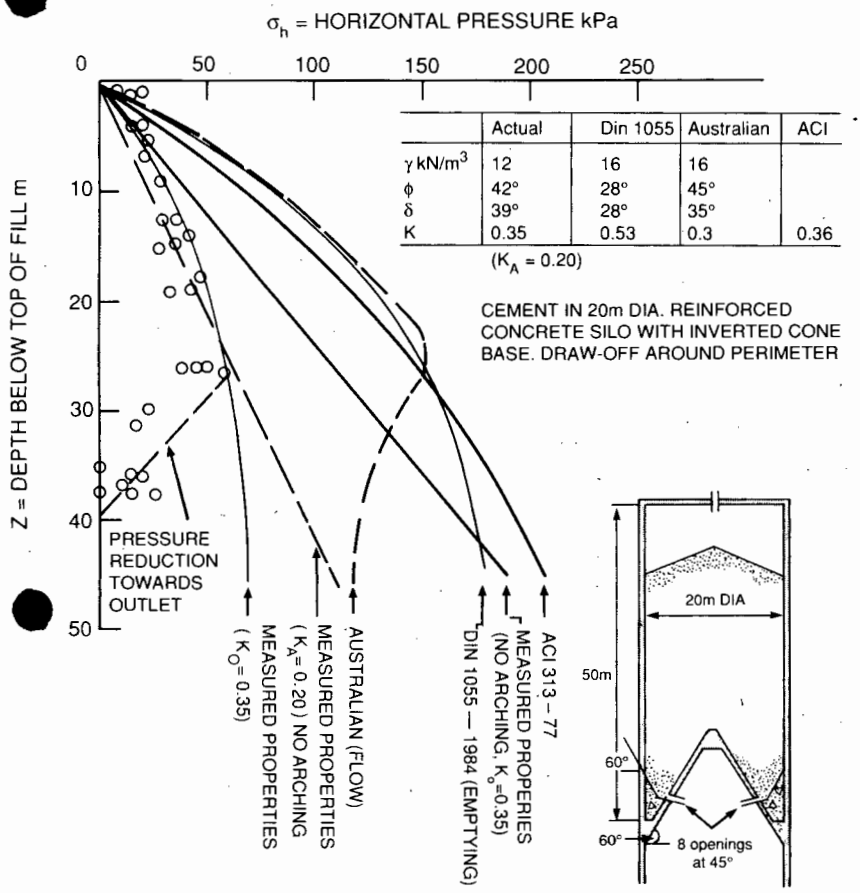

Fig. 4. Horizontal pressures measured during operation of a 20 m dia. by 50 m high reinforced concrete cement storage silo

19. Design pressure envelopes for emptying according to the DIN and ACI codes and the Australian guidelines are also shown in Fig. 3. The envelopes for the DIN and ACI codes have been calculated for the material properties specified in the DIN code; the envelope for the Australian guidelines has been calculated for the properties given in those guidelines. It will be seen that none of the code envelopes describes the measured pressures very well; also, none comes near to predicting the maximum stress actually measured in the silo; and perhaps more importantly, none describes the big range of pressures encountered at a particular level around the perimeter of a silo.

20. Figure 4 shows a set of pressures measured by means of pressure cells built into the walls in a 20 m dia. by 50 m high reinforced concrete cement storage silo.[11] The silo is operated as a load-out facility for bulk cement deliveries and is subject to simultaneous filling and emptying. Even though the height to diameter ratio of the silo is unfavourable, Fig. 4 shows that the relationship between horizontal pressure and depth of material accords with the predictions of the Janssen theory, and that the contents are fully and permanently arched; this illustrates the difficulty of predicting whether or not arching is likely to occur. The various code and guideline pressure envelopes again do not describe the pressures in the silo very well. In this case, much of the discrepancy arises because the materials parameters assumed by the codes are much more severe than the actual materials properties. (The unit weight is 30% higher and the angle of wall friction is lower.)

21. There are many other examples in the literature that illustrate both the unreliability of the arching phenomenon and the difficulty of predicting its occurrence. A number of such examples have been assembled in an earlier paper.[12]

22. Figure 5 shows a final example of stress paths for a silo, in this case a plane plate-welded steel silo storing maize, for which the horizontal pressures and frictional wall loads were measured by means of strain gauges mounted on the walls.[13]

23. Figure 5(a) shows the stress paths measured on four lines—A, B, C, D—separated by 90° around the perimeter of the silo. The symbols A, B, C, D each represent a measurement at positions A, B, C, D. There are twice as many points shown in Fig. 5(a) as in Fig. 5(b) because Fig. 5(a) includes measurements made between erection stiffeners and on the line of stiffeners, and Fig. 5(b) includes only measurements between stiffeners so that they represent wall loads in the unstiffened plate. The stress paths are similar to those shown in Fig. 2 but more variable because this silo is uninsulated and subject to greater diurnal fluctuations of temperature than the insulated sugar silo. Nevertheless, the stress paths fall within envelopes defined by the K_A line and a temperature surcharge line. There is little evidence of any arching in the fill. Figure 5(b) shows the stress paths for the frictional wall load in the silo. The measurements show that, although there was insufficent arching to reduce horizontal stresses, frictional load was being transferred into the silo wall.

24. The correspondence between stress paths D in Fig. 5(a) and (b) should be noted in particular. Line D was always in shade when measurements were taken and, as such, was cooler than the other lines of measurements. The pressures were therefore consistently higher on line D, and the frictional wall loads were lower. The cool section of the silo was prevented from contracting both vertically and horizontally by the presence of the grain, thus increasing the horizontal stress and decreasing the wall load. The mechanism of temperature stressing of silo walls has been more fully described elsewhere.[14]

Radial variations of horizontal pressure in silos

25. The data displayed in Figs 2, 3, and 5 show that the horizontal pressure on a silo's walls, at a given level, can vary considerably around its circumference. Steel silos, which have walls that are relatively flexible in a horizontal plane, may not be much affected by this variation. The pressure variation can, however, cause significant horizontal bending moments in the walls of reinforced concrete silos, and these merit consideration in design.

26. Figure 6 gives some examples of observed radial variations of horizontal pressures in silos. Fig. 6(a) shows the radial variation of pressure observed in the 7 m dia. wheat silo referred to in Fig. 3.[10] Fig. 6(b) shows radial pressure distributions observed on two separate occasions on three separate levels in a reinforced concrete ring silo, storing cement powder.[15] Fig. 6(c) shows radial variations of pressure observed at two different levels at the end of filling the sugar silo referred to in Fig. 2.[8] In the case of Fig. 6(c), it is believed that much of the apparent radial variability of pressure is, in fact, radial variability of strain arising from geometrical imperfections in the silo shell.

27. It will be noted from these examples that radial pressure distributions may be multilobed, that the variation may exceed half of the maximum measured pressure, and that the radial pressure distribution varies with level in a silo and differs on different occasions. Radial pressure may therefore have a highly variable distribution that does not appear to be susceptible to rational prediction.

Calculating temperature surcharge pressures in silos

28. Knowledge of the factors governing the magnitude and occurrence of temperature surcharge pressures is as yet incomplete (see, for example, the ASAE Code[4]). Measurements have shown, however, that the diurnal temperature change experienced by a steel silo wall is less than the corresponding change of air temperature.[16] Hence, temperature surcharge pressures calculated on the basis of air temperature changes will usually be slight overestimates. There do not appear to be any published observations of temperature surcharge pressures in reinforced concrete silos. Because of the insulation provided by the concrete, these pressures may not respond to diurnal changes; but if materials are stored for long periods of time, a seasonal temperature surcharging is possible, and should be considered. There is also no established basis for calculating temperature surcharge pressures: the equation attributable to Andersen[17] has been used, but it appears to give unrealistic reults, mainly because of the difficulty of estimating the parameters necessary for its solution.

29. The Author[13,16] has formulated an equation based on measurements of temperature surcharge pressues in four steel bins storing maize. The equation is

$$TS = \frac{2MEt\alpha\Delta\theta}{MD + 2Et} \qquad (2)$$

where TS is the temperature surcharge pressure; M is the compression modulus of the silo filling; E is the elastic modulus for the material of the silo wall; t is the wall thickness; α is the coefficient of thermal contraction for the material of the silo wall; and D is the silo diameter. The derivation of equation (2) is given in Appendix 1.

30. It appears from the field measurements that M is very dependent on the overburden stress to which the filling material is subjected. Fig. 7 shows the

relationship between M and overburden stress established from measurements on maize-storing silos. Clearly, more research is required on this topic, and, in particular, data enabling the calculation of the compression modulus M for various materials are required.

Pressures at cylinder-to-hopper transitions

31. Work by Jenike,[18] by Jenike and Johanson,[19] and by Walker[20] appeared to show that a 'switch pressure' or 'overpressure' would occur at the start of emptying close to the transition from the parallel-sided section of a silo to the convergent-walled hopper section. According to Jenike and Johanson, the switch pressure is generated because of the transition from an *active* state of stress in the

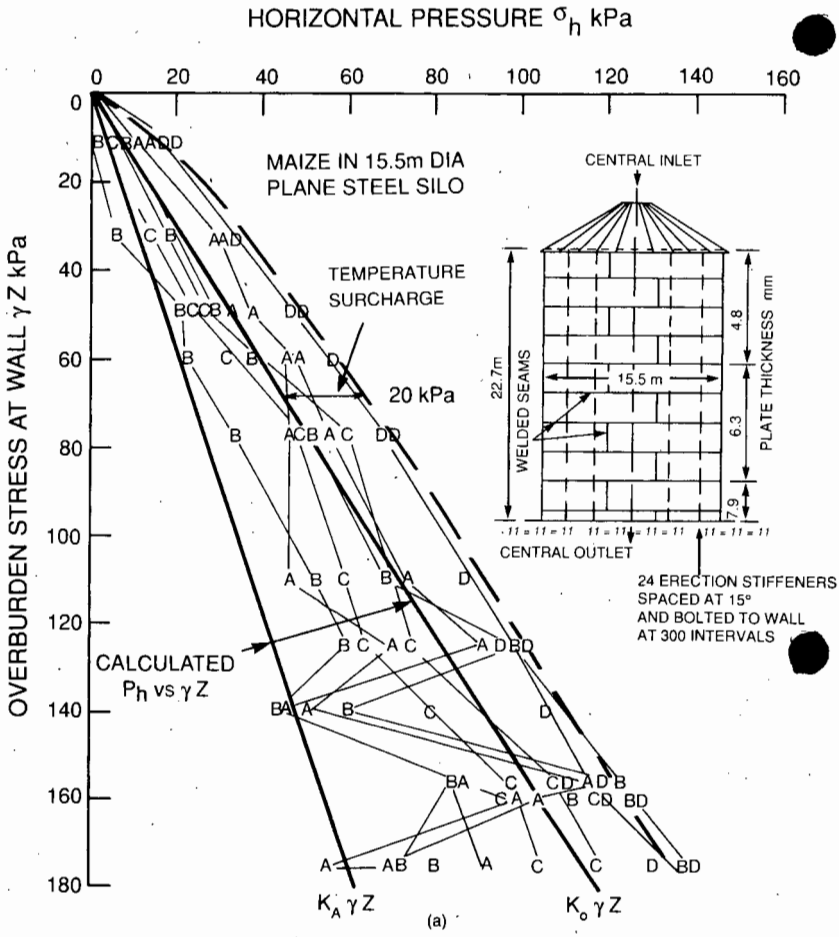

Fig. 5 (above and facing). Stress path for (a) horizontal pressure and (b) frictional wall load in a 15·5 dia. by 22·7 m high steel silo during filling with maize

zone of parallel material flow to a *passive* state in the zone of convergent flow (see quotation from ACI Code commentary in § 3). The switch pressure was postulated to be transient, to act over only a small height of wall at any time, and to travel upwards as the transition from a static condition to one of flow was established. Walker's theory postulates a similar switch from *active* to *passive* conditions at the cylinder-to-hopper transition, and predicts that a peak pressure will act at the transition.

32. There are at least two reasons why these theories do not stand up to close examination.

(*a*) They call for a near-instantaneous transition from the active to passive states, taking no account of the strain required to produce this transition (see Fig. 1(a)).

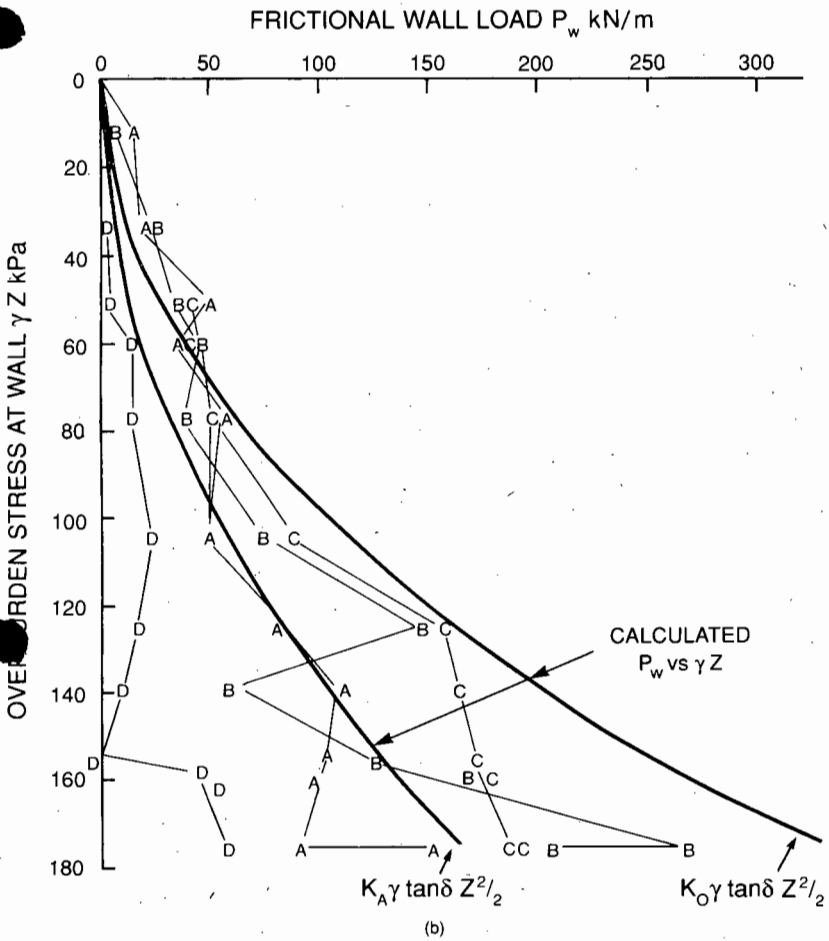

Fig. 5—continued

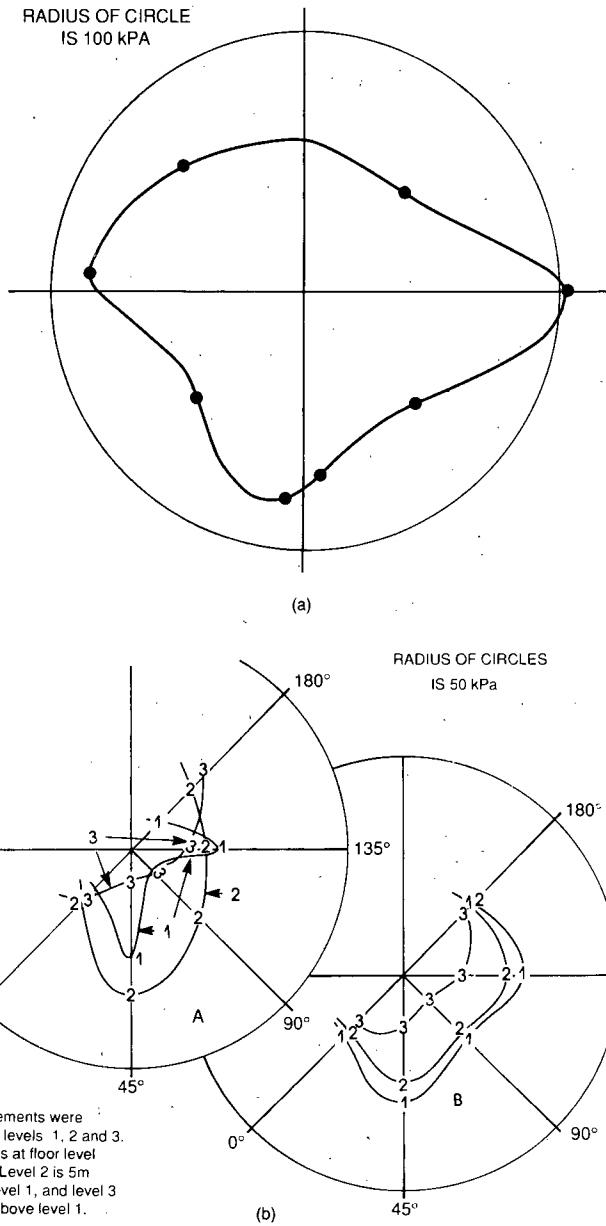

Fig. 6 (above and facing). Radial variations of horizontal pressure observed in silos: (a) 7 m dia. silo referred to in Fig. 3; (b) 24 m outside dia., 15 m inside dia. reinforced concrete ring silo storing cement; (c) 20 m dia. steel sugar silo referred to in Fig. 2 (in each case, horizontal pressures have been plotted radially in plan)

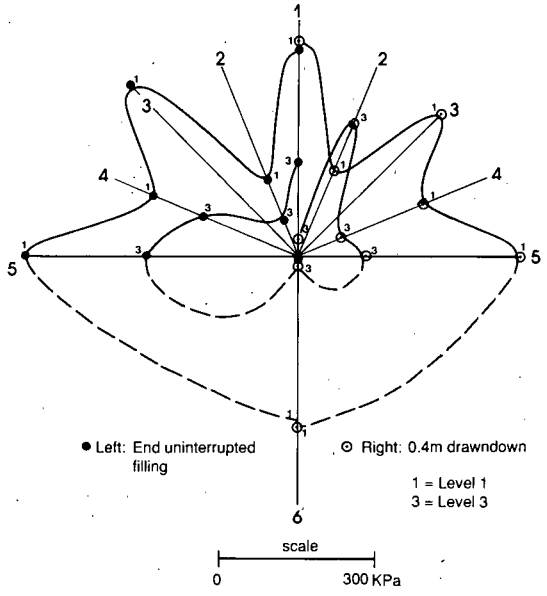

(c)

Fig. 6—continued

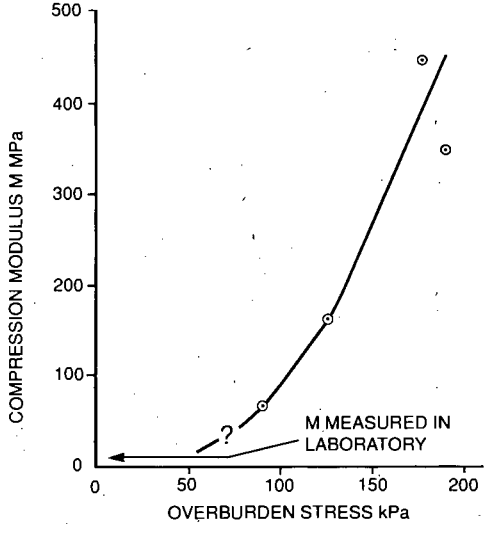

Fig. 7. Relationship between overburden stress and compression modulus for maize, deduced from measurements of temperature strains in four steel silos

(*b*) They assume that plane sections through the silo fill in the zone of parallel flow remain plane in the zone of convergent flow. There are many studies of flow patterns within silos (for example, reference 21) that show that this is not the case. Material flowing from a silo *queues* to get through the available opening, and hence there is no sudden change in pressure. It is probable that the vertical stress in the flow zone reduces considerably. The horizontal stress at the silo wall may also reduce, as shown in Fig. 4. However, measurements to be shown later show that

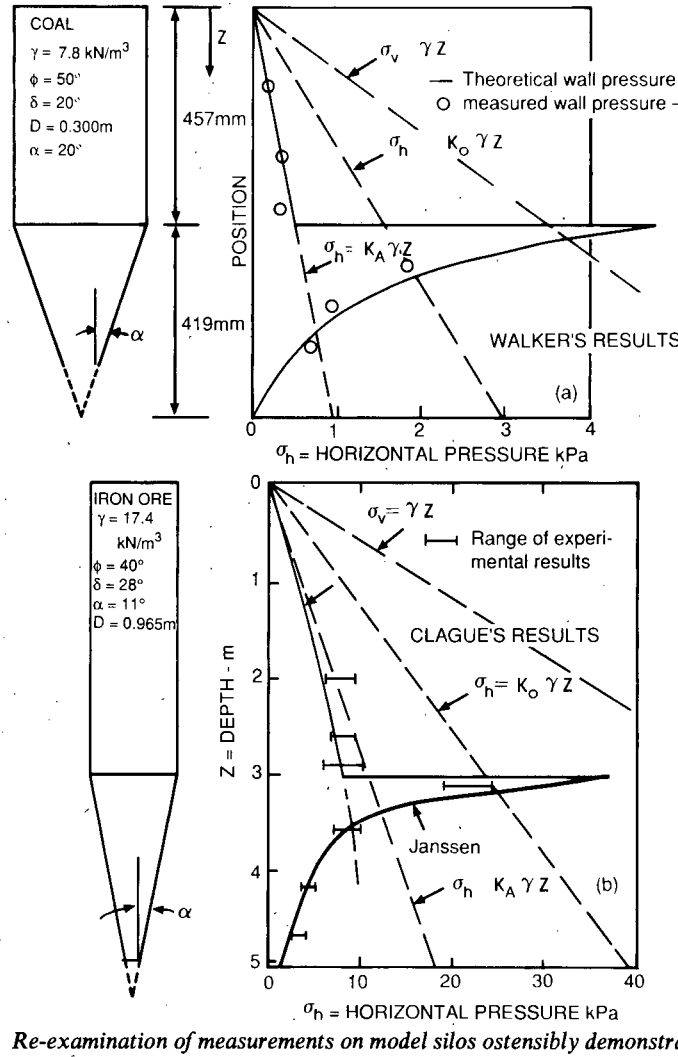

Fig. 8. Re-examination of measurements on model silos ostensibly demonstrating the occurrence of a peak pressure at the start of emptying

horizontal stress at the silo or hopper wall may be unaffected by emptying.

33. The overpressure theory was apparently substantiated by measurements made on model silos by Walker[20] and by Clague.[22] The results of these measurements have been reproduced in Fig. 8. In each case, the theoretical peak pressure is shown together with the experimental observations purported to support the theory. However, if these results are compared with the positions of the K_A and K_0 lines, it becomes apparent that the filling in the model silos was actually following the stress path OAB in Fig. 1(b), with a localized transition from the K_A to the K_0 state in the vicinity of the cylinder-to-hopper transition. This observation will now be substantiated by referring to the results of measurements on full-size hoppers.

Measurements of pressures in full-size hoppers

34. Figure 9 shows pressures measured at the start of emptying by means of pressure cells in the hopper portion of a 20 m dia. by 54 m high coal load-out silo.[23] The figure also shows the positions of the K_A and K_0 lines. The observed pressures fall mostly between the K_A and K_0 lines, with a few measurements

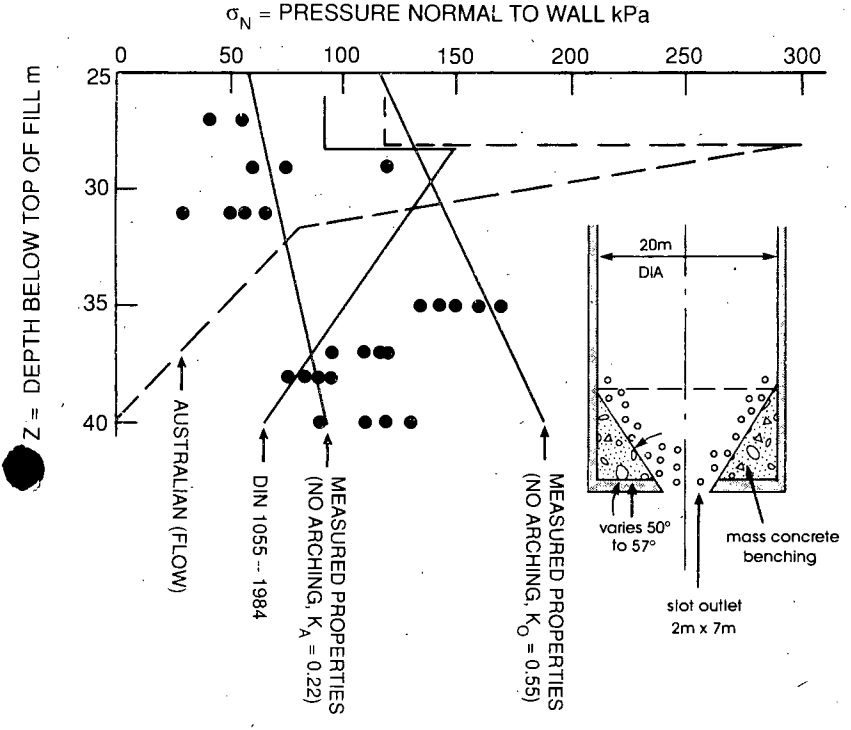

Fig. 9. Comparison of measured pressures normal to the wall of a 20 m dia. by 54 m high, coal load-out silo, at the start of emptying, with pressures predicted by the DIN code and the Australian guidelines

somewhat less than the active condition would predict. There is no evidence of any pressure substantially greater than that corresponding to the K_0 condition; furthermore, no arching occurred in the hopper.

35. Figure 9 also shows the hopper pressures predicted according to the DIN code and the Australian guidelines, the latter making allowance for a peak pressure. As the figure shows, pressure predicted on the basis of the code and guidelines bears little resemblance to the actual pressures.

36. Similar data are shown in Fig. 10 for the hopper of a steel bin, storing maize starch.[12] In this case, the pressures were deduced from strain measurements on the hopper wall. Even though the filling was an extremely fine powder, there

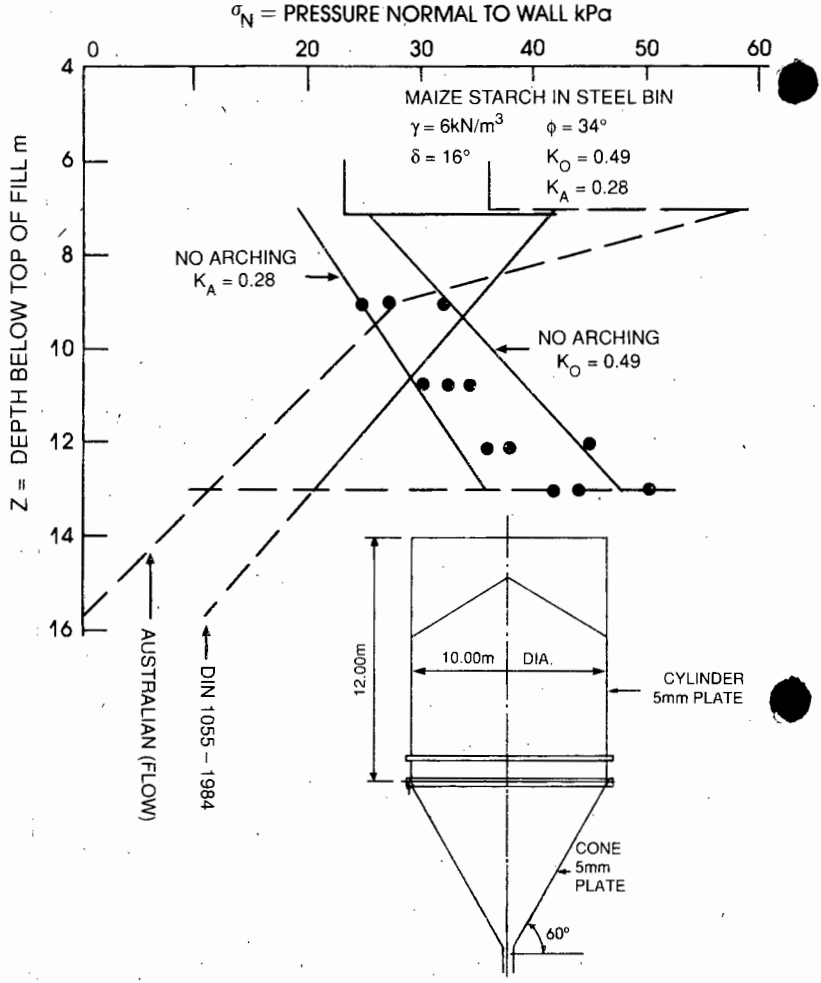

Fig. 10. Comparison of measured and calculated pressures normal to the hopper walls of a 10 m diameter starch bin

was no evidence of arching. The results were very similar to those measured in the coal silo and again bear little resemblance to the code predictions. The pressures shown were those normal to the convergent hopper wall, and the K_A and K_0 lines have been adjusted to allow for this.

37. The final comparison is shown in Fig. 11(a).[24] To improve the outflow from a long reinforced concrete coal staithe or two-dimensional hopper, the outlet was modified by means of a bolt-on slot opening, together with a plough operating

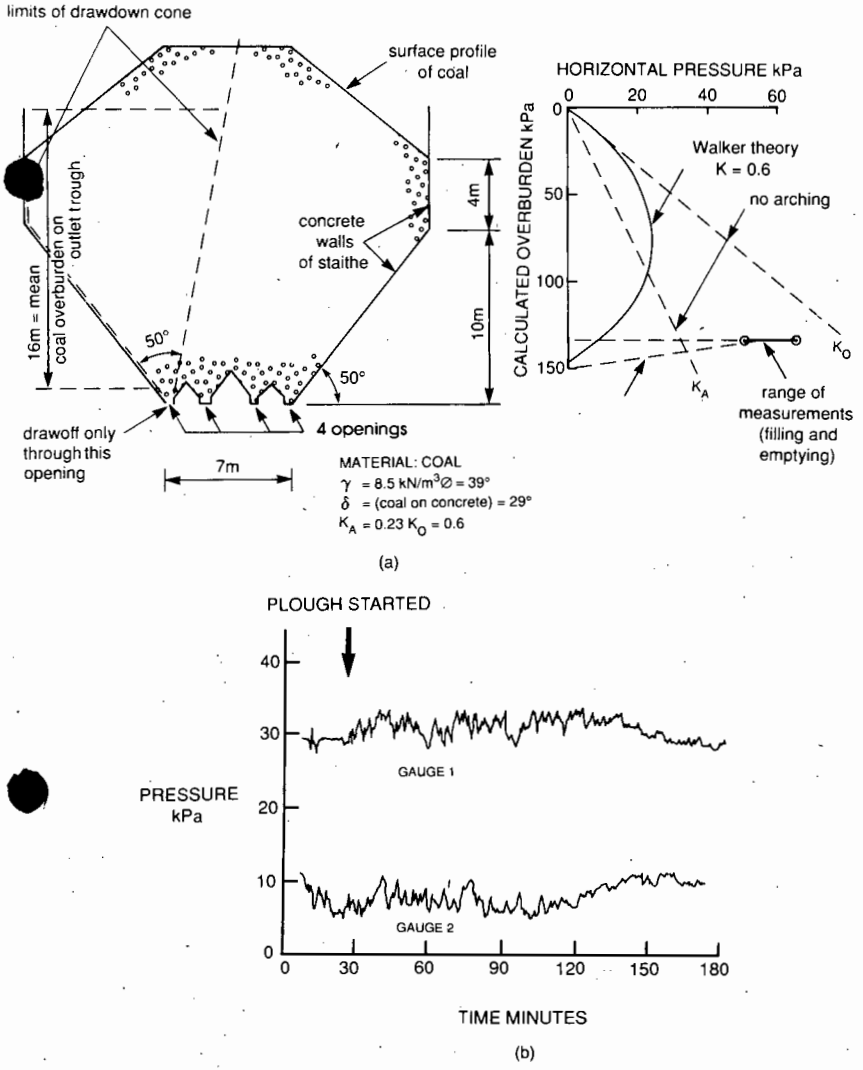

Fig. 11. (a) Pressures measured near the outlet of a reinforced concrete coal staithe; (b) variation of pressure at the start of emptying

along a shelf. The steel bolt-on modification was strain-gauged and test-loaded to check on its design. The horizontal pressure just above the shelf, both at the end of filling and the start of emptying, could then be calculated from the measured strains. The results displayed in Fig. 11(a) showed that the horizontal pressure at this point lay between the K_A and K_0 lines, and hardly changed between the end of filling and the start of emptying. The Walker arching theory appears to be quite inadequate in this case, as no arching appears to occur in the hopper either during filling or at the start of emptying.

38. Figure 11(b) shows the variation of strain with time recorded by strain gauges at two positions along the length of the hopper. Neither gauge showed any substantial change in pressure once the plough was put into operation.

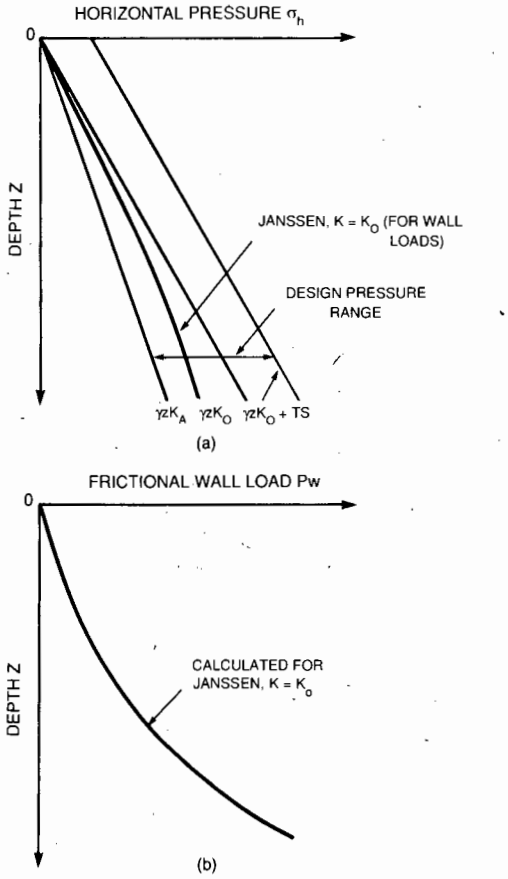

Fig. 12 (above and facing). Suggested basis for estimating design loading on parallel-walled silos: (a) band of horizontal pressure between γzK_A and $\gamma zK_0 + TS$; (b) frictional wall loading based on Janssen theory with $K = K_0$; (c) suggested radial variation of design horizontal pressure; (d) suggested vertical profile of design horizontal pressure

39. From these comparisons, it may be concluded that
(*a*) arching does not necessarily occur in hoppers
(*b*) peak pressures do not occur at cylinder-to-hopper transitions.

Suggested methods of estimating design loading on silos and hoppers

40. Suggestions for more realistic estimates of design loading are summarized in Fig. 12, and are as follows.

41. It should be recognized that arching may not occur in a silo or hopper fill. Even if arching does occur, it may break down at the start of emptying, resulting in

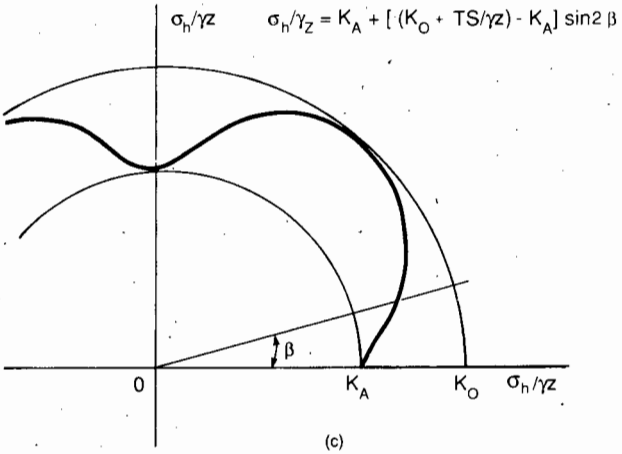

(c)

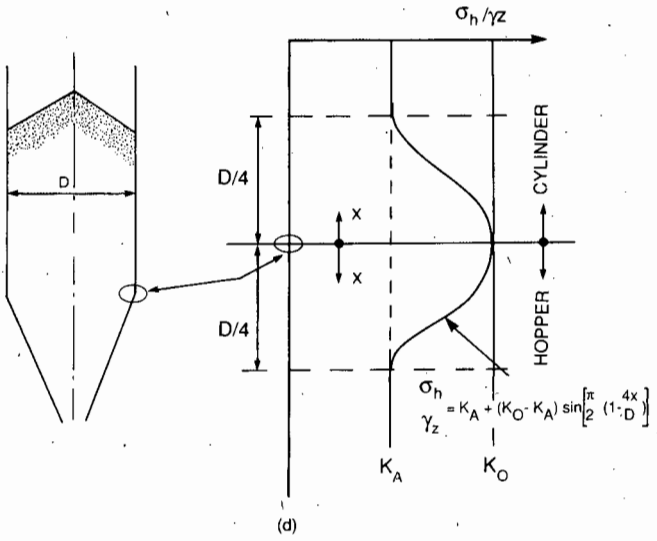

(d)

Fig. 12—continued

the application of pressures that exceed those calculated on the assumption that arching will occur.

42. The hopper portion of a silo should be treated simply as an extension of the silo itself. The design horizontal pressure distribution should extend from the top of the cylinder to the apex of the hopper, without any discontinuity.

43. Temperature surcharge pressures (TS) will occur in steel silos and may also occur in reinforced concrete silos. Temperature surcharges may be calculated according to equation (2), or following the suggestions of the ASAE Code,[4] taking appropriate temperature changes into account.

44. The design maximum horizontal pressure envelope should be the one in Fig. 12(a) labelled

$$\gamma z K_0 + TS$$

45. Frictional wall loads will be at a maximum if arching occurs in the s[illegible] They should therefore be calculated on the basis of a horizontal pressure distribution that assumes arching according to the Janssen theory, with a pressure coefficient of K_0 (Fig. 12(b)).

46. It should be recognized that horizontal pressures will not be uniform around the perimeter of a silo or hopper. Depending on the construction of the silo or hopper, it may be advisable to consider the effect of a hypothetical radial pressure distribution varying between the limits of

$$\sigma_h = \gamma z K_A$$

and

$$\sigma_h = \gamma z K_0 + TS$$

A possible, but arbitrary, distribution for this purpose is that shown in Fig. 12(c), i.e.

$$\sigma_h = \gamma z K_A + [(\gamma z K_0 + TS) - \gamma z K_A]\sin 2\beta \tag{3}$$

where β is defined in Fig. 12(c). This distribution recognizes that both the horizontal pressure due to the filling, and the temperature surcharge pressure may vary around the perimeter of the silo in a multilobed fashion.

47. Irregularities in the horizontal pressure profile, resulting from a localized break-down of arching, may give rise to bending in the vertical direction. This aspect could be considered by assuming that a variation occurs in the vertical profile of horizontal pressure, such as that illustrated in Fig. 12(d). This distribution, also arbitrary, recognizes that a change in pressure conditions appears most likely to occur in the vicinity of the cylinder-to-hopper transition. The profile is given in non-dimensional form, assuming that the relationship between horizontal pressure and overburden is basically linear. A progressive transition is assumed from K_A to K_0 conditions, and back again, over a vertical height of $D/4$ above and below the cylinder-to-hopper transition. The variation is assumed to be described by

$$\frac{\sigma_h}{\gamma z} = K_A + (K_0 - K_A)\sin\frac{\pi}{2}\left(1 - \frac{4x}{D}\right)$$

as shown in Fig. 12(d). In this case, the temperature surcharge TS is not considered, as observations have shown[14] that the temperature surcharge disappears

once the silo contents are put in motion at the start of emptying. The surcharge could, however, be included by adding an appropriate term to give

$$\frac{\sigma_h}{\gamma z} = K_A + \left(K_0 + \frac{TS}{\gamma z} - K_A\right)\sin\frac{\pi}{2}\left(1 - \frac{4x}{D}\right)$$

Conclusions

48. Current codes of practice and guidelines for assessing design loading on silos and hoppers are lacking in some respects. These deficiences have been enumerated and illustrated with reference to measurements on a number of full size silos and hoppers. Suggestions have been made for making silo loading codes more realistic.

Appendix 1. Derivation of temperature surcharge pressure equation

49. If ε is the thermal strain that is prevented from occurring by the presence of the silo fill, α is the coefficient of thermal contraction of the silo wall, $\Delta\theta$ is the change of temperature of the silo wall, TS is the thermal surcharge pressure, and M is the modulus of compressibility of the grain for radial compression, then

$$\varepsilon = \alpha\Delta\theta - (TS/M)$$

Also

$$TS = 2E\varepsilon t/D$$

where E is the elastic modulus of the silo wall, t is the wall thickness and D is the silo diameter. Hence, by eliminating ε

$$TS = 2MEt\alpha\Delta\theta/(MD + 2Et)$$

50. The equation was formulated for silos with corrugated steel walls in which the hoop strain is essentially one-dimensional. It does, however, seem to give a reasonable description of temperature surcharges in steel silos with walls of plane welded plate.

References

1. AMERICAN CONCRETE INSTITUTE. *Recommended practice for design and construction of concrete bins, silos and bunkers for storing granular materials.* Title 72–37. *J. Am. Concr. Inst.*, 1975 Oct., 528–548.
2. DEUTSCHES INSTITUT FÜR NORMUNG. *Lastannahmen für Bauten-Lasten in Silozellen.* DIN, Berlin, 1987, DIN 1055, Part 6.
3. INSTITUTION OF ENGINEERS, AUSTRALIA. *Guildlines for the assessment of loads on bulk solids containers.* The Institution, Melbourne, 1986.
4. AMERICAN SOCIETY OF AGRICULTURAL ENGINEERS. *Loads exerted by free-flowing grains on bins.* ASAE, St Joseph, Michigan, 1989, Engineering Practice: ASAE EP433.
5. JANSSEN H. A. Versuche über Getreidedruck in Silozellen. *VDI Zeitschrift*, 1895, **39**, 1045–1049.
6. REIMBERT M. and REIMBERT A. Silos-Taite Theorique et Pratique. *Editions Eyrolles*, 1961, Paris.
7. REYNOLDS C. E. *Reinforced concrete designer's handbook.* Concrete Publications, London, 1932.
8. BLIGHT G. E. and GARSTANG A. Strains measured in a 7500 t sugar silo. *Bulk Solids Handling* (FRG), 1987, **7** (4), 573–582.
9. BLIGHT G. E. Strains measured in a 7500 t sugar silo, part II. *Bulk Solids Handling* (FRG), 1988, **8** (4), 413–419.

10. HARTLEN J. *The wall pressure in large grain silos.* Swedish Council for Building Research, Stockholm, 1984, Document D2.
11. SCHAFFNER R. H. and BLIGHT G. E. A comparison of design and measured pressures in a large Ibau-type cement storage silo. *Int. J. Bulk Solids Storage in Silos*, 1986, **2** (3), 17–24.
12. BLIGHT G. E. A comparison of measured pressures in silos with code recommendations. *Bulk Solids Handling* (FRG), 1988, **8** (2), 145–153.
13. BLIGHT G. E. Load and temperature strains of a welded plane plate grain silo. *Powder Handling and Processing* (FRG), 1990, **2** (1), 25–29.
14. BLIGHT G. E. Temperature changes affect pressure in steel bins. *Int. J. Bulk Solids Storage in Silos*, 1985, **1** (3), 1–7.
15. FLISS L. and BLIGHT G. E. A comparison of design and measured lateral pressures and temperatures in a large duo-cell cement storage silo. *Int. J. Bulk Solids Storage in Silos*, 1986, **2** (4), 18–28.
16. BLIGHT G. E. Strain and temperature measurements on an externally stiffened corrugated steel grain silo. *Powder Processing and Handling* (FRG), 1989, **1** (4), 343–347.
17. ANDERSON P. Temperature stresses in steel grain storage tanks. *Civil Engineering*, American Society of Civil Engineers, New York, 1966, Jan., 74.
18. JENIKE A. W. *Storage and flow of solids.* Engineering Experiment Station, University of Utah, 1964, Utah, Bulletin 123.
19. JENIKE A. W. and JOHANSON J. R. Bin loads. *J. Struct. Div. Am. Soc. Civ. Engrs*, 1968, **94** (ST4), 1011–1041.
20. WALKER D. M. An approximate theory for pressures and arching in hoppers. *Chem. Engng Sci.*, 1966, **21**, 875–997.
21. DEUTSCH G. P. and CLYDE D. H. Flow and pressure in granular materials in silos. *J. Engng Mech. Div. Am. Soc. Civ. Engrs*, 1967, **93** (EM6), 102–125.
22. CLAGUE K. *The effects of stresses in bunkers.* University of Nottingham, 1973, PhD thesis.
23. BLIGHT G. E. A comparison of design and measured lateral pressures in a large coal load-out silo. *Int. J. Bulk Solids Storage in Silos*, 1986, **2** (2), 1–8.
24. BLIGHT G. E. Pressures exerted by materials stored in silos: part 1, coarse materials. *Géotechnique*, 1986, **36** (1), 33–46.

Proc. Instn Civ. Engrs, Part 1, 1991, **90**, Oct., 1077–1088
9593 DISCUSSION STRUCTURAL ENGINEERING GROUP

Defects in accepted methods of estimating design loading for silos

G. E. Blight

Professor J. M. Rotter and Dr J. Y. Ooi, *University of Edinburgh*

The Author argues that current codes of practice and guidelines for assessing design loading on silos and hoppers are lacking in some aspects. The object is stated as: 'to point out these defects and to suggest how the design approach can be improved.' We agree that current codes have many defects, but we would argue that this Paper does not help code writers very much.

On stress paths

52. In § 8, the Author states that during filling, the solid 'will be compressed vertically and some horizontal extensive strain will occur'. For a smooth-walled rigid cylinder, the horizontal strain will always be zero. For most real silos, including all the silos the Author studied, a uniform radial strain of 0·1% would be extremely large. A glance at Fig. 1(a) shows that the walls are all very stiff. Hence the most likely condition for initial filling is effectively zero lateral strain. The horizontal pressure ratio differs from K_0 because wall friction causes shearing in the solid, and because the test to measure K_0 does not model the stress history to which the solid is subjected.

53. The Author describes next what might happen when emptying begins, which appears to be founded on one experiment by the Author.[25] To say that stress path OA is in 'a metastable stress state' (i.e. in unstable equilibrium: *vide* Oxford English Dictionary) is quite unfounded. To say that the stresses will tend to assume the K_0 condition under vertical (tensile) strains when the lateral strain is prevented has not been demonstrated and is contrary to many known materials test results.

54. The responses of particulate media are known to be stress history dependent. Many experiments on soils and bulk solids have shown that when the solid is allowed to undergo vertical tensile strain, the horizontal stress can be 'locked-in': the ratio of horizontal to vertical stress K increases and can exceed unity. An example of tests on sand is shown in Fig. 13.[26] There is no 'natural' state at K_0, as suggested in § 9.

55. It appears that Fig. 2(a) demonstrates that K increases on discharge, moving towards the K_0 line at three locations around the circumference chosen 'as they are spaced at 90° to each other'. However, it is very instructive to examine Fig. 6(c), where results at two other levels in the same silo are shown. The left side of the figure shows the filling 'pressures', and the right side shows the discharge 'pressures'. At level 1, three 'pressures' fell substantially, while two scarcely changed. At level 3, three 'pressures' fell dramatically while one rose dramatically.

Paper published: *Proc. Instn Civ. Engrs*, Part 1, 1990, **88**, Dec., 1015–1036.

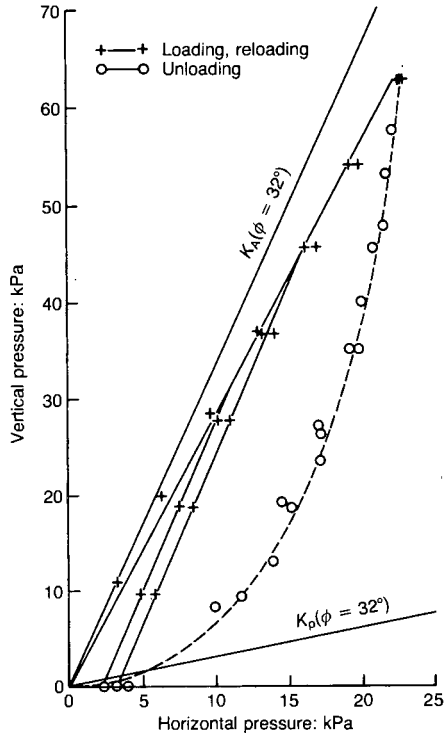

Fig. 13. Stress paths observed in a confined compression test

56. The proposition that the solid is therefore seeking stability under higher pressures resulting from a higher K is clearly untenable. If anything, the mean 'pressure' is falling. Rigorous statistical studies[27] have shown that the mean pressure overall is always close to Janssen, whether the filling or concentric discharge state is being studied. If the Author plotted all the results before he chose to present those of Fig. 2(a), he must have found that there was no general increase in K. It appears that he chose his results very selectively to demonstrate the required proposition.

57. Finally, if a designer were to try to predict the line marked $K_0\,yz$ in Fig. 2(a), using the information in the Paper, he would measure the angle ϕ at 41°[8] and use it in equation (1c) to obtain $K_0 = 0{\cdot}374$. The designer would then underestimate the $K_0\,yz$ line pressures by 32%. Using equations (1), the value of K_A in Fig. 2(a) corresponds to $\phi = 39{\cdot}7°$, while the value of K_0 corresponds to $\phi = 26{\cdot}1°$. Such an inconsistency needs explanation.

Circumferential pressure variation

58. The horizontal pressure variations in silos and their structural consequences have been discussed at some length before.[8, 10, 27–30] They are widely acknowledged to occur, and the German DIN code[2] has included a procedure to

allow for them for several years. The Author appears to have ignored reference 10 and not to be aware of much of the other literature.

59. The real challenge facing code committees is to find a rationally-based simple codifiable method of including horizontal pressure variations. The new suggestion in Fig. 12(c) may well be suitable, but its superiority over the German 'patch' load has not been established.

Deduction of 'equivalent wall pressure' from strain measurements

60. The Author derived the pressures acting on the walls of the two steel silos from the readings of the strain gauges mounted on the wall. The deduction of pressures from strains in the shell is not a straightforward process. The instrumentation of the steel sugar silo of Fig. 2 is given in reference 8. Bending strains in the steel wall were not measured, and the local circumferential stress σ_θ has been simply interpreted through $\sigma_\theta = \sigma_h D/2t$ as a local pressure value.

61. This process results in wall 'pressures' which are wrong by large and variable margins, often by several hundred percent. The Author appears to try to allow for wall bending by writing: 'The calculated horizontal pressure depends on the assumption that the silo cross-section is truly circular.' (§ 12). A truly circular silo would still experience large bending strains if subjected to the pressures plotted in Fig. 6(c).

62. In an attempt to investigate the magnitude of the ignored bending for this case, we analysed the silo of reference 8, subject to the pressure distribution given in Fig. 6(c), and using the geometry defined in reference 8. The bending strains (which were assumed to be zero by the Author) were found to be larger than the circumferential membrane strains (which were assumed to be being measured), so that the inferred pressures are probably wrong by more than 100%.

63. However, to make matters worse, the calculations showed that the strains at level 1 depend quite sensitively on the adjacent boundary condition of the bottom of the silo wall, so any strain measured at this point can be interpreted only if a complete structural analysis of the silo is used. Accordingly, most of the huge variation in pressures which the Author plots in Fig. 6(c) probably arises from bending of the wall under smaller unsymmetrical pressures, and not from large variations in pressure. The variations shown in Fig. 6(a) and (b) are more credible, but the reader is not told whether these are peak values, values at one instant, or maximum and minimum values. It is difficult to know, therefore, how they should be used to develop a design rule.

64. The Author appears to have some inkling of these difficulties when he writes in § 26: 'it is believed that much of the apparent radial variability of pressure is, in fact, radial variability of strain arising from geometrical imperfections'. If the inferred pressures in Fig. 6(c) are in error or exaggerated by geometric imperfections, how can so much faith be placed in the readings shown earlier in Fig. 2?

Misinterpretation of arching and wall friction

65. The proposition that 'arching may or may not occur and may break down' (§ 11) is central to the Paper. Unfortunately, almost all the evidence for the loss of arching is obtained by misunderstanding or misinterpretation.

66. As a first example, § 16 states: 'It will be noted that the angle of wall friction developed on path 5–5 during filling was about 12°, as compared with the full angle of wall friction of 32°.'. If the value at the point marked in Fig. 2(b) is used, together with the density[8] of $\gamma = 8{\cdot}6$ kN/m^3, the value of K which has been

used in backfiguring this wall friction can be found as $K_0 = 0{\cdot}55$. As the silo was being filled, and the pressures were clearly much smaller (Fig. 2(a)) than this $K_0 \gamma z$, it is quite misleading to use this K_0 to backfigure the wall friction, and so to deduce a low wall friction value.

67. If, instead, Janssen's equation is used with a sensible value of K of perhaps 0·3, the full wall friction is found to predict the curves 5 and 6 very closely. Thus, the curves in Fig. 2(b) do not show that wall friction is poorly developed. Instead, they show that Janssen's equation (involving wall friction and arching) gives much better predictions of the measured vertical wall loads than the Author's procedure.

68. Next, the Author infers (e.g. § 18) that high pressures arise from low local wall friction ('the upper limit to the measured horizontal pressures reveals that there was relatively little arching at this depth'). By studying the equilibrium of the entire silo, it can easily be shown that neither the pressures nor the wall load respond quickly to local changes of wall friction (Fig. 14). Loss of arching is not a viable explanation of the high pressures.

69. The most probable reason for the inverse correlation between the measured circumferential strain on the outside of the wall and the deduced value of vertical wall load (§ 13) lies in the structural behaviour of a cylindrical shell under unsymmetrical local normal loads, which induce vertical membrane stresses in the wall as well as circumferential membrane stresses, and both vertical and circumferential bending stresses.[31] The behaviour is very complicated and cannot be described within this discussion.

Mean vertical stress in the stored solid

70. Several plots show the changes to the deduced pressure and the wall vertical load at a point as the 'overburden pressure' (γz) increases.

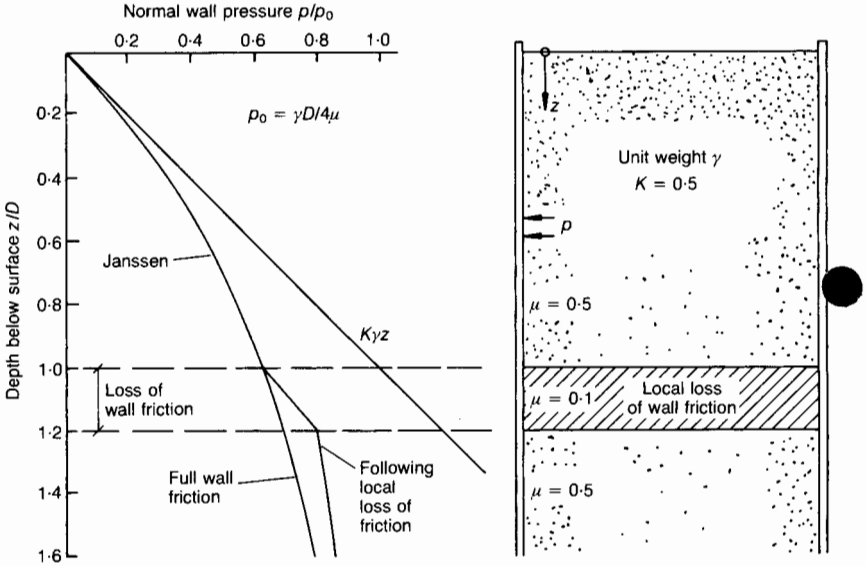

Fig. 14. Effect of local loss of wall friction on pressures

71. If the wall load from friction at a certain level is known, then the mean vertical stress in the solid can be found from the difference between the weight of bulk solid and the frictional wall load at that level, divided by the silo cross-sectional area. Thus, if there is any friction on the wall, the vertical stress at the level will be less than γz.

72. Frictional wall loads developed in all the experiments. It is misleading to plot pressure and wall load against γz and to state that this plot shows a stress path (§ 12). No mention is made of this simplifying approximation.

Wall pressure profiles and plots of 'stress path'

73. Although the assumption is not directly stated, the Author appears to have interpreted the 'stress path' at a point on the wall during filling (e.g. Fig. 5) as identical to the wall pressure profile above that point at the end of filling.

74. Many experimental observations have shown that the changes in wall pressure at a point during filling can be very different from the actual pressure distribution on the silo wall.[32] This can also be demonstrated from the results presented in the Paper. Accordingly, if the curve for generator 5 in Fig. 2(a) (level 2) is used to predict the pressure which this inference indicates should have occurred at the end of filling at level 3, the prediction is found to be 41 kPa. The measured value (Fig. 6) was only 29 kPa, so the inference shows an error of 41%. The wall pressure distribution cannot be inferred from pressure changes at one level.

Linear K_A or K_0 profile

75. The Paper does not distinguish between tall and squat silos. The silos of Figs 2, 4 and 5 are all moderately squat (effective H/D around 1·5). In a squat silo, the linear hydrostatic pressure distribution and the Janssen distribution are experimentally almost indistinguishable. Therefore, these are not good experiments from which to argue about whether or not arching is occurring. For moderately deep and deep silos (Fig. 3), the $K\gamma z$ lines give extremely large wall pressures which are most unlikely to occur in practice. The 'spread' of pressures (§ 17) shown for the silo of Fig. 3 disguises the fact that the mean pressure distribution overall, as found from the original raw data, is very close to the Janssen distribution.

Pressures in hoppers

76. The Author's casual treatment of the mechanics of hoppers (§ 33), even ignoring the orientation of the hopper wall, must be left for others to answer. However, it should be noted that his two main criticisms of earlier work were that the material could not change rapidly from an active to a passive state at the transition, and that existing theories assume that plane sections in the cylinder remain plane in the hopper.

77. It is easy to believe that an active to passive change must occur rapidly below the transition in a normal conical hopper if one examines the change in cross-sectional area which occurs here (Fig. 15). Huge strains (by Fig. 1(a) standards) must occur immediately below the transition. The same is not true for an inverted cone silo (Fig. 4), and the suggestion that no switch may occur in this silo is quite reasonable.

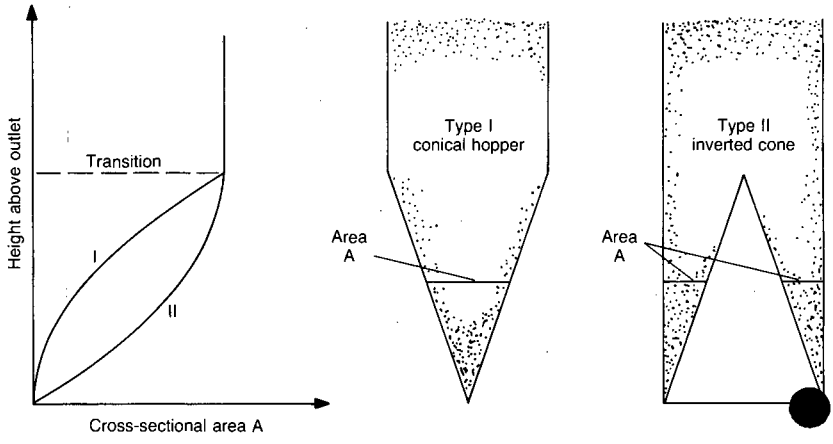

Fig. 15. Variation of cross-sectional area for conical hopper and inverted cone

78. The second criticism muddles static and kinematic considerations. The quoted existing theories make no assumptions about plane sections, but insist merely that equilibrium must exist in any slice of material. They do not exclude material from queuing to exit the silo.

79. The reader should note that the pressure comparisons given with Walker's theory and the Australian code omit their predictions of filling pressures, which are much closer to the test results. It is not clear what the Author means by 'no arching' in a hopper. Can he believe that bulk solid is sliding out of the hopper without the full wall friction developing between the solid and the wall?

Temperature surcharge pressure

80. In § 28, the Author states that the equation attributed to Andersen 'appears to give unrealistic results' and he develops a 'new' equation in the Appendix, based on the assumptions which Andersen used. However, the Author's equation is, in fact, the same as Andersen's equation, with the material parameter M substituted for Andersen's more identifiable but otherwise similar material parameter $E_s(1 - \nu)$.

81. If the 'new' equation (2) is divided top and bottom by $2Mt$, and D is recognized as the radius R, then equation (2) is identical to Andersen's equation, as given in reference 3.

G. Mathieson, *Charles Scott & Partners*

It has been clear for many years that silo design methods have been less accurate than one would like: for instance, close inspection of prestressed concrete silos designed by traditional methods often shows up significant horizontal and vertical cracking that cannot be explained other than as a result of design shortcomings. This Paper represents an important and valuable addition to the literature on the subject.

83. One particular aspect of the problem that is touched on in the Paper is the question of the effect of geometrical irregularities in the silo wall on the theoretical stress distribution. Such irregularities can have a highly significant effect on stress distribution in thin walled structures, as has been shown by work on the design of hyperbolic shell cooling towers.

84. Excessive stress resulting from such dimensional irregularities has probably been responsible for several collapses, including that of the cooling tower at Ardeer some years ago. It is therefore of vital importance to ensure that setting out and construction techniques are suitable to attain the degree of geometrical accuracy that is required. The designer must also consider the effect of inevitable irregularities, and ensure that the contract spells out clearly the dimensional tolerances that must be maintained in each particular case.

Dr M. J. Blackler, *Mott MacDonald*

In the Paper, the Author sets out to highlight, by reference to measurements on full-scale silos, defects in the assumptions behind the derivation of ACI, DIN, Australian and EP silo codes. The Author suggests a method for the prediction of silo wall loads which simplifies existing design methods. However, the benefits of the simplified method to the practising engineer are not convincingly presented, nor are they robustly derived. Some of the reasons are outlined below.

86. It is apparent from Figs 3 and 4 that the simplified formula will result in conservative over-prediction of horizontal pressures on the vertical cylindrical wall, and that existing codes using actual material properties will give more realistic estimates. This may not be too important for small capacity silos, but is critical for the economic design of large-scale installations. It also goes against the successful use of modern silo codes in designing safe and functional structures.

87. Full-scale pressure measurements in silos, taken by the Author and other researchers, represent conditions acting over a small area of the wall only. The occurrence of local peak pressures, which are known to occur in practice, can pose problems with data analysis unless there is sufficient instrumentation to define the rate of pressure variation. This is because the structural significance of local overpressures may be small in comparison with the effects of a more gradual variation that has reduced amplitude. The consequence of ignoring localized pressure peaks, by enveloping the measured data, is to over-design the silo for in-plane loads, but this could misrepresent the bending effects.

88. The results presented in Fig. 6 illustrate that silo pressures may not be radially uniform where nominally concentric flow is deemed to occur. Variations in pressure around the circumference are understood to be influenced by such factors as geometric imperfections, method of filling and discharge, eccentricity of outlets, use of mechanical discharge equipment and inherent variations within the stored medium. Because of these many factors, especially the method of discharge in multi-outlet bins, the sin 2β pressure variation suggested in equation (3) may be inappropriate. For silos with central filling and central discharge, it would be better to specify a nominal design bending moment, and for other configurations, to base the radial variation on consideration of potential flow patterns.

89. Pressures derived from surface strain measurements, such as reported in Fig. 5, can be used to bridge the information gap between measured silo loads and their interaction with the silo structure. However, in using this approach, it is necessary to monitor closely the rate of strain variation over a circumference and

to identify wall bending effects (particularly at points of discontinuity, such as stiffeners, ring beams, lap joints, etc.). Where this is not done, extrapolated pressure profiles may be largely in error because of the nature of the necessary simplifying assumptions.

90. In summary, some of the shortcomings of the Author's suggested design method are seen to be:

(*a*) no readily apparent benefit to the overall design effort over traditional methods which form the basis of modern codes
(*b*) over-prediction of horizontal pressures, against realistic prediction by existing methods when actual material properties are used
(*c*) the need to relate more closely the radial pressure variation to silo flow behaviour.

Professor Blight

In § 52, *Professor Rotter* states that the most likely stress condition for initial filling is one of zero lateral strain. His implication is that if the measured horizontal pressure ratio differs from K_0, the measurements must be wrong. However, he fails to appreciate that the material in most silos is placed in an active (K_A) condition and, in terms of Fig. 1(a), has to undergo strain to reach the K_0 condition. This strain occurs in the silo filling, and not in the wall of the silo.

92. The active state is a state of failure, with shear stresses at the maximum for the prevailing direct stresses. The stable condition for vertical compression under zero lateral strain is the K_0 state, as Rotter states in § 52. If shear stresses in the filling are larger than those corresponding to the K_0 state, as they are along stress path OA in Fig. 1(b), they will, given the opportunity, reduce to those of the K_0 state. The start of emptying causes vertical tensile strain in limited parts of the filling, depending on the flow pattern. It also allows lateral strains to occur in the filling that, in turn, reduce shear stresses and allow stress path AB to occur. This very process is illustrated in Rotter's Fig. 13, where the stress path starts out on the K_A line and progresses towards the K_0 line, reaching the K_0 line only when the vertical stress has been increased to 45 kPa.

93. In § 54, Rotter again demonstrates misunderstanding. If the process depicted in his Fig. 13 were to be followed on a pressure cell set in the wall of a silo, it would be observed that, as emptying starts, the horizontal pressure is virtually unchanged. The observer would have no knowledge of the vertical stress changes and would therefore conclude that the stress ratio was not changing. Studies of strain conditions in silos at the start of emptying (e.g. Deutsch and Clyde,[21] show that strain conditions hardly change in the silo filling, except in the immediate vicinity of the outlet. There must be dramatic stress changes here, but elsewhere the lack of changes in strain shows that all vertical and horizontal stress changes must be modest, as indicated by stress path AB in Fig. 1.

94. In Rotter's §§ 55–57, I am accused of being selective in my choice of data. On reviewing Rotter's evidence for this accusation, I admit that he appears to be correct. However, in attempting to confound, Rotter has committed the very sin of which he accuses me. If he had read reference 8 less selectively, he would no doubt have noticed that an error has been made. The diagram that appears as Fig. 6(c) actually shows radial distributions of frictional wall load, not equivalent horizontal pressure. The correct version of Fig. 6(c) is given here. This figure shows that in

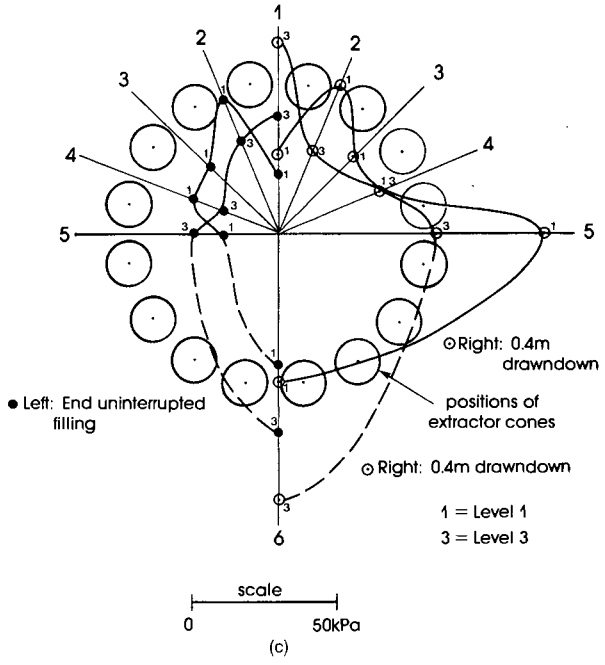

Fig. 6(c). Corrected version

every case, except one, the equivalent horizontal pressure increases on drawdown. Rotter would also have seen that there is a separate figure in reference 8, similar to his Fig. 13, that shows that K_0 for normally consolidated sugar was measured at 0·55. It is hoped that the hypothetical designer would have used this value, rather than equation (1c), which is clearly denoted as empirical and approximate.

95. In Rotter's § 58, I am accused of ignoring reference 10. This is hard to understand as the reference has been listed in the Paper and Fig. 3 is acknowledged as coming from that source. With regard to references 27–30 (three are Rotter's), 27 was published after the Paper was written, 28 appeared in the proceedings of an obscure conference, 29 is in German, and 30 was never published.

96. Rotter's §§ 58–64 were clearly written by an analyst who has never tried to make any sort of field measurement. If he had, Rotter would have known that access to all heights of the outside of a large silo is very difficult to obtain. Access is available only if scaffolding has been erected for the purpose of applying insulation or of painting, or if a tower crane is available, so that one can work dangling from a basket. Access to upper heights of the inside of the wall of a roofed silo is just not practically possible. Application of strain gauges to the inside of the walls of a silo is even more difficult, as the wall frictional forces scrape off the gauges and their connecting leads. Storage silos for foodstuffs and other perishable commodities have to be waterproof. For this reason, owners of these silos are reluctant to allow holes to be drilled in the walls of their structures. One therefore has a dilemma.

Either one accepts that it is not possible adequately to measure strains on working steel silos and interpret them in terms of pressures, or one makes the best possible attempt under the circumstances. The equivalent horizontal pressures and frictional wall loads shown by me in Figs 2, 5, 6(a) and 10 are at least numbers that, if multiplied by suitable factors, will give the principal strains measured on the outside of the relevant silo walls. It follows that strain calculated in a design situation from pressure distributions established by this means will give strains of the same nature as those measured on the outside of the test silo. Despite Rotter's objections—which, it should be noted, are based on approximate theories—these pressures cannot be completely unrealistic.

97. I have now developed a method of protecting strain gauges mounted on the inside of silos having corrugated steel walls. It turns out that pairs of back-to-back readings are quite similar. This casts at least some doubt on the validity of Rotter's criticism. However, do not take my word for it. A recent comparison by Borcz and el Rahim[33] of pressures derived from strains measured on the outside of a steel silo, with pressures measured by means of pressure cells, has shown very good agreement between the two sets of measurements. The fact of the matter is that individual panels composing the walls of circular steel silos are extremely flexible. Initial out of roundness in these large flexible sheets is largely corrected when the internal pressure is first applied and thereafter does not affect strain measurements.

98. If strains measured on one side of the wall of a steel silo cannot be used to estimate internal pressures, why are similar results obtained whether strain measurement or pressure cells are used on steel silos?[8,25,33] Furthermore, why are similar results obtained when pressures are measured using pressure cells on reinforced concrete silos? The data shown in Fig. 3 (which Rotter does not attack) are very similar to those shown in Fig. 5 (which he does attack). Why can the suggested methods be used to calculate reasonable envelopes to data from both pressure cells and strain gauges if the strain gauge method is hopelessly wrong?

99. In § 66, Rotter refers to 'Fig. 2(b)'. It is presumed that he refers to point 5B on the wall load diagram to the right of Fig. 2. A corresponding point 5B is shown on the left-hand diagram for equivalent horizontal pressure. This point lies very close to the $K_0 \gamma z$ line for $K_0 = 0{\cdot}55$. Hence, it was quite correct to back-figure the angle of wall friction for this value of K_0.

100. Rotter's argument in § 68 and his Fig. 14 are not convincing. Fig. 14 shows a 10% increase in horizontal pressure resulting from a hypothetical loss of frictional resistance over a limited height of silo wall. Fig. 3, to which he appears to be referring, shows a 23% increase in pressure at a depth of 30 m. By adjusting the numbers he has selectively used in his example, a 23% increase could equally reasonably be demonstrated.

101. Referring to Rotter's §§ 70–72, the term 'overburden stress' is commonly accepted as meaning 'depth above point considered multiplied by unit weight of material'. This is clearly shown wherever the term has been used in the Paper. Nowhere is there any suggestion that overburden stress equals vertical stress.

102. Rotter's §§ 73 and 74 are also uncalled for: wherever a diagram in the Paper refers to changes of pressure or wall load at a point, it is quite clearly marked as a stress path. Full pressure profiles are not thus marked.

103. Rotter may be correct in saying in § 75, for the specific case illustrated in Fig. 3, that pressures near the base of the silo will never reach the linear $K_A \gamma z$ profile. However, in the vicinity of 30 m, at which depth the H/D ratio is 4 to 4·5,

pressures not only reached the $K_A \gamma z$ line, they exceeded it. Thus it is obviously possible for a linear pressure–depth profile to occur in a tall silo. A linear profile also does not always occur in a squat silo. It does not apply in Fig. 4, where the silo concerned has an H/D ratio of 2 to 2·5.

104. With reference to § 76, I fail to see in what respect I have ignored the orientation of the hopper walls. The slope of the hopper is clearly marked in each case, and the pressure normal to that wall is given. In §§ 77–79, Rotter shows again that he does not understand the implications of his Fig. 13 or how material flows out of a hopper. The flow can occur without significant change of pressure normal to the hopper wall because the material queues to exit and because, in terms of Fig. 13, there is little change in horizontal pressure accompanying a reduction in vertical pressure. Rotter's Fig. 15 becomes relevant only if the material crowds into the outlet, thus undergoing lateral compressive strain and increasing the lateral [illegible]ss ratio in the process. It does not do this, and hence filling pressures remain [illegible]hanged at the start of emptying in structures such as those illustrated in Figs 9–11. In these structures, the material adjacent to the hopper walls is not intentionally disturbed during emptying. However, in the case of the structure shown in Fig. 4, the material is disturbed during discharge by the injection of compressed air. Here there is a marked reduction of pressure towards the outlet.

105. Referring to Rotter's §§ 80 and 81, I have nowhere stated that equation (2) is new. It is different from Anderson's equation in two respects: firstly, it lumps uniaxial elastic and Poisson's ratio effects together into the compression modulus M; secondly, M has so far been derived from field measurements. This recognizes that the compressibility of granular materials is highly strain-dependent and needs, in this instance, to be measured in the range 0–200 microstrain. Although this can now be achieved in the laboratory (e.g. reference 34), the technique is new and I do not yet have the apparatus to carry out this type of measurement.

106. With regard to *Mr Mathieson's* comments on the effects of geometrical irregularities, I would agree that the latter are certainly important for hyperbolic shell cooling towers, but are possibly less so for silos where the loading is to a certain extent supportive of the shell.

107. In respect of *Dr Blackler's* discussion, it is certainly true that the Janssen theory gives results that are quite satisfactory for some silos: Fig. 4 illustrates this. However, the argument is not as convincing for Fig. 3. The difficulty the designer faces is knowing beforehand when Janssen will apply and when not.

108. I would certainly endorse Blackler's remarks concerning the use of actual, [illegible]perly measured material properties, where these are available. Often, however, [illegible]s have to be designed and constructed before the product they are intended to store has been produced. In these circumstances, how does one know if calculated pressures will be conservative?

109. Blackler's point in his § 87 is well-taken. It would, however, be useful to have some suggestions as to how to overcome the difficulties inherent in extrapolating from spot measurements. The same comment applies to his § 89. Unfortunately, there is always a gap between what is practically achievable and what is theoretically desirable. Availability of resources usually dictates the former.

110. Referring to §§ 88 and 90, I have made some suggestions for what I consider to be improvements to existing design codes. Research and learning should be an ongoing process. The suggestions in the Paper are certainly not seen as the last word on the subject, but only as a step on the way to improved engineering knowledge of silos.

References

25. BLIGHT G. E. Performance of a 20 m diameter steel maize storage bin. *Proc. 2nd Int. Conf. on Design of Silos for Strength and Flow, Stratford upon Avon*, 1983, 179–191.
26. ZACHARY L. W. and LOHNES R. A. A confined compression test for bulk solids. *Proc. 13th Ann. Conf. on Powder and Bulk Solids Handling*, Powder Advisory Centre, London, 1988, 483–493.
27. OOI J. Y. *et al.* Systematic and random features of measured pressures on full-scale silo walls. *Engng Structs*, 1990, **12**(2), 74–87.
28. ROTTER J. M. *et al.* On the specification of loads for the structural design of bins and silos. *Proc. 2nd Int. Conf. on Bulk Materials Storage Handling and Transportation, Wollongong*, July 1986, Institution of Engineers, Australia, 241–247.
29. SCHMIDT K. H. and STIGLAT K. Anmerkungen zur Bemessungslast von Silos. *Beton und Stahlbetonbau*, 1987, **9**, 239–242.
30. OOI J. Y. and ROTTER J. M. Unsymmetrical features of measured pressures on prototype grain silos. *Proc. 2nd Europ. Symp. on Stress and Strain Behaviour of Particulate Solids—Silo Stresses*, Prague, August 1990.
31. FLÜGGE W. *Stresses in shells*, Springer-Verlag, Berlin, 1973, 2nd edn.
32. NIELSEN J. and KRISTIANSEN N. O. *Trykmaling pa silo i Karpalund.* Department of Structural Engineering, Technical University of Denmark, Lyngby, 1979, Research Report.
33. BORCZ A. and EL RAHIM H. A. Pressure measurements on silos. *Powder Handling and Processing* (Germany), 1990, **2**(3), 239–246.
34. BURLAND J. B. and GEORGIANNOU V. N. Small strain stiffness under generalised stress changes. *Proc. 10th Europ. Conf. on Soil Mechanics and Foundation Engineering*, Florence, 1991, **1**, 41–44.

bulk solids handling Volume 8, Number 2, April 1988

A Comparison of Measured Pressures in Silos with Code Recommendations

G.E. Blight, South Africa

Summary

The paper examines the evidence for the occurrence of Jenike or Walker-type overpressure in silos by studying the results of pressure measurements in two models and ten full-scale structures. It is shown that although a localized increase in horizontal pressure often occurs in the vicinity of a transition from parallel to convergent flow, increased pressures do not generally exceed a limit defined by the horizontal pressure for the zero lateral strain condition in the silo fill. Pressure distributions predicted by various design codes do not usually represent measured horizontal pressures very well.

1. Introduction

The work of Jenike and Johanson [1] [2] and Walker [3] introduced the concept of the "overpressure", "pressure peak", "switch pressure" or "concentrated force" to the assessment of loads on silos. According to these authors, the phenomenon occurs close to the transition from the parallel walled section of a silo to the hopper portion. The overpressure is generated because of the transition from an "active" state of stress in the zone of parallel material flow to a "passive" state of stress in the zone of convergent flow. It is difficult, Jenike and Johanson say, to measure and record the pressure peak because it acts only over a narrow portion of the wall at any time and travels upwards as the transition from a static to a flow condition is established.

The work of Jenike and Johanson appears to have been supported, quantitatively at least, by that of Walker [3] whose theory postulated the generation of a static pressure peak at the transition from parallel to convergent flow. Walker's theory was apparently substantiated by small-scale model tests that he undertook and also by larger-scale model tests undertaken by Clague [4].

Those working in the field of silo design took these publications seriously and quite soon, the concept of the "overpressure factor" made its appearance in the American Concrete Institute Code for silo loadings [5]. This was followed by the introduction of overpressure factors into the German silo loading code [6] and the very recent Australian guidelines [7].

Dr. G.E. Blight, Professor of Construction Materials, University of the Witwatersrand, Dept. of Civil Engineering, P.O. Wits, 2050, Johannesburg, Republic of South Africa

The object of this paper is to examine the evidence for the occurrence of overpressures in silos and to show that the basis for present concepts appears unsound. This contention will be backed by comparing pressures measured in ten full-scale silos with the pressure distributions postulated by the three sets of guidelines or codes already mentioned [5] [6] [7].

Finally, a much simpler and more rational basis for design will be advanced. This does not mean that the author believes that all problems regarding the assessment of loads on silo walls have now been solved. On the contrary, a number of important problems remain. But, it should now be possible considerably to simplify load assessment procedures.

2. States of Stress in Ensiled Materials

Fig. 1a illustrates the relationship between the stress ratio $K = \sigma_h/\sigma_v$ and lateral strain in a particulate material. If a material can expand laterally without limit when loaded vertically, K reaches a lower limit K_A, the active stress ratio. For a cohesionless material K_A is related to the angle of shearing resistance ϕ by

$$K_A = \frac{1 - \sin\phi}{1 + \sin\phi} \quad (1)$$

If all lateral strain is prevented as the material is loaded vertically, K will tend towards K_0, the "at rest" or "zero lateral yield" stress ratio. For a cohesionless material K_0 is given, empirically, but not exactly, by

$$K_0 = 1 - \sin\phi \quad (2)$$

If a material is compressed laterally while being subject to a constant vertical stress, the stress ratio will increase until it is compressing laterally without limit. In this condition, the stress ratio K will have a value given by K_p, the passive stress ratio. For a cohesionless material K_p is given by the inverse of K_A, i.e.

$$K_p = \frac{1 + \sin\phi}{1 - \sin\phi} \quad (3)$$

When a material is loaded into a silo it comes to rest in an active state with a stress ratio K_A. As further material is loaded and a particular layer becomes buried, lateral strain is prevented by the silo walls. Vertical strain occurs, however, and friction is built up between the material and the walls.

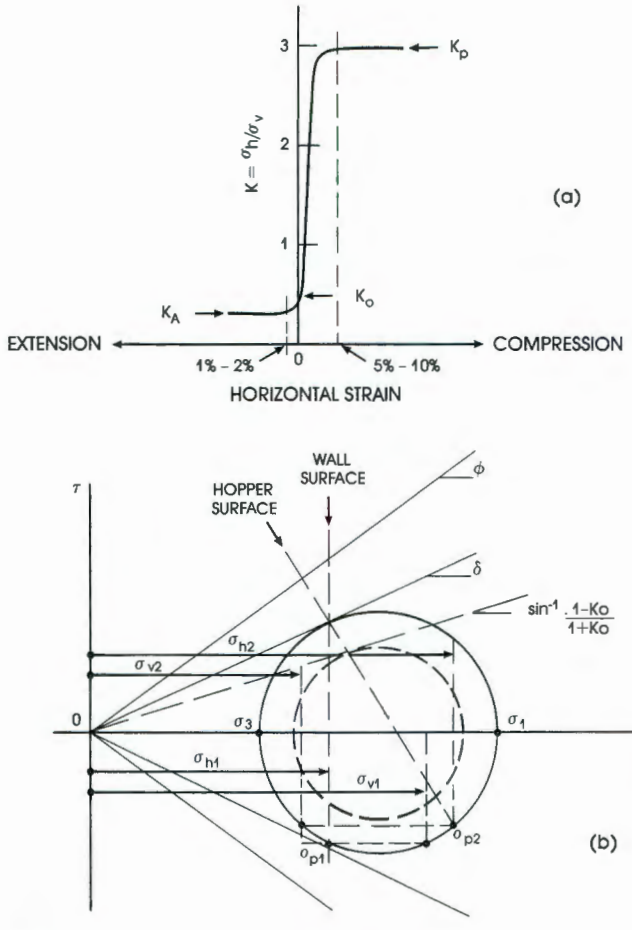

Fig. 1: a - Stress ratios in a silo fill related to horizontal strain
b - Stresses in a silo fill during filling

The stress state in the material adjacent to the walls is illustrated in Fig. 1b. Because the fill is settling relative to the vertical wall, the stress circle is tangent to the wall friction envelope defined by δ, the angle of wall friction. The corresponding horizontal and vertical stresses, σ_{h1} and σ_{v1} have been located by means of the origin of planes construction. Because the fill itself is not in a state of failure, the stress ratio σ_3/σ_1 exceeds K_A and approaches K_0. Similarly, the stress ratio σ_{h1}/σ_{v1} also approaches K_0. The K_0 condition is defined by circles tangent to an envelope rising at an angle

$$\sin^{-1}\frac{1-K_0}{1+K_0}$$

(e.g. the broken circle in Fig. 1b).

In Fig. 1b as drawn σ_{h1}/σ_{v1} actually exceeds K_0.

Now consider what happens when sliding is initiated on an inclined hopper surface. If the same pair of principal stresses σ_1 and σ_3 are considered, and σ_h and σ_v are again located by the origin of planes construction, it will be noted from Fig. 1b that a greater horizontal stress σ_{h2} together with a smaller vertical stress σ_{v2} are required for sliding to occur on the hopper wall*. Note also that the shear stress on the vertical surface has decreased. It would not be unreasonable to expect the stress changes indicated by Fig. 1b to occur in material adjacent to a silo wall at the cylinder-to-hopper transition as the change from filling to emptying occurs. The mechanism for the stress change would be the change in the predominant direction of movement of the fill and the rotation of the direction of maximum shear. Note also, that even during filling it is possible for σ_h/σ_v to exceed K_0.

The major stress σ_1 in Fig. 1b must be closely related to the weight of material overlying the point under consideration. There is no obvious way in which a lateral pressure greater than the overburden pressure could arise without involving environmentally related effects such as temperature or the swelling of wetted grain.

Away from the wall, shearing would have to occur within the material itself. As it is unlikely that σ_1 would increase, it is more likely that σ_3 or σ_1 and $\sigma_3$would decrease to allow the stress circle in Fig. 1b to become tangent to the shearing resistance envelope for the fill material.

At the start of emptying therefore, one would expect the following changes in the stresses on the silo wall in the vicinity of the cylinder-to-hopper transition:

(i) the vertical stress will decrease;

(ii) the horizontal stress will increase; and

(iii) the shear stress will slightly decrease.

Experimental evidence for the occurrence of the process outlined is given in Fig. 2 which shows simultaneous measurements of frictional wall load and horizontal pressure on the wall of a 20 m diameter multi-outlet sugar silo 5 m above the base. It will be noted that both the wall load and the horizontal pressure built up progressively while the silo was being filled. As soon as emptying started, the horizontal pressure increased considerably and the wall load decreased (Blight and Garstang [8]).

On the basis both of theory and observation therefore, one would expect the horizontal pressure in the vicinity of the cylinder-to-hopper transition in a silo to increase moderately at the start of emptying after uninterrupted filling. It appears unlikely that the horizontal pressure could increase beyond the value of the material overburden.

This statement does not conflict with the concepts of Jenike and Johanson [2] and Walker [3] except in the extent to which the horizontal stress is expected to increase.

3. Experimental Results

The experimental results that Walker [3] and Clague [4] used to justify Walker's theory have been reproduced in Fig. 3. Both sets of measurements correspond to emptying of their model silos after uninterrupted filling.

The theoretical pressure line in each case features a large discontinuity in the stress ratio σ_h/σ_v at the cylinder-hopper transition. In the case of Walker's results, this corresponds to an increase by a factor of 9 while for Clague's results the factor of increase is 5. According to the Jenike and Johanson theory (e.g. Johanson [9]) the ratio of peak pressure to the pressure on an adjacent area of wall may be as high as 10.

The experimental results, in both cases, indicate that horizontal pressures remained substantially in accordance with a linear pressure distribution according to which

$$\sigma_h = K_A \gamma Z \qquad (5)$$

(*) An opposite conclusion can be reached by drawing the hopper surface from right to left in Fig. 1b to obtain the conjugate stresses but this possibility seems to be excluded by the experimental evidence.

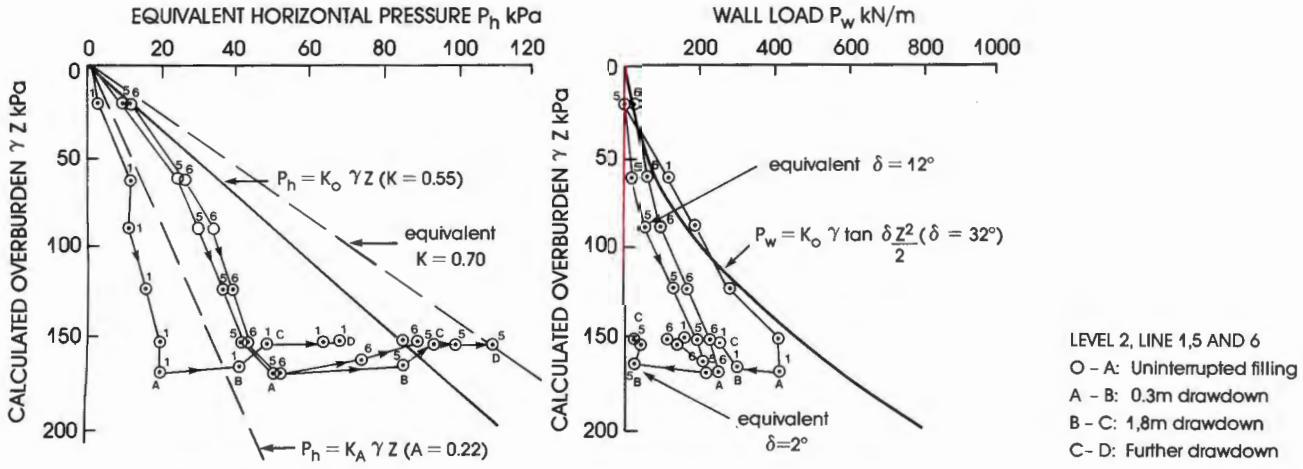

Fig. 2: Breakdown of arching in a silo illustrated by simultaneous measurements of horizontal pressure and wall load. As drawdown starts, wall load decreases and horizontal pressure increases

except in the vicinity of the cylinder-hopper transition, where the horizontal pressure increased to lie on a second linear pressure distribution

$$\sigma_h = K_0 \gamma Z \tag{6}$$

The extravagant peak pressure according to the Walker theory (which depends on the ratio of K values selected) is not needed to explain the results. The actually observed ratio by which K increased was only

$$\frac{K_0}{K_A} = 1 + \sin \phi \tag{7}$$

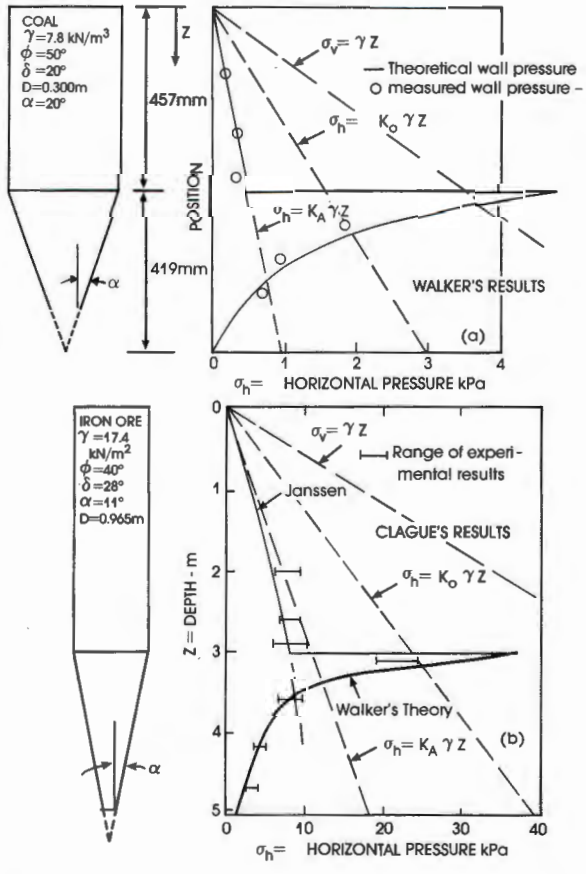

Fig. 3: Re-examination of Walker's and Clague's results purporting to show the existence of "overpressure" during discharge of model silos

This has a value of 1.77 for $\phi = 50°$ which is far less than the 9 assumed for the theory, and quite within the limits suggested by Fig. 1b. Hence a re-examination of Walker's and Clague's experimental results shows that they do not really support Walker's theory.

4. Comparisons of Measured Horizontal Pressures in Vertical Walled Silos With Code Recommendations

A series of comparisons will now be made between pressure distributions during emptying, measured in a series of full-size silos and the pressure envelopes calculated according to the three silo loading codes or guidelines, ACI 313-77 [5], DIN 1055-1984 [6] and the Australian guidelines [7].

Wherever possible, the materials properties listed in the guidelines or codes have been used in the calculations. To give a more direct comparison between the codes, the calculations for ACI and DIN have been made using the properties listed by DIN.

Only case histories where due attention has been given by the authors to accuracy of instrumentation have been included. In one case, the authors appear to have used the wrong calibration for their instruments. However, because the characteristics of the instrument type is known, their readings have been corrected accordingly.

Case 1: 16 m diameter reinforced concrete pulverized fuel ash silo (Nielson [10])

The measured and calculated pressures and the main dimensions published for this silo are shown in Fig. 4. Nielson unfortunately did not document the properties of the fly ash fully and for some of the calculations it has been necessary to assume certain values. The silo appears to operate in funnel flow and the effective cylinder-hopper transition point would occur about 5 m above the silo base, i.e. about the level of the top of the concrete benching.

The material properties listed in Fig. 4 (and in Figs. 5 to 7 and 9 to 12) consist of properties measured on the actual

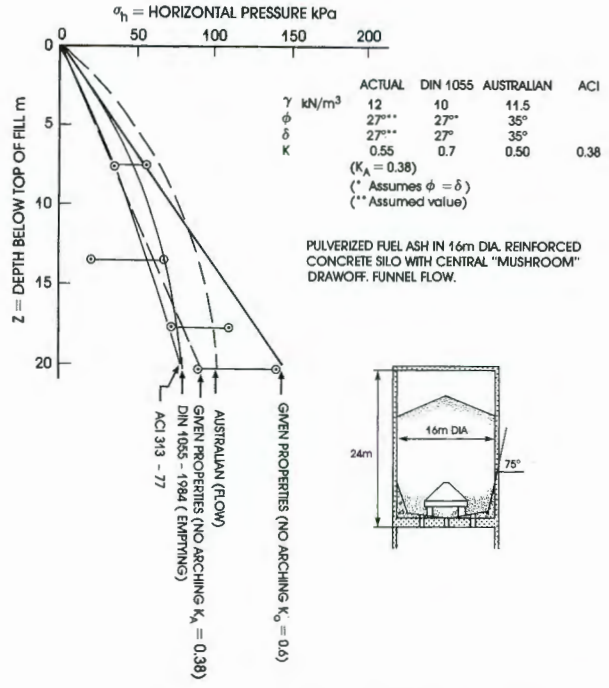

Fig. 4: Comparison of code and measured horizontal pressures for 16 m diameter reinforced concrete pulverized fuel ash silo in Denmark (Nielson)

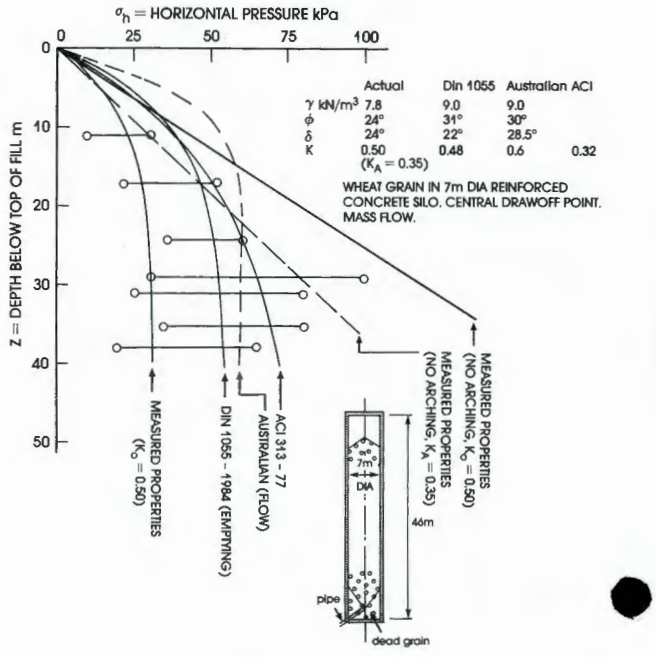

Fig. 5: Comparison of code and measured horizontal pressures for 7 m diameter reinforced concrete wheat silo in Sweden (Hartlén et al.)

filling material of the silo and properties listed in DIN 1055-1984 or the Australian guidelines. As mentioned above, the same properties have been used to calculate the pressure lines for the DIN and ACI codes. The single property listed under ACI on the figures is the active pressure ratio K_A, calculated for the value of ϕ listed under DIN.

As the diagram shows, neither the ACI nor the DIN pressure lines envelope the measured pressures. The Australian guidelines are more successful in their predictions, but even then, do not cover the larger pressures near the base of the silo. The only envelope that contains all the measured emptying pressures is the "no-arching" envelope given by Eq. (6) and calculated with the actual materials properties.

The reader will recall that this is the same envelope that applied in the case of the model tests of Walker and Clague. The increased pressures near the silo bottom occur in the area within which the Walker-type pressure peak would be predicted or the Jenike and Johanson-type switch pressure would supposedly originate.

Case 2: 7 m diameter reinforced concrete wheat silo (Hartlén et al. [11])

Fig. 5 summarizes the dimensions and horizontal pressures on emptying published for this silo. It will be noted that again, not one of the three code pressure lines envelopes the pressures measured in this silo. Also shown in the diagram are a pressure line labelled "measured properties (K_0 = 0.5)" and two "no-arching" lines (one for K_A = 0.35 and for K_0 = 0.50).

The first of these three lines was calculated by means of the Janssen equation with $K = K_0$. Again, it is only the no-arching line with $K = K_0$ that envelopes all the measured pressures.

With the squat dimensions of the fly ash silo of Case 1, it is not surprising that a straight line pressure-depth relationship best describes the observed pressures. In this case, however, with a height to diameter ratio of 7, considerable arching could be expected, and the lower limit of the observed emptying pressures shows that this arching does occur.

The upper limit to the emptying pressures appears to show that there is either a partial or intermittent break-down of arching in the silo and that this, together with the shear plane rotation effect referred to earlier results in the increase of lateral pressure.

Case 3: 26 m diameter reinforced concrete coal silo (Omote and Suekane [12])

The main dimensions for the silo and the pressure depth lines according to the three codes are shown in Fig. 6. Kyowa pressure cells were used as the instrumentation, but the authors make no mention of calibrating the cells for coal. The manufacturers routinely calibrate their cells using sand, and sand gives a higher calibration factor than does coal, which is more compressible (e.g. Blight and Bentel [13]). Hence the published pressure measurements have been corrected to correspond with a calibration for coal.

Again, none of the code pressure-depth lines cover all of the measured pressures, although the Australian guidelines come close to doing this.

Omote and Suekane do not give full properties for the coal, and it has been necessary to assume that K_0 = 0.6. On this basis, the no-arching line envelopes all the measured horizontal pressures except for the upper limit pressure at a depth of 5 m.

Because of the outward tapering of the silo diameter one would not expect arching to occur in the silo and the code provisions are therefore not really applicable.

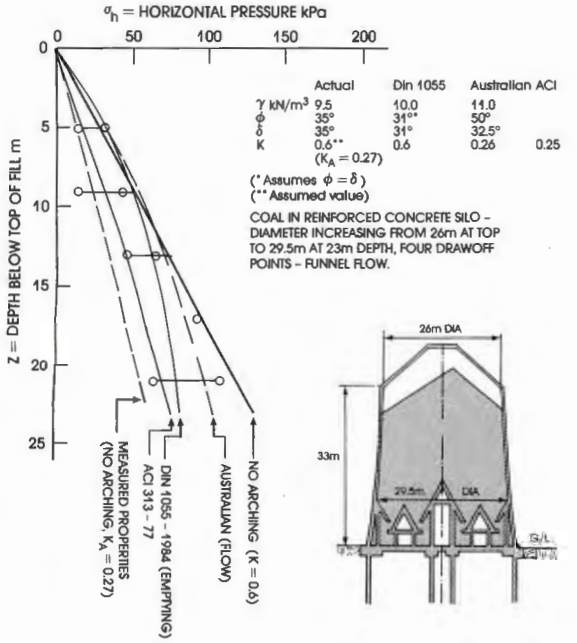

Fig. 6: Comparison of code and measured horizontal pressures for 28 m (approx.) diameter reinforced concrete coal silo in Saijo, Japan (Omote and Suekane)

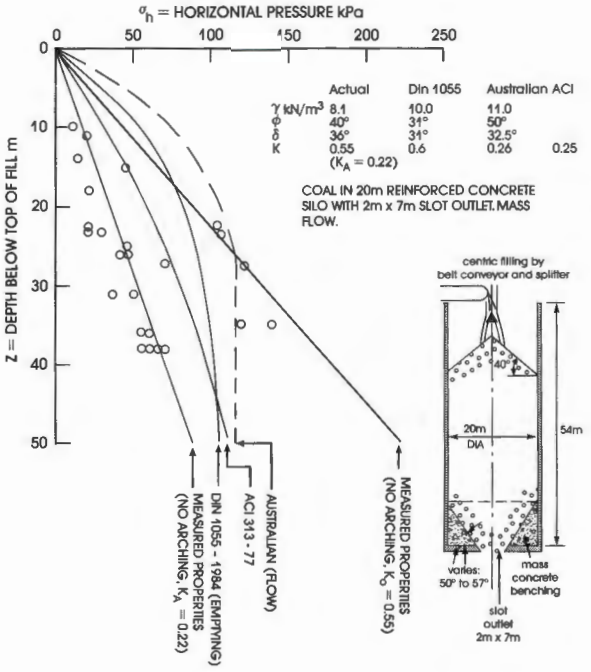

Fig. 7: Comparison of code and measured horizontal pressures for 20 m diameter reinforced concrete coal load-out silo at Optimum, S. A.

Case 4: 20 m diameter reinforced concrete coal load-out silo (Blight [14])

Fig. 7 shows the main dimensions and recorded pressures at the start of emptying for this silo. Because of the squat dimensions, one would not expect much arching to occur in the silo. This is borne out by the fact that the majority of the measured pressures cluster about the no-arching envelope for $K = K_A$. The corresponding envelope for $K = K_0$ contains all the measured emptying pressures.

Of the three code pressure-depth lines, those by ACI and DIN appear inadequate, while the Australian guidelines overestimate the pressure at small depths and underestimate it at larger depths. Only the no-arching line with $K = K_0$ is completely satisfactory.

Case 5: 20 m diameter reinforced concrete coal load-out silo (Blight and Midgley [15])

It will have been noted so far that although horizontal pressures in silos are observed to increase at the start of emptying, extravagant switch pressures such as those predicted by Jenike and Johanson [2] [9] have not been observed.

This may be because, as postulated by Jenike and Johanson, the peak pressure is transient and travels up the height of the bin as the transition from initial emptying to filling occurs. This possibility is explored in Fig. 8 showing pressures recorded on an ultra-violet recorder on two occasions during the first few minutes of emptying from the load-out silo. As the figure indicates, the pressure cells are located at the cylinder-hopper transition and on a vertical line (A) at various distances above the transition. Gauge A 2 is probably located right at the transition from the cylinder to the effective hopper formed in the flowing coal. If either static or transitory peak pressures arise in the bin, they should initially be recorded on gauges A 1 or A 2 and should then be reflected on gauges A 3 and A 4 as the peak travels up the wall.

The recordings in Fig. 8 show that there certainly are dynamic effects at the start of emptying. The pressures at gauges A 1, A 2 and A 3 all decrease, instantaneously in five of six cases, and after a small initial increase in the sixth (gauge A 3 in [a]). Gauge A 4 shows small increases in pressure. There is absolutely no evidence of a pressure peak, even a transitory one.

In case it be said that a pressure peak would not be expected anyway in a funnel flow bin like that of this case, let it be recorded that similar measurements made in the hopper of the silo referred to in Case 4 showed the same complete lack of evidence of a pressure peak.

Case 6: 20 m diameter insulated steel sugar storage silo (Blight and Garstang [8])

Pressures at the start of emptying from this silo are illustrated in Fig. 9. The DIN and ACI pressure-depth lines tend to underestimate horizontal pressures near the bottom of the bin, probably because they overestimate the effects of arching. In this case the Australian guidelines envelope the observed pressures. The no-arching line for $K_0 = 0.55$ envelopes or lies close to most of the observed pressures. There is one measurement, however, that lies well outside this line.

Here again, the general conclusions from Cases 1 to 4 apply, but not quite as satisfactorily. The bin is insulated with 100 mm of polyurethane foam, hence, unlike the next case, the larger than expected pressures cannot be ascribed to diurnal temperature variations.

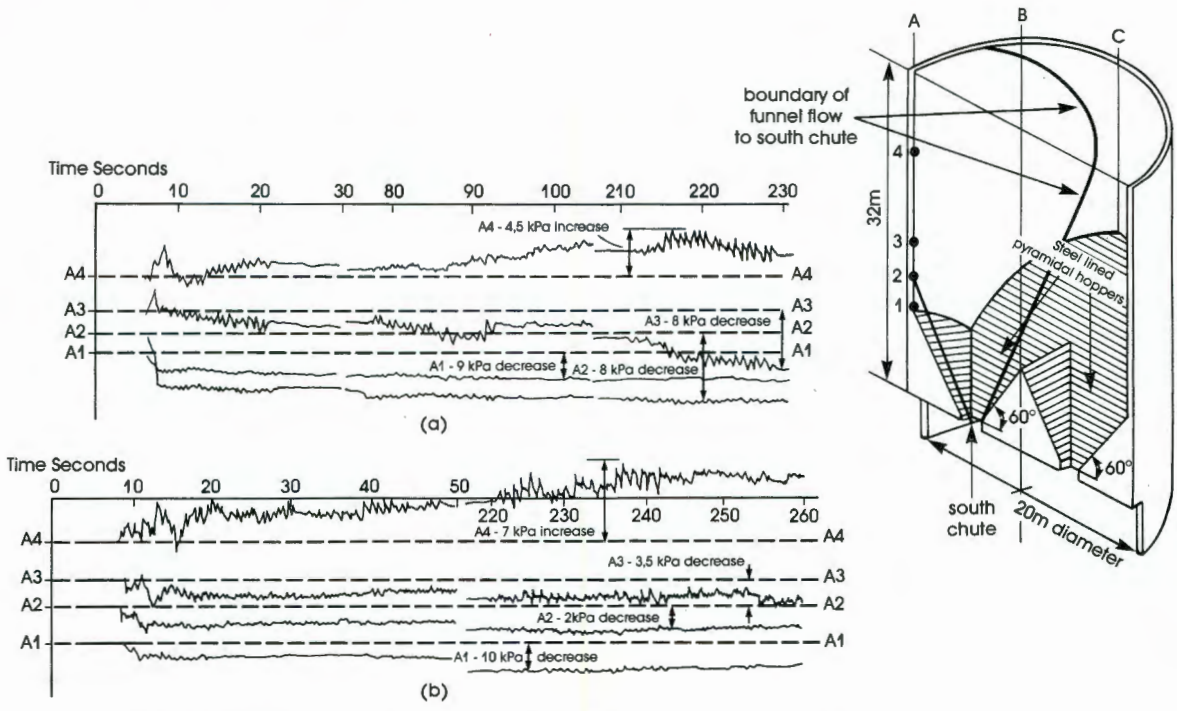

Fig. 8: Dynamic pressure record for start of emptying from south chute of 20 m diameter coal load-out bin

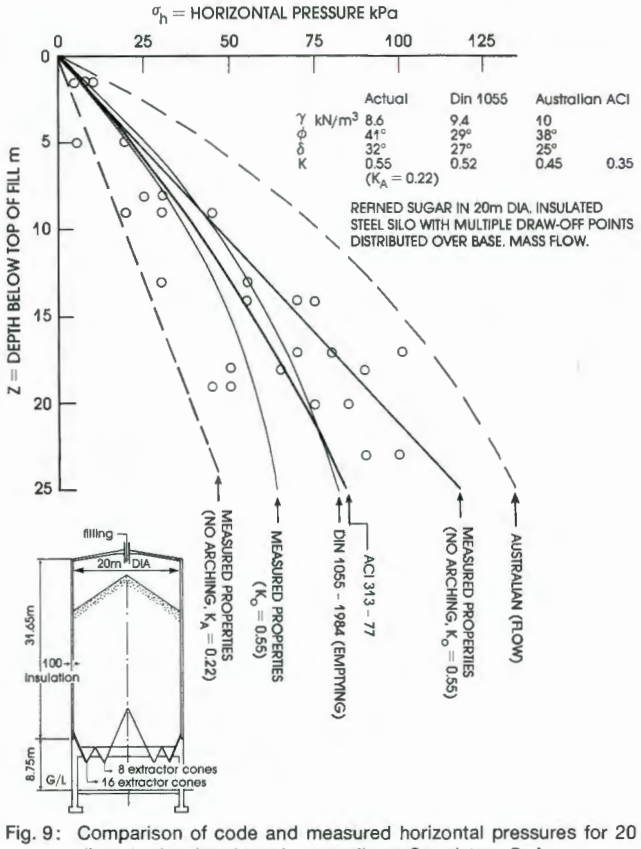

Fig. 9: Comparison of code and measured horizontal pressures for 20 m diameter insulated steel sugar silo at Germiston, S. A.

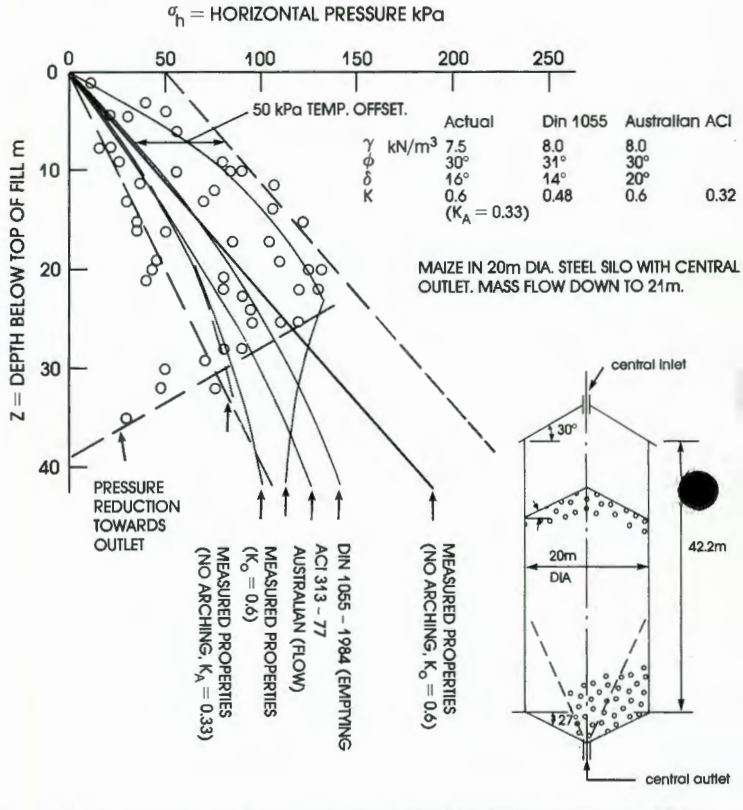

Fig. 10: Comparison of code and measured horizontal pressures for 20 m diameter steel maize silo at Randfontein, S. A.

Case 7: 20 m diameter steel maize storage silo (Bight [16] [17])

The six preceding cases have all concerned horizontal pressure measurements made at the start of emptying, after uninterrupted filling. The three cases that follow in this section deal with silos operated on an intermittent or simultaneous filling and emptying basis.

Fig. 10 shows measured horizontal pressures for a steel maize bin. It will be noted that the measured pressures are considerably, i.e. up to more than 50 kPa, larger than the predictions of either ACI or DIN. The provisions of the Australian guidelines come closest to enveloping the measured pressures, but even they do not cover the whole range. The no-arching envelope with $K = K_0$ in this case does not contain all the measured pressures, by far.

The reason for the unusually large pressures appears to lie with diurnal temperature variations. The bin is not insulated, like the sugar silo of Case 6, and hence temperature variations considerably increase measured horizontal pressures.

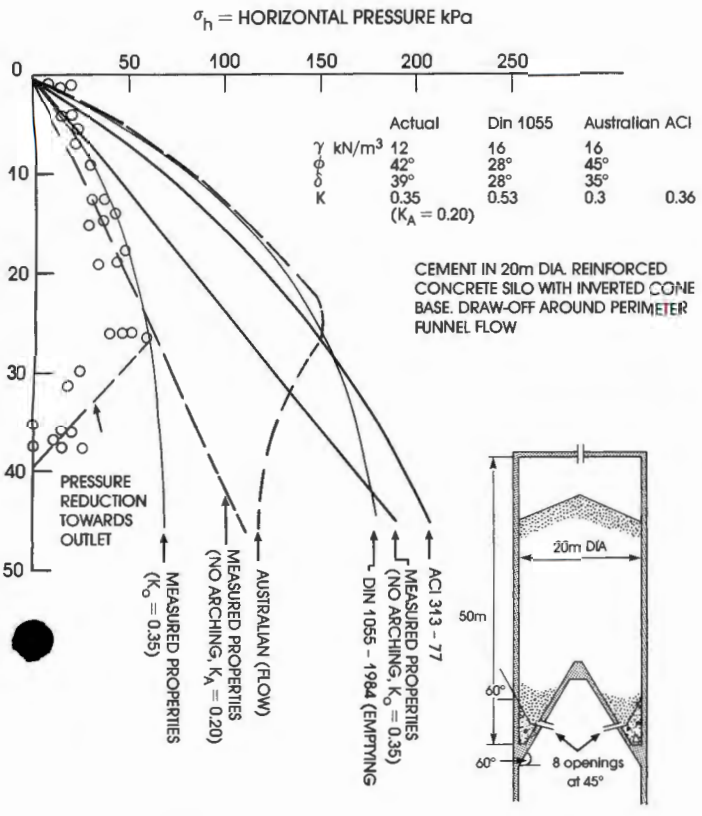

Fig. 11: Comparison of code and measured horizontal pressures for 20 m diameter reinforced concrete cement silo at Jupiter, S. A.

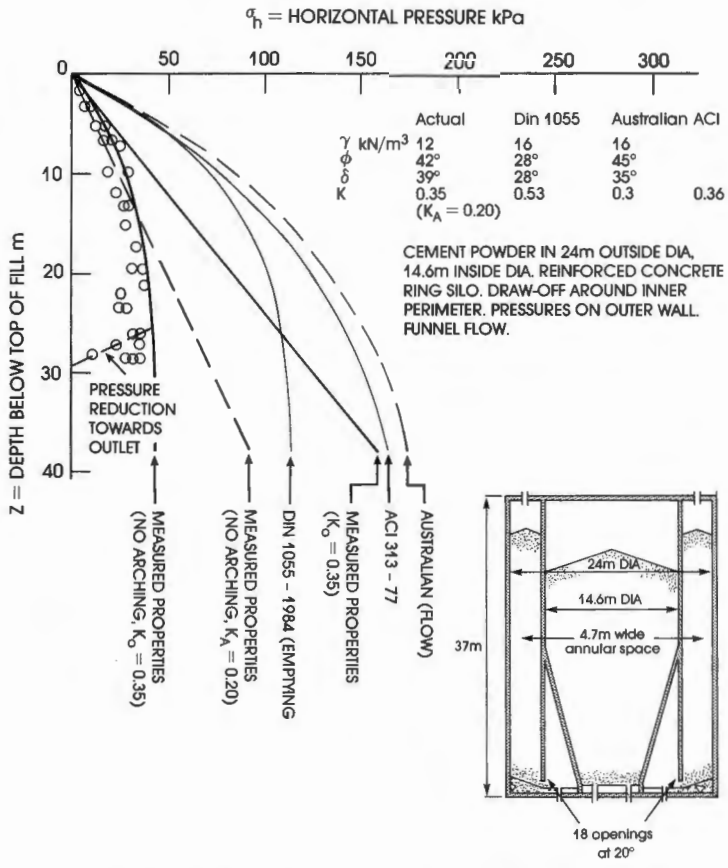

Fig. 12: Comparison of code and measured horizontal pressures for reinforced concrete ring silo storing cement at Lichtenburg, S. A.

The effect of temperature changes on this silo has been studied in reasonable detail and the reader is referred to Ref. [17] for further information on the subject.

For the present purpose, it is sufficient to note that diurnal temperature variations can increase horizontal pressures in the bin by at least 50 kPa. If a 50 kPa surcharge pressure is added to the no-arching K_0 envelope shown in Fig. 10, it will be seen that almost all of the measured pressures are enveloped.

Hence the conclusions stated earlier remain, except that environmental effects such as temperature, and in other cases, effects such as swelling of the silo contents, may have to be superimposed on the basic pressure-depth line. In this regard, note that the fact that the Australian guidelines gave the best result of the three codes is purely coincidental and does not reflect any special rationality of the guideline.

Case 8: 20 m diameter reinforced concrete cement storage silo (Schaffner and Blight [18])

This silo is used to load out road tankers for bulk cement deliveries. It is subject to simultaneous filling and emptying. In this case Fig. 11 shows that all three code pressure-depth curves far overestimate the actual horizontal pressures in the silo. The basic reason for this is that the properties of the cement and, in particular, its density, are very different to the properties listed by the codes.

The no-arching K_0 pressure-depth line also overestimates the actual pressures by far. The reason for this is that whereas the proportions of the silo would indicate that not much arching is likely, the contents actually appear to arch fully. In this case the best containing line to horizontal pressures in the silo is given by the Janssen equation with $K = K_0$ ("measured properties (K_0 = 0.35)" in Fig. 11).

This raises a basic fault with the three codes being considered here. All three list typical materials properties for a wide range of materials. While these are useful for preliminary designs and estimates, there is a strong temptation also to base final designs on these properties.

The authors of the codes clearly recognize this and have deliberately listed properties that err on the side of conservatism. Conservatism may mean safety but it also may mean unjustified expenditure on heavily overdesigned structures. It certainly does not mean good engineering. Codes should enjoin their users to establish the actual properties of the materials for which they are designing and should discourage the use of parameters taken from the literature.

Case 9: A 4.7 m wide, 24 m outside diameter, ring silo for storing cement (Fliss and Blight [19])

Fig. 12 shows the main dimensions and horizontal pressure information for this silo. Like the silo of Case 8, this is used to load out road and rail tankers and also serves a bagging plant. It is subject to simultaneous filling and emptying. As Fig. 12 shows, the results are very similar to those for the previous case. There is clearly strong arching in the silo and the best containing line for the pressure-depth relationship is given by Janssen's equation calculated for the actual cement properties with $K = K_0$.

There appears to be a tendency for fine powders to arch strongly even in silos having a geometry that is unfavourable to arching. Although Nielson's results [10] (Case 1) do not show arching during emptying, they do show arching during filling. Another silo on record (Blight [20]) containing cement raw meal and having a height-to-diameter ratio of 3 also shows strong arching.

Conclusions

1. Many materials do not exhibit a pronounced Janssen-type arching action when stored in a silo. Any arching that does occur may break down, at least locally or intermittently, when a silo is emptied after uninterrupted filling. In general, pressures will increase at the start of emptying, both as a result of the rotation of planes of maximum shear and as a result of the break-down of arching. The increased pressures do not generally exceed a limit defined by the equation

$$\sigma_h = K_0 \gamma z \quad (6)$$

2. Environmental factors, such as diurnal temperature variations may increase lateral pressures beyond the limit defined by Eq. (6). Temperature effects are most likely to affect uninsulated steel silos. Other effects such as the swelling of the silo contents may also affect pressures in steel or reinforced concrete silos (e.g. Blight [21]).

3. Fine powders may exhibit a capability to arch strongly, especially if stored in silos subject to simultaneous filling and emptying. In such cases, pressures may not reach the limit defined by Eq. (6).

4. Predictions of horizontal pressure based on the three codes of practice [5] [6] [7] examined here do not usually represent measured horizontal pressures particularly well. In some cases this is because they assume the development of arching, which does not occur. In other cases, it is because the materials properties listed by the codes are unrealistic. Pressures should always be predicted on the basis of actual measured properties.

5. Comparisons of Measured Normal Pressures in Hoppers With Code Recommendations

Two comparisons will now be made between the design pressures for hoppers according to DIN 1055-1984 and the Australian guidelines, and pressure measured in two hoppers.

Case 1: Hopper to 20 m diameter coal load-out silo

This is the hopper to the silo described in Case 4 of the previous section of this paper. The dimensions of the hopper and the information on normal pressures at the start of emptying are shown in Fig. 13.

The Australian guidelines predict a peak pressure at the cylinder-hopper interface, but the step in the pressure distribution according to DIN results from the change in inclination of the wall. The figure also shows continuations of the no-arching K_A and K_0 envelopes adjusted for the slope of the hopper wall. It will be noted that the measured pressures do not agree with either the Australian guidelines or DIN 1055. Most of the measurements cluster about the no-arching K_A line while the no-arching K_0 line defines an upper limit to the measured normal pressures.

Case 2: Hopper to 10 m diameter steel starch silo

Information on the silo and the results of pressure measurements are shown in Fig. 14. This silo serves a starch bagging plant and is operated on a simultaneous filling and emptying basis. The pressures in the hopper were deduced from strains measured on the hopper wall. Here again, the measured stresses fall between the limits defined by the no-arching K_A and K_0 lines and bear no resemblance to the predictions of either DIN or the Australian guidelines.

One other case of pressures in hoppers that has been investigated by the author [22] agrees with the evidence presented by these two cases.

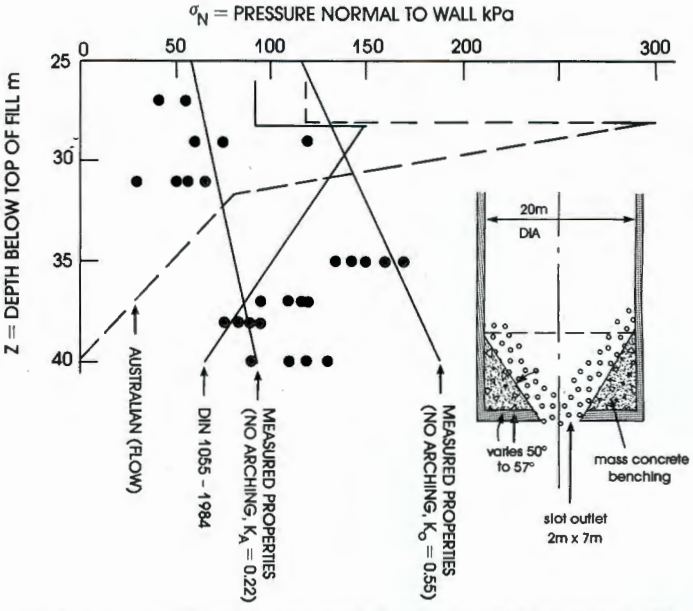

Fig. 13: Comparison of code and measured normal pressures on hopper of 20 m diameter coal load-out silo referred to in Fig. 8

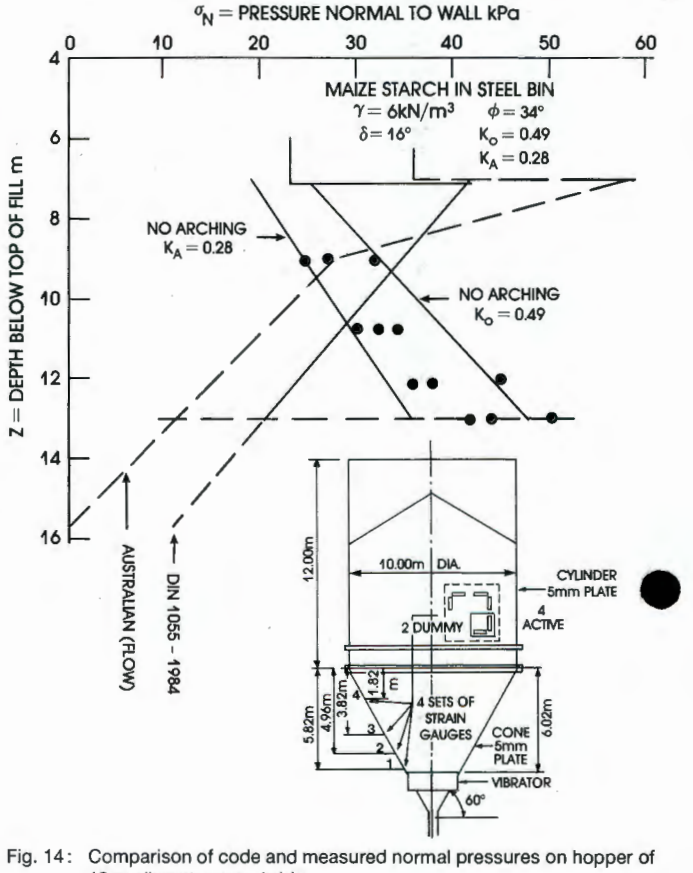

Fig. 14: Comparison of code and measured normal pressures on hopper of 10 m diameter starch bin

Discussion and Conclusions

As seen above, pressures measured in these two hoppers do not agree with the Australian guidelines' predictions in two respects:

(i) there is no peak pressure at the cylinder-hopper transition; and

(ii) the pressure does not decrease towards the outlet, except right at the outlet.

In other cases, however, there is a pressure decrease towards the outlet. In this paper, the effect is shown by Clague's results [4], by Hartlén et al. [11], by the 20 m diameter steel maize silo, and by the two cement silos.

However, for design purposes, this decrease cannot be taken into account as the more severe condition shown in Figs. 13 and 14 might apply, and certainly will apply if the silo-hopper system is filled without interruption.

The latter point is illustrated by Fig. 15. There has only been one opportunity to observe the build-up of lateral pressures in the steel maize silo described in Fig. 10. Fig. 15 shows the results of these measurements, which illustrate that when the silo is filled without interruption, the full pressure described by Eq. (6) acts in the lower part of the silo.

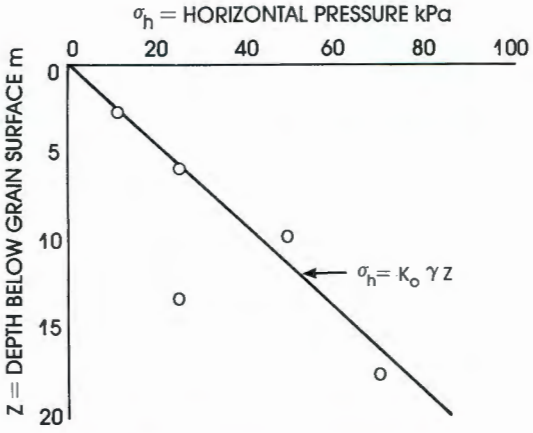

Fig. 15: Relationship between horizontal pressure and depth of grain for uninterrupted filling of maize silo referred to in Fig. 10

6. General Conclusion and Recommendations

(i) There is no evidence for the existence of Jenike and Johanson-type switch pressures or Walker-type peak pressures;

(ii) In the case of most materials, it would be preferable to design silos and hoppers on the basis of a linear horizontal pressure distribution defined by

$$\sigma_h = K_0 \gamma z \qquad (6)$$

In this equation K_0 and γ must be measured for the actual materials to be stored. With fine powders stored in silos subject to simultaneous filling and emptying, it would probably be satisfactory to design on the basis of the Janssen arching theory using actually measured materials properties.

(iii) It may be necessary to surcharge the pressures calculated as above to allow for the effects of diurnal temperature changes or other environmental factors. Temperature effects will affect only uninsulated steel silos.

References

[1] Jenike, A.W.: Storage and flow of solids; University of Utah, Engineering Experiment Station, Bulletin 123, 1964

[2] Jenike, A.W., and Johanson, J.R.: Bin loads; Journal of the Structural Division, ASCE, Vol. 94, No. ST4, 1968, pp. 1011–1041

[3] Walker, D.M.: An approximate theory for pressures and arching in hoppers; Chemical Engineering Science, Vol. 21, 1966, pp. 975–997

[4] Clague, K.: The effects of stresses in bunkers; PhD Thesis, University of Nottingham, 1973

[5] American Concrete Institute: Recommended practice for design and construction of concrete bins, silos and bunkers for storing granular materials; ACI Standard 313-77, 1977

[6] Deutsches Institut für Normung: Lastannahmen für Bauten - Lasten in Silozellen; DIN 1055, Teil 6, 1984

[7] The Institution of Engineers, Australia: Guidelines for the assessment of loads on bulk solids containers; 1986

[8] Blight, G.E., and Garstang, A.: Strains Measured in a 7,500 t Sugar Silo; bulk solids handling, Vol. 7, No. 4, 1987, pp. 573–582

[9] Johanson, J.R.: Effect of initial pressures on flowability of bins; Journal of Engineering for Industry, ASME, May 1969, pp. 395–399

[10] Nielson, J.: Pressure measurements in a full-scale fly ash silo; Proceedings Pacific Region Meeting, Fine Particle Society, Hawaii, 1983

[11] Hartlén, J., Nielson, J., and Ljunggren, L.: The wall pressure in large grain silos; Swedish Council for Building Research, Stockholm, 1984

[12] Omote, Y., and Suekane, M.: Pressure measurements on large-scale coal storage silo at the Saijo power station in Japan; International Journal of Bulk Solids Storage in Silos, Vol. 2, No. 1, 1986, pp. 11–16

[13] Blight, G.E., and Bentel, G.M.: Measurements on Full Size Silos, Part 2 - Pressures; bulk solids handling, to be published, 1988

[14] Blight, G.E.: A comparison of design and measured lateral pressures in a large coal load-out silo; International Journal of Bulk Solids Storage in Silos, Vol. 2, No. 2, 1986, pp. 1–8

[15] Blight, G.E., and Midgley, D.: Pressure measured in a 20 m diameter coal load-out bin; Journal of Powder and Bulk Solids Technology, Vol. 5, No. 2, 1981, pp. 21–31

[16] Blight, G.E.: Performance of a 20 m diameter steel maize storage bin; Proceedings 2nd International Conference on Design of Silos for Strength and Flow, Powder Advisory Centre, London, 1983, pp. 179–191

[17] Blight, G.E.: Temperature changes affect pressure in steel bins; International Journal of Bulk Solids Storage in Silos, Vol. 1, No. 3, 1985, pp. 1–7

[18] Schaffner, R.H., and Blight, G.E.: A comparison of design and measured lateral pressures in a large Ibau-type cement storage silo; International Journal of Bulk Solids Storage in Silos, Vol. 2, No. 3, 1986, pp. 17–24

[19] Fliss, L., and Blight, G.E.: A comparison of design and measured lateral pressures and temperatures in a large duo-cell cement storage silo; International Journal of Bulk Solids Storage in Silos, Vol. 2, No. 4, 1986, pp. 18–28

[20] Blight, G.E.: Pressures exerted by materials stored in silos: part II, fine powders; Geotechnique, Vol. 36, No. 1, 1986, pp. 47-56

[21] Blight, G.E.: Swelling Pressure of Wetted Grain; bulk solids handling, Vol. 6. No. 6, 1986, pp. 1135–1140

[22] Blight, G.E.: Pressures exerted by materials stored in silos: part I, coarse materials; Geotechnique, Vol. 36, No. 1, 1986, pp. 33–46

PAPER #88-4024

DESIGN LOADING FOR GRAIN SILOS - INTENTION AND REALITY

by
G E BLIGHT
Professor of Civil Engineering
(Construction Materials)
University of the Witwatersrand,
Johannesburg,
P O WITS, 2050, South Africa

Written for presentation at the 1988
International Summer Meeting of the
AMERICAN SOCIETY of AGRICULTURAL ENGINEERS

Rushmore Plaza Civic Centre
Rapid City, SD
June 26-29, 1988

SUMMARY:
The case of the failure of a silo that had a sequel in a civil court is described. The conflicting technical evidence on the causes of the failure is reported. When the silo failed it was storing material for which it had not been designed. The primary cause of the failure, however, was that the structure was subjected to eccentric emptying. This generated forces and moments that the silo could not withstand. The intended design loads were exceeded by those that applied in reality.

KEYWORDS:
Design, Grain storage, Load, Silos, Wheat.

American Society of Agricultural Engineers

St. Joseph, MI 49085-9659

1. INTRODUCTION

In 1980 the British colony of Rhodesia became the Republic of Zimbabwe, after a debilitating fifteen year long bush war. In 1981 the President and People of the United States of America made a gift of a ship-load of wheat to the people of the new republic. In July 1982 the ship-load arrived off Africa and was handled through the Port of Durban in the Republic of South Africa, as Zimbabwe is a land-locked country.

The wheat was off-loaded into the silos of a bulk handling facility from where it was to be railed the 1600km to Harare, the capital of Zimbabwe.

Part of the load was stored in the pair of steel silos depicted in Figure 1, one of 10.7m (35 feet) diameter and one of 12.2m (40 feet), both silos being completely filled. The 10.7m diameter silo was emptied, but the 12.2m silo stood undisturbed for a period of 15 days. On the night of the fifteenth day, a worker in the reclaim tunnel under the silo heard a groaning, grinding noise overhead, rushed out of the tunnel and found that the 12.2m silo had canted over and was leaning against the 10.7m silo.

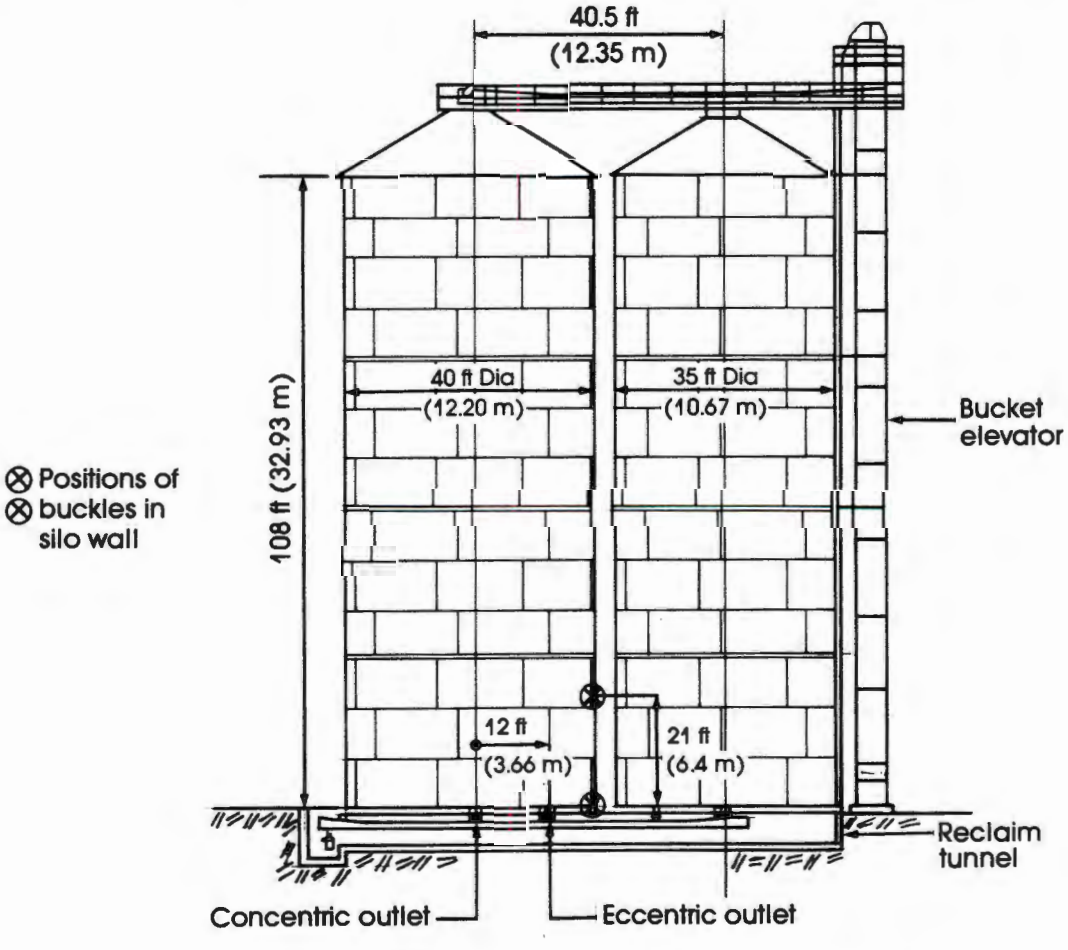

Figure 1: Layout and principal dimensions of silos

The alarm was raised and engineers were summoned to the site. The silos were inspected and the situation was assessed. It was discovered that the silo wall had buckled at the base, and also at a height of 6.4m (21 feet) above the base. It is not known which buckle occurred first.

It was decided that nothing could be done until the silo was emptied, and that the silo should slowly be emptied and the wheat transferred to other silos in the complex. Figure 1 shows that each silo was flat-bottomed and was equipped with a central outlet and an eccentric outlet. Emptying of the 12.2m silo was started through the central outlet and continued for a few hours, until at two in the morning, the 12.2m silo collapsed, knocking over the empty 10.7m silo. The empty silo fell into the adjacent property demolishing a factory building and doing some $2 million damage. Figure 2 is a reconstruction of how the silos fell.

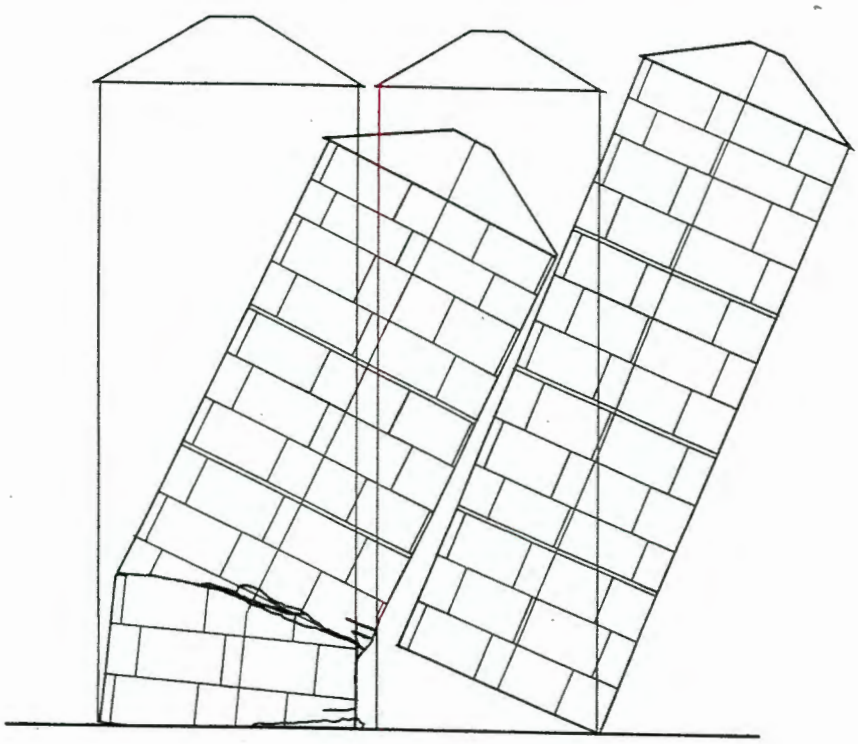

Figure 2: Reconstruction of falling of silos

The accident led to a civil court claim against the owners and operators of the bulk terminal and their consulting engineers, as well as the designers and constructors of the silos. The ensuing court case resulted in the facts given in this paper becoming public.

2. POSSIBLE CAUSES OF FAILURE

As inevitably happens in a court case, the technical witnesses differed in their interpretation of the causes of the failure. As the author was one of those witnesses, the interpretation given in this paper is not necessarily the only possible one.

.1 The plaintiff claimed that the design of the silo was inadequate, particularly with regard to the resistance of the walls to buckling under the frictional wall load. He also maintained that the form and location of the failure was consistent with denting caused by eccentric emptying of the silo. That was why the silo wall buckled in line with the reclaim tunnel. The worker in the reclaim tunnel must have been in the process of drawing grain from the eccentric outlet when he heard the sounds of the failure occurring overhead. Therefore the silos had been negligently operated.

.2 The owner-operator maintained that the failure was caused by faulty design. In particular, the plate thickness of the walls was inadequate to withstand the frictional wall load, and the silo wall buckled at the base. The buckle occurred directly in line with the reclaim tunnel on the side of the eccentric outlet and developed slowly over the 15 day period that the silo stood full. According to the owner-operater no grain whatsoever was drawn from the silo between the time it was filled and the time it collapsed. According to him, the failure process was assisted by the diurnal temperature changes which added to the compressive wall load. That was why the silo failed at night, as the temperature was falling, the mechanism being axisymmetric buckling under the action of the wall load.

.3 The designer-constructor pointed out that his contract with the owner called for the supply of two silos for storing barley malt. When the silo failed it was storing wheat, a material having a unit weight more than 45 per cent greater than that of malt. Records discovered to the court showed that at various times the 12.2m silo had been used to store maize, rice, sunflower seed, wheat and de-fatted maize germ. The designer-constructor agreed with the plaintiff that the primary cause of the failure was eccentric emptying. He disagreed with the owner's explanation of the effects of a fall in temperature, stating that a temperature decrease would have reduced the frictional wall load. It would also have increased the horizontal pressure on the wall, thus improving the buckling resistance of the plates.

This brings the reader back to the title of the paper: "Design loading - intention and reality".

.4 The loads for which a silo is intended are not necessarily those which it will really carry.

.5 According to Murphy's law, if it is possible to operate a silo in a manner for which it was not intended, it will really be so operated.

3. DESIGN AND ACTUAL BUCKLING LOADS CARRIED BY THE SILO WALL

The silos were designed in 1972, when the only silo loading code in use in South Africa was the German DIN 1055 of 1969. The loads quoted in this paper are based on the 1984 version of this code which are more conservative that the 1969 version.

Text books available for the structural design of steel silos in 1972 made little or no mention of the possibility of buckling of a silo wall under concentric load conditions. One well-known text book (Reisner, Ward Rothe) published in 1971 makes no mention at all of the possibility of wall buckling. Another published in 1976(Reimbert) merely says of the subject "This [wall] thickness will be finally checked for resistance to general buckling".

Even in 1988 there is no single, universally recognized criterion for checking the buckling stability of a silo wall. A recent publication(Trahair et al, 1983) puts forward certain expressions that allow for the effects the silo contents have in stabilizing the walls against buckling. As shown in Table 1, this expression predicts an allowable stress that was well exceeded by the calculated stress when the silo was filled with wheat. However, in two more recent papers by some of the same authors(Rotter et al, 1986 and Jumikis et al, 1986) the opinion is advanced that the actual stress at which a silo wall will buckle is larger than that given earlier. On this basis, the silo had a small margin of safety against axisymmetric buckling both at the base and at a height of 6.4m above the base, where the main buckle that led to the silo failure occurred and also where the plate thickness was reduced from 6mm to 5mm.

The data given in the last line of Table 1 casts doubt on the conclusion that the silo failed by axisymmetric buckling of the walls, but it does not rule out the possibility. However, if the temperature changes experienced by the silo are considered, the possibility of failure by axisymmetric buckling is indeed ruled out:

Meteorological records showed that for the month of July, the mean temperature change between noon and midnight is $\Delta\theta = 9°C(16°F)$. Taking the coefficient of thermal expansion for steel as $\alpha = 11.5 \times 10^{-6}/°C$ and regarding the fill as being incompressible, the effect of a temperature fall of 9°C would be to cause the silo wall to contract onto the contents thus increasing the lateral pressures. If the fill is regarded as incompressible and if vertical thermal strain is prevented by wall friction the horizontal pressure induced in the wheat and hence on the wall is given by

$$\Delta\sigma_h = \frac{E\alpha\Delta\theta}{(1-\upsilon)} \cdot \frac{2t}{D} \qquad [1]$$

where E and υ are respectively Young's modulus and Poisson's ratio for steel and t/D is the ratio of wall thickness to silo diameter. Field measurements made

on a 20m diameter steel maize silo(Blight, 1985) illustrated and amplified in Appendix I, have shown that the assumption of incompressible contents gives a good agreement between calculated and measured thermally induced horizontal pressures.

TABLE 1

Calculated and Permissible Vertical Stresses in Silo Wall with Silo Storing Wheat

a = 6.4m above base of silo
b = at base of silo

	a	b
Vertical wall stresses calculated by DIN 1055, 1984 σ_{VW}MPa	61	73
Timoshenko Classical Buckling Stress σ_TMPa	100	120
Australian Institute of Steel Construction Permissible Stress σ_AMPa	57	60
σ_A/σ_{VW} (Trahair et al, 1983)	0.93	0.82
$0.8\sigma_T/\sigma_{VW}$ (Rotter et al, 1986)	1.31	1.32

The increase in horizontal pressure resulting from the fall in temperature, according to equation (1), would be about 25kPa. The fall in temperature would in addition cause the silo wall to contract in a vertical direction also as illustrated in Figure 2. The contraction would be resisted by upward frictional forces between the silo wall and the wheat. Taking the angle of wall friction between steel and wheat at a low value of 15°, the induced upward tensile wall stress would amount to 38MPa both at the base of the silo and at 6.4m above the base. Comparing these figures with the corresponding calculated compressive wall stresses given in Table 1 as 73MPa and 63MPa shows that the net compressive wall stress in the silo would have been more than halved by the fall in temperature. This completely contradicts the case of the silo owner-operator and shows that the silos were quite unlikely to have failed during the night. If a failure by axisymmetric buckling were to have occurred, it would have been most likely to occur in the heat of the day when the frictional wall load would have had its greatest value, and the lateral pressure on the walls would have been at a minimum value.

4. THE EFFECTS OF ECCENTRIC EMPTYING

There was no evidence that more than a very small quantity of grain had been discharged from the eccentric outlet on the night of the failure. The outlet had not been locked, and the rubber skirt, which was used to prevent spillage of the grain from the conveyor belt as it discharged, was found fitted in place at the eccentric outlet. The worker who had been in the reclaim tunnel admitted to "cracking the eccentric outlet open to see if the grain would flow", but denied that "more than a few grains" had actually flowed out of the outlet. However, after the failure, wheat was found on the reclaim conveyor.

It is well established (eg. Jenike, 1967) that withdrawing material from a full silo via an eccentric outlet has the effect of forming a funnel of grain flowing towards the outlet, as indicated in Figure 3. Horizontal pressures in this funnel fall below those in the surrounding static grain, the net result being that where the flowing grain impinges on the wall of the silo, the wall bends inwards. If the bending stiffness and strength of the wall are insufficient, the silo will dent inwards. Once the denting occurs, the frictional wall load will complete the destruction of the silo by collapsing the wall in a vertical direction.

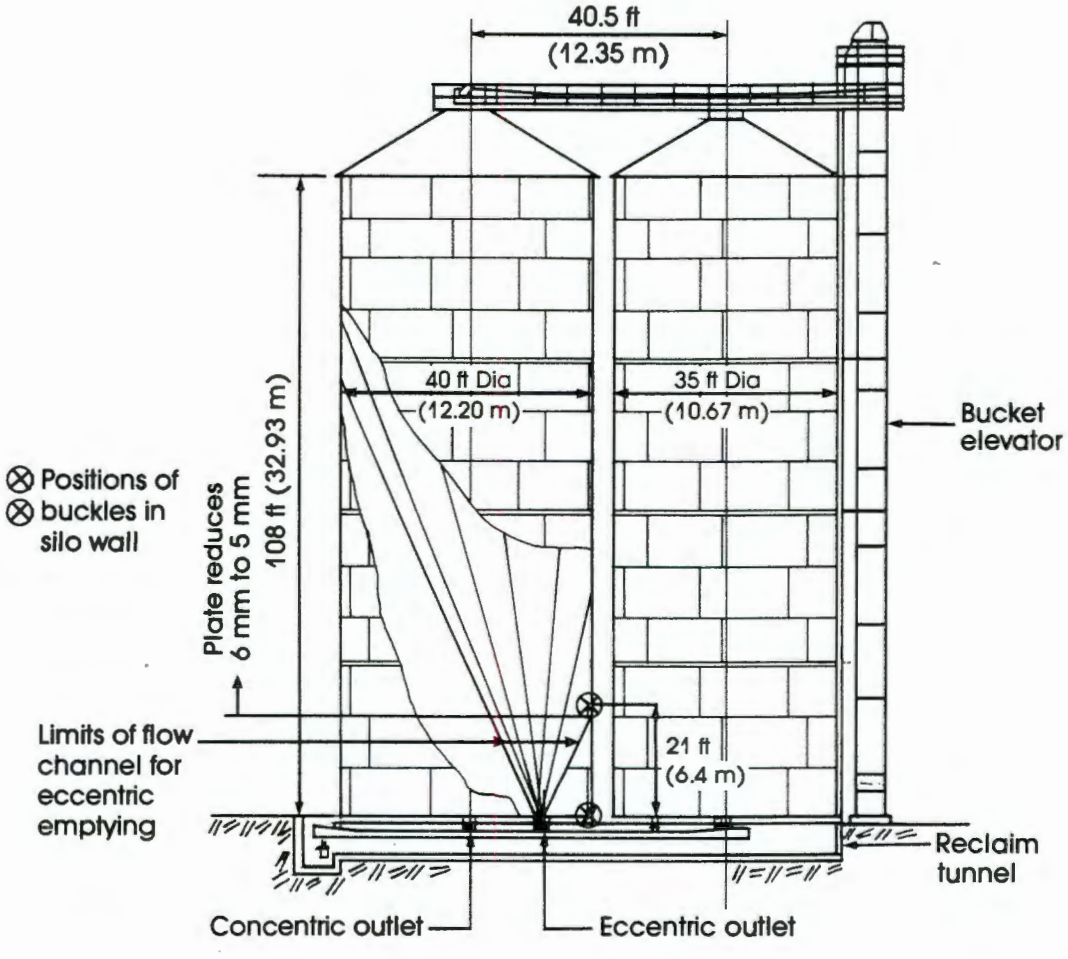

Figure 3: Flow channel for eccentric emptying

Calculations based on Jenike's (1967) paper showed that the silo wall would have been quite unable to resist the forces generated by eccentric outflow. Also, as indicated in Figure 3, the position of the dent at 6.4m above the base of the silo coincides with the height at which the eccentric flow funnel would have impinged on the silo wall. The wall would have dented as soon as sufficient grain had been withdrawn to establish the eccentric flow pattern.

There is no indication in the literature as to how much movement is required to establish the eccentric flow pattern. If the grain is regarded as being incompressible, then in this case, a withdrawal of 1 ton of grain would have caused the fill surface to fall by 10mm (0.4 inch). It seems possible that a withdrawal of even less than 1 ton would have been sufficient to establish the flow funnel. If this is correct, denting of the silo could have been induced within half to one minute of starting eccentric drawoff at the lowest possible reclaim rate of 60 tons per hour. Experiments in the laboratory on model silos (see Appendix 2) consisting of a tube of aluminum foil filled with sand showed that eccentric withdrawal of about a teaspoonful of sand was sufficient to cause the tube to dent visibly. If withdrawal was then continued through a central outlet, the model silos continued to cant over in the direction of the initial dent. Continuing withdrawal through the central outlet of the prototype silo would, on the basis of the model tests, have inevitably led to complete collapse of the silo.

The buckle or bulge at the base of the silo wall accords with deformations reported by Jumikis et al(1986) for experiments on the eccentric emptying of model silos. If the bulge at the base occurred after the dent at 6.4m height it would have been generated by the canting movment of the silo following formation of the dent. As the centre of gravity of the mass of grain above the 6.4m level moved across, vertical pressures on the grain on that side would have increased. This would have increased the vertical stress in the silo wall, resulting in the buckle that was later observed.

5 CONCLUSIONS

The most likely cause of the failure was never pronounced by the court. However, it is highly significant that the matter was settled shortly after the owner-operator's technical witnesses had given evidence and been cross-examined by the plaintiff and the designer-constructor. Costs of the court case were borne by the owner and his consulting engineer. The designer-constructor bore no costs.

The importance of this case history as stated earlier, is that it illustrates that:

.1 The loads for which a silo is designed may be nothing like those it is called to carry during its service life. Current silo design codes still do not pay sufficient attention to such factors as the effects of eccentric emptying or to temperature effects. Operators of silos often appear unaware that a silo is a structure that is highly sensitive to the nature of the material stored in it.

.2 Eccentric outlets should never be provided in a silo, especially a steel silo, unless the structure has been specifically designed to withstand the forces and moments generated by eccentric flow. Of the many hundreds of steel silos built by the designer-constructors mentioned in this paper, the only silos that have ever developed structural problems have been those equipped with eccentric openings.

6. REFERENCES

Blight, G.E. 1985. Temperature changes affect pressures in steel bins. International Journal of Bulk Solids Storage in Silos, 1(3):1-7.

German Standard DIN 1055. 1964 to 1984. Sheet 6: Design loads for buildings: Loads in silo bins.

Jenike, A.W., 1967. Denting of circular bins with eccentric drawpoints. Journal of the Structural Division, ASCE, 93(ST1):27-35.

Jumikis, P.T., Rotter, J.M., Fleming, S.P. and Porter, S.J. 1986. Experiments on the buckling of Thin walled model silo structures. PROCEEDINGS, 2nd International Conference on Bulk Materials Storage, Handling and Transportation, Wollongong, Australia:180-186.

Reimbert, M.A. 1986. Silos - theory and practice. Trans Tech Publications, Clausthal, West Germany.

Reisner, Ward Rothe, M.R. 1971. Bins and bunkers for handling bulk materials. Trans Tech Publications, Clausthal, West Germany.

Rotter, J.M., Ansourian, P. and Trahair, N.S. 1986. A survey of recent buckling research on steel silos. PROCEEDINGS, 2nd International Conference on Bulk Materials Storage, Handling and Transportation, Wollongong, Australia:68-75.

Trahair, N.S., Abel, A., Ansourian, P., Irvine, H.M. and Rotter, J.M. 1983. Structural design of steel bins for bulk solids. Australian Institute of Steel Construction, Sydney, Austrlia.

APPENDIX 1

Figure 4 shows a daily record of temperature changes undergone by a 20m diameter steel maize silo. The accompanying changes of horizontal pressures in the grain and vertical and horizontal strain measured in the silo wall are also shown.

.1 When the temperature fell by 8°C the corresponding increase in horizontal pressure was 18kPa.

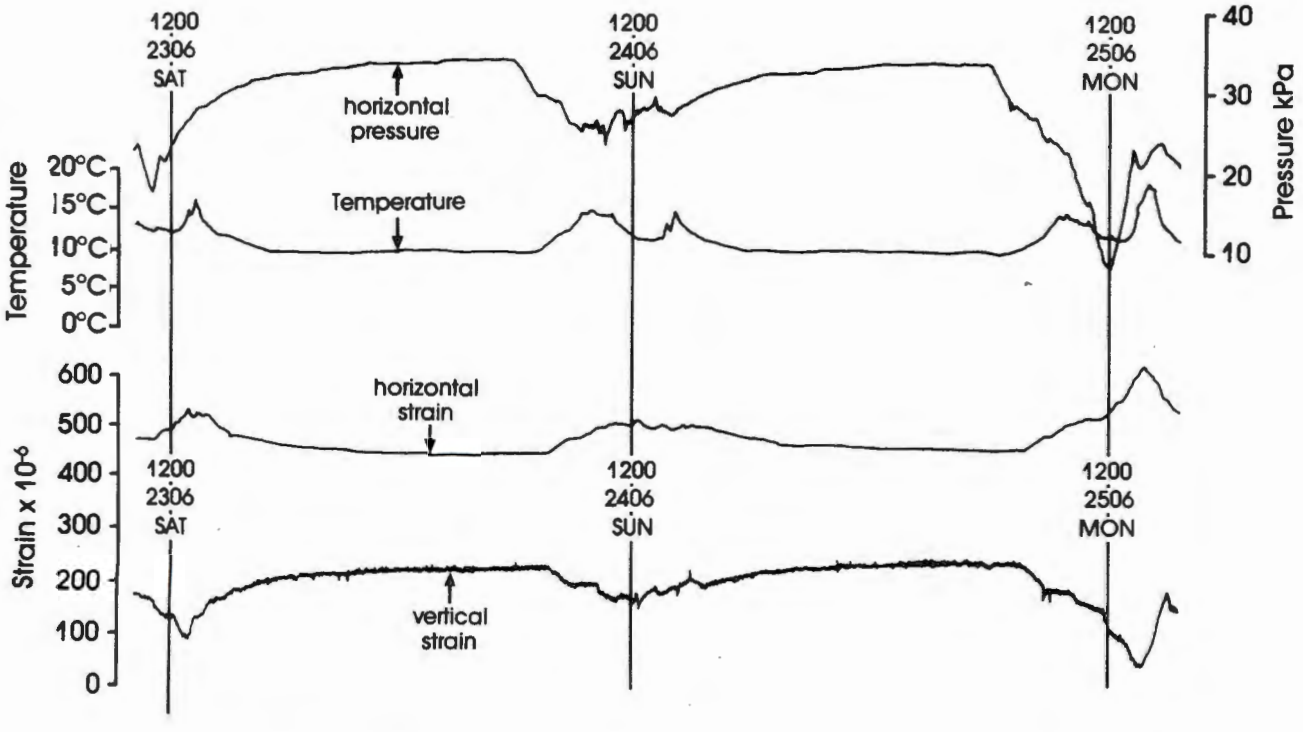

Figure 4: Effect on horizontal pressure and strains of diurnal temperature changes undergone by 20 m diameter steel maize silo

.2 The increase in horizontal pressure calculated from the expression

$$\Delta\sigma_h = \frac{E\alpha\Delta\theta}{1-\upsilon} \cdot \frac{2t}{D} \qquad [A]$$

was 22kPa for the following numerical values:

E	= 200GPa	α	= 11.5×10^{-6}/°C	$\Delta\theta$	= 8°C
t	= 8mm	υ	= 0.33	D	= 20m

.3 The increase in horizontal pressure calculated from the prevented strains in the silo wall was 23kPa.

4. The induced change in vertical stress in the silo wall was a tension of 58MPa.

The stresses reported under .3 and .4 were calculated by applying the generalized Hooke's law to prevented vertical and horizontal strains in the silo wall using the values of E and υ given above.

To summarize:

Measured change in horizontal pressure	: 18kPa
Change in pressure calculated from [A]	: 22kPa
Change in pressure calculated from prevented strains	: 23kPa

These figures are in satisfactory agreement.

APPENDIX 2

Figures 5a (left) and 5b (right) illustrate the mode of failure of a model silo made up of a tube of aluminum foil which was filled with sand and then subjected to eccentric emptying:

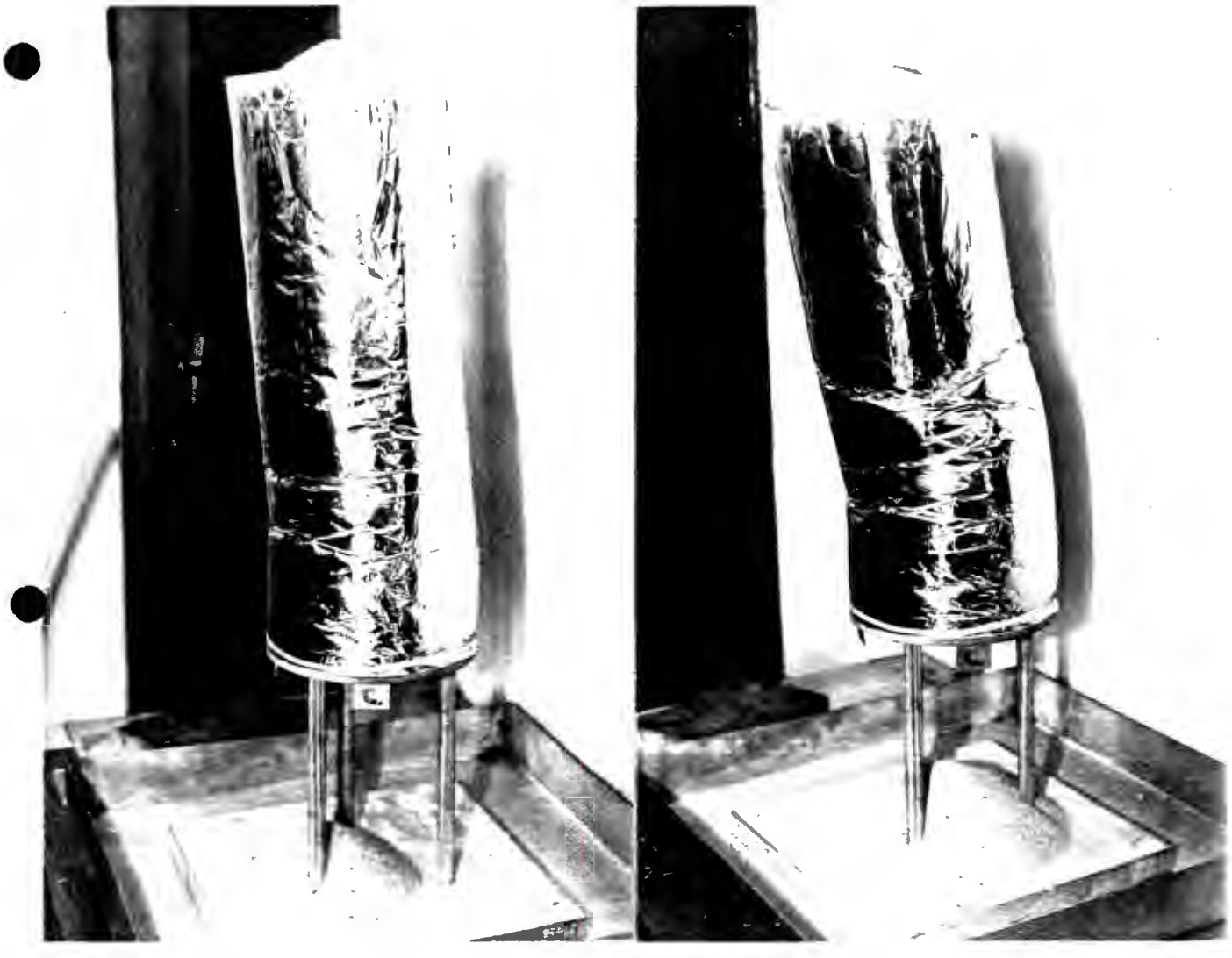

Figure 5: Buckling mode of model silo
(a) After eccentric emptying
(b) After emptying continued centrically

In Figure 5a a small quantity of sand has been withdrawn eccentrically (see the eccentric pile of sand under the model). The buckle adjacent to the eccentric draw-off point became visible after the withdrawal of only about a teaspoonful of sand. Eccentric withdrawal was then stopped and centric withdrawal started. As shown by Figure 5b,the buckling became progressively worse with centric withdrawal (the pile of sand under the model is now centric).

Structural Engineering Review

EDITOR
Dr B.H.V. Topping
Department of Civil Engineering, Heriot-Watt University, Riccarton, Edinburgh EH14 4AS, UK
Telephone: 031-449 5111 Fax: 031-451 3170

9th December 1991

Ref: SER/91/70

Professor GE Blight
Department of Civil Engineering
University of Witwatersrand Johannesburg
Private Bag 3
Wits 2050
South Africa

Dear Professor Blight,

TEMPERATURE INDUCED LOADING ON SILO WALLS

I am pleased to inform you that your paper has been accepted for publication in "Structural Engineering Review". The paper is currently being copy edited and typeset. You will shortly receive proofs. As from January 1992 the journal will be published by Pergamon Press.

I am sorry for the delay in writing to you but this has been caused by the delay in the transfer of the journal to Pergamon Press.

Yours sincerely,

Professor B.H.V. Topping

Published by Chapman and Hall Ltd, 2-6 Boundary Row, London, SE1 8HN, UK
Telephone 071-865 0066 Fax 071-522 9623 Registered in England Number 13655

TEMPERATURE-INDUCED LOADING ON SILO WALLS

G.E. BLIGHT

CIVIL ENGINEERING DEPARTMENT
WITWATERSRAND UNIVERSITY
P O WITS, 2050, JOHANNESBURG
SOUTH AFRICA

ABSTRACT

A brief review is made of guidance concerning temperature-induced loading on silo walls, as given by currently used design codes. The paper goes on to examine the detail of the phenomena resulting in lateral temperature surcharge pressures, and the corresponding temperature effect on frictional wall loads. Thermal bending is also examined in some detail. The explanations in each case are based on observations of temperature, pressure and strain in full size operational industrial silos.

INTRODUCTION AND REVIEW

Primary loading on silo walls consists of the lateral pressure and frictional wall load arising from the weight and friction of the silo contents. A review of primary loading, its characteristics and its variability in full-size silos has been given recently by the author [1]. The term "temperature induced loading" will be used to describe load effects arising from changes of temperature of the silo wall. These changes may result from direct solar heating, changes of air temperature, or from the temperature of the silo contents.

Temperature Surcharge Loads:

Changes of temperature have two distinct effects on silos:

Firstly, as the temperature changes, the perimeter and height of the silo vary. This has an effect both on the lateral wall pressure and the frictional wall load.
Secondly, if there is a gradient of temperature through the thickness of the wall, the wall will be subject to thermal bending.
The guidance given by four current design codes on the subject of temperature loading reveals varying approaches to the problem. The Australian guidelines for the assessment of loads on bulk solids containers [2] recommend using Anderson's [3] expression for lateral pressures caused by a fall in temperature of the wall of a cylindrical silo:

$$TS = \frac{\alpha \, \Delta\theta Ew}{[D/2t + Ew/Es(1-\nu_s)]} \qquad (1)$$

where TS is the temperature surcharge pressure, ie the thermally induced lateral pressure,
α the coefficient of linear thermal contraction of the wall,
$\Delta\theta$ the fall in temperature,
E_w the modulus of elasticity of the silo wall,
D the silo diameter,
t the wall thickness,
E_s the elastic modulus of the stored solid, and
ν_s Poisson's ratio for the stored solid.

The expression is difficult to apply realistically as it requires a knowledge of the elastic modulus and Poisson's ratio for the silo fill material. Values of these parameters have been established by means of conventional triaxial and oedometer laboratory tests. However, equation (1) has not been checked by other authors to any extent against measured values of TS to establish the validity of these moduli for calculating temperature surcharges.

The range of thermal strains experienced by a silo wall in temperate climates probably has a maximum of 300 microstrain. The elastic or compression moduli of granular materials are highly strain dependent, with very much stiffer behaviour being displayed at very low strains than at higher ones. For example, Padfield and Sharrock [4] show that the elastic modulus of a clay is 40 MPa if measured as a secant over the first 500 microstrain, but only 23 MPa if measured over the next 1500 microstrain. If moduli are measured over only a few tens of microstrain, even larger values are obtained (eg. [5]). There does not appear to be a satisfactory method at present of measuring moduli in laboratory tests in the range of 0 to 300 microstrain.

The Guidelines also state that "Additional wall frictional tractions should be expected during the temperature drop" but do not clearly say if this represents an increase or a decrease in the frictional wall load. The word "additional", however, gives the impression that the frictional wall load will increase as the temperature falls.

The American Society of Agricultural Engineers (ASAE) [6] recommends that temperature surcharge pressures for circular steel bins be estimated as 8% of the primary lateral pressure for temperature declines of 10°C per hour and 15% for 20°C per hour. The commentary on this section of the ASAE standard states that tests on model bins indicate that thermally induced lateral pressures vary with static pressures and rates of temperature decline. The recommended figures are based on tests by Manbeck and Muzzelo [7] and Zhang et al [8], who used measurements on small model silos in the strain range 0 to 500 microstrain. These are the most realistically determined laboratory moduli in the literature, but they failed to model the stress range realistically. Thermally induced changes in frictional wall load are not mentioned by the ASAE standard. The older German standard DIN 1055 [9] has nothing to say on the subject of temperature induced loading apart from drawing attention to its existence.

Thermal Bending

The oldest of the four codes, that of the American Concrete Institute (ACI 313) [10] does not mention thermally induced lateral pressures or

frictional wall loads, but does give guidance on thermal bending effects. The usual cause of thermal bending is hot material stored in a silo, but diurnal temperature changes can also cause thermal bending.

The thermal bending moment M_T is given as :

$$M_T = Ew\ t^2\ \alpha\Delta T/12(1-\nu) \qquad (2)$$

Here, ΔT is the difference in temperature between the inner and outer faces of the wall, and ν is Poisson's ratio for the wall material. The other symbols have been defined previously. This expression has short-comings as it ignores the effect of the hoop and vertical reinforcing steel in a reinforced concrete wall (it is, of course, advanced for use in reinforced concrete walls) and assumes an uncracked section.

The Australian Guidelines draw attention to the effects of a temperature gradient across the thickness of a silo wall, but make no recommendations. The ASAE Standard does not mention thermal bending at all, probably because it is mainly concerned with metal silos.

The purpose of the present paper is to illustrate, by means of the results of measurements on full size silos some of the characteristics of temperature-induced loading. The object is to inform the reader and to increase understanding of the various phenomena involved. It is believed that assessment of these loads is subject to many uncertainties and variabilities and that it will never be possible to estimate them with great confidence. Even if the theory for calculation is perfected, there will always be uncertainties and variabilities in the meteorological values (ΔT or $\Delta\Theta$) and materials parameters (E_s, E_w, ν_s, ν, α) to be used. However, the confidence of the designer will be increased if the basic phenomena, and the uncertainties that beset them are more fully understood.

CHARACTERISTICS OF TEMPERATURE SURCHARGE LOADS

Figure 1 illustrates some of the basic features of the development of temperature surcharge loads (Blight [11]). It represents two sets of simultaneous recordings of temperature and pressure on the western side of a 20m diameter steel silo storing 8 000 tons of maize grain. The observations were made over a week-end when the silo was not in use and the grain was static. Hence the observed pressure variations are believed to have arisen only a result of temperature variations and adjustments of the stored grain to these changes. The pressures shown in Figure 1 were recorded on a mercury filled strain gauged diaphragm pressure cell, the strain gauging of which was fully compensated for temperature changes.

It will be seen that the diurnal temperature wave has a double peak. Each peak corresponds to a period during which sunlight fell on the area of measurement. The dip between the peaks corresponds to the time during which the shadow of a neighbouring silo fell on the instrumented area. It will also be seen that the recorded pressure was at a minimum shortly after noon and a maximum at about 6 am. Each successive peak pressure is slightly higher than the last. Hence the temperature-induced pressure tends to "ratchet" upwards from day to day. This is however not quite as serious as it appears. A longer record of observation [11] has shown that after about 5 days an equilibrium is reached and thereafter, provided the daily drop in temperature does not increase, the peak pressure remains constant. Nevertheless the temperature surcharge pressure can represent a large proportion of the total lateral pressure on the silo wall. In the example of Figure 1, the temperature surcharge pressure exceeded the primary lateral pressure by as much as 174 per cent.

Note the jagged stick-slip characteristic of the pressure recordings which presumably arises from intermittent slippage of the grain over the inside surface of the silo wall.

Figure 2 shows a set of strain and temperature measurements made on a 15.5m diameter steel maize silo (Blight [12]). The overall height of the silo is 22.7m and the plate thickness at its base is 7.9mm. Because the electric resistance strain gauges were compensated for changes of temperature, the recorded strain represents stress-inducing strain, ie. that portion of the thermal strain that cannot occur because of the resistance of the silo contents. Note that the microstrain scale in Figure 2 is a scale only, the numbers do not represent absolute values of strain. In the case of both hoop and vertical strains, a fall in temperature induces a tensile strain, and vice versa.

The changes of hoop strain again correspond to appreciable changes in lateral pressure, while the changes in vertical strain correspond to substantial variations in frictional wall load. In fact, for the second temperature cycle in Figure 2, the silo wall went slightly into tension. (Referring to Figure 3b), the strain and temperature records given in Figure 2 were recorded at point B. The absolute wall load corresponding to the second temperature cycle at B just before noon was 250 kN/m, the wall load at dawn would thus have been a tension of about 13 kN/m). Note that the frictional wall load decreases with decreasing temperature. As the temperature falls, the wall tends to shorten, thus moving downwards relative to the silo fill. Hence the wall friction tends to reverse and the frictional wall load decreases.

In considering these measurements, it should be noted that the temperatures represent values at the location of the thermocouple junction. Even though for Figure 1 the thermocouple was located only 200 mm from the pressure cell, it was probably responding to variations of temperature smoothed out by heat conduction in the silo wall. Similarly, the pressure cell was responding to pressure changes in the stored grain that were smoothed to a differing extent. Hence the maxima and minima of the temperature and pressure records shown in Figure 1 do not coincide. Similar phase differences are seen in Figure 2. The junctions for the air and wall temperature thermocouples were only millimetres apart. The wall thermocouple was held against the wall and protected from wind and direct sun. The air thermocouple was 10 mm off the wall surface and exposed to sun and wind. It will be seen that the peaks of the two temperature records do not coincide. Similarly, the

peaks of the strain measurements do not coincide with those of the wall temperature. These phase differences pose unavoidable problems in field measurements.

Figure 3 shows the overall effect of temperature-induced loading on the 15.5m diameter silo referred to by Figure 2. Figure 3 shows stress paths for lateral stress (3a) and frictional wall load (3b) measured on four vertical lines A, B, C, D spaced at 90° around the silo perimeter, at heights of 1.3m and 2.7m above the base. The symbols A, B, C, D each represent a data point on one of these lines. The lower bound to the stress paths for lateral pressure σ_h is defined by the line

$$\sigma_h = K_A \gamma z \qquad (3)$$

where K_A is the active lateral pressure coefficient,
γ is the unit weight of the grain and
z is the depth of grain above the point of measurement.

The upper bound to the stress paths in the absence of temperature stressing would have been the line

$$\sigma_h = Ko\gamma z \qquad (4)$$

where Ko is the lateral pressure coefficient for zero lateral strain.

The difference between the K_A and Ko lines and the actual upper bound represents the temperature surcharge pressure TS which averages about 20 kPa relative to the Ko line, in this case. In Figure 2 values for TS of 30 kPa and 23 kPa are recorded. Note that pressures on line D are consistently higher than the other measurements. This is because the readings were always taken at the same time of day (about noon) when line D was in shade while the other lines were either in sun, or had been in sun earlier that day. Hence, as a result of variable temperatures, lateral pressures can be highly variable around the perimeter of a silo. This is further illustrated by Figure 4. Figure 4a shows the distribution of lateral pressure around the perimeter of the silo. The high values of σ_h on line D are very pronounced.

These measurements have been criticized on the grounds that the strains were measured only on the outside of the silo. Hence part of the strain could have arisen from bending in the wall. Subsequent measurements made on both sides of the wall have shown that differences in inside and

outside strain measurements are very small. The fact that most of the inferred pressures lie between the theoretical limits of the K_A and Ko lines further supports this observation.

Figure 3b shows the stress paths for the frictional wall load. Measurements on lines A, B and C lie more or less within the theoretical limits defined by the lateral pressure coefficients K_A and K_o, but wall loads on line D are consistently low and touch zero at a few points. The corresponding distribution of the wall load Pw around the silo perimeter is shown in Figure 4b. It is obvious that high lateral pressures correspond to low frictional wall loads and vice versa.

Although the data shown in Figure 3 was recorded at two elevations only, it is inferred that similar stress paths, modified by localised temperature conditions (sun and shade patterns) will apply over the entire filled height of the silo. This can be justified by reference to measurements of pressure and wall load distributions on other silos [13, 14], where measurements have proved consistent when made over a considerable height.

The stress paths shown in Figure 3 were recorded while the silo was being filled, and the radial distributions of σ_h and Pw are shown at the end of filling and after 2 weeks of storage. The effect of storage was generally to accentuate the effects of temperature, presumably via the thermal ratchet effect illustrated in Figure 1.

CALCULATING TEMPERATURE SURCHARGE PRESSURES

The difficulty of applying Andersen's equation (1) to the calculation of the temperature surcharge TS is that representative values of E_s are not available. Because the elastic modulus of a granular material is both strain and stress dependent, it is important to define both of these variables when carrying out measurements. While the stress level can probably be defined fairly realistically, the distribution of radial strain within the silo is completely unknown, and considering the non-uniform temperature around the perimeter of a silo, is probably quite indeterminate. Values of elastic modulus measured in the laboratory (eg Puri et al [15] and Blight [5, 16]) are too small to agree with field

measurements of TS when measured at large strains (1000 microstrain) or too large at small strains (10 microstrain). For this reason, the writer decided that it would be more realistic to calculate appropriate moduli from strain and temperature recordings for full size silos, such as those shown in Figure 2. The calculation has the following basis:

The prevented radial strain per unit temperature change (ε) is determined from records like Figure 2, covering several days and taken at two or three points on the perimeter of the silo. Then

$$\Delta\theta\varepsilon = \varepsilon f - TS/M_s \qquad (5)$$

where εf is the thermal strain the silo would have undergone had it been empty, and

$$\varepsilon f = \alpha\Delta\theta$$

M_s is the overall modulus of compressibility of the silo contents for radial compression

$$TS = \frac{2 E_w t}{D} \Delta\theta\varepsilon \qquad (6)$$

and hence

$$M_s = \frac{2Ewt\varepsilon}{D(\alpha-\varepsilon)} \qquad (7)$$

Equations (5), (6) and (7) clearly have the same basis as equation (1) with E_s and ν_s lumped into M_s.

Equation (7) was derived for corrugated steel silos with circumferential corrugations. The walls of these silos, being very flexible in the vertical direction, carry no wall load. The wall load is carried separately by vertical stiffeners. Hence the hoop strain in the wall is uniaxial and Poisson's ratio effects are negligible.

Data on Ms collected by this means is shown in Figure 5. In Figure 5, each data point represents measurements on a different silo, 11 structures in all. So far, data relate mainly to grains of various types. Fortunately, the measurements seem to follow a similar trend with vertical stress, but this can only be confirmed as more data becomes available.

It has been pointed out that the temperature surcharge for the same change in temperature, should, in terms of Figure 5, increase as the

overburden stress increases. This may not appear to be borne out by the data shown in Figure 3a. However, in this figure, TS has been indicated as the difference between the $K_o \gamma z$ line and the largest measured horizontal pressures. Actually as shown in Figure 2, TS is the difference between the pressure on the wall at the highest diurnal temperature and that at the lowest diurnal temperature, with the grain static. In Figure 3a, the fluctuations in pressure as the overburden stress increases, which are thought to result mainly from day to day temperature fluctuations around midday when the measurements were taken, show that TS does increase considerably with increasing overburden stress.

CALCULATION OF THERMAL BENDING MOMENTS

Thermal bending will occur whenever a temperature gradient exists through the thickness of a wall or slab. Because metal silos are thin-walled and metals are good conductors of heat, thermal bending effects will generally not exist. However, reinforced concrete silos are subject to thermal bending arising either from diurnal temperature changes, or from differences in temperature between their contents (usually hot) and the ambient air.

Figure 6 shows the basis for calculating the thermal bending moment, assuming an uncracked symmetrically reinforced wall. Figure 6b shows the assumed strain distribution for increases in temperature of the outside face of $\Delta\theta o$ and of the inside face of $\Delta\theta¿$. The stress diagram will be similar, with local increases in area (shown dotted) to account for the reinforcing steel. If the continuity of the cylindrical wall forces the neutral axis for thermal bending to remain at the centre of the wall thickness, the thermal bending moment will be:

$$M = E_c \alpha (\Delta\theta o - \Delta\theta¿) \left[\frac{t^3}{12} + (m-1) \frac{h^2}{t} As \right] \qquad (8)$$

Where E_c is the elastic modulus of concrete, m is the steel-concrete modular ratio and the remaining terms are defined in Figure 6.

The expression is similar to equation (2) with $(\Delta\theta_o - \Delta\theta¿)$ replacing ΔT and a term included to account for the reinforcing steel. There is no

Poisson ratio effect in this equation, as it is included in the method of measuring α. The equation can be modified for application to a cracked wall.

Reinforced concrete silos are usually designed for hoop tension, on the assumption of a fully cracked section. The contribution of the concrete to carrying tension is completely ignored. However, strain measurements on hoop reinforcing in reinforced concrete silos (e.g. Blight and Dreyer [17]) show that silos may have essentially uncracked walls even after a decade or more in continuous service. Hence it is by no means always incorrect to assume an uncracked section for this analysis, as the ACI [10] have done.

TEMPERATURE SURCHARGE PRESSURES IN REINFORCED CONCRETE SILOS

According to Figure 6, a silo wall subjected to differential temperatures at its inner and outer surfaces will undergo a mean strain

$$\frac{\alpha}{2}(\Delta\theta_i + \Delta\theta_o)$$

Hence if the mean temperature falls, the silo wall should experience a temperature surcharge pressure.

Figure 7 is a set of measurements made on the wall of a 24m diameter reinforced concrete cement storage silo [5,14] that illustrate the development of temperature surcharges in the silo. Temperatures were measured by means of thermocouples built into the silo walls and pressures by means of strain gauged diaphragm-type pressure cells set in the walls. The two sections of record shown in Figure 7 were made at times when the silo was full of cement, but not in use, so that the changes of pressure should be solely a result of diurnal thermal strains in the walls. The figure shows the development of temperature surcharge pressures very clearly, and the corresponding value of M_s is shown on Figure 5. This supports the validity of the assumptions that form the basis of Figure 6.

It should be noted that the average calculated hoop strain in the silo wall under the maximum measured horizontal pressure is less than 50 microstrain, based on the assumption of an uncracked section. Although

confirmatory measurements of strain have not been made, the wall is unlikely to be completely cracked although it has probably partly cracked, as explained below.

CHARACTERISTICS OF THERMAL BENDING

Figure 8 shows a set of measurements of strain in the outer hoop reinforcing of the 450mm thick reinforced concrete wall of a cement raw meal storage silo [18]. Strains were measured while filling the silo from empty, the temperature of the incoming raw meal being about 60°C. Filling was very rapid (average rate of surface rise 7.7 m/h) in order to achieve a measure of blending during filling. The various curves labelled 1423m, 1432m, etc represent changes of strain with time at the corresponding levels.

It was only after a year of service that the walls of this silo showed evidence of having cracked. It is likely that even at levels up to 1437m, the hoop reinforcing was not carrying the full ring tension when these measurements were made.

The fill level started at 1423m, hence the reinforcing at this level was affected by lateral pressure from time zero. Fill only reached the higher levels some time later, yet strain increases were registered immediately at all levels. Level 1437m for example had experienced a strain of 100 microstrain (tension) when the fill reached that level after 2.25 hours. This is clearly the effect of thermal bending, with the inner surface of the wall expanding and forcing the outer surface also to expand. Once the lateral pressure began to increase at that level, the characteristic of the curve changed and strains thereafter were caused by a combination of hoop tension and thermal bending.

Figure 9a shows a set of curves of temperature versus time on the inner and outer surfaces of the wall and 50mm in from the inner surface. Note particularly that the maximum temperature of the inner wall surface was reached when the fill first covered that point. Thereafter the surface began cooling. Figure 9b shows a set of temperature profiles through the wall. Early profiles are completely non linear, but later profiles (eg at 6 hours) approach linearity. Hence during the first 2 hours when

most of the thermal bending was occurring, only the inner 100mm or so of concrete had experienced an appreciable rise of temperature.

Figure 10 shows a set of temperature profiles through the 350mm thick reinforced concrete wall of a cement storage silo [14]. Here thermocouple junctions were positioned on the inner and outer surfaces of the wall and 100mm away from the inner surface in the storage space. A much slower rate of filling (about 0.5m/h) was being used, and the temperature profiles through the wall were probably approximately linear. The observations are similar in nature to those shown in Figure 9b, and show that the wall itself has a cooling effect on the fill adjacent to it that may amount to about 5°C. This is, on the face of it, a far more severe condition than that envisaged by the Australian Guidelines [2] which state, "it may be assumed that the inner surface of the bin wall reaches a temperature 20°C lower than the average temperature of the bulk solid". On the other hand, process engineers' estimates of product temperature generally seem to be too high. For example, in the cases dealt with in Figures 9 and 10 the estimated temperature of the air above the cement and the cement raw meal was 80°C as compared with a measured maximum temperature of 56°.

The maximum tensile strain induced by thermal bending will depend on the temperature difference across the wall. Taking $\alpha = 12 \times 10^{-6}$ per °C and the tensile fracture strain of concrete as 150×10^{-6}, the maximum temperature difference that could be tolerated without the concrete cracking on the cool side would be 25°C. Referring to Figures 9 and 10, it will be seen that in both cases, the concrete must either have cracked on the outside surface of the wall, or have been on the point of cracking.

CONCLUDING REMARKS

The object of the paper has been to inform the reader of some of the detail involved in the phenomena of temperature surcharge pressures, temperature effects on frictional wall loads and thermal bending. The guidance given by current codes of practice on these aspects is basically satisfactory when all advice is taken together. However,

there is a dearth of numerical data derived from measurements on full-scale silos. In some respects available laboratory data does not seem appropriate. Also, it is important to realize the uncertainties involved in estimating temperature-induced loads. It is also important to understand the mechanisms and characteristics of the load-producing phenomena.

REFERENCES

[1] Blight, G.E. (1990) Defects in accepted methods of estimating design loading for silos. Proc. Instn. Civ. Engrs, Part 1, 88, 1015-1036.

[2] Institution of Engineers Australia (1986) Guidelines for the assessment of loads on bulk solids containers. The Institution Melbourne.

[3] Andersen, P.F. (1966) Temperature stresses in steel grain storage tanks. Civil Engineering, ASCE 36 (1), 74.

[4] Padfield, C.J. and Sharrock, M.J. (1983). Settlement of structures on clay soils. CIRIA Special Publication 27, CIRIA, London, p41.

[5] Blight, G.E. (1990) Temperature surcharge pressures in reinforced concrete silos. Powder Handling and Processing 2 (4) 303-5.

[6] American Society of Agricultural Engineers (1989). Loads exerted by free-flowing grains on bins, ASAE Engineering Practice: ASAE EP433, St Joseph, Mo, USA.

[7] Marbeck, H.B. and Muzzelo, LM (1985) Thermally induced pressure in a model grain bin. Trans. Amer. Soc. Agric. Engrs. 28 (4), 1253-1258.

[8] Zhang, Q, Puri, VM, Marbeck, H.B. and Wang, MC (1987). Finite element model for predicting static and thermally induced bin wall pressures. Trans. Amer. Soc. Agric. Engrs 30 (6), 1797-1806.

[9] Deutches Institut Für Normung (1987). Lastannahmen für Bauten-Lasten in Silozellen. DIN Berlin, DIN 1055, Part 6.

[10] American Concrete Institute (1975). Recommended practice for design and construction of concrete bins, silos and bunkers for storing granular materials. Title 72-37. J. Am. Conc. Inst. Oct. 528-548.

[11] Blight, G.E. (1985). Temperature changes affect pressures in steel bins. Int. J. Bulk Solids Storage in Silos. 1(3) 1-7.

[12] Blight, G.E. (1990) Load and temperature strains of a welded plane plate grain silo. Powder Handling and Processing 2(1) 25-29.

[13] Blight, G.E. and Garstang, A. (1987). Strains measured in a 7500t sugar silo. Bulk Solids Handling, 8(4) 413-419.

[14] Fliss, L and Blight, G.E. (1986. A comparison of design and measured lateral pressures and temperatures in a large duo-cell cement storage silo. Int. J. Bulk Solids Storage in Silos, 2 (4) 18-28.

[15] Puri, V.M, Zhang, Q and Marbeck, HB (1986). Influence of granular material properties on thermally induced bin loads. Int. J. Bulk Solids Storage in Silos 2(3) 1-7.

[16] Blight, G.E. (1986) Swelling pressure of wetted grain. Bulk Solids Handling 6 (6) 1135-40.

[17] Blight, G.E. and Dreyer, H.N. (1989) Behaviour of a reinforced concrete coal silo under a design overload. Bulk Solids Handling 9(1) 21-25.

[18] Blight, G.E, Schaffner, R.H. and Gilbert, B. (1982) Strains in a reinforced concrete silo during rapid filling with a fine powder. J. Powder and Bulk Solids Technology 6 (2) 17-27.

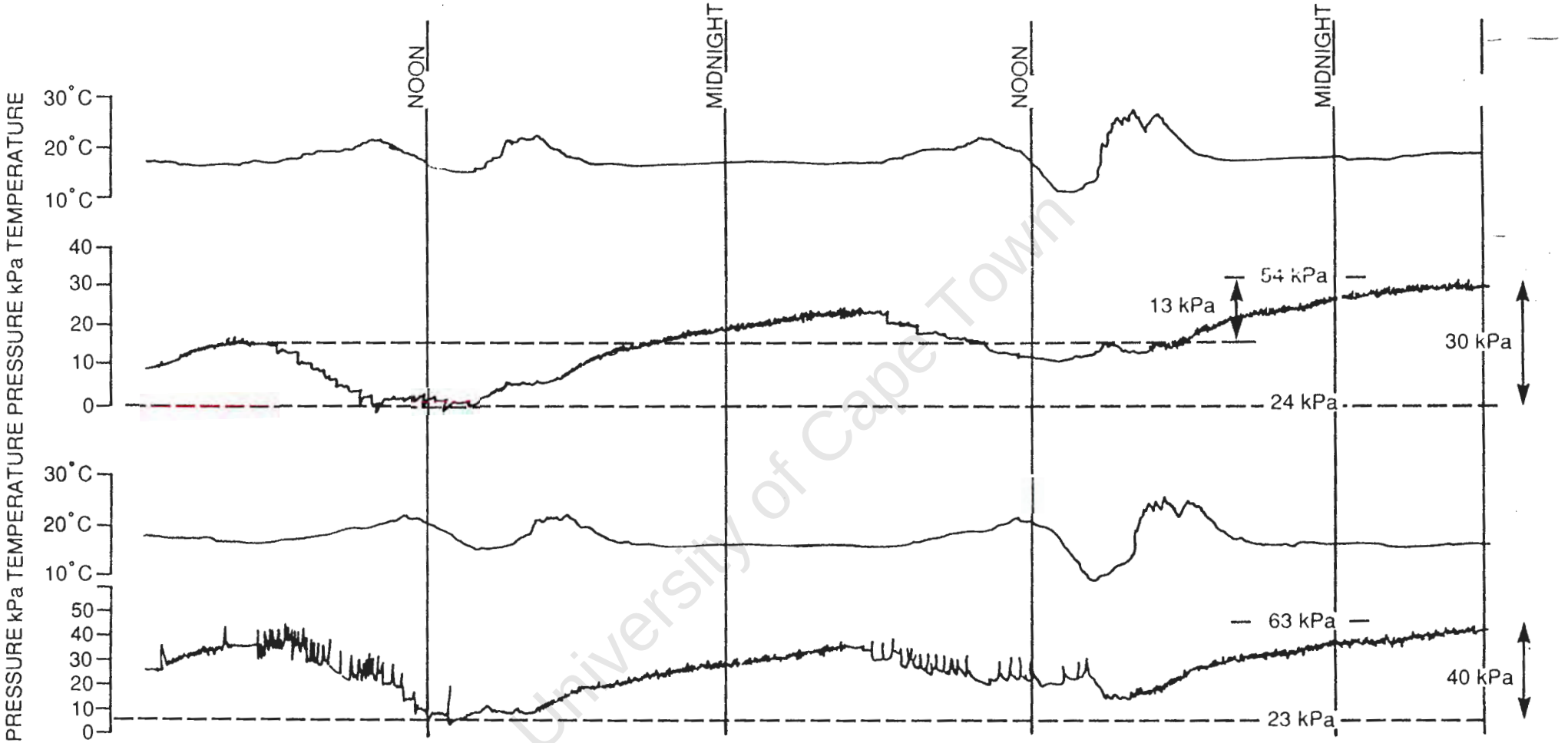

FIGURE 1: Development of temperature-induced loading in a 20m diameter steel silo storing maize.

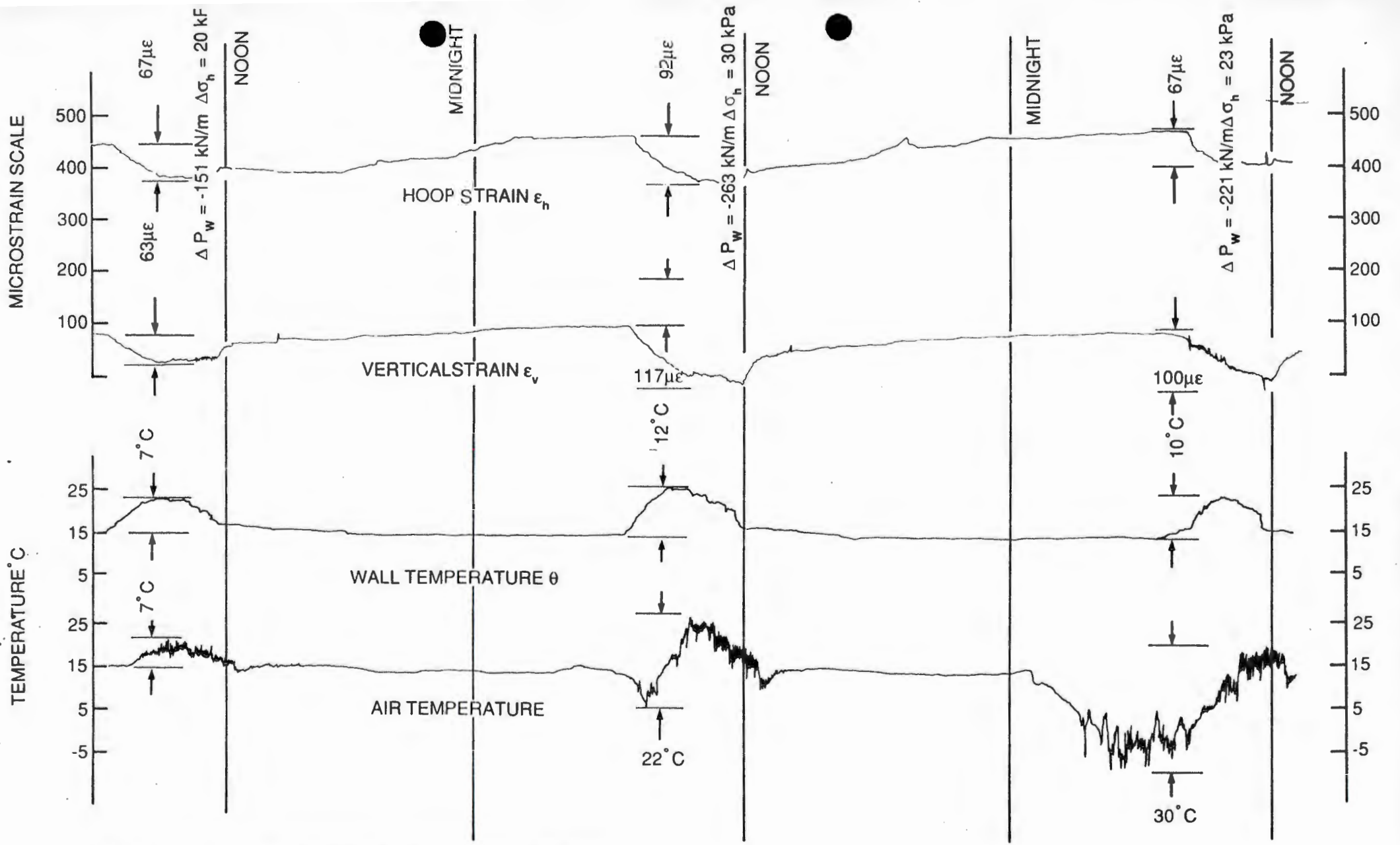

FIGURE 2: Strain and temperature measurements on the wall of a 15.5m diameter steel silo storing maize.

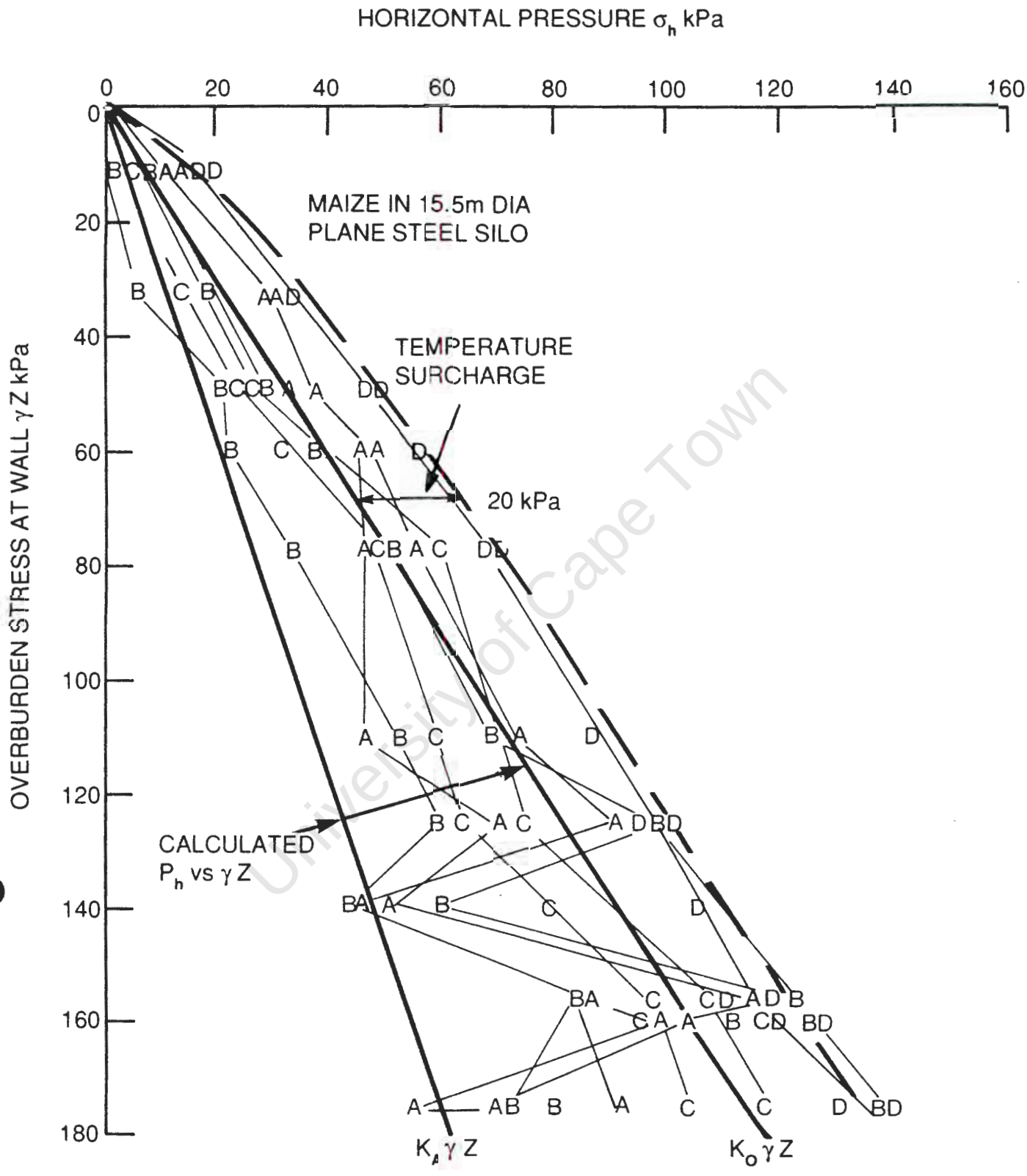

FIGURE 3a: Stress paths for lateral pressure in a 15.5m diameter steel silo storing maize.

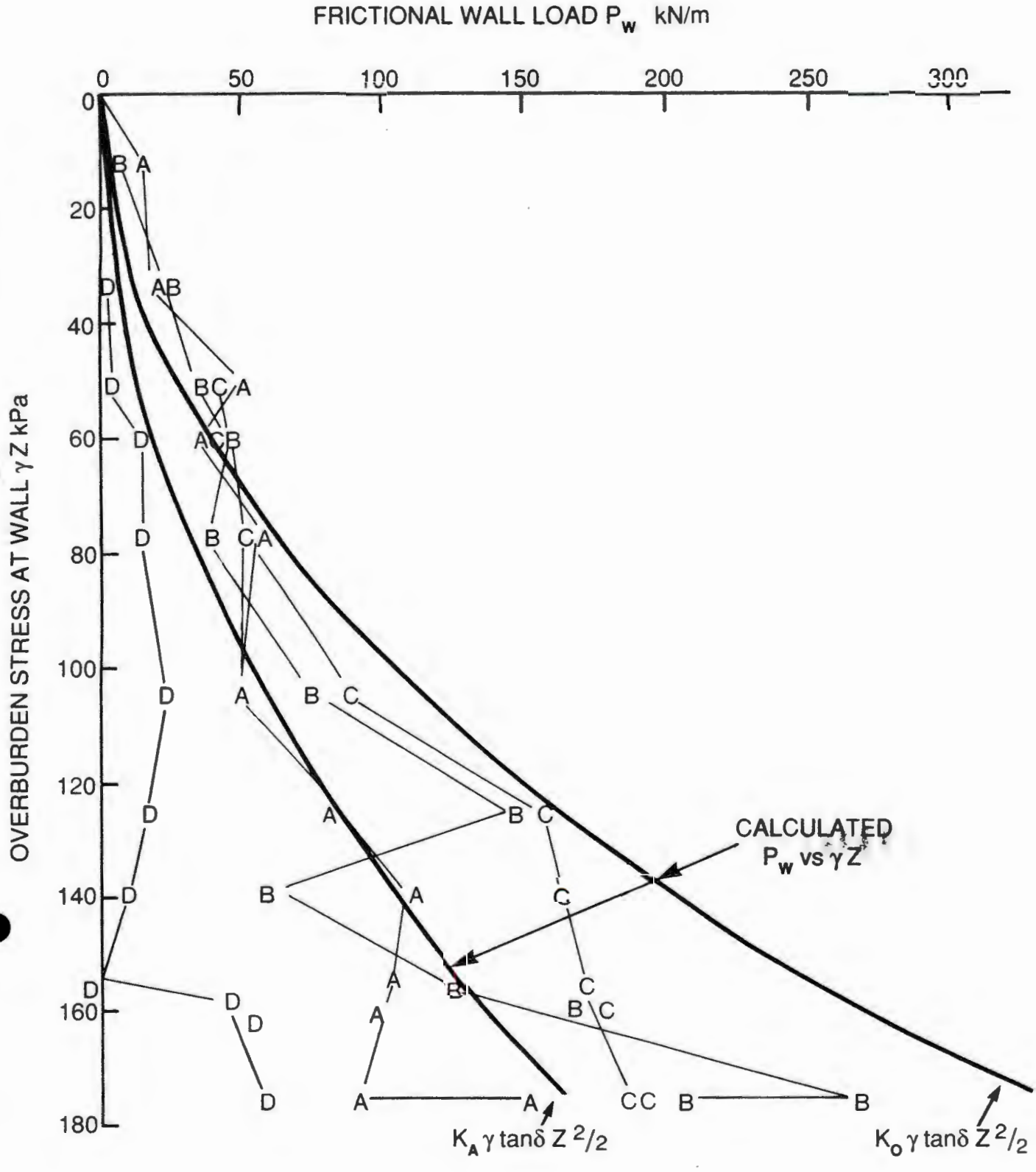

FIGURE 3b: Stress paths for frictional wall load in a 15.5m diameter steel silo storing maize.

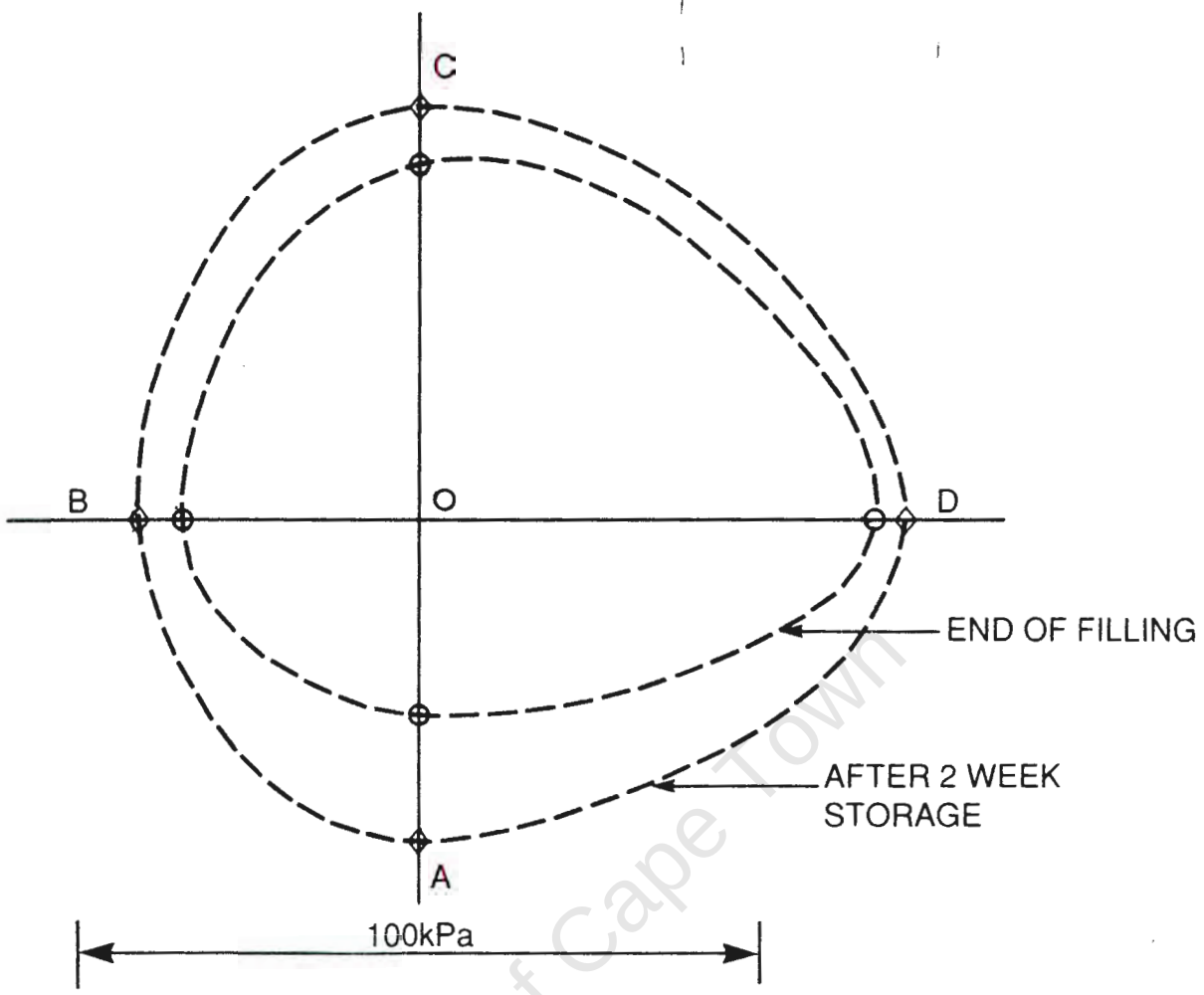

(a) RADIAL VARIATION OF INFERRED LATERAL PRESSURE.

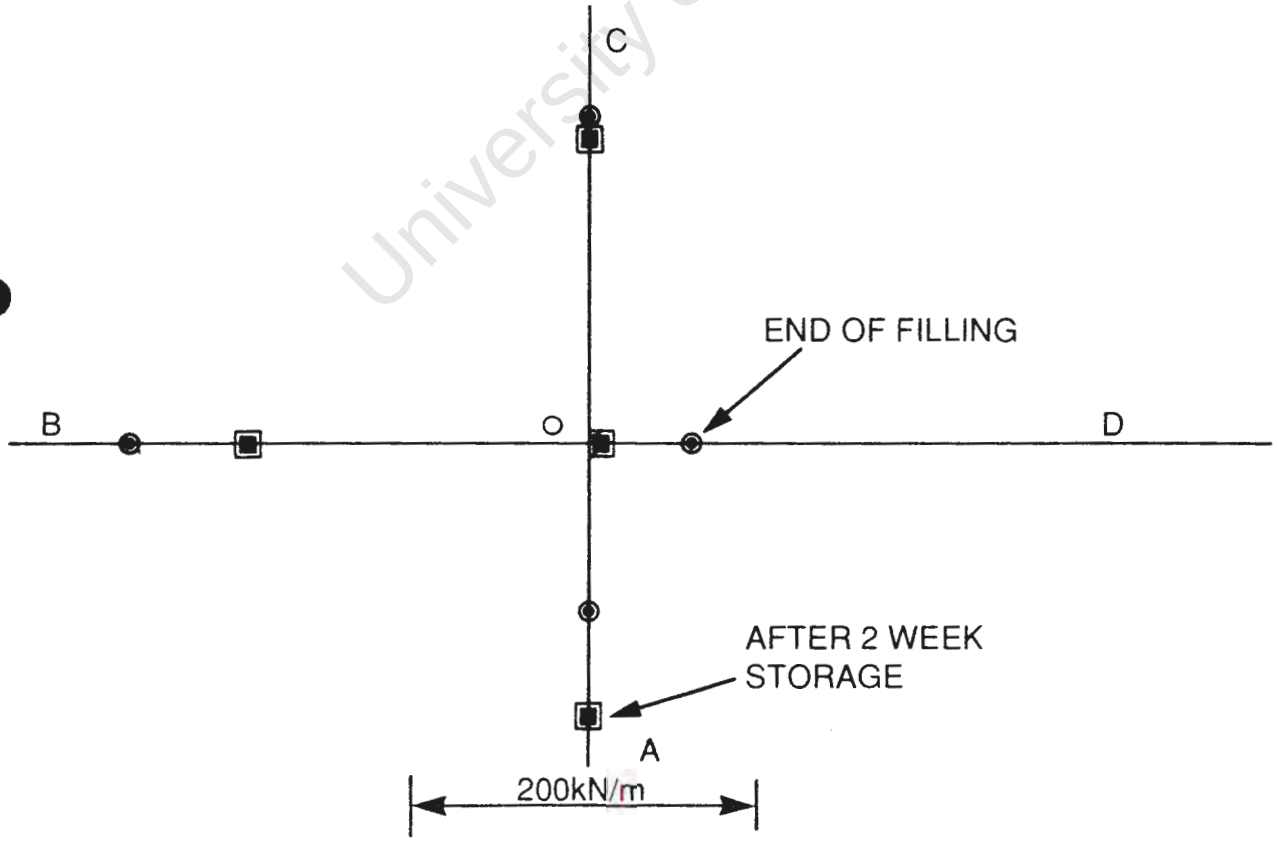

(b) RADIAL VARIATION OF INFERRED FRICTIONAL WALL LOAD

FIGURE 4

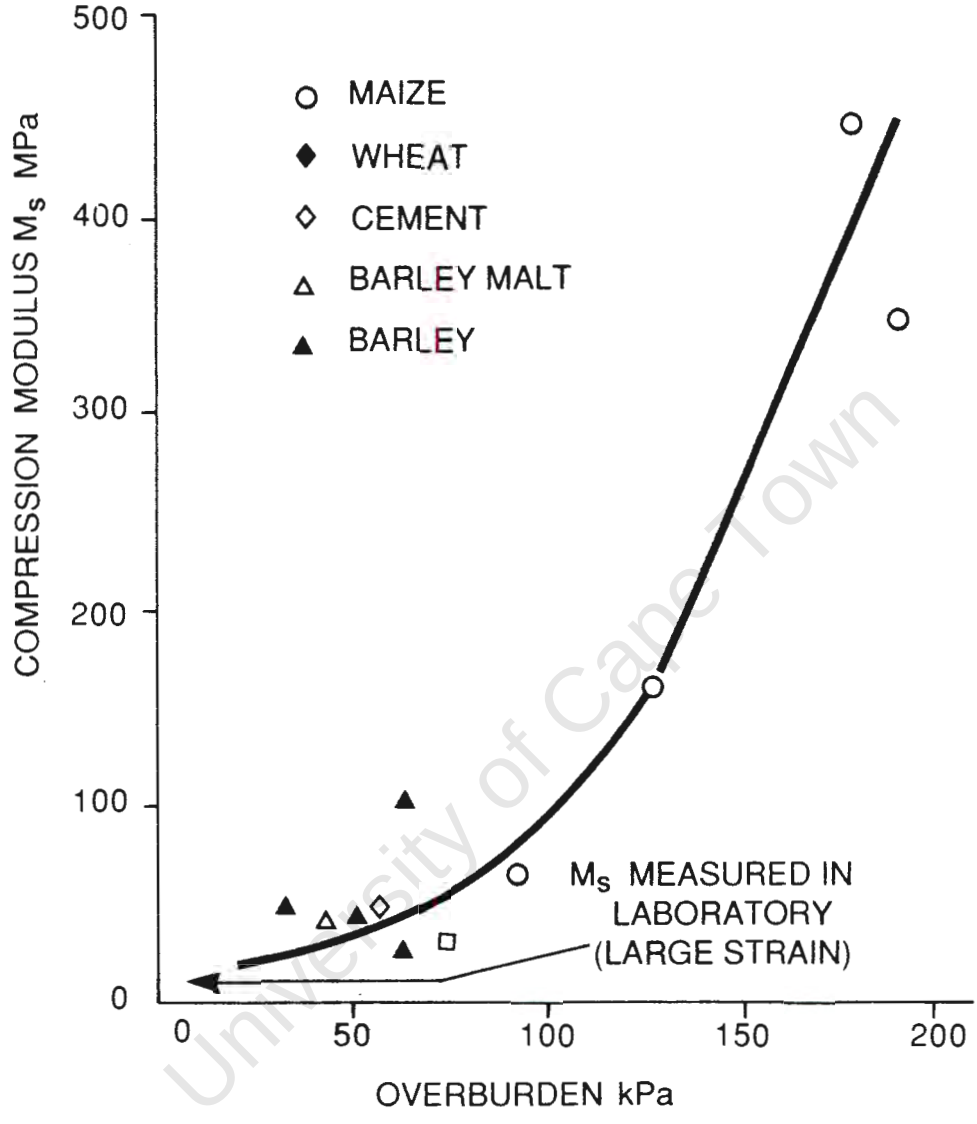

FIGURE 5: Relationship between compression modulus M and overburden stress calculated from measurements on 10 steel grain silos and a reinforced concrete cement silo

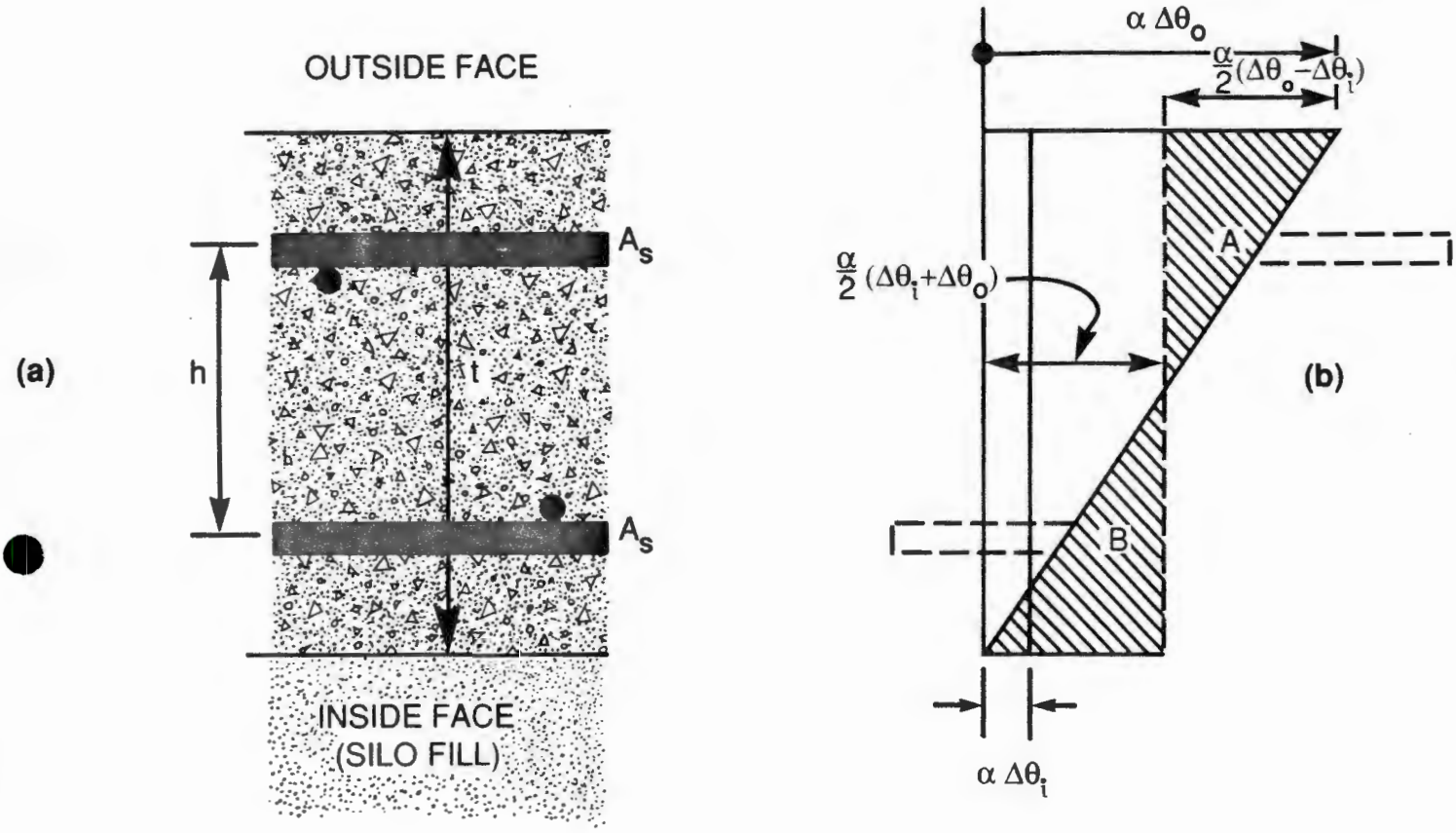

FIGURE 6: Thermal bending in reinforced concrete silo walls.

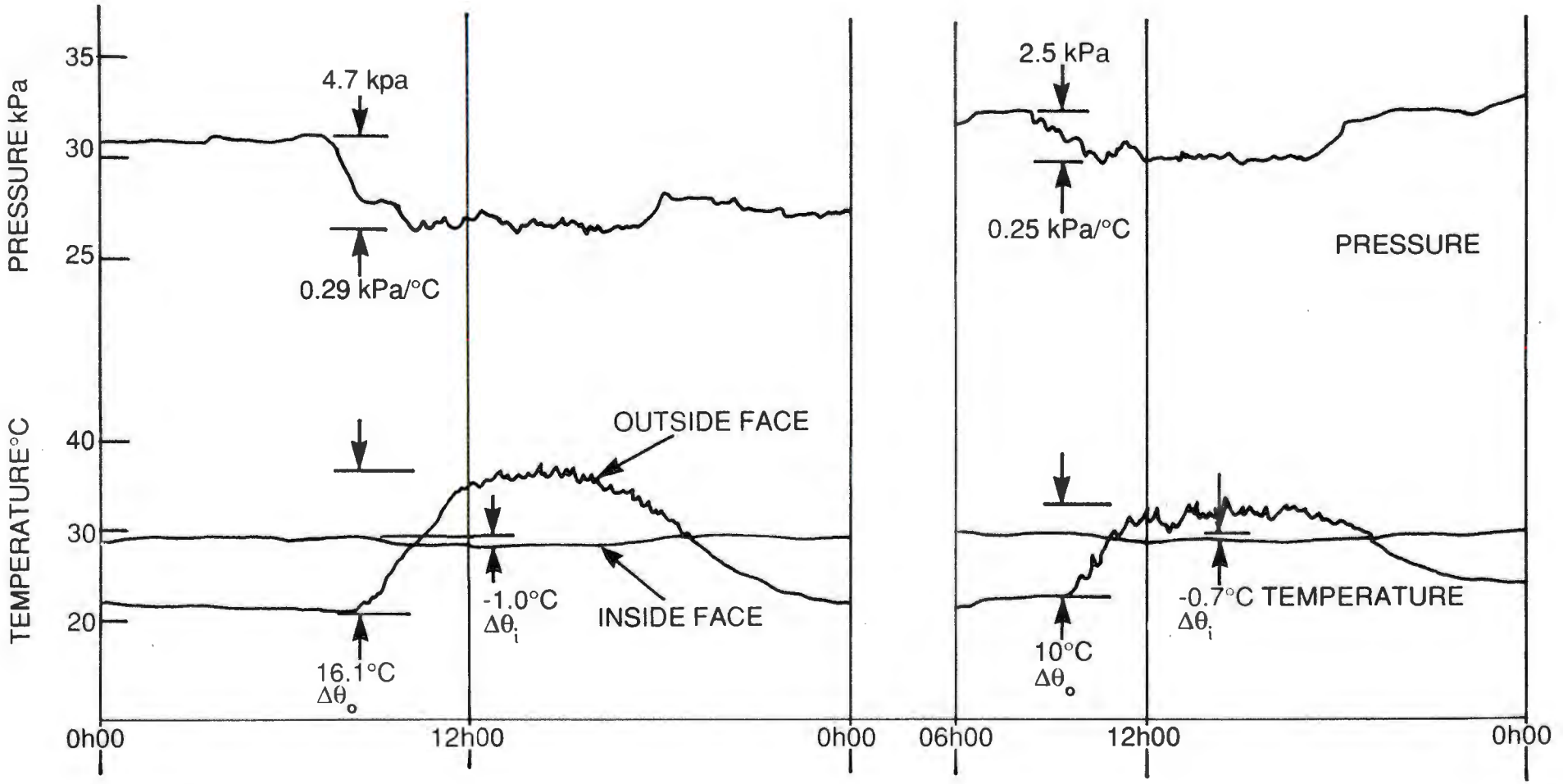

FIGURE 7: Temperature surcharge effect occuring in reinforced concrete wall of a cement storage silo.

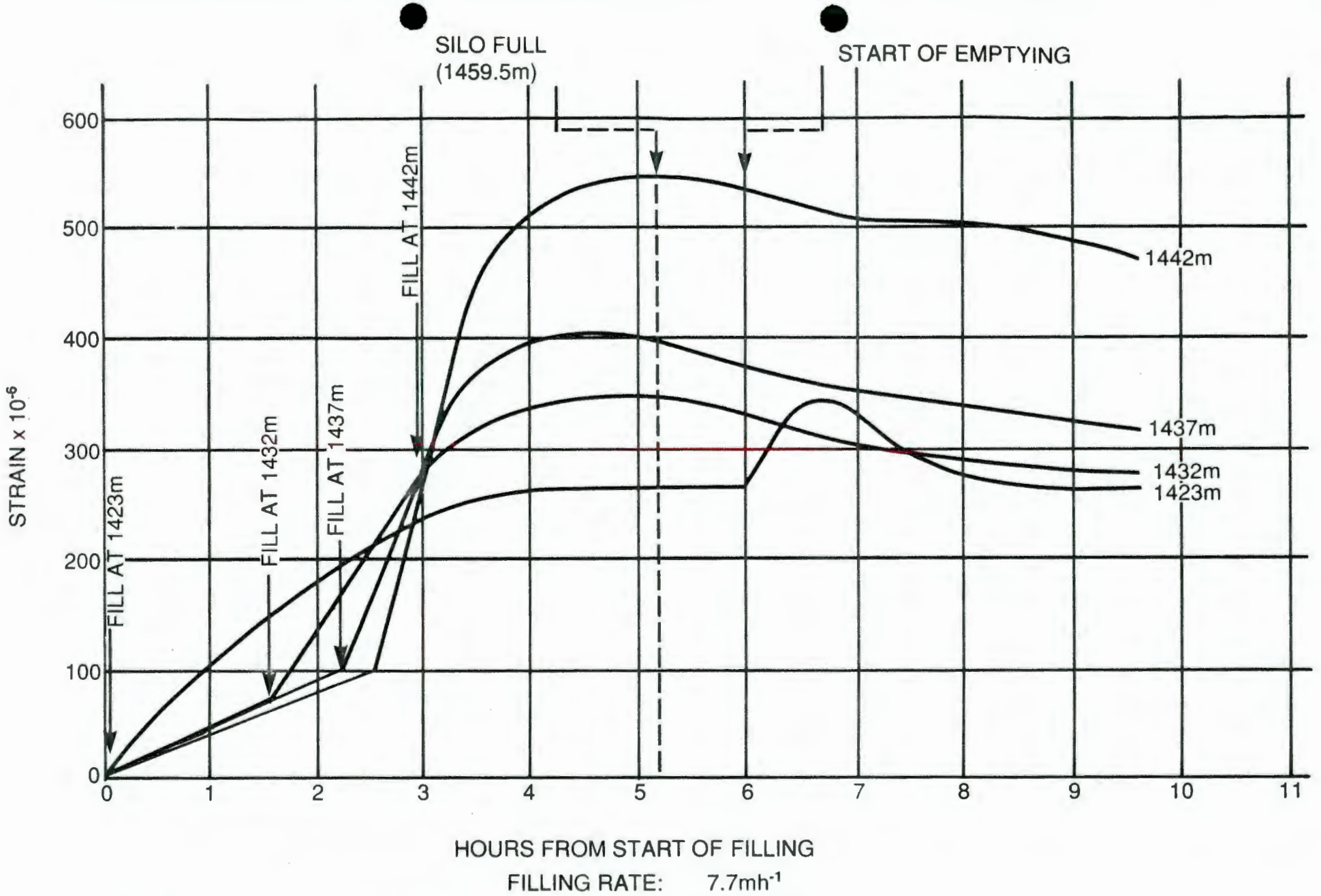

FIGURE 8: Measurements of strain in outer hoop reinforcing of 450mm thick reinforced concrete silo wall during filling with a hot powder.

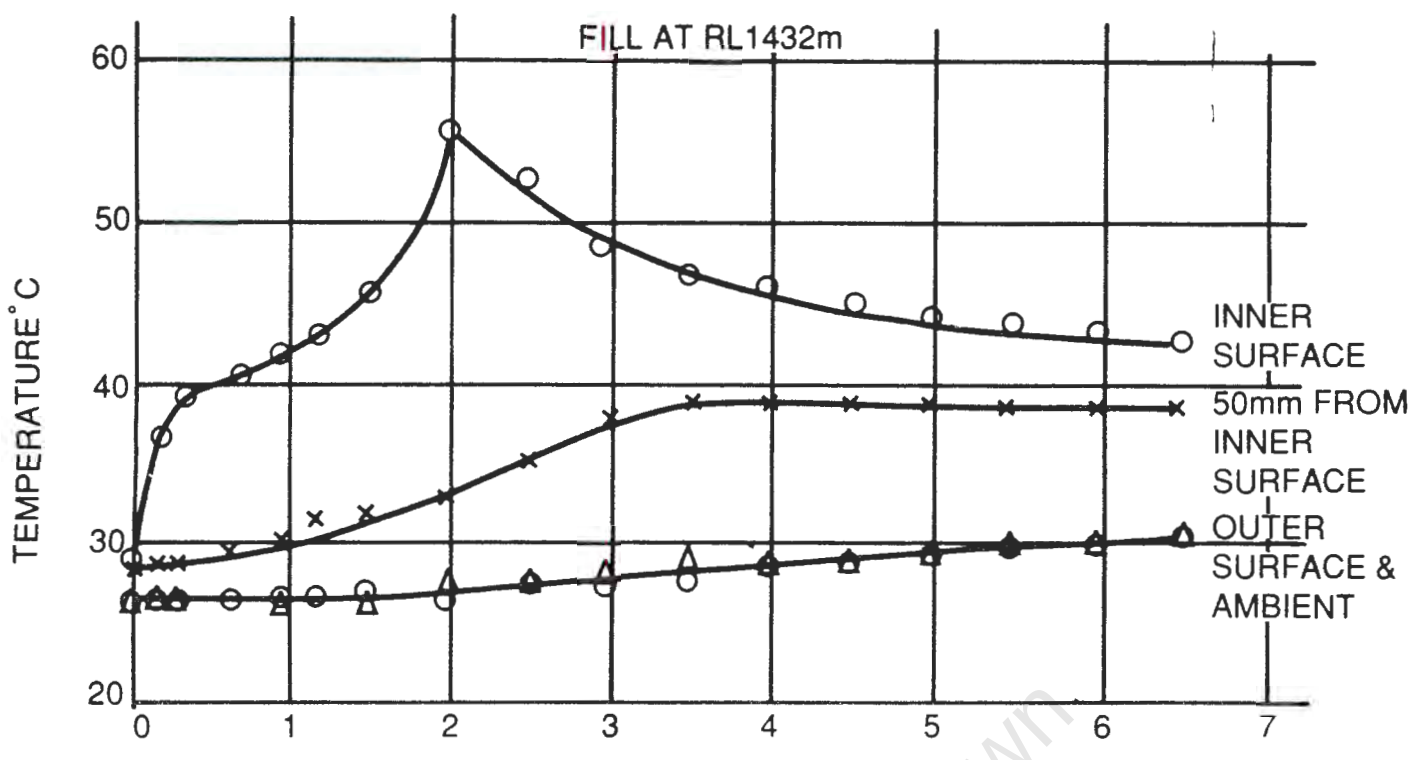

(a)

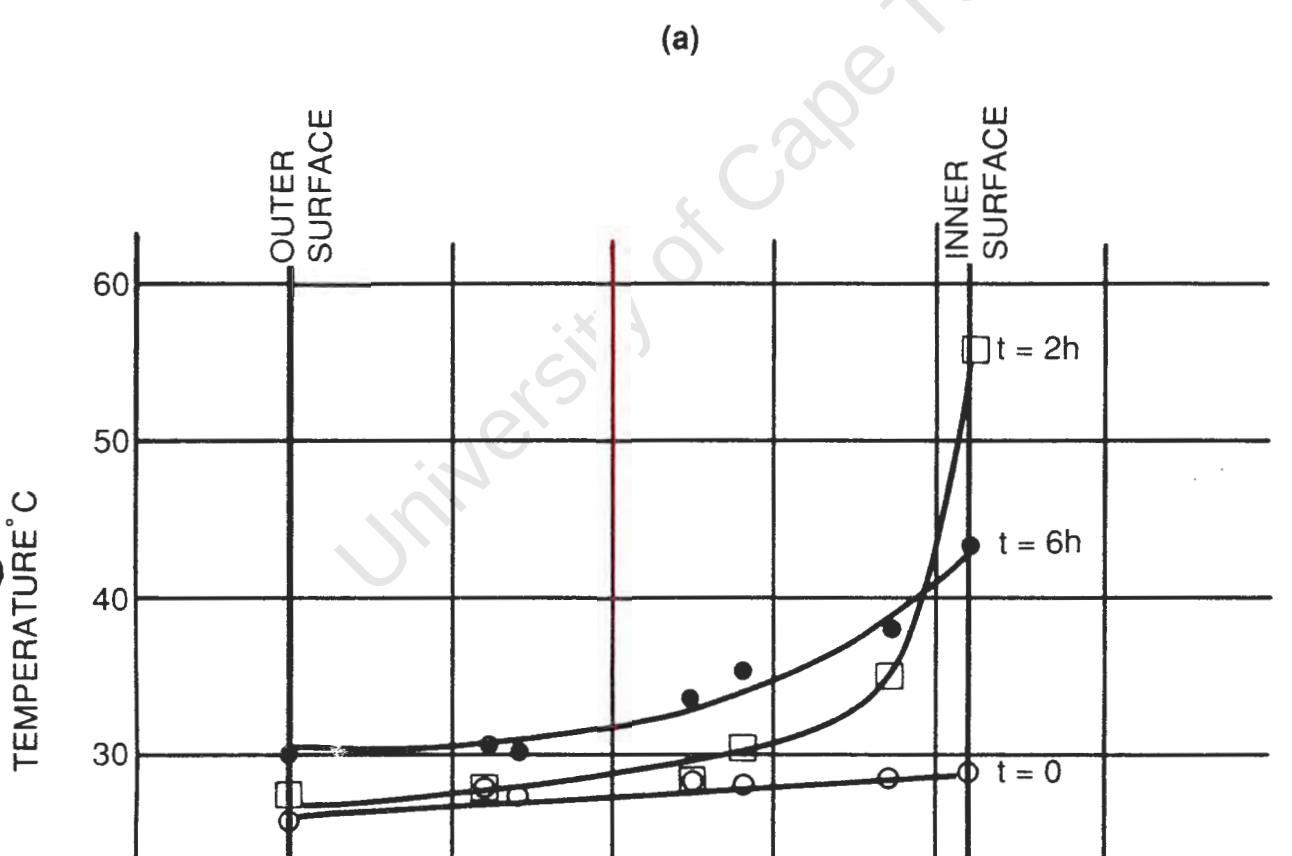

(b)

FIGURE 9: Results of temperature measurements in 425mm thick reinforced concrete silo wall during and after filling with a hot powder.

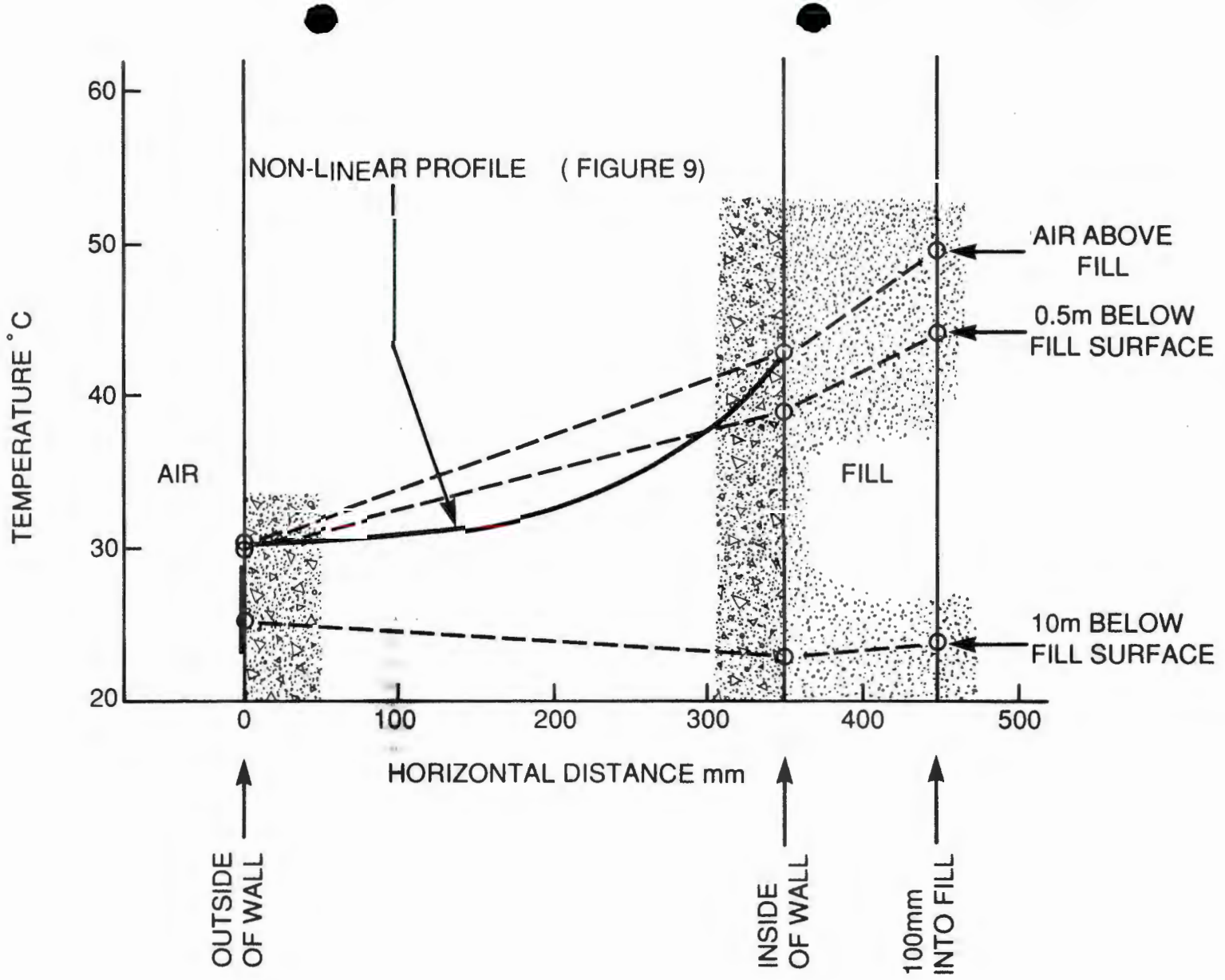

FIGURE 10: Observed temperature profiles through reinforced concrete wall of a cement storage silo filled with hot cement.

7.2 MEASUREMENT OF PRESSURES AND LOADS IN SILOS

CONTRIBUTION TO LEARNING

The two papers in this section summarize the experience built up in instrumenting sixteen full-size silos and storage structures. In particular, the system for installing pressure cells is probably unique.

In general, the techniques developed have resulted in robust, long lasting systems of instrumentation. Some of the strain gauges and thermocouples are fully operational 13 years after installation, while some of the pressure cells are in perfect order eight years after installation.

7.2 MEASUREMENT OF PRESSURES AND LOADS IN SILOS

7.2.1 Blight, G.E. (1987). Measurements on full size silos Part 1 : Temperatures and strains. Bulk Solids Handling, vol 7, No 6, pp 781-786.

7.2.2 Blight, G.E. and Bentel, G.M. (1988). Measurements on full size silos. Part 2 : Pressures. Bulk Solids Handling, vol 8, No 3, pp 343-346.

Dr G.M. Bentel was, at the time, a PhD student who developed the concept of the zero strain pressure cell under my supervision. I wrote the paper, and assess my contribution at 90%.

bulk solids handling Volume 7, Number 6, December 1987

Measurements on Full Size Silos
Part 1: Temperatures and Strains

G.E. Blight, South Africa

Summary

This first part of a two-part paper describes techniques developed for the use of thermocouples and electric resistance strain gauges for measuring temperatures and strains in the walls of full-scale silos, and hence estimating horizontal pressures and wall loads. The paper concentrates on the practicalities of installing instrumentation and on the problems of interpreting observations. Part 2 will treat the use of pressure cells for measuring pressures on the walls of silos.

1. Introduction

The interaction of containing structures and their granular contents has been studied on a rational basis at least since 1776 when Coulomb published his remarkable treatise on retaining walls. Nevertheless there are still many aspects of containment-filling interaction that either are not understood, or at best are understood empirically or imperfectly. Theoretical studies have made great advances in the field of containment-filling interaction especially since the advent of the finite element method. However, theory treats of ideal situations involving idealized structures, and fillings having simplified, idealized properties. Moreover all theory is based on preconceived ideas of structure-filling interaction, and therefore serves mainly to give mathematical expression to these preconceptions (which sometimes turn out to be misconceptions).

An alternative approach to the subject is to carry out measurements on model structures. The great difficulty in this approach is to scale the model correctly and to avoid having effects, that may be minor in the prototype, from having an over-riding effect on the behaviour of the model. For example the zone of interaction between a solid boundary such as a silo wall and a granular fill extends outwards from the wall to a distance of up to 300 mm. This zone is of negligible size in a prototype silo of 20 m diameter, but will affect almost the entire contents of a largish model of 1 m diameter which therefore cannot adequately represent the prototype. The combination of measurements on models that are too small and theory based on preconceptions drawn from model studies has led to belief in phenomena that just do not seem to occur in full-scale structures. For example, the concentrated dynamic switch pressures predicted by Jenike and Johanson [1] and their static overpressure counterpart predicted by Walker [2] appear to be confirmed by observations on models by Clague [3], Deutsch and Schmidt [4], Hartlen et al. [5], and others. Allowance for these predicted loads appears to have found its way into at least one silo design code in the form of the overpressure factors of the American Concrete Institute Code [6]. However, the fact is that neither dynamic switch pressures nor static overpressures appear ever to have been measured in full scale silos (Deutsch [7], Blight [8], [9]).

All of the above reasons make measurements on full-scale silos doubly important as a means of advancing our knowledge of silos and silo-fill interaction. Measurements of loads and pressures in full-scale silos are physically difficult and costly to perform — which accounts for the few sets of such measurements that have been published. The measurements themselves are fraught with difficulties and traps for the unwary that render questionable some of the few sets of measurements that do exist. The object of this paper is to describe some of the methods that have been successfully used to measure temperatures and strains in full-scale silos and hence to infer loads and pressures. Also, to point out some of the pitfalls and difficulties associated with such measurements. The types of measurements that will be described are:

(i) thermocouple measurements of temperature
(ii) measurements of strain on steel silos
(iii) measurements of strain on reinforced concrete and prestressed concrete silos.

Part 2 of this paper will describe the use of pressure cells to measure pressure in full-scale silos directly.

All of these types of measurements use well-established techniques and reasonably inexpensive, readily obtainable components. The skills required are not extraordinary, but there are certain commonsense rules to follow if reliable and dependable results are to be obtained.

2. Measurements of Temperature in the Walls and Contents of Silos

Thermocouples provide a simple, inexpensive, robust and long-lived method of measuring temperatures in the walls and contents of silos. The author has used copper-constantan thermocouples, usually with great success, but with a few notable failures.

Dr. G.E. Blight, Professor of Construction Materials, University of the Witwatersrand, Dept. of Civil Engineering, P.O. Wits, 2050 Johannesburg, Republic of South Africa

Reasonably stout wire of 0.5 to 1 mm diameter should be used. Insulation is usually of braided fibre glass. The most successful and simplest temperature-sensing junction is made simply by stripping the insulation from the wires over a length of about 20 mm and twisting the wires tightly together using pliers. Junctions of this form have never failed. Once, at the insistence of an electrical engineer, junctions were made by brazing the ends of the wires to a small brass disc. The failure rate for the thermocouples in this installation was 80%, presumably because the wires became detached from the disc during installation.

For steel silos, thermocouples can be installed simply by sticking the junction against the steel wall using aluminium-backed, bitumen-adhered sealing strip. Alternatively, a metal or plastic saddle held in place with small self-tapping screws can be used to clamp the junction against the silo wall. As steel is a good heat conductor, there is no need to worry about lateral or transverse temperature gradients local to the junction. The junction must be covered, however, or it will respond to rapid surface temperature fluctuations caused by the wind. The aluminium backing or whatever is used to cover the junction should preferably be painted the same colour as the surrounding silo wall to avoid differences in albedo.

For concrete silos there is usually an interest in measuring temperature gradients through the wall thickness. Hence thermocouples have to be installed at the inner and outer surfaces and possibly at intermediate points within the wall thickness. The simplest way of doing this is to drill or preform a hole (about 20 mm diameter) through the wall. The thermocouples are then taped in their correct relative positions along a wooden dowel stick which is pushed through the hole. The hole is then sealed by injecting a sand-cement grout or alternatively, a sand-epoxy resin grout. As the dowel is itself a good insulator, it may be left in the hole. If a single thermocouple is installed on the outside of a reinforced concrete silo, it is best to protect the junction from the wind by placing it in a shallow (5 mm deep) 3 mm diameter hole drilled in the wall. The hole is plugged with sand-cement or epoxy putty and the thermocouple wire is clamped in position by means of a saddle and steel nails.

The thermocouple wires are taken down the outside of the silo wall to a convenient reading position. It is important to protect the wires where they are exposed to the elements, otherwise the insulation deteriorates in the weather or gets abraded away as the wire is blown back and forth by the wind. If the exposed copper and constantan wires then touch at a point between the sensing junction and the measuring point, the recorded temperature will represent that at the point of touch, rather than that at the junction.

The thermocouples are read by means of a thermocouple bridge or an automatic data logger, or can be recorded continuously by means of a chart recorder. Thermocouples can easily be calibrated over the expected range of measurement by direct comparison with a mercury-in-glass thermometer.

An adequate and long-lasting labelling system for the wires is essential. Labels written or embossed on adhesive tape quickly become illegible. Tie-on labels come off and get lost. The best system, the author has found, consists of small, numbered plastic rings that slip over the wire. The numbers are pressed into the plastic and coloured black. Even if the black colouring should come off, the numbers remain easily readable. After threading on the label rings, a banana plug should be soldered to each wire. This provides a quick and easy means of connecting the wire to the read-out device and also positively retains the label rings.

Figs. 1, 2 and 3 show temperature profiles measured on full scale silos by means of thermocouples.

Fig. 1 (Blight, Schaffner and Gilbert [10], Schaffner and Blight [11]) shows a set of temperatures measured at various points in the thickness of the 450 mm wall of a 15 m diameter cement raw meal silo. The upper diagram shows the variation of temperatures with time as the silo was filled at a rate of 7.4 m of fill per hour. The temperature at the inner surface of the wall rose continuously until the raw meal covered the level at which the thermocouples were installed. Thereafter the temperatures at this point fell continuously while the temperature 50 mm in from the wall inner surface and that at the outside surface slowly rose as the temperature equalised through the wall. The lower diagram shows temperature profiles through the wall at various times. These measurements were taken at the same level, but at two points 30° of arc part on the silo circumference. They show the highly non-linear nature of the temperature profile as the silo was filled, changing to a more linear profile as time progressed.

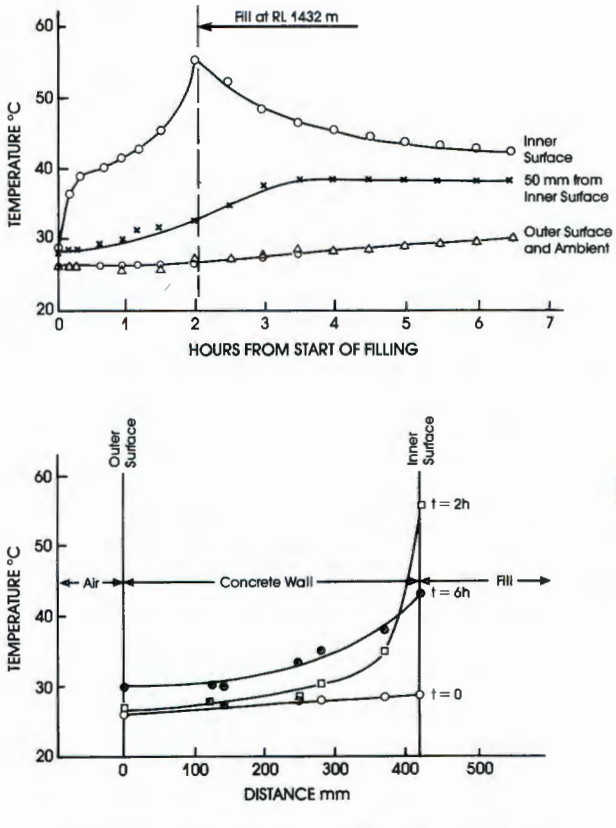

Fig. 1: Temperature measurements in the wall of a cement raw meal silo during filling

Fig. 2 (Fliss and Blight [12]) shows temperature profiles measured at various positions below the surface of the cement in a cement storage silo. In this case thermocouple junctions were positioned at the outer and inner surfaces of the wall and at 100 mm into the filling from the inner surface. These last junctions were housed in metal tubes that projected from the walls and into the filling.

Fig. 3 (also Fliss and Blight [12]) shows temperature profiles with depth in the same silo. Note that the greatest

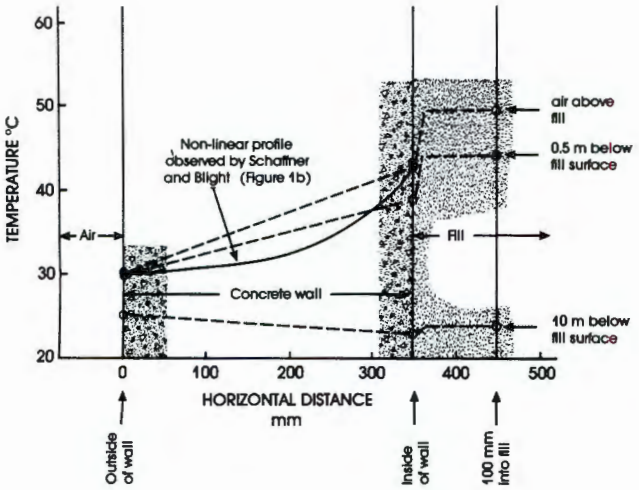

Fig. 2: Observed temperature profiles through the wall of a cement silo during filling

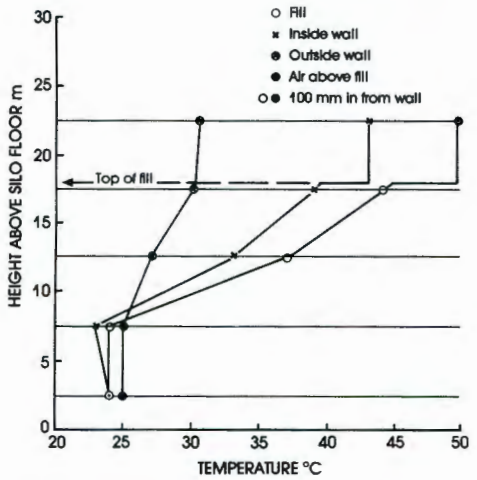

Fig. 3: Observed vertical profiles of temperature in a cement silo

temperature occurred in the air above the cement, while the wall also reached its greatest inside surface temperature above the level of the cement. As was the case with Fig. 1, the cement cooled progressively once it had been deposited in the silo.

Note that the maximum recorded temperature in Figs. 1, 2 and 3 was 55 °C. This was less than half of the 115 ° to 120 ° for which it had been believed necessary to design the silos.

Fig. 4 (Blight [14]) shows a continuous recording of the temperatures at a point on the shell of a steel silo. The figure shows corresponding records of horizontal pressure, and vertical and horizontal strain. It will be noted that the pressure rose as the temperature fell and the silo shell contracted onto the filling (of maize grain). This temperature contraction is shown by the decrease in horizontal strain as the temperature fell. The recorded vertical strain was opposite in sense to that of the horizontal strain i.e. the silo shell went into horizontal ring tension because its thermal contraction was partly prevented by the filling. The shell also went into vertical tension even though it was also tending to contract vertically as the temperature fell. The explanation of this apparent anomaly is that the temperature of the filling remained almost constant because of its large volume and thermal inertia. Its volume therefore remained almost constant. If therefore, the diametral temperature strain was $-\varepsilon$ (contraction), the vertical strain must have been given by:

$$\varepsilon_v - 2\varepsilon = 0$$

$$\varepsilon_v = +2\varepsilon \quad \text{(expansion)}$$

in order for the volumetric strain to remain at zero. In other words, the filling dragged the wall upwards by wall friction. It is important to note that these observations were made while the silo was not in use, so that changes in load-associated strains were eliminated.

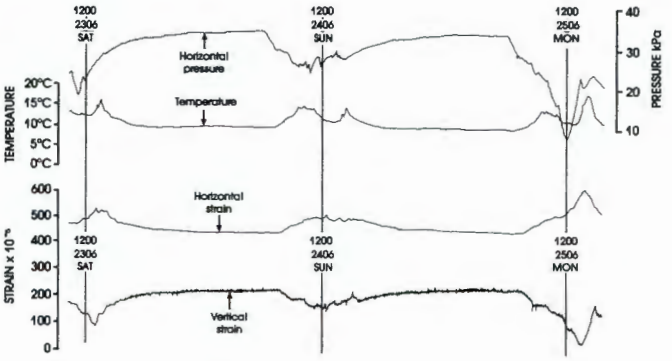

Fig. 4: Continuous record of temperature, strain and horizontal pressure in a steel maize silo

3. Measurement of Strains in Steel Silos

As steel approximates to an elastic isotropic material with clearly defined and constant elastic parameters at working stress, strains measured on a steel silo shell may be used to calculate stresses and hence horizontal hoop tensions and vertical wall loads.

Because of the difficulty of access, gauges that can be read out remotely, such as electric resistance strain gauges are preferable to gauges requiring direct access, such as the demountable demec type.

Ideally, strain gauge rosettes should be used, measuring strains in three known directions. As one is mainly interested in evaluating stresses in horizontal and vertical directions, and because these directions approximately coincide with the principal strain directions in a silo shell, rosettes consisting of a vertical and a horizontal gauge on a common backing are usually adequate.

The author has had good results from electric resistance strain gauges applied directly to the bared steel. Each pair of gauges is read in conjunction with a temperature compensating dummy gauge mounted on a small separate steel plate. This is attached to the silo by means of adhesive foam strips so that it remains stress-free. The gauges are waterproofed with a rubber solution (sold for repairing shoes) and each set of gauges is protected by a small sheet metal cover, also attached to the silo with adhesive foam strips. Various other waterproofers have also been tried, but with less success. Silicone rubber must be avoided as it contains acetic acid that attacks the steel and loosens the gauges. Two component polysulphide rubber has also been used. This works well as a waterproofer, but is difficult to apply and inconvenient to mix.

Connecting wires from the strain gauges are lead to a central reading point where they are labeled and provided with banana plugs, as described earlier.

To read the gauges, each is connected as a half bridge with its dummy gauge. Strains may be read statically using a strain bridge or data logger. Dynamic strains may be recorded by means of an ultra-violet (UV) recorder or a pen recorder if the recorder's dynamic response is sufficiently rapid.

Newly applied electric resistance strain gauges give variable stress-free or zero readings for about three weeks as the solvent in the waterproofing evaporates and the backing strip to the gauge "settles down". After this, zero readings remain stable to within a few tens of microstrain over periods of up to six months. It is, however, always advisable to use electric resistance strain gauges in a situation where the zero readings can be checked at regular intervals, e.g. where a silo is regularly emptied, cleaned and then re-filled (see e.g. Blight and Garstang [14]).

Interpretation of gauge readings as stress changes may be made by applying the generalized equations of elasticity. The vertical and horizontal strains can be interpreted in terms of stress, as follows:

If ε_v and ε_h are the measured vertical and horizontal strains and σ_v and σ_h the corresponding vertical and horizontal stresses in the silo plate, then:

$$\sigma_v = E(\varepsilon_v + \upsilon\varepsilon_h)/(1-\upsilon^2)$$

$$\sigma_h = E(\varepsilon_h + \upsilon\varepsilon_v)/(1-\upsilon^2)$$

where E is the elastic modulus of steel, taken as 200 GPa and υ is Poisson's ratio, taken as 0.33.

The wall load per unit of silo circumference is then calculated as

$$P_w = \sigma_v t$$

where t is the plate thickness, and the equivalent horizontal pressure exerted on the silo wall by the filling as

$$P_h = 2\sigma_h t/D$$

where D is the diameter of the silo shell.

If the strain gauges are fully temperature-compensated, stress-free strains resulting from a change of temperature will not be recorded. If the temperature strain is partly restrained, the restrained portion of the total temperature strain will be recorded, i.e. the gauge set will record the difference between the stress-free temperature strain of the dummy gauge and the actual temperature strain of the structure. For example, the strains recorded in Fig. 4 are the stress-inducing temperature strains in the structure. Because of the existence of stress-inducing temperature strains, it is important to measure and record any changes of temperature that occur as a structure is loaded. Even then, it is usually difficult to differentiate between load-induced and temperature-induced strains.

Ideal situations for strain gauge observations exist where rapid filling with a "cold" material occurs so that temperature changes during the loading period are negligible. Another ideal situation exists if the silo is insulated against temperature change. An example of observations made on an insulated silo is given in Fig. 5 (Blight and Garstang [14]). Here a 7,500 ton 20 m diameter steel sugar silo is insulated with 100 mm of polyurethane foam within an outer cladding of aluminium sheeting. Fig. 5 shows the strain measurements interpreted as the variation of equivalent horizontal pressure and vertical wall load at three corresponding points, each 90° of arc apart and on the same level, as the silo was filled with sugar from empty. The equivalent horizontal pressure, i.e. that calculated from the inferred hoop stress at the points of measurement, increased steadily as the level of sugar rose, while the wall load also increased in reasonable accordance with the theoretical relationship based on the hoop stress. Once the calculated overburden exceeded 140 kPa, the wall load appeared to reduce, apparently as a result of a reduction of friction on the wall. The horizontal pressure increased in sympathy, exactly as would have been anticipated on theoretical grounds.

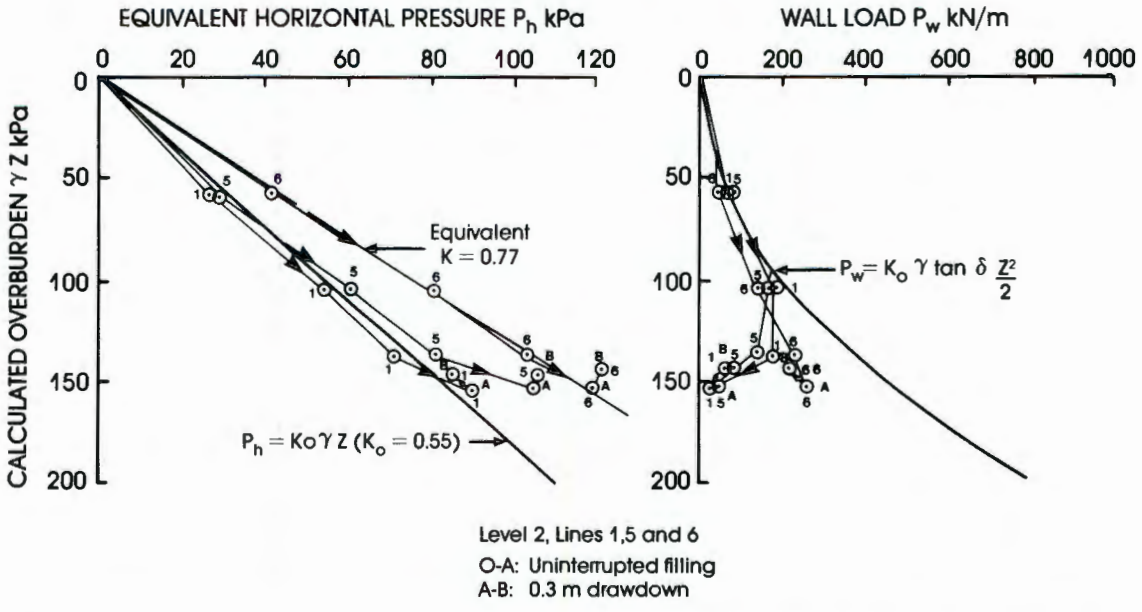

Fig. 5: Build-up of equivalent horizontal pressure and wall load at 3 points on the same level in a sugar silo during filling (assumed γ = 8.6 kN/m³)

4. Measurement of Strains in Reinforced Concrete Silos

When a newly contructed reinforced concrete silo is filled for the first time, the hoop stress is carried partly in tension on the concrete and partly on the hoop steel reinforcing. Over the first few months of service, tensile creep fracture of the concrete gradually occurs, and the hoop load in the concrete of the silo wall is progressively transferred to the reinforcing. There is therefore no point in measuring tensile strains on the concrete, and even tensile strains on the hoop reinforcing are impossible to interpret at first, as there is no way of knowing how the total hoop load is shared between the steel and the partially cracked concrete.

Vertical strains in a concrete silo wall are always small, as the wall remains in compression in a vertical direction and the steel and concrete share the load as a composite section. After about a year of service, the hoop load will have been fully transferred to the steel, and hoop strains then become interpretable in terms of horizontal pressure on the silo wall.

At this stage, hoop strain in the concrete will have become negligible.

The process of transfer of load from concrete to steel as the concrete progressively cracks is illustrated in Fig. 6. The figure shows the results of a tension test on a 150 mm square concrete prism 800 mm long reinforced with a single axial 12 mm diameter steel reinforcing rod. Both the rod and the concrete surface were strain-gauged at 100 mm intervals. The rod was subjected to an axial load and strains in the concrete and steel were observed. At a load of 15 kN (a) strains in both steel and concrete were identical over the central 500 mm length of specimen which was acting as a composite section and sharing the load between steel and concrete. At the ends of the specimen, the concrete strain was zero and over the initial 100 mm to 200 mm of length at either end, bond between steel and concrete was in the process of distributing the load between the two materials.

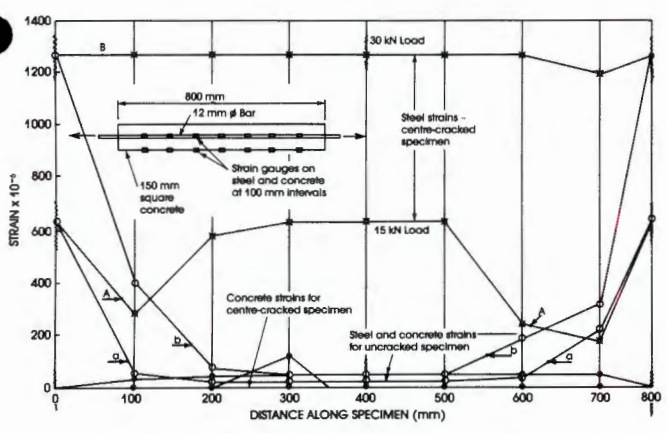

Fig. 6: Effect of cracking and crack spacing on strains in concrete and steel

When the load was increased to 30 kN, a similar strain pattern applied (b) except that the length of the distribution zones increased by about 100 mm. To break the steel-concrete bond, the specimen was then deliberately cracked transversely at its centre by bending it, and the axial loading repeated. The result was that the concrete strains reduced to zero and all of the load was then carried on the steel (*A* and *B*).

Fig. 7 shows how the process of progressive local transfer from the concrete to the steel occurs in a full scale silo. The silo was the 15 m diameter cement raw meal silo referred to earlier (Blight, Schaffner and Gilbert [10]. Fig. 7a shows strains measured on the hoop reinforcing at various levels as the silo was filled for the first time in August 1976. The strains were quite small, and only at level 1,423 m did they approach the cracking strain of concrete (150 to 200 microstrain).

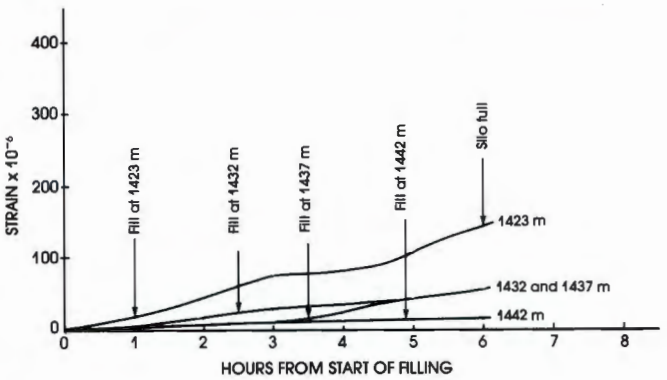

Fig. 7a: Strains measured on first filling of reinforced concrete cement raw meal silo, August 1976.
Filling rates: 0 to 2 1/2 h : 7,3 mh⁻¹
3 to 6 h : 4,3 mh⁻¹
Strains are small as the hoop load is carried on the uncracked wall section

Fig. 7b shows similar measurements taken in August 1977 when the picture was completely different with strains at all the levels of measurement going well above the cracking strain of concrete. At this stage the silo wall had a cracked section, and the hoop load had been transferred to the hoop reinforcing.

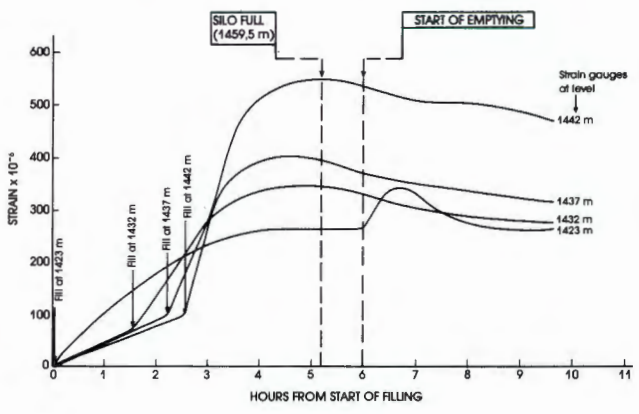

Fig. 7b: Strains measured a year later in August 1977.
Filling rate: 7,7 mh⁻¹
Strains have increased as the concrete has cracked and the hoop steel now carries all the hoop load

The problem of separating restrained temperature strains from load-induced strains arose with the measurements shown in Fig. 7b. It will be noted that strains were observed at various levels before the fill reached that level. The reason for this was that the hoop reinforcing on which the measurements were being made was located 100 mm from the outside of the 450 mm thick wall. As shown in Fig. 1, there was

a very considerable temperature gradient through the wall and the expansion of the concrete on the inside of the wall was inducing tensile strains in the hoop reinforcing on the outside. These were true load-induced strains with the load arising from the restraint of the expansion. However, they were not related to the load of the filling on the wall and had to be separated out.

Fig. 8 illustrates the basis used for correcting for temperature-induced strains:

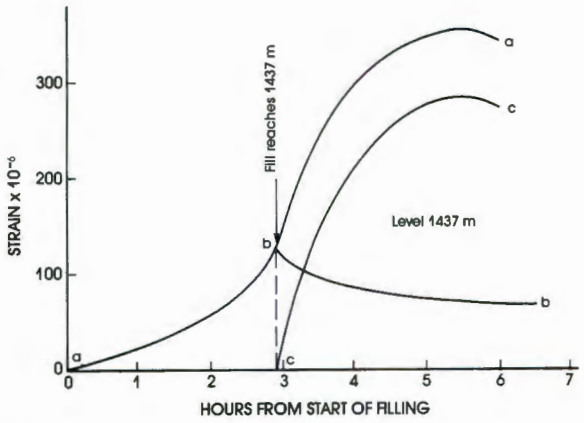

Fig. 8: Correcting observed strains for temperature

aba represents the variation with time of (temperature + load) induced strain. *abb* represents the temperature-induced strain which was known to reach a maximum when the fill reached the level of measurement and to then decline as the temperature gradient evened out, as seen in Fig. 1.

The value of the temperature-induced strain at a time of 6 hours could be calculated as the restrained temperature strain at the position of the hoop reinforcing at this time. The load-induced strain was then represented by the difference between the above two curves, i.e. curve *cc*.

5. Measurement of Strains in Prestressed Concrete Silos

Short term measurements of strain in prestressed concrete silos should be feasible as, on a short term basis, prestressed concrete should behave as an elastic material. Long term measurements would not be feasible because of the difficulty of allowing for the effects of creep, shrinkage and relaxation. The main difficulty in interpreting the strain measurements in terms of stress or load arises from the need to estimate the elastic modulus of concrete. In one attempt to do this (Wolf [15]), the elastic modulus of concrete was estimated by means of Schmidt hammer tests made on the outside of the silo. It is quite unlikely that such a measurement would give a reliable indication of the elastic modulus of the stressed concrete in the direction in which the strains were measured. It would have been better, but still not adequate to have cored the walls and measured the elastic properties of the cores.

6. Concluding Remarks

This paper has described the techniques developed and used by the author and his colleagues over the past 15 years for measuring temperatures and strains in full-scale silos. During this period, eleven full-scale containment structures have been instrumented and observed. Many mistakes have been made and much has been learned the hard way from these mistakes. It is hoped that sharing this experience with the profession will encourage others to follow, so adding to our pool of knowledge and increasing our ability to design silos with confidence.

References

[1] Jenike, A.W., and Johanson, J.R.: On the theory of bin loads. — Journal of Engineering for Industry, ASME, May 1969, pp. 339—344.

[2] Walker, D.M.: An approximate theory for pressures and arching in hoppers. — Chemical Engineering Science, Vol. 21, 1966, pp. 975—997.

[3] Clague, K.: The effects of stress in bunkers. — PhD Thesis, University of Nottingham, 1973.

[4] Deutsch, G.P., and Schmidt, L.C.: Pressures on silo walls. — Journal of Engineering for Industry, ASME, October, 1968, pp. 1—8.

[5] Hartlén, J., Nielsen, J., et al.: The wall pressure in large grain silos. — Swedish Council for Building Research, Document D2:1984.

[6] American Concrete Institute Committee 313: Recommended practice for design and construction of concrete bins, silos and bunkers for storing granular materials. — Journal of the American Concrete Institute, Vol. 71, 1975, pp. 529—565.

[7] Deutsch, G.P.: Discussion. — Session 5, International Conference on Design of Silos for strength and flow, Vol. 2, University of Lancaster, U.K., 1980.

[8] Blight, G.E.: Pressures exerted by materials stored in silos. — Geotechnique, Vol. 36 (1986) 1, pp. 33—46.

[9] Blight, G.E.: A comparison of design and measured pressures in a large coal load load-out silo. — International Journal for Bulk Solids Storage in Silos, Vol. 2 (1986) 2, pp. 1—8.

[10] Blight, G.E., Schaffner, R.H., and Gilbert, B.: Strains in a reinforced concrete silo during rapid filling with a fine powder. — Journal of Powder and Bulk Solids Technology, Vol. 6 (1982), 2, pp. 17—27.

[11] Schaffner, R.H., and Blight, G.E.: Comparison of design assumptions and measured performance for cement works silos. — Proceedings 2nd International Conference on Design of Silos for Strength and Flow, Stratford-on-Avon, U.K., 1983, Vol. 1, pp. 207—216.

[12] Fliss, L., and Blight, G.E.: A comparison of design and measured lateral pressures and temperatures in a large duo-cell cement storage silo. — International Journal for Bulk Solids Storage in Silos, Vol. 2 (1986) 4, pp. 18—28.

[13] Blight, G.E.: Temperature changes affect pressure in steel bins. — International Journal for Bulk Solids Storage in Silos, Vol. 1 (1985) 3, pp. 1—7.

[14] Blight, G.E., and Garstang, A.: Strains measured in a 7,500 ton sugar silo. — bulk solids handling Vol. 7 (1987) 4, pp. 573—582.

[15] Wolf, K.: Messungen an einem Zementsilo in Lägerdorf. — Dr.-Ing. Thesis, Technical University of Brunswick, 1984.

bulk solids handling Volume 8, Number 3, June 1988

Measurements on Full Size Silos

Part 2: Pressures *

G.E. Blight and G.M. Bentel, South Africa

Summary

This second part of a two-part paper describes the factors affecting the performance of pressure cells used for measuring pressures in silos. It also describes the techniques developed for installing such cells in full-scale silos. Finally, a new development, the zero strain cell is described.

1. Introduction

Part 1 of this two-part paper described the use of thermocouples to measure temperatures in the walls and filling of silos, and electric resistance strain gauges to measure strains. Some of the difficulties of interpreting measured strains in terms of corresponding loads and pressures were also described.

Measured strains have the great advantage of giving a direct check on the structural adequacy of a silo. Also, the materials required for strain gauging a structure are relatively inexpensive. However, if the aim of the instrumentation is to check the design loading against the loads actually experienced by the structure, it may be preferable to measure the pressure normal to the silo walls by means of pressure cells. The use of pressure cells requires a considerable amount of pre-planning. Provision must, for example, be made to build them into the silo walls. It quite often happens that the decision to make measurements takes place when the structure has been partly built, or is in service. In these cases, strain gauging is much easier to carry out than installing pressure cells.

This paper will describe the major requirements of a successful pressure cell installation, as well as techniques evolved to install pressure cells. It will also introduce the principle of the zero strain pressure cell and give examples of this type of cell's performance.

2. Factors Affecting the Performance of Pressure Cells

A pressure cell forms part of the silo wall. If it is to register pressures absolutely correctly its characteristics should be identical with those of the wall of which it forms a part.

Dr. G.E. Blight, Professor of Construction Materials, and Mr. G.M. Bentel, University of the Witwatersrand, Dept. of Civil Engineering, P.O. Wits, 2050, Johannesburg, Republic of South Africa

* The first part of this paper was published in bulk solids handling Vol. 7 (1987) No. 6

A number of investigations have been carried out into the factors affecting the correctness of pressure registration by pressure cells. Notable amongst these are the papers by Peattie and Sparrow [1] and Hvorslev [2]. The analysis that follows is largely based on the work reported by Hvorslev and repeats material given in an earlier paper by Blight [3].

Fig. 1 shows a pressure cell of diameter D_c and thickness t_c which is set in a vertical wall so that it protrudes a distance d_c from the general plane of the wall. The filling exerts a pressure σ_{hf} on the wall. Because a conventional pressure cell has to strain away from the fill in order to register, it will register a pressure σ_c which will differ from σ_{hf}, and its deflection will affect the pressure in a zone of fill in the vicinity of the cell face.

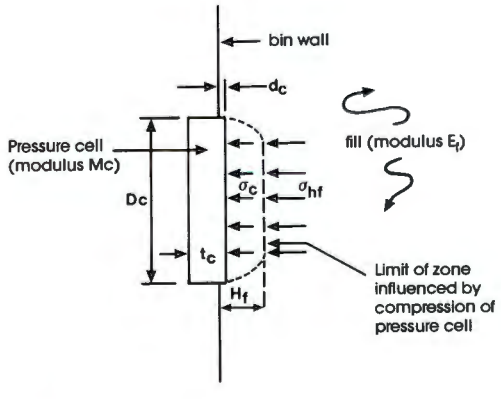

Fig. 1: Factors influencing the performance of a pressure cell

If the modulus of compressibility of the pressure cell is M_c, the cell will compress by an amount:

$$\delta_c = \frac{\sigma_c \, t_c}{M_c} \qquad (1)$$

The strain in the fill affected by the compression of the gauge will average

$$\varepsilon_f = \frac{\delta_c}{H_f} = \frac{\sigma_{hf} - \sigma_c}{E_f} \qquad (2)$$

where H_f is the thickness of the zone of fill affected by the gauge compression, and E_f is the strain modulus of the fill.

The accuracy with which the pressure cell records the pressure in the fill is described by the registration ratio

$$R = \sigma_c / \sigma_{hf}$$

R will be unity for perfect registration, less than unity if the recorded pressure is less than the actual, and more than unity if the recorded pressure exceeds the actual pressure in the silo.

Because δ_c in Eqs. (1) and (2) is the same,

$$R = \frac{1}{1 + \frac{E_f t_c}{H_f M_c}} \qquad (3)$$

The factor E_f/H_f is a characteristic of the fill material and is therefore not controllable. However t_c/M_c is a characteristic of the pressure cell and can be controlled by design. In particular the closer t_c/M_c can be made to approach zero, the closer R will approach the ideal value of 1.0 for perfect registration. This is done most easily by maximizing M_c so that it approaches an infinite value.

If the fill is moving past the face of the pressure cell, which it will do as it compresses under increasing overburden, or as the silo is emptied, the protrusion d_c will cause an additional average strain in the fill of d_c/H_f. Eq. (1) will then become

$$E_f = \frac{\delta_c - d_c}{H_f} \qquad (1a)$$

and the registration ratio will be modified to

$$R = \frac{(1 + d_c E_f)}{\sigma_{hf} H_f} \Big/ \frac{(1 + E_f t_c)}{H_f M_c} \qquad (3a)$$

Hence, other things being equal, the cell will register perfectly if d_c is zero, it will over-register if d_c is positive and under-register if d_c is negative, i.e. set back from the wall surface.

The model of pressure cell operation represented by Eq. (3a) is not perfect, but it does show the role of the most important factors affecting the accuracy of a pressure cell, namely cell modulus or compressibility and accuracy of mounting.

3. Mounting of Pressure Cells in a Full Size Silo Wall

Various systems have been used by the authors to mount pressure cells in silo walls and so minimize the protrusion of the cells, d_c. The system described by Fig. 2 has resulted from many years of trial and error. As described, the method is suitable for reinforced concrete silos. The method could easily be modified for use on steel silos.

A steel pan containing three threaded studs welded to its back plate at 120° intervals is cast into the silo wall during construction. The pressure cell is bolted to a face plate having a diameter 20 mm less than the inside diameter of the pan.

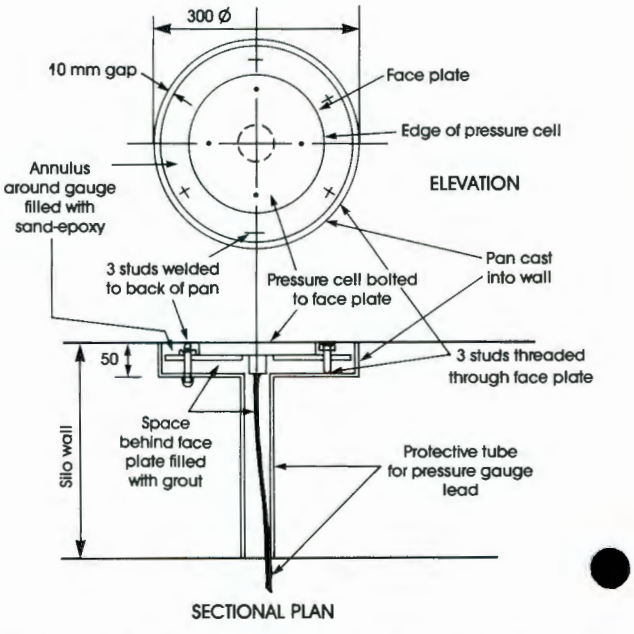

Fig. 2: Method of mounting pressure gauge in wall of reinforced concrete silo

The face plate has three plain clearance holes drilled in it at 120° intervals and three tapped holes, also at 120° and on the same pitch circle as the studs in the pan. Three studs having an overall length slightly less than the depth of the pan are then threaded into the tapped holes. The pressure cell is placed in position with its electrical lead threaded through the pipe which passes to the outside of the wall, and washers and nuts are then placed on the studs welded to the back of the pan.

By tightening or loosening these nuts and adjusting the studs threaded through the face plate, the position of the pressure cell can be adjusted, using a short straight edge, until the face of the cell is as close as possible to co-planar with the inner surface of the silo wall. Fig. 3 shows a pressure cell at this stage of installation.

Fig. 3: View of pressure cell mounted in silo wall, before grouting and smoothing off flush with wall surface

The 10 mm gap between the face plate and the rim of the pan is then stuffed with a length of preformed rubber joint filler and the void behind the face plate filled with a quick-setting cement grout that is poured through a funnel. Once the grout has set, the strip of joint filler is pulled out and the space between the pan and the side of the pressure cell is

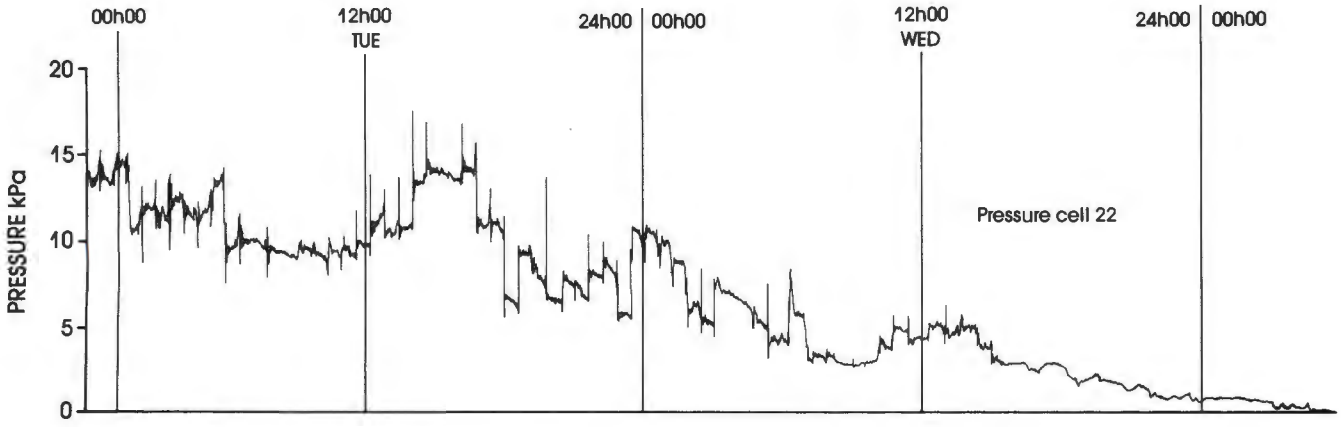

Fig. 4: Pressure variations recorded at a single point during emptying of a cement storage silo

plastered full with a sand-epoxy mortar to finish off the face of the pressure cell flush with the inside surface of the silo wall. Finally, the surface of the pressure cell is painted with epoxy resin and strewn with fine sand to give its surface a texture similar to that of the surrounding concrete.

The electrical lead of each cell is taken down the outside of the silo wall in an electrical conduit to a convenient central reading location. There the ends of the wires are housed in an electrical junction box. Each wire is fitted with a banana plug and is labeled, as described in Part 1 of this paper. The gauges can either be read out manually using a strain bridge, or they can be scanned automatically by means of a data logger. Alternatively, pressure can be recorded continuously using a chart recorder.

Fig. 4 shows an example of a continuous recording of a pressure gauge output made during the emptying of a cement storage silo (Fliss and Blight [4]).

The irregular "spikes" that occur on the record represent localized increases in pressure that arise when compressed air is fed to the aeration pads at the base of the silo. These pressure spikes represent fluctuations of up to 10 kPa. The interval between the spikes corresponds with the regular alternation of draw-off from the 18 openings provided around the perimeter of the silo so as to ensure concentric emptying.

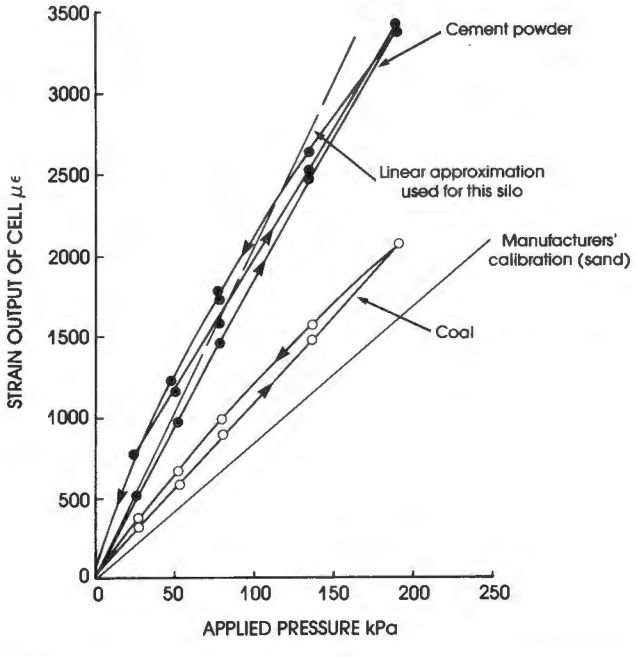

Fig. 5: Calibration of a mercury-filled strain gauged diaphragm pressure cell using various materials in contact with cell face

4. Calibration of Pressure Gauges

Because the registration ratio of a pressure cell depends on the strain modulus of the fill E_f (see Eq. (3)), pressure cells must be calibrated in conjunction with the material that will form the silo fill. Fig. 5 shows typical calibrations of a mercury-filled pressure cell with a fairly rigid material (sand, E probably about 40 MPa), a less rigid material (coal, E = 28 MPa) and a compressible powder (cement, E = 15 MPa). As predicted by Eq. (3) the higher the modulus of the fill material, the lower is the strain output of the cell for a given applied pressure. The calibrations also display hysteresis, presumably because once material has been pressed against the face of the pressure cell, it tends to resist moving back when the pressure is reduced. However, the hysteresis is usually small enough to ignore and to use a single linear calibration.

The method used by the authors for calibrating a pressure cell is as follows:

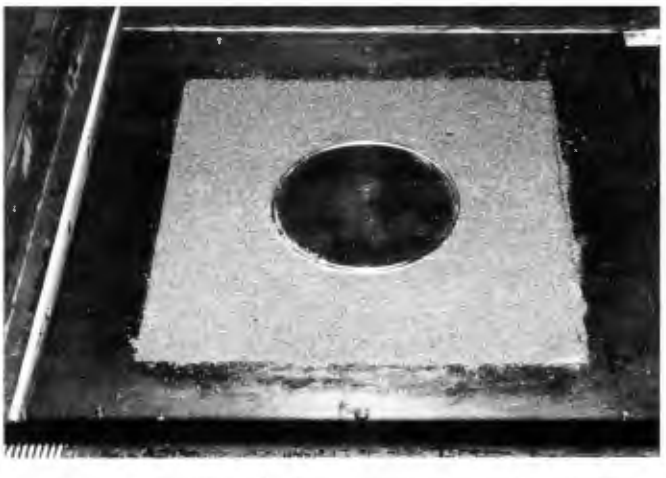

Fig. 6: Pressure cell mounted in base of shear box ready for calibration

The cell is set into the base of a large (350 mm square) shear box by means of a sand-epoxy resin mortar, as shown by Fig. 6. The box is then loosely filled with the silo fill and loads are applied via a rigid top loading platen. Hence the relationship between the strain output of the cell and the known applied pressure can be established (Fig. 5).

5. The Zero Strain Pressure Cell

The zero strain pressure cell is based on the principle that if M_c in Eq. (3) can be made very large, the registration ratio R will approach unity. This can be achieved by balancing the pressure on the face of the pressure cell by means of a fluid pressure applied to the rear of the face. The pressure is continually adjusted to maintain zero strain in the face or diaphragm. Fig. 7 shows the prototype cell that is being used for development studies.

The 0.75 mm thick face diaphragm is strain-gauged as shown and the strain of the face is zeroed or nulled by means of air pressure applied to the inside of the cell.

Fig. 8 shows the calibration curves established:

(a) with the pressure cell used in the zero strain mode;

(b) as a conventional pressure cell with a deflecting diaphragm on the loading cycle; and

(c) as a conventional pressure cell on the unloading cycle.

It will be seen that the registration ratio for operation in the zero strain mode is almost exactly unity for both loading and unloading.

A set of zero strain cells is currently being prepared for the instrumentation of a large model cement storage silo. It is

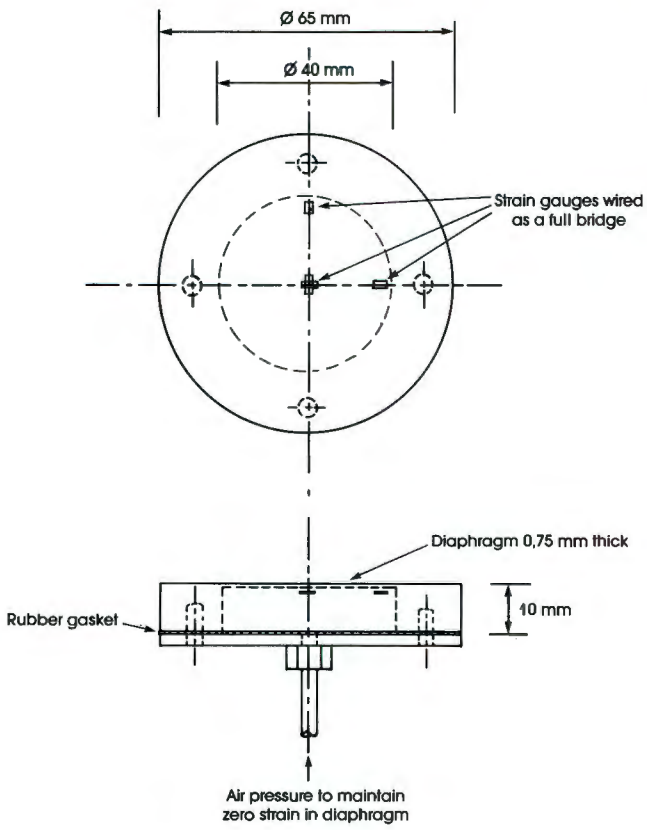

Fig. 7: Prototype of the zero strain pressure cell

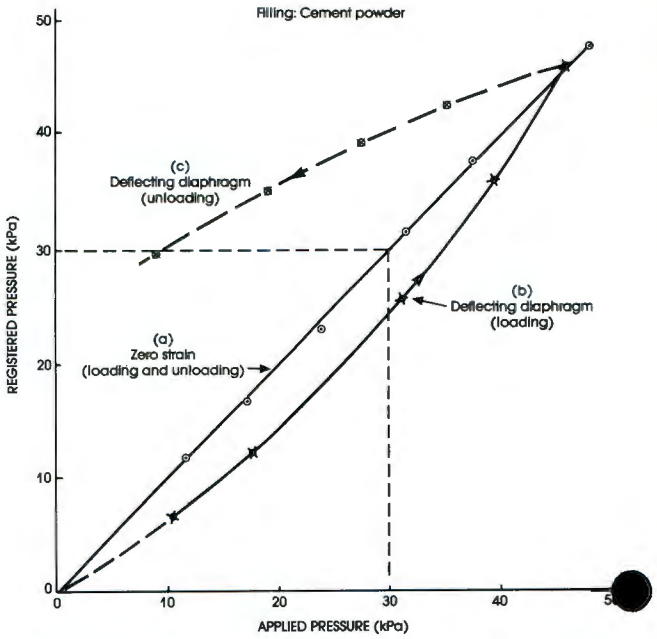

Fig. 8: Calibration curves for a pressure cell operated with a deflecting diaphragm and as a zero strain cell

recognized that development still has some way to go. In particular, compressed air is not the most suitable fluid for maintaining the zero strain condition, especially for a field installation. It would be preferable to use a more incompressible fluid such as an hydraulic oil. Work in this direction is proceeding.

6. Concluding Remarks

This paper described the experience of the authors over the past decade in using pressure cells to measure pressure in full size silos. It is hoped that making this experience available to the industry will encourage others to embark on the difficult, but rewarding course of instrumenting full size silos. The recent development of the zero strain pressure cell should assist considerably in future projects.

References

[1] Peattie, K.R., and Sparrow, R.R.: The fundamental action of earth pressure cells; Journal of the Mechanics and Physics of Solids, Vol. 2 (1954), pp. 141—155.

[2] Hvorslev, M.J.: The changeable interaction between soils and pressure cells; tests and reviews at the Waterways Experiment Station; Technical Report 5-76-7, US Army Engineer Waterways Experiment Station, 1976.

[3] Blight, G.E.: Measuring pressures in silos with pressure cells; Proceedings 2nd International Conference on Design of Silos for Strength and Flow, Stratford-on-Avon, UK, 1983, Vol. 1, pp. 217—229.

[4] Fliss, L. and Blight, G.E.: A Comparison of design and measured lateral pressures and temperatures in a large; duo-cell cement storage silo; International Journal for Bulk Solids Storage in Silos, Vol. 2 (1986) 4, pp. 18—28.

7.3 TEMPERATURES AND PRESSURES MEASURED IN SILOS BY MEANS OF PRESSURE CELLS

CONTRIBUTION TO LEARNING

The seven papers in this section show that design pressure envelopes for silos can be predicted with acceptable accuracy. To do this, materials parameters are measured in the laboratory using the recognized techniques of geotechnical engineering. The parameters are then used with recognized soil mechanics theory to predict the pressure distribution.

The penultimate paper demonstrates that temperature surcharge pressures occur in reinforced concrete silos and can be of appreciable magnitude.

The final paper examines the vexed question of the effect of eccentric emptying on horizontal pressure distributions, and supports a very simple view of the effect.

7.3 TEMPERATURES AND PRESSURES MEASURED IN SILOS BY MEANS OF PRESSURE CELLS

7.3.1 Blight, G E and Midgley, D (1981). Pressure measured in a 20m diameter coal load-out bin. Journal of Powder and Bulk Solids Technology, vol 5, No 2, pp 21-31.

This study was carried out for a firm of consulting civil engineers. Mr D Midgley was the designer of the silo, I designed and installed the instrumentation, took the measurements and drafted the paper. I estimate my contribution to the paper at 75%.

7.3.2 Blight, G E (1986). A comparison of design and measured lateral pressures in a large coal load-out silo. International Journal of Bulk Solids Storage in Silos, Vol 2, pp 1-8.

7.3.3 Schaffner, R H and Blight, G E (1986). A comparison of design and measured lateral pressures in a large Ibau-type cement storage silo. International Journal of Bulk Solids Storage in Silos, vol 2, No 2, pp 17-24.

The situation for this study was similar to that for paper 7.3.1, Mr Schaffner was the designer of the silo. I estimate my contribution to the paper at 75%.

7.3.4 Fliss, L and Blight G E (1986). A comparison of design and measured lateral pressures and temperatures in a large duo-cell cement storage silo. International Journal of Bulk Solids Storage in Silos, vol 2, No 4, pp 18-28.

The situation was similar to that for papers 7.3.1 and 7.3.3. Mr Fliss was the designer of the silo. I estimate my contribution to the paper at 75%.

7.3.5 Blight, G E (1983). Performance of a 20m diameter steel maize storage bin.

Proceedings, 2nd International Conference on Design of Silos for Strength and Flow, Stratford-upon-Avon, UK, pp 179-191.

7.3.6 Blight, G E (1990). Temperature surcharge pressures in reinforced concrete silos. Accepted for publication in Powder Handling and Processing, vol 2, No 3.

7.3.7 Blight, G E (1991). Eccentric emptying of a large coal bin with six outlets. Bulk Solids Handling, vol 11, No 2, pp 451-457.

Journal of Powder & Bulk Solids Technology, **5** (1981) 2; 21-31

PRESSURE MEASURED IN A 20M DIAMETER COAL LOAD-OUT BIN

G. E. Blight,
Department of Civil Engineering,
University of the Witwatersrand,
1 Jan Smuts Avenue,
Johannesburg 2001,
South Africa

D. Midgley,
Ove Arup & Partners,
132 Jan Smuts Avenue, Parkwood,
Johannesburg 2193,
South Africa

As part of a large coal-mining project exporting ten thousand tons of coal a day a reinforced concrete coal load-out bin, having internal diameter of 20m and a maximum storage height of 30m was designed and constructed at Ermelo, South Africa. The bin has a double pyramidal hopper bottom with twin outlets, each of which can be used to load export trains at a rate of 2,800 tons per hour, a 84 truck train carrying 4,800 tons (1 ton = 1,000 kg) of coal being loaded automatically in 110 minutes. To check on the assumptions and applicability of the theories used in the design of the bin, a number of pressure cells were installed in the walls of the bin. There was a particular interest in monitoring possible over-pressures close to the transition between the cylindrical body of the bin and the hopper bottoms. Six sets of static and dynamic pressure measurements were available at the time of writing and the paper presents and analyses these measurements.

Figure 1(a).
The coal load-out bin and associated plant

DESCRIPTION OF BIN

Figure 1a shows the coal load-out bin together with its associated loading conveyor and part of the coal preparation plant at the mine. **Figure 1b** shows a simplified sectional elevation and plan through the bin giving salient dimensions and showing the layout of the twin outlets in the hopper bottom. From this latter figure it will be noted that while the available storage height is 30 metres, the conical top of the stored coal occupies some 8m of the storage height so that the walls of the bin are subjected to lateral pressure over a maximum height of approximately 22 metres. The ratio of maximum fill height to bin diameter is thus close to 1.

OBJECTIVES OF INSTRUMENTATION

The design of the load-out bin was primarily based on the German Code DIN 1055.[1] Certain areas of the walls which were considered to be subject to pressures considerably greater than those predicted by DIN 1055 were evaluated using the theory of Walker[2].

The objectives of the instrumentation study were to:

(i) determine how well the design pressures correlated with the field measurements,
(ii) establish the boundary between the mixed funnel flow and mass flow regimes that were expected to result from eccentric draw-off,
(iii) evaluate the effect that eccentric draw-off has on the development of the flow funnel and on the intensity of pressure around the wall.

The German Code[1] represents an envelope of average maximum pressures and does not differentiate between funnel and mass flow. Walker's theory is based on the assumption of mass flow and enables the peak intensity of pressure to be evaluated. Jenike and Johanson's[3,4] theories also enable a peak pressure intensity to be determined, and in addition would, for the present bin, predict funnel flow for which the wall pressures are significantly lower than those of mass flow.

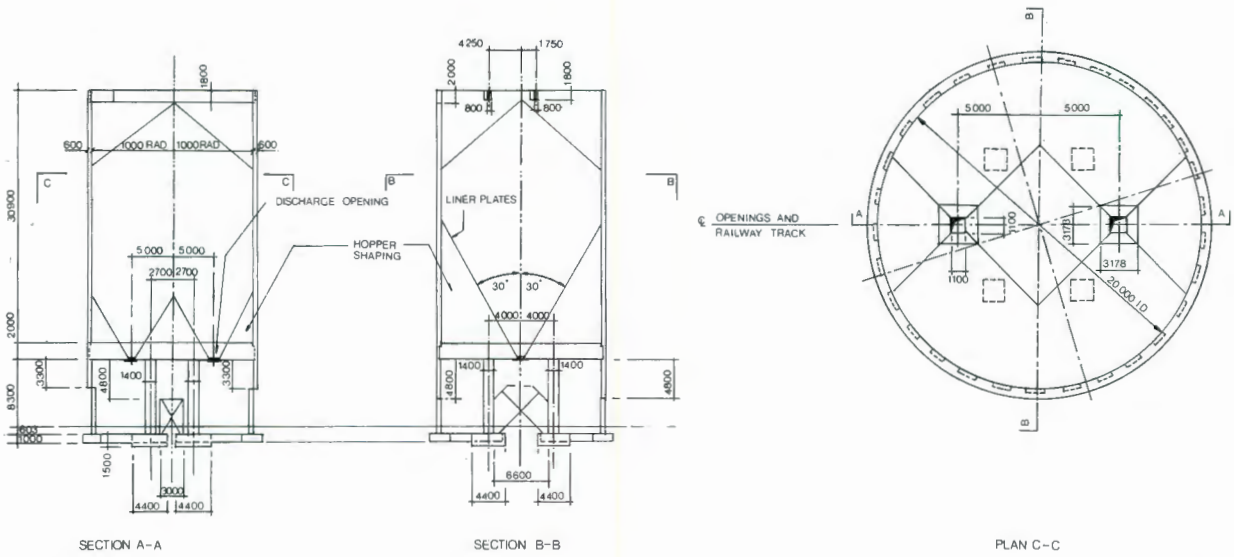

Figure 1(b).
Simplified cross-sectional elevations and plan of load-out bin

It was hoped to determine the position at which the flow channel intersects the silo wall and hence the applicability of the Jenike and Johanson and Walker theories.

PHYSICAL PROPERTIES OF STORED COAL

The coal that passes through the load-out bin is a washed graded product that enters the bin with a water content of 6% to 14% by dry mass. **Figure 2a** shows grading analyses for the coal which has a maximum particle size of between 25 and 50 mm and 3% to 6% of fines passing a 74 micron sieve. **Table 1** summarises the properties of the coal as represented by samples taken on three occasions when pressure measurements were made. The measured properties for the coal are compared with the ranges of design values recommended by the German code DIN 1055 and the American Concrete Institute Committee 313 (Title 72 – 38)[5]. A comparison of the measured and code values shows that the product stored is a reasonably typical coal. The loose bulk density recorded in **Table 1** was measured by pouring the coal loosely into a mould and weighing. The compacted density was achieved by vibrating the mould and contents on a Vebe vibrating table. The measured shear strength parameters recorded in **Table 1** were obtained by means of triaxial compression tests on 100 mm diameter specimens. The specimens were prepared by pouring the coal at the sampled moisture content into a triaxial sleeve which was held in shape by a metal former. Provision was made to allow air to drain when the confining stress was applied and the specimens were sheared with full air drainage to simulate conditions during loading and emptying of the bin.

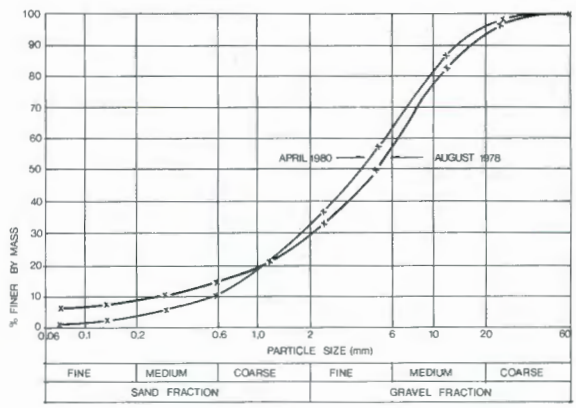

Figure 2(a).
Particle size analyses of coal stored in bin

Figure 2b shows the results of triaxial shear tests on coal at a water content of 13.8% (sampled in April 1980). The open circles represent the results of tests on normally consolidated coal which was sheared at the greatest stress to which it has ever been subjected as a loose aggregate. The effect of reducing the stress or over-consolidating the coal is shown by the filled-in circles. In these tests the coal was first stressed to a particular value of σ_3, say 100 kPa, after which it was sheared at a reduced stress of 10 kPa. The results clearly show the enhancement of strength obtainable by over-consolidation.

Table 1.
Properties of coal

Date Sampled	Water Content %	Bulk Density (kN/m³)		Angle of Shearing Resistance	Capillary Cohesion kPa	Angle of Wall Friction*
		Loose	Compacted			
August 1979	6.4	7.65	9.45	39°	14	
October 1979	8.1	7.99	8.85	43°	10	
April 1980	13.8	7.99	8.85	40°	0	29° to 40°
Design Values DIN 1055		10.0		35°		21° to 26°
ACI 313		8 to 10.4		32° to 44°		27° to 31°

*Coal on Concrete

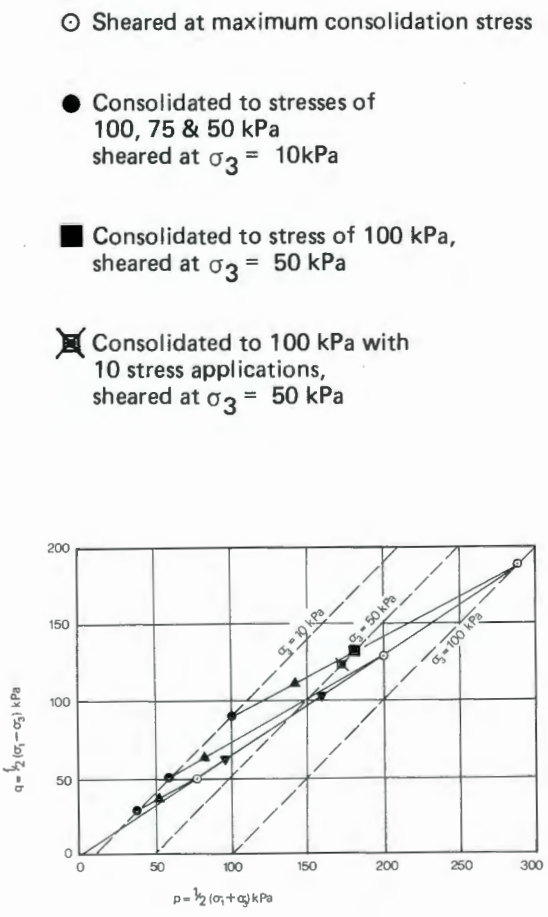

Figure 2(b).
Shear properties of coal at 13.8% water content.

The square filled-in symbol represents the results of consolidating to 100 kPa and shearing at 50 kPA, while the crossed square symbol is the result of a test on a specimen on which σ_3 was increased to 100 kPa and reduced to 50 kPa ten times before shearing at σ_3 = 50 kPa. This result indicates that repeated stressing of coal within the same stress range has little influence on its strength.

The angles of wall friction recorded in **Table 1** were measured in a shear box in which the lower half of the specimen was replaced by a block of concrete. The two limits of 29° and 40° correspond, respectively, to a condition in which the coal is stationary with respect to the concrete surface and a condition in which the coal is sliding across the concrete surface at a constant velocity. Details of the difference between the two states is shown in **Figure 2c**. A constant sliding resistance is developed while the coal and the concrete surfaces are moving relative to each other. When the motion is stopped, the sliding resistance decays to a lower static resistance. The static resistance rapidly increases to the sliding resistance once relative motion is resumed. In the case illustrated, the normal stress across the coal—concrete interface was 60 kPa and the 11.6 kPa change between static and sliding resistance represents a change in the coefficient of friction of 0.19 or a change in the angle of wall friction of 10.9°. The case shown in **Figure 2c** was recorded by means of a UV recorder activated by the load cell used to measure the sliding resistance.

The coefficient of pressure at rest in a granular material (K_o) represents the ratio of the horizontal to the vertical principal stress under conditions of zero lateral strain. This ratio was measured in the triaxial test by varying the vertical stress σ_v, while simultaneously adjusting the horizontal stress so as to maintain a condition of zero lateral strain. This is achieved by using a sensitive lateral strain indicator[6] which was attached across a diameter of the specimen.

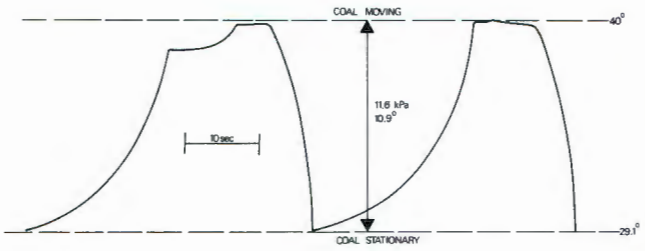

Figure 2(c).
Effect of motion on angle of wall friction.

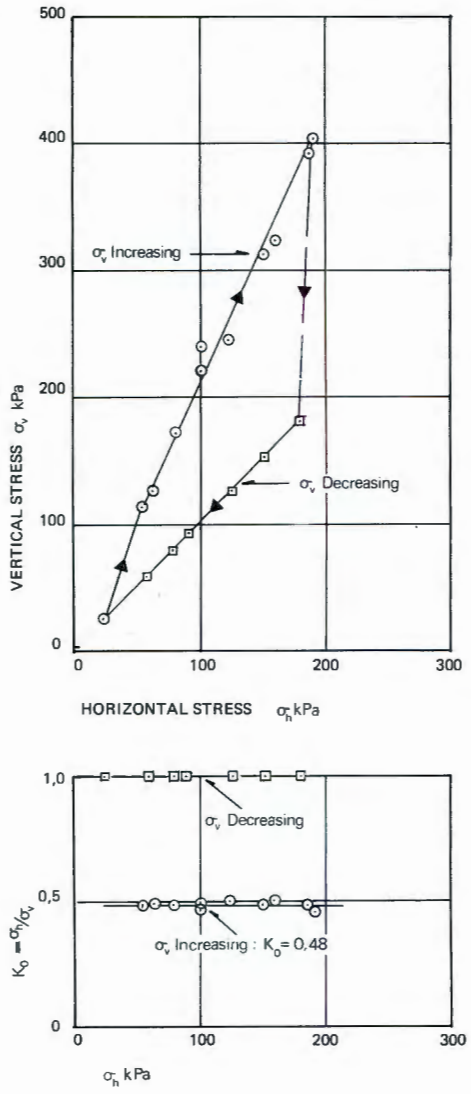

Figure 2(d).
Measurements of the coefficient of pressure at rest for coal at 13.5% water content.

The results of two series of K_o measurements are summarized in **Figure 2d**. The upper diagram shows the relationship between the measured pressures, while the lower one shows the variation of K_o with σ_h while σ_v was first increasing and then decreasing. It will be noted that there is an abrupt discontinuity in the behaviour of the coal when σ_v is decreased and that the value of K_o changes correspondingly. No value for K_o while σ_v was decreasing has been quoted as the actual value appeared to be slightly greater than unity. This could not be measured precisely in the available apparatus. The observed results for σ_v decreasing have been included to illustrate the sudden change in behavior of the coal when the stress regime changes.

INSTRUMENTATION OF BIN

Eight Kyowa pressure cells were installed in the walls in order to measure lateral pressures in the bin during filling and emptying. **Figure 3a** shows the positions of the pressure cells in relation to the outlets and the hopper shaping while **Figure 3b** shows a typical pressure cell during installation with its pressure-sensitive face located flush with the inner face of the bin wall. As shown in **Figure 3a**, four load cells (line A) were positioned in the vertical plane that passed through the axes of the two outlets. The three lower cells were expected to be in a

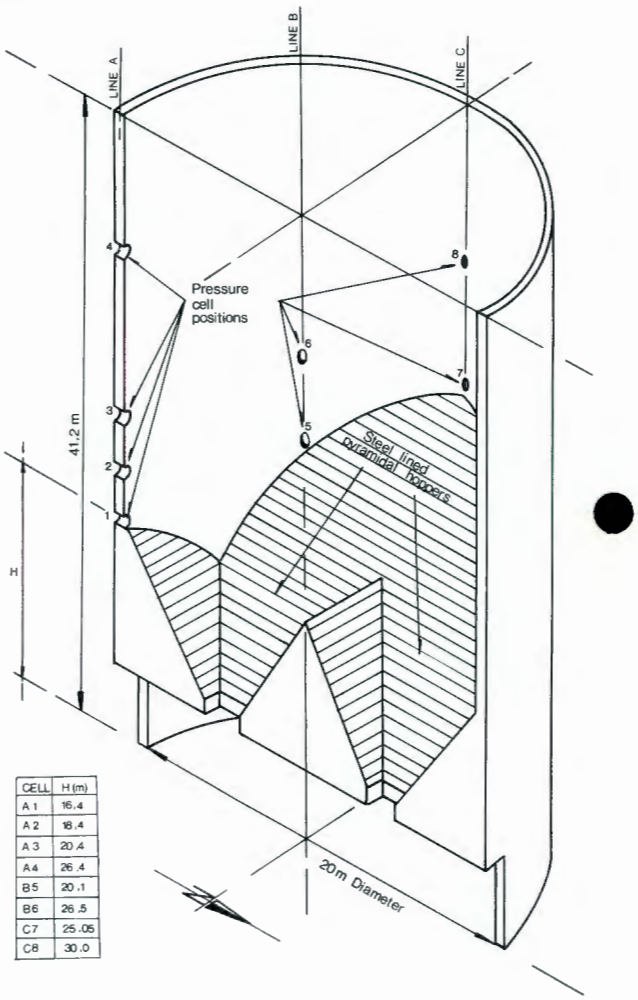

Figure 3(a).
Location of pressure cells in bin wall.

region that would be affected by flow through the south outlet or loading chute. A pair of load cells (line B) were positioned in the vertical plane at 45° to that containing line A, while the remaining two load cells (line C) were positioned in the vertical plane at 90° to that containing line A.

Figure 3(b).
Typical pressure cell during installation.

The pressure cells were installed in cylindrical openings that had been cast in the bin walls during construction. The pressure-sensitive faces of the cells were accurately aligned with the average inner surface profile of the bin walls in the vicinity of each cell and the cells were then grouted in solidly using an epoxy-resin/sand mortar. In this way, the face of each pressure cell presented a minimum of discontinuity on the inner surface of the bin while the perimeter of each cell was protected from the effects of cross-sensitivity resulting from stresses applied in the plane of the strain-gauged diaphragm.

Figure 3c is a diagrammatic cross-section showing the method of installation of the cells.

The manufacturer's calibrations for the load cells were accepted as being correct as a previous experience with Kyowa load cells had shown the calibrations to be accurate and stable. In this previous case a number of similar load cells had been installed in a maize silo for a period of two years[7]. They were removed from the silo and their calibrations were checked by one of the present authors. The values obtained for the recalibration agreed almost exactly with those given by the manufacturer.

The strain gauges on the diaphragms of the load cells are arranged in a full bridge. Static pressure readings on the cells were taken by means of a Huggenberger strain measuring bridge, while dynamic pressure measurements were made using the Huggenberger strain bridge as a balancing box in conjunction with a Rapet portable UV recorder. The pressure cells are connected to the recording equipment by means of fully screened conductor cables to eliminate any interference from electrical equipment operating in the vicinity.

RECORDED LATERAL PRESSURES

Lateral pressures have so far been recorded on five occasions. Further measurements are planned. In August, 1978, part of the filling cycle was recorded followed by the full emptying cycle, for coal discharging from the south outlet chute. In October 1979, a complete filling and emptying cycle was recorded while the north loading chute was in use. In November, 1979, dynamic pressures were recorded while coal was being loaded from both the south and north chutes and in March and April, 1980 dynamic pressures were again recorded using the south and north chutes. **Figure 4** shows a typical time record of the tonnages and approximate volumes of coal discharged from and loaded into the bin during a normal train loading cycle. **Figure 5** shows the variation with time of recorded lateral pressures at various of the load cells, corresponding with the discharge and loading cycles recorded in **Figure 4**. Once the discharge cycle commences the almost immediate changes in pressure

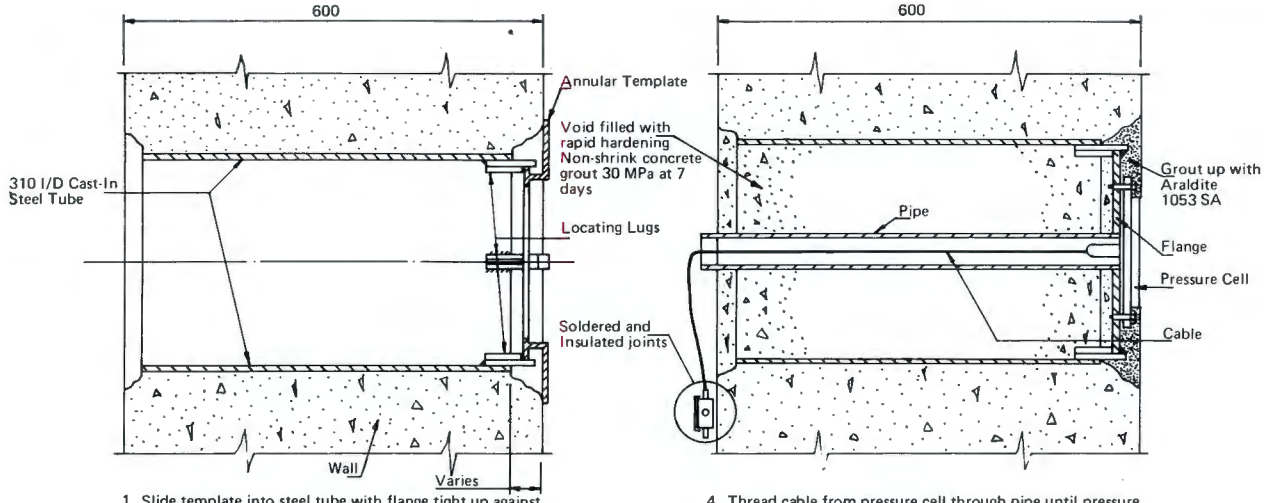

1. Slide template into steel tube with flange tight up against wall (orientation is marked on template)
2. Locate lugs inside steel tube hard against annular ring of template. Weld lugs into position
3. Remove template
4. Thread cable from pressure cell through pipe until pressure cell is located against flange
5. Bolt pressure cell securely to flange
6. Grout recess between pressure cell diaphragm and inside face of silo and finish off flush
7. Hand pack stiff concrete grout (with a non-shrink additive) against rear face of flange and tamp to remove voids. Continue grouting until tube is filled. Screed off smoothly against silo wall
8. Connect conductor cable

Figure 3(c).
Installation of pressure cell in silo wall.

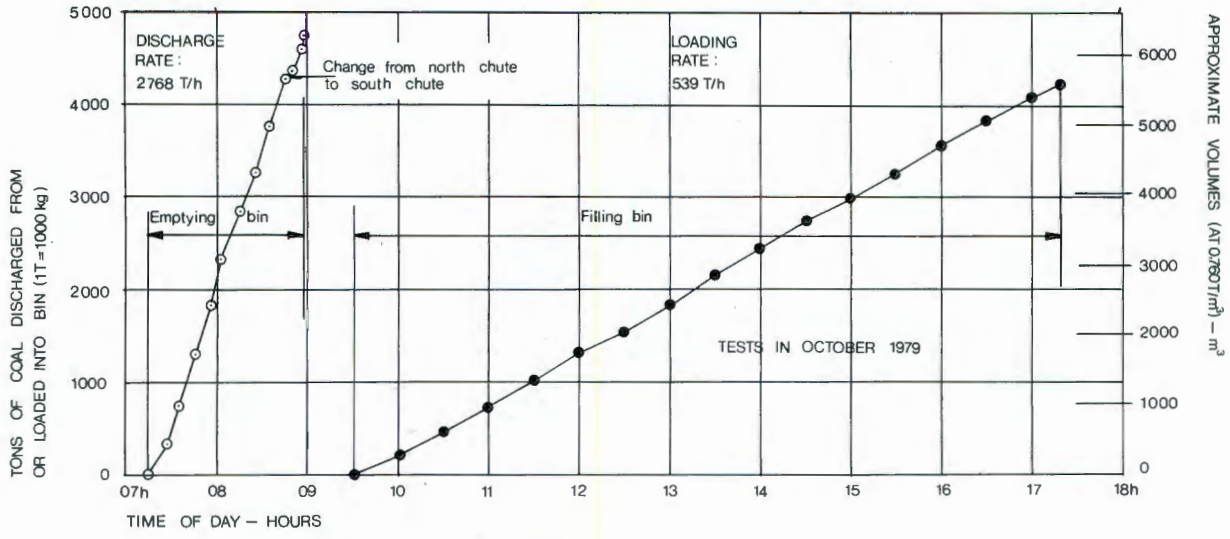

Figure 4.
Typical discharge and loading records for bin tonnages.

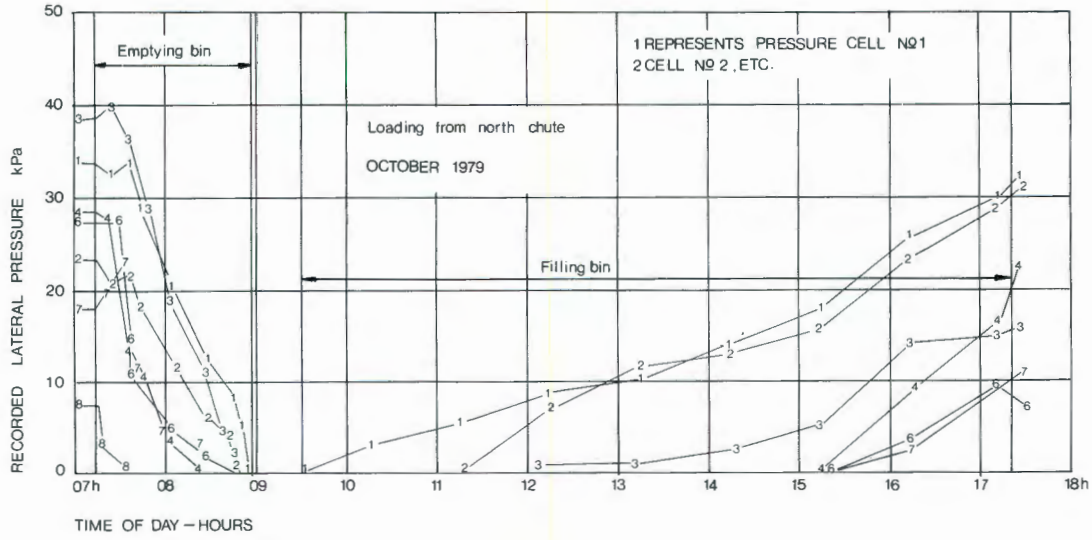

Figure 5.
Typical pressure cell readings during discharge and loading.

recorded by certain of the cells is clearly shown, as are the increases in pressure after completion of the filling cycle. These latter changes presumably occurred as a result of slight settlements of the coal as it compacted into a denser mass. **Figure 6** shows recorded dynamic changes in pressure during discharge from the south and the north chutes. In each case the pressure changes recorded at the lowest pressure cell on each of lines A, B and C is shown. In **Figure 6** zero time corresponds to the first opening of the load-out chute when commencing to load a train. It will be noted that when discharging from the south chute there is a brief time lag of about 12 seconds before any pressure response is observed. This time lag corresponds to the movement of a certain minimum volume of coal before the mass of coal above the chute is activated. At this point there was a slight reduction of pressure at Al and an increase at B5 while the pressure at C7 also increased slightly. The left-hand portion of Figure 6a shows that these pressure changes stabilise within two to three minutes from the start of discharge. When loading out was commenced from the north chute the pressures at cells A1 and B5 were virtually unaffected while the pressure at C7 at first increased, then decreased to slightly less than the initial value. After this the pressure at C7 increased again to a value of 10 kPa above its initial value.

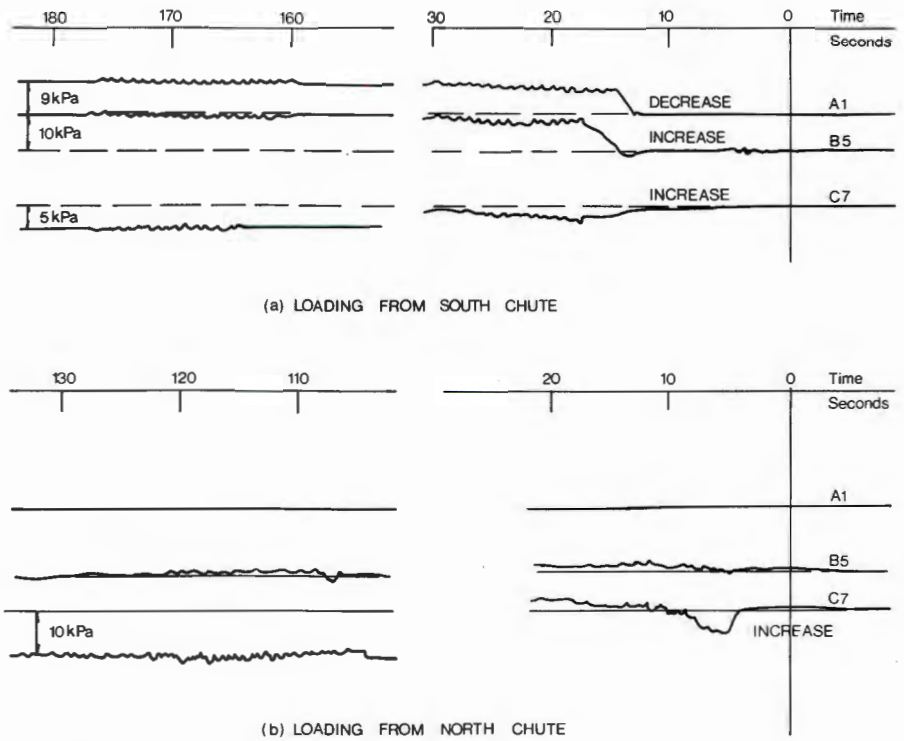

Figure 6.
Dynamic changes in lateral pressure loading from south and north chutes.

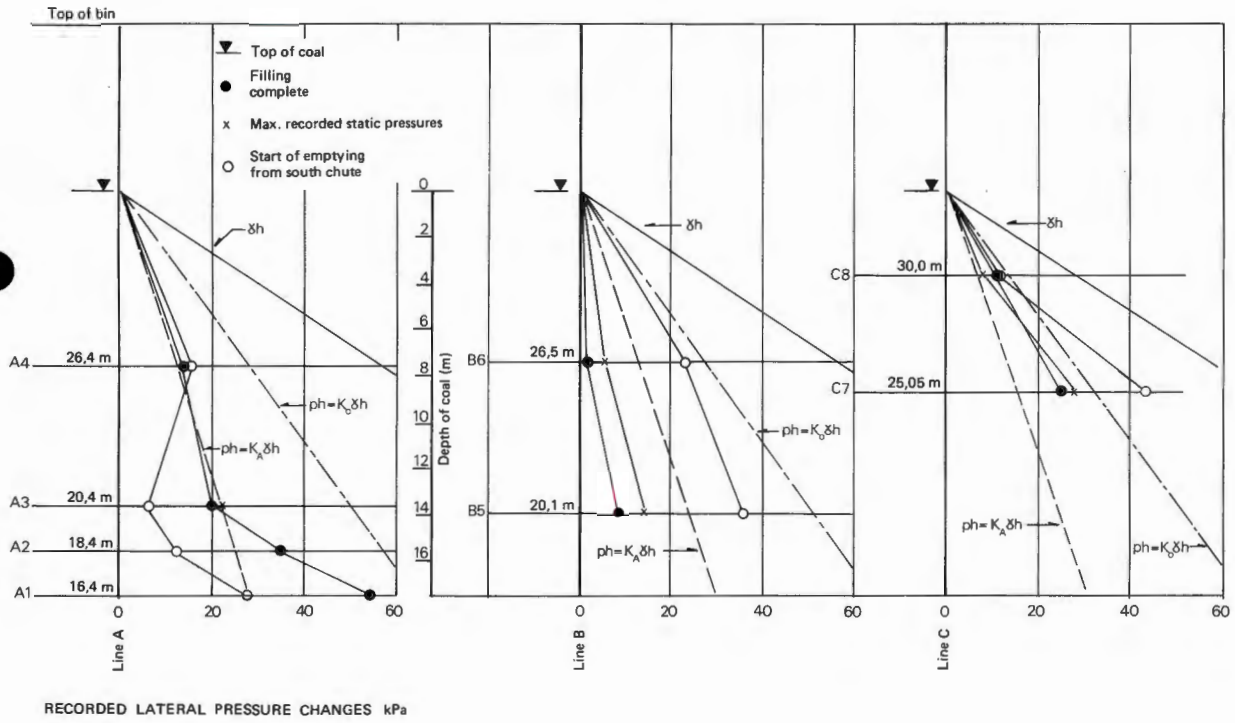

Figure 7(a).
Maximum lateral pressures during discharge from south chute—vertical distribution along lines A, B and C.

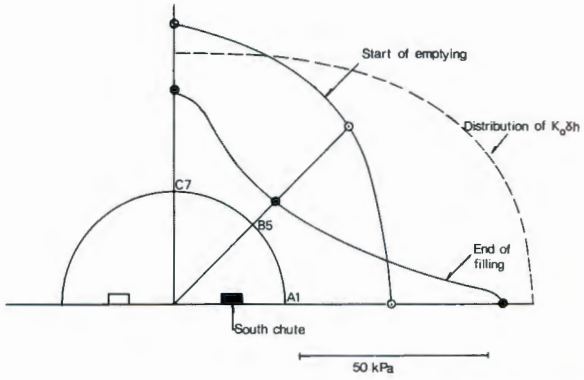

Figure 7(b).
Maximum lateral pressures during discharge from South chute—Radical distribution at cylinder—pyramid transition.

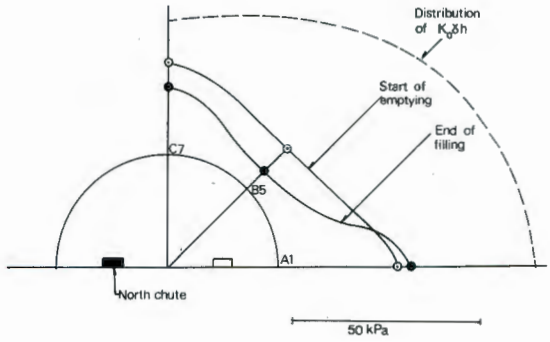

Figure 8(b).
Maximum lateral pressures during discharge from North chute—Radial distribution at cylinder—pyramid transition.

ANALYSIS OF RECORDED PRESSURES

Figure 7a summarises the maximum pressures recorded during discharge from the south loading chute while **Figure 8a** provides similar data for discharge from the north loading chute. In both Figures, the depth of coal is the depth in contact with the wall. It will be seen from **Figure 7a** that pressures on the A line of cells reduced during emptying over a height of 6 to 8 metres above the level of cell A1. The pressures on the B line appear to have increased over a considerable height above the level of cell B5, while similar conclusions apply to the cells on line C. The magnitudes of the changes of pressure shown in **Figure 7a** differ somewhat from those indicated in **Figure 6**. This is probably to be expected as the physical properties, state of compaction, moisture content and hence the flow regime within the coal vary with time.

A considerable quantity of coal remains in the bin after loading a train. The state of compaction of this coal will depend, for example, on whether the bin was being filled while loading was in progress, and on whether the south and north loading chute (or both) has been used during the previous occasion on which the bin was emptied. Bin pressures on refilling will be affected by the state of the coal already in the bin. It is therefore unlikely that the extremes of possible bin pressure are represented by the data shown in **Figure 7a.**

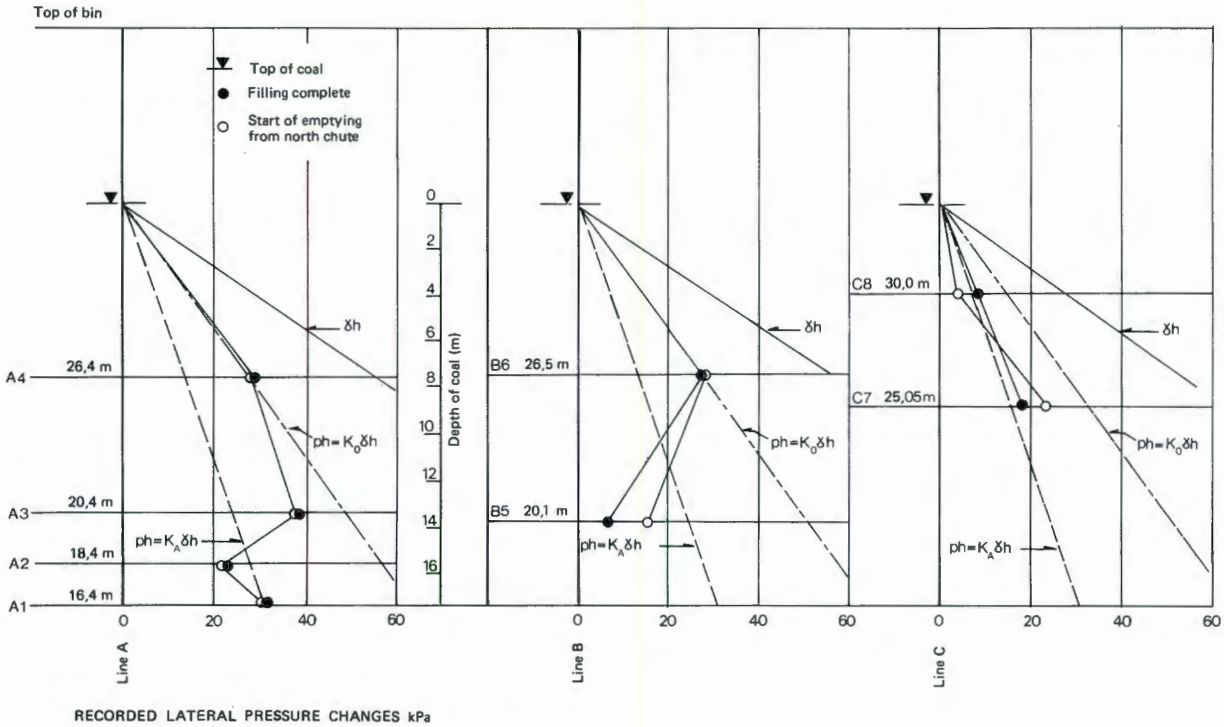

Figure 8(a).
Maximum lateral pressures during discharge from north chute—vertical distribution along lines A, B and C.

Figure 7b shows the radial distribution of horizontal pressure plotted along the transition between the cylindrical bin walls and the pyramidal hopper bottom. The pressure distribution at the end of filling was highly irregular but became considerably more regular when emptying started. The diagram shows that the pressure along an axis at right angles to the centreline of the discharge chutes was greater than that along the centreline. This indicates that there is a tendency for the coal to arch along this axis when discharge occurs from the south chute and for a zone of reduced pressure to form adjacent to the chute.

Figure 8a summarises maximum pressures recorded during emptying of the bin through the north loading chute. This figure confirms the patterns shown by **Figure 6b**, except that in this case cell B5 recorded an increase in pressure instead of no change.

Figure 8b shows recorded pressures during discharge from the north chute plotted on a similar basis to **Figure 7b.** This diagram confirms the highly irregular nature of the lateral pressures at the end of filling and indicates that these pressures can vary considerably from one filling cycle to the next. The pressure distribution in the south half of the bin again became more uniform once emptying was started but as shown earlier was not greatly affected by emptying from the north chute.

PREDICTION OF BIN PRESSURES

As pointed out earlier, if the cone at the top of the bin contents is ignored, the ratio of fill height to bin diameter is close to 1. Hence it would not be reasonable to expect frictional arching of the coal off the walls of the bin, (i.e. silo action) to have any significant effect on either vertical or horizontal pressures, except in the vicinity of the hopper bottoms. It would be reasonable to expect that a granula material filled into a cylindrical container with relatively rigid walls would assume a stress state corresponding to a condition of zero lateral strain and that the lateral pressure within the mass would correspond to the at-rest condition. As shown earlier, the coefficient of pressure at rest for the coal has a value measured in laboratory tests of 0.48 for a condition in which σ_v is increasing. This value compares reasonably well with a value of 0.36 predicted by the empirical relationship[8]

$$K_O = (1 - \sin\phi) \qquad (1)$$

where ϕ is the angle of shearing resistance of coal. If sufficient lateral yield could occur within the mass of coal to cause the material to fail by lateral yielding, the ratio between horizontal and vertical pressures in the bin would reduce to K_A given by the relationship[8]

$$K_A = \frac{1 - \sin\phi}{1 + \sin\phi} \qquad (2)$$

K_A is the active pressure coefficient. Pressure profiles corresponding to the above two relationships have been shown in **Figures 7a** and **8a** for a value of ϕ of 40°. The data recorded on **Figures 7a** and **8a** show that neither Equation (1) nor Equation (2) adequately describe the relationship between depth and lateral pressure for the bin at the end of the filling cycle. However, the at-rest condition seems to represent a stress state that is reasonably close to the observed static pressures. In reaching this conclusion it will be realised that, apart from any other uncertainties, a value for K_o of 0.48 represents conditions for first-time loading of the coal and may not necessarily represent the actual at-rest pressure coefficient for the coal. It is well established[6,8] that the at-rest pressure coefficient is considerably influenced by the previous stress history of the material, namely a material that has experienced loading in its past attains a greater at-rest pressure coefficient than one which has not been pre-loaded. This is clearly illustrated by the measurements shown in **Figure 2d.**

FLOW THROUGH THE ECCENTRIC DISCHARGE CHUTES

Regardless of the mode of flow within the material as the bin is emptied, the confluence towards the outlet can be expected to cause localised arching (eg. Walker[2]) off the walls of the bin. Because of the eccentric location of the outlets and the geometry of the hoppers, it is likely that the state of flow within the bin during emptying will be one of funnel or core flow with the axis of the funnel approximately coincident with the axis of the outlet which is in use. It was difficult to decide conclusively by merely observing the surface of the coal in the bunker during emptying, but the observed changes in the surface profile were not inconsistent with the mechanism just postulated.

Jenike[4] has shown both theoretically and by observation that a zone of reduced pressure should develop when a flow funnel impinges on the wall of a bin. A corresponding increased pressure should develop between the material in the flow funnel and the static material surrounding it. This increased pressure will be transmitted to the walls of the bin, although its effects will be modified by the compressibility and thickness of the material that transmits it.

The existence of the zones of reduced and increased pressure at the start of emptying are indicated by the ovality of the pressure distribution for the start of emptying shown in **Figure 7b.**

In order to further investigate the zone of reduced pressure that develops along the A-line of gauges, a series of dynamic measurements were carried out in March 1980. The results of these measurements are summarized in **Figure 9.**

The south loading chute has been disused for three months as the operators find it more convenient to use the north chute. The dead volume of coal above this chute had therefore been subjected to approximately 140 cycles of loading and unloading and was also hot as a result of oxidation of the coal. **Figure 9a** shows the pressure changes that occurred at gauges A1 to A4 at the start of emptying from this chute.

It will be seen that the pressure changes are similar in character and magnitude to those shown in **Figure 6a.** The age and stress history of the coal apparently having little if any abnormal effect.

Figure 9b shows similar pressure changes recorded 7 hours later when the bin had been refilled with coal. If anything, the pressure record for the freshly filled chute is more irregular and shows greater pressure changes than that for the aged coal.

In both cases the measurements show that a zone of reduced pressure develops to above cell A3, while the pressure at cell A4 increases, presumably because the flow funnel does not impinge on the wall at this level.

Figure 10 summarizes all available information on pressure changes at the start of emptying on lines A and B. The changes have been normalized by dividing by the corresponding values of $K_o\gamma Z$, the at-rest pressure. The Figure shows that the August 1978 measurements, when the bin was emptied for the first time in its service life were abnormal. However, subsequent measurements agree with each other and show:

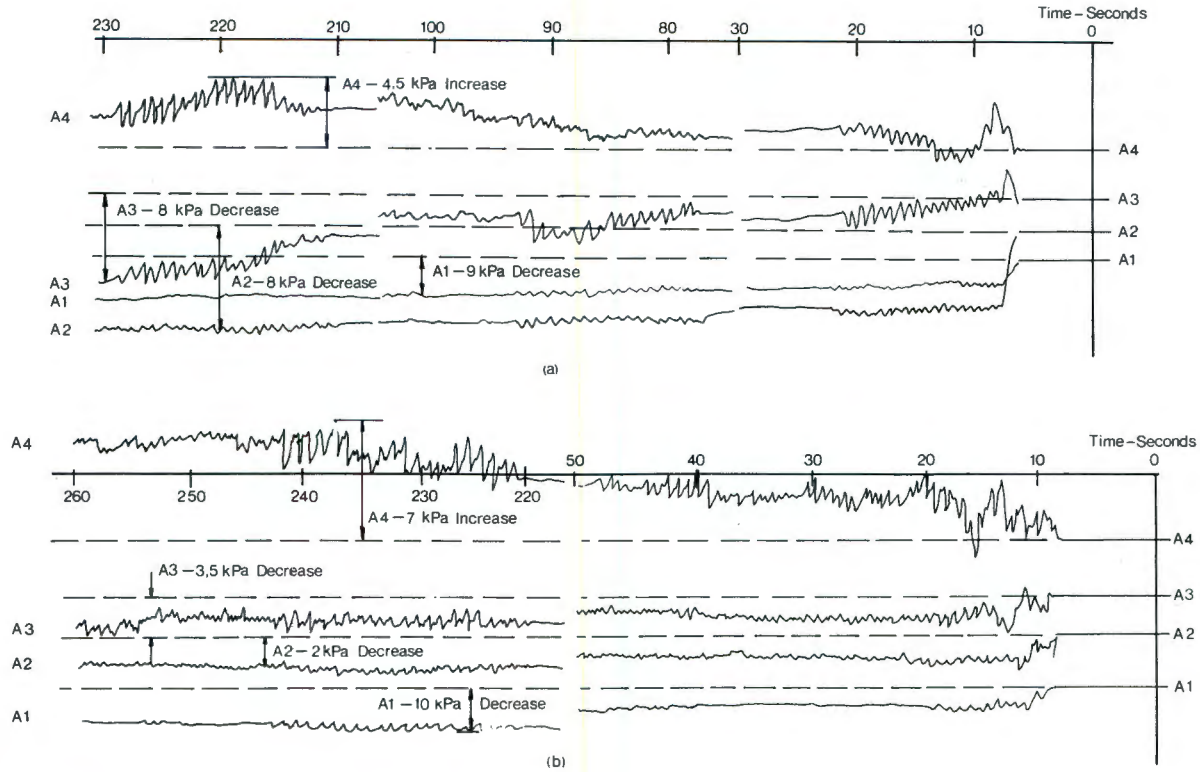

Figure 9.
Dynamic changes in lateral pressure recorded on the A-line pressure cells at the start of emptying from the south chute.

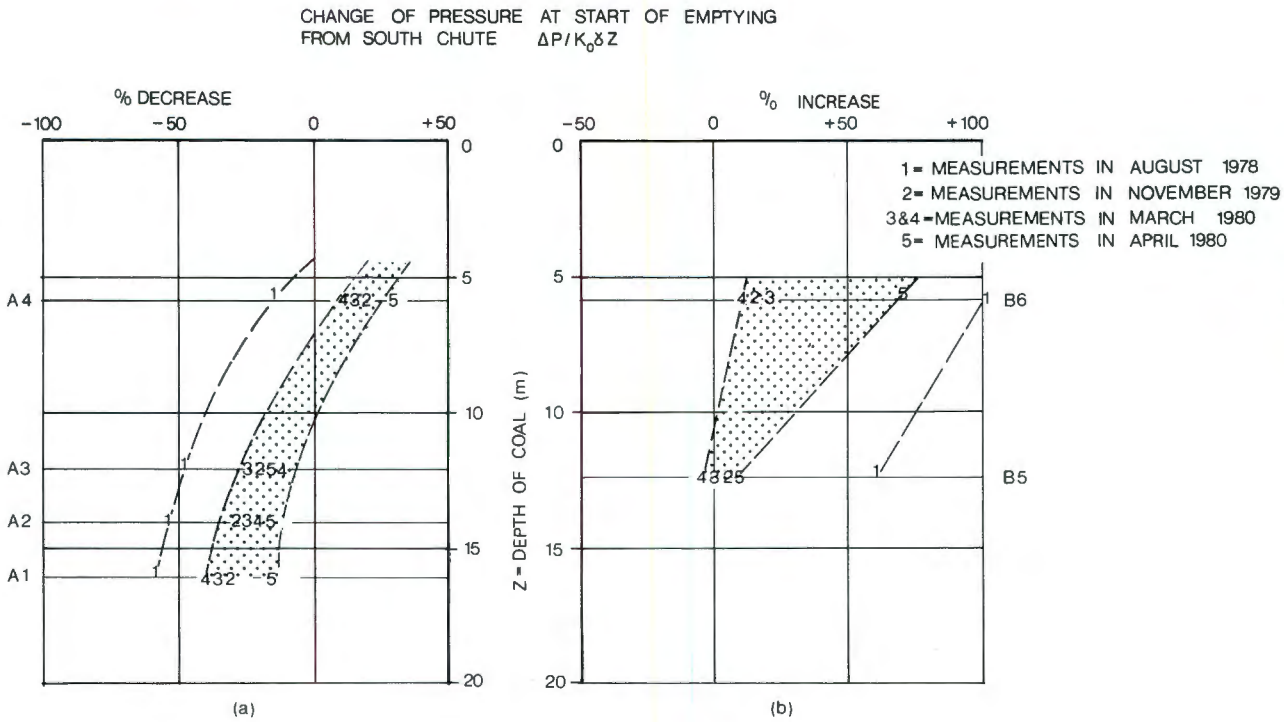

Figure 10.
Variation of pressure changes with height on A and B lines of pressure cells.

(a) that the zone of reduced pressure on the A-line extends to a height of about 8 m above cell A1, and
(b) that the zone of increased pressure on the B-line appears to extend to the surface of the fill.

Figure 10 also shows that the pressure changes are relatively modest and that now that the walls of the bin have been conditioned by use, amount at most to about 40 percent of the filling pressures. Although not shown in **Figure 10**, pressure changes along the C-line are similar in character to those along the B-line.

For the fifth set of measurements shown in **Figure 10**, discharge was started from the north chute, and then, six months later, switched to the south chute. With the exception of cell B6, however, the changes in pressure from the static condition did not appear to be much affected by the change in the flow regime.

According to Jenike,[4], the pressure changes should be roughly in proportion to the diameters of the flow funnel and the complete bin. This prediction appears entirely reasonable in this case, as the diameter of the flow funnel appeared to be 40 to 50 percent of the bin diameter.

It is of great interest and importance to note that no indication of pressure peaks, either static, as predicted by Walker[2], or dynamic, as predicted by Jenike and Johanson[3], were recorded. The authors do not consider this to be proof that such peak pressures do not arise, but merely that they have not been recorded on this particular structure. It would be foolish, and possibly dangerous, to ignore the theoretical prediction of these overpressures or the limited amount of observed evidence on prototype structures that they may, in fact, occur[9]. It is possible that the Walker-type pressure peak is occurring within the hopper bottom of the bin where it would not be recorded by the lowest pressure cells.

CONCLUSIONS

In a relatively wide, shallow bin (height of fill/diameter = 1) the relationship between depth of fill and lateral pressure approximates to the at-rest condition. However, the exact relationship between depth and pressure appears to be influenced by the previous loading history of the bin. For the bin under consideration emptying from the eccentrically placed outlets results in the development of a zone of reduced pressure on the walls of the bin adjacent to the outlet in use, while pressures increase elsewhere.

Measurements have not indicated the occurrence of peak pressures against the bin wall.

ACKNOWLEDGEMENTS

This study was sponsored by General Mining and Finance Corporation and the results are published by courtesy of Ermelo Mine Services (Pty) Ltd.

REFERENCES

1. Deutsche Normenausschuss, *Design Loads for Buildings, Sheet 6, Loads in Silo Bins,* DIN 1055, (1969).
2. Walker, D.M., *An Approximate Theory for Pressures and Arching in Hoppers,* Chemical Engineering Science **21;** 975-997 (1966).
3. Jenike, A.W. & Johanson, J.R., *Bin Loads,* Journal, Structural Division, ASCE, **94,** ST4; 1011-1041 (April 1968).
4. Jenike A.W., *Denting of Circular Bins with Eccentric Drawpoints,* Journal of the Structural Division, **93** ST 1; 27-35 (February 1967)
5. American Concrete Institute, ACI Committee 313, Proposed ACI Standard, *Recommended Practice for the Design and Construction of Concrete Bins, Silos and Bunkers for Storing Granular Materials,* Title No. 72-37, ACI Journal; 529-548 (October 1975).
6. Bishop, A.W. and Henkel, D.J., *The Measurement of Soil Properties in the Triaxial Test,* Arnold, London (1962).
7. De Wet, J., *Processing and Mass Storage of Grain (Part III),* Steel Construction, (South Africa); (12-17 September 1979)
8. Lambe, T.W. and Whitman, R.V. *Soil Mechanics,* Wiley International, New York, p 128 (1968).
9. Wright, H., *Successful Failure? A Reassessment of the Cause of Stress Cracking of the Wall of a 3000 t Capacity Reinforced Concrete Coal Bunker in 1961,* Proceedings International Conference on Design of Silos for Strength and Flow, Lancaster, Powder Advisory Centre (1980).

HEAT EXCHANGER
for Blower Discharge

This unit is designed to cool or heat air on the discharge side of a centrifugal or positive displacement blower. Hot or cold fluid is circuited through the tube side of the coil, and air is passed over the fin side, which provides the required cooling or heating of the air.

Standard sizes from 200-5000 CFM and up to 15 PSIG.

Contact us with your requirements, and we will promptly submit a quotation.

Xchanger Inc.

P.O. Box 810
617 - 14th Avenue South
Hopkins, Minnesota 55343
Phone: (612) 933-2559
Telex: 29-0978

VOLUMETRIC FEEDERS...
featuring "Inter-Auger Action"

...ACRISON'S unique, concentrically mounted, independently driven Double Auger Metering Mechanism for the most accurate metering of even the most difficult products.

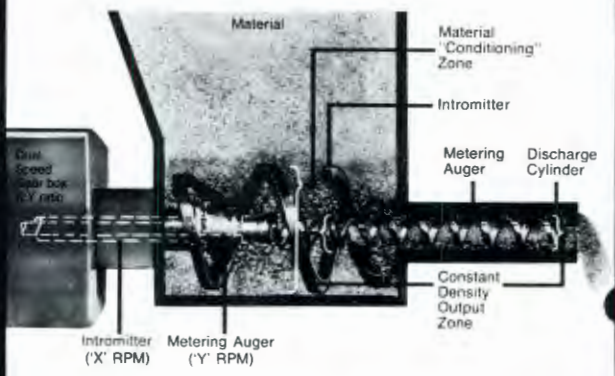

STANDARD FEATURES...

- Highest Accuracy — Generally ±1-2% (total deviation) by weight for most materials.
- Capacities from 0.001 to 3400 cu. ft. per hour.
- Feed Range 30:1
- 304 SS Double Augers, Discharge Cylinder and Seal Components.
- Full Wave SCR — Controlled D.C. Drive.
- Dust-tight, Rugged duty construction.
- Silent operation.

Series 110

With over 30,000 Volumetric Metering Devices in worldwide operation, Acrison has a unit to suit every process requirement.

Series 105

Series 120

Series 140

SEEING IS BELIEVING!

Acrison invites you to witness an actual test in our Laboratory, handling your material with the specific Equipment we recommend for your application. Check the actual performance for yourself. Don't settle for a claim. Prove the fact! No charge or obligation, of course.

Send for Bulletins

At ACRISON, Accuracy is our Business...

acrison, INC.

20 Empire Blvd.,
Moonachie, NJ 07074
201-440-8300 • Telex 134395

Int. J. Bulk Solids Storage in Silos, **2** (2) 1-8, 1986

A COMPARISON OF DESIGN AND MEASURED LATERAL PRESSURES IN A LARGE COAL LOAD-OUT SILO

G. E. Blight,
Professor of Construction Materials,
University of the Witwatersrand,
1 Jan Smuts Avenue,
Johannesburg 2000,
South Africa.

Pressures have been measured in a 10,000 ton coal load-out silo. The measuring system and measurements are described, as well as the flow pattern observed within the silo. The envelope of measured horizontal pressures is compared with the design pressure envelopes, both for the cylindrical and hopper portions of the silo.

It is concluded that little arching occurs within the silo, and that the horizontal pressure envelope can be described by the linear relationship $\sigma_h = K\gamma z$, *in which* γz *is the overburden pressure and K is Ko, the at rest pressure coefficient.*

INTRODUCTION

The reinforced concrete silo that is the subject of this paper is one of a pair of 10,000 ton train rapid load-out silos at the Optimum Colliery in the Transvaal, South Africa. The silos were instrumented with pressure cells in order to check the assumptions made in the design against conditions actually experienced by the silo. This is the second load-out silo owned by the Gencor group of mining companies to be instrumented in this way. The results of the previous study, at the Ermelo mine, were reported by Blight and Midgley[1] in 1981, and will be referred to again in this paper. **Figure 1** is a photograph of the pair of silos with a train passing through them. The open-topped cylindrical silos are 20m in internal diameter, have a wall thickness of 400mm and a storage height of 54m.

PROPERTIES OF COAL

As often happens, the silos had to be designed before the product they were to store became available. Properties for design were therefore selected from the literature. Once the silo was in operation, the coal was sampled on two occasions and subjected to laboratory tests in order to establish its properties. The range of coal properties found in the literature, the properties selected for design and those measured in the laboratory are summarized in **Table 1.**

Figure 2 shows two grading curves for coal sampled from the silo. The maximum particle size is 25mm. (Hence the diaphragm diameter of the pressure cells (see later) of 200mm is just within the range where the effects of individual particles would be negligible). For comparison, **Figure 2** shows the mean grading established for Ermelo Mines coal.

Figure 3 shows the results of measurements of the angle of wall friction, coal on concrete. Most of the measurements were made in a 100mm square shear box which theoretically is too small for the maximum particle size of the coal. However, less detailed repeat measurements made in a 350mm square shear box confirmed the results shown in the Figure.

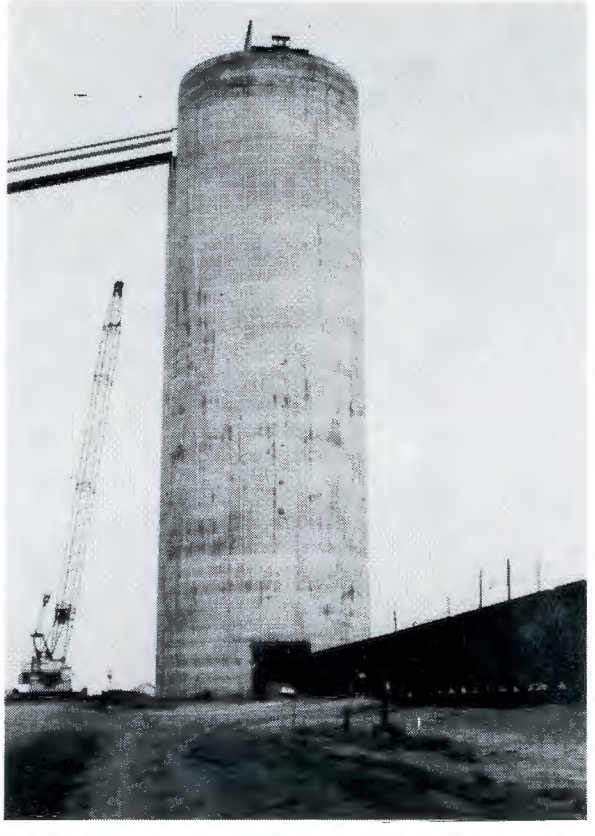

Figure 1.
The Optimum Colliery load-out silos.

Table 1
Comparison of design parameters and parameters measured for coal taken from silo

Parameter	Range from literature	Selected for design	Measured in laboratory
Bulk unit weight	6.8 kN/m³ to 10.4 kN/m³	10 kN/m³	8.08 kN/m³ to 8.83 kN/m³
Lateral pressure coefficient, K_o	0.48	**Filling**: 0.5 **Emptying**: 0.55	0.44 to 0.67
Angle of repose,	32° to 44°	41°	35° to 40°
Angle of shearing resistance, ϕ'	32° to 44°	40°	39°
Angle of wall Friction, $\delta°$	21° to 40°	**Filling**: 27° **Emptying**: 40° or 27°	36° Fill moving relative to wall
Lateral pressure Coefficient, $K_A = \frac{1-\sin\phi'}{1+\sin\phi'}$	0.26 to 0.20		0.23 (for $\phi' = 39°$)

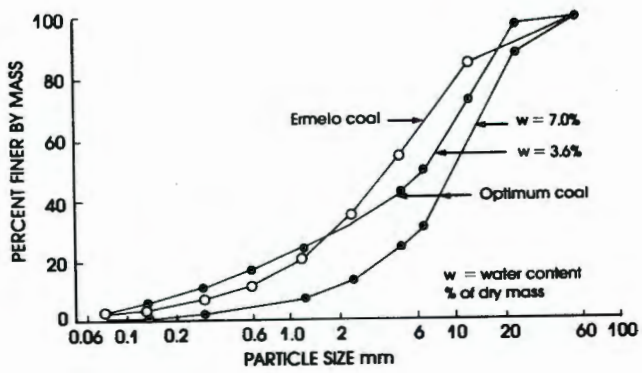

Figure 2.
Grain size analysis of coal.

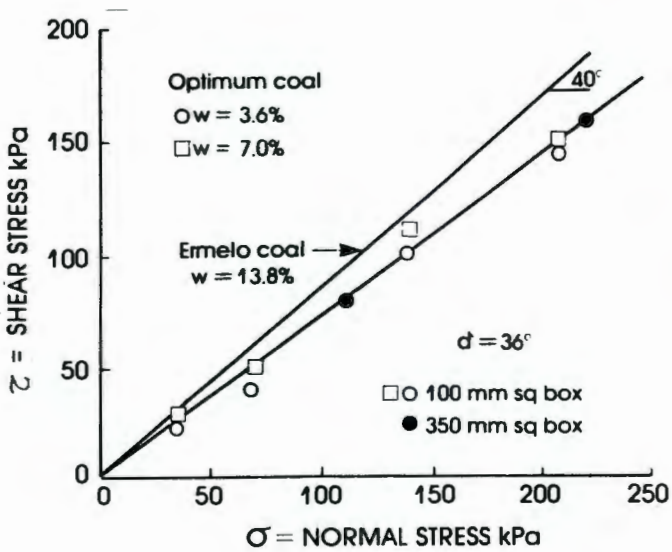

Figure 3.
Measurements of angle of wall friction, coal on concrete, at two water contents.

The measurements show that moisture content has very little effect on the angle of wall friction. For comparison, **Figure 3** also shows the results of wall friction measurements on Ermelo Mines coal. All of the measurements shown in **Figure 3** relate to coal in motion across a concrete surface. The static angle of wall friction is always a little less than the dynamic angle.

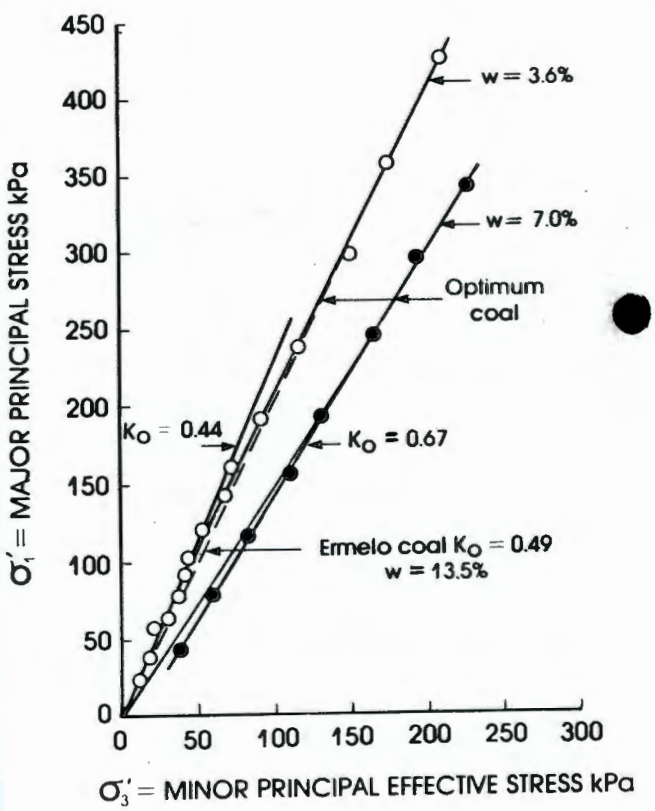

Figure 4.
Measurements of K_o in coal at two water contents.

Figure 4 shows measurements of the at rest pressure coefficient Ko, the ratio of horizontal to vertical stresses, when the coal is compressed vertically without allowing any lateral strain to occur. The measurements were made on 100mm diameter triaxial specimens using a Bishop-type Ko belt[2]. The results show that moisture content and possibly grading have an effect on Ko, the indication being that Ko increases with increasing moisture content. The value of Ko earlier measured on Ermelo Mines coal is included in Figure 4 for comparison.

The angle of shearing resistance of the coal, ϕ^1, was also measured on 100mm diameter triaxial specimens in tests at constant water content and with zero pore air pressure.

DESIGN PRESSURES

The design pressures calculated according to the American Concrete Institute Method[3] and an in-house method of the designers (Messrs. Bateman Engineering Limited) are shown in **Figure 5**. The diagram also shows the largest pressures measured in the Ermelo silo[1].

INSTRUMENTATION

Instrumentation consisted of 10 Kyowa strain gauged mercury-filled diaphragm-type pressure cells, type BE-5KF with a maximum capacity of 500kPa and a sensitivity of 0.2kPa per micro strain. The diameter of the pressure-sensitive diaphragms is 200mm. The performance and calibration of these cells has earlier been described by Blight[4].

The outlet of each silo consists of a slot with semi-circular ends measuring 6.53m long by 2.05m wide overall the opening. Because of the non-symmetric flow this opening was expected to induce, the pressure cells were installed in two vertical lines of 5 cells each, one on the long axis of the slot and one on the short axis.

The hopper section of the silo is formed of concrete benching with a constant height, giving a hopper slope of 50° on the short axis of the opening and 58° on the long axis. There was a particular interest in monitoring the occurrence of Walker[5]-type peak pressures or Jenike[6]-type switch pressures in the vicinity of the cylinder-to-hopper transition, as there is an unresolved controversy as to whether these peak pressures actually occur, and if so, under which circumstances. For this reason, pressure cells were concentrated in the vicinity of the cylinder-hopper transition, and four were installed on the benching below the transition in case the peak pressure only occurred below the transition.

Figure 6 shows the position of the pressure cells on a section through the silo. Line 1 (gauges 11 to 15) was

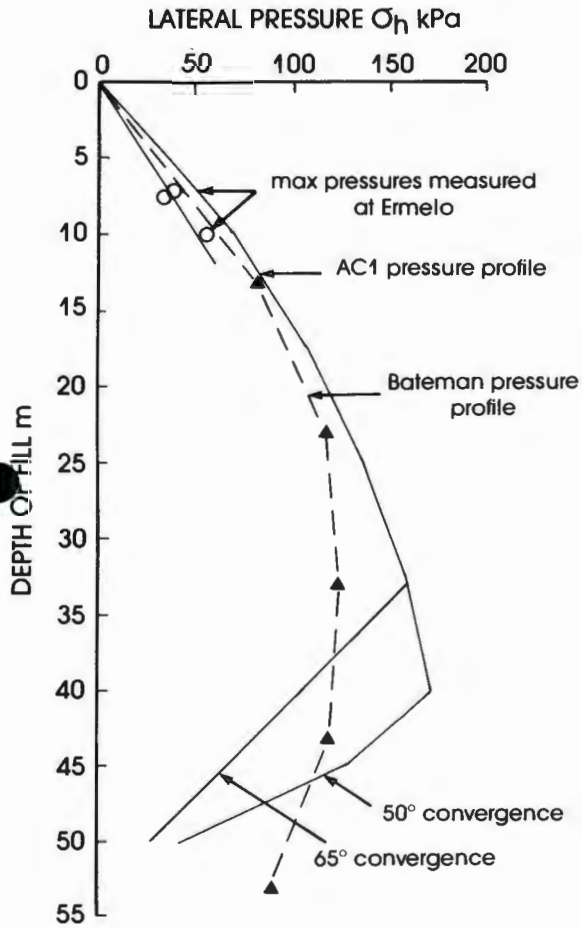

Figure 5.
Design pressures for Optimum silos.

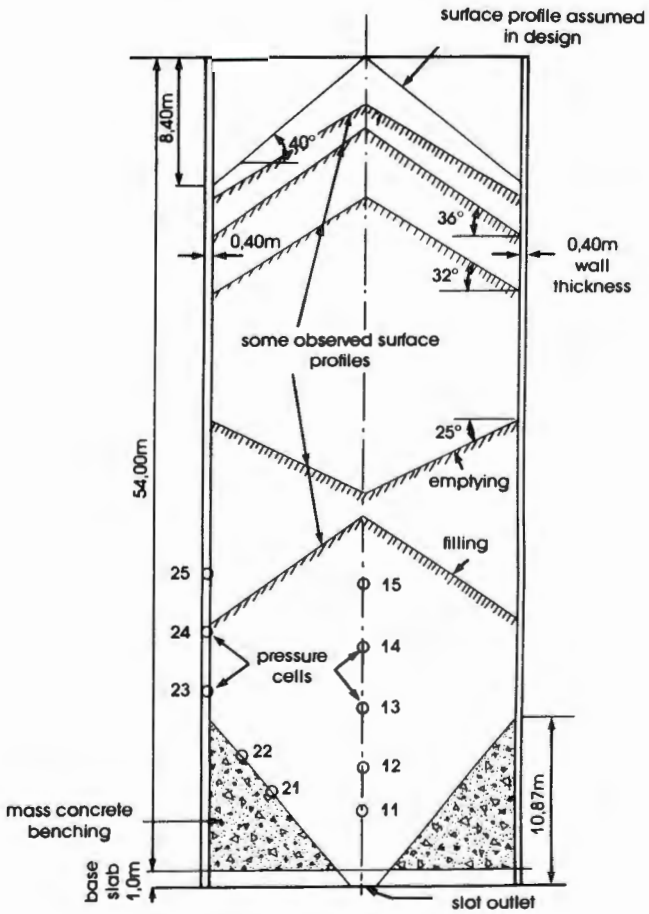

Figure 6.
Layout of pressure cells in elevation and observed and design surface profiles.

installed on the long axis of the outlet, while line 2 (gauges 21 to 25) was installed on the short axis.

The electrical leads from the pressure cells were taken down the outside of the silo walls to a control room below the base of the silo, where they were connected to a multi-point switch box. Pressures were read manually using a Huggenberger strain bridge and in certain cases, recorded via a Toa two pen chart recorder.

INSTALLATION OF GAUGES

Ideally, the gauges should have been installed before the silos had been commissioned. However, because of production requirements the installation was actually only carried out after the silos had been in service for over a year. It was then discovered that some of the steel pans that should have been cast into the silo walls to hold the gauges had been omitted. New pans were made and had to be installed before the gauges could be mounted. Access to line 1 gauge positions was by *sky-climber* platform, the platform being entered from the steel structure that bridges the silo and supports the filling conveyor (see **Figure 1**). Line 2 gauge positions were also accessed by *sky-climber*. To enter this platform, it was necessary to travel to the bottom of the silo down line 1, walk the sky-climber down the concrete benching and then scramble across into the second sky-climber. This then had to be walked up the benching to reach the cylindrical portion of the silo. Travel time from the top of the silo to a position on line 2 was 45 minutes.

The gauge holders that had been cast in during construction of the silo were of the type used earlier at Ermelo mines. These have been fully described previously, and the reader is referred to the paper by Blight and Midgley[1] for details. Lugs were welded into the gauge holders in situ, after which the pressure cell, bolted to a mounting plate was secured to the lugs by welding the mounting plate to the lugs. The lead from the pressure cell was threaded through a pipe leading to the outside of the silo prior to welding it in position. Quick-setting cement grout was then used to fill the cavity behind the gauge and bed it in solidly. Once the grout had set, a sand-epoxy resin mortar was used to fill the annulus around the gauge and to smooth off the surface flush with the surrounding concrete wall surface. Gauge holders installed after construction were of an improved type which did not require any on site welding. Gauge mounting plates were now bolted into position. (See Schaffner and Blight[7] for details). Otherwise the installation procedure was identical.

Installation was made doubly difficult by the presence of coal hung up on the walls and benching of the silo. This hard compacted coal had to be dug away down lines 1 and 2 before access to the concrete could be obtained. The presence of the hung up coal was both dangerous and a nuisance during installation as coal particles and dust rained down continually over the installers (who included the writer) as they worked.

FLOW PATTERN WITHIN SILO

A good indication of the pattern of flow occurring in the silo could be obtained from the disposition of hung up coal around the lower walls and benching. This is sketched in **Figure 7**. A ring of coal of varying height had formed around the perimeter of the silo to form a roughly circular eccentric opening as shown in **Figure 7**. Whereas the slope of the concrete benching varies from

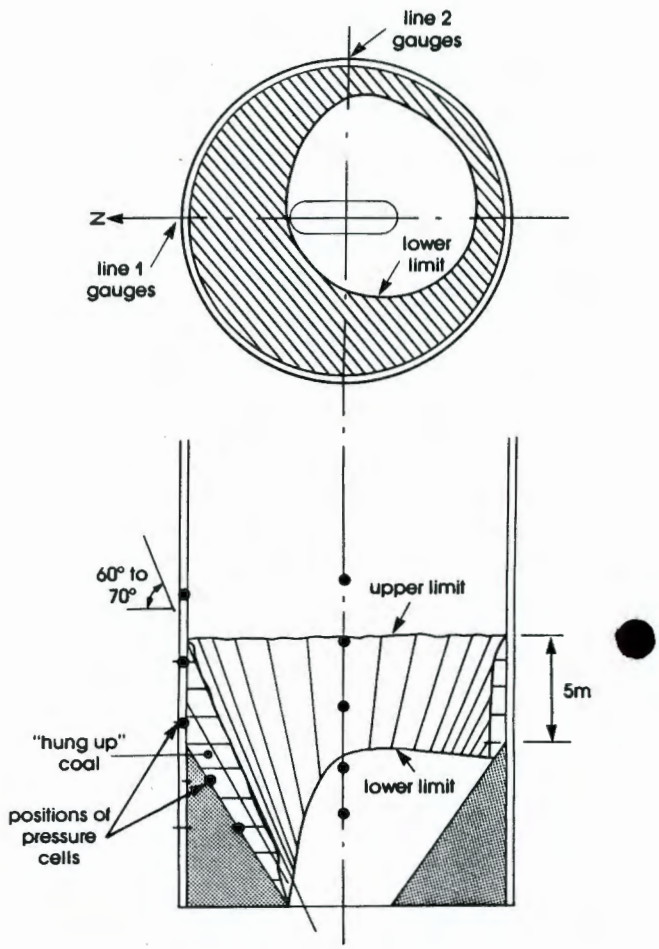

Figure 7.
"Hung-up" coal at outlet of silo.

50° to 58°, the slope of the coal surface varied from 60° to 70° and formed a vertically sided pipe leading to the outlet.

It appears that parallel flow occurs above the upper limit of the dead coal while slightly eccentric convergent flow occurs below this. This flow pattern had been predicted in general terms during design, but, naturally, the eccentricity of flow which must depend on local dimensional and filling pattern irregularities had not.

Because of the presence of the hung up coal, some of the pressure cells are permanently covered by dead material and register pressures transmitted through this material. Others are exposed to actively moving coal. The exposed and covered gauges are indicated in **Figure 7**.

As the observed surface profiles in **Figure 6** show, the plug flow is not completely uniform. The inverted cone assumed by the coal surface during discharge shows that flow on the axis of the silo is more rapid than at the perimeter.

PRESSURES MEASURED DURING FILLING AND EMPTYING

To check out the design assumptions as comprehensively as possible, it was decided to carry out the following measurements and sequence of measurements:

(i) Start with the silo empty and measure pressure during filling, uninterrupted by emptying.
(ii) Measure changes of pressure when emptying is commenced.
(iii) On selected gauges, make continuous recordings of pressure changes when emptying is commenced, in order to detect dynamic effects, transient switch pressures, etc.
(iv) On selected gauges, make continuous recordings of pressures occurring over a period of several days during normal operation of the silo.

These measurements had to be fitted in with the normal revenue-producing operations of the silo and proved unexpectedly difficult to arrange with the operating staff. Even when arranged, measurements did not always go as planned because of break-downs of equipment, unexpected cancellation of trains, etc.

The instrumentation generally performed well. However, gauge 13, although operational at the end of the installation, never functioned thereafter and gauge 22 ceased to operate about 8 months after installation.

Pressures measured during uninterrupted filling, followed by emptying

Figure 8 shows pressures measured on line 1 gauges during uninterrupted filling (long axis of outlet) while **Figure 9** shows corresponding measurements on line 2 gauges (short axis of outlet). In each figure, the design horizontal pressure envelope (the ACI envelope shown in **Figure 5**), has been superimposed on the measurements.

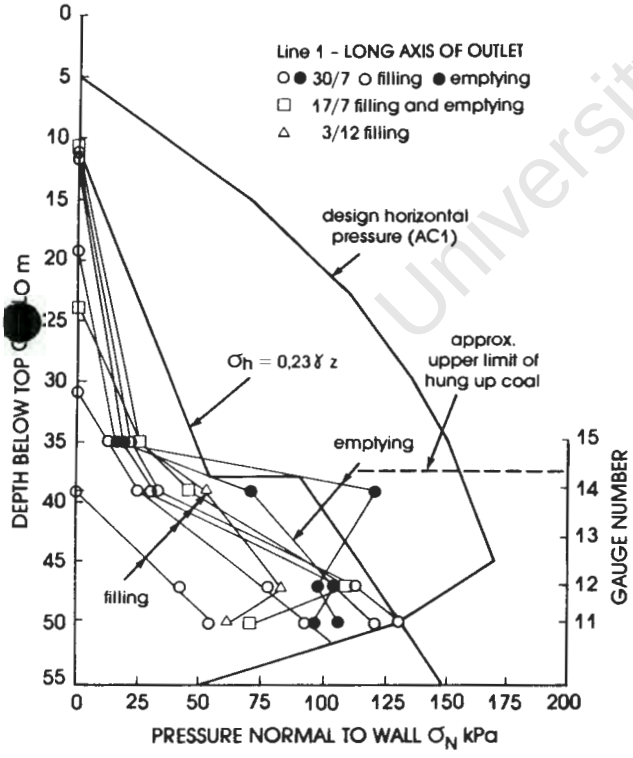

Figure 8.
Pressures observed on long axis of slot outlet.

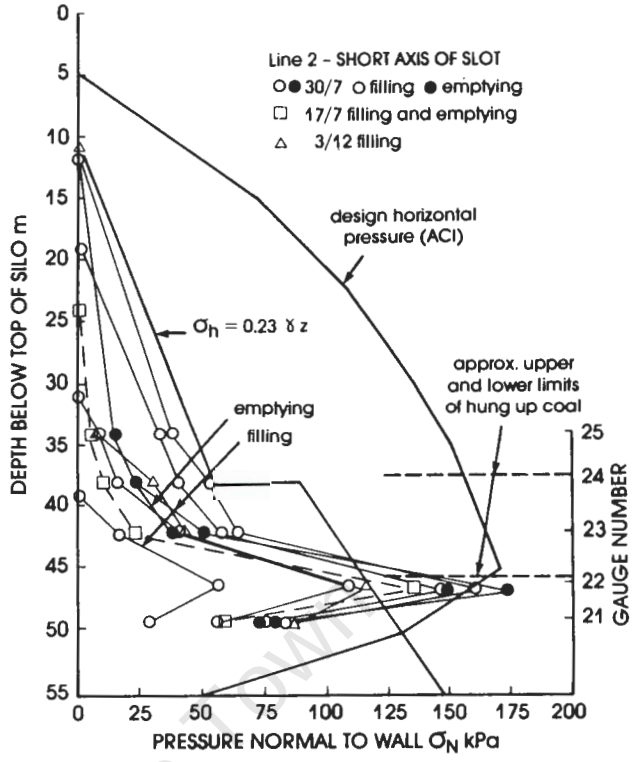

Figure 9.
Pressures observed on short axis of slot outlet.

Pressures measured on gauges 11, 12, 21 and 22 are normal to the slope of the benching and require correction to give equivalent horizontal pressures which can be compared directly with pressures measured on the remaining gauges. The correction factor and the stress circle geometry on which it is based are shown in **Figure 10**. Pressures plotted in **Figures 8 and 9** have not been corrected in this way.

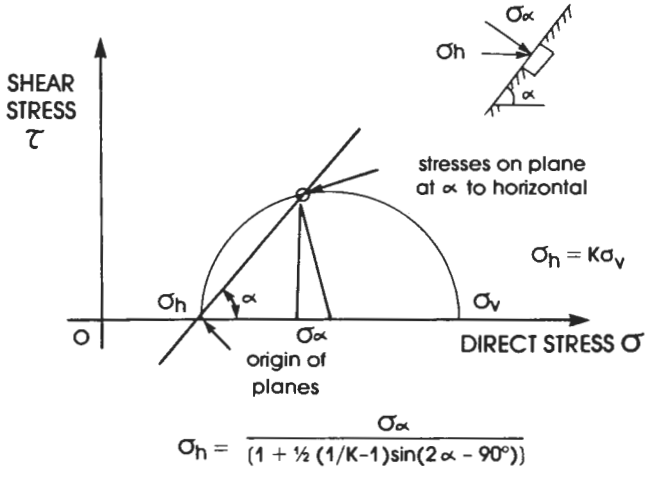

Figure 10.
Correction of pressures normal to benching to equivalent horizontal pressures.

Lateral pressures proved to be surprisingly low during filling. When emptying commenced on 30/7, appreciable and sudden increases in pressure were recorded by gauge 14 (a maximum increase of 88kPa). However, no corresponding changes were recorded by gauge 24. When emptying was commenced on 17/7 the pressure change recorded by gauge 14 was negligible. Continuous recordings of pressure at gauges 14 and 24 did not show any pressure increase at the start of emptying either. It therefore appears that appreciable pressure increases may occur at the point of transition from parallel to convergent flow, but that their appearance is an irregular phenomenon.

All of the readings recorded by gauge 21 appear anomalously high. This may result from a local irregularity in the profile of the concrete or from a high sensitivity of the gauge. The latter explanation is not likely as all of the gauges were calibrated before installation. The profile of the benching was very rough and poorly shaped and local irregularity which caused the gauge to be located on a high spot on the benching is the most likely cause of the anomaly.

To summarize **Figures 8 and 9**, lateral pressures in the silo were generally far lower than expected. There is vague evidence that Walker-type peak pressures may occur, but their appearance and magnitude are irregular.

There is a tendency for pressures measured parallel to the short axis of the slot (line 2) to be slightly larger than those measured normal to the long axis (line 1). This is consistent with the observed eccentricity of flow (see **Figure 7**).

The measurements recorded in **Figures 8 and 9** have been replotted as horizontal stress (σ_h) versus vertical stress (σ_v) in **Figure 11**. The field measurements can thus be compared directly with the laboratory measurements shown in **Figure 4**. In compiling the figure, the vertical stress has been taken as the mean unit weight of 8,4 kPa/m multiplied by the depth below the fill surface.

Most of the measured pressures are considerably less than would be expected on the basis of laboratory Ko measurements. In fact, measured pressures show better agreement with the active condition for which

$$\sigma_h = K_A \sigma_v \qquad (1)$$

Maximum pressures, however, are contained by the Ko condition. The larger recorded pressures have been corrected to equivalent horizontal pressures using a value of K = 0.23. **Figure 11** shows that the correction is valid, as corrected pressures agree with direct measured horizontal pressures. (Pressures measured on gauge 22 have not been included).

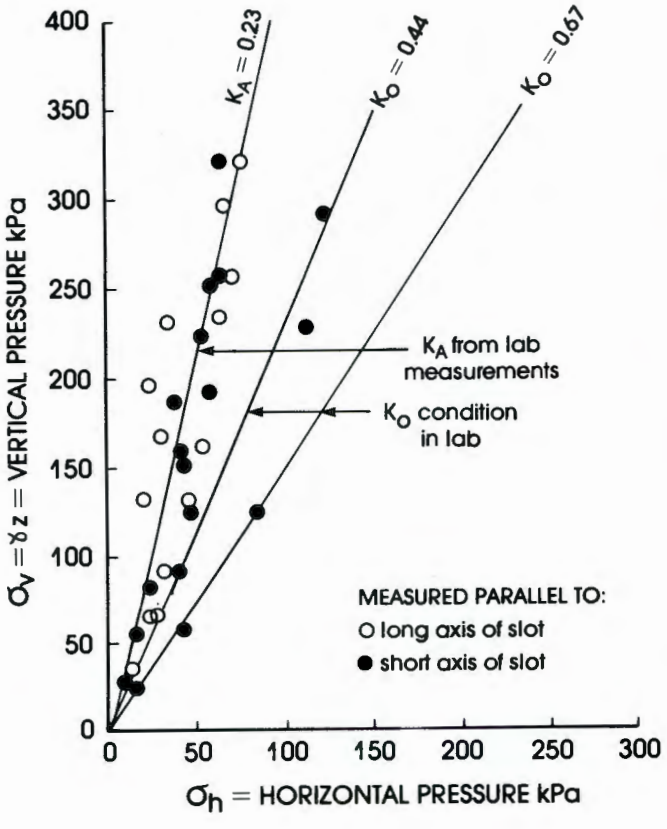

Figure 11.
Relationship between measured horizontal stress and calculated vertical stress during filling.

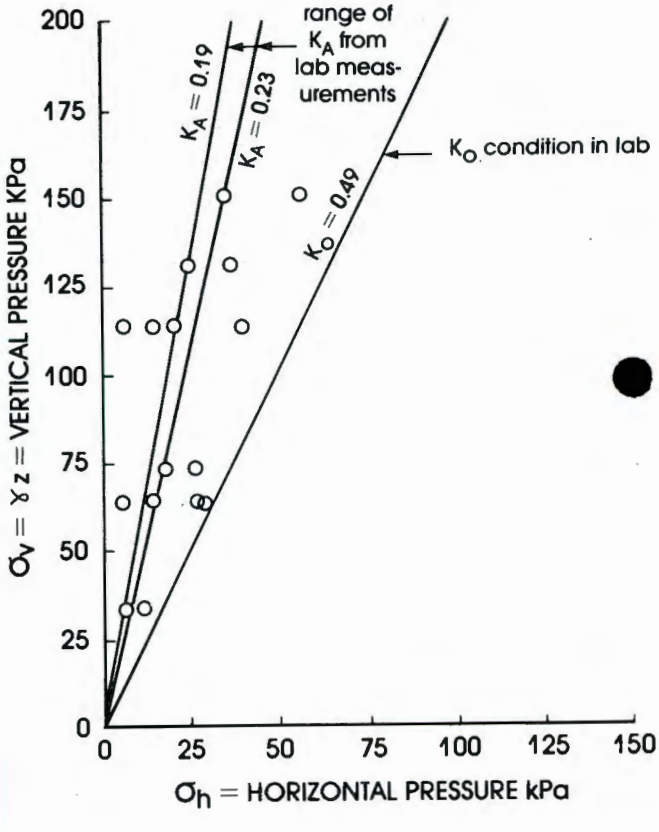

Figure 12.
Ermelo mines silo: relationship between measured horizontal stress and calculated vertical stress during filling.

For comparison, **Figure 12** shows a plot similar to **Figure 11** for the Ermelo Mines silo. The pattern is very similar with the mean relationship between σ_v and σ_h being represented by the active condition and the Ko condition providing a containing envelope to the maximum pressures.

Note in each case there is no differentiation between horizontal pressures measured on vertical walls or on the sides of the hopper. Equation (1) applies equally well to pressures in either zone.

Calculated pressure envelopes

Figures 8 and 9 also show a pressure envelope calculated on the basis of Equation (1) above with σ_v estimated as

$$\sigma_v = \gamma z \text{ and } K = 0.23$$

This simple relationship gives a good containing envelope to all of the data except one observation of gauge 14 and the data recorded by gauge 22, which appears to be anomalous. Arching effects appear to be virtually absent from this silo. This is not surprising when one considers that the ratio of fill depth to silo diameter is only about 2.

As **Figures 8 and 9** show, conventional design pressure envelopes grossly overpredicted horizontal pressures in this case.

PRESSURE CHANGES RECORDED WHEN EMPTYING IS COMMENCED

Figure 13 shows pressure changes recorded on gauges 14 and 24 at the commencement of emptying a silo previously filled from empty without interruption. The first portion of the chart was recorded overnight from 19h30 to 11h30 on the next day and shows that when the silo is left standing in a full condition, very little change in pressure occurs, the maximum change in the reading of gauge 24 being about 3kPa. The *spikes* in the record indicate the start of emptying, each spike representing the opening of the chute to fill a wagon with coal. The 60 second interval between spikes represents the time required to discharge 65T of coal. It is suspected that the short vertical lines recorded at each opening of the chute (representing about 7kPa change in pressure) do not result from pressure changes at all, but represent electrical interference as the motors driving the silo's hydraulic system cut in.

Figure 13 shows that there is a small change in pressure at gauges 14 and 24 when loading is started. The pressure changes are very small but the directions of change are consistent with the larger pressure changes recorded by these gauges on another occasion (see **Figures 8 and 9**).

PRESSURES RECORDED DURING NORMAL WORKING OF THE SILO

Figures 14 and 15 represent portions of a week-long recording of pressures at gauges 14 and 24 as well as the temperature at a point on the outside of the silo wall on gauge line 1. **Figure 14** shows the effects of partly emptying the silo, followed by complete emptying some 14 hours later. The recorded changes of stress of 52kPa at gauge 14 and 30 kPa at gauge 24 agree with pressures recorded for these two gauges in **Figures 8 and 9.** The temperature change recorded in **Figure 14** was only about 4°C and had no effect on pressures in the silo. **Figure 15** shows pressure changes recorded during filling and subsequent emptying. The recorded stress changes again agree reasonably well with those shown in **Figures 8 and 9 and 14**. There are, in **Figure 15,** a couple of unexplained features, mainly a disturbance in the pressure recorded that appears to be associated with a small, but sharp drop in temperature. In no case was anything resembling a switch pressure measured.

CONCLUSIONS

1. The observations made on the Optimum and Ermelo silos have shown that arching effects are negligible in coal silos having a height to diameter ratio of up to 2:1. The relationship between fill depth and lateral pressure can adequately be described by the relationship

$$\sigma_h = K\gamma z \qquad (1a)$$

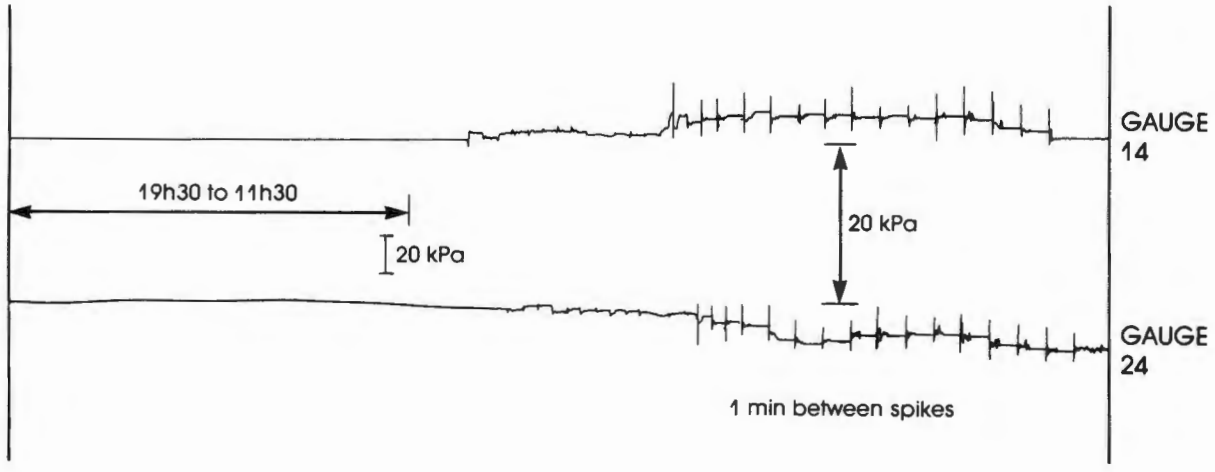

Figure 13.
Pressure record before and at start of load-out.

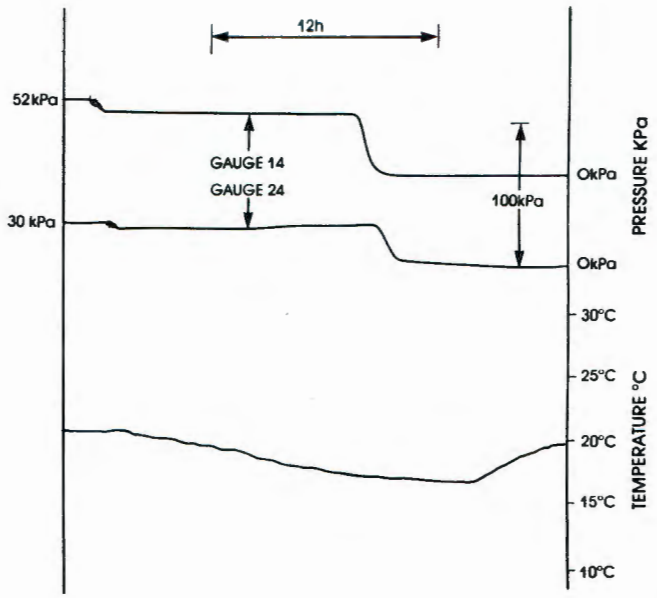

Figure 14.
Recording of pressures at gauges 14 and 24 over 24h period during which silo was completely emptied.

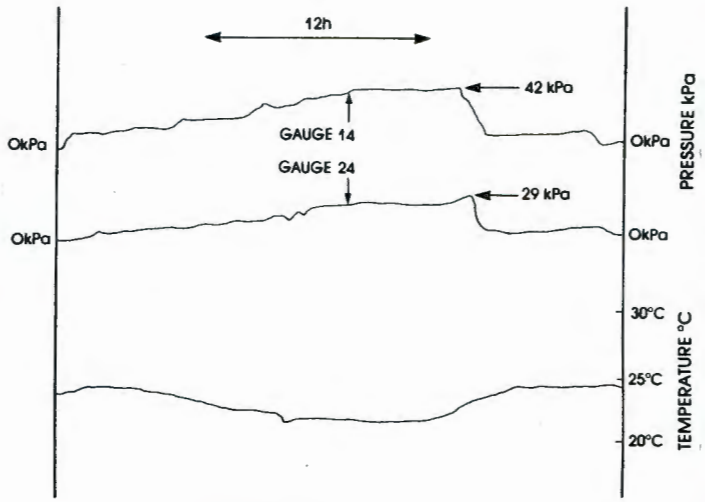

Figure 15.
Recording of pressures at gauges 14 and 24 over 24 h period during which silo was partly filled and then emptied.

Figures 11 and 12 of this paper show that Equation (1a) with $K = K_A$ gives a good description of the average lateral pressure in the silo, whereas if K = Ko, an envelope is obtained which contains all measured values of lateral pressure. This envelope applies both to the cylindrical and hopper portions of the silo.

2. If the silo is filled without interruption and then emptied, lateral pressures increase slightly as emptying starts. There is only vague evidence that anything approaching a switch pressure may develop.

ACKNOWLEDGEMENTS

The paper is published by kind permission of General Mining Union Corporation Limited, owners of the Optimum and Ermelo silos. Thanks are due to Mr. R. Mohle and Mr. P. du Toit for their help and encouragement in carrying out the project.

Thanks are also due to Mr. J. van Zyl for arranging the operation of the silo to enable suitable sets of readings to be taken.

REFERENCES

1. G. E. Blight & D. Midgley, *Pressure Measured in a 20m Diameter Coal Load-out Bin,* Journal of Powder and Bulk Solids Technology, **5** (1981)2;21-31.
2. G. E. Blight, & Z. Ofer, *Laboratory Determination of Ko and Comparison With Prototype Silo Observations,* Proceedings, 4th Australian-New Zealand Conference on Geomechanics, Perth, **1** (1984);83-87.
3. American Concrete Institute, ACI Committee 313, *Proposed ACI Standard, Recommended Practice for the Design and Construction of Concrete Bins, Silos and Bunkers for Storing Granular Materials,* Title No 72-37, ACI Journal, 1975;529-548.
4. G. E. Blight, *Measuring Pressures in Silos with Pressure Cells, Proceedings,* 2nd International Conference on Design of Silos for Strength and Flow, Powder Advisory Centre, London, (1983);217-229.
5. D. M. Walker, *An Approximate Theory for Pressures and Arching in Hoppers,* Chemical Engineering Science Vol **21** (1966);975-997.
6. A. W. Jenike, J. R. Johansen, and J. W. Carson, *Bin Loads Part 3: Mass-Flow Bins,* Journal of Engineering for Industry, ASME, Paper 72-MH-2, (1972);1-7.
7. R. H. Schaffner, & G. E. Blight, *Pressures in a 20m Diameter Ibau-type Cement Storage Silo,* Submitted to International Journal of Bulk Solids Storage in Silos, 1985.

Int. J. Bulk Solids Storage in Silos, **2** (3) 17-24, 1986

A COMPARISON OF DESIGN AND MEASURED LATERAL PRESSURES IN A LARGE IBAU-TYPE CEMENT STORAGE SILO

R.H. Schaffner,
Watermeyer, Legge, Piesold and Uhlmann,
PO Box 221, Rivonia 2128
Republic of South Africa
and
G.E. Blight,*
University of the Witwatersrand
1 Jan Smuts Avenue
Milner Park, Johannesburg 2000,
Republic of South Africa

Measurements have been made of the pressures normal to the walls and inverted conical bottom of an IBAU-type silo that stores cement powder.

The physical properties of the cement powder were measured in the laboratory and used to predict the pressure distributions by means of a modified form of Janssen's theory.

Excellent agreement was obtained between the measured and predicted pressures, both on the vertical walls of the silo and on the sides of the inverted cone.

INTRODUCTION

The Pretoria Portland Cement Company has recently commissioned two 14,000m^3 cement storage silos at their Jupiter works in Germiston, South Africa. The silos are designed to serve road tankers for distribution of cement in the Witwatersrand area. The silos are of the Ibau-type, having an inverted conical base. The principal dimensions of each silo are:

inside diameter: 20m
height of storage cylinder: 50m

Figure 1 shows the structure of one of the silos complete. The second silo is at pedestal level with the internal shuttering of the cone in place.

During the course of designing the silos, a comprehensive investigation was made of the mechanical properties of Portland cement. Pressure cells were installed in the walls and cone of one of the silos to enable service pressures normal to the walls and cone to be measured.

The silos were designed in late 1982, in accordance with the recommendations of the German silo design code DIN1055 Part 6 of November 1964, including the May 1977 amendment and taking into consideration the recommendations of the redrafted version of November 1982.

*To whom all correspondence should be addressed.

Figure 1.
Silo 1 complete, pedestal to silo 2 complete with internal shuttering for cone in place.

The purpose of this paper is to report on the measured pressures on the walls and cone of the one silo, and to give a comparison between the actual pressures and the design pressures calculated at the time of the design.

TESTS ON CEMENT POWDER

Information on the physical characteristics of Portland cement that are relevant to silo design have never been determined for South African cements. Properties recommended by various codes of practice, eg. the German DIN1055, are not necessarily realistic. This is both because South African cements may differ in properties, for example, from European and American cements, and also because "code properties" are designed to give safe values of lateral and vertical pressures when used in conjuncton with the method of calculation advocated by the code. These methods of calculation are formalized so that the designer does not need to have a deep knowledge of how material in silos behaves in order to design safe silos.

In this case it was decided to measure the following properties of some typical Pretoria Portland Cement products:

(i) loose and vibrated unit weight (γ)
(ii) angle of internal friction (ϕ)
(iii) angle of wall friction (δ)
(cement on concrete)
(iv) at rest pressure coefficient K_o
(v) cohesion at low stress after precompression (c)

The tests were carried out on four samples of material that might eventually be stored in the new silos. These comprised:

1. Ordinary Portland Cement (OPC)
2. Portland Blast Furnace Cement (PBFC)
3. OPC plus 5% milled blast furnace slag (JPC5/SL)
4. OPC plus 5% pulverized fuel ash (JPC5/FA)

The angle of internal friction and the angle of wall friction were measured in the shear box apparatus using standard geotechnical methods. The at rest pressure coefficient was measured in a modified oedometer apparatus (Blight and Ofer[1]). The cohesion at low stress was measured after precompressing to a normal stress of 500kPa, a pressure in excess of any likely to be realised in the silo. In every case, the envelopes from which ϕ and δ were measured were perfectly linear up to a normal stress of 250kPa. Comprehensive tests were performed on the OPC, while for the other three products, loose and vibrated unit weights were measured and single measurements of ϕ and δ were made to see if these products have significantly different properties to OPC. As the summarized results in **Table 1** show, differences proved small enough for all four products to be regarded as identical.

The comparison between the "design values" and those actually measured illustrates the points made above concerning "code properties".

The combination of a very high assumed unit weight and a very low angle of wall friction must result in calculated wall pressures that are safe, but in all probability unrealistically large.

During filling of a silo, the material is "at rest", ie. it is compressing vertically, but not straining laterally. The vertical compression is sufficient to set up a shear stress between the walls and the fill and hence silo action can develop. This statement is supported by **Figures 2a and 2b**. **Figure 2a** shows that under a vertical stress of 250kPa (approximately the maximum that will develop under the design assumptions), a vertical compression of 13% occurs, or 130mm per m depth of cement. **Figure 2b** shows that this displacement would be far more than enough to develop full wall shear. One is therefore quite justified in assuming full silo action in calculating wall pressures for cement silos during filling.

CALCULATED WALL PRESSURES

Figure 3 compares pressures normal to the wall and cone of the silo calculated for the design properties and on the basis of actual measured properties for cement powder.

The design pressures were calculated by means of Janssen's theory using a ratio of horizontal to vertical

Table 1
Properties of Various Cements

Cement property	Design values	Type of cement (measured)			
		OPC	PBFC	JPC5/SL	JPC5/FA
Unit weight γ kPa/m					
Loose	17.0	12.3	11.4	11.5	11.9
Vibrated		16.3	14.8	15.0	15.5
Angle of internal friction ϕ	28°	42°	42°	42°	42°
Angle of wall friction cement on concrete δ	22°	39°	39°	37°	38°
At rest pressure coefficient K_o Approximate: $K_o=1-\sin\phi$	0,53	0,29	0,29	0,29	0,29
Measured K_o: Loading	–	0,35-0,37	–	–	–
Unloading		Up to 1,5			
Cohesion after pre-compression c kPa	0	25	–	–	–

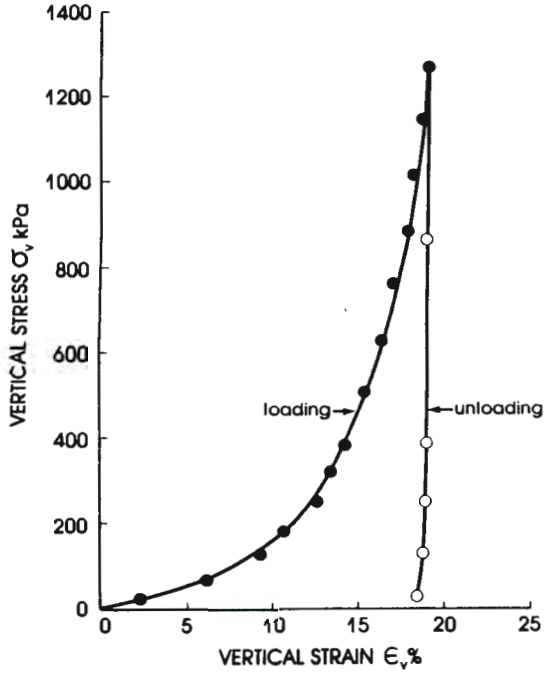

Figure 2a.
Stress-strain relationship for K_o compression of Jupiter OPC Powder.

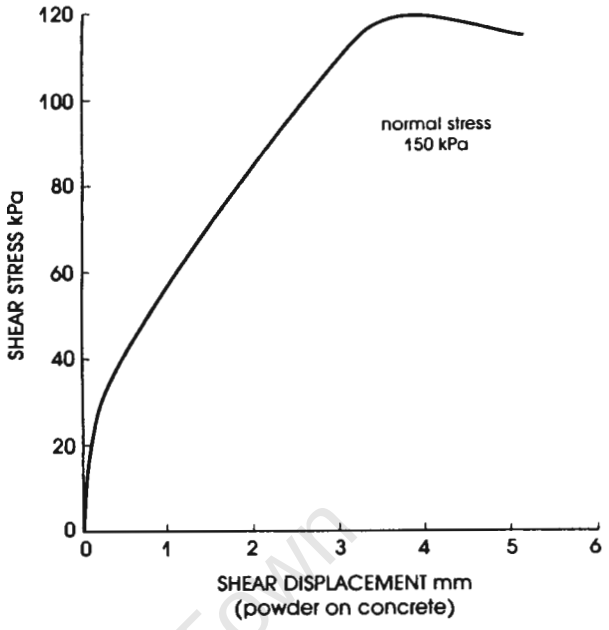

Figure 2b.
Typical stress-shear displacement relationship in wall friction test on Jupiter OPC Powder.

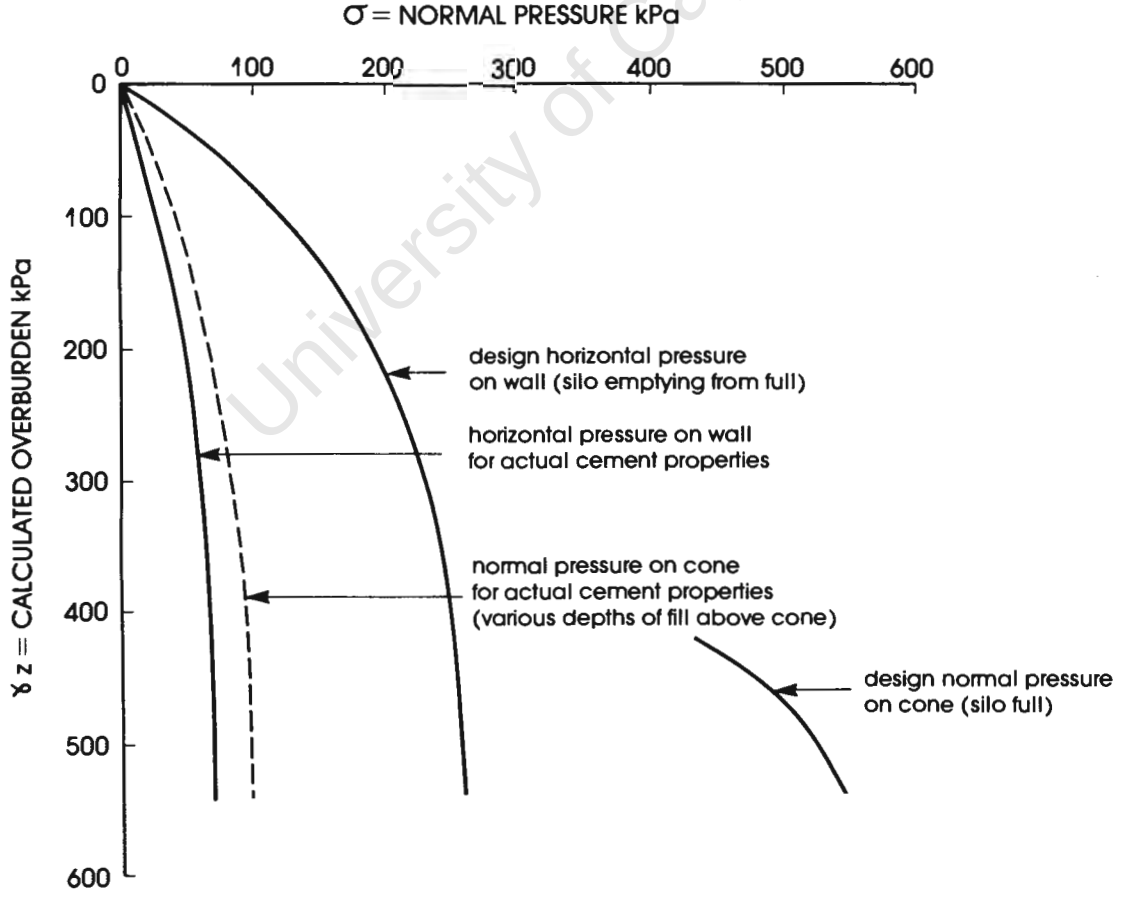

Figure 3.
Comparison of design pressures with pressures calculated for actual cement properties.

stresses of 1.0 for the emptying condition, an angle of wall friction of 22° and a fill unit weight of 17kPa/m. They include an allowance for eccentric discharge in the form of a factor C_1. In this case C_1 was assessed as 1.16. In addition, a computation factor $C_2 = 1.2$ was applied together with a factor to allow for local load peaks, $C_3 = 1.24$. These were based on office practice.

Hence the total extent to which the calculated design pressures was factored was

$$C = C_1.C_2.C_3 = 1.73$$

For design purposes, pressure on the cone was calculated as arising from a vertical pressure equivalent to the full overburden pressure. The vertical and horizontal pressures were combined according to the equation:

$$\sigma_n = \sigma_v \cos^2\alpha + \sigma_h \sin^2\alpha \qquad (1)$$

in which α is the cone angle of 60°. A computational factor of 1.14 was then applied to the result.

Pressures based on actual material properties were later calculated using Janssen's equation together with a loose fill unit weight* of 12kPa/m, an angle of wall friction of 39° and a ratio of horizontal to vertical stresses of Ko = 0.35. the value of Ko for unloading was not used as the measured pressures gave no indication that any significant unloading effect occurs in the silo during operation.

Normal pressures on the cone were calculated from the equation

$$\sigma_n = \sigma_h \left[1 + \left(\frac{1}{K} - 1 \right) \cos^2 60^\circ \right] \qquad (2)$$

again with K = Ko = 0.35.

Justification for these procedures and comment on the comparison between pressures calculated on this basis and the design pressures will be given after considering the pressures measured in the silo.

INSTRUMENTATION

The silo has been instrumented with 11TML strain-gauged mercury-filled diaphragm-type pressure cells (type KD-5B) having a maximum capacity of 500kPa and a sensitivity of 0.05kPa per microstrain.

The pressure cells have a sensitive diameter of 200mm. The performance of this type of pressure cell has been described by Blight[3]. It would obviously have been preferable to have more pressure cells installed. The budget for the research limited the number to 11.

In addition to the pressure cells, three pairs of thermo-couples were installed to measure temperature gradients through the walls of the silo. These proved unsuccessful and will not be referred to again. However, it should be noted that the pressure cells are fully temperature-compensated. Their readings are quite unaffected by temperature fluctuations.

The layout of the instrumentation in relation to the main dimensions of the silo is illustrated in **Figure 4**. Discharge of material takes place via a series of eight symmetrically disposed outlet ports at the apex of the ring-conical hopper formed by the outer walls of the silo and the central inverted cone. The flow pattern within the silo consists of parallel plug-flow in the material above the top of the cone with a transition to ring-convergent flow within the ring-conical hopper portion. Emptying takes place by rotational use of diametrically opposite pairs of outlets and the flow should, on average, be uniform around the periphery of the silo. The silo is filled through the top by a single central pipe so that filling should also be centric.

The pressure cells were positioned in two vertical planes at right-angles so as to detect any major circumferential non-uniformities of flow. The gauges in the outer walls were staggered in height so as to provide a better coverage of the height of the silo. In **Figure 4** gauges W1, W4 and W6 are located midway between outlets. Gauges W2, W3, W5 and W7 are located in the plane of an outlet.

Figure 5a shows the method used to install the pressure cells in the walls of the silo: A pan containing three studs welded to its back plate at 120° intervals was cast into the wall during construction. The cell was bolted to a face plate having a diameter 20mm less than the

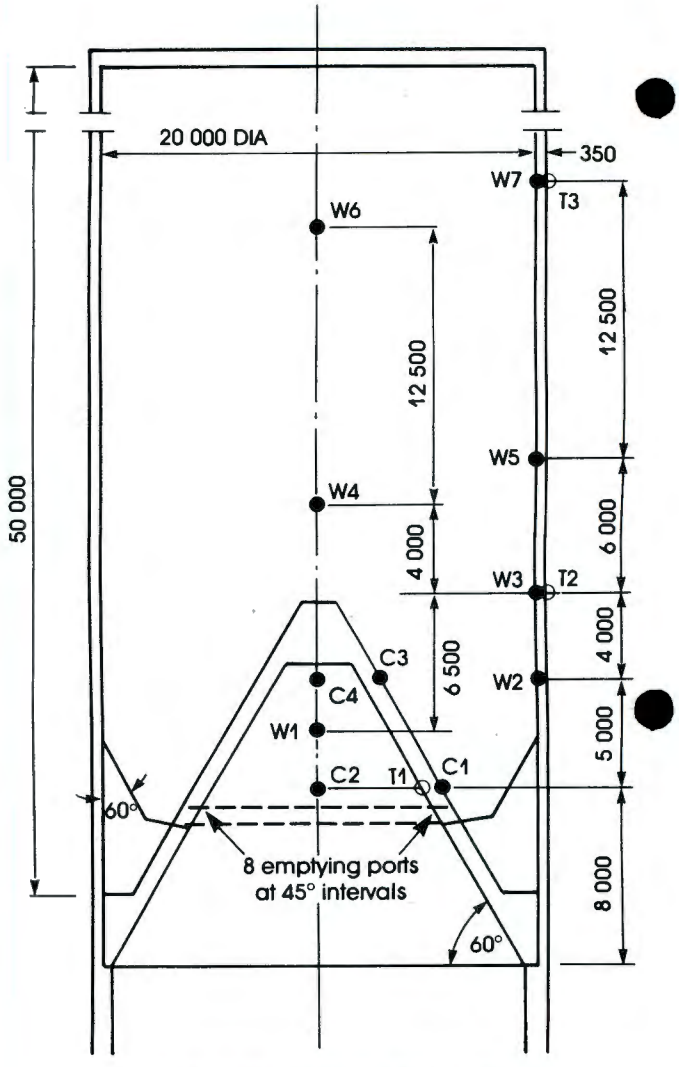

Figure 4.
Layout of instrumentation in silo.

* The loose unit weight was used because measurements on other silos (eg. Blight[2]) have shown that material poured into a silo remains in a loose state.

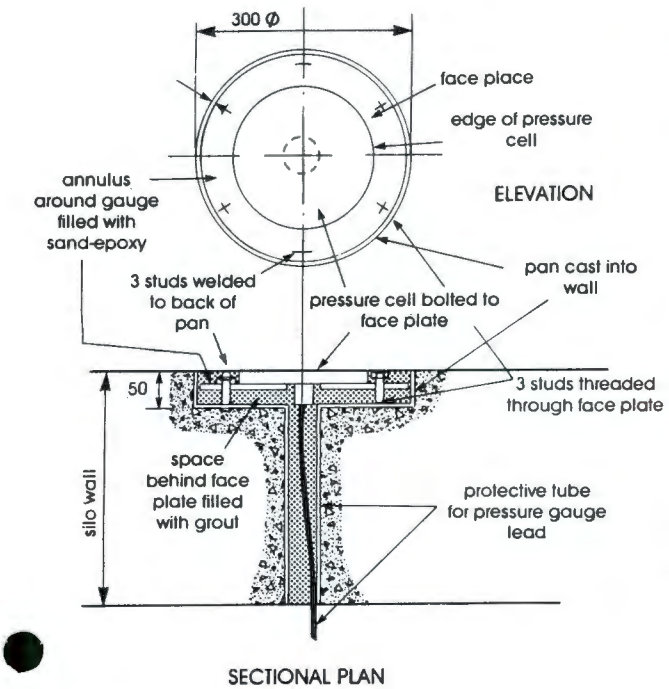

Figure 5a.
Method of mounting pressure gauge in wall of silo.

Figure 5b.
Gauge installed in wall prior to grouting and smoothing off.

inside diameter of the pan. The face plate has three plain clearance holes drilled in it at 120° intervals and three tapped holes also at 120° and on the same pitch circle. Three studs with an overall length slightly less than the depth of the pan were threaded into the tapped holes. The cell was placed in position with its electrical lead threaded through the pipe, passing to the outside of the wall, and nuts and washers were placed on the studs welded to the back of the pan.

By tightening or loosening these nuts and adjusting the studs threaded through the face plate, the position of the pressure cell was then adjusted, using a short straight-edge until the face of the cell was co-planar with the inner surface of the silo. **Figure 5b** shows a pressure cell at this stage of installation.

The space between the face plate and the rim of the pan was then stuffed with a length of pre-formed rubber joint filler and the void behind the face plate poured full of a quick-setting cement grout. Once the grout had set, the strip of joint filler was pulled out and the space between the pan and the side of the pressure cell (seen in **Figure 5**) was plastered full with a sand-epoxy mortar, thus finishing off the face of the pressure cell flush with the inside surface of the silo wall. Finally the surface of the pressure cell was painted with epoxy resin and strewn with fine sand to give its surface a similar texture to that of the surrounding concrete.

PRESSURES ON VERTICAL WALLS

Figure 6a summarizes measurements of pressure on the vertical walls of the silo. The pressures shown in **Figure 6a** have been plotted against the calculated overburden γz. They thus correspond to the depth z of each pressure cell below the surface of the cement in the silo. Also shown in **Figure 6** are two curved pressure envelopes labelled "arching $K_A = 0.20$" and "arching $K_o = 0.35$". These represent the results of calculations by means of the Janssen formula using measured properties for the cement. K_A is the active pressure coefficient

$$K_A = \frac{1-\sin 42^\circ}{1+\sin 42^\circ} = 0{,}2 \qquad (3)$$

while K_o is the at rest pressure coefficient of 0.35 which was measured in the laboratory (see **Table 1**).

Also shown in **Figure 6a** are two straight-line envelopes labelled "no arching" and drawn for the same pressure coefficients. These represent the lines

$$\sigma_h = K\gamma z$$

in which σ_h is the horizontal pressure, K is the pressure coefficient and γz is the calculated overburden pressure at depth z below the surface of the fill.

The silo is filled when cement is available, and emptied on demand. The pressures shown in **Figure 6a** therefore correspond to a condition of mixed filling and emptying. It will be seen later that the transition from a static to an emptying condition causes little change in pressure.

It will be seen from **Figure 6a** that the calculated lines represent containing envelopes to the measured pressures and that most of the measured pressures are considerably less than the calculated values. The arching envelope for K_o gives the best-fitting containing envelope, although at very low overburden stresses, some pressures fall outside this line. The effect of convergent flow is to cause the pressure to decrease linearly towards the outlet. The pressure profiles calculated by means of the Walker theory, for which the "unloading" value for Ko of 1.5 would seem appropriate, just do not seem to apply. This linear pressure reduction towards the outlet is indicated by a dashed inclined line in **Figure 6a**.

Although **Figure 6a** shows that the results of the pressure measurements are scattered, it does not indicate

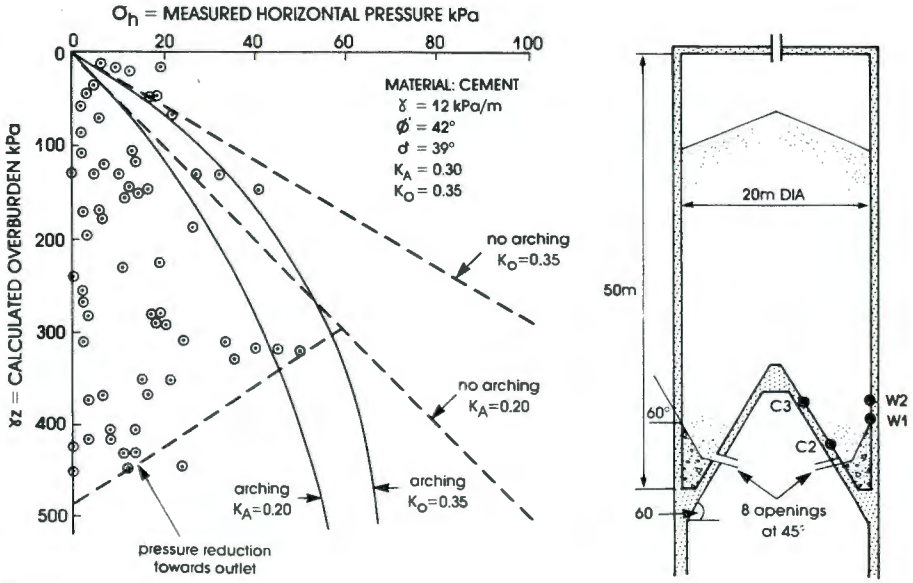

Figure 6a.
Observed pressures on walls.

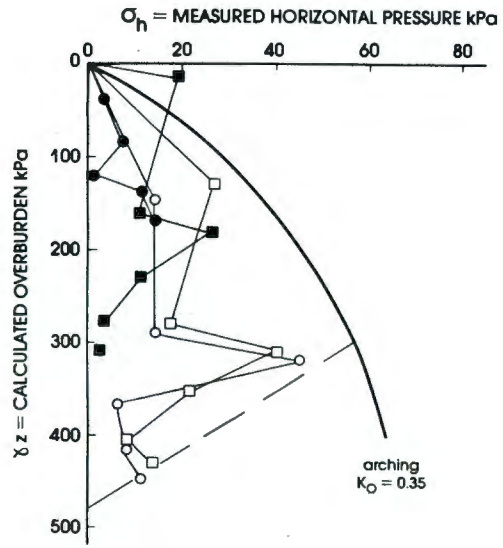

Figure 6b.
Individual profiles for pressure on wall.

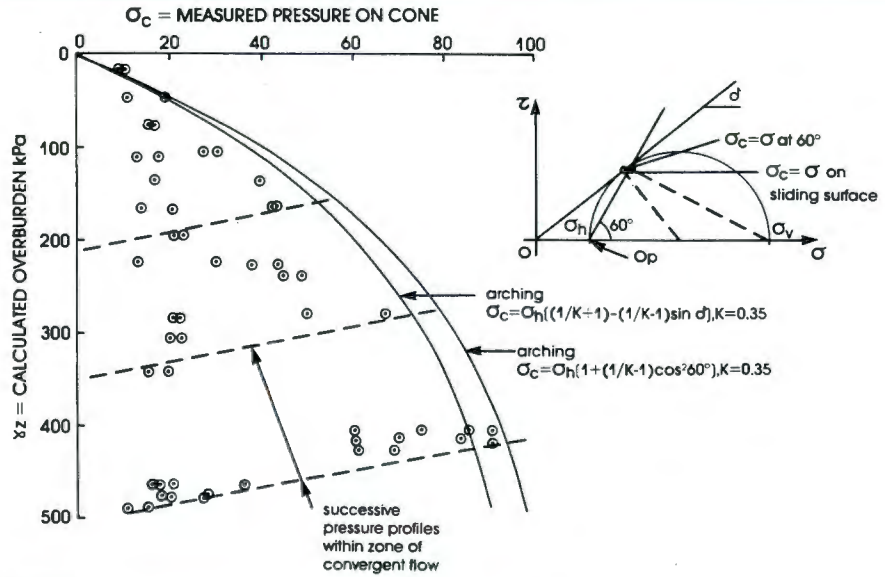

Figure 7a.
Observed pressures on central cone.

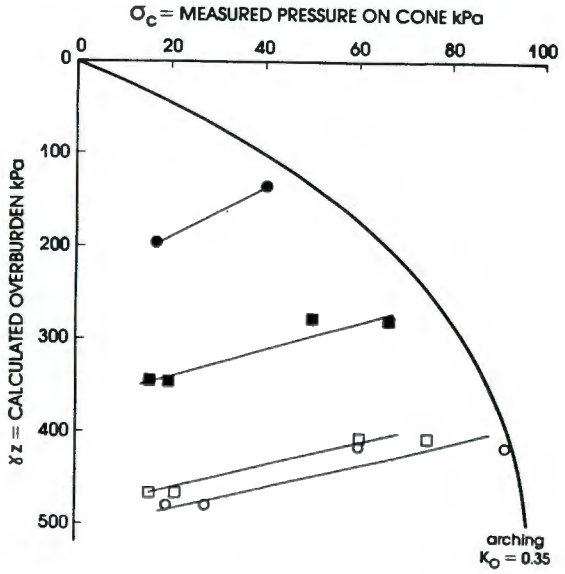

Figure 7b
Individual profiles for pressure on cone.

the shape of individual pressure-depth profiles. **Figure 6b** shows four selected pressure profiles made up of readings taken on both vertical lines of gauges. The irregularity in the profiles results mainly from differences in the pressures recorded over an outlet and between outlets.

Examination of the readings shows that pressures measured midway between outlets always exceed those measured directly above an outlet. There is, therefore, quite an appreciable radial pressure non-uniformity. This cannot be explored in this paper, but will be dealt with in detail in a later paper.

PRESSURES ON THE CONE

All available measurements of pressure on the cone of the silo have been summarized in **Figure 7a**. These include some readings in which the apex of the cone was exposed above the level of the fill and others in which the cone was deeply buried in the fill (whereas the design curve shown in **Figure 3** corresponds to a full silo). The two curved envelopes were calculated from Janssen's formula with $K = K_o = 0.35$.

The calculated horizontal pressures σ_h were modified to give equivalent pressures normal to the cone surface on the following two assumptions:

(i) assuming that the cement was sliding on the surface of the cone:

$$\sigma_c = \sigma_h [(1/K+1) - (1/K-1)\sin\delta] \quad (2a)$$

in which $K = 0.35$ and δ is the angle of wall friction for cement on concrete (39°)

(ii) assuming that sliding occurs through the cement and not on the cone surface:

$$\sigma_c = \sigma_h [1+(1/K-1)\cos^2 60°] \quad (2)$$

As **Figure 7a** shows, the calculated lines fit the measured pressures quite well, again representing containing envelopes to the data.

The inclined lines in **Figure 7a** join measurements on the highest and lowest pressure cells on the cone and again indicate the reduction of pressure that occurs towards the outlets in the zone of convergent flow.

Figure 7b shows four selected pressure-depth profiles for pressure on the cone, that correspond to the profiles of wall pressure shown in **Figure 6b**. The measured points all appear in pairs which relate to the two pairs of pressure cells, one at 90° in plan to the other, that are installed on the cone. These profiles show the very steep reduction in pressure towards the outlet that occurs on the cone.

If measurements at corresponding points on the wall and on the cone are compared, it is found that horizontal pressures on the cone are very similar to wall pressures at corresponding depths.

CONCLUSIONS CONCERNING PRESSURES ON WALL AND CONE

The evidence of **Figures 6 and 7** shows that the upper bound to pressures on the walls and cone of the silo are represented quite accurately by envelopes calculated according to Janssen's formula, using measured properties of the cement. Pressures normal to the cone can be found by modifying the horizontal pressures according to Equation (3) or Equation (3a).

Based on the experimental evidence, there is little justification for adopting the extremely conservative approach of most design codes for the design of a silo to store a fine powder – provided the actual material characteristics are known. It is possible that some

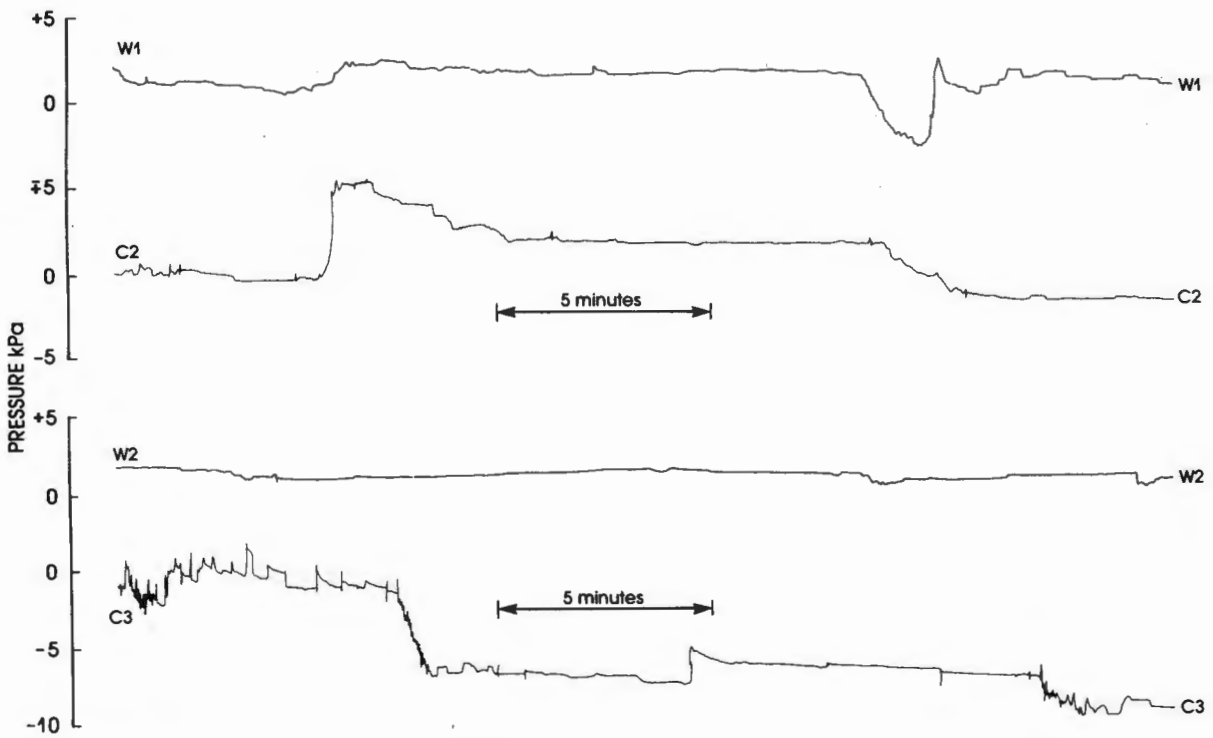

Figure 8.
Pressure variations recorded during discharge from silo.

operating condition may yet arise that will result in more severe pressures than those recorded in the first year of the silo's operation, but that possibility appears remote. Naturally, if the properties of the stored powder are unknown, or are likely to vary widely, or if a silo is to be used to store a variety of products, a more cautious approach is warranted.

PRESSURE VARIATIONS DURING DRAWOFF

Figure 8 shows pressures recorded simultaneously on gauges W1 and C2 and W2 and C3 (see **Figures 4 or 6** for location).

It appears that discharge of cement from the silo can result in either a simultaneous increase in pressure on both wall and cone or a simultaneous decrease (W1 and C2). Alternatively, the pressure on the wall may be relatively unaffected, while that on the cone decreases (W2 and C3).

The changes in pressure during emptying are clearly very complex and unpredictable. The measured changes of up to 10kPa are, however, relatively minor in comparison with the total wall pressures. In particular, there is no evidence of any concentrated transient over-pressures or local load peaks, as referred to in DIN1055 or by Jenike, Johansen and Carson[4], and others.

ACKNOWLEDGEMENTS

This paper is published by kind permission of the Pretoria Portland Cement Company Limited, owners and operators of the silos.

REFERENCES

1. Blight, G.E. and Ofer, Z., *Laboratory Determination of Ko and Comparison with Prototype Silo Observations,* Proceedings, 4th Australian-New Zealand Conference on Geomechanics, Perth, Australia, **1** (1984); pp. 83-87.
2. Blight, G.E., *Performance of a 20m Diameter Steel Maize Storage Bin,* Proceedings, 2nd International Conference on Design of Silos for Strength and Flow, Powder Advisory Centre, London, (1983); pp. 179-191.
3. Blight, G.E., *Measuring Pressures in Silos with Pressure Cells,* Proceedings, 2nd International Conference on Design of Silos for Strength and Flow, Powder Advisory Centre, London, (1983); pp. 217-299.
4. Jenike, A.W., Johansen, J.R., and Carson, J.W., *Bin Loads Part 3: Mass-flow Bins,* Journal of Engineering for Industry, ASME, Paper 72-MH-2, (1972); 1-7.

Int. J. Bulk Solids Storage in Silos, 2 (4) 18-28, 1986

A COMPARISON OF DESIGN AND MEASURED LATERAL PRESSURES AND TEMPERATURES IN A LARGE DUO-CELL CEMENT STORAGE SILO

L. Fliss,
Engineering Management Services Limited,
P O Box 585, Bedfordview 2008,
Republic of South Africa

and

*G.E. Blight,**
University of the Witwatersrand,
1 Jan Smuts Avenue, Milner Park,
Johannesburg 2001,
Republic of South Africa.

The paper describes the results of measurements of horizontal pressure and temperature transferred to the walls of a duo-cell ring silo by the contained freshly milled cement powder. The results of the pressure measurements are compared with pressures calculated by means of the Janssen theory, which in turn were based on measured properties of the cement.

It is shown that the combination of a simple theory and realistic materials parameters results in an accurate prediction of horizontal pressures.

Temperature gradients measured in the walls of the silo were found to conform with the pattern assumed in design.

INTRODUCTION

In 1982-83 a new cement storage complex consisting of two concentric walled Duo-cell silos was erected at the Blue Circle Cement Works at Lichtenburg, Transvaal, South Africa.

For this project the owner, Blue Circle Cement Ltd acting as overall project manager, appointed Babcock S.A. (agents for Claudius Peters in South Africa) as mechanical contractor and Engineering Management Services (EMS) as civil and structural designers and construction managers.

The owner's requirement was to provide storage facilities for 3 different products, as follows:

- Two silo cells of 12,000T capacity each for Ordinary Portland Cement; and
- Two silo cells of 5,000T capacity each for Rapid Hardening Cement and Wallcrete (a proprietary type of cement), respectively.

**To whom all Correspondence should be addressed.*

A preliminary study showed that a pair of Duo-cell silos would be more advantageous than four individual silos, from both operational and economic aspects.

As the Duo-cell silo is a relatively new development in bulk storage technology and the proposed complex at Lichtenburg was claimed to be the world's largest, it was the structural designer's concern to establish the design parameters with utmost possible accuracy. Amongst other design parameters, one which substantially affects the structural safety and cost of a silo shell is the lateral pressure produced by the silo contents.

There are many standards and codes of practice dealing with this subject but none applies specifically to the case of a ring type cell. Available data may only be extrapolated for this particular case.

To carry out the design, certain assumptions had to be made and, to assess the validity of these assumptions, the only practical way was to perform a full scale test of the silo under actual working conditions. For this reason EMS decided that it was worthwhile to instrument one of the ring silos with pressure cells and thermocouples.

Installation of test instruments and monitoring of test data over a period of 2 years have been carried out jointly by EMS and specialists in silo testing from the University of Witwatersrand.

A brief description of the project, including design and construction, is presented to assist the reader to understand the Duo-cell silo system and its structural engineering problems.

HISTORIC BACKGROUND

The concept of dividing a circular silo into two compartments either for storage of two different materials or for two phases of a production process is not new.

For many decades vertical plane partition walls or horizontal slabs were used for this purpose but these

systems proved to be either difficult to construct or expensive, or both. Vertical plane walls introduce large bending moments into the cylindrical shell thus defeating the advantage of a circular shell, that of being mainly a ring tension element.

Horizontal partitioning slabs in silos are difficult to contruct because they require a thicker shell underneath to allow for support and high heavy scaffolding for construction. In addition, for large diameter silos the slab becomes impractically thick since intermediate supports inside the lower silo compartments are not acceptable.

The concept based on a vertical cylindrical partition wall concentric to the silo shell was originated by Prof. J. Peter[1] and used by IBAU for the first time at Wuelfrather Zement Works at Duisburg, Schwelgern – West Germany[2] in 1978.

Since then several concentric silos from 18 to 24m outer shell diameter have been constructed in various parts of the world[3].

From the beginning two main variants of concentric silos were available:

One, with the concentric shells supported by a common conical bottom called the *Ring silo*, was developed by IBAU on Peter's structural concept.

The other, was subsequently developed by Claudius Peters also in West Germany and called the *Duo-cell silo*, has the concentric shells supported on a flat bottom slab.

In South Africa the first Ring silo was built for a cement depot near Cape Town in 1981[4] followed by the two Duo-cell units at Lichtenburg, Transvaal and one at Boksburg Transvaal.

The concentric silo presents several structural advantages such as:

a. The horizontal silo pressures developed in the ring cell are substantially lower than the pressures developed in an equivalent capacity cylindrical silo, due to a reduced hydraulic radius.
b. The inner cell wall, being an internal one, does not need to be designed for limited crack width as a serviceability limit state.
c. The roof of the ring cell, spanning between the two concentric shells, is a very economical small span element.

DESCRIPTION OF SILO COMPLEX

The Duo-cell silo complex at Lichtenburg consists of two identical elevated silos having the following principal dimensions:

	Inner Silo	Outer Silo
Capacity (T)	5000.0	12000.0
Internal diameter (m)	14.0	24.0
Shell height(m)	35.1	35.1
Shell thickness (mm)	300.0	350.0
Total silo height above ground level (m)	51.0	51.0

The arrangement of each silo and its supporting structure is shown in **Figure 1** while **Figure 2** is a photograph taken of the complex during construction.

Each Duo-cell silo consists of five parts:

a. Bottom slab. This is a circular slab of variable thickness from 1.0m to 1.9m, with a radial fall towards the centre, which incorporates trenches, ducts and cast-in-pipes for the aeration extraction system.
b. Outer shell. This is a cylindrical shell supported by the bottom slab and supporting the roof, which ties the inner and outer shells together.
c. Inner shell. This forms the inner silo wall, provides support for the roof and is supported by 18 stub columns. The reason for supporting the inner shell on columns is that openings have to be provided at the bottom of the inner shell to allow the cement from the outer cell to flow into a collecting trench located around the hopper base. Both outer and inner shells were constructed using slip forms.
d. The inner cell hopper is a truncated cone 10m high varying in diameter from 14m at the top to 6m at the bottom. The space between the hopper, the inner shell and the bottom slab is utilised as a de-aeration chamber.
The bottom slab inside the hopper base is provided with a system of airslides and trenches for the discharge of cement.
The conical hopper was made of 18 precast panels joined together by hoop reinforcing bars and cast-in-situ non-shrink concrete. The hopper hangs from the inner shell to prevent transmission of wall friction loads from the shell, through the hopper, to the bottom slab which otherwise would require an impractically large thickness. The joint between the hopper and the bottom slab was sealed by injecting it with polyurethene foam.

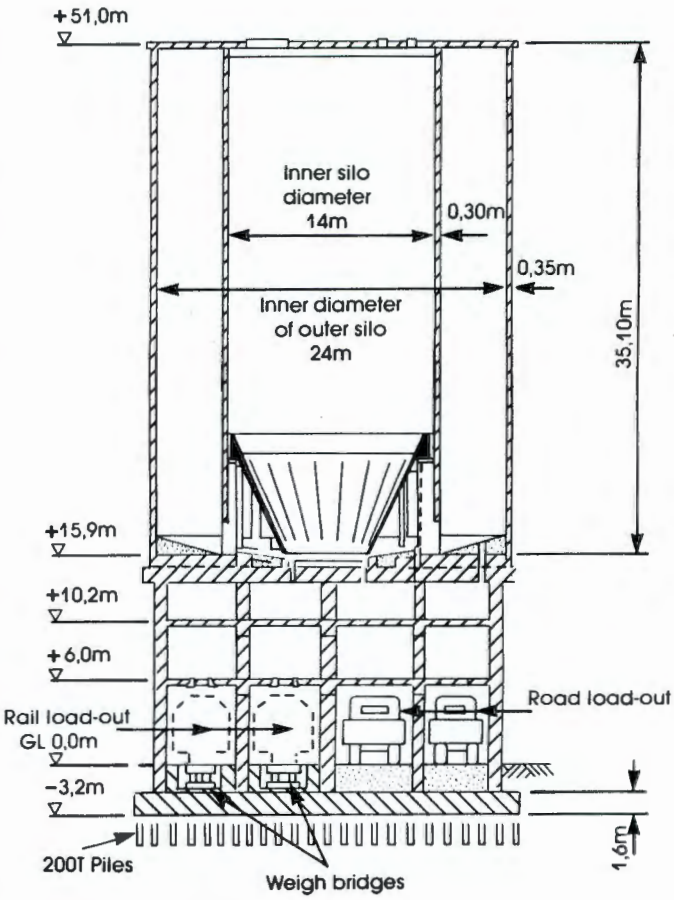

Figure 1.
Vertical cross section through Duo-cell silo.

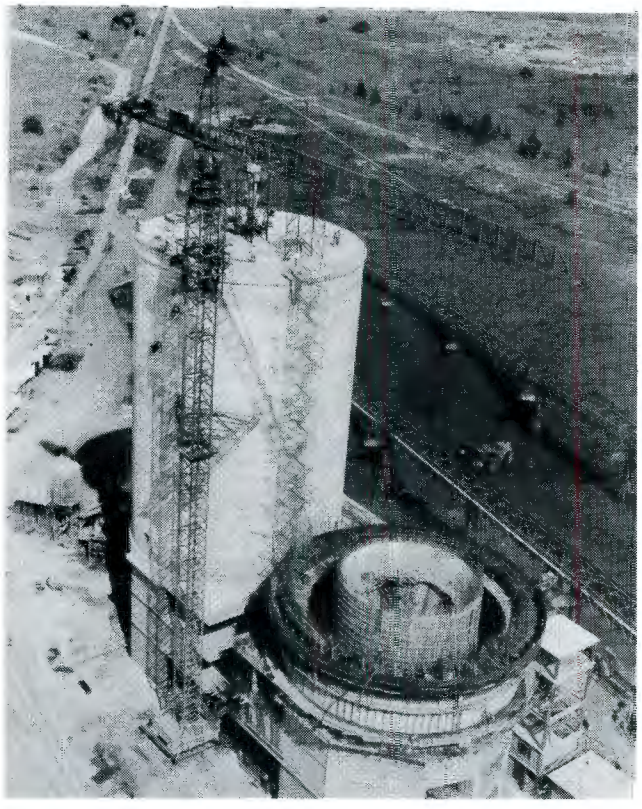

Figure 2a.
View of Duo-cell silo complex. The instrumented silo is that on the right.

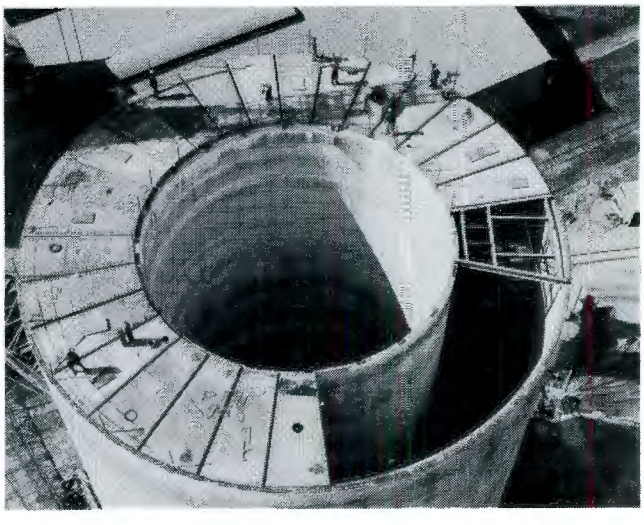

Figure 2b.
View showing inner and outer shells, and roof construction.

e. The roof. In addition to its function as a waterproof and airtight cover to the silo, the roof supports the filling and de-dusting systems and acts as a horizontal diaphragm to tie the inner and outer shells together.
Economics and limited crane lifting capacity contributed to the selection of the roofing structural system which consists of two different parts:

The roof section covering the ring cell, spans 5m between the two concentric shells and was constructed using precast ribbed slabs provided with loop bars at the support ends. The inner cell, 14m in diameter, was covered with a structural grid of steel beams supporting steel QC decking as a permanent shutter.
Both the QC decking over the inner cell and the precast slabs over the outer one, received a reinforced concrete topping 100 to 200mm thick which created a monolithic diaphragm to tie the shells together and at the same time provided adequate support for the reinforced acrylic roof waterproofing.

The total duration for the construction of the two Duo-cell silos, including piling and erection of the adjacent packing plant was 15 months. The cost of the structural works, including the piling, was approximately US$6 million at 1984 prices.

SILO DESIGN LOADS AND STRUCTURAL ANALYSIS

At the time the Lichtenburg silo complex was designed and even to date none of the recognised Standards and Codes of Practice for silos refers specifically to ring cells.

To carry out the design, it was decided to extrapolate the recommendations of DIN 1055 - Part 6 – 1964[5] for the case of ring cells.

The following physical characteristics for cement were used as design data:

Unit Weight γ	17 kN/m^3
Angle of Internal Friction ϕ[1]	20°
Maximum Temperature	+115°C

The density and angle of internal friction are in accordance with DIN 1055 - Part 1 – 1978. The pressures were much lower than the ones calculated by using other Standards such as ACI-313-77[6] (see **Figure 3**).

To allow for eccentric emptying of the ring cell it was assumed possible for the cement surface to slope at 40° along a circumference having the average radius of the annulus.

Using the above design data, the calculated horizontal pressure diagram which has maximum values for the emptying case is as shown in **Figure 3**.

Two load cases for temperature gradients were taken into account:

a. The ring silo partially full with hot cement at +115° and outside air temperature +20°C.
In this case, for the area of the shell above the cement surface, the calculated temperature gradient across the wall thickness was 43°C while for the area below this surface the temperature gradient was considered negligible due to the self-insulation effect of the silo contents as indicated by Koch and Peter[7].

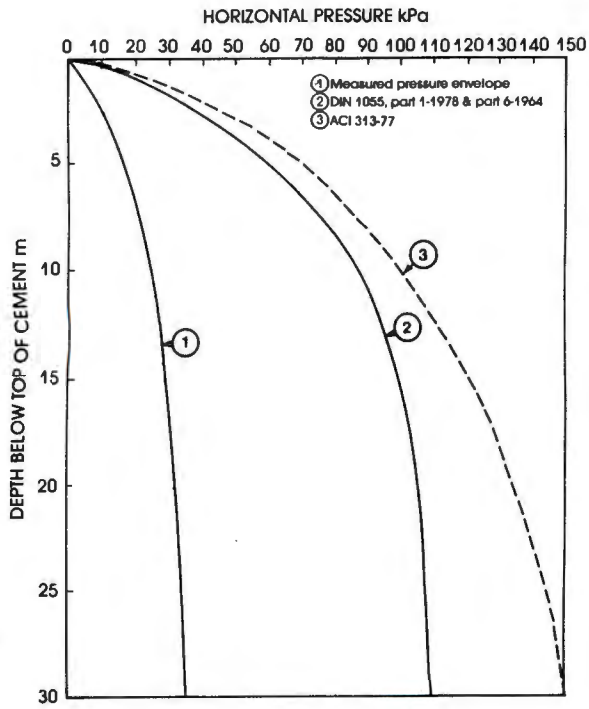

Figure 3.
Comparison of design and measured silo pressures in Duo-cell silo.

b. Silo empty, outside air temperature +40°C and inside air temperature +10°C. The calculated reversed temperature gradient was 25°C.

The structural design model of the outer shell was a cylinder fixed at the bottom and laterally simply supported at the top. The shell was analysed using the finite element method on a 2.5 × 4.5m grid.

The serviceability state was defined by maximum crack width of 0.3mm, an acceptable value for the dry climate and alkaline environment at Lichtenburg Cement Works.

Temperature gradient effects were significant only for the upper quarter of the shell. For the rest the hoop reinforcement was determined by the lateral pressure, as the highest lateral pressures do not occur simultaneously with the highest temperature effects.

Reinforcement consisted of high tensile deformed bars with a specified characteristic strength of 410MPa.

The total amount of hoop reinforcement required for each outer shell was 200T, distributed ⅔ on the outer face of the shell and ⅓ on the inner one to cater for temperature stresses and crack width control.

INSTRUMENTS AND INSTALLATION

The pressure cells used in the installation were TML KD2BS gauges made by Tokyo Sokki Kenkyujo Company Limited. The gauges are rated for pressure measurements in the range 0 to 200 kPa and for temperatures from −20°C to +100°C.

The location of the pressure cells in the silo is shown in **Figure 4**. There are 5 vertical lines of pressure cells, so as to give a good reflection of radial pressure distribution, and 5 horizontal rows of cells. Two of these lines are complete, each having 5 cells installed. The remaining 3 lines each have 3 cells installed. The total number of pressure cells installed in the outer wall is thus 19. A twentieth pressure cell was installed on the inner wall adjacent to the inspection chamber and on the same level as the lowest row of pressure cells on the outer wall. This was placed to study pressure differences between the outer and inner walls. Thermocouples have been installed on one of the lines of pressure cells. The junctions are located as follows:

1. at the end of a short steel tube projecting 100mm into the fill;
2. at the inner face of the wall;
3. at the outer face of the wall.

Instruments were installed from a *sky-climber* platform suspended from the roof of the silo. **Figure 5a** shows work in progress.

Installation proceeded as follows:

(i) Steel 'pans' previously cast into the walls to receive the pressure cells were cleaned out.
(ii) Using a template to ensure a constant distance in from the face of the wall, a series of 6 lugs were welded to the cylindrical rim of the pan.
(iii) The pressure cell, bolted to a mounting plate, was now inserted, its lead passing through the central

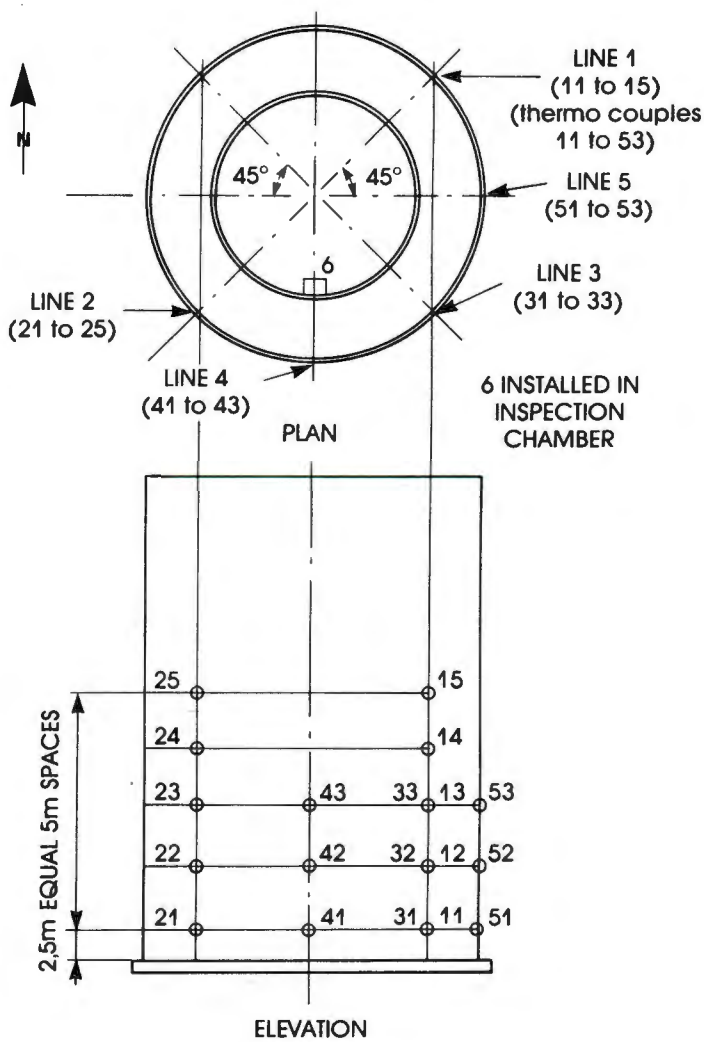

Figure 4.
Location of pressure cells and thermo couples in silo walls.

pipe of the pan. The mounting plate was now welded to the lugs.

(iv) The gaps between the mounting plate and the rim of the pan were plugged with a joint-filling material and the void between the mounting plate and the pan was filled with a quick-setting flowable grout. (This stage is shown in **Figure 5b**).

(v) The annulus around the pressure cell was then filled in with epoxy-sand plaster to give a smooth, uninterrupted surface. **Figure 5c** shows a completed installed pressure cell.

Where thermocouples were installed, the following procedure was adopted:

The thermocouple wire was fed through the hole in the pan prior to installing the pressure cell, with the junctions to the inside of the silo. The 100mm long thermocouple pipe had previously been welded to the mounting plate of the gauge, and the thermocouple No. 1 was fed through the pipe when the cell was installed, with the projecting pipe at the lowest point of the mounting plate.

The junctions of thermocouples 1 and 2 were then fixed in place using epoxy putty, prior to pouring in the grout. Thermocouples 3 were fixed to the outer surface of the wall using a saddle and steel nails. A 5mm deep, 3mm diameter hole was drilled in the concrete. The thermocouple junction was inserted into the hole and fixed with epoxy putty. This is to prevent the thermocouple from reflecting temperature fluctuations caused by the wind.

Figure 5a.
Work in progress on installing instrumentation.

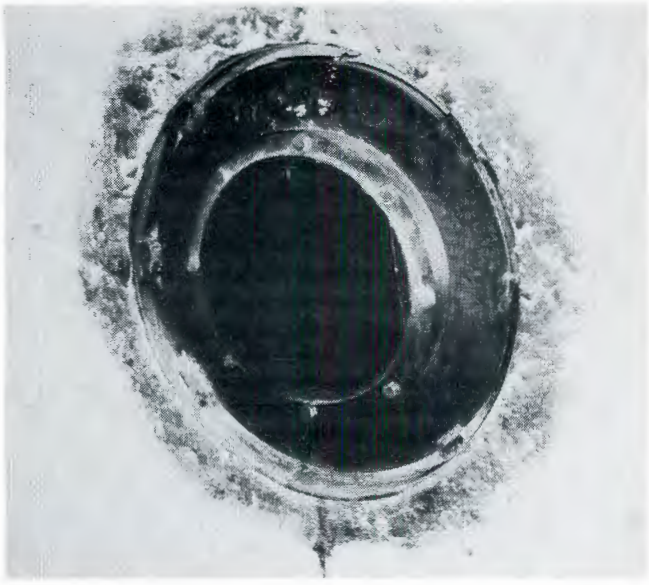

Figure 5b.
Pressure cell installed and ready for grouting.

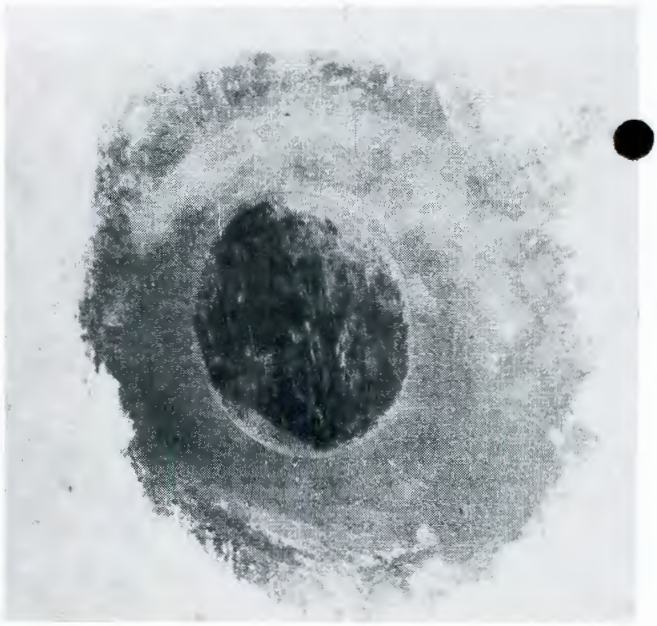

Figure 5c.
Completely installed pressure cell.

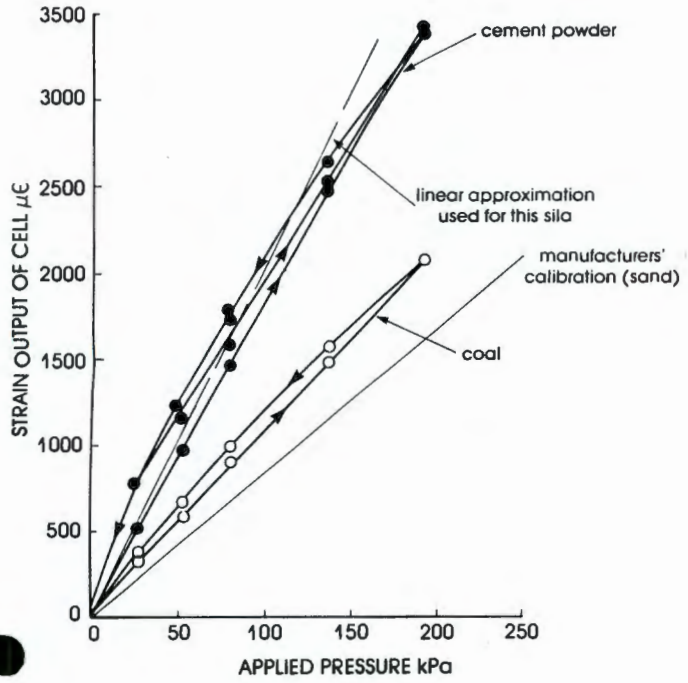

Figure 6.
Calibration of TML pressure cell using various materials in contact with cell face.

CALIBRATION OF PRESSURE CELLS

The calibration of a pressure cell depends on the ratio of the compressibility of the fill it is in contact with and the compressibility of the cell itself[8]. For this reason, all pressure cells must be calibrated using the specific silo fill material. Only one of the cells was calibrated in this case. The manufacturer's calibrations showed that all 20 cells had characteristics that were within 10 per cent of each other and most gauges were closer than that.

The gauge was calibrated by mounting it in the base of a large shear box, in a similar manner to its mounting in the silo wall. The gauge was then covered with a 150mm layer of loose cement powder and a series of known pressures were applied normal to the gauge face by means of dead loads. The resulting calibration curves for first loading, unloading and reloading are shown in **Figure 6**.

A linear approximation, also shown in **Figure 6**, was used to interpret the measurements from the silo. This gave a gauge factor of 1000 $\mu\epsilon$ = 50 kPa. The factor is a good fit with the calibration at pressures up to 100 kPa, somewhat on the conservative side for pressures between 20 to 60 kPa. The maximum pressure so far measured in the silo has only been 32 kPa.

Figure 6 also shows the effect of calibrating a pressure cell with materials of differing compressibilities. The manufacturer's calibration was made with sand and gives a calibration factor that is approx. 2.4 times that established with cement powder.

CALCULATED PRESSURES FOR ACTUAL CEMENT PROPERTIES

Measurements in the laboratory of the actual (as opposed to 'code') values of the physical properties of the cement powder stored in the silo were as follows:

(a) Loose density ρ = 1150 to 1230 kg/m^3
Mean ρ = 1200 kg/m^3
Unit weight γ = 12 kN/m^3

(b) Angle of internal friction $\phi^1 = 42°$

(c) Angle of wall friction $\delta = 37°$ to $39°$ (cement powder on concrete)
mean $\delta = 38°$

(d) At rest pressure co-efficient $K_o = 0.38$ (for normally consolidated powder).

(e) Active pressure co-efficient.

$$\frac{1-\sin\phi'}{1+\sin\phi'} = K_A = 0.20$$

Figure 7 shows pressure curves calculated from the Janssen equation for the following properties:

γ = 12 kN/m^3
δ = 38°
K = 0.20 and 0.35

(These are described as *arching* curves in **Figure 7**).

For a ring silo, of inner and outer diameters, D_i and D_o, respectively, the Janssen equation takes on the form:

$$\sigma_h = \frac{K\gamma}{A}(1-e^{-Az})$$

$$A = \frac{4K\tan\delta}{(D_o-D_i)}$$

where σ_h is the horizontal pressure at depth z below the fill surface.

Figure 7 also shows two lines representing pressure distributions with *no arching* and K = 0.20 and 0.35. For the *no arching* case, the horizontal pressure is calculated from $\sigma_h = K\gamma z$.

0.35 was used rather than 0.38 because measurements on other silos have indicated that K_o in a silo is slightly less than the value measured in laboratory tests.

MEASURED PRESSURES IN SILO

Most of the pressure measurements made to date have been plotted in **Figure 7**. It will be seen that the majority of the measured pressures lie inside the calculated line for γ = 12 kN/m^3 and K = K_o = 0.35. A few measurements, at low values of γz fall outside the *arching* envelope, but are contained by the *no arching* envelope for K_o = 0.35.

The measured pressures are low when compared with the envelope based on parameters recommended by DIN1055, or ACI 313-77 (see **Figure 3**), but agree very reasonably with the curves calculated for actual cement properties.

The very low pressures, well inside the calculated curves, appear to result from emptying of the silo. Emptying also causes significant radial non-uniformity of pressures, as will be seen later.

Figure 8 shows a few individual pressure profiles. These conform quite well to the shape of the theoretical curves. The effect of emptying is shown by the reduced pressures at the bottom of profiles F1 and F2.

Typical variations in radial pressure are shown in **Figures 9 and 10**.

Figure 9 shows the variations possible at a single level (either level 1 or 2) at various times. The effects of emptying or changing the wall pressure are very well demonstrated in the profiles F (compared with E) and A (compared with B).

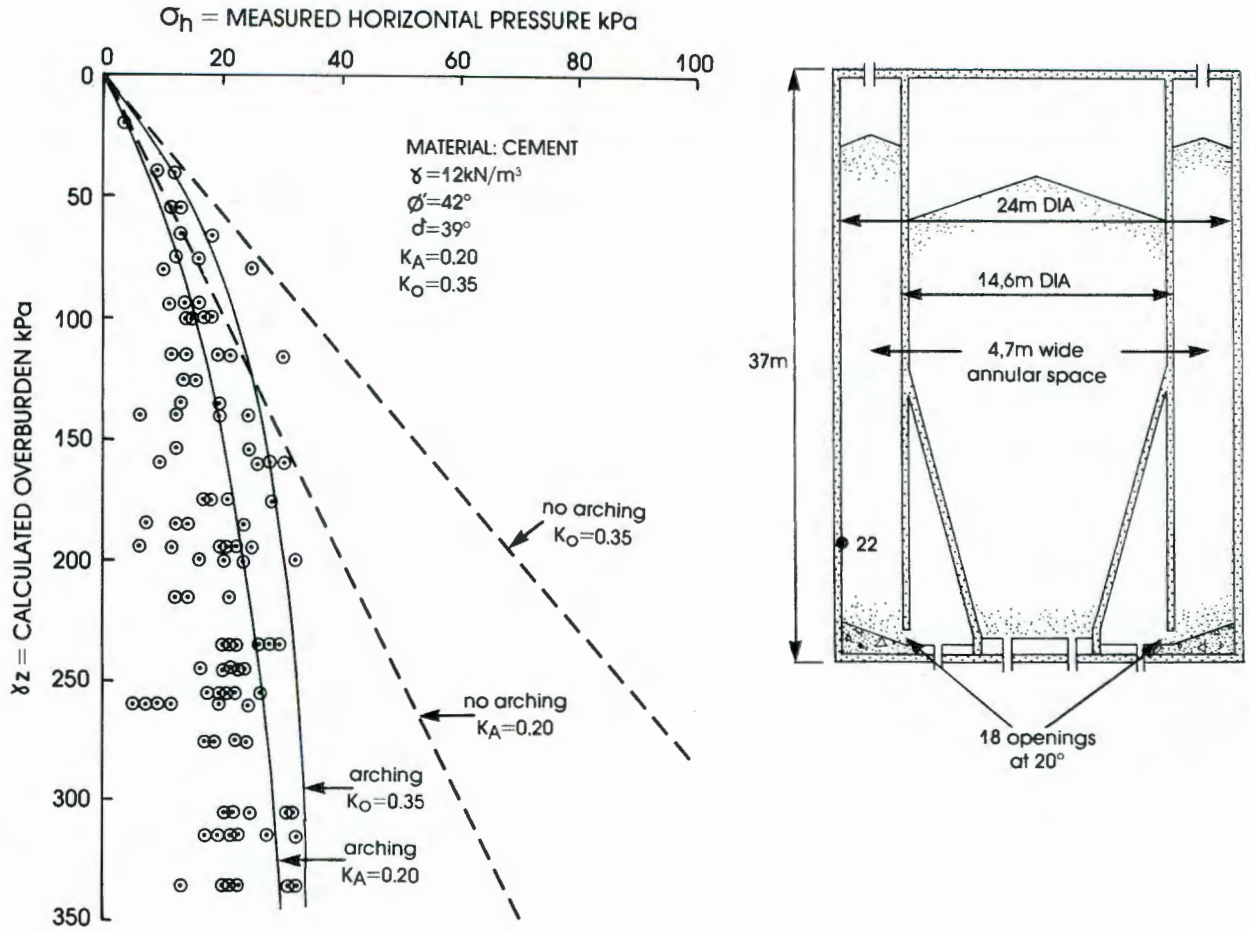

Figure 7.
Summary of measured horizontal pressures.

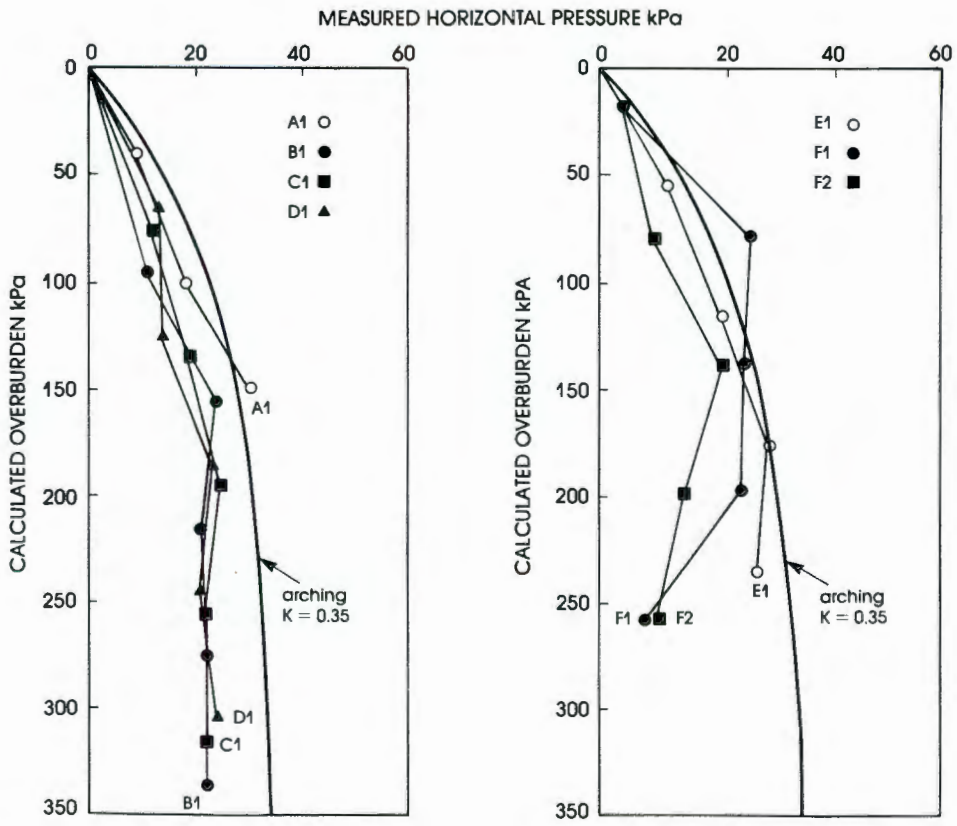

Figure 8.
Individual pressure profiles on lines 1 and 2.

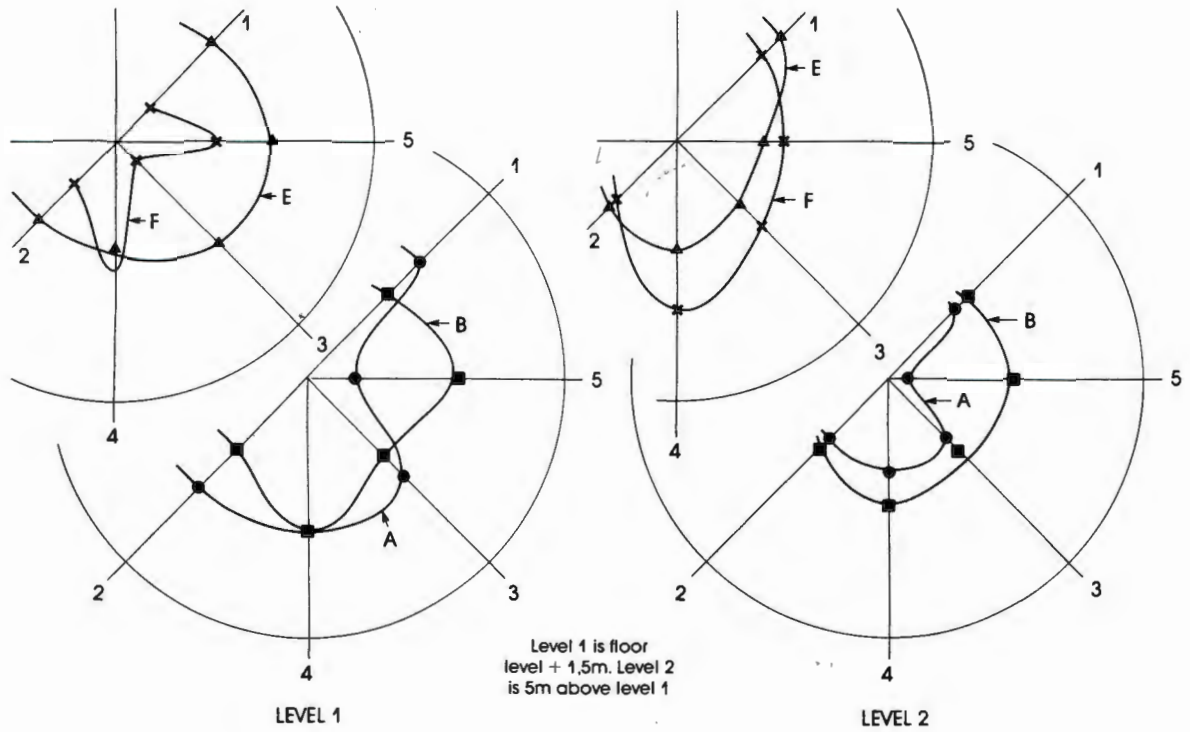

Figure 9.
Radial variation of pressure at levels 1 and 2.

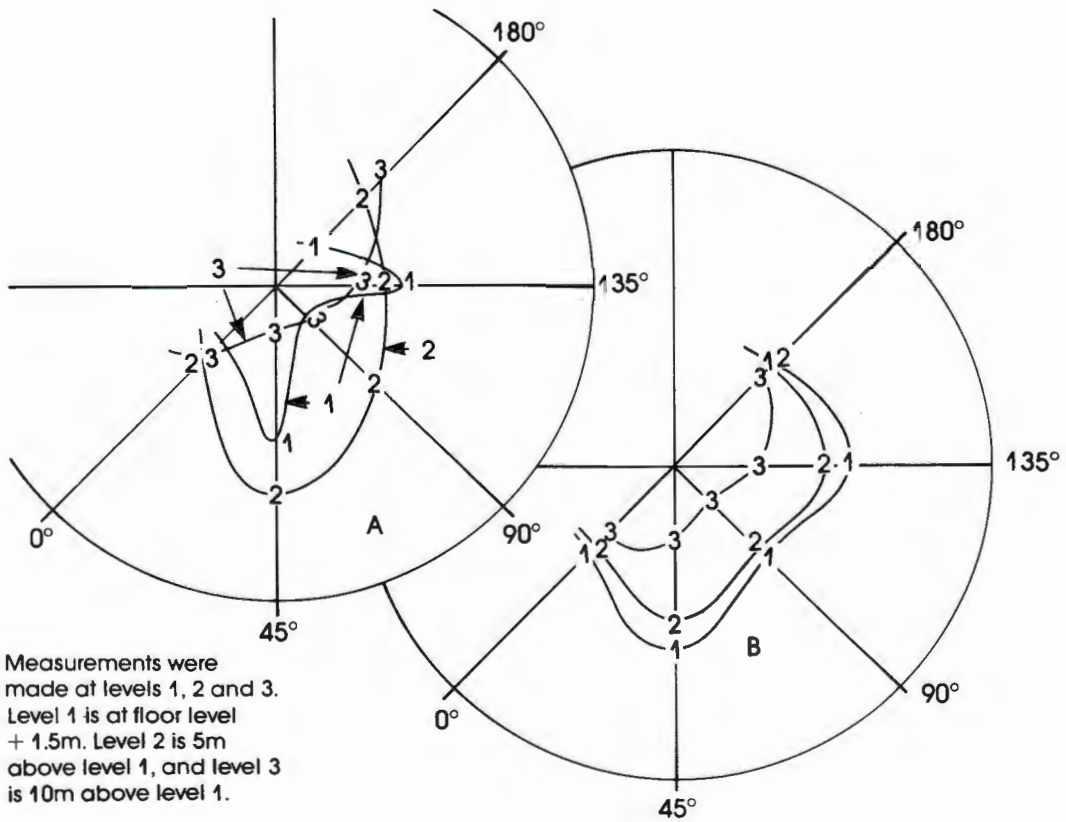

Figure 10.
Variations of radial pressure distribution with height in silo.

Figure 10 shows the variation of radial pressure distribution with height in the silo at a given time. In profiles B, the radial pressure distribution remains similar with height, possibly because the silo had been operating in the same mode for some time. In the case of A, however, the distribution changes drastically between levels 1 and 2 and levels 2 and 3. The profile at level 3, being uniform, probably corresponds to uninterrupted filling, while that at level 1 shows the effect of emptying.

VARIATION OF PRESSURE WITH TIME

Figure 11 shows recorded variations of pressure with time at cell 22 during emptying of the silo. It will be seen from the chart recordings that a series of irregular 'spikes' occur on the recording charts. The *spikes* are caused by a rise in pressure in the silo fill when compressed air is fed to the aeration pads. It will be seen from **Figure 11** that quite major displacements of the pressure record are associated with the *spikes*. The displacements represent pressure changes of up to 10 kPa. It is largely these changes of pressure that introduce so much scatter into the static pressure measurements shown in **Figure 8**. The regularity with which these sudden changes of pressure occur should be noted. The interval corresponds with the alternation of draw-off from the 18 openings around the inner perimeter of the silo. It will also be noted that, after every spike, there is a decay of pressure, caused by localised dissipation of air pressure from the fill.

MEASURED TEMPERATURES

Figure 12 shows two sets of temperature profiles measured in the silo. In case (a), the temperature of the outside wall was reasonably constant with variation of no more than 1°C. The temperature of the inside of the wall was also reasonably constant, while the largest variation of temperature occurred 100m away from the inside of the wall. In case (b), the fill level was lower than that of case (a). It is notable that up to 7.5m above the floor of the silo, the temperatures of the outside and inside of the wall and of the fill have nearly equalised. The cement above this level had obviously been placed more recently and the temperature gradient through the wall was larger. Even the outside surface of the wall had responded to the increased inside temperature. The highest temperatures of all were recorded in the air above the level of the fill, where temperatures reached a maximum of nearly 50°C. This is consistent with other observations[8,9].

Schaffner and Blight[9], for example, observed that the highest temperature on the inside of a wall is reached just as the fill covers it. Thereafter, there is a progressive cooling of the wall. **Figure 13** shows the temperature profiles through the wall:

(i) adjacent to the air space
and
(ii) just under the top surface of the fill.

Also shown in **Figure 13** is the shape of a hypothetical temperature profile sketched by Martens[10], Handcock[11] (and others). The observed temperature data fit the hypothetical profile well. However, it must be remembered (Schaffner and Blight[9]) that the temperature gradient through the wall will not be linear unless a steady state heat flow exists. A steady state is most unlikely to obtain in the wall of a silo during or after filling with a hot material.

The difference between the measured and design gradient appears to result mainly from the fact that the temperature of the cement fed into the silo has never exceeded 80°C instead of the 115°C assumed.

CONCLUSIONS

1. At this stage the available test results could be considered valid only for a particular material, namely cement. To extend the conclusions listed below to other materials similar tests should be carried out.
2. In general it appears that the radial uniform horizontal pressures in a Duo-cell silo correspond to the well-known Janssen's theory.
3. The difference between the measured and design pressures recommended by various Standards may be considered sufficient to cover possible non-uniform pressure effects.

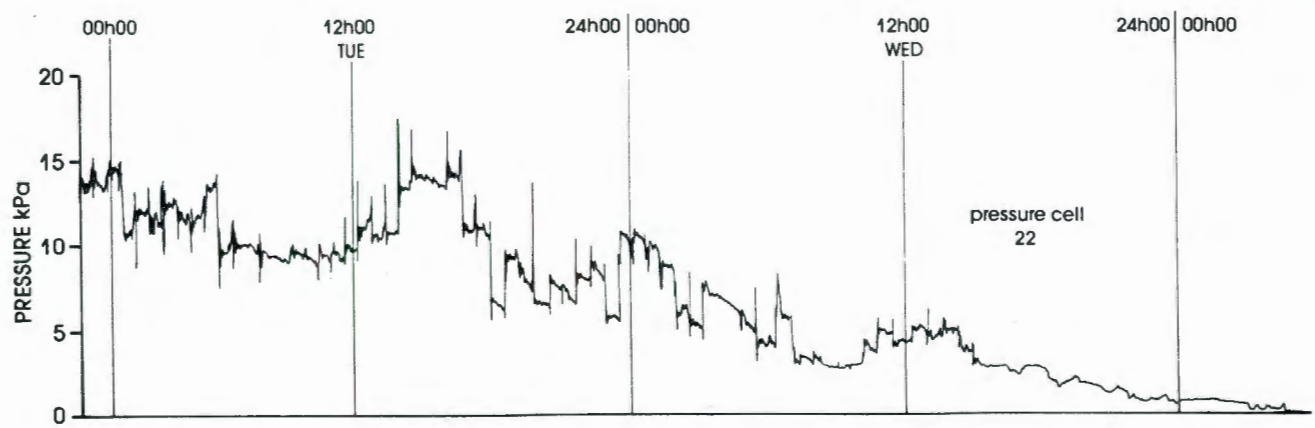

Figure 11.
Pressure variations at a single point during emptying of silo.

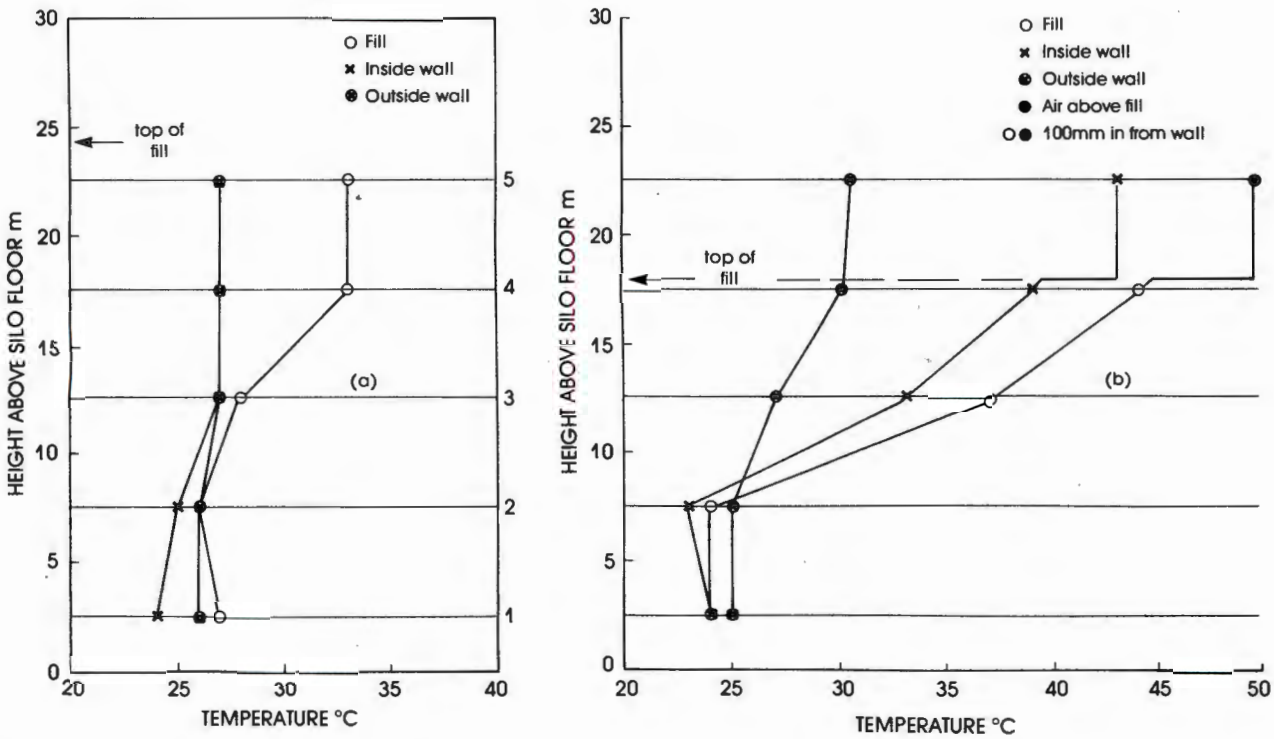

Figure 12.
Observed vertical profiles of temperature.

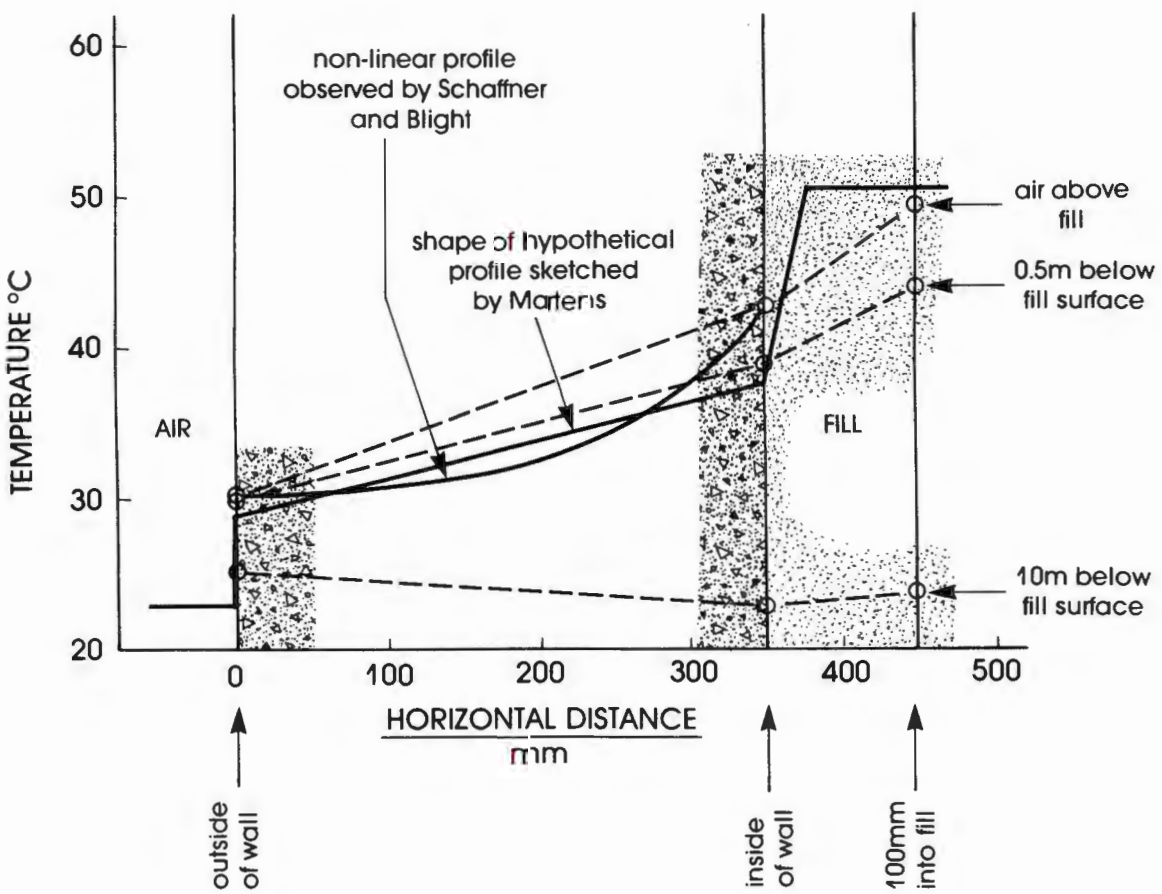

Figure 13.
Observed and hypothetical temperature profiles through silo wall.

During the tests described, no major eccentric discharge or arch breaking overpressures were detected, perhaps due to the limited number of recording sessions. These unpredictable phenomena are the unfavourable effects standards must cover.

4. Measured temperature gradients through the shell proved to correspond with previous observations as published in reference papers.
5. As the intention is to continue the monitoring of silo pressures at Lichtenburg for a couple of years, the experimental data will increase in reliability making it possible to quantify more accurately the safety and economy of the present standards applied to Duo-cell silos.

ACKNOWLEDGEMENTS

This paper is published by kind permission of Engineering Management Services Limited, who sponsored the instrumentation and the test.

Peter und Lochner – Consulting Engineers Stuttgart – West Germany advised EMS on silo loading and checked the design.

Thanks are also due to Blue Circle Cement (Pty) Limited for permitting the silo to be instrumented.

REFERENCES

1. Peter, J., *The central cone silo from the structural point of view,* Zement – Kalk – Gips, **34** (1981); 12.
2. Hilgard, G., *New double circular cement silo at a slag cement grinding plant at Duisburg – Schwelgern,* Zement – Kalk – Gips, **34** (1980); 12.
3. Ernstbrunner, L. and Krauss, W., *New storage possibilities by means of the Duo-cell silo,* Zement – Kalk – Gips, **35** (1981); 4.
4. Smeets, G.J.I.M., and Wilkinson, K.F.D., *Storage, bag packing and loading of two types of cement all in one silo,* Proceedings, 1st International Conference on Design of Silos for Strength and Flow, Powder Advisory Centre, London (1980); p. 26.
5. German Standards Institution, Din 1055, *Design loads for buildings.* Sheet 1/1963 and 1978, Sheet 6/1964.
6. American Concrete Institute ACI Standard 313-77, *Recommended Practice for Design and Construction of Concrete Bins, Silos and Bunkers for storing Granular Materials,* (1975).
7. Koch, R., and Peter, J., *Bemessung fur combinierte Beenspruchung aus Lasten, Vorspannung and Temperaturezwang am Beispiel von Silowanden,* Beton und Stahlbeton, (1978); 4.
8. Blight, G.E., *Measuring pressures in silos with pressure cells.* Proceedings, 2nd Conference on Design of Silos for Strength and Flow, Stratford-upon-Avon, England, (1983); 217-229.
9. Schaffner, R.H., and Blight, G.E. *Comparison of design assumptions and measured performance for cement works silos.* Proceedings, 2nd Conference on Design of Silos for Strength and Flow, Stratford-upon-Avon, England, (1983); 207-216.
10. Martens, P., *Uberschlagige Ermittlung der Temperaturen in Klinkersilos,* Die Bautechnick, (1975); 12: 402-408.
11. Handcock, M.G., *Reinforced concrete storage silos containing hot materials.* Proceedings, 2nd Conference on Design of Silos for Strength and Flow, Stratford-upon-Avon, England, (1983); 82-94.

Second International Conference on

DESIGN OF SILOS FOR STRENGTH AND FLOW

7 - 9 November 1983
STRATFORD-UPON-AVON HILTON

Organised by the
POWDER ADVISORY CENTRE, P O. Box 78. London NW11 0PG. England
Telephone. 01-455 0011 Telex: 8954242 (POWDER G)

PREFACE

This volume comprises the texts of papers, in Programme order, to be presented during the Conference. This material has been directly photo-reduced from author original typescripts.

We are indebted to all our authors for their contributions and sincerely hope that they will stimulate active discussion.

We are also indebted to the members of our Programme Committee - F. E. Weare (Polytechnic of Central London), J. G. M. Wood (Mott, Hay & Anderson, Croydon) and H. Wright (British Steel Corporation, Teesside Laboratories).

Finally, we also acknowledge the support and encouragement of our co-sponsoring professional organisations (as listed on the inside back cover) who have assisted in ensuring a worthwhile Programme and full international participation.

It is hoped, as with the first Conference, to publish a supplementary volume to these Proceedings based on contributions and discussions submitted in writing by Conference participants. The actual Conference discussions will not be recorded so as to stimulate audience participation in a confidential atmosphere.

We sincerely hope that this- the second of our series - event will stimulate searching practical discussion of all aspects of silo design and lead to more efficient and safer constructions and also stimulate international and interdisciplinary contact.

A. S. Goldberg
Conference Chairman

PERFORMANCE OF A 20m DIAMETER STEEL MAIZE STORAGE BIN

by

G.E. Blight
Department of Civil Engineering,
University of the Witwatersrand,
Johannesburg, South Africa

SYNOPSIS

The paper describes an investigation of pressures occurring in a maize storage bin operated by a milling concern. It is shown that measured pressures can be reconciled with calculated values based on laboratory data, provided the flow pattern within the bin is correctly assessed. Duirnal temperature changes are identified as an important cause of pressure variations in a steel bin.

INTRODUCTION

An opportunity recently arose to compare the lateral pressures calculated for the design of a 20 m diameter steel maize storage bin with the pressures to which the bin is actually subjected in everyday use. The bin is used to store maize for a milling operation. It is subject to regular daily withdrawals in a five day working week and random fillings which occur as and when new supplies of grain arrive.

Figure 1 shows the major dimensions of the symmetrical all-welded bin. The plate thicknesses used in its construction are also noted in the figure.

The bin was instrumented by means of seven pressure cells of the mercury-filled strain-gauged diaphragm type. All pressure cells were calibrated in the laboratory prior to installation in the bin, using maize to transmit pressure to the diaphragms.

Access to the side of the bin was only possible at one point on its circumference and for this reason, the cells were installed in a single vertical line at the spacings shown in Figure 1. Because the bin as well as the filling and emptying arrangements are axisymmetric, this is not considered a limitation on the validity of the measurements. Figure 2a is an exterior view of the bin, while Figure 2b shows one of the pressure cells as seen from the outside. Each pressure cell was bolted to a steel adaptor which in turn was clamped to a stiffener ring welded into the bin wall. The surface of the pressure cell was adjusted until its plane coincided with the inside surface of the bin wall before clamping it in its final position. Figure 2b shows the stiffening ring, the rear of the adaptor plate and two of the three cap screws used for clamping.

The profile of the maize surface in the bin could be determined by dropping a tape from the central grain inlet in the roof and also from a second opening in the roof at a radius of 6,5 m from the centreline. Some typical surface profiles have been shown in Figure 1.

The type of operation to which the bin is subjected is further illustrated in Figure 3 which shows fluctuations in bin contents over a 3 month period. The height fluctuation-time relationship was

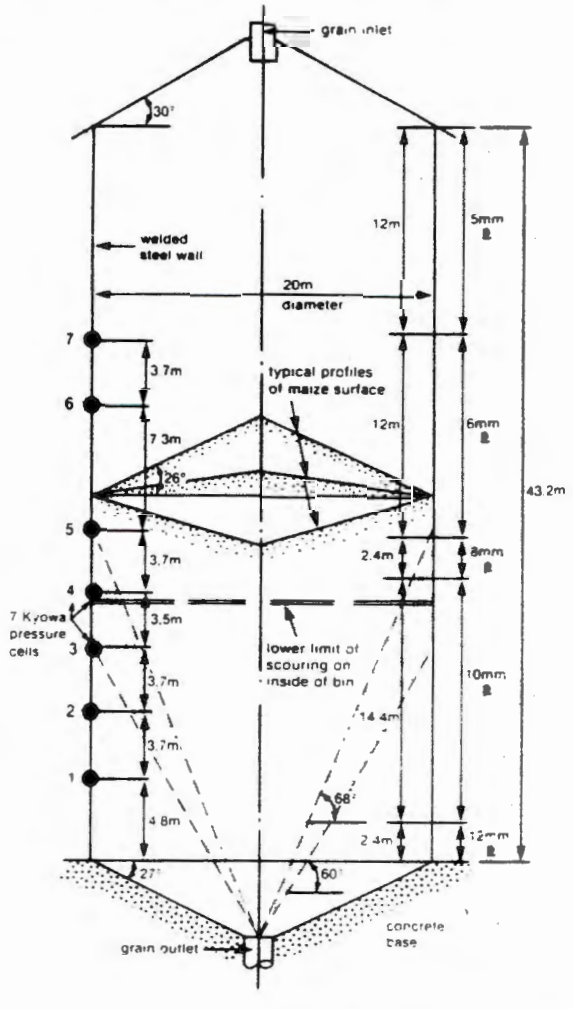

FIGURE 1 : Section through bin showing principal dimensions, plate thicknesses and locations of pressure cells

FIGURE 2a : Photograph of 20m diameter maize bin

FIGURE 2b : Pressure cell installed in bin wall

constructed from daily records of withdrawals and fillings in terms of tons of maize. The tonnage record was reconciled with six tape measurements (A, B, C, etc. in Figure 3) made during the 3 months. This gave an excellent estimate of the average density of the maize in the bin.

It is clear from Figure 3 that the classic design concept that at any time either "filling" or "emptying" conditions apply to the contents of a bin, would be hard to justify in the case of bins of this type where continual and often simultaneous filling and emptying occur.

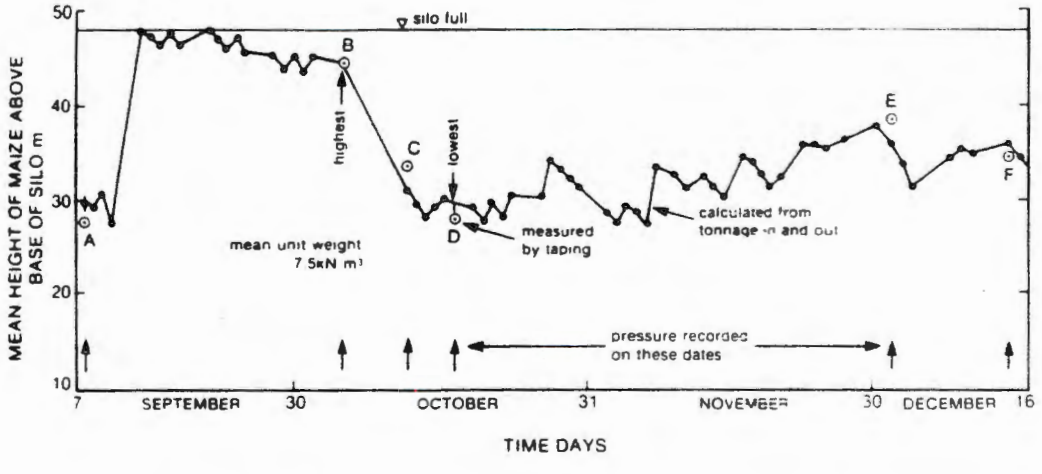

FIGURE 3 : Daily fluctuations over a 3 month period of level of maize stored in bin

PHYSICAL PROPERTIES OF MAIZE

A series of laboratory measurements were made to establish the physical properties of the maize. These included measurements of:

ϕ = the angle of shearing resistance;
δ = the angle of friction for maize on steel;
γ = the loose and compact density; and
K_o = the at rest horizontal pressure coefficient.

ϕ was evaluated by means of drained triaxial shear tests and proved to have a value of 30° as compared with a range of values appearing in the literature (2) of 21° to 37°. Steel surfaces in three different conditions were used to assess δ by means of shear box tests. δ was found to vary between 12° and 17° (the range appearing in the literature is 14° to 23°). The values of ϕ and δ are slightly stress-dependent, reducing with increasing stress. δ is not affected by the condition of the surface. The static value of δ is 3° to 4° less than the dynamic value. This result is similar to one reported earlier for the sliding of coal on steel (3), although the difference between moving and static values for maize is not as large as for coal

The density of the maize in a loose state was determined as 750 kg/m³ which proved to be identical with the value determined from the filling and emptying records for the silo.

The at rest pressure coefficient for the maize was established using the Bishop (4) technique of axially compressing a specimen in a traxial cell while simultaneously adjusting the lateral pressure to maintain a condition of zero lateral strain. The results of the determination are shown in Figure 4.

The at rest pressure coefficient K_o was constant during loading and had a value of 0,67 as compared with 0,5 according to the empirical relationships (5) of

Jaky : $K_o = 1 - \sin\phi$

and Reimbert : $K_o = \frac{45° - \phi/2}{45° + \phi/2}$

On unloading, the ratio increases and approaches asymptotically to a value of 0,95.

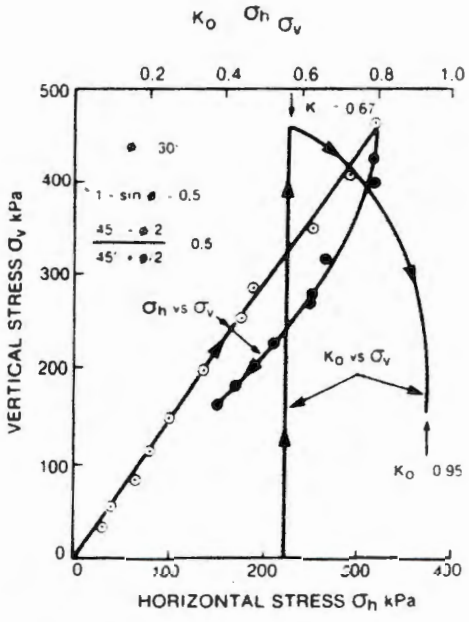

Figure 4 : Relationship between horizontal and vertical stresses in maize during compression and unloading with zero lateral strain

PRESSURES IN BIN DURING FILLING

During the period of observation, only one opportunity arose to measure pressures in the bin during uninterrupted filling. It was discovered that some of the contents had decayed as a result of rain water leaking into the bin around the heads of temporary construction bolts that had not been sealed. The bin was completely emptied, the leaks sealed and the bin was then refilled to 2,5 m above the level of pressure cell 5 (see Figure 1) before any maize was drawn off. Figure 5 shows the pressure profile at the end of the filling stage. The profile agrees with that predicted from the relationship

$$\sigma_h = K_o \gamma z \quad \text{with } K_o = 0,6 \qquad (1)$$

i.e. the effective value of K_o is slightly less than the value given in Figure 4. This confirms a similar conclusion reported earlier (3) for the filling of a bin with coal. (See additional comment later.) As the ratio of depth of contents to bin diameter was close to 1,0 at the end of the filling, silo action had a negligible effect on the pressure distribution.

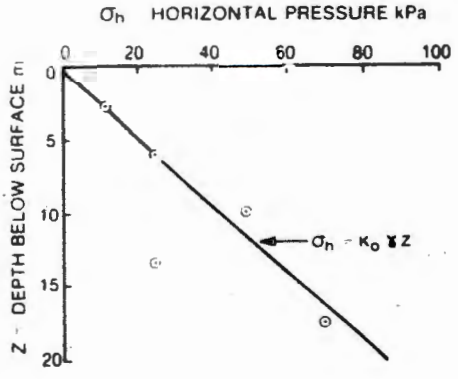

FIGURE 5 : Measured and theoretical relationsips between depth and pressure on filling

PRESSURES IN BIN DURING NORMAL OPERATION

Figure 6 shows the results of a series of pressure measurements taken over a period of a year. The letters A, B, C, etc. (which represent the individual readings) correlate with similar letters in Figure 3. The pressure readings have been plotted at the level of the pressure cells.

Various calculated curves have been superimposed on the diagram. These represent:

(i) the Janssen curve for ϕ = 13° and K = 0,6, i.e. K_o for first loading (Figure 5);

(ii) similar curves for ϕ = 13° and 16° and K = 1,0, i.e. K_o for unloading (Figure 4);

(iii) the Janssen curve for ϕ = 13° and K = 2,0 (this passes through the F measurement at pressure cell 5);

(iv) the Walker (6) curves for K values of 1,0 and 1,25 and a cone half angle α of 20°. These have been drawn for initial pressures of 110 kPa (K = 1,25) and 137 kPa (K = 1,0).

Note that most of the pressures recorded on gauges 5, 6 and 7 are enveloped by the Janssen curves for K = 1,0 and also that a sharp increase in pressure occurs in many of the pressure profiles at gauge 5.

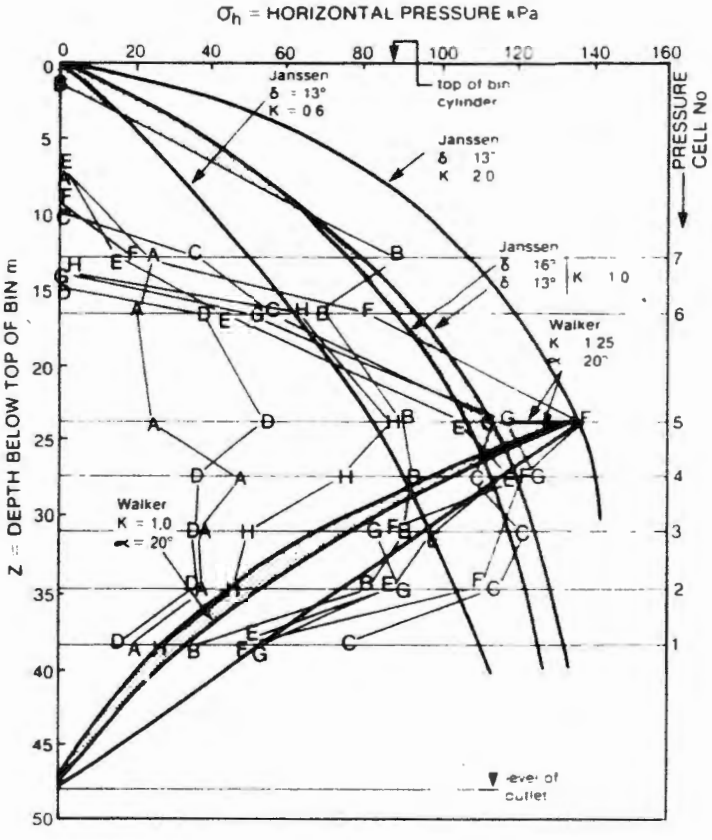

FIGURE 6 : Pressures in bin during normal operation (plotted at the level of each pressure cell)

It is plain from the flat angle of the conical bin bottom that the flow pattern within the bin must consist of two main regions:

a zone of parallel plug flow above, feeding into one of convergent funnel flow towards the outlet. The angle to the horizontal that defines the zone of funnel flow would have a minimum value of 45° + ϕ/2 = 60°. As Figure 1 shows, pressure cells 3, 4 and 5 are located in the zone where the transition from parallel to convergent flow could be expected to occur. Therefore, the increased pressures recorded by these cells probably reflect the increased lateral stresses in the parallel-convergent flow transition zone.

This deduction was confirmed when the bin was emptied and it became

possible to inspect it from the inside. The walls of the bin had been scoured and cleaned by moving grain down to a clearly defined horizontal ring. Below this ring, the plates were rusty and where the water leaks mentioned earlier had occurred, decayed maize adhered to the walls. This was clear evidence that parallel flow of grain was occurring above the ring and that dead material was in contact with the bin walls below the ring.

The inside of a large bin is particularly difficult to photograph, but in Figure 7 maize adhering to the bin walls can clearly be seen and the junction between the rusty plates below and the scoured plates above occurs just above the fourth horizontal plate seam in the photograph. Two of the pressure cells are faintly visible between the second and third vertical stiffeners from the left of the photograph.

FIGURE 7 : Photograph of inside of bin showing dead material adhering to walls and transition between parallel and convergent flow zones

The position of the observed lower limit of the zone of convergent flow is marked on Figure 1 and occurs just below pressure cell 4. It appears from the markings on the bin and the pressure readings that the transition zone is either static or nearly static in position.

The two pressure profiles (Figure 6) calculated by means of Walker's theory (6) follow the general trend of the pressures measured by cells 1 to 4, but the measured pressures show a much wider peak than the calculated values. (Actually, a straight line from the maximum recorded pressure to zero at the outlet fits the recorded data very well.)

The apparently random variation in lateral pressures requires closer examination. Part of the variation may have been caused by the effects reported in Reference (1). However, the variation appears to be far larger than can be attributed to unaccounted errors in cell calibration.

THE EFFECTS OF TEMPERATURE ON PRESSURES IN BINS

One possible explanation for the wide variation of measured pressures is that of the effect of temperature variations. A thin walled steel bin, being a good heat conductor, will respond rapidly to diurnal temperature variations, whereas its contents will not. If the temperature falls, the bin walls will contract onto its contents and lateral stresses will rise. Conversely, pressures will fall when the bin walls expand away from the filling.

To test this hypothesis, continuous recordings of temperature and pressure were made at pressure cells 1 and 2 over a week-end when the pressures would not be affected by filling or emptying from the bin. Because the pressure cells are strain gauged with a full bridge, they should be temperature compensated. Nevertheless, to check that the cells do indeed not respond to changes in temperature, a cell of similar make was connected to a chart recorder and simultaneous recordings of cell reading and temperature were made while the cell was exposed to the outside environment. The results of these measurements confirmed that the cells are completely temperature compensated.

The results of the measurements made on the bin are shown in Figure 8. The thermocouple junctions were taped to the outside of the bin wall adjacent to each pressure cell. The recordings confirm that as the temperature rises, the pressure on the bin falls and vice versa. The difference in the characteristics of the pressure-time relationships when the temperature is rising or falling is of particular interest. As the temperature falls, pressure builds up in a series of small amplitude, relatively high frequency oscillations. When the temperature rises, the pressure decreases in a series of larger amplitude lower frequency steps.

It will be noted that there is a tendency for the pressure to rise progressively as each diurnal cycle of temperature takes place. This is presumably because the grain settles against the sides of the bin as the bin walls move outwards. Subsequent decreasing temperatures therefore result in higher pressures than in the previous temperature cycle.

The measurements shown in Figure 8 were taken in spring when the diurnal temperature cycle is subdued. Bigger diurnal changes in temperature and pressure can be expected to occur in summer and winter.

For the two temperature cycles shown in Figure 8, a pressure coefficient of 0,5 at noon on Saturday would be transformed to between 1,1 and 1,4 by 06h00 on Monday. A K value of 1,0 on Saturday could become 2,8 by Monday. Hence it is not unreasonable to ascribe much of the variation in the pressure profiles shown in Figure 6 to temperature effects. It is also not unreasonable to expect the pressure coefficient K to rise to its maximum value of 3 at times of year when the daily temperature cycle is large.

When emptying of the bin was resumed, the accumulated pressures were relieved and pressures in the bin returned to a "working " condition.

COMPARISON OF MEASUREMENTS WITH CALCULATED VALUES

It is difficult to compare calculated pressure profiles with observed pressures because:

(i) the transition from parallel to convergent flow is static, whereas the surface of the grain that represents the datum for both measured and calculated pressures is variable; and

(ii) the lateral pressure coefficient varies with temperature as well as the state of operation of the bin.

If the bin were being designed ab initio by a designer with some knowledge of the flow of material within bins and silos, it is likely that the flow pattern would have been correctly identified and the region of the transition from parallel to convergent flow correctly located. The design pressure curve would then in all probability have been based on the Janssen curve for K = 1,0 and δ = 13° above the transition and the Walker curve with α = 20° and 30° and K = 1,25 to 1,50 below the transition. As Figure 6 shows, these assumptions would have given a reasonably accurate basis for the design of the silo, especially if a range of possible locations for the parallel-convergent transition were considered.

The conclusion is therefore reached that if correctly measured values of the fill parameters had been used together with a realistic assessment of the flow pattern within the bin, it would have been perfectly possible to predict the limits of actual pressures within the bin.

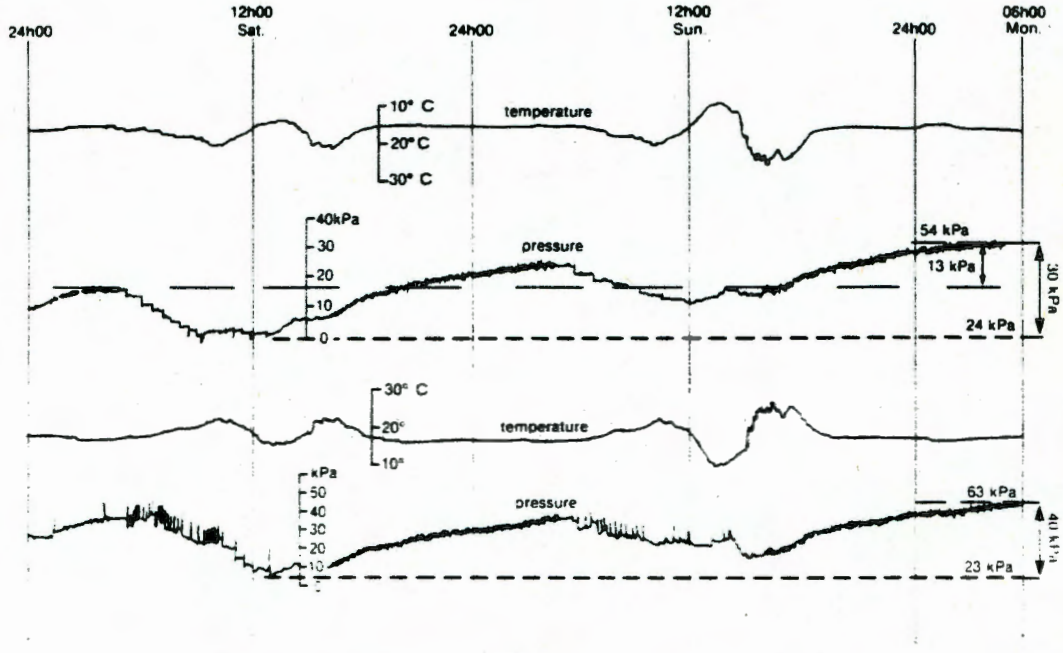

FIGURE 8 : Recorded variation of pressure with temperature while bin contents were constant

CONCLUSIONS

1. It has been shown that when a bin is filled with granular material without any drawoff occurring, lateral pressures correspond to the at rest condition for first loading.

2. Where a transition from parallel to convergent flow occurs in a bin, there is an increase in lateral pressure, as predicted theoretically. The zone of increased pressure is, however, wider than that predicted by theory.

3. Pressures in steel bins are highly variable and diurnal fluctuations of temperature have been identified as a major cause of the fluctuation. The walls of reinforced concrete bins would respond more slowly to temperature variations and consequently would not perform in this way to the same extent.

4. If current theoretical knowledge is rationally applied, it is possible to predict the upper limits to the pressures in a bin with adequate accuracy for design purposes.

ACKNOWLEDGEMENT

The author wishes to thank the management of Nola Industries Limited, owners of the bin, for permission to take the observations reported above. Particular thanks are due to Mr van der Walt and his staff for their kind co-operation. The author also wishes to thank Bessemer Steel Construction (Pty) Ltd., for making the pressure cells available and for installing them in the bin. Particular thanks are due to Mr J.A. de Wet in this regard.

REFERENCES

(1) BLIGHT, G.E. "On Measuring Pressures with Pressure Cells", Paper to this conference.

(2) Collection of published and unpublished data on materials properties maintained by the author.

(3) BLIGHT, G.E. and MIDGLEY, D., "Pressure Measured in a 20m Diameter Coal Load-Out Bin", Journal of Powder and Bulk Solids Technology, vol. 5, 1981, pp 21-31.

(4) BISHOP, A.W. and HENKEL, D.J., "The Measurement of Soil Properties in the Triaxial Test", Arnold, London, 1962.

(5) HARR, M.E., "Mechanics of Particulate Media", McGraw-Hill International, 1977.

(6) WALKER, D.M., "An Approximate Theory for Pressures and Arching in Hoppers", Chemical Engineering Science, vol. 21, 1966, pp 975-997.

powder handling & processing Volume 2, Number 4, November 1990

Temperature Surcharge Pressures in Reinforced Concrete Silos

G.E. Blight, South Africa

Summary

It is fairly well recognised that temperature surcharge pressures do occur in steel bins and silos, although so far, only one silo design code [1] includes these pressures in their specified loading. This short paper shows that temperature surcharge pressures also occur in reinforced concrete silos and reports on measured temperature surcharges in a reinforced concrete cement storage silo.

1. Introduction: Thermal Strains in Silo Walls

Temperature surcharge pressures have been firmly identified as a major component of the loading carried by steel-walled silos [1 – 5]. However, at present only one silo design code, that of the American Society of Agricultural Engineers [1] formally includes temperature surcharge pressures as part of the design loading for silos.

Attention so far has focused on steel silos. However, reinforced concrete silos must also be subject to temperature, surcharge pressures, although this is possibly not so obvious as in the case of steel silos.

Fig. 1a represents a section through a reinforced concrete silo wall of thickness t that is subjected to a temperature change at its outside face of $\Delta\theta_0$ and at its inside face of $\Delta\theta_i$. As indicated in Fig. 1b, $\Delta\theta_0$ and $\Delta\theta_i$ may be opposite in sense, or they may be of like sense.

The requirements of force equilibrium and strain compatibility through its thickness ensure that, if unrestrained by the silo fill the wall would undergo a mean free thermal strain:

$$\varepsilon_f = \frac{\alpha}{2}(\Delta\theta_i + \Delta\theta_0) \qquad (1)$$

where α is the coefficient of thermal expansion or contraction of the wall, and the temperature gradient through the wall is assumed to be linear (Fig. 1b). Hence even if the temperature at the inside face of the wall does not change, the wall as a whole will undergo thermal strain. If, however, the concrete is so thick or has such a high insulating value that the temperature variation does not penetrate through the full thickness of the wall (as indicated in Fig. 1c), the mean free thermal strain would be less than that given by Eq. (1).

In both Figs. 1b and 1c force equilibrium requires that area A equals area B. For Fig. 1c, this results in the conclusion that if the temperature change penetrates a distance of xt into the wall, the mean free thermal strain would be:

$$\varepsilon_f = \frac{x}{2}\alpha\Delta\theta_0 \qquad (2)$$

If $x = 1$, Eq. (2) reduces to Eq. (1) with $\Delta\theta_i = 0$.

For a silo wall subjected to a uniform change in temperature $\Delta\theta$ it can be shown [4] that the temperature surcharge pressure TS is given by

$$TS = \frac{2MEt\ \alpha\Delta\theta}{MD + 2Et} \qquad (3)$$

where

M = modulus of compressibility of the silo filling for radial compression

E = modulus of elasticity for the material of the wall, and

D = mean diameter of silo

Noting that $\alpha\Delta\theta$ is the mean free thermal strain ε_f in the wall, it follows that for a reinforced concrete silo in which the wall is

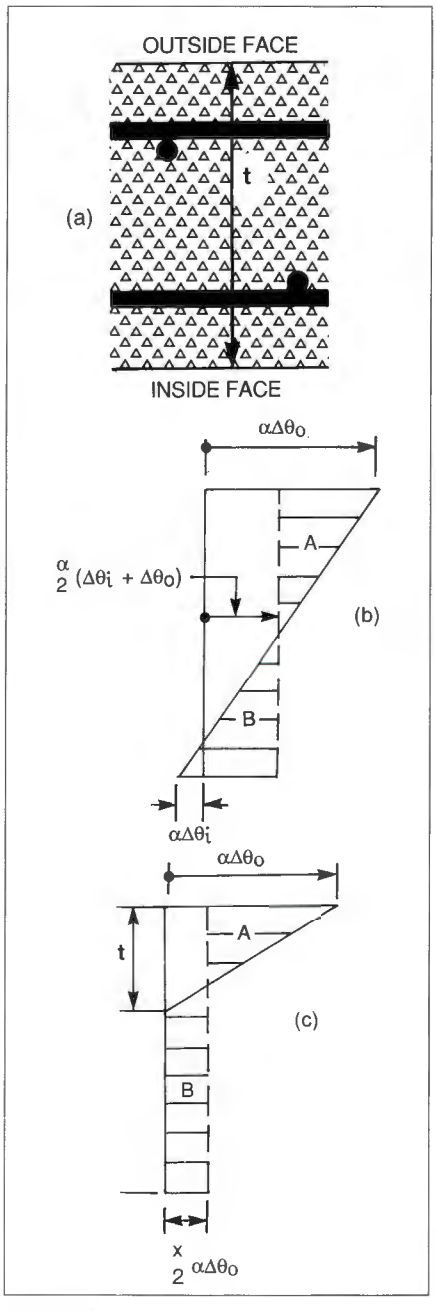

Fig. 1: Thermal strains in reinforced concrete silo walls

Details about the author of this paper on page 386

subjected to a varying temperature change

$$TS = \frac{2MEt\ \varepsilon_f}{MD + 2Et} \qquad (3a)$$

where ε_f is given by Eqs. (1) or (2).

2. Temperature Surcharge Pressures Measured in a Reinforced Concrete Silo Wall

Fig. 2 shows variations of pressure and temperature recorded for the outer wall of a 24 m diameter duocell cement storage silo. This silo and its instrumentation has previously been fully described [6], and is the only one available to the author that has pressure cells and functioning thermocouples that can be used for this type of measurement.

The two periods of record shown in Fig. 2 were periods when the silo was full of cement but not in use, and the recorded changes of pressure were thus solely a result of diurnal thermal strains in the walls.

It will be noted that the temperature of the inner face of the wall varied, although very little, and was at a minimum shortly after noon, when the outside of the wall was hottest. The entire 350 mm thickness of the wall is thus subject to diurnal change of temperature, although it is not known if the temperature gradient is linear.

The pressure on the walls clearly responds to the temperature changes, reducing as the temperature rises and increasing as the temperature falls.

The measured temperature surcharge pressure was equivalent to 0.29 kPa/°C on one occasion and 0.25 kPa/°C on the other. Thus the two available measurements were quite consistent.

It can therefore be concluded that diurnal temperature surcharge pressures do indeed arise in reinforced concrete silos.

On the assumption of a linear temperature gradient through the full thickness of the wall, as in Fig. 1b, and E for concrete of 30 GPa, the value of M for cement powder under a vertical pressure of about 60 kPa is 50 MPa. The corresponding values of M for wheat and maize grain under a similar vertical stress would be about 25 kPa [4]. Hence the moduli for the three materials are not dissimilar.

3. Values of M Measured in the Laboratory

In an earlier paper [7] the author described the use of a special oedometer to measure lateral swelling pressure in wetted grain. In this paper, values were given of the modulus for vertical compression of four types of grain including wheat and maize. The moduli were of the order of 5 and 10 MPa respectively and were far less than values of M subsequently deduced from measurements on silos [4]. Measurements by *Puri*, *Zhang* and *Marbeck* [8] on a 0.9 m diameter model silo lead to values of M for wheat of 8 MPa and maize of 12 MPa. These are also far too small to fit measurements made on full size silos.

The oedometer ring is illustrated in Fig. 3. The oedometer has now been used to measure the modulus of compressibility for radial compression at small strains.

The procedure was as follows:

A vertical pressure was applied to the specimen in the oedometer and the resulting lateral strain was measured via

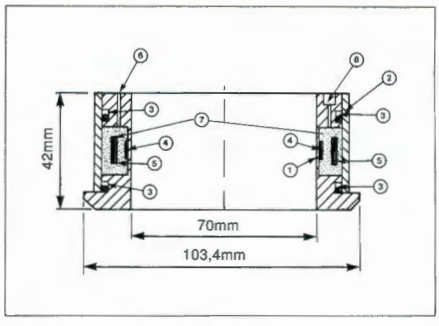

Fig. 3: Section showing principal components of K_0 oedometer ring
1. Thin wall oedometer ring
2. Casing ring
3. O ring seals
4. Strain gauge
5. Temperature compensator
6. Electrical outlet
7. Rubber foam packing
8. Air pressure inlet

strain gauge 4. A lateral pressure was then applied via air pressure inlet 8 and increased progressively until the lateral strain had been eliminated. Thus the lateral pressure Δp corresponding to a particular lateral strain ε_h was determined, and hence

$$M = \frac{\Delta p}{\varepsilon_h} \qquad (4)$$

The results of measurements of M on wheat and cement powder for a range of vertical pressures from 0 to 100 kPa are shown in Fig. 4. Values of M deduced from measurements on 6 full size silos are shown in Fig. 5.

It will be seen from Fig. 4 that values of M measured by means of the special oedometer turned out to be almost constant with vertical pressure and the same for loading and unloading cycles. Fig. 5 shows that the laboratory measurements of M are far larger than values deduced from field measurements. The field measurements present a consistent picture in which the values of M for maize, wheat and cement, at the lower end of the overburden stress range, are of comparable magnitudes.

The laboratory measurements of M were made at radial strains in the range of 5 to 10 microstrain, whereas radial strains in the full size silos were in the range of 100 to 200 microstrain. *Puri* et al.'s [8] measurements were in the strain range 0 to 500 microstrain.

This may be the reason for the lower values of M measured in the field and by *Puri* et al. as it is known that granular materials are extremely stiff at small strains and soften as the strain increases (e.g. [9]). *Puri* et al.'s measurements show that for temperature changes from about 1°C upwards the relationship between temperature drop and temperature surcharge is linear. This is also the assumption made in deriving Eq. (3). Hence if the small strain

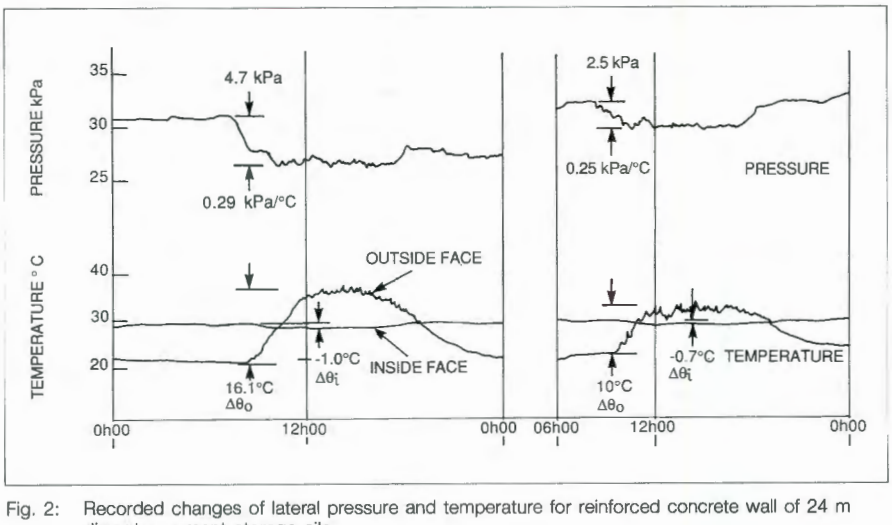

Fig. 2: Recorded changes of lateral pressure and temperature for reinforced concrete wall of 24 m diameter cement storage silo

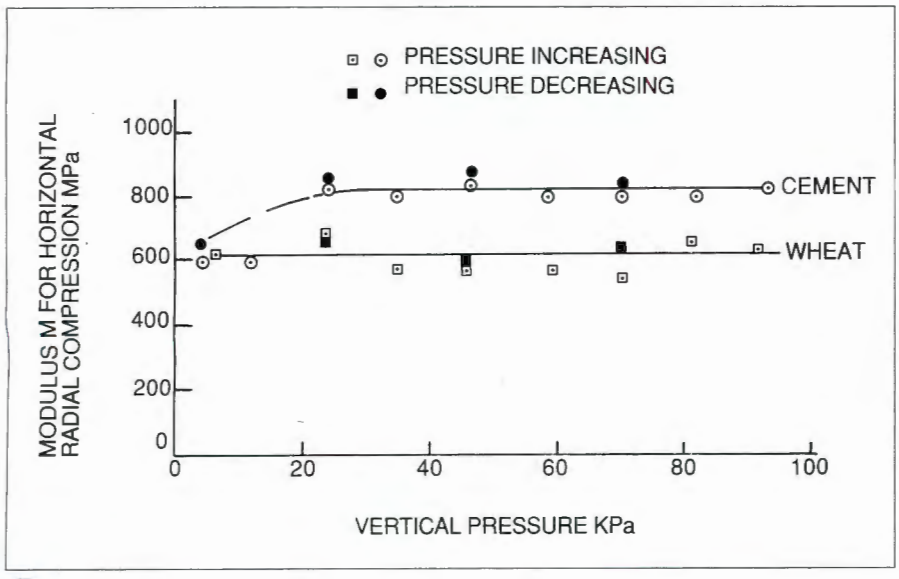

4: Values of *M* for cement and wheat measured in the laboratory

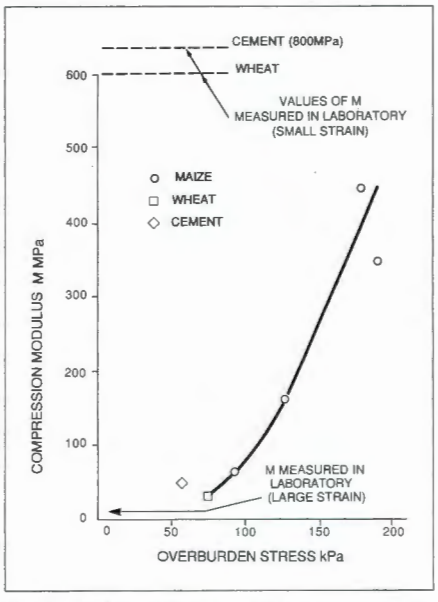

Fig. 5: Relationship between compression modulus M and overburden stress calculated from measurements on 5 steel grain silos and reinforced concrete cement silo

laboratory measurements have any practical relevance, they are relevant only for very small changes of temperature, probably less than 1°C. Whatever the reason for the discrepancy between field and laboratory measurements it is considered that the field data shown in Fig. 5 are realistic for design purposes.

4. Conclusions

It has been demonstrated, both by calculation and observation, that temperature surcharge pressures do occur on the walls of reinforced concrete silos. These pressures can form a very appreciable part of the total pressure loading on the walls of large silos, and should be accounted for in design.

A way has yet to be found to measure the [illegible]al compression modulus by means of small-scale tests in the laboratory, in a realistic way. Present methods of measuring the modulus for vertical compression give results that are far too small, and measurements of the modulus for radial compression at small strains give results that are too large in comparison with moduli deduced from measurements in full size silos. Measurements made on small silos also do not seem to give a realistic result, probably because the range of overburden stresses was not large enough.

5. References

[1] *American Society of Agricultural Engineers*: Loads Exerted by Free-Flowing Grains in Bins; ASAE EP433 (1989)

[2] *Anderson, P.*: Temperature Stresses in Steel Grain Storage Tanks; Civil Engineering; ASCE, (1966), p. 74.

[3] *Blight, G.E.*: Temperature Changes Affect Pressures in Steel Bins; Int. J. Bulk Solids Storage in Silos, Vol. 1 (1985) No. 3, pp. 1-7.

[4] *Blight, G.E.*: Strain and Temperature Measurements on an Externally Stiffened Corrugated Steel Grain Silo; powder handling & processing, Vol. 1 (1989) No. 4, pp. 343-347.

[5] *Blight, G.E.*: Defects in Accepted Methods of Estimating Design Loading for Silos; Proc. Institution of Civil Engineers, Part 1, London 1990.

[6] *Fliss, L.* and *Blight, G.E.*: Comparison of Design and Measured Lateral Pressures and Temperatures in a Large Duo-Cell Cement Storage Silo; Int. J. Bulk Solids Storage in Silos, Vol. 2 (1986) No. 4, pp. 18-28.

[7] *Blight, G.E.*: Swelling Pressure of Wetted Grain; bulk solids handling, Vol. 6 (1986) No. 6, pp. 1135-1140.

[8] *Puri, V.M., Zhang, Q.* and *Marbeck, H.B.*: Influence of Granular Material Properties on Thermally Induced Bin Loads; Int. J. Bulk Solids Storage in Silos, Vol. 2 (1986) No. 3, pp. 1-7.

[9] *Padfield, C.J.* and *Sharrock, M.J.*: Settlement of Structures on Clay Soils; CIRIA Special Publication 27 (1983).

bulk solids handling Volume 11, Number 2, May 1991

Eccentric Emptying of a Large Coal Bin with Six Outlets

G.E. Blight, South Africa

Summary

A run-of-mine coal bin with a diameter of 25 m and a capacity for 15,000 t of coal has been instrumented to study pressure distributions during emptying through its six eccentric outlets.

The measurements have shown that the *Jenkyn* [1] assumptions adequately explain the observed eccentric pressures.

The behaviour of two steel silos under eccentric emptying is also described to show that the *Jenike* theory [2] of pressures under eccentric emptying also seems valid in the vicinity of an eccentric outlet.

1. Introduction

Pressure changes arising during eccentric emptying of bins and silos are one of the least well understood aspects of silo loading. As long ago as 1904 *Jamieson* [3] reported that when a silo is emptied eccentrically the pressure on the wall closest to the eccentric opening decreases, while that on the more remote wall increases. The first attempt at a rational explanation of this phenomenon, and a method of estimating pressure distributions during eccentric emptying appears to have been due to *Jenike* [2] over 60 years later. *Jenike* postulated that eccentric flow generally occurs in a flow channel of diameter less than that of the silo. The ratio of the pressure in the flow channel at any level, to that in the static material around it is equal to the ratio of the diameters of flow channel and silo. Hence the pressure in the flow channel is reduced relative to that in the rest of the silo. Where the flow channel impinges on the silo wall, the wall is subjected to bending in the horizontal plane.

Most later explanations of the effects of eccentric emptying have been based on *Jenike*'s very logical-sounding explanation (e.g. *Wood* [4] and *Rotter* [5]). However, *Jenkyn* [1] adopted an even simpler assumption based on the observation that eccentric emptying draws down the

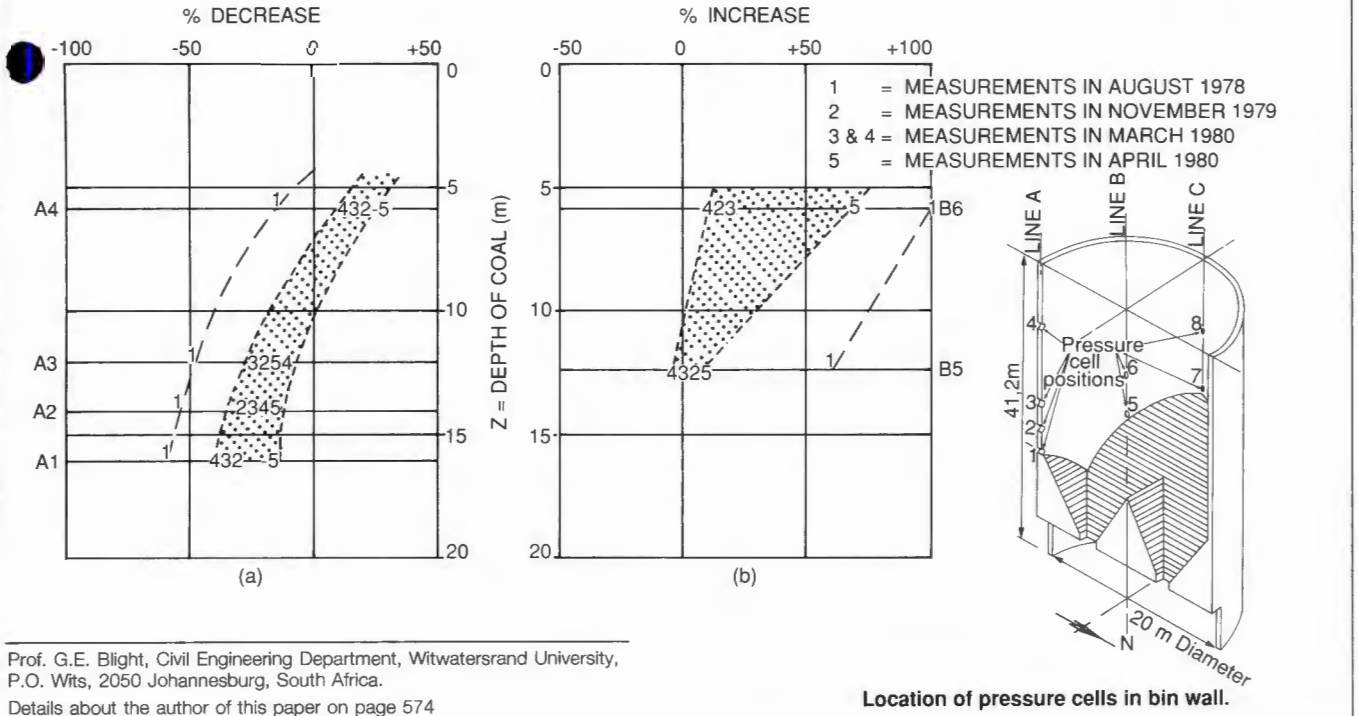

Fig. 1: Variation of pressure changes with height on A and B lines of pressure cells

Location of pressure cells in bin wall.

Prof. G.E. Blight, Civil Engineering Department, Witwatersrand University, P.O. Wits, 2050 Johannesburg, South Africa.

Details about the author of this paper on page 574

surface of the material in a silo unevenly. According to *Jenkyn* the pressures around the perimeter of a silo, at any level, are proportional to the material overburden above that level. Because the surface is drawn down further on the side of the eccentric outlet, the pressure will be lower on that side and higher on the opposite side. There were, however, no measurements offered to support his assumption.

The present author [6] made observations of the changes in pressure that occurred in a large coal load-out bin with twin outlets when emptying was started. The results of these measurements are given in Fig. 1. The pressure cells A1 to A4 were on a vertical line adjacent to the operative outlets, while cells B5 and B6 were on a line displaced by 45° in plan from line A. Pressures were observed to decrease on line A, except high up on the silo wall at cell A4. On line B pressures were found to increase. These were short-term changes (right at the start of emptying) that occurred without any appreciable change in the surface levels of coal in the silo.

Fig. 2 shows the radial distribution of pressures in the silo on two occasions, at the end of uninterrupted filling from empty and at the start of emptying. Fig. 2a corresponds to the emptying situation applicable in Fig. 1. It shows the decrease in pressure adjacent to the outlet and the pressure increase remote from the outlet. Fig. 2b shows the situation when the other outlet was opened. There was again a very slight decrease in pressure on line A and increases in pressure occurred elsewhere.

Because the pressure cells represented in Fig. 2 were mounted on an oblique section through the cylindrical barrel of the silo, a completely uniform pressure distribution would be represented in Fig. 2 by an ellipse like the broken ellipse representing the radial distribution of $K_0\gamma z$ (where K_0 is the at rest pressure coefficient, γ is the density of the coal and z is the depth below the coal surface at the wall). The impression is gained from Fig. 2 that the pressure changes at the start of emptying could have arisen from a tendency for the non-uniform pressure distribution at the end of filling to become more radially uniform once the coal started moving, rather than from the effects of eccentric flow. Certainly, horizontal bending in the silo wall would have decreased once emptying started, rather than increasing as *Jenike*'s approach would predict. Hence these observations appear not to support the *Jenike* hypothesis.

Hartlen et al. [7] studied the effects of eccentric emptying on pressures in a silo measuring 7 m in diameter and 46 m high. Pressure cells were mounted on four vertical lines displaced by 90° in plan, and at vertical intervals of 7 m. The eccentric outlet was at the side of the silo, at the bottom. These tests showed a slight decrease in pressure on the pressure cells closest to the outlet. However, as the nearest pressure cell to the outlet was a full silo diameter above it, the instrumentation was not well placed to record the effects of eccentric emptying on wall pressures. These tests do, however, show that the effect of an opening is localized and may not be felt in areas remote from the opening.

The author was involved, in 1987, in checking the design for a 25 m internal diameter run-of-mine coal bin with six outlets, all of them eccentric. This presented an opportunity for making further observations of the effects of eccentric emptying on wall pressures. The present paper is the outcome of those observations.

Construction of the silo started in 1988 and the pressure cells were installed in March and April 1989. The first coal entered the silo in May 1990 .

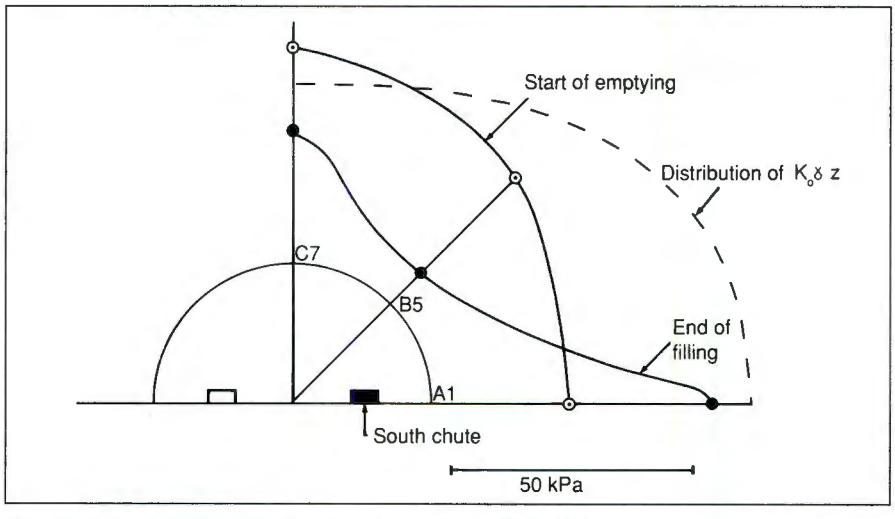

Fig. 2a: Maximum lateral pressures during discharge from South chute – radial distribution at cylinder – pyramid transition

Fig. 2b: Maximum lateral pressures during discharge from North chute – radial distribution at cylinder – pyramid transition

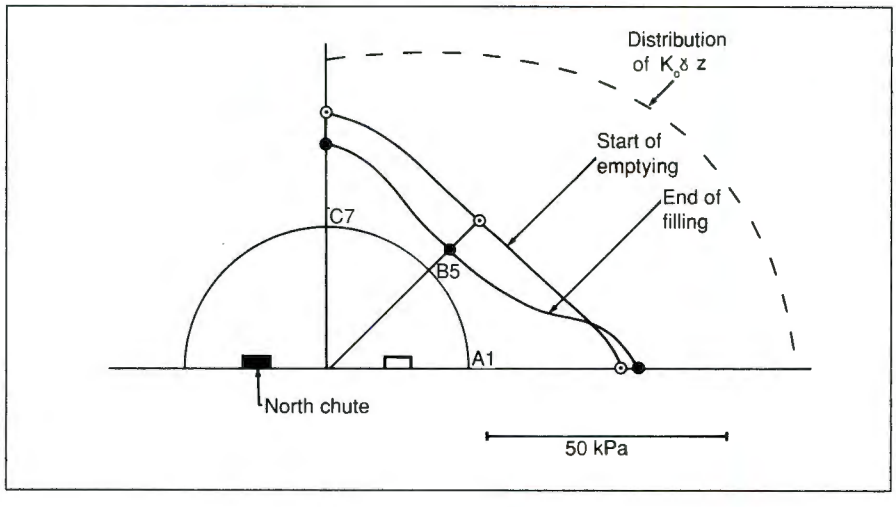

2. Details of 25 m Diameter Coal Bin and Instrumentation

A section through the bin is shown in Fig. 3a. The barrel is 36 m high and 25 m in internal diameter with 650 mm thick walls. The floor containing the 6 outlets is supported independently of the barrel on 8 columns. The interior is benched with mass concrete at a 50° inclination towards the outlets.

Fig. 3b shows the 6 outlets in plan. The outlets will eventually be served by three conveyors, but at present only two have been installed and only two feeders are operative. All of the measurements were made with discharge occurring through both of these outlets.

The instrumentation consists of 12 mercury-filled strain-gauged diaphragm pressure cells with 200 mm diameter pressure-sensitive faces. The silo was built for a new colliery that did not come into production until a year after the bin was completed. Hence the pressure cells were calibrated with coal as similar

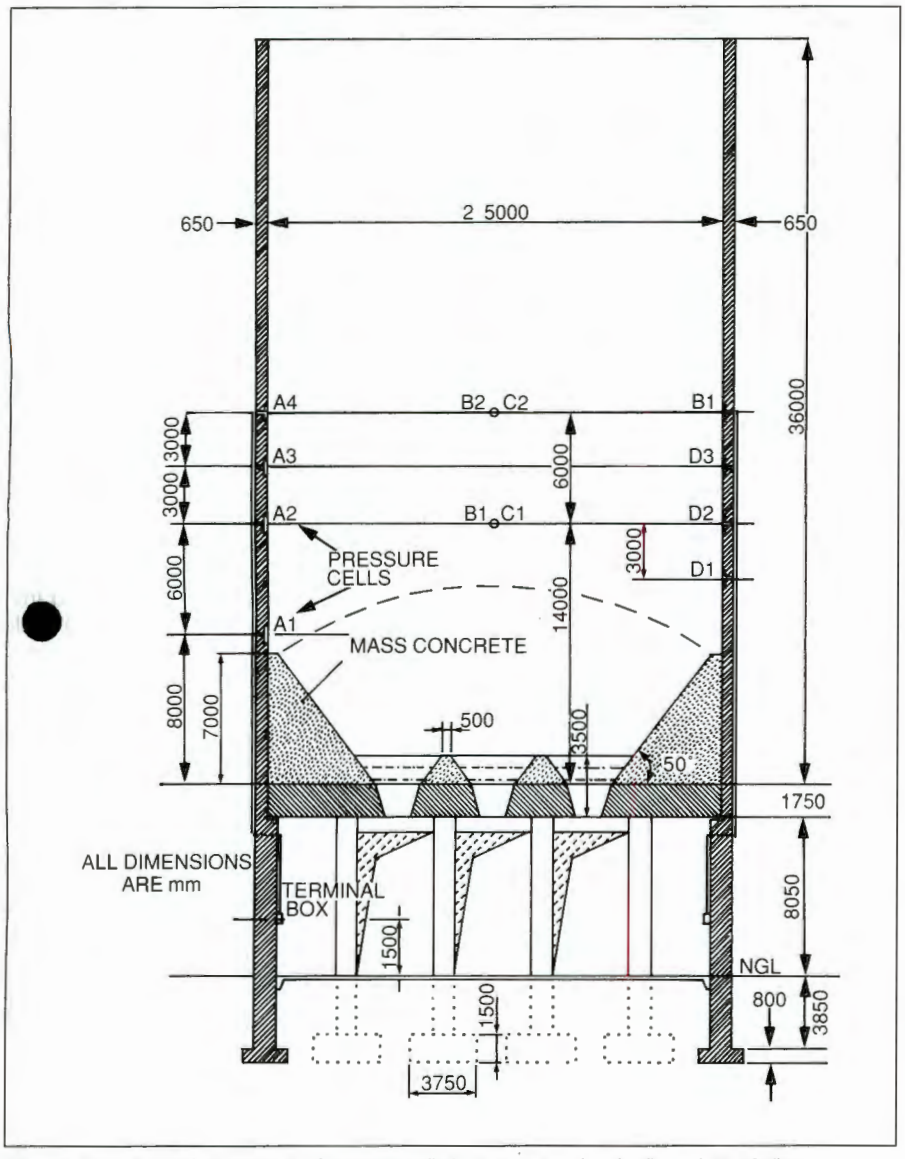

Fig. 3a: Section showing positions of pressure cells in elevation and main dimensions of silo

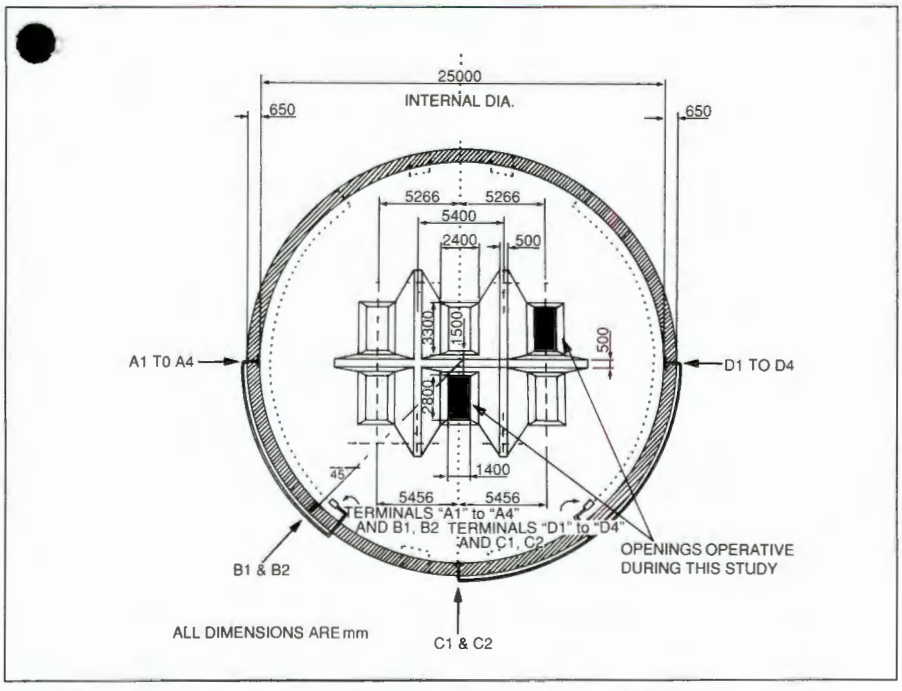

Fig. 3b: Plan showing openings in base of silo and positions of pressure cells in plan

as possible in properties to that expected to be produced.

The calibration of the cells and their installation was carried out in the manner described by *Blight* and *Bentel* [8]. Access for installation was provided by means of a basket hanging from a tower crane.

The layout of the pressure cells in elevation is shown in Fig. 3a and the layout in plan is shown in Fig. 3b. Leads from the pressure cells were taken down the outside of the bin walls to two junction boxes accessible from ground level.

Fig. 4a shows the general appearance of the silo and Fig. 4b shows 3 of the 6 outlets in plan. Two of the pressure cells are just visible as dark spots at 12 o'clock and one-thirty in this photograph.

The limits of the flow zones to the three pairs of outlets are indicated in Fig. 3a. Cell A1 was positioned in a 'dead' zone of material, while cell D1 is close to the boundary of the flow zone to the side outlets.

All of the remaining gauges are either in a flow zone or a dead zone when the side outlets are used, and all are in a dead zone when only the central outlets are used.

3. Observed Wall Pressures

At the time these observations were made, the power station fed by the colliery had not yet been commissioned and the coal-handling circuit was being used to build up a temporary stockpile for future use by the power station.

It was necessary to fit in observations with the operations of the mine.

Three sets of measurements have been made after the bin was filled without interruption from a part empty state and three sets when the bin had been drawn down eccentrically.

The general pressure versus depth behaviour of the bin is illustrated in Fig. 5.

In this figure, measured pressures have been plotted against the depth of each pressure cell below the coal surface. Each letter represents a data point, *A* and *a* for gauges on line A etc. Capital letters represent filling and small letters emptying pressures.

As observed previously in a number of silos, including two coal silos ([6, 9]), measured horizontal pressures σ_h were found to lie between two limiting lines represented by the equations

$$\sigma_h = K_A \gamma z$$

Fig. 4a: General appearance of 15,000 t run of mine coal bin

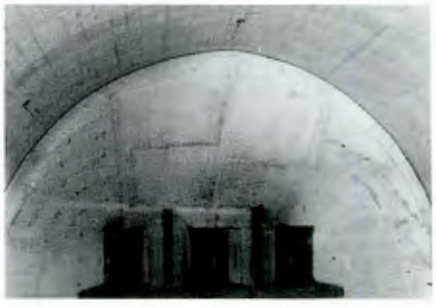

Fig. 4b: View into 15,000 t bin showing 3 of 6 outlets. Pressure cells are visible at 12 o'clock and 1h30 in photograph, on bin wall

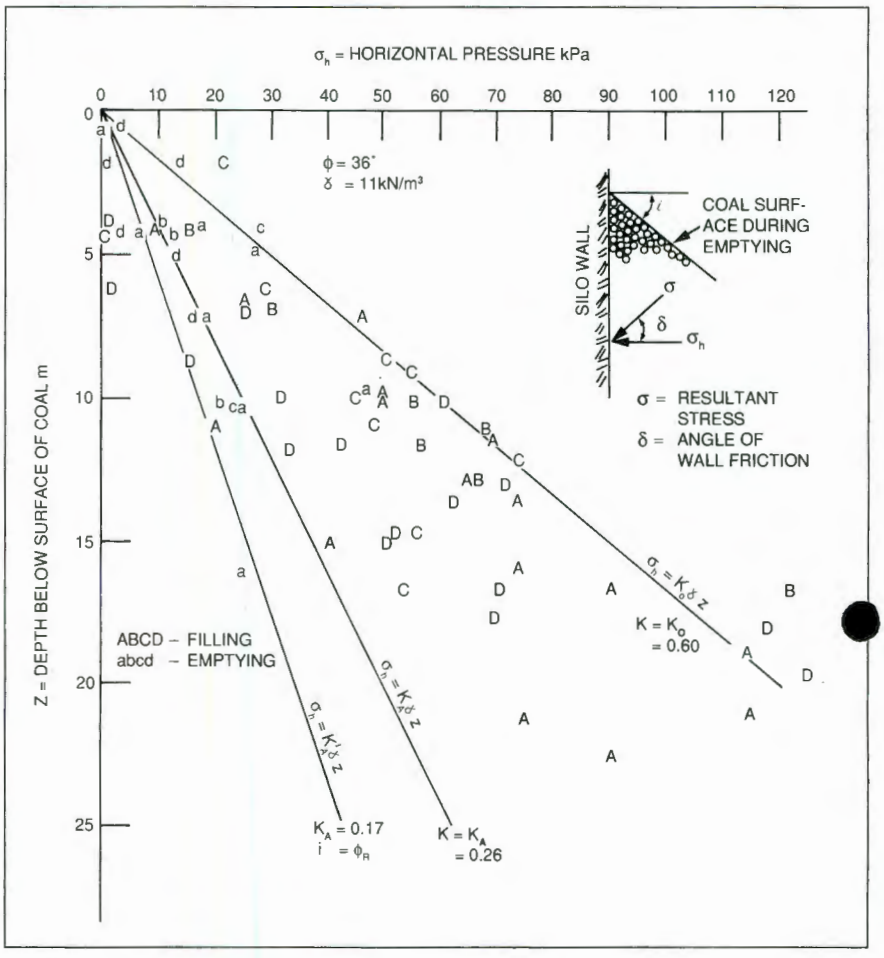

Fig. 5: General relationship between depth of coal and horizontal pressure

and

$$\sigma_h = K_0 \gamma z$$

where K_A is the active pressure coefficient and the other symbols have been defined previously. The active pressure coefficient was determined from the angle of shearing resistance of the coal, $\phi = 36°$, while K_0 was measured in the laboratory (see, e.g. *Blight* and *Ofer* [10]). The bin had been designed for a bulk density of the coal of $\gamma = 8$ kN/m^3. The actual density during the tests averaged 11 kN/m^3.

During emptying, the coal surface slopes away from the wall at an angle *i* equal to the angle of repose $\phi_R = 35°$.

The third pressure-depth line in Fig. 5 corresponds to the *Coulomb* active pressure coefficient K'_A for a negative surcharge angle of ϕ_R.

Fig. 5 shows that this bin behaves very much as would be expected of a squat structure with a maximum depth of filling roughly equal to its diameter.

The pressure varies linearly with depth, there is no *Janssen*-type arching, and the pressure coefficient varies between predictable limits.

4. Pressures During Eccentric Emptying

Figs. 6a and b compare pressures measured at the end of filling on two occasions with those measured after subsequent eccentric emptying. In both figures a cross-section shows the profile of the coal surface in the bin corresponding to each set of measurements. In Figs. 6a and b pressures have been plotted opposite the absolute elevations of the pressure cells.

In Fig. 6a pressures at the end of filling plot between the K_0 and K_A lines while pressures after drawdown plot closer to the K_A line. This is particularly marked for line D gauges where the coal surface was lowest.

The picture in Fig. 6b is similar except that most measured pressures appear to follow the K_0 lines.

Figs. 6a and b also show the design pressure distributions, for which the assumed coal parameters were

$$\gamma = 8 \text{ kN/m}^3; \quad K_0 = 0.5$$

and the angle of wall friction, coal on concrete was $\delta = 30°$.

Even though the actual coal parameters differed from those assumed, the design pressure envelopes contain all but one of the measured pressures.

The important point emerging from Figs. 6a and b is that *Jenkyn*'s assumption [1] appears to be quite correct for this silo. Wherever the pressure is measured, it is directly related to the head of coal above the point of measurement. This is particularly well shown by the measurements on lines D and A after eccentric drawdown.

There may well be some re-distribution of horizontal pressure at the start of eccentric drawdown, such as that shown in Figs. 1 and 2, but once an appreciable change in the position of the fill surface has occurred, *Jenkyn*'s assumption seems to hold.

This is a very important observation, because it means that the eccentricity of the pressure distribution becomes less, as the depth below the fill surface increases.

The eccentricity of loading may be large where the absolute magnitude of the pressure is small, but will be much smaller where the pressure is large. This is illustrated by Fig. 7.

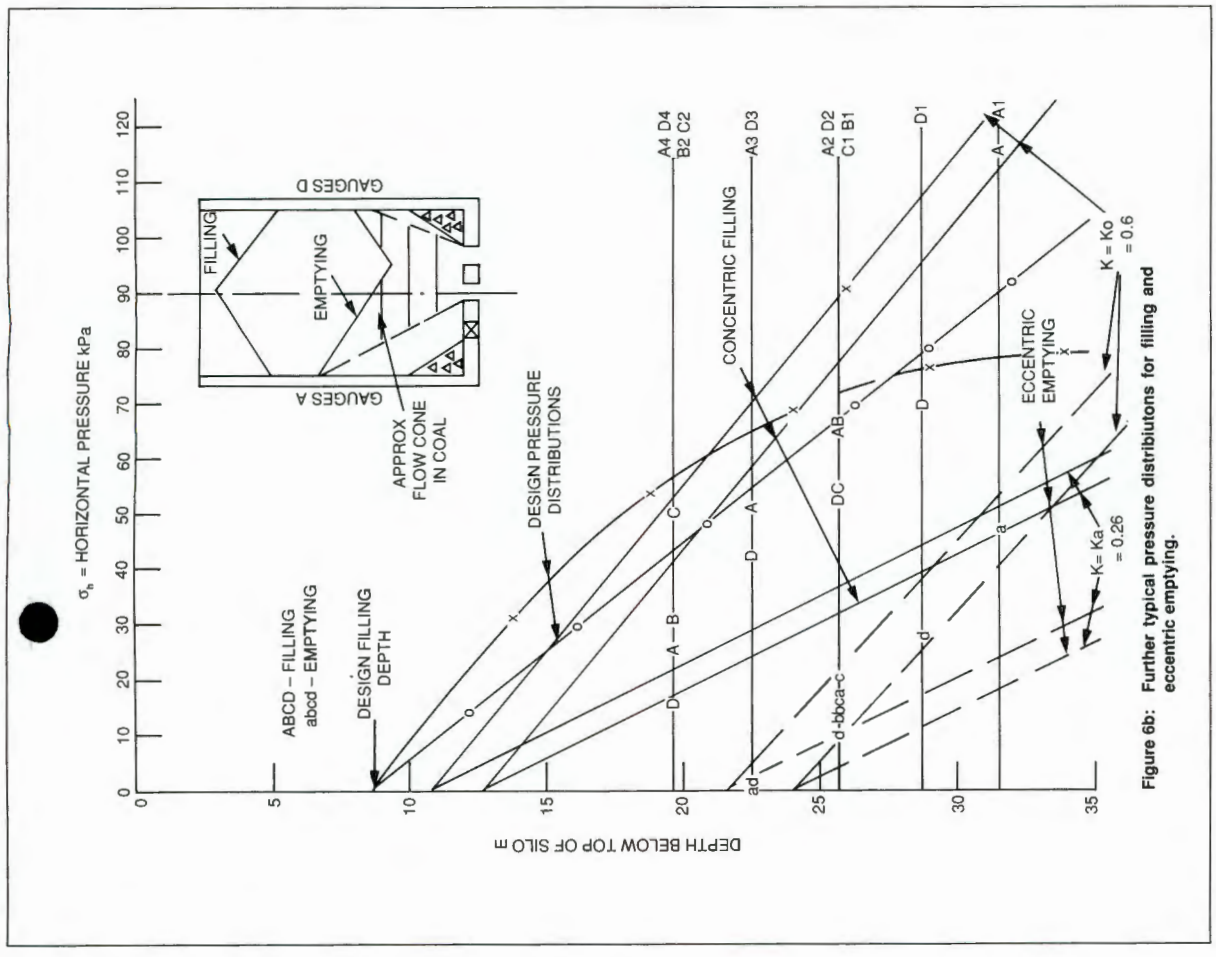

Figure 6b: Further typical pressure distributions for filling and eccentric emptying.

Fig. 6b: Further typical pressure distributions for filling and eccentric emptying

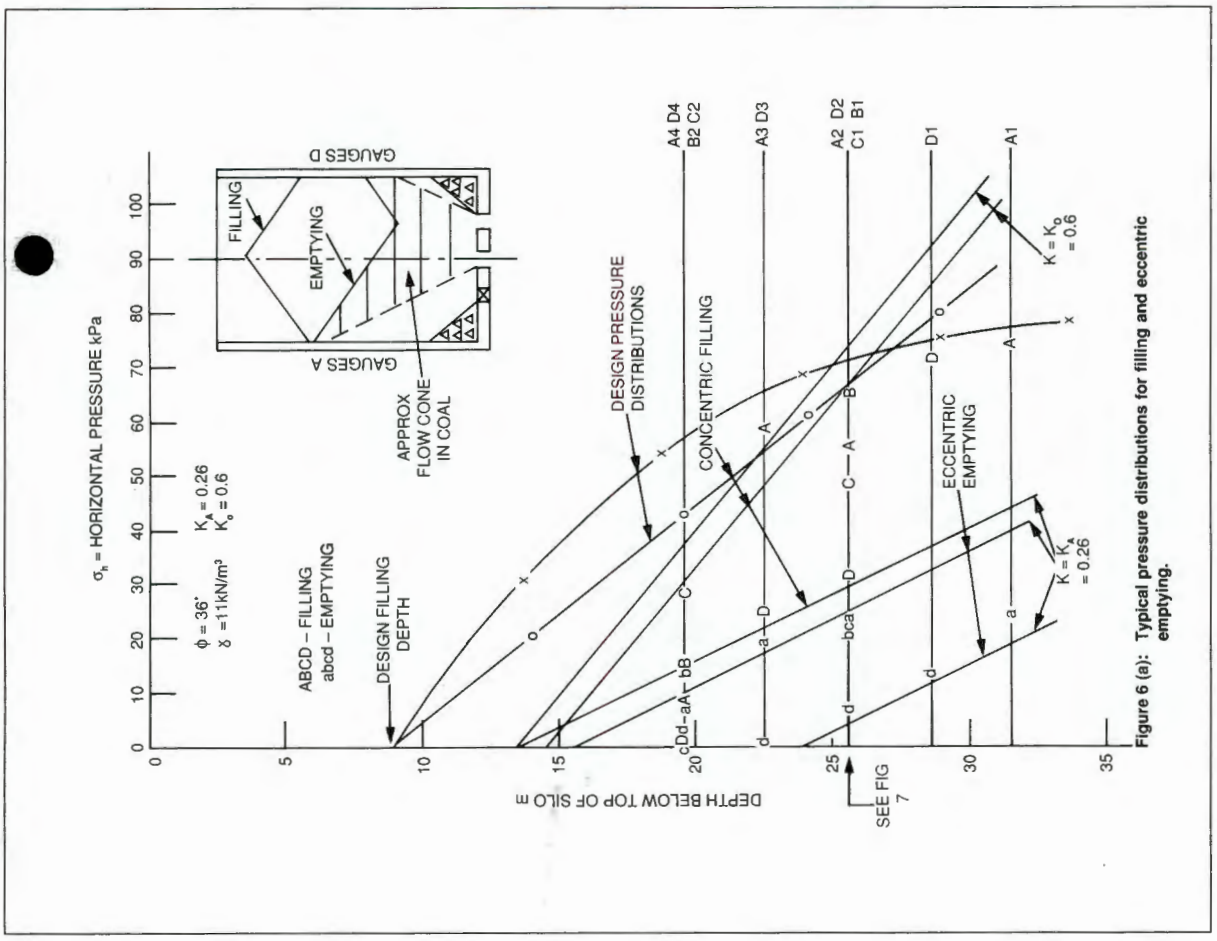

Figure 6 (a): Typical pressure distributions for filling and eccentric emptying.

Fig. 6a: Typical pressure distributions for filling and eccentric emptying

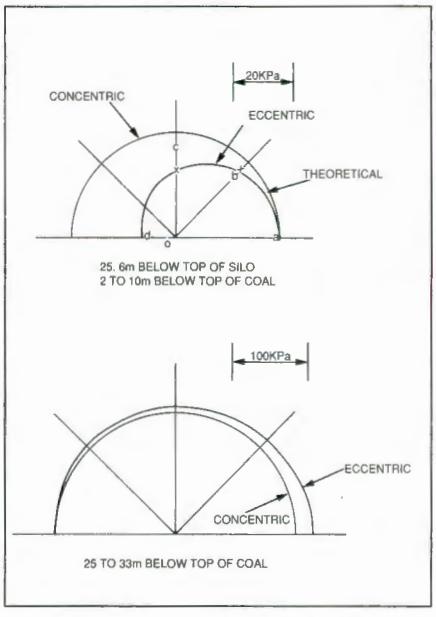

Fig. 7: Typical pressure distributions for filling and eccentric emptying

The upper part of Fig. 7 compares the eccentric pressure distribution predicted by the *Jenkyn* assumption at a depth of 25.6 m below the top of the silo when the coal depth above that level varied from 2 to 10 m. The diagram also shows the pressures measured at this level (from Fig. 6b). The lower part of the diagram shows the pressure distribution that would apply at a depth of 25 to 33 m below the coal surface. The maximum difference in pressure is the same in each case (about 23 kPa), but the eccentricity is very much less at the greater depth, because of the generally higher pressure level there.

5. Consequences of Eccentric Emptying

For a reinforced concrete silo, the main consequence of eccentric emptying lies in the horizontal bending moments induced in the silo shell. Because the wall of the reinforced concrete silo is relatively thick, providing a lever arm to resist the moment usually poses no great design problems. A reinforced concrete wall is also thick enough to resist buckling under vertical wall load.

However, a number of steel silos have either collapsed or their walls have buckled inwards as a result of being emptied eccentrically. It was this phenomenon that led *Jenike* [2] to his analysis of the effects of eccentric flow. Moreover, steel silos have been observed to collapse almost immediately after eccentric flow was initiated, and long before any appreciable changes in level of the fill surface had occurred.

Fig. 8 shows the collapsed remains of a welded plane plate silo [11]. The silo, 12.2 m in diameter and 33 m high, collapsed after wheat grain was accidentally drawn from an eccentric outlet at its base. It is believed that the silo buckled inwards and leaned over towards the buckle on the side of the eccentric outlet after less than a ton of the silo's 3,000 t capacity had been withdrawn. Once the buckle was observed, it was decided to empty the silo by drawing from the central outlet. After withdrawing a few more tons of grain, the silo fell over, knocking over an adjacent empty silo as it came down.

Fig. 8: 12.2 m diameter by 33 m high welded plane plate silo after collapsing and falling over as a result of eccentric emptying

In contrast, Fig. 9 shows an internally stiffened corrugated steel bin 18.2 m diameter and 24 m high that survived eccentric emptying with no damage. The bin had been filled with maize grain that had too high a moisture content and subsequently spontaneously caught fire. The operators decided to remove the burning grain by cutting a hole in the side of the bin at the base. The hole can be seen to the right of the bin in Figure 9. Despite the very severe eccentric emptying condition imposed on the walls, the structure suffered no damage, although the stiffeners were distorted by heat at the top of the bin where the grain was actually burning.

Fig. 9: 18.2 m diameter by 24 m high maize storage bin undamaged after eccentric emptying through opening at base (visible to right of photograph)

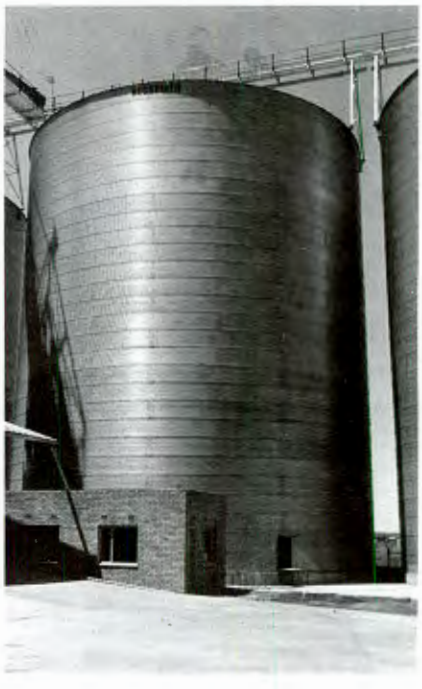

There was obviously a big difference in the behaviour of the two structures. It appears likely that in accordance with *Jenike*'s assumptions, a low pressure zone developed against the walls of both silos, in the immediate vicinity of the eccentric outlet. In the case of the wheat silo the wall was unable to support the frictional wall load and buckled inwards, precipitating the collapse. It was probably not horizontal bending that caused the failure, but buckling under vertical load. Theoretical studies by *Rotter* [5] show that this is a very likely explanation. On the other hand, the maize silo, being adequately stiffened against frictional wall load, was able to survive the removal of lateral support to its wall at the base. There are no signs of any inward bending on its plates in the vicinity of the eccentric opening.

No design calculations investigating the buckling stability of the walls of the wheat silo were available. A subsequent analysis after *Trahair* et al. [12] showed that the silo wall was safe against buckling while supported by the lateral pressure of its contents, but unsafe if this support was removed. This seems to have been exactly what happened as a result of the eccentric emptying.

In contrast, the stiffeners of the maize bin were designed to support the entire frictional wall load without any support from the outward pressure of the contents. The structure was thus able to survive the effects of eccentric emptying.

6. Conclusions

Two main hypotheses have been advanced to explain the effects that eccentric emptying may have on the walls of a bin or silo. It appears that both have validity:

The *Jenkyn* assumption whereby pressures during eccentric emptying are related purely to the head of material above any point of the silo wall seems to be valid in areas remote from the eccentric outlet.

The *Jenike* assumption that postulates the development of a zone of low pressure in the immediate vicinity of an eccentric outlet also appears to be valid.

Whereas *Jenkyn*-type eccentric pressures result in horizontal bending in a silo wall, the *Jenike*-type low pressure zone, by removing lateral support from the silo wall, may precipitate a buckling failure of a steel silo wall if it is inadequately strong or inadequately stiffened to carry the

frictional wall load without the assistance of lateral support from the silo fill.

References

[1] *Jenkyn, R.T.*: Calculation of material pressures for the design of silos; Proc., Institution of Civil Engineers (London) Part 2, Vol. 65, 1978, pp. 821-838.

[2] *Jenike, A.W.*: Denting of circular bins with eccentric draw-points; J. of the Structural Division, ASCE, Vol. 93, 1967, No ST1, pp. 27-35.

[3] *Jamieson, J.A.*: Engineering News, Vol. 51 - Quoted in Handbuch für Eisenbetonbau, Wilhelm Ernst, Berlin, 1924.

[4] *Wood, J.G.M.*: The analysis of silo structures subject to eccentric discharge; Proc., 2nd Int. Conference on Design of Silos for Strength and Flow, Stratford-upon-Avon, U.K., 1983, pp. 132-144.

[5] *Rotter, J.M.*: The analysis of steel bins subject to eccentric discharge; Proc., 2nd Int. Conference on Bulk Materials Storage, Handling and Transportation, Wollongong, Australia, 1986, pp. 264-271.

[6] *Blight, G.E.* and *Midgley, D.*: Pressure measured in a 20 m diameter coal load-out bin; J. of Powder and Bulk Solids Technology, Vol. 5, (1981) No. 2, pp. 21-31.

[7] *Hartlen, J., Nielsen, J., Ljunggren, L., Martensson, G.* and *Wigram, S.*: The wall pressure in large grain silos; Swedish Council for Building Research, Document D2 : 1984, 66 pp.

[8] *Blight, G.E.* and *Bentel, G.M.*: Measurements on full size silos. Part 2: Pressures; bulk solids handling, Vol. 8 (1988) No. 3, pp. 343-346.

[9] *Blight, G.E.*: A comparison of design and measured lateral pressures in a large coal load-out silo; Int. J. of Bulk Solids Storage in Silos, Vol. 2 (1986) No. 2, pp. 1-8.

[10] *Blight, G.E.* and *Ofer, Z.*: Laboratory determination of K_0 and comparison with prototype silo observations; Proc., 4th Australian-New Zealand Conference on Geomechanics, Perth, Australia, 1984, pp. 83-87.

[11] *Blight, G.E.*: Design loading for grain silos - intention and reality; Paper 88-4024, American Society of Agricultural Engineers, International Summer Meeting, 1988, Rapid City, USA, 12 pp.

[12] *Trahair, N.S., Abel, A., Ansourian, P., Irvine, H.M.* and *Rotter, J.M.*: Structural design of steel bins for bulk solids; Australian Institute of Steel Construction, Sydney, 1983, 30 pp.

Silos, Hoppers, Bins & Bunkers for Storing Bulk Materials

The Best of "bulk solids handling" A/86

1986 (reprinted 1989), 66 papers, 480 pages, ISBN 0-87849-060-4, sFr. 90.00

Trans Tech Publications

Segantinistr. 216 CH-8049 Zürich Switzerland

Fax: +41 1 342 05 29

7.4 MEASUREMENTS OF STRAIN IN THE REINFORCING OF REINFORCED CONCRETE SILOS.

CONTRIBUTION TO LEARNING

The first two papers of this section (7.4.1 and 7.4.2) describe the use of measured reinforcement strains in a reinforced concrete silo to estimate pressures resulting from rapid filling with a fine powder. As far as is known, this is the first and only case in which this form of loading has been investigated in a full size silo.

A major problem with this type of measurement is uncertainty as to whether the reinforcing is carrying the full hoop tension, or if the concrete is carrying part of the hoop load. At the time of writing, the author was convinced that the silo walls were fully cracked and that the hoop reinforcing was carrying the full hoop tension.

The third paper (7.4.3) describes an investigation into the behaviour of a 12 year old reinforced concrete coal silo subjected to a design overload. To the author's surprise, the silo behaved as if the wall was uncracked except for a small section that appeared to be partly cracked. This was despite the fact that the silo had been in service continuously for 12 years and had been overloaded continuously for a period of months.

This result has thrown some doubt on the results reported in 7.4.1. Plans are now being made to return to the cement raw meal silo to check on its behaviour 13 years after it was filled for the first time.

7.4 MEASUREMENTS OF STRAIN IN THE REINFORCING OF REINFORCED CONCRETE SILOS.

7.4.1 Blight, G.E., Schaffner, R.H. and Gilbert, B. (1982). Strains in a reinforced concrete silo during rapid filling with a fine powder. Journal of Powder and Bulk Solids Technology, vol 6, No 2, pp 17-27.

The designer of the silo was Mr Schaffner while Mr Gilbert represents the contractor. I estimate my contribution to the paper at 80%.

7.4.2 Schaffner, R.H. and Blight, G.E. (1983). Comparison of design assumptions and measured performance for cement works silos. Proceedings, 2nd International Conference on Design of Silos for Strength and Flow, Stratford-upon-Avon, UK, pp 207-216.

I was commissioned to write this paper by Mr Schaffner, on behalf of his firm. My contribution to the paper was thus 100%.

7.4.3 Blight, G.E. and Dreyer, H.N. (1989). Behaviour of a reinforced concrete coal silo under a design overload. Bulk Solids Handling, vol 9, No 1, pp 21-25.

This study was commissioned for a mining house. Mr Dreyer was head office engineer for the mine. I planned and undertook the investigation and drafted the paper. I estimate my contribution to the paper at 90%.

Journal of Powder & Bulk Solids Technology, **6** (1982) 2; 17-27

STRAINS IN A REINFORCED CONCRETE SILO DURING RAPID FILLING WITH A FINE POWDER

G. E. Blight,
Department of Civil Engineering,
University of the Witwatersrand,
1 Jan Smuts Avenue,
Johannesburg 2001,
South Africa,

R. H. Schaffner,
Watermeyer, Legge Piesold & Uhlmann,
Box 31176, Braamfontein,
South Africa

and *B. Gilbert,*
Techtonics (Pty) Ltd.,
P.O. Box 75102,
Garden View,
2047 Johannesburg,
South Africa.

INTRODUCTION

RAPID FILLING OF SILOS WITH FINE POWDERS

When a fine powder is rapidly loaded into a silo it entrains a large proportion of air. The pressure exerted on the silo walls at any depth is made up of two components: that exerted by pressure in the entrained air and that exerted by the solid particles. Thus the total horizontal pressure σ_h can be written as

$$\sigma_h = p_a + \sigma'_h \qquad (1)$$

where p_a is the pressure in the air (or the pore air pressure) and σ'_h is the intergranular pressure exerted by the solids. The relative magnitude of p_a will vary with the speed of filling. With extremely rapid rates of filling p_a may be large enough to support most of the weight of the solid particles, in which case σ'_h will be small and the powder will be partly fluidized. As time progresses after the depositon of a particular element of fill, the entrained air will escape, p_a will diminish and σ'_h will increase. Simultaneously, as the entrained air escapes, the fill will compress, settle relative to the walls of the silo and develop increasing frictional stresses against the walls. This, in turn, will have the effect of reducing both vertical and horizontal intergranular stresses in the silo.

Martens[1] carried out research into the effects of rapid filling using an instrumented model silo of 0.8 m diameter. The materials he used consisted of powdered limestone, cement and wheat flour. He came to the semi-empirical conclusion that the profile of σ_h in the zone affected by the speed of filling could be represented by two straight-line relationships:

$$\sigma_h = 0.8\,\gamma\,Z \qquad (2a)$$

with a vertical cutoff at depth Z given by

$$Z = (v - v_o)\,t \qquad (2b)$$

In the above γ is the density of the powder ir its loosest state; v is the filling speed or rate of rise of the fill surface in the silo; and v_0 is the limiting filling speed.

If v and v_0 are expressed in mh^{-1}, t is taken as 1h. **Table 1** summarizes the values of γ and v_0 established by Martens for his three materials.

Table 1
Properties of materials tested by Martens[1]

Material	Minimum density γ		Limiting filling speed v_0	
	(kNm^{-3})	($lbft^{-3}$)	(mh^{-1})	(fth^{-1})
Powdered limestone	13.5	84	1.40	4.6
Cement powder	15.5	97	2.60	8.5
Wheat flour	7.0	44	4.80	15.7

Some of the detailed results of Marten's tests were published by Pieper[2] and are reproduced as **Figure 1.** Note in particular that, at large times, the horizontal stresses in the silo became less than those predicted by the equations of DIN 1055 (1964)* and that the pressure was actually found to decrease with increasing depth over some portions of the silo. It should also be noted (see **Figure 1**) that Martens does not appear to have investigated pressures *during* rapid filling, but only the condition at the end of rapid filling and subsequent pressure changes as the fill consolidated.

Marten's work was subsequently extended by Nothdurft[3] who refined Marten's result to

$$\sigma_{ho} = (\min\gamma)v\,t_a\,K_f\sqrt{R}\;3.6 \text{ (in kPa)} \qquad (3)$$

In this expression:
σ_{ho} is the maximum horizontal pressure
$(\min\gamma)$ is the minimum density of the powder
v is the rate of rise of the fill surface
t_a is a characteristic settling or consolidation time for the powder.
R is the hydraulic radius of the silo, and
K_f is the ratio of horizontal to vertical stresses in the silo during filling.

Values for these variables recommended by Pieper, Martens and Nothdurft[3] are given in **Table 2.**

*Although the DIN curves were calculated for a higher density than that which actually obtained.

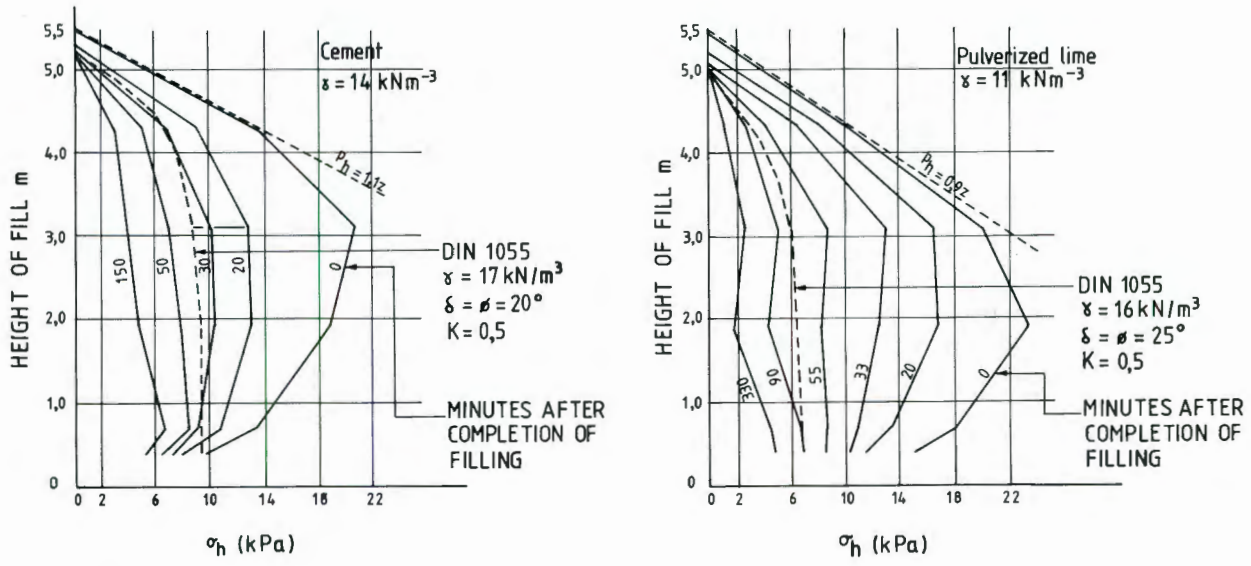

Figure 1.
Pieper's and Martens' observations on pressures after rapid filling of a model silo.

Table 2
Values of (minγ) t_a and K_f according to Pieper, Martens and Nothdurft[3]

Material	(minγ) (kN/m³)	(lb/ft³)	t_a (h)	K_f
Powdered limestone	11	62	0.24	0.55
Cement powder	13	81	0.19	0.53
Wheat flour	6	37	0.14	0.31

Recently, Martens[4] has indicated his opinion that Equation(2a) could be refined to

$$\sigma_h = 0.6\,\gamma z \qquad (2c)$$

The only other work in this field appears to be that of Murfitt and Bransby[5,6] who studied the dissipation of pore air pressures after filling small (1.83m diameter by 4.24m high and 2.44m diameter by 4.21 m high) hoppers with a fine chalk powder. The filling speeds were 23mh^{-1} for the small hopper and 12mh^{-1} for the larger hopper. Murfitt and Bransby recorded virtually full hydrostatic pressures in their bins at the end of filling, i.e.

$$\sigma_h = \gamma z \qquad (4)$$

and recommended that silos filled rapidly with fine powders be designed for full hydrostatic pressures. Murfitt and Bransby's work post-dates that of Nothdurft by some seven years. Hence there is still considerable confusion as to the true state of stress in rapidly filled silos.

No measurements on full-scale silos subjected to rapid filling appear to have been reported. In particular, there appear to have been no measurements of pressures *during* filling either on model or full-scale silos. The present paper will report on strains measured in the walls of a full size silo (15 m diameter (49.2ft) by 43 m high (141ft)). The silo forms part of a blending and storage complex for cement raw meal at the Slurry works of the Pretoria Portland Cement Company. **Figure 2** shows a vertical section through one of the pair of blending and storage silos. The blending silos form the upper one third of the height of the structure. When both blending silos are full, their contents can be discharged simultaneously into one of the two storage silos at filling rates of up to 10mh^{-1}.

The objective of the observations on the Slurry silos has been:

(a) to gather information on pressures generated during rapid filling at various rates, via measurements of strain in the reinforcing steel;
(b) to resolve the present confusion regarding the relationship between rate of filling and the envelope of maximum pressure at the end of filling;
(c) to investigate the possible existence of transitory overpressures at the start of emptying the silo (e.g. Walker[7] and Johanson[8]).

With reference to (c), there are theoretical grounds for believing that an increase in pressure occurs when the contents of a silo become constricted as they flow towards the outlet. The existence of these "switch pressures" as the flow pattern switches from one of vertical parallel flow to radial converging flow has been a point of argument for many years. Switch pressures have been measured in model silos (e.g. Walker[7]) and their existence has been used to explain structural failures that have occurred in hoppers, bins and silos (e.g. Wright[9]). However, these overpressures do not appear to have been *measured* in a full-scale silo.

THE INSTRUMENTATION AT SLURRY

Ideally, the pressures developed in a silo should be measured by means of calibrated pressure cells [e.g. 10 and 11]. However, at Slurry it was decided instead to measure the strains in the hoop reinforcing of the silo. This method has the advantage of providing a direct check on the design strains (or stresses) in the reinforcing. However, the approach suffers from the considerable disadvantage that in a composite structure such as a

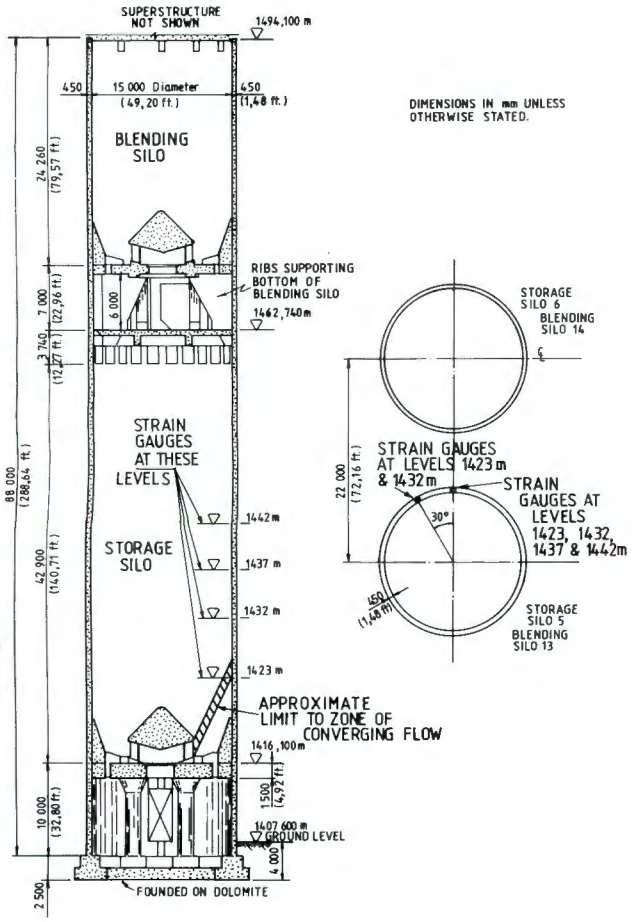

Figure 2.
Sections through silos and positions of strains gauges.

reinforced concrete wall in hoop tension, there are severe difficulties in interpreting the measured strains in terms of pressure. The layout of the instrumentation is shown in **Figure 2.**

Electric resistance strain (ERS) gauges were installed on the hoop reinforcing of the silo at levels 1423m (2 positions) 1432m, 1437m and 1442m. At each instrumentation point at least two reinforcing hoops were exposed in a pocket cast into the concrete and measuring 450mm square by 100mm deep. Each exposed bar was instrumented with two pairs of gauges; each gauge pair consisting of a longitudinal and a transverse gauge. In this way each gauge pair is compensated for the effects of temperature on the resistance of the gauges and a slight magnification of the recorded strain is obtained, the gauge readings representing $(1 + \nu)\varepsilon$ where ε is the longitudinal strain in the bar and ν is Poisson's ratio for steel. The gauges were waterproofed and protected from mechanical damage by a thick layer of polysulphide rubber.

Two sets of four thermocouples each were installed in the silo walls at level 1432m. A 20mm diameter hole was drilled through the thickness of the wall and the thermocouples were inserted, taped to a wooden dowel stick to maintain them in their correct positions. A disc of stiff rubber fastened to the end of the dowel was used to close off the inner end of the drilled hole, and the hole was then filled with an epoxy-sand grout. Thermocouples were also attached to the exposed hoop reinforcing at levels 1423m, 1432m and 1437m. Unfortunately, at the time the thermocouples were installed, level 1442m was inaccessible. It would have been desirable to have installed strain gauges at a level above 1442m, but higher levels were inaccessible.

The level of fill in the storage silo was measured by sounding from an opening in the roof slab at level 1462,7m using a steel measuring tape weighted with a 100mm square steel plate at its zero end. Similar soundings were taken as a check from openings in the roof slabs of the east and west blending silos at level 1494m.

As far as the measurement of switch pressures is concerned, the approximate limits of the zone of radial flow are indicated on **Figure 2.** Level 1423m just falls within these limits. In retrospect, it is unfortunate that strain gauges were not also installed at a level slightly below 1423m, say at level 1420m.

THE INTERPRETATION OF STRAINS IN REINFORCING STEEL

Reinforced concrete sections subjected to axial or hoop tension are usually designed on the assumption that the concrete will crack under load and the steel will carry all the load. Actual load-sharing between steel and concrete is illustrated by the data shown in **Figure 3.** A 150mm (6 inch) square concrete prism 800mm (31,5 inches) long, reinforced with a single axial 12mm (½ inch) diameter reinforcing rod was subject to axial tension applied via the ends of the reinforcing rod. The steel rod and the concrete prism were instrumented with electric resistance strain gauges at 100mm intervals.

At a load of 15kN, strains in both steel and concrete were identical over the central 500mm length of specimen, which was clearly acting as a truly composite steel-concrete section. At the ends of the specimen, concrete strains fell to zero, while steel strains increased. In these zones, about 100mm long at one end of the specimen and 200mm long at the other, bond between steel and concrete was in the process of distributing the load between the two materials.

When the load was increased to 30kN, a similar pattern of strains obtained, except that the length of the load transference zones increased by about 100mm.

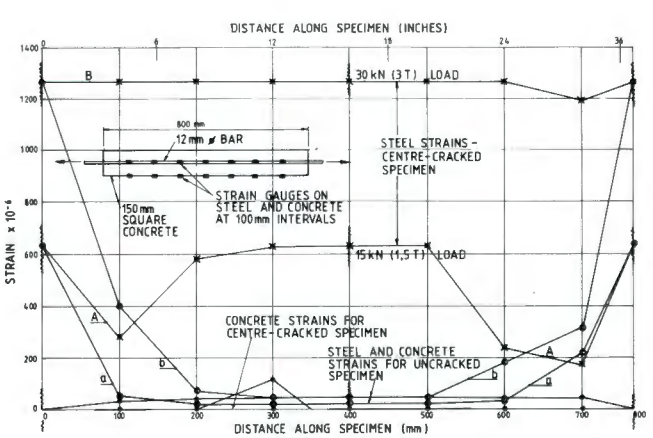

Figure 3.
Effect of cracking and crack spacing on strains in concrete and steel.

The concrete was then deliberately cracked at a distance of 400mm from one end and the measurements were repeated. **Figure 3** shows that at this stage, the concrete virtually ceased to carry load and almost the entire load was carried by the steel.

In the initial stage, while the reinforced concrete was acting as a composite section, strains measured in the steel could not be used to give an indication of the total load carried by the section, unless the elastic modulus of the concrete was known. In the final stage, steel strains could be used to indicate the load in the section. At intermediate stages (for example the strains measured in the cracked specimen at a distance of 700mm along the specimen) the load in the member was indeterminate from strains measured in the steel. The question that now arises is: "Can strains measured on reinforcing bars in a full-scale structure be assumed to represent the determinate state of a fully cracked section?" This question will be answered by reference to a case history:

A battery of eight free-standing reinforced concrete asbestos ore storage silos have internal diameters of 7m, storage depths of 23m and wall thicknesses of 250mm. They are emptied through diametral slots by means of a plough that runs the length of the row of silos. Early in their working life, the silos suffered severe vertical cracking which ultimately extended to about 15m above the base of the silos. In order to check stresses in the reinforcing steel of the silos, the hoop steel was exposed in six places around the perimeter of one of the silos and the bars were instrumented with electric resistance strain gauges in the manner described previously. Strains were then measured as the silo was filled and emptied. The filling rate of 1.33m/h (4.4 ft/h) ensured that no pore air pressures could have developed in the relatively coarse ore stored in the silo.

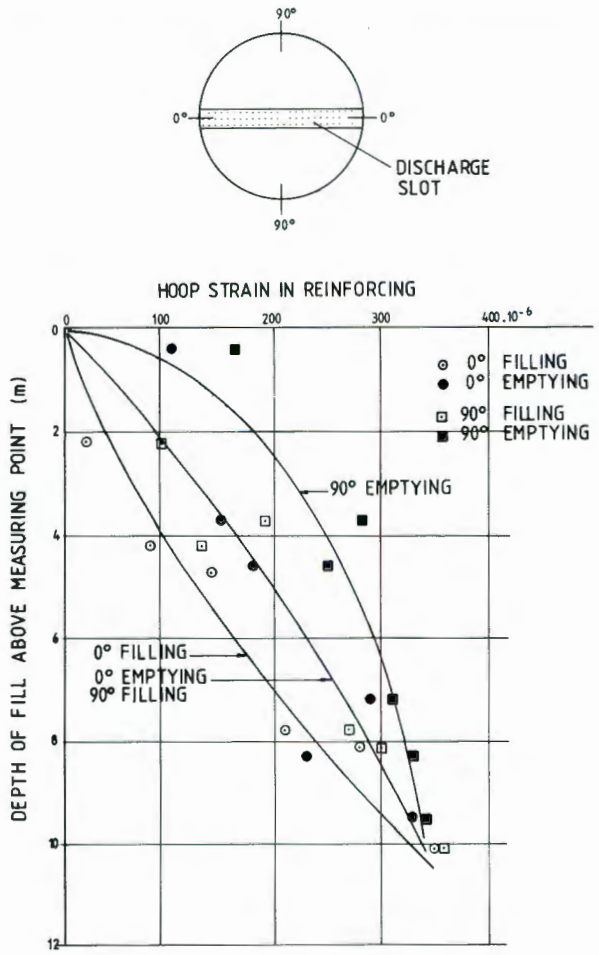

Figure 4.
Strains measured in reinforcing of cracked 7m dia asbestos ore storage silo.

Some of the results of the strain measurements are illustrated in **Figure 4.** Although the results are somewhat scattered, it is evident that

a) strains for emptying were slightly larger than those for filling; and
b) strains measured in line with the emptying slot were slightly less than those measured at right angles to the slot. This is consistent with the theory of eccentric-emptying suggested by Jenike[12].

Strains in the silo at depths of 5m and 10m at 90° to the direction of the slot were analysed by means of the Janssen equation

$$\sigma_h = \sigma_{(max)} (1 - e^{-\{K\gamma z/\sigma_{h(max)}\}}) \quad (5a)$$

$$\sigma_h(max) = \frac{\gamma D}{4 \tan \delta} \quad (5b)$$

In these equations K is the ratio of horizontal to vertical stresses in the silo fill, D is the internal diameter of the silo; and δ is the angle of friction of the fill on the silo walls.

δ for asbestos ore on concrete was measured at 31°, while γ was measured at 16kN/m³ (100lb/ft³).

Calculating σ_h on the assumption that the hoop reinforcing carried all the hoop load and solving Equation (5a) for K gave the values of K summarized in **Table 3:**

Table 3
Values of $K = \sigma_h/\sigma_v$ calculated from measured strains in asbestos ore silo

Condition	Depth	K	K_0	K_A
Filling	5m	0.27	0.32	0.19
	10m	0.26		
Emptying	5m	0.36		
	10m	0.26		
Average		0.29		

During filling, K should lie between the coefficient of lateral pressure at rest, K_o, and the active pressure coefficient K_A for the fill (see e.g. Blight and Midgley[10]). K_o is given approximately by

$$K_o = 1 - \sin \phi \quad (6a)$$

while K_A is given by $K_A = (1 - \sin \phi)/(1 + \sin \phi)$ (6b)

in which ϕ, the angle of shearing resistance of the fill was 43°. The agreement between the value of K derived from the measured strains and the values given by Equations (6a) and (6b) is close enough to conclude that the hoop reinforcement must have been carrying the entire hoop force in the cracked reinforced concrete walls of the silo.

OBSERVATIONS AT SLURRY

The programme of observations at Slurry was designed to study the effect of different filling rates on strains in the silo walls and hence to investigate the validity of existing information on pressures generated during rapid filling with fine powders. **Table 4** summarizes the dates on which observations were made and the rates of filling used on those occasions:

Table 4
Dates and rates of filling for which strains have been measured at slurry

Date	Rate of filling (mh^{-1})	Rate of filling (fth^{-1})	Remarks
August 1976	5.3	14.4	First filling. Rate varied from $7.3mh^{-1}$ to $4.3mh^{-1}$
August 1977	7.7	25.3	1 year of service
November 1977	4.2	13.8	
January 1978	10.1	33.1	
October 1980	7.4	24.3	Lapse of 2.7 years

Figure 5 summarizes the strains measured on the Slurry silo in August, 1976, when the silo was filled for the first time. **Figures 6a and 6b** show similar data recorded a year later (August 1977 and January 1978).

Two things will be noted on comparing the three sets of results:

(i) The strains on first filling of the silo were considerably less than those recorded at a similar filling rate a year later. For example, the maximum strain recorded at level 1432m changed from 55×10^{-6} to 345×10^{-6}. It appears that a year of service had caused the concrete in the silo walls to crack and that the hoop steel was probably now carrying all, or certainly most of the hoop tension.

(ii) Quite large strains occurred even before the fill had reached a particular level. The temperature of the raw meal varies from 55°C to 65°C whereas ambient air temperatures vary from 0°C to 30°C, depending on the time of year and time of day. Hence these strains can be ascribed to the temperature gradient through the silo wall, although they may also include a component due to vertical bending in the walls.

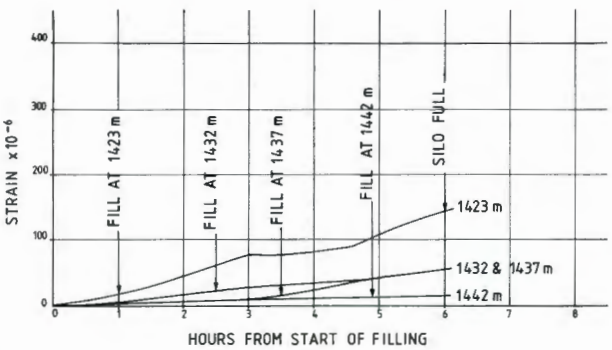

Figure 5.
Strains measured on first filling of silo — August 1976
Filling rates { 0 to 2½ Hours : 7.3mh⁻¹ (23.9fth⁻¹)
3 to 6 hours : 4.3mh⁻¹ (14.1fth⁻¹)

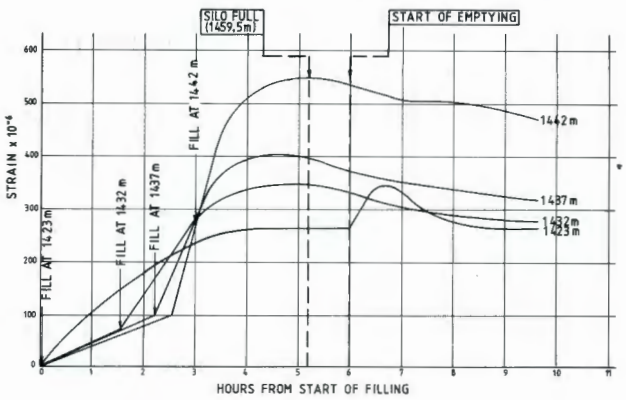

Figure 6a.
Strains measured in August 1977
Filling rate : 7.7mh⁻¹ (25.3fth⁻¹)

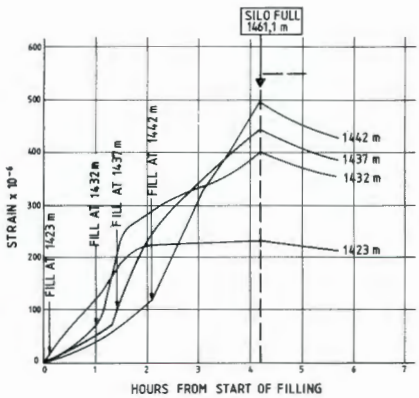

Figure 6b.
Strains measured in January 1978
Filling rate : 10.1mh⁻¹ (33.1fth⁻¹)

Typical temperature data for the walls at Slurry are shown in **Figures 7a and 7b:**

Figure 7a shows the variation of temperature with time at the inner surface of the silo, 50mm in from the inner surface and at the outer surface as the silo was filled at a rate of $7.36mh^{-1}$ ($24.3fth^{-1}$). It will be noted that the temperature of the inside surface reaches a maximum as the raw meal covers the thermocouple and that thereafter cooling occurs progressively with time. The temperature of other points within the thickness of the wall rises to a maximum, after a considerable time lag, and then also slowly falls as a result of cooling.

Figure 7b shows the temperature profiles through the wall at three different times, and also shows that two separately measured profiles coincide almost exactly.

The strains induced by a temperature gradient in a reinforced concrete wall are difficult to evaluate, especially when there is no way of deducing the position of the neutral axis. Hence it has been assumed that the temperature-induced strains in the outer reinforcement of the wall are proportional to the temperature difference between the inner and outer surfaces. The initial temperature-induced strain is given by the strain that occurs in the steel before the fill surface reaches the level

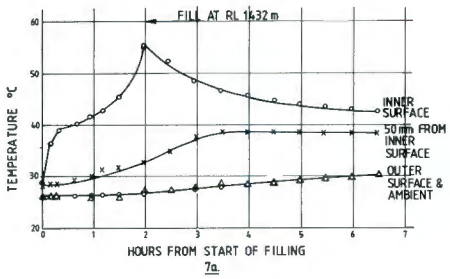

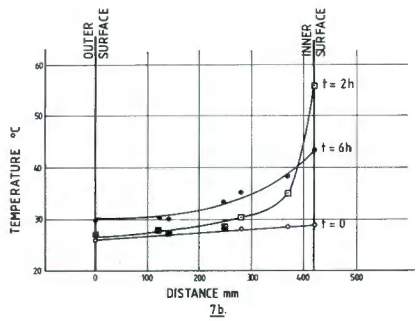

Figures 7a & 7b.
Results of temperature measurements in silo wall

at which the strains are being measured. Once the surface of the fill has passed the level of measurement, the temperature-induced strain must fall as the temperature gradient reduces.

The principle adopted for correcting the measured strains for temperature is illustrated by **Figure 8:**

aba represents the variation of total, i.e. (temperature-induced + pressure-induced) strain.

ab represents the temperature-induced strain which reaches a maximum at b.

bb represents the reducing value of the temperature-induced strain as deduced from cooling curves such as those shown in **Figure 7a.**

cc represents the corrected curve of pressure-induced strain.

Figure 6a, which is typical of the strain measured from August 1977 onwards, shows that strains actually start reducing slightly before the silo is completely full. This presumably results from the dissipation of pore air pressures from the fill.

There was a significant increase in the strain recorded at level 1423m once emptying of the silo was started. This may represent the effects of convergent flow of the silo fill, but equally may represent the effects of compressed air introduced at the base of the silo to facilitate emptying. A similar pattern of strain increases just after the start of emptying was also observed on other occasions.

During rapid filling, vibration of the silo can be felt when standing at level 1462.7m. To see if rapid filling results in dynamic components of strain, an ultra-violet light (UV) recorder was linked to the strain gauges at each level during filling at a rate of 10.1mh^{-1}. Typical recorder traces are shown in **Figure 9** and show that dynamic strains, if present at all, are less than 10x10^{-6} in magnitude.

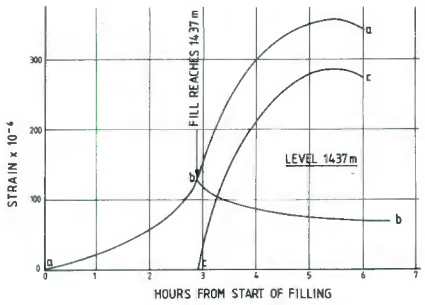

Figure 8.
Correcting observed strains for temperature

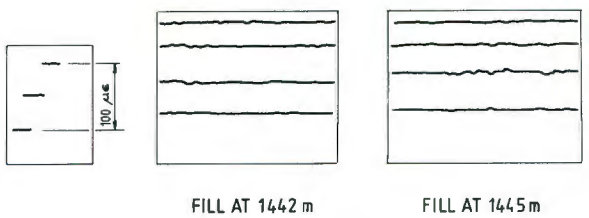

Figure 9.
Attempt to record dynamic strains during filling at 10.1mh^{-1} (33.1fth^{-1}) UV traces show largest recorded dynamic strains at level 1442.

ENVELOPES OF MAXIMUM STRAIN AND CORRESPONDING PRESSURE ENVELOPES

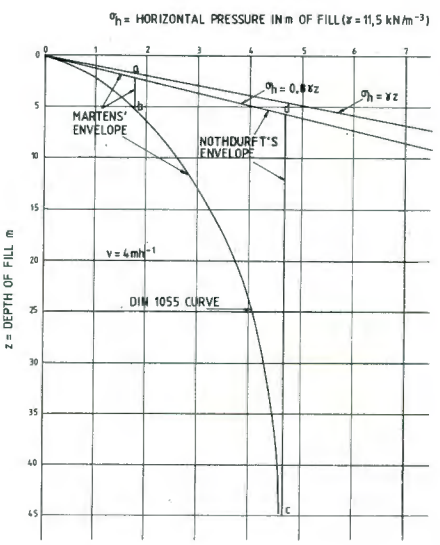

Figure 10.
Comparison of Martens' and Nothdurft's pressure envelopes for a filling speed of 4mh^{-1} (13.1fth^{-1}).

Figure 10 shows the Equations (2) and (3) applied to the Slurry silo for a filling speed of 4mh^{-1} (13.1fth^{-1}) assuming that cement raw meal has properties intermediate between those of powdered limestone and cement, viz:

(minγ) or γ	=	11.5 kN/m^3	(72lb/ft^3)
v_o	=	2.0 mh^{-1}	(6.6 fth^{-1})
t_a	=	0.22h	
K_f	=	0.52	
δ	=	angle of wall friction = 38°*	

In this diagram Marten's pressure envelope for a filling speed of 4mh^{-1} is given by o a b c while that according to Nothdurft is o a d c.

Figure 11a shows the envelope of maximum pressure-induced strain recorded when the silo was first filled. In interpreting this envelope it should be remembered that the drying shrinkage of concrete, if restrained by the presence of reinforcing steel is itself sufficient to crack the material. (A typical range of shrinkage strains would be 300x10^{-6} to 500x10^{-6} while the failure strain of concrete in axial tension is between 100×10^{-6} and 200x10^{-6} (Neville[13]). Hence when the silo was first filled, it was probably already in a partly cracked state.

The validity of this statement can be demonstrated as follows: Suppose that at level 1423m the horizontal pressure is assumed to be given by the DIN 1055 curve shown in **Figure 10.** The elastic modulus of the concrete E_c is estimated to be 24GPa (3.5x10^{-6}lb/in^2) and the transformed thickness t of the uncracked wall, based on this estimate, is 490mm.

Treating the silo as thin-walled cylinder, the hoop strain ε_h can be calculated from:

$$\varepsilon_h = \sigma_h D/2tE_c \qquad (7)$$

to be 30×10^{-6}.

It will be noted that the actual strain at level 1423m was 140x10^{-6} which is far in excess of this. Hence it appears that when the silo was first filled, the concrete was in a partly cracked state and pressures were not determinate from strains.

The alternative assumption that the silo walls were uncracked would require lateral pressures of 4½ times the DIN 1055 values. Pressures as high as this can only be rationally explained by assuming a value of δ of very much less than the measured value for the raw meal of 38°. The requisite value of δ can be calculated from Equation (5b) to be 12°. In the absence of better information, the value of δ that had actually been used in the design of the silo was 20°.

Figure 11b summarizes the results of all the maximum strains measured in the silo walls since August 1977. In addition to the experimental results, the diagram shows the maximum pressure line of 0.6γZ suggested by Martens[4] as well as the vertical cut-off line given by Equation (3) for v = 4.2mh^{-1}. The theoretical curves in **Figure 11b** have been calculated by simultaneous solution of the differential equations for the Janssen pressure equation and consolidation of the raw meal as its entrained air escapes. This analysis is given in **Appendix II.**

* See **Appendix I**

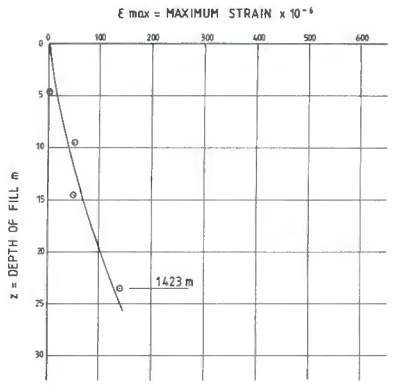

Figure 11a.
Profile of maximum strain measured in silo on first filling.

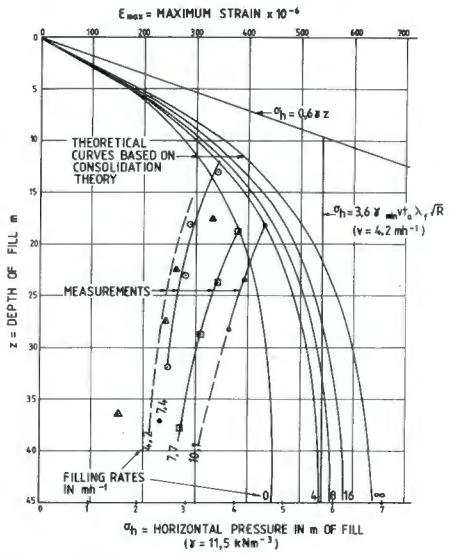

Figure 11b.
Summary of measured and theoretical dept — pressure relationships at the end of filling

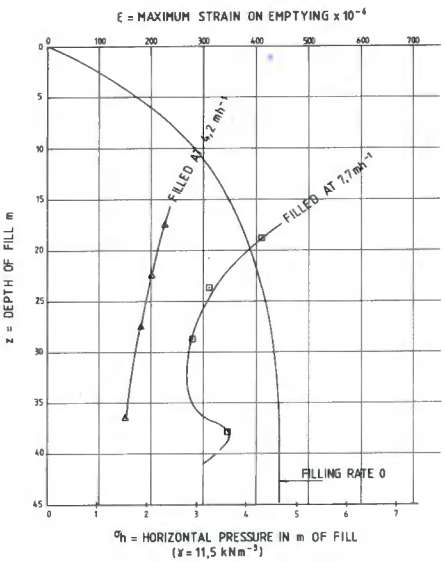

Figure 11c.
Pressure — depth relationships at maximum strain after start of emptying

The effects of a variable filling speed is shown very clearly by these results. It will also be seen that maximum strains

(a) decrease with depth; and
(b) are generally less even than the strains predicted theoretically for zero filling speed.

Both of these features are evident in Marten's results shown in **Figure 1.**

It was first thought that the pattern of maximum strains that reduce with depth may have resulted from uneven cracking of the silo. However, the repeated application of strains well in excess of 200×10^{-6} over a period of more than four years must have thoroughly cracked the concrete. The latest measurements (October 1980) are actually less than corresponding measurements made 3½ years earlier. Hence it appears reasonable to assume that all the measurements shown in **Figure 11b** correspond to a determinate state in which strains measured on the reinforcing steel may be used to evaluate silo pressures.

This, however, does not explain either the reduction of strain with depth or the low values of the pressures. It will be noted from **Figure 6** that strains at all levels reduce with time. Also, the level of the surface of the fill subsides as the entrained air escapes. Hence the entire mass of fill shrinks continuously as the silo is filled. It is probably this shrinkage that results in the form and low values of the observed pressure envelopes.

Figure 11c shows two pressure profiles drawn for the maximum strains that occurred after the start of emptying. Comparing these profiles with the corresponding ones for the end of filling, it will be seen that in both cases strains in the upper part of the profile have declined, while strains at level 1423m have increased, probably as a combined result of the effects of convergent flow and aeration.

CONCLUSIONS

The measurements made at Slurry are apparently the only observations available of the effects of rate of filling on strains in a full-scale silo.

It has been demonstrated that strains measured on the reinforcing steel of a reinforced concrete silo can be interpreted in terms of internal horizontal pressures. It also appears that the strain measurements made at Slurry from August 1977 onwards can be thus interpreted.

Pressures deduced in this way are generally less than those predicted on the basis of Janssen's theory modified for the effects of entrapped air pressure. However, agreement between the *maximum* deduced pressures and the theoretical predictions are quite close.

It will be seen from **Figure 11b** that maximum pressures can be predicted reasonably accurately by the procedure of simultaneous solution of the differential equations for the Janssen pressure distribution and the consolidation of the silo fill. However, this procedure is tedious and for design purposes, the equation of Nothdurft probably gives a sufficiently accurate and conservative envelope of maximum pressures.

ACKNOWLEDGEMENTS

The authors thank the Pretoria Portland Cement Company Limited and Techtonics (Pty) Ltd., for permission to publish the data contained in this paper.

APPENDIX I — PHYSICAL PROPERTIES OF CEMENT RAW MEAL

The raw meal was sampled on two occasions, August 1977 and October, 1980. Physical properties were determined for both samples.

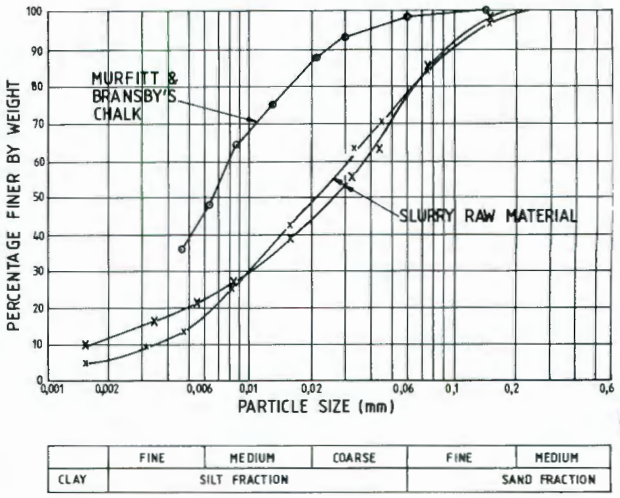

Figure 12.
Particle size distribution of cement raw meal and chalk powder.

The particle size distribution of the meal is shown in **Figure 12.** Although there was some variation between the two samples, the grading has, as would be expected, remained essentially constant.

Figure 12 also shows the grading of the chalk used by Murfitt and Bransby[5,6] which is very much finer than the cement raw meal and would therefore be expected to retain entrapped air for longer.

Figure 13 illustrates the frictional characteristics of the raw meal. **Figure 13a** shows a typical relationship between the major principal strain and the principal stress ratio $(\sigma_1 - \sigma_3)/\sigma_3$ measured in a drained triaxial shear test, while **Figure 13b** shows the results of drained triaxial shear tests (black dots) and wall friction tests (white dots). The wall friction tests were conducted in a shear box in which the lower half of the specimen was replaced by a concrete block.

These results show:

(a) that a considerable amount of strain is required to mobilize the shear strength of the raw meal; and
(b) that the angle of shearing resistance ϕ^1 is sensibly equal to the angle of wall friction δ for raw meal on concrete.

Figure 13c shows the influence of relative movement between the fill and the wall on the angle of wall friction. When the raw meal is moving relative to the concrete, the angle of wall friction rises to about 2° above the static value. These results are similar to those reported for coal[10], but in the case of coal the difference between static and moving values was 11°.

The consolidation characteristics of the raw meal are illustrated by **Figure 14. Figure 14a** shows a typical time-consolidation curve for triaxial consolidation of the raw meal, while **Figure 14b** shows a series of void ratio — consolidation stress curves for the meal starting from four different initial void ratios. It is evident from the parallelism of these curves that the compressibility of the meal is only slightly affected by the initial void ratio.

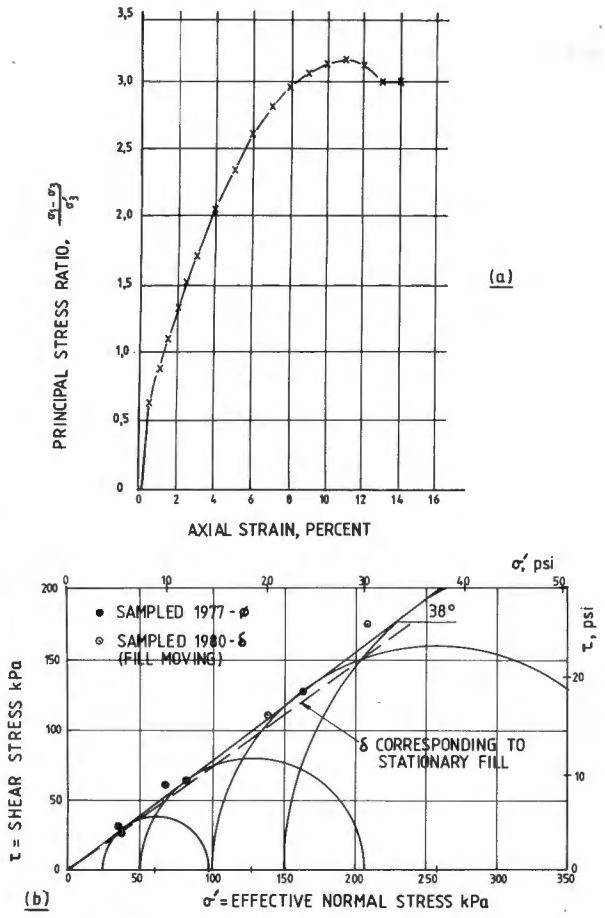

Figure 13.
Shear strength characteristics of raw meal
(a) typical stress ratio — axial strain relationship
(b) Mohr strength envelope.

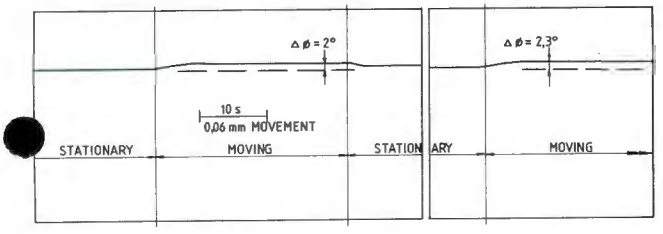

Figure 13c.
Effect of movement between raw meal and wall on angle of wall friction

Figure 15 shows the relationship between horizontal and vertical principal stresses during consolidation of the cement raw meal with zero lateral yield. The ratio of the two stresses represents K_o, the coefficient of lateral pressure at rest. At low stresses K_o is about 0.65, declining as the stress increases to a value of 0.5. The approximate value of $K_o = 1 \sin\phi$ is about 0.4. In the stress range of interest for the Slurry silo, K_o would have a value of about 10 kPa and K_o would therefore be about 0.65. However, a separate set of measurements of K_o using a slightly different technique gave a value in this stress range of 0.38. Hence calculated pressures were based on an average value of 0.52.

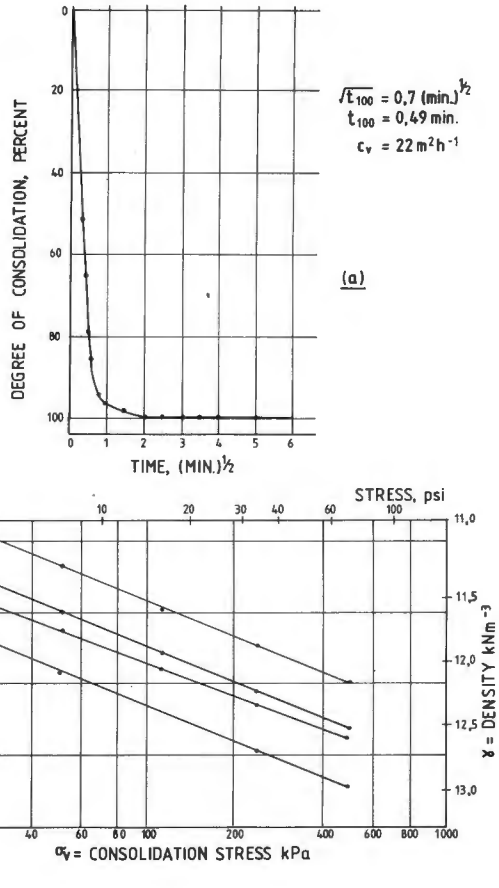

Figure 14.
Consolidation characteristics of raw meal:
(a) typical consolidation — time curve
(b) void ratio — consolidation stress relationships

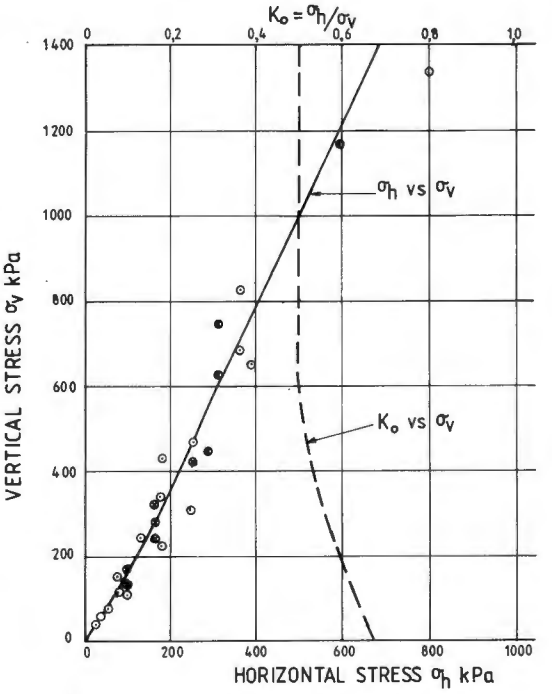

Figure 15.
Relationship between horizontal and vertical principal stresses for consolidation of cement raw meal with zero lateral yield.

APPENDIX II — CALCULATION OF THE EFFECTS OF RATE OF FILLING ON SILO PRESSURES

Gibson[14] showed that the progress of consolidation in a water saturated clay layer increasing in thickness with time could be represented by the differential equation

$$\frac{\partial pw}{\partial t} = c_v \frac{\partial^2 pw}{\partial x^2} + \gamma B_w \frac{dh}{dt} \qquad (8a)$$

In which p_w is the water pressure at a point distant x above the impermeable base of the clay at time t, h is the height of the surface of the clay above the base; c_v is a coefficient, the coefficient of consolidation, that depends on the permeability and compressibility of the clay; and $B_w = (1/\gamma)$. (dpw/dh) is the ratio of the pore pressure to the corresponding increment of overburden stress under undrained conditions.

Blight[15] showed experimentally that the same basic form of differential equation could be used to describe the unsteady flow of air in a dry powder. For the flow of air the equation would be re-written as

$$\frac{\partial pa}{\partial t} = c_v \frac{\partial^2 pa}{\partial x^2} + \gamma B_a \frac{dh}{dt} \qquad (8b)$$

B_a can be calculated from the compressibility characteristics of the powder. Using Boyle's law it can be shown that

$$\frac{\Delta p_a}{p_a} = \frac{-\Delta e}{e + \Delta e} \qquad (9)$$

In which Δp_a is the increment in p_a that results from a decrease Δe in the void ratio e* of the powder. The increment of total stress $\Delta\sigma_v$ required to reduce the void ratio from e to (e-Δe) can be found from the measured relationship between e and σ_v (see **Figure 14b**).

Hence

$$B_a = - \frac{p_a}{\Delta\sigma_v} \cdot \frac{\Delta e}{e + \Delta e} \qquad (10)$$

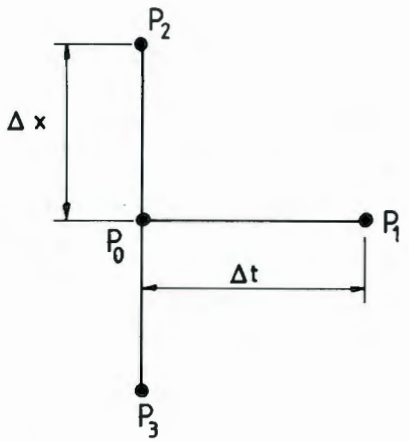

Figure 16.
Finite difference grid for solving Equations (8a) and (11).

*e is defined as the ratio of the volume of voids contained by the powder to the volume of solids.

For the range of stresses that are of interest (p_a from 100kPa to 200kPa, σ_v up to 1000kPa) B_a for the Slurry raw meal is about 0.1. γ can be found from the σ_v versus e relationship for the raw meal as shown in **Figure 14b.** In the calculations described below a value of γ of 12kNm^{-3} was used. c_v can be found from the time-compression relationships for the raw meal, a typical example of which is shown in **Figure 14a.** The average c_v for the raw meal was 20m^{2}h^{-1}. The reader is referred to a standard textbook on soil mechanics (e.g. Lambe and Whitman[16]) for further details of these tests.

Equation (8b) must be solved simultaneously with the differential equation for the Janssen analysis, viz.

$$\frac{d\sigma_v}{dh} = \gamma - \frac{4}{D}(1-\sin\phi)\tan\delta(\sigma_v - p_a) \qquad (11)$$

This is done by writing Equations (8b) and (11) in finite difference form as follows (see **Figure 16**)

$$P_1 = P_o \frac{c_v \Delta t}{(\Delta h)^2}(p_2 + p_3 - 2p_o) + B_a \Delta\sigma_v \qquad (12a)$$

$$\Delta\sigma_v = \Delta h \left\{\gamma - \frac{4}{D}(1-\sin\phi)\tan\delta(\sigma_v - p_a)\right\} \qquad (12b)$$

Suitable values of Δx and Δt are chosen and Δh is then fixed by the speed of filling for which the calculation is being performed. The procedure for solution is as follows:

(i) Use the theoretical curves given by Gibson[14] to set up an initial distribution of p_a down to a depth of one silo diameter, ignoring silo action. (i.e.$\Delta\sigma_v = \gamma\Delta h$)
(ii) Calculate the initial stress profile from Equation (12b)
(iii) Introduce an increment of fill Δh and calculate $\Delta\sigma_v$ for each node of the finite difference grid.
(iv) Calculate values of p_a from Equation (12a).
(v) Repeat iii).

Continue until the silo is full.

REFERENCES

1. Martens, P., *Silolasten aus staubförmigen Schuttgütern und aus Luftzufuhr,* Dr. Ing. Dissertation, Technische Universität Carolo — Wilhelmina zu Braunschweig, (1969).
2. Pieper, K., *Investigation of Silo Loads in Measuring Models,* Journal of Engineering for Industry, ASME (May 1969); 365-372.
3. Pieper, K., Martens, P. and Nothdurft, K., *Silolasten aus Mehl,* Aufbereitungs — Technik, **16** (1975) 11; 579-584.
4. Martens, P., Personal Communication.
5. Murfitt, P. G. and Bransby, P. L., *Deaeration of Powders in Hoppers,* Proceedings Powder Europa 80 Conference, Wiesbaden, published by the International Powder Institute, London.
6. Murfitt, P. G. and Bransby, P. L., *Pressures in Hoppers Filled with Fine Powders,* Proceedings International Conference on Design of Silos for Strength and Flow, Powder Advisory Centre, London (1980).
7. Walker, D. M., *An Approximate Theory for Pressures and Arching in Hoppers,* Chemical Engineering Science, **21** (1966); 975-997.
8. Johanson, J. R., *Effect of Initial Pressures on Flowability of Bins,* Journal of Engineering for Industry, ASME (May 1969); 395-399

9. Wright, H., *Successful Failure? A Reassessment of the Cause of Stress Cracking of the Wall of a 3000t Capacity Reinforced Concrete Coal Bunker in 1961,* Proceedings International Conference on Design of Silos for Strength and Flow, Powder Advisory Centre, London (1980).
10. Blight, G. E. and Midgley, D., *Pressures Measured in a 20m Diameter Coal Load-out Bin,* Proceedings International Conference on Design of Silos for Strength and Flow, Powder Advisory Centre, London (1980).
11. Nielsen, J and Kristiansen, N. O., *Related Measurements of Pressure Conditions in Full-scale Barley Silo and in Model Silo,* Proceedings International Conference on Design of Silos for Strength and Flow, Powder Advisory Centre, London (1980).
12. Jenike, A. W., *Denting of Bins With Eccentric Drawpoints,* Journal of the Structural Division, ASCE, **93** (1967) ST1; 27-35.
13. Neville, A.M., *Properties of Concrete,* Pitman International London (1975).
14. Gibson, R. E., *The Progress of Consolidation in a Clay Layer Increasing in Thickness with Time,* Geotechnique, **8** (1958); 171-182.
15. Blight, G. E., *Flow of Air through Soils,* Journal of the Soil Mechanics and Foundations Division, ASCE, **97** (1971) SM4; 607-624.
16. Lambe. T. W., and Whitman, R. V., *Soil Mechanics,* Wiley, New York, (1969).

Second International Conference on

DESIGN OF SILOS FOR STRENGTH AND FLOW

7 - 9 November 1983
STRATFORD-UPON-AVON HILTON

Organised by the
POWDER ADVISORY CENTRE, P.O. Box 78, London NW11 0PG, England
Telephone: 01-455 0011 Telex: 8954242 (POWDER G)

PREFACE

This volume comprises the texts of papers, in Programme order, to be presented during the Conference. This material has been directly photo-reduced from author original typescripts.

We are indebted to all our authors for their contributions and sincerely hope that they will stimulate active discussion.

We are also indebted to the members of our Programme Committee - F. E. Weare (Polytechnic of Central London), J. G. M. Wood (Mott, Hay & Anderson, Croydon) and H. Wright (British Steel Corporation, Teesside Laboratories).

Finally, we also acknowledge the support and encouragement of our co-sponsoring professional organisations (as listed on the inside back cover) who have assisted in ensuring a worthwhile Programme and full international participation.

It is hoped, as with the first Conference, to publish a supplementary volume to these Proceedings based on contributions and discussions submitted in writing by Conference participants. The actual Conference discussions will not be recorded so as to stimulate audience participation in a confidential atmosphere.

We sincerely hope that this- the second of our series - event will stimulate searching practical discussion of all aspects of silo design and lead to more efficient and safer constructions and also stimulate international and interdisciplinary contact.

A. S. Goldberg
Conference Chairman

The Pretoria Portland Cement Company in this instance sited the blending silos above the storage silos. The meal can then be rapidly decanted from the blending silos into the storage silos below. In the process more blending occurs and this results in a more homogenous feedstock for the kiln.

A complex consisting of twin blending and storage silos was required, to feed a new nominal 2500 ton per day rotary kiln having a four-stage suspension pre-heater system. Each of the two blending/storage silos is housed in a continuously slid reinforced concrete cylinder having an internal diameter of 15 m, a wall thickness of 450 mm and an overall height of 88 m. Figure 1a shows the completed complex while Figure 1b shows detailed dimensions of one of the cylinders. Each blending silo has a volume of 4100 m^3 while the volume of each storage silo is 8000 m^3. Each storage silo can be filled directly from the blending silo above it and is also connected by an air slide to the blending silo on top of the adjacent storage silo. It was assumed that filling rates of up to 6000T/h (or a rate of rise of the meal surface of up to 30m/h, assuming a meal density of 1,15T/m^3 could occur by direct vertical flow, while 1000T/h (5m/h) could be transferred by transverse flow from the adjacent blending silo. Hence a maximum of rise of up to 35 m/h (7000T/h) was considered possible.

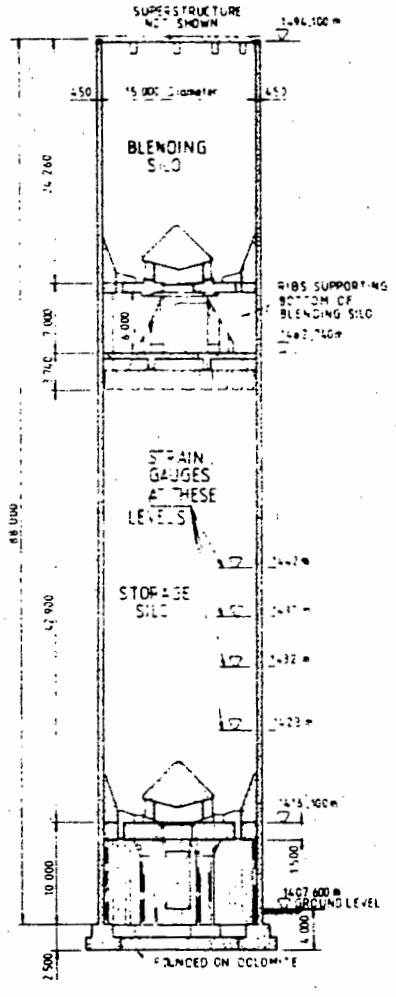

Figure 1a (above) :

View of twin blending/storage silo complex

Figure 1b (right) :

Section through combined blending and storage silo cylinder

DESIGN PRESSURES

For the blending silos, in which pneumatic homogenizing takes place, horizontal pressures p_h were calculated on the basis of DIN 1055 as:

$$p_h = 0{,}6\gamma z \quad \ldots\ldots (1)$$

with $\gamma = 1{,}15 T/m^3$ and z the depth below the fill surface.

For the storage silos the following filling possibilities were assumed to exist:

(i) Discharge into an empty storage silo at a rate of 35 m/h from two full blending silos until the blending silo directly above the storage silo was empty, followed by transverse discharge at 5m/h until the adjacent blending silo was empty.

(ii) Filling of an empty storage silo by vertical discharge at 30 m/h followed by filling at 5 m/h by transverse discharge.

(iii) The reverse of (ii).

(iv) Starting at any stage of filling of a storage silo and discharging into it at any rate from 5 m/h to 35 m/h.

At the time of the design, the only known work available on the effects of rapid filling of silos with fine powders was that due to Martens (2) who gave the following equation for pressures under rapid filling rates:

$$p_h = 0{,}8\gamma z_o \quad \ldots\ldots (2)$$

where z_o is the depth below the surface at which the horizontal pressure reaches a maximum and below which it is constant with depth

$$z_o = (v - v_o) \quad \ldots\ldots (3)$$

in which v = rate of filling in m/h and
v_o = limiting filling rate in m/h.

Martens gave v_o for powdered limestone as 1,4 m/h and this was assumed to be applicable also to cement raw meal.

Once the material had been deposited in the silo, the horizontal pressure was assumed to revert to that predicted by the Janssen expression

$$p_h = p_h(max)\{1 - e^{-K\gamma z/p_h(max)}\} \quad \ldots\ldots (3a)$$

$$p_h(max) = \frac{\gamma D}{4\tan\delta} \quad \ldots\ldots (3b)$$

in which K was taken as the active pressure coefficient K_A, and

$$K_A = (1-\sin\phi)/(1+\sin\phi)$$

γ is the density of the settled raw meal, taken as 1,7T/m³

δ is the angle of wall friction, taken equal to the angle of shearing resistance ϕ, as 20°.

In addition to the normal filling and emptying pressures in the storage silo, it was considered prudent to design the walls to withstand a nominal minimum pressure of 100 kPa that could be transmitted from the blending silo above.

Figure 2 shows the resultant envelope of maximum horizontal pressures, which was made up as follows:

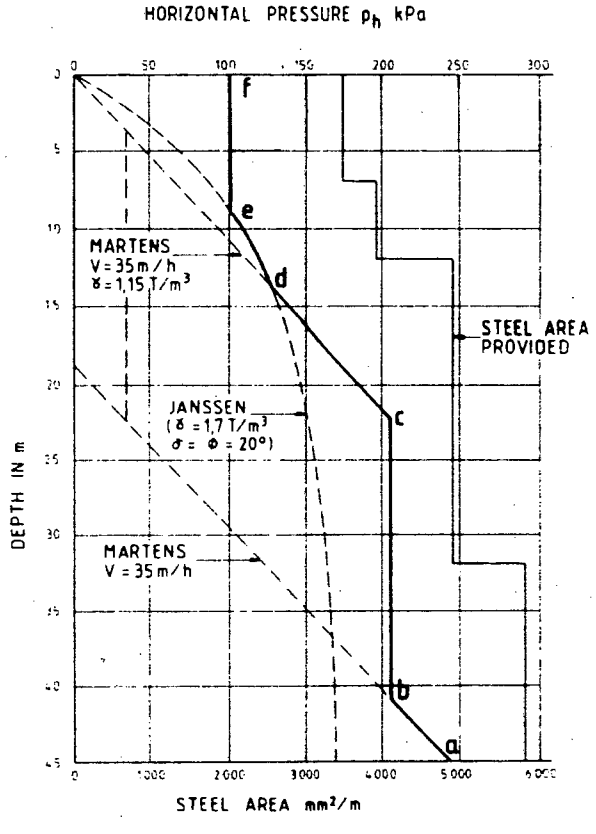

Figure 2 : Design horizontal pressure envelope and steel area provided

ab represents the pressure produced by filling the silo to just more than half (26,25m) at a rate of 35 m/h (z_o = 33,6m)

bcd represents the pressure produced by filling the upper half of an initially half-full silo at a rate of 35 m/h

de represents portion of the static pressure curve

ef represents the minimum pressure referred to above.

Figure 2 also shows the area of hoop steel reinforcing provided to resist the lateral pressures. High tensile steel having a yield stress of 450 MPa was used for the reinforcement. The maximum stress in the steel under assumed static pressures occurs between depths of 25 m and 32 m and amounts to 250 MPa. The maximum transient stress would occur between depths of 22,5 m and 32 m and amounts to approximately 345 MPa, giving a minimum design factor of safety of 1,30 against yield of the steel. (Thermal stresses would have reduced the stress in the inner layer of hoop steel to 295 MPa and increased that in the outer steel to 395 MPa.)

MEASURED PRESSURES

As the greatest uncertainty in the design pressures appeared to relate to those generated during rapid filling of the storage silos, it was decided to instrument one silo by mounting strain gauges on the hoop reinforcing at intervals up its height. Access to the outside of the silo was only available through the elevator and dust filter housing to be seen between the twin cylinders in Figure 1a. This limited the positions at which strain gauges could be mounted. These positions are indicated in Figure 1b. The reader is referred to ref (1) for details of the instrumentation, the development of strain during filling of the silo and the interpretation and correction for temperature effects of the measured strains.

Initially, flow into the silos was throttled by means of orifice plates in the connecting ducts to give a maximum rate of filling of 5 m/h under combined vertical and transverse discharge. Larger orifices were then inserted in the filling ducts, and ultimately the orifice plates were removed completely. It transpired that the maximum attainable rate of flow was only 10,1 m/h instead of 35 m/h assumed at the design stage. At this filling rate it was noted that the dust extracting plant that de-dusted the air space above the fill in the storage silos worked so effectively that a partial vacuum existed above the fill.

Figure 3 superimposes the maximum recorded strains (expressed as an envelope of equivalent actual horizontal pressures) on the design pressure envelope. The actual pressures for a filling rate of 10,1 m/h are compared with Marten's theory in this figure.

REASONS FOR DISCREPANCIES BETWEEN DESIGN AND MEASURED PRESSURES

As Figure 3 shows, the actual lateral pressures in the silo during rapid filling proved to be very much less than the design pressure envelope. It was unfortunately not possible, due to mechanical constraints, to fill at a faster rate to investigate the theory to the limit of 35m/h. As Figure 3 shows, Marten's theory, when applied to the maximum attainable rate of filling of 10,1 m/h, gives a pressure envelope which still exceeds observed pressures, but by no means as much as the design envelope.

A source of discrepancy lay in the assumed characteristics of the raw meal. Measurements on material stored in the silo showed that the settled density is only 1,15 T/m³ while the angles of shearing resistance and wall friction are 38°. The static pressure envelope shown in Figure 3 is based on these parameters with $K = K_o = 1-\sin\phi$. Marten's work appears to have encompassed filling rates of up to about 10 m/h. Because his relationships and those of Nothdurft (3) are empirical, one is probably not justified in extending the use of their expressions to filling rates greater than this without further experimental work. An analysis given in ref (1) in which the consolidation of the raw meal is considered as it is filled into the silo indicates that even with very large filling rates, horizontal pressures would be less than those predicted by Marten's expression. The pressure profile labelled "dynamic envelope" in Figure 3 is generally 50% of the design Janssen curve for the assumed raw meal characteristics and less than 40% of the Martens curve for v = 35 m/h, given in Figure 2.

WALL-TEMPERATURES

The milling process raises the temperature of the raw meal to the vicinity of 100°C and the temperature is still high when the meal is decanted into the storage silos. The walls therefore have to be designed to resist the thermal bending moment that results from the temperature difference between the inner and outer hoop reinforcing in the wall. The design assumptions were:

Maximum temperature of meal : 100°C

Minimum ambient air temperature : 5°C

Internal wall surface temperatures:

space above stored meal : 80% of meal temperature
below surface of meal: 60% of meal temperature

Taking a centre-to-centre distance between the inner and outer hoop reinforcing of the wall of 400 mm, the design thermal bending stress in the steel would be proportional to a temperature difference of $\frac{400}{450}(60-5) = 49°C$.

Thermocouples installed in the wall of the silo were used to measure actual temperature differences through its thickness. Figure 4 shows temperatures measured as the silo was filled at a rate of 7,36 mh^{-1}.

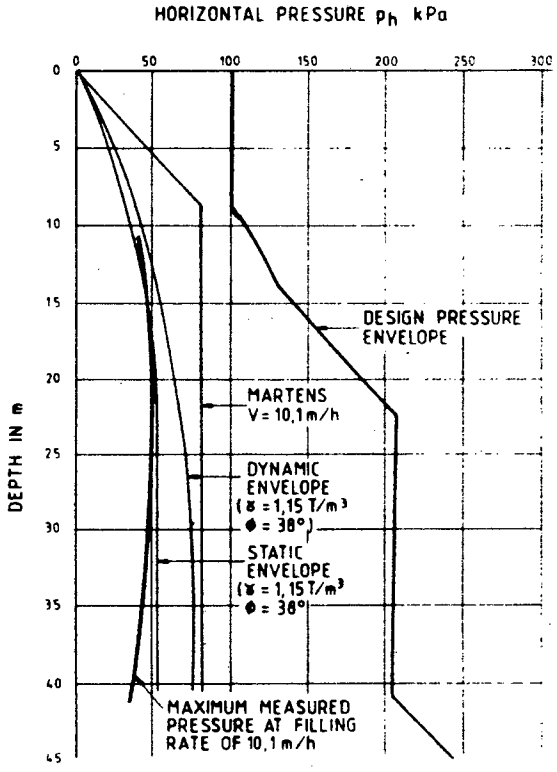

Figure 3 : Comparison between design and measured pressure envelopes

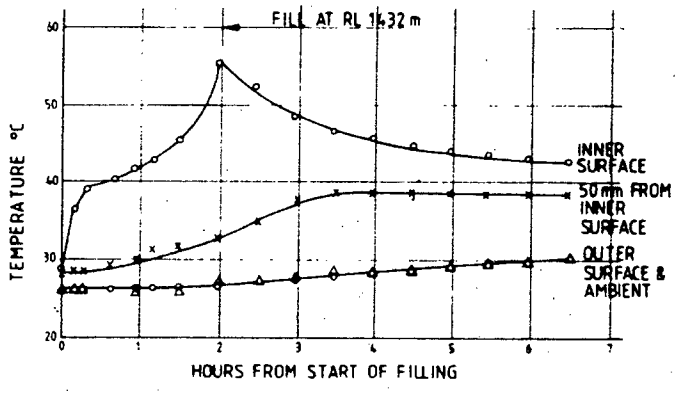

Figure 4a : Temperatures in silo wall during filling at 7,36 mh^{-1}

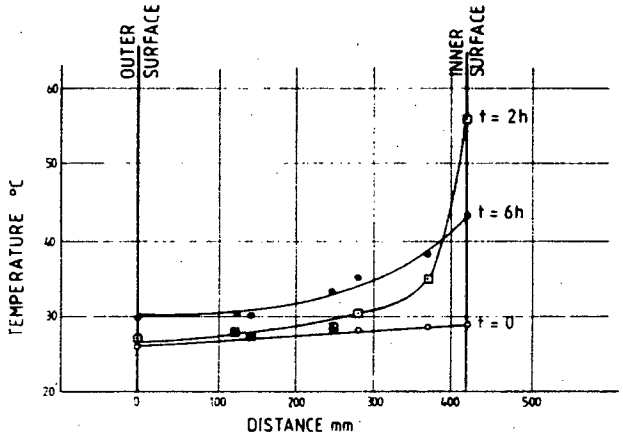

Figure 4b : Temperature profiles through silo wall at various times from start of filling

It will be seen that the temperature at the inner surface rose continuously until the meal surface covered the point at which the thermocouple junction was mounted. The temperature at this instant was 56°C which represented the temperature of the meal. Thereafter the temperature at the inner surface fell until it levelled out at 43°C (77% of the temperature of the meal). At this stage, 6 hours after the start of filling, the temperature gradient through the wall was approximately linear, and the temperature difference over the central 400 mm of thickness was 12°C. (Note that the actual wall thickness at this point was only 420 mm and not the design value of 450 mm). However, at a time of 2 hours on Figure 4, the maximum temperature difference between inner and outer steel reinforcing was 18°C and could have been as much as $18.\frac{(80-5)}{(56-26)} = 45°C$ had the temperature of the meal been a full 100°C with the ambient temperature as low as 5°C. Comparing the design value of 49°C with the above figure of 45°C, it is seen that the design assumptions were not unrealistic.

CONCLUDING REMARKS

A major point to emerge from this comparison is the extent to which the design of a silo may depend on information, not always accurate, or even correct, but given in good faith by a third party such as a mechanical equipment supplier. Another difficulty that the silo designer has to face is that many industrial silos have to be designed and constructed before the product which they will store has been produced. The designer therefore has to depend on available information, which again may be unreliable. It is only by carrying out comparisons such as the one above that the large discrepancies that may exist between assumption and reality come to light.

ACKNOWLEDGEMENTS

The authors thank the Pretoria Portland Cement Company Limited, Johannesburg, for permission to publish the data contained in this paper.

REFERENCES

(1) BLIGHT, G E, SCHAFFNER, R H and GILBERT, B, "Strains in a Reinforced Concrete Silo During Rapid Filling with a Fine Powder", Journal of Powder and Bulk Solids Technology, vol. 6, no. 2, 1982, pp 17-27.

(2) MARTENS, P, "Silolasten aus staubförmigen Schuttgütern und aus Luftzufuhr", Dr Ing. Dissertation, Technische Universität Carolo - Wilhelmina zu Braunschweig, 1969.

(3) PIEPER, K, MARTENS, P and NOTHDURFT, K, "Silolasten aus Mehl, Aufbereitungs - Technik, vol. 16, no. 11, 1975, pp 579-584.

bulk solids handling Volume 9, Number 1, February 1989

Behaviour of a Reinforced Concrete Coal Silo Under a Design Overload

G.E. Blight and H.N. Dreyer, South Africa

Summary

In situ strain measurements were made on the reinforcing of a reinforced concrete coal storage silo in order to decide if the silo could safely be loaded beyond its design load. The results of the measurements showed that the silo wall was still carrying load as an uncracked section after eleven years of service. It could be shown that it is quite safe to overload the structure to the extent required.

1. Introduction

The reinforced concrete silo concerned is one of a pair of identical silos for the storage of run-of-mine coal at Bank Colliery, South Africa, built in 1976. The silos had been designed to be filled to a level such that the apex of the filling cone came level with the top of the silo wall. The conveyor gantry was much higher above the top of the silos than is usual, because the silos had originally been equipped with central spiral loading chutes to minimize breakage of the coal. These chutes had recently been removed. The height of the conveyor made it possible to fill each silo completely, with the apex of the filling some 6 m above the top of the wall. The object of the investigation was to establish whether the silos can be filled completely with safety.

The two silos have unusually large dead volumes at the base. The extent of the dead zones is indicated on the section in Fig. 1. The cone forming the lower portion of the dead zone rises at 65° (theoretically $(45° + \phi/2)$ where ϕ, the angle of shearing resistance is 40°). This lower cone or funnel is cut off by an upper cone with a flatter angle of 38° which is the angle of repose of the coal.

When filled to the original design level, the silos each store a live capacity of 1,400 t. When filled to the proposed maximum level, the live capacity increases to 2,400 t each, i.e. an increase of 71 % of the original capacity. If the silos could be filled to this extent the cost of an additional storage silo could be saved.

Manuscript received: April 1, 1988.

2. Investigation Undertaken

It was decided to expose the hoop reinforcing of the silo at selected points on the outside of the wall and to strain gauge the bars thus exposed. The strain gauged silo would then be test-loaded by filling it to the required level, from empty, and observing the strains in the reinforcing. Hence the margin of safety of the silo under the proposed new loading could be assessed. The procedure was safe because the filling could be stopped instantly if the measured strains showed up any distress in the structure. Investigations of strains in two other reinforced concrete silos have previously been carried out using a similar technique. One silo is at King Mine, Mashaba, Zimbabwe and the other at the Pretoria Portland Cement works near Mafikeng, South Africa [1].

Exposing the reinforcing proved very difficult as the 11-year old concrete is extremely strong. Also, at some of the chosen positions the hoop reinforcing had been displaced towards the inside of the silo, with the result that the concrete cover is as much as 100 mm.

3. Instrumentation

Fig. 1 shows the positions of the ten strain gauge points (1 to 10) in elevation and in plan. At each point, the exposed high yield steel bar was prepared by grinding a small flat on it, on which to mount the strain gauges. The gauges were mounted on two vertical lines, one approximately on the north side of the silo, the other on the east.

The gauges used were 2 mm gauge length Kyowa right angle rosettes consisting of two gauges at right angles on a single piece of backing. The rosettes were mounted with one gauge parallel to the bar and one at right angles. After mounting, each rosette was waterproofed using a rubber solution and further protected against the weather by means of a piece of aluminium foil-backed bitumen sealing strip. Four-core shielded cable was used for connecting leads and these were anchored by tieing them around the exposed steel bar. The leads were then taken down the side of the silo to a central reading station at ground level. The pair of gauges forming each rosette were connected as a half bridge. This arrangement gives temperature compensation and a 30% magnification of strain. The strain read-

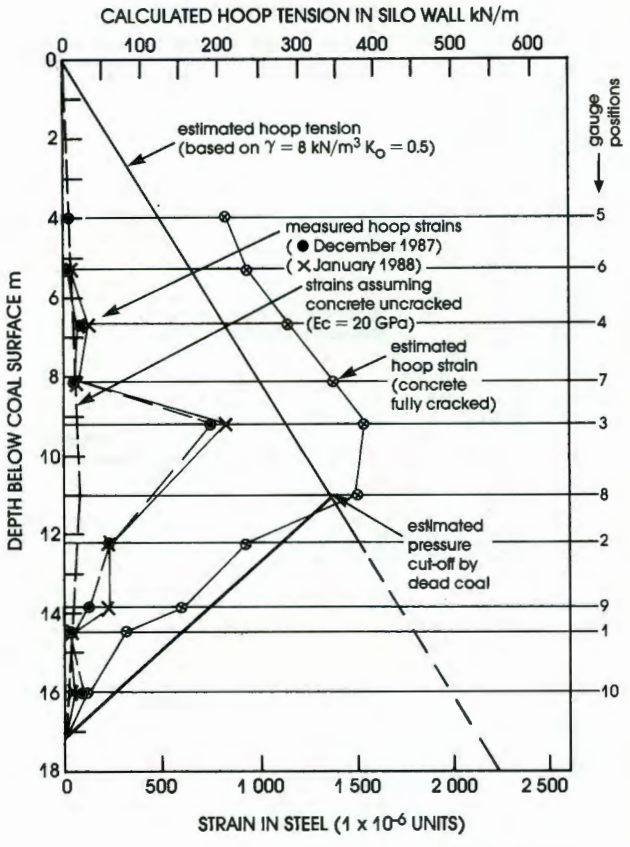

Fig. 4: Comparison of calculated and measured hoop strains in silo

The ring tension is shared, in general, between the concrete and the reinforcing steel, the usual design assumption being that the concrete carries no tension and that all the tension is carried on the hoop steel. In this case the tensile strain in the steel would be given by:

$$\varepsilon = \frac{T \cdot s}{A_s E_s} \qquad [3]$$

in which s is the vertical spacing of the hoop steel, A_s is the cross-sectional area of the bars at the level considered and E_s is Young's modulus for steel.

It is usually found that in a new concrete silo, the load is shared between the steel and the concrete, but that within a few years, the concrete has shed its load, and all (or most of) the tension is carried by the steel. This principle has been illustrated recently by Blight [5].

Fig. 4 shows the estimated hoop strains based on Eq. 3. Reference to Fig. 3 will show that actual steel strains might vary considerably from these estimated values, depending on the actual values of K and γ and also on the actual position of the cutoff for the pressure distribution AB.

The maximum calculated hoop strain on the basis of loading line OAB in Fig. 4 is about $1{,}500 \times 10^{-6}$ which corresponds to a steel stress of 300 MPa. This is the maximum stress that could occur for the assumed loading. The yield stress of the high tensile reinforcing steel is 450 MPa hence on this "worst case" basis, there is no danger of the reinforcing yielding.

Fig. 4 also shows the measured strains in the silo which, with the exception of gauge position 3, were very much less than the calculated strains. Even the strain at position 3 was only half than calculated.

As Fig. 3 indicates, it is possible that the loading could considerably exceed that represented by line OAB, but the risk that this would occur was considered small enough to accept. The cutoff pressure line AB depends on the presence of the well compacted dead zone in the base of both silos. The cutoff would disappear if, for any reason, the dead coal were to be removed from the silo. It is essential, therefore, that it be regarded as part of the structure of the silos and be left undisturbed in place.

Referring back to Fig. 2, it was noted that the measured strain at position 3 was only 260×10^{-6} when the coal reached its original maximum level. The strain elsewhere in the silo would have been far less than this as can be seen from the line in Fig. 4 representing strains in the uncracked silo. These strains were based on a value for the elastic modulus of concrete of 20 GPa which is probably less than the actual value. Hence the strains in the uncracked wall have probably been overestimated. As the cracking strain of concrete in tension is about 150×10^{-6} to 200×10^{-6} and the maximum calculated strain in the uncracked section was only 85×10^{-6}, it appears that at the other positions monitored the concrete was still sharing the hoop tension with the steel, and in fact carrying the major portion of the hoop load.

Even on the first filling of the silo eleven years ago, when the loading condition was similar to line CD in Fig. 3, the maximum calculated strain in the silo was only 85×10^{-6}, and probably less than this, because of the constraint applied to the silo walls by the floor.

The situation is expected progressively to change in the future as the silo is repeatedly filled to maximum capacity. However, the strains cannot increase to more than the hoop strains estimated on the assumption that the hoop steel carries all the load.

This was the main reason that the strain measurements on the silo were repeated after a period of 6 weeks. The silo was filled to capacity several times per week during that period. It had been anticipated that as a result, the concrete would crack and the strains in the steel would increase. As seen on Figs. 2 and 4 this did not happen to any extent. The strains in most of the steel remained small. However, there were indications that cracking was progressively occurring and the concrete was shedding its load at positions 2, 4 and 9. Strains can be expected eventually to increase considerably throughout the silo. It was only the concrete in the vicinity of position 3 that appeared to have cracked fully at the time the measurements were made. The strain at this position was 55% of the calculated strain, which means that for a value of $\gamma = 8$ kN/m^3, the horizontal pressure coefficient is 0.28. If this is taken to be an active pressure coefficient K_A, the corresponding angle of shearing resistance would be 35° which is a very possible value. Hence if the steel at position 3 is regarded as a load cell, it indicates that the lateral loading on the silo walls is actually less than represented by load line OAB in Fig. 3.

6. Conclusions

1. Measured strains in the hoop reinforcing of the silo when filled to maximum capacity were generally low. With the exception of position 3 (where the maximum strain was 850 $\times 10^{-6}$) the strains had a greatest value of 225×10^{-6} which

is about equal to the cracking strain of concrete. This indicates that most of the silo wall was still behaving as an uncracked section and that the ring tension was partly being carried in tension on the concrete.

2. The estimated hoop strains, on the assumption that the hoop reinforcing carries all the ring tension, indicated that the maximum stress in the reinforcing will not exceed 300 MPa. This stress is safe, although it exceeds the usual design stress for high yield reinforcing.

This conclusion depends on the assumption that the load diagram for the silo is represented by line OAB in Fig. 3.

Strains measured at position 3 on the silo indicated that the actual lateral loading was probably less than that assumed.

3. The ring tension near the base of the silo is considerably reduced by the presence of a large zone of dead coal. This cannot be removed without the ring tensions increasing very considerably.

4. It is probable that as the silo is repeatedly filled to maximum capacity, the concrete will gradually transfer its hoop load to the reinforcing. The measured strains will then move toward the calculated strains shown in Fig. 4.

5. Based on the two sets of measurements described in this paper, it was decided that the silo may be filled to maximum capacity without in any way endangering the structures.

Acknowledgement

This paper is published by kind permission of Amcoal Collieries Limited.

References

[1] Blight, G.E., Schaffner, R.H., and Gilbert, B.: Strains in a reinforced concrete silo during rapid filling with a fine powder; Journal of powder and bulk solids technology, Vol. 6 (1982) No. 2, pp. 17–27.

[2] Deutsches Institut für Normung: Lastannahmen für Bauten - Lasten in Silozellen: DIN 1055, Teil 6 (1984).

[3] American Concrete Institute: Recommended practice for design and construction of concrete bins, silos and bunkers for storing granular materials; ACI Standard 313–77 (1977).

[4] Blight, G.E.: Pressures Exerted by Materials Stored in Silos: Part 1, Coarse Materials; Geotechnique, Vol. 36 (1986) No. 1, pp. 33–46.

[5] Blight, G.E.: Measurements on Full Size Silos, Part 1: Temperatures and Strains; bulk solids handling, Vol. 7 (1987) No. 6, pp. 781–786.

About the Authors

Geoffrey E. Blight is Professor of Construction Materials in the Department of Civil Engineering at the University of Witwatersrand, Johannesburg, Republic of South Africa.

G.E. Blight has a long-standing interest in the art of obtaining engineering design information by means of measurements on full-scale structures. His interest has been pursued in the field of geotechnical engineering, mining and reinforced concrete structures, as well as silos and other containment structures.

Hector Neville Dreyer was born in South Africa in 1944. His tertiary education includes a National Diploma in Electrical Engineering and an M.Sc. in Mechanical Engineering.

The whole career of H.N. Dreyer has been tied to the mining industry which included gold, copper and coal. Since his first appointment in 1970 as a Maintenance Engineer he was promoted to Chief Engineer in 1977, and in 1980 to Consultant.

SKAKO makes bulk solids mobile ....but the dust is enclosed

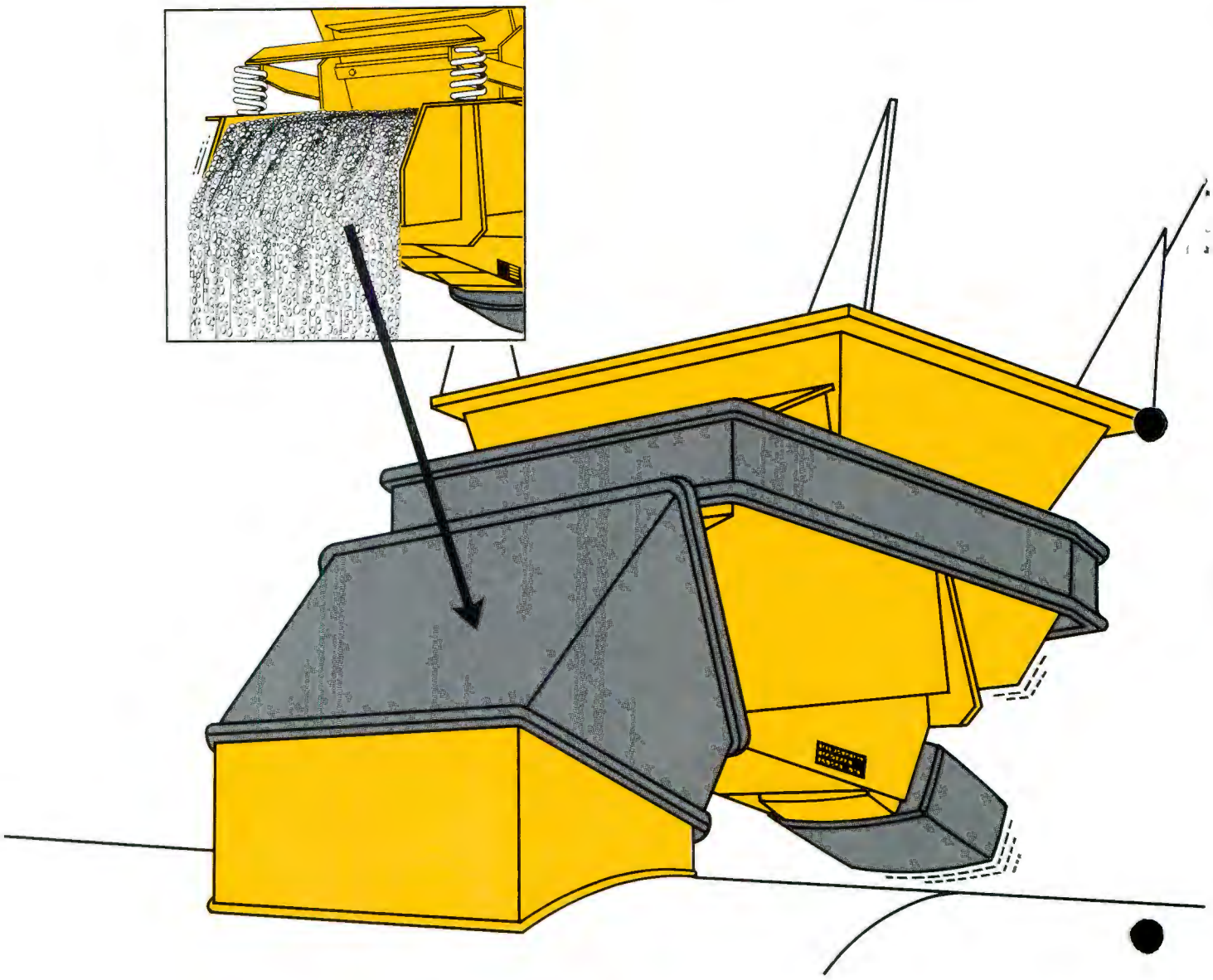

SKAKO for good vibrations

BRD, EVATEC Wiege- und Verpackungsautomaten GmbH
Tel.: +49 23 64 13 191 - Tlx.: 829671
Fax.: +49 23 64 16 707

España, COMESSA ESPAÑA S.A.
Tel.: +34 1 448 99 55 - Tlx.: 49 864
Fax.: +34 1 447 54 77

France, SKAKO COMESSA S.A.
Tel.: +33 88 40 12 00 - Tlx.: 871016
Fax.: +33 88 39 24 80

Island, STRAUMUR Umbods- og Heildsverlun
Tel.: +354 1 67 24 44 - Tlx.: 2299
Fax.: +354 1 68 84 41

Norge, AGDERMASKIN A/S
Tel.: +47 42 81 044 - Tlx.: 21358
Fax.: +47 42 81 840

Suomi Finland, OY TANSKAKO AB
Tel.: +358 02 87 636
Fax.: +358 02 91 13 28

Sverige, SKAKO AB
Tel.: +46 40 22 00 80 - Tlx.: 33660
Fax.: +46 40 21 92 00

United Kingdom, SKAKO Vibration Ltd.
Tel.: +44 532 42 05 95
Fax.: +44 532 42 21 84

USA/Canada,
TABOR Machine Company
Tel.: +1 304 327 2431
Fax.: +1 304 325 6953

TABOR Machine Company
Tel.: +1 412 37 37 065
Fax.: via phone

SKAKO A/S
VIBRATION
DK-5600 Faaborg – Denmark
Tel. +45 9 61 97 61 -Telex 50307
Fax: +4 59 61 82 70

RIBER REKLAME/OFFSET - FAABORG

89 B1 UK-INT.

7.5 MEASUREMENT OF LOADS IN STEEL SILOS VIA ELECTRIC RESISTANCE STRAIN GAUGES

CONTRIBUTION TO LEARNING

The author was originally forced into using strain gauges, rather than pressure cells by budgetary constraints. The fall in the value of the Rand against the Yen has now made pressure cell prohibitively expensive to purchase.

It was soon realised that strain gauges had considerable advantages over pressure cells for measurements on steel silos. Strain gauges are self calibrating, provided the gauge factor is correct, and can be used to measure frictional wall loads, which conventional pressure cells cannot do.

The main contributions of this group of eight papers have been as follows:

.1 Temperature surcharge pressures have been investigated and a method developed for calculating the surcharge.

.2 The effect of temperature changes on frictional wall loads has been demonstrated. Under certain circumstances it is possible for a steel silo wall to go into vertical tension as a result of a decrease in ambient temperature.

.3 The sharing of load between the sheeting and the stiffeners of corrugated steel silos has been elucidated.

In the penultimate paper (7.5.7) strain measurements have been used to illustrate and confirm the conclusions (reached on other evidence) stated in the summary paper number 7.1.6.

The final paper shows that the broad concepts of 7.1.6 can be predicted for a given filling material used in a series of silos of varying geometry.

7.5 MEASUREMENT OF LOADS IN STEEL SILOS VIA ELECTRIC RESISTANCE STRAIN GAUGES

7.5.1 Blight, G E (1985). Temperature changes affect pressures in steel bins. International Journal of Bulk Solids Storage in Silos, vol 1, No 3, pp 1-7.

7.5.2 Blight, G E and Garstang, A (1987). Strains measured in a 7,500t sugar silo. Bulk Solids Handling, vol 7, No 4, pp 573-582.

Mr Garstand was designer of the silo. I planned and carried out the investigation and drafted the paper. My contribution to the paper is assessed at 80%.

7.5.3 Blight, G E (1988). Strains measured in a 7,500t sugar silo, Part II. Bulk Solids Handling, vol 8, No 4, pp 413-419.

7.5.4 Blight, G E (1989). Behaviour of a bolted corrugated steel grain silo. Powder Handling and Processing, vol 1, No 2, pp 143-149.

7.5.5 Blight, G E (1989). Strain and temperature measurements on an externally stiffened corrugated steel grain silo. Powder Handling and Processing, vol 1, No 4, pp 343-347.

7.5.6. Blight, G E (1990). Load and temperature strains of a welded plane plate grain silo. Powder Handling and Processing, vol 2, No 1, pp 25-29.

7.5.7 Blight, G E (1990). Measured loading on a small steel grain silo. Powder Handling and Processing, vol 2, No 2, pp 1-6.

7.5.8 Blight, G E (1991). Structure-fill interaction in steel grain silos. Powder Handling and Processing, vol 3, No 1, pp 43-48.

Int. J. Bulk Solids Storage in Silos, **1** (3) 1-7, 1985

TEMPERATURE CHANGES AFFECT PRESSURES IN STEEL BINS

G. E. Blight,
Department of Civil Engineering,
University of Witwatersrand,
Hillman Building, East Campus,
1 Jan Smuts Avenue,
Johannesburg 2001,
South Africa.

Strains, pressures and temperatures in the walls of a steel storage bin have been recorded in the field. The measurements illustrate the large effect of diurnal temperature changes on wall pressures and wall loads in a steel bin. Wall pressures generally increase as temperatures fluctuate, while wall loads are decreased by falling temperature and vice versa.

INTRODUCTION

This paper deals with pressures measured in a steel maize storage bin and the effect that temperature changes have on these pressures. A complete description of the bin, of which a photograph is shown in **Figure 1**, has been given in a previous paper[1].

Measurements of pressure were made by means of mercury-filled strain-gauged pressure cells mounted in a vertical line up the side of the bin. The pressure-sensitive faces of the cells are aligned flush with the inner face of the bin so that there is no interruption in the continuity of the interior surface.

Figure 2 shows the main dimensions of the bin and also summarizes measurements of horizontal pressure on its walls. The measurements are presented as a plot of horizontal pressure versus calculated overburden, i.e. the unit weight of the maize γ multiplied by the depth z to the point of measurement.

Also shown in **Figure 2** are a series of theoretical relationships between pressure and overburden. The line labeled "arching K_o (NC)" represents the relationship calculated from the well-known Janssen theory[2] using a lateral pressure coefficient

$$\sigma_v / \sigma_h = K_o$$

K_o is the pressure coefficient corresponding to vertical compression with zero lateral strain, and σ_v and σ_h are respectively the vertical and horizontal pressures. The coefficient K_o was measured in the laboratory.

The straight lines labeled "no arching" correspond to relationships in the form

$$\sigma_h = K\gamma z$$

in which γz is the calculated overburden. K_A is the active pressure coefficient which is theoretically the minimum value K can have.

Figure 1.
20m Diameter steel maize storage bin referred to by paper.

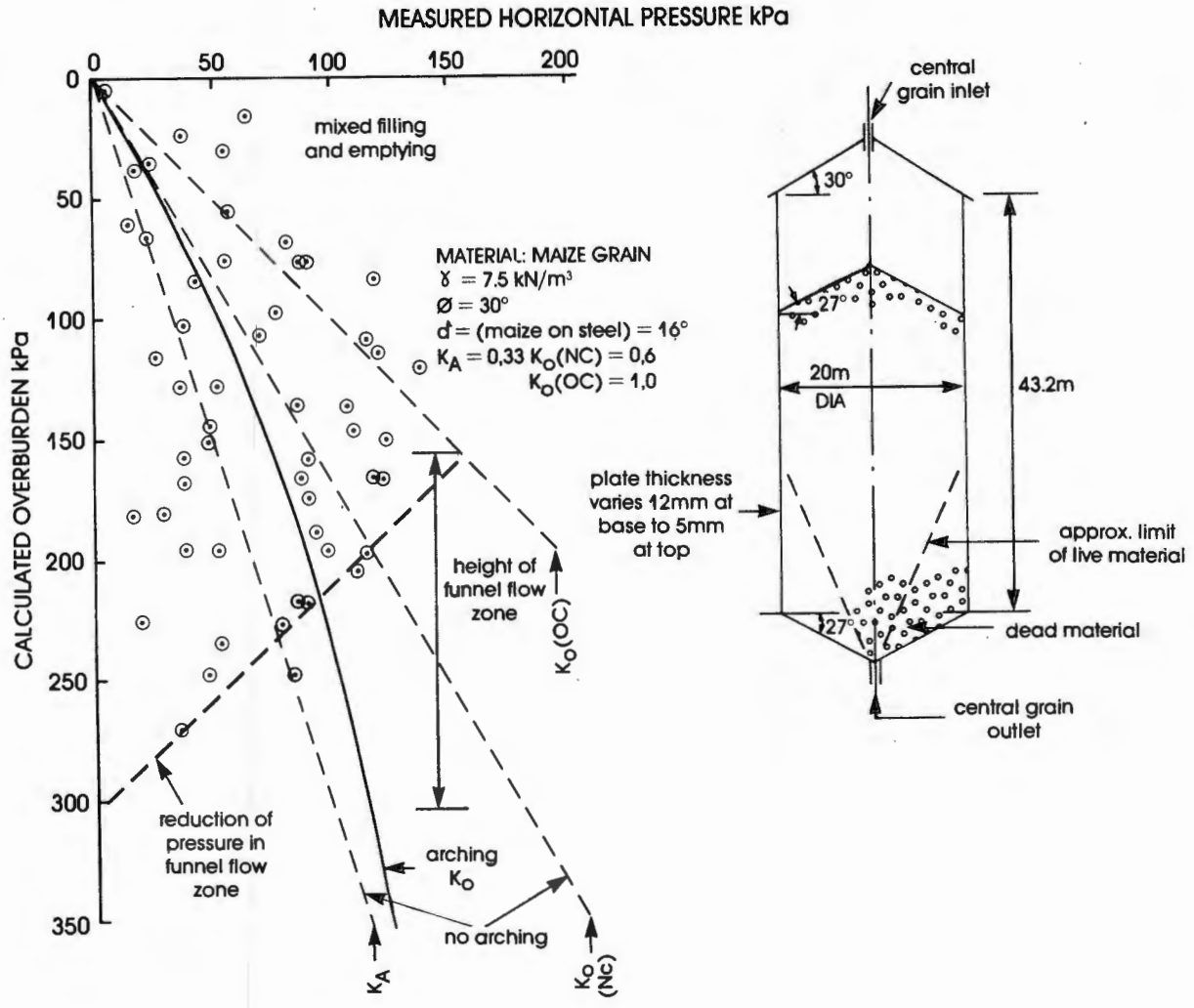

Figure 2.
Dimensions of storage bin and summary of measured horizontal pressures.

K_o (NC) corresponds to normally consolidated grain, i.e. material in which the stress has continuously increased. As the bin's contents pass through it from top to bottom they should remain normally consolidated until the zone of convergent or funnel flow to the outlet is reached. Within this zone, as indicated in **Figure 2,** the vertical and horizontal stresses generally decrease and the grain becomes overconsolidated. K_o (NC) can be expected to increase towards K_o (OC) which is the upper limit to the pressure coefficient for the overconsolidated grain. As **Figure 2** indicates K_o (OC) may be considerably greater than K_o (NC).

Pressures in the grain above the zone of funnel flow were found regularly to exceed even those corresponding to K_o (OC). Hence some additional mechanism appears to operate to increase the lateral stresses in the bin. As the measurements will show, the increased pressures result from the effect of temperature changes of the steel walls of the bin.

A steel bin or silo has a thin wall consisting of material that is a good thermal conductor. It contains a relatively large mass of filling that is usually a poor conductor of heat. Hence one can expect the wall of the bin to react to external temperature changes without much time lag, while its contents remain inert to short-term, e.g. diurnal temperature changes and will only react to longer period, eg. seasonal changes.

The temperature at any point on the wall of a bin will undergo a diurnal temperature cycle. However, the cycle at any other point will be different. For example, the eastern side of a bin will reach a maximum temperature earlier in the day than the western side. Shading by adjacent structures, cooling by rain showers, etc. will modify the temperature cycle at any point. Hence the temperature history of the bin wall will be extremely complex and so will the effect of these temperature variations on pressures generated in the contained fill.

This paper presents a series of recordings of temperature, pressure and strain made on the 20m diameter steel maize storage bin. The recordings demonstrate the response of the bin and its contents to changes in temperature and show how complex is this response.

Because the measurements were made at a series of points on the surface of the bin, whereas the bin wall responds to the average environment, the recordings can only be analyzed qualitatively and semi-quantitatively. Nevertheless, it is believed that they help to elucidate

several rather obscure aspects of bin behaviour.

OBSERVATIONS OF TEMPERATURE-RELATED PRESSURE CHANGES

In simple terms, if the bin wall cools while its contents remain at constant temperature, the contraction of the wall will squeeze the contents. An increased pressure will result, and vice-versa. When the bin wall expands, one can expect the fill to settle so as to occupy the increased diameter. On the next cooling cycle, therefore, the wall will be unable to return to its previous diameter, and the pressure in the fill will further increase.

Figure 3 shows an example of temperature-related pressure changes recorded by means of two pairs of pressure cells and thermocouples, mounted on the western side of the storage bin. The observations were made over a week-end during which the silo was not operated, hence the observed changes are only a result of temperature variations and adjustment of the filling to these changes. The pressure cells are fully temperature compensated and measurements have shown that changes of temperature have no effect on their reading.

The thermocouple junctions were mounted on the outside of the bin wall adjacent to each pressure cell and were covered by aluminium foil-backed adhesive strip to provide a similar surface texture and colour to that of the aluminium-painted silo.

Figure 3 illustrates the pattern of rising pressures as the temperature falls and falling pressures as the temperature rises. It also shows an apparent *"thermal-ratchet"* effect, whereby the maximum pressure in each diurnal cycle progressively increases. This presumably occurs because of settlement of the grain against the sides of the bin when its diameter increases.

It will be noted that the recorded temperatures and pressures are slightly out of phase. The pressure is often still falling while the temperature is rising, and vice-versa. This is probably because the recorded temperature represents conditions at a point, whereas the pressure responds to average conditions over a larger area of the bin wall.

The different nature of the pressure-time record when the pressure is falling or rising should also be noted. Both exhibit a "stick-slip" characteristic, but whereas pressure increases take place in a series of relatively high frequency, low amplitude fluctuations, pressure decreases have lower frequency, higher amplitude fluctuations.

When operation of the bin was resumed on Monday morning (not shown in **Figure 3**) the *"ratchet"* cycle was broken and pressures in the bin fluctuated more randomly in response to the influence of filling and emptying operations.

The ratchet effect illustrated in **Figure 3** prompts the question: "If a bin is left undisturbed for a period of several weeks or months (as storage bins sometimes are), will the pressure continue to ratchet upwards to a dangerous level, or will an equilibrium be reached within a short period?"

It can be argued that an equilibrium must soon be reached if the diurnal temperature cycles repeat themselves and do not increase in amplitude. As the minimum pressure in the bin rises, a stage will soon be

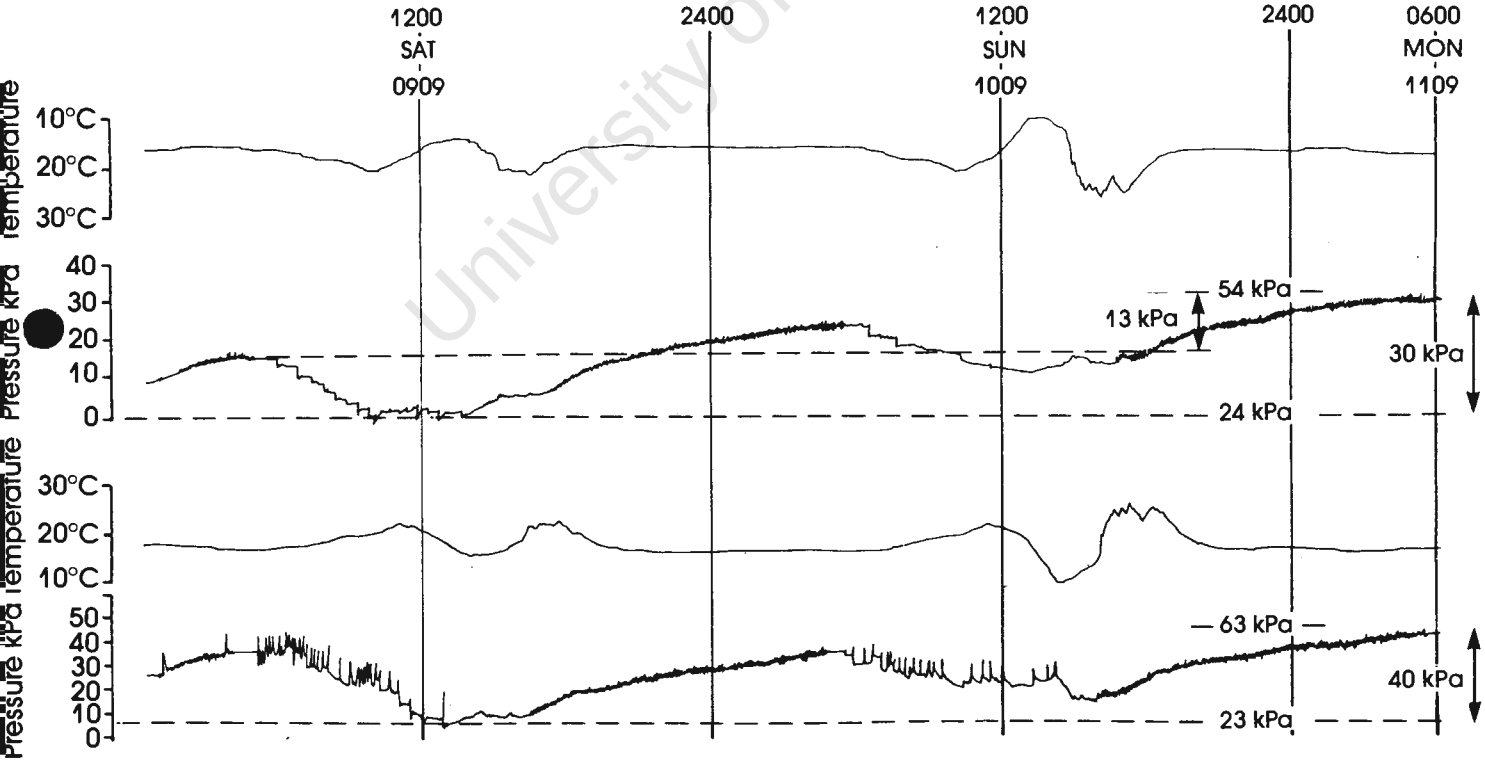

Figure 3.
Variation of horizontal pressure on bin wall and temperature with time at constant fill level.

reached where the wall friction will be sufficient to support the filling and prevent it from slipping downwards. At this stage, with the wall contracting and expanding onto a static mass of filling, an equilibrium will exist and the pressure cycle will repeat itself without ratchetting as long as the temperature cycle does not increase in amplitude.

At this point it should be noted that the temperature cycles shown in **Figure 3** increase progressively in amplitude, so the apparent ratchet effect shown in the figure could be expected.

Even without thermal ratchetting, the increases in pressure caused by thermal cycles can be surprisingly large. As pointed out earlier[1] in the case illustrated in **Figure 3**, a pressure coefficient of 0.5 at noon on Saturday would increase to between 1.1 and 1.4 by early on Monday morning.

Figure 4a shows data similar to that of **Figure 2**, but the record covers a longer period. The first point to note is the relatively large increase of pressure that occurred on Thursday night, followed by a decrease as maize was extracted on Friday. A similar large increase of pressure occurred on Friday night and the pressure continued to increase until Saturday night, even though the temperature remained almost static.

From Sunday morning onwards the pressure tended to fluctuate in sympathy with the temperature. However, the Sunday temperature cycle was slightly more subdued than that of Saturday, and there was no evidence of a thermal ratchet effect.

Figure 4b does bring out another aspect of the time-dependence of pressures in silos, viz. that settlement and readjustment of the filling after emptying may result in larger changes of pressure than those caused by temperature.

The record of **Figure 4a** is continued in **Figure 4b**. During Tuesday, simultaneous filling and emptying occurred with a net increase in fill level over the day. Nevertheless, there was a net decrease in pressure, even allowing for the time-dependent increase that occurred on Tuesday night. This shows that the pressure at a point in a bin is by no means uniquely related to the head of material above the point, as assumed by all available theories for silo pressures. This is, of course, well known, but **Figure 4b** provides a graphic description of the statement.

RELATIONSHIP BETWEEN TEMPERATURE, HORIZONTAL STRAIN AND HORIZONTAL PRESSURE

Figure 5 shows simultaneous recordings of horizontal pressure, temperature and horizontal or hoop strain made at a point on the bin wall.

The measurements of horizontal strain were made by glueing 5mm gauge-length electric resistance strain gauges to the bared steel. Temperature compensation was provided by means of separate dummy strain gauges mounted on small squares of steel plate. The plates were glued to the wall of the silo and both active and dummy gauges were covered by the same strip of water-proofing material (bitumen bonded to an aluminium foil backing) so that both would be subject to the same changes of temperature. To see how repeatable the measurements were, the hoop strain measurements were duplicated by mounting one strain gauge pair on either side of the pressure cell at a distance of 1m away from it. The distance was chosen to avoid the strain-raising effect of the 200mm diameter hole in the silo wall through which the pressure cell is mounted.

Figure 5 shows that the readings of the horizontal strain gauges are almost exactly duplicated, while the shape of the strain, temperature and horizontal pressure records are closely related. (The silo was not in operation while these measurements were being recorded, hence they represent a constant fill level).

The temperature, strain and pressure fluctuations are not quite in phase, but in general, a fall in hoop strain is reflected by a rise in pressure and vice-versa, while a rise in temperature is accompanied by a rise in hoop strain and a fall in pressure.

One should not expect quantitatively to relate the observations as the pressure and strain measurements probably reflect average conditions over a segment of the silo perimeter, whereas the temperature measurements more nearly represent conditions at a point.

Theoretically, the observed strain and the strains resulting from changes in temperature and silo pressure should be related as follows:

i.e. $\varepsilon_n = \varepsilon_t - \varepsilon_p$

where ε_n = net observed change in hoop strain

ε_t = temperature strain and

ε_p = strain resulting from change of silo pressure.

As an example, consider the period just after noon on 8th June (see **Figure 5**):

(i) The recorded pressure fell by about 7kPa. As the plate thickness at the level of the measurements is 6mm, this should correspond to a change of about 60 microstrain ($= \varepsilon_p$) in hoop strain (a decrease in hoop stress of 12MPa).

(ii) The temperature rose by about 9°C which should correspond to an increase of about 110 microstrain in hoop strain (ε_t).

(iii) The observed change of hoop strain was an increase of 80 microstrain (ε_n) which should equal the difference between the temperature-and pressure-related strains. (Actually, $(\varepsilon_t - \varepsilon_p) = 50$ microstrain).

Hence in this example, quantitative agreement between the observations is not achieved, although there is qualitative agreement.

RELATIONSHIP BETWEEN TEMPERATURE, HORIZONTAL STRAIN AND VERTICAL STRAIN

Figure 6 shows simultaneous recordings of horizontal pressure, horizontal strain and vertical strain measured at the same point on the silo as represented in **Figure 5**. The record of vertical strain is a near mirror image of the horizontal strain. It is apparent that if the horizontal strain decreases (i.e. the silo diameter contracts), the vertical strain increases (i.e. the height of the silo expands). Hence the grain must tend to move upwards relative to the silo wall as the temperature falls and downwards as the temperature rises. Note that the vertical strain in the silo wall is thus the opposite of what one would expect if the strain were governed by the temperature alone.

The maximum recorded change of vertical strain shown in **Figure 6** amounts to a decrease of 200 microstrain. The corresponding rise in temperature was about 8°C. Hence the total compressive strain in the wall must have been close to 300 microstrain ie. total strain = net observed strain + temperature strain (a stress change of 60MPa). Even the smaller of the three diurnal changes in vertical strain corresponds to a stress change in the

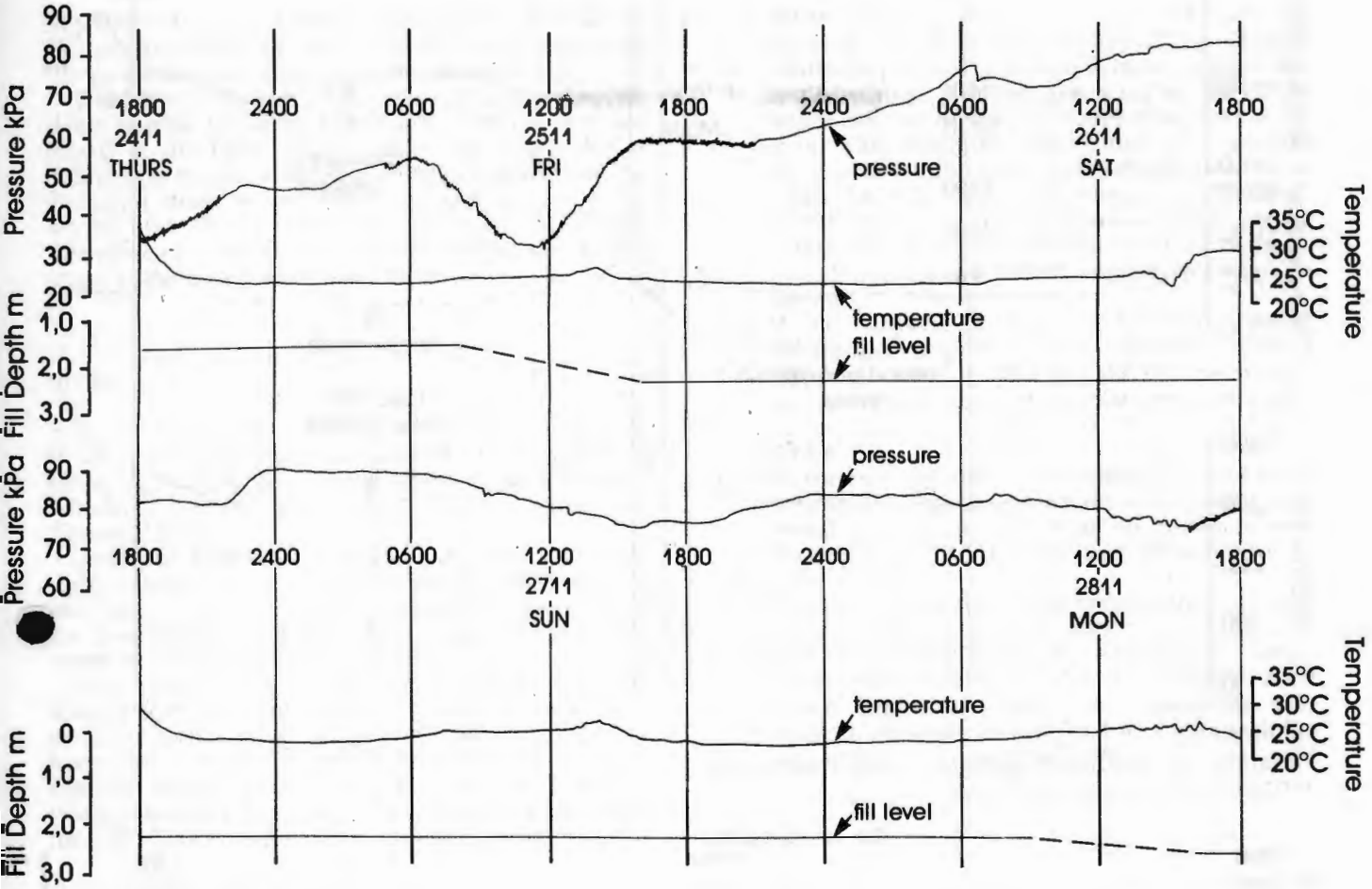

Figure 4a.
Variation of horizontal pressure, temperature and fill level in bin with time.

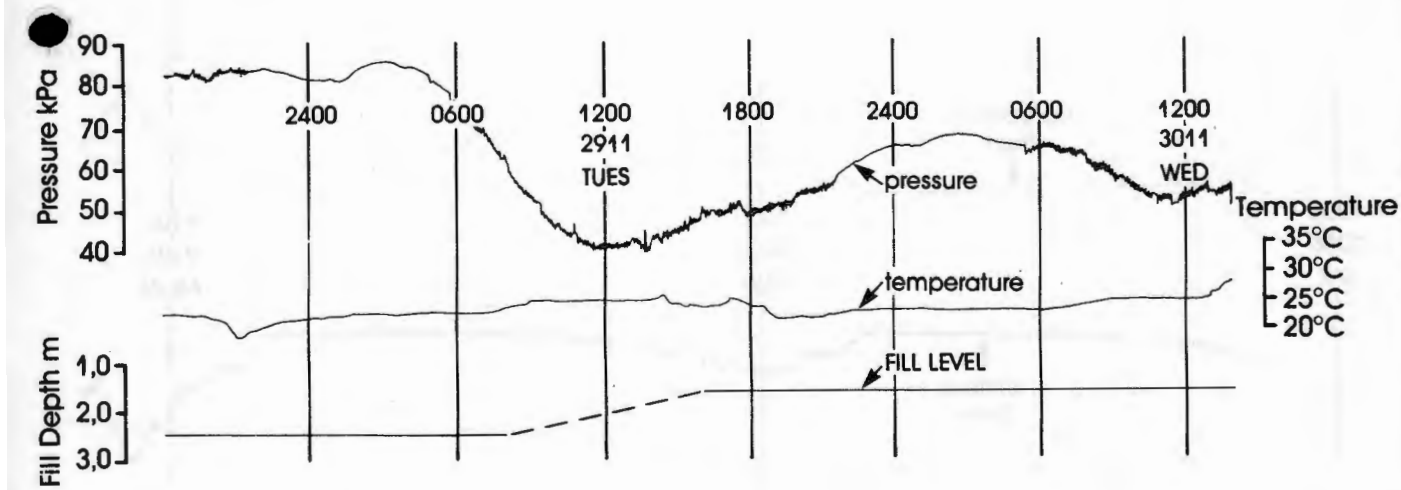

Figure 4b.
Continuation of record shown in Figure 4a.

A truly important new book:

Sampling and Weighing of Bulk Solids

by Jan W. Merks, Canada

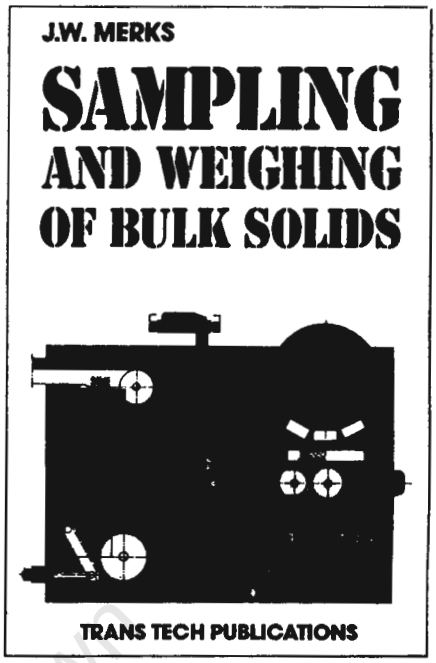

1985, 420 pages, 200 figures & tables,
92 references
Price: US$ 45.00 ISBN 87849-053-1

Contents:

Excerpts from the Preface:

"This text is written for the specific purpose of providing guidelines in the field of quality evaluation and mass measurement, loss prevention and loss control for bulk solids such as coal and concentrates, ores and industrial minerals, chemicals and fertilizers, and many others. Its central theme is to create understanding for the concepts of accuracy and precision of measurements in weighing, sampling, preparation and analysis of bulk solids.

Therefore, the most important tests and techniques will be introduced and their use demonstrated with practical examples from a wide range of experiences and experiments at coal mines, hard rock mines, mineral processing and coal preparation plants, steel plants and base metal smelters, power utilities and bulk handling terminals in different parts of the world.

Efforts have also been made to eliminate statistical jargon and to use simple prose. The most important concepts, and their symbols, are defined and listed in a glossary. Many numerical examples have been included to put into perspective the basic concepts of probability and statistics, and to encourage the use of these powerful techniques.

About the Author:

Jan W. Merks was Vice President, Quality Control Services, with the SGS organization, a worldwide network of inspection companies that act as referee between buyers and sellers. He joined Cominco Ltd. in the position of Assistant to the Chairman for the purpose of reviewing their procedures for the determination of quality and weight and compiling an internal manual on weighing, sampling and analysis. Currently he is President of Matrix Consultants Ltd., a Canadian company that provides consulting services to the resource industry in the field of sampling and weighing.

Please send me. . . .copy(ies) of the book **Sampling and Weighing of Bulk Solids** immediately after publication.

I enclose a check drawn on a U.S. bank in the amount of US$ 45.00 per copy which includes postage and handling if the check accompanies the order.

Check Number: _____

Please send me your Pro-Forma invoice for. . .copy(ies) of the book **Sampling and Weighing of Bulk Solids.**

I am interested in further details on the book **Sampling and Weighing of Bulk Solids.**

Name: _____

Position, Job or Title: _____

Company or Organization Name: _____

Address: _____

City, State or Province: _____

Country: _____ Date: _____

TRANS TECH PUBLICATIONS
P.O. Box 266 · D-3392 Clausthal-Zellerfeld · West Germany
16 Bearskin Neck · Rockport, MA 01966 · USA

bulk solids handling Volume 7, Number 4, August 1987

Strains Measured in a 7,500t Sugar Silo

G.E. Blight and A. Garstang, South Africa

Synopsis

The paper describes the result of strain measurements on the walls of a free-standing cylindrical steel sugar silo. The measurements were made to study the interactive behaviour of the bulk sugar and the silo and to confirm the assumptions made for the design. The strains indicated that in general the silo behaved as expected. However, the wall load for the silo was found to decline to unexpectedly low values at the start of emptying. This phenomenon has not been satisfactorily explained.

1. Introduction

Two free-standing cylindrical steel silos, each of 7,500 t capacity, have recently been commissioned at a bulk sugar depot at Germiston, Republic of South Africa. An opportunity arose for instrumenting one of the silos during construction. The objective of the instrumentation was to study the structural behaviour of the silo during normal operation and also to check on the assumptions made in its design.

The paper will comprise of the following:

1. A brief summary will be given of the expected behaviour and properties of the sugar, as measured for the design of the silo.

2. The silo and instrumentation will be described.

3. Strains measured in the silo walls, interpreted in terms of vertical wall friction loads and equivalent horizontal fill pressures, will be described for the first and second fillings of the silo. These will be compared with the loadings calculated for the design.

Dr. G.E. Blight, Professor of Construction Materials, University of the Witwatersrand, Dept. of Civil Engineering, 1 Jan Smuts Ave., Johannesburg 2001, and Mr. A. Garstang, Consulting Engineer, Bosch & Associates, Inc., Durban, Republic of South Africa

2. Expected Behaviour of Sugar in the Silo

During filling of the silo, it was expected on the basis of earlier measurements [1] that stresses in sugar away from the influence of the walls (see Fig. 1) would be geostatic. That is, vertical and horizontal stresses, σ_v and σ_h, would be principal stresses related by:

$$\sigma_h = K_0 \sigma_v = K_0 \gamma z \quad (1)$$

where:

K_0 — lateral pressure coefficient for compression with zero lateral strain
γ — unit weight of the sugar
z — depth below the sugar surface.

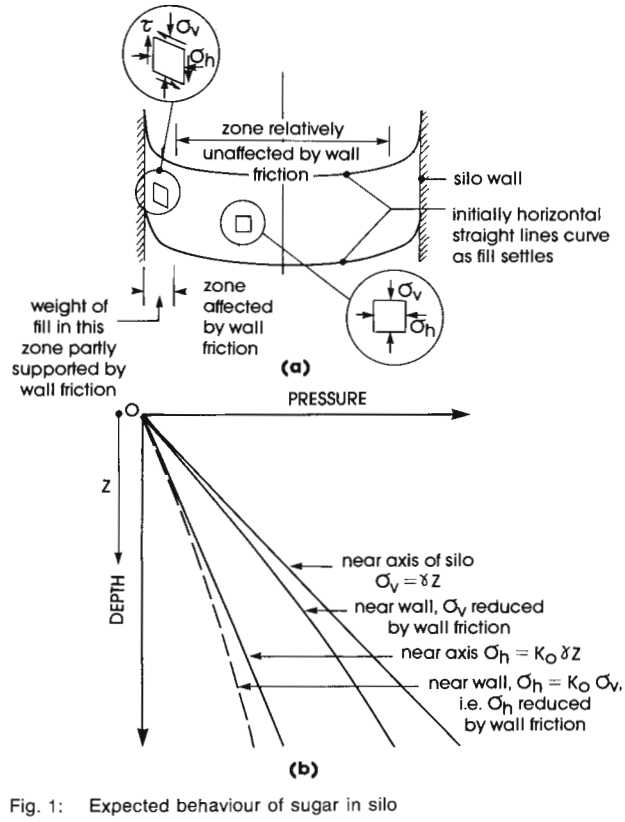

Fig. 1: Expected behaviour of sugar in silo

Near the walls of the silo, friction was expected to retard the settlement of the sugar under its self-weight, thus transferring some of the weight of the sugar into the wall and locally reducing σ_v. σ_h would still be related to σ_v by an equation similar to Eq. (1), but the equivalent value of K_0 might be changed. Fig. 1 shows the process described above in diagrammatic form.

The frictional wall load P_w in the silo can be calculated as:

$$P_w = K_0 \gamma \tan\delta \frac{z^2}{2} \quad (2)$$

where:

δ — angle of wall friction.

3. Properties of Sugar

Two samples of sugar were tested, one from each of the refineries that will serve the silos.

The following properties of the sugar, which are relevant to this paper, were measured by means of conventional soil engineering test techniques:

1. Moisture content
2. Unit weight γ
3. Angle of wall friction δ
4. Angle of shearing resistance φ
5. Lateral pressure coefficient K_0.

3.1 Moisture Content

The moisture contents of the two sugars were measured by drying in an oven at 105°C for 24 h. The moisture content on this basis was between 0.03 and 0.04 %, which is comparable with the moisture content of the conditioned sugar that will be delivered to the silos.

3.2 Unit Weight γ

A cylinder 150 mm in diameter and 150 mm high was filled with sugar by pouring loosely from a scoop. The sugar was struck off level with the top of the cylinder using a straightedge and the cylinder was weighed to get the loose unit weight. The full cylinder was then vibrated and more sugar added until no more could be accommodated. Re-weighing of the cylinder gave the vibrated density. Measured values varied from 8.36 kN/m³ (loose) to 10.28 kg/m³ (vibrated).

Previous measurements [2] have shown that the unit weight of silo fills remains close to the loose condition.

Hence a unit weight of 8.6 kN/m³ was adopted as a basis for analysing the measurements described later.

3.3 Angle of Wall Friction δ

The angle of wall friction was measured by means of a shear box apparatus. For this purpose the lower half of the box was occupied by a square of steel plate representing the wall, with its upper surface accurately coinciding with the plane of shearing. A series of simulated wall materials was tested. The material actually used for the silo was represented by a carbon steel specimen prepared by shot-blasting and painted with 75 μm of abrasion-resistant paint.

The results of the wall friction tests have been summarized in Fig. 2. It will be seen that the angles of wall friction for the two sugars are very similar and a value for the angle of $\delta = 32°$ appeared to be a good average. The maximum horizontal pressure in the silo has been measured at less than 120 kPa. It will be noted that the relationship between normal stress and shear stress over this range is quite linear.

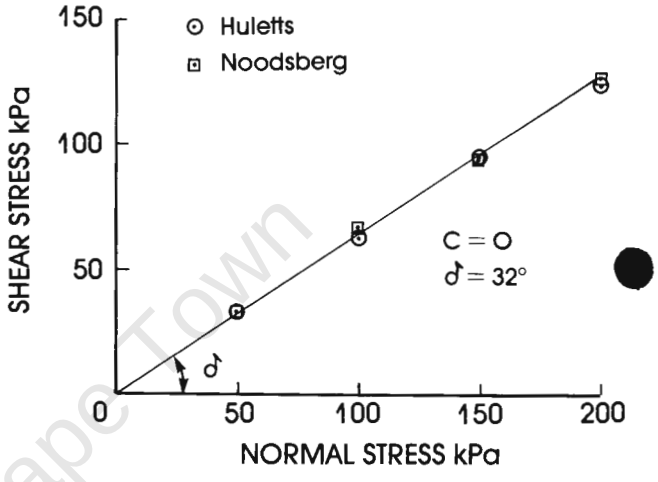

Fig. 2: Angle of wall friction — sugar on shot-blasted carbon steel painted with 75 μm dimetcote 4

3.4 Angle of Shearing Resistance φ

The shear box apparatus was also used to measure the angle of shearing resistance. The results of the measurements are shown in Fig. 3.

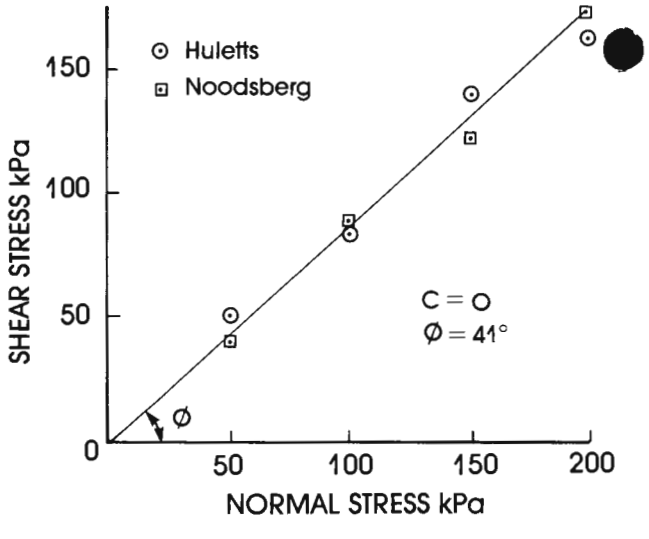

Fig. 3: Angle of shearing resistance of sugar

An angle of $\varphi = 41°$ represents a good average value for both sugars. Again, this series of tests indicates a linear relationship between the shear stress at failure in the sugar and the normal stress on the shear surface.

The active pressure coefficient K_A is given by:

$$K_A = (1 - \sin\varphi)/(1 + \sin\varphi) \quad (3)$$

which in this case has an average numerical value of 0.22.

3.5 Lateral Pressure Coefficient K_0

K_0 represents the ratio of horizontal to vertical stress in a material which is being compressed vertically with zero lateral strain. In a silo, during filling, the lateral pressure usually lies between K_A and K_0 times the vertical pressure, with K_0 defining the upper limit to the lateral pressure [1].

K_0 was measured in the laboratory by means of the triaxial apparatus [3]. The results of the K_0 measurement are shown in Fig. 4. The figure shows the relationship between the vertical stress and the corresponding horizontal stress under a condition of zero lateral strain. The slope of a straight line joining the origin to any measured point represents K_0. K_0 for both sugars averaged 0.55 for loading, but increased towards 1.0 during unloading.

For comparison, the active pressure line having a slope K_A is also shown in the figure.

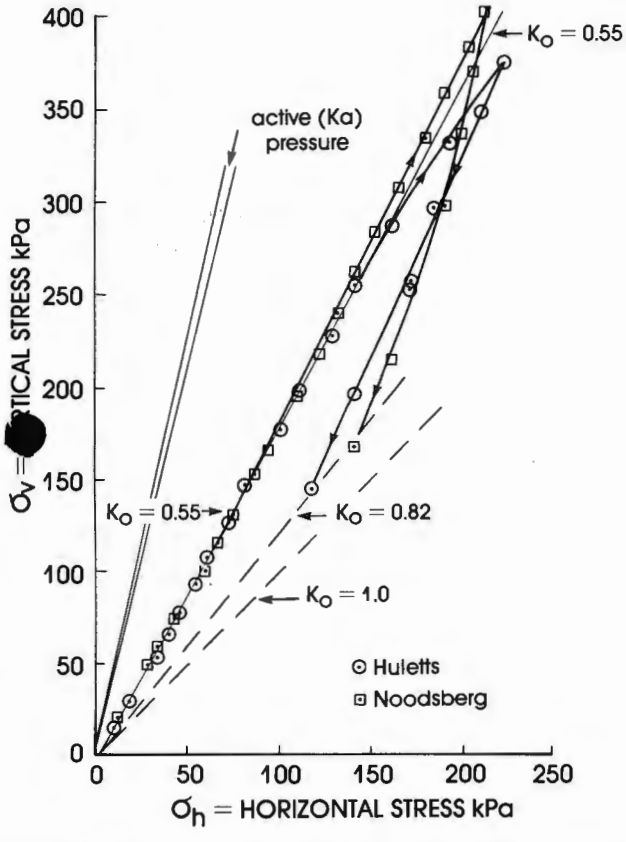

Fig. 4: Measurements of the lateral pressure coefficient K_0 of sugar

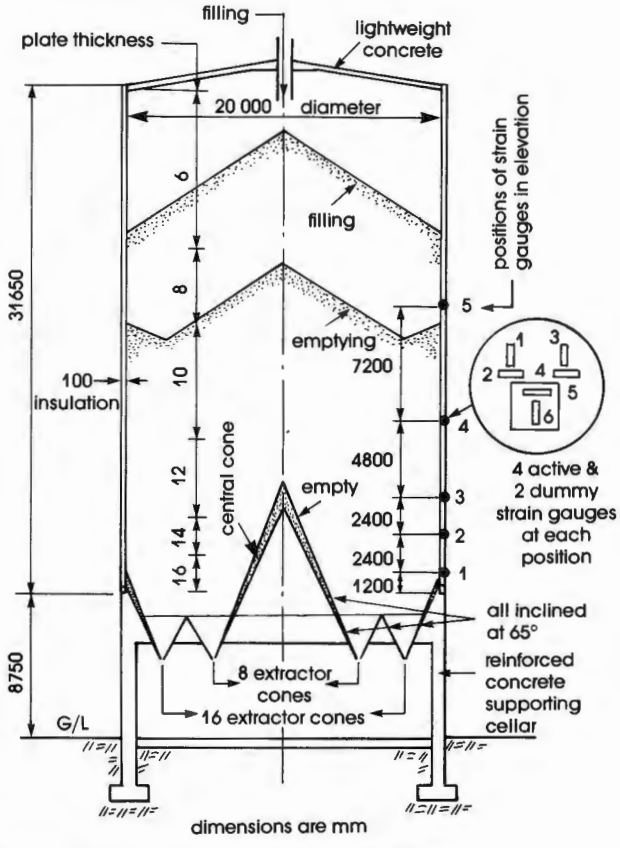

Fig. 5a: Layout of silo and instrumentation in elevation

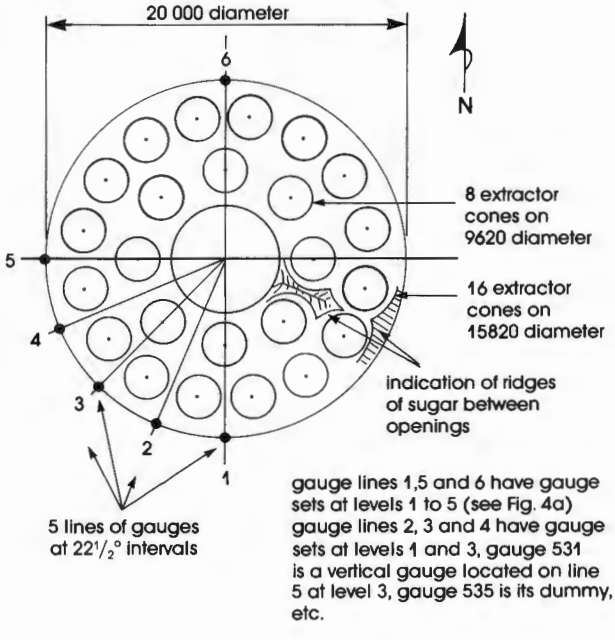

Fig. 5b: Layout of extractor cones in base of silo and layout of instrumentation in plan

4. Layout of Silo and Instrumentation

Fig. 5a shows the layout of the silo, its principal dimensions and plate thicknesses. Fig. 5b shows the arrangement in plan of the multiple extractor cones and the central deflector cone.

Also indicated in Fig. 5a are the shapes of the sugar surface during filling and emptying, as well as the layout of the instrumentation in elevation. The layout of the instrumentation in plan is shown in Fig. 5b.

The instrumentation at each location consisted of two pairs of strain gauges applied to the steel shell of the silo (see Fig. 5a). The gauges were read in conjunction with a set of dummy gauges mounted on a small separate steel plate, which was attached to the silo wall by means of adhesive foam strips so that it remained stress-free.

Each set of gauges was waterproofed with a rubber solution and protected by means of a galvanized sheet steel cover, also attached to the silo wall with adhesive foam strips. Each of the vertical and horizontal gauges was connected in turn with the same dummy gauge to form a half-bridge. The leads from the gauges were taken down the side of the silo to three reading points housed in the cellar. Static readings were taken by means of a Huggenberger strain bridge and dynamic strains were recorded on a Toa chart recorder connected to the Huggenberger bridge. The silo is insulated with 100 mm of polyurethane foam insulation within an outer cladding of ribbed aluminium sheeting. The strain gauges are therefore completely protected from the weather and well insulated from ambient temperature variations.

Fig. 6 is a general view of the silo while the gauges and the insulation were being installed. The vertical strips from which the insulation has been omitted mark the positions of the strain gauge lines.

Fig. 6: View of silo while instrumentation was being installed (note man on tenth level of scaffolding)

5. Interpretation of Strain Readings

It was assumed that the measured vertical and horizontal strains, ε_v and ε_h, represented principal strains. The vertical and horizontal stresses σ_v and σ_h in the silo plate were then calculated from:

$$\sigma_v = E\,(\varepsilon_v + \nu\varepsilon_h)/(1 - \nu^2) \quad (4a)$$

$$\sigma_h = E\,(\varepsilon_h + \nu\varepsilon_v)/(1 - \nu^2) \quad (4b)$$

where:

E — elastic modulus of steel (taken as 200 GPa)
ν — Poisson's ratio (taken as 0.33).

The wall load P_w per unit of circumference was then calculated from:

$$P_w = \sigma_v\, t \quad (5)$$

where:

t — plate thickness.

The horizontal stresses were interpreted as equivalent horizontal pressures p_h exerted by the sugar on the silo walls, via the equation:

$$p_h = 2\,\sigma_h\, t/D \quad (6)$$

where:

D — diameter of the silo shell.

This interpretation is not strictly correct as it assumes that p_h is uniform across a diameter of the silo. As will be seen later, p_h varies quite considerably around the circumference of the silo. For this reason, p_h will be referred to as the equivalent horizontal pressure.

6. Long-Term Stability of Instrumentation

Previous experience with strain gauge instrumentation had shown that newly applied gauges give varying zero readings for a period of about three weeks. After this period the zero readings remain stable to within a few tens of microstrain over long periods. The silo was filled for the first time starting in mid-October 1985 and was empty again in mid-May 1986, giving an opportunity to check on the zero readings. Most of the gauges returned to within 50 microstrain of their October 1985 readings. There were, however, a number of gauges for which the discrepancy was larger than this, for some unknown reason. The gauges appear still to be in good working order and a new zero was taken for measurements associated with the second filling of the silo.

Fig. 7 shows readings with time for a horizontal gauge (gauge 122) and a vertical gauge (gauge 611). The figure shows how readings on a typical horizontal gauge increase as the sugar level rises and hoop strain at that level increases and how readings on a vertical gauge decrease as the silo wall goes into compression under the increasing wall load.

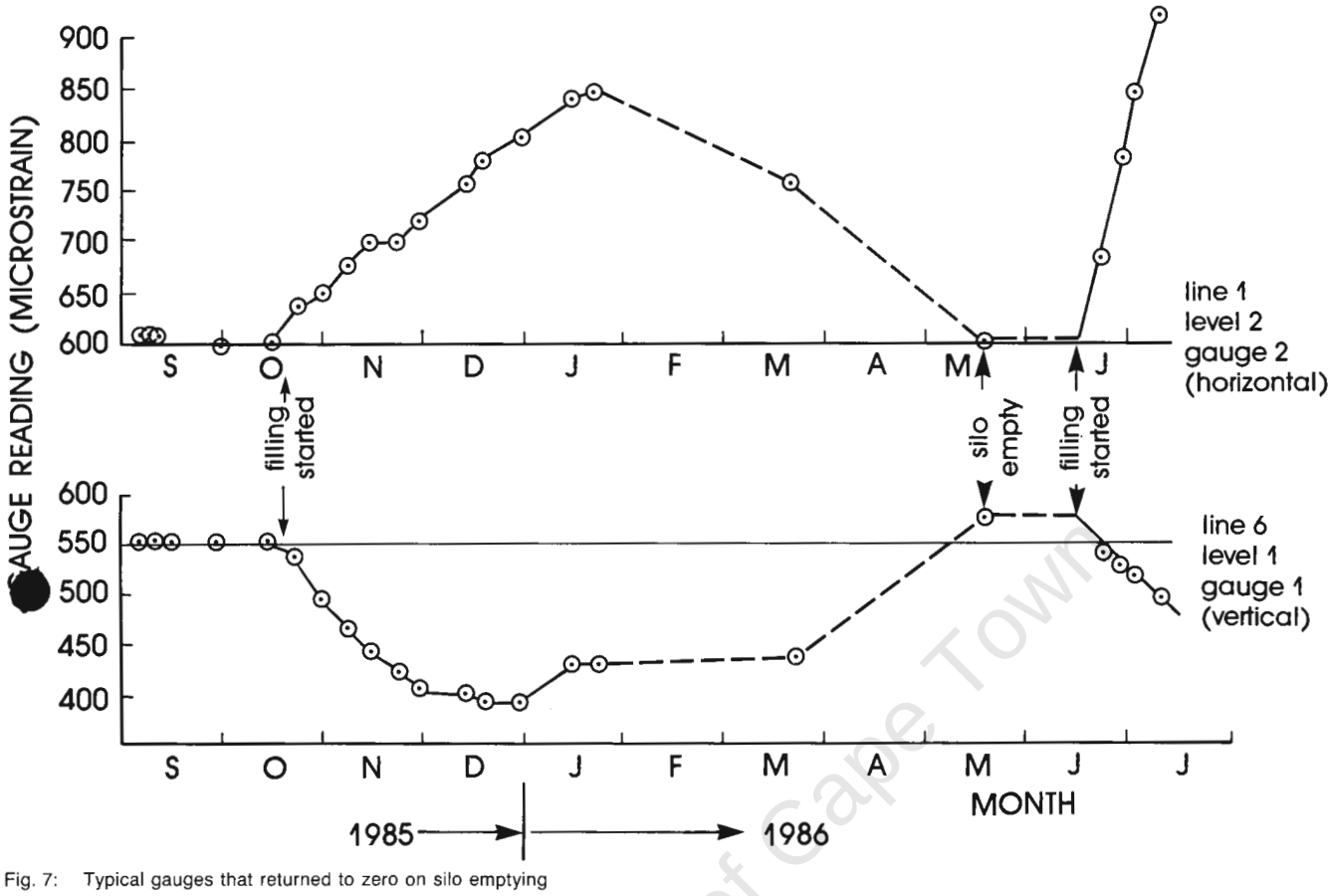

Fig. 7: Typical gauges that returned to zero on silo emptying

7. Profiles of the Sugar Surface in the Silo

A number of detailed measurements were made of the profile of the sugar within the silo to establish how concentric the filling and emptying of the silo are and to get some idea of the flow pattern within the sugar. These are summarized in Fig. 8.

The upper part of Fig. 8 shows two circumferential profiles measured 1 m in from the silo wall during filling and emptying. They show that the maximum deviation from a mean circumferential level is never more than 150 mm. Hence for both filling and emptying the surface is extraordinarily uniform.

The lower part of Fig. 8 shows cross-sections of the fill surface taken on north-south and east-west lines. The profiles measured during filling are completely symmetrical and the slope of the sugar surface (33° to 33.5°) is very close to the angle of repose of 34°±0.5° measured in the laboratory.

In the early stages of emptying (2 m drawdown) the sugar surface remains conical, but its angle flattens. As drawdown continues, a circumferential valley develops around a central cone. These two basic surface profiles are also shown in Fig. 5a.

It appears from the profiles that a "ring funnel flow" develops in the silo with the sugar moving most rapidly over the circles of extractor cones and least rapidly over the central deflector cone. The flow pattern, however, is almost perfectly symmetrical.

When the silo was empty in May 1986, the inside was inspected. It was found that, notwithstanding the steep 65° angle of the central deflector cone and the sides of the silo immediately above the floor, sugar had caked on the surface, at an angle estimated at about 70°. This caked material is indicated in Fig. 5a. Ridges of caked sugar had also formed between the extractor cones, as indicated in Fig. 5b. However, there is very little "dead" sugar in the silo which does not move during emptying.

8. Observed Equivalent Horizontal Pressures and Wall Loads

Fig. 9 shows the build-up of equivalent horizontal pressure and wall load measured at level 2 on lines 1, 5 and 6 (see Fig. 5) as the sugar overburden above this level increased. Reference to Fig. 5a will show that level 2 is well within the "live" sugar in the silo. Readings at level 1 have not been shown, as the gauges at level 1 may just lie within the zone of "dead" static sugar.

Measurements of equivalent horizontal pressure on lines 5 and 6 are consistent, one with the other, and indicate that the lateral pressure coefficient in the vicinity was intermediate between K_A and K_0. Similar observations have been made in other silos filled with various materials [1]. The equivalent horizontal pressure on line 1, however, was initially consistent with a lateral pressure coefficient K_A, but later, during filling, indicated a value of K considerably less than K_A.

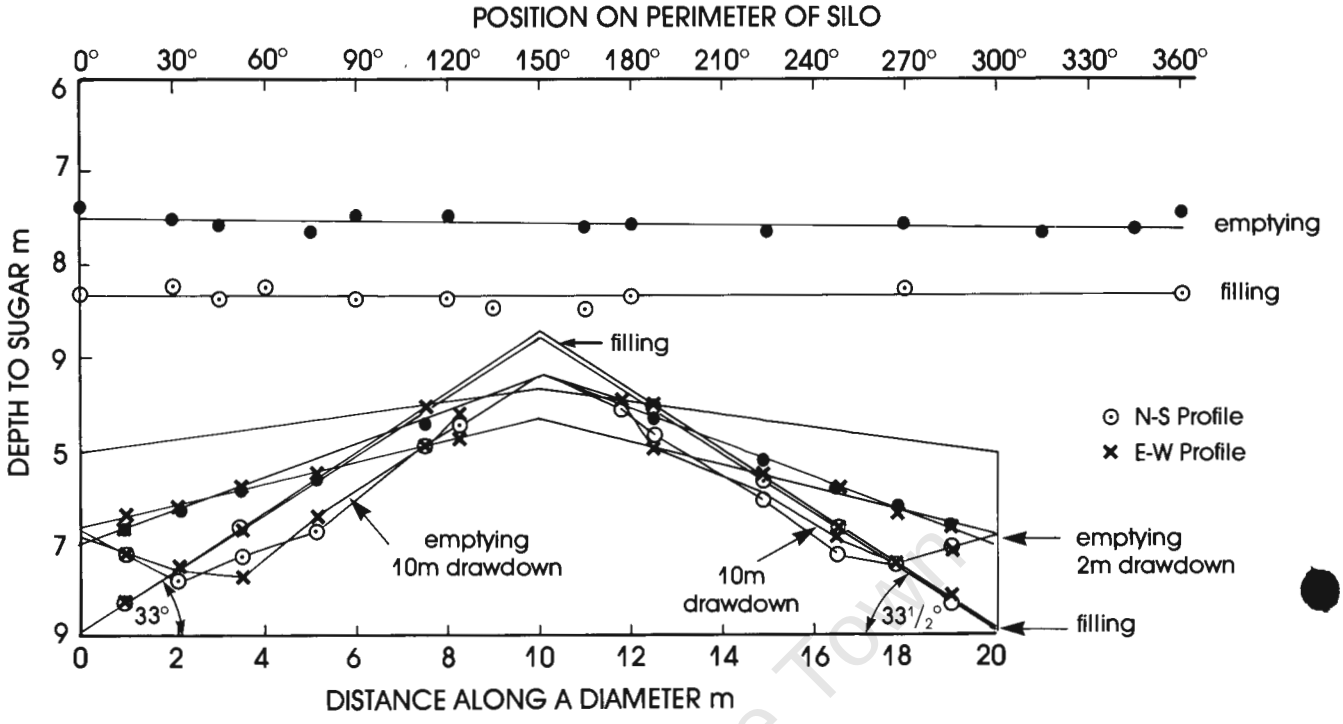

Fig. 8: Surface profiles during silo filling and emptying

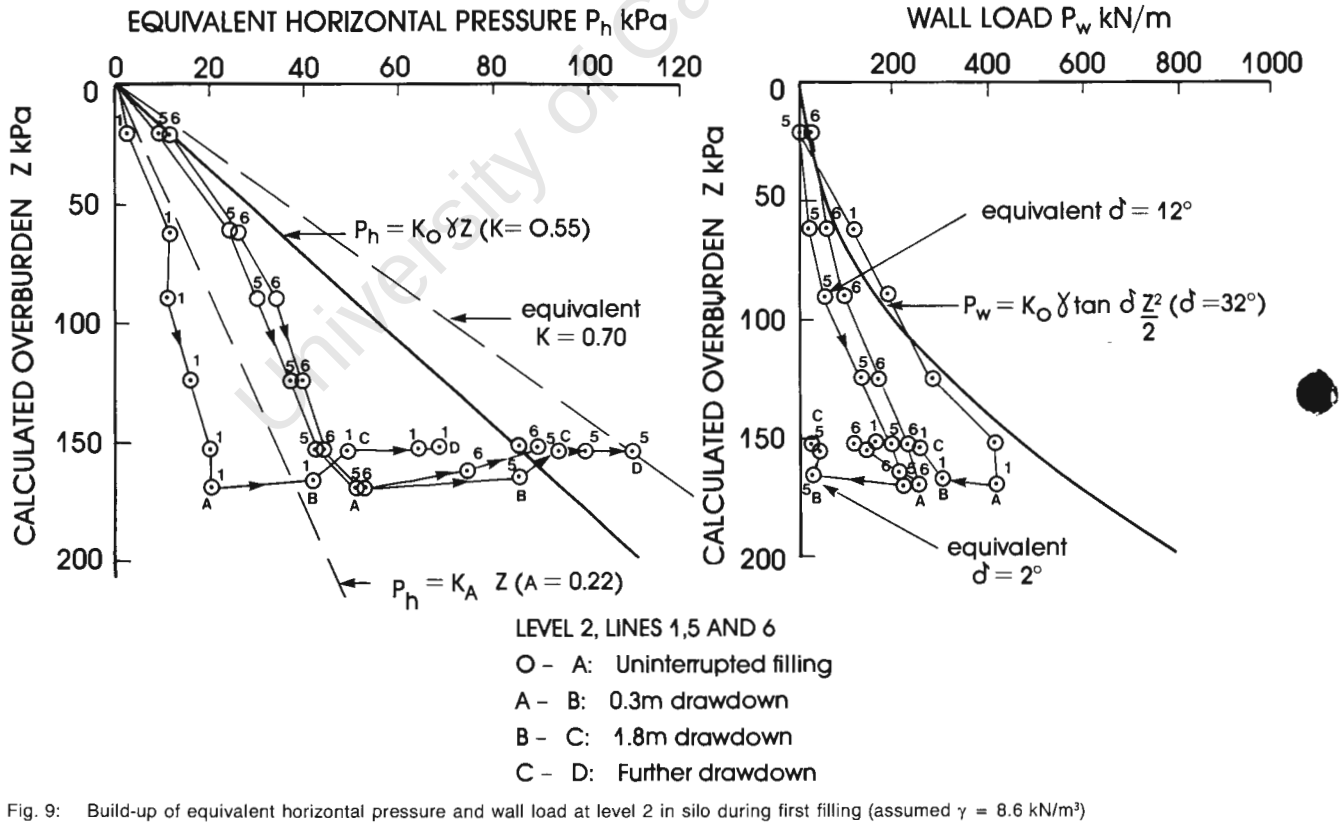

Fig. 9: Build-up of equivalent horizontal pressure and wall load at level 2 in silo during first filling (assumed γ = 8.6 kN/m³)

When emptying was started, p_h increased sharply at all three positions, with K on line 1 approaching K_0 and K on lines 5 and 6 reaching a value of 0.7.

The wall loads on lines 5 and 6 (Fig. 9) were also very similar. It is clear that full wall friction was not developed, but that the developed angle of wall friction was about 12°. On line 1, however, the measurements indicate that full wall friction was developed. The frictional load carried by the wall probably accounts for the low lateral pressure coefficient indicated by the measurements of p_h. The reason for the radial non-uniformity of the wall load is not known.

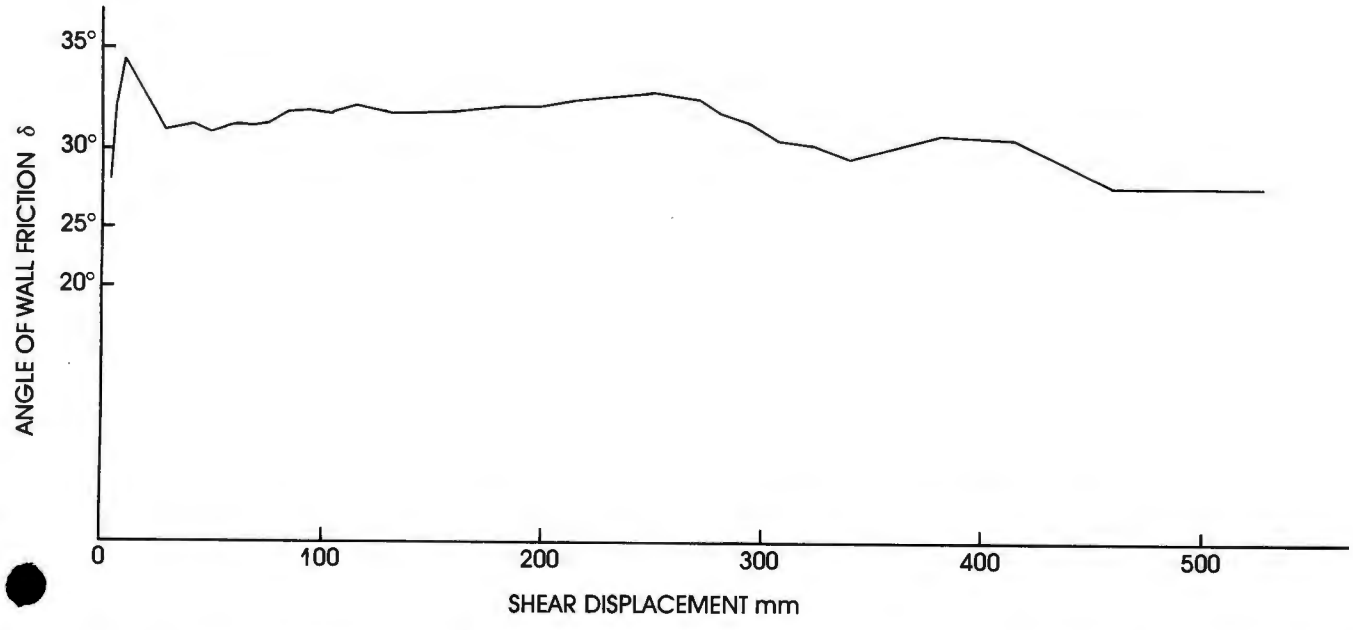

Fig. 10: Variation of angle of wall friction of sugar with shear displacement in a ring shear apparatus — shear velocity 300 mm/h; maximum shear velocity in silo 370 mm/h

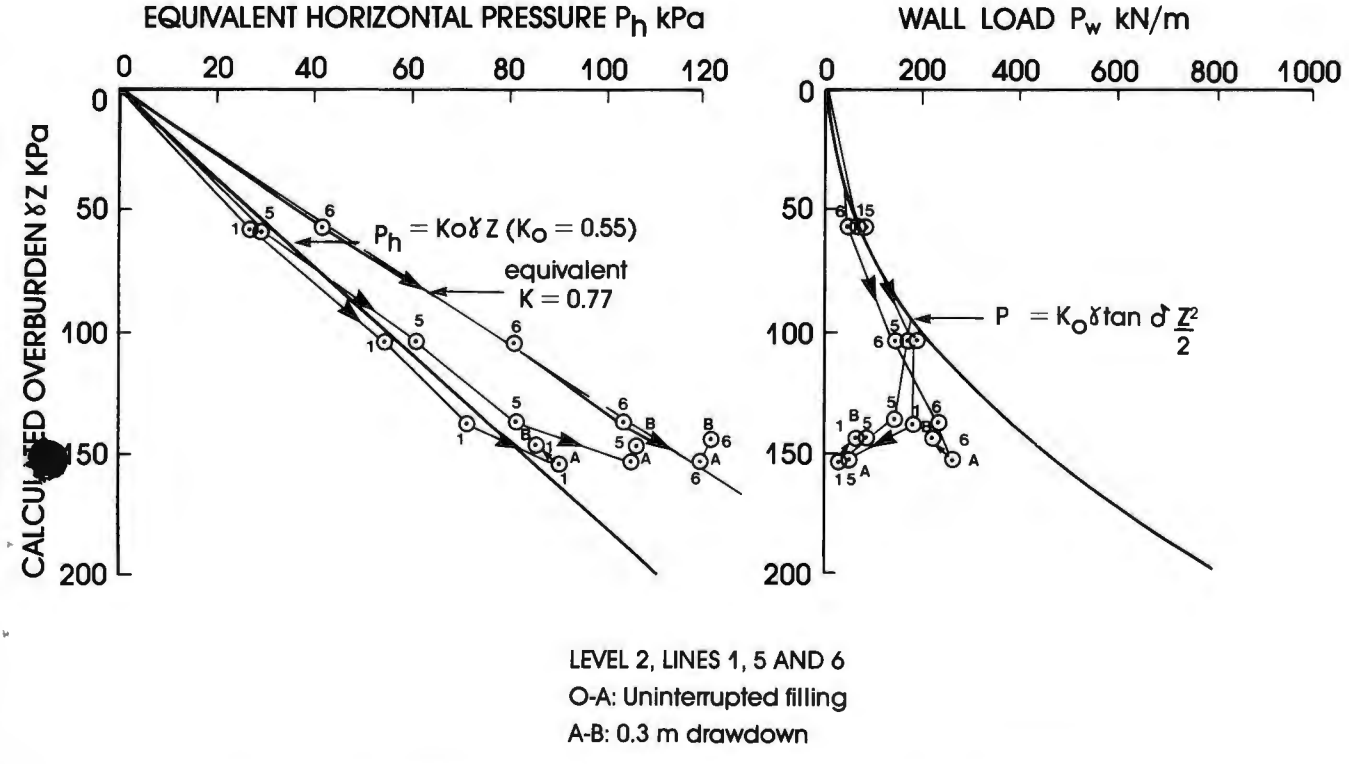

Fig. 11: Build-up of equivalent horizontal pressure and wall load at level 2 in silo during second filling (assumed γ = 8.6 kN/m³)

As soon as emptying began, the friction load declined to very low values on lines 1, 5 and 6. This is consistent with the corresponding increases in p_h, but also apparently anomalous in that, as the sugar moved downward relative to the silo walls, one would have expected the angle of wall friction to develop to a maximum. Instead, δ appeared to decline to a lower residual value. The shear box tests used to evaluate δ gave no indication that this apparent breakdown in δ was a possibility (Fig. 2).

Fig. 10 shows the results of tests in a ring shear apparatus to see whether the angle of wall friction declines at large shear displacements. The results showed no dramatic decrease such as that indicated by Fig. 9.

Fig. 11 shows data similar to those for Fig. 9 for the second filling of the silo. In this case, the data for lines 5 and 6 are very much closer together. During filling, the increase in p_h followed the K_0 line fairly closely at lines 1 and 5, with line 6 following a line equivalent to a value of K = 0.77.

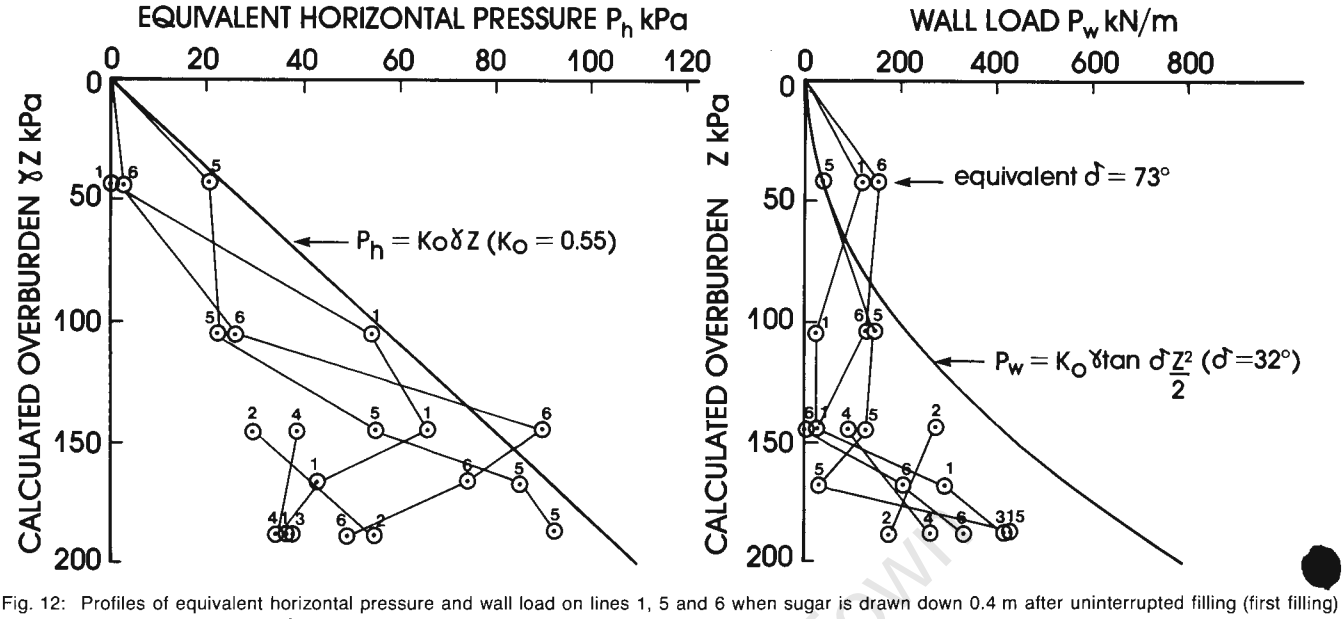

Fig. 12: Profiles of equivalent horizontal pressure and wall load on lines 1, 5 and 6 when sugar is drawn down 0.4 m after uninterrupted filling (first filling) (assumed γ = 8.6 kN/m³)

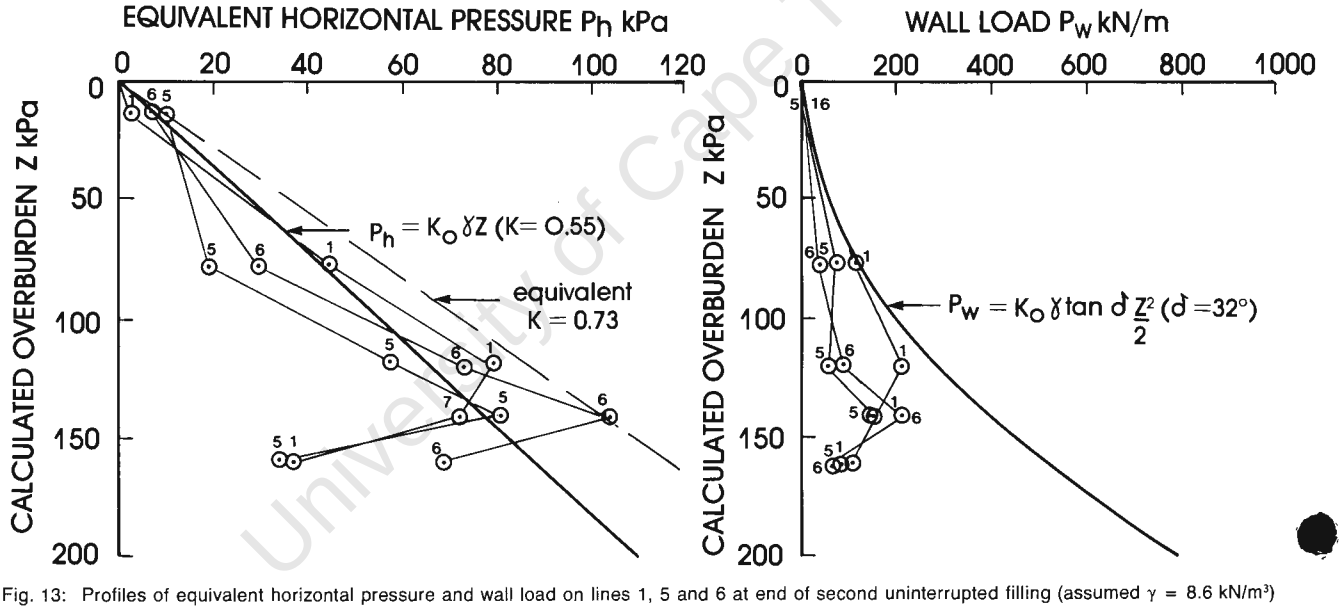

Fig. 13: Profiles of equivalent horizontal pressure and wall load on lines 1, 5 and 6 at end of second uninterrupted filling (assumed γ = 8.6 kN/m³)

When a small drawdown occurred at the end of filling, small increases of pressure were recorded at lines 5 and 6 and a small decrease at line 1.

The wall load was also very similar at all three positions and showed that almost the full angle of wall friction was being developed until the overburden exceeded 110 kPa. There was a decline in wall load at lines 1 and 5 towards the end of filling, which corresponded to a slight increase in p_h. At the start of emptying the wall load decreased, but not dramatically, as on the first emptying.

An apparently low value of K associated with high wall loads can be explained as the result of a reduction of vertical stress by load transfer into the wall. An apparently higher value during filling can only be explained in terms of a change in material properties — either an increase in unit weight or an increase in K_0. In this case, the unit weight would have had to increase to 12 kN/m³, which is probably not possible. However, an increase in unit weight to 10 kN/m³, together with an increase in K_0 to 0.66, would account for the discrepancy. Hence the result shown in Fig. 11 does not appear to need any special explanation.

Fig. 12 shows profiles of equivalent horizontal pressure and wall load for gauge lines 1, 5 and 6 and partial profiles for lines 2, 3 and 4 when the sugar had been drawn down by 0.4 m after the first filling. There is a lot of variation in the value of p_h at any level (as seen in Fig. 7), but the design profile of $p_h = K_0 \gamma z$ provides a reasonable envelope to the measured values. The wall loads also generally fall within the design envelope of $p_w = K_0 \gamma \tan\delta\, z^2/2$, although anomalous values were recorded on lines 1 and 6 at gauge level 5. The equivalent δ of 73° recorded at this level cannot be realistic.

Fig. 13 shows data similar to those of Fig. 12, at the end of the second uninterrupted filling. The form of the data is very similar to that shown in Fig. 12, except that the containing envelope to values of p_h corresponds to a higher value of K (0.73) (which is consistent with Fig. 11) and there are no anomalous wall load measurements.

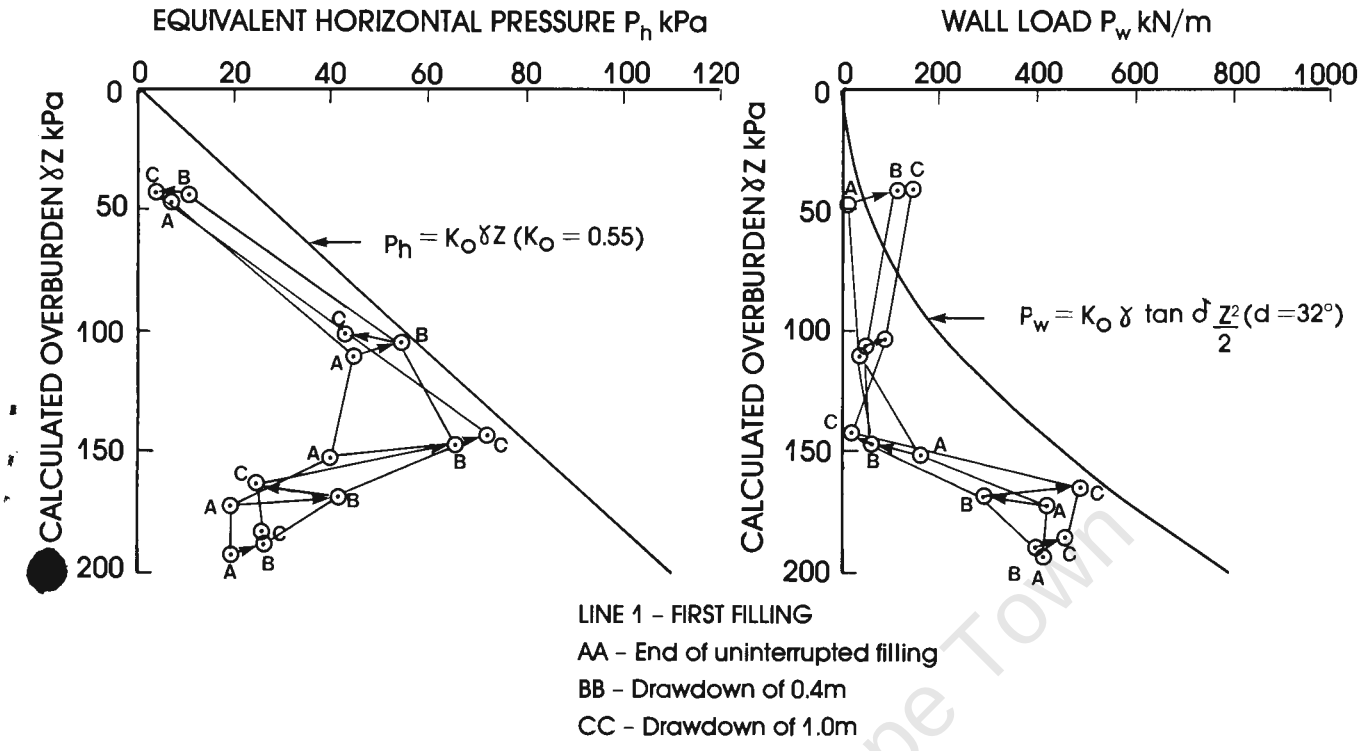

Fig. 14: Change in pressure profiles from condition at end of filling to start of emptying

Fig. 14 shows how the profiles of equivalent horizontal pressure and wall load in the silo varied from the end of the first uninterrupted filling to the start of emptying. The initial response to emptying is that equivalent horizontal pressures increase, accompanied by a simultaneous decrease in wall loads. Thereafter, horizontal pressures tend to decrease again, while wall loads show a corresponding small increase.

With the exception of the anomalous wall friction observations, the sugar behaved as expected and fairly closely as predicted from the measured properties.

Radial Variability of Equivalent Horizontal Pressures and Wall Loads

As already indicated by Figs. 9 to 14, equivalent horizontal pressures and wall loads in the silo were far from being radially uniform. The actual radial distributions of these two variables have been plotted in Figs. 15 and 16 for levels 1 and 3. The positions of the extractor cones in the outer circle have also been shown as it appeared possible that their positions might have some influence on the radial distribution of the horizontal pressure and hence of the wall load. As it happens, all of the gauge lines fall between the outer extractor cones; hence the positions of the cones cannot have influenced the strains.

Figs. 15 and 16 show measurements at two stages — at the end of uninterrupted filling and after a 0.4 m drawdown.

Measurements are shown for two levels in the silo — level 1, where the sugar in contact with the silo walls probably forms a dead zone, and level 3, which is in a live zone. As the figures show, the radial distribution of equivalent horizontal pressure and wall load is highly non-uniform. The distribution changes in going from the filling to the emptying condition, but the radial non-uniformity remains.

The explanation for this behaviour is obscure. It does not appear to arise from non-uniformities of either the filling or the emptying patterns. The only other likely explanation lies in non-uniformities of the texture of the silo plates. If this is the case, the effect can be expected to gradually disappear as the silo is used and the wall surface is abraded to a uniform texture.

Wall loads for the second filling (not shown due to lack of space) seem to be slightly more uniform than for the first filling.

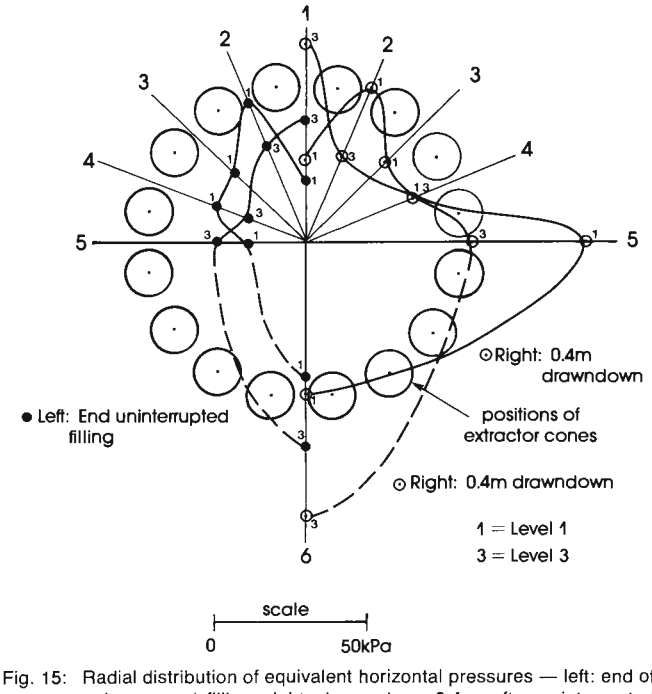

Fig. 15: Radial distribution of equivalent horizontal pressures — left: end of uninterrupted filling; right: drawn down 0.4 m after uninterrupted filling

Measurements made on subsequent fillings will show whether the silo characteristics do become more uniform in the longer term.

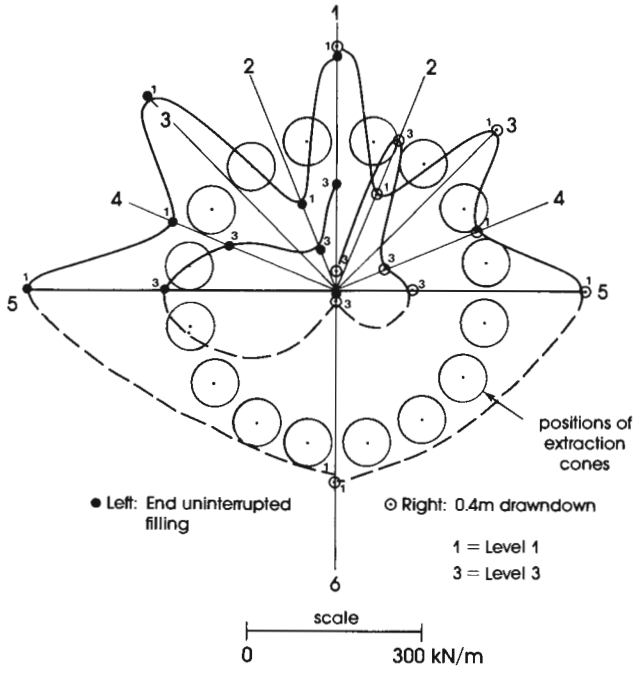

Fig. 16: Radial distribution of wall loads — left: end of uninterrupted filling; right: drawn down 0.4 m after uninterrupted filling

10. Dynamic Effects on Emptying

To study dynamic strain effects when sugar is drawn from the silo, the gauges on line 3, level 2, were connected through the strain bridge to a chart recorder. The results shown in Fig. 17 were recorded when sugar was first drawn from the silo after the completion of the first filling. While the fill is static, there is no significant variation in strain. When emptying was started, the recording shows a decrease in vertical strain (i.e. an increased compression), which indicates an increase in the wall load as the sugar moved downwards. This corresponds with a decrease in the horizontal strain, i.e. the equivalent horizontal pressure decreased as load was transferred onto the wall. When draw-off was stopped, both strains re-established themselves at a higher level. Note that in Fig. 17 two recorder chart speeds have been used. Note also that at this early stage of emptying the wall load was still increasing as the full angle of wall friction was developed. There was no evidence then of the dramatic decrease in wall friction shown in Fig. 9.

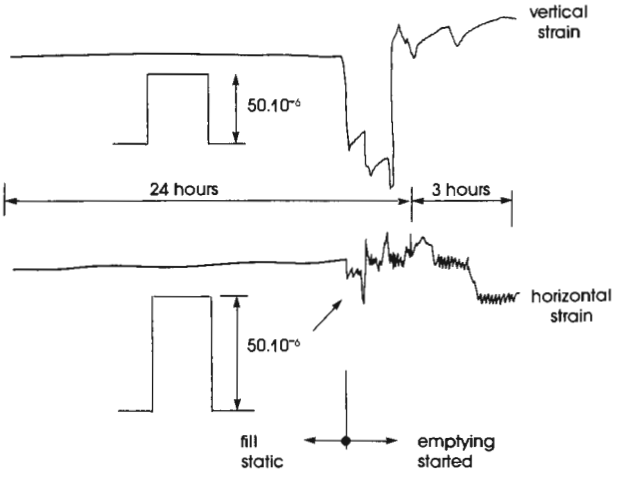

Fig. 17: Effect of emptying on vertical and horizontal strains at line 3, level 2

11. Conclusions

The measurements described in this paper have shown the following:

1. The behaviour of the sugar in the silo conformed quite closely with expectations at the design stage. The one unexpected aspect of its behaviour has been the large decrease in the wall load on emptying and the corresponding increase in equivalent horizontal pressure. Further research is required into this aspect of sugar properties.

2. Even though the silo is filled almost perfectly concentrically and the flow pattern during emptying is also concentric, wall loads and equivalent horizontal pressures were radially non-uniform on the first and second filling and emptying. It is expected that pressures will become more uniform as the walls of the silo are abraded to a uniform texture.

3. The most important conclusion is that the conditions assumed for design have largely been met in the silo. The critical case for design of the walls was the wall load. Wall loads were generally less than the design value. Equivalent horizontal pressures became greater than the design values during emptying and during the second filling. This should perhaps have been catered for by adopting a higher value for the unit weight of sugar for design purposes.

Acknowledgements

The study described here was made possible by the cooperation of and partial funding by the South African Sugar Association.

References

[1] Bl i g h t, G.E.: Pressures Exerted by Materials Stored in Silos — Part I: Coarse Materials, and Part II: Fine Powders; Geotechnique Vol. 36 (1986) No. 1, Jan., pp. 33 — 56.

[2] Bl i g h t, G.E.: Performance of a 20 m Diameter Steel Maize Storage Bin. Proc. 2nd Int. Conf. on Design of Silos for Strength and Flow, Powder Advisory Centre, 1983, London, pp. 179 — 191.

[3] Bl i g h t, G.E., and Z. O f e r: Laboratory Determination of K_0 and Comparison with Prototype Silo Observations. Proc. 4th Australia-New Zealand Conf. on Geomechanics, 1984, Perth, Vol. 1, pp. 83 — 87.

bulk solids handling Volume 8, Number 4, August 1988

Strains Measured in a 7,500 t Sugar Silo

Part II

G.E. Blight, South Africa

Summary

The paper describes the results of a further set of strain measurements on the walls of a free-standing cylindrical insulated steel sugar silo. The strains are interpreted in terms of the equivalent horizontal pressure exerted by the sugar, and the frictional load transferred into the silo walls. The paper provides further data to support measurements published earlier and illustrates some previously unsuspected and unrecorded aspects of the behaviour of this silo. In particular, these aspects are the effect of daily temperature changes on wall loads and horizontal pressures.

1. Introduction

A recent paper [1] described the results obtained from strain measurements made on a 7,500 t capacity free-standing cylindrical steel sugar silo. The measurements reported then related to the first and second annual fillings of the silo and the following conclusions are quoted from that paper:

1. The behaviour of the sugar in the silo conformed quite closely with expectations at the design stage. The one unexpected aspect of its behaviour was the large decrease in the wall load on emptying and the corresponding increase in equivalent horizontal pressure. Further research is required into this aspect of sugar properties.

2. Even though the silo is filled almost perfectly concentrically and the flow pattern during emptying is also concentric, wall loads and equivalent horizontal pressures were radially non-uniform on the first and second filling and emptying. It was expected that pressures will become more uniform as the walls of the silo are abraded to an even texture.

3. The most important conclusion was that the conditions assumed for design had largely been met in the silo. The critical case for design of the walls was the frictional wall load. Wall loads were generally less than the design values.

Dr. Geoffrey E. Blight, Professor of Construction Materials, University of the Witwatersrand, Johannesburg. Department of Civil Engineering, P.O. Wits, 2050, Republic of South Africa.
The first part of this paper was published in *bulk solids handling* Vol. 7 (1987) No. 4, pp. 573–582.
Manuscript received: March 14, 1988

Equivalent horizontal pressures became greater than the design values during emptying and during the second filling. This should perhaps have been catered for by adopting a higher value for the unit weight of sugar for design purposes.

The purpose of the present paper is to present the results of strain measurements made during the third annual filling of the silo, and to consider these results in relation to the above conclusions. Also, quantitative credibility of the measurements will be considered in the light of appropriate laboratory measurements of the properties of sugar.

A full description of the insulated silo and its instrumentation was given earlier [1]. For the present purpose, Fig. 1 shows the layout and principal dimensions of the silo both in elevation and in plan, as well as the location of the measurement points.

As explained in the earlier paper, each strain that is converted to a corresponding stress is the average reading of two strain gauges. It has been assumed that the measured vertical and horizontal strains ε_v and ε_h represent principal strains in the silo wall. The vertical and horizontal stresses in the silo wall were calculated from:

$$\sigma_v = \frac{E(\varepsilon_v + \upsilon\varepsilon_h)}{(1 - \upsilon^2)} \quad (1a)$$

$$\sigma_h = \frac{E(\varepsilon_h + \upsilon\varepsilon_v)}{(1 - \upsilon^2)} \quad (1b)$$

where:

E: elastic modulus of steel (taken as 200 GPa)
υ: Poisson's ratio (taken as 0.33).

The wall load P_w per unit of circumference was taken as

$$P_w = \sigma_v t \quad (2a)$$

where t is the plate thickness.

The horizontal stresses were interpreted as equivalent horizontal pressures p_h exerted by the sugar on the silo walls, via the equation:

$$p_h = \frac{2\sigma_h t}{D} \quad (2b)$$

where D is the diameter of the silo shell.

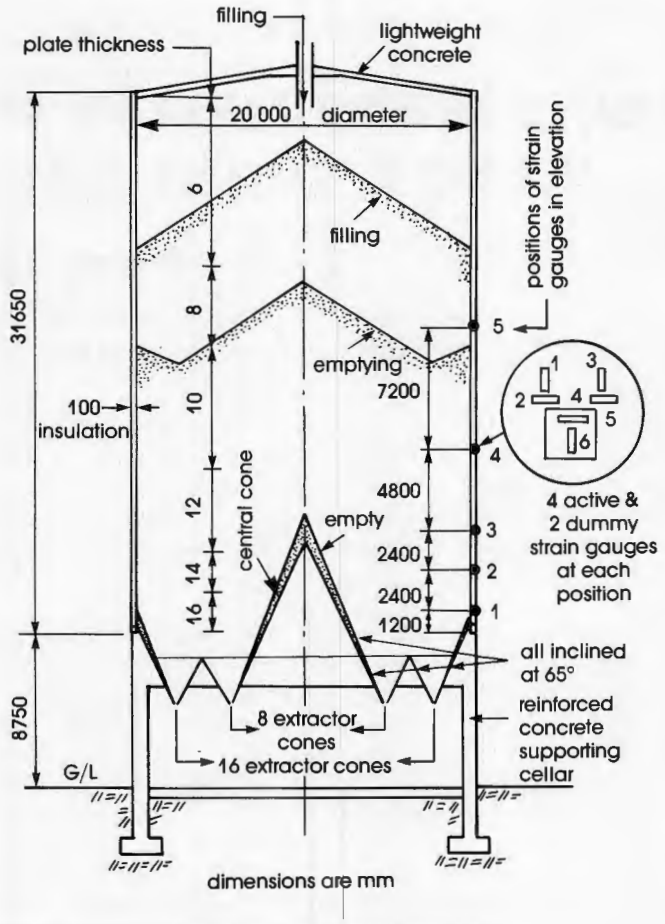

Fig. 1a: Layout of silo and instrumentation in elevation

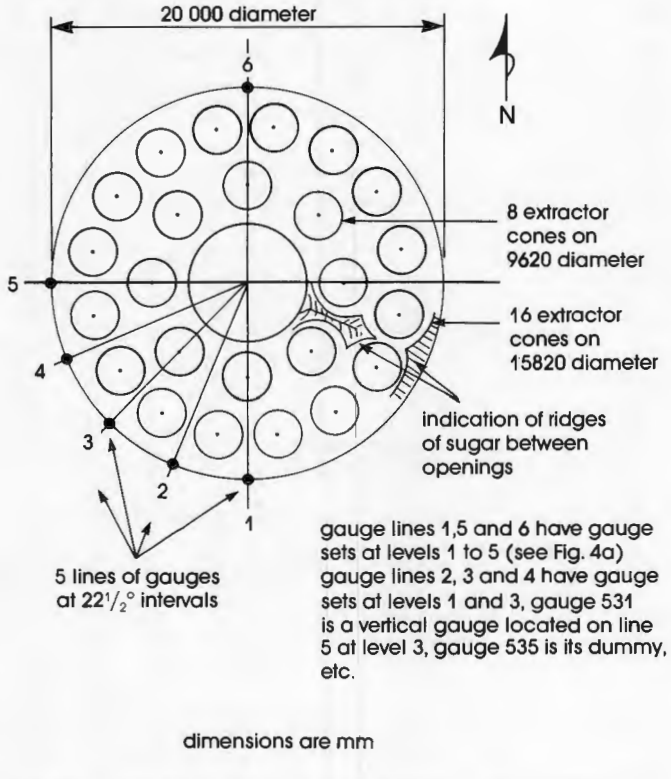

Fig. 1b: Layout of extractor cones in base of silo and layout of instrumentation in plan

The properties of the sugar as established in the laboratory and given in the earlier paper [1] were as follows:

Moisture content: 0.03 to 0.04%
Unit weight γ: 8.6 kN/m^3
Angle of wall friction δ: 32°
Angle of shearing resistance ϕ: 41°
At rest lateral pressure coefficient K_o: 0.55
Active lateral pressure coefficient K_A: 0.22.

More recent tests have shown that the properties of sugar produced by a single mill may vary from season to season. The following variations in sugar properties have been observed:

Moisture content: 0.03% to 0.10%
Unit weight γ: 8.3 kN/m^3 to 9.9 kN/m^3
Angle of wall friction δ: 22° to 39°
Angle of shearing resistance ϕ: 35° to 41°
At rest lateral pressure coefficient K_o: 0.44 to 0.55
Active lateral pressure coefficient K_A: 0.22 to 0.27.

2. Variation of K_o With Time Under Load

During the second filling of the silo, it appeared that the at-rest-pressure coefficient K_o could be as high as 0.77, as compared with the 0.55 measured in short-term laboratory tests. A possible explanation of this was that K_o for sugar might be time-dependent and might increase with time under load.

A second possible explanation is that the unit weight of the sugar was larger than that assumed. To account for a value of K_o as high as 0.77, the unit weight would have had to be as high as 12 kN/m^3 which does not appear likely, even considering the observed variations of this property. A higher unit weight may, however, be a partial explanation for the higher lateral pressures.

A special test was set up to measure K_o under long-term sustained loading. The strain-gauged oedometer technique described by Blight and Ofer [2] was used. The results of this test are shown in Fig. 2. As the diagram shows, there were slight random fluctuations in the measured value of K_o, but over a period of nearly 60 days under constant load there was no tendency for K_o to increase. The value at the end of the loading period was 0.54 which is very close to the mean value of 0.55 measured earlier in short term tests. The explanation of the high apparent lateral stress ratios must therefore be sought in a different direction.

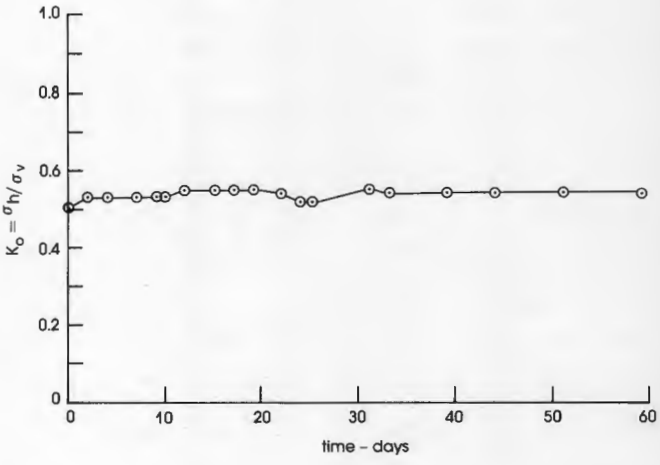

Fig. 2: Variation of K_o for sugar with time under constant load

Fig. 3 shows a third possible explanation: the lateral pressure coefficient K_o is usually taken as the ratio of horizontal to vertical principal stresses. The diagram shows a Mohr stress circle with principal stresses p_{ho} and p_v scaled to correspond to $K_o = 0.50$. The circle which is tangent to the Mohr failure envelope has a ratio of p_{hA} to p_v equal to K_A, the active pressure coefficient (0.33 in this case). As the diagram shows, if the vertical and horizontal stresses are not principal stresses (and they will not be principal stresses if there are wall friction stresses) — then the ratio of horizontal to vertical stress may exceed K_o. In the example shown the ratio p^*_{ho} to p^*_{vo} is 0.71. Hence the presence of wall friction may result in unexpectedly high values of the lateral pressure coefficient adjacent to the walls of a silo. However, as will now be seen, there is a fourth possible explanation that appears even more likely in the present case.

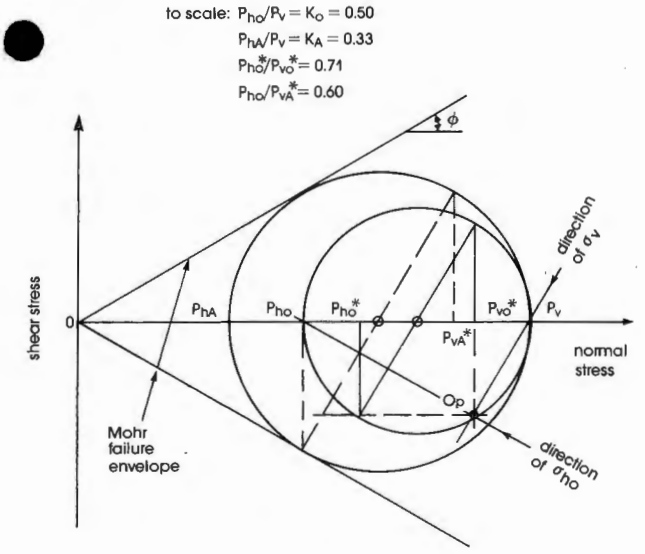

Fig. 3: Mohr diagram illustrating how $K = p_h/p_v$ can exceed either K_A or K_o, even though the principal stress ratios equal either K_A or K_o

3. Expected Pressures and Wall Loads

In the absence of arching, one would conventionally expect the equivalent horizontal pressure to increase roughly linearly with increasing overburden stress (γz) and to lie between the limits defined by

$$p_h = K_A \gamma z \quad (3a)$$

$$p_h = K_o \gamma z \quad (3b)$$

The sugar is deposited into the silo in an active stress state and as it is compressed by the increasing overburden, the stress state moves towards the at-rest condition. This occurs because the lateral strains possible in the ensiled fill are less than those necessary to maintain the active stress state. Any friction between the walls and the sugar tend to modify the increase of p_h with z. If the full angle of wall friction δ develops between the sugar and the wall, the horizontal pressure can be expected to develop according to the Janssen curve, in this case, the wall load P_w would develop according to the equation

$$P_w = \frac{K_o \gamma \tan \delta z^2}{2} \quad (4)$$

It is quite possible that less than the full angle of wall friction will develop in which case the wall load will be less than that indicated by Eq. 4. Alternatively, if the lateral pressure coefficient K is less than K_o, the wall load will be less than that predicted by Eq. 4.

4. Strains Measured During Third Annual Filling

Figs. 4, 5 and 6 show the build-up of equivalent horizontal pressure and wall load in the silo as it was filled without interruption from empty for the third time.

Fig. 4 shows the build-up of equivalent horizontal pressure and wall load at level 3 on instrument lines 1, 2, 4, 5 and 6 (the gauges on level 3, line 3 were not in working order).

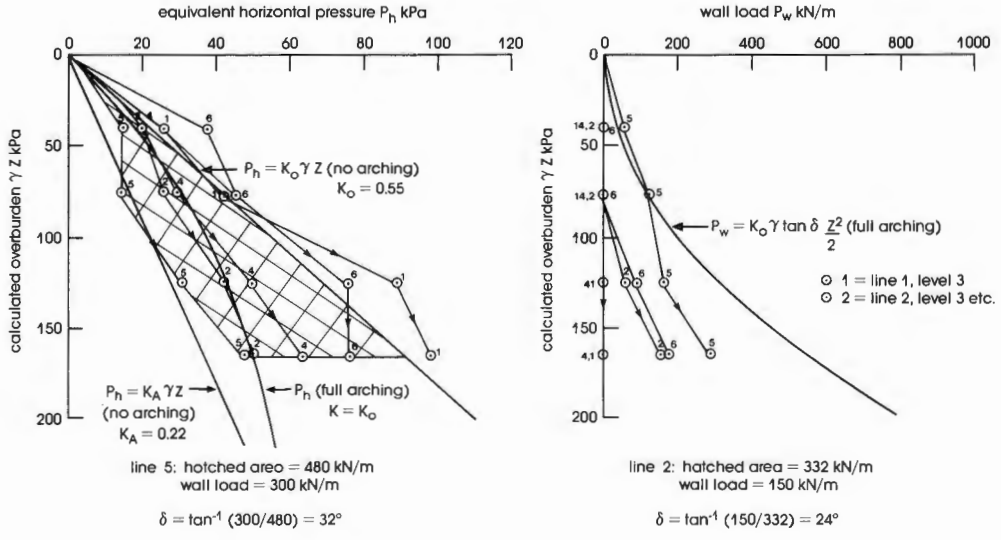

Fig. 4: Build-up of equivalent horizontal pressure and wall load at level 3, lines 1, 2, 4, 5 and 6 during uninterrupted filling

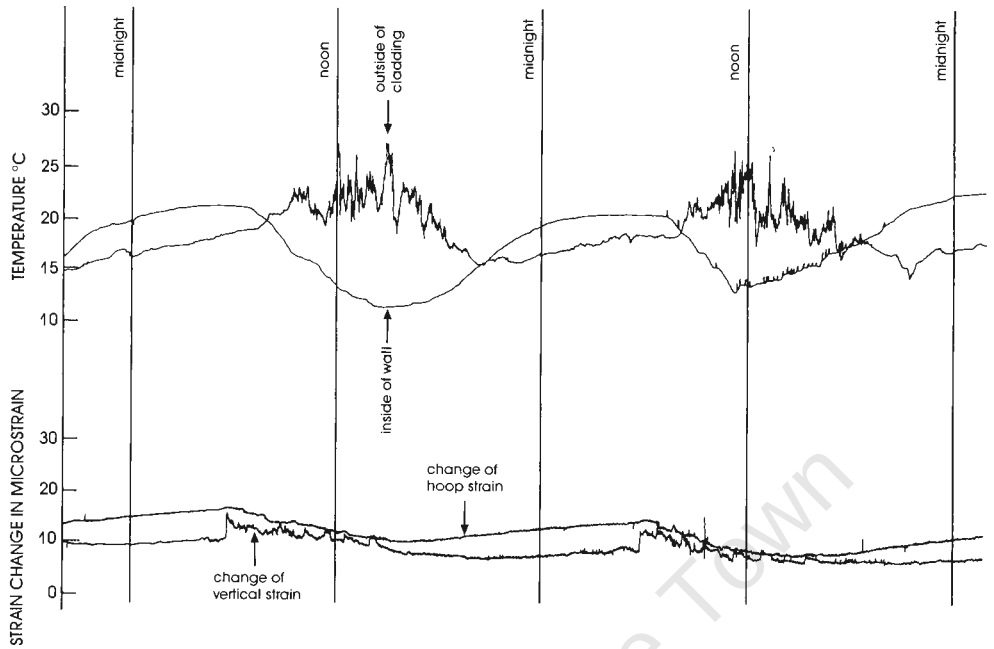

Fig. 5: Continuous record of temperatures of silo wall and outside of cladding and hoop and vertical strains

4.1 Wall Loads

An interesting feature of the present set of measurements was that no frictional wall load appeared to develop throughout the filling process at gauges 1 and 4, while only limited wall friction developed at gauges 2 and 6. The observation of zero wall load did not mean that there was no vertical strain in the wall at these points, but referring to Eq. 1a, that

$$\varepsilon_v < -\upsilon\varepsilon_h \qquad (1c)$$

Reasonably large wall frictions were observed at line 5, but these were also less than the theoretical maximum wall loads.

The phenomenon of zero wall friction was quite unexpected, but has occurred repeatedly during this set of measurements. Zero wall loads were not recorded in previous measurements on the silo, although unexpectedly small wall frictions were recorded.

The unexpected observations did not result from faulty instruments, because later measurements with the same strain gauges showed wall loads of a more expected magnitude. The most likely explanation appeared to be one of daily temperature change. This possibility had not previously been considered because the silo is insulated and it had been assumed that the inner structural wall of the silo would only be affected by slow seasonal temperature changes. When it was suspected that temperature changes in the silo wall were not negligible, thermocouples were attached to the inner wall and to the adjacent outside of the cladding. Fig. 5 shows a pair of continuous temperature recordings on the cladding and structural wall. As the figure shows, the peak temperature of the steel wall lags behind that of the cladding by 10 to 14 hours. Also, the amplitude of temperature change of the wall is almost the same as that of the cladding. Most of the readings in the present series of tests were taken in the early to mid afternoon. This was purely for convenience. The effect of this was that the wall was always about 10°C cooler when the strains were measured than it would have been about midnight.

The physical effect of this 10° temperature change would have been that the wall daily tried to shorten by a maximum of about 3 mm. This shortening would have been resisted by friction between the sugar and the wall with the result that the wall friction would have been considerably reduced.

The phenomenon of low or even tensile wall loads induced by diurnal low temperatures has previously been observed on uninsulated steel silos, e.g. [3]. This appears to be the first time that similar effects have been recorded on an insulated steel silo.

Fig. 6 shows the relationship between shear displacement and shear stress in a laboratory test to measure the angle of wall friction of sugar against steel. As the figure shows, 1 mm of relative displacement is enough to account for most of the wall frictional stress. A 1 to 2 mm vertical contraction of the wall would have been enough virtually to nullify the wall frictional load.

4.2 Horizontal Pressures

On instrument line 4 (see Fig. 4) the equivalent horizontal pressure increased linearly, with a lateral pressure coefficient greater than K_A but less than K_o. On line 1, however, the equivalent lateral pressure increased with a lateral pressure coefficient that exceeded K_o. This implies either that lateral strains were restricted in the vicinity of line 4 or that the unit weight of sugar may have been greater than that assumed. It appeared likely that horizontal compressional strains had occurred as a result of the same thermal contraction of the silo wall that had resulted in the reduced frictional wall loads.

Fig. 5 also shows a continuous record of horizontal and vertical strain variations caused by the varying temperature

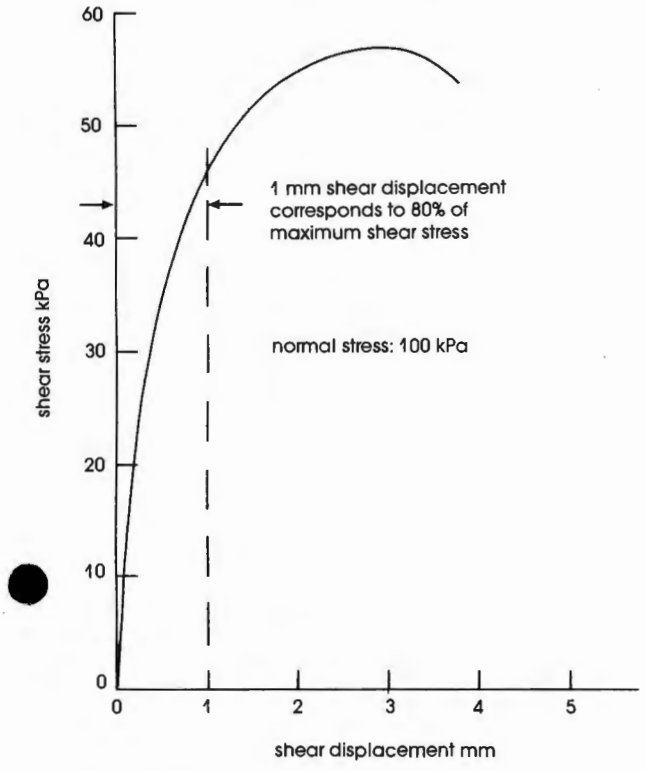

Fig. 6: Shear stress/displacement curve for sugar on steel plate

of the silo wall. The measurements were made on line 6 at level 3. This is on the same vertical line as the thermocouples, but some 25 m below their points of attachment. The two positions were separated because of difficulty of access. No sugar was loaded into or withdrawn from the silos while the measurements of Fig. 5 were being made, hence the strain changes are purely due to temperature effects.

If it is accepted that the form of the temperature wave at level 3 is the same as that measured higher up on the wall, the wall load and horizontal pressure variations caused by the temperature changes can be calculated from Eqs. 1 and 2. The actual strains occurring in the wall were of the order of 10×10^{-6} whereas the free temperature strains would be about 110×10^{-6}. Hence the silo contents are causing prevented strains in the horizontal and vertical directions of about 100×10^{-6}. If these strains are transposed into horizontal pressure and wall load via Eqs. 1 and 2, it will be seen that the horizontal pressure may vary by 40 kPa and the vertical wall loads by 400 kN/m as a result of the temperature variation.

If these variations are compared with the theoretical values of horizontal pressure and wall load shown in Fig. 4 it will be seen that they can easily account for the observed phenomena of zero wall load and larger than expected horizontal pressure. This observation does not invalidate the results of the strain measurements, as all were taken at approximately the same temperature. It does illustrate, however, that temperature effects may be just as important as the effects of materials loading.

4.3. Credibility of Measurements

In the left hand diagram of Fig. 4, the area between the line $p_h = K_o \gamma z$ and a line such as that for line 5 can be interpreted as representing the reduction in horizontal load transferred by the sugar to the wall of the silo, per metre width of wall, by the effects of wall friction. This would apply if in the absence of wall friction, the pressure line 5 would have followed the line $p_h = K_o \gamma z$.

The hatched are in Fig. 4 represents a horizontal load of 480 kN/m width of silo wall down to a level representing an overburden stress of 165 kPa (a depth of 165 kPa/8.6 kN/m^3 = 19.2 m).

The corresponding wall load at this level was 300 kN/m. Hence the equivalent angle of wall friction is given by

$$\delta = \arctan\left(\frac{300}{480}\right) = 32°$$

Repeating the exercise for the area up to line 2 gives

$$\delta = 24°$$

Both are credible average values for δ as compared with the 22° to 39° measured in the laboratory. Hence in this light the measurements shown in Fig. 4 appear qualitatively credible.

Note that the calculation just described depends on the assumption that the equivalent horizontal pressure line lies below the line defined by Eq. 3 because of the effects of wall friction. This assumption obviously cannot apply in a case such as line 6, where wall friction was recorded, but the horizontal pressure line lay beond the $K_o \gamma z$ line.

5. Other Measurements

Fig. 7 shows the build-up of equivalent horizontal pressure and wall load on gauge line 1 at levels 1, 2, 3 and 4, while the silo was being filled without interruption.

The equivalent horizontal pressure at level 1 lies below the line defined by Eq. 3. This is because of the proximity of the floor of the silo. It should also be noted that line 3 on Fig. 7 appeared as line 1 on Fig. 4.

Once again, the phenomenon of zero measured wall friction is apparent in the observations taken at levels 3 and 4, although significant wall friction developed at levels 1 and 2. This is not inconsistent, as levels 2 and 1 lie successively below levels 4 and 3, and at any time, the wall load at level 1 exceeded that at level 2. At points marked "A" on Fig. 7 filling was completed and a small tonnage of sugar was then withdrawn from the silo. It will be seen that the wall friction at levels 1 and 2 showed an immediate decrease while the equivalent horizontal pressure at level 1 increased. This pattern of stress change has been observed before [1]. However, at level 2 the reverse occurred — a slight decrease of wall load was accompanied by a decrease of equivalent horizontal pressure.

At levels 3 and 4, withdrawal of sugar produced quite large values of wall friction with simultaneous decreases in horizontal pressure (paths "AB" on Fig. 7). This occurrence confirms that the strain gauges were fully operational, and that the earlier absence of wall friction was not the result of an instrument problem.

The quantitative credibility of the measurements shown in Fig. 7 can further be checked by calculating the angle of wall friction as was done for Fig. 4. For level 1, δ was calculated as 26° and 32.6° for level 2. Both are quite credible values.

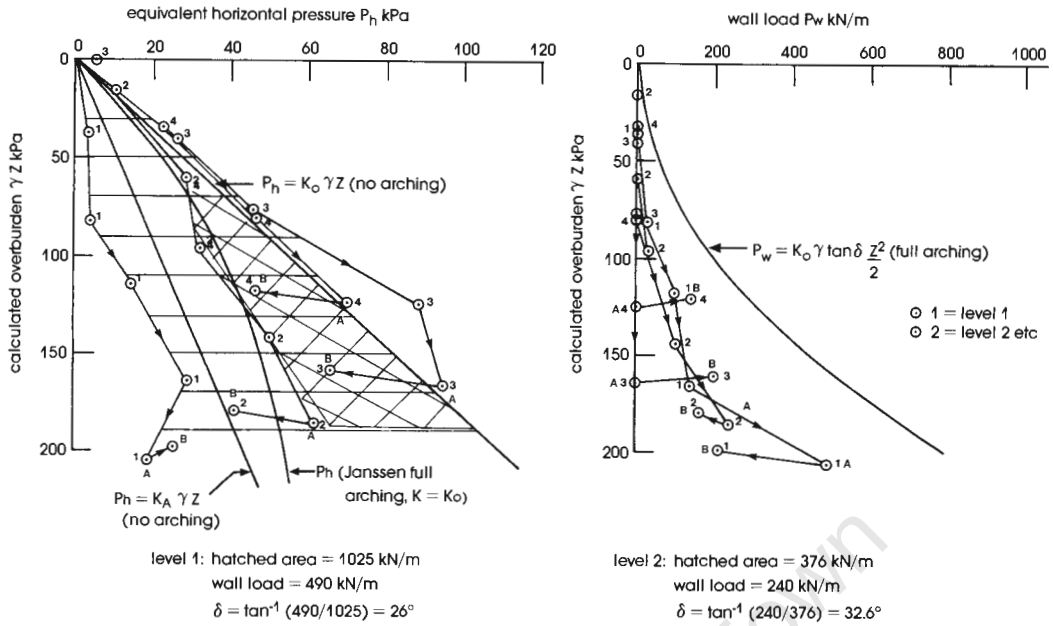

Fig. 7: Build-up of equivalent horizontal pressure and wall load on line 1, levels 1, 2, 3 and 4 during uninterrupted filling (from O to *A*)

Fig. 8 shows profiles of equivalent horizontal pressure and frictional wall load drawn for gauge lines 1, 5 and 6 when the fill reached maximum height after uninterrupted filling from empty. The profiles are very similar to those recorded at the end of the first and second fillings of the silo [1]. The figure also records angles of wall friction calculated on the same basis as for Figs. 4 and 7. Quite reasonable values were derived for δ for lines 5 and 6. The check on credible values for δ does not, however, apply to the profiles for line 1.

The final set of measurements is shown in Fig. 9. This represents a similar set of profiles to those shown in Fig. 8, with the fill at maximum height, but during recirculation of the sugar with simultaneous filling and emptying. A comparison of Figs. 8 and 9 shows that as a result of the recirculation, frictional wall loads have generally increased while horizontal pressures have decreased. Some of the wall loads now exceed the theoretical upper limit given by Eq. 4. As recorded on Fig. 9, the frictional wall load now appears to exceed the reduction in normal load assumed to be caused by the friction.

Movement of the sugar in the silo as a result of emptying would nullify the effects of temperature in two ways:

1. by allowing sugar to move downwards relative to the wall it would allow normal wall friction to develop, and
2. it would allow the lateral pressure coefficient to adopt a normal (lower) value.

Both of these effects are evident in Fig. 9.

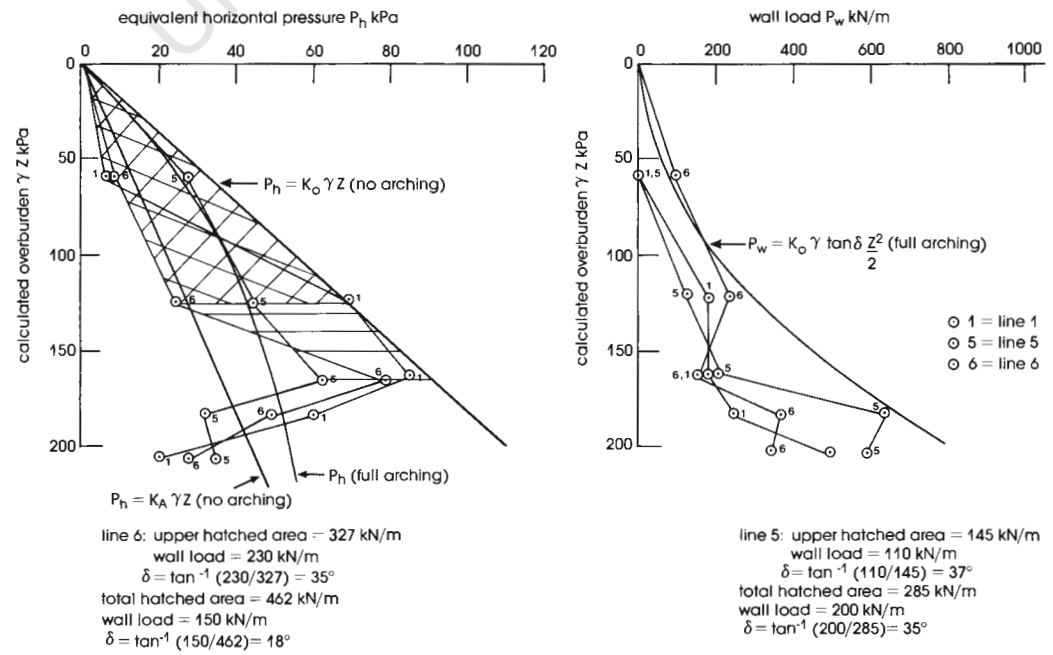

Fig. 8: Fill at maximum height after uninterrupted filling — profiles of equivalent horizontal pressure and frictional wall load on line 1, 5 and 6

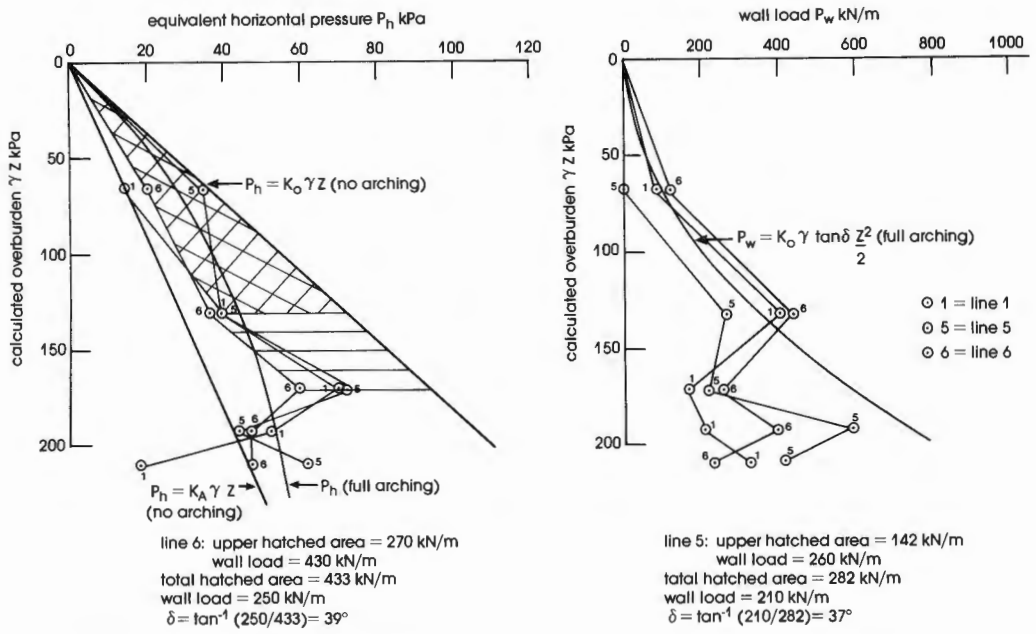

Fig. 9: Fill at maximum height after recirculation with simultaneous filling and emptying — profiles of equivalent horizontal pressure and frictional wall load on lines 1, 5 and 6

From the point of view of the silo design, this condition is clearly the least favourable reached in this series of measurements. The frictional wall load is usually critical in deciding the required plate thickness for a steel walled silo, and the permissible wall stress is positively influenced by the lateral stress [4]. Hence the critical design condition would be represented by the lowest lateral stress in combination with the highest frictional wall load.

It will have been noted from the measurements shown in Figs. 4, 7, 8 and 9 that there is still a considerable radial non-uniformity in both equivalent horizontal pressure and frictional wall load.

6. Conclusions

The measurements presented in this paper have again illustrated the extreme complexity of the interaction between a silo and its contained fill. The measurements also emphasize the relative inadequacy of the available theories to predict the loading on a silo wall.

2. The measurements on this silo have, a number of times, recorded equivalent horizontal pressures in the sugar that exceed those predicted by

$$p_h = K_o \gamma z \qquad (3b)$$

Tests have shown that the at-rest lateral pressure coefficient K_o does not vary appreciably with time up to 60 days under constant load. Three possible alternative explanations have been advanced:

2.1 that the lateral pressure coefficient comes to exceed K_o because of the effects of friction between the silo walls and the fill

2.2 that the effect arises from daily thermal contraction of the silo shell as the silo is filled without interruption

2.3 that the apparent increase results from an increase of the unit weight of the sugar.

Daily temperature changes seem to be the most likely explanation.

3. In a number of instances, no or very low frictional wall loads have been measured at points on the silo wall, both during filling and during subsequent intermittent recirculation of the sugar. These effects are also ascribed to daily temperature changes. Where frictional wall loads have been registered, it is usually possible to calculate a reasonable angle of wall friction from a combination of the assumed reduction in horizontal stress as a result of transfer of load to the wall by friction and the frictional wall load.

4. The worst situation from the point of view of the design of the silo wall appears to occur during circulation of the contents of the full silo with the occurrence of simultaneous filling and emptying. This process appears to result in higher frictional wall loads together with reduced lateral pressures.

7. Acknowledgements

The study described here was made possible by the cooperation of and partial funding by the South African Sugar Association.

References

[1] Blight, G.E., and Garstang, A.: Strains Measured in a 7,500 t Sugar Silo; bulk solids handling Vol. 7 (1987) No. 4, pp. 573–582.

[2] Blight, G.E., and Ofer, Z.: Laboratory Determination of K_o and Comparison with Prototype Silo Observations; Proc. 4th Australia - New Zealand Conf. on Geomechanics, Perth, 1984, Vol. 1, pp. 83–87.

[3] Blight, G.E.: Temperature Changes Affect Pressures in Steel Bins; Int. J. of Bulk Solids Storage in Silos, Vol. 1 (1985) No. 3, pp. 1–7.

[4] Trahair, N.S., Abel, A., Ansourian, P., Irvine, H.M., and Rotter, J.M.: Structural Design of Steel Bins for Bulk Solids; Australian Institute of Steel Construction, 1983, p. 13.

E & F Dust Control and Loading Equipment

E & F Services Ltd. of Leicester, U.K., process plant and associated equipment specialists, now manufacture a complete range of dust control equipment. Following their expansion programme it was a logical step to produce a range of dust control equipment to use in assiociation with their own plants and to market in its own right.

One example of this new range of dust control equipment being used in conjunction with E & F's handling equipment is the recently commissioned Mobile Loader (Fig. 1) for the dust free loading of open top wagons. The loader in this case is fed by an overhead grab.

Fig. 1: Mobile Loader of E & F Services Ltd.

This particular loader is a completely self-contained vehicle which can be driven to the most convenient loading point, and is suitable for a wide variety of loose bulk materials.

The main hopper is a wind-free enclosure fitted with internal baffles, the hopper is then tapered downwards to terminate in a mass flow bin type discharger. The dust is removed by a series of dust filter units and returned via gravity and screw conveyor into the system.

The road vehicles enter and leave through a curtain wall and are filled in dust free conditions. Fill rate is between 250 to 350 t/h depending on materials. Several patents are pending on these units.

The Manutube from E & F Services Ltd. offers a completely enclosed dust-free loading facility (Fig. 2). The Manutube is available in various sizes catering for a range of throughputs up to and in excess of 600 t/h.

These units can be installed as a static handling system, or mounted on a chassis as a mobile unit. The larger mobile units can also be supplied as motorised units for one-man operation.

Telescopic swivel discharge chutes can be fitted at the discharge point enabling material to be spread evenly with the vessels hold. The Manutube is also able to move at right angles in a parallel line to the vessel being loaded, adding to its versatility.

Actual loading of the Manutube can be by various methods,

Fig. 2: Lorry tipping Manutube unit for ship loading

but on ship loading applications it is usually by direct lorry tip. Various forms of inlet hoppers and feeders can be provided depending on how fast a vehicle turn round is required.

The Manutube follows the principle of a traditional belt conveyor, replacing the conventional troughing idlers with a tube manufactured from high density polycarbonate which is corrosion-free and has a very high impact resistance.

The belt is supported on air carried into the tube by the belt movement.

Improved Jetline V Dust Filter

The Jetline V from Neu Engineering Ltd. of Woking, Surrey, U.K., is a proven, high performance filter, designed to cost effectively meet a wide range of industry's dust control needs. Based on multiple rows of square section, needlefelt filter sleeves and incorporating an integral reverse jet compressed air cleaning system, these fully automatic, compact units provide proficient filtration with low operating costs and high efficiency.

Now, as part of Neu Engineering's policy of continuous product development, the company has introduced a new modified 100 mm square sleeve design, which results in an even more compact unit and a lower pressure drop during the cleaning cycle, with consequent reduction in power consumption.

Jetline V uses square-section, equally-spaced, needlefelt filter bags, which clean most effectively and are not subject to clogging. The benefits of the square bag configuration include a lower pressure drop, longer bag life and high air to cloth ratios, even on difficult dusts.

The integral Neu-designed "Venturi Economiser" minimises compressed air usage during the pulsed cleaning operation, which is programmed automatically. This adjustable cycle takes place without any detectable drop in air flow through the filter. These and other design features mean that high filter speeds are possible and up to 300 m^3/h of dust laden air per m^2 of filter can be handled. High levels of filtration efficiency also lead to low emission levels, normally not exceeding 10 mg/m^3.

Jetline V is one of a range of Neu purpose-designed dust control products.

powder handling & processing Volume 1, Number 2, June 1989

Behaviour of a Bolted Corrugated Steel Grain Silo

G.E. Blight, South Africa

Summary

The paper describes a series of strain measurements made on a bolted corrugated steel maize silo. The object of the measurements was to discover how the main structural components of the silo, the corrugated sheeting wall and the vertical stiffeners, function. In particular, to find what proportions of the vertical frictional wall load are carried by the sheeting and the stiffeners.

The measurements showed that the corrugated wall carries hoop tension, but a negligible fraction of the frictional wall load. The wall load is carried almost entirely by the vertical stiffeners.

1. Introduction

Bolted corrugated steel grain silos have proved to be economically competitive with forms of construction such as welded plane steel plate and slid reinforced concrete. Although many hundreds of corrugated steel silos have been built in various parts of the world, to very large sizes (at least 37 m diameter), there seems to be some uncertainty as to how the structural system functions. The horizontally corrugated plates that form the silo wall cannot be expected to carry much of the vertical frictional wall load. This must almost entirely be carried by internal or external vertical stiffeners that are provided for this purpose.

An alternative view is that the silo wall provides a horizontal radial constraint to the silo contents. This material is then able to support the vertical gravitational stress and in effect becomes self-supporting by developing internal shear stresses. On this basis, the stiffeners should carry relatively little load. The familiar grain sack or bag is pointed to as an example of this principle. The bag has no stiffness in the vertical direction, yet the walls of the bag do not buckle when it is filled with grain. Therefore, the argument goes, the radial restraint provided by hoop tension in the bag allows the grain to be self-supporting in the vertical direction.

To investigate just how bolted corrugated steel silos do function, it was decided to carry out a series of measurements on one. A suitable silo was located with the active assistance of Iscor Ltd. and the Northern Transvaal Co-operative Ltd. The latter body very kindly placed one of its silos at the writer's disposal for experimental purposes. The designer-builders of the silos, Bessemer Steel Construction (Pty) Ltd., kindly provided structural drawings of the silo and a test specimen of the corrugated steel wall plate.

2. Details of Test Silo

Fig. 1a shows the silo complex at Naboomspruit of which the test silo forms part. The test silo is the one closest to the camera. The silos are 18.19 m in diameter and 23.69 m high to the eaves. Each is stiffened by means of 60 equally spaced internal vertical stiffeners to which the corrugated strakes forming the walls are bolted. Fig. 1b is an internal view of the test silo showing the series of vertical stiffeners.

The layout of the silos in elevation and their principal dimensions are shown in Fig. 2a which also shows the double-skinned construction of the top-hat section vertical stiffeners. The stiffeners are bolted to the corrugated walls, but simply abut on each other in the vertical direction.

Fig. 1a: View of silo complex; test silo is on left closest to camera

Fig. 1b: View of inside of silo showing stiffeners

The flat-bottomed silos are emptied by gravity flow through the central outlet until the grain forms a cone, at its angle of repose, around the outlet. The remaining grain is then extracted using a sweeping auger. The housing for the motor driving this auger appears in the centre foreground in Fig. 1b.

The properties of the maize with which the silo was filled were established in the laboratory and were as follows:

Unit weight: $\gamma = 7.5$ kN/m^3

Coefficient of lateral pressure with zero lateral strain: $K_o = 0.65$

Angle of internal friction: $\phi = 30°$

The angle of wall friction δ between the maize and the corrugated galvanized wall sheeting was assumed also to be 30°.

3. Details of Instrumentation

Because the greatest interest lay in assessing the maximum loads in the stiffeners, and because of difficulty of access, it was decided to concentrate the instrumentation around the perimeter of the silo at a height of 1.5 m above the base.

Four stiffeners at 90° intervals in plan around the silo were strain-gauged. Each stiffener was strain-gauged in three positions, using electric resistance gauges as indicated in Fig. 2a.

As the inner skins of the stiffeners were inaccessible, only the outer skins were strain-gauged. The vertical and horizontal gauges of each pair were connected as a half-bridge to form a temperature-compensated pair. This was done on the assumption that there would be no (or negligible) transverse compression or bending on the stiffener section. On this assumption, measured axial strains would exceed true axial strains by a factor of $(1 + \nu)$ where ν is Poisson's ratio for steel. The layout in plan of the instrumented stiffeners is shown in Fig. 2b.

Electric resistance strain-gauges were mounted on the outside of the silo wall in each of four places to measure hoop strains at the same height as the stiffener strain measurements. At each point, two strain gauges were mounted horizontally, one in a trough and one on a ridge of the corrugations.

A copper-constantan thermocouple was also mounted at each gauging point. The junction of one thermocouple in each position was fixed to the stiffener inside the silo, and the junction of the other to the outside of the silo wall. To prevent wind from affecting the readings of the outside thermocouple, the junction was covered with a piece of aluminium-backed adhesive tape. This has a similar colour to the galvanized steel and is a good heat conductor. Hence it shielded the junction from the wind, but did not unduly impede heat flow.

The strain gauges and thermocouples were waterproofed using a rubber solution. The strain gauges on the stiffeners were protected from abrasion by the

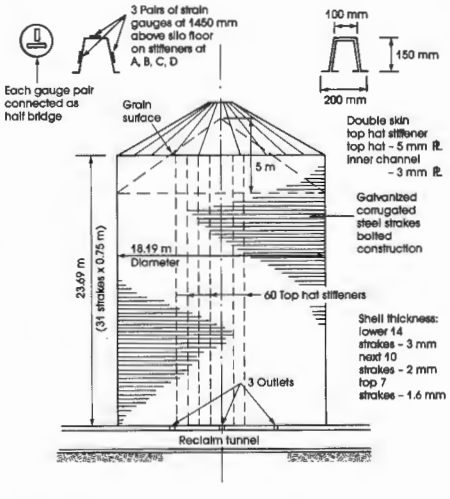

Fig. 2a: Silo layout in elevation showing principal dimensions

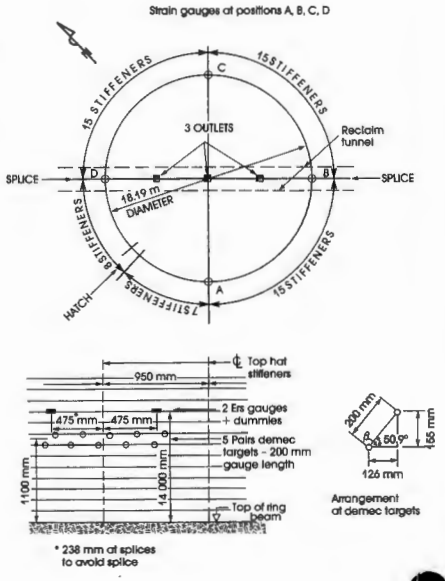

Fig. 2b: Silo layout in plan and layout of instrumentation on wall

grain by covering them with a sheet of galvanized steel fastened to the stiffener and the silo wall using small self-tapping screws. The protection to gauges on a stiffener is shown in Fig. 3a which also shows the stiffener in more detail. The strain gauge and thermocouple leads were taken through the wall sheeting to a water-proof box fixed to the outside of the silo. This is shown in Fig. 3b. This figure also shows the strain gauges to measure the hoop strain (on either side of the box), the outside thermocouple lead (to the right) and the separate stress-free steel tag on which was mounted the temperature-compensating dummy gauges for the hoop strain gauges. The vertical lines of bolts show the position of the stiffener.

To measure the vertical strain in the silo wall, a demountable Demec strain gauge with a gauge length of 200 mm was used. Electric resistance strain gauges could not be used because they would record vertical bending strains that might arise in the corrugated steel, as a result of vertical compression by the wall load. It appeared possible that these might be larger than the purely compressional vertical strain in the wall. It was necessary to mount the targets for the Demec gauge on ridges of the corrugations. As these did not fit in with the 200 mm gauge length, each pair of targets (5 pairs at each measuring position) had to be mounted diagonally, as shown in Fig. 2b. The Demec targets may just be discerned in Fig. 3b on the second and fourth ridges below the terminal box.

Fig. 3a: Steel sheet protecting strain gauges on internal stiffener

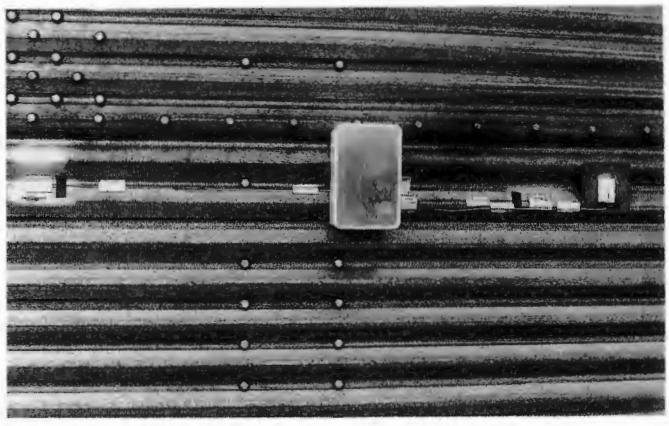

Fig. 3b: Terminal box and hoop strain gauges on outside of silo

4. Evaluation of Instrumentation

The effects of temperature must be expected to play an important role in any measurements on an uninsulated steel structure that is exposed to the weather. In fact, temperature can play a considerable role even in steel structures that are insulated [1]. In the present case, the test silo is partly in sun and partly in shade throughout the day. Hence apart from any day-night temperature differences, the structure is subjected to a temperature wave that moves around the structure as the day progresses.

In theory, if electric resistance gauges are compensated for temperature, they will register only stress-induced strains, but it is known that the temperature compensation is not perfect. Therefore it was considered important to investigate the extent to which the temperature compensation of the gauges was effective. To do this, two strain gauges were mounted on a small steel tag, together with the junction of a copper-constantan thermocouple. The strain gauges were connected as a half-bridge and the output of the strain gauges and the thermocouple on the stress-free tag were recorded while the tag was exposed to the weather over a period of four days. Part of these recordings are shown in Fig. 4, with the tag screened from the sun and wind (above) by sandwiching it between two slabs of polystyrene foam, and unscreened (below). The recordings for the screened tag show far less fluctuation than for the unscreened tag, but the two records are basically very similar. If temperature compensation had been perfect, the strain traces would not have deviated from a horizontal straight line.

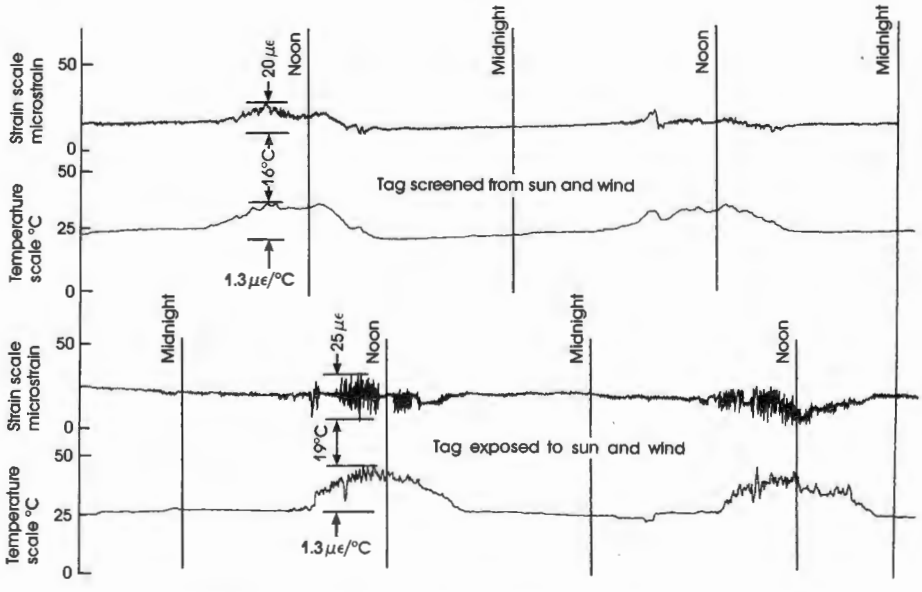

Fig. 4: Tests on temperature compensated gauge pair mounted on 50 mm square steel tag

The recorded value of the ratio of strain to temperature was 1.3 με/°C (*) whereas the coefficient of linear expansion for steel is about 12 με/°C. This indicates that almost 10% of thermal strains are not compensated; alternatively, that temperature compensation is 90% effective.

5. Restraint of Thermal Strains in the Empty Structure

Having established the extent to which the electric resistance strain gauges were likely to be temperature compensated, it was considered important to study the extent to which the structure itself would restrain the occurrence of thermal strains. Because of the daily solar temperature wave that travels around the wall of the silo, it appeared likely that thermal expansion of heated stiffeners might be restrained, via the silo wall and roof, by cooler stiffeners on either side. It did not seem likely however, that thermal hoop strains would be restrained in the empty silo. This effect was studied by recording the diurnal variation of strains and temperatures while the silo was empty.

Fig. 5 shows sets of simultaneous recordings of the variations of hoop strain and the temperature with time, and vertical stiffener strain and temperature with time. In the case of the recordings for the stiffener, the temperature was recorded by the thermocouple junction mounted on the stiffener.

It will be seen that the ratio of recorded hoop strain to temperature change was only 1 με/°C. Hence it can be concluded that thermal hoop strains are not restrained by the structure, although

(*) $1\mu\varepsilon = 1 \times 10^{-6}$ mm/mm = 1 microstrain.

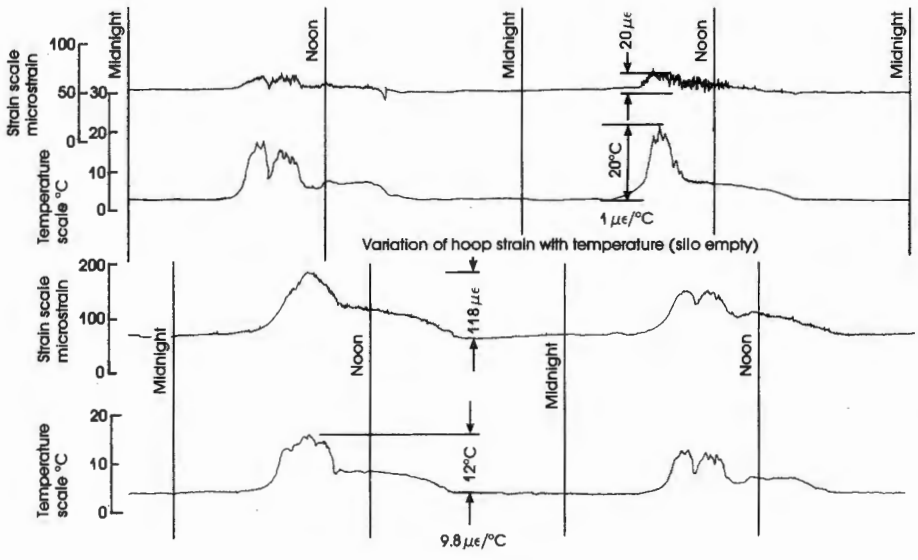

Fig. 5: Variation of longitudinal strain in stiffener with temperature (silo empty)

they will be restrained by the silo contents when the silo is full.

The ratio of recorded strain in the stiffener to change in temperature was nearly 10 με/°C. This indicates that thermal strains in the stiffeners are restrained to the extent of about (10−1)/12 or 75% when the structure is empty. This prevented thermal strain will add to the load in the stiffeners when the silo is full, it if occurs to the same extent.

6. Hoop Strains Measured During Filling with Maize

Strains in the silo were measured at roughly weekly intervals as the silo was filled with maize from empty over a period of 6 weeks. The results of the strain measurements are shown in Fig. 6 where they have been plotted against the overburden stress at the wall of the silo.

As the figure shows, there was a considerable spread of results. At any one position, such as A, the readings on the two gauges, one in the corrugation trough, the other on the ridge, differed considerably. There was also a considerable difference in the strain measured at different positions around the perimeter of the silo. For example, strains measured at position C are consistently higher than those measured at position B. This non-uniformity of strain and the corresponding pressure around the perimeter of a silo has been observed and recorded before, e.g. [2], [3] and probably applies to all full-size silos. Regarding the positions of the strain-gauges, those located in troughs generally appeared to read higher than those on ridges. The reason for this is not known.

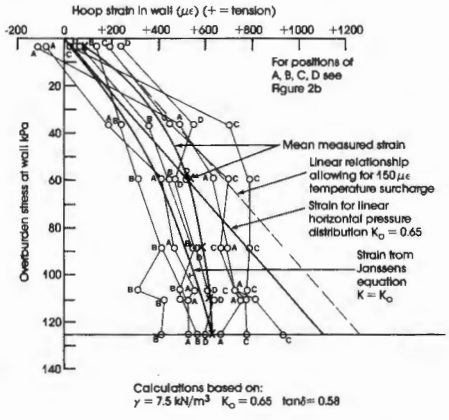

Fig. 6: Hoop strains observed in silo wall during uninterrupted filling

Three solid lines have been superimposed on Fig. 6. Two of these represent the variation in hoop strain with overburden, one calculated from the Janssen equation with $K = K_o$ and the other on the assumption that the horizontal pressure varies linearly with depth according to the relationship:

$$p_h = K_o \gamma z \qquad (1)$$

where:

p_h = horizontal pressure at depth z
γ = unit weight of the grain
K_o = the coefficient of lateral pressure under conditions of zero lateral strain.

The hoop strain was then calculated from:

$$\varepsilon_h = \frac{p_h D}{2tE} \qquad (2)$$

where:

D = silo diameter
t = equivalent thickness of the corrugated steel wall
E = Young's modulus for steel.

This assumes that the vertical strain in the corrugated steel is zero, which is probably not correct, but the error is believed to be acceptably small. The third line represents the arithmetic mean of the measured hoop strains. Neither of the two calculated relationships matches the distribution of mean observed hoop strain very well.

The effect of temperature on hoop strain when the silo is full is shown in Fig. 7. Two typical daily cycles of temperature and the corresponding variation of prevented hoop strain are shown. Each cycle of strain represents the reduction in hoop strain that would have occurred in going from the highest to the lowest temperature, had the contents of the silo not restrained and prevented it. The greatest value of this prevented temperature strain recorded during the tests was about 140με, but obviously, larger values are potentially possible, depending on the variation in temperature.

The greatest variation in temperature on the outer surface of the silo occurred while the sun was on it, between about 07h and 13h. Strangely enough, during the rest of the 24 hours, very little variation of temperature was recorded on the surface of the silo. It will be noted that the minimum temperature recorded in Fig. 7 was about 10 and the maximum just over 25°C. During the same period, a mercury-in-glass thermometer in the shade showed a minimum air temperature of 3°C and a maximum of 30°C. It was at first thought that either the calibration of the thermocouple, or the recorder were faulty. However, careful checks of these showed no fault. It is now thought that the daily variation of temperature in the silo wall is subdued by the combined effects of insulation of the inside of the wall by the grain and conduction of heat within the wall. Both of these would tend to reduce the amplitude of the daily temperature wave. Reference to temperatures recorded on other uninsulated steel silos, e.g. [4], shows a similarly subdued daily temperature variation. It is only the relatively concentrated heating by the sun that cannot be evenly distributed as it occurs, and results in the marked temperature variation shown in Fig. 7.

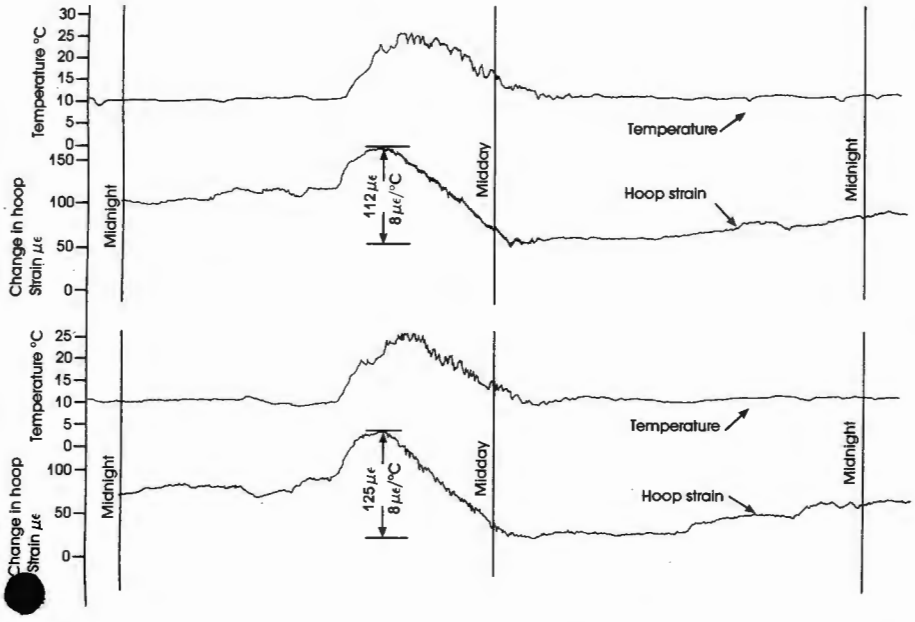

Fig. 7: Variation of hoop strain in silo with temperature when silo was full

It will be noted from Fig. 6 that if a "temperature surcharge" of 150 με is superimposed on the calculated linear strain distribution, all but four of the observed strains are contained below the surcharged relationship. Hence this relationship could be used to design a corrugated steel silo for hoop stresses.

7. Strains in Stiffeners Measured During Filling

Fig. 8 summarizes the measurements of strain made on the four instrumented stiffeners as the silo was filled from empty. The values plotted in Fig. 8 are the strains as they were recorded. True strains are $1/(1+\nu)$ or 3/4 times the observed values. There was a considerable variation in the measurements, both from stiffener to stiffener and even on a single stiffener (see, e.g. the measurements on stiffener B). It is apparent that the strain distribution across the section of each stiffener is completely non-uniform.

Not all of the strain gauges were working as the silo was filled. All the gauges at B were registering but only 2 each at A and D and one at C.

Fig. 8 also shows the arithmetic mean of the observed strains which, as it happens, coincides very closely with the single measurement at C and other single measurements at A, B and D.

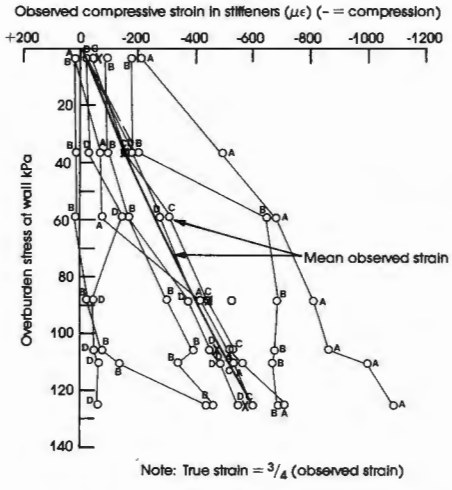

Fig. 8: Strains in stiffeners observed during uninterrupted filling

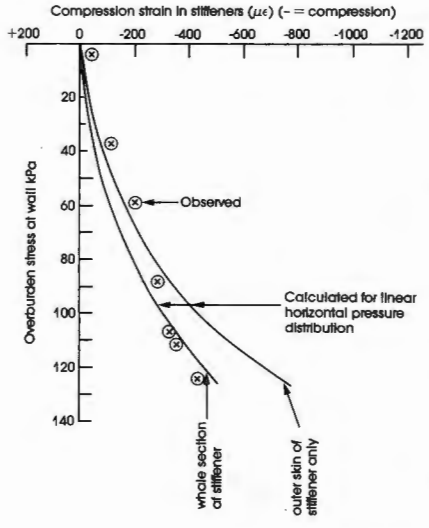

Fig. 9: Comparison of average observed strains in stiffeners with calculated strains; calculations based on $\gamma = 7.5$ kN/m^3, $K_o = 0.65$, $\tan\delta = 0.58$

To eliminate the clutter shown in Fig. 8, the mean true strains have been replotted in Fig. 9. The figure also shows two theoretical relationships between strain in the stiffeners and overburden stress. These were calculated assuming the linear relationship between horizontal pressure and depth given by Eq. (1), and also that the entire wall load is carried by the stiffeners. The wall load per stiffener is given by:

$$p_s = K_o \gamma \tan\delta \frac{z^2}{2} \frac{\Pi D}{S} \qquad (3)$$

in which δ is the angle of wall friction, S the number of stiffeners and the other symbols are as defined earlier. The strain in the stiffener is then given by:

$$\varepsilon_s = \frac{p_s}{A_s E} \qquad (4)$$

where:

A_s = cross-sectional area of the stiffener.

The two curves shown in Fig. 9 assume that either the complete section of the stiffener is carrying the load, or only the outer skin. The agreement between the mean observed and predicted strains is remarkably close. It gives the impression that initially only the outer skin of the stiffener carries the load but that as the load increases, the inner skin begins to carry its share. However, it must be remembered that the actual strain at points in the stiffener cross-section may be much larger (or smaller) than the mean strain.

The diurnal variation of strain in a stiffener as the temperature varies is shown in Fig. 10. The temperature in this case was measured on the stiffener. Whereas the ratio of prevented strain to temperature in the empty silo was nearly 10° με/°C (Fig. 5), the ratio recorded in Fig. 10 is only about 4 με/°C. Hence temperature fluctuations have relatively little effect on loads in the stiffeners when the silo is full.

It appears from Fig. 9 that the stiffeners do indeed carry all, or almost all of the frictional wall load in the silo. However, vertical strains in the corrugated silo wall must be examined before this can be stated as a firm conclusion.

8. Vertical Strains in the Silo Wall

Vertical strains in the corrugated silo wall were assessed by combining the mean hoop strain at each of the po-

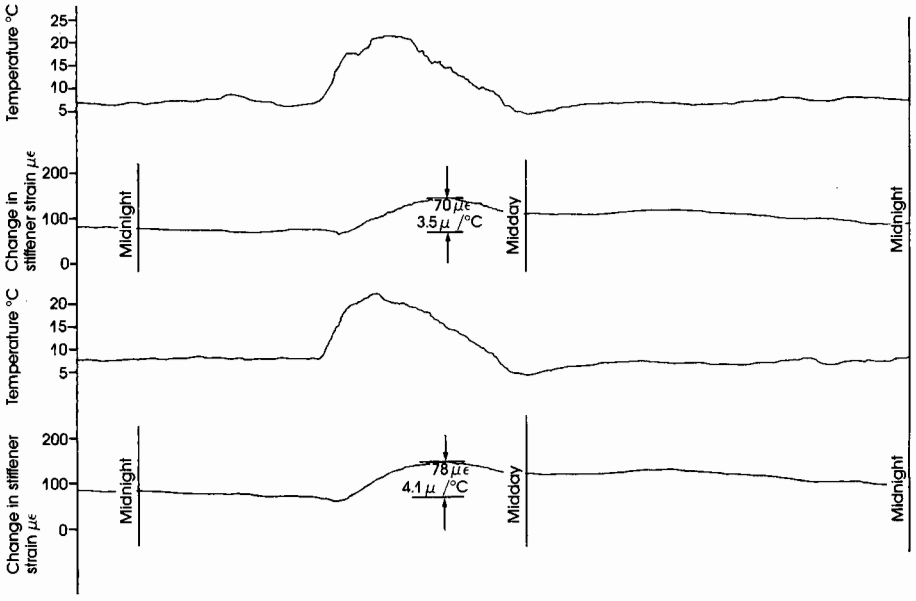

Fig. 10: Variation of stiffener strain in silo with temperature (silo full)

sitions A to D with the mean strain measured diagonally by using the Demec gauge (Fig. 2b) The geometry of the Mohr strain circle was used to do the combination.

The resulting variation of vertical strain with increasing overburden stress is shown in Fig. 11. It will be noted that the strains are rather small, a maximum of 250 με as compared with a maximum hoop strain of about 800 με. The hoop strain takes place parallel to the currugations where the elastic modulus of the plate is 200 GPa, but the vertical strain takes place across the corrugations, where the modulus of the plate is very low.

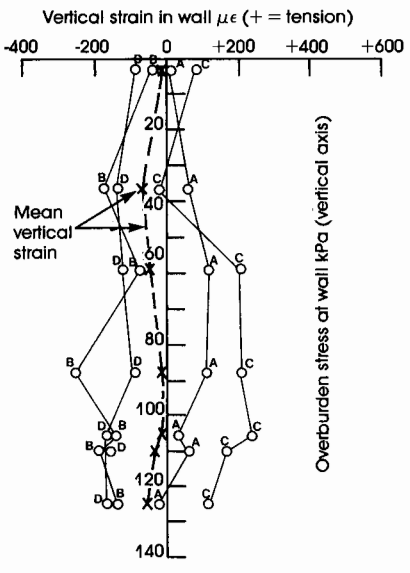

Fig. 11: Vertical strains in silo wall observed during uninterrupted filling

As with the other sets of measurements, the vertical strains are scattered, and some strains appear to be tensile. As stated earlier the strains plotted in Fig. 11 are a combination of tensile hoop strains measured by means of electric resistance strain gauges, and diagonal strains measured by a Demec gauge. It should be noted that all of the diagonal strains were small and tensile, showing qualitatively that the vertical strains must have been very small. The mean vertical strain in the wall was indeed close to zero.

The compression characteristics of the wall across the corrugations was measured in the laboratory by compressing specimens of 3 mm thick corrugated plate. The specimens measured 190 mm long and 150 mm wide and the load was applied across the corrugations in the mean plane of the corrugation wave form. The results of these measurements have been expressed as axial load in kN per m width (measured parallel to the corrugations) versus compressive strain across the corrugations, and are shown in Fig. 12.

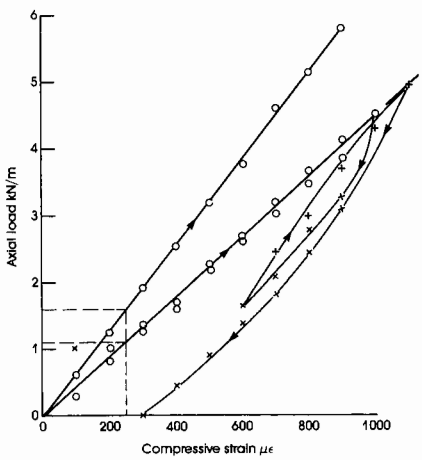

Fig. 12: Load-strain characteristics of three specimens of 3 mm corrugated steel plate compressed in the plane of the plate and across the corrugations

If the maximum measured strain of 250 με is superimposed on the diagram, it will be seen to correspond to a wall load of about 1.5 kN/m. The calculated maximum wall load at the level of the instrumentation is 400 kN/m. Hence it is quite plain that the corrugated wall sheeting carries almost no frictional wall load.

9. Conclusions

The following conclusions can be drawn from the measurements and their analysis:

1. The stiffeners carry almost the entire frictional wall load in the silo and the wall itself carries very little. The wall sheeting distributes the frictional wall load into the stiffeners as it arises and also carries the hoop tension caused by the radial pressure of the silo contents.
2. The functioning of the silo shell is very complex: the hoop strain caused by the pressure of the silo contents is highly variable around the silo perimeter and is affected by the temperature wave that travels around the silo each day as a result of the sun's heating.
   The strains, and therefore the loads in the stiffeners also vary around the silo perimeter, and the cross-section of each stiffener is not uniformly strained.
3. However, on average, hoop strains, surcharged for temperature, agree reasonably well in magnitude with strains predicted on the basis of simple silo theory.
   Average strains in the stiffeners also agree reasonably well with those calculated from simple silo theory.
   A sample calculation of design loads for this silo is included as an appendix.

Acknowledgements

As recorded earlier, the writer acknowledges the assistance of Iscor Ltd., Northern Transvaal Co-operative Ltd.

and Bessemer Steel Construction (Pty) Ltd. Particular thanks go to Mr Johan de Wet who brought together the four parties concerned in the work.

References

[1] Blight, G.E.: Strains Measured in a 7,500 t Sugar Silo, Part II; bulk solids handling, Vol. 8 (1988) No. 4, pp. 413–419

[2] Blight, G.E. and Garstang, A.: Strains Measured in a 7,500 t Sugar Silo; bulk solids handling, Vol. 7 (1987) No. 4, pp. 573–582

[3] Fliss, L. and Blight, G.E.: A Comparison of Design and Measured Lateral Pressure and Temperatures in a Large Duo-Cell Cement Storage Silo; International Journal of Bulk Solids Storage in Silos, Vol. 2 (1986) No. 4, pp. 18–28

[4] Blight, G.E.: Temperature Changes Affect Pressures in Steel Bins; International Journal of Bulk Solids Storage in Silos, Vol. 1 (1985) No.3, pp. 1–7

Appendix

Sample Calculation of Design Loads Based on Conclusions from Strain Measurements

Materials parameters: $\gamma = 7.5$ kN/m^3, $K_o = 0.65$, $\delta = 30°$

Silo dimensions: $D = 18.19$ m; z_{max} = maximum depth of grain against silo wall = 23 m

Horizontal pressure at base of silo: $p_h = K_o \gamma z_{max} = 0.65 \times 7.5 \times 23 = 112$ kPa

Hoop tension at base of silo:

$$\sigma_h = \frac{p_h D}{2} = \frac{112 \times 18.19}{2} = 1{,}019 \text{ kN per m height}$$

Wall load at base of silo:

$$P_w = K_o \gamma \tan \delta \frac{(z_{max})^2}{2} = \frac{0.65 \times 7.5 \times \tan 30° \times (23)^2}{2}$$

$$= 744 \text{ kN per m perimeter}$$

Wall load per stiffener (60 stiffeners):

$$P_s = \frac{P_w \Pi D}{S} = \frac{744 \times 18.19\ \Pi}{60} = 709 \text{ kN per stiffener}$$

IN SEPTEMBER BRITAIN WILL AGAIN HAVE TWO WORLD LEADERS

For the International Handling and Storage Exhibition — IHSE — returns to The National Exhibition Centre, Birmingham. But this time at the heart of a new event:

INTERACTION 89

Three years ago IHSE '86 was one of the biggest and most successful materials handling exhibitions ever staged, with one of the best displays of working handling equipment ever seen. Interaction '89 — which links IHSE '89 with five other complementary exhibitions is more than twice the size of IHSE '86 — and its six shows now cover every aspect of materials movement, storage and control. With over 1200 exhibiting companies occupying 50,000 + square metres of net stand space, Interaction '89 now leads the world as the largest indoor materials movement exhibition ever held.

The six Interaction events are:

HANDLING & STORAGE

IHSE — over 500 companies from around the world displaying the latest technology for the movement and storage of unit loads.

INTERBULK 89

The products of almost 300 companies make this the world's largest exhibition on the subject of bulk solids, handling and processing.

POWER TRANSMISSION 89

A comprehensive display of the products to generate, transmit and control motive power for plant and machinery.

DISTRIBUTION 89

Covers every aspect of the logistics of moving goods between locations.

INDUSTRIAL BUILDINGS 89

Features products and services for the difficult tasks of locating, constructing and equipping factories and warehouses.

SITE HANDLING 89

A wide range of plant to move materials on external sites.

For more information on Interaction '89 or the four major conferences that are being staged during the event contact the organisers: Trinity International Ltd, Trinity House, Hercies Road, Hillingdon, Middlesex UB10 9NA, England. Tel: (0895) 56751/2. Fax: (0895) 71946. Telex: 8813047 Trinty G.

Getting there is easy. There are daily flights direct to the NEC's own airport — Birmingham International, from many parts of the world. For travel and hotel arrangements contact the official travel agent for West Germany: Deutches Reiseburg Gmbh on 49-69 1566377.

INTERACTION 89

Six Exhibitions One Event

NEC, Birmingham, UK, 18-22 September

powder handling & processing Volume 1, Number 4, November 1989

Strain and Temperature Measurements on an Externally Stiffened Corrugated Steel Grain Silo

G.E. Blight, South Africa

Summary

The paper describes a series of measurements made on an externally stiffened corrugated steel grain silo. The measurements were undertaken to confirm the results of earlier measurements [1] made on an internally stiffened corrugated steel silo, and to investigate possible differences between the behaviour of internally and externally stiffened corrugated silos. The results confirmed the earlier measurements and showed that internally and externally stiffened silos behave in a very similar manner. The measurements have emphasized the important role played by temperature-induced loads in total silo loading.

1. Introduction

A recent paper [1] described the results of measurements made on an internally stiffened bolted corrugated steel grain silo measuring 18.19 m in diameter by 23.7 m high.

The measurements showed that the stiffeners in the silo carry almost the entire frictional wall load. The corrugated sheeting forming the silo wall distributes the wall load into the stiffeners as it arises and also carries the hoop tension caused by the radial pressure of the silo contents.

The investigation also showed that the cross-section of each stiffener was not uniformly loaded, and also that the pressure of the silo contents appeared to vary significantly around the perimeter of the wall. Hoop strains (and hence horizontal pressures) were considerably affected by the temperature wave that travels around the silo each day as a result of solar heating and also by overall diurnal temperature changes.

Although the investigation on the 18.2 m silo successfully identified the loads carried by the various components and showed that these can be estimated by a simple calculation procedure, the results needed to be confirmed. As the silo is filled and emptied once each year, it was originally intended to obtain confirmation by repeating the measurements in the following year. However, an opportunity arose to repeat the measurements on a different type and size of silo. This was recognised as a better means of confirmation as it would provide a completely independent check on the earlier set of measurements.

The author is indebted to the Northern Transvaal Co-operative Ltd. for their active co-operation in making their Pienaarsrivier silo facility available for the performance of the measurements.

2. Details of Silo

Whereas the silo described in the previous paper [1] has a capacity of 4,600 t of maize, the silo treated in this paper has a capacity of only 1,200 t of maize. Details of the layout of the silo are shown in Fig. 1; Fig. 2 is a view of the complex of which the test silo forms part. (The test silo is the fourth silo from the right).

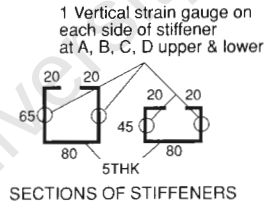

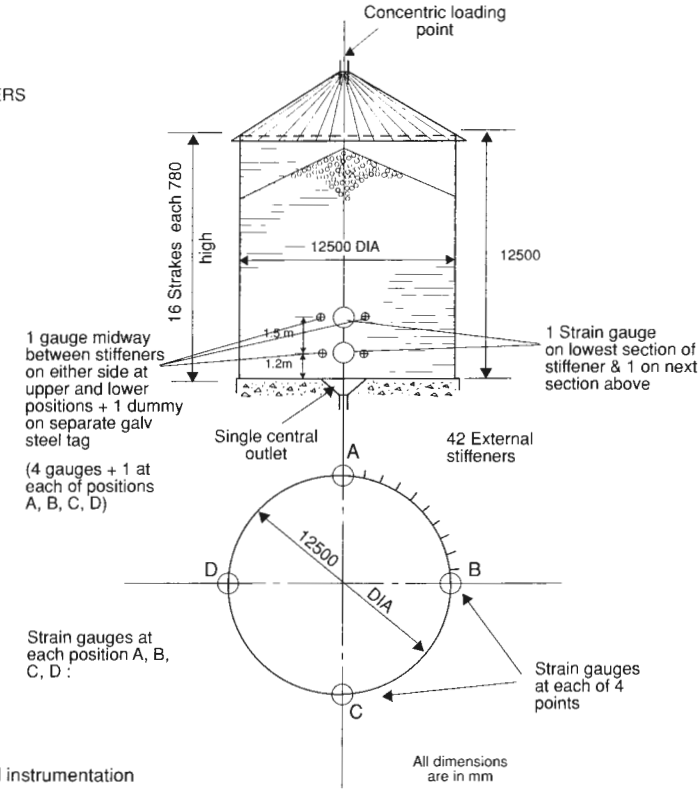

Fig. 1: Layout of silo and instrumentation

For information on author – see page 442

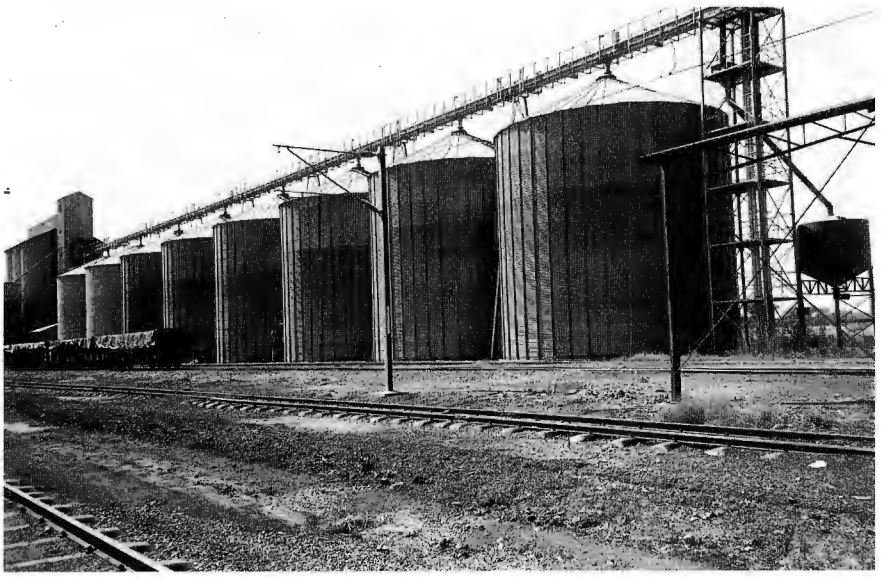

Fig. 2: View of Pienaarsriver silo facility; the test silo is fourth from the right

The silo has a diameter of 12.5 m, a wall height of 12.5 m, and is of all bolted construction. It is filled concentrically by means of a conveyor belt and has a single central outlet discharging into a conveyor tunnel.

The wall consists of 2.5 mm thick galvanised corrugated steel plate and is stiffened by 42 equally spaced external stiffeners.

The stiffeners (visible in Fig. 2) consist of galvanized lipped channels made of 5 mm thick steel. The lowest section of stiffener measures 80 mm wide by 65 mm deep overall, while higher sections measure 80 mm wide by 45 mm deep.

The stiffeners are bolted directly onto the corrugated wall. Each stiffener section butts onto and rests on the section below, but is located only by the sheeting of the silo wall.

The properties of the maize which the silo stores were as follows:

Unit weight:	$\gamma = 7.5$ kN/m^3
Coefficient of lateral pressure with zero lateral strain:	$K_0 = 0.65$
Coefficient of lateral pressure for active condition:	$K_A = 0.33$

The angle of wall friction δ between the maize and the galvanized corrugated wall sheeting was assumed to be equal to the angle of internal friction ø:

$$ø = \delta = 30°$$

3. Details of Instrumentation

The layout of instrumentation was very similar to that used previously on the 18.19 m dia. silo and is shown in Fig. 1.

Fig. 3: Close-up of instrumentation on wall and stiffener of 12.5 m diameter silo

Strain gauges were attached at four positions A, B, C, D separated by 90° in plan. At each of these positions gauges were mounted at two different heights: 1.2 m above the concrete base of the silo, and 2.7 m above the base. Four gauges were mounted at each height:

- two on the stiffener, one on either side as shown in Fig. 1; and
- two on the corrugated sheeting, midway between stiffeners, one in a trough of the corrugations and the other on a ridge.

A separate dummy gauge for temperature compensation was used for each of positions A to D. This was mounted on a small tag of galvanized steel sheeting which was attached to the wall of the silo by means of mirror-mounting tape to ensure that it was stress-free. Strain gauges on the stiffeners were mounted in a vertical orientation and those on the silo walls were aligned horizontally. All strain gauges were waterproofed by means of rubber solution and then further waterproofed and protected by means of an aluminum foil-backed rubber bitumen sealing strip.

Fig. 3 is a photograph showing the installation at the lower level for a typical instrument position. The dummy gauge, attached, to its tag, is to the right above one of the horizontal gauges to measure hoop strain in the silo wall.

One of the gauges on the stiffener is visible just under the terminal box. The latter is an ordinary plastic freezer box with an airtight press-on lid.

The measurements on the 18.19 m dia. silo had shown that vertical strains in the corrugated sheeting are negligible and therefore that measured hoop strains would be unaffected by Poisson ratio effects.

The same applies to strains measured parallel to the length of the stiffeners. Strains could thus be measured by connecting each active gauge in turn into a half-bridge with the dummy gauge. Most of the strain measurements were carried out manually by means of a Huggenberger strain bridge.

Temperature-associated strains and the corresponding temperatures were recorded by means of a Toa electronic pen recorder.

Copper-constantan thermo-couples arranged in pairs were used for measuring temperatures. One had its junction in contact with the silo wall, so as to measure the temperature of the wall. The other had its junction 5 mm off the wall so as to measure the temperature of the air in close proximity to the wall. Both junctions were shielded from the wind by means of aluminum-backed adhesive tape.

4. Horizontal Pressures Deduced from Measured Strains

Strains were measured at intervals as the silo was filled from empty. Knowing that measured strains are temperature-dependent because of the restraint to movement of the silo imposed by the grain, readings were taken at approximately the same time (between 12h00 and 13h00) on each occasion to minimize temperature differences. The depth of grain in the silo was measured by means of a tape dropped in from the apex of the silo roof.

The horizontal pressure corresponding to a particular hoop strain was calculated as follows:

Horizontal pressure:

$$P_h = \frac{2E\varepsilon_h t}{D} \qquad (1)$$

where:

P_h = horizontal pressure

E = elastic modulus of steel

ε_h = measured hoop strain

t = equivalent thickness of silo sheeting allowing for the effect of the corrugations

D = silo diameter.

The observed variation of the horizontal pressure with overburden stress at the wall of the silo is shown in Fig. 4. In this figure, each experimental point represents an individual strain measurement. If the pair of readings taken at a particular position and level had been averaged, the scatter of points would have been reduced by as much as half. In contrast to the measurements made on the 18.19 m dia. silo, the scatter of measurements is remarkably small.

Three calculated pressure versus overburden stress lines have been superimposed on the measurements shown in Fig. 4. These correspond to:

- a linear distribution of horizontal pressure with overburden stress:

$$P_h = K_0 \gamma z \qquad (2)$$

where:

K_0 = coefficient of lateral pressure for zero lateral strain

γz = overburden of grain at the wall

- two distributions calculated from Janssen´s theory [2], one for a coefficient of lateral pressure for zero lateral strain (K_0), the other for the active lateral pressure coefficient (K_A).

It appears from the results that there is sufficient arching in the silo, notwithstanding its 1 to 1 height to diameter ratio, for the Janssen equation to apply, with a lateral pressure coefficient between the limits K_A and K_0. This is completely consistent with observations on other silos [1, 3, 4] storing coarse granular materials.

The small scatter of the observations on this silo is quite remarkable. The scatter of strain observations in previous projects of this nature (e.g. [1], [5]) has been far greater.

The data shown in Fig. 4 is for filling of the silo from empty without interruption. Because of the squat dimensions of the silo, the funnel of flow that develops on emptying does not intersect with the wall. Hence no change in hoop stain or horizontal pressure would be expected at the start of emptying. In fact no change in hoop strain was observed at the start of emptying.

5. Stiffener Loads Deduced From Measured Strains

Strains in the stiffeners were measured at the same times as the hoop strains. The stiffener load P_s corresponding to a particular strain was calculated from:

$$P_s = \varepsilon_s E A_s \qquad (3)$$

where:

ε_s = measured strain in the stiffener

A_s = stiffener cross-sectional area.

The observed stiffener loads have been plotted against overburden stress in Fig. 5. Here again, the scatter of observations is remarkably small. Each individual strain reading had been used to calculate a stiffener load. The scatter of observations would have been halved if each pair of strains on a particular stiffener, at a particular height had been averaged.

The lines representing calculated stiffener loads that appear in Fig. 5 were based on the Janssen theory and were calculated by the method given in DIN 1055 (1984) [2] for the two lateral pressure coefficients K_A and K_0. The DIN calculation gives the frictional wall load P_w in load per m perimeter of silo. The stiffener load P_s was then calculated from:

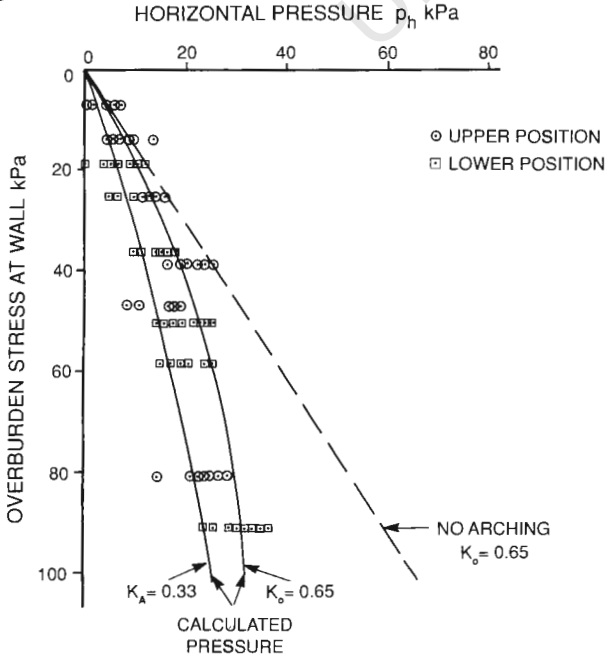

Fig. 4: Relationship between horizontal pressure and overburden stress

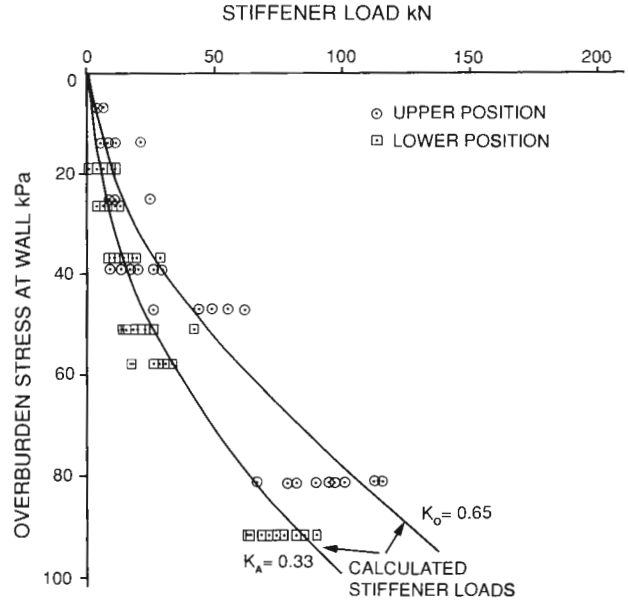

Fig. 5: Relationship between stiffener loads and overburden stress

$$P_s = \frac{P_w \pi D}{S} \qquad (4)$$

where:

S = number of stiffeners.

The observed stiffener loads agree remarkably well with the calculated loads. In particular, the agreement is better than that obtained with the 18.19 m dia. silo. The better agreement is at least partly because the stiffeners on the 12.5 m dia. silo have a simple section. Those in the 18.19 m dia. silo are double-skinned. Only the outer skin was accessible for strain-gauging and strains in the inner skin had to be assumed equal to those in the outer skin.

Because the grain in contact with the walls of the silo does not move when emptying is started, no change in stiffener loads was observed at the start of emptying.

6. Temperature Effects on Horizontal Pressure

Previous measurements on steel silos (e.g. [1], [6]) have shown that restrained temperature changes play a considerable part in the loads imposed on the silo walls. In general, if the temperature of the wall of a full silo falls, the hoop tension is increased and the frictional wall load reduced. In extreme cases, it is possible for the wall to go from compression into vertical tension. The opposite effect takes place when the temperature rises.

In the tests on the 18.19 m dia. silo, the greatest observed value of the prevented (i.e. load-inducing) hoop strain was 140 microstrain which would have corresponded with a change in horizontal pressure of 9.2 kPa.

After the tests on the 18.19 m dia. silo, it was noticed that the temperature variation of the silo wall appeared to be considerably less than that of the air adjacent to the silo. It was decided to check this observation in the tests on the 12.5 m dia. silo.

Fig. 6a shows the variation of prevented thermal hoop strain and air temperature 5 mm from the silo wall, recorded over two days while the silo stood completely full, with no grain being added or withdrawn. Fig. 6b shows the corresponding recording of the temperature of the silo wall and the prevented thermal strain in a stiffener. The data in the figures show that the temperature in the silo wall varies by about 10°C less than does the air temperature. This confirms the earlier similar observations on the 18.19 m dia. silo. The subduing of the diurnal temperature wave in the silo wall is a most important observation, as it shows that thermally induced loads are considerably less (in this case, about one third less) than those that would be expected on the basis of air temperature variations.

The cause of the lower temperature variation in the silo wall has not been established, but must result from the insulating and warming effect of the grain in contact with the wall and the ability of the steel wall to even out temperature variations by conduction of heat.

As indicated on Fig. 6a, the variation in horizontal pressure P_h as a result of prevented thermal strain is in the range of 9 to 12 kPa. As the prevented thermal strains were measured at the lower instrument level, this comprises between 35 and 46 % of the mean calculated horizontal pressure (at that level) of 26 kPa. Hence thermal effects comprise a major component of the hoop loading in the silo wall.

If the grain were regarded as being incompressible the horizontal pressure P_h induced by a temperature change $\Delta\theta$ would be given by the expression

$$\Delta P_h = E\alpha\Delta\theta \cdot \frac{2t}{D} \qquad (5)$$

where:

α = coefficient of linear thermal contraction of the steel silo walls

υ = Poisson´s ratio.

This assumes zero vertical stress which is justified by the low vertical stiffness of the corrugated steel.

For a temperature change of 26°C (see Fig. 6b) and taking

α = 11 x 10 $^{-6}$/°C
E = 200 GPa
υ = 1/3
ΔP_h = 23 kPa

The difference between the calculated and measured values of ΔP_h (shown in Fig. 6a) arises from the lateral compressibility of the grain.

The compressibility of the grain can be calculated by applying the following equality:

$$\varepsilon = \alpha\Delta\theta - \frac{\Delta P_h}{M} \qquad (6)$$

where:

ε = prevented thermal strain

M = modulus of compressibility of the grain for radial compression

ΔP_h = resulting increase in horizontal pressure.

ε and $\Delta\theta$ have been measured, ΔP_h can be calculated from Eq. (1), and hence M can be calculated from a re-arranged Eq. (6):

$$M = \frac{2Et\varepsilon}{D(\alpha\Delta\theta - \varepsilon)} \qquad (7)$$

Three cases of measured thermally induced horizontal pressures in maize are available for analysis. These cases and the corresponding values of M are as follows:

Silo diameter [m]	Modulus M [MPa]	Overburden Stress [kPa]
12.5	65	90
18.19	165	125
20 [6]	350	190

The values above are 10 to 100 times larger than values of the modulus of compressibility measured in the laboratory, of about 5 MPa (e.g. [7], [8]).

As indicated in the tabulation, M is dependent on the overburden stress, and Fig. 7 shows the experimental relationship between these two variables.

If the values of $\Delta\theta$ and M are known, Eq. (7) can be re-arranged to give:

Fig. 6a: Variation of hoop strain with temperature of air 5 mm from wall

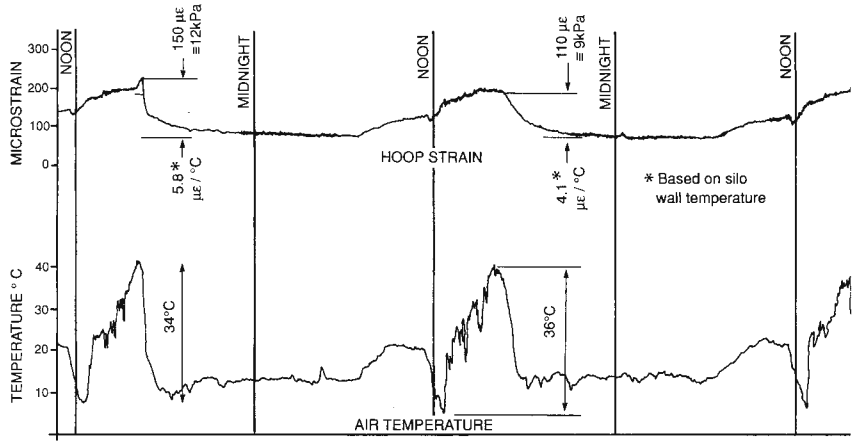

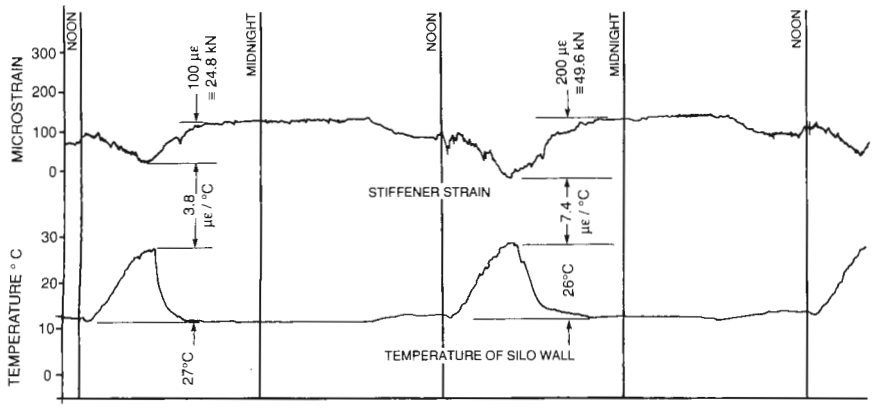

Fig. 6b: Variation of stiffener strain with silo wall temperature

$$\Delta P_h = \frac{2MEt\alpha\Delta\theta}{MD + 2Et} \qquad (8)$$

This equation is similar, but not identical to that given by Andersen [9].

It should be noted here that laboratory measurements, (e.g. [7], [8]) indicate that the moduli of compressibility of grains such as wheat and maize are not dissimilar. Hence the moduli for maize given in this paper give some guidance to the moduli applicable to other hard grains.

7. Temperature Effects on Stiffener Loads

Fig. 6b shows that the variation in stiffener load as a result of prevented thermal strain can be as much as 50 kN, or 50% of the mean calculated stiffener load of 102 kN at the lower instrumentation level. Hence, thermal effects can also comprise a major component of the stiffener loading. However, there is a difference between thermal hoop loads and thermal stiffener loads. When the temperature falls, the hoop load increases, but the stiffener loads decrease. Also, because stiffener loads are induced by downward frictional drag on the wall, thermal effects cannot increase stiffener loads beyond a maximum value dictated by the downward frictional drag between the silo walls and the stored contents.

Fig. 7: Relationship between overburden stress and compression modulus for maize

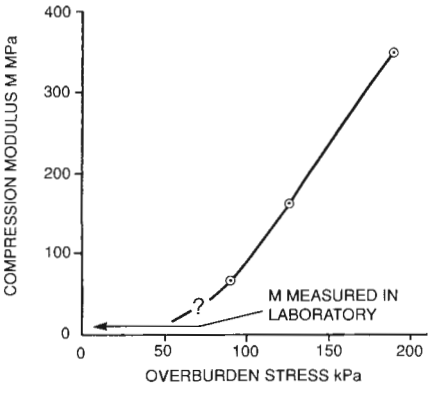

The reason why stiffener loads decrease when the temperature of the silo shell falls is as follows:

The wall contracts radially onto the contents. Because of the relative incompressibility of the grain and its thermal inertia, its volume remains approximately constant. If the radial strain of the shell is ε_h, and the vertical strain ε_v, the condition for zero volume change of the silo contents would be:

$$\varepsilon_v + 2\varepsilon_h = 0$$

$$\text{i.e. } \varepsilon_v = -2\varepsilon_h$$

Hence, if the radial strain is compressive, the vertical strain will be tensile, i.e. the grain will move upwards relative to the silo wall and the wall friction will reduce or even reverse in direction.

8. Conclusions

This study has confirmed the findings reported previously for the 18.19 m dia. silo. Moreover, because of the small scatter of the measurements, the confirmation has strengthened the confidence with which the conclusions can be stated:

1. In a corrugated steel silo, the stiffeners, whether external or internal, carry almost the entire frictional wall load.
2. The corrugated wall carries the hoop tension arising from the lateral pressure exerted by the silo contents.
3. Both the stiffener loads and the hoop tension in the wall can be calculated by accepted calculation procedures (e.g. [2] or the method shown in [1]).
4. Prevented thermal strains result in loads being induced in steel silos that comprise an important part of the total loading. A method, and numerical information has been given for calculating thermally induced hoop loads in silos filled with maize.
5. Whereas thermal effects can increase hoop loads beyond values arising from gravity loading this does not apply to stiffener loads. A fall in temperature will increase hoop loads but decrease stiffener loads.

Acknowledgements

The research was funded by the S.A. Foundation for Research Development. The assistance of the Northern Transvaal Co-operative Ltd. and the friendly collaboration of their staff at the Pienaarsriver depot is gratefully acknowledged. The silos were instrumented and many of the readings taken by Messrs. Bob Anderson and Mark Oelofse of the Witwatersrand University.

References

[1] Blight, G.E.: Behaviour of a Bolted Corrugated Steel Grain Silo; powder handling & processing, Vol. 9 (1989) No. 2, pp. 143 - 149.

[2] German Standards Institute: DIN 1055, Lasten in Silozellen, Teil 6; 1984, 8 pp.

[3] Blight, G.E.: A Comparison of Measured Pressures in Silos with Code Recommendations; bulk solids handling, Vol. 8 (1988) No. 2, pp. 145–153.

[4] Blight, G.E.: Pressures Exerted by Materials Stored in Silos: Part I, Coarse Materials; Geotechnique, Vol. 36 (1986) No.1, pp. 33–46.

[5] Blight, G.E. and Garstang, A.: Strains Measured in a 7,500 t Sugar Silo; bulk solids handling, Vol. 7 (1987) No. 4, pp. 573–582.

[6] Blight, G.E.: Temperature Changes Affect Pressures in Steel Bins; Int. J. Bulk Solids Storage in Silos, Vol. 1 (1985) No. 3, pp. 1–7.

[7] Blight, G.E.: Swelling Pressure of Wetted Grain; bulk solids handling, Vol. 6 (1986) No. 6, pp.1135–1140.

[8] Manbeck, H.B. and Puri, V.M.: Predicting Thermally Induced Loads in Thin-Walled Grain Bins: State-of-the-Art; Int. J. Bulk Solids Storage in Silos, Vol. 1 (1985) No.3, pp. 9–13.

[9] Andersen, P.: Temperature Stresses in Steel Grain Storage Tanks; Civil Engineering, ASCE, (1966), January, p. 74.

Powder & Bulk Solids™ 15 YEARS

CONFERENCE / EXHIBITION

Conference: June 4–7, 1990 Exhibition: June 5–7, 1990
O'Hare Exposition Center Rosemont (Chicago), Illinois

POWERFUL FOCUS

Powder & Bulk Solids is the largest and most complete exhibition and conference in the world dedicated to solutions for the processing, handling, packaging, instrumentation and control, transportation, and storage of particulate matter and bulk solids.

POWERFUL MARKETING OPPORTUNITIES

Meet thousands of decision makers from many different industries with the authority to buy your equipment, products, and services. In 1989, more than 7,000 attendees sought solutions to specific business problems at Powder & Bulk Solids.

POWERFUL PRODUCT SHOWCASES

Responding to attendee demand, Powder & Bulk Solids '90 will introduce the Packaging Showcase and the Instrumentation and Control Showcase, covering nearly 10,500 square feet of the exhibition and focusing on the latest innovations in two of the hottest product areas in the powder and bulk solids field.

SEIZE THE POWER OF POWDER & BULK SOLIDS '90!

For more information about attending or exhibiting please call Show Management at (708) 299-9311, or contact: **Cahners Exposition Group** ■ 1350 East Touhy Avenue ■ P.O. Box 5060 ■ Des Plaines, IL 60017-5060 ■ Telephone: (708) 299-9311 ■ FAX: (708) 635-1571

powder handling & processing Volume 2, Number 1, March 1990

Load and Temperature Strains of a Welded Plane Plate Grain Silo

G.E. Blight, South Africa

Summary

Technical argument in two recent court cases concerning the collapse of two welded plane plate silos, showed that the role of construction stiffeners in carrying frictional wall load is not clear.

Also unclear is the effect on wall stresses of construction defects. This paper describes measurements made to investigate these two areas of uncertainty.

The measurements showed that the presence of construction stiffeners should be ignored and also that construction defects can considerably modify wall stresses in a silo.

1. Introduction

The writer has recently been involved in two civil court cases that arose from the collapse of flat bottomed welded plane plate grain silos.

In each case the silo concerned collapsed by buckling of the wall. Also, in each case the silo was equipped with two eccentric outlets provided to clear the grain from the bottom of the silo once emptying had, as far as possible, been completed through the central outlet.

In both cases there was evidence to show that an eccentric outlet had been opened while the silo was full and the appearance of the collapse was consistent with localized buckling induced by eccentric emptying.

As opening of one eccentric outlet in a full silo would have indicated negligence in operating the silo, the cases each resolved into an argument as to whether the silo had failed during emptying through the central outlet by buckling of the wall under axisymmetric frictional wall loads, or if eccentric emptying had led to the failure.

Both cases were settled before the judges gave their verdicts, leaving the arguments both legally and technically inconclusive.

Both silos had been erected from the top down: The partly-built structures were supported on a series of vertical erection stiffeners while a strake or ring of plates was welded into place.

The structures were then jacked up high enough to enable the next strake to be welded in, and so on. These vertical erection stiffeners remained in place in the completed silos, but their presence had been ignored in the design.

Much of the argument in the court case revolved about the extent to which the erection stiffeners carried frictional wall load.

For information on author - see page 98

The designs were both apparently safe, under concentric emptying conditions, if it could be assumed that the erection stiffeners carried a share of the frictional wall load in proportion to their cross-sectional area.

On the other hand, the spacing of the stiffeners was too large for them to be regarded as acting truly compositely with the wall plates. They were also not fastened to the wall plates at sufficiently close intervals for true composite load sharing.

A lot of argument also attempted to consider the effects on the failure, of construction defects such as vertical misalignment of plates, and the effect of changing the plate thickness on the buckling propensities of the silo walls.

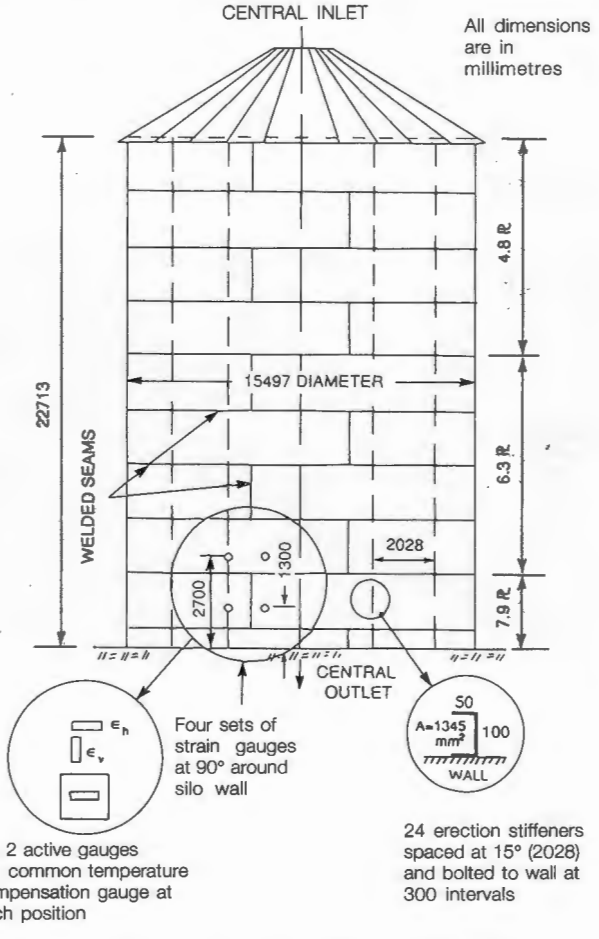

Fig. 1: Principal dimensions and details of instrumentation of silo

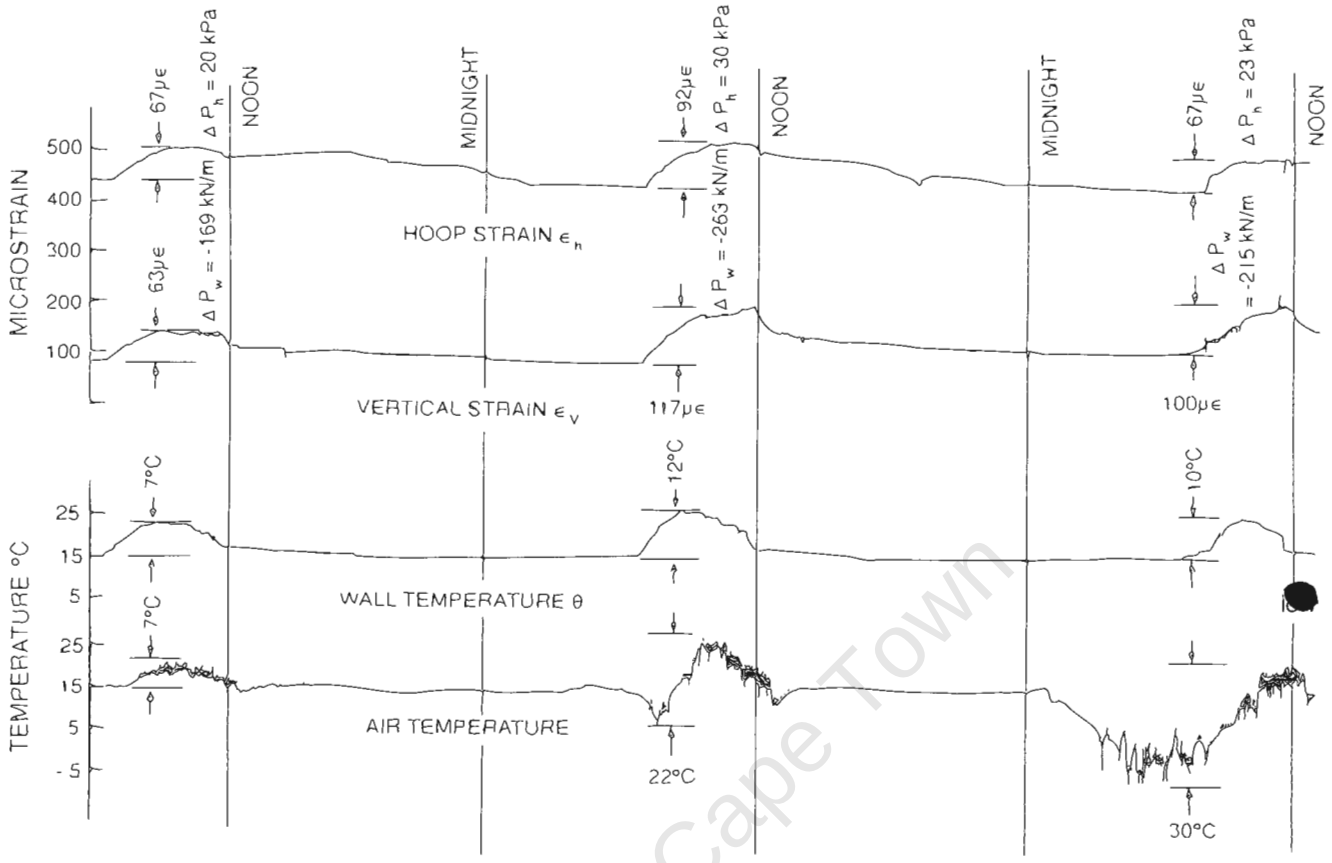

Fig. 5: Variation of vertical and horizontal strain as a function of temperature

calculated values of ΔP_w are compared with the measurement shown in Fig. 4, it will be seen that when the temperature was at a minimum, the frictional wall load at *B* was very low. In fact, for the second temperature cycle recorded in Fig. 5, the wall at *B* probably went slightly into tension. These observations all confirm what has been measured previously [1, 4].

It should be emphasized that as the sun moves over the surface of the silo, each point on the silo circumference experiences a temperature wave such as those shown in Fig. 5, and there is a corresponding cyclic fluctuation in the strains and stresses in the wall. The lateral pressures and wall loads in the silo can therefore only ever be expected to be uniform around its circumference at times when the temperature of the whole silo wall is uniform. For South African conditions this probably only occurs for an hour or two shortly before dawn in windless conditions.

In a recent paper [3] the writer put forward an expression for calculating the change of horizontal pressure Δp_h corresponding to a change of temperature $\Delta\theta$:

$$\Delta P_h = \frac{2MEt\alpha\Delta\theta}{MD + 2Et}$$

where:

M = compression modulus of grain in silo
E = elastic modulus for material of silo wall
t = wall thickness
α = coefficient of linear expansion for material of silo wall
D = silo diameter.

A diagram was also presented (reproduced as Fig. 6) relating the compression modulus *M*, derived from measurements on full size silos, to the overburden stress above the point of measurement. Applying the equation and a modulus $M = 300$ MPa for a temperature change of 10°C gives a value for $\Delta P_h = 13$ kPa which is somewhat lower than the values of Δp_h recorded in Fig. 5. The measured unit weight of the maize was in this case 8.7 kN/m^3 as compared with 7.5 kN/m^3 for the other data.

The difference appears to arise from the fact that the earlier measurements had referred to silos filled with white maize, whereas the present silo was filled with yellow maize having a smaller, apparently denser kernel.

As the compression modulus of a granular material is usually related to its density, values of *M* for this silo have been recalculated from the data shown in Fig. 5. The average calculated value of *M* has been included in Fig. 6.

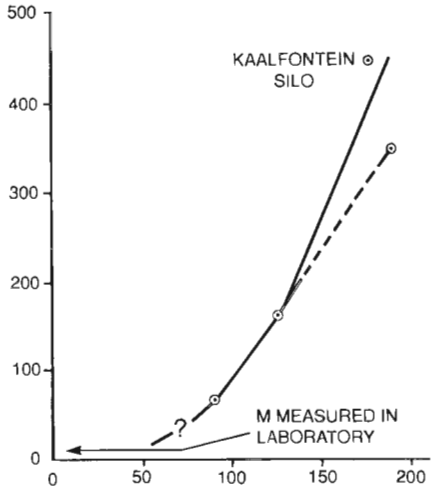

Fig. 6: Relationship between overburden stress and compression modulus for maize

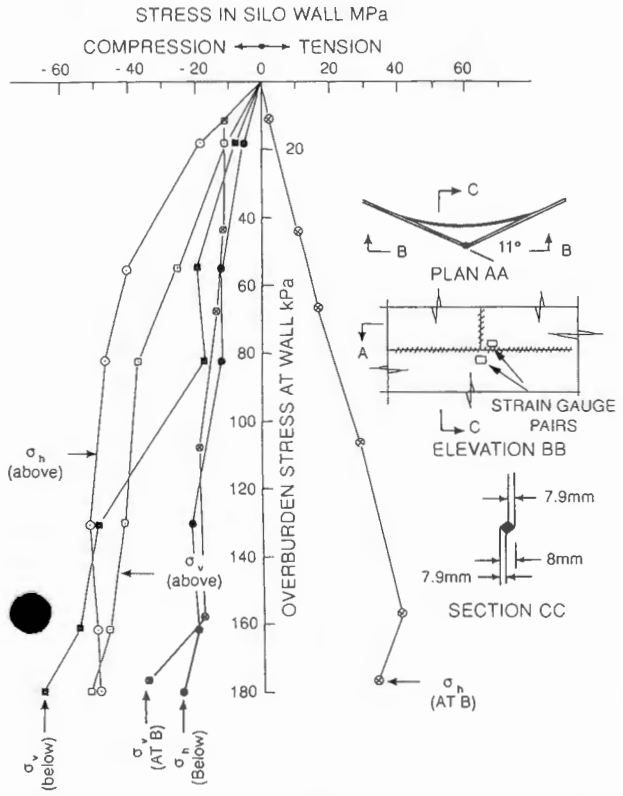

Fig. 7: Strains at a construction defect expressed as stresses in the silo wall

7. The Effect on Strains of a Construction Defect

The worst-appearing construction defect on the silo wall within easy access was strain gauged to study its effect on vertical and horizontal strains. This point (*E* in Figs. 3 and 4) was just below the lower level of the main instrumentation. The form and dimensions of the defect have been illustrated in Fig. 7.

The straight ends of two pre-curved plates meet at this point to form a prow at an angle of 11° (plan *AA*). In vertical section (*CC*) this introduces an eccentricity in the vertical alignment of the plates of 8 mm which equals the thickness of the plates involved. Strain gauge pairs were mounted above and below this eccentricity in the positions indicated in elevation *BB*.

The strain measurements have been expressed as vertical and horizontal stresses in Fig. 7. As a basis of comparison σ_v and σ_h measured at the defect have been displayed alongside σ_v and σ_h measured at the lower point *B*, midway between construction stiffeners. At *B* the hoop stress σ_h was tensile throughout the filling of the silo while σ_v, the frictional wall stress, was compressive.

However, both σ_h and σ_v, both above and below the defect were compressive throughout. Values of σ_v were not dissimilar to those measured at *B*. The fact that σ_h, the hoop stress on the outside of the plate above and below the defect was compressive shows that the internal horizontal pressure tends to reduce the 11°angle of the prow thus introducing a severe horizontal bending moment.

If the hoop tension at *B* in defect-free plates was about 40 MPa, and the outside of the plates of the silo at the defect was about 50 MPa, the tension at the inside surface of the plates at the defect must, for force equilibrium, have been 90 to 100 MPa. (The precise value cannot be determined). Hence, while the defect appears to have no marked effect on vertical stresses in the silo wall, it also appears to result in a doubling of the maximum tensile stress in the wall.

If the *von Mises* criterion for yield of the wall is

$$\sigma_v^2 - \sigma_v\,\sigma_h + \sigma_h^2 = \sigma_{vm}^2 = \sigma_y^2$$

where:

σ_{vm} = *von Mises* stress
σ_y = yield stress of the plate in uniaxial tension,

then inserting values

$$\sigma_v = -50 \text{ MPa and } \sigma_h = 40 \text{ MPa}$$

gives

$$\sigma_{vm} = 78 \text{ MPa}$$

If, however

$$\sigma_v = -50 \text{ MPa and } \sigma_h = 100 \text{ MPa}$$

$$\sigma_{vm} = 132 \text{ MPa}$$

Hence the *von Mises* stress is considerably increased. However, as the yield stress of the plate is probably about 300 MPa, there is no danger of yield occurring.

8. Conclusions

The strain measurements taken on this silo have generally confirmed the results of earlier measurements on steel silos:

1. No *Janssen*-type arching developed in this silo, and the relationship between horizontal pressure and depth or overburden was linear, with a temperature surcharge.
2. Measurements of frictional wall load again revealed the sensitivity of this load to wall temperature. The measurements indicated that the stiffeners may relieve the wall load carried by the plate, but this relief is localized and variable in extent.
3. Measurements of the effects of temperature change on wall stresses confirmed earlier observations and added data to the relationship between the compression modulus of ensiled maize and the overburden stress.
4. Construction defects were shown, in this case, to have a large effect on horizontal stresses in the silo wall in the vicinity of the defect. Vertical stresses were almost unaffected.

Acknowledgements

The writer thankfully acknowledges the cooperation and assistance received from the Eastern Transvaal Co-operative Ltd., owners of the test silo and of Bessemer Steel Construction Ltd., the silo designer-erectors.

References

[1] *Blight, G. E.* and *Garstang, A.*: Strains Measured in a 7,500 t Sugar Silo; bulk solids handling, Vol. 7 (1987) No. 4, pp. 573-582.
[2] *Blight, G. E.*: Behaviour of a Bolted Corrugated Steel Grain Silo; powder handling & processing, Vol. 1 (1989) No. 2, pp. 143-149.
[3] *Blight, G. E.*: Strain and Temperature Measurements on an Externally Stiffened Corrugated Steel Grain Silo; powder handling & processing, Vol. 1 (1989) No. 4, pp. 343 - 347.
[4] *Blight, G. E.*: Temperature Changes Affect Pressures in Steel Bins; Int. J. Bulk Solids Storage in Silos, Vol. 1 (1985) No. 3, pp. 1-7.
[5] *Blight, G. E.*: Design Loading for Grain Silos – Intention and Reality; American Society of Agricultural Engineers, Paper No. 88 - 4024, 1988, p. 12.

P.A. Shamlou:

Handling of Bulk Solids

– Theory and Practice –

1988, 200 pp, 143 figs & tables, 270 refs, DM 118,- / US$ 59.50

Contents:

Excerpts from book reviews:

"The increasing importance of basic knowledge on solids storage, handling and conveying is reflected by this book.

The book is divided into 8 chapters from which the first 4 deal with:

- bulk solids flow and handling properties (particle size, shape distribution, particle interaction as electrostatic, van der Waal´s and capillary forces, fluidization behaviour and flow properties of powders)
- pressure profiles in bulk solids storage vessels (flow profiles, pressure distribution during filling and discharge, Janssen´s and Walter´s equation, Mohr stress circle, comparison of formulae with published measurements)
- design of storage vessels for particulate solids (critical width of an outlet for no-arching and no-piping with consideration of time consolidation, measurement of bulk solids flow properties including wall friction)
- gravity flow of particulate solids (discharge rates for coarse and fine solids)

The remaining 4 chapters are devoted to:

- pneumatic conveying of bulk solids (positive pressure systems, dilute-phase and dense-phase systems, pressure drop, choking conditions)
- hydraulic transport of particulate solids (settling of solids from suspensions, non-settling slurries, rheology, pressure drop, equipment components)
- mechanical conveyors (screw feeders, belt, bucket and en-masse conveyors and elevators, mechanical feeders)
- safety in bulk solids handling (dust explosions, explosion prevention, health hazards, dust control equipment as cyclones, filters and scrubbers).

Each chapter is extended by an example and a literature survey. The book gives a good survey into the state of the art without providing too many theoretical details. Therefore, it is a good introduction and book accompanying a basic course or seminar. It is one of the few books suitable for such a course without originating from a seminar held previously. As is stated in the preface, this book "fills a gap between the experienced researcher and those new to the work".

"For the serious student and the practical safety and process management team who wish to plan through a reasoned, calculated approach, rather than by unquestioned tradition and guesswork, this volume is an excellent investment."

Trans Tech Publications P.O. Box 12 54 D-3392 Clausthal-Zellerfeld F.R. Germany
Trans Tech Publications Old Post Road Brookfield, VT 05036 USA

powder handling & processing Volume 2, Number 2, June 1990

Measured Loading on a Small Steel Grain Silo

G.E Blight, South Africa

Summary

A [illegible] t steel maize silo of bolted construction has been strain-gauged in order to confirm certain premises concerning design loading for silos.

The measurements have confirmed:

1. That *Janssen*-type arching which may develop in silos during filling will break down at the start of emptying;
2. that there are no switch pressures at the silo-to-hopper transition in a silo;
3. that the horizontal pressure distribution in the hopper forms an extension to that in the cylinder of a silo.

The measurements have also confirmed a method proposed for calculating temperature surcharge pressures.

1. Introduction

In a recent paper [1] the author made proposals concerning the loading to be assumed for the design of silos. The proposals are based on in-situ measurements of pressures and wall loads in a large number of steel and reinforced concrete silos [2, 3]. P[illegible]sures on these structures have been measured by a number of workers, in addition to the author, and measuring instruments have included strain-gauged diaphragm pressure cells and electric resistance strain gauges.

The premises on which the proposals were based are as follows:

(a) *Janssen*-type arching is an unreliable phenomenon that may or may not occur during filling of a silo, depending on such factors as geometry, conditions of wall friction and the characteristics of the silo filling.

(b) Any arching that occurs during uninterrupted filling of a silo is likely to break down, at least locally, at the start of emptying. This will result in pressures on the structure increasing, either generally or locally.

(c) Pressures at a given level will vary around the perimeter of a silo. This variation should be considered in design.

d) Pressure profiles with depth in the hopper portions of silos form a continuation of the pressure profile in the cylindrical portion. Switch pressures do not occur at the transition from the cylindrical to the hopper portion.

(e) Pressures in steel silos, and possibly also in reinforced concrete silos, are subject to temperature surcharges. The temperature surcharge pressure should also be considered in design.

An opportunity has recently arisen to test these premises by making a series of measurements on a small steel grain silo. This paper describes the results of these measurements and show how they support the various premises.

2. Description of Silo and Instrumentation

Fig. 1 shows the layout of the silo in vertical section as well as giving its main dimensions. Fig. 2 is a view of the silo complex of

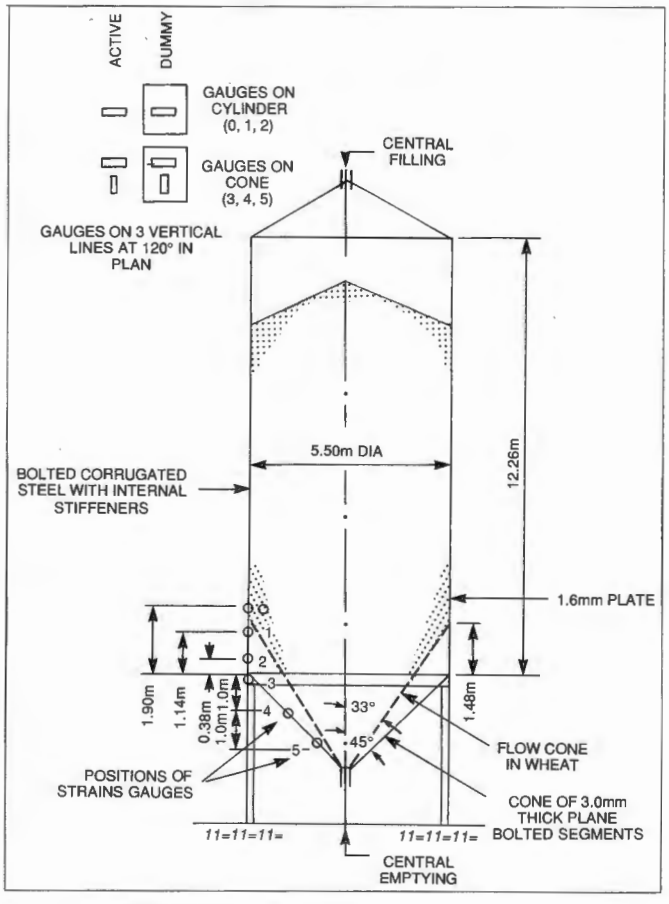

Fig. 1: Main dimensions and layout of silo; layout of strain gauges in elevation

For information on author - see page 196

Fig. 2: View of silo complex at Bethlehem, South Africa

Fig. 3: View of conical hopper at base of test silo

which the test silo forms part (the test silo is in the rear row in the photograph). The silos are of all-bolted construction. Fig. 3 is a view of the conical hopper at the base of the silo.

The upper cylindrical portion of each silo is of galvanized corrugated steel and has 12 internal stiffeners that bear on the supporting legs visible in the two photographs. The base of the cylinder rests on a ring beam (also visible in the photographs).

The conical 45° hopper is made up of 24 segments of plane galvanized steel. The thickness of the corrugated plates at the base of the cylinder is 1.6 mm and the hopper segments are 3.0 mm thick.

Fig.1 shows the layout of the instrumentation in elevation. Strain gauges were placed at three elevations on the cylinder and three on the hopper. As one of the objectives of the investigation was to check on the presence of a switch pressure at the cylinder-to-hopper transition, the gauges were positioned to cover the intersection with the cylinder of the effective hopper or flow cone that would form within the grain during emptying.

As access to the internal stiffeners was not possible, only hoop strains were measured on the cylinder. Earlier work [4, 5] has shown that strain in a cylindrical corrugated wall is essentially uniaxial and hence the gauges were placed horizontally, each active gauge being connected with a temperature-compensating dummy gauge to give a half strain bridge.

Strains in the conical hopper are two-dimensional. Hence strain gauges were mounted in pairs with the axis of one gauge horizontal, and the other vertical. Each active gauge was connected with a temperature-compensating dummy gauge, as indicated in Fig.1.

The instrumentation was repeated on three vertical lines separated by 120° in plan. One line of strain gauges on the hopper can be seen as light patches in Fig. 3. It transpired later that the gauges at level 3 were placed too close to the very rigid ring beam, where the plate of the cone was acting compositely with the beam. Consequently, strains measured on level 3 could not be interpreted and are not referred to in this paper.

The silos are loaded through a central filling point via an overhead conveyor. A big advantage of working on such a small silo (which holds only 250 t) is that it can be filled from empty in 8 h, whereas the larger multi-thousand ton silos the author is used to working on take several weeks or months to fill.

3. Properties of Grain

The silo is used for storing wheat. The unit weight of the wheat was obtained from weighbridge records and the corresponding volume of the silo occupied by the grain. The unit weight, measured in this way and averaged over two fillings of the silo was $\gamma = 8.2$ kN/m^3.

Unit weights measured in the laboratory varied from 7.9 kN/m^3 for loosely poured grain to 8.4 kN/m^3 for grain compacted by vibration. For the purposes of this paper the unit weight determined in the silo, e.g. 8.2 kN/m^3 has been adopted.

The angle of shearing resistance of the wheat measured in shear box tests was

$$\phi = 25°$$

giving an active pressure coefficient of

$$K_A = 0.41$$

and an at rest pressure coefficient of

$$K_0 = 0.58$$

The angle to the vertical of the effective hopper or flow cone in the wheat would be

$$45° - \phi/2 = 33°$$

The angle of wall friction of wheat on smooth galvanized steel sheet was measured as

$$\delta = 16°$$

However, as a recent paper [6] has shown, the effective angle of wall friction for the corrugated barrel of the silo would be

$$\delta = \phi = 25°$$

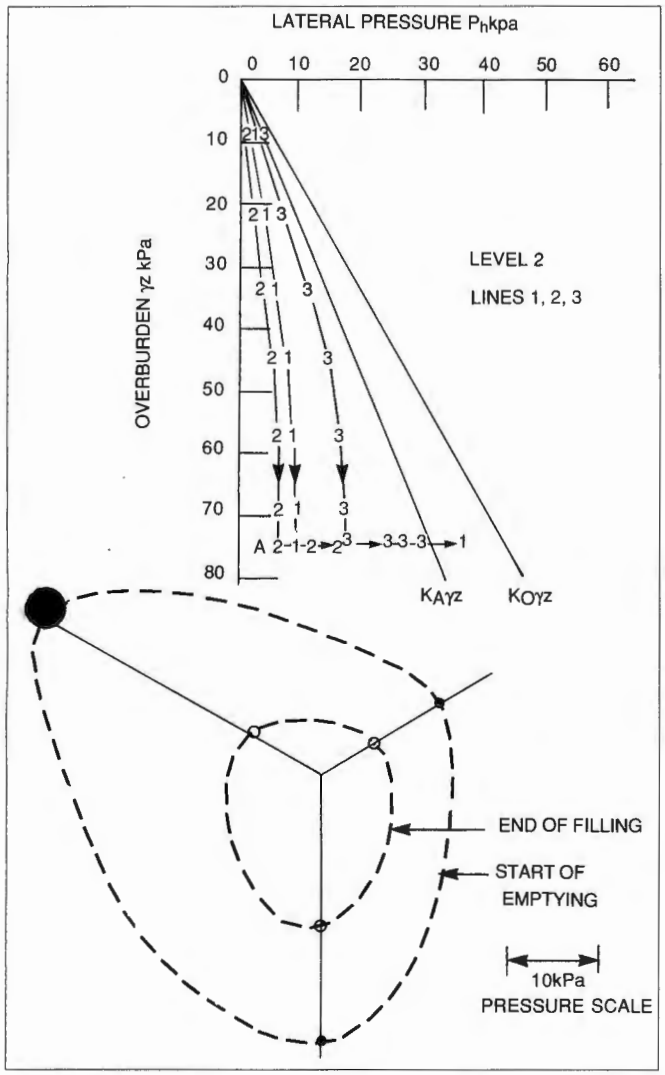

Fig. 4: Stress paths and profile in horizontal plane for p_h around perimeter of silo during filling and at start of emptying

4. Stress Paths for Silo Barrel

Fig. 4 shows the stress paths (i.e. the variation of lateral pressure with overburden) observed at level 2 on each of the three vertical lines 1, 2 and 3.

It is obvious from the curvature of the stress paths and the fact that they fall below the $K_A\gamma z$ line that *Janssen*-type arching developed in the silo as it was filled. At *A* in Fig. 4, emptying was started and the lateral pressures increased as shown in the diagram, with the final pressure at lines 1 and 3 being close to the $K_A\gamma z$ line. As the $K_A\gamma z$ line represents a stress path for a no-arching condition, this shows that the start of emptying caused the arching to break down and hence the lateral pressure to increase to that corresponding to the no-arching condition.

The diagram also shows that pressures do not appear to be uniform around the perimeter of the silo. The lower part of Fig. 4 gives an indication of the apparent radial pressure distribution both at the end of filling and at the start of emptying.

In considering this diagram, it must be remembered that what is being portrayed is hoop strain expressed as lateral pressure. At least part of the apparent variation of pressure around the silo perimeter is probably caused by geometrical imperfections in the silo shell. The shell is unlikely to be perfectly circular in cross-section when not under load, but being flexible, will take up a near-perfect circularity when loaded. If a particular plate when unloaded, has a radius that is more than the radius when

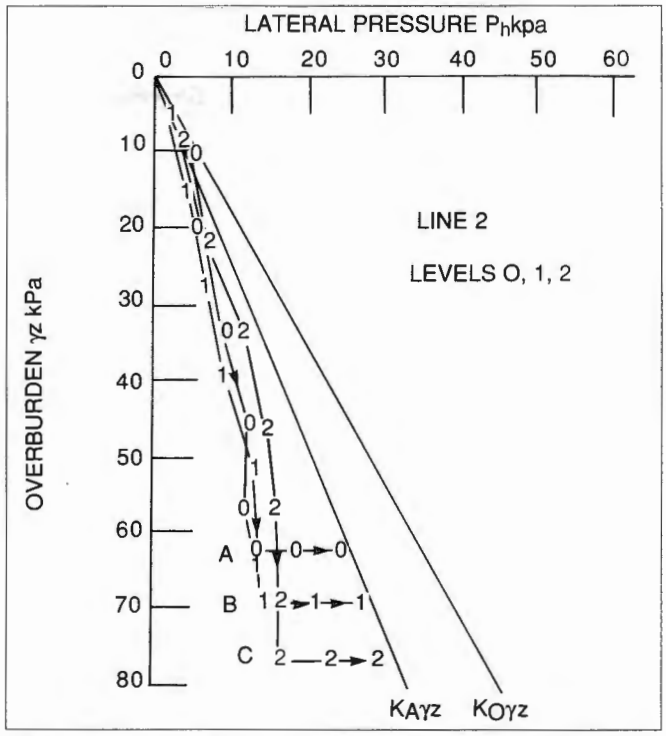

Fig. 5: Lateral pressure in cylinder of silo - stress paths showing variation of p_h at different levels on same meridian line during filling and at start of emptying

loaded, a strain gauge affixed to its outside surface will record more than the average strain, and *vice-versa*. The reason why low strains were recorded on lines 1 and 2 during filling may be that the unloaded plates have a sharper curvature than the average for the silo. However, whether the variation of lateral pressure around the circumference is real or only apparent, there is a real variation of hoop strain. Hence this effect should be considered in design.

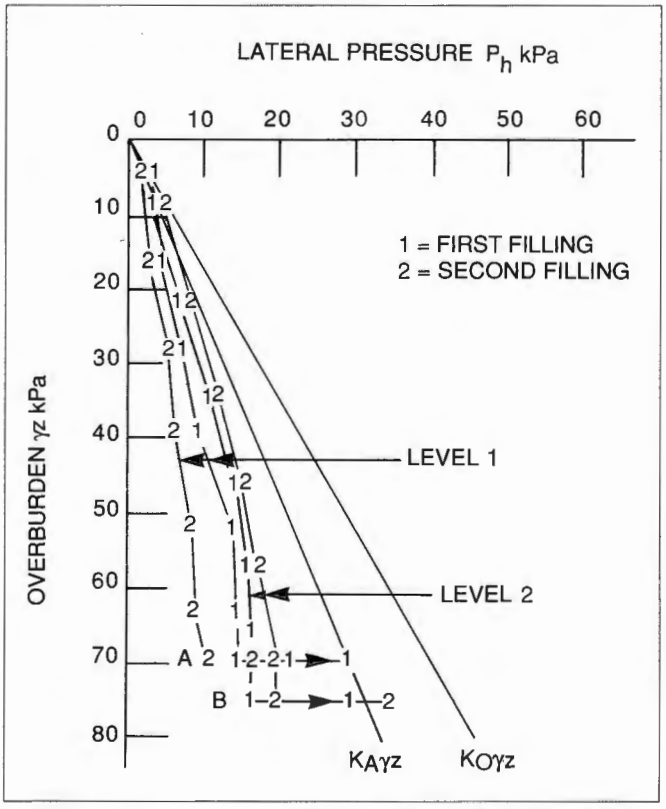

Fig. 6: Lateral pressure in cylinder of silo - stress paths showing variation of p_h from one filling and start of emptying to another

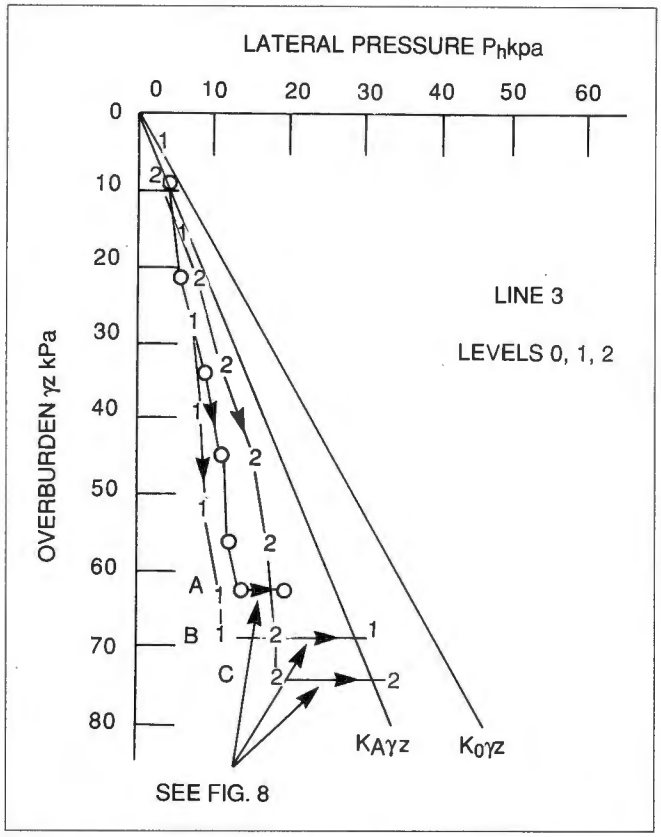

Fig. 7: Lateral pressure in cylinder of silo - stress paths showing variation of p_h at different levels on the same meridian. Details of change of p_h at start of emptying shown in Fig. 8

Fig. 5 shows stress paths measured at levels 0, 1 and 2 on line 2. Filling was completed at points *A*, *B* and *C*. The stress paths lie very close together and all show a break-down of arching at the start of emptying, with pressures increasing to lie on the $K_A\gamma z$ line.

Fig. 6 compares stress paths observed at levels 1 and 2 on lines 1 and 2 for two successive fillings of the silo. It will be seen that the behaviour of the silo is essentially the same and measurements are repeatable on successive fillings.

Fig. 7 shows similar stress paths to those shown in Figs. 4, 5 and 6. In this case recordings were made of the change in pressure with time from the start of emptying.

These recordings are shown in Fig. 8. After a slight initial decrease the pressure was found to increase gradually over a period of 5 to 20 minutes to reach a maximum value. There is no sign of any sudden switch in pressure, no sign of any transient pressure wave, or dynamic pressure, as postulated by certain authors, e.g. [7].

5. Stress Paths for Hopper

Fig. 9 shows stress paths measured for pressures normal to the hopper wall at level 4. The *Mohr* stress diagram in the lower part of Fig. 9 shows how the corresponding lateral pressures were deduced, assuming that full wall friction had developed with an angle of wall friction of

$$\delta = 16°$$

Because the three measured normal stress paths were so close, Fig. 9 shows only the mean values of p_h, the deduced lateral pressure.

In the unloaded condition, a horizontal cross-section of the hopper is polygonal rather than circular although the faces of the "polygon" are curved, not plane. The cross-section becomes truly circular when loaded. As explained above, the effect of this change of geometry is to cause strains that are larger than those arising in a truly circular hopper cross-section. There is no way of rigorously correcting for the effect of the change in geometry.

However, Fig. 9 shows a corrected stress path based on the reasonable assumption that the application of load when the first strains were measured (γz = 12 kPa) was sufficient to cause the hopper to go circular and that thereafter no correction was necessary. As Fig. 9 shows, the corrected stress path for p_h then follows the $K_A\gamma z$ line.

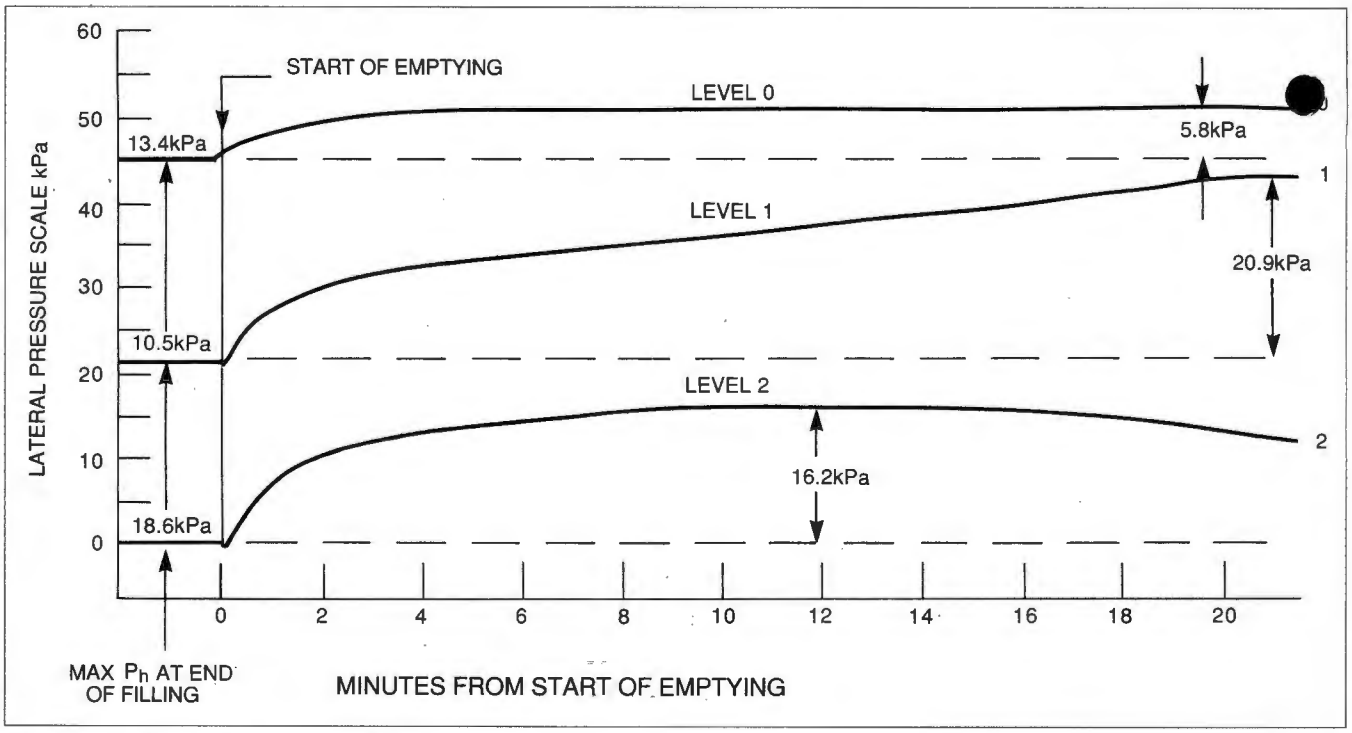

Fig. 8: Variation of lateral pressure at start of emptying

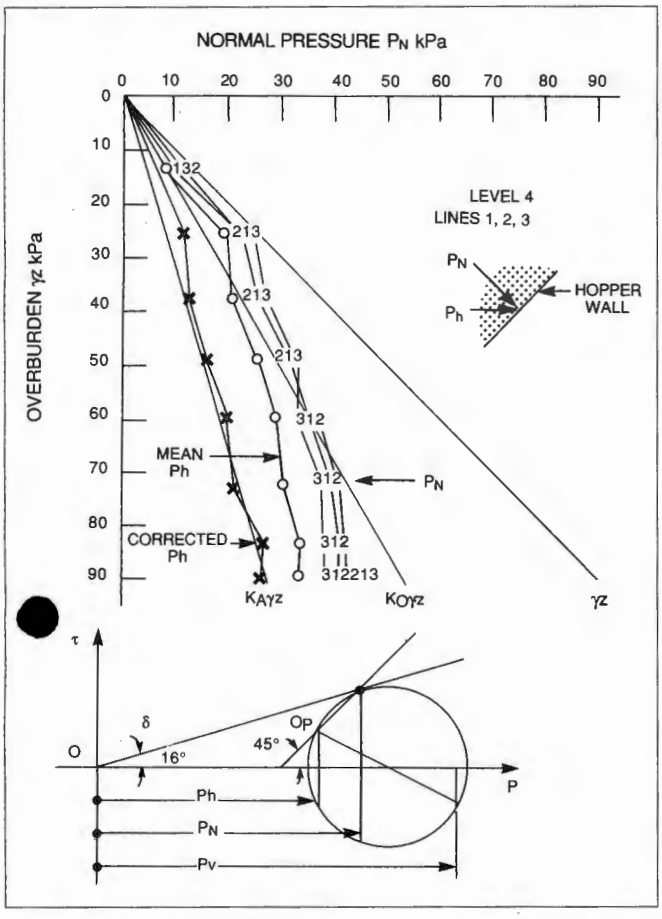

Fig. 9: Pressures in hopper of silo - stress paths showing variation of p_N and p_h at level 4

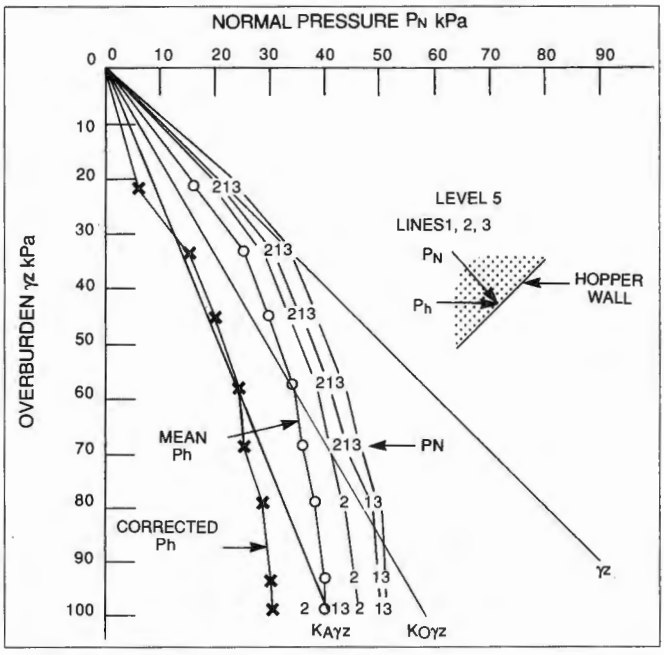

Fig. 10: Pressures in hopper of silo - stress paths showing variation of p_N and p_h at level 5

Fig. 10 shows a similar set of measurements at level 5. The corrected stress path for p_h again follows the $K_A\gamma z$ line quite closely. It will thus be seen that stress paths for lateral stress in the hopper are very similar to the stress paths for lateral stress in the cylinder.

It should be noted that the angle of wall friction (δ) in the hopper is probably greater than 16° because of the roughening effect of the many bolt heads [6]. If the effective δ for the hopper wall exceeds 16°, then p_h for a given p_N will decrease.

Hence the corrected stress paths of p_h shown in Figs. 9 and 10 probably represent maximum values of p_h and the actual stress paths for lateral pressure in the hopper are even closer to those for lateral pressure in the cylinder.

Note also that at the start of emptying there is very little change of pressure in the hopper. This supports the conclusion that the stress path for lateral pressure in the hopper lies on the $K_A\gamma z$ line, i.e. that little arching occurs in the hopper.

6. Temperature Surcharge

Fig. 11 shows recordings of prevented or stress-inducing thermal strain and temperature of the silo wall at level 2, line 3 on

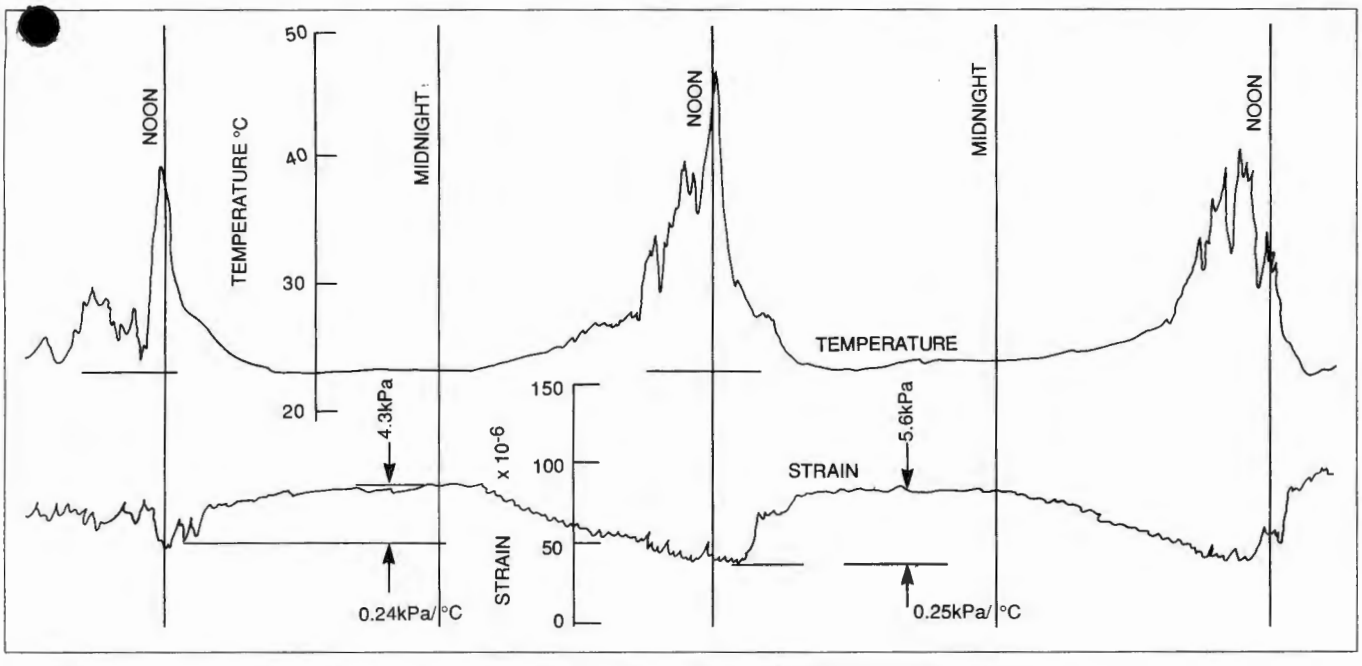

Fig. 11: Simultaneous recording of wall temperature and prevented thermal strain made at level 2, line 3 after second filling

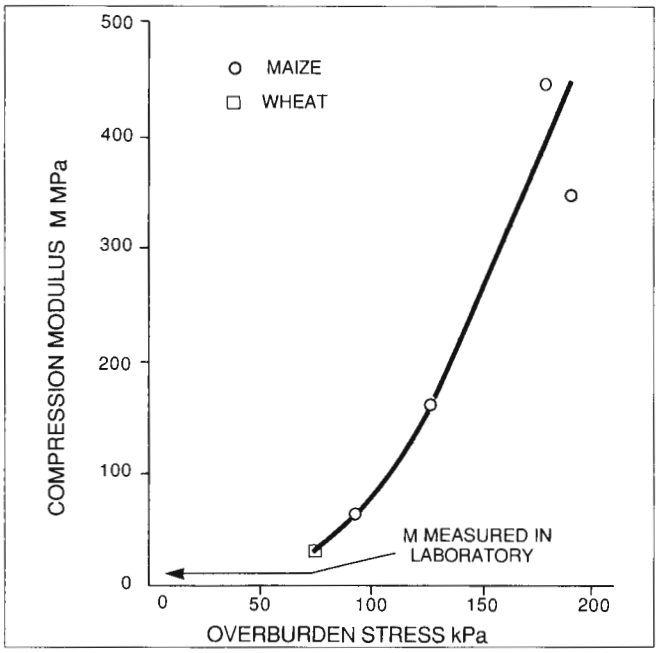

Fig. 12: Relationship between compression modulus M and overburden stress calculated from measurements on five steel grain silos

three successive days. During this period the silo stood static, full of wheat, but no grain was added or withdrawn.

As a result of the diurnal fluctuation of temperature, a temperature surcharge of about 6 kPa, or 0.25 kPa per °C change in temperature arose.

In earlier papers, e.g. [8], the following relationship has been derived between

α = coefficient of thermal contraction of the silo wall

$\Delta\theta$ = change in temperature of the wall

E = elastic modulus of the silo wall

t = wall thickness

D = silo diameter

M = modulus of compressibility of the grain for radial compression, and

TS = temperature surcharge pressure:

$$TS = \frac{2MEt\ \alpha\Delta\theta}{MD + 2Et} \qquad (1)$$

Measurements by the author supporting this relationship have so far been made on fairly large steel silos storing maize. However, laboratory measurements [9] have shown that the value of M for wheat is probably not too dissimilar to that for maize.

Fig. 12 shows the value of M calculated for wheat from the present measurements, superimposed on a relationship between M and overburden stress established from measurements on maize silos. It appears that the data for maize and wheat could be reasonably well represented by a single curve.

Hence the temperature surcharge measurements made on the silo support those made earlier on other steel grain silos.

7. Conclusions

Measurements made on this 5.5 m diameter wheat silo have fully confirmed the premises stated in the introduction:

(i) *Janssen*-type arching does occur in this silo, during filling, but breaks down at the start of emptying, at which stage the pressure profile with depth in the silo can accurately be represented by

$$p_h = K_A \gamma z$$

at any depth z.

(ii) Pressures at any level vary around the perimeter of the silo. It may be necessary to take consideration of this variation during design.

(iii) The pressure profile with depth in the hopper portion of a silo forms an extension to the pressure profile in the cylinder. Switch pressures do not occur at the cylinder-to-hopper transition.

(iv) Pressures in steel silos are subject to temperature surcharges if the silo contents are left static for any length of time. The magnitude of the temperature surcharge pressure may be calculated from Eq. 1 in conjunction with the data on the compression modulus of grain shown in Fig. 12.

Acknowledgement

The research reported in this paper would not have been possible without the cooperation and assistance of Messrs Sasko Limited, Millers of Bethlehem, Republic of South Africa.

The author was placed in contact with Sasko by Bessemer Steel Construction, builders of the silo.

References

[1] *Blight, G.E.*: Defects in accepted methods of estimating design loading for silos; Submitted to Proceedings, Institution of Civil Engineers, London, Part 1, 1990.

[2] *Blight, G.E.*: Pressure exerted by materials stored in silos; Part 1: Coarse materials, and Part 2: Fine powders; Geotechnique, Vol. 36 (1986) No. 1, pp. 33-57.

[3] *Blight, G.E.*: A Comparison of Measured Pressures on Silos with Code Recommendations; bulk solids handling, Vol. 8 (1988) No. 2, pp. 145-153.

[4] *Blight, G.E.*: Behaviour of a Bolted Corrugated Steel Grain Silo; powder handling and processing, Vol. 1 (1989) No. 2, pp. 143-149.

[5] *Blight, G.E.*: Strain and Temperature Measurements on an Externally Stiffened Corrugated Steel Grain Silo; powder handling and processing, Vol. 1 (1989) No.4, pp. 343-347.

[6] *Blight, G.E.*: Silo Wall Friction and Wall Roughness; powder handling and processing, Vol. 2 (1990), submitted.

[7] *Schmidt, L.C.* and *Wu, Y.H.*: Prediction of Dynamic Wall Pressures on Silos; bulk solids handling, Vol. 9 (1989) No. 3, pp. 333-338.

[8] *Blight, G.E.*: Load and Temperature Strains of a Welded Plane Plate Grain Silo; powder handling and processing, Vol. 2 (1990) No. 1, pp. 25-29.

[9] *Blight, G.E.*: Swelling Pressure of Wetted Grain; bulk solids handling, Vol. 6 (1986) No. 6, pp. 1135-1140.

powder handling & processing Volume 3, No. 1, March 1991

Structure–Fill Interaction in Steel Grain Silos

G.E. Blight, South Africa

Summary

Lateral pressures and stiffener loads have been measured in three internally stiffened corrugated steel silos of bolted construction. The object was to study the interaction between the barley stored in all three silos and the containing structures. The complexity of this interaction was illustrated by the measurements, although it was found that all three silos behaved in an essentially similar manner.

Further information on temperature surcharge pressures was also obtained from measurements on the barley silos, and on a fourth silo storing barley malt.

1. Introduction

The interaction between filling and structure of three steel silos storing barley has been studied. The silos, all of bolted corrugated steel with internal stiffeners, each have slightly different dimensions and different structural details. The factor common to all of them is that they all store barley. The study of this silo group, part of the storage facility of a barley malt extract company, was undertaken to see the effects that differing sizes and proportions of silo have on wall loads, lateral pressures and temperature effects for the same filling material. In addition to the three barley silos, temperature effects were also measured on a fourth silo, storing barley malt.

It is believed to be the first time that a comparative study of this type has been undertaken. Studies of full size silos are relatively rare. Usually, only a single silo is studied and where there is a group of silos, all are usually identical, so that there seems to be little point in instrumenting more than a single typical one (e.g. [1]). In the malt factory complex, however, there are a variety of silos of many sizes. Their common characteristics are that they all store barley or barley malt.

As usual in this type of study, it was necessary to fit the experimental work in with the normal operation of the factory. Usually, only three to four days were available during which a particular silo was empty and available for instrumentation. The silos were not usually cleaned out completely, and the barley remaining inside after emptying limited access for instrumenting to certain sectors of the silo interior. Another limitation was that some of the silos are set very close together, or close to walls, so that access is not possible to the whole of their exterior perimeter.

2. Description of Silos and Instrumentation

Only one silo will be described in detail. The others are similar, but with different details. The factory numbers of the barley silos studied are 1, 8 and 10. The malt silo is number 9. These numbers will be used in this paper.

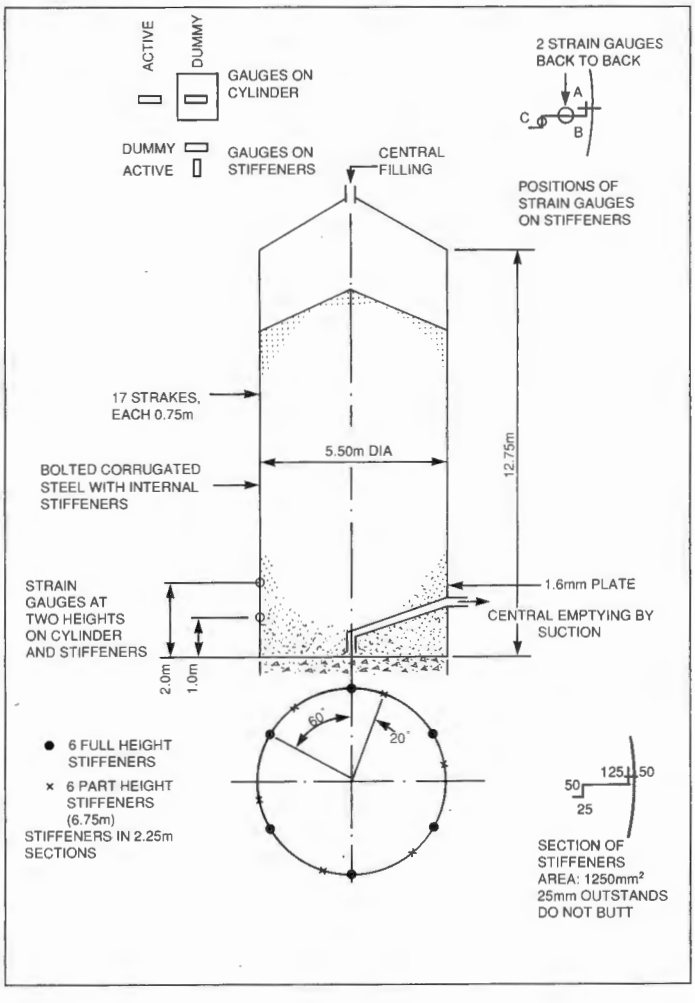

Fig. 1:
Main Dimensions and layout of the silo. Layout of strain gauges in elevation and plain

Professor *Geoff E. Blight*, Department of Civil Engineering, University of Witwatersrand, Johannesburg, South Africa.

Details about the author(s) of this paper on page 94

Fig. 1 shows the detailed dimensions of silo 10, while Fig. 2 is a photograph of the structure. The horizontally corrugated cylinder is supported on a concrete slab base and is stiffened by means of 6 full height z-shaped stiffeners and 6 part-height stiffeners. The silo is filled centrically by pneumatic pumping and emptied centrically by the same means.

The instrumentation covered the 120° arc of the silo circumference that was accessible from the outside, and consisted of electric resistance strain gauges. Strain gauges were mounted at two levels near the base of the silo. On the corrugated cylinder, active gauges were mounted horizontally and connected as a half bridge with separate temperature compensating dummy gauges. The dummy gauges were mounted on separate small tags of galvanized steel which were stuck to the silo shell using double sided adhesive foam tape. Gauges on the silo cylinder were duplicated inside and outside of the silo. The gauges inside were protected from the scouring action and pressure of the grain against the silo walls, by means of strips of galvanized steel. Great care had to be taken to ensure that the dummy gauges remained stress-free and that their mounting tags did not become subject to bending from the pressure of the grain.

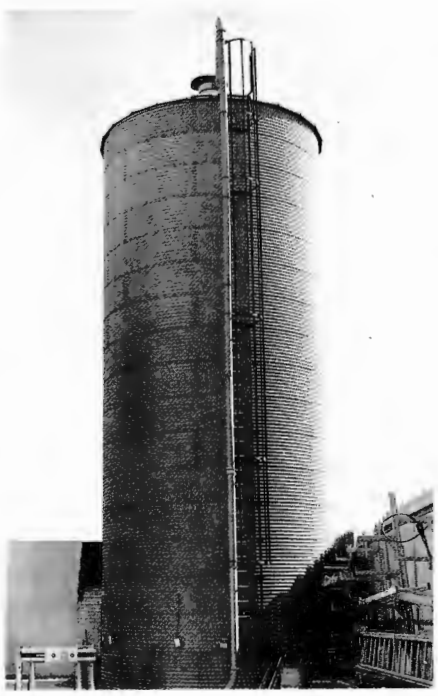

Fig. 2: Appearance of barley silo No. 10

Fig. 3 shows four of the instrumented stiffeners inside silo 10 while Fig. 4 shows the sheet steel protection over the strain gauges on a stiffener. The leads from the upper level of strain gauges and the plastic terminal boxes can be seen near the base of silo 10 in Fig. 2.

On the stiffeners, strain gauges were mounted in pairs, one vertical, one horizontal. This arrangement gives a temperature compensated half bridge that records $(1 + \upsilon)$ times the true longitudinal strain of the stiffener, where υ is Poisson's ratio for steel. Strain gauges on the stiffeners were also protected against scour by skirts of galvanized steel. Connecting wires for the internal strain gauges were brought to the outside through bolt holes, and thence to the reading positions. External gauges were fully waterproofed by means of a rubber solution as well as bitumen-backed aluminium tape.

As shown in Fig. 1, silo 10 has a diameter of 5.5 m and a height of 12.75 m. (It is, in fact, identical with the upper part of the wheat silo described in an earlier paper [2]).

Silo 8 has a diameter of 7.3 m and a height of 10 m. It is stiffened internally by means of 8 equally spaced angles measuring 50 mm x 50 mm x 5 mm thick. Instrumentation was applied to three stiffeners and the adjacent cylinder, equally spaced at 120° in plan.

Silo 1 has a diameter of 6.37 m and is 7.7 m high. It is also stiffened by 8 equally spaced 50 mm x 50 mm x 5 mm thick angles. Silo 1 forms part of a cluster of 4 similar silos inside a building. Because of the walls and the other silos, only three adjacent stiffeners were accessible from the outside, and only two stiffeners, separated by 90° in plan, were strain-gauged.

Silo 9, the barley malt silo, is also inside a building. It has a diameter of 11 m, and is 7 m high. Access to the inside of Silo 9 has not been possible as it is an operating silo that is kept partially full at all times. The cylinder of the silo was strain-gauged at two points to study the effects of temperature variations on lateral pressure.

3. Properties of Barley and Barley Malt

The properties of the barley and barley malt were measured in the laboratory with the following results:

Unit weight:
barley $\gamma = 6.8$ kN/m^3
malt $\gamma = 5.6$ kN/m^3

Angle of shearing resistance:
barley $\phi = 27°$
malt $\phi = 30°$

Active pressure coefficient:
barley $K_A = 0.38$
malt $K_A = 0.33$

At rest pressure coefficient:
barley $K_o = 0.56$
malt $K_o = 0.45$

Because of the corrugated walls of the four silos, the angle of wall friction δ was not measured separately as it was assumed that ϕ would represent δ for the corrugated wall.

Fig. 5 shows a curve of shear stress versus shear displacement for a shear box test on barley under a normal stress of 50 kPa. Note that to develop an angle of shearing resistance of 27° requires a shear displacement of 9 mm, while to

Fig. 3: Instrumented stiffeners inside silo 10

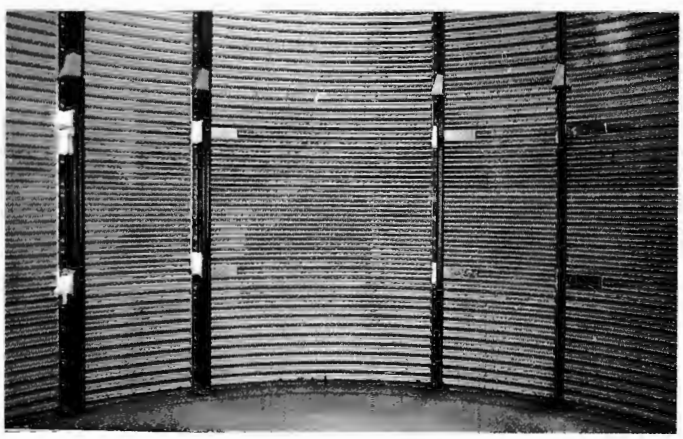

Fig. 4: Sheet steel protection to strain gauges on a stiffener

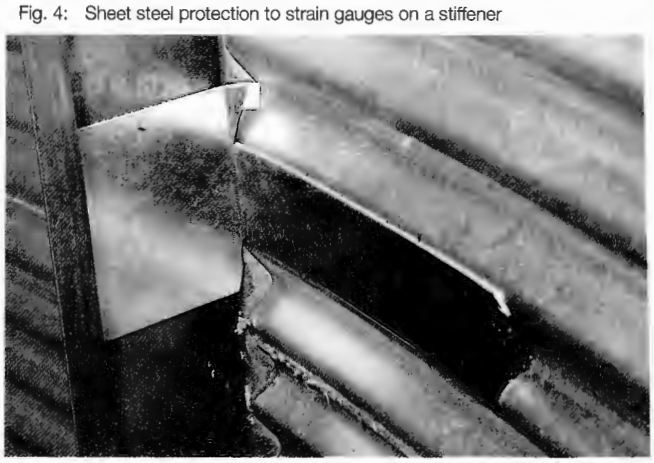

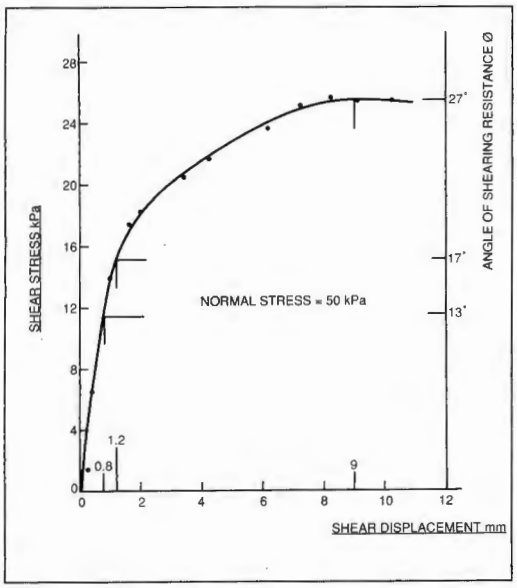

Fig. 5 (left): Shearing curve for barley

Fig. 6 (right): Lateral pressures and stiffener loads observed for silo 10

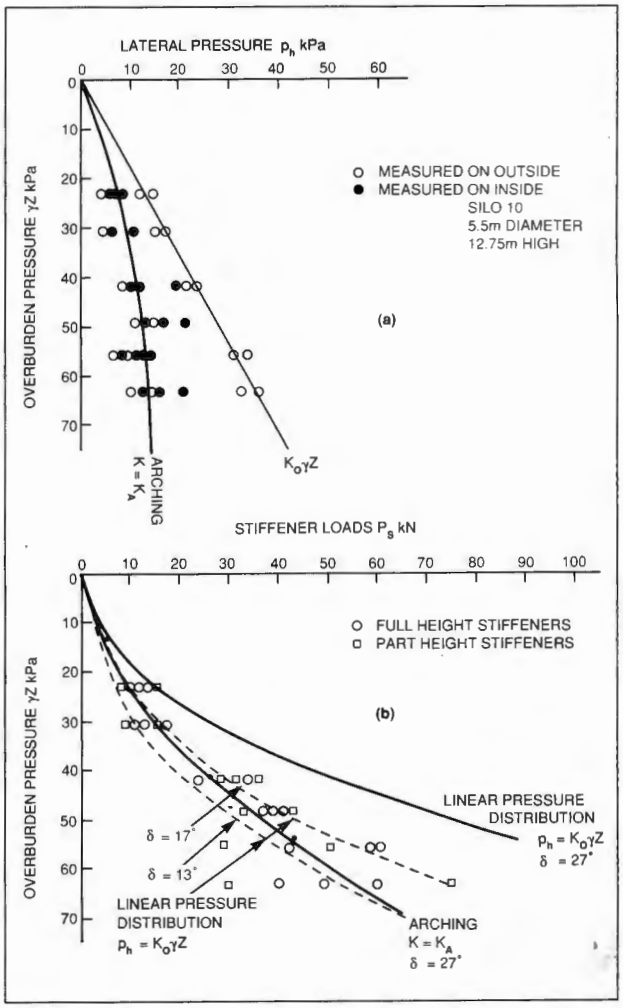

Fig. 7 (right): Radial distribution of lateral pressure and stiffener load

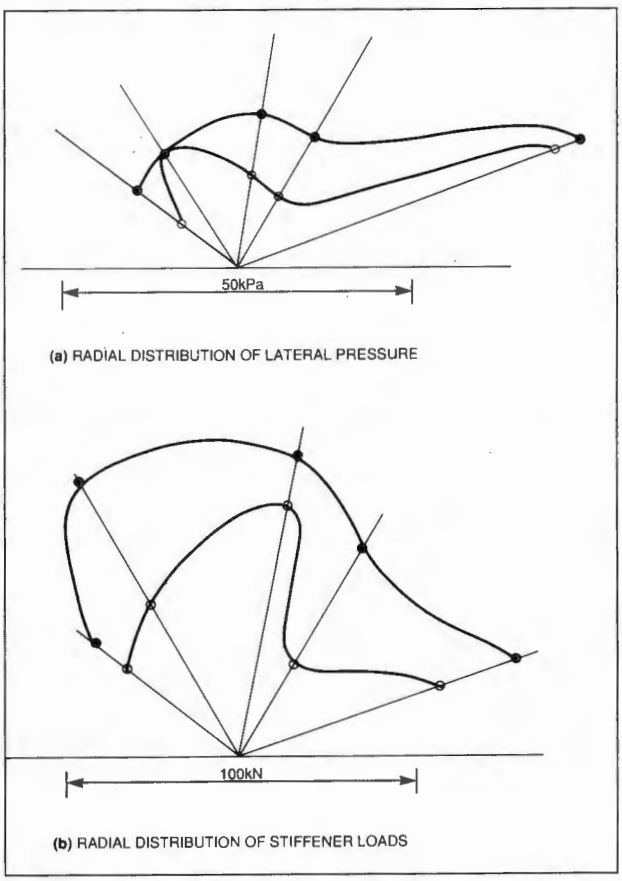

develop half that angle requires less than 1 mm of shear displacement.

4. Pressures and Stiffener Loads for Silo 10

The lateral pressures and stiffener loads calculated from strain readings made during filling of silo 10 are plotted in Fig. 6. Values of P_h were calculated from the expression:

$$p_h = \frac{2Et\varepsilon_h}{D} \qquad (1)$$

in which

p_h = the lateral pressure on the silo wall

E = elastic modulus of steel

t = wall thickness

ε_h = measured lateral strain

D = silo diameter

The validity of this expression depends on the observation [3] that vertical strains in the corrugated silo wall are essentially zero. The stiffener loads P_s were calculated from:

$$P_s = \frac{\bar{\varepsilon}}{(1+\nu)} EA_s \qquad (2)$$

in which $\bar{\varepsilon}$ is the average compressive strain over the section of the stiffener and A_s is the stiffener's cross-sectional area.

As indicated in Fig. 1, $\bar{\varepsilon}$ was the average of three strain measurements. Typical distributions between gauges A, B and C (see Fig. 1) were as follows:

Upper gauges: (microstrain)	A - 441
	B - 260
	C - 250
Lower gauges: (microstrain)	A - 540
	B - 425
	C - 295

It is clear from these values that

1. the stiffeners are subject to bending (A compared with B) and
2. the section is far from being uniformly stressed.

It will be noted from Fig. 6a that measurements made on the inside of the cylinder agree reasonably well with those made on the outside. There are small differences that result from minor bending in the silo shell.

Fig. 7 shows the radial distribution of lateral pressures and stiffener loads at the lower level of strain gauges, when the silo was full, both at the end of filling, and after a month of storage. Figs. 6 and 7 need to be studied together, as the radial variation in Fig. 7 explains the variation of measurements shown in Fig. 6. It will be seen from Fig. 6a that while some of the measurements of lateral pressure follow the Janssen pressure line calculated for the

active lateral pressure coefficient K_A, (labeled "arching K = K_A), others follow the linear no-arching distribution corresponding to the at-rest pressure coefficient K_o. Fig. 7 shows that generally, low values of lateral pressure are associated with large stiffener loads, and vice versa. Fig. 6b shows that near the base of the silo, the part-height stiffeners carry as much load as the full-height ones.

It is clear from Figs. 6a and 7a that Janssen-type arching does not occur right round the perimeter of the silo, but that in certain areas there is insufficient transfer of load to the walls to affect the linear at-rest pressure distribution. In other areas, sufficient load transfer occurs to reduce the lateral pressure to the Janssen values.

It can be seen from Fig. 6b that the stiffener loads can be predicted reasonably well from the Janssen pressure distribution (arching, K = K_A) but that stiffener loads corresponding to a linear lateral pressure distribution can only be reconciled with the development of a reduced angle of wall friction of 17° to 13° or less. Hence it appears that full wall friction developed over sectors of the silo wall, giving rise to full Janssen-type arching. Over other sectors a reduced wall friction developed. This, in turn, reduced frictional load transfer to the walls and a linear (K_o) pressure distribution resulted. Fig. 6a shows that yet other sectors must have developed conditions intermediate between K_A arching and K_o no-arching, while certain sectors must have approached K_o arching. Hence the structure-fill interaction in so seemingly simple a structure as a silo is exceedingly complex. The complex behaviour may to a large extent result from differences in compressibility of the barley as it is placed. The extent to which wall friction develops (see Fig. 5) depends on the shear displacement between the fill and the wall. Hence differential compression will result in differential wall friction, differential stiffener loads and differential lateral pressures. The radial profiles in Fig. 7 show that lateral pressures and wall loads generally increased in the period of storage that followed the end of filling. This is probably as a result of temperature variations causing a thermal ratchetting effect [4] on lateral pressures and a consequent increase in developed friction on the silo walls.

A possible alternative explanation for the apparent low developed angle of wall friction is that the stiffeners may not be carrying all of the frictional wall load. Earlier measurements [3] have demonstrated the low stiffness of corrugated sheeting when subjected to compression across the corrugations. These measurements showed that at cross-corrugation strains comparable with the compressive strains in the stiffeners, 3 mm thick corrugated sheeting can support a load of only 1 to 1,5 kN/m. The sheeting of silo 10 is 1.6 mm thick and would therefore be able to support even less load than the 3 mm sheeting. Referring to Fig. 6a, the frictional wall load corresponding to a stiffener load of 50 kN is 35 kN/m, hence it is unlikely that load-carrying by the silo wall sheeting could have influenced the results to any significant extent.

5. Pressures and Stiffener Loads for Silo 8

The lateral pressures and stiffener loads observed for silo 8 are shown in Fig. 8. In contrast to the wide variability of lateral pressure and stiffener load observed in Silo 10, conditions in Silo 8 appeared almost uniform around its perimeter. Silo 8 was filled with barley drawn from other storage silos in the complex, whereas Silo 10 was filled from train-loads of new grain coming into the factory. In the case of Silo 8 there was probably some blending of product that produced a more uniform fill than was loaded into Silo 10.

The distribution of lateral pressure was linear with depth with pressures varying between $K_A\gamma z$ and $K_o\gamma z$. There was no evidence of Janssen-type arching, but

Fig. 8: Lateral pressures and stiffener loads observed for silo 8

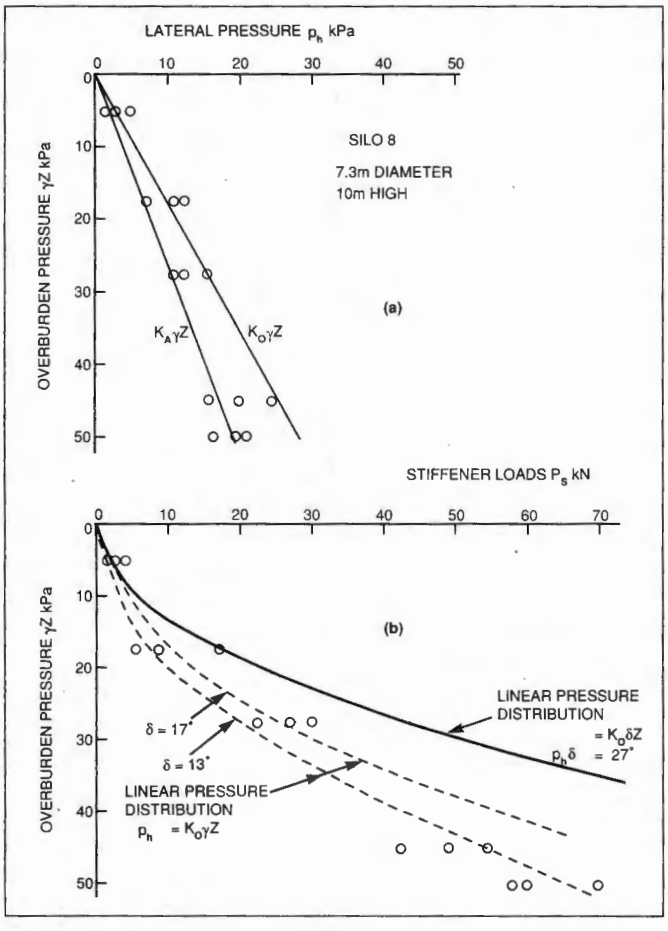

Fig. 9: Lateral pressures and stiffener loads observed for silo 1

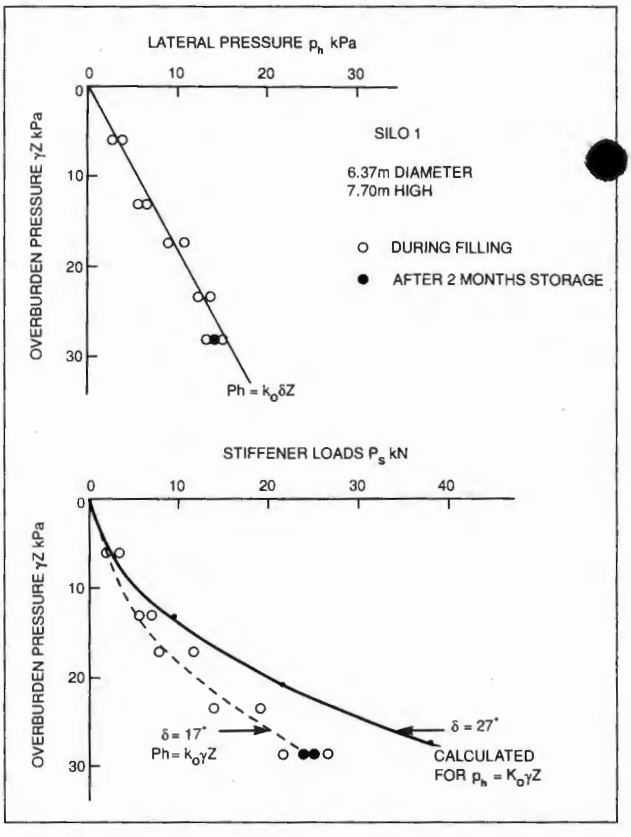

the height-to-diameter ratio for this silo is less than that of Silo 10. The variation of stiffener load with overburden pressure also shows the development of a reduced angle of wall friction - again 17° to 13° or less. Hence apart from the absence of arching, the results for Silo 8 are not dissimilar to those for Silo 10.

6. Pressures and Stiffener Loads for Silo 1

The final set of lateral pressure and stiffener load measurements shown in Fig. 9, is for Silo 1. Silo 1 is inside a building and therefore protected from rapid temperature fluctuations. It was filled by transferring grain from other silos in the complex. Hence one might expect little variation between one set of measurements and another. This was indeed so. As Fig. 9 shows, the pressure distribution was linear with depth and stiffener loads correspond to a developed angle of wall friction of about 17°. Hence this set of measurements is very similar to that for Silo 8. Note from Fig. 9 that the lateral pressure and stiffener loads were almost unchanged after 2 months of storage. Contrast this with the change of pressure and stiffener loads that occurred in Silo 10 during 1 month of storage (Fig. 7). This confirms the conclusion that increases of loads during storage are largely a result of diurnal temperature variations. Although Silo 1 is subject to diurnal temperature variations, these are muted because the silo is indoors, whereas Silo 10 is fully exposed to the elements.

7. Temperature-induced Strains and Pressures

An expression enabling temperature surcharge pressures on the walls of silos to be predicted has been developed [5] and appears as equation (3):

$$TS = \frac{2MEt\varepsilon_f}{MD + 2Et} \qquad (3)$$

in which

- TS is the temperature surcharge pressure,
- M is the modulus of compressibility of the silo contents for radial compression,
- ε_f is the thermal strain the silo would have undergone had it been empty,

and E, t and D are as defined in section 4 of this paper.

There is at present no satisfactory method of measuring M in the laboratory.

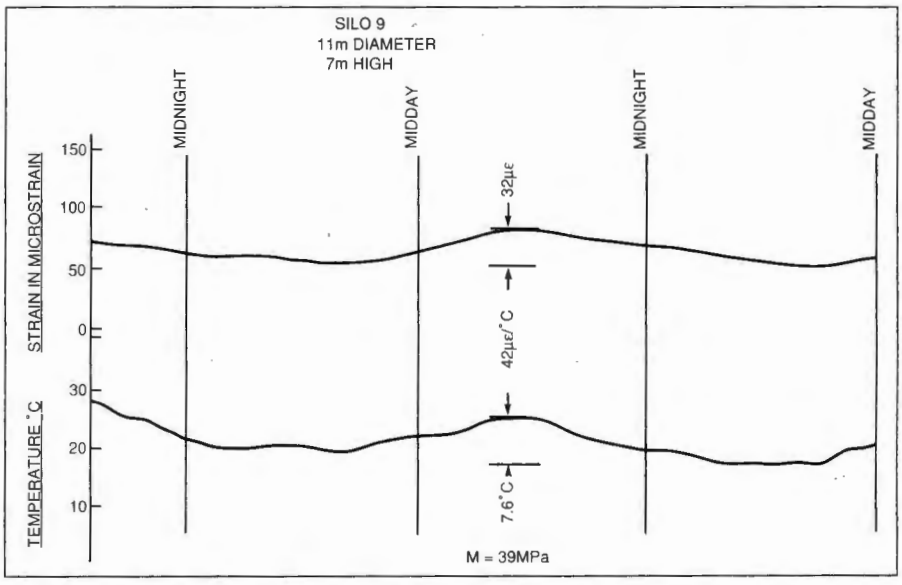

Fig. 10: Simultaneous recordings of temperature and prevented thermal strain for silo 9 – storing barley malt

Hence the author has for the past 5 years been assembling information on M from measurements on full size silos. The present exercise has provided values of M for barley and malt.

The type of measurement is shown in Fig. 10. This represents simultaneous recordings of prevented thermal strain and temperature at a point on the wall of Silo 9 - storing barley malt. Because the silo is indoors, the changes in temperature are subdued, without the sharp peaks in temperature that result from the sun shining on a silo wall.

The strain gauges were compensated for temperature, hence they record the thermal strain that is prevented by the presence of the silo contents. This strain, per unit temperature change $\Delta\theta$ is $\dot{\varepsilon}$ where

$$\Delta\Theta\dot{\varepsilon} = \varepsilon_f - \frac{TS}{M} \qquad (4)$$

$$TS = \frac{2Et\Delta\Theta\dot{\varepsilon}}{D} \qquad (5)$$

$$M = \frac{2Et\dot{\varepsilon}}{D(\alpha - \dot{\varepsilon})} \qquad (6)$$

Fig. 11 shows the data on M resulting from measurements on 9 steel grain silos, as well as a reinforced concrete silo storing cement powder. Fortunately, values of M for the grains dealt with so far: maize, wheat, barley and malt, seem to lie close to a common relationship between M and overburden stress.

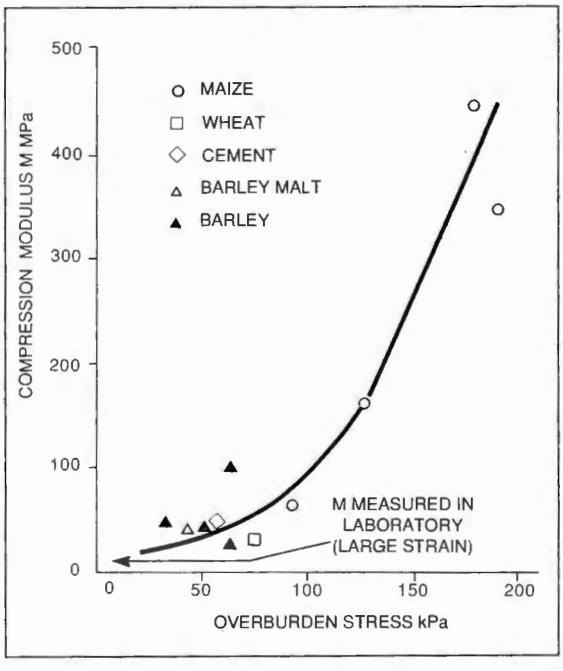

Fig. 11: Relationship between compression modulus M and overburden stress calculated from measurements on 10 steel grain silos and a reinforced concrete cement silo

8. Conclusions

1. This study of the lateral pressures and stiffener loads in three similar silos, storing nominally the same grain has again demonstrated the complexity of the interaction between a silo and its filling.
2. It has shown that Janssen-type arching can occur over part of the perimeter of a silo, but need not occur over the whole perimeter. This has confirmed earlier observations of the behaviour of a steel sugar silo and a steel maize silo [6, 7]. It has further demonstrated the radial non-uniformity that may apply to lateral pressures and frictional wall or stiffener loads.
3. It has emphasized the dependence of stress on strain by showing that the full angle of wall friction need not develop between the silo and its contents if insufficient shear displacement occurs.

Acknowledgement

The experimental work took place by courtesy of King Food Corporation of Johannesburg. The author was introduced to King Food Corporation by Bessemer Steel Construction, designers and builders of the silos.

The instrumentation was installed and many of the measurements were taken by Mr. *Bob Anderson.*

References

[1] *Borcz, A.* and *El Rahim, H.A.*: Pressure measurements on cement silos; powder handling and processing Vol. 2 (1990) No. 3, pp. 239-246.

[2] *Blight, G.E.*: Measured loading on a small steel grain silo; powder handling and processing; Vol. 2 (1990) No. 2, pp. 153-158.

[3] *Blight, G.E.*: Behaviour of a bolted corrugated steel grain silo; powder handling and processing, Vol. 1 (1989) No. 2, pp .143-149.

[4] *Blight, G.E.*: Temperature changes affect pressures in steel bins; Int. Jnl. Bulk Solids Storage in Silos, Vol. 1 (1985) No. 3, pp. 1-7.

[5] *Blight, G.E.*: Defects in accepted methods of estimating design loading for silos; Proc. Inst. Civ. Engrs. (U.K.) Part 1, Vol. 88 (1990), pp. 1015-1036.

[6] *Blight, G.E.*: Strains measured in a 7500t sugar silo. Part II; bulk solids handling, Vol. 8 (1988) No. 4, pp. 413-419.

[7] *Blight, G.E.*: Load and temperature strains of a welded plane plate grain silo; powder handling and processing, Vol, 2 (1990) No, 1, pp, 25-29.

Correction and Explanation

powder handling & processing No. 4/90, Article: "Temperature Surcharge Pressures in Reinforced Concrete Silos" by G.E. Blight.

– Fig. 1: dimension "*t*" should be "*xt*"

– In deriving eq. (2) of the paper, it may appear that the transformed area of the reinforcing steel has been left out of consideration. In practice, the inner and outer hoop reinforcing areas in a reinforced concrete silo are usually equal and symmetrically placed. Therefore areas A and B in Figs. 1b and 1c would each include the transformed area of half of the total hoop steel and eq. (2) would be unaffected. The effect of the hoop steel would only be felt if either,

- the inner and outer hoop steel areas were unequal, or
- the temperature gradient through the wall did not penetrate beyond the outer cover of concrete.

Only the first of these conditions is likely to be one of practical concern.